Advanced membrane science and technology for sustainable energy and environmental applications

© Woodhead Publishing Limited, 2011

Related titles:

Advanced power plant materials, design and technology
(ISBN 978-1-84569-515-6)

Fossil-fuel power plants generate the majority of the world's power, but many plants are ageing and cannot meet rising global energy demands and increasingly stringent emissions criteria. To ensure security and economy of supply, utilities are building a new generation of advanced power plants with increased output and environmental performance. This book initially reviews improved plant designs for efficiency and fuel flexibility, including combined-cycle technology and utilisation of lower-grade feedstocks. Coverage extends to advanced material and component use, and the incorporation of alternative energy conversion technology.

Developments and innovation in carbon dioxide (CO_2) capture and storage technology: Volume 1: Carbon dioxide (CO_2) capture, transport and industrial applications
(ISBN 978-1-84569-533-0)

Carbon dioxide (CO_2) capture and storage (CCS) is the one advanced technology that conventional power generation cannot do without. CCS technology reduces the carbon footprint of power plants by capturing and storing the CO_2 emissions from burning fossil fuels and biomass. This volume provides a comprehensive reference on the state of the art of research, development and demonstration of carbon capture technology in the power sector and in industry. It critically reviews the range of post- and pre-combustion capture and combustion-based capture processes and technology applicable to fossil-fuel power plants.

Oxy-fuel combustion for power generation and carbon dioxide (CO_2) capture
(ISBN 978-1-84569-671-9)

Oxy-fuel combustion is currently considered to be one of the major technologies for carbon dioxide (CO_2) capture in power plants. The advantages of using oxygen (O_2) instead of air for combustion include a CO_2-enriched flue gas that is ready for sequestration following purification and low NO_x emissions. This book critically reviews the fundamental principles, processes and technology of oxy-fuel combustion.

Details of these and other Woodhead Publishing materials books can be obtained by:

- visiting our web site at www.woodheadpublishing.com
- contacting Customer Services (e-mail: sales@woodheadpublishing.com; fax: +44 (0) 1223 832819; tel.: +44 (0) 1223 499140 ext. 130; address: Woodhead Publishing Limited, 80 High Street, Sawston, Cambridge CB22 3HJ, UK).

If you would like to receive information on forthcoming titles, please send your address details to: Francis Dodds (address, telephone and fax as above; e-mail: francis.dodds@woodheadpublishing.com). Please confirm which subject areas you are interested in.

http://avaxhome.ws/blogs/ChrisRedfield

Woodhead Publishing Series in Energy: Number 25

Advanced membrane science and technology for sustainable energy and environmental applications

Edited by

Angelo Basile and Suzana Pereira Nunes



Oxford Cambridge Philadelphia New Delhi

© Woodhead Publishing Limited, 2011

Published by Woodhead Publishing Limited,
80 High Street, Sawston, Cambridge CB22 3HJ, UK
www.woodheadpublishing.com

Woodhead Publishing, 1518 Walnut Street, Suite 1100, Philadelphia,
PA 19102-3406, USA

Woodhead Publishing India Private Limited, G-2, Vardaan House,
7/28 Ansari Road, Daryaganj, New Delhi – 110002, India
www.woodheadpublishingindia.com

First published 2011, Woodhead Publishing Limited
© Woodhead Publishing Limited, 2011
The authors have asserted their moral rights.

This book contains information obtained from authentic and highly regarded sources. Reprinted material is quoted with permission, and sources are indicated. Reasonable efforts have been made to publish reliable data and information, but the authors and the publisher cannot assume responsibility for the validity of all materials. Neither the authors nor the publisher, nor anyone else associated with this publication, shall be liable for any loss, damage or liability directly or indirectly caused or alleged to be caused by this book.

Neither this book nor any part may be reproduced or transmitted in any form or by any means, electronic or mechanical, including photocopying, microfilming and recording, or by any information storage or retrieval system, without permission in writing from Woodhead Publishing Limited.

The consent of Woodhead Publishing Limited does not extend to copying for general distribution, for promotion, for creating new works, or for resale. Specific permission must be obtained in writing from Woodhead Publishing Limited for such copying.

Trademark notice: Product or corporate names may be trademarks or registered trademarks, and are used only for identification and explanation, without intent to infringe.

British Library Cataloguing in Publication Data
A catalogue record for this book is available from the British Library.

Library of Congress Control Number: 2011934921

ISBN 978-1-84569-969-7 (print)
ISBN 978-0-85709-379-0 (online)
ISSN 2044-9364 Woodhead Publishing Series in Energy (print)
ISSN 2044-9372 Woodhead Publishing Series in Energy (online)

The publisher's policy is to use permanent paper from mills that operate a sustainable forestry policy, and which has been manufactured from pulp which is processed using acid-free and elemental chlorine-free practices. Furthermore, the publisher ensures that the text paper and cover board used have met acceptable environmental accreditation standards.

Typeset by Replika Press Pvt Ltd, India
Printed by TJI Digital, Padstow, Cornwall, UK

© Woodhead Publishing Limited, 2011

Contents

Contributor contact details *xv*

Woodhead Publishing Series in Energy *xxi*

Preface *xxvii*

Part I Introduction to membrane science and engineering

1 Fundamental membrane processes, science and engineering 3
V. Calabrò, University of Calabria, Italy and A. Basile, Institute on Membrane Technology of the Italian National Research Council (ITM-CNR), Italy

1.1 Introduction 3
1.2 Membrane processes 4
1.3 Conclusions and future trends 18
1.4 References 18

2 Fundamental science of gas and vapour separation in polymeric membranes 22
Y. Yampolskii, A.V. Topchiev Institute of Petrochemical Synthesis, Russian Academy of Sciences, Russia

2.1 Introduction 22
2.2 Basic principles and definitions of separation processes 23
2.3 Effects of the properties of penetrants and polymers 32
2.4 Effects of pressure on transport parameters 39
2.5 Effects of temperature on transport parameters 45
2.6 Gas permeability of polymers: objects of membrane gas separation 47
2.7 References 49
2.8 Appendix: list of symbols 54

© Woodhead Publishing Limited, 2011

3 Characterization of membranes for energy and environmental applications 56
M. Campo, A. Tanaka and A. Mendes, University of Porto, Portugal and J. M. Sousa, University of Trás-os-Montes e Alto Douro, Portugal

3.1 Polymer and carbon molecular sieve membranes 56
3.2 Zeolite and mixed matrix membranes 64
3.3 Mass transport characterization 71
3.4 Conclusions 80
3.5 References 80
3.6 Appendix: list of symbols 88

4 Economic analysis of membrane use in industrial applications 90
V. Calabrò, University of Calabria, Italy and A. Basile, Institute on Membrane Technology of the Italian National Research Council (ITM-CNR), Italy

4.1 Introduction 90
4.2 Economic analysis 91
4.3 Case studies 96
4.4 Conclusions and future trends 106
4.5 References 107

Part II Membranes for coal and gas power plants: carbon dioxide (CO_2) capture, synthesis gas processing and oxygen (O_2) transport

5 Membrane technology for carbon dioxide (CO_2) capture in power plants 113
A. Basile, A. Gugliuzza, and A. Iulianelli, Institute on Membrane Technology of the Italian National Research Council (ITM-CNR), Italy and P. Morrone, University of Calabria, Italy

5.1 Introduction 113
5.2 Reasons for using membranes for carbon dioxide (CO_2) separation and sequestration 123
5.3 A short review of membrane technology for CO_2 separation 124
5.4 Performance of membrane processes for CO_2 sequestration 137
5.5 Membrane modules for CO_2 sequestration 139
5.6 Design for power plant integration 141
5.7 Cost considerations and membrane technology at the industrial scale 142
5.8 Modelling aspects of gas permeation membrane modules 144
5.9 Conclusion and future trends 150

© Woodhead Publishing Limited, 2011

5.10	References	151
5.11	Appendix: list of symbols	158
6	Polymeric membranes for post-combustion carbon dioxide (CO_2) capture W. Yave and A. Car, GKSS-Research Centre Geesthacht GmbH, Germany	160
6.1	Introduction	160
6.2	Basic principles of flue gas membrane separation	163
6.3	Membrane development and applications in power plants	166
6.4	Operation and performance issues and analysis	176
6.5	Advantages and limitations	179
6.6	Future trends	179
6.7	References	180
7	Inorganic membranes for pre-combustion carbon dioxide (CO_2) capture A. Iulianelli and A. Basile, Institute on Membrane Technology of the Italian National Research Council (ITM-CNR), Italy and H. Li and R. W. van den Brink, ECN Hydrogen Production and CO_2 Capture, The Netherlands	184
7.1	Introduction	184
7.2	Inorganic membranes for carbon dioxide (CO_2) separation	187
7.3	Membrane reactors for CO_2 capture	197
7.4	Techno-economic analysis of the integrated gasification combined cycle (IGCC) and natural gas combined cycle (NGCC)	205
7.5	Conclusions and future trends	207
7.6	References	207
8	Inorganic membranes for synthesis gas processing S. Smart, L. P. Ding and J. C. Diniz da Costa, University of Queensland, Australia	214
8.1	Introduction	214
8.2	Basic principles of membrane operation	218
8.3	Membrane materials and development	223
8.4	Application and integration in industry	230
8.5	Membrane modules	237
8.6	Future trends	241
8.7	Conclusions	244
8.8	References	244
8.9	Appendix: list of symbols	253

© Woodhead Publishing Limited, 2011

9 Oxygen transport membranes: dense ceramic membranes for power plant applications 255
S. Smart and J. C. Diniz da Costa, University of Queensland, Australia, and S. Baumann and W. A. Meulenberg, Forschungszentrum Jülich, Germany

9.1 Introduction 255
9.2 Oxygen transport membrane materials, development and design 256
9.3 Principles of oxygen membrane separation 263
9.4 Application and integration in power plants 267
9.5 Oxygen transport membranes 275
9.6 Future trends 282
9.7 Conclusions 284
9.8 Acknowledgements 285
9.9 References 286

Part III Membranes for the petrochemical industry: hydrocarbon fuel and natural gas processing, and advanced biofuels production

10 Membranes for hydrocarbon fuel processing and separation 295
A. Gugliuzza, A. Iulianelli and A. Basile, Institute on Membrane Technology of the Italian National Research Council (ITM-CNR), Italy

10.1 Introduction 295
10.2 Membrane materials, development and design for hydrocarbon processing 297
10.3 Separation of olefins and paraffins 314
10.4 Removal of hydrocarbons from liquid streams 317
10.5 Nanotechnologies from fundamental research to large-scale industry 322
10.6 References 329
10.7 Appendix: list of symbols 338

11 Polymeric membranes for natural gas processing 339
S. E. Kentish, CRC for Greenhouse Gas Technologies (CO2CRC), University of Melbourne, Australia

11.1 Introduction 339
11.2 Polymeric membrane operations in natural gas processing 339
11.3 Membrane materials, development and design for natural gas processing 341
11.4 Operation and performance issues and analysis 346

© Woodhead Publishing Limited, 2011

11.5 Application and integration into natural gas operations 349
11.6 Advantages and limitations 351
11.7 Future trends 352
11.8 Sources of further information and advice 355
11.9 References 356
11.10 Appendix: list of symbols 360

12 Membranes for advanced biofuels production 361
S. Curcio, University of Calabria, Italy

12.1 General overview of second-generation biofuels 361
12.2 Hydrolysis of biomass to produce sugars 367
12.3 Key role of process engineering for second-generation biofuels production 371
12.4 Membrane bioreactors 372
12.5 Biocatalyst continuously separated by a membrane system and recirculated into the reaction tank 374
12.6 Biocatalyst immobilized onto the membrane surface 378
12.7 Continuous stirred tank reactor with biocatalyst immobilized on the membrane surface (CSTMB) 382
12.8 Single pass membrane bioreactor 384
12.9 Hollow fibre membrane bioreactor with recycling of unreacted substrate 396
12.10 Conclusions 402
12.11 Sources of further information and advice 403
12.12 References 403
12.13 Appendix: list of symbols 406

Part IV Membranes for alternative energy applications: batteries, fuel cells and hydrogen (H_2) production

13 Ion exchange membranes for vanadium redox flow batteries 413
S. S. Hosseiny, Aachener Verfahrenstechnik-Chemische Verfahrenstechnik, RWTH-Aachen University, Germany and M. Wessling, Aachener Verfahrenstechnik-Chemische Verfahrenstechnik, RWTH-Aachen University, Germany and University of Twente, The Netherlands

13.1 Electrochemical energy storage 413
13.2 Vanadium redox flow batteries 418
13.3 Membranes 423
13.4 Conclusions 430
13.5 References 430

© Woodhead Publishing Limited, 2011

14 Membranes for lithium batteries 435
R. Bongiovanni and J. R. Nair, Politecnico di Torino, Italy, C. Gerbaldi, Italian Institute of Technology and Politecnico di Torino, Italy and A. M. Stephan, Central Electrochemical Research Institute, India

14.1 Introduction 435
14.2 Types of lithium battery and basic operating principles 436
14.3 Polymer electrolyte membranes for advanced lithium batteries 441
14.4 Conclusions and future trends 455
14.5 Sources of further information and advice 456
14.6 References 458

15 Proton exchange membranes for fuel cells 465
V. Arcella, L. Merlo and A. Ghielmi, Solvay Solexis S.p.A., Italy

15.1 Introduction 465
15.2 Basic operating principles and types of fuel cell 466
15.3 Membrane materials, design and fabrication processes 468
15.4 Membrane performance in operation: issues and analysis 487
15.5 Integration and application of proton exchange membrane (PEM) fuel cell systems 489
15.6 Advantages and limitations of PEM fuel cells 491
15.7 Future trends 491
15.8 Sources of further information and advice 492
15.9 References 492
15.10 Appendix: list of symbols 494

16 Functional ceramic hollow fibre membranes for catalytic membrane reactors and solid oxide fuel cells 496
Z. T. Wu, M. H. D. Othman, B. F. K. Kingsbury and K. Li, Imperial College London, UK

16.1 Introduction 496
16.2 Membrane materials issues 499
16.3 Membrane development routes and macrostructure control 501
16.4 A multifunctional dual-layer hollow fibre membrane reactor (DL-HFMR) for methane conversion 507
16.5 Dual-layer hollow fibres for a micro-tubular solid oxide fuel cell (SOFC) 518
16.6 Other ways of improving ceramic dual-layer hollow fibres 535
16.7 Conclusions 537
16.8 References 538

© Woodhead Publishing Limited, 2011

17 Proton-conducting ceramic membranes for solid oxide fuel cells and hydrogen (H_2) processing 541
W. A. Meulenberg, M. E. Ivanova, Forschungszentrum Jülich GmbH, Germany, J. M. Serra, Instituto de Technologia Química (UPV-CSIC), Spain and S. Roitsch, Ernst-Ruska Centre for Microscopy and Spectroscopy with Electrons, RWTH Aachen University and Forschungszentrum Jülich GmbH, Germany

17.1 Introduction 541
17.2 Operation principle of proton-conducting ceramic membranes and demands on materials 542
17.3 Protons and proton conductance in ceramics 545
17.4 Conductivity and hydrogen (H_2) flux of selected classes of ceramic membrane materials 549
17.5 Structure of selected classes of proton-conducting materials 555
17.6 Chemical stability of selected classes of ceramic membrane materials 559
17.7 Conclusions 561
17.8 Acknowledgements 562
17.9 References 562

18 Membrane electrolysers for hydrogen (H_2) production 568
P. Millet, University of Paris, France

18.1 Introduction 568
18.2 Basic principles of electrolysis 571
18.3 Membrane materials 574
18.4 Membrane performance 580
18.5 Application and integration of electrolyser systems 586
18.6 Some advantages and limitations of current membrane materials 601
18.7 Future trends 605
18.8 Sources of further information and advice 605
18.9 References 606
18.10 Appendix: nomenclature 608

19 Biomimetic membrane reactors for hydrogen (H_2) production 610
S. Bensaid and G. Saracco, Politecnico di Torino, Italy

19.1 Introduction 610
19.2 General background to the concept 613
19.3 An ambitious goal with numerous challenges 614
19.4 Thermodynamic limitations and device design 622
19.5 Integrated engineering approach for solar-to-fuel conversion 635

© Woodhead Publishing Limited, 2011

19.6 Conclusions 638
19.7 References 640

Part V Membranes for industrial, environmental and nuclear applications

20 Membranes for industrial microfiltration and ultrafiltration 647
A. Cassano and A. Basile, Institute on Membrane Technology of the Italian National Research Council (ITM-CNR), Italy

20.1 Introduction 647
20.2 Basic principles of microfiltration and ultrafiltration 648
20.3 Membrane materials and membrane preparation technology 649
20.4 Module configuration and process design 652
20.5 Concentration polarization and membrane fouling 661
20.6 Applications 668
20.7 Microfiltration and ultrafiltration in integrated processes 673
20.8 Advantages and limitations 676
20.9 Future trends 676
20.10 Sources of further information and advice 677
20.11 References 677

21 Membranes for forward osmosis in industrial applications 680
N. K. Rastogi and C. A. Nayak, Central Food Technological Research Institute, India

21.1 Introduction 680
21.2 Mechanism of forward osmosis 683
21.3 Membranes for forward osmosis 688
21.4 Forward osmosis membrane modules 692
21.5 Effect of various parameters on transmembrane flux 695
21.6 Applications of forward osmosis 703
21.7 Conclusions 711
21.8 Acknowledgements 712
21.9 References 712

22 Degradation of polymeric membranes in water and wastewater treatment 718
A. Antony and G. Leslie, The University of New South Wales, Australia

22.1 Introduction 718
22.2 Polymer materials and module design 719

© Woodhead Publishing Limited, 2011

22.3	Membrane failure and operational issues	720
22.4	Membrane degradation mechanisms	724
22.5	Identification and monitoring of membrane degradation	731
22.6	Materials degradation control strategies	737
22.7	Future trends	739
22.8	Sources of further information and advice	739
22.9	Acknowledgements	740
22.10	References	740
23	Membranes for photocatalysis in water and wastewater treatment V. Loddo and L. Palmisano, Università di Palermo, Italy and T. Marino and R. Molinari, Università della Calabria, Italy	746
23.1	Introduction	746
23.2	Basic principles of heterogeneous photocatalysis	747
23.3	Membrane materials developments and design for photocatalysis	749
23.4	Membrane operations performance issues and analysis: case studies	759
23.5	Future trends	765
23.6	Sources of further information and advice	765
23.7	References	765
24	Membranes for nuclear power applications S. Tosti, ENEA, Italy and C. Rizzello, Tesi Sas, Italy	769
24.1	Introduction	769
24.2	Membranes for nuclear fission applications	771
24.3	Membranes for nuclear fusion applications	776
24.4	Conclusions	785
24.5	Future trends	787
24.6	References	788
	Index	*792*

© Woodhead Publishing Limited, 2011

Contributor contact details

(* = main contact)

Editors

A. Basile (also Chapters 1, 4, 5, 7, 10 and 20)
Institute on Membrane Technology
Italian National Research Council (ITM-CNR)
c/o University of Calabria
via P. Bucci, cubo 17/C
87030 Rende (CS)
Italy

E-mail: a.basile@itm.cnr.it

Ast-Engineering s.r.l.
via Portuense n. 95
I-00153
Rome
Italy

S. Pereira Nunes
King Abdullah University of Science and Technology (KAUST)
Water Desalination and Reuse Center
23955-6900 Thuwal
Kingdom of Saudi Arabia

E-mail: suzana.nunes@kaust.edu.sa

Chapter 1

V. Calabrò
Department of Engineering Modeling
University of Calabria
via P. Bucci, cubo 39/c
87030 Rende (CS)
Italy

E-mail: vincenza.calabro@unical.it

A. Basile
ITM-CNR
University of Calabria
Via P. Bucci, cubo 17/C
87030 Rende (CS)
Italy

E-mail: a.basile@itm.cnr.it

Chapter 2

Y. Yampolskii
A. V. Topchiev Institute of Petrochemical Synthesis
Russian Academy of Sciences
Moscow 119991
Leninsky Prospect 29
Russia

E-mail: Yampol@ips.ac.ru

© Woodhead Publishing Limited, 2011

Chapter 3

M. Campo, A. Tanaka, A. Mendes* and J. M. Sousa
LEPAE – Department of Chemical Engineering
Faculty of Engineering of University of Porto
Rua Roberto Frias S/N
4200-465 Porto
Portugal

E-mail: mendes@fe.up.pt

J. M. Sousa
School of Life and Environmental Sciences - Chemistry Department
University of Trás-os-Montes e Alto Douro
Apartado 1013, 5001-801 – Vila Real Codex
Portugal

E-mail: jsousa@utad.pt

Chapter 4

V. Calabrò*
Department of Engineering Modeling
University of Calabria
Via P. Bucci, cubo 39/C
87030 Rende (CS)
Italy

E-mail: vincenza.calabro@unical.it

A. Basile
ITM-CNR
University of Calabria
Via P. Bucci, cubo 17/C
87030 Rende (CS)
Italy

E-mail: a.basile@itm.cnr.it

Chapter 5

A. Basile*, A. Gugliuzza and A. Iulanelli
Institute on Membrane Technology
Italian National Research Council (ITM-CNR)
c/o University of Calabria
via P. Bucci, cubo 17/C
87030 Rende (CS)
Italy

E-mail: a.basile@itm.cnr.it

P. Morrone
Department of Mechanical Engineering
Via Pietro Bucci 45/C
University of Calabria
I-87030 Rende
Italy

Chapter 6

W. Yave and A. Car*
formerly of
Institute of Materials Research
GKSS-Research Centre Geesthacht GmbH
Max-Planck Strasse 1
21502 Geesthacht
Germany

E-mail: car_anja@hotmail.com

© Woodhead Publishing Limited, 2011

Chapter 7

A. Iulanelli* and A. Basile
Institute on Membrane Technology
Italian National Research Council (ITM-CNR)
c/o University of Calabria
via P. Bucci, cubo 17/C
87030 Rende (CS)
Italy

E-mail: a.iulianelli@itm.cnr.it

H. Li and R. W. Van den Brink
ECN Hydrogen Production & CO_2 Capture
P.O. Box 1
NL1755 ZG Petten
The Netherlands

Chapter 8

S. Smart, L. P. Ding and J. C. Diniz da Costa*
FIMLab – Films and Inorganic Membrane Laboratory
School of Chemical Engineering
Chemical Engineering Building (74)
The University of Queensland
Brisbane
Queensland 4072
Australia

E-mail: j.dacosta@eng.uq.edu.au

Chapter 9

S. Smart and J. C. Diniz da Costa*
FIMLab – Films and Inorganic Membrane Laboratory
CCETech – Centre for Coal Energy Technology
School of Chemical Engineering
Chemical Engineering Building (74)
The University of Queensland
Brisbane
Queensland 4072
Australia

E-mail: j.dacosta@eng.uq.edu.au

S. Baumann and W. A. Meulenberg
Forschungszentrum Jülich
Institute of Energy and Climate Research
IEK-1: Materials Synthesis and Processing
52425 Jülich
Germany

E-mail: sbaumann@fz-juelich.de
w.a.meulenberg@fz-juelich.de

Chapter 10

A. Gugliuzza*, A. Iulianelli and A. Basile
Institute on Membrane Technology
Italian National Research Council (ITM-CNR)
c/o University of Calabria
via P. Bucci, cubo 17/C
87030 Rende (CS)
Italy

E-mail: a.gugliuzza@itm.cnr.it

© Woodhead Publishing Limited, 2011

Chapter 11

S. E. Kentish
CRC for Greenhouse Gas Technologies (CO2CRC)
Department of Chemical and Biomolecular Engineering
The University of Melbourne
Victoria 3010
Australia

E-mail: sandraek@unimelb.edu.au

Chapter 12

S. Curcio
Department of Engineering Modeling
University of Calabria
Ponte P. Bucci, cubo 39/C
Rende (CS)
87036
Italy

E-mail: j.dacosta@eng.uq.edu.au

Chapter 13

S. S. Hosseiny and M.Wessling*
Aachener Verfahrenstechnik-Chemische Verfahrenstechnik
RWTH-Aachen University
Turmstrasse46
52064 Aachen
Germany

E-mail: m.wessling@tnw.utwente.nl

M. Wessling
University of Twente
P.O. Box 217
7500 AE Enschede
The Netherlands

Chapter 14

R. Bongiovanni* and J. R. Nair
Department of Materials Science and Chemical Engineering
Politecnico di Torino
C. Duca degli Abruzzi 24
10129 Torino
Italy

E-mail: roberta.bongiovanni@polito.it

C. Gerbaldi
Center for Space Human Robotics @ POLITO
Italian Institute of Technology
and
Department of Materials Science and Chemical Engineering
Politecnico di Torino
Italy

A. M. Stephan
Electrochemical Power Systems Division
Central Electrochemical Research Institute
Karaikudi
India

Chapter 15

V. Arcella*, L. Merlo and A. Ghielmi
Solvay Solexis S.p.A.
Viale Lombardia 20
20021 Bollate (MI)
Italy

E-mail: vincenzo.arcella@solvay.com

© Woodhead Publishing Limited, 2011

Chapter 16

Z. T. Wu, M. H. D. Othman, B. F. K. Kingsbury and K. Li*
Department of Chemical Engineering and Chemical Technology
Imperial College London
South Kensington Campus
London
SW7 2AZ
UK

E-mail: Kang.Li@Imperial.ac.uk

Chapter 17

W. A. Meulenberg* and M. E. Ivanova
Forschungszentrum Jülich GmbH
Institute of Energy and Climate Research
IEK-1: Materials Synthesis and Processing
52425 Jülich
Germany

E-mail: w.a.meulenberg@fz-juelich.de
m.ivanova@fz-juelich.de

J. M. Serra
Instituto de Tecnología Química (UPV - CSIC)
av. los Naranjos s/n
46022 Valencia
Spain

E-mail: jmserra@itq.upv.es

S. Roitsch
Ernst Ruska Centre for Microscopy and Spectroscopy with Electrons
RWTH Aachen University and Forschungszentrum Jülich GmbH
Leo-Brandt-Str.
52425 Jülich
Germany

E-mail: s.roitsch@fz-juelich.de

Chapter 18

P. Millet
Institut de Chimie Moléculaire et des Matériaux d'Orsay
UMR 8182
Université Paris Sud
Centre d'Orsay
Bâtiment 410
91405 Orsay Cedex
France

E-mail: pierre.millet@u-psud.fr

Chapter 19

S. Bensaid* and G. Saracco
Department of Materials Science and Chemical Engineering
Politecnico di Torino
Corso Duca degli Abruzzi 24
10129 Torino
Italy

E-mail: samir.bensaid@polito.it

© Woodhead Publishing Limited, 2011

Chapter 20

A. Cassano* and A. Basile
Institute on Membrane Technology
Italian National Research Council (ITM-CNR)
c/o University of Calabria
via P. Bucci, cubo 17/C
87030 Rende (CS)
Italy

E-mail: a.cassano@itm.cnr.it

Chapter 21

N. K. Rastogi* and C. A. Nayak
Department of Food Engineering
Central Food Technological Research Institute
Council of Scientific and Industrial Research
Mysore - 570 020
India

E-mail: nkrastogi@cftri.res.in
nkrastogi@yahoo.com

Chapter 22

A. Antony and G. Leslie
UNESCO Centre for Membrane Science and Technology
The University of New South Wales
Sydney 2052
Australia

E-mail: alicea@unsw.edu.au
g.leslie@unsw.edu.au

Chapter 23

V. Loddo and L. Palmisano*
Schiavello Grillone
Photocatalysis group
Dipartimento di Ingegneria Elettrica, Elettronica e delle Telecomunicazioni
Università di Palermo
Viale delle Scienze
Ed. 6
90128 Palermo
Italy

E-mail: leonardo.palmisano@unipa.it

T. Marino and R. Molinari
Dipartimento di Ingegneria Chimica e dei Materiali
Università della Calabria
via P. Bucci
cubo 45/A
87030 Rende (CS)
Italy

Chapter 24

S. Tosti*
ENEA
Unità Tecnica Fusione
C.R. ENEA Frascati
Via E. Fermi 45
Frascati (RM) I-00044
Italy

E-mail: silvano.tosti@enea.it

C. Rizzello
Tesi Sas
Via Bolzano 28
Roma
Italy

© Woodhead Publishing Limited, 2011

Woodhead Publishing Series in Energy

1 **Generating power at high efficiency: Combined cycle technology for sustainable energy production**
Eric Jeffs

2 **Advanced separation techniques for nuclear fuel reprocessing and radioactive waste treatment**
Edited by Kenneth L. Nash and Gregg J. Lumetta

3 **Bioalcohol production: Biochemical conversion of lignocellulosic biomass**
Edited by K.W. Waldron

4 **Understanding and mitigating ageing in nuclear power plants: Materials and operational aspects of plant life management (PLiM)**
Edited by Philip G. Tipping

5 **Advanced power plant materials, design and technology**
Edited by Dermot Roddy

6 **Stand-alone and hybrid wind energy systems: Technology, energy storage and applications**
Edited by J.K. Kaldellis

7 **Biodiesel science and technology: From soil to oil**
Jan C.J. Bart, Natale Palmeri and Stefano Cavallaro

8 **Developments and innovation in carbon dioxide (CO_2) capture and storage technology Volume 1: Carbon dioxide (CO_2) capture, transport and industrial applications**
Edited by M. Mercedes Maroto-Valer

9 **Geological repository systems for safe disposal of spent nuclear fuels and radioactive waste**
Edited by Joonhong Ahn and Michael J. Apted

© Woodhead Publishing Limited, 2011

10 **Wind energy systems: Optimising design and construction for safe and reliable operation**
Edited by John D. Sørensen and Jens N. Sørensen

11 **Solid oxide fuel cell technology: Principles, performance and operations**
Kevin Huang and John Bannister Goodenough

12 **Handbook of advanced radioactive waste conditioning technologies**
Edited by Michael I. Ojovan

13 **Nuclear safety systems**
Edited by Dan Gabriel Cacuci

14 **Materials for energy efficiency and thermal comfort in buildings**
Edited by Matthew R. Hall

15 **Handbook of biofuels production: Processes and technologies**
Edited by Rafael Luque, Juan Campelo and James Clark

16 **Developments and innovation in carbon dioxide (CO_2) capture and storage technology Volume 2: Carbon dioxide (CO_2) storage and utilisation**
Edited by M. Mercedes Maroto-Valer

17 **Oxy-fuel combustion for power generation and carbon dioxide (CO_2) capture**
Edited by Ligang Zheng

18 **Small and micro combined heat and power (CHP) systems: Advanced design, performance, materials and applications**
Edited by Robert Beith

19 **Hydrocarbon fuel conversion technology: Advanced processes for clean fuel production**
Edited by M. Rashid Khan

20 **Modern gas turbine systems: High efficiency, low emission, fuel flexible power generation**
Edited by Peter Jansohn

21 **Concentrating solar power (CSP) technology: Developments and applications**
Edited by Keith Lovegrove and Wes Stein

22 **Nuclear corrosion science and engineering**
Edited by Damien Féron

© Woodhead Publishing Limited, 2011

23 **Power plant life management and performance improvement**
Edited by John Oakey

24 **Direct-drive renewable energy systems**
Edited by Markus Mueller and Henk Polinder

25 **Advanced membrane science and technology for sustainable energy and environmental applications**
Edited by Angelo Basile and Suzana Pereira Nunes

26 **Irradiation embrittlement of reactor pressure vessels (RPVs) in nuclear power plants**
Edited by Naoki Soneda

27 **High temperature superconductors (HTS) for energy applications**
Edited by Ziad Melhem

28 **Infrastructure and methodologies for the justification of nuclear power programmes**
Edited by Agustín Alonso Santos

29 **Waste to energy (WtE) conversion technology**
Edited by Marco Castaldi

30 **Polymer electrolyte membrane and direct methanol fuel cell technology Volume 1: Fundamentals and performance**
Edited by Christoph Hartnig and Christina Roth

31 **Polymer electrolyte membrane and direct methanol fuel cell technology Volume 2: In situ characterisation techniques**
Edited by Christoph Hartnig and Christina Roth

32 **Combined cycle systems for near-zero emission power generation**
Edited by Ashok Rao

33 **Modern earth buildings: Materials, engineering, construction and applications**
Edited by Matthew R. Hall, Rick Lindsay and Meror Krayenhoff

34 **Handbook of metropolitan sustainability: Understanding and improving the urban environment**
Edited by Frank Zeman

35 **Functional materials for energy applications**
Edited by John Kilner, Stephen Skinner, Stuart Irvine and Peter Edwards

© Woodhead Publishing Limited, 2011

36 **Nuclear decommissioning: Planning, execution and international experience**
Edited by Michele Laraia

37 **Nuclear fuel cycle science and engineering**
Edited by Ian Crossland

38 **Electricity transmission, distribution and storage systems**
Edited by Ziad Melhem

39 **Advances in biodiesel preparation: Second generation processes and technologies**
Edited by Rafael Luque and Juan Antonio Melero

40 **Biomass combustion science, technology and engineering**
Edited by Lasse Rosendahl

41 **Ultra-supercritical coal power plant: Materials, technologies and optimisation**
Edited by Dongke Zhang

42 **Radionuclide behaviour in the natural environment: Science, impacts and lessons for the nuclear industry**
Edited by Horst Geckeis and Christophe Poinssot

43 **Calcium and chemical looping technology for power generation and carbon dioxide (CO_2) capture: Solid oxygen- and CO_2-carriers**
P. Fennell and E.J. Anthony

44 **Materials ageing and degradation in light water reactors: Mechanisms, modelling and mitigation**
Edited by K.L. Murty

45 **Structural alloys for power plants: Operational challenges and high-temperature materials**
Edited by Amir Shirzadi, Rob Wallach and Susan Jackson

46 **Biolubricants: Science and technology**
Jan C.J. Bart, Emanuele Gucciardi and Stefano Cavallaro

47 **Wind turbine blade design and materials: Improving reliability, cost and performance**
Edited by Povl Brøndsted and Rogier Nijssen

48 **Radioactive waste management and contaminated site clean-up: Processes, technologies and international experience**
Edited by William E. Lee, Michael I. Ojovan, Carol M. Jantzen

© Woodhead Publishing Limited, 2011

49 **Probabilistic methods of strength reliability and their application for optimum nuclear power plant life management (PLiM)**
Gennadij V. Arkadov, Alexander F. Getman and Anderi N. Rodionov

50 **Coal utilization in industry: Towards cleaner production**
Edited by D.G. Osborne

51 **Coal power plant materials and life assessment: Developments and applications**
Edited by Ahmed Shibli

© Woodhead Publishing Limited, 2011

Preface

The world is still mostly powered by fossil fuels. There is an urgent call for renewable resources and new energy conversion technologies that could provide humanity with a safe and sustainable future after the oil reserves have gone. Besides fuel scarcity, the alarming increase in CO_2 emissions caused by anthropogenic activity is at least as important. Alternative energy conversion has therefore become highly topical, with research initiatives being launched all over the world, including the Gulf countries and Saudi Arabia, where petroleum is abundant.

The road to a society completely powered by sustainable, clean and renewable energy is long and the most probable eventual scenario will be a world operating with a combination of several energy conversion methodologies, fitting the possibilities provided by the natural resources in each particular region. Countries such as Brazil can be seen to be leading in this field, with hydropower supplying more than 85% of the country's energy demand, while the majority of cars are fuelled with bioethanol and, more recently, with biodiesel. This progressive renewable energy picture is shared with Scandinavian countries such as Norway, where hydropower is also substantial, and Denmark, which is a worldwide leader in wind energy, while nations with large desert areas are starting to invest more heavily in solar energy. Other countries have to find solutions more suitable to their geographical situation.

This book is dedicated to emerging applications of membrane technology in the fields of energy and the environment. The main motivation for the book is to show how membrane technology could help to reduce greenhouse gas emissions and contribute to energy security. To this end, the editors invited an international field of experienced membrane scientists to report the state-of-the-art of membrane processes, science and engineering. We are, of course, aware that additional relevant activities are continuously emerging and that many other excellent groups are working on related topics. This book is therefore designed to enable the reader to gain a clear and up-to-date insight into this important field and to direct them to additional and valuable sources of further information on the research, development and demonstration of advanced membranes.

© Woodhead Publishing Limited, 2011

The first part of the book is designed as an introduction to general aspects of membrane technology, which is relevant to understanding the more specific topics discussed in later sections. Chapter 1 (Calabrò and Basile) presents a general introduction to membrane processes, while Chapter 2 (Yampolskii) builds on this coverage to describe the fundamental science of gas and vapour separation by membranes. Standard membrane characterization methods and modelling procedures are summarized in Chapter 3 (Campo, Tanaka, Mendes and Sousa), and economic analysis of the appropriate selection and utilization of membrane technologies is covered in Chapter 4 (Calabrò and Basile).

Worldwide changes in energy strategy do not take place from one day to the next. The coming decades will first be characterized by a more gradual transition, in which conventional power plants and refineries have to be modernized to become more effective with a substantial reduction in CO_2 emissions. Membranes can make a core contribution in this phase. Examples of how this will be possible are demonstrated in the second and third parts of the book, which include coverage of membranes under consideration for the modernization of coal power plants and refineries.

In Part II, a general introduction of membrane technology used for CO_2 separation is given in Chapter 5 (Basile, Gugliuzza, Morrone and Iulianelli), which also charts strategic projects in this field in Europe, USA and Australia. More detailed information on the development and application of polymeric membranes for the separation of CO_2 from flue gas, where membrane technology competes with amine absorption, is provided in Chapter 6 (Yave and Car). Inorganic membranes for precombustion separation of CO_2 and synthesis gas processing are considered in Chapters 7 (Iulianelli, Basile, Li and van den Brink) and 8 (Smart, Ding and da Costa); systems that are being developed to fit the intermediate CO_2 capture and fuel processing steps in integrated gasification combined cycle (IGCC) coal plants. Oxygen transport membranes also have a potential application in the precombustion and oxyfuel combustion processes in a power plant, as discussed in Chapter 9 (Smart, da Costa, Baumann and Meulenberg).

Part III deals with the integration of membrane processes in petrochemical refineries, which is quite straightforward, and in biofuels production. Membrane technologies for hydrocarbon separation are reviewed in Chapter 10 (Gugliuzza, Iulianelli and Basile). Membranes are industrially used for removal of hydrocarbons from liquid streams and to recover gasoline vapours in tank farms as well as in 'green' tank stations. The motivation increases as the environmental legislation becomes stricter, but there are also economic reasons for this. Membranes for natural gas processing and purification, which is becoming increasingly relevant owing to the growing application of cleaner burning gas in energy systems, are covered in Chapter 11 (Kentish). The demand for biofuels that will effectively replace fossil

© Woodhead Publishing Limited, 2011

fuels is also increasing and the application of membranes in this field is presented in Chapter 12 (Curcio).

Part IV is dedicated to the direct application of membranes in clean energy conversion and energy storage. In the transport sector, electric cars are becoming an increasing reality. Lighter and more effective batteries are required. Membranes are important components of advanced batteries as discussed in Chapters 13 (Hosseiny and Wessling) and 14 (Bongiovanni, Nair, Gerbaldi and Stephan). Membranes are also core components of fuel cells. Chapters 15 (Arcella, Merlo and Ghielmi), 16 (Wu, Othman, Kingsbury and Li) and 17 (Meulenberg, Ivanova, Serra and Roitsch) discuss membranes for proton-exchange membrane fuel cells (PEMFC) and solid oxide fuel cells (SOFC), including more recent developments in proton-conducting SOFC membranes. Hydrogen is one of the cleanest energy carriers, however 95% of the available hydrogen is currently still produced from natural gas. The implementation of hydrogen as sustainable fuel requires its production by renewable technologies. Chapters 18 (Millet) and 19 (Bensaid and Saracco) discuss the membrane role in two alternative hydrogen production methods: electrolysis and water splitting.

Finally in Part V membranes are considered to provide an energy-saving and efficiency-improving technology for industrial, environmental and nuclear applications. Chapter 20 (Cassano and Basile) focuses on industrial microfiltration and ultrafiltration and Chapter 21 (Rastogi and Nayak) discusses emerging processes like forward osmosis for water treatment and pressure retarded osmosis, which has an application as an energy conversion technology by placing membrane between seawater and fresh water and using the osmotic pressure to move turbines. Issues related to water and wastewater treatment are discussed in Chapters 22 (Antony and Leslie) and 23 (Loddo, Palmisano, Marino and Molinari), respectively covering membrane degradation issues and photocatalytic applications for a cleaner environment. The use of membranes for a cleaner environment is also the topic of Chapter 24 (Tosti and Rizzello), which is dedicated to nuclear applications.

The editors would like to take this opportunity to thank the chapter authors for their expert contributions to this important new volume. It is our hope that this comprehensive work will help to serve the scientific community through promoting the development of increasingly efficient and effective membrane technology and applications for a cleaner, safer and more sustainable future.

Suzana Pereira Nunes
Angelo Basile

© Woodhead Publishing Limited, 2011

1

Fundamental membrane processes, science and engineering

V. CALABRÒ, University of Calabria, Italy and
A. BASILE, Institute on Membrane Technology of the Italian National Research Council, ITM-CNR, Italy

Abstract: In this chapter a brief overview of membrane processes is presented, where the most significant parameters and processes have been pointed out, including descriptions of the industrial applications of membrane processes, membrane configurations and membrane operations.

Key words: membrane processes, filtration, membrane configurations and separation, membrane performance, bioreactors, membrane reactors.

1.1 Introduction

Membrane operation or membrane processes may be regarded as a unit operation in chemical engineering. They are largely used in industrial applications in different fields like chemicals, food, gas, water and wastewater treatment, pharmaceuticals and more. Membrane systems are based on the use of synthetic membranes that permit the concentration and separation of solutions without thermal damage. Particles are separated on the basis of their molecular size and shape using pressure and specially designed synthetic and semi-permeable membranes.

Membrane processes play an important role in separation industry, nevertheless, they were not considered technically important until mid-1970. In fact synthetic membranes have been successfully used for small and large-scale industrial processes since the middle of the twentieth century. A wide variety of synthetic membranes is known (Osada and Nakagawa, 1992). They can be produced from organic materials such as polymers and liquids, as well as from inorganic materials. Most commercially utilized synthetic membranes in the separation industry are made of polymeric structures. They can be classified based on their surface chemistry, bulk structure, morphology and production method. Three types of synthetic membranes are commonly used in the separation industry: dense membranes, porous membranes and asymmetric membranes (Pinnau and Freeman, 1999).

The selection of synthetic membranes for a targeted separation process is usually based on few requirements. Membranes have to provide enough

© Woodhead Publishing Limited, 2011

mass transfer area to process large amounts of feed stream. The selected membrane has to have high selectivity (rejection) properties for certain particles, it has to resist fouling and to have high mechanical stability. It also needs to be reproducible and to have low manufacturing costs (Mulder, 1996). The success of membrane processes is related to their performances and feasibility of use. In this chapter a brief description of membrane processes, configurations, operating conditions and applications is reported.

1.2 Membrane processes

Membrane filtration represents a very efficient and economical way of separating components that are suspended or dissolved in a liquid. The membrane plays the role of a physical barrier that allows certain compounds to pass through, depending on their physical and/or chemical properties. Membranes generally consist of a porous support layer with a thin dense layer on top that forms the actual membrane. The components that pass through the membranes represent the permeate, the solute retained is the retentate.

The retention capability is related to the molecular weight cut-off (MWCO) of the membrane, which is related to the pore size of the membrane. Membrane pore sizes can vary from 0.1 nm to 5000 nm depending on filter type. Particle filtration removes particles of 1 μm or larger. Microfiltration (MF) removes particles of 50 nm or larger. Ultrafiltration (UF) removes particles of roughly 3 nm or larger. Nanofiltration (NF) removes particles of 1 nm or larger. Reverse osmosis (RO) is in the final category of membrane filtration and removes particles larger than 0.1 nm.

Both polymeric and inorganic materials are used to produce membranes, which might have a homogeneous or composite structure with both a dense layer and a skin layer which have different porosities and compositions. Also dense or porous membranes might be produced depending on their use and applications. Further research is related to the production of functionalized membranes or coated membranes, also depending on the field of application.

Membrane processes provide efficiency and operational simplicity, high selectivity and permeability for the transport of specific components. It is possible to achieve high compatibility as between different membrane operations as between membrane operations and traditional industrial applications in integrated systems. In order to analyse their economic impact, it is necessary for membrane processes to be characterized by low energetic requirements, good stability under operative conditions, environment compatibility, great flexibility, easy scale-up and good control of effectiveness with the possibility of reaching advanced levels of automation and remote control.

© Woodhead Publishing Limited, 2011

The chemical and physical properties of synthetic membranes and separated particles as well as the choice of driving force define a particular membrane separation process (Mulder, 1996). According to the driving force of the operation it is possible to distinguish:

- pressure driven operations (that includes MF, UF, NF, RO, gas separation, pervaporation)
- concentration driven operations (like dialysis and osmosis)
- operations in electric potential gradient (like electrodialysis, membrane electrolysis and electrophoresis)
- operations in temperature gradient (membrane distillation).

MF and UF are widely used in food and beverage processing (beer MF, apple juice UF), biotechnological applications and pharmaceutical industry (antibiotic production, protein purification), water purification, desalination and wastewater treatment, microelectronics industry and others (Zeman and Zydney, 1996). NF and RO membranes are mainly used for water purification purposes. Dense membranes are utilized for gas separations (removal of CO_2 from natural gas, separating N_2 from air, organic vapour removal from air or nitrogen stream) and sometimes in membrane distillation. The later process helps in separating azeotropic compositions reducing the costs of distillation processes. A very concise description of membrane processes is necessary, in order to introduce the most important fields of applications and problems related to their use in industrial applications.

1.2.1 Microfiltration

MF allows particles or biological substances in the range of 0.025 μm to 10.0 μm to be removed from liquid solutions and fluids by permeation through a microporous medium such as a polymeric or inorganic membrane filter. Although micrometre-sized particles can be removed by use of non-membrane or depth materials such as those found in fibrous media, only a membrane filter that has a precisely defined pore size can ensure quantitative retention. Membrane filters can be used for final filtration or prefiltration, whereas a depth filter is generally used in clarifying applications where quantitative retention is not required or as a prefilter to prolong the life of a downstream membrane. Membrane and depth filters offer certain advantages and limitations. They can complement each other when used together in a UF process system or fabricated device. The retention boundary defined by a membrane filter can also be used as an analytical tool to validate the integrity and efficiency of a system. For example, in addition to clarifying or sterilizing filtration, fluids containing bacteria can be filtered to trap the microorganisms on the membrane surface for subsequent culture and analysis. MF can also be used in sample preparation to remove intact cells and some cell debris from the

© Woodhead Publishing Limited, 2011

lysate. Membrane MWCO used for these types of separation are typically in the range 0.05–1.0 μm. The module can be in a submerged configuration or a pressure vessel configuration, whereas the membrane configuration can be hollow fibres, flat sheet, tubular, spiral wound, hollow fine fibre or track etched (Crittenden *et al.*, 2005). Low energy requirements and easy cleaning systems permit the use of a MF system where the economic impact is less significant in comparison with other membrane process. Membrane cleaning represents a critical point in order to reduce membrane replacement costs.

1.2.2 Ultrafiltration

UF permits the separation of small particles and dissolved molecules from fluids. The separation depends on molecular size and the permeability might be affected by the chemical, molecular or electrostatic properties of the sample. UF is a membrane filtration technique in which hydrostatic pressure forces a liquid against a semipermeable membrane. Suspended solids and solutes with a high molecular weight are retained, while water and low molecular weight solutes pass through the membrane. It is possible to retain molecules of 1–1000 kDa by UF, while salts and water will pass through. Colloidal and particulate matter can also be retained. UF membranes can be used both to purify material passing through the filter and to collect material retained by the filter. The retention capability is also related to the MWCO of the membrane in this case.

All particles and molecules significantly smaller than the MWCO pass through the filter: consequently UF might be used in order to clarify and separate solutions from high molecular weight contaminants. Molecules and particles larger than the MWCO are retained by the membrane and can be concentrated or separated from low molecular weight contaminants. UF is typically used to separate proteins from buffer components for buffer exchange, desalting or concentration. Ultrafilters are also ideal for removal or exchange of sugars, non-aqueous solvents, the separation of free from protein-bound ligands, the removal of materials of low molecular weight or a rapid change in the ionic and/or pH environment. Depending on the proteins to be retained, the most frequently used membranes have a nominal MWCO ranging from 3–100 kDa. UF is far gentler to solutes than processes such as precipitation. UF is more efficient because it can simultaneously concentrate and desalt solutes. It does not require a phase change, which often denatures labile species and can be performed either at room temperature or in a cold room. UF is not fundamentally different from MF, NF or gas separation, except in terms of the size of the molecules it is able to retain. UF is applied in cross-flow or dead-end mode and separation in UF undergoes concentration polarization.

UF is used as a pretreatment for spiral wound membranes for effluent and

© Woodhead Publishing Limited, 2011

wastewater treatments, with sub-products recovery (Turano *et al.*, 2002). The alternative would require an extensive train of several treatment steps with the associated high investment and operating costs, while RO feed water quality cannot be guaranteed 100% of the time. UF guarantees a constant water quality at low cost, virtually independent of the feed water quality.

Multiple large scale plants are today in operation in The Netherlands, Belgium, Germany, Spain, Namibia, Singapore, Kuwait and the USA (Futselaar *et al.*, 2004; Von Gottberg *et al.*, 2003; Menge *et al.*, 2001; Lim, 2005). UF has also been accepted as an alternative to conventional pretreatment for brackish surface water RO systems. This application was piloted first by the company PWN (http://www.pwntechnologies.nl) in The Netherlands during the 1990s (De Bruin *et al.*, 2002). UF pretreatment to sea water reverse osmosis (SWRO) has been piloted in many places in the world. Despite the technical success, very few dual membrane desalination plants are in operation; fewer than half a dozen plants are in operation or under construction in Saudi Arabia, Bahrain and China (Basha *et al.*, 2005; Galloway *et al.*, 2003; Burashid *et al.*, 2005).

From an energetic point of view, UF is less expensive than traditional pretreatments, because the driving force of the filtration process is a small pressure difference of 0.1–0.5 MPa. As a consequence the most significant costs are related to the membrane equipment and membrane replacement. These aspects might be reduced with an effective cleaning system (Curcio *et al.*, 2002).

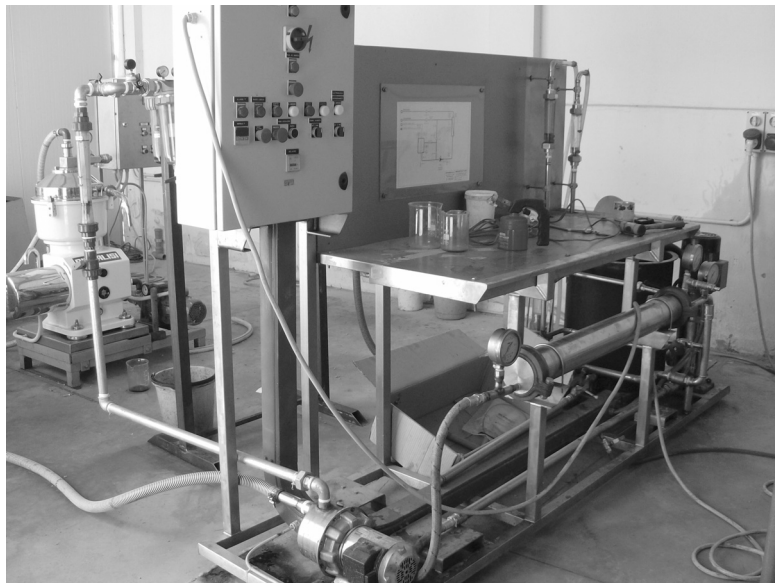
In Fig. 1.1 a UF module with a polymeric membrane used for the treatment of food industry wastewater is reported (Calabrò *et al.*, 2008a).

1.2.3 Reverse osmosis and nanofiltration

RO separates salts and small molecules from low molecular weight solutes (generally less than 100 Da) at relatively high pressures (more then 3 MPa), usually using membranes with MWCO lower then 1 kDa. RO membranes are normally rated by their retention of sodium chloride while UF membranes are characterized according to the molecular weight of retained solutes. NF, similar to RO, uses membranes with MWCO of 1–2 kDa (Kock Company, 2010). The driving force is the difference between the applied transmembrane pressure difference and the osmotic pressure.

The equipment for NF and RO are almost the same. The applied pressure might range from 3–10 MPa, depending on the solutions that are treated and on the desired level of concentration or purification. Usually RO systems are primarily used to purify tap water to purities that exceed distilled water quality. UF systems ensure that ultrapure water is free from endotoxins as well as nucleases for critical biological research. Millipore water purification systems, for example, employ both RO membranes as well as UF membranes.

© Woodhead Publishing Limited, 2011



1.1 Ultrafiltration system for food industry wastewater, implemented by ECOTEC, Italy (adapted from Calabrò *et al.*, 2008a).

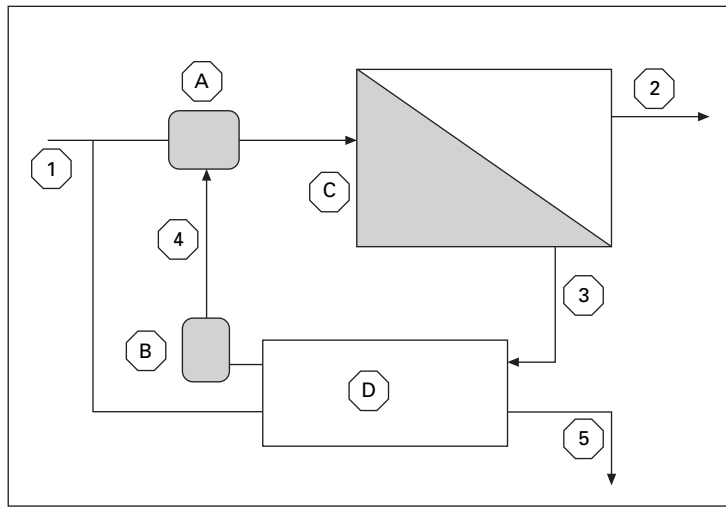
The membranes used for RO have a dense barrier layer in the polymer matrix where most separation occurs. In most cases, the membrane is designed to allow only water to pass through this dense layer, while preventing the passage of solutes (such as salt ions). This process requires high pressure on the high concentration side of the membrane, usually 0.2–1.7 MPa for fresh and brackish water and 4.0–7.0 MPa for seawater, which has around 2.4 MPa natural osmotic pressure that must be overcome. This process is well known for its use in desalination (removing the salt and other minerals from sea water to get fresh water), but since the early 1970s it has also been used to purify fresh water for medical, industrial and domestic applications. In Fig. 1.2, a schematic of RO system for desalination applications is shown.

High pressure requirements, equipment and energetic costs are more relevant in RO than other membrane processes. It is also very important to use a pretreatment in order to reduce the time and cost of membrane cleaning and replacement.

1.2.4 Applications of reverse osmosis

RO systems are used in different industrial fields and applications; the most relevant are discussed here in order to give some indications and details so that an economic analysis can be carried out (Fritzmann *et al.*, 2007).

© Woodhead Publishing Limited, 2011



1.2 Schematic of a reverse osmosis system (desalination). 1, Sea water inflow; 2, fresh water flow (40%); 3, concentrate flow (60%); 4, sea water flow (60%); 5, concentrate (drain); *A*, high pressure pump flow (40%); *B*, circulation pump; *C*, osmosis unit with membrane; *D*, pressure exchanger.

Drinking water purification

Around the world, household drinking water purification systems, which include a RO step, are commonly used to improve water for drinking and cooking. Such systems typically include a number of steps:

- a sediment filter to trap particles, including rust and calcium carbonate
- optionally, a second sediment filter with smaller pores
- an activated carbon filter to trap organic chemicals and chlorine, which will attack and degrade thin film composite RO membranes
- a RO filter, which is a thin film membrane (TFM) or thin film composite (TFC)
- optionally, a second carbon filter to capture those chemicals not removed by the RO membrane
- optionally an ultraviolet lamp to disinfect any microbes that may escape filtering by the RO membrane.

In some systems, the carbon prefilter is omitted and a cellulose triacetate membrane (CTA) is used. The CTA membrane is prone to rot unless protected by chlorinated water, while the TFC membrane is prone to break down under the influence of chlorine. In CTA systems, a carbon post-filter is needed to remove chlorine from the final product water.

© Woodhead Publishing Limited, 2011

In the USA military, RO water purification units (ROWPU) are used on the battlefield and in training. Capacities range from 6.8–680 m^3/day, depending on the need. The most common of these are the 2.7 and 13.5 m^3 h^{-1} units; both are able to purify salt water and water contaminated by chemical, biological, radiological and nuclear agents. During a 24-hour period, at normal operating parameters, one unit can produce 55–270 m^3 of water, with a required 4-hour maintenance window to check systems, pumps, RO elements and the engine generator. A single ROWPU can sustain the size of a battalion, or roughly 1000–6000 service members (http://www.globalsecurity.org/military/systems/ground/rowpu.htm).

Water and wastewater purification

Rain water collected from storm drains is purified with RO water processors and used for landscape irrigation and industrial cooling in Los Angeles and other cities, as a solution to the problem of water shortages. In industry, RO is used to remove minerals from boiler water at power plants. The water is boiled and condensed repeatedly. It must be as pure as possible so that it does not leave deposits on the machinery or cause corrosion. The deposits inside or outside the boiler tubes may result in under-performance of the boiler, reducing its efficiency and resulting in poor steam production and hence poor power production at the turbine. It is also used to clean effluent and brackish groundwater. The effluent in larger volumes (more than 500 m^3/day) is treated preliminarily in an effluent treatment plant and then the clear effluent is subjected to RO system. Treatment cost is reduced significantly and the membrane life of the RO system is increased.

The process of RO can be used for the production of deionized water. In 2002, Singapore announced that a process named NEWater (the brand name given to reclaimed water produced by Singapore's Public Utilities Board) would be a significant part of its future water plans. The Singapore Water Reclamation Study (NEWater Study) was initiated in 1998 by the Public Utilities Board and the Ministry of the Environment and Water Resources. NEWwater involves the use of RO for the treatment of domestic wastewater (NEWater web site, 2010).

Desalination

Areas that have either no or limited surface water or groundwater may choose to desalinate seawater or brackish water to obtain drinking water. RO is the most common method of desalination, although 85% of desalinated water is produced in multistage flash plants. Large RO and multistage flash desalination plants are used in the Middle East, especially Saudi Arabia. The energy requirements of the plants are large, but electricity can be produced

© Woodhead Publishing Limited, 2011

relatively cheaply with the abundant oil reserves in the region. Desalination plants are often located adjacent to the power plants, which reduces energy losses in transmission and allows waste heat to be used in the desalination process of multistage flash plants, reducing the amount of energy needed to desalinate the water and providing cooling for the power plant.

Sea water reverse osmosis (SWRO) is a RO desalination membrane process that has been commercially used since the early 1970s. Its first practical use was demonstrated by Sidney Loeb and Srinivasa Sourirajan at the University of California in Coalinga, California (Glater, 1998). Because no heating or phase changes are needed, energy requirements are low in comparison to other processes of desalination, but are still much higher than those required for other forms of water supply (including RO treatment of wastewater).

The Ashkelon SWRO desalination plant in Israel is the largest in the world (Kronenberg, 2004). The project was developed as a BOT (build-operate-transfer). The typical single-pass SWRO system consists of the following steps and components:

- intake
- pretreatment
- high pressure pump
- membrane assembly
- remineralization and pH adjustment
- disinfection
- alarm/control panel.

The pump supplies the pressure needed to push water through the membrane, even as the membrane rejects the passage of salt through it. Typical pressures for brackish water range from 1.6–2.6 MPa. In the case of seawater, they range from 6–8 MPa. This requires a large amount of energy.

1.2.5 Gas separation

A very interesting application of membrane processes is related to gas separation: in this case the feed gas is separated as permeate and retentate through the membrane layer. The most common membrane device is based on the different diffusivity and solubility which individual gases show when passing through non-porous polymers. A few membranes also operate by sieving effects or under a Knudsen flow. The first large application was used to separate U^{235} from U^{238}, but membranes became economically feasible only in the 1980s with some applications for the separation of H_2, acid gases CO_2/CH_4 and N_2 production from air (Pandey and Chauhan, 2001).

Membranes not only operate by a different mechanism from other separation methods, but in most cases they also perform a separation at a lower cost, provide more valuable products and show fewer undesirable side effects than

© Woodhead Publishing Limited, 2011

older gas separation methods. In a gas separation, a membrane is selective because some components permeate much more rapidly than others; the more permeable gas is called *fast gas* and it is the one enriched in the permeate flow. All the processes involved in a membrane are supported by a wide background of mass transfer theory (Morrone *et al.*, 2008).

Gas separation membranes are mainly used today for recovering hydrogen, separation of methane–carbon dioxide mixtures and separation of oxygen and nitrogen. Hydrogen recovery was the first large commercial membrane gas separation. Applications include recovery of H_2 from ammonia purge gas, hydrogen production from biomass and extraction of H_2 from petroleum cracking streams. Membrane reactors for hydrogen production are becoming more and more important: dense palladium-based membrane reactors are able to carry out both the fuel to H_2 conversion and the hydrogen separation in the same device (Basile, 2008; Iulianelli *et al.*, 2010; Basile and Calabrò, 2010). A gas separation membrane might be used in a membrane reactor for the steam reforming of ethanol or methanol in the production of hydrogen (Basile *et al.*, 2008; Iulianelli *et al.*, 2011).

Much of the natural gas produced in the world contains acid gas, commonly CO_2 or H_2S. Membrane separation is a commercially successful device for the separation of CO_2 and CH_4, especially for small installations. Methane CH_4 is a slow gas; CO_2, H_2S and H_2O are fast gases.

In oxygen–nitrogen separation, a membrane might be used because of higher solubility properties; O_2 is faster than N_2 in many polymers by a factor of 5. Since simple industrial single-stage air compressors provide sufficient pressure to drive an air-separating membrane, moderate purity N_2 (95–99.5%) may be produced in low to moderate quantities quite economically by membrane separation.

Another interesting application of membranes in this field is related to the fuel cells (Basile and Iulianelli, 2007) and gas shift reactions (Basile *et al.*, 1996). Other minor examples involve helium separation, gas dehydration and vapour recovery.

As a technology competing with chemical absorption with amines, such as monoethanolamine (MEA absorption), the CO_2/N_2 gas separation membrane process for post-combustion capture of CO_2 is attracting more and more attention around the world (Koros, 2004; Herzog, 2001; Powell and Qiao, 2006). In comparison with the above-mentioned weaknesses of chemical absorption, CO_2 gas separation membranes are characterized by their lower environmental impact; furthermore they can be designed as turnkey CO_2 separation equipment both for new-build power plants and as a retrofit for existing power plants. These are eminently important properties of the gas separation membrane process, distinguishing it from other post-combustion capture technologies.

© Woodhead Publishing Limited, 2011

1.2.6 Membrane bioreactors

A membrane bioreactor (MBR) is the combination of a membrane process like MF or UF with a suspended growth bioreactor and is now widely used for municipal and industrial wastewater treatment. MBR is an advanced wastewater treatment technology that has been successfully applied at an ever increasing number of locations around the world and which is also increasing in terms of scale. A number of plants with a treatment capacity of around 5000 to 10000 m^3/day have been in operation for several years whilst the next generation have design capacities up to 45000 m^3/day (Chapman *et al.*, 2010).

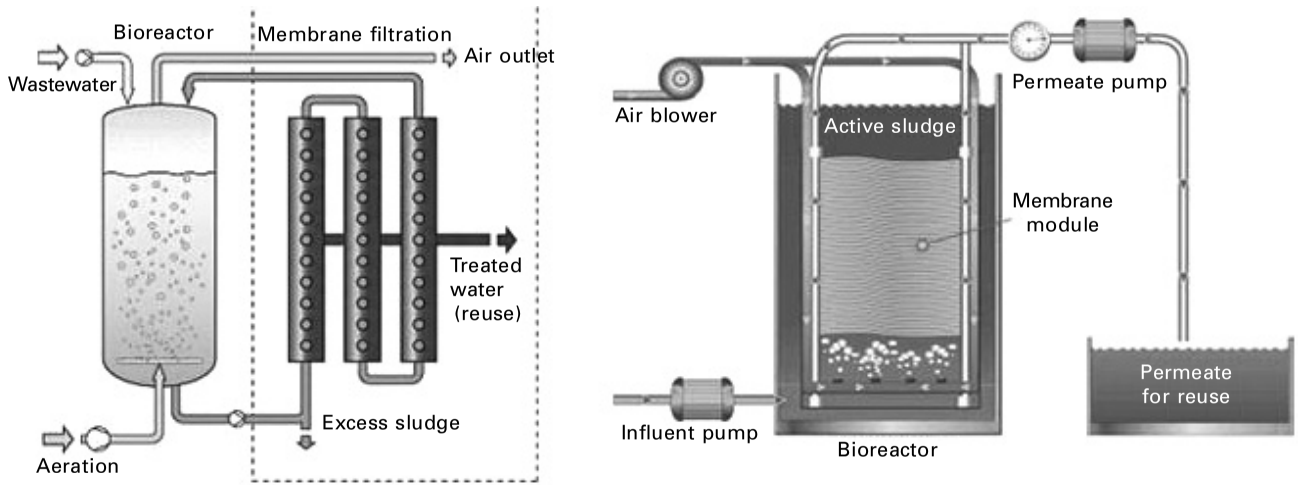
The MBR process is a suspended growth activated sludge system that utilizes microporous membranes for solid/liquid separation instead of secondary clarifiers. A detailed holistic cost comparison may reveal reasonably comparable results between the costs of the MBR option versus advanced treatment options, especially if land value is also considered.

In Fig. 1.3 two schemes of membrane bioreactors are reported (Basile and Calabrò, 2010). A bioreactor may refer to any device or system that supports a biologically active environment. In one case, a bioreactor is a vessel in which a chemical process is carried out which involves organisms or biochemically active substances derived from such organisms. This process can either be aerobic or anaerobic. These bioreactors are commonly cylindrical, ranging in size from litres to cubic metres, and are often made of stainless steel. Furthermore a membrane bioreactor is a reactor in which separation and reaction catalysed by enzymes or whole cells may occur (Cheryan and Mehaia, 1986). A membrane bioreactor may also refer to a device or system meant to grow cells or tissues in the context of cell culture, used in tissue engineering (Giorno *et al.*, 2003). On the basis of mode of operation, a bioreactor may be classified as batch, fed batch or continuous (e.g. a continuous stirred-tank reactor model). A further example of a continuous bioreactor is the chemostat. Organisms growing in bioreactors may be suspended or immobilized (Messing, 1975). A simple method, where cells are immobilized, is a Petri dish with agar gel.

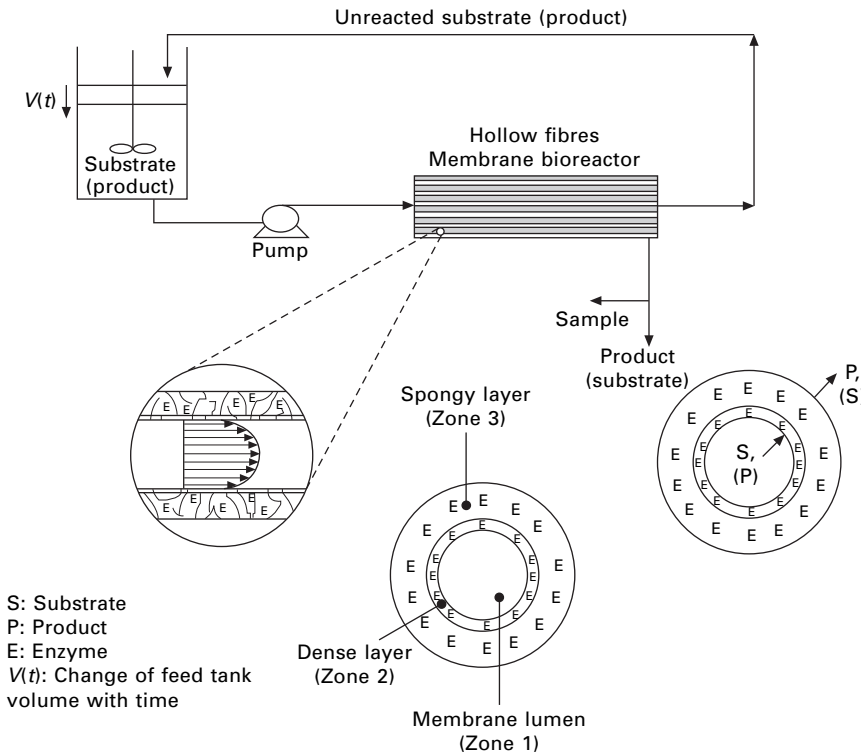
Membranes have been extensively used as a support for biocatalysts (enzymes or whole cells) immobilization with the aim of implementing membrane bioreactors (Atkinson, 1974; Bailey and Ollis, 1986). Different kinds of membrane bioreactors do actually exist (Belfort, 1989; Calabrò *et al.* 2008b), namely:

- enzyme membrane reactors (EMR)
- enzyme gel-layer membrane reactors
- membrane segregated enzyme reactors
- membrane bound enzymes in continuous flow reactors
- whole cells or enzymes immobilized in capillary membrane reactors (as depicted in Fig. 1.4).

© Woodhead Publishing Limited, 2011



1.3 Schemes showing membrane bioreactors for wastewater treatment (adapted from Basile and Calabrò, 2010).



1.4 Scheme-showing membrane bioreactor with enzyme immobilized in the membrane (adapted from Calabrò *et al.*, 2008b).

Large scale immobilized cell bioreactors are:

- moving media, also known as a moving bed biofilm reactor (MBBR)
- packed bed
- fibrous bed
- membrane bioreactor.

In Fig. 1.5 the scheme for cellulosic ethanol research is shown. The mobile pilot-plant fermentor shown here has a 90 litre capacity and currently is used to generate large volumes of cells and cell products such as outer membrane vesicles under highly controlled conditions. Future generations of fermentors will be more highly instrumented with sophisticated imaging and other analytical devices for analysing interactions between cells in microbial communities under an array of conditions. Biofuels production represents an interesting field of application of membrane bioreactors (Calabrò *et al.*, 2010; De Paola *et al.*, 2009). Furthermore, a membrane bioreactor might be used in integrated systems in order to achieve the wastewater treatment with bioconversion of sub-products (Calabrò *et al.*, 2009).

© Woodhead Publishing Limited, 2011



1.5 Bioreactor used in cellulosic ethanol production (research-pilot scale) (adapted from Calabrò *et al.*, 2010).

1.2.7 Membrane configurations

Typical membrane module configurations are plate and frame, spiral wound, tubular and hollow fibres.

Spiral wound module

This consists of large consecutive layers of membrane and support material rolled up around a tube. This configuration permits maximization of the surface area and is less expensive. However, it is more sensitive to pollution.

Tubular membrane

The feed solution flows through the membrane core and then the permeate is collected in the tubular housing. Generally it is used for viscous or bad

© Woodhead Publishing Limited, 2011

quality fluids. The system is not very compact and has a high cost per membrane area installed.

Hollow fibres membrane

The modules contain several small (0.6–2 mm diameter) tubes or fibres. The feed solution flows through the open cores of the fibres and then the permeate is collected in the cartridge area surrounding the fibres. The filtration can be carried out either 'inside-out' or 'outside-in'.

1.2.8 Operating membrane systems

Dead-end filtration

The most basic form of filtration is dead-end filtration. The complete feed flow is forced through the membrane and the filtered matter is accumulated on the surface of the membrane. The dead-end filtration is a batch process as accumulated matter on the filter decreases the filtration capacity, owing to clogging. A next process step to remove the accumulated matter is required. Dead-end filtration can be a very useful technique for concentrating compounds.

Cross-flow filtration

In cross-flow filtration a constant turbulent flow along the membrane surface prevents the accumulation of matter on the membrane surface. The membranes used in this process are commonly tubes with a membrane layer on the inside wall of the tube. The feed flow through the membrane tube is at an elevated pressure providing the driving force for the filtration process and a high flow speed to create turbulent conditions. The process is referred to as *cross flow* because the feed flow and the filtration flow direction are at a 90° angle. Cross-flow filtration is an excellent way to filter liquids with a high concentration of filterable matter.

Hybrid-flow filtration

The hybrid flow process combines the dead-end and the cross-flow principle. The filtration process has two phases: the production phase and the flushing phase. During the production phase, the tubes are closed on one side and a dead-end filtration is performed. During the flushing phase, the tube is open on both sides and the fraction that did not pass through the membranes is removed in order to clean the membrane surface as in cross-flow filtration. This filtration technique is especially suitable for treating water streams

© Woodhead Publishing Limited, 2011

containing suspended solids in low concentrations (polishing). A control system might be adopted in such a configuration (Curcio *et al.*, 2002).

Submerged filtration

In submerged membrane filtration, the membranes are submerged in the liquid that has to be filtered. The filtration is performed from the outside to the inside of the membrane (the filtering layer is on the outer side of the tube or plate). Shear forces along the membrane surface are created by a flow of air bubbles along the surface. In some cases the airflow also results in a liquid flow created by the airlift principle. The driving force is a vacuum applied on the inner side of the membrane.

1.3 Conclusions and future trends

A general description of most common membrane processes and applications has been provided, in order to anticipate some important concepts presented in this book, related to their applications, engineering aspects, environmental impact, economic considerations, future developments and perspectives which will be discussed in the following chapters. Membrane processes can significantly increase the performance while reducing the cost of separation and recovery processes when compared to conventional processes. Furthermore, improvements in both pretreatment UF and MF membranes as well as the RO membranes will reduce the energy requirements and maintenance costs related to membrane replacement. The lifetime of the membrane represents a critical point in membrane operations; consequently an overall analysis of the process is required, studying all the operating parameters, as well as making an engineering and economic analysis of the overall process.

Integrated membrane processes represent an attractive opportunity because of their synergic effects, the simplicity of using single units and the possibility of advanced levels of automation and remote control. Last, but not the least, the development of new materials to make membranes more stable and resistant to chemicals will permit an increase in their performance and lifetime.

1.4 References

Atkinson B (1974), *Biochemical Reactor*, Pion Ltd, London, UK.

Bailey J E and Ollis D F (1986), *Biochemical Engineering Fundamentals*, McGraw Hill Book Company, Singapore, MA.

Basha K, Saud M, Gulamhusein A, Nicoll P and Boda R (2005), 'Design and construction challenges of the Kindasa SWRO desalination plant expansion', in *Proceedings IDA World Congress on Desalination and Water Reuse*, Singapore, 11–16 September 2005.

© Woodhead Publishing Limited, 2011

Basile A (2008), 'Hydrogen production using Pd-based membrane reactors for fuel cells', *Topics in Catalysis*, **51**, 107–22.

Basile A and Calabrò V (2010), *Sustainable Hydrogen and Energy Production from Renewable Sources – Catalytic and Bio-catalytic Membrane Reactors – Fuel Cells*, Università della Calabria by Centro Editoriale e Librario, Rende (Italy).

Basile A and Iulianelli A (2007), 'Alternative sulfonated polymers to Nafion for PEM fuel cell', in *Fuel Cell Research Trends*, L.O. Vasquez (ed), Nova Science Publishers, New York, Chapter 3, 135–60.

Basile A, Criscuoli A, Santella F and Drioli E (1996), 'Membrane reactor for water gas shift reaction', *Gas Separation and Purification*, **10**(4), 243–54.

Basile A, Gallucci F, Iulianelli A, Tereschenko GF, Ermilova M M and Orekhova V (2008), 'Ti–Ni–Pd dense membranes: The effect of the gas mixtures on the hydrogen permeation', *Journal of Membrane Science*, **310**, 44–50.

Belfort G (1989),'Membrane and bioreactors: a technical challenge in biotechnology', *Biotechnology Bioengineering*, **33**, 1047–66.

Burashid K, Hashim A, Kannari T, Tada K and Iwahori H (2005), 'Ultrafiltration membrane performance experience at Addur: expectation, reality and prospects', in *Proceedings IDA World Congress on Desalination and Water Reuse*, Singapore, 11–16 September 2005.

Calabrò V, Curcio S, Sansonetti S and Iorio G (2008a), 'Integrated membrane system for agro-food wastewater treatment: two industrial case studies in the southern Italy', in *Proceedings of ICOM 2008*, Honolulu (USA), 12–18 July 2008, 699.

Calabrò V, Curcio S and Iorio G (2008b), 'Membrane bioreactors: modelling and analysis', in *Membrane Reactors*, Basile A and Gallucci F (eds), Nova Science Publications, New York.

Calabrò V, Curcio S, De Paola M G and Iorio G (2009), 'Optimization of membrane bioreactor performance during enzymatic oxidation of waste bio-polyphenols', *Desalination*, **236**, 30–8.

Calabrò V, Di Bari I, Verardi A, Saraceno A, Curcio S and Liuzzi F (2010), 'Integrated bioreactor/pervaporation system, for bioethanol production from lignocellulosic biomasses', in *Proceeding of AMS6 – IMSTEC10 The 6th Conference of the Aseanian Membrane Society in Conjunction with the 7th International Membrane Science and Technology Conference*, Sydney Australia, 22–26 November 2010, P-712.

Chapman S, Leslie G and Law I (2010), *Membrane Bioreactors (MBR) for Municipal Wastewater Treatment – An Australian Perspective*, www.ch2.com.au.

Cheryan M and Mehaia M A (1986), 'Membrane bioreactors' in *Membrane Separations in Biotechnology*, Mc Gregor W C (ed.), Marcel Dekker, New York, USA.

Crittenden J, Trussel R, Hand D, Howe K and Tchobanoglous G (2005), *Water Treatment Principles and Design*, 2nd edition, John Wiley and Sons, New Jersey.

Curcio S, Calabrò V and Iorio G (2002), 'Monitoring and control of TMP and feed flow rate pulsatile operations during ultrafiltration in a membrane module', *Desalination*, **146**, 217–22,

De Bruin F, Kamp P, Eddy D and Kools R (2002), 'Jan- Lagrand WTW: UF/RO from technological novelty to full size application', in *Proceeding IWA Enviro 2002*, Melbourne, Australia.

De Paola MG, Ricca E, Calabrò V, Curcio S and Iorio G (2009), 'Factor analysis of transesterification reaction of waste oil for biodiesel production', *Bioresource Technology*, **100**, (21), 5126–31.

Fritzmann C, Löwenberga J, Wintgensa T and Melina T (2007), 'State-of-the-art of reverse osmosis desalination', *Desalination*, **216**, (1–3), 1–76.

© Woodhead Publishing Limited, 2011

Futselaar H, Van Hoof S and Rosberg R (2004), 'Ultrafiltration technology for potable, process and waste water treatment', in *Proceedings 9th World Filtration Congress*, New Orleans, USA, 18–22 April 2004.

Galloway M, Von Gottberg A and Mahony J (2003), 'Ultrafiltration for seawater RO pretreatment', in *Proceedings AWWA Membrane Technology Conference*, Atlanta, USA, 2–5 March 2003.

Giorno L, De Bartolo L and Drioli E (2003), 'Membrane bioreactors for biotechnology and medical application', in *New and Insight into Membrane Science and Technology: Polymeric and Biofunctional Membranes*, Bhattacharya D and Butterfield DA (eds), Elsevier, Netherlands, NL, Chap. 9.

Glater J (1998), 'The early history of reverse osmosis membrane development', *Desalination*, **117**, 297–309.

Herzog H J (2001), 'What future for carbon capture and sequestration', *Environmental Science and Technology*, **35**, 148–53.

Iulianelli A, Liguori S, Calabrò V, Pinacci P and Basile A (2010), 'Partial oxidation of ethanol in a membrane reactor for high purity hydrogen production', *International Journal Hydrogen Energy, special issue Bio-hydrogen Production)*, **35**, 12626–34.

Iulianelli A, Seelam P K, Liguori S, Longo T, Keiski R, Calabrò V and Basile A (2011), 'Hydrogen production for PEM fuel cell by gas phase reforming of glycerol as byproduct of bio-diesel. The use of a Pd–Ag membrane reactor at middle reaction temperature', *International Journal of Hydrogen Energy*, **36**, 3827–34.

Kock Company, (2010), http://www.kochmembrane.com/archived_papers.html

Koros W J (2004), 'Evolving beyond the thermal age of separation processes: membranes can lead the way', *AIChE Journal*, **50**, 2326–34.

Kronenberg G (2004), 'The largest SWRO plant in the world – Ashkelon 100 million m^3/y BOT project', *Desalination*, **166**, 457–63.

Lim C G (2005), 'NEWater, closing the water loop', in *Proceedings IDA World Congress on Desalination and Water Reuse*, Singapore, 11–16 September 2005.

Menge J, Haarhoff J, Konig E, Mertens R and Van der Merwe B (2001), 'Occurence and removal of giardia and cryptosporidium at the Goreangab Reclamation Plant,' *Water Science Technology, Water Supply*, **1** (1), 97–106.

Messing RA (1975), *Immobilised Enzymes for Industrial Reactors*, Academic Press, New York, USA.

Morrone P, Amelio M, Gallucci F and Basile A (2008), 'Separation of gaseous mixtures', in *Simulation of Membrane Reactors*, Nova Science Publishers, New York.

Mulder M (1996), *Basic Principles of Membrane Technology*, Kluwer Academic Publishers, Netherlands.

NEWater web site (2010), http://www.pub.gov.sg/about/historyfuture/Pages/NEWater.aspx.

Osada Y and Nakagawa T (1992), *Membrane Science and Technology*, Marcel Dekker, New York.

Pandey P and Chauhan R S (2001), 'Membranes for gas separation', *Progress in Polymer Science*, **26**(6), 853–93.

Pinnau I and Freeman B D (1999), *Membrane Formation and Modification*, ACS Symposium Series, Vol. 744, USA.

Powell C E and Qiao G G (2006), 'Polymeric CO_2/N_2 gas separation membranes for the capture of carbon dioxide from power plant flue gases', *Journal Membrane Science*, **279**, 1–49.

Turano E, Curcio S, De Paola M G, Calabrò V and Iorio G (2002), 'An integrated

© Woodhead Publishing Limited, 2011

centrifugation-ultrafiltration system in the treatment of olive mill wastewater', *Journal Membrane Science*, **209**(2), 519–31.

Von Gottberg A, Gagne D, Vaccaro G and Elyanow D, (2003), 'World's largest membrane-based reuse project', in *Proceedings AWWA Membrane Technology Conference*, Atlanta, USA, 2–5 March 2003.

Zeman L J and Zydney A L (1996), *Microfiltration and Ultrafitration, Principles and Applications*, Marcel Dekker, New York.

© Woodhead Publishing Limited, 2011

2

Fundamental science of gas and vapour separation in polymeric membranes

Y. YAMPOLSKII, A.V. Topchiev Institute of Petrochemical Synthesis (TIPS), Russian Academy of Sciences, Russia

Abstract: This chapter discusses the principles of gas and vapour permeation and separation in non-porous polymeric membranes. The dependence of permeability, diffusion and solubility coefficients on the parameters of gaseous penetrants and properties of polymers are considered. Special sections deal with the effects of pressure and temperature on the transport parameters. A brief survey is given on membrane gas separation materials and the problems of gas separation that can be solved using membranes.

Key words: diffusion coefficients, membrane gas separation, permeability coefficients, solubility coefficients.

2.1 Introduction

Today, membrane separation of gases and vapour has become a highly efficient technological process that successfully competes with more traditional processes of separation such as distillation, adsorption or extraction or is used in combination with these processes aiming to accomplish better technological parameters. The creation of any feasible and viable membrane process is preceded by extensive work by specialists in various fields of knowledge. Work begins with the selection of an appropriate membrane material thought to be suitable because of its intrinsic properties for the solution of a particular separation task. Positive results from such a selection are necessary but are by no means sufficient for the successful solution of the whole problem. At the next stage, it is necessary to establish how films or laboratory membranes based on this material behave during the separation of model mixtures that simulate the real feed streams of the process and to test the process under realistic conditions (temperature and pressure) of separation. The key questions at this stage of investigation are What is the real selectivity? How robust are these films or membranes? Are they susceptible to mechanical or thermal destruction? The next stage involves making a decision on a desirable configuration of membranes (flat sheet or hollow fibre) and preparation of representative batches of such defect-free membranes that will eventually be used in the manufacture of the modules.

© Woodhead Publishing Limited, 2011

Successful field tests are the final stage in process development. Somewhere in between an economic analysis should be performed in order to estimate the probable economic parameters and to compare the material with other competing membrane or non-membrane processes.

Other chapters of this book will discuss the various stages of this long but necessary activity in more length and depth using as examples diverse separation problems and different membranes. This chapter considers the theoretical background of the separation of gases and vapours.

2.2 Basic principles and definitions of separation processes

2.2.1 Historical background

The most basic discovery in this field, made in the middle of the nineteenth century, was recognition of the fact that mass transfer of gases and liquids through polymeric films or membranes (at that moment mainly of natural origin), liquid films and inorganic (e.g. clay) septa can proceed even in the absence of opened pores, that is, the idea of non-porous, permeable membranes was introduced. The basic observations that different gases can penetrate through rubbery films or 'animal membranes' were made by Thomas Graham and John Mitchell. Thus, Mitchell (1831) wrote 'Substances formed of organic matter are generally penetrable by gases of all kinds'. However more than 30 years were necessary before Graham (1866) understood that different rates of penetration of different gases were determined by their relative ability to dissolve in membrane material and the rate of diffusion in the membrane. Thus, in membrane science, the basic idea of a so-called 'solution–diffusion mechanism' was formulated. This and other articles from early history of membrane science have been reproduced, in part, in a special issue of the *Journal of Membrane Science* (Boeddeker, 1995).

An important contribution to the quantitative investigation of the process of gas permeation through membranes was made by von Wroblewski (1879) who proposed the equation for the gas permeation rate or flux J (mol m^{-2} s^{-1}):

$$J = P\,(\Delta p/l) \qquad [2.1]$$

where Δp is the pressure drop across the membrane and l is its thickness. The proportionality coefficient in this equation P was defined as the permeability or permeability coefficient. However, this empirical equation does not reveal the molecular basis of permeation and the complicated nature of this quantity.

© Woodhead Publishing Limited, 2011

2.2.2 Solution–diffusion mechanism

Let us consider a steady state isothermal flux through a homogeneous (uniform) polymer film with thickness l that separates two gas phases containing a single gas with pressure $p_2 > p_1$ (Fig. 2.1). According to Fick's first law applied to the polymer–sorbed gas system:

$$J = -D(\mathrm{d}C/\mathrm{d}x) \qquad [2.2]$$

where C is concentration, x is the coordinate across the film and the diffusion coefficient D in the first approximation does not depend on C and x. This equation predicts a linear concentration profile within the membrane (Crank, 1975). It can easily be integrated, but boundary conditions $C(x = 1)$ and $C(x = 0)$ are usually unknown (in contrast to pressure p_1 and p_2). So one must address the relationship $C(p)$ or the sorption isotherm. The simplest case of sorption isotherms is Henry's law:

$$C = Sp \qquad [2.3]$$

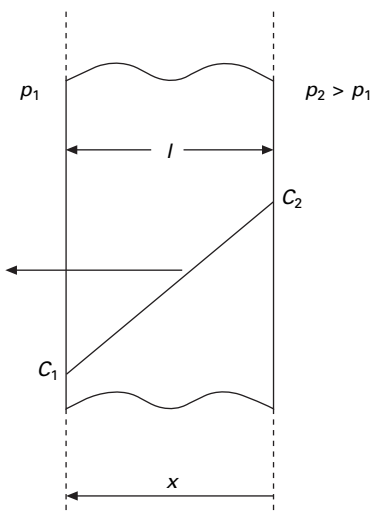
where S is the solubility coefficient. Replacing C by p in Equation [2.2] one obtains:

$$J = DS(p_2 - p_1)/l = DS\,\Delta p/l \qquad [2.4]$$

By comparing Equations [2.1] and [2.4] it is clear that:

$$P = DS \qquad [2.5]$$

This means that P includes two seemingly independent terms that characterize



2.1 Scheme of gas transport through a non-porous polymeric membrane.

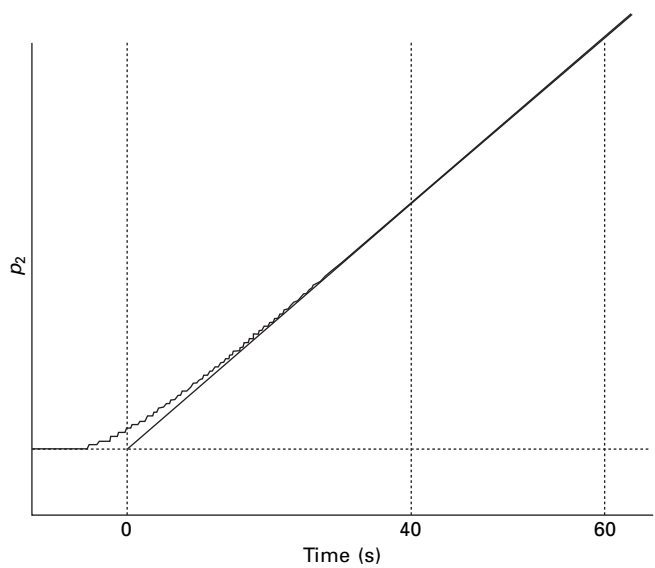
© Woodhead Publishing Limited, 2011

a gas–polymer system: a thermodynamic term S that determines the driving force within the membrane (induced by certain pressure drop Δp) and a kinetic or mobility term D that characterizes the response of the system to the superimposed driving force. Equation [2.5] shows that high P values can be caused either by D or by S terms (or both); some so-called 'fast' gases may display either large diffusion coefficients (e.g. He or H_2) or great solubility coefficients in polymers (e.g. CO_2).

The permeability coefficient characterizes the steady-state flux across the membrane. However, in order to estimate the diffusion coefficient, an analysis of the data from transients experiments is necessary. Daynes (1920) carried out and analysed experiments where the gas permeated through a polymer film into a closed volume. After solving Fick's second law under appropriate initial and boundary conditions, he showed that extrapolation of the line obtained, after steady-state conditions are established, to the time axis gives a time lag θ that is directly related to the diffusion coefficient:

$$\theta = l^2/6D \qquad [2.6]$$

as illustrated in Fig. 2.2. The curvature of the line in the transient regime is such that the steady-state conditions are attained after time equal to 3–4 θ. The conclusions made by Daynes actually defined the future trends of membrane science. He wrote 'The process of diffusion of a gas through a film is determined by two more or less separate processes… Measurements



2.2 Determination of permeability and diffusion coefficients by the Daynes–Barrer method.

© Woodhead Publishing Limited, 2011

must be made simultaneously on the permeability, absorption coefficients, and diffusion constants, or, as a minimum, any two of these three quantities.'

2.2.3 Definitions

When discussing membrane separation, it is necessary to give a definition of membranes. Different definitions can be found in the literature and some of them are given below.

'A membrane is any essentially two-dimensional structure which lies at the boundary between two separate three-dimensional phases and is physically or chemically distinct from both of them.' (Lonsdale, 1989)

'A membrane is a phase or a group of phases that lies between two different phases, which are physically and/or chemically distinctive from both of them and which, due to its properties and the force field applied, is able to control the mass transport between these phases.' (Meares, 1961)

'A membrane is nothing more than a discrete, thin interface that moderates the permeation of chemical species in contact with it.' (Baker, 2007)

In the polymer membrane literature, two notions, membrane and film, are used indiscriminately and this can result in confusion. It should be remembered that a membrane is a device, whereas a film (or so-called dense film) is, as a rule, a molecularly homogeneous object that is completely uniform in composition and structure. Measuring the permeability of a film results in the determination of the transport properties of the polymer–gas system as specified by the permeability coefficient or the flux normalized by the film thickness. On the other hand, in the case of membranes there can be no specific uniform thickness of the selective separating layer.

A widely accepted unit of the permeability coefficient is 1 barrer which equals 10^{-10} cm^3(STP) cm/(cm^2 s cm Hg) or mol/(m s Pa) in SI units. Permeability coefficients of common gases in polymers span a range of more than seven orders of magnitude, from 10^{-3} to 10^4 barrer (see more details later on).

The quantity that characterizes the gas permeation rate of a membrane, permeance Q (or P/l), is expressed in the units cm^3(STP)/(cm^2 s cm Hg) or m^3(STP)/m^2 h atm or mol/m^2 s Pa. Permeance is also often expressed in gas permeation units (GPU), where 1 GPU = 10^{-6} cm^3(STP)/(cm^2 s cm Hg). In the SI system the unit of permeance is mol/(m^2 s Pa).

It should be noted that the solution–diffusion mechanism in the general case includes three steps that can provide a contribution to resistance of the observed flux: (1) adsorption onto the 'inlet' surface of the film/membrane, (2) diffusion across the membrane and (3) desorption from the 'outlet' surface of the membrane. However, the fulfillment of Equation [2.5] (i.e. dependence of P on two parameters, D and S, which characterize the bulk properties of the film and inverse proportional dependence of the flux on film thickness l

© Woodhead Publishing Limited, 2011

indicate that in commonly tested films (thickness in the range 30–300 μm) steps (1) and (3) can be neglected. However, for membranes with an extremely thin selective layer that have a thickness of about 50–100 nm this may not be true. In composite membranes, the resistance of the porous sub-layers can provide a noticeable additional contribution to the total resistance of the flux.

Under real conditions of gas separation, the idealized assumption made in deriving Equations [2.4] and [2.5] may be not fulfilled. In cases where the composition of the film or membrane is not constant across its full thickness, D can be a function of the coordinate within the membrane. Much more important and frequent complications are related to non-linear sorption isotherms $C(p)$ (deviations from Henry's law) and the concentration dependence of diffusion coefficient $D(C)$, which can occur when upstream pressure is displaced from the low pressure limit, $p \to 0$. In this case (Koros and Chern, 1987):

$$P = -D(C)\ \mathrm{d}C/\mathrm{d}x\ [(p_2 - p_1)/l] \qquad [2.7]$$

and

$$P = 1/\Delta p \int_{p_1}^{p_2} D(C)\ (\mathrm{d}C/\mathrm{d}p)\ \mathrm{d}p \qquad [2.8]$$

In practice, this analysis is often difficult to perform. Thus, instead of a low pressure limit solubility coefficient defined by Equation [2.3], the finite pressure solubility coefficient $S = C/p$ at $p > 0$ is used, that is, a secant of the sorption isotherm at a certain pressure (often at 2–10 atm). As another possibility, mean values of D and S in a certain range of concentration and pressure can be used:

$$P = \bar{D}(C)\bar{S}(C) \qquad [2.9]$$

2.2.4 Selectivity

Another key characteristic of membranes is their selectivity in gas separation. There are several definitions of this property. If permeation of different gases proceeds independently, that is, the permeability of one gas is not sensitive to the presence of other permeating gases, then the ideal separation factors defined as:

$$\alpha_{AB} = P_A/P_B \qquad [2.10]$$

are useful for characterization of separation of gas mixtures. Here P_A and P_B are the permeability coefficients of gases A and B measured in runs with individual permeation. Commonly, a 'fast' gas is taken as A, that is, α_{AB}

© Woodhead Publishing Limited, 2011

>1. Bearing in mind Equation [2.5], one can partition the ideal selectivity α_{AB} into diffusivity and solubility selectivity:

$$\alpha_{AB} = (D_A/D_B)\ (S_A/S_B) = \alpha^D_{AB}\ \alpha^S_{AB} \qquad [2.11]$$

Analysis of α^D_{AB} and α^S_{AB} is very helpful in understanding the mechanism of gas permeation in polymers. Ideal separation factors can be also considered for membranes as the ratios $\alpha_{AB} = Q_A/Q_B$.

The magnitude of separation factors α_{AB} strongly depends on, strictly speaking, the tentative choice of gas pairs. Thus, for air separation the values of $\alpha(O_2/N_2)$ vary in the range 2–15 in different polymers. For gas pair H_2 and CH_4 the separation factors $\alpha(H_2/CH_4)$ are in the range 5–1000 or even more.

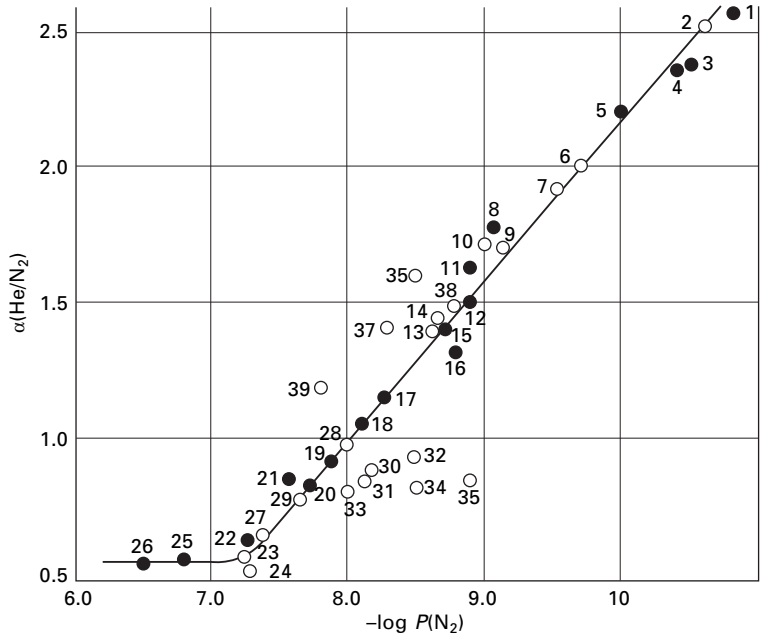
If the components of a mixture exert mutual influence on transport in the membrane, directly or indirectly (via their effects on polymer matrix), ideal separation factors become a rather rough measure of the selectivity of a separation process. For strongly interacting gases and vapours the separation factors should be a characteristic of actual separation process:

$$\alpha^m_{AB} = (y_A/y_B)/(x_A/x_B) \qquad [2.12]$$

where y_A and y_B are mole fractions of the components in the permeate and x_A and x_B are their mole fractions in the feed stream. Selectivity defined in this way depends not only on the properties of the gas–polymer system but also on process parameters, like upstream and downstream pressure, stage-cut (the ratio of permeate and feed streams) and so forth. More detailed consideration of mixed gas selectivity can be found in Matteucci *et al.* (2006).

Many researchers have paid attention to a certain trade-off behaviour of permeability and permselectivity in various polymers: statistically, the more permeable a polymer is with respect to a gas (P_A) the smaller the separation factors $\alpha_{AB} = P_A/P_B$ it reveals. Examples of early correlations of this type are shown in Fig. 2.3 and Fig. 2.4 (Kapanin *et al.*, 1972; Durgaryan and Yampolskii, 1983). A peculiar feature of the correlation shown in Fig. 2.3 is that here the selectivity $\alpha(He/N_2)$ is plotted against the permeability coefficient of the slow component, nitrogen. Systematically for various gas pairs this regularity was demonstrated by Robeson (1991), who also showed that in all permeability–permselectivity diagrams there exist certain lines (upper bounds) which limit the whole 'clouds' of the data points from above. In a subsequent paper, Robeson (2008) showed that the positions of such upper bounds move to higher values of α_{AB} and P_A as soon as the data for more efficient membrane materials have been accumulated (Fig. 2.5). The mean slope of the whole clouds of data points can be rationalized on the basis of a free volume model (Alentiev and Yampolskii, 2000). The position of the upper bounds for several permeability–permselectivity diagrams was predicted on the basis of the activated diffusion model (Freeman, 1999), although the

© Woodhead Publishing Limited, 2011

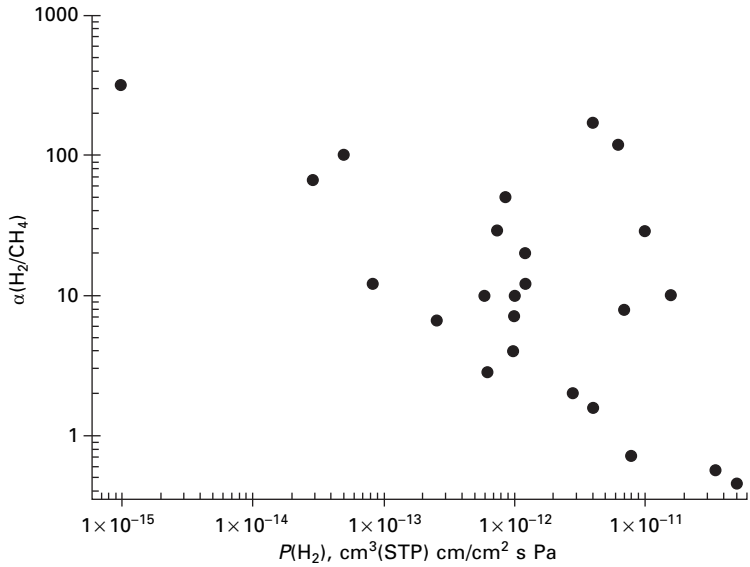


2.3 Permeability–selectivity diagram for the He/N_2 pair in polymers (adapted from Kapanin *et al.*, 1972). Permeability coefficient P is expressed in cm^3 (STP) · cm/cm^2 · s · atm. Open points are the data of the authors (Kapanin *et al.*, 1972), filled points are taken from the literature. Polymers: 1, polyvinylidene chloride; 2 and 4, polyethylene terephtalate; 3, polyvinylfluoride; 5, polyvinylchloride; 6, polyimide; 7, plasticized polyvinylidene chloride; 8, nitrocellulose; 9, polypropylene; 10, fluoroplast-26; 11, copolymer of isoprene (74%) and acrylonitrile (26%); 12, 18 and 20, copolymers of butadiene and acrylonitrile; 13, polyarylate D-4P; 14, polycarbonate; 15, polyisobutylene; 16, butyl rubber; 17, copolymer of vinyl chloride and vinyl acetate; 19 and 37, acetobutylate cellulose; 21, copolymer of ethylene and vinylacetate; 22, polybutadiene; 23, SKI-3 rubber; 24, natural rubber; 25, nitrile siloxane rubber; 26, phenyl siloxane rubber; 27, SKS-30 rubber; 28, copolymer of butadiene and α-methylstryrene; 29, SKMS-30 rubber; 30, 31, 34 and 35 polyethylene; 32, copolymer of ethylene (90%) and propylene (10%); 33, copolymer of ethylene (96.5%) and vinyl acetate (3.5%); 36, cellulose triacetate; 38, acetylcellulose; 39, polystyrene.

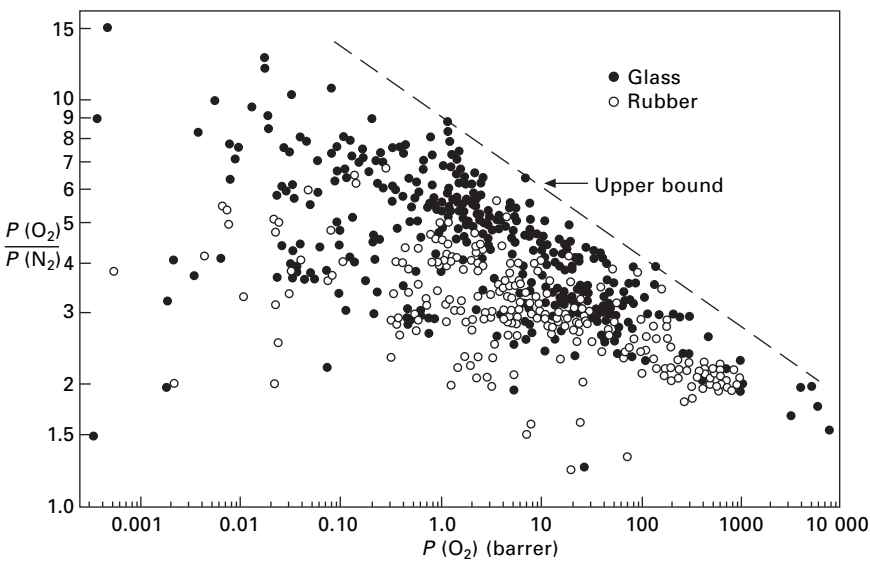
variation of the upper bounds in time reported by Robeson (2008) modifies the parameters used in this model.

This tradeoff behaviour of permeability and permselectivity is characteristic of gas polymer systems where P values are mainly determined by the mobility component of permeability (D). There are examples where increases in permeability are accompanied by growth in permselectivity. This occurs in the separation of mixtures of vapours and permanent gases (e.g. air) or in the

© Woodhead Publishing Limited, 2011



2.4 Permeability–selectivity diagram for the H_2/CH_4 pair in polymers (adapted from Durgaryan and Yampolskii, 1983).



2.5 Permeability–selectivity diagram for the O_2/N_2 pair in polymers (adapted from Robeson, 1991).

separation of hydrocarbon molecules of different mass. The most spectacular example of such behaviour is the separation of alkanes C_1–C_4, which is a very important technical problem in the treatment of natural and associated

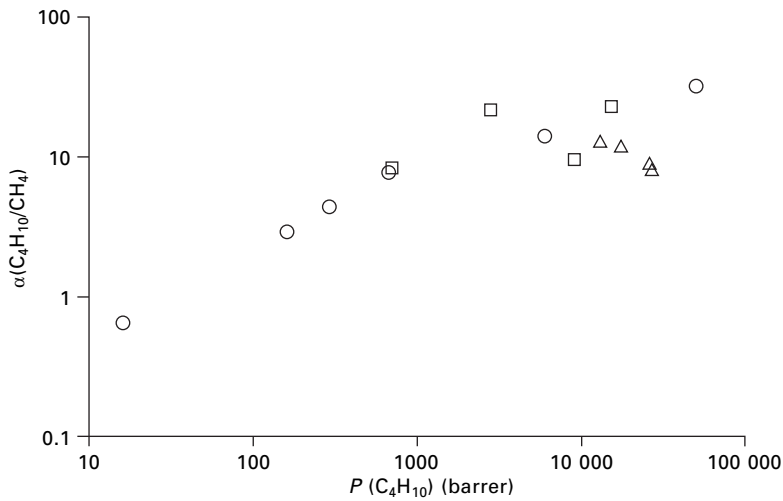
© Woodhead Publishing Limited, 2011

petroleum gases. Figure 2.6 gives an example of such a reverse-selective separation. Butane is more soluble in all the polymers than methane. When the variation of the diffusion coefficients, which decrease with molecular size and mass, is weaker than the variation of the solubility coefficients, which increase when molecular mass of penetrants increases, then a simultaneous increase in P and α are observed. This subject will be discussed in more detail in subsequent sections.

Two theoretical approaches are employed to explain and describe diffusion and permeation of gases in polymers. The first one, the transition state theory (see e.g. Glasstone *et al.*, 1941) is based on the concept that diffusion in condensed media is an activated process like the rate of chemical reactions. Hence, the Arrhenius equation is applicable to the temperature dependence of the diffusion coefficients:

$$D = D_0 \exp(-E_D/RT) \qquad [2.13]$$

Although this approach is mainly qualitative, because no straightforward method has been proposed for prediction of activation energy of diffusion E_D and, especially the pre-exponential term D_0, its application can be very useful, for example for description of permeability–permselectivity diagrams (Freeman, 1999). An advanced development of the activated diffusion approach (Gusev and Suter, 1993) is extensively used in contemporary simulations of mass transfer in polymers.



2.6 Permeability–selectivity diagram for the pair C_4H_{10}/CH_4 in polymers: ○, mixed gas permeation, polyacetylenes (Pinnau *et al.*, 2004); △, individual gas permeation, glassy norbornene polymers (Finkelshtein *et al.*, 2006); □, individual gas permeation, rubbers (van Amerongen, 1964; Robb, 1968).

© Woodhead Publishing Limited, 2011

Another approach, the free volume theory is based on the concept that all condensed (amorphous) media contain a free volume (holes, microcavities) that is either fluctuating in nature (liquid, rubbers) or is embedded in a rigid matrix (inorganic glasses, glassy polymers). The presence, size and/or mobility of these microcavities is a prerequisite for diffusion of small particles in the medium. The concept of free volume was introduced long ago (Frenkel, 1959; Cohen and Turnbull, 1959), but in these works free volume was considered as an abstract notion. Today, free volume theory is the leading approach for understanding and description of nanostructure in polymers. It is very helpful that several direct methods are now available for estimation of free volume in polymers (Theodorou, 2006; Yampolskii, 2007) and in numerous works free volume (its size and size distribution) is related to the observed values of D and P.

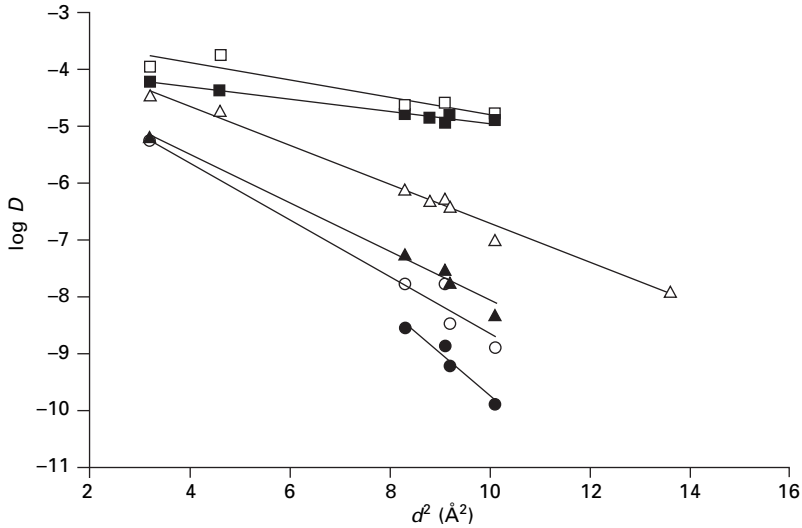
2.3 Effects of the properties of penetrants and polymers

As has been mentioned, permeability is an intrinsic property of the 'gas–polymer' system. Gases are much simpler objects than polymers, so different correlations apply that relate various diffusion and solubility coefficients (and hence the P values) of different gases in a given polymer. The situation with polymers is more complicated. Nonetheless, some properties of polymers also correlate with the D, S and P values (for a given gas). However, universal correlations are often worse than those valid for limited sets of polymers (rubbers and glasses, certain chemical polymeric classes, etc.).

2.3.1 Effects of gas parameters

The diffusion coefficients of different gas molecules characterize their dynamics or mobility in a polymer and therefore, they should be larger for smaller molecules. This intuitive assumption which is valid in all media is consistent with numerous data reported both for glassy and rubbery polymers. The square of the cross-section d^2 of diffusing molecules was successfully used as a scaling parameter for D (Michaels *et al.*, 1963; van Amerongen, 1964; Teplyakov and Durgaryan, 1984; Teplyakov and Meares, 1990; Shantarovich *et al.*, 2000) (Fig. 2.7). However sometimes d or d^3 functions were also employed. These linear correlations $\ln D(d^2)$ are especially good for spherical molecules, such as inert gases. Different scales can be used for d, specifically based on gas viscosity, Lennard-Jones parameters or adsorption in zeolites (Hirschfelder *et al.*, 1954; Breck, 1974). It was noted that systematic deviations are observed for non-spherical molecules, like CO_2, so a special scale that is convenient for predicting the diffusivity of gases in polymers was suggested (Teplyakov and Meares 1990). For a homologous

© Woodhead Publishing Limited, 2011



2.7 Correlation of the diffusion coefficients D (cm^2s^{-1}) in polymers with the cross-section of diffusants: □, polytrimethylsilyl propyne (Masuda *et al.*, 1988); ■, polydimethylsiloxane (Robb, 1968); △, polyvinyltrimethylsilane (Paul and Yampolskii, 1994); ▲, polycarbonate (Pixtone and Paul, 1994); ○, tetrabrompolycarbonate (Pixton and Paul, 1994); ●, polyimide Kapton (Data base, A.V. Topchiev Institute of Petrochemical Synthesis, TIPS, 1998).

series of penetrants (e.g. n-alkanes) it is convenient to use a single parameter, the number of carbon atoms in the molecule, because this allows similar correlations to be plotted for *D*, *S* and *P* (Fujita *et al.*, 1960; Yampolskii *et al.*, 1979). If a wide range of penetrants with varying sizes and shapes is considered, the most convenient scale is van der Waals volume or critical volume of penetrants. However, the resulting correlations are non-linear (Berens and Hopfenberg, 1982; Merkel *et al.*, 1999).

For many polymers, gas solubility coefficients over short ranges of critical temperature of penetrants are well described by a linear relationship between the logarithm of *S* and any quantity that can serve as a measure of solute condensability, critical temperature T_c, boiling point T_b, (Barrer and Scirrow, 1948) and Lennard-Jones energy parameter ε/k (Van Krevelen, 1990). Such an empirical relationship for gas solubility follows from simple classical solution thermodynamics (Gee, 1947; Petropoulos, 1994). The enthalpy of sorption ΔH_s in the van't Hoff equation for gas dissolution in Henry's law (low pressure) limit:

$$S = S_0\, e^{-\Delta H_s/RT} \qquad [2.14]$$

can be presented as the sum

$$\Delta H_s = \Delta H_c + \Delta H_m \qquad [2.15]$$

© Woodhead Publishing Limited, 2011

where $\Delta H_c = -\Delta H_v$ (enthalpy of vaporization) is the enthalpy of condensation and ΔH_m is partial molar enthalpy of mixing. It was assumed (Petropoulos, 1994) that:

$$\Delta H_v/R = a_b T_b = a_c T_c = a_e(\varepsilon/k) \quad [2.16]$$

If ΔH_m is close to zero, which is the case for rubbers (Braun and Guillet, 1976), then one obtains:

$$\ln S = \ln S'_0 + a_b T_b = \ln S'_0 + a_c T_c = \ln S'_0 + a_e(\varepsilon/k) \quad [2.17]$$

However, complications may arise for glassy polymers and for solutes (in both rubbery and glassy polymers) with large values of ΔH_c. In glassy polymers, partial molar enthalpies of sorption are negative and can have large absolute value (Bondar *et al.*, 1999). More importantly, for heavier solutes $|\Delta H_c| >> |\Delta H_m|$ and ΔH_c is directly proportional to T_c^2 (Stull *et al.*, 1969). Indeed, it has been shown that for penetrants with widely ranging T_c the correlations of the type:

$$\ln S = M + N T_c^2 \quad [2.18]$$

$$\ln S = M' + N'(T_c/T)^2 \quad [2.19]$$

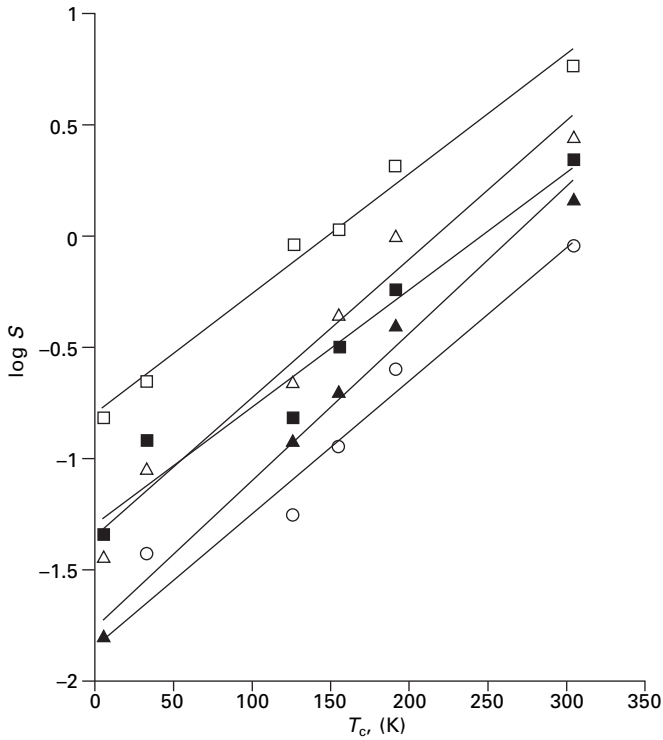
are observed (Stern *et al.*, 1969; Bondar *et al.*, 1999). However, for light gases the correlations in Equation [2.17] are fulfilled with sufficient accuracy and can be used to predict solubility. An example of such a correlation is shown in Fig. 2.8.

If van der Waals forces dominate in gas–polymer interactions during dissolution then solubility coefficients should be proportional to appropriately defined surface areas of the molecules. Excellent correlations between ln S and van der Waals (using the universal functional activity coefficient method, UNIFAC) and solvent accessible surface areas have been demonstrated for numerous polymers (both rubbery and glassy) (Yampolskii *et al.*, 2000). In contrast to Equation [2.17], they are linear for a wide range of solutes.

In penetrants series, when the size of the diffusing molecule d or V_c (and as well T_c and ε/k) increases, the D values should decrease and S should grow. So the resulting permeability coefficients P can be determined predominantly by either D or S. As can be seen from Fig. 2.7, the slopes of the dependences $D(d^2)$ (or mean diffusivity selectivity) reveal substantial differences for polymers in the rubbery and glassy state. For polymers above their glass transition temperature, the size of diffusants exerts weak effects on the D values. On the other hand, much greater diffusivity selectivity or size sieving effects can be observed for glassy polymers. Meanwhile, solubility selectivity (see Fig. 2.8) is approximately the same for rubbery and glassy polymers.

If one takes a single scaling parameter for correlations of D, S and P, for example the critical volume of penetrants (Fig. 2.9), it can be concluded that

© Woodhead Publishing Limited, 2011



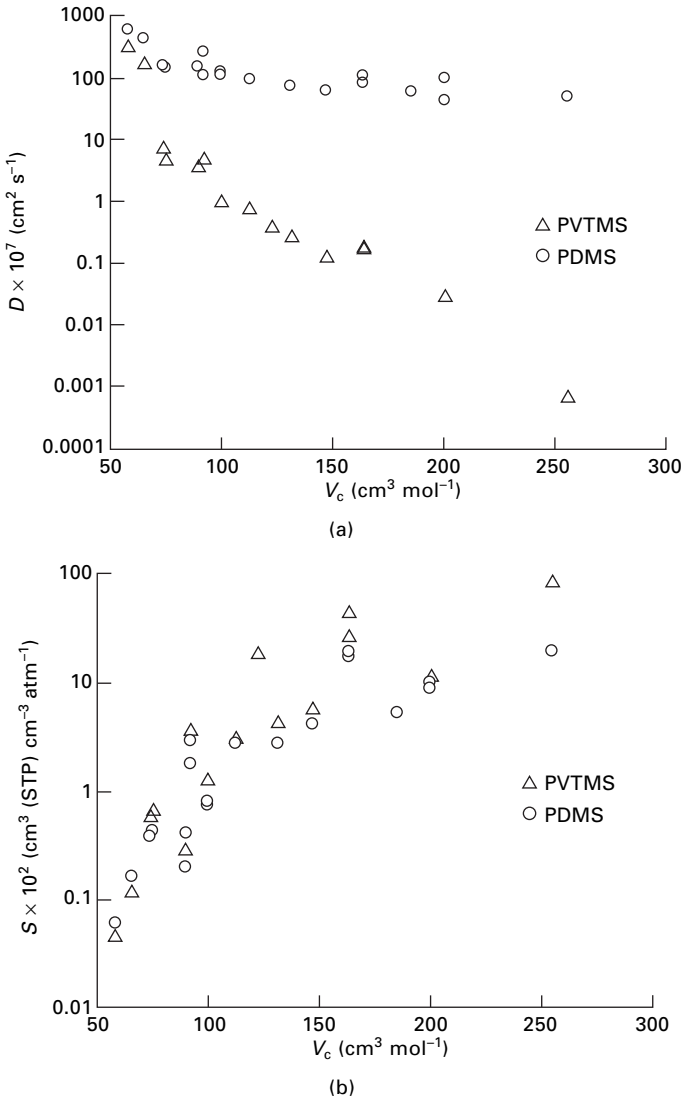
2.8 Correlation of the solubility coefficients S (cm^3 (STP) cm^{-3} atm^{-1}) with critical temperature T_c of penetrants in rubbery and glassy polymers. □, polytrimethylsilyl propyne (Masuda *et al.*, 1988); ■, polydimethylsiloxane (Robb, 1968); △, polyvinyltrimethylsilane (Paul and Yampolskii, 1994); ▲, polycarbonate (Pixton and Paul, 1994); ○, natural rubber (van Amerongen, 1964).

for glassy polymers similar dependences $D(V_c)$ and $P(V_c)$ are observed. So it is possible to speak about diffusivity or mobility controlled permeation below T_g. This means that in membranes based on glassy polymeric materials, permeates are always enriched by lighter components of feed mixtures (gases having a larger D). In contrast, in rubbers the dependence $P(V_c)$ is governed by $S(V_c)$ (see Fig. 2.9), and one can speak about solubility controlled permeation. Hence, if a membrane material works above its T_g, the permeate should be enriched by heavier components in the feed stream that have greater solubility coefficient in the membrane material although lower diffusivity. This important circumstance is always taken into account in selection of membrane materials for certain separations (Freeman and Pinnau, 1997).

A notable exception from this regularity are highly permeable polyacetylenes (in particular poly(trimethylsilyl propyne) (PTMSP)) and some other highly

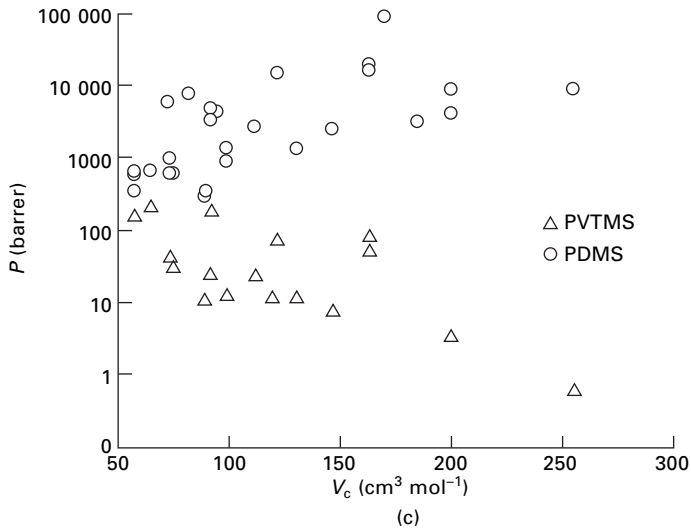
© Woodhead Publishing Limited, 2011

permeable polymers (Nagai *et al.*, 2001; Finkelshtein *et al.*, 2006). These glassy polymers are characterized by low size sieving selectivity. Hence, in these polymers solubility controlled permeation is realized and membranes based on them can be used for enrichment of heavier components of gas streams, for example extraction of higher hydrocarbons from natural gas.



2.9 Correlations of (a) diffusion, (b) solubility and (c) permeability coefficients with the critical volume V_c of penetrants in polydimethylsiloxane (PDMS) and polyvinyltrimethylsilane (PVTMS).

© Woodhead Publishing Limited, 2011



2.9 Continued

2.3.2 Effects of polymer parameters

Glass transition temperature

The effects of the glass transition temperature T_g are especially evident for rubbers or semi-crystalline polyolefins when T_g is below room temperature. In elastomers, segmental mobility is responsible for diffusion. The free volume in such media, like in liquids, is fluctuating in nature, so apparently the displacement of the measurement temperature (or room temperature) T_m from T_g (or the difference $T_m - T_g$) can serve as a measure of the segmental mobility at T_m. Indeed, good correlations of D and P with T_g have been demonstrated by several authors (van Amerongen, 1964; Yampolskii *et al.*, 1982; Fitch *et al.*, 1993), while S values rarely depend on T_g. The values ln P and ln D linearly decrease when T_g, the glass transition temperature, increases in rubbers. This trend disappears when T_g becomes higher than T_m: in glassy polymers one can find examples of very large and very small diffusivity and permeability in polymers with a high T_g (e.g. PTMSP and polyimide Kapton). Raising T_g in a group of structurally related glassy polymers that differ, for instance, via alkyl substitution often results in increases in P and D (Pixton and Paul, 1994). However, attempts to find a general correlation of this type for a big set of polymers have failed. It can be explained by complex nature of T_g. On the one hand, the glass transition temperature is a characteristic of the rigidity of isolated polymeric chain, on the other hand, it should depend on interchain interactions in the polymer matrix.

It seems to be plausible that smaller scale main or side chain motions that determine sub-T_g behavior can also affect gas permeation in polymers.

© Woodhead Publishing Limited, 2011

In fact, low temperature transitions T_γ in substituted polysulfones correlate with the permeability coefficients of these materials. However, more careful consideration shows that the reasons for this correlation can be induced by intramolecular packing or free volume affecting both T_γ and P values (Pixton and Paul, 1994).

Recently an attempt was made to predict permeability coefficients via an empirical equation including T_γ (Bas *et al.*, 2010), but such predictions only apply to polyimides. In addition, one may suspect that this correlation reflects on the indirect effects of the glass transition temperature T_g, because T_g and T_γ are strongly interrelated.

Molecular mass

The molecular mass of polymers is not among the key factors that influence gas permeation parameters. In the range of molecular masses, where one can anticipate the strongest effects, poor film forming properties make this question insignificant. Fairly weak effects of molecular mass of polymers on P and D values have been reported (see e.g. Berens and Hopfenberg, 1982; Merkel *et al.*, 1999). Toi and Paul (1982) reported some variations in the solubility coefficients of CO_2 in polystyrene samples with molecular masses in the range 3600–850 000. However, these effects can be partly ascribed to a concomitant increase of T_g from 345–374 K.

Free volume

Permeability is sensitive to various parameters that can characterize chain packing such as polymer density (Pilato *et al.*, 1975) or mean interchain distance (*d*-spacing deduced from wide angle X-ray diffraction, WAXD, studies) (Charati *et al.*, 1991; Hirayama *et al.*, 1996). However, the most relevant measure of chain packing efficiency is free volume. According to free volume theory (Cohen and Turnbull, 1959):

$$D = D_o \exp(-V^*/V_f) \qquad [2.20]$$

where V_f is free volume and the parameter V^* characterizes the size of diffusing molecules. Strictly speaking this equation holds only for diffusivity. However, since solubility coefficients in different polymers vary over a much narrower range and the effects of free volume on solubility are usually assumed to be weaker than those for diffusivity, an empirical equation for permeability is also often considered:

$$P = P_0 \exp(-B/V_f) \qquad [2.21]$$

Today, there are many methods for determination of free volume in polymers: positron annihilation lifetime spectroscopy (PALS), inverse gas

© Woodhead Publishing Limited, 2011

chromatography (IGC) (Yampolskii, 2007) and use of photochromic probes (Jansen *et al.*, 2009). The simplest and the most common way to examine correlations of the transport parameters of free volume employs the definition suggested by Bondi (1968). Accordingly, free volume V_f ($cm^3\ g^{-1}$) can be represented as the difference between the specific volume of polymers $V_{sp} = 1/\rho$, where ρ ($g\ cm^{-3}$) is the polymer density and V_{oc} the occupied volume. Bondi proposed calculating V_{oc} as 1.3 V_w, where V_w is the sum of the increments of van der Waals volumes of the groups that form the repeat unit of the polymer. The V_w values are tabulated, for example by Van Krevelen (1990). Hence:

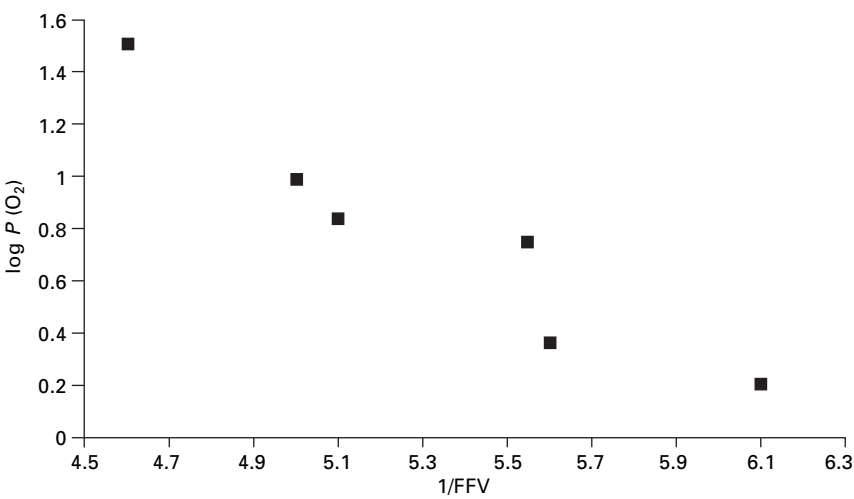
$$V_f = V_{sp} - 1.3\ V_w \qquad [2.22]$$

The value 1.3 corresponds to the random packing coefficients for cylinders. In most cases, an application of a dimensionless reduced value of fractional free volume FFV = V_f/V_{sp} gives better correlation results. The Bondi method gives rather rough statistics for free volume influencing gas diffusion and permeation in polymers. However, good correlations for P and D are often reported for structurally related polymers (Fig. 2.10).

2.4 Effects of pressure on transport parameters

2.4.1 Sorption

Sorption of gases and vapours in polymers is characterized by the solubility coefficient S or by sorption isotherms, that is, the pressure dependence of the



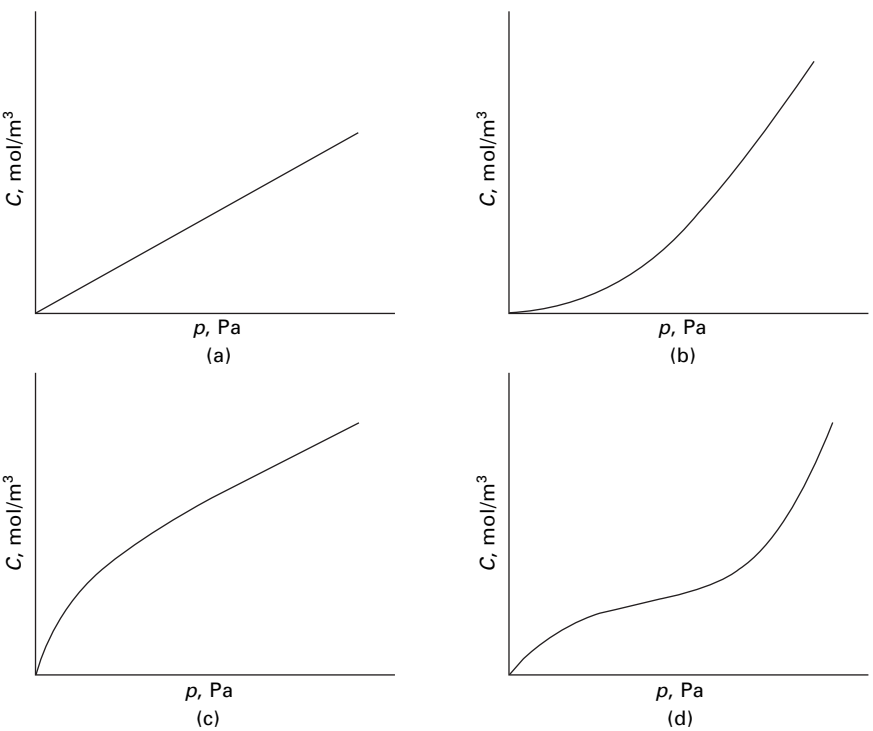
2.10 Correlation of the $P(O_2)$ (barrer) values for polycarbonates with fractional free volume FFV (Pixton and Paul, 1994).

© Woodhead Publishing Limited, 2011

concentration of sorbed component C (cm^3(STP)/cm^3 polymer or cm^3(STP)/g polymer) at constant temperature. The shape of sorption isotherms $C(p)$ depends on the nature of gas and polymer. At sufficiently low pressures all the sorption isotherms can be approximated by Henry's law:

$$C = Sp \qquad [2.23]$$

For light gases that have relatively low solubility, Henry's law isotherms can be observed up to a high pressure. If a process of membrane gas separation is performed far from the low pressure limit, strong deviation from Henry's law and non-linear sorption isotherms are observed as a rule. Figure 2.11 shows schematically different types of sorption isotherms. The sorption isotherm convex to the pressure axis is specifically characteristic of vapour dissolution in polymers above their glass transition temperatures and is well described by Flory–Huggins equation (Petropoulos, 1994; Flory, 1969)



2.11 Typical shapes of sorption isotherms $C(p)$: (a) and (b), for example solubility of methane in silicone polymers (Shah *et al.*, 1986); (c) solubility of different gases in glassy polymers (Paul, 1979); (d) solubility of CO_2 in glassy polymers at high pressure (Kamiya *et al.*, 1989).

© Woodhead Publishing Limited, 2011

$$\ln(a) = \ln(p/p_s) = \ln \phi_v + (1 - \phi_v) + \chi(1 - \phi_v)^2 \quad [2.24]$$

where a is activity, p and p_s are pressure and saturated vapour pressure, respectively, ϕ_v is the volume fraction of penetrant and χ is the so-called Flory–Huggins (interaction) parameter. When $\chi > 2$ interactions are small, and if $\chi \leq 0.5$ interactions are so strong that non-cross-linked polymer dissolves in the penetrant. Numerous examples of such isotherms can be found in the literature. For example similar behaviour was observed for sorption of acetone in polydimethylsiloxane (Singh *et al.*, 1998). Another typical case of isotherms convex to the pressure or activity axis is realized by the sorption of water or lower alcohols in hydrophobic polymers and this type of isotherm is evidence of solute cluster formation which becomes progressively more important at higher activities (Tokarev *et al.*, 2006).

Another form of sorption isotherm is typical of glassy polymers: the isotherms are concave to the pressure axis. The three parameters dual mode sorption isotherm describes well (Paul, 1979) gas dissolution below T_g:

$$C = k_D p + C'_H \frac{bp}{1 + bp} \quad [2.25]$$

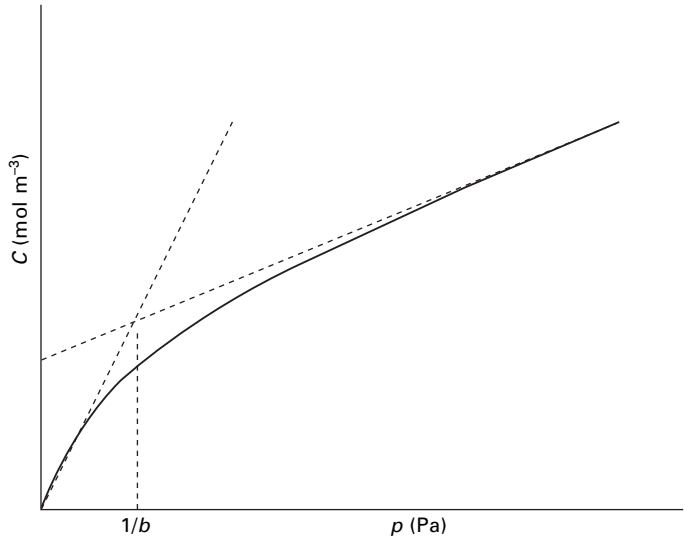
where k_D is the Henry's law parameter characterizing sorption in the densified equilibrium matrix of the glassy polymer, C'_H is the Langmuir sorption capacity, which characterizes sorption in the non-equilibrium excess volume associated with the glassy state and b is the Langmuir affinity parameter. It is assumed in this model that there are the two 'populations' of sorbed species, adsorbed in free volume elements and dissolved in more densely packed regions within polymers. At the low pressure limit $p \rightarrow 0$, one obtains the infinite dilution gas solubility coefficient:

$$S = k_D + C'_H b \quad [2.26]$$

which determines the initial slope of the isotherms (Fig. 2.12). At higher pressures, the slope is determined by Henry's law solubility coefficient k_D and the transition between these two parts of the isotherm occurs at $p = 1/b$. Analysis of numerous data on gas sorption in glassy polymers (Paterson and Yampolskii, 1999) indicates that the main contributors to S values are provided by the Langmuir term in Equation [2.26]: $C'_H b >> k_D$, especially in polymers with a high T_g. The k_D and b values behave as equilibrium constants: they obey van't Hoff plots with negative enthalpies of sorption ΔH_s (usually $\Delta H_s(b)$ is more negative (exothermic) than $\Delta H_s(k_D)$). Both k_D and b values reflect the condensability of penetrants as correlations with the critical temperature indicate.

The Langmuir sorption capacity constant C'_H can be considered as a measure of non-equilibrium or unrelaxed volume in polymers. Kanehashi and Nagai (2005) have demonstrated that rather good correlations of the

© Woodhead Publishing Limited, 2011



2.12 Dual mode sorption model isotherm in glassy polymers.

transport parameters with C'_H values are observed for various polymers. In these cases the term $1/C'_H$ behaves just like $1/V_f$ in other correlations. The C'_H parameters determined by analysis of experimental sorption isotherms are often consistent with the independently obtained C'_H values estimated via specific volume in glassy V_g and rubbery V_r states (Koros and Chern, 1987). According to this interpretation, C'_H should be temperature dependent, that is, decrease when the temperature increases and vanish when the experimental temperature T becomes equal to T_g. For 'one gas–different polymers' systems, C'_H must increase with T_g. These types of behaviour are well documented in the literature (Paul, 1979; Koros and Chern, 1987; Pixton and Paul, 1994). If one considers 'one polymer–different gases' systems, for gases below their critical temperature T_c, the observed C'_H values are smaller the larger the molecular size (e.g. the critical volume V_c) of the solute (or when the difference T_c–T increases) (Volkov *et al.*, 1985; Bondar *et al.*, 1999; Tokarev *et al.*, 2006). It means that larger gas sorption 'probes' sample progressively smaller fractions of available unrelaxed (free) volume in glassy polymers.

At sufficiently high pressure of strongly sorbed solute (typically CO_2 or hydrocarbons) deviation from the dual mode sorption shapes is observed in sorption isotherms as shown in Fig. 2.11(d). This phenomenon is interpreted as an isothermal glass transition in the system 'gas–polymer'. Owing to the high concentration of solutes and plasticization effects caused by them, glassy polymers become rubbery at temperatures much lower than T_g values for neat polymers (Kamiya *et al.*, 1989; Bondar and Yampolskii, 1995).

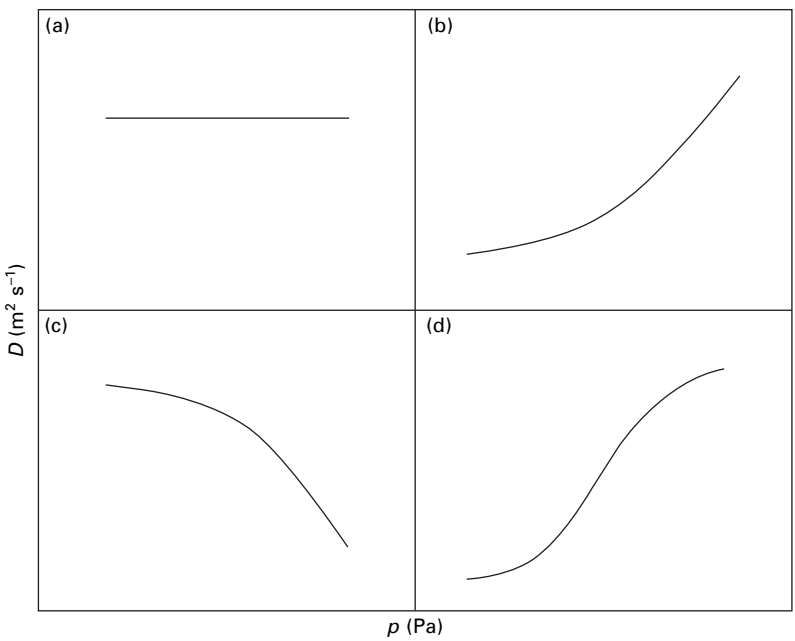
In spite of intuitive consistency of the dual mode sorption model it must be considered only as a phenomenological model that gives excellent fit of

© Woodhead Publishing Limited, 2011

the experimentally measured isotherms but lacks a fundamental physical basis. It has no prediction ability, its parameters depend to some extent on the history of the sample treatment, especially when working at higher pressure, and also depend on the range of pressures used in the measurement of sorption (Bondar *et al.*, 1996). Modern models of sorption thermodynamics (Sanchez and Lacomb, 1978; Vrentas and Vrentas, 1991; Kirchheim, 1992; Petropoulos, 1994; Doghiri *et al.*, 2006) take into account the equations of state of the polymer matrix and other relevant parameters. They consider the gas sorption process in more depth. Their obvious advantage in many cases is good predictability.

2.4.2 Diffusion

Figure 2.13 shows different types of concentration (or pressure) dependence of diffusivity. For low sorbing light gases (permanent gases or even carbon



2.13 Different types of dependence of diffusion coefficients on penetrant concentration: (a) light gases in polymers, for example diffusivity of CO_2 in polybenzylmethacrylate at 75°C (Wang *et al.*, 1996); (b) organic vapours in polymers, for example acetone, chloroform and hexane in amorphous Teflon AF2400 at 25°C (Tokarev *et al.*, 2006); (c) decreasing curve $D(c)$ due to clustering, for example MeOH and EtOH in amorphous Teflon AF2400 at 25°C (Tokarev *et al.*, 2006); (d) dual mode behaviour in glassy polymers, for example CO_2 in polycarbonate at 35°C (Koros *et al.*, 1976).

© Woodhead Publishing Limited, 2011

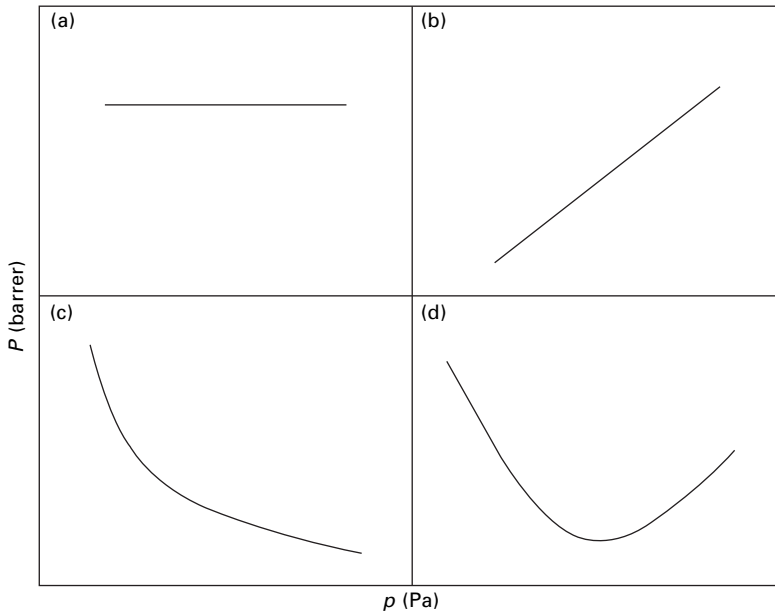
dioxide) the diffusion coefficients in polymers usually are pressure independent, as illustrated in Fig. 2.13(a). Numerous examples of such dependence can be found in the literature, for example as shown by Wang *et al.* (1996) for diffusion of CO_2 in polybenzylmethacrylate. Plasticization caused by high concentration of penetrants such as organic vapours in polymers often results in linear or exponential growth of D (Fig. 2.13(b)) while clustering is accompanied by effective increase in the mean size of diffusing species and is manifested in a dramatic decrease in the D values (Fig. 2.13(c)). The dependence of D on concentration allows one to distinguish between the two possible mechanisms of sorption isotherms convex to the pressure axis: Flory–Huggins behaviour is accompanied by increases in D, whereas clustering phenomena lead to reduced diffusion coefficients with greater vapour activity and solute concentration. Finally, Fig. 2.13(d) is characteristic of diffusion coefficients of gases in glassy polymers (Koros *et al.*, 1976). The shape of such a curve is consistent with the dual mode sorption and mobility model.

2.4.3 Permeability

Different forms of dependence of $C(p)$ and $D(p)$ determine pressure and concentration effects on permeability. The permeability of low sorbing penetrants reveals little or no change of the P values as a function of the pressure or concentration of penetrant. This is illustrated in Fig. 2.14(a). This dependence was reported for example for the system N_2–PDMS (Merkel *et al.*, 2000). However, some penetrants (carbon dioxide, hydrocarbons) are sorbed in polymers to such an extent that they can plasticize the polymer matrix, increase diffusion coefficients and in this way strongly affect the permeability coefficients. An example of such behaviour (Fig. 2.14(b)) can be found for example in the study of permeation of CO_2 at low temperatures in cross-linked poly(ethylene glycol diacrylate (Lin *et al.*, 2006). Another reason for this form of the dependence of the curve $P(C)$ can be the shape of sorption isotherm that obeys the Flory–Huggings equation. The dual mode sorption and mobility model for glassy polymers predicts a decrease in P with pressure (Fig. 2.14(c)), which is confirmed by many studies (e.g. Paul, 1979). However, sometimes plasticization at higher penetrant concentrations leads to increases in the P values, as shown in Fig. 2.14(d). (e.g. Starannikova *et al.*, 2008).

So far we have considered the effects of various penetrants on $P(C)$ that are exerted by their own pressure and concentration in the membrane. There is, however, a group of important phenomena where permeability and permselectivity are sensitive to the presence of strongly sorbed impurities (residual solvents that remain in the membranes after their casting procedure and higher hydrocarbons in feed streams during the separation of methane-

© Woodhead Publishing Limited, 2011



2.14 Different types of dependence of the permeability coefficients on penetrant concentration: (a) and (b) for example see Stern *et al.* (1987); (c) see for example Paul (1979); (d) see for example Starannikova *et al.* (2008).

hydrogen mixtures, etc.). In such cases, the permeation rates of the components of the mixtures to be separated increase, the stronger effects being observed for 'slower' penetrants (e.g. CH_4 in its mixture with H_2). These effects are of great concern to the engineers who want to perform real membrane processes, because the observed separation factors (see Equation [2.12]) are much lower than ideal separation factors (Equation [2.10]). A possible way to overcome these difficulties is to use perfluorinted polymers that show reduced solubility of hydrocarbons as membrane materials (Merkel *et al.*, 2006).

2.5 Effects of temperature on transport parameters

Diffusion of gases in polymers is an activated process, described by the Arrhenius equation:

$$\ln D = \ln D_0 - E_D/RT \qquad [2.27]$$

In combination with the van't Hoff equation for the solubility coefficients:

$$\ln S = \ln S_0 - \Delta H_s/RT \qquad [2.28]$$

This results in the Arrhenius equation for permeability coefficients:

© Woodhead Publishing Limited, 2011

$$\ln P = \ln P_0 - E_P/RT \quad [2.29]$$

The parameters of these equations are related by a simple formula: $E_P = E_D + \Delta H_s$. The values of E_D are always positive, while the sign of E_P depends on relative magnitudes of E_P and ΔH_s. For light gases, typically $E_D > |\Delta H_s|$, the resulting values $E_P > 0$ and permeability increases when temperature increases. However, there are frequent situations when $E_P < 0$: this occurs in vapour sorption, when ΔH_s has a large absolute value or in polymers with rigid main chains and unusually low energy barriers for diffusion (small E_D values) such as polyacetylenes (Masuda *et al.*, 1988; Nagai *et al.*, 2001) or derivatives of polynorbornene (Starannikova *et al.*, 2008). It should be noted that E_P and E_D values are constant during transport in glassy polymers, while temperature dependence of these activation energies is often observed in rubbers (Van Amerongen, 1964). When the experimental temperature range includes glass transitions, in most cases a marked break in Arrhenius dependence is observed, when the temperature of the measurements passes through T_g (Yasuda and Hirotsu, 1977). Higher activation energies E_D and E_P observed above T_g seem to be consistent with an assumption that segmental mobility in rubbers is responsible for diffusion and the size of kinetic segment is substantially larger than the sizes of diffusing gas molecules.

The parameters of Arrhenius equations [2.27] and [2.29] are strongly interrelated due to the so-called compensation effect: larger pre-exponential factors correspond to higher activation energies. For rubbers with temperature-dependent activation energies, the pre-exponential factor can be expressed as (Barrer and Chio, 1965):

$$\ln D_0 = a' - b' (E_D/RT) \quad [2.30]$$

while in glassy polymer a simpler formula holds true:

$$\ln D_0 = a - bE_D \quad [2.31]$$

Parameters of these equations that were first discovered long ago (Van Amerongen, 1946) were recently confirmed (see Prabhakar *et al.*, 2004).

Equation [2.31] enables activation energies to be estimated when the D or P values are known at a single temperature; hence, the values of D and P in the whole range of temperatures can be evaluated from an observation at one temperature (Yampolskii *et al.*, 1998).

The parameters E_D, E_P and ΔH_s are strong functions of the molecular size of penetrants. A simple interpretation of this phenomenon was given by the Meares' equation (1954):

$$E_D = 0.25\, N_o \pi d^2 \lambda\, CED \quad [2.32]$$

where N_o is the Avogadro number, d is the kinetic cross-section of a diffusant, CED is the cohesion energy density in a polymer and λ (adjustable parameter) is a diffusion jump length. This equation not only explains the dependence

© Woodhead Publishing Limited, 2011

of E_D on V_c or d^2 but also the decreases in diffusivity of gases with larger d sizes or critical volumes (Fig. 2.7 and Fig. 2.9). However, it is not predictive, because the λ values are unknown.

Traditionally, temperature dependence of D and activation energy E_D are interpreted based on the transition state theory (Glasstone *et al.*, 1941). On the other hand, it is known that activation energies E_D and E_P correlate with free volume: polymers with a large free volume reveal fairly low activation energies and vice versa (Yampolskii *et al.*, 1998). There were attempts to propose a unified model that encompasses both transition state and free volume theories such as:

$$D = A \exp(-E_D/RT) \exp(-V^*/V_f) \quad [2.33]$$

Recently, Lin and Freeman (2005) have developed the following relation between the activation energy of diffusion and fractional free volume:

$$E_D = [A + b - (B/FFV)]/[(a/R) - (1/RT)] \quad [2.34]$$

where the parameters A and B are characteristics of free volume model and are constants in the linear free energy relation, like Equation [2.31].

Analysis of the Meares Equation [2.32] in conjunction with data from positron annihilation on the size and concentration of free volume elements in polymers led to the conclusion (Alentiev and Yampolskii, 2002) that the diffusion jump length λ is close to the average distance between adjacent free volume elements in glassy polymers, that is, this quantity has a specific physical meaning.

2.6 Gas permeability of polymers: objects of membrane gas separation

Polymers with different chemical structures and physical states (rubbery and glassy) exhibit substantially different values of gas permeability. Table 2.1 shows that the range of variation of permeability coefficients in different polymers is as large as eight orders. This range depends to some extent on the nature of a gas: for hydrogen or helium it is narrower, for 'heavier' gases like C_4H_{10} it is wider. For glassy polymers, the effects of chemical structure on permeability are stronger than for rubbers. Among glassy polymers one can find low permeability (barrier) materials, as well as polymers with extra-large gas permeability. This reflects the possible richness of the nano-structure of polymeric glasses.

Table 2.2 gives the list of gas mixtures that can be separated by membrane methods. The most obvious and traditional object of these separations is air: obtaining pure oxygen and nitrogen. The incentive to obtain a membrane that provides sufficiently pure oxygen stems from the aim to replace the inefficient energy processes of cryogenic separation of air via distillation.

© Woodhead Publishing Limited, 2011

Table 2.1 Permeability of polymers

Polymer	$P(O_2)$ (barrer)
Copolyester Vectra	0.0005
Polymethylmethacrylate	0.09
Polystyrene	2.9
Polycarbonate	1.6
Polyimide 6FDA-ODA	2.4
Polyethylene	3
Polydimethylsiloxane	900
Polyvinyltrimethylsilane	44
Amorphous Teflon AF2400	1140
Polytricyclononen with 2 $Si(CH_3)_3$ groups	2400
Polytrimethylsilylpropyne	8000
Indan-containing poly(diphenylacetylene)	18000

Table 2.2 Problems in membrane gas separation

Main problems		Other problems of gas separation	
Mixture	Target component/process	Most important	Others
O_2/N_2	N_2 (99+%) Oxygen enriched air ($[O_2]$ = 30–50%)	He/CH_4	He/N_2
H_2/N_2 H_2/CO	H_2: Ammonia synthesis H_2: C_1 chemistry, MeOH synthesis	CO_2/O_2	CO_2/CO
H_2/CH_4	H_2: Petrochemistry, refinery		
CO_2/CH_4	CO_2: enhanced oil recovery	CO_2/H_2	C_2H_4/C_3H_6
C_1/C_{4+}	Separation of natural gases	H_2S/CO_2	C_3H_6/C_3H_8
H_2O/CH_4 H_2O/air	Dehumidification of various gases	SO_2/N_2	n-C_4H_{10}/i-C_4H_{10}
Vapours (solvents, fuels)	Removal of organic vapours from permanent gases	H_2S/CH_4	C_6H_6/C_6H_{12} vapours

However, one stage in obtaining a permeate that contains 99% O_2 requires a separation factor $\alpha(O_2/N_2) = 370$, a feat presently unattainable by modern membranologists. On the other hand, streams containing 30–50% of oxygen can be obtained using existing membranes and these gas mixtures can find limited applications in medicine and in the intensification of combustion and oxidation processes. Meanwhile, the production of gas streams containing 99% nitrogen using membranes is a much simpler problem. Normally, designing a membrane process always requires a compromise between the necessary composition of the obtained streams (permeate and retentate) and a reasonable stage-cut (ratio of permeate and feed streams or retentate

© Woodhead Publishing Limited, 2011

and feed streams). In the case of air, it is possible to obtain virtually pure nitrogen (retentate stream) at very low stage-cuts. So membrane production of technical nitrogen streams is common practice today.

The largest industrial application is the membrane separation of hydrogen from the stream containing H_2 in mixtures with nitrogen (ammonia synthesis), methane (various processes of petrochemistry and refinery) and carbon monoxide (so-called chemistry C_1). Separation of the mixtures of CO_2/CH_4 was one of the first successful industrial membrane gas separation processes. Originally permeate streams enriched with carbon dioxide were used in the EOR (enhanced oil recovery) process, returning them to the oil wells in order to increase oil output. Now general attention to membrane separation of various mixtures containing CO_2 is related to the universal problem of global warming. Several chapters of this book deal with these separations. A detailed description and analysis of industrial processes of membrane gas separation can be found in the review by Baker (2002).

The two right hand columns in Table 2.2 present separations that have not yet found practical application. Among them I would like to emphasize the extraction of helium from its mixtures with nitrogen and especially methane. Helium is present in relatively small concentrations in natural gases (0.4–0.5% are considered exceptionally large), so large volumes of He are lost if the produced natural gas is not treated to obtain pure He or He-enriched streams. This problem is not new (see for example Stern *et al.* (1965)), however, it has not been solved on the industrial scale in spite of the fact that He is a strategic gas urgently needed in nuclear, electronic and other industries.

Two other separations (SO_2/air and H_2S/CH_4) are of great environmental importance. The difficulties of membrane removal of SO_2 from the flue gases of coal power stations are caused by unpleasant conditions for membrane separation of the streams to be separated: low pressure, low concentration of SO_2 and high temperature.

A variety of different separations of hydrocarbon-containing mixtures will be very beneficial for various processes in petrochemistry. However, so far there has not been successful industrial realization of such membrane processes.

2.7 References

Alentiev A Yu and Yampolskii Yu P (2000), 'Free volume model and tradeoff relations of gas permeability and selectivity in glassy polymers', *J Membr Sci*, **165**, 201–16.

Alentiev A Yu and Yampolskii Yu P (2002), 'Meares equation and the role of cohesion energy density in diffusion in polymers', *J Membr Sci*, **206**, 291–306.

Baker R W (2002), 'Future directions of membrane gas separation technology', *Ind Eng Chem Res*, **41**, 1393–411.

Baker R W (2007), *Concise Encyclopedia of Polymer Science and Technology*, third edition, Wiley, Hoboken, 657.

© Woodhead Publishing Limited, 2011

Barrer R M and Chio H T (1965), 'Solution and diffusion of gases and vapors in silicone rubber membranes', *J Polym Sci C*, **10**, 111.

Barrer R M and Skirrow G (1948), 'Transport and equilibrium phenomena in gas elastomer sytems. Part II. Equilibrium phenomena', *J Poly Sci*, **3**, 564–75.

Bas C, Mercier R, Charles Dauwe C and Alberola N D (2010), 'Microstructural parameters controlling gas permeability and permselectivity in polyimide membranes', *J Membr Sci*, **349**, 25–34.

Berens A R and Hopfenberg H B (1982), 'Diffusion of organic vapors at low concentrations in glassy PVC, polystyrene and PMMA', *J Membr Sci*, **10**, 283–303.

Boeddeker K W (1995), 'Commentary tracing membrane science', *J Membr Sci*, *Special Issue*, **100**, 1–68.

Bondar V I and Yampolskii Yu P (1995), 'S-shaped sorption isotherms: Effect of the nature of polymers and gases', *Proceedings Euromembrane'95*, Bowen W R, Field R W and Howell J A (eds), European Society for Membrane Science, Bath, V.II, 141–6.

Bondar V I, Kamiya Y and Yampolskii Yu (1996), 'On pressure dependence of the parameters of the dual-mode sorption model', *J Polym Sci, Part B: Polym Phys*, **34**, 369–78.

Bondar V I, Freeman B D and Yampolskii Yu P (1999), 'Sorption of gases and vapors in an amorphous glassy perfluorodioxole copolymer', *Macromolecules*, **32**, 6163–71.

Bondi A (1968), *Physical Properties of Molecular Crystals*, *Liquids and Glasses*, Wiley, New York.

Braun J M and Guillet J E (1976) 'Study of polymers by inverse gas chromatography', *Adv Polym Sci*, **21**, 107–45.

Breck D W (1974), *Zeolite Molecular Sieves*, Kriegere Publishing, Malabar.

Charati S G, Houde A Y, Kulkarni S S and Kulkarni M G (1991), 'Transport of gases in aromatic polyesters: correlation with WAXD studies', *J Polym Sci*, *Part B: Polym Phys*, **29**, 921–31.

Cohen M and Turnbull T (1959), 'Molecular transport in liquids and glasses', *J Chem Phys*, **31**, 1164–69.

Crank J (1975), '*The Mathematics of Diffusion*', Clarendon Press, Oxford.

Data base (1998), *Gas Permeation Parameters of Glassy Polymers*, #3585, Informregistr RF, TIPS database, Moscow.

Daynes H A (1920), 'The process of diffusion through a rubber membrane', *Proc R Soc Ser A*, **97**, 286–307.

Doghieri F, Quinzi M, Rethwish D G and Sarti G C (2006), 'Predicting gas solubility in membranes through non-equilibrium thermodynamics for glassy polymers', in *Materials Science of Membranes for Gas and Vapor Separation*, Yampolskii Yu, Pinnau I and Freeman B D (eds), Wiley, Chichester, 137.

Durgaryan S G and Yampolskii Yu P (1983),'Membrane gas separation processes in petrochemistry and refinery', *Neftekhimia*, **23**, 579–95.

Finkelshtein E, Makovetskii K, Gringolts M, Rogan Yu, Golenko T, Starannikova L, Yampolskii Yu, Shantarovich V and Suzuki T (2006)'Addition-type polynorbornene with $Si(CH_3)_3$ side group: synthesis, gas permeation and free volume', *Macromolecules*, **39**, 7022–9.

Fitch M W, Koros W J, Nolen R L and Carnes J R (1993), 'Permeation of several gases through elastomers, with emphasis on the D_2/H_2 pair', *J Appl Polym Sci*, **47**, 1033–46.

Flory P J (1969), *Statistical mechanics of chain molecules*, Wiley, New York.

Freeman B D (1999), 'Basis of permeability/selectivity tradeoff relations in polymeric gas separation membranes', *Macrolmolecules*, **32**, 375–80.

© Woodhead Publishing Limited, 2011

Freeman B and Pinnau I (1997) 'Separation of gases using solubility-selective polymers', *Trends Polym Sci*, **5**, 167–73.

Frenkel Ya I (1959), *Collected Works*, *V. 3*, *Kinetic Theory of Liquids*, Izd AN SSSR, Moscow.

Fujita H, Kishimoto A and Matsumo K (1960), 'Concentration and temperature dependence of diffusion coefficients for systems polymethylacrylate and n-akyl acetates', *Trans Faraday Soc*, **56**, 424–37.

Gee G (1947), 'Some thermodynamic properties of high polymers and their molecular interpretation', *Quart Rev Chem Soc*, **1**, 265–98.

Glasstone S, Laidler K J and Eyring H (1941), *The Theory of Rate Processes*, McGraw-Hill, New York and London.

Graham T (1866), 'On the absorption and dialitic separation of gases by colloid septa. Action of a septum of caoutchouc', *Phil Mag*, **32**, 401–20.

Gusev A A and Suter U W (1993), Dynamics of small molecules in dense polymers subjected to thermal motion, *J Chem Phys*, **99**, 2228–34.

Hirayama Y, Yoshinaga T, Kusuke Y, Nonomiya K, Sakakibara T and Tamari T (1996), 'Relation of gas permeability with structure of aromatic polyimides', *J Membr Sci*, **111**, 169–82.

Hirschfelder J O, Curtiss C F and Bird R B (1954), *Molecular Theory of Gases and Liquids*, John Wiley, New York.

Jansen J C, Macchione M, Tocci E, De Lorenzo L, Yampolskii Yu P, Sanfirova O, Shantarovich V P, Heuchel M, Hofmann D and Drioli E (2009), 'Comparative study of different probing techniques for the analysis of the free volume distribution in amorphous glassy perfluoropolymers', *Macromolecules*, **42**, 7589–604.

Kamiya Y, Mizoguchi K, Hirose T and Naito Y (1989), 'Sorption and dilation in poly(ethylmethacrylate)-carbon dioxide system', *J Polym Sci, Part B: Polym Phys*, **27**, 879–92.

Kanehashi S and Nagai K (2005), 'Analysis of dual-mode model parameters for gas sorption in glassy polymers', *J Membr Sci*, **253**, 117–38.

Kapanin V V, Chalykh A E and Reitlinger S A (1972), 'Selectivity of gas permeation and polymer structure', *Dokl Acad Sci USSR*, **203**, 147–50.

Kirchheim R (1992), 'Sorption and partial molar volume of small molecules in glassy polymers', *Macromolecules*, **25**, 6952–60.

Koros W J and Chern R T (1987), 'Separation of gaseous mixtures using polymer membranes', in *Handbook of Separation Progress Technology*, Rousseau R W (ed), Wiley, New York, 862.

Koros W J, Paul D R and Rocha A A (1976), 'Carbon dioxide sorption and transport in polycarbonate', *J Polym Sci, Part B: Polym Phys*, **14**, 687–702.

Lin H and Freeman B D (2005), 'Gas permeation and diffusion in cross-linked poly(ethylene glycol diacrylate)', *Macromolecules*, **38**, 8394–407.

Lin E, van Wagner E, Freeman B D, Toy L G and Ragubir P (2006), 'New membrane materials for CO_2/H_2 separation and a model for pure and mixed gas permeability', *Science*, **311**, 639–42.

Lonsdale H K (1989), 'What is membrane? Part II', *J Membr Sci*, **43**, 1–3.

Masuda T, Iguchi Y, Tang B-Z and Higashimura (1988), 'Diffusion and solution of gases in substituted polyacetylene membranes', *Polymer*, **29**, 2041–9.

Matteucci S, Yampolskii Yu, Freeman B D and Pinnau I (2006), 'Transport of gases and vapors in glassy and rubbery polymers', in *Materials Science of Membranes for Gas and Vapor Separation*, Yampolskii Yu, Pinnau I and Freeman B D (eds), Wiley, Chichester, p 1.

© Woodhead Publishing Limited, 2011

Meares P (1954), 'The diffusion of gases through polyvinyl acetate', *J Amer Chem Soc*, **76**, 3415–22.

Meares P (1961), *Encyclopedic Dictionary of Physics*, Volume 4, Pergamon Press, Oxford, 561.

Merkel T C, Bondar V, Nagai K, Freeman B D and Yampolskii Y P (1999), 'Gas sorption, diffusion and permeation in poly(2,2-bis(trifluoromethyl)-4,5-difluoro-1,3-dioxole-co-tetrafluoroethylene)', *Macromolecules*, **32**, 8427–40.

Merkel T C, Bondar V, Nagai K, Freeman B D and Pinnau I (2000), 'Gas sorption, diffusion, and permeation in poly(dimethylsiloxane)', *J Polym. Sci, Part B: Polym Phys*, **38**, 415–34.

Merkel T C, Pinnau I, Prabhakar R and Freeman B D (2006), 'Gas and vapor transport properties of perfluoropolymers', in *Materials Science of Membranes for Gas and Vapor Separation*, Yampolskii Yu, Pinnau I and Freeman B D (eds), Wiley, Chichester, 251.

Michaels A S, Vieth W R and Barrie J A (1963), 'Diffusion of gases in polyethylene terephthalate', *J Appl Phys*, **34**, 13–21.

Mitchell J K (1831), 'On the penetrativeness of fluids', *J Roy Inst Great Britain*, **101** (no IV), 307.

Nagai K, Masuda T, Nakagawa T, Freeman B D and Pinnau I (2001), 'Poly[1-(trimethylsilyl)-1-propyne] and related polymers, synthesis, properties and functions', *Prog Polym Sci*, **26**, 721–98.

Paterson R and Yampolskii Yu (1999), 'Solubility of gases in glassy polymers', *J Phys Chem Ref Data*, **28**, 1255–450.

Paul D R (1979), 'Gas sorption and transport in glassy polymers', *Ber Bunsenges Phys Chem*, **83**, 294–302.

Paul D R and Yampolskii Yu (eds) (1994), *Polymeric Gas Separation Membranes*, CRC Press, Boca Raton, 177.

Petropoulos J H (1994), 'Mechanisms and theories for sorption and diffusion of gases in polymers', *Polymeric Gas Separation Membranes*, Paul D R and Yampolskii Yu P (eds), CRC Press, Boca Raton, 17.

Pilato L A, Litz L M, Haritay B, Farnham A G, Kawakami J H, Fritze P E and McGrath J E (1975), 'Polymers for permselective membrane gas separations', *Am Chem Soc Div Polym Chem, Polym Preprints*, **16**, 41–6.

Pinnau I, Morisato A and He Z (2004), 'Influence of side-chain length on the gas permeation properties of poly(2-alkylacetylenes)', *Macromolecules*, **37**, 2823–8.

Pixton M R and Paul D R (1994), 'Relationships between structure and transport propoerties for polymers with aromatic backbones', in *Polymeric Gas Separation Membranes*, Paul D R and Yampolskii Yu P (eds), CRC Press, Boca Raton, 83.

Prabhakar R, Freeman B D and Roman I (2004), 'Gas and vapor sorption and permeation in poly(2,2,4-trifluoro-5-trifluoromethoxy-1,3-dioxole-co-tetrafluoroethylene)', *Macromolecules*, **37**, 7688–97.

Robb W L (1968), 'Silicon membranes, their permeability and application', *Ann NY Acad Sci*, **146**, 119–37.

Robeson L M (1991), 'Correlation of separation factor versus permeability for polymeric materials', *J Membr Sci*, **62**, 165–85.

Robeson L M (2008), 'The upper bound revisited', *J Membr Sci*, **320**, 390–400.

Sanchez I C and Lacomb R H (1978), 'Statistical thermodynamics of polymer solutions', *Macromolecules*, **11**, 1145–56.

Shah V M, Hardy B J and Stern S A (1986), 'Solubility of carbon dioxide, methane and propane in silicone polymers: effect of polymer side chains', *J Polym Sci, Part B: Polym Phys*, **24**, 2033–47.

© Woodhead Publishing Limited, 2011

Shantarovich V P, Kevdina I B, Yampolskii Yu P and Alentiev A Yu (2000), 'Positron annihilation lifetimes of high and low free volume glassy polymers: effects of free volume sizes on the permeability and permselectivity', *Macromolecules*, **33**, 7453–66.

Singh A, Freeman B D and Pinnau I (1998), 'Pure and mixed gas acetone/nitrogen permeation properties of polydimethylsiloxane', *J Polym Sci, Part B: Polym. Phys*, **36**, 289–301.

Starannikova L, Pilipenko M, Belov N, Yampolskii Yu, Gringolts M and Finkelshtein E (2008), 'Addition type polynorbornene with $Si(CH_3)_3$ side group: detailed study of gas permeation and thermodynamic properties', *J Membr Sci*, **323**, 134–43.

Stern S A, Sinclair T F, Gareis P J, Vahldiek N P and Mohr P H (1965), 'Helium recovery by permeation', *Ind Eng Chem*, **57**(2), 49–60.

Stern S A, Mullhaupt J T and Garries P J (1969), 'The effect of pressure on the permeation of gases and vapors through polyethylene. Usefulness of the corresponding states principle', *A I Ch E Journal*, **15**, 64–73.

Stern S A, Shah V M and Hardy B J (1987), 'Structure-permeability relationships in silicone polymers', *J Polym Sci, Part B: Polym Phys*, **25**, 1263–98.

Stull D R, Westrum E F and Sinke G C (1969), *The Chemical Thermodynamics of Organic Compounds*, Wiley, New York.

Teplyakov V V and Durgaryan S G (1984), 'Correlation analysis of gas permeation parameters for polymers', *Vysokomol Soed A*, **26**, 1498–505.

Teplyakov V and Meares P (1990), 'Correlation aspects of the selective gas permeabilities of polymeric materials and membranes', *Gas Sep Purif*, **4**, 66–74.

Theodorou, D (2006), 'Principles of molecular simulation of gas transport in polymers', in *Materials Science of Membranes for Gas and Vapor Separation*, Yampolskii Yu, Pinnau I and Freeman B (eds), Wiley, Chichester, 49.

Toi K and Paul D R (1982), 'Effect of polystyrene molecular weight on the carbon dioxide sorption isotherm', *Macromolecules*, **15**, 1104–107.

Tokarev A, Friess K, Machkova J, Sipek M and Yampolskii Yu (2006), 'Sorption and diffusion of organic vapors in amorphous teflon AF2400', *J Polym Sci, Part B: Polym Phys*, **44**, 832–44.

van Amerongen G J (1946), 'The permeability of different rubbers to gases and its relation to diffusivity and solubility', *J Appl Phys*, **17**, 972–85.

van Amerongen G J (1964), 'Diffusion in elastomers', *Rubber Chem Technol*, **37**, 1065–153.

Van Krevelen D W (1990), *Properties of Polymers*, Elsevier, Amsterdam.

Volkov V V, Bokarev A K, Durgaryan S G and Nametkin N S (1985), 'Sorption of low-molecular-weight compounds in glassy PVTMS in vicinity and below the critical temperature of the solute', *Dokl Akad Nauk SSSR*, **282**, 641–4.

von Wroblewski S (1879), 'Ueber die nature der absorption der gase durch flussigkeiten unter hochen drucken', *Ann Physik u Chem*, **8**, 29–52.

Vrentas J S and Vrentas C M (1991), 'Sorption in glassy polymers', *Macromolecules*, **24**, 2404–12.

Wang J-S, Naito Y and Kamiya Y (1996), 'Effect of penetrant-induced isothermal glass transition on sorption, dilation, and diffusion behavior of polybenzylmethacrylate/CO_2', *J Polym Sci, Part B: Polym Phys*, **34**, 2027–33.

Yampolskii Yu P (2007), 'Methods for investigation of the free volume in polymers', *Rus Chem Rev*, **76**, 59–78.

Yampolskii Yu P, Durgaryan S G and Nametkin N S (1979), 'Permeability, diffusivity and solubility of n-alkanes in polymers', *Vysokomol Soed B*, **21**, 616–21.

© Woodhead Publishing Limited, 2011

Yampolskii Yu P, Durgaryan S G and Nametkin N S (1982), 'Translational and rotational mobility of low molecular mass compounds in polymers with different glass transition temperatures', *Vysokomol Soed A*, **24**, 536–41.

Yampolskii Yu, Shishatskii S, Alentiev A and Loza K (1998), 'Correlations with and predictions of activation energies of gas permeation and diffusion in glassy polymers', *J Membr Sci*, **148**, 59–69.

Yampolskii Y, Wiley D and Maher C (2000), 'Novel correlation for solubility of gases in polymers: effect of molecular surface area of gases', *J Appl Polym Sci*, **76**, 552–60.

Yasuda H and Hirotsu T (1977), 'The effect of glass transition on gas permeabilities', *J Appl Polym Sci*, **21**, 105–12.

2.8 Appendix: list of symbols

2.8.1 Latin

a	activity
A'	characteristics of free volume model
a'	parameter in equation relating D_0 and E_D
a_b, a_c, a_e	empirical parameters
B	parameter in equation of free volume for permeability coefficient
B'	characteristics of free volume model
b	Langmuir affinity parameter, atm^{-1}
b'	parameter in equation relating D_0 and E_D
C	concentration of penetrant in the membrane
C'_H	Langmuir sorption capacity, $cm^3(STP)/cm^3$
CED	cohesion energy density, J cm^{-3}
D	diffusion coefficient, $cm^2\ s^{-1}$
d	kinetic cross-section of a diffusant, Å
D_0	pre-exponential factor of the Arrhenius equation of diffusion coefficient, $cm^2\ s^{-1}$
D'_0	pre-exponential factor of the free volume equation of diffusion coefficient, $cm^2\ s^{-1}$
E_D	activation energy of diffusion, kJ mol^{-1}
ΔH_c	enthalpy of condensation, kJ mol^{-1}
ΔH_m	partial molar enthalpy of mixing, kJ mol^{-1}
ΔH_s	enthalpy of sorption, kJ mol^{-1}
J	flux across the membrane, mol $m^{-2}\ s^{-1}$
k_D	Henry's law solubility coefficient, $cm^3(STP)/cm^3$ atm
l	thickness of the film, μm
M	constant in equation relating solubility coefficient and T_c^2
M'	constant in equation relating solubility coefficient and $(T_c/T)^2$
N	constant in equation relating solubility coefficient and T_c^2
N'	constant in equation relating solubility coefficient and $(T_c/T)^2$
N_0	Avogadro number

© Woodhead Publishing Limited, 2011

P	permeability coefficient, Barrer; 1 Barrer = 10^{-10} cm^3(STP)·cm/(cm^2·s·cm Hg)
p	pressure, atm
Δp	pressure drop across the membrane
P_0	pre-exponential factor of the Arrhenius equation of permeability coefficient, Barrer
P'_0	pre-exponential factor of the free volume equation of permeability coefficient, Barrer
p_s	saturated vapour pressure, mm Hg
Q	permeance of the membrane, l m^{-2} s^{-1} atm^{-1}
R	universal gas constant, J mol^{-1} K^{-1}
S	solubility coefficient, cm^3(STP)/cm^3 atm
S_o	pre-exponential factor of the vant'Hoff equation of the solubility coefficient, cm^3(STP)/cm^3 atm
T	temperature, K
T_b	boiling point, K
T_c	critical temperature, K
T_g	glass transition temperature (K)
T_m	measurement or room temperature (K)
V^*	characteristics of the size of diffusing molecules
V_f	free volume, cm^3 g^{-1}
V_w	van der Waals volume of repeat unit
x	coordinate across the membrane
x_A	mole fraction of the component A in the feed stream
x_B	mole fraction of the component B in the feed stream
y_A	mole fraction of the component A in the permeate
y_B	mole fraction of the component B in the permeate

2.8.2 Greek

$\alpha_{AB} = P_A/P_B$	permselectivity (ideal separation factor) in respect of gas A and B
α^D_{AB}	selectivity of diffusions defined as D_A/D_B
α^S_{AB}	selectivity of sorption defined as S_A/S_B
$\alpha'_{AB} = Q_A/Q_B$	ideal separation factor of the membrane in respect of gases A and B
ε/k	energy constant of the Lennard Jones potential, K
θ	time lag, s
λ	diffusion jump length, Å
ϕ_v	volume fraction of penetrant
χ	Flory–Huggins (interaction) parameter

© Woodhead Publishing Limited, 2011

3

Characterization of membranes for energy and environmental applications

M. CAMPO, A. TANAKA and
A. MENDES, University of Porto, Portugal and
J. M. SOUSA, University of Trás-os-Montes e Alto Douro, Portugal

Abstract: Industrial use of membranes for gas separation has been increasing over the past two decades. The most common gas separations are oxygen enrichment from air, carbon dioxide separation and hydrogen purification. Membranes for gas separation can have various natures, namely polymer, ceramic (e.g. zeolite), metallic, carbon or mixed matrix. For their development and application it is necessary to characterize these membranes according to their surface and inner morphologies, surface chemistry, mass transport parameters and mechanical and chemical stability. This chapter presents the most common characterization techniques of polymer, ceramic, metal and carbon membranes, with regard to morphology and mass transport parameters. It also provides some phenomenological models normally used to describe the permeating mass transport.

Key words: mass transport parameters, membrane characterization, modelling, physical structure, surface chemistry.

3.1 Polymer and carbon molecular sieve membranes

Morphological and chemical characterization of membranes is of great importance and can be carried out using several techniques. The primary characterization usually involves determination of the morphology and chemical composition. Scanning electron microscopy (SEM) is used to analyse the morphology and surface quality, while the crystallinity is normally analysed by X-ray diffraction (XRD). Transmission electron microscopy (TEM) is used to analyse nanoparticles or very thin (< 2 nm) samples that need to be transparent to the electron beam; it also allows analysis of the crystallinity. Furthermore, some of the main characterization techniques of polymer (porous, microporous and dense), carbon, zeolite and metal membranes are discussed.

© Woodhead Publishing Limited, 2011

3.1.1 Polymer membranes

Polymer membranes were the first membranes to enter into the gas separation market. Usually they are integrally skinned asymmetric membranes with a dense skin layer made from a glassy polymer, while a few are made from rubbery polymers. The structural characterization of polymer membranes includes (Khulbe *et al.*, 2008):

- the chemical nature of the polymer at a molecular level
- the microcrystallinity, which influences the mechanical properties of the membrane and its mass transport performance
- the colloidal level, which accounts for the aggregation of macromolecules, influencing the void/free volume and density and their pore size.

The morphological characterization of polymer membranes is normally performed by SEM, scanning force microscopy (SFM) and atomic force microscopy (AFM). The latter has the advantage of not requiring sample treatment. Even when studying non-conducting surfaces, the sample is not affected by the electron beam as it is in electron microscopes and the samples can be managed in air or under liquid (Khulbe *et al.*, 2008). Furthermore, AFM analyses surface structures with a superior spatial resolution down to the nano-scale; very small differences at the surface, like single atoms that were previously imperceptible, are observed clearly with this technique. Besides giving information on the local surface molecular composition, AFM is also applied to analyse mechanical properties like the nanostructure and chain packing of polymers (Khulbe *et al.*, 2008).

The permeation properties of glassy polymer membranes are directly related to their structural properties, namely to the free volume. The polymer free volume represents the volume not occupied by the electronic clouds of the polymer (Bernardo *et al.*, 2009). These 'pores' of different sizes and topologies may be interconnected forming channels through the membrane, creating its 'microporosity'. The overall free-volume fraction or the size of a free-volume element itself is meaningless or of very little relevance. It is more important to understand how free-volume elements link to each other, creating a pore network with a particular pore size distribution (Budd and McKeown, 2010; Jansen *et al.*, 2009). The free-volume network has a major role in the permeation properties of the membrane.

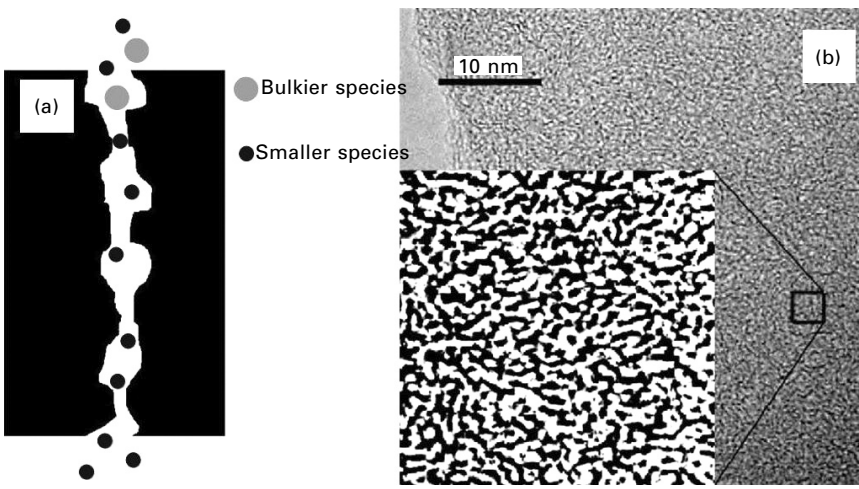
For a long time, this free-volume network was nothing more than a theoretical hypothesis, but with the development of new analytical techniques it was possible to confirm this theory experimentally. The analytical techniques usually employed to determine the average free-volume size and its distribution are positron annihilation lifetime spectroscopy (PALS), inverse gas chromatography (IGC), nuclear magnetic resonance (NMR) and electrochromic, spin and photochromic probe (PCP) methods (Yampolskii and Shantarovich, 2006, Hofmann *et al.*, 2003).

© Woodhead Publishing Limited, 2011

PALS is the most advanced and reliable technique and has been applied widely. This is a non-destructing radioactive technique where the lifetime of an anti-particle of an injected electron into the polymeric material is measured, probing the free volume at the angstrom size-scale. IGC is a dynamic method traditionally used to study polymers above their glass transition temperature, but later on used for glassy polymers, allowing the indirect determination of free-volume average sizes. More detailed information about these techniques can be found elsewhere (Bernardo *et al.*, 2009; Jansen *et al.*, 2009; Yampolskii and Shantarovich, 2006). Besides the experimental approach, molecular dynamic simulations (Jansen *et al.*, 2009) are gaining importance for describing the membrane inner structure.

3.1.2 Carbon molecular sieve membranes

Carbon molecular sieve membranes (CMSM) result from carbonization of polymer precursors under a controlled atmosphere following a specific temperature protocol. During this heat treatment, heteroatoms (essentially oxygen and hydrogen) from the polymeric chains are progressively removed forming a porous and amorphous carbon skeleton, consisting of disordered graphene layers. The pore system derives from the pathways created between adjacent graphene sheets, creating a network of interconnected pores: larger pore sections (cavities) are linked by very narrow pores, called constrictions, responsible for the molecular sieving effect, as illustrated in Fig. 3.1(a) (Song



3.1 Porous structure of a CMSM. (a) Schematic representation of a pore showing the molecular sieving effect. (b) TEM micrographs of poly(furfuryl alcohol) based carbon membranes (reproduced from Song *et al.* (2010) with permission from Elsevier).

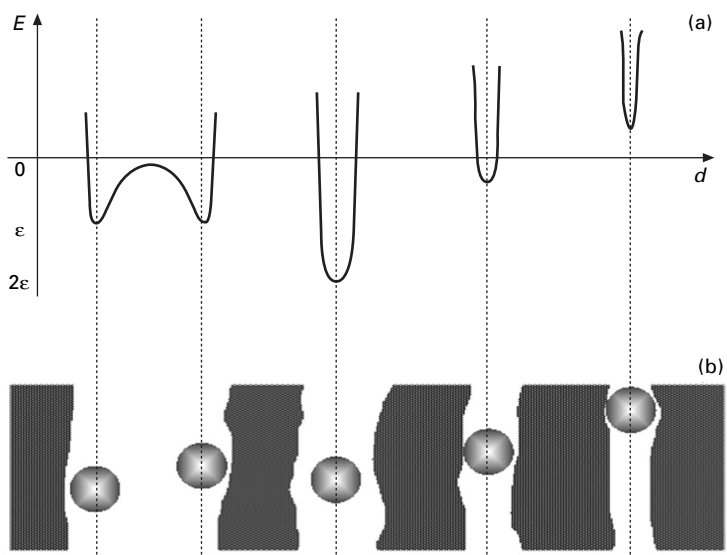
© Woodhead Publishing Limited, 2011

et al., 2010). The constrictions are very important and impose selectivity on the membrane, while the cavities contribute to increase the membrane adsorption capacity, allowing moderate fluxes through the membrane (Lagorsse *et al.*, 2004). A distinct feature of CMSM is that the pore network can be tailored or adjusted by employing different heat treatments, or combining a set of pre- or post-heat treatments (Saufi and Ismail, 2004), tuning the permeation properties of the membrane in order to suit a given application.

Pore network

The pore network of CMSM is the core of these membranes and is responsible for their sieving properties. Molecular sieving takes place when the pore size is close to that of the permeating species (< 0.3–0.5 nm); smaller species are allowed to pass through very narrow constrictions, whereas larger species are retained (Fig. 3.1(a)).

In CMSM, species are confined to the space between two carbon walls and are subjected to a potential energy field as illustrated in Fig. 3.2. If the pores are wide enough, two minimum potentials occur close to each wall. As the pore gets narrower, the two contributions from opposite walls start to become significant, resulting in one minimum. This continues until the potential becomes positive and the pore becomes impermeable to the species.



3.2 Schematic representation of a species/wall interaction within a micropore or constriction. (a) Potential energy, *E*, of a species within pores of different dimensions.(b) Sketch of the species in the respective pores (adapted from Koresh and Soffer (1980)).

© Woodhead Publishing Limited, 2011

However, there is still an intermediate pore size where the species cannot be adsorbed, but with enough energy, they pass constrictions by an activated process. In order to understand the mass transport mechanism of CMSM it is essential to understand their pore structure (Campo *et al.*, 2010b). Relevant analytical techniques are described below.

Topography and integrity

Several techniques are usually used for a preliminary characterization of the CMSM structure. SEM provides a global indication on the membrane's integrity. This technique is very useful for detecting the presence of mesoscopic defects or cracks, assessing the overall homogeneity of the surface and also determining the membrane thickness.

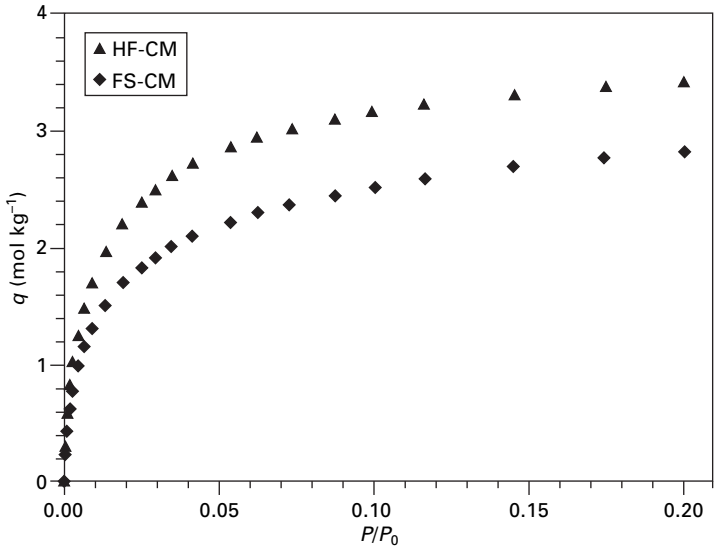
Permeation of probing species

One technique for characterizing the sieving character of the membranes is to perform single component permeation experiments using, for example, SF_6 as a probing species. SF_6 has a molecular size of 0.502 nm (Koresh and Soffer, 1980) (based on liquid molar volume) and should not permeate since constrictions should have a mean pore width close to 0.4 nm if gas separations such as O_2/N_2 are envisioned. This procedure can be performed with gas species of increasing molecular sizes in order to determine the critical pore width of the membrane.

To perform a deeper analysis of the microporosity of CMSM, utilizing the physical adsorption of gases is a very common procedure. The adsorption of N_2 at 77K has been used for a long time as an indirect method of characterizing the microporosity of carbonaceous materials, but with diffusional limitations occurring for pores narrower than 0.7 nm (Cazorla-Amoros *et al.*, 1996). Therefore, the adsorption of CO_2 at 273K appeared to be a good alternative for characterizing carbon molecular sieve materials (membranes or adsorbents); the higher temperature overcomes the diffusional limitations, favouring access into smaller pores. Surface area, micropore volume, pore size distribution and mean pore width can be found from adsorption equilibrium isotherms. A CO_2 adsorption isotherm can be obtained either by volumetric or gravimetric methods (Lozano-Castello *et al.*, 2004).

The adsorption equilibrium isotherm of CO_2 on CMSM at 273K exhibits type I behaviour. The typical plateau of these isotherms corresponds to maximum adsorption capacity, which usually occurs at relative pressures around 0.2, as shown in Fig. 3.3 (Campo *et al.*, 2010a, 2010b); this means that there is a significant volume fraction of narrow micropores (Cazorla-Amoros *et al.*, 1998).

© Woodhead Publishing Limited, 2011



3.3 Adsorption equilibrium values (q) of CO_2 at 273K as a function of CO_2 relative pressure P/P_0 for carbon hollow fibre membranes (HF-CM) and carbon flat sheet membranes (FS-CM) obtained from different cellulosic precursors.

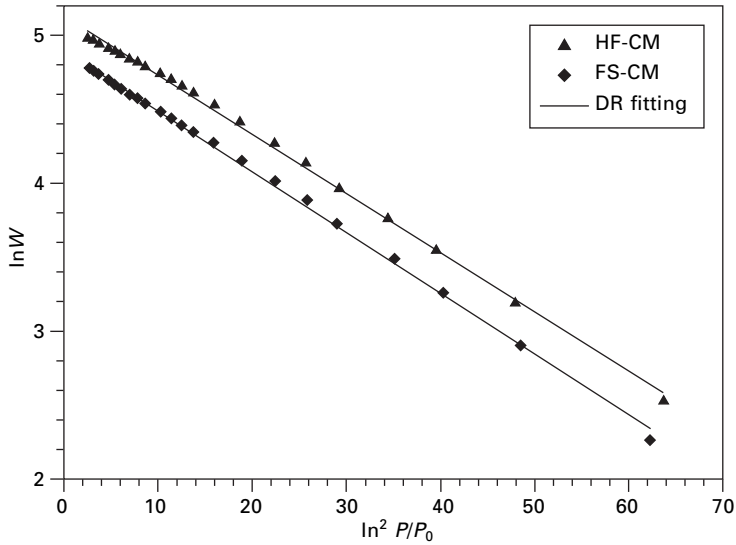
Micropore volume and mean pore width

Despite the eventual existence of mesoporosity to some extent, the adsorption capacity of CMSM is mostly determined by its microporosity. The equation normally used to determine the volume of microporous materials, W_0, is the well known Dubinin–Radushkevich (DR) equation (Hutson and Yang, 1997):

$$W = W_0 \exp\left(-\left(\frac{RT\ln(P_0/P)}{\beta E_0}\right)^2\right) \quad [3.1]$$

where W is the volume filled at temperature T and at a certain relative pressure P/P_0 (P_0 is the saturation pressure), R is the gas constant, β is the affinity coefficient for carbon (considered to be 0.35) and E_0 is the characteristic energy (Stoeckli *et al.*, 2002; Cazorla-Amoros *et al.*, 1996). This equation lacks consistency at very low pressures (does not follow the Henry law) but it provides important information concerning the porosity of these materials in a straightforward way. Plotting the adsorption equilibrium isotherm in logarithmic scale and fitting the DR equation to the experimental data, as exemplified in Fig. 3.4, the intercept of the linear regression represents the micropore volume of the material, W_0. The activation energy, which can

© Woodhead Publishing Limited, 2011



3.4 Characteristic curves of CO_2 at 273K for hollow fibre carbon membranes (HF-CM) and flat sheet carbon membranes (FS-CM); solid lines represent DR fitting.

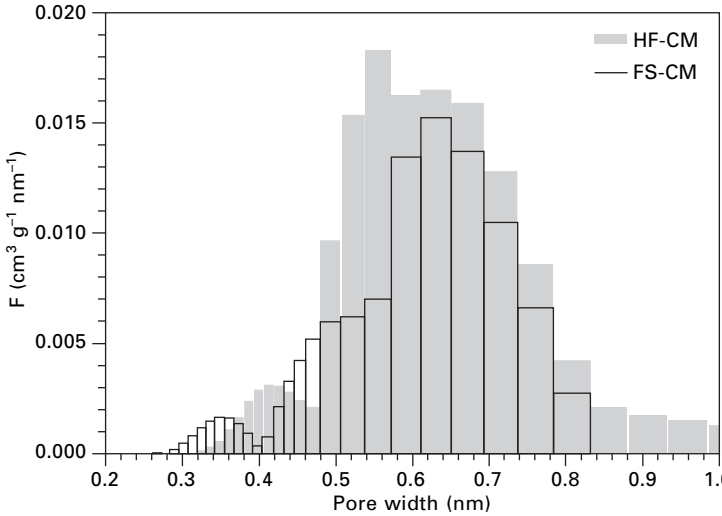
be related to the mean pore width, can be calculated from the slope of the linear fitting.

Micropore size distribution

In contrast to zeolite membranes which have a well defined pore structure, CMSM present a disordered microporous structure. Knowledge of the overall micropore volume is not sufficient to relate the porous structure to mass transport in these membranes. But the micropore size distribution does provide meaningful information, since it qualifies and quantifies a range of pores from the smallest constrictions to the largest cavities. There are powerful molecular simulation algorithms for determining the pore size distribution (PSD) of microporous materials, but these methods are complex and time consuming. In the last decade, however, a structural-based method that can be easily implemented was developed by Do's group (Nguyen and Do, 1999; Nguyen *et al.*, 2003). Similar to the DR analysis, the method by Do uses the adsorption equilibrium data determined for CO_2 at 273K. A typical pore size distribution for CMSM is shown in Fig. 3.5.

A more recent technique that is now being developed to describe the internal morphology of non-regular materials is based on a three-dimensional (3D) reconstruction from microscope photos. The 3D reconstruction can then be used to obtain the pore size distribution and, afterwards, a description

© Woodhead Publishing Limited, 2011



3.5 Pore size distribution obtained from the CO_2 adsorption equilibrium isotherms at 273K. Carbon hollow fibre membranes (HF-CM) in grey filling and carbon flat sheet membranes (FS-CM) in black lines.

of mass transport in micropores, mesopores and macropores (Hamzehpour *et al.*, 2007; Hamzehpour and Sahimi, 2006; Capek *et al.*, 2009).

Surface chemistry

The surface chemistry plays an important role in mass transport (Campo *et al.*, 2010b). These carbon materials are mainly made up of carbon atoms placed as random graphene sheets that exhibit hydrophobic behaviour. However, it is known that these structures present traces of oxygen, usually in the form of hydroxyl, carboxyl, quinone, peroxide or aldehyde functional groups (Brennan *et al.*, 2001; Foley *et al.*, 1997; Harding *et al.*, 1998) therefore conferring hydrophilic character to these materials. This can be crucial if the membranes are used to treat humidified streams. The hydrophilic character of CMSM can be assessed from the adsorption isotherm of water vapour at room temperature. The adsorption of water vapour in carbon materials with oxygen-based functional groups normally follows an S-shaped curve (Do and Do, 2000; Alcaniz-Monge *et al.*, 2002; Nan and Levan, 2005), which corresponds to a type V isotherm. The existence of hysteresis is usually attributed to differences in the mechanism of adsorption and desorption rather than to capillary condensation in the mesopores.

© Woodhead Publishing Limited, 2011

3.2 Zeolite and mixed matrix membranes

3.2.1 Zeolite membranes

Zeolite membranes are hydrated aluminosilicates with a very ordered (crystalline) and regular microporous structure. These micropores are in the molecular size range, conferring a molecular sieving effect to the membranes (Coronas, 2010). Several Al/Si ratios can be combined yielding zeolite membranes that exhibit different chemical interactions with adsorbable species (Mallada and Menéndez, 2008). Thus, zeolite membranes exhibit different adsorption, catalytic and ion exchange properties and for this reason they are attractive to use in several gas and vapour separations. Zeolite membranes are able to separate difficult mixtures and to promote both reaction and separation at the same time (Coronas and Santamaria, 2004); they can withstand harsh chemical and thermal conditions. However, these membranes are brittle and, therefore, they are typically prepared on porous inorganic supports (alumina, titania, stainless steel, etc).

Morphology

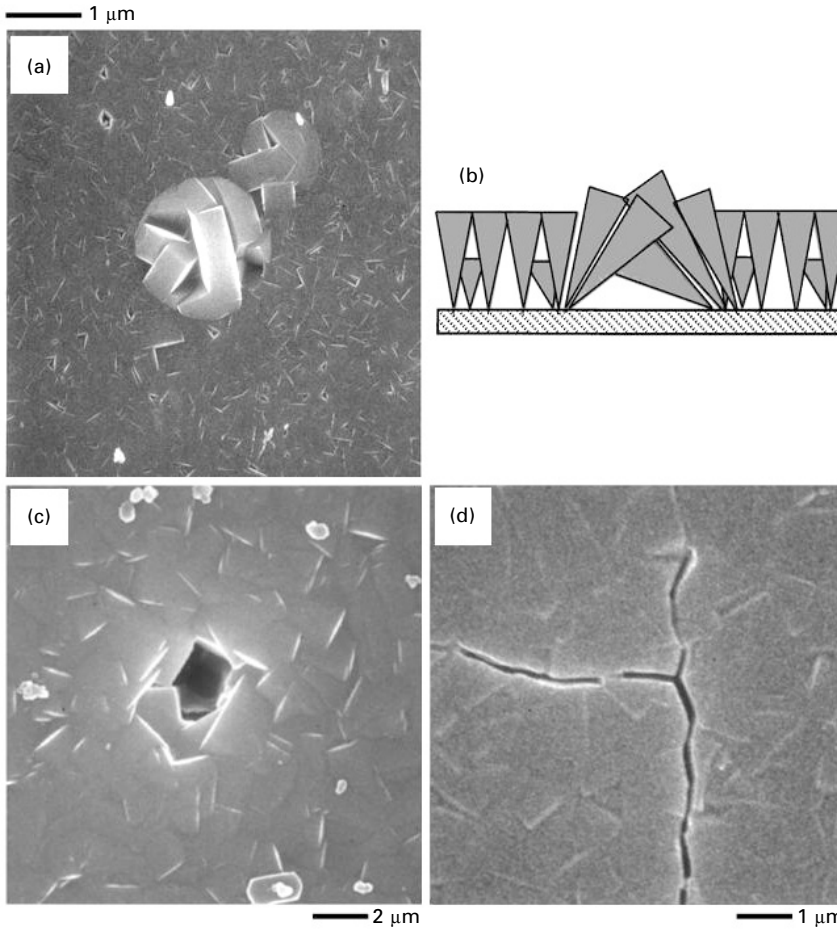
SEM is a very useful technique for assessing the topography of the membrane surface. It analyses the shape and size of the zeolite crystals and their distribution along the surface, detecting the existence of intercrystalline defects, pinholes or cracks (Xomeritakis *et al.*, 1999) as shown in Fig. 3.6. Furthermore, it allows membrane thickness to be obtained (selective layer, support layer, or selective layer plus support layer).

Together with SEM, X-ray photoelectron spectroscopy (XPS) and electron-probe microanalysis (EPMA) provide quantification of the Al/Si ratio and their concentration profile along the membrane thickness. Using AFM, it is possible to obtain surface and cross-section views of the membrane. There are other important analytical techniques such as TEM, which can be used to identify the formation of zeolite-support nanocomposites, and field energy scanning electron microscopy (FESEM) which provides a greater resolution than SEM (Mallada and Menéndez, 2008). XRD is widely employed to analyse the zeotype synthesized during membrane formation and the degree of crystallinity, crystal sizes and interplanar distance. PALS is also employed to study the sizes of the cages and the characteristics of the active sites (Dutta *et al.*, 2005; Nakanishi and Ujihira, 1982).

Pore structure and permeation mechanism

Permeation measurements are the most important experiments for quantifying the separation performance of a membrane for a gas mixture. Single-component permeation experiments with several probe species with different kinetic

© Woodhead Publishing Limited, 2011



3.6 SEM pictures of MFI polycrystalline films showing: (a) typical dome-like defects, (b) model of their formation, (c) pinholes, (d) cracks (reprinted from Xomeritakis *et al.* (1999) with permission from Elsevier).

diameters make it possible to estimate the effective pore size of the membrane (Guan *et al.*, 2001). In zeolite membranes with molecular sieve behaviour, smaller species should penetrate the membrane more easily than bulkier ones which should be retained. Therefore, single-component permeation is an easy way to depict the existence of intercrystalline defects.

Depending on the size of the pores and on the temperature, the mass transport mechanism results from the combination of adsorption and diffusion through the membrane. Adsorption is an exothermic process that should decrease as the temperature increases. On the other hand, the activated diffusion when crossing the constrictions is enhanced by temperature. Thus, determining the

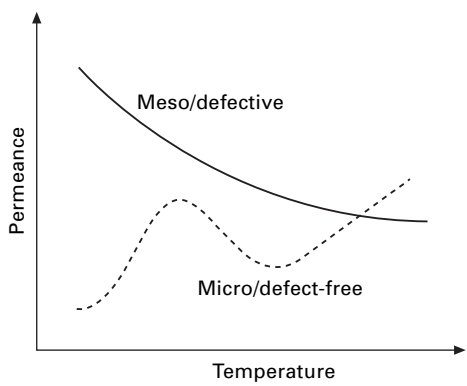
© Woodhead Publishing Limited, 2011

single-component permeance as a function of the temperature, it is possible to investigate the controlling mass transport mechanisms (Piera *et al.*, 1999). As Fig. 3.7 shows, this procedure can be employed to assess defective membranes as well. In a microporous membrane, permeance should increase with temperature since the mass transport is controlled by diffusion in this temperature range. Afterwards, permeance decreases since the adsorption affinity decreases. Finally, permeance increases again for high temperatures, controlled by diffusion. At this stage the adsorption becomes residual.

Adsorption studies (equilibrium and kinetic) using different probe species may also be performed, providing valuable information on the porous structure. This information may be used to simulate the permeation. In addition, using probe species with different sizes, polarities and shapes, the membrane can be characterized in terms of pore size and chemical properties, like the hydrophilic character. In this way, an appropriate choice between different zeolites for a particular application would be possible (Bowen *et al.*, 2004). However, it should be noted that adsorption studies, using either gravimetric or volumetric methods, do not discriminate between effective and dead-end pores.

Permporosimetry

Zeolite membranes present undesirable intercrystalline defects, in addition to selective cages through which permeation takes place. In order to assess and quantify the flux through the defects, permporosimetry is commonly employed (Ernst, 2009). This technique consists of evaluating the flux of a certain non-adsorbing species (usually He or N_2) when a mixture of the non-adsorbing species with a strongly adsorbing one is fed to the membrane. The



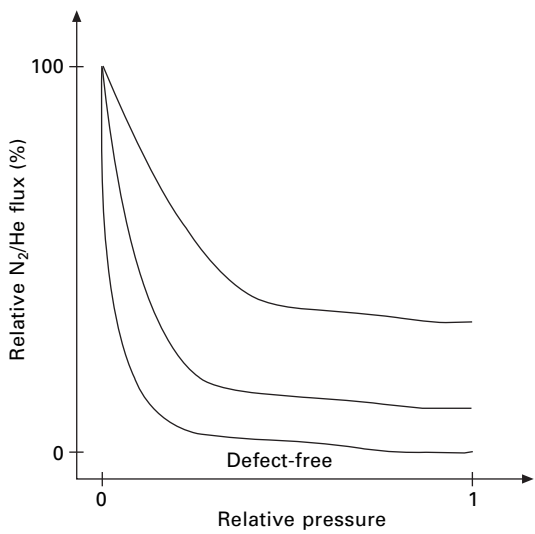
3.7 Schematic representation of generic permeation patterns for microporous defect-free and mesoporous defective zeolite membranes.

© Woodhead Publishing Limited, 2011

selection of the strongly adsorbing species relates to the nature of the zeolite being studied. For instance, n-butane (or benzene) is usually selected for a highly hydrophobic zeolite membrane, rather than water which is commonly selected to characterize highly hydrophilic membranes. The experiment is performed by scanning the flux of the non-adsorbing species for increasing relative pressures of the strongly adsorbing species. The final representation should picture the relative decrease in the flux of the non-adsorbing species as a function of P/P_0 of the adsorbing one, as illustrated in Fig. 3.8.

3.2.2 Palladium and palladium alloy membranes

Palladium-based membranes have attracted enormous interest for use in hydrogen separations and in membrane reactors owing to their high flux and exclusive hydrogen permselectivity. Their production can be achieved in a variety of configurations by several methods (Paglieri and Way, 2002; Uemiya, 1999). Self-supported palladium alloy membranes have been used successfully to obtain high purity hydrogen (Tosti and Bettinali, 2004; Tosti *et al.*, 2000a, 2000b). However these membranes are very thick (> 25 μm). In order to obtain high hydrogen flux and minimize material costs, thin palladium membranes have been supported on various tubular asymmetric substrates, including stainless steel and ceramic materials. The usual methods for depositing palladium include electroless plating (Uemiya *et al.*, 1991), electrodeposition (Nam *et al.*, 2009), chemical vapour deposition (Xomeritakis



3.8 General permporosimetry patterns for assessing membrane defects.

© Woodhead Publishing Limited, 2011

and Lin, 1998) and physical vapour deposition (Peters *et al.*, 2009); of these, the electroless plating technique provides advantages, particularly with respect to the homogeneity of surface coverage, operational flexibility, simple equipment and cost performance (Mallory, 1990, Paglieri and Way, 2002).

Membrane characterization

The physical and chemical characterization of membranes, namely with respect to morphology, thickness, grain size, and types and amounts of surface or grain boundary contamination, is very important. These properties may depend on the fabrication method, or result from testing history, and influence the performance of the membrane. So, the knowledge acquired by such analysis may be used to improve the membrane performance during its production. Some of the most commonly used techniques for analysing palladium films include SEM, AFM, XRD, TEM, EPMA, XPS, energy dispersive X-ray analysis (EDX), Auger-electron spectroscopy (AES) and thermal desorption spectroscopy (TDS) (Paglieri and Way, 2002).

Since gas permeance depends on the thickness of the membrane, this is an important parameter to be characterized. Sometimes, the thickness is calculated from the weight of the support before and after metal deposition considering the density of the metal and the area of deposition; this method is not accurate, especially when thin membranes are produced (Paglieri *et al.*, 1999).

SEM is a direct method for the determination of the thickness; several sections of the membrane should be measured and the error in the measurements reported. Special caution should be taken when a diamond cutter is used in the preparation of samples; owing to the friction between the membrane and the cutter disc, the membrane may suffer deformation and look thicker than it really is.

Energy-dispersive X-ray spectroscopy analysis conducted by means of SEM analysis (SEM-EDX) gives information concerning the distribution and composition of the elements in the membrane. The metal composition of Pd alloy membranes can be also determined by dissolving the membrane in aqua regia or concentrated nitric acid and analysing the metals by atomic absorption spectroscopy (AAS) or inductively coupled plasma optical emission spectroscopy (ICPOES).

XRD gives information about the composition of the membrane, as the lattice constant of Pd alloy membranes varies with alloy composition according to Vegard's law (Denton and Ashcroft, 1991). Therefore, the composition of the alloy can be estimated by the peak position. Thin Pd alloy membranes are prepared by sequential or simultaneous deposition of the metals followed by thermal treatment. Time and temperature needed for complete alloying

© Woodhead Publishing Limited, 2011

can be determined by monitoring the inter-phase diffusion of the two metals by XRD-analysis.

As Pd or Pd alloy membranes are permeable only to hydrogen, the permeation of any other gas indicates the presence of defects. Very large leaks can be detected by bubbles produced when pressurized helium is used. The presence of defects can be evaluated by permeation experiments with nitrogen (Uhlhorn *et al.*, 1992; Mardilovich *et al.*, 1998; Jayaraman and Lin, 1995), helium (Guazzone *et al.*, 2006; Mardilovich *et al.*, 1998; Jayaraman and Lin, 1995) or other non-condensable gases (Mardilovich *et al.*, 1998). Analysis of the defects in terms of pore size can be made by analysing the permeance, Π (ratio between the permeability and the membrane thickness; see Section 3.3.1), as a function of the average pressure across the membrane, P_{av}, according to the Equation [3.2] (Uhlhorn *et al.*, 1992; Mardilovich *et al.*, 1998; Guazzone *et al.*, 2006; Jayaraman and Lin, 1995):

$$\Pi = U + ZP_{av} \qquad [3.2]$$

where U and Z represent the Knudsen and viscous flow constants, respectively. If the permeance is independent of the mean pressure ($Z \approx 0$), the dominant contribution comes from Knudsen diffusion, indicating the presence of mesopores; otherwise, macropores are also present in the membrane. Details of the fundamentals of Equation [3.2], namely the meaning of parameters U and Z, are presented below in Section 3.3.2.

3.2.3 Mixed matrix membranes

For several years, the scientific community tried to improve polymer membrane properties by dispersing inorganic particles into the membrane matrix. This new category of membranes is named mixed matrix membranes (MMM) (Koros and Mahajan, 2000). This approach guarantees a simple manufacturing procedure, characteristic of a pure polymer membrane. Furthermore, hybrid membranes present superior membrane performance: membranes benefit from mass transport properties of the dispersed inorganic fillers overcoming, therefore, the permeability-selectivity trade-off characteristic of the polymer matrix (Perez *et al.*, 2009; Car *et al.*, 2006). MMM are mechanically more resilient, easier to reproduce and provide low cost manufacturing (Cong *et al.*, 2007). Frequently, zeolites were used as fillers to prepare MMM for gas separation. However, researchers then started to develop new families of materials such as (1) organic–inorganic hybrids, known as metal–organic frameworks (MOF) and (2) polymers with intrinsic microporosity (PIM). These new materials have been successfully applied to the preparation of membranes and are discussed below.

© Woodhead Publishing Limited, 2011

Metal-organic framework (MOF) membranes

MOF membranes consist of transition metal ions linked by organic ligands (Car *et al*., 2006). MOFs belong to a very large family of highly selective crystalline nanoporous materials with tailorable topologies and organic functionalities (Li *et al*., 2010). MOFs are chemically combined in many different ways, making it possible to change their pore size and chemical properties. They are of special interest for gas storage and catalysis, gas separation, molecular recognition, and lately, in high temperature fuel cells, owing to their controlled and high porosity, increased affinity towards certain gases and proton exchange ability (Kitagawa *et al*., 2004; Yaghi *et al*., 2003; Li *et al*., 2010; Liu and Smit, 2009). It was then just a short step until MOF were incorporated into polymer membranes. The resulting MMM combine the high sorption properties of MOFs with the good permeabilities and mechanical properties of a polymeric matrix, improving the selectivity of the resulting MMM (Adams *et al*., 2010; Car *et al*., 2006).

However, there are delicate challenges to be overcome when dealing with MOFs. The first challenge concerns the controlled development of MOF nanocrystals (size and shape) (Li *et al*., 2010): the average particle size can be determined by TEM and high resolution TEM (HRTEM) can even provide information about the lattice planes of the visualized nanocrystals (Li *et al*., 2010). X-ray diffraction is useful to infer the crystallinity of the MOF structure (Li *et al*., 2010; Perez *et al*., 2009). The second challenge concerns the MOF membrane as a whole. One of the problems here is the defects or non-selective voids that are created at the interface of the MOF–polymer matrix owing to the low affinity or poor contact between them (Perez *et al*., 2009). This produces an increase in the membrane permeance, but selectivity can be severely compromised; in this case, MOF crystals act simply as fillers owing to a poor wetting by the polymer (Husain and Koros, 2007, 2009). The existence of such voids at the particle interface can be visualized by scanning electron microscopy (Shu *et al*., 2007; Moore and Koros, 2007).

Polymers with intrinsic microporosity (PIM) membranes

Unlike conventional polymers, polymers with intrinsic microporosity have an amorphous nanoporous structure derived from a continuous network of interconnected free volumes (Budd *et al*., 2004, 2005a, 2006; McKeown and Budd, 2006). This microporosity is defined by the shape and rigidity of the molecular chains; the incorporated rings impair the rotation of the bonds in the polymeric backbone, inhibiting conformational changes (Budd *et al*., 2004, 2005a, 2006, McKeown and Budd, 2006). Still, PIM are chemically well defined but with high surface areas, close to those of activated carbons (Budd *et al*., 2004). The development of PIM led to a new generation of membranes,

© Woodhead Publishing Limited, 2011

high free-volume polymer membranes with chemical functionalities (Budd and McKeown, 2010; Budd *et al.*, 2005b).

The most important features of PIM membranes are (Ghanem *et al.*, 2009):

- relatively high permeabilities
- good permselectivities
- large free volume
- low activation energies of permeation
- weak tendency to age.

Furthermore, PIM membranes combine all these previously mentioned features with the great benefit of being solution processable, which is one of the greatest advantages of polymers (McKeown and Budd, 2010; Ghanem *et al.*, 2010; Emmler *et al.*, 2010).

The characterization of the free-volume network, that is, microporosity and pore structure, is usually assessed using:

- gas sorption analysis, namely N_2 adsorption at 77K, in order to determine microporosity and surface areas (McKeown and Budd, 2010; Budd *et al.*, 2005b).
- PALS, which allows, as mentioned before, the determination of the distribution of free-volume elements, confirming their existence in the size range associated with microporosity (McKeown and Budd, 2010; Emmler *et al.*, 2010).
- atomistic computer simulation, like the grand canonical Monte Carlo method (McKeown and Budd, 2010; Heuchel *et al.*, 2008), which can also be used to determine pore size distributions.

For these membranes 3D reconstitution to characterise the inner morphology and molecular simulation analysis based on the 3D reconstitution that allows determination of the mass transport parameters are of special interest.

3.3 Mass transport characterization

To help in developing new membranes and optimize the operation of membrane systems, it is essential to understand and model the mass transport mechanism. This allows mass transport to be described in a wide range of operating conditions, for complex mixtures of gases, based on a few parameters obtained from experimental characterization. To perform this task, the materials to be analysed should be separated in two main groups: dense (non-porous) membranes and porous membranes, depending on the internal 'voidage'. If this empty space allows there to be a continuous gas phase, the membrane is defined as porous. Otherwise it can be described as microporous or dense.

© Woodhead Publishing Limited, 2011

Dense membranes comprise materials like pure metals or alloys and polymeric materials. Polymer membranes, in turn, can be divided in two groups: the glassy ones, which have interconnected microcavities (free-volume) that generate a pore network responsible for the permeability, and the rubbery ones which have 'dynamic porosity', that is, ultramicropores (more correctly, free-volume elements) that are changing continuously (appearing, disappearing, shrinking and expanding) on a similar timescale to the motion of the permeant traversing the membrane (Yampolskii and Shantarovich, 2006; Hofmann *et al.*, 2003); mass transport through these materials is usually described by the sorption–diffusion model. According to this model, the permeant sorbs into the membrane surface at the higher partial pressure side (more rigorously, higher chemical potential), diffuses through the membrane down a gradient of the driving force (concentration of the sorbed species) and, finally, desorbs on the other side (Bernardo *et al.*, 2009; Wijmans and Baker, 1995).

Porous membranes, which comprise a diversity of materials (polymers, ceramics, carbon) are characterized with regard to mass transfer according to a variety of models, from the simplest 'lumped' global mass transfer coefficient (Schlunder *et al.*, 2006; Krishna and van Baten, 2009) to the more complex based on the Maxwell–Stefan equations (van den Broeke *et al.*, 1999; Yang *et al.*, 2005; Li *et al.*, 2007; Krishna and Wesselingh, 1997; Bakker *et al.*, 1996).

3.3.1 Models for dense membranes

Polymer membranes

The simplest model used to describe the mass transport of gas species permeating through a dense membrane assumes that the sorbed permeant diffuses through the membrane according to Fick's first law of diffusion, defined in Equation [3.3] for a pure component (Barrie and Munday, 1983; Shah *et al.*, 2006; Koros *et al.*, 1977):

$$J = -D\frac{\mathrm{d}C}{\mathrm{d}x} \qquad [3.3]$$

where J is the molar flux, D is the diffusivity (constant or dependent on the permeant concentration) and $\mathrm{d}C/\mathrm{d}x$ is the sorbed concentration gradient of the sorbed species across the membrane thickness. Assuming a constant diffusion coefficient, which is usually the case for rubbery membranes when there is no swelling, Equation [3.3] can be integrated, giving:

$$J = \frac{D(C^{\mathrm{h}} - C^{\mathrm{l}})}{\delta} = \frac{D\Delta C}{\delta} \qquad [3.4]$$

© Woodhead Publishing Limited, 2011

where the superscripts h and l refer to the high and low concentration, respectively, and δ is the membrane thickness. If the diffusion is a function of the permeant concentration, more complex models are needed to describe such coupling and the integration of Equation [3.3] may be much more complicated (Bode, 1990; Shah *et al.*, 2006).

Normally, it is assumed that the mass transport kinetics is controlled by the diffusion step; this means that the sorption/desorption process can be considered always to be at equilibrium with the gas phase (retentate and permeate sides). The concentration of the species at the membrane surfaces may then be defined as a function of the respective pressure on the retentate/permeate sides according to a sorption isotherm, which can be described by different models. The simplest model considers a linear relationship between the gas and sorbed phases, Henry's law (Merkel *et al.*, 2000; Jansen *et al.*, 2011; George *et al.*, 1999):

$$C = k_D P \qquad [3.5]$$

where k_D is the Henry's constant (sorption coefficient) and P is the pressure of the species at the corresponding membrane/gas interface. This linear relationship is usually verified for ideal systems, or where the solubility is very low and independent of the concentration, as is the case for some permanent non-interacting gases in rubbery polymers. This being the case, the diffusivity can also be assumed as constant (Mulder, 1996; Jansen *et al.*, 2011). In this way, Equation [3.5] may be substituted into Equation [3.3], giving:

$$J = -Dk_D \frac{dP}{dx} = -L\frac{dP}{dx} = L\frac{P^h - P^l}{\delta} = \frac{L}{\delta}\Delta P \qquad [3.6]$$

where L is the permeability coefficient and P^h and P^l are the pressures at the retentate (higher partial pressure) and permeate (lower partial pressure) sides, respectively. Sometimes, the membrane thickness is unknown. In these cases, a new parameter, the permeance, can be defined: $\Pi = L/\delta$.

For some simple gases up to moderate pressures (20–30 bar) or organic vapours in glassy polymers, the sorption isotherm is non-linear, usually with a negative deviation from Henry's law behaviour, described by dual sorption theory (Paul and Koros, 1976; Koros *et al.*, 1977; Vieth *et al.*, 1976; Duthie *et al.*, 2007). This model assumes that the global sorption capacity is the result of two different sorption mechanisms occurring simultaneously, one according to Henry's law and the other of the Langmuir type:

$$C = k_D P + \frac{C'_H b P}{1 + bP} \qquad [3.7]$$

where C'_H is the maximum void sorption concentration and b is an affinity constant. Considering constant diffusivity as well, a global permeability

© Woodhead Publishing Limited, 2011

coefficient can also be defined, although it is no longer constant. Alternatively, multilayer adsorption may be considered in some glassy polymers, characterized by the BET (Brunauer, Emmett, Teller) adsorption isotherm (Rutherford, 2001a).

The sorption isotherm of organic vapours and gases in rubbery membranes is also usually non-linear, but with a positive deviation from Henry's behaviour, which has been assigned to the swelling of the membrane. In these cases, both the sorption and the diffusivity are strongly dependent on the penetrant concentration, both increasing with the concentration. In these cases, more complex models are needed to describe the permeation mechanism (Deng and Hägg, 2010; George *et al.*, 1999; Shah *et al.*, 2006).

Metal membranes

In the case of metal membranes (e.g. Pd and Pd-alloys) the sorption isotherm is usually described by the Sieverts' law (these membranes are selective only for H_2):

$$C_{H_2} = k_{H_2}(P_{H_2})^{0.5} \qquad [3.8]$$

where k_{H_2} is the Sieverts constant. In this case, the flux is described by the following equation:

$$J_{H_2} = L_{H_2}\frac{(P^{h}_{H_2})^{0.5} - (P^{l}_{H_2})^{0.5}}{\delta} \qquad [3.9]$$

known as Richardson's equation. However, this relationship holds only for specific operating and system conditions. In general, the flux of hydrogen can be influenced by factors such as temperature, partial pressure difference, membrane diffusivity, membrane thickness, existence of a support, existence of pinholes and cracks, grain size, surface or grain boundary contamination, concentration polarization at the surface, and adsorption/desorption (surface processes) kinetics. In most of the reported studies, the influence of these factors is accounted for by considering a parameter n in Equation [3.9] instead of exponent '0.5'. This parameter is obtained from the fitting of this equation to the experimental data (Gielens *et al.*, 2004, 2007; Tong *et al.*, 2004; Wilhite *et al.*, 2004; Jayaraman and Lin, 1995; Morreale *et al.*, 2003; Paglieri and Way, 2002; Guazzone *et al.*, 2006; Mardilovich *et al.*, 1998; Zhang *et al.*, 2006; Keurentjes *et al.*, 2004; Mejdell *et al.*, 2008). Usually, n takes a value between 0.5 and 1, but still higher values have been reported (Gielens *et al.*, 2004, 2007; Keurentjes *et al.*, 2004). Alternatively, some authors have reported more complex models to describe the permeation (Ward and Dao, 1999, McLeod *et al.*, 2009a, 2009b; Caravella *et al.*, 2010).

© Woodhead Publishing Limited, 2011

Determination of the sorption and diffusion parameters

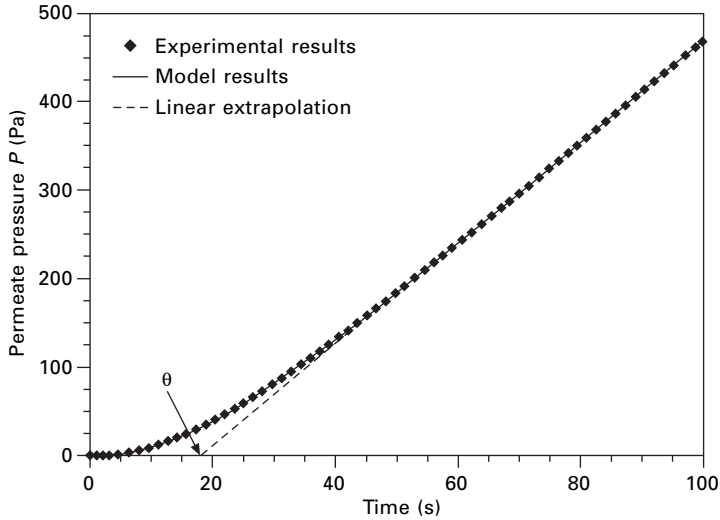
A direct method of determining the sorption parameters needed to describe mass transport is to perform sorption equilibrium measurements. A sample of material is brought into contact with a pure gas at a given known pressure and the amount of sorbed gas is obtained from the difference between the final and initial pressure values (volumetric method) (Koros *et al.*, 1977; Yu *et al.*, 2006; Zhou *et al.*, 2007) or simply using a high precision balance (gravimetric method) (Jansen *et al.*, 2011; Vopicka *et al.*, 2009; Giacinti Baschetti *et al.*, 2009; Yu *et al.*, 2006; Duthie *et al.*, 2007). The equilibrium isotherm is obtained by increasing stepwise the pressure of the contacting gas. Considering a suitable transport model in transient state, the diffusion coefficient can also be determined (Giacinti Baschetti *et al.*, 2009; Vopicka *et al.*, 2009; Krykin *et al.*, 1999).

Another way to calculate the sorption and diffusion parameters is from permeation experiments (Vopicka *et al.*, 2009; Yeom *et al.*, 1999). Experimental methods for gas permeation can be divided into the integral permeation method (Yasuda and Rosengren, 1970; Felder, 1978; Illing *et al.*, 2005; Liu *et al.*, 2001; Wang *et al.*, 2007; Xu *et al.*, 2002), in which the permeation pressure history is measured, and the differential permeation method (Yasuda and Rosengren, 1970; Felder, 1978; Burggraaf *et al.*, 1998; Kong *et al.*, 2006; Hasbullah *et al.*, 2011; Friess *et al.*, 2004), in which the measured variable is the steady state permeation rate through the membrane. Integral methods use unsteady state mass transport models, while differential methods use steady state mass transport models. The most commonly used method for determining mono-component permeabilities is the so-called time lag, which is an integral method (Shah *et al.*, 2006; Wang, 2005; Ye *et al.*, 2006; Ash, 1996, 2001, 2004; Rutherford and Do, 1997, 1999; Perry *et al.*, 1989; Lape *et al.*, 2004; Nuxoll *et al.*, 2005; DeRocher *et al.*, 2005; Kruczek *et al.*, 2005; Rutherford, 2001b; Taveira *et al.*, 2003). The time lag considers a step perturbation in the high pressure chamber of a two-chamber permeation cell (initially evacuated) separated by the membrane. The total pressure on the low pressure chamber is measured with time. A typical time-lag response is represented in Fig. 3.9. The time lag, θ, is defined by the interception of the extrapolated steady state linear region to the time axis.

For membranes where the sorption and diffusion coefficients are constant, the transient mass balance equation used with the time-lag method has an analytical solution. The diffusion coefficient is determined from the value of θ and the permeability from the slope of the steady state linear region. The sorption coefficient is subsequently calculated from the relation $Dk_D = L$ (Illing *et al.*, 2005; Liu *et al.*, 2001; Wang *et al.*, 2007; Xu *et al.*, 2002).

For cases where the sorption and/or diffusion coefficients are not constant, or the membrane is not homogeneous, mass transport model parameters can be calculated directly from the model equations in case they have analytical

© Woodhead Publishing Limited, 2011



3.9 Representation of the permeate pressure against time in an integral permeation experiment (see text for details of the results).

solution (Ye *et al.*, 2006; Paul and Koros, 1976; Rutherford, 2001b; Ash, 2001, 2004; Wang, 2005; Kruczek *et al.*, 2005) or through global fitting of the model to the experimental data (Jansen *et al.*, 2011; Ye *et al.*, 2006; Shah *et al.*, 2006; Sousa *et al.*, unpublished).

An example of a time-lag experiment where a step perturbation with hydrogen was performed in a poly(dimethylsiloxane) (PDMS) membrane with nanoclusters of palladium catalyst built-in is presented in Fig. 3.9. This figure shows also the respective global fitting curve. The unsteady state mass transport model for this case is (Sousa *et al.*, unpublished):

$$(1-\phi)\frac{\partial C^{\mathrm{P}}}{\partial t} + \phi\frac{\partial C^{\mathrm{C}}}{\partial t} = \frac{(1-\phi)D}{\tau}\frac{\partial^2 C^{\mathrm{P}}}{\partial x^2} \qquad [3.10]$$

where C^{P} and C^{C} are the concentrations of the species in the polymer and metallic phases, respectively, D is the diffusion coefficient of the pure polymer (obtained in previous experiments with a pure PDMS membrane), τ is a tortuosity factor that takes into account the influence on the diffusivity of the solid barrier created by the nanoclusters and ϕ is the volume fraction of catalyst, which is calculated from the mass fraction, density of the clusters and density of the polymer. This model assumes constant diffusion of the permeant in the polymeric phase and accumulation in both the polymer phase and metal clusters. It is also assumed that Henry's law is obeyed in the interface gas/membrane and then $C^{\mathrm{P}} = k_{\mathrm{D}}P$, where P is the pressure of a hypothetical gas phase in equilibrium with C^{P}, and k_{D} is the Henry's sorption coefficient for the pure polymer (also obtained in previous experiments with a pure PDMS

© Woodhead Publishing Limited, 2011

membrane), as described above. The relation between C^C and C^P, which are assumed to be in equilibrium, is described by the phenomenological equation $C^C = k_C\rho_C(C^P)^n = k_C\rho_C(k_D P)^n$, where ρ_C is the density of the clusters, k_C is a partition coefficient between the polymeric phase and the metallic clusters and n is the parameter described above in Section 3.3.1.

Equation [3.10] can thus be rewritten as:

$$\frac{\partial P}{\partial t} = \frac{1}{1 + \phi(\rho_C k_C n(k_D P)^{n-1} - 1)} \frac{D(1-\phi)}{\tau} \frac{\partial^2 P}{\partial x^2} \qquad [3.11]$$

subjected to the initial and boundary conditions:

$$t < 0\ (\forall\ x),\ P = 0; \quad t \geq 0\ (x = 0),\ P = P^h;$$
$$t \geq 0\ (x = \delta),\ P = P_l\ (t) \qquad [3.12]$$

where P^h and P^l are the pressures in the high and low pressure chambers, respectively. P^h is constant, while P^l is calculated from the following mass balance equation in the permeate chamber:

$$\frac{V}{RT}\frac{\partial P^l}{\partial t} = -\frac{(1-\phi)ADk_D}{\tau}\left.\frac{\partial P}{\partial x}\right|_{x=\delta} \qquad [3.13]$$

where V is the volume of the permeate chamber and A is the membrane surface area.

This model has three parameters, k_C, τ and n, whose values were obtained from a global fitting of the model to the experimental data. For the present example, $\tau = 1.44$, $n = 1.5$ and $k_C = 3195$ (mol kg_{Pd}^{-1}) · (mol m_{Pol}^{-3})$^{-1}$.

Whenever a total pressure difference between feed and permeate sides is not recommended, the differential method should be used. This method should also be used for multicomponent experiments. In this case, the composition is determined using a gas analyser (Mendes *et al.*, 2010; Xomeritakis and Lin, 1997).

3.3.2 Models for porous membranes

The transport of a gas through porous membranes results from different mass transport mechanisms, which may be grouped into a diffusive component (activated, surface, Knudsen and bulk) and in a viscous component (Poiseille flow) (de Lange *et al.*, 1995; Rao and Sircar, 1996; Krishna and Wesselingh, 1997; Schlunder *et al.*, 2006; Burggraaf, 1999; Tuchlenski *et al.*, 1998). Some of these mechanisms can coexist simultaneously or not, depending on the operating conditions. For example, Knudsen diffusion is the controlling mechanism whenever the mean free path of the travelling species (λ) is much higher than the pore radius (r). For pore radius between 1 nm and 50 nm, Knudsen diffusion is normally the predominant mass transfer mechanism

© Woodhead Publishing Limited, 2011

(Jansen *et al.*, 2011; de Lange *et al.*, 1995; Rao and Sircar, 1996; Hinds *et al.*, 2004; Gilron and Soffer, 2002). However, some care should be taken in determining the parameters from experimental data in the Knudsen region when weak adsorption is present (Bhatia and Nicholson, 2011).

The Knudsen flux is described by the following equation (Uchytil *et al.*, 2000; Veldsink *et al.*, 1994; Tuchlenski *et al.*, 1998; Keizer *et al.*, 1988; Thomas *et al.*, 2001):

$$J^{\mathrm{Kn}} = -\frac{4k_0}{3RT}\sqrt{\frac{8RT}{\pi M}}\frac{\mathrm{d}P}{\mathrm{d}x} \qquad [3.14]$$

where M is the molar mass of the gas and k_0 is the Knudsen coefficient related to the porous matrix, according to Equation [3.15] (Veldsink *et al.*, 1994; Uchytil *et al.*, 2000; Thomas *et al.*, 2001):

$$k_0 = \frac{\varepsilon}{\tau}\frac{r_{\mathrm{p}}}{2} \qquad [3.15]$$

where ε, τ and r_{p} are the porosity, tortuosity and pore radius of the porous matrix.

Another important mechanism present in the mass transfer is the viscous flow, which is described by the Poiseuille equation. This mechanism is present whenever there is a transmembrane total pressure gradient, especially in the case of macroporous membranes (Uchytil *et al.*, 2000; Veldsink *et al.*, 1994; Keizer *et al.*, 1988; Thomas *et al.*, 2001):

$$J^{\mathrm{Vs}} = -\frac{1}{RT}\frac{B_0}{\mu}P\frac{\mathrm{d}P}{\mathrm{d}x} \qquad [3.16]$$

where μ is the viscosity of the gas and B_0 is the viscous flow parameter related to the porous matrix structure, according to Equation [3.17] (Veldsink *et al.*, 1994; Uchytil *et al.*, 2000; Thomas *et al.*, 2001):

$$B_0 = \frac{\varepsilon}{\tau}\frac{r_{\mathrm{p}}^2}{8} \qquad [3.17]$$

Surface diffusion is relevant when micropores are present and for species that adsorb significantly (de Lange *et al.*, 1995; Tuchlenski *et al.*, 1998; De Vos and Verweij, 1998). For example, it plays a relevant role in mass transport in zeolite membranes that show strong adsorption properties, in particular for hydrocarbons (Abdel-Jawad *et al.*, 2009). When this mechanism is the only one considered for the mass transfer, a sorption–diffusion model is usually employed, with the flux described by the following equation (de Lange *et al.*, 1995; Tuchlenski *et al.*, 1998):

$$J^{\mathrm{SD}} = -\frac{1-\varepsilon}{\tau}\rho_{\mathrm{s}}D^{\mathrm{S}}\frac{\mathrm{d}q}{\mathrm{d}x} \qquad [3.18]$$

© Woodhead Publishing Limited, 2011

where ρ_s is the solid density, D^S is the surface diffusion coefficient and dq/dx is the surface concentration gradient.

The simplest model frequently used to describe mass transport through porous membranes considers a 'lumped' global mass transfer coefficient, called the global permeability or global permeance, as described by Equation [3.19] (Schlunder *et al.*, 2006):

$$J = \frac{L}{\delta}(P^h - P^l) \quad \text{or} \quad J = \Pi(P^h - P^l) \qquad [3.19]$$

However, the permeability or the permeance parameter does not have the same meaning as in the case of dense membranes, where it represents the product of the sorption and diffusion coefficients (Equation [3.6]). In this case, it means simply a 'lumped' mass transfer coefficient for the respective component, without any relation to the membrane characteristics.

Characterization of the porous matrix structure, considering pores that are roughly of the same size, may be performed from permeation experiments with single non-condensable gases (to avoid the surface diffusion contribution). In this case, we may assume that the total flux results from the contribution of the Knudsen diffusion and viscous flow. Considering Equations [3.14] and [3.16] in the integral form, and assuming steady-state conditions (constant flux) we may write (Uchytil *et al.*, 2000; Veldsink *et al.*, 1994):

$$J^{tot} = J^{Kn} + J^{Vs} = \frac{1}{RT}\left(\frac{4k_0}{3}\sqrt{\frac{8RT}{\pi M}} + \frac{B_0}{\mu}\frac{(P^h + P^l)}{2}\right)\frac{P^h - P^l}{\delta} \qquad [3.20]$$

This equation can be rearranged in the following form:

$$\frac{J^{tot}}{P^h - P^l} \equiv \frac{J^{tot}}{\Delta P} = \frac{4k_0}{3\delta RT}\sqrt{\frac{8RT}{\pi M}} + \frac{B_0}{\mu\delta RT}\frac{(P^h + P^l)}{2}$$
$$= U + Z\frac{(P^h + P^l)}{2} \equiv U + ZP_{av} \qquad [3.21]$$

Representing $J^{tot}/\Delta P$ (which is the permeance, Π) as a function of P_{av}, a linear relationship should be obtained. The slope and the intercept allow the determination of the structural parameters k_0 and B_0, providing the thickness is known. The ε/τ and pore radius of the porous matrix can be calculated from Equations [3.15] and [3.17], respectively. We should call the reader's attention to Equation [3.20] which was obtained from integration of Equations [3.14] and [3.16] assuming a constant permeating area (flat membrane). However, for different geometries, slightly different equations are obtained (Thomas *et al.,* 2001; Tuchlenski *et al.*, 1998).

© Woodhead Publishing Limited, 2011

3.4 Conclusions

Commonly used characterization techniques for surface and inner morphologies, surface chemistry and transport/separation parameters for different classes of membranes, namely polymer (porous, microporous and dense), zeolite, carbon molecular sieve and metal, were presented and discussed. Single component mass transport models usually employed to describe the permeating transport were also presented. These models are used to obtain the transport parameters as well as to understand the phenomena better.

3.5 References

Abdel-Jawad, M. M., Macrossan, M. N. and Da Costa, J. C. D. (2009). 'Modelling gas purification systems employing molecular sieve silica membranes'. *Separation and Purification Technology*, **66**, 559–64.

Adams, R., Carson, C., Ward, J., Tannenbaum, R. and Koros, W. (2010). 'Metal organic framework mixed matrix membranes for gas separations'. *Microporous and Mesoporous Materials*, **131**, 13–20.

Alcaniz-Monge, J., Linares-Solano, A. and Rand, B. (2002). 'Mechanism of adsorption of water in carbon micropores as revealed by a study of activated carbon fibers'. *Journal of Physical Chemistry B*, **106**, 3209–16.

Ash, R. (1996). 'Transient-state transport in some finite systems. 3. Some historical and hitherto largely-unexplored aspects of time-lag theory'. *Journal of Membrane Science*, **117**, 79–108.

Ash, R. (2001). 'A note on permeation with boundary-layer resistance'. *Journal of Membrane Science*, **186**, 63–9.

Ash, R. (2004). 'Transport with time-dependent boundary conditions in a nu-dimensional membrane'. *Journal of Membrane Science*, **232**, 9–18.

Bakker, W. J. W., Kapteijn, F., Poppe, J. and Moulijn, J. A. (1996). 'Permeation characteristics of a metal-supported silicalite-1 zeolite membrane'. *Journal of Membrane Science*, **117**, 57–78.

Barrie, J. A. and Munday, K. (1983). 'Gas-transport in heterogeneous polymer blends. 1. Polydimethylsiloxane-g-polystyrene and polydimethylsiloxane-b-polystyrene'. *Journal of Membrane Science*, **13**, 175–95.

Bernardo, P., Drioli, E. and Golemme, G. (2009). 'Membrane gas separation: A review/state of the art'. *Industrial and Engineering Chemistry Research*, **48**, 4638–63.

Bhatia, S. K. and Nicholson, D. (2011). 'Some pitfalls in the use of the Knudsen equation in modelling diffusion in nanoporous materials'. *Chemical Engineering Science*, **66**, 284–93.

Bode, E. (1990). 'A simple method to derive activity profiles and diffusivities of permeants in a membrane from steady-state permeation measurements'. *Journal of Membrane Science*, **50**, 1–17.

Bowen, T. C., Noble, R. D. and Falconer, J. L. (2004). 'Fundamentals and applications of pervaporation through zeolite membranes'. *Journal of Membrane Science*, **245**, 1–33.

Brennan, J. K., Bandosz, T. J., Thomson, K. T. and Gubbins, K. E. (2001). 'Water in porous carbons'. *Colloids and Surfaces A, Physicochemical and Engineering Aspects*, **187**, 539–68.

© Woodhead Publishing Limited, 2011

Budd, P. M. and McKeown, N. B. (2010). 'Highly permeable polymers for gas separation membranes'. *Polymer Chemistry*, **1**, 63–8.

Budd, P. M., Ghanem, B. S., Makhseed, S., McKeown, N. B., Msayib, K. J. and Tattershall, C. E. (2004). 'Polymers of intrinsic microporosity (PIMs): robust, solution-processable, organic nanoporous materials'. *Chemical Communications*, **2**, 230–1.

Budd, P. M., McKeown, N. B. and Fritsch, D. (2005a). 'Free volume and intrinsic microporosity in polymers'. *Journal of Materials Chemistry*, **15**, 1977–86.

Budd, P. M., Msayib, K. J., Tattershall, C. E., Ghanem, B. S., Reynolds, K. J., McKeown, N. B. and Fritsch, D. (2005b). 'Gas separation membranes from polymers of intrinsic microporosity'. *Journal of Membrane Science*, **251**, 263–9.

Budd, P. M., McKeown, N. B. and Fritsch, D. (2006). 'Polymers of intrinsic microporosity (PIMs): High free volume polymers for membrane applications'. *Macromolecular Symposia*, **245**, 403–5.

Burggraaf, A. J. (1999). 'Single gas permeation of thin zeolite (MFI) membranes: theory and analysis of experimental observations'. *Journal of Membrane Science*, **155**, 45–65.

Burggraaf, A. J., Vroon, Z. A. E. P., Keizer, K. and Verweij, H. (1998). 'Permeation of single gases in thin zeolite MFI membranes'. *Journal of Membrane Science*, **144**, 77–86.

Campo, M. C., Magalhaes, F. D. and Mendes, A. (2010a). 'Carbon molecular sieve membranes from cellophane paper'. *Journal of Membrane Science*, **350**, 180–8.

Campo, M. C., Magalhaes, F. D. and Mendes, A. (2010b). 'Comparative study between a CMS membrane and a CMS adsorbent: Part I Morphology, adsorption equilibrium and kinetics'. *Journal of Membrance Science*, **346**, 15–25.

Capek, P., Hejtmanek, V., Brabec, L., Zikanova, A. and Kocirik, M. (2009). 'Stochastic reconstruction of particulate media using simulated annealing: improving pore connectivity'. *Transport in Porous Media*, **76**, 179–98.

Car, A., Stropnik, C. and Peinemann, K. V. (2006). Hybrid membrane materials with different metal–organic frameworks (MOFs) for gas separation. *Desalination*, **200**, 424–6.

Caravella, A., Scura, F., Barbieri, G. and Drioli, E. (2010). 'Sieverts law empirical exponent for Pd-based membranes: critical analysis in pure H_2 permeation'. *Journal of Physical Chemistry B*, **114**, 6033–47.

Cazorla-Amoros, D., Alcaniz-Monge, J. and Linares-Solano, A. (1996). 'Characterization of activated carbon fibers by CO_2 adsorption'. *Langmuir*, **12**, 2820–4.

Cazorla-Amoros, D., Alcaniz-Monge, J., De La Casa-Lillo, M. A. and Linares-Solano, A. (1998). 'CO_2 as an adsorptive to characterize carbon molecular sieves and activated carbons'. *Langmuir*, **14**, 4589–96.

Cong, H. L., Radosz, M., Towler, B. F. and Shen, Y. Q. (2007). 'Polymer-inorganic nanocomposite membranes for gas separation'. *Separation and Purification Technology*, **55**, 281–91.

Coronas, J. (2010). 'Present and future synthesis challenges for zeolites'. *Chemical Engineering Journal*, **156**, 236–42.

Coronas, J. and Santamaria, J. (2004). 'State-of-the-art in zeolite membrane reactors'. *Topics in Catalysis*, **29**, 29–44.

De Lange, R. S. A., Keizer, K. and Burggraaf, A. J. (1995). 'Analysis and theory of gas transport in microporous sol–gel derived ceramic membranes'. *Journal of Membrane Science*, **104**, 81–100.

De Vos, R. M. and Verweij, H. (1998). 'Improved performance of silica membranes for gas separation'. *Journal of Membrane Science*, **143**, 37–51.

© Woodhead Publishing Limited, 2011

Deng, L. and Hägg, M.-B. (2010). 'Swelling behavior and gas permeation performance of PVAm/PVA blend FSC membrane'. *Journal of Membrane Science*, **363**, 295–301.

Denton, A. R. and Ashcroft, N. W. (1991). 'Vegard Law'. *Physical Review A*, **43**, 3161–4.

DeRocher, J. P., Gettelfinger, B. T., Wang, J. S., Nuxoll, E. E. and Cussler, E. L. (2005). 'Barrier membranes with different sizes of aligned flakes'. *Journal of Membrane Science*, **254**, 21–30.

Do, D. D. and Do, H. D. (2000). 'A model for water adsorption in activated carbon'. *Carbon*, **38**, 767–73.

Duthie, X., Kentish, S., Powell, C., Nagai, K., Qiao, G. and Stevens, G. (2007). 'Operating temperature effects on the plasticization of polyimide gas separation membranes'. *Journal of Membrane Science*, **294**, 40–9.

Dutta, D., Chatterjee, S., Ganguly, B. N. and Pillai, K. T. (2005). 'Structural aspects of synthetic zeolite: A comparative assay through positron annihilation and gas adsorption methods'. *Journal of Applied Physics*, **98**, 033509.

Emmler, T., Heinrich, K., Fritsch, D., Budd, P. M., Chaukura, N., Ehlers, D., Ratzke, K. and Faupel, F. (2010). 'Free volume investigation of polymers of intrinsic microporosity (PIMs): PIM-1 and PIM1 copolymers incorporating ethanoanthracene units'. *Macromolecules*, **43**, 6075–84.

Ernst, S. (ed.) (2009). *Advances in Nanoporous Materials*, Elsevier, Oxford, UK.

Felder, R. M. (1978). 'Estimation of gas transport coefficients from differential permeation, integral permeation, and sorption rate data'. *Journal of Membrane Science*, **3**, 15–27.

Foley, N. J., Thomas, K. M., Forshaw, P. L., Stanton, D. and Norman, P. R. (1997). 'Kinetics of water vapor adsorption on activated carbon'. *Langmuir*, **13**, 2083–9.

Friess, K., Sípek, M., Hynek, V., Sysel, P., Bohatá, K. and Izák, P. (2004). 'Comparison of permeability coefficients of organic vapors through non-porous polymer membranes by two different experimental techniques'. *Journal of Membrane Science*, **240**, 179–85.

George, S. C., Knörgen, M. and Thomas, S. (1999). 'Effect of nature and extent of crosslinking on swelling and mechanical behavior of styrene-butadiene rubber membranes'. *Journal of Membrane Science*, **163**, 1–17.

Ghanem, B. S., McKeown, N. B., Budd, P. M., Al-Harbi, N. M., Fritsch, D., Heinrich, K., Starannikova, L., Tokarev, A. and Yampolskii, Y. (2009). 'Synthesis, characterization, and gas permeation properties of a novel group of polymers with intrinsic microporosity: PIM-polyimides'. *Macromolecules*, **42**, 7881–8.

Ghanem, B. S., Hashem, M., Harris, K. D. M., Msayib, K. J., Xu, M. C., Budd, P. M., Chaukura, N., Book, D., Tedds, S., Walton, A. and McKeown, N. B. (2010). 'Triptycene-based polymers of intrinsic microporosity: Organic materials that can be tailored for gas adsorption'. *Macromolecules*, **43**, 5287–94.

Giacinti Baschetti, M., Doghieri, F., Freeman, B. and Sarti, G. C. (2009). 'Transient and steady-state effective diffusivity in high free volume glassy polymers'. *Journal of Membrane Science*, **344**, 144–54.

Gielens, F. C., Tong, H. D., Van Rijn, C. J. M., Vorstman, M. A. G. and Keurentjes, J. T. F. (2004). Microsystem technology for high-flux hydrogen separation membranes. *Journal of Membrane Science*, **243**, 203–13.

Gielens, F. C., Tong, H. D., Vorstman, M. A. G. and Keurentjes, J. T. F. (2007). 'Measurement and modeling of hydrogen transport through high-flux Pd membranes'. *Journal of Membrane Science*, **289**, 15–25.

© Woodhead Publishing Limited, 2011

Gilron, J. and Soffer, A. (2002). 'Knudsen diffusion in microporous carbon membranes with molecular sieving character'. *Journal of Membrane Science*, **209**, 339–52.

Guan, G. Q., Kusakabe, K. and Morooka, S. (2001). 'Synthesis and permeation properties of ion-exchanged ETS-4 tubular membranes'. *Microporous and Mesoporous Materials*, **50**, 109–20.

Guazzone, F., Engwall, E. E. and Ma, Y. H. (2006). 'Effects of surface activity, defects and mass transfer on hydrogen permeance and n-value in composite palladium-porous stainless steel membranes'. *Catalysis Today*, **118**, 24–31.

Hamzehpour, H. and Sahimi, M. (2006). 'Development of optimal models of porous media by combining static and dynamic data: The porosity distribution'. *Physical Review E*, **74**, 026308.

Hamzehpour, H., Rasaei, M. R. and Sahimi, M. (2007). 'Development of optimal models of porous media by combining static and dynamic data: The permeability and porosity distributions'. *Physical Review E*, **75**, 056311.

Harding, A. W., Foley, N. J., Norman, P. R., Francis, D. C. and Thomas, K. M. (1998). 'Diffusion barriers in the kinetics of water vapor adsorption/desorption on activated carbons'. *Langmuir*, **14**, 3858–64.

Hasbullah, H., Kumbharkar, S., Ismail, A. F. and Li, K. (2011). 'Preparation of polyaniline asymmetric hollow fiber membranes and investigation towards gas separation performance'. *Journal of Membrane Science*, **366**, 116–24.

Heuchel, M., Fritsch, D., Budd, P. M., McKeown, N. B. and Hofmann, D. (2008). 'Atomistic packing model and free volume distribution of a polymer with intrinsic microporosity (PIM-1)'. *Journal of Membrane Science*, **318**, 84–99.

Hinds, B. J., Chopra, N., Rantell, T., Andrews, R., Gavalas, V. and Bachas, L. G. (2004). 'Aligned multiwalled carbon nanotube membranes'. *Science*, **303**, 62–5.

Hofmann, D., Entrialgo-Castano, M., Lerbret, A., Heuchel, M. and Yampolskii, Y. (2003). 'Molecular modeling investigation of free volume distributions in stiff chain polymers with conventional and ultrahigh free volume: Comparison between molecular modeling and positron lifetime studies'. *Macromolecules*, **36**, 8528–38.

Husain, S. and Koros, W. J. (2007). 'Mixed matrix hollow fiber membranes made with modified HSSZ-13 zeolite in polyetherimide polymer matrix for gas separation'. *Journal of Membrane Science*, **288**, 195–207.

Husain, S. and Koros, W. J. (2009). 'Macrovoids in hybrid organic/inorganic hollow fiber membranes'. *Industrial and Engineering Chemistry Research*, **48**, 2372–9.

Hutson, N. D. and Yang, R. T. (1997). 'Theoretical basis for the Dubinin–Radushkevitch (D–R) adsorption isotherm equation'. *Adsorption*, **3**, 189–95.

Illing, G., Hellgardt, K., Schonert, M., Wakeman, R. J. and Jungbauer, A. (2005). 'Towards ultrathin polyaniline films for gas separation'. *Journal of Membrane Science*, **253**, 199–208.

Jansen, J. C., Macchione, M., Tocci, E., De Lorenzo, L., Yampolskii, Y. P., Sanfirova, O., Shantarovich, V. P., Heuchel, M., Hofmann, D. and Drioli, E. (2009). 'Comparative study of different probing techniques for the analysis of the free volume distribution in amorphous glassy perfluoropolymers'. *Macromolecules*, **42**, 7589–604.

Jansen, J. C., Friess, K. and Drioli, E. (2011). 'Organic vapour transport in glassy perfluoropolymer membranes: A simple semi-quantitative approach to analyze clustering phenomena by time lag measurements'. *Journal of Membrane Science*, **367**, 141–51.

Jayaraman, V. and Lin, Y. S. (1995). 'Synthesis and hydrogen permeation properties of ultrathin palladium-silver alloy membranes'. *Journal of Membrane Science*, **104**, 251–62.

© Woodhead Publishing Limited, 2011

Keizer, K., Uhlhorn, R. J. R., Van Vuren, R. J. and Burggraaf, A. J. (1988). 'Gas separation mechanisms in microporous modified [gamma]-Al_2O_3 membranes'. *Journal of Membrane Science*, **39**, 285–300.

Keurentjes, J. T. F., Gielens, F. C., Tong, H. D., Van Rijn, C. J. M. and Vorstman, M. A. G. (2004). 'High-flux palladium membranes based on microsystem technology'. *Industrial and Engineering Chemistry Research*, **43**, 4768–72.

Khulbe, K. C., Feng, C. Y. and Matsuura, T. (eds.) (2008). *Synthetic Polymeric Membranes: Characterization by Atomic Force Microscopy*, Springer, Heidelberg, Germany.

Kitagawa, S., Kitaura, R. and Noro, S. (2004). 'Functional porous coordination polymers'. *Angewandte Chemie, International Edition*, **43**, 2334–75.

Kong, C., Lu, J., Yang, J. and Wang, J. (2006). 'Preparation of silicalite-1 membranes on stainless steel supports by a two-stage varying-temperature *in situ* synthesis'. *Journal of Membrane Science*, **285**, 258–64.

Koresh, J. and Soffer, A. (1980). 'Study of molecular-sieve carbons. 2. Estimation of cross-sectional diameters of non-spherical molecules'. *Journal of the Chemical Society Faraday Transactions I*, **76**, 2472–85.

Koros, W. J. and Mahajan, R. (2000). 'Pushing the limits on possibilities for large scale gas separation: which strategies?' *Journal of Membrane Science*, **181**, 141.

Koros, W. J., Chan, A. H. and Paul, D. R. (1977). 'Sorption and transport of various gases in polycarbonate'. *Journal of Membrane Science*, **2**, 165–90.

Krishna, R. and Van Baten, J. M. (2009). 'An investigation of the characteristics of Maxwell-Stefan diffusivities of binary mixtures in silica nanopores'. *Chemical Engineering Science*, **64**, 870–82.

Krishna, R. and Wesselingh, J. A. (1997). 'The Maxwell-Stefan approach to mass transfer'. *Chemical Engineering Science*, **52**, 861–911.

Kruczek, B., Frisch, H. L. and Chapanian, R. (2005). 'Analytical solution for the effective time lag of a membrane in a permeate tube collector in which Knudsen flow regime exists'. *Journal of Membrane Science*, **256**, 57–63.

Krykin, M. A., Zinovieva, O. M. and Zinoviev, A. B. (1999). 'Sorption and diffusion of low molecular weight gases and vapors in classy polymers at high concentration of sorbate'. *Journal of Polymer Science Part B, Polymer Physics*, **37**, 2314–23.

Lagorsse, S., Magalhaes, F. D. and Mendes, A. (2004). 'Carbon molecular sieve membranes: Sorption, kinetic and structural characterization'. *Journal of Membrane Science*, **241**, 275–87.

Lape, N. K., Nuxoll, E. E. and Cussler, E. L. (2004). 'Polydisperse flakes in barrier films'. *Journal of Membrane Science*, **236**, 29–37.

Li, S. G., Falconer, J. L., Noble, R. D. and Krishna, R. (2007). 'Interpreting unary, binary, and ternary mixture permeation across a SAPO-34 membrane with loading-dependent Maxwell–Stefan diffusivities'. *Journal of Physical Chemistry C*, **111**, 5075–82.

Li, Y. S., Bux, H., Feldhoff, A., Li, G. L., Yang, W. S. and Caro, J. (2010). 'Controllable synthesis of metal–organic frameworks: from MOF nanorods to oriented MOF membranes'. *Advanced Materials*, **22**, 3322.

Liu, B. and Smit, B. (2009). 'Comparative molecular simulation study of CO_2/N_2 and CH_4/N_2 separation in zeolites and metal–organic frameworks'. *Langmuir*, **25**, 5918–26.

Liu, Y., Wang, R. and Chung, T.-S. (2001). 'Chemical cross-linking modification of polyimide membranes for gas separation'. *Journal of Membrane Science*, **189**, 231–9.

Lozano-Castello, D., Cazorla-Amoros, D. and Linares-Solano, A. (2004). 'Usefulness of CO_2 adsorption at 273 K for the characterization of porous carbons'. *Carbon*, **42**, 1233–42.

© Woodhead Publishing Limited, 2011

Mallada, R. and Menéndez, M. (eds.) (2008). *Inorganic Membranes: Synthesis, Characterization and Applications*, Elsevier, Oxford, UK.

Mallory, G. O. (1990). *Electroless Plating: Fundamentals and Applications*, American Electroplaters and Surface Finishers Society, Orlando, FL.

Mardilovich, P. P., She, Y., Ma, Y. H. and Rei, M.-H. (1998). 'Defect-free palladium membranes on porous stainless-steel support'. *AiChE Journal*, **44**, 310–22.

McKeown, N. B. and Budd, P. M. (2006). 'Polymers of intrinsic microporosity (PIMs): organic materials for membrane separations, heterogeneous catalysis and hydrogen storage'. *Chemical Society Reviews*, **35**, 675–83.

McKeown, N. B. and Budd, P. M. (2010). 'Exploitation of intrinsic microporosity in polymer-based materials'. *Macromolecules*, **43**, 5163–76.

McLeod, L. S., Degertekin, F. L. and Fedorov, A. G. (2009a). 'Determination of the rate-limiting mechanism for permeation of hydrogen through microfabricated palladium–silver alloy membranes'. *Journal of Membrane Science*, **341**, 225–32.

McLeod, L. S., Degertekin, F. L. and Fedorov, A. G. (2009b). 'Non-ideal absorption effects on hydrogen permeation through palladium–silver alloy membranes'. *Journal of Membrane Science*, **339**, 109–14.

Mejdell, A. L., Klette, H., Ramachandran, A., Borg, A. and Bredesen, R. (2008). 'Hydrogen permeation of thin, free-standing Pd/Ag23% membranes before and after heat treatment in air'. *Journal of Membrane Science*, **307**, 96–104.

Mendes, D., Chibante, V., Zheng, J.-M., Tosti, S., Borgognoni, F., Mendes, A. and Madeira, L. M. (2010). 'Enhancing the production of hydrogen via water–gas shift reaction using Pd-based membrane reactors'. *International Journal of Hydrogen Energy*, **35**, 12596–608.

Merkel, T. C., Bondar, V. I., Nagai, K., Freeman, B. D. and Pinnau, I. (2000). 'Gas sorption, diffusion, and permeation in poly(dimethylsiloxane)'. *Journal of Polymer Science Part B-Polymer Physics*, **38**, 415–34.

Moore, T. T. and Koros, W. J. (2007). 'Gas sorption in polymers, molecular sieves, and mixed matrix membranes'. *Journal of Applied Polymer Science*, **104**, 4053–9.

Morreale, B. D., Ciocco, M. V., Enick, R. M., Morsi, B. I., Howard, B. H., Cugini, A. V. and Rothenberger, K. S. (2003). 'The permeability of hydrogen in bulk palladium at elevated temperatures and pressures'. *Journal of Membrane Science*, **212**, 87–97.

Mulder, M. (1996). *Basic Principles of Membrane Technology*, Kluwer Academic Publishers, Dordrecht.

Nakanishi, H. and Ujihira, Y. (1982). 'Application of positron-annihilation to the characterization of zeolites'. *Journal of Physical Chemistry*, **86**, 4446–50.

Nam, S.-E., Seong, Y.-K., Lee, J. W. and Lee, K.-H. (2009). 'Preparation of highly stable palladium alloy composite membranes for hydrogen separation'. *Desalination*, **236**, 51–5.

Nan, Q. and Levan, M. D. (2005). 'Adsorption equilibrium modeling for water on activated carbons'. *Carbon*, **43**, 2258–63.

Nguyen, C. and Do, D. D. (1999). 'Adsorption of supercritical gases in porous media: Determination of micropore size distribution'. *Journal of Physical Chemistry B*, **103**, 6900–8.

Nguyen, C., Do, D. D., Haraya, K. and Wang, K. (2003). 'The structural characterization of carbon molecular sieve membrane (CMSM) via gas adsorption'. *Journal of Membrane Science*, **220**, 177–82.

Nuxoll, E. E., Siegel, R. A. and Cussler, E. L. (2005). 'Layered reactive barrier films'. *Journal of Membrane Science*, **252**, 29–36.

© Woodhead Publishing Limited, 2011

Paglieri, S. N. and Way, J. D. (2002). 'Innovations in palladium membrane research'. *Separation and Purification Methods*, **31**, 1–169.

Paglieri, S. N., Foo, K. Y., Way, J. D., Collins, J. P. and Harper-Nixon, D. L. (1999). 'A new preparation technique for Pd/alumina membranes with enhanced high-temperature stability'. *Industrial and Engineering Chemistry Research*, **38**, 1925–36.

Paul, D. R. and Koros, W. J. (1976). 'Effect of partially immobilizing sorption on permeability and diffusion time lag'. *Journal of Polymer Science Part B, Polymer Physics*, **14**, 675–85.

Perez, E. V., Balkus, K. J., Ferraris, J. P. and Musselman, I. H. (2009). 'Mixed-matrix membranes containing MOF-5 for gas separations'. *Journal of Membrane Science*, **328**, 165–73.

Perry, D., Ward, W. J. and Cussler, E. L. (1989). 'Unsteady diffusion in barrier membranes'. *Journal of Membrane Science*, **44**, 305–11.

Peters, T. A., Tucho, W. M., Ramachandran, A., Stange, M., Walmsley, J. C., Holmestad, R., Borg, A. and Bredesen, R. (2009). 'Thin Pd-23%Ag/stainless steel composite membranes: Long-term stability, life-time estimation and post-process characterisation'. *Journal of Membrane Science*, **326**, 572–81.

Piera, E., Bernal, M. P., Salomon, M. A., Coronas, J., Menendez, M. and Santamaria, J. (1999). 'Preparation and permeation properties of different zeolite tubular membranes'. *Porous Materials in Environmentally Friendly Processes*, **125**, 189–96.

Rao, M. B. and Sircar, S. (1996). 'Performance and pore characterization of nanoporous carbon membranes for gas separation'. *Journal of Membrane Science*, **110**, 109–18.

Rutherford, S. W. (2001a). 'Mechanism of sorption and diffusion in a high free-volume polymer'. *Industrial and Engineering Chemistry Research*, **40**, 1370–6.

Rutherford, S. W. (2001b). 'Polymer permeability and time lag at high concentrations of sorbate'. *Journal of Membrane Science*, **183**, 101–7.

Rutherford, S. W. and Do, D. D. (1997). 'Review of time lag permeation technique as a method for characterisation of porous media and membranes'. *Adsorption-Journal of the International Adsorption Society*, **3**, 283–312.

Rutherford, S. W. and Do, D. D. (1999). 'Permeation time lag with multilayer adsorption and surface diffusion'. *Chemical Engineering Journal*, **74**, 155–60.

Saufi, S. M. and Ismail, A. F. (2004). 'Fabrication of carbon membranes for gas separation: A review'. *Carbon*, **42**, 241–59.

Schlunder, E. U., Yang, J. and Seidel-Morgenstern, A. (2006). 'Competitive diffusion and adsorption in Vycor glass membranes: A lumped parameter approach'. *Catalysis Today*, **118**, 113–20.

Shah, M. R., Noble, R. D. and Clough, D. E. (2006). 'Analysis of transient permeation as a technique for determination of sorption and diffusion in supported membranes'. *Journal of Membrane Science*, **280**, 452–60.

Shu, S., Husain, S. and Koros, W. J. (2007). 'A general strategy for adhesion enhancement in polymeric composites by formation of nanostructured particle surfaces'. *Journal of Physical Chemistry C*, **111**, 652–7.

Song, C., Wang, T., Jiang, H., Wang, X., Cao, Y. and Qiu, J. (2010). 'Gas separation performance of C/CMS membranes derived from poly(furfuryl alcohol) (PFA) with different chemical structure'. *Journal of Membrane Science*, **361**, 22–7.

Stoeckli, F., Slasli, A., Hugi-Cleary, D. and Guillot, A. (2002). 'The characterization of microporosity in carbons with molecular sieve effects'. *Microporous and Mesoporous Materials*, **51**, 197–202.

Taveira, P., Mendes, A. and Costa, C. (2003). 'On the determination of diffusivity and

© Woodhead Publishing Limited, 2011

sorption coefficients using different time-lag models'. *Journal of Membrane Science*, **221**, 123–33.

Thomas, S., Schäfer, R., Caro, J. and Seidel-Morgenstern, A. (2001). 'Investigation of mass transfer through inorganic membranes with several layers'. *Catalysis Today*, **67**, 205–16.

Tong, H. D., Gielens, F. C., Gardeniers, J. G. E., Jansen, H. V., Van Rijn, C. J. M., Elwenspoek, M. C. and Nijdam, W. (2004). 'Microfabricated palladium–silver alloy membranes and their application in hydrogen separation'. *Industrial and Engineering Chemistry Research*, **43**, 4182–7.

Tosti, S. and Bettinali, L. (2004). 'Diffusion bonding of Pd–Ag rolled membranes'. *Journal of Materials Science*, **39**, 3041–6.

Tosti, S., Bettinali, L. and Violante, V. (2000a). 'Rolled thin Pd and Pd–Ag membranes for hydrogen separation and production'. *International Journal of Hydrogen Energy*, **25**, 319–25.

Tosti, S., Violante, V., Basile, A., Chiappetta, G., Castelli, S., De Francesco, M., Scaglione, S. and Sarto, F. (2000b). 'Catalytic membrane reactors for tritium recovery from tritiated water in the ITER fuel cycle'. *Fusion Engineering and Design*, **49–5**, 953–8.

Tuchlenski, A., Uchytil, P. and Seidel-Morgenstern, A. (1998). 'An experimental study of combined gas phase and surface diffusion in porous glass'. *Journal of Membrane Science*, **140**, 165–84.

Uchytil, P., Schramm, O. and Seidel-Morgenstern, A. (2000). 'Influence of the transport direction on gas permeation in two-layer ceramic membranes'. *Journal of Membrane Science*, **170**, 215–24.

Uemiya, S. (1999). 'State-of-the-art of supported metal membranes for gas separation'. *Separation and Purification Methods*, **28**, 51–85.

Uemiya, S., Sato, N., Ando, H., Kude, Y., Matsuda, T. and Kikuchi, E. (1991). 'Separation of hydrogen through palladium thin film supported on a porous glass tube'. *Journal of Membrane Science*, **56**, 303–13.

Uhlhorn, R. J. R., Intveld, M. H. B. J. H., Keizer, K. and Burggraaf, A. J. (1992). 'Synthesis of ceramic membranes. 1. Synthesis of non-supported and supported gamma-alumina membranes without defects'. *Journal of Materials Science*, **27**, 527–37.

Van Den Broeke, L. J. P., Bakker, W. J. W., Kapteijn, F. and Moulijn, J. A. (1999). 'Binary permeation through a silicalite-1 membrane'. *AIChE Journal*, **45**, 976–85.

Veldsink, J. W., Versteeg, G. F. and Van Swaaij, W. P. M. (1994). 'An experimental study of diffusion and convection of multicomponent gases through catalytic and non-catalytic membranes'. *Journal of Membrane Science*, **92**, 275–91.

Vieth, W. R., Howell, J. M. and Hsieh, J. H. (1976). 'Dual sorption theory'. *Journal of Membrane Science*, **1**, 177–220.

Vopicka, O., Hynek, V., Zgazar, M., Friess, K. and Sipek, M. (2009). 'A new sorption model with a dynamic correction for the determination of diffusion coefficients'. *Journal of Membrane Science*, **330**, 51–6.

Wang, K. (2005). 'Gas permeation in hollow fiber membranes with nonlinear sorption isotherm and concentration dependent diffusion coefficient'. *Journal of Membrane Science*, **267**, 99–103.

Wang, L., Cao, Y., Zhou, M., Zhou, S. J. and Yuan, Q. (2007). 'Novel copolyimide membranes for gas separation'. *Journal of Membrane Science*, **305**, 338–46.

Ward, T. L. and Dao, T. (1999). 'Model of hydrogen permeation behavior in palladium membranes'. *Journal of Membrane Science*, **153**, 211–31.

Wijmans, J. G. and Baker, R. W. (1995). 'The solution-diffusion model: a review'. *Journal of Membrane Science*, **107**, 1–21.

© Woodhead Publishing Limited, 2011

Wilhite, B. A., Schmidt, M. A. and Jensen, K. F. (2004). 'Palladium-based micromembranes for hydrogen separation: Device performance and chemical stability'. *Industrial and Engineering Chemistry Research*, **43**, 7083–91.

Xomeritakis, G. and Lin, Y. S. (1997). 'Fabrication of thin metallic membranes by MOCVD and sputtering'. *Journal of Membrane Science*, **133**, 217–30.

Xomeritakis, G. and Lin, Y.-S. (1998). 'CVD synthesis and gas permeation properties of thin palladium/alumina membranes'. *AIChE Journal*, **44**, 174–83.

Xomeritakis, G., Gouzinis, A., Nair, S., Okubo, T., He, M. Y., Overney, R. M. and Tsapatsis, M. (1999). 'Growth, microstructure, and permeation properties of supported zeolite (MFI) films and membranes prepared by secondary growth'. *Chemical Engineering Science*, **54**, 3521–31.

Xu, Z.-K., Dannenberg, C., Springer, J., Banerjee, S. and Maier, G. (2002). 'Novel poly(arylene ether) as membranes for gas separation'. *Journal of Membrane Science*, **205**, 23-31.

Yaghi, O. M., O'Keeffe, M., Ockwig, N. W., Chae, H. K., Eddaoudi, M. and Kim, J. (2003). 'Reticular synthesis and the design of new materials'. *Nature*, **423**, 705–14.

Yampolskii, Y. P. and Shantarovich, V. (2006). 'Positron annihilation lifetime spectroscopy and other methods for free volume evaluation in polymers'. In: Pinnau, I., Freeman, B. D. and Yampolskii, Y. P. (eds) *Materials Science of Membranes for Gas and Vapor Separation*. Wiley, London, England.

Yang, J. H., Cermakova, J., Uchytil, P., Hamel, C. and Seidel-Morgenstern, A. (2005). 'Gas phase transport, adsorption and surface diffusion in a porous glass membrane'. *Catalysis Today*, **104**, 344–51.

Yasuda, H. and Rosengren, K. (1970). 'Isobaric measurement of gas permeability of polymers'. *Journal of Applied Polymer Science*, **14**, 2839–77.

Ye, X., Lv, L., Zhao, X. S. and Wang, K. (2006). 'Permeation time lag in polymeric hollow fiber membranes'. *Journal of Membrane Science*, **283**, 425–9.

Yeom, C. K., Kim, B. S. and Lee, J. M. (1999). 'Precise on-line measurements of permeation transients through dense polymeric membranes using a new permeation apparatus'. *Journal of Membrane Science*, **161**, 55–66.

Yu, M., Hunter, J. T., Falconer, J. L. and Noble, R. D. (2006). 'Adsorption of benzene mixtures on silicalite-1 and NaX zeolites'. *Microporous and Mesoporous Materials*, **96**, 376–85.

Zhang, Y., Gwak, J., Murakoshi, Y., Ikehara, T., Maeda, R. and Nishimura, C. (2006). 'Hydrogen permeation characteristics of thin Pd membrane prepared by microfabrication technology'. *Journal of Membrane Science*, **277**, 203–9.

Zhou, W., Wu, H., Hartman, M. R. and Yildirim, T. (2007). 'Hydrogen and methane adsorption in metal–organic frameworks: A high-pressure volumetric study'. *Journal of Physical Chemistry C*, **111**, 16131–7.

3.6 Appendix: list of symbols

3.6.1 Symbols

A	Area	(m^2)
b	Affinity constant (Equation [3.7])	
B_0	Viscous flow parameter	
C	Concentration	($mol\,m^{-3}$)

© Woodhead Publishing Limited, 2011

C'_H	Maximum void sorption concentration	$(mol\,m^{-3})$
D	Diffusion coefficient	$(m^2\,s^{-1})$
E_0	Characteristic energy (Equation [3.1])	$(J\,mol^{-1})$
J	Molar flux	$(mol\,m^{-2}\,s^{-1})$
k_C	Partition coefficient	$((mol\,kg^{-1})\cdot(mol\,m^{-3})^{-1})$
k_D	Henry's sorption coefficient	$(mol\,m^{-3}\,Pa^{-1})$
k_{H_2}	Sieverts' constant	$(mol\,m^{-3}\,Pa^{-1/2})$
L	Permeability coefficient	$(mol\,m\,m^{-2}\,s^{-1}\,Pa^{-1})$
M	Molar mass	$(g\,mol^{-1})$
n	Parameter	
P	Pressure	(Pa)
P_0	Saturation pressure	(Pa)
P_{av}	Average pressure across the membrane	(Pa)
q	Concentration in the adsorbed phase	$(mol\,m^{-3})$
r_p	Pore radius	(m)
R	Gas constant	$(J\,mol^{-1}\,K^{-1}))$
t	Time	(s)
T	Absolute temperature	(K)
U	Parameter (Equation [3.2])	
V	Volume	(m^3)
x	Membrane spatial coordinate	(m)
W	Volume of micropores	(m^3)
W_0	Total volume of micropores	(m^3)
Z	Parameter (Equation [3.2])	

3.6.2 Greek symbols

β	Affinity coefficient for carbon (Equation [3.1])	
ε	Porosity	
δ	Membrane thickness	(m)
ρ	Density	$(kg\,m^{-3})$
Π	Permeance	$(mol\,m^{-2}\,s^{-1}\,Pa^{-1})$
τ	Tortuosity	
ϕ	Volume fraction	
μ	Viscosity	

Superscripts

h	Relative to the high concentration/pressure side
l	Relative to the low concentration/pressure side

© Woodhead Publishing Limited, 2011

4

Economic analysis of membrane use in industrial applications

V. CALABRÒ, University of Calabria, Italy and
A. BASILE, Institute on Membrane Technology of the Italian National Research Council, ITM-CNR, Italy

Abstract: In this chapter an economic analysis applied to different membrane systems and applications is discussed. Methods used for economic analysis of new investment or for comparison between different choices for existing plants are also reported. The applications of these methods are then shown with analysis of a few case studies relating to existing industrial applications, where membranes are substituted for conventional treatment.

Key words: economic analysis, membrane performances, membrane process investment.

4.1 Introduction

Membrane processes are largely used in industrial applications in different fields like chemicals, food, gas, water and wastewater treatment, pharmaceutical and more. Their success is related to their performance and feasibility of use. It is interesting to make an analysis of the economic aspects relating to membrane processes, by evaluating the possibility of using some typical economic methods or new ones and by evidencing the most important parameters that are needed for the economic analysis.

In this chapter the most important costs related to membrane processes like gas separation, ultrafiltration (UF), reverse osmosis (RO), microfiltration (MF), nanofiltration (NF) and pervaporation as well as their integration are investigated utilizing economic analysis methods. The most important parameters are cited and described and their values have been reported for the specific cases. It is important to include evidence that the economic analysis of membrane processes is strictly related to an energetic analysis of the overall process. This requires a global evaluation of the overall process in order to raise a correct economic evaluation of the feasibility and convenience of introducing membrane systems into existing industrial processes or plant as well as introducing membranes into new plant design.

© Woodhead Publishing Limited, 2011

4.2 Economic analysis

Economic analysis has been done with reference to methods based on different economic parameters. The methods used are reported in order to offer a complete description of all the parameters used in the different cases studied.

4.2.1 Internal return rate (IRR) method

An economic evaluation method based on the internal return rate (IRR) is considered suitable for an initial estimate of economic feasibility of industrial processes (Castilho *et al.*, 2000). This method is based on evaluating the discount rate that causes the present value of the cash flow, projected for the life of the plant, to be equal to the invested capital. The basic idea of the IRR evaluation is to obtain a single value that synthesizes the merits of the project for its lifetime. Since this value does not depend on market interest rates, it is labelled internal return rate. The IRR is intrinsic to the project and does not depend on anything other than the project cash flow. As a hypothesis for the application of the method, the annual net profit was assumed to be constant during the lifetime of the plant.

To evaluate the feasibility of the project a minimum return rate (MRR) expected by the investor must be set. This tax is usually between 8% and 18% for chemical industry projects (Rudd and Watson, 1968). If the internal return rate is higher than the minimum return rate expected, the investment is considered to be economically feasible. The method for finding this is based on the calculation of the so-called net present value (NPV) of the investment which is required in order to estimate the effect of the discount rate (DR) on this value. The discount rate for NPV = 0, representing the expected investment return rate IRR as:

$$IRR = DR \qquad [4.1]$$

when NPV = 0

The IRR method requires the MRR to be lower than the expected return rate

$$IRR > MRR \qquad [4.2]$$

The NPV might be calculated as follows:

$$NPV = \sum_{m=1}^{\text{plant life}} \frac{NPAT}{(1 + DR)^m} - I_{\text{total}} \qquad [4.3]$$

where NPAT is the net profit after the income tax, related to the income tax (IT), whereas I_{total} is the total investment cost, which might be calculated by

© Woodhead Publishing Limited, 2011

summing capital and non-capital investment costs, (I_{cap} and I_{ncap}, respectively), working capital costs (I_{wcap}) and start cost (I_{start}):

$$I_{total} = I_{cap} + I_{ncap} + I_{wcap} + I_{start} \quad [4.4]$$

To calculate NPAT, the net profit before income tax (NPBT), related to the gross profit (GP) and the depreciation (DP), have to be evaluated:

$$NPAT = NPBT - IT \quad [4.5]$$

$$NPBT = GP - DP \quad [4.6]$$

$$IT = 0.25NPBT \quad [4.7]$$

In order to evaluate the total investment costs I_{total} as well as the NBPT, it is necessary to calculate all the costs reported in Equation [4.4]. To do this the total equipment cost TEC, related to the sum of the costs of all equipment (I_{equip}), should be introduced:

$$TEC = \sum I_{equip} \quad [4.8]$$

It is possible to calculate the I_{cap} as:

$$I_{cap} = 1.45L_f\ TEC \quad [4.9]$$

where L_f represents the Lang factor (Groot *et al.*, 1993) which depends on the process and equipment.

For the other investment costs it is possible to use the following relationships:

$$I_{ncap} = 0.25I_{cap} \quad [4.10]$$

$$I_{wcap} = 0.15I_{total} \quad [4.11]$$

$$I_{start} = 0.10(I_{cap} + I_{ncap}) \quad [4.12]$$

Equation [4.13] shows how to calculate the gross profit (GP) from the total costs (TC) and the total revenue (TR) as:

$$GP = TR - TC \quad [4.13]$$

where the total costs might be calculated from the direct costs (C_{direct}) and fixed costs (C_{fix}):

$$TC = C_{direct} + C_{fix} \quad [4.14]$$

$$C_{fix} = 0.03\ (I_{cap} + I_{ncap}) \quad [4.15]$$

$$C_{direct} = C_{raw} + C_{util} + C_{maint} + C_{sup} + C_{lab} + C_{adm} \quad [4.16]$$

where C_{raw} and C_{util} represent the raw material and utilities costs, respectively and depend on the processes involved in the system, C_{maint} is the maintenance cost and it is related to the total equipment costs as:

© Woodhead Publishing Limited, 2011

$$C_{maint} = 0.04 L_f \cdot TEC \quad [4.17]$$

C_{sup} represents the value of the supplies cost that is calculated as:

$$C_{sup} = 0.006\ (I_{cap} + I_{ncap}) \quad [4.18]$$

C_{lab} is the labour cost and is a fraction of the total costs TC:

$$C_{lab} = 0.20 TC \quad [4.19]$$

C_{adm} is the administrative cost and might be estimated as function of the labour costs as

$$C_{adm} = 0.20\ C_{lab} \quad [4.20]$$

Depreciation depends on the capital investment costs as:

$$DP = 0.07 I_{cap} \quad [4.21]$$

The calculation requires process data in terms of raw materials, utilities, equipments with their costs. Then it is possible to choose operating parameters for the economic analysis by evaluating the optimal value that permits the desired IRR to be attained. Membrane costs represent one of the most important parameters used for this analysis. A more detailed analysis will be done in the case studies that will be presented next.

4.2.2 Comparative analysis

In some applications it is necessary to perform a comparison among different membrane systems and other processes. In some cases it will be enough to perform the analysis strictly in relation to the membrane processes. This is frequently the case in the study of seawater desalination or in the use of UF as pretreatment, where membrane systems are largely used and new configurations are also studied.

4.2.3 Total cost ownership (TCO) methods

Total cost of ownership (TCO) is the cost calculated over the lifecycle of a desalination plant. This can either be the contract period of a build own operate transfer (BOOT) project (typically 20 years) or the technical life of the mechanical and civil constructions. This cost might be compared for sea water reverse osmosis (SWRO) desalination plants that are presently in operation, under construction or being planned and the calculation might also be applied to large-scale desalination plants (Pankratz, 2006; Fichtner, 2005) showing that the trend in TCO for sea water reverse osmosis (SWRO) based large scale desalination plants is to 0.85–0.90 US$/m^3 of water produced.The TCO might be, in general, split as follows (Menge *et al.*, 2001; Henthorne, 2005; Caneja *et al.*, 2005):

© Woodhead Publishing Limited, 2011

- 17% pretreatment
- 6% membrane replacement and cleaning
- 27% other fixed costs (amortization of other equipment etc.)
- 50% other variable costs (energy costs etc.).

If the sum of the individual parts of the TCO for UF is lower than the TCO for conventional plants (0.85–0.90 US$/m^3), this implies that UF is not only technically feasible, but also economically attractive. It has to be noted that not only the actual cost of the pretreatment system has to be taken into consideration, but also the impact of the pretreatment system on the other costs (both fixed as well as variable).

Pretreatment

The pretreatment costs can be split into amortization of investment and operating costs (mainly chemicals for coagulation and for disinfection). When UF is selected as pretreatment for SWRO instead of conventional technology, this will change the split in the TCO: the investment costs for the pretreatment will increase and the fixed costs associated with pretreatment will increase too. The costs of chemicals (mainly coagulant) will decrease, but a new cost arises, the cost of UF membrane replacement.

Membrane replacement and cleaning

When UF is selected as a pretreatment option over conventional technology, the RO cleaning frequency will be greatly reduced. Pilots have shown that with UF as pretreatment, RO cleaning frequency can be virtually eliminated. The typical cleaning frequency can be reduced from once every 2–3 months to once every 6–12 months. Because of reduced RO fouling and because of the reduced chemical attack caused by RO cleaning, the RO membrane lifetime will increase when UF is selected. Typical RO lifetime can be increased from 6 years to at least 7 years (conservative) or 8 years or longer (Knops *et al.*, 2007).

Other fixed costs

Fixed costs are calculated in a fixed currency divided by the total net filtrate production over the complete lifecycle, so they depend on the on-line time of the desalination plant: the shorter the on-line time the higher the fixed costs will be. When the plant is not producing water this reduces the net water production over its lifetime and thus increases the fixed costs expressed as cost per cubic metre.

Compared to conventional technology, UF will provide the following benefits:

© Woodhead Publishing Limited, 2011

- Shorter construction time: the plant can be produce water for a longer time. If the construction time can be reduced by 3–6 months, for a typical lifetime of 20 years, this means an increase in net production of 1–2%.
- RO plant will have more operational days per year as consequence of decreased RO cleaning frequency. Assuming that the RO cleaning duration is decreased by 5 days per year, this increases the net RO output by approximately 2%.
- Other fixed costs, such as land purchase, will be reduced as well.

Other variable costs

Variable costs will be reduced when conventional pretreatment is replaced by UF membrane technology because less RO fouling will lead to a lower flux decline and consequently in a lower RO operating pressure. A UF plant has a higher degree of automation, thus the labour requirement will be smaller.

4.2.4 Detailed costs

The previously described analysis refers to some costs and their details are reported here. Analysis based on annual costs requires evaluation of the following economic parameters: amortization factor a (years^{-1}), interest rate I (%), plant life n (years), plant capacity m (m^3/day), plant availability f, specific consumption of electric power w (kWh/m^3), electric energy cost c (US$/kWh), heating steam cost s (US$/kg), specific chemicals cost k (US$/m^3), specific cost of operating labour γ (US$/m^3), specific maintenance and spare parts cost p (US$/m^3),

For desalination plants two more parameters are necessary: salts price flowrate $SPFi$ (US$/kg) and specific cost of brine disposal b (US$/m^3).

During process or plant design, the amortization factor might be evaluated as:

$$a = \frac{I(1+I)^n}{(1+I)^n - 1} \qquad [4.22]$$

and the unit product cost (UPC) on the basis of total annual cost (TAC), is calculated too:

$$UPC = \frac{TAC}{fm\ 365} \qquad [4.23]$$

$$TAC = \sum AC = AC_{\text{fixed}} + AC_{\text{el–en}} + AC_{\text{vapour}} + AC_{\text{chemicals}} + AC_{\text{labour}} + AC_{\text{maint}} + AC_{\text{membrane}} + AC_{\text{process}} \qquad [4.24]$$

© Woodhead Publishing Limited, 2011

where AC_{fixed} is the annual fixed cost and might be calculated as function of direct and indirect capital costs, (DCC and ICC respectively):

$$AC_{\text{fixed}} = a\ DCC + ICC \quad [4.25]$$

In the case of desalination, the ICC is calculated as 10% of DCC (Macedonio *et al.*, 2007). $AC_{\text{el-en}}$ is the annual electric power cost related to the specific consumption of electric power and plant capacity as:

$$AC_{\text{el–en}} = cwfm\ 365 \quad [4.26]$$

AC_{vapour} is the annual steam cost related to the steam flow rate feed to the plant G (kg/day)

$$AC_{\text{vapour}} = sGf\ 365 \quad [4.27]$$

$AC_{\text{chemicals}}$ is the annual cost of chemicals and is related to the chemicals required for the processes:

$$AC_{\text{chemicals}} = kfm\ 365 \quad [4.28]$$

AC_{labour} is the annual labour cost:

$$AC_{\text{labour}} = \gamma fm\ 365 \quad [4.29]$$

AC_{maint} is the annual maintenance and spare parts cost:

$$AC_{\text{maint}} = pfm\ 365 \quad [4.30]$$

During desalination the brine annual disposal costs AC_{brine}, and the costs of all disposal sub-products related to their flow rate B (kg/day) have to be evaluated:

$$AC_{\text{brine}} = bBf\ 365 \quad [4.31]$$

In desalination as well as other separation processes the annual costs of salts AC_{salts}, is calculated from the sum of the specific salts costs SPF:

$$AC_{\text{salts}} = \left(\sum_i SPF_i\right) f\ 365 \quad [4.32]$$

4.3 Case studies

The case studies reported in this section relate to existing plants as well as to new plants where membrane processes have to be introduced. The choice of cases reported here has been made in order to offer an overview of the applications of all the cited membrane processes, that is UF, RO, gas separation, bioreactors and their integration. The field of application is usually where membrane processes are actually used (like bioconversions, desalination, gas separation and recovery).

© Woodhead Publishing Limited, 2011

4.3.1 Integrated fermentation, ultrafiltration and pervaporation systems

An interesting application relates to the production of ethanol from sugar cane, coupled to the recovery of fructose. Di Luccio *et al.* (2002) suggest an economic analysis of a continuous selective fermentation coupled to pervaporation for ethanol removal. The system design consists of selective fermentation of a mixture of sugars in a bioreactor coupled to pervaporation for ethanol removal. Experiments using a mutant strain of *Saccharomyces cerevisiae* (ATCC36859) were performed using batch, semi-batch and semi-batch coupled to pervaporation and vacuum membrane distillation processes. The fermentation medium contained glucose, fructose, yeast extract and peptone. In this study economic analysis was carried out considering the different plant configurations by the IRR method already described.

In order to perform the economic analysis it is necessary to define, preliminarily, the capability and performance of the plant. It has been decided that the ethanol plant can operate on 330 days/year and produce 6000 m^3/year of ethanol and 10000 t/year of fructose. Data for the analysis have been supplied by the producers or obtained from the economic literature: the prices of raw materials were obtained from ethanol producers in the State of Sao Paulo (Brazil), the estimate of utilities costs was obtained from literature data and the average price of the products was obtained from the Exterior Commerce Institute of Brazil. Information about equipment costs from industry equipment manufacturers has also been used.

All the data relating to the performance of the systems require a preliminary experimental analysis coupled with a predictive or theoretical analysis (Calabrò *et al.*, 2002). The latter permits simulation of the process giving a complete description of the system performance; furthermore it permits evaluation of the operating conditions to enable an estimation of the operating range of the process parameters, and to find the optimal control system (Curcio *et al.*, 2009).

When different plant or process configurations might be considered, it is useful to perform a comparison not only in terms of performance but also in terms of the economic and energetic validity and in terms of the possibility of recovering the residual (Calabrò *et al.*, 2008). Di Luccio *et al.* (2002) used the following data:

- *Raw materials:* cell concentration, 2.5 g l^{-1}, glucose concentration 100 g l^{-1}, fructose concentration 100 g l^{-1}, glucose in the feed, 150 g l^{-1}, fructose in the feed 150 g l^{-1}.
- *Operating conditions:* initial volume 50 m^3, total volume 120 m^3, feed rate 4.29 m^3 h^{-1}.
- *Membrane systems:* membrane area 2000 m^2, ethanol flux 50 g/m^{-2} h^{-1}, ethanol in permeate 3.5 wt%.

© Woodhead Publishing Limited, 2011

- *Fermentor conditions:* ethanol in fermentor 44 g l^{-1}, fructose yield in the bioreactor, higher than 90%, fructose in bioreactor, 131 g l^{-1}.
- *Distillation column:* top product, ethanol 95%, bottom ethanol less than 0.005%.
- *Productivity:* ethanol 9.5% flow rate, 6000 m^3/year, fructose final product, more than 95% of fructose in dry basis, with 770 g l^{-1} of solids, fructose flow rate (770 g l^{-1}), 10000 t/year, fructose recovery in the extraction column, 95%.

These quantities have been integrated with the following costs data:

- *Raw materials*: invert sugar 0.035 US$/l, nutrients 0.02 US$/l.
- *Utilities:* steam 0.008 US$/l, electricity 0.08 US$/l, air 0.015 US$/l, cooling water 0.07 US$/l.
- *Cost of products:* ethanol 0.37 US$/l, fructose 1.50 US$/kg.

A further step relates to the analysis of equipment costs. In the case studied, three bioreactors operating in parallel to maintain continuous ethanol production have been taken in consideration. The distillation column was operated with two feed inlets, one stream that leaves the membrane unit and one that leaves the bioreactor bleed.

- *Equipment costs*: fermentor (3 units) US$ 450 000, seed tank (2 units) US$ 35 000, storage tanks (3 units) US$ 90 000, mixing tank (1 unit) US$ 15 000, pumps (12 units) US$ 2500, vacuum pumps (3 units) US$ 20 000, cryostate (1 unit) US$ 58 780, distillation column (1 unit) US$ 68 400, fructose extraction column (1 unit) US$ 410 400.
- *Lifetime:* plant: 15 years, membranes 5 years.

In the cited paper, Di Luccio *et al*. (2002) follow the IRR method, which is considered suitable for an initial estimation of the economic feasibility of industrial processes, where a MRR of 17% and a Lang factor $L_f = 4.5$ were considered (Groot *et al*., 1993). For the calculation of IRR Equations [4.1] to [4.21] have all been used.

Two projects were considered:

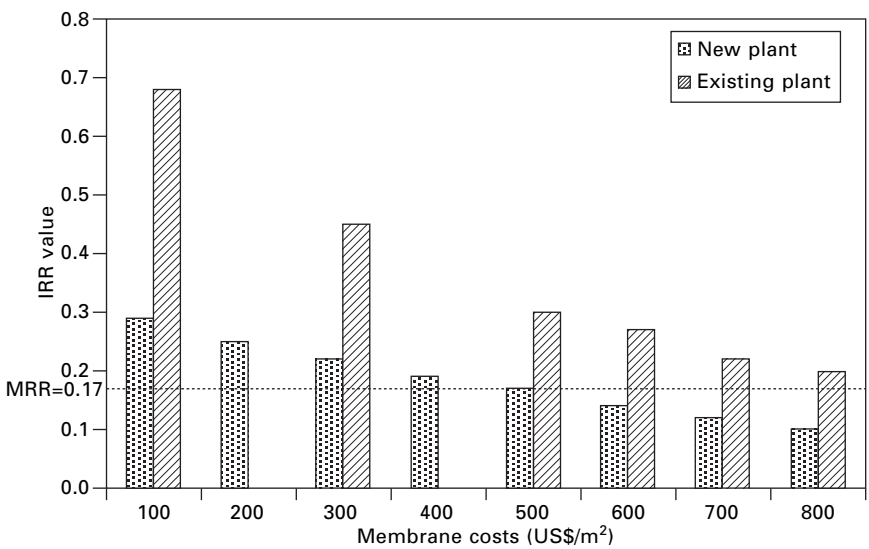
(1) There is no plant installed and investment in all equipment is necessary.
(2) The plant already exists and has to be adapted for a selective fermentation process, in this case the investment in equipment is less than in case (1).

For membrane systems, the different costs of membranes have been taken into account in order to estimate their impact on the IRR. For case (1) a preliminary analysis has been performed with reference to an assumed membrane cost of 300 US$/$m^2$. A second analysis has been repeated using

© Woodhead Publishing Limited, 2011

membrane costs ranging from 100 to 800 US$/m^2. For case (2) membrane costs for the analysis range from 100 to 800 US$/m^2.

The results of the analysis, in terms of NPV and consequently IRR (Equations [4.1 and 4.3]) for each case are reported in fig. 4.1. It is evident that for case (1) NPV ≥ 0 for IRR < 21.7%. This result shows that up to a return rate of 21.7%, the project is still economically feasible, since the NPV is still positive. On the other hand, for expected rates of return higher than 21.7%, the project is not feasible. Considering that MRR was set to 17%, one can conclude that the installation of a new plant for ethanol and fructose production is economically viable, given that the NPV is positive with IRR > MRR (Equation [4.2]). The same considerations may be applied using the membrane costs and the conditions where IRR > MRR, following the Equation [4.1] (the value of IRR where NPV = 0), will be obtained for membrane costs lower than 500 US$/m^2. Higher membrane costs cause the return rate to be lower than the expected 17%, characterizing a non-feasible project. The same analysis was carried out for the case (2), with membrane costs in the same range as case (1). In this case, even for a membrane cost of US$ 800/m^2, the project is still viable, since the IRR is about 20%, quite a bit higher than the minimum return rate expected (17%).



4.1 Internal return rate (IRR), calculated by plotting the net present value (NPV) versus discount rate (*I*) at different membrane costs (in US$/m^2) for different investments. IRR is the value of *I* where NPV = 0.

© Woodhead Publishing Limited, 2011

4.3.2 Ultrafiltration as pretreatment in sea water reverse osmosis (SWRO)

The second case study relates to the study of UF as a pretreatment for SWRO (Knops *et al*., 2007). The main obstacle to the use of UF membranes in SWRO pretreatment has always been the higher operating cost of UF compared to conventional pretreatment. The general perception is that UF as a pretreatment for SWRO is technically feasible but economically unviable and only a few references quote lower costs for UF systems (Burashid *et al*., 2005; Clunie *et al*., 2005; Gleuckstern and Priel, 2003; Mody *et al*., 2005; Coté *et al*. 2005).

In Knops *et al*. (2007) the analysis has been performed to test the possibility of using a new membrane that has been designed with the aim of tailoring it towards lowest total cost of ownership. Typical operating conditions have been used to quantify the parameters for a potentially large scale desalination system (UF + SWRO). The parameters taken into account are those introduced previously in the general description of the TCO method, for example amortization of investment in UF membranes and equipment; the operating costs of the UF system; the reduction in operating costs of the SWRO desalination plant when compared to a conventional pretreatment for the SWRO system and the increased output of the SWRO desalination plant due to greater availability and shorter construction time. The analysis permits calculation of the total cost of ownership of a UF-based SWRO desalination plant determined and expressed in US$/m^3 of water produced. Taking all these factors into account, the total cost of ownership of a dual membrane desalination plant (Seaguard UF + SWRO) will be 2–7% lower than the total cost of ownership of a SWRO plant based on a conventional pretreatment.

The economic evaluation of different SWRO desalination plants, either with conventional pretreatment or with UF pretreatment, has been performed following the TCO method (Equations [4.22] to [4.32]). Instead of fixed currency the costs are being expressed per volume of water being produced in order to make proper comparison of different sizes in desalination capacity, with the assumption that the economies of scale are negligible for plants over a certain net filtrate capacity.

Pretreatment with UF permits a reduction of 25–50% in the costs of chemical dosing (0.07–0.08 US$ of the total, almost 0.15 US$) during pretreatment. The costs of amortization (in the conventional case equal to 0.15 US$) will increase by 10–20%. The new additional cost for membrane replacement is approximately 0.01 US$/m^3 (taking into account a membrane lifetime of 8 years). With UF technology, the TCO part of 'pretreatment' will be approximately 0.12–0.16 US$ /m^3. Considering RO membrane replacement and cleaning, with conventional pretreatment technology as

© Woodhead Publishing Limited, 2011

the RO replacement and RO cleaning part of the TCO is approximately 6% of 0.85–0.90 US$/m^3, equalling approximately 0.05 US$/m^3. Membrane replacement and membrane cleaning each make up 50% of the cost; with UF pretreatment, RO cleaning will be reduced by 50% and RO replacement will be reduced by 15–30%. The weighted average of both costs will be reduced by 30–40%. With UF technology the part of the TCO related to RO membrane replacement and RO membrane cleaning will be approximately 0.03–0.04 US$/m^3.

In comparing of UF with conventional technology as pretreatment it is observed that:

- the 'fixed costs' part of the TCO is approximately 27% of 0.85–0.90 US$/m^3, equalling 0.23–0.24 US$/m^3. With UF technology the 'other fixed costs' part of the TCO will be approximately 0.22–0.23 US$/m^3, assuming an overall reduction of approximately 4% in the other fixed costs;
- the 'variable costs' part of the TCO is approximately 50% of 0.85–0.90 US$/m^3, equalling 0.42–0.45 US$/m^3. The same value has been assumed with UF as pretreatment.
- the TCO of the SWRO desalination plant is approximately 0.85–0.90 US$/m^3.

With UF as pretreatment the TCO of the dual membrane desalination plant will be 0.79–0.88 US$/m^3. This provides a reduction in TCO of 2–7% compared with conventional pretreatment. Table 4.1 gives a résumé of these results.

4.3.3 Integrated membrane systems for seawater desalination

This case relates to the comparison of different integrated membrane systems for seawater desalination using RO, with recovery of salts. In the last few years the reliability of RO integrated with other membrane separation systems

Table 4.1 Split of total costs of ownership (TCO) for various pretreatments of SWRO

	Conventional pretreatment (%)	Ultrafiltration pretreatment (%)
Pretreatment	17	17
RO membrane replacement and RO membrane cleaning	6	4
Other fixed costs	27	26
Other variable costs	50	50
Cost savings		3

© Woodhead Publishing Limited, 2011

has greatly increased. MF, UF and NF can be combined in pretreatment steps with RO (Macedonio et al., 2007).

It is also useful to compare different integrated membranes for seawater desalination when membrane distillation (MD) and membrane crystallization (MCr) techniques are used. In sea and brackish water desalination processes, the optimization and integration of various membrane units could contribute to reaching goals of better water quality, an increase in the recovery factor and marginal or zero brine production, with a consequent reduction in the environmental problems related to its disposal. Furthermore costs might be reduced and the quality of water increased. This approach is related to the process intensification that consists in the development of novel equipment and avant-garde techniques which, compared to those commonly used today, are expected to bring drastic improvements in manufacturing and processing, by decreasing the equipment size/production capacity ratio, energy consumption and waste production. In order to estimate the energy saving made in the processes, a methodology based on energy and exergy analysis has been used to establish, respectively, the energy requirements of the membrane integrated systems and their exergetic efficiency evaluated in terms of entropic losses.

In the study reported by Macedonio et al. (2007), seven flow sheets (FSs) for seawater desalination have been proposed, analysed and compared. In each of them, different membrane units have been integrated in pretreatment and post-treatment stages in order to reach the process intensification goals, overcoming the limits of the single units and, thus, improving the performance of the overall desalination process. The first three FSs work with 'conventional' membrane processes, such as MF, UF, NF and RO:

- FS1: constituted only by the RO unit,
- FS2: RO operates on NF permeate;
- FS3: both MF and NF have been introduced for the feed water pretreatment and load reduction to the following RO unit, with the aim of increasing the quantity of desalted fresh water produced with solid salts production

The other four FSs, integrate with the basic flow sheet represented by FS3, a membrane crystallizer module MCr:

- FS4: MCr operates on NF brine;
- FS5: MCr operates on RO brine;
- FS6: MCr operates both on RO and NF brines;
- FS7: MCr has been introduced on NF brine while MD operates on RO brine.

Economic analysis has been performed after a complete energetic and exergetic analysis that permits estimation of all the costs of raw materials, utilities and equipments, as described in Equation [4.22] to [4.32]. For the systems with

© Woodhead Publishing Limited, 2011

the MCr unit, it is necessary to add an equation to calculate the profit from the sale of the salts, in terms of annual profit for the salts (AP_{salts}):

$$AP_{salts} = SP\ SFR\ f\ 365 \quad [4.33]$$

where SP = salt price, SFR = salt flow rate and AP_{salts} is calculated in US$/year.

In further calculations, the following values have also been used: interest rate $I = 5\%$, plant life $n = 30$ years, amortization factor $a = 0.0651$ year^{-1}, plant availability $f = 0.9$, electric cost $c = 0.09$ US$/kWh, heating steam cost $s = 0.007$ US$/kg, specific chemicals cost $k = 0.025$ US$/m^3, by introducing MF as pretreatment $k = 0.018$ US$/m^3, specific cost of operating labour $\gamma = 0.05$ US$/m^3, by introducing MF as pretreatment $\gamma = 0.03$ US$/m^3, specific cost of brine disposal $b = 0.0015$ US$/m^3, specific maintenance and spare parts cost $p = 0.033$ US$/m^3.

Salts price:

- Na_2CO_3 price = 0.068 US$/kg
- NaCl price = 30 US$/t
- $MgSO_4 \cdot 7H_2O$ price = 570 US$/t
- $CaCO_3$ price = 62 US$/t.

Pumping and energy recovery system cost:

$$C_{pump\ or\ turbine} = 0.0151\ Ge\ P \quad [4.34]$$

where P = pressure (atm), Ge = flow rate (kg h^{-1}); NF/RO membrane cost = 30 US$/m^2, MF/MD membrane cost = 90 US$/m^2.

The membrane replacement rate varies between 20% per year for membranes treating high-salinity seawater to 10% per year for membranes treating low-salinity water supported by pretreatment systems. The unit cost of fresh water produced and the gain for the salts sale have been calculated. In all the flow sheets examined, the fresh water cost is lower than that of thermal desalination processes (about 1.5 US$/m^3) and ranges from 0.39 US$/m^3 for FS3 to 0.74 US$/m^3 for FS7. If the water stream is already available at the temperature needed to carry out the MCr operation or the thermal energy is available in the plant, the water cost is reduced to about 0.47–0.55 US$/m^3.

Thermal energy consumption depends on flow rate and temperature of the MCr feed: these parameters influence heater and membrane crystallizer size too and consequently they also affect membranes purchase and replacement cost. Furthermore, when the MCr feed flow rate rises, the unit water cost increases; when the temperature of the MCr feed grows, the fresh water cost is a minimum as a consequence of the increase in annual steam cost and transmembrane flux and the decrease in membrane replacement costs (Macedonio *et al.*, 2007).

© Woodhead Publishing Limited, 2011

4.3.4 Gas separation membrane in CO_2 post-combustion capture

Gas separation membranes used for post-combustion capture have been investigated by several authors (Favre, 2007; Hussain and Hägg, 2010; Car *et al.*, 2008). In a recent paper Zhao *et al.* (2010) describe a detailed parametric study for multi-stage membrane systems used in a coal-fired power plant, using CO_2/N_2 gas separation membranes for post-combustion capture. Both energy consumption and capture cost analyses have been carried out. The economic analysis process was explored for a cascade membrane system and a cost model was also developed in order to make a further analysis of the cascade variant; the correlation between membrane parameters (selectivity, permeability) and system performance (energy consumption, capture cost) has been also performed.

The whole simulation process has been divided into two steps. In the first step, two analyses have been carried out: the influence of membrane parameters on membrane area in order to achieve the specified target is analysed and the evaluation of various process parameters, components and membrane arrangements on energy consumption has also been done.

In the second step, the effect of the variation of membrane area and energy consumption on the capture cost has been analysed, with the aim of finding a correlation between the membrane parameters (selectivity and permeability) and the capture performance (energy consumption and capture cost). A comparison of the costs of capture cost for MEA absorption in the range 30–50 euro/$t_{\text{separated CO}_2}$ has been performed.

The reference power plant, in North Rhine-Westphalia (RKW-NRW) was chosen for the analyses. According to the different conditions of the feed gas and different capture purposes, two forms of staged membranes can be distinguished: the enricher (serial connection on the permeate side) and the stripper (parallel connection on the permeate side). The parameters used for the analysis were:

- Compressors and vacuum pumps have a pressure of 0.8 MPa and 3 kPa.
- Membrane CO_2/N_2 selectivity = 43, CO_2 permeance = 0.5 $Nm^3m^{-2}\ h^{-1}\ bar^{-1}$.
- The feed flow rate for each variant remains constant at 100 $Nm^3\ h^{-1}$;
- The degree of CO_2 separation of each variant is defined as 70%.

The depreciation time for the components of compressor, expander, vacuum pump, heat exchanger and membrane module was fixed at 25 years, and the lifetime of the membrane is 5 years.

The operations and maintenance (O&M) costs of the components of compressor, expander, vacuum pump and heat exchanger were assumed

© Woodhead Publishing Limited, 2011

to be 3.6% of the capital cost, and for the membrane and membrane frame the O&M cost is taken as 1% of the capital cost. The membrane cost is set at 50 euro/m^2 and the electricity price 3.37 euro cents/kWh. It should be emphasized that this price is the current power cost.

Total costs (TC) per year have been analysed in terms of capital cost (C_{cap}), including membrane, frame, compression equipment and heat exchanger, O&M costs ($C_{O\&M}$) and energy costs C_{en}; (all the costs are in euro/year):

$$TC = C_{cap} + C_{en} + C_{O\&M} \quad [4.35]$$

where:

$$C_{cap} = IC_c + IC_{vp} + IC_{ex} + IC_{he} + IC_m + IC_{mf} \quad [4.36]$$

$$C_{en} = t_{op}\,(h)\; P_{tot}(MW)\; 3.37 \text{ (euro cent/kWh)} \quad [4.37]$$

$$C_{O\&M} = 0.036\,(IC_c + IC_{vp} + IC_{ex} + IC_{he}) + 0.01\,(IC_m + IC_{mf}) \quad [4.38]$$

where IC_c estimates the investment cost of the compressor, IC_{vp} estimates the investment cost of the vacuum pump, IC_{ex} estimates the investment cost of the expander, depending on the energy recovered by the expanders, P_{ex}, IC_{he} estimates the investment cost of the heat exchanger and cooling facilities, IC_m estimates the investment cost of the membrane, depending on membrane area A_m (m^2) and IC_{mf} estimates the investment cost of the permanent membrane frame.

In Equation [4.37], Zhao *et al.* (2010) have introduced operation time t_p and total energy consumption P_{tot}, whereas in the Equations [4.36] and [4.38] they introduced specific investment costs (euro and million euro) as:

$$IC_c = 3 \text{ (Meuro) } 1.8 + 30 \text{ (Meuro) } 1.8 \quad [4.39]$$

$$IC_{vp} = 4.3 \text{ (Meuro) } 1.8 \quad [4.40]$$

$$IC_{ex} = P_{ex}(\text{MW})\; 0.3 \text{ (Meuro/MW) } 1.8 \quad [4.41]$$

$$IC_{he} = 3.5 \text{ (Meuro)} \quad [4.42]$$

$$IC_m = 0.064\; A_m(m^2)\; 50 \text{ (euro/}m^2\text{) } 0.225 \quad [4.43]$$

$$IC_{mf} = \left(\frac{A_m}{2000}\right)^{0.7} 0.25 \text{ (Meuro)} \quad [4.44]$$

On the basis of TC and of the total amount of CO_2 captured each year (TA_{CO_2}), the specific CO_2 separation cost SC_{CO_2} may be calculated, in euro/($t_{\text{separated } CO_2}$ y):

$$SC_{CO_2} = TC/TA_{CO_2} \quad [4.45]$$

Two cases have been taken into account relatively to different separation

© Woodhead Publishing Limited, 2011

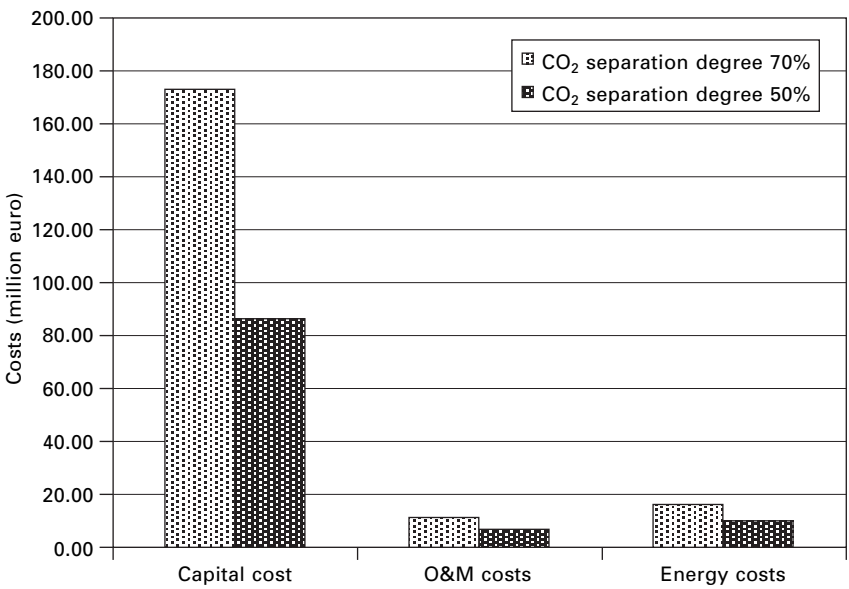
degrees, 70% and 50%. In the case of a 70% separation degree, the specific costs are higher than the 50% case. When the separation degree is 70%, *TC* = 201 Meuro and SC_{CO_2} = 110 euro/($t_{\text{separated } CO_2}$ *y*).

When the separation degree is 50%, *TC* = 105 Meuro and SC_{CO_2} = 80 euro/($t_{\text{separated } CO_2}$ *y*);

In Figs 4.2 and 4.3, comparison of the costs with a separation degree of 70% and one of 50% and the detail of capital costs are reported, respectively. The capture cost calculated shows the CO_2 separation expense using the existing infrastructure. The purpose is to reduce CO_2 emissions to the atmosphere. According to this view it is not the amount of carbon dioxide captured per unit of production (e.g. per kWh electricity) that is important, but the amount of carbon dioxide emission avoided. The amount of CO_2 avoided is less than the amount of CO_2 captured, so that the cost per ton of CO_2 avoided will be higher than the cost per ton of CO_2 captured. This aspect is also relevant for the processes where waste or pollutant compounds will be reused or avoided.

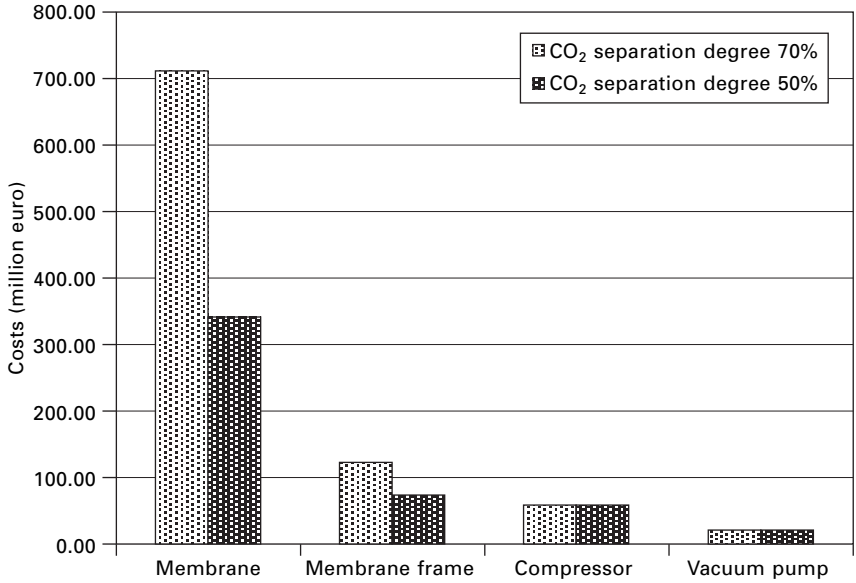
4.4 Conclusions and future trends

The analysis reported in this chapter using case studies already described offers an idea of the methods that might be applied for membrane applications in industrial situations. New investment as well as the introduction of membrane



4.2 Comparison of costs of a gas separation membrane for CO_2 capture with two different degrees of separation.

© Woodhead Publishing Limited, 2011



4.3 Comparison of detailed capital costs of a gas separation membrane for CO_2 capture with two different degrees of separation.

processes in existing plants have been taken into account, in order to offer a general view of possible membrane processes integration. The economic methods suggested can be applied to systems where the operating parameters have to be chosen or where the integration of membrane systems is required. The analysis presented in this chapter must be considered as just a starting point for economic analysis, which must be integrated at any time with optimization of the membrane processes as well as with the complete energetic evaluation of the whole process. Improvement in membrane properties, new material for membranes and optimization of the processes with new modelling approaches will permit better performances and consequently the costs of the processes where membrane systems are used should be reduced, with significant saving for processes innovations.

4.5 References

Burashid K, Hashim A, Kannari T, Tada K and Iwahori H (2005), 'UF membrane performance experience at Addur: expectation, reality and prospects', in *Proceedings IDA World Congress on Desalination and Water Reuse*, Singapore, 11–16 September 2005.

Calabrò V, Curcio S and Iorio G (2002), 'A theoretical analysis of mass transfer phenomena in a hollow fiber membrane bioreactor with immobilized biocatalyst', *Journal of Membrane Science*, **206**(1–2), 215–39.

Calabrò V, Curcio S and Iorio G (2008), 'Membrane bioreactors: modelling and analysis',

© Woodhead Publishing Limited, 2011

in *Membrane Reactors,* Basile A and Gallucci F (eds), Nova Science Publishers, Hauppauge, NY, USA.

Caneja J, Farinas M and Jimenez A (2005), 'Spanish cost data illustrate RO's competitiveness', *Desalination & Water Reuse*, **15**(1), 10–17.

Car A, Stropnik C, Yave W and Peinemann K V (2008), 'Pebax/polyethylene glycol blend thin film composite membranes for CO_2 separation', *Separation and Purification Technology*, **62**, 110–17.

Castilho L R, Polato C M S, Baruque E A, Sant' Anna G L Jr and Freire D M G (2000), 'Economic analysis of lipase production by Penicillium restrictum in solid state and submerged fermentations', *Biochemistry Engineering Journal*, **4**, 239–47.

Clunie W, Van deVenter L, Williams S and Garana E (2005), 'Comparison of pre-treatment alternatives for seawater reverse osmosis', in *Proceedings AWWA Membrane Technology Conference*, Phoenix, USA, 6–9 March 2005.

Côté P, Siverns S and Monti S (2005), 'Comparison of membrane-based solutions for water reclamation and desalination', *Desalination,* **182**, 245–51.

Curcio S, Calabrò V and Iorio G (2009), 'Reduction and control of flux decline in cross-flow membrane processes modeled by artificial neural networks and hybrid systems', *Desalination*, **236**, 234–43.

Di Luccio M, Borgesb C P and Alves T L M (2002), 'Economic analysis of ethanol and fructose production, by selective fermentation coupled to pervaporation: effect of membrane costs on process economics', *Desalination*, **147**, 161–6.

Favre E (2007), 'Carbon dioxide recovery from post-combustion processes: can gas permeation membranes compete with absorption?', *Journal Membrane Science*, **294**, 50–9.

GHD Fichtner (2005), *Sydney Water Planning for Desalination*, July 2005, http://www.sydneywater.com.au/EnsuringTheFuture/Desalination/DesalinationPlanning.cfm.

Gleuckstern P and Priel M (2003), 'Comparative cost of UF vs. conventional pretreatment for SWRO systems', *Desalination & Water Reuse*, **12**(4) and **31**(1), 34–9.

Groot W J, Kraayenbrink M R, van der Lans R GJ.M and Luyben K Ch A M (1993), 'Ethanol production in a integrated fermentation/membrane system. Process simulations and economics', *Bioprocess Engineering*, **8**, 189–201.

Henthorne L (2005), 'Economic evaluation of membrane and conventional SWRO pretreatment results from pilot study', in *Proceedings AWWA Membrane Technology Conference*, Phoenix, USA, 6–9 March 2005.

Hussain A and Hägg M B, (2010), 'A feasibility study of CO_2 capture from flue gas by a facilitated transport membrane', *Journal Membrane Science*, **359**, 140–8.

Knops F, van Hoof S, Futselaar H, and Broens L (2007), 'Economic evaluation of a new ultrafiltration membrane for pretreatment of seawater reverse osmosis', *Desalination*, **203**, 300–6.

Macedonio F, Curcio E and Drioli E (2007), 'Integrated membrane systems for seawater desalination: energetic and exergetic analysis, economic evaluation, experimental study', *Desalination,* **203**, 260–76.

Menge J, Haarhoff J, Konig E, Mertens R and Van der Merwe B (2001), 'Occurence and removal of Giardia and Cryptosporidium at the Goreangab Reclamation Plant,' *Water Science Technology, Water Supply*, **1** (1), 97–106.

Mody A, Dietrich J, Reiss R, Coates M, Owen C and McIntyre D (2005), 'Alternative pretreatment considerations for the Tampa Bay water gulf coast desalination project', in *Proceedings AWWA Membrane Technology Conference*, Phoenix, USA, 6–9 March 2005.

© Woodhead Publishing Limited, 2011

Pankratz T, (2006), *Water Desalination Report*, 42, (2), Texas Water Development Board, Texas, USA.

Rudd D F and Watson C C (1968), *Strategy of Process Engineering*, John Wiley and Sons, New York.

Zhao L, Riensche E, Blum L and Stolten D (2010), 'Multi-stage gas separation membrane processes used in post-combustion capture: Energetic and economic analyses', *Journal Membrane Science*, **359**, 160–72.

© Woodhead Publishing Limited, 2011

5

Membrane technology for carbon dioxide (CO_2) capture in power plants

A. BASILE, A. GUGLIUZZA and A. IULIANELLI, Institute on Membrane Technology of the Italian National Research Council, ITM-CNR, Italy and P. MORRONE, University of Calabria, Italy

Abstract: Polymeric membranes are mainly used today for CO_2 capture by membrane technology to produce clean fuel from a gas mixture (from coal gasification or steam reforming processes). Furthermore, gas separation using polymeric membranes is commercially available; nevertheless, CO_2 capture in large-scale power production by means of polymeric membranes still presents an inadequate performance owing to their lack of high-temperature stability. CO_2 capture using membranes is an ongoing innovative solution that can be applied in combination with all types of power plants, since its main benefit is the possibility of using membranes in combination with small-scale modular fuel cells. In contrast, the main drawback of the removal of carbon dioxide using commercially available membranes is the higher energy penalties on power generation efficiency with respect to a conventional chemical absorption process.

Key words: CO_2 capture, membrane modules, polymeric membrane.

5.1 Introduction

In the 1820s, Joseph Fourier (Grattan-Guinness, 1969) indicated that gases in the atmosphere might trap energy in the form of visible light received from the sun, which easily penetrates the atmosphere and heats up the surface. This represents the well known 'greenhouse effect'. In 1859, Tyndall identified several gases in the atmosphere, such as water vapour, carbon dioxide and methane, which can trap heat rays (Hulme, 2009). The most important gas is water vapour, which, however, as it has a very short atmospheric lifetime (about 10 days), is not a forcing gas in the context of global warming (Keeling *et al.*, 2008). In contrast, CO_2 is effective in altering the balance of heat radiation through the entire atmosphere. In fact, a good part of the radiation that rises from the surface is absorbed by CO_2 in the middle levels of the atmosphere. Its energy is transferred into the air itself rather than escaping directly into space.

In the 1960s, Keeling *et al.* (2008) directed a programme to measure the concentrations of CO_2 in the atmosphere. With a painstaking series of

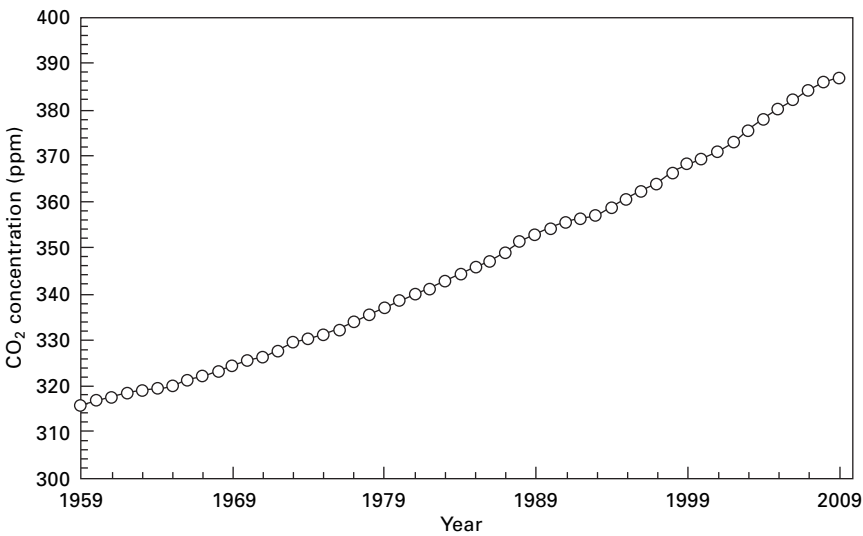
© Woodhead Publishing Limited, 2011

measurements in the pristine air of Antarctica and high atop the Mauna Loa volcano in Hawaii, a stable baseline level of CO_2 in the atmosphere was determined precisely. In 1960, with only two full years of Antarctic data, Keeling reported that this baseline level had risen. The rate of the rise was approximately what would be expected if the oceans were not swallowing up most industrial emissions.

Figure 5.1 reports the 'Keeling curve' of CO_2, measured at Mauna Loa, Hawaii into the twenty first century. The exponential trend points out, in particular, that the amount of gas added to the atmosphere is doubling every 30–35 years. Consequently, the observed increase in CO_2 concentration, most probably, has caused the increase in global average temperatures since the mid-twentieth century, as reported by the Intergovernmental Panel on Climate Change (IPCC) (Anon. 1; Anon. 2; Anon. 3; Keeling *et al.*, 2008).

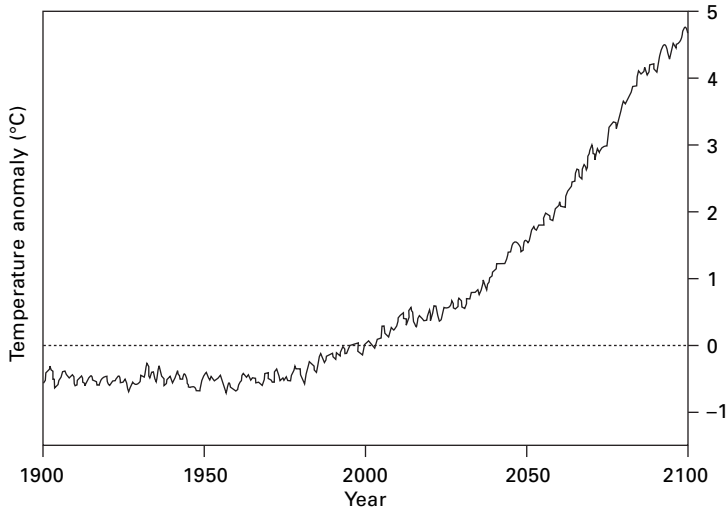
In particular, as shown in Fig. 5.2, the IPCC predicted an average global rise in temperature from 1.4–5.8°C between 1990 and 2100 (Anon. 1).

The detrimental effects of CO_2 and, in general, all greenhouse gases can be partially alleviated by reducing their emissions (Smith *et al.*, 2001). These reductions can occur by increasing the use of non-fossil fuel power sources, improving soil management, and so on (Pacala and Socolow, 2004). In particular, the Kyoto Protocol (Anon. 2) attributes greenhouse gas emissions to eight main economic sectors highlighting power stations (most burning coal or other fossil fuels), industrial processes (among them, cement production is a dominant contributor), transportation fuels (generally, fossil fuels) and

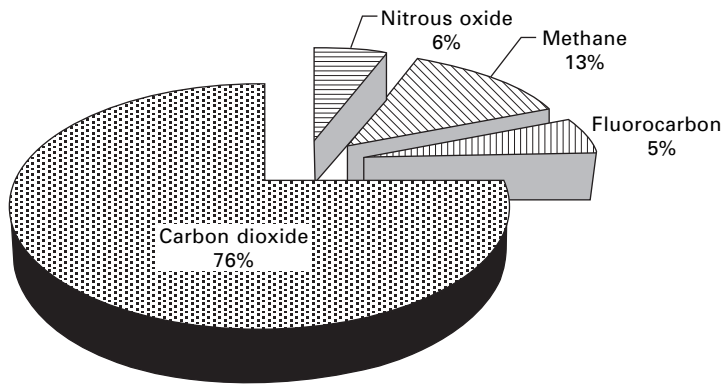


5.1 The 'Keeling curve' of atmospheric CO_2 concentrations measured at Mauna Loa, Hawaii, 1959–2009.

© Woodhead Publishing Limited, 2011



5.2 Predicted global warming at the end of the twenty first century.



5.3 Distribution of greenhouse gases in Earth's atmosphere.

agricultural by-products (mainly, methane from enteric fermentation and nitrous oxide from fertilizer use) as the largest contributors.

In this chapter, since CO_2 represents one of the most prominent greenhouse gases in Earth's atmosphere (Anon. 5), as shown in Fig. 5.3, particular attention is paid to the methods of reducing CO_2 emissions, particularly focusing on CO_2 sequestration using membrane technology. Emphasis is put on polymeric membranes since they are commercially attractive owing to the ease of processability, low operation temperature and reasonable costs with respect to the inorganic membranes.

© Woodhead Publishing Limited, 2011

5.1.1 Carbon dioxide (CO_2) sequestration and environmental problems

The IPCC expects that annual greenhouse gas emissions will double in the next 50–100 years. This will result in a cascade of environmental effects such as:

- melting of polar ice and oceanic expansion
- cold and warm gulf stream alteration caused by desalination of the Atlantic Ocean
- increase in the number and severity of tropical storms and cyclones
- flooding and erosion of agricultural plots
- major shifts in ecosystems and decreasing biodiversity
- saltwater penetration of groundwater zones.

In order to avoid these dramatic environmental effects, the scientific community is strongly involved in studying new technologies to reduce the greenhouse gases and, in particular, the amount of CO_2 (Kerr, 2007; Kintisch, 2007; Kluger, 2007). There are three strategies for lowering CO_2 emissions and mitigating climate change (Schrag, 2007):

(1) reduction of global energy use
(2) development of low or no-carbon fuel
(3) sequestration of CO_2 from point sources or atmosphere through natural and engineering techniques.

The first option requires an efficient use of energy, whereas the second option requires switching to using non-fossil fuels such as hydrogen and renewable energy. Thus, in order to meet mid-to-long term CO_2 reduction targets, CO_2 capture from fossil fuel use and the subsequent sequestration need to be evaluated. A brief description of sequestration methods is reported in the following:

- Geological sequestration involves capture, liquefaction, transport and injection of industrial CO_2 into deep geological strata. The CO_2 may be injected in coal seams, old oil wells (to increase yield), stable rock strata or saline aquifers. A by-product of coal and oil sequestration is enhanced methane production, which can be recovered and used to offset sequestration costs. In fact, the amount of methane is approximately half (by mol) that of CO_2 sequestered (Klara *et al.*, 2003; Tsang *et al.*, 2002).
- Ocean sequestration: the ocean is a primary component of the natural carbon cycle, acting as a reservoir that balances atmospheric CO_2 levels. Several ocean sequestration methods have been proposed:
  - ♦ Dissolution: CO_2 is injected by ship or pipeline into the water column at depths of 1000 m or more and is subsequently dissolved.

© Woodhead Publishing Limited, 2011

- Lake: CO_2 is deposited directly onto the sea floor at depths greater than 3000 m, where CO_2 is denser than water and it is expected to form a 'lake' that would delay dissolution of CO_2 into the environment.
- Convert CO_2 into bicarbonates (using limestone).
- Store the CO_2 in solid clathrate hydrates already existing on the ocean floor or grow more solid clathrate.

- Mineral sequestration aims to trap carbon in the form of solid carbonate salts. This process occurs slowly in nature and is responsible for the deposition and accumulation of limestone (calcium carbonate) over geologic time. Carbonic acid in groundwater slowly reacts with complex silicates to dissolve calcium, magnesium, alkalis and silica and leave a residue of clay minerals (Schuiling, 2006). The dissolved calcium and magnesium react with bicarbonate to precipitate calcium and magnesium carbonates. Ongoing research aims to speed up similar reactions involving alkali carbonates (Schuiling, 2006).
- Terrestrial sequestration is the net removal of CO_2 from the atmosphere or the avoidance of CO_2 emissions from terrestrial ecosystems into the atmosphere. The removal process includes CO_2 uptake from the atmosphere by all chlorophyllous plants, through photosynthesis (Lehmann *et al.*, 2006). This C is stored as plant biomass (in the trunks, branches, leaves and roots of the plants) and organic matter in the soil.

Carbon sequestration is a two-step process where the capture of CO_2 from a gas stream is followed by its permanent storage. The capture step contributes 75% to the overall carbon sequestration process cost (Anon. 3). For this reason, the scientific community has paid a great attention to the development of new processes for CO_2 capture. Currently, there are a wide range of technologies to separate CO_2 from gas streams, as shown in Fig. 5.4, although they have been not designed for power-plant scale operations (Desideri and Corbelli 1998).

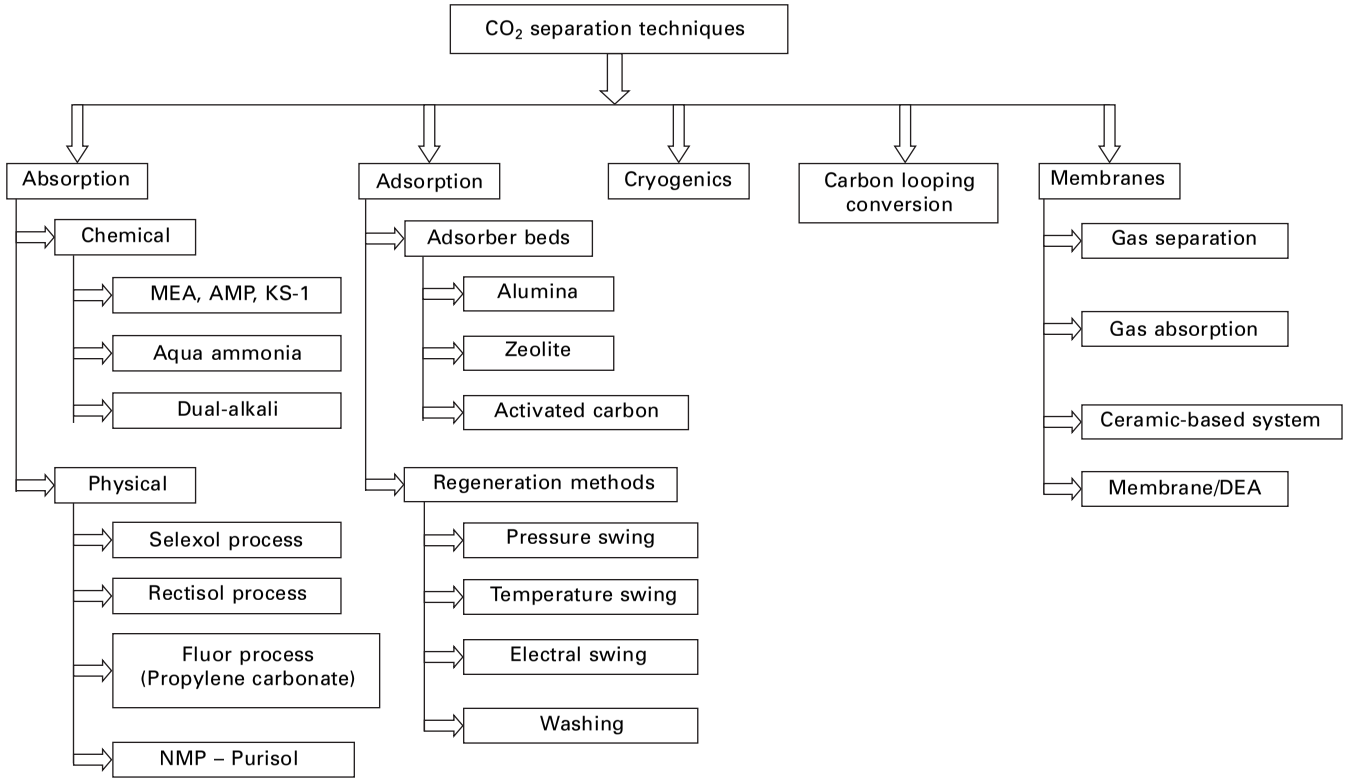
They are based on different physical and chemical processes including absorption, adsorption, cryogenics and membrane technology (Jeremy, 2000; Olajire, 2010). The choice of a suitable technology depends on the characteristics of the flue gas stream and, as a consequence, on the power-plant technology.

5.1.2 Conventional systems for CO_2 capture

Conventionally, CO_2 capture is the process for removing CO_2 produced by hydrocarbon combustion (coal, oil and gas) before entering into the atmosphere. It is an existing industrial technology widely used on a smaller scale in the manufacture of fertilizers, the food-processing industry and within the oil and gas sector (Gielen *et al.*, 2008). Nevertheless, CO_2 capture could

© Woodhead Publishing Limited, 2011

© Woodhead Publishing Limited, 2011

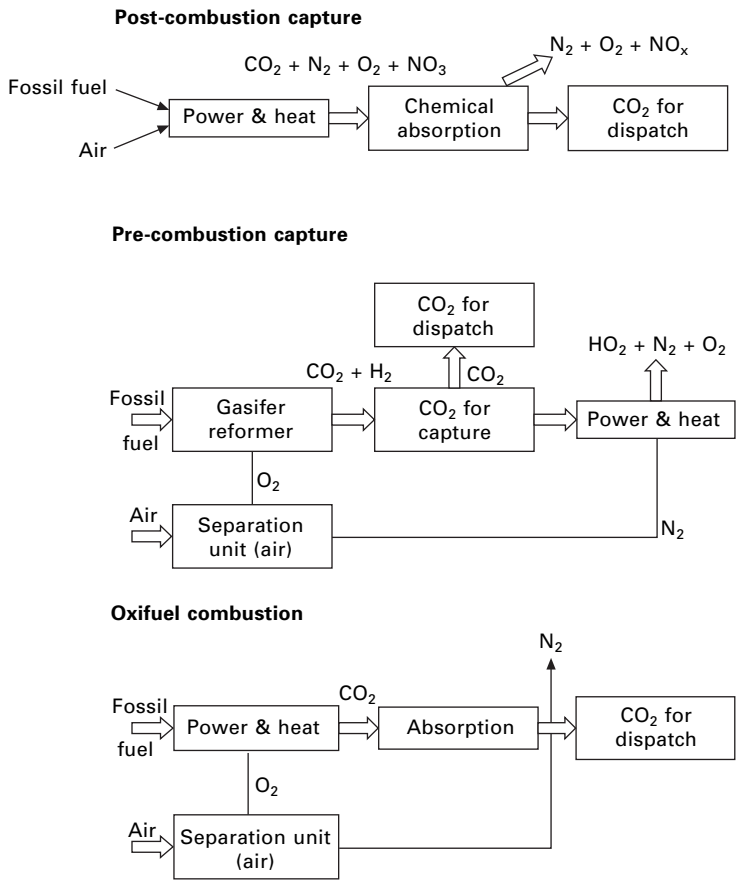


5.4 Technology options for CO_2 separation. AMP = aminomethyl propanol, DEA = diethanolamine, MEA = monoethanolamine, NMP = *N*-methyl pyrrolidone.

be most cost effective when it is used on large point sources of CO_2 such as power stations and industrial plants, which currently make up more than half of all man-made CO_2 emissions (Anon. 4).

The main challenge for any capture process is the low concentration of CO_2 in the flue gas. Depending on the industrial source, CO_2 content can vary from a few percent to over 50%. Other contaminant gases such as oxygen, sulphur oxides, water vapour and nitrogen can also be present in flue gases. Owing to both economic and energy costs, it would be impossible to compress and store all of them. Therefore CO_2 must be preferentially separated from the other flue gases by the capturing process.

There are currently three main methods for capturing CO_2 (Fig. 5.5) (Chiesa *et al.*, 2005; Figuero *et al.*, 2008; Gibbins and Chalmers, 2008; Haszeldine, 2007; Meisen and Shuai, 1997; Pennline *et al.*, 2008; Yang *et al.*, 2008):



5.5 Three different methods of CO_2 capture.

© Woodhead Publishing Limited, 2011

Oxy-fuel combustion capture

In oxy-fuel combustion capture, the fuel is combusted in the presence of nearly pure (approximately 98%) oxygen to ensure that the products of combustion (flue gas) contain CO_2 and water with only trace amounts of other gases. In this way, CO_2 recovery by means of condensation from a purge stream rich in CO_2 and water and with a very low nitrogen content is easier than from flue gas produced in conventional combustion, in which CO_2 is typically combusted in air made up of roughly 79.9% N_2 (Simbeck and Roekpooritat, 2009). The main problem with this method is separating oxygen from air. This separation is usually completed cryogenically, requiring a lot of energy. However, a promising new technology, 'chemical looping combustion' is under development. With this technique the oxygen in the air is removed through oxidation of a metallic compound, which can be reduced during combustion allowing the oxygen to be released. This process has a potential for 100% CO_2 capture.

Pre-combustion capture

Pre-combustion capture involves CO_2 removal prior to combustion. The capture process consists of three stages:

- the hydrocarbon fuel (typically methane, or gasified coal) is converted into hydrogen and carbon monoxide to form a synthesis gas;
- CO is converted into CO_2 by water gas shift reaction;
- CO_2 is separated from hydrogen, which could be combusted cleanly. The CO_2 can be compressed into liquid and transported to a storage site.

The benefits of this process are:

- verified industrial scale technology in oil refineries
- 90–95% of CO_2 emissions capture
- applicable to natural gas and to coal fired integrated gasification combined cycle (IGCC) power plants.
- lowest technology risk with the possibility of becoming the most efficient method
- it can produce H_2 as a transportable energy carrier or liquid fuels from coal, but paying penalties for efficiency.

Nevertheless, pre-combustion capture requires high investment costs for dedicated new-build plant as well as high NO_x emissions, requiring expensive scrubbers.

© Woodhead Publishing Limited, 2011

Post-combustion capture (PCC)

Post-combustion capture is useful for separating CO_2 from exhaust gases created by burning fossil fuel. The exhaust gases, a mixture of CO_2, nitrogen and some oxygenated compounds (SO_2, NO_2 and O_2) are first treated to remove particulate matter and the oxides of nitrogen and sulphur. Generally, they are in contact with a liquid solvent, typically an aqueous amine solution. The amine selectively absorbs the CO_2, capturing more than 85% of the CO_2 and enabling nitrogen and oxygen to be released into the atmosphere. A CO_2-rich amine is regenerated by stripping the CO_2 out of the liquid with steam, allowing the lean amine to be recycled to the absorber while producing a concentrated CO_2 stream. The CO_2 is compressed and cooled in liquid form. The benefits of this process are.

- PCC can be typically built into existing industrial plants and power stations (known as retro-fitting) without significant modifications to the original plant.
- PCC can be integrated into new plants to achieve a range of greenhouse gas intensity reductions near to zero emissions.
- In contrast to competing technologies, PCC offers high operational flexibility (partial retrofit, zero to full capture operation) and it can match market conditions for both existing and new power stations.
- PCC offers a lower technology risk compared to competing technologies; this is further enhanced by the ability for staged implementation, which is not possible with competing technologies.
- Renewable technologies can be integrated in the PCC process, in particular, PCC allows the use of low-cost solar thermal collectors to provide the necessary heat to separate CO_2 from sorbents, effectively reducing the loss of electrical output caused by capture.
- PCC can be applied to capture CO_2 from natural gas fired power stations and other large stationary sources of CO_2, for instance, smelters, cement kilns and steelworks.

The potential of these technologies are summarized in Table 5.1.

In particular, separation techniques for CO_2 capture such as pressure swing adsorption, amine absorption and cryogenic separation have been widely used in industry for CO_2 separation in chemical and petrochemical applications (Drioli and Romano, 2001; Simmonds *et al.*, 2003). For example, the amine-based absorption with an aqueous monoethanolamine (MEA) solution is the most common technology used for post-combustion capture, since it is capable of achieving a high level of CO_2 capture (more than 90%) from flue gas owing to fast kinetics and a strong chemical reaction. Nevertheless, the amines are corrosive, predisposed to degradation by trace flue gas constituents such as sulphur oxides and require a considerable amount of energy, mainly in the regeneration step (Choi *et al.*, 2009; Maneeintr *et al.*, 2010).

© Woodhead Publishing Limited, 2011

Table 5.1 Potential of CO_2 capture technologies

Post-combustion	Pre-combustion	Oxyfuel combustion
• Applicable to the majority of existing coal-fired plants • Low CO_2 partial pressure • Significantly higher performance or circulation volume is required for high capture levels. • CO_2 produced at low pressure compared to sequestration requirements. • Retrofit technology option • Improved solvents may reduce energy losses. • Significant cost savings are possible.	• Generally higher CO_2 concentration than for post-combustion capture • Higher driving force for CO_2 separation • Fuel processing is needed. • Potential for reduction in compression costs/loads • For coal plants, efficiency and cost penalties are generally lower than for post-combustion capture • Barriers to commercial application of gasification are common in pre-combustion capture • Extensive supporting systems requirements	• Very high CO_2 concentration in flue gas • Combustors would be fairly conventional • Large cryogenic oxygen production requirement may be cost prohibitive • Need to recycle large quantities of flue gas to avoid excessively high combustion temperatures • CO_2 is recycled to the compressor to provide the expansion medium, instead of air • Novel turbine cycles have been proposed, which eliminate shift reaction/fuel gas CO_2 separation • Potential for advanced oxygen separation membranes with lower energy consumption • Decreased process efficiency

Cryogenic CO_2 capture is constituted by many steps, some of them reported below:

- cooling of CO_2-laden flue gas to desublimation temperatures (from –100 to –135°C)
- separation of solid CO_2 formed from flue gas
- use of the cold products to cool incoming gases in a recuperative heat exchanger
- compression of the solid/liquid CO_2 to final pressures (100–200 atm; 10.13–20.27 MPa)
- delivering of a compressed CO_2 stream separated from an atmospheric pressure light-gas stream.

The overall energy and economic costs appear to be at least 30% lower than most competing processes involving air separation units, solvents or similar technologies. In addition, the cryogenic CO_2 capture process shows several benefits (Bolland and Undrum, 2003), including:

- no chemical absorbents are required;
- it can be operated at atmospheric pressure;

© Woodhead Publishing Limited, 2011

- it provides highly efficient removal of many pollutants (Hg, SO_x, NO_2, HCl, etc.);
- possible energy storage capacity, and
- potential water savings.

Cryogenic separation is widely used commercially for streams that have high CO_2 concentrations (typically > 90%), but it is not used for more dilute CO_2 streams. In fact, the major disadvantage of CO_2 cryogenic separation is the amount of energy required to provide the refrigeration necessary for the process, particularly for dilute gas streams.

5.2 Reasons for using membranes for carbon dioxide (CO_2) separation and sequestration

As an alternative to conventional processes for CO_2 separation and capture, membrane technology shows great potentiality for CO_2 capture (Abertz *et al.*, 2006; Basu *et al.*, 2004) owing to its easy applicability, efficiency, flexibility, ability to maintain high CO_2 pressure and to perform separations at low energy penalties (Kohol and Nielsen, 1997). CO_2-selective membranes allow separation of CO_2 from different gas streams, such as:

- flue gas (post-combustion system)
- natural gas (natural gas processing)
- hydrogen (pre-combustion systems) or oxygen from nitrogen (in an oxyfuel combustion system).

Furthermore, membranes have a number of innate advantages over other separation techniques, including simple design with no moving parts, limited maintenance, single-step separation, exceptional reliability (Mazur and Chan 1982) and they can be retrofitted easily onto the tail end of power-plant flue gas streams without requiring complicated integration (Perry *et al.*, 2006). Moreover, membranes do not need to have chemicals added to them or to regenerate an absorbent/adsorbent.

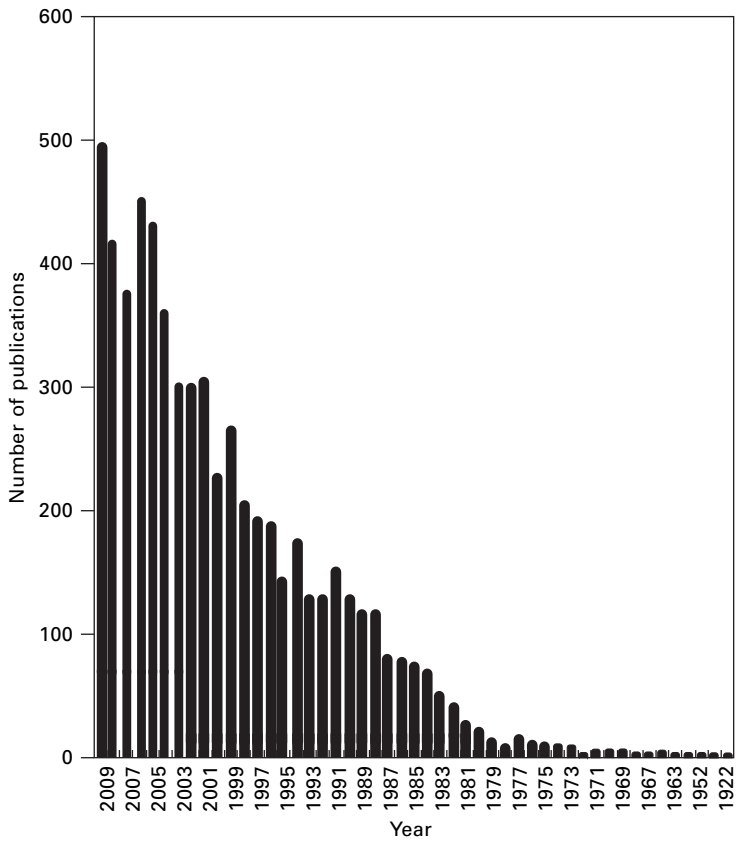
The aforementioned benefits, mainly the energy efficiency and easiness in applicability, have allowed membranes to make significant commercial advances in some CO_2 removal applications such as natural gas sweetening (Abertz *et al.*, 2006; Basu *et al.*, 2004; Feron, 1992). In contrast, membrane technology is not yet used commercially to recover CO_2 from flue gas, although membranes seem a natural choice for carbon capture from flue gas, where pressures and CO_2 concentrations are high (Coady and Davis, 1982; Mazur and Chan, 1982; Spillman, 1989). In particular, their widespread application on the industrial scale is limited by the fact that most membranes have been tested on the bench scale and under relatively ideal conditions rather than in a real industrial environment. Another reason for their relatively little use

© Woodhead Publishing Limited, 2011

today is that pressure swing adsorber (PSA) and cryogenic distillation are mature technologies based upon well-established industrial knowledge.

5.3 A short review of membrane technology for CO_2 separation

The growing interest in the membrane processes utilized in industry, biomedical engineering and space science is reflected by the consistent number of publications in the scientific open literature (Anon. 5), Fig. 5.6. In particular, the concept of membrane separation was originally proposed by Graham in 1866 for separating a solution into its components (Graham, 1866). Initially, the main application of membrane separation was reverse osmosis (Jawad, 1989; Podall, 1971). Subsequently, from the 1980s to 1990s, substantial innovations in membrane materials were studied such as



5.6 Number of published papers per year on membrane applications in the gas separation field (Elsevier Scopus database).

© Woodhead Publishing Limited, 2011

an improvement in the gas separation efficiency and membrane durability, making membrane gas separation commercially competitive with respect to the existing separation technologies (Coady and Davis, 1982; Mazur and Chan, 1982; Paul and Yampolskii, 1994).

Membranes for gas separation can be classified as:

- polymeric (organic)
- inorganic (metallic and porous)
- mixed-matrix (hybrid)
- supported-liquid/facilitated transport.

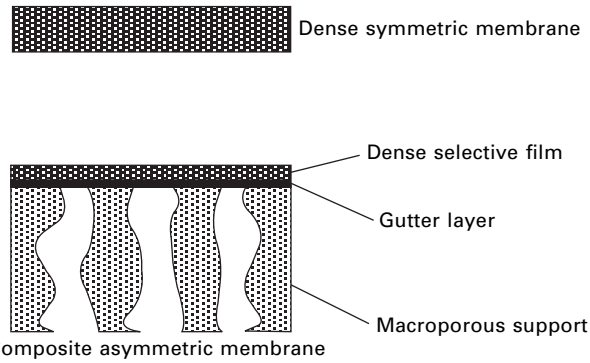
5.3.1 Polymeric membranes: from glassy to rubbery membranes

Four types of membrane are usually operated in gas separation, including metallic, ceramic, carbon and polymeric. Despite limited robustness and relatively high sensitivity to ageing and swelling, their use in gas separation finds large application, especially when mild operating conditions are requested. Their utilization takes advantage of low capital cost of fabrication, good processability, ability to cope with high pressure-drops, long-term operation under mild conditions and good scalability. All these aspects make them extremely attractive and more economically competitive than inorganic membranes. Keeping in mind the benefits and shortcomings of the various categories, the development of high-performance polymeric membranes for CO_2 separation will be a key issue in the coming years.

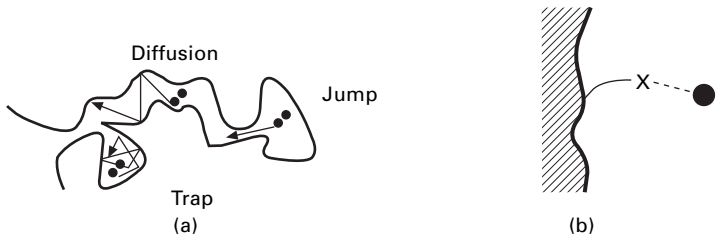
In gas separation, dense polymeric films with integrated skin or composite systems involving a thicker microporous support adjacent to the dense layer are normally used. In composite asymmetric systems, the porous support offers simply a mechanical reinforcement for thin dense selective film. Sometimes, a highly permeable gutter layer is interspaced between the support and selective layer (Fig. 5.7). In this second case, a less thick membrane can be realised, preventing rupture and formation of defects that cause the efficiency abatement of the active layer. Depending on the composition of gaseous streams and the operating conditions, the development of polymeric membranes for a desired gas separation necessarily requires a careful assessment of both materials and assembly procedures.

In this respect, CO_2 removal and sequestration can be achieved by polymeric membranes according to different controlling mechanisms based on diffusivity or solubility selectivity, respectively. Considering a binary gas mixture, the ideal selectivity can be regarded as a result of the thermodynamic and kinetic contributions to the overall selectivity, if the solution–diffusion model ($P = DS$) is considered. The solubility selectivity depends on the penetrant condensability, interaction of the penetrant–polymer chains and,

© Woodhead Publishing Limited, 2011



5.7 Scheme of different morphologies of polymeric membranes used in gas separation.



5.8 Scheme representing mobility of the penetrant in the bulk of the matrix (a) and membrane affinity for the penetrant (b).

in some cases, fractional free volume (FFV) of the polymeric network where the penetrating molecules can be allocated (Fig. 5.8(a)). In contrast, the diffusivity selectivity is strongly affected by the penetrant size and shape, the cohesive energy density of the polymer, the mobility of the polymer chains and '*d*-spaces' for diffusional jumps through the inter-segmental distance between the polymer chains (Fig. 5.8(b)). Depending on the materials, one contribution can override another one.

CO_2 transport through glassy membranes is governed by the movement of the gas through gaps, provisional cavities and *d*-spaces embedded in the rigid polymer networks. This means that diffusivity predominates over selectivity. The major difficulty is just to achieve membranes with D_x/D_y larger than S_x/S_y. For this reason, much effort in the development of glassy membranes has been addressed at reducing the distribution of free volume and improving the degree of interconnectivity of the channels in order to create small and stable *d*-spaces for diffusional jumps of the penetrant and yield enhanced molecular discrimination (Fig. 5.8(b)). The majority of existing polymeric membranes exhibit unfavourable selective properties with respect to the upper-bound relationships by Robeson (2008). However, keynote investigations

© Woodhead Publishing Limited, 2011

have recently offered new insights into the development of polymer-based gas separation membranes with the desired selectivity properties. Tailor-made polymer membranes have been realised through molecular design and chemical modification of polymers, including polyamides (Table 5.2), polycarbonates (Table 5.3), polyarylates (Table 5.4), polypyrrolones (Table 5.5) and polysulphones (Table 5.6).

Among the various polymers, the polyimides (Matrimid®) are of particular interest for the rigidity and stiffness of their fused ring structures. Matrimid® hollow fibre membranes, prepared by imidization of polyamic acid, exhibited CO_2 permeability of 12.7 Barrer with an ideal CO_2/CH_4 selectivity of 40 at a pressure of 20 bar. For a binary mixture feed of 5 mol% CO_2 in CH_4, a reduction of the permeability to 7.4 Barrer and selectivity to 21 were achieved, respectively (Sridhar *et al*., 2007). High-performance membranes from polyimides with intrinsic microporosity have been proposed by Ghanem *et al*. (2008). High permeability and good selectivity have been combined with excellent thermal stability, yielding CO_2/N_2 of 23 and CO_2/CH_4 of 19 with CO_2 permeability up to 3700 Barrer. Although Matrimid® membranes behave like glassy matrixes, the nano cavities enable the allocation of larger amount of penetrant, causing an enhancement in permeability without loss of selectivity. Of particular interest is the effect of cross-linking Matrimid® membranes by a *p*-xylenediamine solution at ambient temperature (Tin *et al*., 2003). As expected, cross-linking reduced the permeability of CO_2 and CH_4 when mixed, but a surprising greater selectivity was achieved for mixed gases than pure gases. This was ascribed to a reduction of the free volume, mobility of the polymer segment chains and related *d*-spaces which have a different impact on the diffusivity of the linear CO_2 and spherical CH_4. Similarly, Matrimid® cross-linked with poly(propylene glycol), block poly(ethylene glycol) and block poly(propylene glycol) diamine (PPG/PEG/PPGDA) produced an ideal CO_2/N_2 selectivity of 52.49 (Zhao *et al*., 2008a). Undoubtedly, cross-linking revealed itself to be a promising strategy for enhancing the H_2/CO_2 gas pair selectivity (Chung *et al*., 2006). A value of 101 was achieved for pure gas, far superior to the other polymeric membranes and above the Robeson's upper-bound curve, while a smaller separation factor (42 for mixed gases) was ascribed to the highest solubility of CO_2 (Fig. 5.9 and 5.10).

Recently, it was demonstrated that the molecular design of polymides coupled with modified amine can direct the selectivity (up to 120) for the H_2/CO_2 gas pair by controlling polymer free volume and chain stiffness, leading to modified polymer networks with restricted mobility of the polymer segments and, consequently, optimized molecular discrimination (Low *et al*., 2009).

Another strategy used to improve the performance of Matrimid® for gas separation is blending (Hosseini *et al*., 2008). Mixtures of Matrimid® with

© Woodhead Publishing Limited, 2011

Table 5.2 CO_2 and N_2 gas permeability data for dense films incorporating polyimides

Name	Feed pressure (atm)	Temperature (°C)	P_{CO_2} (Barrer)	P_{N_2} (Barrer)	α_{CO_2/N_2}	Ref.
PMDA-BAPHF	6.8	35	11.8	0.66	17.8	Stern *et al.* (1989)
PMDA-4.4′-ODA	10	35	2.71	0.10	27.1	Stern *et al.* (1989)
PMDA-MDA	10	35	4.03	0.20	20.2	Kim *et al.* (1988)
DMeCat-durene	1	30	63	2.05	31	Al Masri *et al.* (2000)
BPDA-mTrMPD	10	35	137	8.42	16.3	Tanaka *et al.* (1992a)
BTDA-4.4′-ODA	10	35	0.63	0.02	26.5	Tanaka *et al.* (1992b)
TMMPD	3	–	600	35.1	17.1	de Abajo *et al.* (2003)
IMDDM	3	–	196	10.8	18.1	de Abajo *et al.* (2003)
6FDA-FDA/ HFBAPP(1/1)	–	30	465	19.9	23.4	Chun *et al.* (1994)
6FDA-BAFL	1	25	98	3.3	29.7	Kazama *et al.* (2002)
Matrimid 5218	10	35	6.5	0.25	25.6	Tin *et al.* (2003)

PMDA = pyromelletic daihypride; BAPHF = 2,2-bis(4-(4-aminophenoxy)phenyl)hexafluoropropane; ODA = dianhydride/oxydianiline; MDA = 3,3-methylenedianiline; DMeCat = dimethylethercatecholate dianion; BPDA = biphenyltetracarboxylic dianhydride; TrMPD = 2,4,6-trimethyl-1,3-phenylene diamine; BTDA = 3,3′,4,4′-tetracarboxylicbenzophenone dianhydride; TMMPD = 4,6-trimethyl-1,3-phenylenediamine; IMDDM = methylene bis(3isopropyl-5-methyl-4-aminobenzene); HFBAPP = 2-bis[4-(4-aminophenoxy)phenyl] hexafluoropropane; BAFL = 9,9-bis(4-aminophenyl)fluorine.

© Woodhead Publishing Limited, 2011

Table 5.3 CO_2 and N_2 gas permeability data for dense films incorporating polycarbonates

Name	Feed pressure (atm)	Temperature (°C)	P_{CO_2} (Barrer)	P_{N_2} (Barrer)	α_{CO_2/N_2}	Ref.
PC	1	35	6.0	0.289	21	Hellums *et al*. (1989)
	10		6.8	0.32		
TMPC	1	35	17.58	1.09	16.1	Hellums *et al*. (1989)
	10		18.6	1.0	18.6	
TBPC	1	35	4.23	0.182	23.2	Muruganandam and Paul (1987)
HFPC	10	35	24	1.6	15.0	Hellums *et al*. (1989)
TMHFPC	10	35	111	7.4	15.0	Hellums *et al*. (1989)
FBPC	2	35	15.1	0.592	25.5	Aguilar-Vega and Paul (1993)

TMPC = tetramethyl bisphenol-A polycarbonate; TBPC = tetrabromo polycarbonate; HFPC = hexafluorobisphenol A polycarbonate; TMHFPC = tetramethylhexafluoropolycarbonate; FBPC = fluorene bisophenol polycarbonate.

Table 5.4 CO_2 and N_2 gas permeability data for polyarylate dense films

Name	Temperature (°C)	P_{CO_2} (Barrer)	P_{N_2} (Barrer)	α_{CO_2/N_2}	Ref.
BPA/IA	35	5.4	0.24	22.5	Pixton and Paul (2003)
HFBPA/IA	35	19.1	1.11	17.2	Pixton and Paul (2003)
PhTh/tBIA	35	23.8	1.09	21.8	Pixton and Paul (2003)
HFBPA/tBIA	35	56.9	3.88	14.7	Pixton and Paul (2003)
TBFBP/IA	35	20.4	0.70	29.1	Pixton and Paul (1995)
TBFBP/tBIA	35	69.5	2.94	23.6	Pixton and Paul (1995)
TBHFBPA/tBIA	35	85.1	4.47	19.0	Pixton and Paul (1995)

BPA/IA = bisphenol A isophthalate; HFBPA = hexafluoro bisphenol A tertiary butyl; PhTh/tBIA = phthalate/5-tert-butylisophthaloyl dichloride; TBFBP = tetrabromofluorene bisphenol; TBHFBPA = tetrabromo hexafluoro bisphenol A tertiary butyl.

Table 5.5 CO_2 and N_2 gas permeability data for polypyrrole dense films

Name	Temperature (°C)	P_{CO_2} (Barrer)	P_{N_2} (Barrer)	α_{CO_2/N_2}	Ref.
6FDA-TAB	35	54.0	2.6	20.8	Zimmerman and Koros (1999a)
6FDA-TADPO	35	27.6	1.2	23.0	Walker and Koros (1991)
BBL	35	0.12	0.0026	46.3	Zimmerman and Koros (1999b)

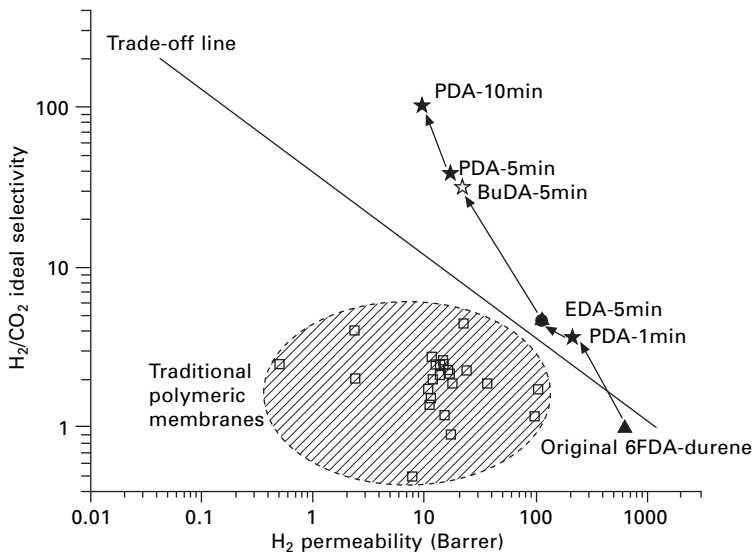
TAB = tetramino benzene; TADPO = tetramino diphenyl ether; BBL = benzimidazo benzophenanthroline-type ladder polymer.

© Woodhead Publishing Limited, 2011

Table 5.6 CO_2 and N_2 gas permeability data for dense films incorporating polysulphones

Name	Temperature (°C)	P_{CO_2} (Barrer)	P_{N_2} (Barrer)	α_{CO_2/N_2}	Ref.
PSF	35	5.6	0.25	22.4	McHattie *et al.* (1991)
TMBIPSF	35	31.8	1.21	26.3	Aitken *et al.* (1992)
2.6-NPSF	35	1.5	0.051	29.4	Aitken and Paul (1993)
HMBIPSF	35	25.5	1.2	23.3	Aitken *et al.* (1992)
FBPSF	35	13.8	0.484	28.5	Aguilar-Vega and Paul (1993)

PSF = polysulphone; TMBIPSF = tetramethylbiphenol polysulphone; NPSF = naphthalenepolysulphone; HMBIPSF = hexamethyl biphenol polysulphone; FBPSF = fluorene bisphenol polysulphone.

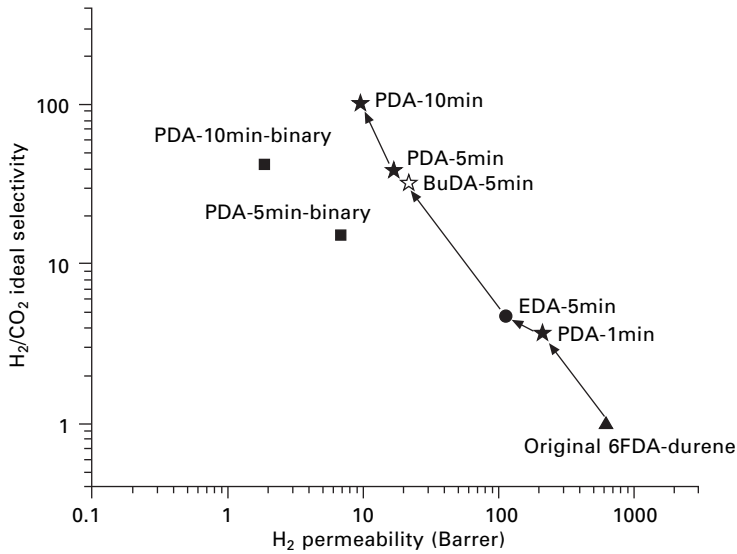


5.9 Pure gas separation properties of H_2/CO_2 for membranes derived from 6FDA-durene with respect to the upper-bound curve (Chung *et al.*, 2006). PDA = phenylenediamine, EDA = ethylenediamine, FDA = fluoropropanediimide, BuDA = diaminobutane.

polybenzimidazole (PBI) 25/75 brought about an improvement of H_2/CO_2 (9.43) and CO_2/CH_4 (59.79) selectivity with respect to more traditional membranes prepared from pure Matrimid®. A factor of separation of 9 was also achieved by doping polyanilines with counter ions, causing changes in the *d*-spacing within the polymer network.

Although the previous methodology brought about an improvement in selectivity, a significant reduction in permeability has often been observed, whereas it should be desirable to obtain a compromise between high selectivity and high permeability. Preliminary studies carried out on

© Woodhead Publishing Limited, 2011



5.10 Comparison between pure gas and mixed gas separation properties of H_2/CO_2 for membranes derived from 6FDA-durene (Chung *et al.,* 2006).

mixed composite membranes encourage further research in this direction. Polysulphone/zeolite 3A MMM membranes have been prepared by using aminopropyltrimethoxysilane as a coupling agent to improve the adhesion between the organic and inorganic phases and a H_2/CO_2 selectivity of 72 and a corresponding H_2 permeability of 7.1 Barrer have been achieved (Guiver *et al*., 2002). Khan *et al*. (2010) prepared mixed matrix membranes from derivatized polysulphone and zeolite particles, increasing the H_2/CO_2 separation from 1.53 for pure polysulphone to 3.57 for 40% zeolite loading. The dispersion of multi-walled carbon nanotubes MWCNTs in a poly(bisphenol A-*co*-4-nitrophthalicanhydride-*co*-1,3-phenylene diamine) (PBNPI) brought about a H_2 permeability of 14 Barrer with a H_2/CO_2 selectivity of 6 at 15% loading. Also, polyimides mixed with silica exhibited a CO_2 permeability of 150 with a CO_2/N_2 selectivity of 28 (Suzuki and Yamada 2005), whereas an abatement of the permeability (0.21 Barrer) versus a selectivity of 31 was estimated for polyetherimides/zeolite membranes (Husain and Koros, 2007). Matrimid-containing carbon aerogel exhibits enhanced separation for CO_2/CH_4 gas pairs (51.9 vs 46.9 for pure gas), owing to penetration being facilitated in the polymer chain in mesopores, whose shape and size lead to higher molecular discrimination (Zhang *et al*., 2008).

Undoubtedly, nanoparticles embedded in polymer matrix affect the polymer chain packing density, causing gaps through which the penetrant can easily diffuse. On the other hand, well-functionalized nanoparticles can improve

© Woodhead Publishing Limited, 2011

the solubility discrimination of specific membranes, resulting in better solubility selectivity. This approach is attracting more attention, but there are shortcomings to overcome in order to obtain efficient and productive membranes. One of them is to obtain uniform dispersion of the nanoparticles in the polymer matrixes, preventing them from leaching or adhering to each other. One approach could be to connect the particles to the polymers via covalent bonds or functionalize them in order to improve compatibility with the attractive interactions of polymer chains through van der Waals forces or hydrogen-bonds via blending (Akagi *et al.*, 2010; Jeon and Baek, 2010), *in situ* polymerization (Li and Sun, 2010; Sun and Yang, 2008), sol–gel (Schmidt *et al.*, 2000) and layer-by-layer (Kotov, 2003) methods.

Considering that selectivity through rubbery polymers is governed by solubility, while separation through glassy polymers is mainly directed by diffusivity selectivity, the intrinsic properties of the gases forming the stream are evaluated and it is decided whether to favour thermodynamic or kinetic separation. Considering the high condensability of CO_2, its competitive ability to dissolve itself in polymer matrixes and to form intermolecular interactions with polar moieties, CO_2 capture via mechanisms directed by the solubility selectivity appear to be attractive. CO_2-selective membranes, known as 'reverse-selective-membranes', are usually derived from rubbery materials and promote separation where the thermodynamic selectivity predominates over the kinetic selectivity. A class of rubbery membranes with a singular ability to separate CO_2 from gaseous streams is that of block copolymers, resulting in higher performance than homopolymer analogues (Guan and De Simone, 1994).

Poly(ethylene oxide) (PEO) is, for example, one of the most interesting materials for CO_2 separation, especially when cross-linked to another polymer or inserted in block copolymers (Lin *et al.*, 2006; Pethe *et al.*, 2008). Because of its amorphous character and flexibility, it suitably directs the permselectivity of CO_2 through polymeric matrixes, especially when segment length, molecular weight and ratio with the other hard blocks of the copolymer are changed. Bondar *et al.* (2000) observed that the CO_2 permeability increased with the amount of polyether (PEO or poly(tetramethyleneoxide), PTMEO) incorporated in polyether-*b*-polyamide segmented block copolymers, where the hard phase is formed by nylon-6 (PA6) or nylon-12 (PA12). Specifically, they observed that 57PEO/PA6 and 55PEO/PA12 copolymers exhibit the best pure gas selectivity for CO_2/N_2 56 (P_{CO_2} 66 Barrer) and CO_2/H_2 9.8 (P_{CO_2} 20 Barrer), respectively, compared with more conventional rubbery and glassy polymers. A higher performance is observed as more polar units (PEO and PA6) are incorporated into the polymer segment chains, suggesting a critical role of attractive polar intermolecular interactions at the polymer chain/penetrating molecule.

Tailor-made PEO/PBT (poly(butylene terephthalate)) membranes have been

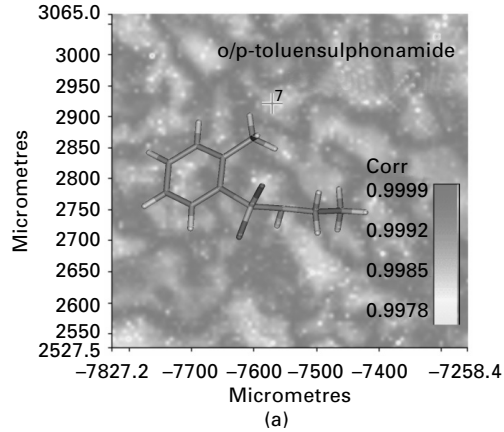
© Woodhead Publishing Limited, 2011

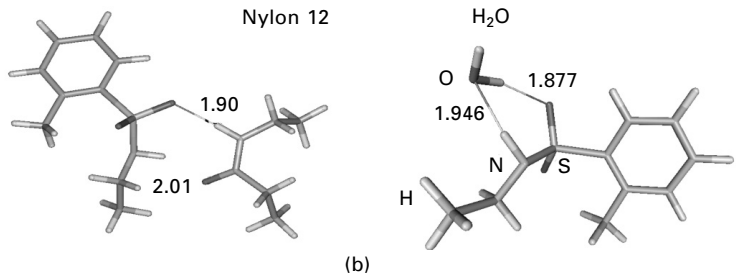
designed to achieve high-performance block copolymers for CO_2 separation (Car *et al.*, 2008a). Separation factors for CO_2/H_2 10.6, CO_2/N_2 50 and CO_2/CH_4 20 gas-pairs have been achieved at different soft/hard ratios of polymer segment chains. When blended with poly(etherglycol) (PEG), a significant improvement in permeability and selectivity has also been observed for various block copolymers. A CO_2/H_2 selectivity of 11 and CO_2 permeability of 150 Barrer have been estimated for polyether-*b*-polyamide segmented block copolymers, whereas an increase in CO_2 permeability and selectivity for the CO_2–H_2 gas-pair has been measured for PEO–PBT (500PEO77PBT23) at 30 wt% of PEG (Yave and Peinemann 2010). The addition of a physical solvent for acid gas absorption such as PEG-dimethylether (PEG-DME) to the polyether-*b*-polyamide copolymer resulted in an eight-fold increase in the carbon dioxide permeability and CO_2/H_2-selectivity increased simultaneously from 9.1 to 14.9 (Car *et al.*, 2008b; Zhao *et al.*, 2008b). Indeed, PEG affinity to quadrupolar gas is large enough to change the selectivity mechanism in Matrimid® membranes, moving from H_2-selective membranes to reverse H_2-selective membranes with CO_2/H_2 7.3 (Simmons, 2005; Zhao *et al.*, 2008b).

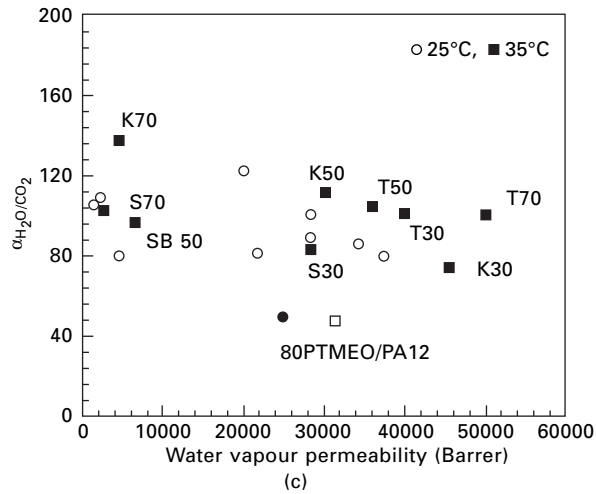
Poly(etherurethane) and poly(etherurea) block copolymers containing PEG (P_{CO_2} 590 Barrer), exhibited a CO_2/H_2 selectivity of 7.7 (Lie *et al.*, 2007), confirming once more the strategic role of PEO and PEG in favour of a solubility discrimination-based transport. On the other hand, polar motifs in the polymer network seem to be crucial for highly CO_2 permselective transport. Lie *et al.* (2007) demonstrated how amine groups in the polymer backbone work as fixed site carriers, yielding relevant productivity and selectivity, that is CO_2/CO 140, CO_2/N_2 160 and CO_2/H_2 175. The permselectivity in favour of CO_2 was ascribed to the water-assisted formation of the HCO_3^- ion which has mobility comparable to that of the mobile carriers. The decisive role of polar motifs in establishing a favourable intermolecular interaction between membrane and guest penetrant has been discussed widely (De Luca *et al.*, 2009; Gugliuzza *et al.*, 2006, 2007). The incorporation of organic nanofillers bringing sulphonamide, hydroxyl and ester motifs into a polyether-*b*-polyamide matrix yielded enhanced solubility discrimination in the order $H_2O>>CO_2>CH_4>N_2$ through competitive host–host and host–guest interactions between polymer segment chains, modifier and penetrant, resulting in attractive interfaces for CO_2 current dehydration (Fig. 5.11) (Gugliuzza and Drioli 2003, 2004, 2005).

Increasing interest in the incorporation of nanofillers into polymeric matrixes reflects a tendency to include it as a viable alternative to simple organic and inorganic membranes. Tailor-made polymer nanoparticles composite membranes represent an attractive challenge for the future, because they may combine the basic properties of apparently conflicting materials, yielding high-performance artificial membranes with excellent transport properties,

© Woodhead Publishing Limited, 2011

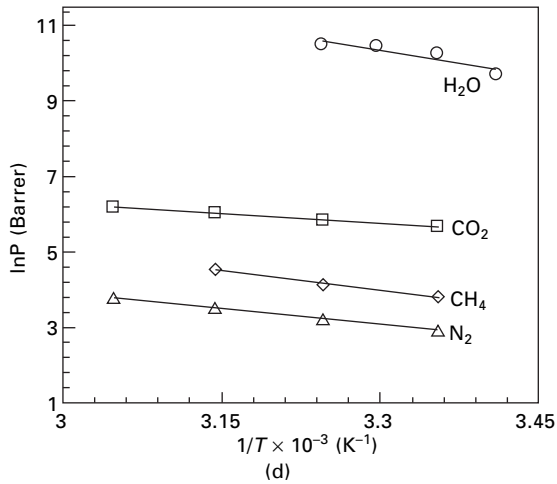






5.11 (a) FT-IR chemical imaging representing the uniform distribution of *o*/*p*-toluensulphonamide in 80PTMEO/PA12; (b) modelling molecules representative of the functional linkage of 80PTMEO/PA12-modifier and water-modifier; (c) ideal selectivity H_2O–CO_2 vs water vapour permeability; (d) permeability of penetrant at increasing condensability through 80PTMEO/PA12/triethylcitarte50 (De Luca *et al.*, 2009; Gugliuzza *et al.*, 2004, 2005, 2006).

© Woodhead Publishing Limited, 2011



5.11 Continued

good thermal and chemical resistance, adaptability to harsh conditions and scalability. Recently, successful attempts to disperse inorganic nanoparticles such as silica in polyether and polyether-*b*-polyamide have been made (Ardestani *et al.*, 2010; Xu *et al.*, 2009). A separation factor CO_2/N_2 of 81 has been estimated for poly(amide-6-*b*-ethylene oxide) blended with silica (Kim and Lee, 2001), while values of selectivity for a CO_2/H_2 gas pair exceeding 11 with a corresponding CO_2 permeability of 83 Barrer have been estimated at 12 atm (1.22 MPa) for nanocomposite PEG membranes (Patel *et al.*, 2003).

5.3.2 Inorganic membranes

Inorganic membranes are generally subdivided into porous and non-porous (metallic). In particular, porous inorganic membranes offer high ability to operate at high temperatures, for example, in the separation of CO_2 from hydrogen in syngas processes (Lu *et al.*, 2007). Simple molecular sieving can be used to separate CO_2 owing to the large size of CO_2 with respect to hydrogen and/or other gases (Kluiters, 2001). Recent patents (Gobina, 2006; Ku *et al.*, 2008) describe inorganic membranes consisting of a ceramic support, such as Al_2O_3, onto which a porous separating layer is deposited, often silica, alumina or zirconia. A further functional layer like $BaTiO_3$ or MgO is even added. These functional groups have high chemical affinity for CO_2 and, therefore, the pore walls become saturated, which increases the permeability. A major difficulty with this approach is to achieve an efficient trap of the particles within the pores. Both the pore and sieve sizes must be well-known and sufficiently similar to ensure strong packing of the

© Woodhead Publishing Limited, 2011

pores. Otherwise, the gaps between the sieves and the pore walls will allow bulk diffusion of gas molecules, diminishing the selectivity performance (Berger, 1971).

5.3.3 Mixed matrix membranes

Mixed matrix membranes are made from an inorganic material in the form of micro or nano-particles (discrete phase) incorporated into a polymeric matrix (continuous phase). The use of two materials provides the possibility of designing a better membrane for CO_2 capture, allowing the synergic combination of polymers and superior gas separation performance of inorganic materials (Mahajan *et al.*, 1999). The presence of inorganic materials in a polymeric matrix allows physical, thermal and mechanical properties to be enhanced in aggressive environments as well as stabilizing the polymeric membrane against change in permselectivity with temperature. The dispersed particles can affect the permeability of gases in different modes:

- Discrete particles can act as molecular sieves, altering the permeability in relation to molecular size;
- Particles can disrupt the polymeric matrix resulting in increased microcavities and hence increasing permeability;
- Particles can act as a barrier to gas transport and reduce permeability.

For these membranes, high affinity between the sieve and the polymeric phase is necessary. Otherwise, during casting the polymer can dissociate from the sieve's surface leaving microcavities throughout the membrane, enhancing the permeability of gas and limiting the sieving mechanism (Michaels, 1990).

5.3.4 Facilitated transport membranes

Facilitated transport membranes are based on a chemical reaction occurring between the gas of interest and a component of the membrane (carrier). The reacted species is readily carried across the membrane, whereas diffusion of non-reactive gases is inhibited. The active carrier is generally a base, because of the acidic nature of CO_2. The driving force for gas transportation remains the partial pressure difference across the membrane. However, the facilitator carrier increases both the permeability and selectivity of the membrane through increased loading. The facilitator carrier can be either fixed-sited within the polymeric matrix or mobile (Ohyanagi *et al.*, 1988). Moreover, the inclusion of catalysts (such as arsenite salts) into the facilitator membrane can increase the rate of reaction between the carrier and CO_2 and, thus, the permeability and selectivity (Gaikar and Sharma, 1987; Shao *et al.*, 2009).

© Woodhead Publishing Limited, 2011

5.4 Performance of membrane processes for CO_2 sequestration

Typically, membranes used for CO_2 capture have to possess properties like:

- high CO_2 permeability
- high CO_2/N_2 selectivity
- thermal and chemical resistance
- plasticization resistance
- ageing resistance
- cost effectiveness
- ability to be cheaply manufactured into different membrane modules.

In fact, the key parameters dictating membrane performance are:

- permeability, the flux of a specific gas through the membrane:

$$\frac{P}{l} = \frac{Q}{A\Delta p} \quad [5.1]$$

  where l is the effective thickness of the membrane, Q the gas flow rate through the membrane, A the membrane surface area and Δp is the pressure difference across the membrane;
- ideal gas selectivity, the membrane preference for passing one gas species and not another:

$$\alpha_{ij} = \frac{P_i}{P_j} \quad [5.2]$$

For many membranes, there is a trade-off between selectivity and permeability. A highly permeable membrane tends to have low selectivity and vice versa. Robeson (2008) suggested that this trade-off may be represented by a graph, where the 'log' of the selectivity is represented against the 'log' of the permeability of the more permeable gas in a binary mixture. For example, Fig. 5.12 shows the correlation for CO_2/N_2 separation.

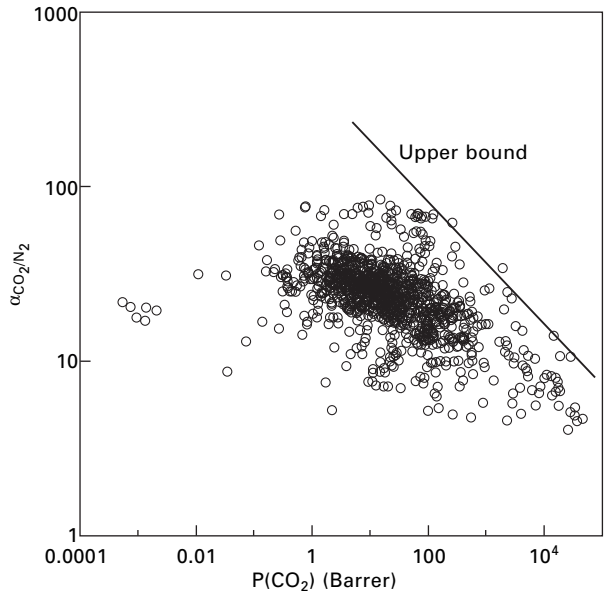
In this graph, the upper-bound represents the limit for achieving the desired result of a high selectivity combined with a high permeability for polymeric membranes. The upper-bound relationship is expressed by Equation [5.3]:

$$P_i = k\alpha_{ij}^n \quad [5.3]$$

where P_i is the permeability of the more permeable gas, k is constant and n is the slope of the log–log limit. Methods allowing the upper-bound limits to be exceeded can be, for example, the following:

- surface modification (Robeson *et al.*, 1994)
- UV surface modification (Hsu *et al.*, 1993)

© Woodhead Publishing Limited, 2011



5.12 Upper bound correlation for CO_2/N_2 separation (Robeson, 2008).

- ion beam surface carbonization (Won *et al.*, 2000)
- surface fluorination (LeRoux *et al.*, 1994)
- mixed matrix approach (Zimmerman *et al.*, 1997)
- carbon molecular sieving membranes produced by carbonization of aromatic polymer membranes (Youn *et al.*, 2005).

Moreover, as the permeability and selectivity improve, the membrane materials have to be thermally and chemically robust. In particular, long-term stability of the polymeric membranes at elevated temperatures is necessary to maintain the robustness of the membrane-based systems. Polymers with superior intrinsic thermal stability may be beneficial for use in H_2/CO_2 separation. A good example is PBI, which was studied for elevated temperature applications (> 400°C) (Khare *et al.*, 2005; Young *et al.*, 2006).

Lastly, the membranes have to be resistant to plasticization, which changes the polymer configuration by increasing the free volume of mixtures. The polymer matrix swells due to sorption of one species, accelerating the permeation of the other. As a consequence, the polymer membrane loses its selectivity. For example, in CO_2/CH_4 separations, CO_2 acts as a plasticizer. A typical effect of plasticization is that the permeability versus pressure curves go through a minimum. The pressure, corresponding to the minimum of permeability, is called 'plasticization pressure'. For some polyimides with outstanding permeation performance, a partial pressure of CO_2 of 8–10 bar is often sufficient to induce plasticization (Koros and Walker, 1991). However, not all polymers show the same tendency to be plasticized (Bos, 1996).

© Woodhead Publishing Limited, 2011

5.5 Membrane modules for CO_2 sequestration

Conventionally, the membrane must be packed in a proper device called a 'membrane module', which should offer:

- low production costs
- high packing density
- low energy consumption
- good control of concentration polarization.

For the application of the membranes in gas separation processes, several configurations are conventionally used for the membrane housing such as hollow and capillary fibre systems and spiral wounds. In Table 5.7, the benefits and drawbacks of these different membrane modules are summarized.

It should be stated that the commercial membrane modules available today are specifically designed for a specific membrane process application. However, the choice of a module configuration depends on:

- type of separation problem
- ease of cleaning
- ease of maintenance
- ease of operation
- compactness of the system
- scale
- possibility of membrane replacement.

5.5.1 Modules based on hollow fibre membranes

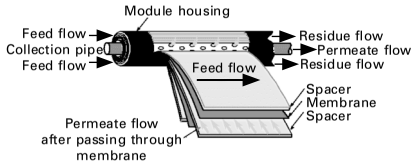
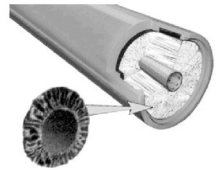
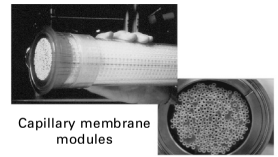
Hollow fibre membranes are made from extremely thin polymeric tubes, with a diameter of 50–200 μm (Baker, 2004). The selective layer is on the outside surface of the fibres, facing the high-pressure gas. A hollow fibre membrane module normally contains tens of thousands of parallel fibres deposited at both ends in epoxy tube sheets (Baker, 2004). These kinds of membrane play an important role in gas separation owing to their high separation area and selectivity. Hollow fibres are stable and show high flux with moderate selectivity in a full scale system. The high flux of hollow fibres is due to the combination of high transfer or separation areas and a thin membrane wall. Moreover, they also possess a low surface energy (Sandru *et al.*, 2010).

5.5.2 Modules based on capillary fibre membranes

Capillary fibres are produced using similar equipment to hollow fibres, but they have a larger diameter, typically, 200–400 μm (Baker, 2004). The selective layer is formed on the inside surface of the fibres. The free ends of the capillaries are potted agents such as epoxy resins, polyurethanes. In

© Woodhead Publishing Limited, 2011

Table 5.7 Advantages and disadvantages of different kinds of membrane housing

Membrane module	Spiral wound	Hollow fibre	Capillary fibre
			
Advantages	• Compact • Good membrane surface/ volume ratio • Minimum energy consumption • Low capital/operating cost	• Compact • Excellent membrane surface/volume ratio • Low energy consumption	• Good membrane surface/ volume ratio • Low capital/operating cost
Disadvantages	• Not suitable for very viscous fluids • Difficult to clean • Faulty membrane – change whole module	• Cleanable by reversing permeate flow • Well-developed equipment • Low area cost • Low holdup volume	• Susceptible to end-face fouling • Susceptible to plugging by particulates • Single fibre damage – replace entire module • Pre-treatment required to prevent plugging • Intolerant of capillary rupture

© Woodhead Publishing Limited, 2011

a capillary fibre module, the feed gas flows through the bore of the fibres. The pressure difference feed-to-permeate, which capillary fibres can support, is limited and typically it does not exceed 10–15 bar. Higher pressures may rupture fibres and even a single defective fibre can seriously degrade the separation capability of the module. Capillary membrane modules are not as expensive or compact as hollow fibre modules, but they are still very economical. Their principal drawback is the pressure that the fibres can support. This limitation means capillary modules cannot be used at the high pressures that are necessary for hydrogen or natural-gas processing applications (Buysse *et al.*, 2010).

5.5.3 Spiral wound modules

Generally, sheets of membrane 1–2 m long are cut and folded and then packaged as spiral wound modules (Kashemekat *et al.*, 1991). A single module may contain as many as 30 membranes. Spiral wound elements are generally the most economical to operate (Bartels *et al.*, 2007). Spiral systems are:

- Compact – high membrane packing density results in more efficient utilization of floor space;
- Energy efficient – lower power consumption compared to other membrane configurations;
- Lower capital cost, when extensive feed pretreatment is not required;
- Robust – high pressure spiral elements can withstand pressures in excess of 1000 psi (6.89 MPa).

5.5.4 Comparison between different membrane modules

It is difficult to quantify correctly the cost of a module because the same module design varies widely depending on the application considered. Generally, hollow fibre modules are cheaper than the others even if they are produced for very high-volume applications in order to justify the expense of developing and building the spinning and module fabrication equipment. Hollow-fibre and spiral-wound modules are very common mainly owing to their higher area to volume ratio. Spiral-wound modules have distinct advantages over the hollow-fibre elements in important applications, although the latter can offer higher packing density.

5.6 Design for power plant integration

The design of power stations requires simultaneous consideration of heat integration and power generation. Simulation models for gas separation

© Woodhead Publishing Limited, 2011

membranes have to consider, generally, an equation describing the gas transport across the membrane, a mass balance equation for each component of the gas mixture, the pressure drops occurring on both sides of the membrane and the boundary conditions (Ahmad *et al.*, 2010; Hwang and Kammermeyer, 1975; Lababidi *et al.*, 1996; Safari *et al.*, 2009). The major impediment to the engineering analysis of membrane processes in CO_2 separation is the large number and range of process variables. The mixture is often treated as a binary system (generally CO_2 and H_2) and, therefore, the role of impurities (water, SO_2, NO_x, particles, etc.) has not yet been investigated in detail. Another common assumption is that the constant feed mixture temperature is either close to or slightly above ambient temperature (e.g. 40°C). Moreover, the most important parameter, that must be considered, is the efficiency of a membrane separation process. The efficiency depends on three major variables:

- the membrane selectivity α;
- the pressure ratio between feed and permeate streams;
- the stage cut θ, the ratio of permeate flow rate to feed flow rate.

Particular attention is paid to the calculation of the CO_2 recovery ratio, the fraction of CO_2 in the feed captured in the permeate side:

$$R = \theta \frac{y_p}{x_{in}} \qquad [5.4]$$

where y_p is the mole fraction of CO_2 in the permeate and x_{in} is the mole fraction of CO_2 in the feed. In general, an increase in θ (and so an increase of the membrane area) is not linear with the recovery of CO_2. For this reason, in a problem like CO_2 capture, one major objective of scientific studies is to determine the relationship between the CO_2 recovery ratio (R) and the corresponding permeate composition (y_p).

The International Energy Agency (IEA) guidelines require R to be above 80% or 90% (Davison and Thambimuthu, 2004), because values below this do not offer a sufficient decrease in CO_2 released to the atmosphere. The permeate CO_2 mole fraction y_p must also be in the range 0.8–0.95, both to minimize the compression and transportation costs (Davison and Thambimuthu, 2004) and to prevent problems related to deep ocean or geological disposal (Davison and Thambimuthu, 2004). Unfortunately, the recovery ratio R and permeate composition y_p seem to be inversely related, such that an increase in R implies a decrease in y_p and vice versa.

5.7 Cost considerations and membrane technology at the industrial scale

Economic analysis includes not only the costs for capture, but also the costs of injection and storage into a geological site, allowing a full comparison

© Woodhead Publishing Limited, 2011

of 'end-to-end' sequestration costs. The total production costs in membrane processes depend on the fixed charges and the repayment of the plant investment cost and of operating costs (energy, membrane replacement, maintenance). In particular, quantitative analysis of the costs strongly depends on the specific application, plant and location as well as on the characteristics of membranes and modules.

In fact, the costs of capture using gas separation membrane systems can be reduced by increasing the membrane permeability and selectivity. Improvements in the permeability reduce the capture cost because less membrane area is required for the same CO_2 recovery rate. By increasing the CO_2/N_2 selectivity, the mole fraction of CO_2 in the permeate increases. As the capture cost includes the compression of CO_2 after separation, a higher CO_2 fraction in the permeate stream requires less compression and, thus, less energy; therefore, both the capital expenditure and operating costs are lower.

In contrast, the cost of membranes affects only marginally the capture costs (Ho *et al.*, 2006). Therefore, reductions in membrane costs will improve the overall competitiveness of gas separation membrane systems slightly.

Another important aspect of CO_2 separation costs is the driving force, which, by using membrane technology, depends on the partial pressure difference between both sides of the membrane. By increasing the pressure across the membrane or reducing the feed gas pressure, the capture cost decreases. This is because a lower feed pressure requires a smaller compressor, thereby reducing both the capital costs and the total energy consumption (Ho *et al.*, 2006). Nevertheless, decreasing the feed pressure, the driving force across the membrane decreases (Ho *et al.*, 2006). Therefore, to obtain the same CO_2 recovery from the feed gas, the membrane area required must increase. Globally, it is better to increase the costs of the membrane than to use a bigger compressor.

Moreover, just to give a very brief overview of the work in CO_2 capture direction, some European projects (in the UE FP6 and FP7 only) are reported in the following:

- Innovative CO_2 capture (iCap: 2010–2013). This project is coordinated by the Norwegian University of Science and Technology. The aim of the project is to develop breakthrough technologies that can be applied to post-combustion CO_2 capture. These technologies include the use of phase change solvents, the combination of SO_2 and CO_2 absorption, the use of CO_2-selective low-temperature membranes and the development of new energy production cycles with CO_2 capture.
- CO_2 enhanced separation and recovery (CESAR: 2008–2011. For: CESAR: http://www.co2cesar.eu/index.php). This aims for a breakthrough in the development of low-cost post-combustion CO_2 capture technology in

© Woodhead Publishing Limited, 2011

order to provide an economically feasible solution for both new large scale power plants and retrofit of existing power plants. For this project, the research is charged with the development of new membrane contactors, development carried out by SME Polymem and ENSIC-Nancy.

- Nanoglowa is a project based on CO_2 capture trough nanostructured membranes, see: http://www.nanoglowa.com. In this project, the application of nanostructured membranes for CO_2 capture and separation brings down the energy penalty related to conventional absorption with amines.

5.8 Modelling aspects of gas permeation membrane modules

In 1950, before the development of practical membranes, Weller and Steiner (1950) studied gas separation by membranes. The simplest model proposed was complex mixing. The hypothesis is that the concentration and total pressure are almost constant in both permeate and retentate streams. However, when convective transport in the direction parallel to the membrane is prevalent with respect to molecular diffusion, the gas stream is in plug flow and the concentration of the species in the direction perpendicular to the membrane can be assumed to be uniform. In particular, the low pressure permeate and the high pressure retentate streams can flow perpendicular to the membrane surface, obtaining a so-called cross flow. Moreover, both the permeate and retentate streams can flow parallel to the membrane surface, obtaining a parallel flow (Baker, 2004; Hwang and Kammermeyer, 1975; Javaid, 2005; Nunes and Peinemann, 2001; Vansant and Dewolf, 1990).

In this section, a numerical model for the simulation of a multi-component gas separation process through dense polymeric membrane modules is described (complete mixing, co-current flow and cross-flow modes). Furthermore, some consideration of the iterative procedure for the counter-current flow is given. For more details see (Basile and Gallucci, 2009).

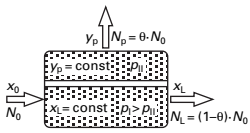
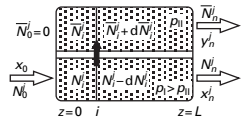
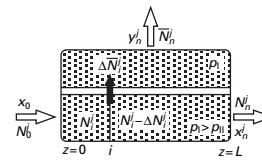
In order to understand better the influence of permeability and selectivity on the surface membrane (and so on the costs) of operating a requested gas separation, three different polymers are considered (Powell and Qiao 2006):

- poly(ethylene)oxide (PEO) membrane with a very low CO_2 permeability and a very high CO_2/N_2 separation factor;
- poly(trimethyl-prop-1-ynyl-silane) with a very high CO_2 permeability and a low CO_2/N_2 separation factor;
- PMDA-BAPHF (a dense film incorporating polyimides) with a low CO_2 permeability and a low CO_2/N_2 separation factor.

In Table 5.8, the main characteristics of the three model flows considered

© Woodhead Publishing Limited, 2011

Table 5.8 Complete mixing, parallel co-current flow and cross flow: main characteristics

Complete mixing	Parallel co-current flow	Cross flow
The concentration and total pressure are assumed to be constant in both permeate and retentate streams.	The components of velocity perpendicular to the membrane are negligible with respect to the longitudinal ones on both sides. Moreover the Peclet number is great enough so that plug flow can be assumed.	In cross flow, the transversal velocity is prevalent and the Peclet number is high enough so the flux is in plug flow.
		
Let us consider a binary gas feed. The transport rate of the two species (1 refers to the more permeable component):	For a multi-component gas feed, the retentate and permeate composition of the species *j* between two consecutive segments, *i*-1 and *i* are, respectively:	The permeated flux is rapidly removed perpendicularly to the membrane surface so that the molecular diffusion is negligible.
$\begin{cases} N_p^1 = \dfrac{P^1}{l} S(p_I x_L - p_{II} y_p) \\ N_p^2 = \dfrac{P^2}{l} S[p_I(1-x_L) - p_{II}(1-y_p)] \end{cases}$	$\begin{cases} \bar{N}_i^j = \bar{N}_{i-1}^j + \Delta\bar{N}_i^j \\ N_i^j = N_{i-1}^j + \Delta N_i^j \end{cases}$	The additive term in the permeate molar flow rate equations for the parallel co-current flow mode is not present. For this reason, the transport equation for the *j*-th gas species for retentate is the same as in the co-current flow model, whereas for the permeate side becomes:
where $x_L = \dfrac{N_L^j}{\sum_j N_L^j} \quad y_p = \dfrac{N_p^j}{\sum_j N_p^j}$	the variation of molar flow rate due to the permeation of the species *j* at the step *i* is $\Delta N_i^j = \dfrac{P^j L}{l} S_A (p_I x_i^j - p_{II} y_i^j)$	$\begin{cases} \bar{N}_i^j = \Delta\bar{N}_i^j \\ N_i^j = N_{i-1}^j + \Delta N_i^j \end{cases}$
Dividing the two transport equations we obtain: $\dfrac{y_p}{1-y_p} = \alpha \dfrac{p_I x_L - p_{II} y_p}{p_I(1-x_L) - p_{II}(1-y_p)}$	A predictor–corrector method has been used. The procedure can be summarized as follows.	Finally, the outlet molar flow rate, on the permeate side, for the *j*-th species is $\bar{N}^j = \sum_{j=1}^{N_{species}} \bar{N}^j$
The solution is: $y_p = \dfrac{-A + \sqrt{A^2 + 4(1-\alpha)\alpha\varphi x_L}}{2(1-\alpha)}$	Starting from the boundary condition $\bar{N}_0^j = 0$, we can predict the values of $\bar{N}_i^j$ and N_i^j with the known values of molar flow rate at the previous step $\bar{N}_{i-1}^j$ and N_{i-1}^j. The temporary predicted values of molar flow rates on both sides are used in the corrector step, which provides the final value of ΔN_i^j as a function of the predicted values.	
where $A = (\alpha - 1)\,\varphi x_L + \varphi + (\alpha - 1)$		
Finally, the relation between stage cut and x_L, x_0 and y_p can be obtained by the overall material balance: $x_0 = \theta y_p + (1-\theta) x_L$		

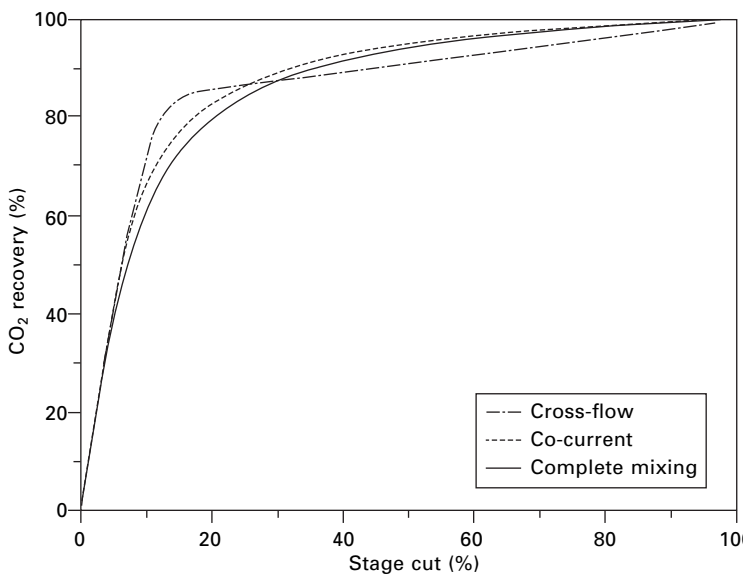
© Woodhead Publishing Limited, 2011

are summarised. Applying the three cited models to a simple one-stage removal plant, let us consider a membrane system for the carbon dioxide separation from a mixture of N_2 (90%) and CO_2 (10%). A PEO dense film membrane is considered (Table 5.9); the pressure ratio is 20. As already seen (see Equation [5.4]), the CO_2 recovery ratio is the fraction of carbon dioxide in the feed actually captured in the permeate side and is a better independent variable with respect to the stage cut (Bounaceur *et al.*, 2006; Corti *et al.*, 2004). In fact, the increase in θ, and so the increase in the membrane area, is not linear with the recovery of the most permeable species. Figure 5.13 depicts the recovery ratio with respect to the stage cut. Complete CO_2 recovery is reached for stage cut values less than 100%. For example, when the fraction of feed flow that permeates through the membrane $\theta = 50\%$, the CO_2 recovery fraction is more than 90% for all the flow modes analysed. Therefore, a further increase in stage cut (and so in membrane area), does not provide a significant increase in CO_2 actually recovered.

Table 5.9 Poly(ethylene)oxide membrane properties

Permeability (Barrer)		Selectivity
CO_2	N_2	CO_2/N_2
8.1	0.07	116

1 barrer = 10^{10} cm^3 (STP) cm/(cm^3s cmHg).



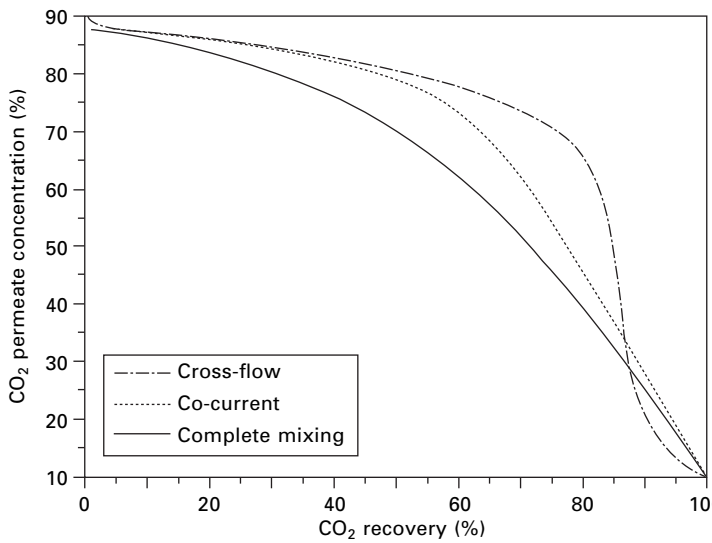
5.13 CO_2 Recovery ratio versus stage cut for three different flow mode patterns: complete mixing, co-current and cross flow.

© Woodhead Publishing Limited, 2011

Figure 5.14 shows the CO_2 permeate concentration with respect to recovery. It is clear that a concentrated permeate product can be obtained with low values of CO_2 recovery, whereas an increase in recovery produces a significant decrease in purity. This means that it is not possible to obtain simultaneously high recovery and high purity in a one-stage only membrane system. Moreover, it is also clear that the cross-flow mode is more efficient with respect to both complete mixing and co-current flow mode. As an example, with a 30% carbon dioxide recovery, the purity is 80% for complete mixing flow mode, and nearly 85% for cross-flow and co-current flow patterns.

Two membranes with low selectivity (10.6 and 17.7) but with very different values of permeability are now considered (see Table 5.10). In particular, the values of permeability (in barrer) are 19 000 and 11.8 for CO_2 and 1800 and 0.66 for N_2, respectively.

The results of the simulation are shown in Fig. 5.15, where the CO_2 permeate concentration is plotted against the CO_2 recovery for both membranes and for the three flow models.

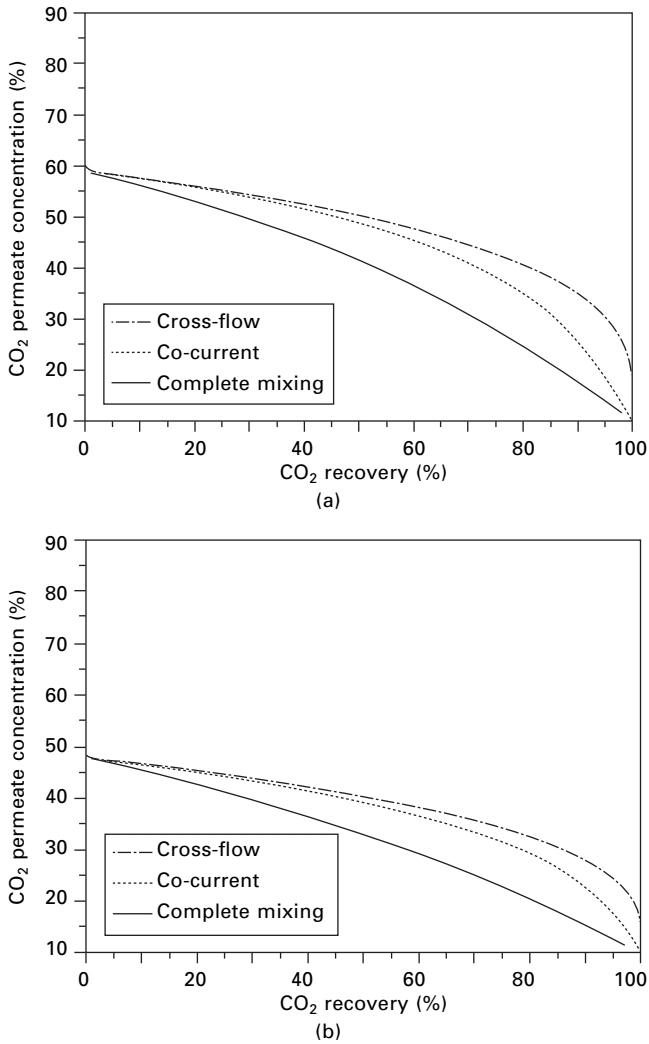


5.14 CO_2 permeate concentration for three flow patterns: complete mixing, co-current and cross flow. CO_2 feed concentration 10%; PEO membrane.

Table 5.10 Membrane properties

	Permeability (Barrer)		Selectivity
	CO_2	N_2	CO_2/N_2
Poly(trimethyl-prop-1-ynyl-silane)	19000	1800	10.6
PMDA-BAPHF	11.8	0.66	17.7

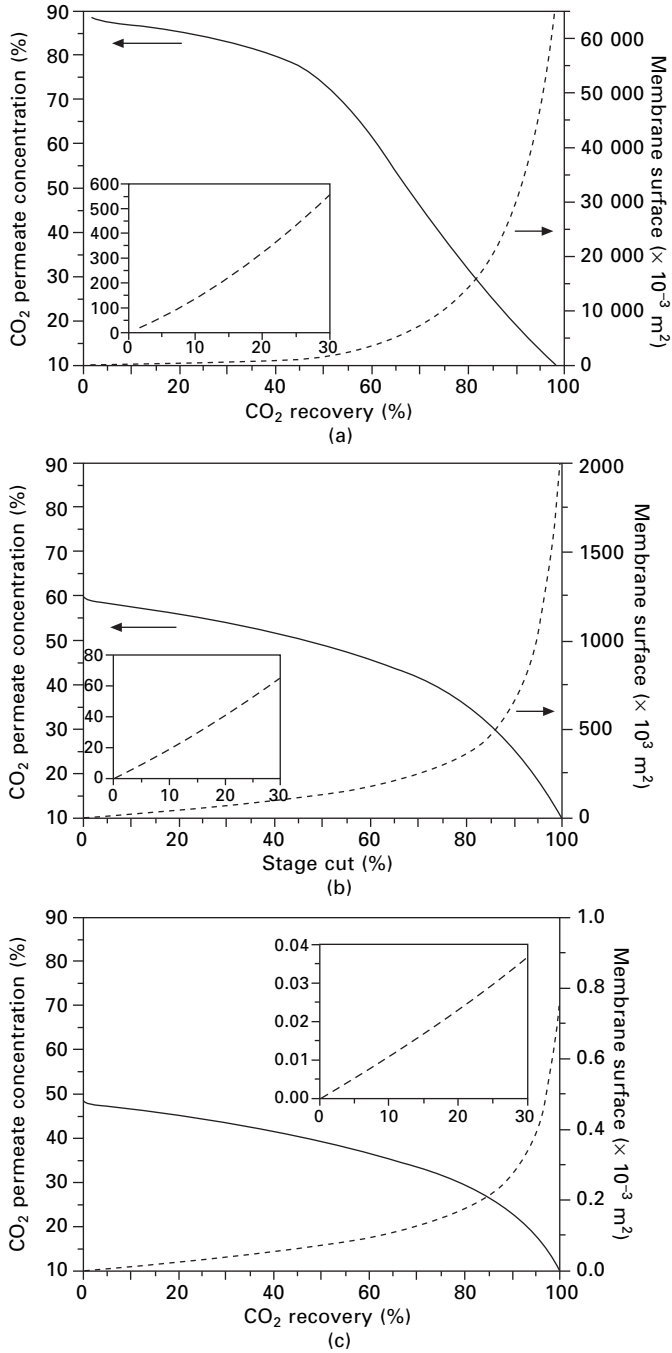
© Woodhead Publishing Limited, 2011



5.15 CO_2 permeate concentration versus carbon dioxide recovery fraction for all flow patterns. (a) PMDA–BAPHF, (b) poly(trimethyl-prop-l-ynyl-silane).

The better performances (in terms of purity) are reached by the polymide membrane PMDA-BAPHF, which is characterized by the higher selectivity. Nevertheless, these simulation results are significantly lower with respect to the value registered for the PEO membrane, Fig. 5.14, which shows a selectivity 6.5 times higher. However, the simulation results of Fig. 5.15 show the effect of the selectivity in terms of product purity, but do not illustrate the membrane surface required. To this end, Fig. 5.16 depicts the

© Woodhead Publishing Limited, 2011



5.16 Membrane area and CO_2 permeate concentration versus carbon dioxide recovery fraction for the three membranes considered and for a co-current flow pattern. (a) PEO, selectivity 115, (b) PMDA-BAPHF, selectivity 17.7, (c) poly(trimethyl-prop-l-ynyl-silane), selectivity 10.6.

© Woodhead Publishing Limited, 2011

comparison between membrane area required (related to the permeability) and carbon dioxide concentration on the permeate side (the purity, related to the selectivity). In particular, the membrane surface rises remarkably with the carbon dioxide recovery, and the values of the membrane with the higher permeability are significantly lower. For 30% CO_2 recovery the membrane area required is 560×10^3, 65×10^3 and 0.0365×10^3 for PEO, PMDA-BAPHF and poly(trimethyl-prop-1-ynyl-silane), respectively.

To summarize, selectivity is related to purity and it is evident that it is not possible to obtain simultaneously high recovery and high purity in only one-stage membrane system. The addition of further units/modules will increase both capital and operating cost owing to the additional membrane area required and the recompression needed between the various stages. Investment costs for compressor, vacuum pump and membrane area have to be balanced with the operating costs (Baker, 2004; Basile and Gallucci, 2009; Nunes and Peinemann, 2001). On the other hand, it is important to stress that the membrane area required is not related to the selectivity, but only to the permeability (Fig. 5.16): an increase of the permeability reduces the membrane area required for a fixed purity.

5.9 Conclusions and future trends

Membrane-based technology has several advantages over conventional separation approaches for CO_2 capture, such as:

- lower capital cost
- ease of skid-mounted installation
- lower energy consumption
- ability to be applied in remote areas, especially offshore
- flexibility.

Nevertheless, there are many relevant factors determining the appropriateness of each membrane type for each specific application. When selecting a suitable membrane for CO_2 separation, the operating temperature and pressure are of paramount importance since they directly affect the separation performance of the membrane. In addition, the composition of the gas mixture to be separated, the material and fabrication costs of the membranes as well as the overall process design need to be taken into account. Moreover, the energy reduction required and the corresponding costs must be addressed.

Currently, chemical modification of polymeric membranes is one of the most promising approaches for greatly enhancing separation performance. Therefore, further development of existing modification methods (e.g. identifying better cross-linking agents) or the invention of new modification techniques for existing gas-separation materials may accelerate the commercialization of polymeric membranes for CO_2 separation. However, long term stability and

© Woodhead Publishing Limited, 2011

performance of polymeric membranes at elevated temperatures are necessary to maintain the robustness of the membrane-based systems. In addition to membrane materials selection, membrane configuration and module design are important considerations for industrial applications.

5.9.1 Remarks

Membrane separation is an attractive and promising technology, which can be applied in combination in all types of power plants. Nevertheless, although membrane technology is widely applied for gas separation, it is not yet used on the scale of power plants. For this reason, a potential objective could be the development of innovative membrane-based technologies capable of reducing the cost of CO_2 capture, producing, for example, hydrogen from natural gas fuel. This could be, for example, obtained by producing higher selective membranes, such as hybrid membrane–absorbent (or solvent) systems, which use very high surface area to volume ratios for mass exchange between a gas stream and a solvent, resulting in a very compact system. Overall, even though the separation of CO_2 using polymer-based membranes is a complex undertaking, it is necessary to address the challenges and continue to explore new approaches that will produce the next generation of high-performance membranes.

5.10 References

Abertz V, Brinkmann T and Dijkstra M (2006), 'Developments in membrane research: from material via process design to industrial application', *Adv Eng Mater*, **8**, 328–58.

Aguilar-Vega M and Paul D R (1993), 'Gas transport properties of polycarbonates and polysulfones with aromatic substitutions on the bisphenol connector group', *J Polym Sci Part B: Polym Phys*, **31**, 1599–610.

Ahmad F, Lau K K and Shariff A M (2010), 'Removal of CO_2 from natural gas using membrane separation system: Modeling and process design', *J Applied Sci*, **10**, 1134–9.

Aitken C L and Paul D R (1993), 'Gas transport properties of polysulfones based on dihydroxynaphthalene isomers', *J Polym Sci Part B: Polym Phys*, **31**, 1061–5.

Aitken C L, Koros W J and Paul D R (1992), 'Gas transport properties of biphenol polysulfones', *Macromolecules*, **25**, 3651–8.

Akagi T, Watanab K, Kim H and Akashi M (2010), 'Stabilization of polyion complex nanoparticles composed of poly(amino acid) using hydrophobic interactions', *Langmuir*, **26**, 2406–13.

Al-Masri M, Fritsch D and Kricheldorf H R (2000), 'New polyimides for gas separation. 2. Polyimides derived from substituted catechol bis(etherphthalic anhydrides)s', *Macromolecules*, **33**, 7127–35.

Anon. 1: 'Projections of future climate change', Chapter 9 of *Climate Change 2001: the scientific basis*, http://www.grida.no/climate/ipcc_tar/wg1/339.htm.

Anon. 2: *The Kyoto Protocol*, UNFCCC, http://unfccc.int/resource/docs/convkp/kpeng.html.

© Woodhead Publishing Limited, 2011

Anon. 3: US Department of Energy, *Carbon Sequestration Technology Roadmap and Program Plan*, (2007), http://www.netl.doe.gov/sequestration.

Anon. 4: *Storing CO_2 Underground*, http://www.ieaghg.org/docs/general_publications/storingCO.pdf.

Anon. 5: http://scopees.elsevier.com.

Ardestani M A, Babaluo A A, Peyravi M, Razavi Aghjeh M K and Jannatdoost E (2010), 'Fabrication of PEBA/ceramic nanocomposite membranes in gas sweetening', *Desalination*, **250**, 1140–3.

Baker R W (ed) (2004), *Membrane Technology and Applications*, John Wiley and Sons, Chichester, UK, 538.

Bartels C, Hirose M and Fujioka H (2007), 'Performance advancement in the spiral wound RO/NF element design', *EDS Conference Halkidiki*, Greece, 1–9.

Basile A and Gallucci F (2009), *Simulation of Membrane Reactors*, Nova Science, New York.

Basu A, Akhtar J, Rahman M and Islam M (2004), 'A review of separation of gases using membrane systems', *Petrol Sci Techn*, **22**, 1343–68.

Berger C (1971), *Separation Means*, US patent 3567666.

Bolland O and Undrum H (2003), 'A novel methodology for comparing CO_2 capture options for natural gas-fired combined cycle plants', *Adv Env Res*, **7**, 901–11.

Bondar V I, Freeman B D and Pinnau I (2000), 'Gas transport properties of poly(ether-b-amide) segmented block copolymers', *J Polym Sci: Part B: Polym Phys*, **38**, 2051–62.

Bos A (1996), *High Pressure CO_2/CH_4 Separation with Glassy Polymer Membranes: Aspects of CO_2-induced plasticization*, PhD Thesis, University of Twente, The Netherlands.

Bounaceur R, Lape N, Roizard D, Vallieres C and Favre E (2006), 'Membrane processes for post-combustion carbon dioxide capture: A parametric study', *Energy*, **31**, 2556–70.

Buysse C, Kovalevsky A, Snijkers F, Buekenhoudt A, Mullens S, Luyten J, Kretzschmar J and Lenaerts S (2010), 'Fabrication and oxygen permeability of gastight, macrovoid-free $Ba_{0.5}Sr_{0.5}Co_{0.8}Fe_{0.2}O_{3-\delta}$ capillaries for high temperature gas separation', *J Membrane Sci*, **359**, 86–92.

Car A, Stropnik C, Yave W and Peine K V (2008a), 'Tailor-made polymeric membranes based on segmented block copolymers for CO_2 separation', *Adv Funct Mater*, **18**, 2815–23.

Car A, Stropnik C, Yave W and Peinemann K V (2008b), 'PEG modified poly(amide-b-ethylene oxide) membranes for CO_2 separation', *J Membrane Sci*, **307**, 88–95.

Chiesa P, Consonni S, Kreutz T and Williams R (2005), 'Co-production of hydrogen, electricity and CO_2 from coal with commercially ready technology. Part A: Performance and emissions', *Int J Hydrogen Energy*, **30**, 747–67.

Choi W J, Seo J B, Jang S Y, Jung J H and Oh K J (2009), 'Removal characteristics of CO_2 using aqueous MEA/AMP solutions in the absorption and regeneration process', *J Env Sci*, **21**, 907–13.

Chun B W, Ishizu C, Itatani H, Haraya K and Shindo Y (1994), 'Characterization and gas permeability of a three-component polyimide series', *J Polym Sci Part B: Polym Phys*, **32**, 1009–16.

Chung T S, Shao L and Tin P S (2006), 'Surface modification of polyimide membranes by diamines for H_2 and CO_2 separation', *Macromol Rapid Commun*, **27**, 998–1003.

Coady A B and Davis J A (1982), 'CO_2 recovery by gas permeation', *Chem Eng Prog*, **78**, 44–9.

© Woodhead Publishing Limited, 2011

Corti A, Fiaschi D and Lombardi L (2004), 'Carbon dioxide removal in power generation using membrane technology', *Energy*, **29**, 2025–43.

Davison J and Thambimuthu K (2004), 'Technologies for capture of carbon dioxide', *Proceedings of the 7th Greenhouse Gas Technology Conference*, Vancouver, Canada, http://uregina.ca/ghgt7/PDF/papers/peer/597.pdf.

de Abajo J, de la Campa J G, Lozano A E, Espeso J and Garcia C (2003), 'Designing aromatic polyamides and polyimides for gas separation membranes', *Macromol Symp*, **199**, 293–306.

De Luca G, Gugliuzza A and Drioli E (2009), 'Competitive host–host, guest–host interactions in modified polymer membranes: a density functional theory investigation on the availability of polymer polar moieties', *J Phys Chem B*, **113**, 5473–7.

Desideri U and Corbelli R (1998), 'CO_2 capture in small size cogeneration plants: technical and economic considerations', *Energy Conversion Management*, **339**, 857–67.

Drioli E and Romano M (2001), 'Progress and new perspectives on integrated membrane operations for sustainable industrial growth', *Ind Eng Chem Res*, **40**, 1277–300.

Feron P (1992), *CO_2 Capture: The Characterization of Gas Separation/Removal Membrane Systems Applied to the Treatment of Flue Gases Arising from Power Generation using Fossil Fuel*, IEA Greenhouse Gas R & D Programme, Report IEA/92/0E8, Cheltenham, UK.

Figuero J D, Fout T, Playnski S, McIlvried H and Srivastava R D (2008), 'Advances in CO_2 capture technology – The U.S. Department of Energy's carbon sequestration program', *Int J Greenhouse Cont*, **2**, 9–20.

Gaikar V G and Sharma M M (1987), 'New strategies for separations through reactions', *Sadhana*, **10**, 163–83.

Ghanem B S, McKeown N B, Peter M B, Selbie J D and Fritsch D (2008), 'High-performance membranes from polyimides with intrinsic microporosity', *Adv Mater*, **20**, 2766–71.

Gibbins J and Chalmers H (2008), 'Carbon capture and storage', *Energy Policy*, **36**, 4317–22.

Gielen D, Newman J and Patel M K (2008), 'Reducing industrial energy use and CO_2 emissions: the role of materials science', *MRS Bull*, **33**, 471–8.

Gobina E (2006), *Apparatus and Method for Separating Gases*, US patent 2006112822.

Graham T (1866), *Philos Mag*, **32**, 402.

Grattan-Guinness I (1969), 'Joseph Fourier and the revolution in mathematical physics', *IMA J Appl Math,* **5**, 230–53.

Guan Z and De Simone J M (1994), 'Fluorocarbon-based heterophase polymeric materials: 1 block copolymers surfactants for carbon dioxide applications', *Macromolecules*, **27**, 5527–32.

Gugliuzza A and Drioli E (2003), 'New performance of a modified poly(amide-12-b-ethyleneoxide)', *Polymer*, **44**, 2149–57.

Gugliuzza A and Drioli E (2004), 'Role of additives in the water vapor transport through block co-poly(amide/ether) membranes: effects on surface and bulk polymer properties', *Eur Polym J*, **40**, 2381–9.

Gugliuzza A and Drioli E (2005), 'Evaluation of the CO_2 permeation through functional assembled monolayers: relationships between structure and transport', *Polymer*, **46**, 9994–10003.

Gugliuzza A, Fabiani R, Garavaglia MG, Spisso A and Drioli E (2006), 'Study of the surface character as responsible for controlling interfacial forces at membrane-feed interface', *J Colloid Interface Sci*, **303**, 388–403.

© Woodhead Publishing Limited, 2011

Gugliuzza A, De Luca G, Tocci E, De Lorenzo L and Drioli E (2007), 'Intermolecular interactions as controlling factor for water sorption into polymer membranes', *J Phys Chem B*, **111**, 8868–78.

Guiver M D, Thi N L and Robertson G P (2002), *Composite Gas Separation Membranes*, US Patent 20020062737.

Haszeldine S (2007), 'Carbon capture and storage: How to bury the problem', Chemistry World, 42–46, http://www.geos.ed.ac.uk/research/subsurface/diagenesis/How_To_Bury_The_Problem_Chemistry_World_Oct07.pdf

Hellums M W, Koros W J, Husk G R and Paul D R (1989), 'Fluorinated polycarbonates for gas separation applications', *J Membrane Sci*, **46**, 93–112.

Ho M T, Allinson G and Wiley D E (2006), 'Comparison of CO_2 separation options for geo-sequestration: are membranes competitive?', *Desalination*, **192**, 288–95.

Hosseini S S, Teoh M M and Chung T S (2008), 'Hydrogen separation and purification in membranes of miscible polymer blends with interpenetration networks', *Polymer*, **49**, 1594–603.

Hsu K K, Nataraj S, Thorogood R M and Puri P S (1993), 'O_2/N_2 selectivity improvement for polytrimethylsilylpropyne membranes by UV irradiation and further enhancement by subambient temperature operation', *J Membrane Sci*, **79**, 1–10.

Hulme M (2009), 'On the origin of "the greenhouse effect": John Tyndall's 1859 interrogation of nature', *Wheater,* **64**, 121–3.

Husain S and Koros W J (2007), 'Mixed matrix hollow fibre membranes made with modified HSSZ-13 zeolite in polyetherimide polymer matrix for gas separation', *J Membrane Sci*, **288**, 195–207.

Hwang S T and Kammermeyer K (1975), *Membranes in Separation. Techniques of chemistry*, Vol VII, Wiley Interscience, New York.

Javaid A (2005), 'Membranes for solubility-based gas separation applications', *Chem Eng J*, **112**, 219–26.

Jawad M (1989), 'Future for desalination by reverse osmosis', *Desalination*, **72**, 23–8.

Jeon I Y and Baek J B (2010), 'Nanocomposites derived from polymers and inorganic nanoparticles', *Materials*, **3**, 3654–74.

Jeremy D (2000), *Economic Evaluation of Leading Technology Options for Sequestration of Carbon Dioxide*, MS Thesis, MIT, Cambridge, MA.

Kashemekat J, Baker R W and Wijmans J G (1991), *A Membrane Module*, US Patent 5069793.

Kazama S, Teramoto T and Haraya K (2002), 'Carbon dioxide and nitrogen transport properties of bis(phenyl)fluorene-based cardo polymer membranes', *J Membrane Sci*, **207**, 91–104.

Keeling R F, Piper S C, Bollenbacher A F and Walker J S (2008), 'Atmospheric carbon dioxide record from Mauna Loa', CDIAC (Carbon Dioxide Information Analysis Center) doi: 103334/CDIAC/atg035. http://www.ornl.gov/~webworks/cppr/y2001/rpt/118259.pdf

Kerr R A (2007), 'Scientists tell policy makers we're all warming the world', *Science*, **315**, 754–7.

Khan A L, Cano-Odena A, Gutiérrez B, Minguillón C and Vankelecom I F J (2010), 'Hydrogen separation and purification using polysulfone acrylate–zeolite mixed matrix membranes', *J Membrane Sci*, **350**, 340–6.

Khare V P, Greenberg A R, Balakrishnan A, Diani J and Brahmandam S (2005), 'Gas transport and mechanical behavior of polymeric dense films at elevated temperatures', *Proceedings of the 230th ACS National Meeting*, Washington, DC.

© Woodhead Publishing Limited, 2011

Kim J H and Lee Y M (2001), 'Gas permeation properties of poly(amide-6-b-ethyleneoxide)-silica hybrid membranes', *J Membrane Sci*, **193**, 209–25.

Kim T H, Koros W J, Husk G R and O'Brien K (1988), 'Relationship between gas separation properties and chemical structure in a series of aromatic polyimides', *J Membrane Sci*, **37**, 45–62.

Kintisch E (2007), 'New congress may be warming up to plans for capping emissions', *Science*, **315**, 444.

Klara S M, Srivastava R D and McElvried H G (2003), 'Integrated collaborative technology development program for CO_2 sequestration in geologic formations', *Energy Conversion Management*, **44**, 2699–712.

Kluger J (2007), 'Global warming: what now? Our feverish planet badly needs a cure', *Time Mag*, **9**, 50–109.

Kluiters S C A (2001), 'Status review on membrane systems for hydrogen separation', Intermediate Report EU project MIGREYD NNE5-2001-670, http://www.ecn.nl/docs/library/report/2004/c04102.pdf

Kohol A L and Nielsen R (1997), *Gas Purification*, 5th edn, Gulf Publishing, Houston, TX.

Koros W J and Walker D R B (1991), 'Gas separation membrane material selection criteria: differences for weakly and strongly interacting feed components', *Fluid Phase Equilib*, **53**, 339–54.

Kotov N A (2003), *Multilayers Thin Films*, Decher G and Schlenoff J B (eds), Wiley-VCH, Weinheim, 207–36.

Ku A Y C, Ruud J A, Molaison J L, Schick L A and Ramaswamy V (2008), *Functionalized Inorganic Membranes for Gas Separation*. US Patent 20087396382.

Lababidi H, Al-Enezi G A and Ettouney H M (1996), 'Optimization of module configuration in membrane gas separation', *J Membrane Sci*, **112**, 185–97.

Lehmann J, Gaunt J and Rondon M (2006), 'Bio-char sequestration in terrestrial ecosystems: A review', *Mit Adapt Strat Global Chan*, **11**, 395–419.

LeRoux J D, Teplyakov V V and Paul D R (1994), 'Gas transport properties of surface fluorinated poly(vinyltrimethylsilane) films and composite membranes', *J Membrane Sci*, **90**, 55–68.

Li Y and Sun X S (2010), 'Preparation and characterization of polymer–inorganic nanocomposites by *in situ* melt polycondensation of l-lactic acid and surface-hydroxylated MgO', *Biomacromolecules*, **11**, 1847–55.

Lie J A, Vassbotn T, Hagg M B T, Grainger D, Kim T J and Mejdell T (2007), 'Optimization of a membrane process for CO_2 capture in the steelmaking industry', *Int J Greenhouse Gas Control*, **1**, 309–17.

Lin H, Van Wagner E, Swinnea J S, Freeman B D, Pas S J, Hill A J, Kalakkunnath S and Kalika D S (2006), 'Transport and structural characteristics of crosslinked poly(ethylene oxide) rubbers', *J Membrane Sci*, **276**, 145–61.

Low B T, Xiao Y and Chung T S (2009), 'Amplifying the molecular sieving capability of polyimide membranes via coupling of diamine networking and molecular architecture', *Polymer*, **50**, 3250–8.

Lu G Q, da Costa J C D, Duke M, Giessler S, Socolow R, Williams R H and Kreutz T (2007), 'Inorganic membranes for hydrogen production and purification: A critical review and perspective', *J Colloid Interface Sci*, **314**, 589–603.

Mahajan R, Zimmerman C M and Koros W J (1999), 'Fundamental and practical aspects of mixed matrix gas separation membranes', *ACS Symp Series*, **733**, 277–86.

Maneeintr K, Idem R O, Tontiwachwuthikul P and Wee A G H (2010), 'Comparative

© Woodhead Publishing Limited, 2011

mass transfer performance studies of CO_2 absorption into aqueous solutions of DEAB and MEA', *Ind Eng Chem Res*, **49**, 2857–63.

Mazur W H and Chan M C (1982), 'Membranes for natural gas sweetening and CO_2 enrichment', *Chem Eng Prog*, **78**, 38–43.

McHattie J S, Koros W J and Paul D R (1991), 'Gas transport properties of polysulphones 1 Role of symmetry of methyl group placement on bisphenol rings', *Polymer*, **32**, 840–50.

Meisen A and Shuai X (1997), 'Research and development issues in CO_2 capture', *Energy Conversion Management*, **38**, 37–42.

Michaels A S (1990), 'Membranes, membrane processes, and their applications: Needs, unsolved problems, and challenges of the 1990s', *Desalination*, **77**, 5–34.

Muruganandam N and Paul DR (1987), 'Evaluation of substituted polycarbonates and a blend with polystyrene as gas separation membranes', *J Membrane Sci*, **34**, 185–98.

Nunes S P and Peinemann K V (2001), *Membrane Technology in the Chemical Industry*, Wiley–VCH, Weinheim (Germany).

Ohyanagi M, Nishide H, Suenaga K and Tsuchida E (1988), 'Effect of polymer matrix and metal species on facilitated oxygen transport in metalloporphyrin (oxygen carrier) fixed membranes', *Macromolecules*, **21**, 1590–4.

Olajire A A (2010), 'CO_2 capture and separation technologies for end-of-pipe applications: A review', *Energy*, **35**, 2610–28.

Pacala S and Socolow R (2004), 'Stabilization wedges: solving the climate problem for the next 50 years with current technologies', *Science*, **305**, 968–72.

Patel N P, Miller A C and Spontak R J (2003), 'Highly CO_2-permeable and selective polymer nanocomposite membranes', *Adv Mater*, **15**, 729–33.

Paul D and Yampolskii Y (1994), *Polymeric Gas Separation Membranes*, CRC Press, Baton rouge:

Pennline H W, Luebke D R, Jones K L, Myers C R, Morsi B I, Heintz Y J and Ilconich J B (2008), 'Progress in carbon dioxide capture and separation research for gasification-based power generation point sources', *Fuel Proc Technol*, **89**, 897–907.

Perry J D, Nagai K and Koros W J (2006), 'Polymer membranes for hydrogen separations', *MRS Bull*, **31**, 745–9.

Pethe V V, Wang H P, Hiltner A, Baer E and Freeman B D (2008), 'Oxygen and carbon dioxide permeability of EAA/PEO blends and microlayers', *J Appl Polym Sci*, **110**, 1411–19.

Pixton MR and Paul DR (1995), 'Gas transport properties of polyarylates Part II Tetrabromination of the bisphenol', *J Polym Sci Part B: Polym Phys*, **33**, 1353–64

Pixton M R and Paul D R (2003), 'Gas transport properties of polyarylates. Part I Connector and pendant group effects', *J Polym Sci Part B: Polym Phys*, **33**, 1135–49.

Podall H (1971), 'Recent advances in reverse osmosis membranes for desalination', *Chem Eng Prog*, **67**, 260–6.

Powell C E and Qiao G (2006), 'Polymeric CO_2/N_2 gas separation membranes for the capture of carbon dioxide from power plant flue gases', *J Membrane Sci*, **279**, 1–49.

Robeson L M (2008), 'The upper bound revisited', *J Membrane Sci*, **320**, 390–400.

Robeson L M, Burgoyne W F, Langsam M, Savoca A C and Tien C F (1994), 'High performance polymers for membrane separation', *Polymer*, **35**, 4970–8.

Safari M, Ghanizadeh A and Montazer-Rahmati M M (2009), 'Optimization of membrane-based CO_2-removal from natural gas using simple models considering both pressure and temperature effects', *Int J Greenhouse Gas Control*, **3**, 3–10.

Sandru M, Haukebø S H and Hägg M B (2010), 'Composite hollow fibre membranes for CO_2 capture', *J Membrane Sci*, **346**, 172–86.

© Woodhead Publishing Limited, 2011

Schmidt H, Jonschker G, Goedicke S and Mennig M (2000), 'The sol–gel process as a basic technology for nanoparticle-dispersed inorganic-organic composites', *J Sol–Gel Sci Tech*, **19**, 39–51.

Schrag D P (2007), 'Preparing to capture carbon', *Science*, **315**, 812–13.

Schuiling R D (2006), 'Mineral sequestration of CO_2 and recovery of the heat of reaction', in *Macro-Engineering: A challenge for the future*, Badescu V, Cathcart R B and Schuiling R D (éds), Springer, Dordrecht, The Netherlands, Vol 54, 21–9.

Shao L, Low B T, Chung T S and Greenberg A R (2009), 'Polymeric membranes for the hydrogen economy: Contemporary approaches and prospects for the future', *J Membrane Sci*, **327**, 18–31.

Simbeck D and Roekpooritat W (2009), 'Near-term technologies for retrofit CO_2 capture and storage of existing coal-fired power plants in the United States', White paper for *MIT Coal Retrofit Symposium*, Mountain View, CA, USA, SFA Pacific Inc. http://webmit.edu/mitei/docs/reports/simbeck-near-term.pdf.

Simmons J W (2005), *Block Polyurethane–Ether and Polyurea–Ether Gas Separation Membranes*, US Patent 6843829.

Simmonds M, Hurst P, Wilkinson M B, Watt C and Roberts C A (2003), 'A study of very large scale post combustion CO_2 capture at a refining & petrochemical complex', http://www.co2captureproject.org

Smith A, Schellnhuber H J and Mirza M M Q (2001), *Climate Change 2001: Impacts, adaptation, and vulnerability*, McCarthy J J, Canziani O F, Leary N A, Dokken D J and White K S (eds), Cambridge, University Press, Cambridge.

Spillman R W (1989), 'Economics of gas separation membranes', *Chem Eng Prog*, **85**, 41–62.

Sridhar S, Veerapur R S, Patil M B, Gudasi K B and Aminabhavi T M (2007), 'Matrimid polyimide membranes for the separation of carbon dioxide from methane', *J Appl Polym Sci*, **106**, 1585–94.

Stern S A, Mi Y, Yamamoto H and St Clair A K (1989), 'Structure/permeability relationships of polyimide membranes. Applications to the separation of gas mixtures', *J Polym Sci Part B: Polym Phys*, **27**, 1887–909.

Sun H Z and Yang B (2008), '*In situ* preparation of nanoparticles/polymer composites', *Science in China Series E: Tech Sci*, **51**, 1886–901.

Suzuki T and Yamada Y (2005), 'Physical and gas transport properties of novel hyperbranched polyimide-silica hybrid membranes', *Polymer Bull*, **53**, 139–46.

Tanaka K, Okano M, Toshino H, Kita H and Okamoto K I (1992a), 'Effect of methyl substituents on permeability and permselectivity of gases in polyimides prepared from methyl-substituted phenylenediamines', *J Polym Sci Part B: Polym Phys*, **30**, 907–14.

Tanaka K, Kita H, Okano M and Okamoto K I (1992b), 'Permeability and perm-selectivity of gases in fluorinated and non-fluorinated polyimides', *Polymer*, **33**, 585–92.

Tin P S, Chung T S, Liu Y, Wang R, Liu S L and Pramod K P (2003), 'Effects of cross-linking modification on gas separation performance of Matrimid membranes', *J Membrane Sci*, **225**, 77–90.

Tsang C F, Benson S M, Kogelski B and Smith R E (2002), 'Scientific considerations related to regulation development for CO_2 sequestration in brine formations', *Environ Geol*, **42**, 275–81.

Vansant E F and Dewolf R (1990), 'Gas separation technology', *Proceedings International Symposium on Gas Separation Techniques*, Antwerp (Belgium), Elsevier.

Walker D R B and Koros W J (1991), 'Transport characterization of a polypyrrolone for gas separations', *J Membrane Sci*, **55**, 99–117.

© Woodhead Publishing Limited, 2011

Weller S and Steiner W A (1950), 'Separation of gases by fractional permeation through membranes', *J Appl Phys*, **21**, 279–83.
Won J, Kim M H, Kang Y S, Park H C, Kim U Y, Choi S C and Koh S K (2000), 'Surface modification of polyimide and polysulfone membranes by ion beam for gas separation', *J Appl Polym Sci*, **75**, 1554–60.
Xu Z, Yu L and Han L (2009), 'Polymer-nanoinorganic particles composite membranes: a brief overview', *Front Chem Eng China*, **3**, 318–29.
Yang H, Xu Z, Fan M, Gupta R, Slimane R B, Bland A E and Wright I (2008), 'Progress in carbon dioxide separation and capture: A review', *J Env Sci*, **20**, 14–27.
Yave W, Car A and Peinemann K V (2010), 'Nanostructured membrane material designed for carbon dioxide separation', *J Membrane Sci*, **350**, 124–9.
Youn K K, Ho B P and Young M L (2005), 'Preparation and characterization of carbon molecular sieve membranes derived from BTDA-ODA polyimide and their gas separation properties', *J Membrane Sci*, **255**, 265–273.
Young J S, Long G S and Espinoza B F (2006), *Sulfolane-Cross-Polybenzimidazole Membrane for Gas Separation*, US Patent 6997971.
Zhang Y, Musselman I H, Ferraris J P and Balkus Jr K J (2008), 'Gas permeability properties of mixed-matrix matrimid membranes containing a carbon aerogel: A material with both micropores and mesopores', *Ind Eng Chem Res*, **47**, 2794–802.
Zhao H Y, Cao Y M, Ding X L, Zhou M Q and Yuan Q (2008a), 'Effects of cross-linkers with different molecular weights in cross-linked Matrimid 5218 and test temperature on gas transport properties', *J Membrane Sci*, **323**, 176–84.
Zhao Y, Cao Y M, Ding X L, Zhou M Q, Liu J H and Yuan Q (2008b), 'Poly(ethylene oxide) induced cross-linking modification of Matrimid membranes for selective separation of CO_2', *J Membrane Sci*, **320**, 179–84.
Zimmerman C M and Koros W J (1999a), 'Polypyrrolones for membrane gas separations I Structural comparison of gas transport and sorption properties', *J Polym Sci Part B: Polym Phys*, **37**, 1235–49.
Zimmerman C M and Koros W J (1999b), 'Comparison of gas transport and sorption in the ladder polymer BBL and some semi-ladder polymers', *Polymer*, **40**, 5655–64.
Zimmerman C M, Singh A and Koros W J (1997), 'Tailoring mixed matrix composite membranes for gas separations', *J Membrane Sci*, **137**, 145–54.

5.11 Appendix: list of symbols

5.11.1 Symbols

D diffusivity (cm s^{-1})
FFV fraction free volume
k constant (mol $cm_{membrane\ thickness}$ cm^{-2} Pa^{-1} s^{-1})
l thickness (μm)
N molar flow rate (mol s^{-1}), $\overline{N}$ refers to the permeate flow (mol s^{-1})
P gas permeability (mol $cm_{membrane\ thickness}$ cm^{-2} Pa^{-1} s^{-1})
p gas pressure (Pa)
Q gas permeation flow rate (mol s^{-1})
Δp pressure difference across the membrane (Pa)
R efficiency of the membrane separation process

© Woodhead Publishing Limited, 2011

S gas solubility selectivity
n slope of the log-log limit
S_A cross-sectional area of the membrane (m^2)
x retentate CO_2 molar fraction
x_{in} mole fraction of CO_2 in the feed
y_P mole fraction of CO_2 in the permeate
y permeate CO_2 molar fraction
z axial coordinate (m)

5.11.2 Subscripts

i gas species 'i'
j gas species 'j'
I retentate side
II permeate side
L membrane outlet
0 membrane inlet
tot total

5.11.3 Greek symbols

α_{ij} ideal gas selectivity between gas 'i' and gas 'j'
θ stage cut as a ratio between permeate and feed flow rates
φ pressure ratio

© Woodhead Publishing Limited, 2011

6

Polymeric membranes for post-combustion carbon dioxide (CO_2) capture

W. YAVE and A. CAR, GKSS-Research Centre Geesthacht GmbH, Germany

Abstract: This chapter focuses on membranes from block copolymers (e.g Pebax and Polyactive) and their potential application for flue gas processing in power plants. The development of membranes and their advantages and limitations are clearly presented. Recently developed polymeric membranes are reviewed from critical point of view, and some results under real conditions are also reported. A new approach for obtaining tailor-made polymeric membranes with a CO_2-phillic surface, manufactured as thin films is described. The membranes developed by this approach exhibit outstanding separation performance with promising results for flue gas treatment.

Key words: block copolymers, CO_2-phillic surface, flue gas, polymeric membranes.

6.1 Introduction

Global warming is mainly caused by exhaust or flue gases that are the result of the combustion of coal and fossil fuels (in power plants, industry, agriculture, home heating and transport). Flue gas typically consists of nitrogen (N_2), water vapour (H_2O), carbon dioxide (CO_2) and small quantities of other gases. CO_2 is considered to be one of the largest contributors to global warming and owing to population growth during last century, the concentration of CO_2 in the atmosphere stayed higher than 350 ppm and until September 2010 was higher than 388 ppm.[1] According to the Intergovernmental Panel on Climate Change (IPCC) of the United Nations (UN), the global climate will be dramatically changed by 2050 if CO_2 emission continues to rise at current rates.[2] Actually, we are already seeing many climate change disasters such as floods, hurricanes, droughts, forest fires, and so on. The control and reduction of CO_2 emissions are therefore important policies to stop climate change right now.

To reduce CO_2 emission and not depend on fossil fuels, new and efficient technologies for producing energy are being developed (e.g. solar energy and laser-fusion).[3–5] The efficient use of energy is another alternative to control and reduce CO_2 emission, that is sharing excess energy and changing our lifestyles.[6] Although these alternatives could lead to a reduction or at least to

© Woodhead Publishing Limited, 2011

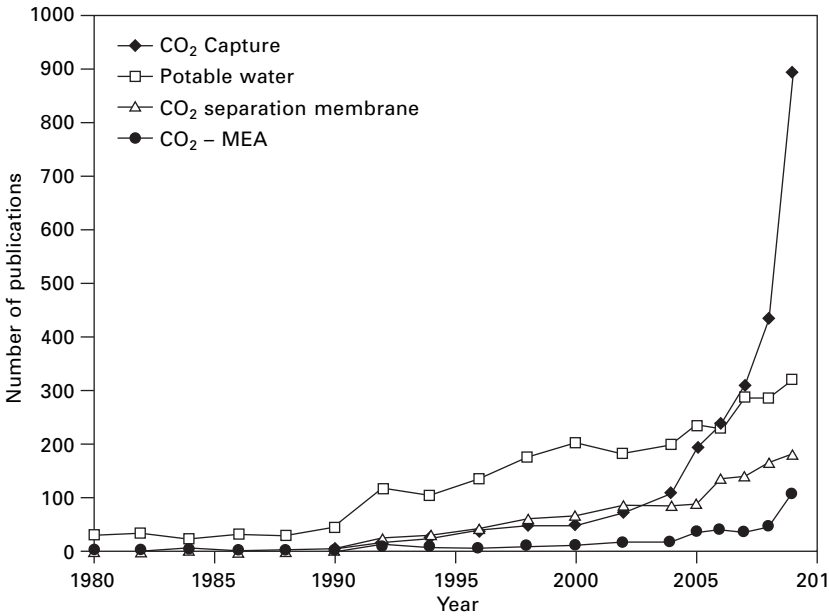
maintain the CO_2 concentration in the atmosphere, energy demand (electricity) is increasing every day, showing that the use of fuels and the construction of new power plants will continue for many years. It is known, that more than one-third of CO_2 emission comes from power plants, cement plants, refineries and steel mills;[7] the integration of CO_2 capture technologies in these facilities is therefore being strongly investigated and is believed probably to be cheaper than transition to new nuclear, wind and solar energy.[8]

The IPCC in fact reported in 2005 that the CO_2 capture and storage (CCS) might considerably reduce CO_2 emissions.[9] The first and largest pilot plant for the CO_2 capture and storage following this recommendation was launched in Denmark (2006); this project is at the Elsam power station and will demonstrate the reliability and efficiency of the post-combustion capture process.[10] In this unit, the flue gas is directed to an absorber (solvent), where ~90% of CO_2 is captured, the solvent–CO_2 mixture is then sent to a regenerator (> 100°C) to separate the CO_2 from the solvent, the regenerated solvent is used again later and the CO_2 is transported to storage. The challenge in this project is to find an adequate absorbent which can lower the CO_2 capture costs. The CO_2 capture cost by a conventional absorption process is between US$ 50 and 70 per metric tonne of CO_2 captured; by developing new absorbents it might be reduced up to US$ 30 per metric tonne. The CO_2 capture costs could be also lowered if heat integration is considered (by utilizing feed-water preheating heat flow and heat generated during CO_2 compression), since an analysis has shown that without heat integration the process would not be economically viable.[11]

Nowadays, the search for CO_2 capture technologies is attracting researchers from different fields including nanotechnology. Although the absorption process is still considered to be the best technology for CO_2 capture,[12] 'membranologists' believe that membrane technology is an attractive candidate for CO_2 capture. Membrane technology has its own advantage over the absorption process such as less environmental impact, small footprints, low investment cost, energy efficiency and ease of integration into existing power plants.[13] The membrane process for CO_2 capture had already been suggested in the 1980s.[14, 15] Later many authors focused their researches on improving CO_2 selectivity and permeability (development of novel membrane materials).[16, 17] Recently, studies on the opportunities and feasibility of CO_2 capture from flue gases using membranes have been also reported,[18–20] and separately these authors[18–20] concluded that with an optimal process design and an advanced CO_2-selective membrane, the membrane process is technically and economically feasible. Much information on CO_2 capture by membranes either organic or inorganic can be found in the literature.

In general, a schematic view of the importance of CO_2 capture (research and development) in the last years can be seen in Fig. 6.1. The CO_2 capture problem has become much more important than the issue of potable water,

© Woodhead Publishing Limited, 2011



6.1 Number of publications vs year on different topics: CO_2 capture, potable water, CO_2 separation membrane and CO_2 separation by MEA. The number of publications was extracted from the ISI web of knowledge[SM] for each topic (20 August 2010).

which is a basic problem that concerns millions of people worldwide. For instance, the number of publications related to CO_2 capture in the last few years has increased tremendously in comparison with the topic of potable water. The number of publications relating to CO_2 separation by membranes (Fig. 6.1) has also grown (1995–2009) more than those about the amine absorption process (MEA). Investigations relating to CO_2 capture by membranes were almost double those about absorbents in 2009, which demonstrates that membrane technology is becoming an important option for CO_2 capture.

This chapter is only devoted to CO_2 capture using polymeric membranes in power plants; CO_2 capture in general is discussed in the other chapters of this book. However, recent advances in CO_2 capture from air are worthy of description here, since this topic is not discussed in any other chapters and is important because the amount of global CO_2 also includes CO_2 that already exists in the atmosphere (produced by transportation). Keith and co-workers from the University of Calgary (Canada), for example, developed a device that removes CO_2 directly from the air.[21, 22] The process captures CO_2 with alkali hydroxide solutions, in a similar manner to commercial technology. Although this process can eliminate the additional separation processes, its adoption on the large scale is not yet feasible. Lackner's group at Columbia

© Woodhead Publishing Limited, 2011

University (USA) is also developing technologies to capture CO_2 from the air.[23, 24] They created a so-called synthetic tree and claimed that it collects CO_2 1000-times faster than anything else; the process is similar to that used for capturing CO_2 in power plants but with the difference that it can operate at anytime and anywhere. Like Keith's group, they found that CO_2 capture from the air is almost impossible owing to the low concentrations (~0.039%). However, they also found that CO_2 capture from the atmosphere is very important, because the CO_2 generated by cars and airplanes contribute to global warming as well. Other alternatives for capturing CO_2 from the air are also being developed, such as those at PARC (Palo Alto Research Center), Max-Planck Institute (Potsdam) and Sandia National Laboratories (New Mexico) among others.

6.2 Basic principles of flue gas membrane separation

The basic principles of flue gas membrane separation mainly depend on the membrane material, gas composition in the feed side and process conditions. Developing a high performance membrane for flue gas processing involves designing a membrane material with high permeability, high selectivity which is stable under wet conditions (water vapour), at temperatures not less that 50°C. A limitation of membrane material design however is the existence of the permeability–selectivity trade-off proposed by Robeson,[25] which means that membranes with higher permeability usually present lower selectivity (only for dense polymeric film excluding facilitated transport membranes).

The gas flux (J) through a dense polymeric membrane is described by Fick's law, where J is directly proportional to the gas diffusivity (D) and a driving force (dc/dx) which is a concentration gradient through the thickness (l) of dense film, Equation [6.1]:

$$J = -D\frac{dc}{dx} \qquad [6.1]$$

Under steady-state conditions, Equation [6.1] can be integrated taking into account the limits c_{if} and c_{ip} (concentration of gas i on the feed or permeate side) for 'c', and $x = 0$ and $x = l$ for 'x', thereby Equation [6.1] becomes:

$$J_i = D_i \times \frac{(c_{if} - c_{ip})}{l} \qquad [6.2]$$

The concentrations c_{if} and c_{ip} of gas 'i' can be replaced by its partial pressure (p_i) according to Henry's law, Equation [6.3]:

$$c_i = S_i \times p_i \qquad [6.3]$$

where S_i is the solubility coefficient of gas 'i'.

© Woodhead Publishing Limited, 2011

Inserting Equation [6.3] into Equation [6.2], the gas flux J becomes:

$$J_i = D_i \times S_i \times \frac{(p_{if} - p_{ip})}{l} \quad [6.4]$$

The term '$D_i \times S_i$' in Equation [6.4] represents the gas permeability (P_i); hence the permeability has been defined as the product of diffusion and solubility coefficients for the gas in the membrane material.

The ratio between two gas permeabilities (pure gas) is defined as intrinsic selectivity (α):

$$\alpha = \frac{P_i}{P_j} \quad [6.5]$$

Because P can be expressed as a product of D and S, the intrinsic selectivity can be also written as:

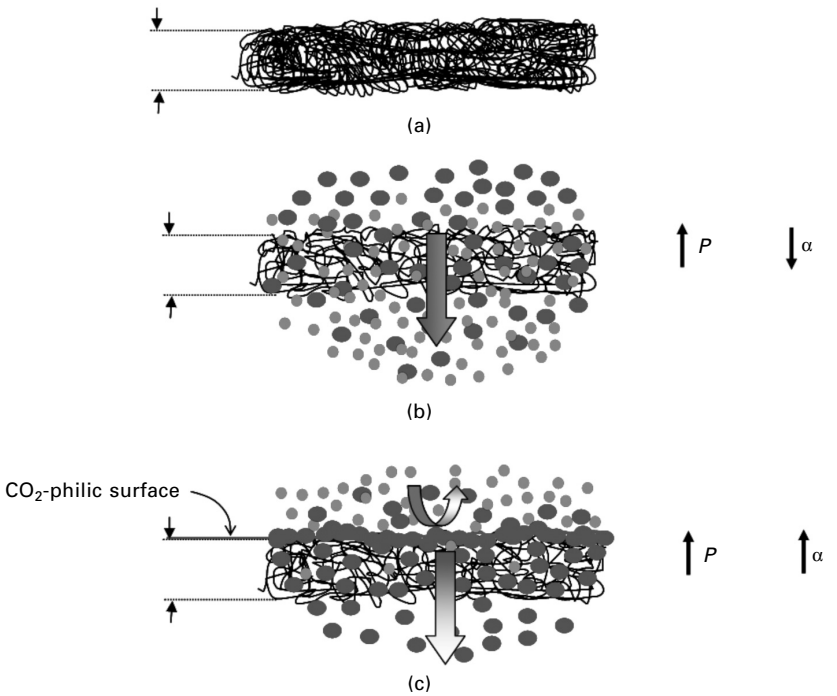
$$\alpha = \frac{D_i \times S_i}{D_j \times S_j} = \frac{D_i}{D_j} \times \frac{S_i}{S_i} \quad [6.6]$$

where the diffusivity and solubility selectivity are defined.

The permeability definition in Equation [6.4] allows the development of strategies for designing new membrane materials with high permeability, that is the higher the diffusivity and solubility, the higher the permeability of the polymeric material. However, in order to improve the gas diffusivity in dense polymeric membranes, the free volume and fractional free volume of polymer must be enhanced, thereby displacing the gas molecule more easily. Improving the fractional free volume also improves the gas solubility, since it means a less crystalline structure in the polymeric material and improves the interaction of gas molecules with the polymer. The gas solubility coefficient can be also increased by designing a specific monomeric unit or by modifying the polymer chemically, that is making the polymer more CO_2-philic. On the other hand, both the diffusivity and solubility selectivity allow membranes to be designed with better selectivity. Improving simultaneously both selectivities is a key challenge in developing advanced membrane materials. For CO_2 capture as described above, the polymer must be CO_2-selective with high permeability, stable to water vapour and easy to process when making membranes. Although CO_2-selective membranes are the most studied, N_2-selective membranes have also been proposed for flue gas processing,[26, 27] but this reverse selective membrane is still viewed as a scientific curiosity.

Figure 6.2 shows a schematic representation of a strategy to develop a highly CO_2-selective membrane (rubbery-like). As known, a polymer is formed by amorphous and crystalline structure (semi-crystalline materials); the polymer matrix, especially the amorphous phase is formed by small spaces called free volume and by the polymer chains through which the

© Woodhead Publishing Limited, 2011



6.2 Schematic representation of a strategy to develop CO_2-selective membranes with high permeability and selectivity; (a) a typical polymer structure with a low free volume membrane matrix; (b) a polymer with a high free volume membrane matrix and (c) a polymer with high free volume membrane matrix and a CO_2-philic surface (the spheres represent the CO_2 and H_2 molecules).

gas permeates, the amount of these spaces is the fractional free volume and depends on crystallinity of polymer. Tailoring the free volume and the fractional free volume are keys to improve simultaneously the selectivity and permeability.

As shown in Fig. 6.2, when the free volume size and the fractional free volume are increased, the permeability can be greatley enhanced, but because of the permeability–selectivity trade-off, the selectivity is lowered. Nevertheless, if the polymer is CO_2-philic and this feature is somehow directed towards the membrane surface, both the permeability and selectivity can be simultaneously improved. It is important to note, however, that CO_2-selective membranes have a diffusivity selectivity of less than one, which limits the improvement of the membrane. New insights (tailor-made CO_2-philic membrane) in developing advanced membrane materials may overcome this limitation or at least to have a diffusivity selectivity as high as possible (close to one).

© Woodhead Publishing Limited, 2011

After developing the membrane material, producing it on large scale as composite membrane and studying it under different operating condition (under high and low pressure, high temperature, wet condition, gas mixtures, etc.) is important for its real application. For flue gas processing, the membrane must be highly permeable, since an enormous volume of gas has to be treated at low pressure. Thus, for a membrane to have extremely high flux, the gas permeability must be high, the driving force increased and the thickness of the membrane minimized (Equation [6.4]). Using a thin film membrane with a thickness less than 100 nm would be appropriate to enhance the gas flux, but the membrane selectivity must be maintained (defect-free), and the thin film must be protected from the ash and particle matter, which could degrade the separation performance of membrane (discussed later).

6.3 Membrane development and applications in power plants

As flue gas is mainly the result of the combustion of coal and fossil fuels in power plants and in industry, the CCS concept is being applied in these facilities and it is planned to inject the captured CO_2 into a suitable underground geological formation. Currently, an important goal for industrialized and developing countries is to have the appropriate technology for CO_2 capture (economically and environmentally effective), which is clearly observed by the numbers of projects supported by various foundations worldwide and by the amount of research reported in the last few years (Fig. 6.1).

It is very important to know the flue gas characteristic when designing a membrane for CO_2 capture from flue gases. There is usually an enormous volume flue gas which contains low concentrations of CO_2 (< 20 vol%), moreover it is at atmospheric pressure, which means that the driving force for CO_2 separation is small. Typical CO_2 concentrations in different gas streams are shown in Table 6.1.

The CO_2 concentration in flue gas from power plants is not more than 14 vol% (Table 6.1), which means there is only 0.14 bar of CO_2 partial

Table 6.1 Typical CO_2 concentrations in different gas streams (flue gas)

Facility	CO_2 concentration (vol%)
Power plant	
– coal	~14
– fuel gas	~9
– fuel gas (combined cycle)	~4
– fuel oil	~12
Cement kiln	14–33
Blast furnace gas	18–20
Petrochemical industry (heaters)	~8

© Woodhead Publishing Limited, 2011

pressure (flue gas pressure equal to atmospheric pressure), thus the driving force for the separation process is too small. The small value of CO_2 partial pressure and the enormous volume of flue gas make CO_2 separation from power plants difficult, especially using membranes. The current membranes, for example, are in many cases not competitive for CO_2 separation from flue gas (on a large scale); the flux for CO_2 is not high enough and would require a large membrane area. State-of-the-art membranes exhibit a CO_2 flux of ~0.3 m^3 (STP) m^{-2} h^{-1} bar^{-1}; an increase in flux of an order of magnitude will drastically increase the market share of CO_2 selective membranes and thereby make CO_2 capture from power plants feasible.

The process of CO_2 capture in a power plant should take place after dust removal and desulfurization unit and before entering the stack. After desulfurization, the flue gas is usually saturated with water, implying that the membrane must be resistant to vapour water as well (at ~55°C). CO_2 separation must be performed by an appropriate process design, which can be a multi-step or multi-stage membrane process, to obtain the desired product (i.e. CO_2 recovery and purity).[19] Although CO_2 capture from power plants is not a reality at the moment, there are a great variety of projects and research on separation techniques around the world, such as gas separation technology, absorption and adsorption processes as well as hybrid processes (absorption/membrane).

One of the first analyses of CO_2 separation from flue gas using membranes was carried out by Van Der Sluijs and co-workers in 1992.[28] Using a computer program based on the cross-flow model, they found that membranes with a CO_2/N_2 selectivity of 200 are needed to make the membranes competitive with other separation processes. Moreover, with the existing membranes (in 1992), CO_2 removal could be achieved up to 75% (50% purity) and the capture cost would be about US$ 50 per tonne. Later, in 2007, Favre[29] reported a critical comparison of CO_2 capture by polymeric membrane and the amine absorption process (for post-combustion applications). For flue gases containing 10% CO_2, the energy requirement for CO_2 capture by a polymeric membrane was found to be much larger than the absorption process and even if the membrane had high selectivity (> 120) the required energy was high. However, they concluded that if the flue gas had 20% CO_2 (cement kiln and blast furnace gas fleets), membrane technology could compete with the absorption process. Another important conclusion was that the selectivity of the membrane is not necessarily the most important factor for improvement.

A polymeric membrane from the RITE institute (Japan)[30] was presented as being the first promising membrane for CO_2 capture due to its high gas flux. However, because of its membrane structure (hollow fibre) and material (chemically modified cardo-polyimide type) production on large scale seemed to be difficult. Laboratory scale studies have shown that membranes with a

© Woodhead Publishing Limited, 2011

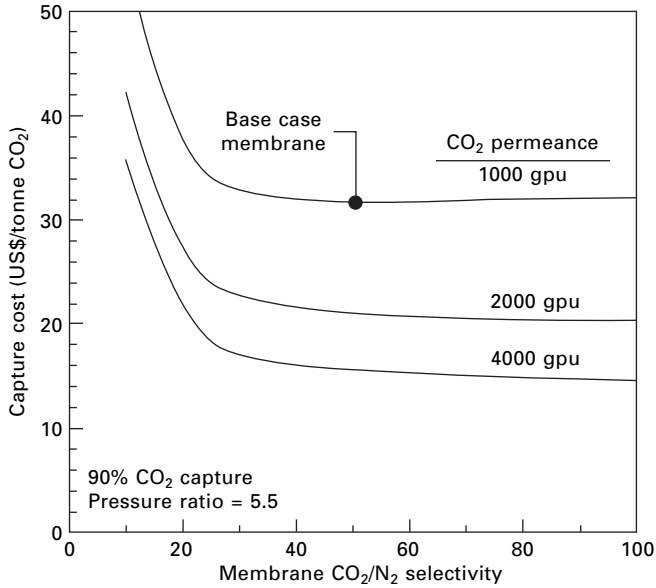
CO_2/N_2 selectivity of 35 effectively recovered CO_2 from flue gas. The cost of CO_2 separation and subsequent liquefaction was also found to be cheaper than the amine absorption process. Another membrane which also seems to be promising is the CO_2-selective membrane with a facilitated transport mechanism developed by May-Britt Hägg's group.[18] This membrane was studied for the capture of CO_2 from flue gas mixtures and the results showed that it is feasible even for low CO_2 concentrations (< 10%). They also showed that 90% CO_2 can be recovered and a purity of up to 90% can be reached. The energy requirement and gas processing cost seem to be competitive compared with the amine absorption process.

Membrane Technology and Research (MTR) Inc, working together with the US Department of Energy (DoE) presented the Polaris™ Membrane,[19] whose performance was similar to the membrane from the RITE institute which was the best membrane to that date. The CO_2 flux of these membranes is around 2.7 m^3 (STP) m^{-2} h^{-1} bar^{-1}. The Polaris™ membrane was examined for CO_2 capture from a power plant and it was concluded that membrane selectivity is not really a factor that controls the final cost of CO_2 capture. The CO_2 flux was found to be more important and, by appropriate design of the separation process, the cost of CO_2 capture could be lowered up to about US$ 32 per tonne of CO_2 captured. This analysis has shown that the membrane process can effectively compete or even replace the absorption process. However, the membrane must have an extremely high CO_2 flux. The developed membrane is based on a rubbery-like membrane (polyether-polyamide copolymer 'Pebax®') and has CO_2 fluxes greater than those described above; the flux is ten times higher than commercial CO_2-selective membranes.[31] The goal of MTR was to develop a thin film membrane with extremely high flux; thereby they could reduce the required membrane area. Combined with a novel process design this membrane could meet DOE targets (reduction of energy costs in a CO_2 recovery system). As evidence, Fig. 6.3 illustrates the effect of membrane properties on CO_2 capture cost elaborated by MTR scientists. To generate this plot, a two-step counter-flow/sweep membrane process was used and the pressure ratio was 5.5, which corresponded to a feed pressure of 1.1 bar and 0.2 bar in the permeate vacuum.

Figure 6.3 shows that membranes with a higher flux result in lower CO_2 capture cost, if a membrane with a much higher flux (>10 m^3 (STP) m^{-2} h^{-1} bar^{-1}) was developed, the CO_2 capture cost would be lowered to less than US$ 20 per tonne. As predicted by Favre,[29] the selectivity effectively did not have an affect on CO_2 capture cost; a CO_2/N_2 selectivity of about 30 is enough to lower the costs. MTR expects to use 12% of the energy from an electricity plant and they planned to test in the real field in 2009 at Arizona Public Service's coal-fired Cholla plant.

It is worthwhile mentioning that Pebax® which was used by MTR had already been identified as a promising CO_2-selective material by Blume and

© Woodhead Publishing Limited, 2011

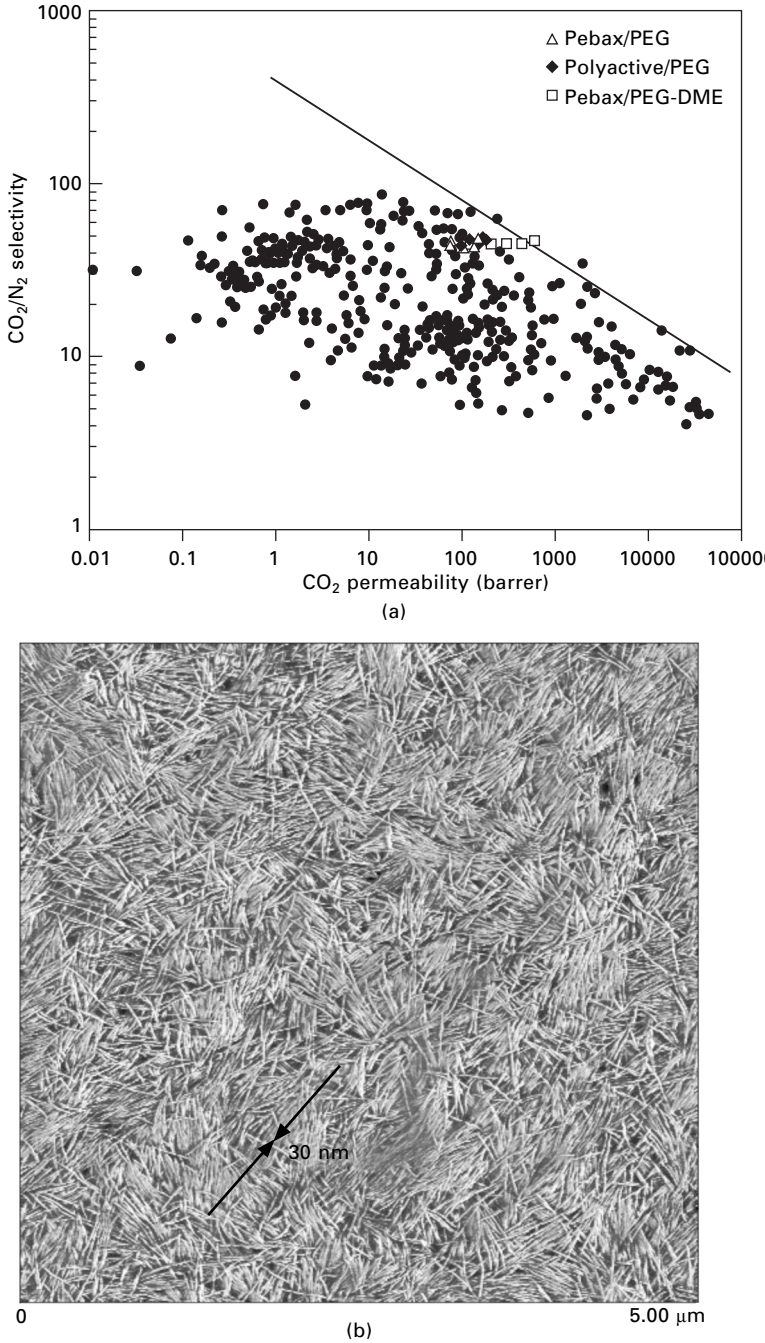


6.3 Effect of membrane properties on the cost of capturing 90% CO_2 from flue gas.[19] Copyright: *Journal of Membrane Science*.

Pinnau in 1990.[32] However, researches showed up the difficulty of producing thin film membranes owing to solubility problems and hence no further work was reported. In 2008, GKSS Research Centre Geesthacht GmbH (Germany) ran the Gas Separation Membranes for Zero-Emission Fossil Power Plants Project. This project is supported by the Helmholtz-Alliance MemBrain and the main goal is to develop CO_2-selective membranes for CO_2 capture.[33] Following the targets set by the MemBrain projects we investigated Pebax® polymer again and found that a mixture of ethanol/water (70/30 wt%) can easily dissolve a Pebax® (Pebax® MH 1657 from Arkema).[34] After this study, we developed dense membranes with extremely high performance,[35, 36] and thin film membranes with CO_2 fluxes higher than 1.0 m^3 (STP) m^{-2} h^{-1} bar^{-1}.[36, 37] Figure 6.4 shows the performance of Pebax® membranes developed in that period. It was interesting during this study to find that the nanostructure formed on the surface seemed to affect the membrane performance. Thus, the high CO_2 flux combined with good selectivity was attributed to a strong increase in the diffusivity and solubility coefficients, as well as to the mikado-like nanostructure on the surface. This membrane overcame the permeability–selectivity trade-off, but did not present long-term stability under real conditions.[36]

Membranes developed from Pebax® have ultimately gained importance owing to its advantages such as high permeability and selectivity, low cost (because it is a commercial polymer) and good mechanical and thermal

© Woodhead Publishing Limited, 2011



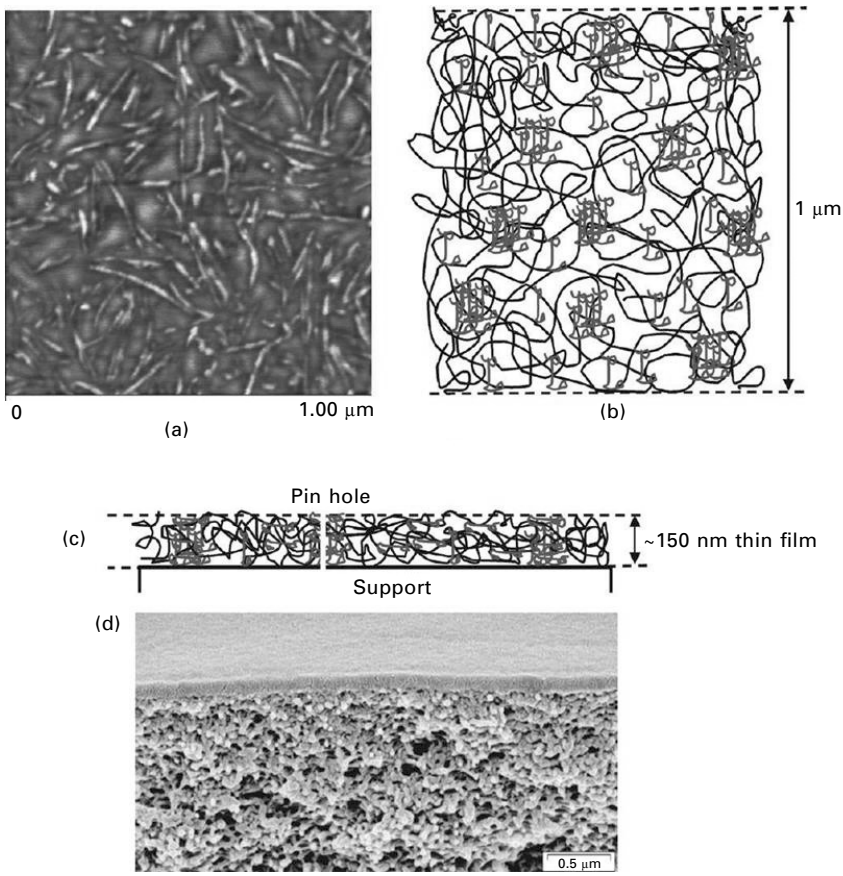
6.4 (a) CO_2/N_2 selectivity as a function of CO_2 permeability (updated from Robeson's upper bound),[25] and (b) AFM micrograph of Pebax®/PEG-DME membrane (blend containing 50 wt% PEG-DME).[36] Copyright: *Journal of Membrane Science*.

© Woodhead Publishing Limited, 2011

properties.[38–40] Moreover, the fabrication of the membrane as a composite is simple for producing on large volumes. Although it became a reality for Pebax® to be used in membranes for CO_2 capture (demonstrated by MTR), other polymers with a similar structure were also reported to constitute promising membrane material, with even better performance than Pebax®. One of these materials is known as Polyactive®, which was first investigated by Metz and co-workers.[41] Their study showed that polymeric membranes (CO_2-selective) from Polyactive® give good separation performance. Later Car and co-workers together with IsoTis OrthoBiologics (USA)[42] developed a tailor-made Polyactive® with better performance than the existing commercial polymer. The pristine polymer and the blend with polyethylene glycol (PEG) gave a better performance than Pebax® communicating to the scientific community that polymeric material with a higher performance can be developed by tailoring the polymer structure. Based on this work and the idea of fabricating thin film membranes with better performance than those developed by MTR, Polyactive® was studied intensively and blended with a special additive (PEG with functionalized end group), which had structural similarity to segments of Polyactive® (butyl group and ethylene oxide units).[43] The polymeric material presented CO_2 permeability five-fold higher than pristine polymer and the CO_2/N_2 selectivity remained almost constant; thus the thin film membrane fabricated on the pilot scale presented a similar performance to the membranes developed by MTR and the RITE institute (~2.7 m^3 (STP) m^{-2} h^{-1} bar^{-1}). Laboratory studies have shown that this membrane is promising for CO_2 capture from flue gas and experiments with gas mixtures under different operating conditions have given an indication of its performance. The main conclusion was that thin films with a thickness on the nanometre scale give outstanding gas separation performance, but long-term performance can deteriorate owing to thinning and microphase separation between Polyactive® and PEG. Figure 6.5 shows the thin film membrane developed from Polyactive®, as well as the proposed structure of the membranes and the appearance of defects caused by the presence of the low molecular weight PEG.

Recently, a nanometric thin film membrane with the highest performance for CO_2 capture was reported.[44] Using the tailor-made Polyactive® and controlling the nanofabrication conditions defect-free ultra-thin film membranes (far thinner than 100 nm) with unmatched CO_2 fluxes were produced on the square metre scale. Figure 6.6(a) presents a SEM image of a nanometric thin film membrane and Fig. 6.6(b) shows the performance of these membranes compared with other state-of-the-art membranes including the Pebax® membrane developed by GKSS, the Polaris™ membrane from MTR and the cardo-polyimide from RITE institute. These polymeric membranes represent membranes with the highest performance to date for CO_2 separation from flue gas.

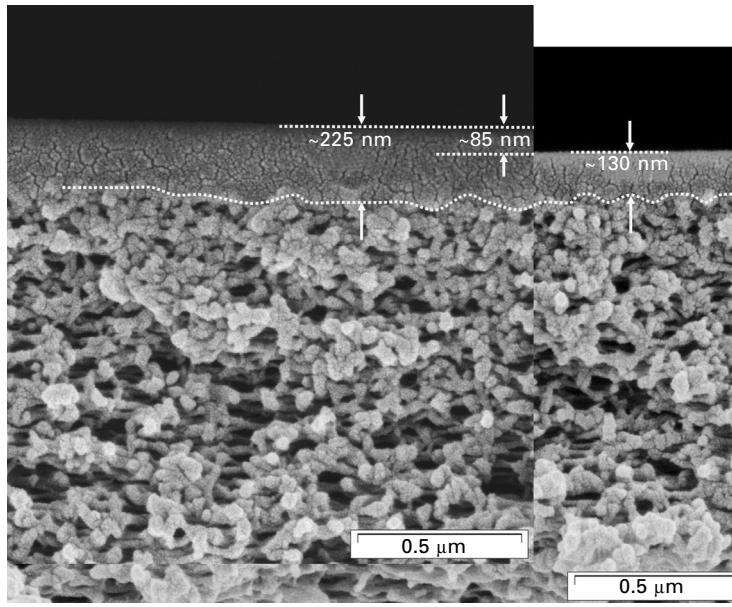
© Woodhead Publishing Limited, 2011



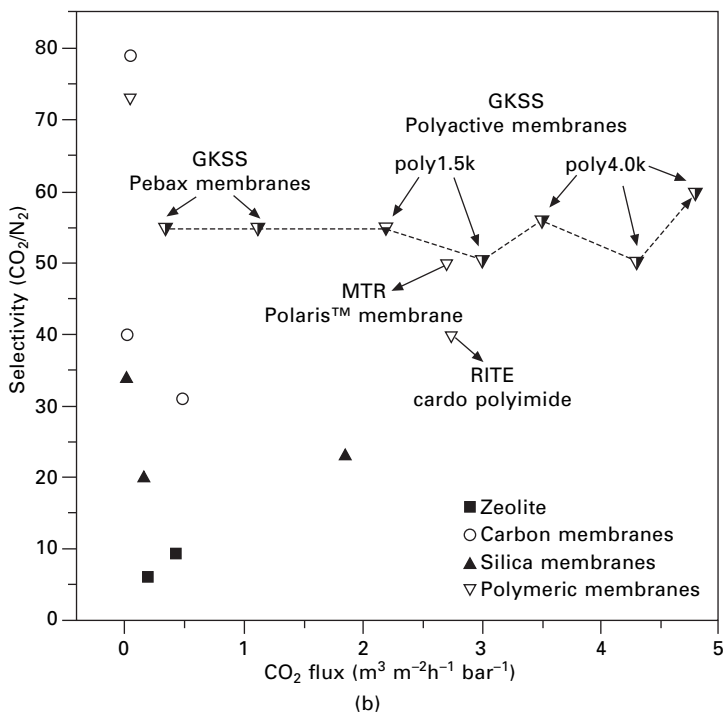
6.5 (a) Atomic force microscopy (AFM) phase image of Polyactive® membrane blended with polyethylene glycol dibutylether, (b) schematic representation of AFM image showing the microphase separation, (c) schematic representation of thin film membrane showing the possible pin hole, and (d) scanning electron microscopy (SEM) image of a Polyactive® membrane (thickness approximately 150 nm).[43] Copyright: *Macromolecules*.

For application in power plants, the performance of these membranes was studied with a single gas and with gas mixtures under different operating conditions (different temperatures and pressures). Moreover, the best membrane (the most stable and highly reproducible) was produced on square metre scale and is under evaluation on the pilot scale in the German MemBrain project.[33] This thin film membrane has potential application in the treatment of large streams under low pressure. However, its stability in the long-term still has to be investigated (protection of the thin film from particle matter), since it was found that the flue gas contains large quantities

© Woodhead Publishing Limited, 2011



(a)



(b)

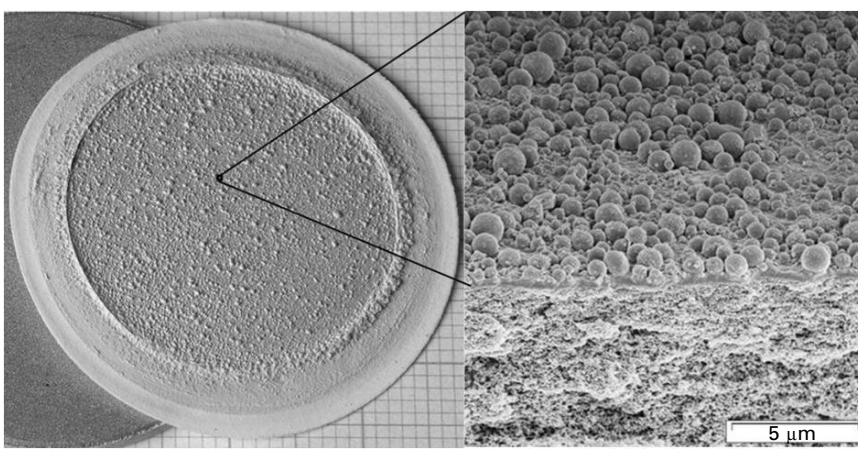
6.6 (a) SEM image of a nanometric thin film membrane and (b) performance of different polymeric membranes (thin film) compared with those from other materials.[44] Copyright: *Nanotechnology*

© Woodhead Publishing Limited, 2011

of particle matter which is difficult to remove before gas treatment by the membranes. The accumulation of this matter might damage the thin film if it is not well protected (Fig. 6.7), resulting in lower selectivity and flux.

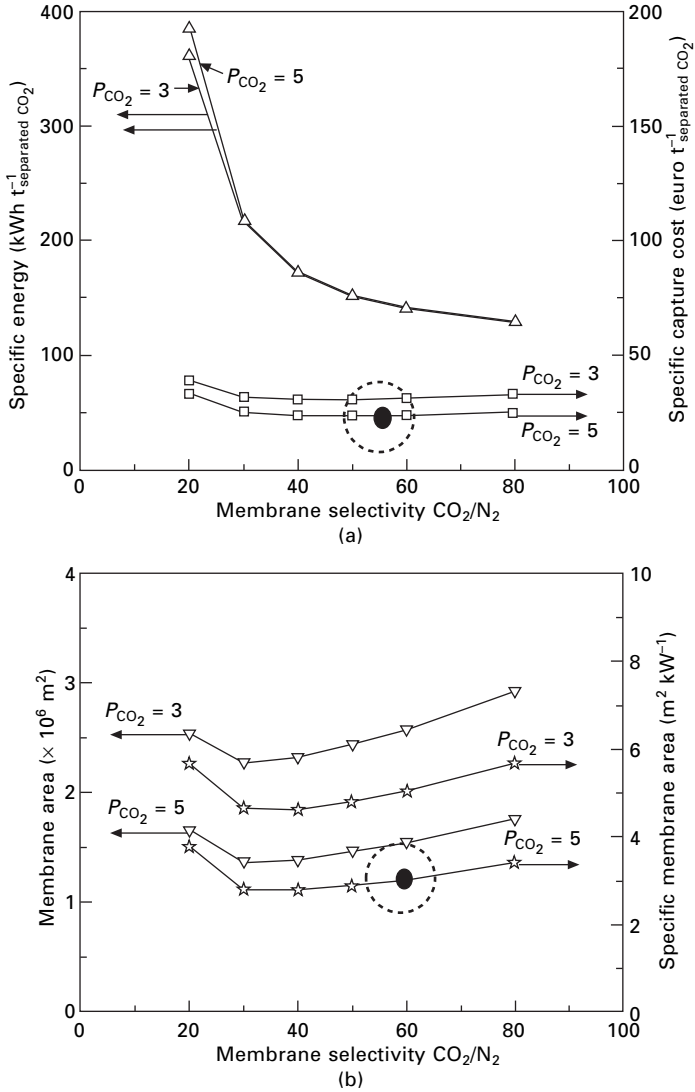
Membranes containing these particle matters (exposed to real flue gas) presented extremely low CO_2 flux after 42 days, but after cleaning with ultrasonic in water for 3 min, the separation performance was immediately recovered and was almost the same as the new sample (the decrease in the CO_2 flux and selectivity were not more than 20%). This means that the thin film was not physically damaged and its stability was demonstrated. In the longer term and on a large scale however, the thin film membrane must be protected and tested again. This is now a challenge for the MemBrain project.

A detailed parametric study was also done using these membranes (developed by GKSS).[20] A multi-stage membrane system was used to analyse the energy consumption and capture cost and the system was integrated in the 600 MW North-Rhine-Westphalia power plant and compared with the chemical absorption process. In attempting to fulfil the targets of 95% of purity and 70% degree of separation, the conclusions of this investigation were similar to those reported by MTR scientists who demonstrated that the values estimated and optimized might be the actual reality when membrane technology is integrated on the large scale (power plants). The simulation results showed, for example, that membranes with a CO_2/N_2 selectivity of ~40 and a CO_2 flux of 5 m^3 (STP) m^{-2} h^{-1} bar^{-1} are really attractive and the CO_2 capture cost could be less than 25 Euro per tonne. To decrease the CO_2 capture cost further, the CO_2 flux must be improved. Figure 6.8 shows the



6.7 Photographic image (left) of a Polyactive® thin film membrane after testing under real flue gas (after 42 days of testing) and its magnification (right) observed by SEM (surface of the membrane exposed to the gas).

© Woodhead Publishing Limited, 2011



6.8 Polyactive® membrane performances vs specific energy and cost (a) and membrane area (b); the best membrane developed by GKSS is highlighted (spot) in the graphs.[20] Copyright: *Journal of Membrane Science*.

results of this study, where membranes with 3 and 5 m^3 (STP) m^{-2} h^{-1} bar^{-1} are analysed.

Based on these analyses, membrane technology could even present lower CO_2 capture costs if we could consider that the membranes will work at 60°C (the values of CO_2 flux are experimentally determined at 30°C) and under

© Woodhead Publishing Limited, 2011

wet conditions (typical exhaust gas in power plants). The CO_2 flux at 60°C is approximately twice that at 30°C under wet conditions. This conclusion is based on CO_2 permeability (CO_2 permeability of Polyactive® under wet conditions at 30°C is 164 barrer and at 60°C is 250 barrer, the CO_2/N_2 selectivity is ~30). Therefore, if we could use the same design proposed by Merkel *et al.*[19] or Zhao *et al.*[20] the CO_2 capture cost might be ≤ US$ 20 per tonne of captured CO_2 (analysis by simple inclusion of estimated graphical data).

It is important to emphasise the required membrane area (millions of square metres). Although this seems to be too big, it is not impossible to build up membrane systems of such a size, since nowadays desalination plants use millions of square metres of membranes.

6.4 Operation and performance issues and analysis

CO_2 separation and its capture from power plants presents difficulties not only for membrane technology, but also for other separation technologies such as the absorption process. These difficulties arise because the flue gas contains low concentration of CO_2 at low pressures and the volume to be treated is extremely high (described above). Hence investigating the separation membrane process and membrane performance is absolutely essential.

6.4.1 Pressure ratio

Because the flue gas is at atmospheric pressure and the CO_2 concentration is low, additional energy must be used for generating a sufficient driving force for the separation process. There are four alternatives for creating additional driving force: (1) compressing the flue gas to pressures higher than 10 bar, (2) creating a vacuum on the permeate side (< 0.1 bar), (3) increasing the CO_2 concentration on the feed side and (4) using a sweep gas. The first two alternatives use additional energy (use of compressor and vacuum pump), the third one can be achieved by an appropriate process design and the last can be carried out using air or water vapour.

The pressure ratio between the feed pressure and permeate pressure is important in order to effect the separation of gas mixtures; for practical applications this ratio is between 5 and 15.[13] Gas separation through the membrane only occurs if the partial pressure of a gas on the feed side is greater than the partial pressure in the permeate side. A higher partial pressure on the feed side (for better separation performance) can be achieved by using a compressor on the feed side or a vacuum pump on the permeate side of membrane. In general, when the pressure ratio is low, more energy is required for the separation.[19, 20] Higher pressure ratios give high CO_2 purity and a high degree of separation.[45] Thus, a requisite for an optimal membrane

© Woodhead Publishing Limited, 2011

system is higher pressure ratios (single-step membrane system). Merkel *et al.*[19] reported that for a single-step membrane driven by a compressor and by a vacuum pump (same membrane) the required membrane area differs; when compression is used, recovery of a portion of the energy of compression is used at the feed side. However, although the area of the membrane is less when a compressor is used; the system which uses the vacuum is still better owing to the low energy consumption. For more detail see Merkel *et al.*[19], Zhao *et al.*[20] and Van Der Sluijs *et al.*[28]

6.4.2 Carbon dioxide concentration in the flue gas

As described above, the driving force through the membrane is very important in the separation process, so that higher partial pressures on feed side are needed for better gas separation performance. One way to increase the partial pressure is by increasing the concentration of CO_2 on the feed side; this can be done by engineering the process system, for example by recycling part of CO_2 or by feeding the boiler (power plant) with CO_2-enriched air (proposed by Merkel *et al.*)[19]

Favre[29] investigated a single-stage separation process and found that for a 10% mol fraction of CO_2 on the feed side, the required CO_2 recovery and purity cannot be reached simultaneously. For a state-of-the-art selective membrane (CO_2/N_2 selectivity) for example, only with a 20% mol fraction of CO_2 (feed side) was it possible to achieve ~80% CO_2 on the permeate side with a recovery of ~40%. However, by increasing the membrane selectivity up to 200 and/or increasing the CO_2 concentration on the feed side, the recovery and purity can be enhanced. From this analysis, Favre concluded that for the required recovery (90%) and purity (> 80%), no solution can be found and thus only a multi-stage separation process might overcome this limitation. That is why multi-stage processes were studied later.

The water vapour content in the flue gas is another important issue that must be taken into account during the design of the membrane process. Water vapour may condense and, together with acid gases, can corrode some parts of the separation fleet (installation), thus the lifetime of the equipment can be greatly reduced. Water vapour can be separated from flue gas by different methods such as condensation and dehydration (by using desiccants). Reheating the flue gas is also an option to prevent the water condensation and thus water vapour and flue gas leave the stacks. Water vapour from flue gas can also be removed by membranes. However the problem is that almost all CO_2-selective membranes swell and the separation performance can be greatly damaged. There are several studies on this topic.[46–48] and many strategies have been proposed to hinder this process, one being the use of chemical cross-linked polymers. Cross-linked polymers show good separation properties,[49] but a high degree of cross-linking can reduce the

© Woodhead Publishing Limited, 2011

CO_2 permeability. Other strategies are, for example, to use a physical cross-link, that is to use block copolymers, especially multi-block copolymers. The design of a block copolymer with CO_2-philic features is key to solving these problems. The advantage of block copolymers is that one block is CO_2-philic and the other one provides stability (it can crystallize).[42, 50, 51]

Water vapour permeability is extremely high in polymeric membranes (thousands of barrer),[52] but owing to the water vapour content (~11%) and low temperature (~55°C, which is below evaporation temperature) it can condense on the membrane surface and destroy it. The presence of water vapour in the flue gas can also benefit the separation properties of membranes (due to its activity),[46] because CO_2 permeability or flux can be increased through the membrane and following from this water is also CO_2-philic and the selectivity over N_2 can remain constant as in dry gases; hence the separation performance can even be better. In fact, for Polyactive® membranes we found that CO_2 permeability doubled in the presence of water vapour and the selectivity remained constant.

6.4.3 Membrane performance

As the membrane process needs a membrane, this must be the best, that is it must have high permeability, high selectivity and be very stable under different operating conditions. High permeability in dense films means high flux (Equation [6.4]) in composite membranes, which improves the separation performance, as reported by Merkel.[19] Higher CO_2 fluxes reduce the required membrane area and greatly lower the capture costs. CO_2/N_2 selectivity was initially considered to be an important factor, which led to thinking that membranes with selectivities higher than 200 are needed,[28] but later it was found that a moderate selectivity of ~30 is enough to reach 90% CO_2 purity with > 80% recovery.[19, 20]

The stability of the membrane is another important factor. As described above, the presence of water vapour and particle matter, among other contaminants can damage the membrane performance. Thus membrane material that is stable under wet conditions and at ~55°C must be developed, or the selective thin film must be protected during membrane fabrication without altering the separation performance of membrane.

6.4.4 Membrane configuration

Membranes for gas separation can be configured in several ways into the module. The modules are specifically designed for each application and each configuration has its own advantage. During module design compactness, separation problem and maintenance must be considered. Details of a membrane configuration for gas separation is described in Chapter 5.

© Woodhead Publishing Limited, 2011

6.5 Advantages and limitations

As mentioned in the introduction, membrane technology has advantages over the absorption process such as less environmental impact, a smaller carbon footprint, low investment cost, energy efficiency and ease of integration into the existing power plants. Membrane technology is chosen in many applications because it has a very high energy efficiency compared to conventional separation processes, but a limitation is the permeability–selectivity trade-off. Nevertheless, nowadays advanced membrane materials are being developed. These new polymeric membranes are overcoming the upper bound limit and they are promising for future applications.[49, 53] Novel polymeric membranes however also have some limitations such as their high cost and limited reproducibility on large scale. Another limitation of polymeric membranes is their stability (> 50°C) and durability, since their lifetime is usually no more than 5 years. In application in a power plant, the lifetime of a membrane could be even less than expected (2 years) owing to the presence of water vapour (water vapour can destroy the selective thin film, as well as inducing plasticization which reduces the selectivity) and particle matter (which physically damage the thin film). To date there are no real data on membrane lifetimes in power plants, but MTR's project and other research groups will most probably soon demonstrate the feasibility of membranes in power plants.

Another advantage for the environment is that membrane technology does not cause too much damage, because it is simple and does not use chemicals. The only pollution arises from the energy consumption during operation. The absorption process, for example, suffers from high solvent losses caused by evaporation (high temperature). The absorption process also has a high consumption of energy (during regeneration of solvent), which is a disadvantage over membrane technology. Energy demands are estimated to be 330–340 kWh per tonne of CO_2 captured for chemical absorption, 160–180 kWh for pressure swing absorption, 600–660 kWh for cryogenic methods and ~70 kWh for membrane technology.[54] Thus, membrane technology demands far lower energy than the other technologies.

Another advantage of membrane process is its size. It can be built in different sizes and can be easily incorporated into existing power plants. Although the amount of membrane required is huge, the membrane process is still potentially able to compete with other separation processes.

6.6 Future trends

Everyone expects that an efficient separation technology must be developed very soon to capture CO_2 from all emission points. As researchers we believe that only by working hand in hand with people in all research fields and

© Woodhead Publishing Limited, 2011

industries, will the appropriate technology for CO_2 capture be developed and demonstrated. In fact, several multidisciplinary projects relating to CO_2 capture (worldwide) have timelines that hope to demonstrate CO_2 capture from power plants on the pilot scale by 2015; hence as membranologists we should still seek innovative and advanced membranes materials.

Today the efficiency of membrane technology for CO_2 capture has been demonstrated on the laboratory and pilot scale, but many tasks are still unresolved. These problems mainly concern the lifetime and performance of membranes. In the next few years these two problems should be resolved.

The lifetime of a membrane can be only determined through experiment with real flue gas (in power plants). The MTR project, MemBrain and other research projects are proceeding in this direction. The performance of different membranes is being studied around the world, but in the future we should concentrate more on the fabrication of thin film membranes, since fabrication methods must be improved in order to produce large areas of ultra thin films with thicknesses less than 50 nm, as well as developing methods of protecting these thin films, since the nanometric thickness can be damaged during operation or during configuration into the modules. Ultra thin membranes must be defect-free and highly stable and these membranes are required because high CO_2 fluxes are needed for power plant applications. Therefore, CO_2-philic membranes with a CO_2 flux higher than 10 m^3 (STP) m^{-2} h^{-1} bar^{-1} and CO_2/N_2 selectivity no less than 30 must be developed. Moreover, these membranes must have long-term stability under flue gas conditions.

6.7 References

1 http://co2now.org
2 http://www.ipcc.ch
3 http://photovoltaics.sandia.gov
4 http://www.eupvplatform.org
5 https://lasers.llnl.gov
6 *Technologies, Policies and Measures for Mitigating Climate Change*, IPCC Technical Paper I. http://www.ipcc.ch/pdf/technical-papers/paper-I-en.pdf
7 International Energy Agency (2004), *Prospects for CO_2 Capture and Storage, Energy Technology Analysis*, OECD Publishing, Paris.
8 Lackner K S, 'A guide to CO_2 sequestration science', 2003, **300**, 1677–8.
9 Metz B, Davidson O, de Coninck H, Loos M and Meyer L (2005), *Carbon Dioxide Capture and Storage*, Cambridge University Press, UK.
10 http://www.ens-newswire.com/ens/mar2006/2006-03-15-06.asp
11 Lively R P, Chance R R and Koros W J, 'Enabling low-cost CO_2 capture via heat integration', *Ind. Eng. Chem. Res.*, 2010, **49**, 7550–62.
12 Rochelle G T, 'Amine scrubbing for CO_2 capture', *Science*, 2009, **325**, 1652–4.
13 Baker R W (2004), *Membrane Technology and Applications*, 2nd edition, Wiley, New York.

© Woodhead Publishing Limited, 2011

14 Hendricks C A, Blok K and Turkenburg W C (1989), 'The recovery of carbon dioxide from power plants', Okken P A, Swart R J and Swerver S (eds), *Climate and Energy*, Kluwer Academic, Dordrecht.
15 Van Der Sluijs J P, Hendriks C A and Blok K, 'Feasibility of polymer membranes for carbon dioxide recovery from flue gases', *Energy Conversion Manage*, 1992, **33**, 429–36.
16 Shekhawat D, Luebke D R and Pennline H W, *A Review of Carbon Dioxide Selective Membranes: A Topical Report*, National Energy Technology Laboratory, US Department of Energy (DOE) http://www.osti.gov/bridge/product.biblio.jsp?osti_id=819990
17 Lin H and Freeman B D, 'Materials selection guidelines for membranes that remove CO_2 from gas mixtures', *J. Mol. Struct.*, 2005, **739**, 57–74.
18 Hussain A and Hagg M B, 'A feasibility study of CO_2 capture from flue gas by a facilitated transport membrane, *J. Membr. Sci.*, 2010, **359**, 140–8.
19 Merkel T C, Lin H, Wie X and Baker R, 'Power plant post-combustion carbon dioxide capture: an opportunity for membranes', *J. Membr. Sci.*, 2010, **359**, 126–39.
20 Zhao L, Riensche E, Blum L and Stolten D, 'Multi-stage gas separation membrane process used in post-combustion capture: energetic and economic analyses', *J. Membr. Sci.*, 2010, **359**, 160–72.
21 Keith D W, 'Why capture CO_2 from the atmosphere?' *Science*, 2009, **325**, 1654–5.
22 Keith D W, Homepage: http://people.ucalgary.ca/~keith/AirCapture.html
23 *Synthetic Trees could Purify Air*: http://news.bbc.co.uk/2/hi/science/nature/2784227.stm
24 Lackner K S, Homepage: http://www.earth.columbia.edu/articles/view/2523
25 Robeson L M, 'The upper bound revisited', *J. Membr. Sci.*, 2008, **320**, 390–400.
26 Kumar P, Kim S, Ida J and Guliants V V, 'Comments on the origins of N_2/CO_2 selectivity of gas separation membranes', *Ind. Eng. Chem. Res.*, 2009, **48**, 3702.
27 Favre E, Roizard D, Bounaceur R and Koros W J, 'CO_2/N_2 reverse selective gas separation membranes: Technological opportunities and scientific challenges', *Ind. Eng. Chem. Res.*, 2009, **48**, 3700–1.
28 Van Der Sluijs J P, Hendriks C A and Blok K, 'Feasibility of polymer membranes for carbon dioxide recovery from flue gases', *Energy Conversion Manage*, 1992, **33**, 429–36.
29 Favre E, 'Carbon dioxide recovery from post-combustion processes: can gas permeation membranes compete with absorption?' *J. Membr. Sci.*, 2007, **294**, 50–9.
30 Kasama S, Duan S, Ohno C, Kouketsu T, Shimada Y, Chowdhury F A, Fujiwara I, Haraya K, Nagai K, Freeman B and Yamada K, 'Molecular gate membrane for CO_2 capture', *Greenhouse Gas Control Tech.*, 2005, **7**, 1947–50.
31 Figueroa J D, Fout T, Plasynski S, McIlvried H and Srivastava R D, 'Advances in CO_2 capture technology: The US Department of Energy's carbon sequestration program', *Int. J. Green. Gas Contr.*, 2008, **2**, 9–20.
32 Blume I and Pinnau I, *Composite Membrane, Method of Preparation and Use*, US Patent 4 963 165, 1990.
33 *Gas Separation Membranes for Zero-Emission Fossil Power Plants*: http://www2.fz-juelich.de/ief/ief-1/membrain (in German).
34 Car A, Stropnik C, Yave W and Peinemann K V, 'PEG modified poly(amide-b-ethylene oxide) membranes for CO_2 separation', *J. Membr. Sci.*, 2008, **307**, 88–95.

© Woodhead Publishing Limited, 2011

35 Yave W, Car A, Peinemann K V, Shaikh M Q, Raetzke K and Faupel F, 'Gas permeability and free volume in poly(amide-b-ethylene oxide)/polyethylene glycol blend membranes', *J. Membr. Sci.*, 2009, **339**, 177–83.
36 Yave W, Car A and Peinemann K V, 'Nanostructured membrane material designed for carbon dioxide separation', *J. Membr. Sci.*, 2010, **350**, 124–9.
37 Car A, Stropnik C, Yave W and Peinemann K V, 'Pebax/polyethylene glycol blend thin film composite membranes for CO_2 separation: performance with mixed gases', *Sep. Purif. Tech.*, 2008, **62**, 110–17.
38 Reijerkerk S R, Knoef M H, Nijmeijer K and Wessling M, 'Poly(ethylene glycol) and poly(dimethyl siloxane): combining their advantages into efficient CO_2 gas separation membranes', *J. Membr. Sci.*, 2010, **352**, 126–35.
39 Shishatskiy S, Pauls J R, Nunes S and Peinemann K V, 'Quaternary ammonium membrane materials for CO_2 separation', *J. Membr. Sci.*, 2010, **359**, 44–53.
40 Murali R S, Sridhar S, Sankarshana T and Ravikumar Y V L, 'Gas permeation behavior of Pebax-1657 nanocomposite membrane incorporated with multiwalled carbon nanotubes', *Ind. Eng. Chem. Res.*, 2010, **49**, 6530–8.
41 Metz S J,. Mulder M H V and Wessling M, 'Gas-permeation properties of poly(ethylene oxide)-poly(butylene terephthalate) block copolymers', *Macromolecules*, 2004, **37**, 4590–7.
42 Car A, Stropnik C, Yave W and Peinemann K V, 'Tailor-made polymeric membranes based on segmented block copolymers for CO_2 separation', *Adv. Funct. Mater.*, 2008, **18**, 2815–23.
43 Yave W, Car A, Funari S S, Nunes S P and Peinemann K V, 'CO_2-philic polymer membrane with extremely high separation performance', *Macromolecules*, 2010, **43**, 326–33.
44 Yave W, Car A, Wind J and Peinemann K V, 'Nanometric thin film membranes manufactured on square meter scale: ultra-thin films for CO_2 capture *Nanotechnology*', 2010, **21**, 395301.
45 Zhao L, Riensche E, Memzer R, Blum L and Stolten D, 'A parametric study of CO_2/N_2 gas separation membrane processes for post-combustion capture', *J. Membr. Sci.*, 2008, **325**, 284–94.
46 Metz S J, van de Ven W J C, Potreck J, Mulder M H V and Wessling M, 'Transport of water vapor and inert gas mixtures through highly selective and highly permeable polymer membranes', *J. Membr. Sci.*, 2005, **251**, 29–41.
47 Sijbesma H, Nyneijer K, van Marwijk R, Heijboer R, Potreck J and Wessling M, 'Flue gas dehydration using polymer membranes', *J. Membr. Sci.*, 2008, **313**, 263–76.
48 Potreck J, Nijmeijer K, Kosinski T and Wessling M, 'Mixed water vapor/gas transport through the rubbery polymer PEBAX 1074', *J. Membr. Sci.*, 2009, **338**, 11–16.
49 Lin H, Van Wagner E, Freeman B D, Toy L G and Gupta, R P, 'Plasticization-enhanced hydrogen purification using polymeric membranes', *Science*, 2006, **311**, 639–42.
50 Reijerkerk S R, Arun A, Gaymans R J, Mijmeijer K and Wessling M, 'Tuning of mass transport properties of multi-block copolymers for CO_2 capture applications', *J. Membr. Sci.*, 2010, **359**, 54–63.
51 Yave W, Szymczyk A, Yave N and Roslaniec Z, 'Design, synthesis, characterization and optimization of PTT-b-PEO copolymers: a new membrane material for CO_2 separation', *J. Membr. Sci.*, 2010, **362**, 407–16.
52 Nunes S P and Peinemann K V (2006), *Membrane Technology in the Chemical Industry*, 2nd edition, Wiley-VCH, Weinheim.

© Woodhead Publishing Limited, 2011

53 Berchtold K A, 'Novel polymeric–metallic composite membranes for CO_2 separation at elevated temperatures', *American Filtration and Separation Society Fall Topical Conference*, Pittsburg, PA, 2006,
54 Khoo H H and Tan R B H, 'Life cycle investigation of CO_2 recovery and sequestration', *Environ. Sci. Tech.*, 2006, **40**, 4016–24.

© Woodhead Publishing Limited, 2011

7

Inorganic membranes for pre-combustion carbon dioxide (CO_2) capture

A. IULIANELLI and A. BASILE, Institute on Membrane Technology of the Italian National Research Council (ITM-CNR), Italy and H. LI and R.W. VAN DEN BRINK, ECN Hydrogen Production and CO_2 Capture, The Netherlands

Abstract: Both polymeric and inorganic membranes are used for CO_2 gas separation in CO_2 capture by membranes. In the last few decades, considerable effort has been directed towards the development of inorganic membranes at the scientific level because of their applicability at higher operating temperatures than polymeric membranes. For CO_2 and hydrogen separation, active transport systems are also under development and both porous and dense inorganic membranes are being developed. In this context, dense Pd or Pd-alloy membranes on ceramic or metallic supports are the most-developed membrane types. Furthermore, water–gas shift (WGS) or methane steam reforming (MSR) reactions may be performed using inorganic membrane reactor technology. Indeed, these reactions can be incorporated in both integrated gasification combined cycle (IGCC) and natural gas combined cycle (NGCC) for electricity production with CO_2 capture. Hydrogen selective membrane reactors are capable of concentrating CO_2 at both relatively lower costs and energy consumption than conventional pre-combustion CO_2 capture, although inorganic membrane technology has not yet been developed on the industrial scale.

Key words: CO_2 capture inorganic membrane, inorganic membrane, membrane reactor, palladium membrane.

7.1 Introduction

The overabundance of CO_2 in the atmosphere constitutes one of the main contributors to global climate change. In fact, it is responsible for about 64% of the greenhouse effect and global warming (Zhou *et al.*, 2009). This has led to scientific interest in the development of new methods for considerably reducing the amount of CO_2 emitted into the atmosphere from industry or fossil fuel power plants. In particular, carbon capture and storage (CCS) technology consists of the capture of CO_2 from industrial installations, its transport to a storage site and its injection into a suitable underground geological formation for permanent storage. Nowadays, no full-scale power plants exist with CCS technology, but the construction of several large-scale demonstration plants is ongoing (e-net 1; e-net 2). The CO_2 capture step

© Woodhead Publishing Limited, 2011

represents 60–80% of the total CCS cost and, hence, is the most critical issue in any economic analysis (Drioli and Giorno, 2009).

There are basically three families of processes for CO_2 capture, based on existing technology: sorption (absorption in solvents or adsorption on solid sorbents), membrane and cryogenic processes (e-net 3; e-net 4). Absorption in solvents is, today, the most diffuse technique on the industrial scale, in natural gas treatment and in experimental plants for CO_2 capture. In particular, the amine-based absorption with an aqueous monoethanolamine (MEA) solution is capable of achieving a high level of CO_2 capture (more than 90%) from flue gas. Nevertheless, amines are corrosive, predisposed to degradation owing to the action of sulphur oxides and require a considerable amount of energy, mainly in the regeneration step (Choi *et al.*, 2009; Maneeintr *et al.*, 2010).

In all pathways that can be pursued for CO_2 capture from coal-derived power generation such as post-combustion capture, pre-combustion capture and oxy-combustion, membranes can offer several advantages over conventional separation techniques, such as low capital investment, compactness, ease of installation and operation, simplicity, flexibility, and so on (Adhikari and Fernando 2006; Mix, 1987).

Taking into account that pre-combustion capture offers several advantages such as the production of a carbon-free fuel and capture of CO_2 at high pressure, in this chapter particular attention is paid to the benefits and drawbacks of inorganic membranes, which are useful in pre-combustion fuel decarbonization, with respect to the conventional systems used for CO_2 separation. Then, the inorganic membrane technology applied to pre-combustion capture has the scope both to generate and separate hydrogen and concentrate CO_2 for further storage.

Over the last two decades, a growing interest in inorganic membranes for gas separation has been justified by the different benefits, such as high resistance to chemical degradation, a well-defined stable pore structure (in the case of porous inorganic membranes), high mechanical stability and elevated resistance at high operating temperatures. In fact, inorganic membranes are stable between 300 and 800°C and, in the case of ceramic membranes, they can operate at temperatures over 1000°C (Van Veen *et al.*, 1996). However, despite many scientific studies involving inorganic membrane applications for CO_2 capture, industrially only polymeric membrane technology is currently applied (Table 7.1).

When fossil fuels are reformed into synthesis gas (syngas), mainly hydrogen and carbon monoxide are formed. Carbon monoxide could be converted into further hydrogen and CO_2 through the water–gas shift (WGS) reaction. The resulting hydrogen and CO_2 mixture can be separated using solvents or pressure swing adsorption (PSA). Alternatively, inorganic membrane separators or reactors can be used to separate the hydrogen from the other

© Woodhead Publishing Limited, 2011

Table 7.1 Characteristics of the current membrane CO_2 capture industry (Drioli and Giorno, 2009)

Separation	Principal producers	Membrane/module	Market size (US$million/year)
CO_2 from natural gas	Cynara Medal Grace, Separex MTR	Cellulose triacetate/fine fibre Polyaramide/fine fibre Cellulose acetate/spirals Perfluoro polymers/spirals	100

gases. The benefits of membrane reactors are that separation could be carried out at higher temperatures. Conventional solvent and PSA processes operate at ambient temperatures, which means that the gases from the WGS reactor need to be cooled down first. The hydrogen fuel resulting from the separation section subsequently needs to be heated up to approx. 250°C before entering the combustion chamber of the gas turbine (de Bruijn *et al.*, 2007). By using membrane separation, these heating and cooling steps can be eliminated. Membranes also offer the possibility of integrating the WGS or methane steam reforming reaction with the separation of hydrogen and CO_2. This reduces the number of process steps and increases hydrogen production by removing one of the reaction products from these equilibrium reactions.

Specific demands on membranes for use in pre-combustion CO_2 capture for power production are:

- Selectivity must be sufficient to reach the targeted CO_2 capture ratio (> 90%);
- Fluxes should be high to minimize the reactor size and membrane costs;
- The membrane should be resistant to carbon monoxide, steam, and in the case of application in coal-derived syngas, sulphur;
- The hydrogen fuel should be delivered at a pressure suitable for entering the gas turbine combustion chamber (approx. 22–25 bar) (Dijkstra *et al.*, 2010).

7.1.1 Statistic evaluation of scientific studies of membrane-based processes with respect to conventional systems for carbon dioxide (CO_2) separation

Since the 1960s, a significant commercial application of membrane technology has grown up in the field of gas separation. Today, gas separation membranes are used in industry for:

- separation of nitrogen from air

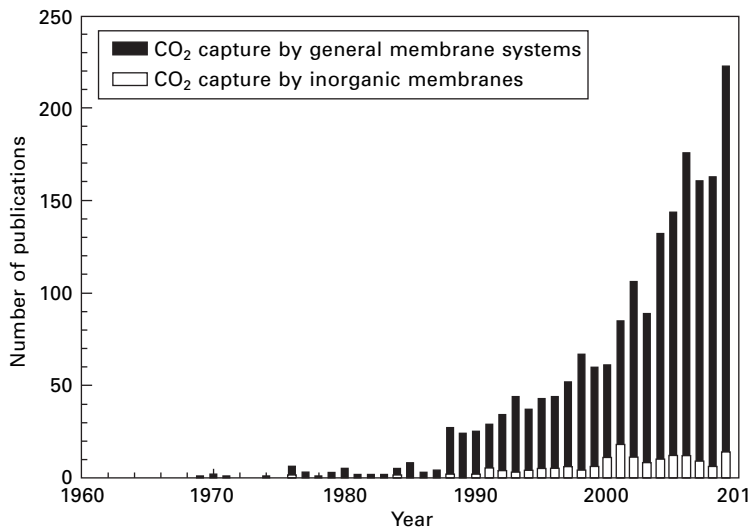
© Woodhead Publishing Limited, 2011

- production of dry air
- separation of hydrogen
- natural gas treatment
- separation of carbon dioxide
- separation of heavy hydrocarbons
- separation of vapour/gas in petrochemical operations
- separation of organic vapour mixtures.

Among these applications, in the last few years, particular attention has been devoted to CO_2 separation with regard to the reduction of greenhouse gas emissions. In order to understand the growing interest of the scientific community in membrane system applications in this field, Fig. 7.1 summarizes the statistic evaluation of scientific studies of CO_2 capture by inorganic membranes over the generality of membrane applications in this field.

7.2 Inorganic membranes for carbon dioxide (CO_2) separation

Gas permeation through membranes depends on the membrane's physical and chemical properties as well as on the nature of the permeant species (Shekhawat *et al.*, 2003). With particular reference to CO_2 capture in pre-combustion fuel decarbonization, in order to obtain a sufficiently concentrated stream of CO_2, both permeability and selectivity are important parameters in selecting the membrane. The higher the permeability the lower the membrane



7.1 Number of published papers per year on CO_2 capture with both conventional and membrane systems; Elsevier Scopus database.

© Woodhead Publishing Limited, 2011

area required for a given separation and, therefore, the lower the system cost. Unfortunately, high permeability does not correspond to high selectivity and the achievement of this combination is a goal for membrane scientists. The usual membrane choice is based on a highly selective material and making it as thin as possible to increase the permeability. However, a reduced membrane thickness could lower its mechanical resistance and, therefore, make the membranes unusable.

Owing to similarities between the membrane materials and their texture and structure, we will divide the survey into:

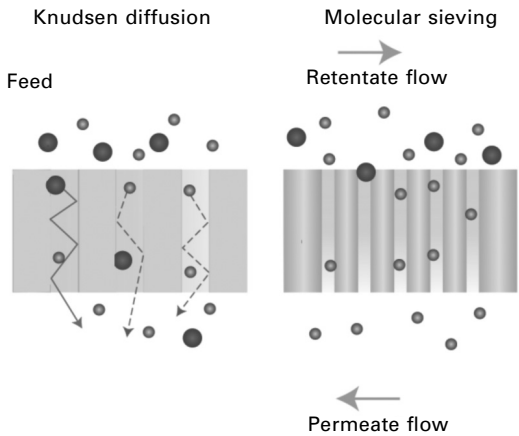
1. porous inorganic membranes for H_2 or CO_2 separation
2. dense inorganic membranes for H_2 separation.

7.2.1 Porous inorganic membranes

In porous inorganic membranes, a thin porous top layer is cast onto a porous metal or ceramic support, which provides mechanical strength, offering minimum mass-transfer resistance. Carbon, glass, silicon carbide, titania, zeolite membranes, and so on are mainly adopted as porous inorganic membranes supported on different substrates, such as α-alumina, γ-alumina, zirconia, zeolite, or porous stainless steel (Rao and Sircar 1993; Petersen *et al.*, 1997). Surface modification by covalently bonding a layer of selected compounds with appropriate functional groups is one of the more convenient routes for altering membrane performance. Such modifications can increase the performance by changing the mean pore size and promoting an eventual specific interaction between the surface of the membrane and the permeating molecules in order to enhance permeation. The main transport mechanisms for porous inorganic membranes are reported in the following (some of them are schematically illustrated in Fig. 7.2):

- *Knudsen mechanism* takes place when the average pore diameter is similar to the average free path of fluid molecules. In this case, the collisions of the molecules with the porous wall are very frequent.
- *Surface diffusion* is achieved when one of the permeating molecules is adsorbed on the pore wall owing to the presence of active sites in the membrane. This diffusion can take place even in the presence of Knudsen transport. This mechanism is made less significant by increasing the temperature owing to the progressive decrease of the bond strength between molecules and surface.
- *Capillary condensation* occurs when one of the components condenses within the pores caused by capillary forces, which are sufficiently strong only at low temperature and in presence of small pores. If the pore dimension is small and homogeneous and the pores are uniformly distributed on the membrane, this mechanism can offer high selectivity.

© Woodhead Publishing Limited, 2011



7.2 Schematic representation of two of the different possible mechanisms for membrane gas separation.

Generally, capillary condensation favours the transfer of relatively large molecules.

- *Multi-layer diffusion* is developed when the molecule/surface interactions are strong. This mechanism is similar to an intermediate flow regime between surface diffusion and capillary condensation.
- *Molecular sieving* takes place when the pore diameters are very small, allowing the permeation of only smaller molecules.

Zeolites are crystalline aluminosilicates with a uniform pore structure and a minimum channel diameter ranging from 0.3 to 1.0 nm. The presence of molecular-sized cavities and pores make the zeolites effective as shape-selective materials for a wide range of separation applications. This ability to adsorb molecules selectively by size and polarity is the key factor in the efficiency of synthetic zeolites as a basis for gas separation. Separation in zeolite membranes occurs by molecular sieving and/or surface diffusion mechanisms. Zeolites have good thermal stability, but under hydrothermal conditions the stability appears to be limited owing to dissolution of aluminium from the zeolite framework. Hydrothermal stability improvement can be obtained by using low aluminium content zeolites or titano-silicate membranes (Bredesen *et al.*, 2009). By using these membranes, CO_2 preferentially permeates in CO_2/N_2, CO_2/CH_4 and CO_2/H_2 mixtures at low temperatures, because CO_2 adsorbs more strongly on zeolites than the other gases.

Kusakabe *et al.* (1997) studied the variations in CO_2 selectivity and permeance in CO_2/N_2 mixtures by comparing Y-type zeolite, C-based and SiO_2 membranes. In Y-type zeolites, which have a high affinity for CO_2, the CO_2 molecules migrating along the pore walls are able to overcome the few N_2 molecules migrating along the pore centre. At temperatures around

© Woodhead Publishing Limited, 2011

140°C, CO_2/N_2 selectivity is >10, with a permeance of CO_2, approximately equal to 1.4×10^{-7} mol $m^{-2}s^{-1}$ Pa^{-1}.

Furthermore, some other zeolites can selectively separate CO_2 only via molecular sieving (Dyer, 1988). For example, zeolite 4A, with pore sizes of ~4 Å, allows separation of CO_2 from nitrogen and methane (Guiver *et al.*, 2004). Molecular sieving-based inorganic membranes incorporate such materials into the pores of a porous support. This integrates the size exclusion properties of the molecular sieve within the pores, providing selective gas separation (Suzuki, 1986). A major difficulty with this approach is achieving an efficient trap of the sieve particles within the pores. Both the pore and sieve sizes have to be well-known and similar enough to ensure strong packing of the pores, otherwise, the gaps between the sieves and the pore walls will allow bulk diffusion of gas molecules, diminishing the selectivity performance (Figueroa *et al.*, 2008). The molecular sieve framework forms a well-defined repeating structure of regular channels and cages. Gas separation is dependent on the size of these channels and cages relative to the kinetic diameter of the gas. The difference in the kinetic diameter of gas molecules dictates which molecular sieves are useful and provides an indication of selectivity.

Microporous zeolite membranes can also be used to separate H_2. However, the hydrogen fluxes of zeolite membranes are one order of magnitude lower than for the sol–gel silica membranes discussed in a recent review by Caro *et al.* (2000). The high thickness required to form a pinhole free zeolite membrane, for example in the range of 2-50 μm, is believed to be the reason for the low H_2 flux. Currently, research efforts on the zeolite membranes are not focused on hydrogen separation.

Recently, silica membranes have been shown to have promising properties in terms of both permeability and selectivity, particularly towards H_2/CO_2 separation. In these membranes, which may be fabricated by two methods, sol–gel and chemical vapour deposition (CVD) methods, separation is based on a sieving effect through small pores (about 3–4 Å). The final membrane properties depend strongly on the preparation conditions (gas composition, temperature and pressure) and the support structure. In sol–gel silica membranes, defects, like pinholes and cracks in the support surface, are not tolerated, because the silica layer is not able to repair them and, moreover, a clean environment during the membrane preparation is necessary to obtain membranes with high selectivity. Compared to sol–gel membranes, CVD membranes have lower permeance and higher selectivity. They may also be produced on supports with larger pores and, thus, with higher support resistance. Silica is a viable starting material for the fabrication of CO_2 selective membranes, mainly because of its stability and easy modification of structures. Unlike alumina, which tends to undergo phase transition at relatively low temperatures, or carbon, which can exhibit substantial changes in pore size

© Woodhead Publishing Limited, 2011

in oxidizing environments, silica shows exceptional thermal, chemical and structural stability in both oxidizing and reducing environments (Yang *et al.*, 2008). However, some studies show that silica membranes are not stable at higher temperatures, especially in steam-containing atmospheres (Fotou *et al.*, 1995). Many studies on silica membranes deal with flat samples, given the relatively simpler preparation procedure of this type of shape (Ciora *et al.*, 2004; Iwamoto *et al.*, 2005; Volger *et al.*, 2006).

For example, Kuraoka *et al.* (2000) prepared a multi-layer microporous silica xerogel membrane by the sol–gel method. They found that the selectivity CO_2/N_2 attained for this membrane is more than 60 at 25°C. This value is considerably higher than the theoretical Knudsen value ($CO_2/N_2 = 0.8$). Moreover, the authors also investigated the application of this membrane to enrichment of CO_2 from the air. CO_2 in the air (about 380 ppm) was concentrated to more than 1000 ppm by using the membrane at 25°C, demonstrating that this membrane can be applied to the recovery of CO_2 from gases with low CO_2 concentration. Furthermore, Cuffe *et al.* (2006) studied the application of ultra-thin (~5–25 nm) nanoporous silica for separating CO_2 from exhaust streams. They showed that ultra-thin nanoporous membranes exhibit CO_2 selectivities over nitrogen higher than 36:1 in one case and 75:1 in another case at a working temperature of 600°C. At the University of New Mexico, researchers produced a microporous inorganic silica membrane containing amine functional groups for the separation of CO_2 from flue gas, by sol–gel dip processing (Figueroa *et al.*, 2008). By modifying the membrane, the strong interactions between the permeating CO_2 molecules and the amine functional membrane pores enhance the selective diffusion of CO_2 along the membrane pore wall with subsequent blocking of the transport of other gases, such as O_2, N_2 and SO_2. Thus, this novel membrane should have better CO_2 selectivity than a pure siliceous membrane, if a balance between permeance and selectivity can be achieved.

Currently, the application of hydrogen separation is the main focus of silica membranes as it is promising to achieve a high H_2 permeance without compromising the H_2 selectivity. H_2 permeance and selectivity of silica membranes reported in the literature showed a large spread in values (Table 7.2) depending on the preparation conditions and support structure (Vos de *et al.*, 1999; Prabhu and Oyama 2000). A major hurdle for the application of silica-based membrane materials is chemical stability when sintering at high temperature, especially in a steam-containing environment. For example, pore volume and surface area reductions of 75% have been reported for the unsupported sol–gel silica material at 600°C (Fotou *et al.*, 1995). Thus, further work is needed to improve the hydrothermal stability and to identify the temperature–gas composition stability window (Bredesen *et al.*, 2004). Metal-doped silica membranes have recently attracted a lot of attention as they offer the promise to enhance durability without reducing permeation

© Woodhead Publishing Limited, 2011

Table 7.2 General overview of properties of H_2-selective porous inorganic membranes

Membrane type	Main transport mechanism	H_2 permeance	T (appl, T_c)	H_2/other relevant gas (e.g. N_2 or CO_2)	References
Silica	Molecular sieving	Large spread in values	$T_{appl.}$ 200–825°C	8–10 000	Ciora *et al.* (2004); Fotou *et al.* (1995); Kanezashi and Asaeda (2006); Prabhu and Oyama (2000); Yang *et al.* (2008); Uhlmann *et al.* (2009); Vos de *et al.* (1999)
Zeolite, carbon (MSCM), Si—O—C, SiC and glass membranes	Molecular sieving	Zeolite: one order of magnitude lower than silica, Carbon: fairly low, Si—O—C, SiC: close to silica Glass: close to silica	Large spread in values	Unclear	Bredesen *et al.* (2009); Caro *et al.* (2000); Koresh and Soffer (1986); Lee and Tsai (1999); Nam and Gavalas (1989); Sea *et al.* (1998); Shelekhin *et al.* (1992, 1995);
Metal membranes dispersed in porous supports	Surface diffusion	Close to Pd-based membranes	$T_{appl.}$ 100–500°C	10–300	Chen *et al.* (2003); Kikuchi *et al.* (2000); Liu *et al.* (1999)

flux, for example nickel or cobalt-doped silica membranes have shown high flux and selectivity and particularly good hydrothermal stability in the presence of steam at temperatures above 400°C (Kanezashi and Asaeda 2006; Uhlmann *et al.*, 2009).

Carbon membranes for gas separation can be classified into two types: molecular sieve carbon membranes (MSCM) and adsorption selective carbon membranes (ASCM). MSCM have small pores and can be used to separate small molecules such as hydrogen from larger ones (Koresh and Soffer, 1986). ASCM, characterized by larger pores, separate heavy molecules on the basis of an adsorption–surface migration mechanism, making possible their use for CO_2 separation (Sircar *et al.*, 1999). Alternatively, organic silane precursors can be pyrolysed to obtain Si—O—C and SiC microporous membranes (Sea *et al.*, 1998; Lee and Tsai 1999), which may have a better

© Woodhead Publishing Limited, 2011

stability than pure SiO_2 membranes in H_2/CO_2 separation (Nam and Gavalas 1989).

It has been found that microporous glass can provide high H_2 permeability (Shelekhin *et al.*, 1992), and in particular excellent thermal and chemical stability (Shelekhin *et al.*, 1992, 1995). The major disadvantage of these membranes is their fragility and, in addition, it is difficult to develop cheap modules with a high production capacity for densely packed glass fibres.

The hydrogen permeation characteristics of the porous support can be significantly changed by depositing metal, for example Pd (Chen *et al.*, 2003) or Rh (Liu *et al.*, 1999), on the surface or in the pore structure of the support (Kajiwara *et al.*, 2000). For example, Kikuchi *et al.* (2000) prepared a CVD platinum on a commercially available alumina tube with an average pore size of 200 nm which showed H_2/N_2 selectivity as high as 280 and excellent performance similar to the electroless-plating palladium membrane. Chemical stability is the major obstacle for the application of such metal membranes dispersed in a porous support as is the case for Pd-based membranes (Gao *et al.*, 2004), since the contaminants in the process streams such as H_2S and CO have a high affinity for the metal.

A Li_2ZrO_3 membrane was reported to exhibit absorption enhanced selectivity towards CO_2 at high temperatures (Nair *et al.*, 2002; Olivares-Marìn *et al.*, 2010). For example, the Li_2ZrO_3 membrane showed a CO_2 permeance of about $1–2 \times 10^{-8}$ mol $m^{-2}s^{-1}Pa^{-1}$) between 500 and 600°C and a selectivity of around 4–5 in CO_2:CH_4 (1:1) at 600°C (Nair *et al.*, 2002). It is a significant advantage of the Li_2ZrO_3 membrane that it can be applied at such a high temperature, but its CO_2 selectivity still needs to be further improved.

Recently, several patents have described the application of inorganic membranes to CO_2 separation/capture with particular reference to those consisting of a ceramic support, such as Al_2O_3, onto which a porous separating layer is added, often silica, alumina or zirconia (Ku *et al.*, 2008; Gobina, 2006). $BaTiO_3$ (Ku *et al.*, 2008) or MgO (Gobina, 2006) have been added to this functional layer (Gobina, 2006). These functional groups have a high chemical affinity for CO_2 and, therefore, the pore walls become saturated, which increases the permeability. For example, $BaTiO_3$ on alumina, with 5 nm pores, has a CO_2/H_2 selectivity of 3.1 at 500°C, whereas with 1 nm pores it has a CO_2/H_2 selectivity of 18.4 (Ku *et al.*, 2008). Similarly, for MgO, a CO_2/N_2 selectivity of 120 is obtained with a CO_2 permeability > 0.02 barrer at 350°C (Gobina, 2006).

Table 7.2 and Table 7.3 give a general overview of properties of H_2-selective and CO_2-selective porous inorganic membranes.

7.2.2 Dense inorganic membranes

Dense inorganic membranes are conventionally used for hydrogen separation from gas mixtures and in membrane reactors. Metal membranes can be

© Woodhead Publishing Limited, 2011

Table 7.3 General overview of properties of CO_2-selective porous inorganic membranes

Membrane type	Main transport mechanism	CO_2 permeance	T (appl, T_c)	CO_2/N_2, CO_2/O_2 CO_2/CH_4, CO_2/H_2	References
Silica	Surface diffusion and molecular sieving	4.3×10^{-8} to 8.4×10^{-7} mol $m^{-2}s^{-1}Pa^{-1}$	$T_{appl.}$25°C	CO_2/N_2: 4–92	Cuffe *et al.* (2006); Figueroa *et al.* (2008); Kuraoka *et al.* (2000)
Zeolite	Surface diffusion and molecular sieving	Unclear	$T_{appl.}$ 22–140°C	CO_2/N_2, CO_2/CH_4, CO_2/H_2 : 7–110	Bredesen *et al.* (2009); Dyer (1988); Guiver *et al.* (2004); Kusakabe *et al.* (1997); Shekhawat *et al.* (2003); Suzuki (1986)
Carbon (ASCM)	Surface diffusion and molecular sieving	2.7×10^{-9} mol $m^{-2}s^{-1}Pa^{-1}$	$T_{appl.}$30°C	CO_2/N_2: 34.4 CO_2/O_2: 3.1	Sircar *et al.* (1999)
Li_2ZrO_3	Surface diffusion	1×10^{-8} to 2×10^{-8} mol $m^{-2}s^{-1}Pa^{-1}$	$T_{appl.}$ 500–600°C	CO_2/CH_4: 4–5	Nair *et al.* (2002); Olivares-Marín *et al.* (2010)
$BaTiO_3$/ Al_2O_3 MgO/ silica/ ceramic support	Surface diffusion	Unclear	$T_{appl.}$ 350–500°C	CO_2/H_2: 3.1–18.4 CO_2/N_2: 120	Ku *et al.* (2008); Gobina (2006)

classified into two groups: palladium-based membranes and those containing group IVB and VB metals. Actually, palladium and its alloys are the dominant materials for preparing inorganic membranes owing to the high solubility and permeability of hydrogen through them (Van Delft *et al.*, 2007). Exploiting this ability, a CO_2/H_2 stream or, more generally, a reformed stream containing mainly H_2 and CO_2 could be further concentrated in CO_2 owing to the selective permeation of hydrogen through the Pd-based membranes.

In the case of dense metallic membranes, molecular transport occurs through a solution–diffusion mechanism. In particular, in a dense palladium-based membrane, hydrogen atoms interact with palladium metal. Hydrogen permeation through the membrane is a complex process with several stages (Adhikari and Fernando 2006; Dittmeyer *et al.*, 2001):

© Woodhead Publishing Limited, 2011

- dissociation of molecular hydrogen at the gas–metal interface
- adsorption of atomic hydrogen on the membrane surface
- dissolution of atomic hydrogen into the palladium matrix
- diffusion of atomic hydrogen toward the opposite side of the membrane
- recombination of atomic hydrogen to form hydrogen molecules at the gas/metal interface
- desorption of hydrogen molecules.

Dense Pd-based membranes can be classified as supported (a thin Pd-based layer supported onto a dense or porous support) or laminated. Porous supports are typically made by binary oxides like SiO_2, Al_2O_3 and B_2O_3, giving an excellent anchor effect and adherence (Mallada and Menéndez, 2008). Porous stainless steel (PSS) can also be considered as a valid support owing to its mechanical durability, thermal expansion coefficient close to that of palladium and ease of gas sealing. The thermomechanical properties of stainless steel supports fit the membrane film better than ceramics and glass (Bredesen *et al.*, 2004). For these membranes, there is a relationship between the thickness limit and pore size. In particular, the thickness limit increases with increasing pore size in the support's top layer. Nevertheless, by considering the permeance, the decrease of the membrane thickness is balanced by the necessity to use smaller pores in the support. Therefore, for a certain Pd-alloy thickness and support pore size, the hydrogen flux is limited by the support resistance (Goto *et al.*, 2000). A method of avoiding this problem can consist of separating the membrane layer preparation from the integration procedure between the layer and the support (Bredesen and Klette, 2000). Generally speaking, the upper temperature limits of the supported membranes depend on the material, the chemical environment and the support characteristics such as porosity and pore diameter (Uemiya, 1999). Overall, it is desirable that the support does not contribute significantly to the flow resistance. Therefore, the support is typically built up by a porous structure, where the main part has relatively large pores (commonly 2–20 μm) and one or more thin layers of decreasing pore size are used to provide an adequate surface for the top layer. In contrast, the dense support is an integrated part of the membrane structure. For this reason, its properties have a decisive impact on the membrane performance. In the case of membranes with dense support, several metals possess higher permeability for hydrogen than palladium, such as the refractory group V metals (Buxbaum and Kinney, 1996). These metals are cheaper than palladium, but they are unstable in many environments, since they can be easily oxidized or carburized. Therefore, they are used as a mechanical support material, whereas a thin Pd-alloy may conveniently be used as a separating layer. Moreover, interdiffusion between the refractory metal and Pd-alloy can cause a reduction of the hydrogen permeance (Hsu and Buxbaum, 1986). Thus, interfacial barrier

© Woodhead Publishing Limited, 2011

layers like oxides have been applied to limit this interdiffusion (Edlund *et al.*, 1994; Edlund and McCarthy, 1995). In laminated membranes, a thin palladium (or palladium alloys) layer avoids the formation of oxides on the metallic surfaces resulting in a reduction in the hydrogen adsorption activation energy and, consequently, in an increase in the hydrogen permeation flux.

Pure palladium membranes suffer from hydrogen embrittlement caused by phase transition from α to β palladium hydride at temperatures below 573K and pressures below 2 MPa (Lewis, 1995). By alloying with other metals, for example Ag, the α–β phase transition of the Pd-based membranes can be minimized (Okazaki *et al.*, 2006) with the critical temperature significantly lowered (Shu *et al.*, 1991). Many Pd alloy membranes have been examined, such as a binary alloy with Pt (Dudek, 2001), Ni (Jun and Lee, 2000), Ag (Shu *et al.*, 1991; Keuler and Lorenzen, 2002; Peters *et al.*, 2009) and Cu (Roa *et al.*, 2003; Yuan *et al.*, 2007) and a ternary alloy with Ni and Ti (Basile *et al.*, 2008), of which the Pd/Ag and Pd/Cu alloy membranes are the most extensively studied. Compared to pure Pd membranes, Pd–Ag composite membranes show a higher hydrogen permeance but they are still expensive and prone to segregate upon heat treatment (Roa *et al.*, 2003). Recently, 60 wt% Pd–40 wt% Cu alloy membranes attracted a lot of attention as they exhibit a high H_2 permeance while offering great potential for cost reduction (Basile *et al.*, 2008; Yuan *et al.*, 2007).

Chemical stability is one of the major challenges for the commercial application of Pd-based membranes, since they are susceptible to modification by carbon-containing or sulphur-bearing gases, for example CO and H_2S, as reviewed recently by Gao *et al.* (2004). CO can inhibit the H_2 permeation of the membranes through competitive adsorption. In particular, a level of H_2S of only parts per million can result in a dramatic decrease of the H_2 permeance of Pd-based membranes on a short timescale, followed by the formation of Pd_4S or bulk silver-palladium sulphide ($Ag_5Pd_{10}S_5$) (Mundschau *et al.*, 2006; Kajiwara *et al.*, 1999). The issue of sulphur tolerance is challenging but critical for the application of Pd-based membranes, for which a lot of research has been carried out.

A fcc (face centred cubic) Pd–Cu alloy membrane has been found to exhibit superior resistance to H_2S (Kamakoti *et al.*, 2005; Kajiwara *et al.*, 1999; McKinley 1967, 1969; Morreale *et al.*, 2004). For example, 1000 μm thick 80 wt% Pd–20 wt% Cu and 60 wt% Pd–40 wt% Cu alloy foils were tested in the presence of either pure hydrogen or a 1000 ppm H_2S/balance H_2 mixture (Kamakoti *et al.*, 2005). At temperatures corresponding to the fcc phase, the membranes showed minimal decreases in H_2 permeance while at temperatures related to the bcc (body centred cubic) phase of the 60 wt% Pd–40 wt% Cu alloy, a significant decrease in H_2 permeance was observed for H_2S containing mixtures, up to two orders of magnitude. Nevertheless,

© Woodhead Publishing Limited, 2011

a fcc Pd–Cu alloy membrane showed a major drawback of relatively low H_2 permeance compared to a pure Pd membrane.

Besides the fcc Pd–Cu alloy, McKinley (1969) has also indicated that a Pd–Au membrane exhibited better H_2S resistance compared to a pure Pd membrane, which also offers promise for the future application of Pd-based membranes in a sulphur-containing environment. Ceramic membranes also show some prospect in the field of H_2 separation, especially silica membranes, which can achieve a H_2 permeance equal to or even above that of Pd-based membranes, and particularly possess the great advantage of H_2S tolerance. The major shortcoming of silica membranes is the hydrothermal stability and further work is required to clarify the temperature–gas composition stability window (Bredesen *et al.*, 2004).

The properties of H_2-selective dense inorganic membranes are listed in the Table 7.4.

7.3 Membrane reactors for CO_2 capture

7.3.1 Water–gas shift membrane reactors

Considering the IUPAC definition (Koros *et al.*, 1996), a membrane reactor (MR) is a device for simultaneously performing a reaction (steam reforming, water–gas shift (WGS), autothermal reforming, etc.) and a membrane-based

Table 7.4 General overview of properties of H_2-selective dense inorganic membranes

Membrane type	Transport mechanism	H_2 permeance	T (appl., T_c) °C	H_2/other relevant gas (e.g. N_2 or CO_2)
Pd	Solution–diffusion	High H_2 permeation	$T_{appl.}$ <600, T_c: 300	∞
Pd–Ag	Solution–diffusion	Higher than Pd	$T_{appl.}$ <400, T_c<< 300	∞
fcc Pd–Cu	Solution–diffusion	Lower than bcc Pd–Cu	$T_{appl.}$300–600, T_c: << 300	∞
bcc Pd–Cu	Solution–diffusion	Possibly higher than Pd (depends on composition)	$T_{appl.}$300–600, T_c: << 300	∞
Pd:M1:M2*	Solution–diffusion	Possibly higher than Pd		∞
M1:M2:M3*	Solution–diffusion	Much lower than Pd-based membranes	$T_{appl.}$200–400	∞

*M1, M2 or M3 metal ∞ = infinity.

© Woodhead Publishing Limited, 2011

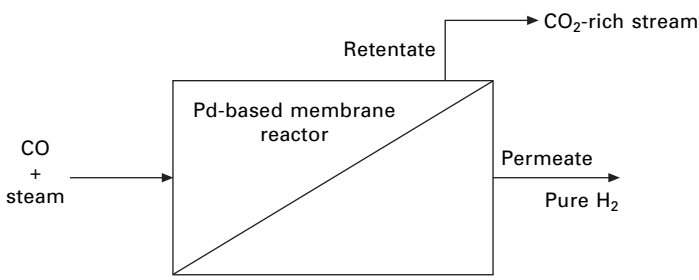
separation in the same physical device. In the field of pre-combustion CO_2 capture processes, to obtain the maximum conversion of syngas into hydrogen and CO_2 as well as the separation of high purity hydrogen associated to CO_2 capture, the WGS reaction (Equation [7.1]) combined with Pd-based MR technology could be very effective. As previously discussed in this chapter, theoretically, dense Pd-based membranes offer full hydrogen permselectivity, allowing a pure hydrogen stream to be obtained on one side of the membrane ('permeate') and a CO_2-rich stream on the other side of the membrane ('retentate'), as shortly schematized in Fig. 7.3.

$$CO + H_2O = CO_2 + H_2 \quad \Delta H°_{298\ K} = -41.1\ kJ\ mol^{-1} \qquad [7.1]$$

Moreover, the ability of a dense Pd-based membrane to remove hydrogen continuously is advantageous for the WGS reaction, because it overcomes the thermodynamic constraints of the reaction, resulting in higher CO conversion to hydrogen and CO_2. In addition, the combination of the WGS reaction and hydrogen separation in the same unit reduces both operating and capital costs.

The WGS membrane reactor can be integrated into the NGCC (natural gas combined cycle) or IGCC (integrated gasification combined cycle) process for power production with pre-combustion CO_2 capture. It may, for example, be located downstream of an oxygen-fed autothermal reformer and a WGS reactor (NGCC) (as shown in Fig. 7.4) or an oxygen blown gasification and subsequent WGS reactor (IGCC). The H_2 separated from the WGS membrane reactor will be sent to the power plant to generate electricity while simultaneously non-permeable CO_2 can be captured on the retentate side. To feed the hydrogen into a gas turbine combustion chamber, a pressure of approx. 25 bar is needed, so the feed pressure of the membrane reactor needs to be considerably higher. To achieve a CO_2 purity of more than 95% to be stored underground, the target H_2 recovery for the WGS membrane reactor is 98% (Koros *et al.*, 1996).

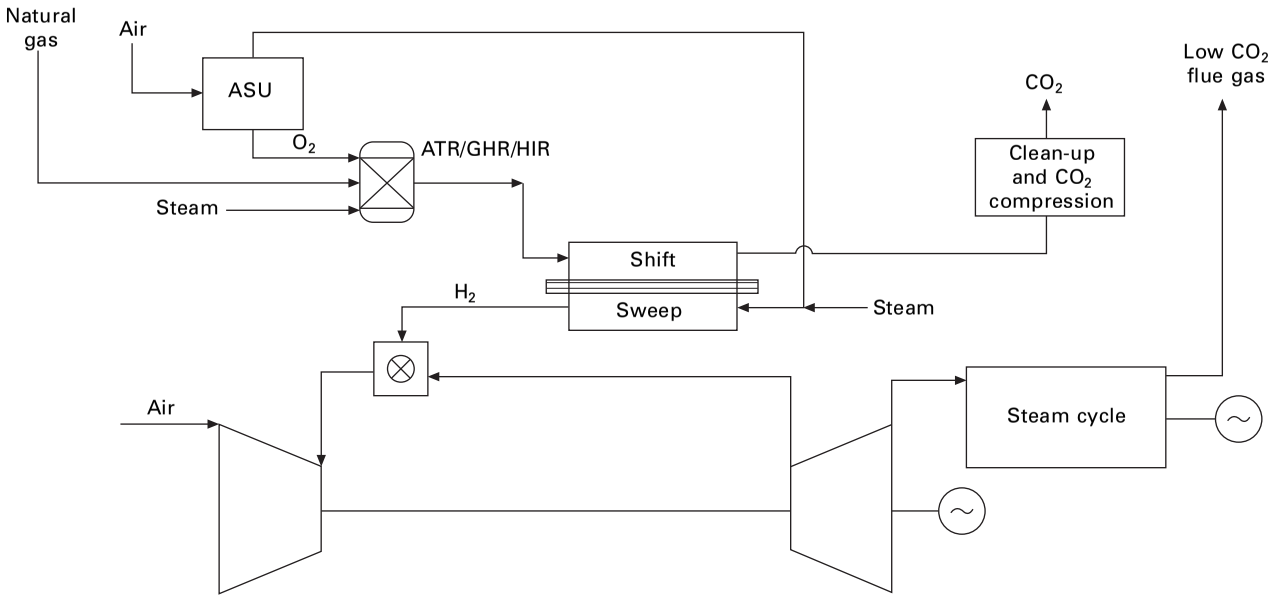
From the beginning of the twentieth century until today, the use of WGS reaction has followed the increased industry demand for hydrogen



7.3 Scheme of a dense Pd-based membrane reactor for WGS reaction.

© Woodhead Publishing Limited, 2011

© Woodhead Publishing Limited, 2011



7.4 Simplified system schematic of natural gas fired power plants with a membrane WGS (right) for CO_2 capture (Koros *et al.*, 1996). ATR/GHR/HIR is the auto thermal or gas heated reformer or the heated infrared reactor.

production. In particular, the growing scientific interest in the application of a WGS reaction in Pd-based MRs is due to the capability of dense Pd-based membranes to produce and separate pure hydrogen with the further advantage of concentrating and capturing CO_2 produced during the reaction. In Table 7.5, a very short overview of the WGS reaction, carried out in Pd-based MRs on the lab scale, is reported, showing CO conversion values under different operating conditions. By observing these values, it is possible to conclude that the Pd-based MRs allow almost complete CO conversion to be obtained at higher temperatures than in conventional industrial operations.

As an example of what is reported above, Jordal *et al*. (2004) found that it is thermodynamically possible to integrate a MR in a combined cycle in a way that enables pre-combustion capture of 80–100% of the produced CO_2, depending on whether microporous or dense Pd-based membranes are employed. However, most of the existing studies of WGS membrane reactor still remain on the lab scale.

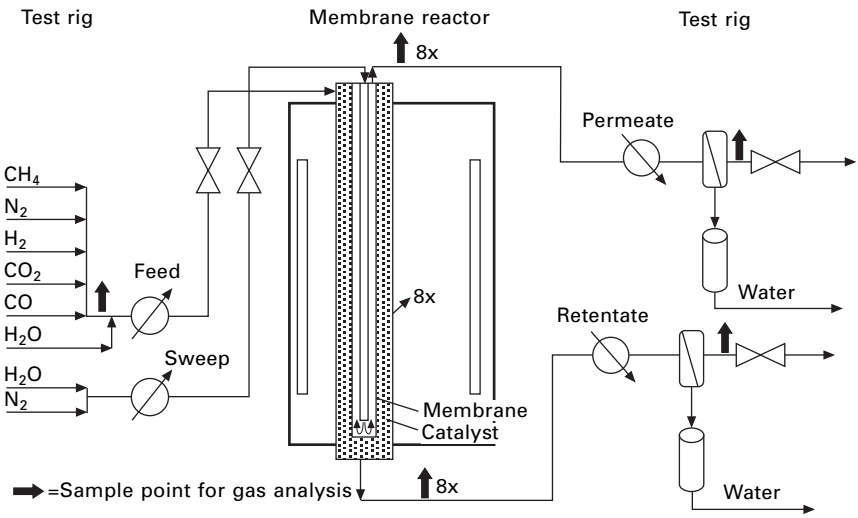
Recently, ECN (Energy research Centre of the Netherlands) has constructed a process development unit (PDU) for testing membrane reactors as shown in Fig. 7.5 (Li *et al*., 2010). It has a capacity of 8 tubular membranes of 44 cm long (effective length) and can be operated up to 40 bar and 600°C. A maximum membrane surface area of 1550 cm^2 can be reached. The PDU will demonstrate the feasibility of MRs on the bench scale size and under the conditions that are present in power plants with pre-combustion CO_2 capture using hydrogen membranes. The scale of the membrane tests in terms of hydrogen production capacity, typically 8.5 $Nm^3\ h^{-1}$ product H_2, exceeds typical lab scale testing by orders of magnitude and provides an important step towards full scale demonstration of the membrane technology and industrial application.

Li *et al*. (2010) describe a membrane-enhanced WGS reaction with three parallel highly permselective Pd composite membranes in the PDU with a length of 50 cm (44 cm effective) and with a palladium layer of *ca*. 5.6 μm,

Table 7.5 Operative conditions and performance of MRs used to carry out the WGS reaction

Membrane	T (°C)	$p_{reaction}$ (bar)	MR conversion (%)	References
Pd/Vycor	400	1.0	92	Kikuchi *et al*. (1989)
Pd on porous glass	400	1.0	98	Uemiya *et al*. (1991)
Pd on ceramic	320	1.0	98	Basile *et al*. (1995)
Pd-composite	322	1.2	99.9	Basile *et al*. (1996)
Pd/γ–Al_2O_3	320	1.1	100	Basile *et al*. (2001)
Pd-based	900	2.4	93	Iyoha *et al*. (2007)
Pd-Ag	325	1.0	100	Tosti *et al*. (2000)
Pd(60%)–Cu	350	–	94	Flytzani-Stephanopoulos *et al*. (2004)

© Woodhead Publishing Limited, 2011



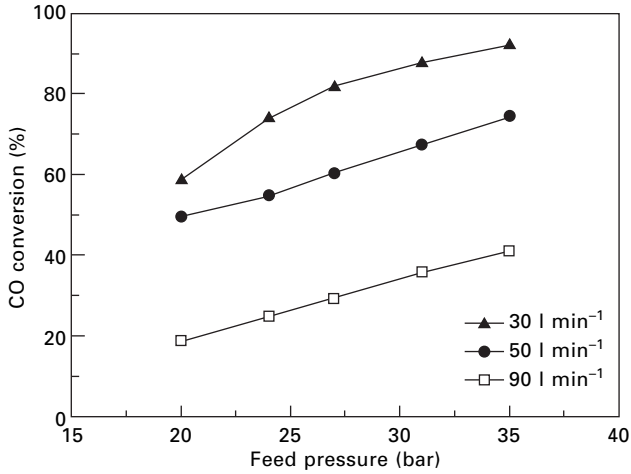
7.5 Schematic diagram of a bench-scale membrane reactor setup process development unit at ECN.

reaching a total membrane surface area of 580 cm^2 configuration. Working conditions were 400°C and 20–35 bar feed pressure, composition: 4.01% CO, 19.24% CO_2, 15.43% H_2O, 1.20% CH_4 and 60.12% H_2. A commercial noble metal WGS catalyst was inserted at the feed side of the reactor tubes. The pure H_2 permeance of the three membranes was measured as 2.7×10^{-6} mol m^{-2} s^{-1} Pa^{-1} at 400°C at a feed/permeate pressure of 2.1/1.1 bar under no-sweep conditions and remained stable for 27 days during the WGS reaction test, while the pure N_2 permeance of the the three membranes was 2.6×10^{-9} mol m^{-2} s^{-1} Pa^{-1} at 400°C. CO conversion was observed to be far beyond the equilibrium conversion at 400°C and increased with feed pressure and decreased with feed flow rate (see Fig. 7.6). CO conversion and H_2 recovery amounted to 92% at a feed/sweep flow rate of 30/19.6 Nl min^{-1} (space velocity of about 3000 Nm^3 m^{-3} h^{-1} and feed/permeate pressure of 35/15 bar. Higher conversion and H_2 recovery over 95% are within reach using longer membranes. Stability tests showed that CO conversion remained stable for about 9 days under different feed pressures and under reduced steam content in the feed, indicating that membrane degradation due to carbon formation was not observed, and a high carbon formation tendency did not result under low steam conditions.

7.3.2 Methane steam reforming membrane reactors

Besides the WGS reaction, the Pd membranes can also be integrated into the methane steam reforming reaction for pre-combustion CO_2 capture in a NGCC as illustrated in Fig. 7.7 (Koros *et al.*, 1996).

© Woodhead Publishing Limited, 2011



7.6 CO conversion as function of the feed pressure and flow rate.

The main reactions in the steam reforming reaction are as follows:

$$CH_4 + H_2O \leftrightarrow CO + 3H_2 \quad \Delta H^0 = 206.2 \text{ kJ mol}^{-1} \qquad [7.2]$$

$$CO + H_2O \leftrightarrow CO_2 + H_2 \quad \Delta H^0 = -41.2 \text{ kJ mol}^{-1} \qquad [7.3]$$

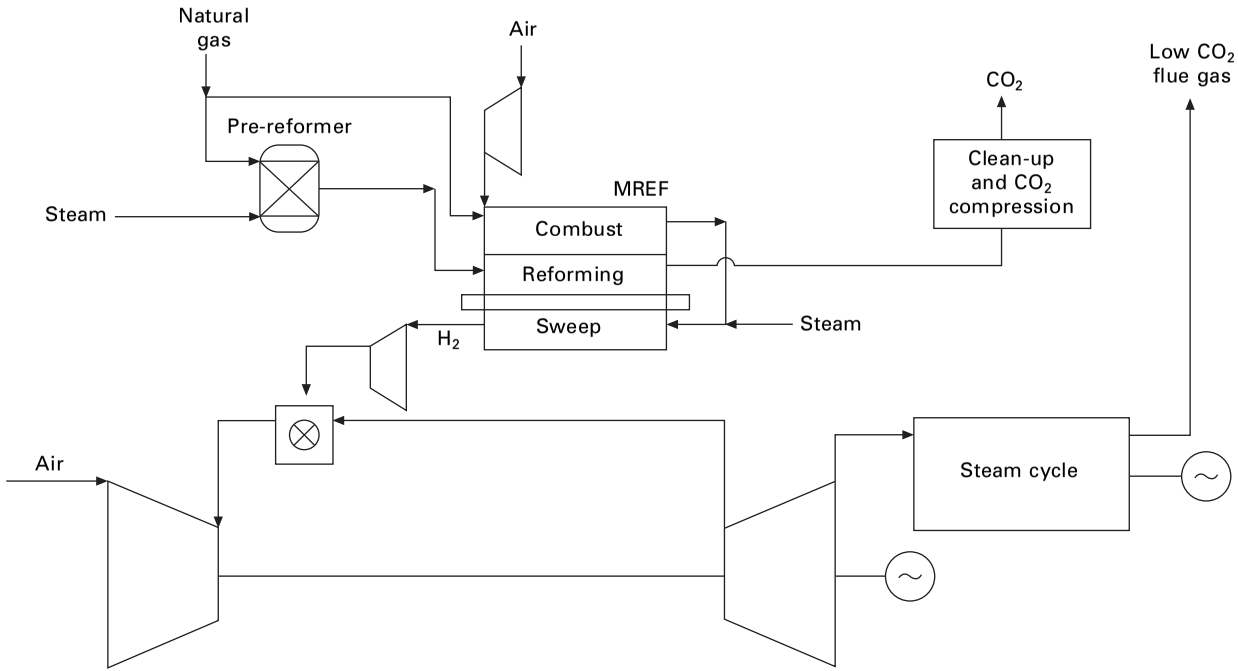
H_2 is selectively removed by the Pd-based membrane both from reaction [7.2] and [7.3] and, thus, not only CH_4 in the feed but also the CO produced from reaction [7.2] is converted to CO_2, which is a great benefit for CO_2 capture. To achieve a CO_2 purity target of 95% (the optimum value is 98.5%), the target CH_4 conversion and H_2 recovery factor are 98% and 95%, respectively.

Until now, there have been many studies on the methane steam reforming in Pd-based MRs both experimentally and theoretically (Shu *et al.*, 1994; Chen *et al.*, 2008a, 2008b; Pieterse *et al.*, 2010). In general, enhanced CH_4 conversion was reported in the MR owing to the extraction of H_2 through the membranes, compared to CH_4 conversion in the conventional reactor or the equilibrium conversion predicted by modelling.

Recently, an improved CH_4 conversion of 84–98% was achieved by Tong *et al.* (2005) with a 6 μm thick Pd composite membrane prepared by a multidimensional plating mechanism at 723–823K, and the superior performance was mainly ascribed to the better separation efficiency of the membrane and proper operating parameters. The highest methane conversion of 98.8% was reported by Chen *et al.* (2008a) with a 4 μm thick Pd/α-Al_2O_3 membrane prepared via electroless plating method (Hou *et al.*, 2005) under mild working conditions: $T = 823$K, $p_{feed} = 9$ bar, GHSV = 4000 ml/g_{cat}.h and a steam-to-methane ratio of 3.0, which was attributed to superior membrane permeance, good catalyst activity and the counter-current sweep gas design.

© Woodhead Publishing Limited, 2011

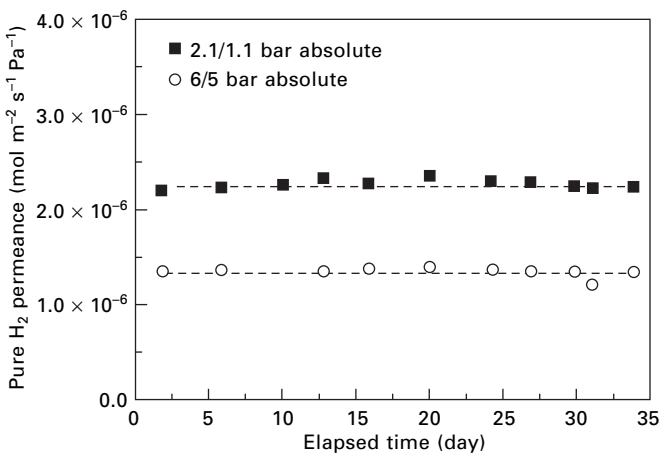
© Woodhead Publishing Limited, 2011



7.7 Simplified system schematic of natural gas fired power plants with a membrane reformer (MREF) for CO_2 capture.

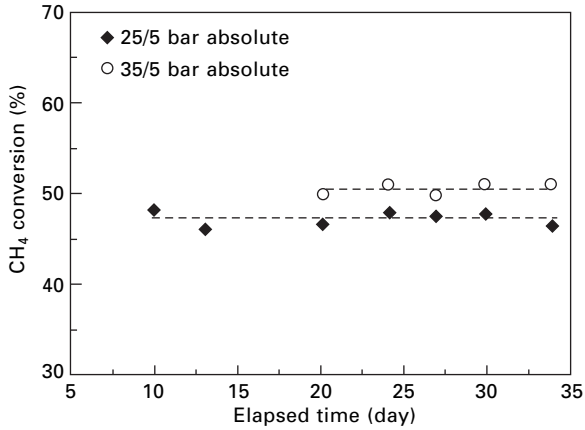
However, most of the present studies remain on a lab scale. Only very few demonstrations of the membrane reformer beyond laboratory scale have been reported to date, for example, MRT (Membrane Reactor Technologies, Canada) has constructed a pure hydrogen generator with capacities in the 15–50 $Nm^3\ h^{-1}$ range using natural gas, propane or renewable feeds (e-net 5), while Tokyo Gas has built and operated a 40 Nm^3-$H_2\ h^{-1}$-class packaged membrane reformer system and successfully demonstrated its technical feasibility (Kameyama *et al.*, 2009). In this section, particular attention is devoted to the demonstration of a bench-scale multi-tubular membrane reformer in ECN, where the test scale in terms of hydrogen production capacity, typically 8.5 $Nm^3\ h^{-1}$ product H_2, exceeds the typical lab scale testing by orders of magnitude.

In the PDU described above, eight Pd membranes with an effective length of 44 cm were incorporated in a parallel configuration, reaching a total membrane surface area of 1550 cm^2. The eight parallel membranes with a thickness of 10.9–13.8 μm were prepared by the electroless plating method (Pieterse *et al.*, 2010), achieving a pure H_2 permeance of 2.2×10^{-6} mol $m^{-2}\ s^{-1}\ Pa^{-1}$ and an ideal H_2/N_2 selectivity up to 30 000 at 823K. A stability of more than 30 days was observed both for the eight parallel membranes and the MSR membrane reactor under challenging NGCC conditions for CO_2 capture (Fig. 7.8 and Fig. 7.9). A reasonable CH_4 conversion can be achieved at a feed/permeate pressure of 35/5 bar at 823K, indicating that the membrane reformer is a promising option for H_2 production. However, upon increasing the permeate pressure from 5 bar to 25 bar the CH_4 conversion



7.8 Evaluation of the stability of the eight membranes during the experimental programme: the pure H_2 permeance of the eight membranes was measured at 823 K and a feed/permeate pressure of 2.1/1.1 bar(a) and 6/5 bar(a).

© Woodhead Publishing Limited, 2011



7.9 Membrane reactor stability test during an experiment of 33 days duration: CH_4 conversion was measured at 823K at a feed/permeate pressure of 25/5 bar(a) and 35/5 bar(a), a space velocity of 1030 Nm^3 m^{-3} h^{-1} and a N_2 sweep flow of 19.6 Nl min^{-1}.

becomes too low to meet the overall CO_2 capture target of > 90%, rendering the membrane reformer a less attractive process for CO_2 capture in power plants. Ongoing research efforts are devoted to the development of high temperature membranes, working at > 923K to increase flux and, therefore, allow working at higher permeate pressures.

7.4 Techno-economic analysis of the integrated gasification combined cycle (IGCC) and natural gas combined cycle (NGCC)

Until now, there has been some techno-economic analysis of the IGCC and NGCC using high temperature inorganic membranes for CO_2 capture. For example, Amelio *et al.* (2007) built a mono-dimensional computational model of the membrane reactor to simulate and evaluate the capability of the $IGCC^M$ plant (integrated gasification gas combined cycle plant with membrane reactor) to capture carbon dioxide. A comparison was made between $IGCC^*$ (integrated gasification gas combined cycle plant with traditional shift reactors and CO_2 solvents) and $IGCC^M$ plants in terms of energetic performance, efficiency and net power. The $IGCC^M$ plant was proven to have an economic advantage over the $IGCC^*$ taking into account a carbon tax, predicting a COE (cost of electricity production) of approx. 60 US$/MWh for $IGCC^M$ systems, higher than that of IGCC plant without CO_2 capture which is 45 US$/MWh and lower than that of $IGCC^*$ at 62US$/MWh.

Jordal *et al.* (2004) set up a model and demonstrated the CO_2 capture in

© Woodhead Publishing Limited, 2011

natural gas fired power cycles through a methane-steam reforming membrane reactor with an integrated H_2-separating membrane. Two types of membrane were investigated: Pd membranes, which could allow zero-emission power cycles and microporous membranes that allow 20% of the generated CO_2 to be emitted into the atmosphere. They predicted a thermal efficiency of 47% for the combined cycles with an integrated membrane reactor and suggested an extensive investigation of the impact of various cycle parameters to find the optimum process parameters and the most suitable gas turbine type.

Dijkstra *et al*. (2009) evaluated two process schemes for a Pd-based H_2 MR integrated into natural gas combined cycles: (1) an integrated membrane WGS combined cycle and (2) an integrated membrane reformer combined cycle. They found that the integration of the WGS-MR gives a lower cost compared to the membrane reformer case, based on membrane performance data after several years of membrane development.

Recently, Doukelis and Beavis (2010) gave a summary of the final performance and economic analysis as reported in Table 7.6 from the EU FP6 CACHET project. The technologies investigated by these researchers showed that they meet the CACHET target of reducing CO_2 emissions by 90% or more. Simulation results, supported by experimental results, show that all the CACHET technologies have the potential to increase the energy efficiency beyond the state-of-the-art base case for pre-combustion CO_2 capture, with membrane WGS showing the highest energy efficiency of 47.1% (lower heating value). Achieving the CACHET objective of reducing the cost of CO_2 capture by 50% has proved to be extremely challenging. The technology with the lowest CO_2 avoidance cost has shown a 31% projected

Table 7.6 Performance and economic analysis of MemWGS (membrane water gas shift combined cycle) and MemREF (integrated membrane reformer combined cycle) from the CACHET project

	Reference	Base case	MemREF	MemWGS
Efficiency (%)	57.2	40.9	46.2	47.1
CACHET target (49.05%)	49.05	49.05	49.05	49.05
Avoidance rate (%)	–	92.6	91.9	92.1
Capture rate (%)	–	94.8	93.5	93.5
CACHET target (90% CO_2 avoided)	90	90	90	90
Cost of capture (€/t CO_2)	–	82.1	96.1	65.9
Cost of avoidance (€/t CO_2)	–	117.5	121.1	81.2
CACHET target (€58.75/t)	58.75	58.75	58.75	58.75
Total fixed investment (€m)	194.9	461.8	530	476
Power output (MWe)	389.8	366	352	392
Break even electricity price (€/MWh)	55.9	86.6	87.4	74.4
Fixed cost (€/MWh)	9	22	23.5	18.8
Variable cost (€/MWh)	46.9	64.6	63.9	55.6
Specific investment	0.5	1.26	1.51	1.21
CACHET target (0.88 €M/MWe)	0.88	0.88	0.88	0.88

© Woodhead Publishing Limited, 2011

cost reduction. Although this is less than the objective, it still represents a significant benefit which should provide industry with sufficient incentive to continue to develop and scale up the technology.

7.5 Conclusions and future trends

Organic membrane separation technology is an emerging technology that has been subject to a rapid growth in attention during the past few decades, as membrane systems offer opportunities to integrate reaction and separation at elevated temperatures. Inorganic membranes are in development for both CO_2 and hydrogen separation. For CO_2 separation, active transport systems are in development and for hydrogen separation both porous and dense membranes are being developed. Dense Pd or Pd-alloy membranes on a ceramic or metallic support are the most developed membrane types.

The WGS or methane steam reforming reactions have been analysed in a membrane reactor. These reactions can be incorporated in the IGCC or NGCC for electricity production with CO_2 capture. Hydrogen membrane reactors are suggested to be able to capture CO_2 at relatively lower costs and lower energy consumption than conventional pre-combustion CO_2 capture technologies. Recently, a bench scale membrane reactor test for both the membrane WGS and membrane reforming reaction have been carried out, showing that the membrane WGS is currently the most promising technology for pre-combustion CO_2 capture in power plants. Further work is required to improve the sulphur tolerance and long-term stability of the Pd-based membranes.

The number of industrial-scale pilots and demonstrations of inorganic membrane technologies is still limited. The next step in the advancement of membrane technologies should be long-term testing in an industrial environment.

7.6 References

Adhikari S. and Fernando S. (2006), 'Hydrogen membrane separation techniques', *Ind. Eng. Chem. Res.*, **45**, 875–81.

Amelio M., Morrone P., Gallucci F. and Basile A. (2007), 'Integrated gasification gas combined cycle plant with membrane reactors: Technological and economical analysis', *Energy Convers. Manage.*, **48**, 2680–93.

Basile A., Violante V., Santella F. and Drioli E. (1995), 'Membrane integrated system in the fusion reactor fuel cycle', *Catal. Today*, **25**, 321–6.

Basile A., Criscuoli A., Santella F. and Drioli E. (1996), 'Membrane reactor for water gas shift reaction', *Gas Separation Purification*, **10**, 243–54.

Basile A., Chiappetta G., Tosti S. and Violante V. (2001), 'Experimental and simulation of both Pd and Pd/Ag for a water gas shift membrane reactor', *Sep. Purif. Techn.*, **25**, 549–71.

© Woodhead Publishing Limited, 2011

Basile A., Gallucci F., Iulianelli A., Tereschenko G.F., Ermilova M.M., and Orekhova N.V. (2008), 'Ti–Ni–Pd dense membranes–The effect of the gas mixtures on the hydrogen permeation', *J. Membrane Sci.*, **310**, 44–50.

Bredesen R. and Klette H. (2000), *Method of Manufacturing Thin Metal Membranes*, US Patent US 6086729.

Bredesen R., Jordal K. and Bolland O. (2004), 'High-temperature membranes in power generation with CO_2 capture', *Chem. Eng. Process.*, **43**, 1129–58.

Bredesen R., Kumakiri I. and Peters T. (2009), 'CO_2 capture with membrane systems', *Membrane Operations*, E. Drioli and L. Giorno (eds), Wiley-VCH, Weinheim, chap. **9**, 195–220.

Buxbaum R.E. and Kinney A.B. (1996), 'Hydrogen transport through tubular membranes of palladium-coated tantalum and niobium', *Ind. Eng. Chem. Res.*, **35**, 530–7.

Caro J., Noack M., Kölsch P. and Schäfer R. (2000), 'Zeolite membranes – state of their development and perspective', *Microporous Mesoporous Mater.*, **38**, 3–24.

Chen H.I., Shiau J.D., Chu C.Y. and Huang T.C. (2003), 'Synthesis and characterization of palladium clusters dispersed alumina membranes', *Sep. Purif. Techn.*, **32**, 247–54.

Chen Y.Z., Wang Y.Z., Xu H.Y. and Xiong G.X. (2008a), 'Efficient production of hydrogen from natural gas steam reforming in palladium membrane reactor', *Appl. Catal. B: Env.*, **81**, 283–94.

Chen Y.Z., Wang Y.Z., Xu H.Y. and Xiong G.X. (2008b), 'Hydrogen production capacity of membrane reformer for methane steam reforming near practical working conditions', *J. Membrane Sci.*, **322**, 453–9.

Choi W.J., Seo J.B., Jang S.Y., Jung J.H. and Oh K.J. (2009), 'Removal characteristics of CO_2 using aqueous MEA/AMP solutions in the absorption and regeneration process', *J. Env. Sci.*, **21**, 907–13.

Ciora R.J., Fayyaz B., Liu P.K.T., Suwanmethanond V., Mallada R., Sahimi M. and Tsotsis T.T. (2004), 'Preparation and reactive applications of nanoporous silicon carbide membranes', *Chem. Eng. Sci.*, **59**, 4957–65.

Cuffe L., Don MacElroy J.M., Tacke M., Kozachok M. and Mooney D.A. (2006), 'The development of nanoporous membranes for separation of carbon dioxide at high temperatures', *J. Membrane Sci.*, **272**, 6–10.

de Bruijn F.A., Rietveld B. and van den Brink R.W. (2007), 'Hydrogen production and fuel cells as bridging technologies towards a sustainable energy system', in *Catalysis for Renewables: From Feedstock to Energy Production*, G. Centi and R.A. van Santen (eds), Wiley-VCH Verlag, Weinheim.

Dijkstra J.W., Jansen D., van den Brink R.W., Peters T.A., Stange M., Bredesen R., Goldbach A., Xu H., Gottschalk A., Tlatlik S. and Doukelis A. (2009), 'Development of hydrogen membrane reactors for CO_2 capture', *Carbon Dioxide Capture for Storage in Deep Geologic Formations*: *Results from CO_2 capture projects*, Volume 3, L. I. Eide (Series ed), CPL Press, chapter 11.

Dijkstra J.W., Pieterse J.A.Z., Li H., Boon J., van Delft Y.C., Raju G., Peppink G., van den Brink R.W. and Jansen D. (2010), 'Development of membrane reactor technology for power production with pre-combustion CO_2 capture', *En. Procedia*, submitted.

Dittmeyer R., Höllein V. and Daub K. (2001), 'Membrane reactors for hydrogenation and dehydrogenation processes based on supported palladium', *J. Mol. Catal. A: Chem.*, **173**, 135–84.

Doukelis A. and Beavis R. (2010), 'Technical project results of CACHET, *CCS Ready to Go? European Conference on CCS Research, Development and Demonstration*, April 19–22, Rotterdam, Netherlands.

© Woodhead Publishing Limited, 2011

Drioli E. and Giorno L. (2009), *Membrane Operations*, Wiley-VCH.

Dudek D. (2001), 'Diffusion coefficients of hydrogen in a $Pd_{81}Pt_{19}$ membrane with time dependent boundary conditions', *J. Alloys Compd.*, **329**, 1–7.

Dyer A. (1988), *An Introduction to Zeolite Molecular Sieves*, J Wiley & Sons, New York.

Edlund D.J. and McCarthy J. (1995), 'The relationship between intermetallic diffusion and flux decline in composite-metal membranes: Implications for achieving long membrane lifetime', *J. Membrane Sci.*, **107**, 147–53.

Edlund D.J., Friesen D.J., Johnson B.M. and Pledger W.A. (1994), 'Hydrogen-permeable metal membranes for high-temperature gas separations', *Gas Sep. Purif.*, **8**, 131–6.

e-net 1 (2007), *European Technology Platform for Zero Emission Fossil Fuel Power Plants*, http://www.zero-missionplatform.eu/website/docs/ETP%20ZEP/EU%20Flagship%20Programme%20for%20CCS.pdf.

e-net 2 (2007), *Near-term Opportunities for Carbon Dioxide Capture and Storage: Global assessments workshop*, International Energy Agency (IEA). IEA Publications, Paris, France.

e-net 3 (2004), *Prospects for CO_2 Capture and Storage*, International Energy Agency (IEA). IEA Publications, Paris, France.

e-net 4 (2005), *IPCC Special Report on Carbon Dioxide Capture and Storage*, Working group III of IPCC, B. Metz, O. Davidson, H.C. de Coninck, M. Loos and L.A. Meyer (eds), Cambridge University Press, Cambridge, UK.

e-net 5: http://www.membranereactor.com/products.html.

Figueroa J.D., Fout T., Plasynski S., McIlvried H. and Srivastava R.D. (2008), 'Advances in CO_2 capture technology—The U.S. Department of Energy's Carbon Sequestration Program', *Int. J. Greenhouse Gas Control*, **2**, 9–20.

Flytzani-Stephanopoulos M., Qi X. and Kronewitter S. (2004), 'Water-gas shift with integrated hydrogen separation process', Final report to DOE, Department of Chemical and Biological Engineering, Tufts University, MA, USA, 1–38.

Fotou G.P., Lin Y.S. and Pratsinis S.E. (1995), 'Hydrothermal stability of pure and modified microporous silica membranes', *J. Mater. Sci,.* **30**, 2803–08.

Gao H.Y., Lin Y.S., Li Y.D. and Zhang B.Q. (2004), 'Chemical stability and its improvement of palladium-based metallic membranes', *Ind. Eng. Chem. Res.*, **43**, 6920–30.

Gobina E. (2006), *Apparatus and Method for Separating Gases*, US Patent 2006112822.

Goto S., Assabumrungrat S., Tagawa T. and Praserthdam P. (2000), 'The effect of direction of hydrogen permeation on the rate through a composite palladium membrane', *J. Membrane Sci.*, **175**, 19–24.

Guiver M.D., Robertson G.P. and Thi H.N.L. (2004), 'Composite gas separation membranes', Canadian Patent: CA2421875.

Hou S.F., Jiang K., Li W.Z., Xu H.Y., Yuan L.X. (2005), *A Metal Palladium Composite Membrane or Alloy Palladium Composite Membrane and Their Preparation Methods*, WO Patent 2005/065806 A1.

Hsu C. and Buxbaum R.E. (1986), 'Palladium-catalyzed oxidative diffusion for tritium extraction from breeder-blanket fluids at low concentrations', *J. Nucl. Mater.*, **141–3**, 238–41.

Iwamoto Y., Sato K., Kato T., Inada T. and Kubo Y. (2005), 'A hydrogen-permselective amorphous silica membrane derived from polysilazane', *J. Eur. Ceramic Soc.*, **25**, 257–64.

© Woodhead Publishing Limited, 2011

Iyoha O., Enick R., Killmeyer R., Howard B., Morreale B. and Ciocco M. (2007), 'Wall-catalyzed water-gas shift reaction in multi-tubular Pd and 80 wt%Pd-20 wt%Cu membrane reactors at 1173 K', *J. Membrane Sci.*, **298**, 14–23.

Jordal K., Bredesen R., Kvamsdal H.M. and Bolland O. (2004), 'Integration of H_2-separating membrane technology in gas turbine processes for CO_2 capture', *Energy*, **29**, 1269–78.

Jun C.S. and Lee K.H. (2000), 'Palladium and palladium alloy composite membranes prepared by metal-organic chemical vapor deposition method (cold-wall)', *J. Membrane Sci.*, **176**, 121–30.

Kajiwara M., Uemiya S. and Kojima T. (1999), 'Stability and hydrogen permeation behavior of supported platinum membranes in presence of hydrogen sulfide', *Int. J. Hydrogen Energy*, **24**, 839–44.

Kajiwara M., Uemiya S., Kojima T. and Kikuchi E. (2000), 'Rhodium- and iridium-dispersed porous alumina membranes and their hydrogen permeation properties', *Catal. Today,* **56**, 83–7.

Kamakoti P., Morreale B.D., Ciocco M.V., Howard B.H., Killmeyer R.P., Cugini A.V. and Sholl D.S. (2005), 'Prediction of hydrogen flux through sulfur-tolerant binary alloy membranes', *Science*, **307**, 569–73.

Kameyama H., Nishio S., Kurokawa H., Shirasaki Y., Yasuda I., Xue Z.Q., Yamada T. and Matsuoka T. (2009), *Assessment of Distributed Carbon Capture and Sequestration in Japan ~ Distributed CCS for City Gas System in Japan*, http://www.igu.org/html/wgc2009/papers/docs/wgcFinal00222.pdf

Kanezashi M. and Asaeda M. (2006), 'Hydrogen permeation characteristics and stability of Ni-doped silica membranes in steam at high temperature', *J. Membrane Sci.*, **271**, 86–93.

Keuler J.N. and Lorenzen L. (2002), 'Developing a heating procedure to optimise hydrogen permeance through Pd-Ag membranes of thickness less than 2.2 μm', *J. Membrane Sci.*, **195**, 203–13.

Kikuchi E., Uemiya S., Sato N., Inoue H., Ando H. and Matsuda T. (1989), 'Membrane reactor using microporous glass supported thin film of palladium. Application to the water gas shift reaction', *Chem. Lett.*, **18**, 489–92.

Kikuchi E., Nemoto Y., Kajiwara M., Uemiya S. and Kojima T. (2000), 'Steam reforming of methane in membrane reactors: comparison of electroless-plating and CVD membranes and catalyst packing modes', *Catal. Today*, **56**, 75–82.

Koresh J.E. and Soffer A. (1986), 'Mechanism of permeation through molecular sieve carbon membrane: Part 1. The effect of adsorption and the dependence on pressure', *J. Chem. Soc. Faraday Trans.*, **82**, 2057–63.

Koros W.J., Ma Y.H. and Shimidzu T. (1996), 'Terminology for membranes and membrane processes', *J. Membrane Sci.*, **120**, 149–59.

Ku A.Y.C., Ruud J.A., Molaison J.L., Schick L.A. and Ramaswamy V. (2008), 'Functionalized inorganic membranes for gas separation', US Patent US 20087396382.

Kuraoka K., Kubo N. and Yazawa T. (2000), 'Microporous silica xerogel membrane with high selectivity and high permeance for carbon dioxide separation', *J. Sol-Gel Sci. Techn.,* **19**, 515–18.

Kusakabe K., Kuroda T., Murata A. and Morooka S. (1997), 'Formation of a Y-type zeolite membrane on a porous α-alumina tube for gas separation', *Ind. Eng. Chem. Res.*, **36**, 649–55.

Lee L.L. and Tsai D.S. (1999), 'Hydrogen-permselective silicon oxycarbide membrane derived from polydimethylsilane', *J. Am. Ceram. Soc.*, **82**, 2796–800.

© Woodhead Publishing Limited, 2011

Lewis F.A. (1995), 'The palladium-hydrogen system: Structures near phase transition and critical points', *Int. J. Hydrogen Energy*, **20**, 587–92.

Li H., Dijkstra J.W., Pieterse J.A.Z., Boon J., van den Brink R.W. and Jansen D. (2010), 'Towards full-scale demonstration of hydrogen-selective membranes for CO_2 capture: Inhibition effect of WGS-components on the H_2 permeation through three Pd membranes of 44 cm long', *J. Membrane Sci.*, **363**, 204–11.

Liu B., Wu G., Niu G. and Deng J.F. (1999), 'Rh-modified alumina membranes: preparation, characterization and reaction studies', *Appl. Catal. A: Gen.,* **185**, 1–10.

Mallada R. and Menéndez M. (2008), 'Inorganic membranes: synthesis, characterization and applications', *Membrane Science and Technology*, R. Malada and M. Menéndez (eds), Elsevier, Oxford, UK. 460.

Maneeintr K., Idem R.O., Tontiwachwuthikul P. and Wee A.G.H. (2010), 'Comparative mass transfer performance studies of CO_2 absorption into aqueous solutions of DEAB and MEA', *Ind. Eng. Chem. Res.*, **49**, 2857–63.

McKinley D.L. (1967), *Metal Alloy for Hydrogen Separation and Purification*, US Patent US 3350845.

McKinley D.L. (1969), *Method for Hydrogen Separation and Purification*, US Patent US 3439474.

Mix T.W. (1987), 'Advanced separation techniques for petrochemicals', *Energy*, **12**, 1121–33.

Morreale B.D., Ciocco M.V., Howard B.H., Killmeyer R.P., Cugini A.V. and Enick R.M. (2004), 'Effect of hydrogen-sulfide on the hydrogen permeance of palladium–copper alloys at elevated temperatures', *J. Membrane Sci.*, **241**, 219–24.

Mundschau M.V., Xie X., Evenson IV C.R. and Sammells A.F. (2006), 'Dense inorganic membranes for production of hydrogen from methane and coal with carbon dioxide sequestration', *Catal. Today*, **118**, 12–23.

Nair B.N., Yamaguchi T., Kawamura H., Nakagawa K. and Nakao S. (2002), *Proceedings of the ICOM*, Toulouse, France.

Nam S.W. and Gavalas G. (1989), 'Stability of H_2-permselective SiO_2 films formed by chemical vapor deposition', *AIChE Symp. Ser.*, **85**, 68–74.

Okazaki J., Tanaka D.A.P., Tanco M.A.L., Wakui Y., Mizukami F. and Suzuki T.M. (2006), 'Hydrogen permeability study of the thin Pd-Ag alloy membranes in the temperature range across the alpha-beta phase transition', *J. Membrane Sci.*, **282**, 370–4.

Olivares-Marín M., Castro-Díaz M., Drage T.C. and Maroto-Valer M.M. (2010), 'Use of small-amplitude oscillatory shear rheometry to study the flow properties of pure and potassium-doped Li_2ZrO_3 sorbents during the sorption of CO_2 at high temperatures', *Sep. Purif. Techn.*, **73**, 415–20.

Peters T.A., Tucho W.M., Ramachandran A., Stange M., Walmsley J.C., Holmestad R., Borg A. and Bredesen R. (2009), 'Thin Pd -23%Ag/stainless steel composite membranes: Long-term stability, life-time estimation and post-process characterisation', *J. Membrane Sci.*, **326**, 572–81.

Petersen J., Matsuda M. and Haraya K. (1997), 'Capillary carbon molecular sieve membranes derived from Kapton for high temperature gas separation', *J. Membrane Sci.*, **131**, 85–94.

Pieterse J.A.Z., Boon J., van Delft Y.C., Dijkstra J.W. and van den Brink R.W. (2010), 'On the potential of nickel catalysts for steam reforming in membrane reactors', *Catal. Today*, **156**, 153–64.

Prabhu A.K. and Oyama S.T. (2000), 'Highly hydrogen selective ceramic membranes: application to the transformation of greenhouse gases', *J. Membrane Sci.*, **176**, 233–48.

© Woodhead Publishing Limited, 2011

Rao M.B. and Sircar S. (1993), 'Nanoporous carbon membrane for gas separation', *Gas Sep. Purif.*, **7**, 279–84.

Roa F., Way J.D., McCormick R.L. and Paglieri S.N. (2003), 'Preparation and characterization of Pd-Cu composite membranes for hydrogen separation', *Chem. Eng. J.*, **93**, 11–22.

Sea B.K., Ando K., Kusakabe K. and Morooka S. (1998), 'Separation of hydrogen from steam using a SiC-based membrane formed by chemical vapor deposition of triisopropylsilane', *J. Membrane Sci.*, **146**, 73–82.

Shekhawat D., Luebke D.R. and Pennline H.W. (2003), *A Review of Carbon Dioxide Selective Membranes–A Topical Report*, National Energy Technology Laboratory, United States Department of Energy.

Shelekhin A.B., Dixon A.G. and Ma Y.H. (1992), 'Adsorption, permeation, and diffusion of gases in microporous membranes. II. Permeation of gases in microporous glass membranes', *J. Membrane Sci.*, **75**, 233–44.

Shelekhin A.B., Pien S. and Ma Y.H. (1995), 'Permeability, surface area, pore volume and pore size of V_{ycor} glass membrane heat-treated at high temperature', *J. Membrane Sci.*, **103**, 39–43.

Shu J., Grandjean B.P.A., Van Neste A. and Kaliaguine S. (1991), 'Catalytic palladium based membrane reactors: a review', *Can. J. Chem. Eng.*, **69**, 1036–60.

Shu J., Grandjean B.P.A. and Kaliaguine S. (1994), 'Methane steam reforming in asymmetric Pd- and Pd-Ag/porous SS membrane reactors', *Appl. Catal. A: Gen.*, **11**, 305–25.

Sircar S., Waldron W.E., Rao M.B. and Anand M. (1999), 'Hydrogen production by hybrid SMR-PSASSF membrane system', *Sep. Purif. Techn.*, **17**, 11–20.

Suzuki H. (1986), *Composite having a Zeolite, a Layered Compound or a Crystalline-Lattice Material in the Pores of a Porous Support and Processes for Production Thereof*, European Patent EP 0180200.

Tong J.H., Matsumura Y., Suda H. and Haraya K (2005), 'Experimental study of steam reforming of methane in a thin (6 μm) Pd-based membrane reactor', *Ind. Eng. Chem. Res.*, **44**, 1454–65.

Tosti S., Violante V., Basile A., Chiappetta G., Castelli S., De Francesco M., Scaglione S. and Sarto F. (2000), 'Catalytic membrane reactors for tritium recovery from tritiated water in the ITER fuel cycle', *Fusion Eng. Des.*, **49–50**, 953–8.

Uemiya S. (1999), 'State-of-art-the-art of supported metal membranes for gas separation', *Sep. Purif. Methods*, **28**, 51–85.

Uemiya S., Sato N., Ando H. and Kikuchi E. (1991), 'The water gas shift reaction assisted by a palladium membrane reactor', *Ind. Eng. Chem. Res.*, **30**, 585–9.

Uhlmann D., Liu S., Ladewig B.P. and Diniz da Costa J.C. (2009), 'Cobalt-doped silica membranes for gas separation', *J. Membrane Sci.*, **326**, 316–21.

van Delft Y.C., Correia L.A., Overbeek J.P., Meyer D.F., de Groot A., Dijkstra J.W. and Jansen D. (2007), 'Palladium membrane reactors for large scale production of hydrogen', *8th International Conference on Catalysis in Membrane Reactors*, Kolkata, India.

Van Veen H.M., Bracht M., Hamoen E. and Alderliesten P.T. (1996), 'Feasibility of the application of porous inorganic gas separation membranes in some large-scale chemical processes', *Fundamentals of Inorganic Membrane Science and Technology*, A.J. Burggraaf and L. Cot (eds), Elsevier, Vol. 14, 641–81.

Volger K.W., Hauser R., Kroke E., Riedel R., Ikuhara Y.H. and Iwamoto Y. (2006), 'Synthesis and characterization of novel non-oxide sol–gel derived mesoporous amorphous Si-C-N membranes', *J. Ceramic Soc. Jap.*, **114**, 567–70.

© Woodhead Publishing Limited, 2011

Vos de R.M., Maier W.F. and Verweij H. (1999), 'Hydrophobic silica membranes for gas separation', *J. Membrane Sci.*, **158**, 277–88.

Yang H., Xu Z., Fan M., Gupta R., Slimane R.B., Bland A.E. and Wright I. (2008), 'Progress in carbon dioxide separation and capture: A review', *J. Env. Sci.*, **20**, 14–27.

Yuan L.X., Goldbach A. and Xu H.Y. (2007), 'Segregation and H_2 transport rate control in body-centered cubic PdCu membranes', *J. Phys. Chem. B,* **111**, 10952–8.

Zhou Q., Chan C.W. and Tontiwachiwuthikul P. (2009), 'A monitoring and diagnostic expert system for carbon dioxide capture', *Exp. Systems Appl.*, **36**, 1621–31.

© Woodhead Publishing Limited, 2011

8

Inorganic membranes for synthesis gas processing

S. SMART, L. P. DING, and J. C. DINIZ DA COSTA, The University of Queensland, Australia

Abstract: This chapter discusses the research and development of inorganic membranes for syngas processing, which is a critical step in H_2 production. The chapter presents an introduction to syngas processing, followed by the basic principles of membrane and membrane reactor operation. Of particular importance here is the coupling of catalysts with membranes as membrane reactor unit operations which shifts the CO conversion of the water gas shift reaction above its equilibrium. The inherent advantages of inorganic membranes for syngas processing and the current challenges that must be overcome for their successful integration and application within industry are then discussed.

Key words: hydrogen purification, membrane reactor, palladium-based membranes, silica-based membranes, water gas shift reaction.

8.1 Introduction

Synthesis gas, commonly known as syngas, is a mixture of hydrogen (H_2) and carbon monoxide (CO) which is formed by reforming or gasification of a hydrocarbon feedstock. Syngas is a vitally important chemical feedstock for producing synthetic fuels including H_2 and higher hydrocarbons, chemicals including alcohols, ethers and ammonia among others and can be used as a fuel source in its own right. Research into the production and processing of syngas has increased dramatically in the last few decades as the evidence and impact of anthropogenic climate change and the corresponding search for clean energy vectors becomes stronger. Syngas features prominently in two areas of these discussions. First, H_2 is seen by many as the ideal clean energy vector and the reforming of fossil fuels, where syngas features as an intermediate, is the most common and most economic method of H_2 production. Second, gasification-based power generation technologies, such as the integrated gasification combined cycle (IGCC) which produces syngas as an intermediate, show great potential for the integration of carbon capture and storage (CCS) processes into fossil fuel fired power plants. However, current syngas production and processing technologies utilize traditional reaction and separation unit operations that are economically unsuitable for

© Woodhead Publishing Limited, 2011

a carbon constrained economy. Inorganic membranes offer many advantages for syngas processing and H_2 production, including higher energy and process efficiencies and the ability to couple reaction and separation into a single unit operation through membrane reactors. This chapter will focus on the research and development of inorganic membranes, their inherent advantages for syngas processing and the current challenges that must be overcome for their successful integration and application within industry.

8.1.1 Syngas production

Syngas may, in theory, be produced from any hydrocarbon and this is reflected by the wide variety of feedstocks utilized in large industrial-scale syngas production including natural gas, liquid hydrocarbons, biomass and coal (Wilhelm *et al.*, 2001; Basini, 2005; Kolb, 2008). There are three main reactionary pathways commonly used in industry for syngas generation: steam reforming, partial oxidation and oxidative steam reforming or autothermal reforming.

Steam reforming (SR) is the conversion of gaseous hydrocarbons into a mixture of CO and H_2 through the addition of steam and heat. SR most commonly operates at temperatures between 700 and 1000°C, is catalysed by a nickel based catalyst, uses natural gas (methane) as a feedstock and proceeds as shown in Equation [8.1].

$$CH_4 + H_2O \leftrightarrow CO + 3H_2 \quad \Delta H°_{298K} = 253.7 \text{ kJ mol}^{-1} \qquad [8.1]$$

There are several side reactions that occur in parallel, the most significant of which is the water gas shift (WGS) reaction, Equation [8.2], which serves to increase the amount of H_2 in the syngas. The reaction is reversible, mildly exothermic and equilibrium limited and so does not achieve high conversions within the reformer itself (Benson, 1981).

$$CO + H_2O \leftrightarrow CO_2 + H_2 \quad \Delta H°_{298K} = -41.1 \text{ kJ mol}^{-1} \qquad [8.2]$$

SR operates at the lowest process temperature and produces syngas with the highest H_2/CO ratio (≥ 3) of any production method. It has been utilized very effectively by industry for more than a century in the production of H_2, ammonia, methanol and higher hydrocarbons via the Fischer–Tropsch process. However, as the main reaction is endothermic, SR requires an external source of heat and contributes more carbon dioxide CO_2 emissions to the atmosphere than other syngas generation processes.

Partial oxidation (POX) is the conversion of hydrocarbons into syngas under an oxygen (O_2) deficient atmosphere as in Equation [8.3]. The reaction is slightly exothermic and can proceed at high temperatures (> 1200°C) without a catalyst or at lower temperatures (800–1000°C) with a catalyst:

$$C_nH_m + n/2\ O_2 \rightarrow nCO + 2H_2 \qquad [8.3]$$

© Woodhead Publishing Limited, 2011

The process requires O_2 rather than steam and this can be supplied either through air or pure O_2. Downstream processing requirements can be hindered by nitrogen (N_2) and so the use of air as an O_2 source is not always advisable; however, both feedstocks are used within industry. The syngas produced via the POX process has a lower H_2/CO ratio (<2) than SR and is more suited to methanol production and Fischer–Tropsch process.

Oxidative steam reforming or autothermal reforming (ATR) is production of syngas via the combination of steam reforming and partial oxidation in a single reaction chamber. In theory the O_2 feed is balanced so that the energy produced via the partial oxidation reaction is equivalent to the energy required in the steam reforming reaction, making the process self-sustaining (Kolb, 2008). An example of the reaction for methane is given in Equation [8.4].

$$CH_4 + O_2 + 2H_2O \rightarrow 4CO + 10H_2 \quad [8.4]$$

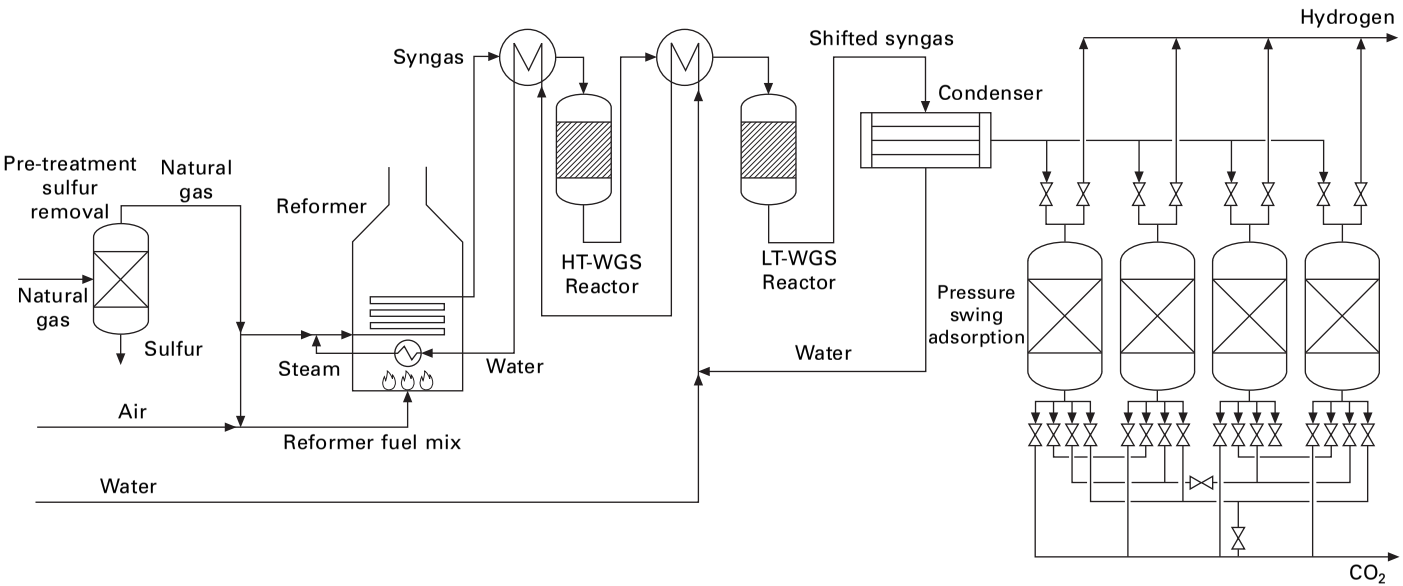
The process operates at approximately 950–1100°C and can be adjusted to give a H_2/CO ratio that ranges from 1 to 2.5 and is therefore able to supply all downstream applications with appropriate quality syngas. As with POX, both air and pure O_2 can be utilized as a feedstock, although air offers more challenges in downstream processing. Despite the flexibility of both the POX and ATR syngas production methods, they are not suited to large scale production facilities, with the cost of a large oxygen plant being prohibitively expensive.

A process flow diagram of a traditional syngas production and processing plant, with a view towards H_2 production, is shown in Fig. 8.1. Syngas leaves the reactor at high temperatures (> 800°C) regardless of the synthesis method. The initial processing step following syngas generation is gas clean up which involves the removal of particulates and trace contaminants like sulfur and heavy metals. The most important unit operation in the downstream processing of the raw syngas is the shift reactor, where the WGS reaction is used to increase the H_2/CO ratio of the syngas. The WGS reaction is a mild exothermic reversible reaction and the reaction conversion is controlled by thermodynamic equilibrium (Benson, 1981). The equilibrium constant of the WGS reaction decreases with increasing temperature; therefore low temperatures favour higher conversion. In contrast, the catalytic reaction rate increases with temperature. Therefore the WGS reaction is normally operated in two stages at different temperatures, with the assistance of catalysts suitable for both the low (~200°C) and high (~350°C) temperature reactors, respectively (Ratnasamy and Wagner, 2009). Through careful operation of the syngas generator and the WGS reactors the H_2/CO ratio of the syngas can be adjusted to suit any application.

Gas separation is the final stage of syngas processing and involves the purification of H_2 or removal of CO_2 from the syngas mixture. There are

© Woodhead Publishing Limited, 2011

© Woodhead Publishing Limited, 2011



8.1 Process flow diagram of steam methane reforming plant for hydrogen production.

several mature technologies that can be employed as gas separation processes including cryogenics, solvent extraction (amines), adsorbents (zeolites) and polymeric membranes (polydimethylsiloxane), all of which are restricted to sorption mechanisms and operate best at low temperatures (< 50°C). These processes are capital and energy intensive. Emerging alternatives to these traditional technologies are inorganic membranes and membrane reactors that will allow syngas processing at elevated temperatures and pressures. Membranes can be integrated into both the production and processing of syngas. This chapter will focus heavily on the use of inorganic membranes and membrane reactors for the purification of H_2 from syngas. The use of membranes, particularly as membrane reactors for the production of syngas via the POX method is the focus of much research; however it will not be discussed in detail here. For more information on the use of membrane reactors for syngas generation, readers are directed to Kolb's book (Kolb, 2008) and a recent review from Caro *et al*. (2007).

8.2 Basic principles of membrane operation

The goal of syngas processing is dependent on the end use of the syngas but most commonly involves altering the H_2/CO ratio, purification of hydrogen and the removal carbon dioxide and other trace elements to obtain high purity fuel gases, H_2 and CO, for utilization downstream. Dense metallic membranes and porous silica and zeolite membranes have been extensively studied for hydrogen purification and gas separation at high temperature. The transport mechanisms and operation principles of syngas processing membranes will be discussed in this section.

8.2.1 Dense membranes

Metals and alloys have long been established as gas permeable. Solute atoms, such as hydrogen, oxygen and nitrogen, are much smaller than the atoms of the metallic lattice and can therefore occupy the interstices inside the metal crystal and form interstitial solid solutions (Mehrer, 2007). The interstitial sites and hence diffusion mechanisms are defined by the geometry of the metal lattice. The diffusion and transfer of H_2 through metallic membranes can be described by the solution–diffusion mechanism (Bitter, 1991). There are five consecutive steps taking place during gas transport. First, the gas molecules diffuse from the bulk phase and adsorb on the surface of the metal. The adsorbed H_2 molecules are then dissociated to form hydrogen atoms. The hydrogen atoms dissolve into the metal lattice to form a metal hydride and diffuse to the opposite side of the metal. Finally the hydrogen atoms recombine to reform the H_2 molecule on the surface and desorb from the permeate side.

© Woodhead Publishing Limited, 2011

The diffusion through a dense metallic membrane of x thickness can be described by Fick's first law (Equation [8.5]) as:

$$J = -D_H \frac{dC_H}{dx} \quad [8.5]$$

where D_H is the diffusion coefficient of hydrogen and C_H is the hydrogen concentration in the metal solution. At low concentrations, it is known that C_H is proportional to the square root of H_2 partial pressure P_H, resulting in Sieverts' law (Equation [8.6]) for hydrogen dissolution in metals given by:

$$C_H = S_H P_H^{0.5} \quad [8.6]$$

Under high temperature conditions, hydrogen diffusion through the bulk metal is the rate-limiting step for gas transport. Therefore the steady-state flux of hydrogen through metallic membranes can be calculated by combining Equations [8.5] and [8.6] to obtain Equation [8.7]:

$$J = \frac{Perm}{\Delta x} (P_f^{0.5} - P_p^{0.5}) \quad [8.7]$$

where the H_2 permeability $Perm$, is equal to the product of hydrogen solubility S_H, and the diffusion coefficient D_H. The solubility value can be obtained from the pressure–composition isotherm measurement by various methods (Wicke and Brodowsky, 1978) and hence the hydrogen diffusion coefficient in a metallic membrane can be calculated according to Equation [8.7] together with the flux measurement. The thickness of metallic membranes has a significant effect on H_2 flux, as does the H_2 solubility in the metal (Grashoff *et al.*, 1983). The relationship between flux and pressure has been found to deviate from the square root law given in Equation [8.7], when the metal surface was contaminated (Yamakawa *et al.*, 2001). Furthermore, at high H_2 feed pressures, the experimental results for flux and pressure gradient do not follow Sieverts' law either (Andrew and Haasz, 1992; Hara *et al.*, 2009). These deviations can be attributed to surface adsorption or diffusion rate limitations under the above conditions.

8.2.2 Porous membranes

Gas transport through porous membranes is controlled by the porous structure of the membrane material (de Lange *et al.*, 1995b). For transport through macro- and mesopores, molecular diffusion, Knüdsen diffusion and viscous flow all contribute to the total transport, while the activated surface flow of the adsorbed phase will affect microporous transport. The pore sizes of silica and silica-derived membranes are in the mesopore and micropore range, therefore Knüdsen and activated diffusion or molecular sieving should be

© Woodhead Publishing Limited, 2011

considered. For Knüdsen flow, a permeating molecule is more likely to collide with the pore wall than colliding with another molecule inside the pore, and the Knüdsen diffusivity D_k can be described by Equation [8.8]:

$$D_k = \frac{d_0}{3}\sqrt{\frac{8RT}{\pi M}} \quad [8.8]$$

In Equation [8.8], M is the molecular weight of the diffusing molecule and d_0 is the pore diameter (Bird *et al.*, 2002). For strongly adsorbed gas molecules on very small pores, such as below 2 nm, the transport of preferentially adsorbed molecules is not negligible and the surface diffusivity should be considered as given by Equation [8.9]:

$$D_s = D_{s,0}\Gamma\frac{dC_{ads}}{dP} \quad [8.9]$$

where $D_{s,0}$ is the intrinsic diffusivity of the adsorbed phase, C_{ads} is the adsorbed concentration and P is the pressure. Γ takes into account the thermodynamic effect determined by the adsorption isotherm. Therefore the total diffusivity in the porous structure can be obtained by combining the gas phase diffusion and surface diffusion described by Equations [8.8] and [8.9], together with the adsorption equation.

By incorporating adsorption and diffusion, the expression [8.10] for permeating flux through microporous silica membranes was proposed (de Lange *et al.*, 1995b):

$$J = \frac{\mu}{x} D_0^* K_0 q_s \exp\left[\frac{E_d - Q_a}{RT}\right]\Delta P \quad [8.10]$$

Where μ is a correction factor related to the porous structure of the silica membrane and x is the membrane thickness. D_0 and K_0 are the pre-exponential factors for the diffusivity and adsorption constant, respectively, while E_d and Q_a are the activation energies for diffusion and isosteric heat of adsorption, respectively, q_s is the adsorbed amount at saturation and ΔP is the pressure gradient. To obtain Equation [8.10], gas adsorption is assumed to take place according to Henry's law. Both the diffusivity and the Henry's law constant are expressed by the Arrhenius form.

For the transport of gas mixtures, the generalized Maxwell–Stefan equation (Krishna and Wesselingh, 1997) has been widely adopted to describe multi-component diffusion. Although quantitative descriptions of gas diffusion in silica membranes and silica mesopores based on statistical mechanics theory (Oyama *et al.*, 2004) or molecular dynamic simulation (Krishna, 2009) have been reported, the prediction of gas permeation in silica membranes remains a challenging task, owing to the difficulty of generating an accurate description of the porous network of the membrane.

© Woodhead Publishing Limited, 2011

The transport mechanism in zeolite membranes is very similar to that in molecular sieving silica membranes and the surface flow of the adsorbed phase should also be considered because of the small pore size. Therefore Equation [8.6] can also be used to describe gas permeation through zeolite membranes. For weakly adsorbed molecules or at high temperatures, Equation [8.11] (Lin *et al.*, 2002; Kanezashi and Lin, 2009) has been proposed for permeation through zeolite membranes:

$$J = \frac{\varphi d_0}{x}\sqrt{\frac{8}{\pi MRT}}\exp\left[\frac{-E_\mathrm{d}}{RT}\right]\Delta P \qquad [8.11]$$

where φ is a membrane structural factor relating to membrane density, porosity and tortuosity. This correlation is derived from gas translational diffusion model (Xiao and Wei, 1992) for small gas diffusion through zeolite pores.

8.2.3 Membrane operation

Transport mechanisms are different in dense metallic membranes and microporous molecular sieve membranes. However, the diffusing flux through different membranes can be adequately described by Fick's law, indicating that gas transport through both dense and porous membranes is driven by a cross membrane pressure gradient. Based on the differences in partial pressures, gas diffusivities, molecular sizes and shapes, gases can be separated when they flow through a membrane. For low temperature separation in molecular sieve type membranes, the adsorption of gas molecules in membrane pores will also exert significant effects on gas transport.

The parameters utilized for membrane evaluation are permeability and permselectivity. Permeability or the permeability coefficient P_e, is the transport flux per unit of cross membrane driving force (pressure difference) per unit membrane thickness (mol m m^{-2} s^{-1} Pa^{-1}). Because the membrane thickness is not readily available for porous membranes like silica and zeolite membranes, permeance, Q (mol m^{-2} s^{-1} Pa^{-1}), is normally utilized to characterize membrane performance. Permselectivity, or ideal selectivity, is often represented by the permeability ratio of two components as given by Equation 8.12:

$$S_{ij} = \frac{\mathrm{Perm_i}}{\mathrm{Perm_j}} \qquad [8.12]$$

where $Perm_i$ and $Perm_j$ are the permeabilities of components i and j, respectively, obtained from single component permeation measurements. For membrane transport of mixed components, the interactions among different components and the interaction between molecules and membrane will affect the transport of each component. The true separation ability of membrane

© Woodhead Publishing Limited, 2011

materials for mixed components will deviate from the value defined by the ideal selectivity and should be described by the separation coefficient, S_c^{ij}, as given by Equation [8.13] (Koros *et al.*, 1996):

$$S_c^{ij} = \frac{x_i / x_j}{y_i / y_j} \quad [8.13]$$

where x_i and y_i are the composition of component i in the permeate and feed streams, respectively. Permeation is also dependent on operation temperatures and the Arrhenius law can be used to describe the temperature dependency of permeance Q as:

$$Q = Q^0 \exp\left[\frac{-E}{RT}\right] \quad [8.14]$$

In Equation [8.14], Q^0 is the pre-exponential coefficient, and E is the activation energy. The gas flow rate through porous membranes can be calculated by:

$$F = QA(P_f - P_p) \quad [8.15]$$

where A is the membrane area and P_f and P_p are the pressure at the feed and permeate side, respectively. Equation [8.15] suggests that the increase of membrane flux can be achieved by increasing gas permeance, membrane area and pressure gradient.

8.2.4 Membrane reactor operation

One of the effective applications of membranes in syngas processing is their use in membrane reactors. A membrane reactor is a unit operation that combines the traditionally separate reaction and separation steps into a single piece of process equipment. If the WGS reaction can be conducted in membrane reactors permselective to hydrogen, significant economic and environmental benefits will be obtained by combining the reaction and separation into a single stage operation. Moreover, it is possible to enhance reaction conversion beyond equilibrium, owing to the lower product concentration in the membrane reactor than in the conventional reactor. Hence the WGS reaction can be conducted at high temperature with a high reaction rate and still attain high conversion.

The performance of a membrane reactor depends on the reaction rate, permeation rate and operating conditions. Various WGS reaction rate equations have been empirically expressed by the Langmuir-type model or the power law form and the parameters, activation energy and rate constant were determined by fitting the experimental data to the equation (Lloyd *et al.*, 1996). For example, Equation [8.16], originally proposed for the low temperature WGS reaction (Moe, 1962), has been successfully applied to the

© Woodhead Publishing Limited, 2011

membrane reactor model for a wide range of temperatures (Barbieri *et al.*, 2005).

$$r_0 = k\left(P_{CO}P_{H_2O} - \frac{P_{CO_2}P_{H_2}}{K_{eq}}\right) \quad [8.16]$$

Where r_0 is the reaction rate, P_i is the partial pressure of component i, k is the rate constant and K_{eq} is the equilibrium constant of the WGS reaction. The product of Damköhler (*Da*) and Peclet (*Pe*) number is an important parameter to check the performance of membrane reactors. Essentially, if the membrane is almost non-permeable, the membrane reactor operates like a conventional packed bed reactor. Similar effects are also observed if the membrane is unable to separate gases. Hence, a membrane reactor in syngas processing will be efficient only in the situation that the membrane will be able to process all the H_2 produced by the WGS. Hence, the *Da* number associated with the reactor must be balanced by the *Pe* number linked to the membrane performance. The *DaPe* number is defined in Equation [8.17] as:

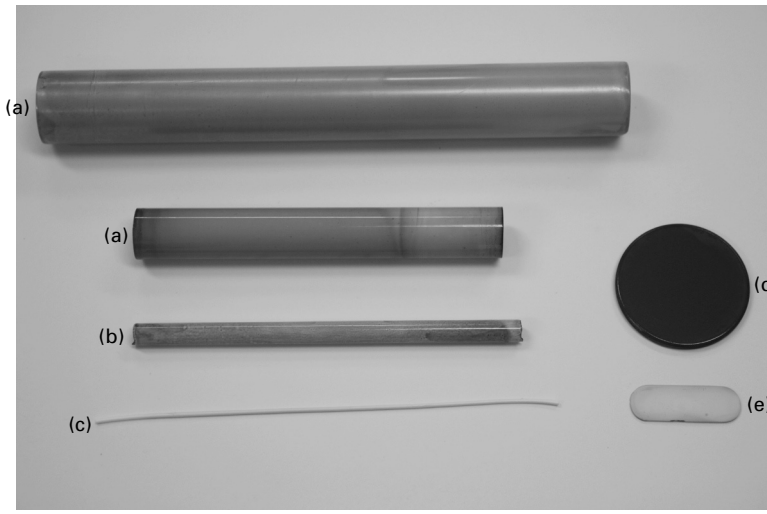
$$DaPe = \frac{r_0 W_{cat}}{Q_H A \Delta P} \quad [8.17]$$

Where W_{cat} is the catalyst mass, Q_H is hydrogen permeance, A the membrane area and ΔP is the cross-membrane pressure difference. *DaPe* represents the reaction rate to permeation rate ratio and can therefore be used to evaluate the effectiveness of a membrane reactor. Previous investigations of dehydrogenation reactions have shown that there is a maximum improvement in conversion for a membrane reactor at *DaPe* =1 (Battersby *et al.*, 2006), indicating that membrane reactors will experience optimum operation when the reaction rate is the same as the permeation rate. Simulation of a membrane reactor for the WGS reaction has also demonstrated that maximum CO conversion was achieved at *DaPe* close to one (Boutikos and Nikolakis, 2010).

8.3 Membrane materials and development

Inorganic membranes for gas separation can be fabricated in a variety of shapes and sizes from simple platelets and discs (Fig. 8.2 (d) and (e)) to porous tubes (Fig. 8.2 (a) and (b)) to hollow fibre capillaries (Fig. 8.2 (c)). Conventionally, they are synthesized with an asymmetric structure. The porous substrate provides the mechanical strength required for the membrane to operate at high pressures. Interlayers, of which there are several varieties, are used to make the transition from the large pores and rough surface of the substrate to the thin, defect-free film responsible for gas separation. This asymmetric structure allows the thinnest membrane layer possible, whilst still retaining the strength and robustness required for industrial applications.

© Woodhead Publishing Limited, 2011



8.2 Cobalt silica membranes coated onto various substrates (a) tubular porous alumina substrates, (b) tubular porous metallic substrate, (c) porous ceramic hollow fibre, (d) porous metallic disc, (e) porous ceramic platelet.

8.3.1 Dense metal membranes

Palladium (Pd) and palladium–metal alloy membranes have been extensively studied for H_2 separation from syngas mixtures owing to their high permeability and perfect permselectivity of H_2 at high temperatures. At temperatures below 300°C, Pd metal can be embrittled by the α–β palladium hydride phase transition caused by H_2 absorption (Lewis, 1967). This problem can be solved by alloying Pd with other metals, such as copper (Cu), silver (Ag), and other rare earth metals (Hunter, 1956; Grashoff *et al.*, 1983). Pd alloys also demonstrate improved mechanical strength and increased permeability to H_2 compared to pure palladium (Cabrera *et al.*, 1995). Because of the high selectivity of Pd-based membranes towards H_2, they can be utilized for processing syngas feedstocks with a low hydrogen composition either to adjust the H_2/CO ratio in the syngas or obtain high purity H_2.

The performance of Pd or Pd alloy membranes for H_2 separation is closely related to the membrane structure and composition (McCool and Lin, 2001; Roa and Way, 2003; Zhang Y *et al.*, 2006). The experimental results of H_2 flux through different Pd or Pd alloy membranes are listed in Table 8.1, together with the experimental conditions at which the results were obtained.

The results listed in Table 8.1 demonstrate that Pd or Pd alloy membranes can produce high H_2 permeance flux at low partial pressure gradients and high temperatures. One of the major obstacles facing Pd and Pd alloy membranes

© Woodhead Publishing Limited, 2011

Table 8.1 H_2 flux through different Pd-based membranes

Membrane	Support	Thickness (μm)	H_2 flux (mol m^{-2} s^{-1})	T (K)	ΔP (kPa)	Reference
Pd	Stainless steel	3	0.409	773	100	Tong *et al.* (2005)
Pd[a]	α-alumina hollow fibre	2	0.48	773	100	Tong *et al.* (2008)
Pd	α-alumina hollow fibre	5	0.33	773	100	Tong *et al.* (2008)
Pd–10%Cu[b]	Zirconia on α-alumina	11	0.8	723	345	Roa and Way (2003)
Pd–9%Cu[c]	α-alumina	3	0.31	753	100	Zhang X *et al.* (2008)
Pd–20%Ag	Stainless steel	2	0.28	773	100	Tong *et al.* (2006)
Pd–22%Ag	Silicon wafer	1	3.6	723	83	Gielens *et al.* (2004)
Pd–23%Ag	Alumina	5.8	0.57	773	196	Uemiya *et al.* (1991)
Pd–Ag	Self-support	60	0.23	593	200	Barbieri *et al.* (2008)

[a]H_2/N_2 separation factor = 150; [b]H_2/N_2 separation factor = 1400; [c]H_2/N_2 separation factor = 840.

is that they are easily poisoned by sulfur compounds, and as such significant pretreatment of the raw syngas maybe required before processing in a Pd-based membrane module (Saracco *et al.*, 1999). Previous studies also indicated that at less than 500°C, CO and steam can deactivate Pd-Ag membranes resulting in reduced H_2 permeance (Hou and Hughes, 2002, Arstad *et al.*, 2006). Pd-based membranes deposited on porous metal substrates may also experience intermetallic diffusion at high temperatures; however a barrier layer formed on the exterior surface of the substrate can alleviate this problem. It has been reported that a Pd-based membrane prepared with an oxide barrier layer was stable in the temperature range of 350–450°C for over 6000 hours (Sholl and Ma, 2006). There are other amorphous metal alloys also being considered for syngas processing and H_2 separation at high temperatures, as presented in a review conducted by Dolan *et al.* (2006). For example, Ni-based membranes have attracted some research interest because of their cheaper price compared with Pd (Phair and Donelson, 2006), and also their catalytic effect on H_2 dissociation and re-association reaction (Burchardt, 2000).

8.3.2 Molecular sieving silica membranes

Molecular sieving silica (MSS) membranes are microporous ceramic membranes that operate via an activated diffusion mechanism (de Lange *et al.*, 1995b), sieving gas molecules based on their adsorption behaviour and kinetic diameters. As discussed in Section 8.2.2, an activated transport

© Woodhead Publishing Limited, 2011

mechanism implies that the flux of smaller gases with positive activation energies, such as H_2, will increase with temperature whilst the flux of larger gas molecules with negative activation energies, such as CO and CO_2, will decrease with temperature. This, taken in combination with their excellent thermal, mechanical and chemical stability, has ensured MSS-based membranes have garnered significant interest for processing syngas into H_2.

The performance of MSS membranes for hydrogen separation is highly dependent on the membrane synthesis conditions, composition, thickness and the membrane support properties. The preparation of MSS membranes for hydrogen separation is most commonly accomplished through sol–gel chemistry or chemical vapour deposition (CVD) (Kim and Gavalas, 1995; de Lange *et al*., 1995a; Lee *et al*., 2004). Silica membranes derived through the sol–gel process are generally produced by dip coating a membrane support in a polymeric silica solution. The coated support is then dried and calcined to fix the silica structure into a microporous membrane. A membrane layer synthesized in this manner is typically on the order of tens of nm thick, but often contains several pin-hole defects and microcracks caused by surface roughness and contamination. Defects can be repaired by multilayer deposition (de Lange *et al*., 1995a; Kusakabe *et al*., 2003; Gu and Oyama, 2007a) and the quality of the final membrane can also be improved by dip-coating in a clean environment (de Vos and Verweij, 1998a, 1998b). A comprehensive comparison of all MSS-derived membranes suitable for syngas processing can be found in Table 8.2. As with all inorganic membranes, the morphology of the substrate materials also affects the membrane performance for gas separation.

The major drawback of MSS-derived membranes is the susceptibility of silica to degrade when exposed to water. It was first shown in 1991 that exposure to steam markedly reduced the surface area and increased average pore diameter of sol–gel derived mesoporous silica (Leboda and Mendyk, 1991) and similar hydrothermal instability was observed soon after in microporous silica membranes (Fotou *et al*., 1995). The hydrothermal degradation process occurs via sorption of water onto the surface silica, followed by the breaking of available siloxane bonds (Si–O–Si) to form silanol groups (Si–OH) (Michalske and Freiman, 1982). As a result, silica becomes mobile inside the pore and migrates to the lowest energy points within the structure (Duke *et al*., 2006; Wei *et al*., 2008). This results in the widening of large pores and eventual collapse of small pores, effectively destroying the molecular sieving capability of the membrane.

Various methods have been explored to improve the stability of silica membranes at high temperature with moisture. Initial attempts focused on producing hydrophobic membranes either through functionalizing the silica with alkyl side chains using organic–inorganic precursors (Raman and Brinker, 1995; Raman *et al*., 1996; Cao *et al*., 1996; de Vos *et al*., 1999) or

© Woodhead Publishing Limited, 2011

© Woodhead Publishing Limited, 2011

Table 8.2 H_2 permeance of MSS-based membranes synthesized by various techniques

Membrane	Substrate	Thickness (μm)	H_2 permeance (mol m^{-2} s^{-1} Pa^{-1})	T(K)	Selectivity (H_2/N_2)	Reference
Silica	γ-alumina interlayer	0.03	2×10^{-6}	573	64	De Vos and Verweij (1998b)
Silica	γ-alumina tube	0.02–0.03	10^{-7}	873	> 1000 (H_2/CO_2)	Lee *et al.* (2004)
Ni-doped silica	α-alumina tube	< 0.5	10^{-6}	773	160	Kanezashi and Asaeda (2006)
Methylated silica	γ-alumina interlayer	0.03	8×10^{-6}	573	40	De Vos *et al.* (1999)
Co-doped silica	α-alumina tube with γ-alumina interlayer	–	5×10^{-9}	523	1000	Battersby *et al.* (2009b)
Silica	γ-alumina capillary	0.01–0.05	6×10^{-7}	873	2300	Gopalakrishnan *et al.* (2007)
Silica with surfactant	α-alumina coated with Locron alumina	0.25–0.3	1.5×10^{-6}	473	18	Giessler *et al.* (2003)
Silica–titania	γ-alumina	0.01–0.02	2.3×10^{-7}	873	57 (H_2/CO_2)	Gu and Oyama (2007b)

by incorporating cationic surfactants into the sol–gel synthesis process (Tsai *et al.*, 2000; Giessler *et al.*, 2001; Duke *et al.*, 2004b, 2006). The membranes are then calcined under either an inert atmosphere or a vacuum, preserving the template or carbonizing the surfactant within in the silica matrix. Whilst these templated membranes demonstrated increased hydrothermal stability, the pore size was slightly enlarged and resulted in increased permeance and decreased selectivity (de Vos *et al.*, 1999). Later synthesis procedures were able to incorporate surfactant-based templates without significantly altering the hydrophobicity of the membranes (Duke *et al.*, 2004b, 2006). It was proposed that the carbon conferred hydrothermal stability to the structure by inhibiting the mobility of the mobile silica phase once formed (Duke *et al.*, 2006).

Recent efforts to improve both hydrothermal stability and H_2 flux have focused on the modification and development of metal and metal oxide doped silica membranes (Kanezashi and Asaeda, 2006). Various metal oxides such as TiO_2, ZrO_2, Fe_2O_3, Al_2O_3, NiO and Co_3O_4 have been trialled and in most cases offer membranes with a lower cost, higher flux and enhanced durability (Fotou *et al.*, 1995; Yoshida *et al.*, 2001; Asaeda *et al.*, 2003, Kanezashi and Asaeda, 2005, 2006; Gu *et al.*, 2008b; Gu and Oyama, 2009). The metals and metal oxides can be incorporated either through CVD (Gu *et al.*, 2008b; Gu and Oyama, 2009) or sol–gel techniques (Kanezashi and Asaeda, 2005, 2006; Kanezashi *et al.*, 2005; Ikuhara *et al.*, 2007; Uhlmann *et al.*, 2009; Battersby *et al.*, 2009a, 2009b). It has also been shown that the inclusion of cobalt as a dopant reduces water adsorption, offering increased resistance by decreasing the hydrophilicity of silica (Battersby *et al.*, 2009a).

8.3.3 Zeolite membranes

Zeolites have been applied as adsorbents and catalysts which has been attributed to their aluminosilicate framework. Zeolitic materials exhibit mono-disperse, uniform pore structures owing to their crystallinity, which enables them to be both size and shape selective (Lai *et al.*, 2003; Bowen *et al.*, 2004). These properties, combined with good thermal and chemical stability have seen zeolite-based membranes attract growing research interest in recent years (McLeary *et al.*, 2006; Caro and Noack, 2008). Zeolite membranes can be prepared by a secondary growth method (Xomeritakis *et al.*, 1999) or by *in situ* crystallization (Wang and Yan, 2001). Seeded synthesis tends to produce continuous films with improved reproducibility owing to better control over nucleation site density (Nair and Tsapatsis, 2003). These methods are laborious and scale up to industrial sizes remains the primary obstacle to the use of zeolite membranes for industrial syngas processing. The permeance of H_2 in zeolite membranes is in the range 10^{-8}–10^{-7} mol m^{-2} s^{-1} Pa^{-1} (Nishiyama *et al.*, 2007). Light gas separation by SAPO–34

© Woodhead Publishing Limited, 2011

membranes at room temperature has demonstrated permeance values of 10^{-8} mol m^{-2} s^{-1} Pa^{-1} for H_2.

Most studies on zeolite membranes for syngas processing have focused on low temperature gas separation and large discrepancies have been observed in predicting binary permeation from single permeation values at low temperature, owing to adsorption and interaction between different molecules and the zeolite crystals (Bakker *et al.*, 1996). Indeed, early work on MFI-type zeolite membranes showed that the adsorption of permeating gases affected the fluxes (Geus *et al.*, 1992). The applicability of pure zeolite membranes for medium to high temperature H_2 separation has only undergone limited testing (Table 8.3) (Masuda *et al.*, 2001; Hong *et al.*, 2005; Gu *et al.*, 2008a; Tang *et al.*, 2010). The ability of all gas molecules to diffuse through the intercrystalline openings in zeolite membranes decreases the selectivity of small gas molecules. There are several modification methods that have been developed to close the gaps. For example, CVD deposition of silica was used on silicalite (Nomura *et al.*, 1997), MFI and DDR type zeolite membranes (Kanezashi *et al.*, 2008, Kanezashi and Lin, 2009). Gas permeance decreased after modification, but the selectivity of H_2 over other gases increased, indicating a reduction in intercrystalline gaps. Catalytic cracking of methyldioxy silane (MDES) in different types of zeolite membranes using N_2 as a carrier gas was also studied (Masuda *et al.*, 2001, Hong *et al.*, 2005). More recently, similar approaches using a H_2/CO_2 mixture as the

Table 8.3 H_2 permeance of zeolite membranes

Membrane	Substrate	H_2 permeance (mol m^{-2} s^{-1} Pa^{-1})	T (K)	Selectivity (H_2/CO_2)	Reference
Al-ZSM-5; modified by catalytic cracking of MDES	α-Alumina	4×10^{-8}	383	90–140	Masuda *et al.* (2001)
B-ZSM-5 zeolite; modified by catalytic cracking of MDES	α-Alumina	1×10^{-7}	673	47	Hong *et al.* (2005)
MFI-type zeolite; modified by catalytic cracking of MDES	α-Alumina	3.96×10^{-7}	723	141	Tang *et al.* (2009)

© Woodhead Publishing Limited, 2011

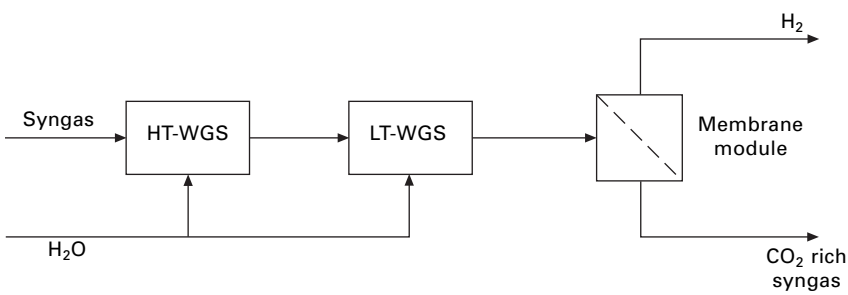
carrier gas were also tested (Gu *et al.*, 2008a; Tang *et al.*, 2009), resulting in a H_2 permeance of 3.96×10^{-7} mol m^{-2} s^{-1} Pa^{-1} and H_2/CO_2 selectivity of 141 at 450°C for a modified MFI zeolite membrane (Tang *et al.*, 2009). The improvement was attributed to the controlled partial modification of the sub-nanometer channels in the MFI-type zeolite membrane. Similarly synthesized membranes were subsequently used in a WGS membrane reactor and were able to deliver hydrogen with a purity of > 95% and increase CO conversion by 25% over the equilibrium conversion (Tang *et al.*, 2010).

8.4 Application and integration in industry

Inorganic membranes can be integrated into syngas processing in two main areas. The first is in gas separation where membranes could be used to replace traditional sorption-based processes in the purification of H_2. The second is as a membrane reactor by coupling the WGS reactor and subsequent separation systems into a single unit. In this section we assess the integration of membranes by taking into consideration a conventional SR syngas processing train (Fig. 8.1) using high temperature (HT) and low temperature (LT) WGS reactors followed by a pressure swing adsorption (PSA) separation unit downstream.

8.4.1 Membrane modules in syngas processing

Membrane modules can be integrated into a syngas processing unit to separate H_2 from the syngas stream. There are three potential designs that incorporate membrane modules into the syngas processing train and they are discussed below. The first integration option is illustrated in the process flow diagram in Fig. 8.3. In this approach, the separation unit in a conventional SR process, which is generally a PSA unit, is replaced by a membrane module. The main advantages of this include increased energy recovery, a reduced unit footprint and a reduction in process complexity. The PSA unit, which



8.3 Process flow diagram of SR syngas processing train incorporating a membrane unit.

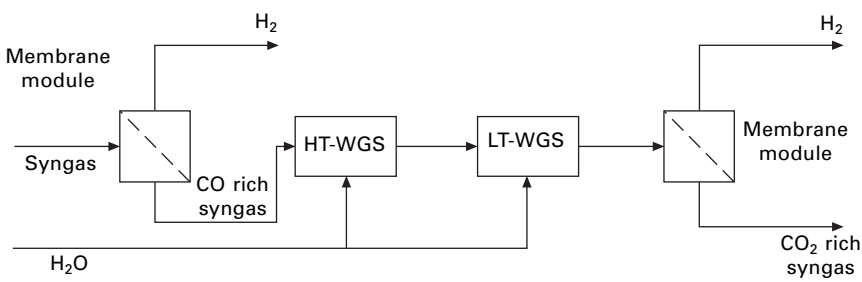
© Woodhead Publishing Limited, 2011

comprises several adsorption columns, requires the syngas stream be cooled to below 50°C to operate efficiently; there is however, no such need using inorganic membranes. Therefore, the integration of a membrane module will deliver improved energy efficiencies compared to other gas separation technologies. The temperature of the syngas stream at the back end of the LT-WGS reactor may range between 200 and 250°C, which favours the application of silica, metal silica and zeolite membranes. At this temperature range, palladium alloys may be poisoned by even low concentrations of CO remaining in the syngas (Amandusson *et al.*, 2000; Catalano *et al.*, 2010) resulting in a significant decrease in H_2 permeation.

The second integration design for consideration is shown in Fig. 8.4. The difference here is that a second membrane module is integrated at the front end of the HT-WGS reactor. The advantage of this approach is the delivery of a CO-rich syngas stream to the reactor. The WGS reaction is equilibrium limited, so high concentrations of H_2 will limit the reaction. By separating the H_2 from the syngas stream prior to the reactor, this allows a high conversion of CO via the WGS reaction and translates to a higher production of H_2. The syngas temperature prior to the WGS reactors will be in the range of 400–500°C or higher, which favours the application of palladium alloy membranes. At temperatures above 500°C, silica membranes undergo densification and loss of flux, although metal silica membranes tend to be more robust to oppose thermal effects (Kanezashi and Asaeda, 2005; Igi *et al.*, 2008).

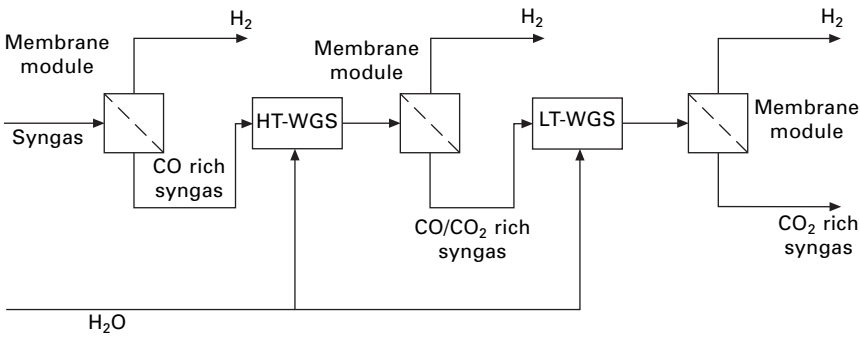
The third and last integration option is shown in Fig. 8.5. In this case, a third membrane module is sandwiched between the HT-WGS and LT-WGS reactors. Similar to the advantages in the second integration approach in Fig. 8.4, separating the hydrogen prior to the LT-WGS reactor can overcome conversion limitations imposed by the equilibrium conditions of the WGS reaction.

The placement of the membrane module within the process, traditionally either before, between or after the WGS reactors, will be largely controlled



8.4 Process flow diagram of SR syngas processing train incorporating two membrane units.

© Woodhead Publishing Limited, 2011



8.5 Process flow diagram of SR syngas processing train incorporating three membrane units.

by the syngas generation method and its end use. These factors ultimately control the H_2 partial gradient across the syngas processing operations and the effectiveness of a membrane module within a given system. Inorganic membranes for H_2 separation are of particular benefit when the syngas has an intrinsically high H_2/CO ratio, as with steam reforming of natural gas, and especially when H_2 production is the primary end use of the syngas. In the case of IGCC, there is high pressure at the feed side of the membrane and the partial pressure of H_2 may be in the order of 9–10 bar (30–35% vol) and 15–18 bar (45–50% vol) before and after the WGS reactor. Separating H_2 from the syngas prior to the WGS reactor allows a higher conversion of CO, as the WGS reaction is equilibrium limited. There are economic incentives in this approach including reduced catalyst loadings and smaller WGS reactors which will reduce capital and operating costs.

8.4.2 Membrane reactor modules in syngas processing

The advantages of integrating inorganic membranes into the syngas processing train are only fully realized through the utilization of a WGS membrane reactor unit operation. As with all processing industries, the two most important and expensive stages are the reaction and separation of the product stream (Dixon *et al.*, 2003). The conventional dual reactor setup shown in Fig. 8.1 is used to overcome the equilibrium and kinetic limitations of the WGS reaction. The HT-WGS has more efficient reaction kinetics but lower CO conversion, whilst the LT-WGS favours high CO conversion, but with slower reaction kinetics. This means that the HT-WGS reactor will allow CO to be converted at a fast rate, whilst the LT-WGS reaction will allow the remaining CO to be converted but at a much slower rate than the HT-WGS. In contrast, a membrane reactor is a single unit operation that incorporates simultaneous reaction and product separation and, by utilising Le Châtelier's principle, can enhance CO conversion through product (H_2)

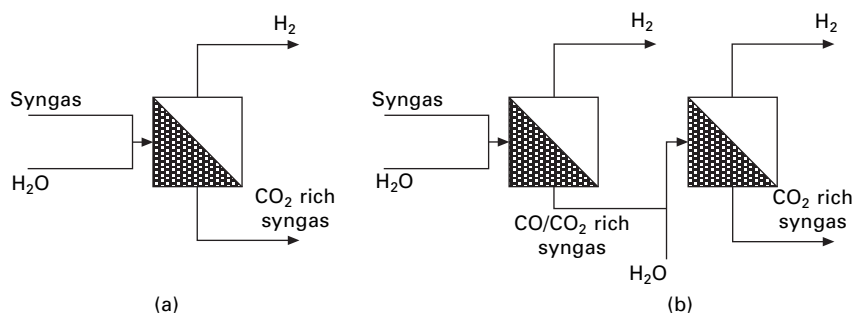
© Woodhead Publishing Limited, 2011

removal. Additionally, CO_2 can be retained in the retentate stream of the membrane reactor and incorporated into a CO_2 capture and sequestration process (Bracht *et al.*, 1997). Ultimately the increased CO conversion in the membrane reactor translates into a reduced unit size, operating costs and catalyst loadings (Battersby *et al.*, 2007).

Figure 8.6 shows two process arrangements for the integration of membrane reactors to process syngas: (a) a single membrane reactor and (b) as HT and LT WGS membrane reactors. As with a traditional WGS reactor, a WGS membrane reactor will be controlled by the reaction kinetics, related to temperature and catalyst characteristics (Newsome, 1980), and CO conversion, related to H_2 concentration. As such, both the reaction rate and H_2 permeance must be considered when analysing membrane reactor performance. The optimum membrane reactor operation dictates that the H_2 permeation is in balance with the reaction rate (Yeung *et al.*, 1994). From an engineering design perspective the traditional dual reactor setup raises the question of whether two sets of membrane reactors, operating at high and low temperatures, or a single membrane reactor operating at a single temperature, will be most advantageous in a syngas processing train.

Equilibrium CO conversion is closely related to temperature and feed composition, particularly the steam to CO (S/C) ratio. For the LT-WGS, equilibrium CO conversions using a S/C feed molar ratio of 1:1 can be as high as 90% or more and a membrane reactor will deliver up to 7% conversion improvements (Battersby *et al.*, 2009a). Water is a cheap reactant in the WGS reaction and if excess water is used in the reaction (S/C feed molar ratio >1), the CO conversion approaches 100% for both a LT-WGS packed bed reactor and membrane reactor. Indeed a LT-WGS membrane reactor will be only advantageous in situations where water supply is limited, thus requiring operation at low S/C feed molar ratio. (Newsome, 1980).

The thermodynamics suggest, therefore, that a membrane reactor will be more advantageous for high temperature operation (> 350°C) as there is a



8.6 Integration of membrane reactor in syngas processing train (a) as a single WGS membrane reactor or (b) as high temperature and low temperature WGS membrane reactors.

© Woodhead Publishing Limited, 2011

greater capacity to improve above the equilibrium CO conversion, in some cases by 20% or more (Smart *et al.*, 2010). Initially, the major obstacle is the high operating temperatures (> 350°C) which may affect the catalyst activity (Chinchen *et al.*, 1984), although advances in catalyst development have seen commercial HT-WGS catalysts operating at 450°C or more (Ratnasamy and Wagner, 2009). Hence, provided gas cleaning can be conducted at high temperatures (≥ 500°C), a single HT-WGS membrane reactor offers significant economic incentives over existing syngas processing systems. This is especially true for IGCC type applications where the HT-WGS/LT-WGS/H_2 separation setup results in significant energy losses caused by the cooling of large volume of gases to meet the operating temperatures of the WGS reaction.

Despite the obvious advantages of a HT-WGS membrane reactor, most research has focused on the membrane and catalyst performance of LT-WGS membrane reactors with a particular focus on how operational parameters such as membrane performance, temperature, S/C feed ratio and space velocity affect conversion. Feasibility studies on Pd-based membrane reactors (Shu *et al.*, 1991; Criscuoli *et al.*, 2001) concluded that current membrane preparation methods are extremely expensive owing to the low productivity per unit membrane area. Therefore finding less expensive Pd-alloys that are more permeable to H_2 and less susceptible to degradation from trace contaminants will make Pd-based membrane reactors feasible on an industrial scale (Hughes, 2001). Similarly, several research groups have conducted WGS membrane reactor studies with MSS-based membranes (Basile *et al.*, 2001; Giessler *et al.*, 2003; Brunetti *et al.*, 2007; Battersby *et al.*, 2008, 2009a). In most instances the hydrothermal stability of the silica matrix, which affects both H_2 flux and selectivity, is the main challenge to be overcome.

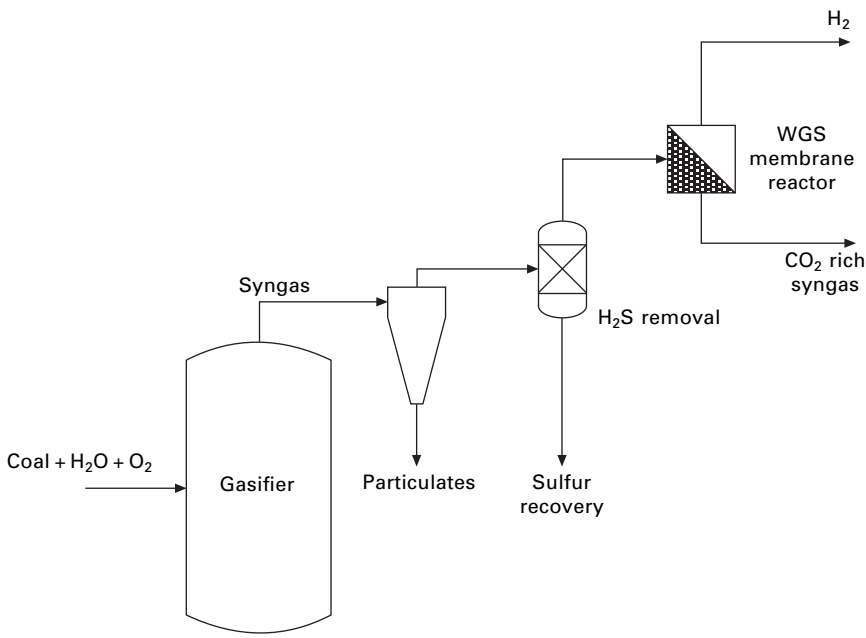
In contrast, current knowledge of HT-WGS membrane reactors is quite limited. There are very few published studies into HT-WGS membrane reactors operating above 400°C and all have been performed using Pd-based membranes (Iyoha *et al.*, 2007). In the most notable case, CO conversions were enhanced considerably above equilibrium values, with a maximum of 93% obtained in a Pd membrane reactor integrated into a coal gasification process at 900°C. After approximately 200 hours of operation, membrane performance declined and surface pitting was observed from prolonged gas exposure at high temperature. Despite the success of several research groups in testing inorganic membranes for single gas permeance at high operating temperatures (> 400°C); there are additional engineering considerations related to sealing, heat management, and mechanical design that have hampered research efforts into HT-WGS membrane reactors (Armor, 1995; Saracco *et al.*, 1999; Smart *et al.*, 2010). Unless these challenges are overcome, the integration of inorganic membranes into syngas processing trains is unlikely to be successful.

© Woodhead Publishing Limited, 2011

8.4.3 Process integration limitations and opportunities

The quality of the syngas and operating conditions will limit the type of membrane to be integrated in syngas processing. Water is a common element in both SR and IGCC, coupled with high temperatures. This has serious implications for silica membranes which undergo densification owing to hydrothermal instability at the operating conditions described. The same applies to the 'hydrostable' metal silica membranes as reported in the literature (Kanezashi and Asaeda, 2006; Igi *et al.*, 2008; Battersby *et al.*, 2009a). Although the literature shows that functionalized silica membranes are hydrostable, this is the case generally at lower temperatures and lower steam vapour pressures. These conditions are far milder than those expected at the front end of the WGS reactor (Smart *et al.*, 2010).

The quality of the syngas, with respect to contaminants, also has major implications particularly for systems integrated into the IGCC syngas process. In coal gasification, contaminants will be present in the syngas in the form of particulates, like many of the heavy metals, in the vapour phase such as mercury (Hg) or selenium (Se); or they may react like sulfur to form H_2S. Although gas cleaning and guard beds are employed after the gasifier in Fig. 8.7, these unit operations are not perfect and trace amounts are likely to remain. The effect and interaction of these compounds at high temperatures on



8.7 Syngas clean up train for IGCC process with a WGS membrane reactor.

© Woodhead Publishing Limited, 2011

inorganic membranes can be significant. For instance, H_2S has a detrimental effect on palladium based membranes by reducing H_2 fluxes (Kajiwara *et al.*, 1999; Kulprathipanja *et al.*, 2005; Mundschau *et al.*, 2006).

In addition, these contaminants can adversely affect the performance of the catalysts employed in the WGS reaction. Currently, the majority of syngas production utilizes natural gas with a very low sulfur content as a feedstock; however, syngas generated from the gasification of coal will contain much higher concentrations of H_2S. Commercial copper-based catalysts for the LT-WGS reaction are highly sensitive to sulfur poisoning and desulfurization to less than 100 ppb is required (Rhodes *et al.*, 1995). By contrast, the iron oxide/chromium-based catalysts used in the HT-WGS reaction display a much higher sulfur resistance (Newsome, 1980), in some cases up to 50 ppm (Hla *et al.*, 2009). However, at H_2S concentrations between 160 and 250 ppm, commercially available Fe/Cr catalysts can lose up to half their activity, through the sulfidation of Fe_3O_4 (Hla *et al.*, 2009). The same study also determined detrimental effects of H_2S plateau at concentrations above 700 ppm, with catalyst activity constant at ~20% of its original activity. Therefore, to avoid being the limiting factor in successful HT-WGS membrane reactor deployment in high sulfur syngas streams, the membranes themselves should be able to tolerate at least 50 ppm of H_2S.

A smaller, but nonetheless important obstacle to high temperature operation in an industrial setting is the start up, shutdown and emergency operation procedures for the membrane module. The membrane layer, interlayers and ceramic substrate are, for most inorganic membranes, brittle and susceptible to thermal shock. As a result, research groups typically employ heating and cooling rates of < 2°C/min to avoid cracking the membrane layer during synthesis and testing. Whilst it should be possible, if inconvenient, to maintain these heating and cooling rates during regular start up and shut down procedures, uncontrolled shutdown of the unit may see thermal shock and high pressure combine to produce catastrophic failure of the membranes within the module.

The long-term stability of inorganic membranes is crucial for the successful integration of the technology into the syngas processing industry. The membranes themselves will need to display good thermal, chemical and mechanical stability over their expected lifespan. This includes not only maintaining high flux and gas purity but also being robust enough to endure the high flow rates, pressures, vibrations and thermal cycles associated with process start up, normal operation and shut down. The mechanical robustness of the underlying membrane support has been discussed previously in this chapter; suffice to say that porous metallic supports are favoured over traditional ceramic supports. The mechanical stability of the membrane layer itself is an area that has received minimal attention from the research community. If the supports remain stable whilst the membrane layer cracks, or develops

© Woodhead Publishing Limited, 2011

pin hole defects, the entire membrane or membrane reactor module will suffer from reduced performance. Of most interest is the ability to withstand exposure to particulates in the syngas stream, without compromising membrane integrity. In the only study to date of inorganic membrane performance in an industrial setting, the accumulation of flyash was not detrimental to the performance of a cobalt silica membrane (Brands *et al.*, 2010). However, as the authors noted, testing was conducted in a low temperature (< 80°C), low pressure flue gas stream and continual online monitoring of the H_2 flux and selectivity was not possible. The effects of particulate contamination under high temperature, high pressure processing conditions may be more abrasive.

8.5 Membrane modules

8.5.1 Sealing

For a membrane module or membrane reactor to separate H_2 from syngas effectively and efficiently, the sealing of the membranes themselves must be gas tight. Sealing ceramic membranes into steel process units is not a trivial task even at low temperatures. The geometry, compressive strength of the membrane and its support and ease of assembly for repair and replacement must all be taken into consideration. As inorganic membranes and their supports are brittle and susceptible to fracture, particularly in scaled-up designs (Duke *et al.*, 2004a), soft polymeric o-rings used in compression, are the most common design currently employed by research groups in this field. However, at the temperatures required for effective integration of inorganic membranes into syngas processing, these polymer seals will melt or decompose and thus sealing the membranes in an industrial setting poses a serious challenge. Unfortunately the research effort into effective means of sealing inorganic membranes for high temperature syngas processing has been small in comparison to the research effort into the membranes themselves. Several possible solutions are postulated below.

The first option is to design the membrane module in such a fashion as to isolate the seals from the hot feed gas and primary heating zone of the module. In terms of industrial applications, this option is unattractive as it would attract complex mechanical design in addition to uneconomical cooling requirements. The second option is to replace the conventional polymeric sealing compounds with ones that can withstand the elevated temperatures and mildly oxidizing environment of the WGS. The primary design requirement for the sealing compound is that it remains gas tight during operation. There are several materials worth consideration and these fall broadly into three main categories–graphitic, silicate and metallic materials. Graphite is a soft, compressible material that is easily capable of withstanding temperatures in

© Woodhead Publishing Limited, 2011

excess of 1000°C. The main concern is that graphite can be slowly consumed by reaction with steam and even CO_2 under certain conditions to produce CO and H_2.

The use of silicate and metallic materials as high temperature sealing compounds has grown with the development of solid oxide fuel cells (SOFC) and oxygen transport membranes (OTM). Metallic materials such as silver (as a solid ring or liquid paste) and gold (as a solid ring) have also been used as a sealant for OTMs (Xu and Thomson, 1998; Kim and Lin, 2000; Kobayashi *et al.*, 2006). Both classes of material could, in theory, be adapted to inorganic membranes for syngas processing. However there are serious concerns over both their reactivity and ability to withstand repeated thermal cycling. At high temperatures, diffusion of the sealant material into the membrane (altering the Pd-alloy composition), or onto the membrane surface (reducing the effective surface area) are possibilities that may lead to performance degradation of the membranes (Qi *et al.*, 2001).

The final option is to alter the membrane support from a porous ceramic substrate to a porous metallic substrate. Metallic supports can be manufactured with dense metal ends that can be conveniently welded into a membrane or membrane reactor module, overcoming the sealing limitations experienced with ceramic supports. Porous metallic supports are commercially available, although their utilization in gas separation applications is limited. Additionally whilst they are more mechanically robust, they do not offer the same level of chemical inertness as ceramic supports and may suffer from corrosion problems.

8.5.2 Scale-up and module design

The process of scaling up an embryonic technology like inorganic membranes from laboratory experiments to full industrial operation is a challenging one. In principle, membrane modules for separation are simple to design, with the required flux and purity of the permeate stream determining the surface area and module size. However, the membrane geometry and arrangement within the module is highly variable and dependent on both the performance and mechanical properties of the membranes themselves. For syngas processing, inorganic membranes are available in two distinct geometries – planar and tubular.

Planar membranes are straightforward to manufacture, exhibit uniform thermal expansion and are compatible with a range of seal designs including both compression and permanent adhesion. However, they have a low surface area to volume ratio and a large sealing area per membrane which serves to increase module size and capital expenditure. Tubular membranes offer a higher surface area to volume ratio and smaller sealing area, reducing module size. In addition, they have a higher packing density and encourage more turbulent

© Woodhead Publishing Limited, 2011

convective flow within the module than planar membranes. However, module assembly, especially sealing, is more complex, as is membrane fabrication, which is likely to result in a higher cost per membrane compared to planar geometries. A subset of tubular membranes are those with so-called hollow fibre geometry where the fibre diameter is orders of magnitude smaller than the membrane length. Hollow fibres offer the highest packing density, surface area to volume ratio and lowest sealing area per membrane and overall module size of any geometry. However, high convective transport through the interior of the fibre will induce significant and unnecessary pressure drops across the unit and the likely erosion of the membrane walls. In addition, no work has been reported for syngas processing using silica or Pd-based membranes supported on hollow fibre geometries.

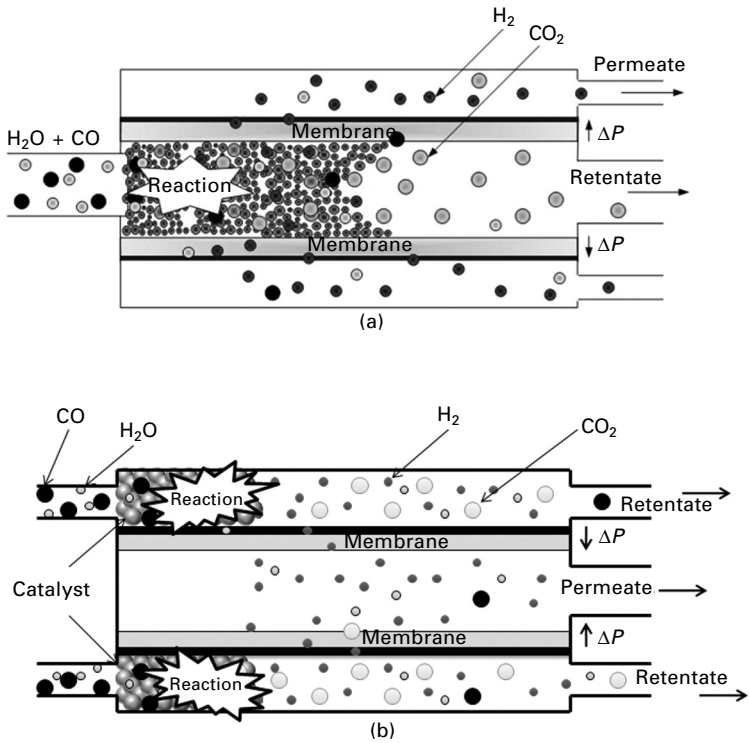
Membrane reactors have additional design requirements over and above those for a membrane module as they must consider both the reaction and separation unit operations simultaneously. The relationships between these two parts determine whether the membrane reactor is an effective replacement for the reactor and separation unit operations. For the case of a WGS membrane reactor, the reactor component is best considered as a packed bed operating in plug-flow, where the ratio of the rate of reaction to the rate of convective transport of the feed, the Damkohler number (*Da*), is an important design parameter (Dixon *et al.*, 2003). For membrane performance, the Peclet number (*Pe*) describes the ratio between the convective transport of the feed and permeation through the membrane. Balancing these two design parameters is crucial for effective and efficient membrane reactor operation as they determine the relationship between the reaction rate and the permeation rate per reactor volume (Moon and Park, 2000; Battersby *et al.*, 2006). For example, if permeation of H_2 through the membrane is low relative to the production rate of H_2, then the WGS membrane reactor behaves like a conventional packed bed reactor and minimal enhancement of CO conversion and reaction rate is observed. In contrast, if the permeation of H_2 is large relative to H_2 production then the membrane reactor will serve to shift the equilibrium and enhance CO conversion. Hence balancing the *Da* and *Pe* numbers will ensure the membrane reactor is correctly sized for catalyst requirements and membrane surface area.

This is a simplified analysis in that it uses the average partial pressure drop of H_2 across the membrane and does not take into account the change in the partial pressure as a feed 'plug' moves through the membrane reactor. In this case computational fluid dynamics are required to analyse the axial differences in driving force along the membrane (Abdel-Jawad *et al.*, 2007, 2009) and the effect of these differences on membrane reactor performance. For example, if the membrane reactor configuration is such that the feed gases do not contact the catalyst until the beginning of the membrane, there will be no initial driving force and the initial portion of the membrane will

© Woodhead Publishing Limited, 2011

be wasted. As a result the final membrane reactor design may require a pre-reaction zone which operates as a conventional reactor increasing the partial pressure of H_2 so that an appropriate driving force exists when the feed gases come into contact with the membrane (Smart *et al.*, 2010). Similarly, if the membrane permeation is too high or the membrane itself is too long, the partial pressure gradient of hydrogen across the membrane may collapse, rendering the latter surface area of the membrane ineffectual and in extreme cases H_2 may flow back into the reactor reducing H_2 flux and recovery.

The final design consideration for a WGS membrane reactor unit operation is the placement of the catalyst within the module. For planar membrane geometries this is not such a concern but for tubular membranes, catalyst placement can either be inside the membrane tube or outside the membrane in the shell of the module (Fig. 8.8). Most research groups favour catalyst placement outside the membrane tube for reasons of heat management and assembly (Barbieri *et al.*, 2008; Abdollahi *et al.*, 2010; Adrover *et al.*, 2010; Pinacci *et al.*, 2010). The WGS reaction is exothermic and heat management is complicated in this scenario and can result in cracking of the membrane



8.8 Options for catalyst placement in a WGS membrane reactor: (a) catalyst placed inside membrane, (b) catalyst placed between membrane and shell.

© Woodhead Publishing Limited, 2011

support. Thus industrial operation would also favour catalyst placement outside the membrane, in the shell of the module as this would afford better heat management and reduced assembly costs.

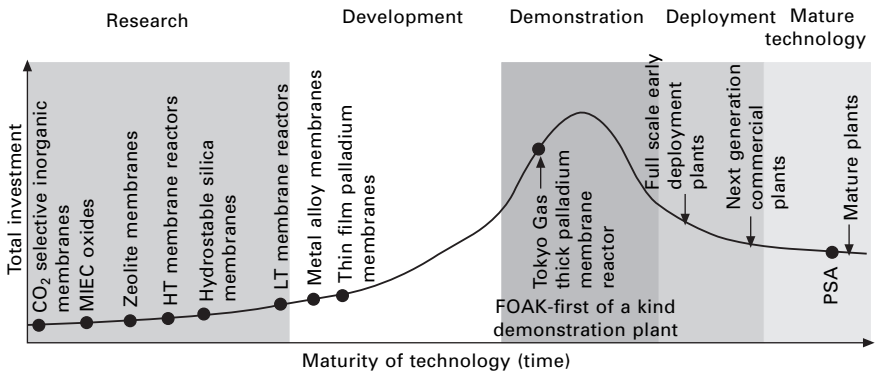
8.6 Future trends

Currently there is a raft of technology options available for syngas processing. The maturity of each technology is categorized into 'research', 'development', 'demonstration', 'deployment' and 'mature technology' and is shown in Fig. 8.9, the so-called technology 'demonstration hump'. At this stage, no membrane technology has overcome the 'demonstration hump' and further development is warranted for the future deployment of membranes or membrane reactors in syngas processing. The only technology which is considered mature is PSA and this is conventionally deployed by the industry, particularly for hydrogen production from the steam reforming of natural gas. Future trends of inorganic membranes for syngas processing will be assessed in terms of technology development, which is generally driven by the promise of increased performance of a system, balancing benefits against costs.

For early stage or novel technologies there is a significant risk associated with the probability of a technology successfully maturing toward an operational state as a function of time. In the early research stages the activities are relatively inexpensive, but the deployment risk is commensurately very high (Duke *et al.*, 2010). In this category there are two very early stage technologies namely: CO_2 selective inorganic membranes and mixed ionic electronic conducting (MIEC) oxide membranes for H_2 separation. In syngas processing, H_2 separation is equally as important as CO_2 separation. If the CO_2 is separated from the syngas stream, then H_2 is similarly concentrated in the retentate stream. Inorganic membranes for CO_2 separation from syngas have been difficult to develop, the exception being zeolite membranes. Early attempts were based on layered double hydroxides (LDHs), which are clay-type materials. LDHs show good CO_2 adsorption at high temperatures (Yong *et al.*, 2001; Reddy *et al.*, 2008), thus favouring CO_2 separation from other gases. However, LDH materials do not translate into good membranes, as particles of clay tend to deliver large inter-particle pores in the mesoporous and macroporous regions. As a result, LDH membrane research has been discontinued, although the LDH concept in syngas processing has evolved towards the concept of a sorption enhanced water gas shift (SEWGS) reactor (van Selow *et al.*, 2009).

Although silica membranes preferentially separate H_2, the embedding of niobia into a silica matrix has been recently reported to separate CO_2 from N_2 (Boffa *et al.*, 2008). Although the separation factor was low, this latest development may open a window of opportunity to develop hybrid silica membranes for CO_2 separation from H_2. The second very early stage

© Woodhead Publishing Limited, 2011



8.9 Technology maturity vs total investment for syngas processing.

technology is based on MIEC oxide membranes. These ceramic membranes are dense and transport through the membrane occurs via proton diffusion, similar to fuel cells. Mixed conductors such as tungstanates (Shimura *et al.*, 2001; Haugsrud, 2007), cerates, zirconates (Matsumoto *et al.*, 2006) and non-stoichiometric perovskites (Norby, 1999) separate H_2 from gas streams at high temperatures (> 700°C), whilst being stable under CO_2 exposure. Nevertheless, H_2 permeance is too low even at high temperatures and future development will need to focus on improving H_2 fluxes preferentially below 500°C to find application in syngas processing.

The pore size of crystalline zeolite membranes has traditionally been higher than 5 Å and, owing to strong CO_2 adsorption, zeolite membranes have preferentially separated CO_2 from syngas rather than H_2. However, modification of the zeolite pore structure by catalytic cracking of silane precursors has enabled zeolite membranes to achieve true molecular sieving, thus allowing permeation of hydrogen instead of CO_2 (Masuda *et al.*, 2001; Hong *et al.*, 2005; Tang *et al.*, 2009). These modified zeolite membranes have been tested as WGS membrane reactors, delivering CO conversions above equilibrium at 500–550°C (Tang *et al.*, 2010). The H_2/CO_2 selectivity was reduced following WGS operation, possibly indicating that the silica modified zeolite is not stable under hydrothermal conditions.

Metal silica membranes produced by doping with nickel (Kanezashi and Asaeda, 2006) or cobalt salts (Igi *et al.*, 2008; Uhlmann *et al.*, 2009) have demonstrated improved hydrothermal stability. Nevertheless, recent work with cobalt silica reported that at high temperatures (500°C) and long-term steam exposure, the metal embedded in the silica film oxidizes, thus forming metal oxide particles (Uhlmann *et al.*, 2010). In addition the metal silica membranes undergo densification at a higher rate than the metal oxide silica membranes. Hydrothermal stability of hybrid silica membranes has yet to be fully realized and future development may focus on steam conditioning of the thin films (Igi *et al.*, 2008), or clever assembly of metal oxides into a silica matrix containing ligand templates.

© Woodhead Publishing Limited, 2011

Palladium and palladium alloy membranes are the most commercially advanced of the membrane technologies for syngas processing. The development of robust, thin films (< 5 μm) that are highly resistant to H_2S contamination will play a crucial role in determining whether a Pd-based membrane will crest the 'development hump'. If such protective coatings prove their effectiveness during long-term operation, they will alleviate the stringent sulfur resistance requirements for the Pd-based membranes themselves, accelerating development of the technology.

The mechanical design of membrane reactors on the large scale is an area that requires further development. The mechanical and sealing problems are of concern and a favoured approach to solve this problem is to use porous metal substrates where both ends of the tube are made of dense metal. Hence, these tubes can be easily sealed by welding or conventional metal ferrule compression seals. However, a balance must be attained between the thermal coefficient of expansion of the porous metal substrate, the metal oxide interlayers and the top membrane thin films, whether made of metal alloys, zeolites or silica. In addition, oxidation of the metal substrate can propagate stress through the membrane structure; resulting in cracks developing in both the interlayers and top separation layer (Brands *et al.*, 2010). These issues become important in wet syngas processing at high temperatures and under reaction conditions where unwanted thermal stresses and corrosion are most likely to develop, thus materials selection becomes paramount in the development of robust membrane and membrane reactor modules.

Finally, demonstration leads to the technical and economic viability of new technologies. Prior to reaching the 'demonstration hump', first of a kind (FOAK) pilot scale units are tested. In this case, a FOAK unit employing thick palladium alloy membranes was developed by Tokyo Gas Co, for processing H_2 from natural gas reforming, which was designed to deliver 20 $Nm^3\ h^{-1}$ (Shirasaki *et al.*, 2001). Although successful in its operation for a period in excess of 2 years, Tokyo Gas discontinued their thick palladium alloy membrane operation in early 2000, with a shift towards thinner membrane design to reduce costs. To make the jump towards deployment, the capital and operating costs of the new technology unit must be reduced. These costs tend to increase for several years (e.g. the demonstration hump) until the technology is fully understood, optimized and intensified.

Recently Tokyo Gas demonstrated a scaled-up reformer with a nominal H_2 production of 40 $Nm^3\ h^{-1}$, ostensibly the largest operation of its type in the world (Shirasaki *et al.*, 2009). The system operated for more than 3100 hours producing H_2 with less than 3 ppm impurities. Future development will focus on improving the energy efficiency of the process to greater than 80%, enabling it to have a clear advantage over conventional sorption-based systems.

© Woodhead Publishing Limited, 2011

Despite the recent progress in inorganic membrane technologies, it is likely that mature and ageing technologies (e.g. chemical/physical sorption-based processes) will continue to be employed in the first generation of syngas processing facilities. However, the significant energy penalties and operating costs of these technologies combined with a limited, incremental scope for improvement open the door for embryonic and growth technologies, such as inorganic membranes, to transform syngas processing, although there is an obvious economic risk attached to their development for demonstration.

8.7 Conclusions

Research into the production and processing of syngas using inorganic membranes has increased dramatically in the last few decades, mirroring the push for clean energy delivery and a H_2-based economy. Dense palladium-based membranes and porous silica membranes are at the forefront of technological development and, when incorporated in a membrane reactor in the case of the water gas shift reaction or natural gas reforming, demonstrate clear advantages over existing, mature technologies. However, mechanical robustness and resistance to both steam densification and poisoning from trace components remain some of the major impediments to commercialization. For palladium-based membranes, alloying with other metals improves performance, increases resistance to poisoning compounds and reduces capital costs, although further development and long-term operation of newer, thin film modules is required to overcome the 'demonstration hump'. The incorporation of organic templates or metal oxides into the silica matrix increases H_2 production and the hydrothermal stability of silica-based membranes, but the fragility of the ceramic supports limits current industrial feasibility. Further materials development in conjunction with porous metallic substrates will accelerate the technology towards long-term demonstration scale projects. Furthermore, integration of inorganic membranes into syngas processing will require clever engineering design of the membrane and membrane reactor modules themselves. Sealing membranes at elevated (> 400°C) temperatures and pressures remains a high risk endeavour, whilst the placement of the membrane module or membrane reactor within the process will be dependent on the end use of the syngas. These materials science and engineering challenges will provide many research and development opportunities in the decades to come.

8.8 References

Abdel-Jawad, M. M., Gopalakrishnan, S., Duke, M. C., Macrossan, M. N., Schneider, P. S. and Diniz Da Costa, J. C. (2007) 'Flowfields on feed and permeate sides of tubular molecular sieving silica (MSS) membranes'. *Journal of Membrane Science*, **299**, 229–35.

© Woodhead Publishing Limited, 2011

Abdel-Jawad, M. M., Macrossan, M. N. and Diniz Da Costa, J. C. (2009) 'Modelling gas purification systems employing molecular sieve silica membranes'. *Separation and Purification Technology*, **66**, 559–64.

Abdollahi, M., Yu, J., Liu, P. K. T., Ciora, R., Sahimi, M. and Tsotsis, T. T. (2010) 'Hydrogen production from coal-derived syngas using a catalytic membrane reactor based process'. *Journal of Membrane Science*, **363**, 160–9.

Adrover, M. E., Anzola, A., Schbib, S., Pedernera, M. and Borio, D. (2010) 'Effect of flow configuration on the behavior of a membrane reactor operating without sweep gas'. *Catalysis Today*, **156**, 223–8.

Amandusson, H., Ekedahl, L. G. and Dannetun, H. (2000) 'The effect of CO and O_2 on hydrogen permeation through a palladium membrane'. *Applied Surface Science*, **153**, 259–67.

Andrew, P. L. and Haasz, A. A. (1992) 'Models for hydrogen permeation in metals'. *Journal of Applied Physics*, **72**, 2749–57.

Armor, J. N. (1995) 'Membrane catalysis: Where is it now, what needs to be done?' *Catalysis Today*, **25**, 199–207.

Arstad, B., Venvik, H., Klette, H., Walmsley, J. C., Tucho, W. M., Holmestad, R., Holmen, A. and Bredesen, R. (2006) 'Studies of self-supported 1.6 μm Pd/23 wt.% Ag membranes during and after hydrogen production in a catalytic membrane reactor'. *Catalysis Today*, **118**, 63–72.

Asaeda, M., Kanezashi, M., Yoshioka, T. and Tsuru, T. (2003) 'Gas permeation characteristics and stability of composite silica–metal oxide membranes'. *MRS Fall Meeting*, *Symposium AA – Membranes – Preparation*, *Properties and Applications*, V. N. Burganos, R. D. Noble, M. Asaeda, A. Ayral and Leroux, J. D. (eds), Boston, Massachusetts.

Bakker, W. J. W., Kapteijn, F., Poppe, J. and Moulijn, J. A. (1996) 'Permeation characteristics of a metal-supported silicalite-1 zeolite membrane'. *Journal of Membrane Science*, **117**, 57–78.

Barbieri, G., Brunetti, A., Granato, T., Bernardo, P. and Drioli, E. (2005) 'Engineering evaluations of a catalytic membrane reactor for the water gas shift reaction'. *Industrial and Engineering Chemistry Research*, **44**, 7676–83.

Barbieri, G., Brunetti, A., Tricoli, G. and Drioli, E. (2008) 'An innovative configuration of a Pd-based membrane reactor for the production of pure hydrogen: experimental analysis of water gas shift'. *Journal of Power Sources*, **182**, 160–7.

Basile, A., Chiappetta, G., Tosti, S. and Violante, V. (2001) 'Experimental and simulation of both Pd and Pd/Ag for a water gas shift membrane reactor'. *Separation and Purification Technology*, **25**, 549–71.

Basini, L. (2005) 'Issues in H_2 and synthesis gas technologies for refinery, GTL and small and distributed industrial needs'. *Catalysis Today*, **106**, 34–40.

Battersby, S., Teixeira, P. W., Beltramini, J., Duke, M. C., Rudolph, V. and Diniz Da Costa, J. C. (2006) 'An analysis of the Peclet and Damkohler numbers for dehydrogenation reactions using molecular sieve silica (MSS) membrane reactors'. *Catalysis Today*, **116**, 12–17.

Battersby, S. E., Miller, D., Zed, M., Patch, J., Rudolph, V., Duke, M. C. and Diniz Da Costa, J. C. (2007) 'Silica membrane reactors for hydrogen processing'. *Advances in Applied Ceramics*, **106**, 29–34.

Battersby, S., Duke, M. C., Liu, S., Rudolph, V. and Diniz Da Costa, J. C. (2008) 'Metal doped silica membrane reactor: Operational effects of reaction and permeation for the water gas shift reaction'. *Journal of Membrane Science*, **316**, 46–52.

© Woodhead Publishing Limited, 2011

Battersby, S., Smart, S., Ladewig, B., Liu, S., Duke, M. C., Rudolph, V. and Diniz Da Costa, J. C. (2009a) 'Hydrothermal stability of cobalt silica membranes in a water gas shift membrane reactor'. *Separation and Purification Technology*, **66**, 299–305.

Battersby, S., Tasaki, T., Smart, S., Ladewig, B., Liu, S., Duke, M. C., Rudolph, V. and Diniz Da Costa, J. C. (2009b) 'Performance of cobalt silica membranes in gas mixture separation'. *Journal of Membrane Science*, **329**, 91–8.

Benson, H. E. (1981) 'Processing of gasification products'. *Chemistry of Coal Utilization*, Elliott, M. A. (ed), John Wiley and Sons, New York.

Bird, R. B., Stewart, W. E. and Lightfoot, E. N. (2002) *Transport Phenomena*, Wiley, New York.

Bitter, J. G. A. (1991) *Transport Mechanisms in Membrane Separation Processes*, Plenum Press, New York.

Boffa, V., Blank, D. H. A. and Ten Elshof, J. E. (2008) 'Hydrothermal stability of microporous silica and niobia-silica membranes'. *Journal of Membrane Science*, **319**, 256–63.

Boutikos, P. and Nikolakis, V. (2010) 'A simulation study of the effect of operating and design parameters on the performance of a water gas shift membrane reactor'. *Journal of Membrane Science*, **350**, 378–86.

Bowen, T. C., Noble, R. D. and Falconer, J. L. (2004) 'Fundamentals and applications of pervaporation through zeolite membranes'. *Journal of Membrane Science*, **245**, 1–33.

Bracht, M., Alderliesten, P. T., Kloster, R., Pruschek, R., Haupt, G., Xue, E., Ross, J. R. H., Koukou, M. K. and Papayannakos, N. (1997) 'Water gas shift membrane reactor for CO_2 control in IGCC systems: techno-economic feasibility study'. *Energy Conversion and Management*, **38**, S159–S164.

Brands, K., Uhlmann, D., Smart, S., Bram, M. and Diniz Da Costa, J. C. (2010) 'Long-term flue gas exposure effects of silica membranes on porous steel substrate'. *Journal of Membrane Science*, **359**, 110–14.

Brunetti, A., Barbieri, G., Drioli, E., Lee, K. H., Sea, B. and Lee, D. W. (2007) 'WGS reaction in a membrane reactor using a porous stainless steel supported silica membrane'. *Chemical Engineering and Processing*, **46**, 119–26.

Burchardt, T. (2000) 'The hydrogen evolution reaction on NiPx alloys'. *International Journal of Hydrogen Energy*, **25**, 627–34.

Cabrera, A. L., Morales-Leal, E., Hasen, J. and Schuller, I. K. (1995) 'Changes in crystallographic orientation of thin foils of palladium and palladium alloys after the absorption of hydrogen'. *Catalysis Letters*, **30**, 11–23.

Cao, G. Z., Lu, Y. F., Delattre, L., Brinker, C. J. and Lopez, G. P. (1996) 'Amorphous silica molecular sieving membranes by sol-gel processing'. *Advanced Materials*, **8**, 588–91.

Caro, J. and Noack, M. (2008) 'Zeolite membranes – recent developments and progress'. *Microporous and Mesoporous Materials*, **115**, 215–33.

Caro, J., Caspary, K. J., Hamel, C., Hoting, B., Kolsch, P., Langanke, B., Nassauer, K., Schiestel, T., Schmidt, A., Schomacker, R., Seidel-Morgenstern, A., Tsotsas, E., Voigt, I., Wang, H. H., Warsitz, R., Werth, S. and Wolf, A. (2007) 'Catalytic membrane reactors for partial oxidation using perovskite hollow fiber membranes and for partial hydrogenation using a catalytic membrane contactor'. *Industrial and Engineering Chemistry Research*, **46**, 2286–94.

Catalano, J., Giacinti Baschetti, M. and Sarti, G. C. (2010) 'Hydrogen permeation in palladium-based membranes in the presence of carbon monoxide'. *Journal of Membrane Science*, **362**, 221–33.

© Woodhead Publishing Limited, 2011

Chinchen, G. C., Logan, R. H. and Spencer, M. S. (1984) 'Water-gas shift reaction over an iron oxide/chromium oxide catalyst. II: Stability of activity'. *Applied Catalysis*, **12**, 89–96.

Criscuoli, A., Basile, A., Drioli, E. and Loiacono, O. (2001) 'An economic feasibility study for water gas shift membrane reactor'. *Journal of Membrane Science*, **181**, 21–7.

De Lange, R. S. A., Hekkink, J. H. A., Keizer, K. and Burggraaf, A. J. (1995a) 'Formation and characterization of supported microporous ceramic membranes prepared by sol-gel modification techniques'. *Journal of Membrane Science*, **99**, 57–75.

De Lange, R. S. A., Keizer, K. and Burggraaf, A. J. (1995b) 'Analysis and theory of gas transport in microporous sol–gel derived ceramic membranes'. *Journal of Membrane Science*, **104**, 81–100.

De Vos, R. M. and Verweij, H. (1998a) 'High-selectivity, high-flux silica membranes for gas separation'. *Science*, **279**, 1710–11.

De Vos, R. M. and Verweij, H. (1998b) 'Improved performance of silica membranes for gas separation'. *Journal of Membrane Science*, **143**, 37–51.

De Vos, R. M., Maier, W. F. and Verweij, H. (1999) 'Hydrophobic silica membranes for gas separation'. *Journal of Membrane Science*, **158**, 277–88.

Dixon, A. G., Nijemeisland, M. and Stitt, E. H. (2003) 'CFD simulation of reaction and heat transfer near the wall of a fixed bed'. *International Journal of Chemical Reactor Engineering*, **1**, A22.

Dolan, M. D., Dave, N. C., Ilyushechkin, A. Y., Morpeth, L. D. and McLennan, K. G. (2006) 'Composition and operation of hydrogen-selective amorphous alloy membranes'. *Journal of Membrane Science*, **285**, 30–55.

Duke, M., Rudolph, V., Lu, G. Q. and Diniz Da Costa, J. C. (2004a) 'Scale-up of molecular sieve silica membranes for reformate purification'. *AIChE Journal*, **50**, 2630–4.

Duke, M. C., Diniz Da Costa, J. C., Lu, G. Q., Petch, M. and Gray, P. (2004b) 'Carbonised template molecular sieve silica membranes in fuel processing systems: permeation, hydrostability and regeneration'. *Journal of Membrane Science*, **241**, 325–33.

Duke, M. C., Diniz Da Costa, J. C., Do, D. D., Gray, P. G. and Lu, G. Q. (2006) 'Hydrothermally robust molecular sieve silica for wet gas separation'. *Advanced Functional Materials*, **16**, 1215–20.

Duke, M. C., Ladewig, B., Smart, S., Rudolph, V. and Da Costa, J. C. D. (2010) 'Assessment of postcombustion carbon capture technologies for power generation'. *Frontiers of Chemical Engineering in China*, **4**, 184–95.

Fotou, G. P., Lin, Y. S. and Pratsinis, S. E. (1995) 'Hydrothermal stability of pure and modified microporous silica membranes'. *Journal of Materials Science*, **30**, 2803–8.

Geus, E. R., Den Exter, M. J. and Van Bekkum, H. (1992) 'Synthesis and characterization of zeolite (MFI) membranes on porous ceramic supports'. *Journal of the Chemical Society, Faraday Transactions*, **88**, 3101–9.

Gielens, F. C., Tong, H. D., Van Rijn, C. J. M., Vorstman, M. A. G. and Keurentjes, J. T. F. (2004) 'Microsystem technology for high-flux hydrogen separation membranes'. *Journal of Membrane Science*, **243**, 203–13.

Giessler, S., Diniz Da Costa, J. C. and Lu, G. Q. (2001) 'Hydrophobicity of templated silica xerogels for molecular sieving applications'. *Journal of Nanoscience and Nanotechnology*, **1**, 331–6.

Giessler, S., Jordan, L., Diniz Da Costa, J. C. and Lu, G. Q. (2003) 'Performance of hydrophobic and hydrophilic silica membrane reactors for the water gas shift reaction'. *Separation and Purification Technology*, **32**, 255–64.

© Woodhead Publishing Limited, 2011

Gopalakrishnan, S., Yoshino, Y., Nomura, M., Nair, B. N. and Nakao, S. I. (2007) 'A hybrid processing method for high performance hydrogen-selective silica membranes'. *Journal of Membrane Science*, **297**, 5–9.

Grashoff, G. J., Pilkington, C. E. and Corti, C. W. (1983) 'Purification of hydrogen'. *Platinum Metals Review*, **27**, 157–69.

Gu, Y. and Oyama, S. T. (2007a) 'High molecular permeance in a poreless ceramic membrane'. *Advanced Materials*, **19**, 1636–40.

Gu, Y. and Oyama, S. T. (2007b) 'Ultrathin, hydrogen-selective silica membranes deposited on alumina-graded structures prepared from size-controlled boehmite sols'. *Journal of Membrane Science*, **306**, 216–27.

Gu, Y. and Oyama, S. T. (2009) 'Permeation properties and hydrothermal stability of silica-titania membranes supported on porous alumina substrates'. *Journal of Membrane Science*, **345**, 267–75.

Gu, X., Tang, Z. and Dong, J. (2008a) 'On-stream modification of MFI zeolite membranes for enhancing hydrogen separation at high temperature'. *Microporous and Mesoporous Materials*, **111**, 441–8.

Gu, Y., Hacarlioglu, P. and Oyama, S. T. (2008b) 'Hydrothermally stable silica-alumina composite membranes for hydrogen separation'. *Journal of Membrane Science*, **310**, 28–37.

Hara, S., Ishitsuka, M., Suda, H., Mukaida, M. and Haraya, K. (2009) 'Pressure-dependent hydrogen permeability extended for metal membranes not obeying the square-root law'. *Journal of Physical Chemistry B*, **113**, 9795–801.

Haugsrud, R. (2007) 'Defects and transport properties in Ln6WO12 (Ln = La, Nd, Gd, Er)'. *Solid State Ionics*, **178**, 555–60.

Hla, S. S., Duffy, G. J., Morpeth, L. D., Cousins, A., Roberts, D. G. and Edwards, J. H. (2009) 'Investigation of the effect of H_2S on the performance of an iron/chromium-based high-temperature water-gas shift catalyst using simulated coal-derived syngas'. *Catalysis Communications*, **10**, 967–70.

Hong, M., Falconer, J. L. and Noble, R. D. (2005) 'Modification of zeolite membranes for H_2 separation by catalytic cracking of methyldiethoxysilane'. *Industrial and Engineering Chemistry Research*, **44**, 4035–41.

Hou, K. and Hughes, R. (2002) 'The effect of external mass transfer, competitive adsorption and coking on hydrogen permeation through thin Pd/Ag membranes'. *Journal of Membrane Science*, **206**, 119–30.

Hughes, R. (2001) 'Composite palladium membrane for catalytic membrane reactors'. *Membrane Technology*, 9–13.

Hunter, J. B. (1956) 'Silver-palladium film for separation and purification of hydrogen'. US Patent 2773561.

Igi, R., Yoshioka, T., Ikuhara, Y. H., Iwamoto, Y. and Tsuru, T. (2008) 'Characterization of co-doped silica for improved hydrothermal stability and application to hydrogen separation membranes at high temperatures'. *Journal of the American Ceramic Society*, **91**, 2975–81.

Ikuhara, Y. H., Mori, H., Saito, T. and Iwamoto, Y. (2007) 'High-temperature hydrogen adsorption properties of precursor-derived nickel nanoparticle-dispersed amorphous silica'. *Journal of the American Ceramic Society*, **90**, 546–52.

Iyoha, O., Enick, R., Killmeyer, R., Howard, B., Morreale, B. and Ciocco, M. (2007) 'Wall-catalyzed water-gas shift reaction in multi-tubular Pd and 80 wt%Pd–20 wt%Cu membrane reactors at 1173 K'. *Journal of Membrane Science*, **298**, 14–23.

Kajiwara, M., Uemiya, S. and Kojima, T. (1999) 'Stability and hydrogen permeation

© Woodhead Publishing Limited, 2011

behavior of supported platinum membranes in presence of hydrogen sulfide'. *International Journal of Hydrogen Energy*, **24**, 839–44.

Kanezashi, M. and Asaeda, M. (2005) 'Stability of H_2-permeselective Ni-doped silica membranes in steam at high temperature'. *Journal of Chemical Engineering of Japan*, **38**, 908–12.

Kanezashi, M. and Asaeda, M. (2006) 'Hydrogen permeation characteristics and stability of Ni-doped silica membranes in steam at high temperature'. *Journal of Membrane Science*, **271**, 86–93.

Kanezashi, M. and Lin, Y. S. (2009) 'Gas permeation and diffusion characteristics of MFI-type zeolite membranes at high temperatures'. *Journal of Physical Chemistry C*, **113**, 3767–74.

Kanezashi, M., Fujita, T. and Asaeda, M. (2005) 'Nickel-doped silica membranes for separation of helium from organic gas mixtures'. *Separation Science and Technology*, **40**, 225–38.

Kanezashi, M., O'Brien-Abraham, J., Lin, Y. S. and Suzuki, K. (2008) 'Gas permeation through DDR-type zeolite membranes at high temperatures'. *AIChE Journal*, **54**, 1478–86.

Kim, J. and Lin, Y. S. (2000) 'Synthesis and oxygen permeation properties of ceramic-metal dual-phase membranes'. *Journal of Membrane Science*, **167**, 123–33.

Kim, S. and Gavalas, G. R. (1995) 'Preparation of H_2 permselective silica membranes by alternating reactant vapor deposition'. *Industrial and Engineering Chemistry Research*, **34**, 168–76.

Kobayashi, K., Nishioka, M., Sato, K., Inoue, T., Hamakawa, S. and Tsunoda, T. (2006) 'Synthesis and oxygen permeation properties of 75 mol% Ce0.75Nd0.25O1.875–25 mol% Nd1.8Ce0.2CuO4 composite'. *Journal of Solid State Electrochemistry*, **10**, 629–34.

Kolb, G. (2008) *Fuel Processing for Fuel Cells*, Wiley-VCH, Weinheim, Germany.

Koros, W. J., Ma, Y. H. and Shimidzu, T. (1996) 'Terminology for membranes and membrane processes'. *Pure and Applied Chemistry*, **68**, 1479–89.

Krishna, R. (2009) 'Describing the diffusion of guest molecules inside porous structures'. *Journal of Physical Chemistry C*, **113**, 19756–81.

Krishna, R. and Wesselingh, J. A. (1997) 'The Maxwell–Stefan approach to mass transfer'. *Chemical Engineering Science*, **52**, 861–911.

Kulprathipanja, A., Alptekin, G. O., Falconer, J. L. and Way, J. D. (2005) 'Pd and Pd-Cu membranes: inhibition of H_2 permeation by H_2S'. *Journal of Membrane Science*, **254**, 49–62.

Kusakabe, K., Shibao, F., Zhao, G., Sotowa, K.-I., Watanabe, K. and Saito, T. (2003) 'Surface modification of silica membranes in a tubular-type module'. *Journal of Membrane Science*, **215**, 321–6.

Lai, Z. P., Bonilla, G., Diaz, I., Nery, J. G., Sujaoti, K., Amat, M. A., Kokkoli, E., Terasaki, O., Thompson, R. W., Tsapatsis, M. and Vlachos, D. G. (2003) 'Microstructural optimization of a zeolite membrane for organic vapor separation'. *Science*, **300**, 456–60.

Leboda, R. and Mendyk, E. (1991) 'Hydrothermal modification of porous structure of silica adsorbents'. *Materials Chemistry and Physics*, **27**, 189–212.

Lee, D., Zhang, L., Oyama, S. T., Niu, S. and Saraf, R. F. (2004) 'Synthesis, characterization, and gas permeation properties of a hydrogen permeable silica membrane supported on porous alumina'. *Journal of Membrane Science*, **231**, 117–26.

Lewis, F. A. (1967) *The Palladium Hydrogen System*, Academic Press, London.

© Woodhead Publishing Limited, 2011

Lin, Y. S., Kumakiri, I., Nair, B. N. and Alsyouri, H. (2002) 'Microporous inorganic membranes'. *Separation and Purification Methods*, **31**, 229–379.

Lloyd, L., Ridler, D. E. and Twigg, M. V. (1996) 'The water-gas shift reaction'. *Catalyst Handbook*, Twigg, M. V. (ed) 2nd edn, Manson Publishing, London.

Masuda, T., Fukumoto, N., Kitamura, M., Mukai, S. R., Hashimoto, K., Tanaka, T. and Funabiki, T. (2001) 'Modification of pore size of MFI-type zeolite by catalytic cracking of silane and application to preparation of H_2-separating zeolite membrane'. *Microporous and Mesoporous Materials*, **48**, 239–45.

Matsumoto, H., Shimura, T., Iwahara, H., Higuchi, T., Yashiro, K., Kaimai, A., Kawada, T. and Mizusaki, J. (2006) 'Hydrogen separation using proton-conducting perovskites'. *Journal of Alloys and Compounds*, **408–12**, 456–62.

McCool, B. A. and Lin, Y. S. (2001) 'Nanostructured thin palladium-silver membranes: effects of grain size on gas permeation properties'. *Journal of Materials Science*, **36**, 3221–7.

McLeary, E. E., Jansen, J. C. and Kapteijn, F. (2006) 'Zeolite based films, membranes and membrane reactors: Progress and prospects'. *Microporous and Mesoporous Materials*, **90**, 198–220.

Mehrer, H. (2007) *Diffusion in Solids Fundamentals, Methods, Materials*, *Diffusion-controlled Processes*, Springer, Berlin.

Michalske, T. A. and Freiman, S. W. (1982) 'A molecular interpretation of stress-corrosion in silica'. *Nature*, **295**, 511–12.

Moe, J. M. (1962) 'Low temperature CO processing'. *Chemical Engineering and Processing*, **58**, 33.

Moon, W. S. and Park, S. B. (2000) 'Design guide of a membrane for a membrane reactor in terms of permeability and selectivity'. *Journal of Membrane Science*, **170**, 43–51.

Mundschau, M. V., Xie, X., Evenson IV, C. R. and Sammells, A. F. (2006) 'Dense inorganic membranes for production of hydrogen from methane and coal with carbon dioxide sequestration'. *Catalysis Today*, **118**, 12–23.

Nair, S. and Tsapatsis, M. (2003) 'Synthesis and properties of zeolitic membranes'. *Handbook of Zeolite Science and Technology*. Auerbach, S. M., Carrado, K. A. and Dutta, P. K. (eds), Marcel Dekker, New York.

Newsome, D. S. (1980) 'The water-gas shift reaction'. *Catalysis Reviews: Science and Engineering*, **21**, 275–318.

Nishiyama, N., Yamaguchi, M., Katayama, T., Hirota, Y., Miyamoto, M., Egashira, Y., Ueyama, K., Nakanishi, K., Ohta, T., Mizusawa, A. and Satoh, T. (2007) 'Hydrogen-permeable membranes composed of zeolite nano-blocks'. *Journal of Membrane Science*, **306**, 349–54.

Nomura, M., Yamaguchi, T. and Nakao, S. I. (1997) 'Silicalite membranes modified by counterdiffusion CVD technique'. *Industrial and Engineering Chemistry Research*, **36**, 4217–23.

Norby, T. (1999) 'Solid-state protonic conductors: principles, properties, progress and prospects'. *Solid State Ionics*, **125**, 1–11.

Oyama, S. T., Lee, D., Hacarlioglu, P. and Saraf, R. F. (2004) 'Theory of hydrogen permeability in nonporous silica membranes'. *Journal of Membrane Science*, **244**, 45–53.

Phair, J. W. and Donelson, R. (2006) 'Developments and design of novel (non-palladium-based) metal membranes for hydrogen separation'. *Industrial and Engineering Chemistry Research*, **45**, 5657–74.

© Woodhead Publishing Limited, 2011

Pinacci, P., Broglia, M., Valli, C., Capannelli, G. and Comite, A. (2010) 'Evaluation of the water gas shift reaction in a palladium membrane reactor'. *Catalysis Today*, **156**, 165–72.

Qi, X., Akin, F. T. and Lin, Y. S. (2001) 'Ceramic-glass composite high temperature seals for dense ionic-conducting ceramic membranes'. *Journal of Membrane Science*, **193**, 185–93.

Raman, N. K. and Brinker, C. J. (1995) 'Organic "template" approach to molecular sieving silica membranes'. *Journal of Membrane Science*, **105**, 273–9.

Raman, N. K., Anderson, M. T. and Brinker, C. J. (1996) 'Template-based approaches to the preparation of amorphous, nanoporous silicas'. *Chemistry of Materials*, **8**, 1682–701.

Ratnasamy, C. and Wagner, J. (2009) 'Water gas shift catalysis'. *Catalysis Reviews – Science and Engineering*, **51**, 325–440.

Reddy, M. K. R., Xu, Z. P., Lu, G. Q. and Diniz Da Costa, J. C. (2008) 'Influence of water on high-temperature CO2 capture using layered double hydroxide derivatives'. *Industrial and Engineering Chemistry Research*, **47**, 2630–5.

Rhodes, C., Hutchings, G. J. and Ward, A. M. (1995) 'Water-gas shift reaction: finding the mechanistic boundary'. *Catalysis Today*, **23**, 43–58.

Roa, F. and Way, J. D. (2003) 'Influence of alloy composition and membrane fabrication on the pressure dependence of the hydrogen flux of palladium-copper membranes'. *Industrial and Engineering Chemistry Research*, **42**, 5827–35.

Saracco, G., Neomagus, H. W. J. P., Versteeg, G. F. and Swaaij, W. P. M. V. (1999) 'High-temperature membrane reactors: potential and problems'. *Chemical Engineering Science*, **54**, 1997–2017.

Shimura, T., Fujimoto, S. and Iwahara, H. (2001) 'Proton conduction in non-perovskite-type oxides at elevated temperatures'. *Solid State Ionics*, **143**, 117–23.

Shirasaki, Y., Yasuda, I., Kobayashi, K., Fujimoto, Y. and Kuroda, K. (2001) 'New concept hydrogen production system based on the membrane reformer'. *Proceedings International Conference on Power Engineering*, Xi'an, China, Chinese Society of Power Engineering, Japanese Society of Mechanical Engineers and American Society of Mechanical Engineers.

Shirasaki, Y., Tsuneki, T., Ota, Y., Yasuda, I., Tachibana, S., Nakajima, H. and Kobayashi, K. (2009) 'Development of membrane reformer system for highly efficient hydrogen production from natural gas'. *International Journal of Hydrogen Energy*, **34**, 4482–7.

Sholl, D. S. and Ma, Y. H. (2006) 'Dense metal membranes for the production of high-purity hydrogen'. *MRS Bulletin*, **31**, 770–3.

Shu, J., Grandjean, B. P. A., Van Neste, A. and Kaliaguine, S. (1991) 'Catalytic palladium-based membrane reactors. A review'. *Canadian Journal of Chemical Engineering*, **69**, 1036–60.

Smart, S., Lin, C. X. C., Ding, L., Thambimuthu, K. and Diniz Da Costa, J. C. (2010) 'Ceramic membranes for gas processing in coal gasification'. *Energy and Environmental Science*, **3**, 268–78.

Tang, Z., Dong, J. and Nenoff, T. M. (2009) 'Internal surface modification of MFI-type zeolite membranes for high selectivity and high flux for hydrogen'. *Langmuir*, **25**, 4848–52.

Tang, Z., Kim, S.-J., Reddy, G. K., Dong, J. and Smirniotis, P. (2010) 'Modified zeolite membrane reactor for high temperature water gas shift reaction'. *Journal of Membrane Science*, **354**, 114–22.

© Woodhead Publishing Limited, 2011

Tong, J., Kashima, Y., Shirai, R., Suda, H. and Matsumura, Y. (2005) 'Thin defect-free Pd membrane deposited on asymmetric porous stainless steel substrate'. *Industrial and Engineering Chemistry Research*, **44**, 8025–32.

Tong, J., Su, L., Kashima, Y., Shirai, R., Suda, H. and Matsumura, Y. (2006) 'Simultaneously depositing Pd–Ag thin membrane on asymmetric porous stainless steel tube and application to produce hydrogen from steam reforming of methane'. *Industrial and Engineering Chemistry Research*, **45**, 648–55.

Tong, J., Su, L., Haraya, K. and Suda, H. (2008) 'Thin Pd membrane on α-Al_2O_3 hollow fiber substrate without any interlayer by electroless plating combined with embedding Pd catalyst in polymer template'. *Journal of Membrane Science*, **310**, 93–101.

Tsai, C.-Y., Tam, S.-Y., Lu, Y. and Brinker, C. J. (2000) 'Dual-layer asymmetric microporous silica membranes'. *Journal of Membrane Science*, **169**, 255–68.

Uemiya, S., Matsuda, T. and Kikuchi, E. (1991) 'Hydrogen permeable palladium-silver alloy membrane supported on porous ceramics'. *Journal of Membrane Science*, **56**, 315–25.

Uhlmann, D., Liu, S., Ladewig, B. P. and Diniz Da Costa, J. C. (2009) 'Cobalt-doped silica membranes for gas separation'. *Journal of Membrane Science*, **326**, 316–21.

Uhlmann, D., Smart, S. and Diniz Da Costa, J. C. (2010) 'High temperature steam investigation of cobalt oxide silica membranes for gas separation'. *Separation and Purification Technology*, **76**, 171–8.

Van Selow, E. R., Cobden, P. D., Van Den Brink, R. W., Hufton, J. R. and Wright, A. (2009) 'Performance of sorption-enhanced water-gas shift as a pre-combustion CO_2 capture technology'. *Energy Procedia*, **1**, 689–96.

Wang, Z. and Yan, Y. (2001) 'Controlling crystal orientation in zeolite MFI thin films by direct *in situ* crystallization'. *Chemistry of Materials*, **13**, 1101–7.

Wei, Q., Wang, Y.-L., Nie, Z.-R., Yu, C.-X., Li, Q.-Y., Zou, J.-X. and Li, C.-J. (2008) 'Facile synthesis of hydrophobic microporous silica membranes and their resistance to humid atmosphere'. *Microporous and Mesoporous Materials*, **111**, 97–103.

Wicke, E. and Brodowsky, H. (1978) 'Hydrogen in palladium and palladium alloys'. *Hydrogen in Metals II. Application-oriented properties*. Alefeld, G. and Volkl, J. (eds), Springer-Verlag, Berlin.

Wilhelm, D. J., Simbeck, D. R., Karp, A. D. and Dickenson, R. L. (2001) 'Syngas production for gas-to-liquids applications: technologies, issues and outlook'. *Fuel Processing Technology*, **71**, 139–48.

Xiao, J. and Wei, J. (1992) 'Diffusion mechanism of hydrocarbons in zeolites--I. Theory'. *Chemical Engineering Science*, **47**, 1123–41.

Xomeritakis, G., Gouzinis, A., Nair, S., Okubo, T., He, M., Overney, R. M. and Tsapatsis, M. (1999) 'Growth, microstructure, and permeation properties of supported zeolite (MFI) films and membranes prepared by secondary growth'. *Chemical Engineering Science*, **54**, 3521–31.

Xu, S. J. and Thomson, W. J. (1998) 'Stability of La0.6Sr0.4Co0.2Fe0.8O3-delta perovskite membranes in reducing and nonreducing environments'. *Industrial and Engineering Chemistry Research*, **37**, 1290–9.

Yamakawa, K., Ege, M., Ludescher, B., Hirscher, M. and Kronmüller, H. (2001) 'Hydrogen permeability measurement through Pd, Ni and Fe membranes'. *Journal of Alloys and Compounds*, **321**, 17–23.

Yeung, K. L., Aravind, R., Zawada, R. J. X., Szegner, J., Cao, G. and Varma, A. (1994) 'Nonuniform catalyst distribution for inorganic membrane reactors: Theoretical

© Woodhead Publishing Limited, 2011

considerations and preparation techniques'. *Chemical Engineering Science*, **49**, 4823–38.

Yong, Z., Mata, V. and Rodriguez, A. E. (2001) 'Adsorption of carbon dioxide onto hydrotalcite-like compounds (HTlcs) at high temperatures'. *Industrial and Engineering Chemistry Research*, **40**, 204–9.

Yoshida, K., Hirano, Y., Fujii, H., Tsuru, T. and Asaeda, M. (2001) 'Hydrothermal stability and performance of silica-zirconia membranes for hydrogen separation in hydrothermal conditions'. *Journal of Chemical Engineering of Japan*, **34**, 523–30.

Zhang, X., Wang, W., Liu, J., Sheng, S., Xiong, G. and Yang, W. (2008) 'Hydrogen transport through thin palladium-copper alloy composite membranes at low temperatures'. *Thin Solid Films*, **516**, 1849–56.

Zhang, Y., Gwak, J., Murakoshi, Y., Ikehara, T., Maeda, R. and Nishimura, C. (2006) 'Hydrogen permeation characteristics of thin Pd membrane prepared by microfabrication technology'. *Journal of Membrane Science*, **277**, 203–9.

8.9 Appendix: list of symbols

A = membrane area
C_i = concentration of component i
C_{ads} = adsorbed concentration
Da = Damköhler number
$DaPe$ = Damköhler Peclet number
D_i = diffusion coefficient of component i
D_k = Knüdsen diffusion coefficient
D_s = surface diffusion coefficient
$D_{s,0}$ = intrinsic diffusivity of the adsorbed phase
D_0 = pre-exponential factor for diffusivity
d_0 = pore diameter
E = activation energy
E_d = activation energy of diffusion
F = flow rate
J_i = flux of component i
K_0 = pre-exponential factor for adsorption
K_{eq} = equilibrium constant
k = rate constant
M = molecular mass
P_i = partial pressure of component i
P_f = pressure of feed stream
P_p = pressure of permeate stream
$Perm_i$ = permeability of component i
Pe = Peclet number
Q_a = isosteric heat of adsorption
Q_i = permeance of component i
Q^0 = pre-exponential coefficient

© Woodhead Publishing Limited, 2011

q_s = adsorbed amount at saturation
r_0 = reaction rate
R = gas constant
S_i = solubility of component i in the membrane
S^{ij} = permselectivity or ideal selectivity of component i from component j
S_c^{ij} = separation coefficient of component i from component j
x = membrane thickness
x_i = composition of component i in the permeate
y_i = composition of component i in the feed
Γ = thermodynamic factor of the adsorption isotherm
μ = correction factor related to the porous structure of the silica membrane
φ = membrane structural factor relating to density, porosity and tortuosity

© Woodhead Publishing Limited, 2011

9

Oxygen transport membranes: dense ceramic membranes for power plant applications

S. SMART and J. C. DINIZ DA COSTA,
The University of Queensland, Australia and
S. BAUMANN and W. A. MEULENBERG,
Forschungszentrum Jülich, Germany

Abstract: This chapter addresses the latest developments in ceramic materials for use in oxygen transport membranes. Oxygen production is a multibillion dollar business with applications in clean energy, petrochemicals and metallurgical processes. The chapter describes the transport mechanisms involved and possible integration of these membranes in oxyfuel coal combustion and coal gasification. The chapter finishes with a discussion of the most appropriate membrane geometries and considerations for the development of membrane modules for industrial applications.

Key words: ceramic materials, coal gasification, ionic transport, oxyfuel coal combustion, oxygen transport membranes.

9.1 Introduction

Oxygen production is a multibillion dollar industry and oxygen is an important reactant in the production of a wide range of consumable products derived from glass, metals, chemicals and petrochemical processes. The oxygen production market is expected to expand rapidly in the near future because virtually all large scale clean fossil fuel power generators will require oxygen as a feed. This is reflected in national and international policies for maintaining security of energy supply and reducing the anthropogenic effects associated with greenhouse gas emissions via carbon capture and storage (CCS) processes. As an example, new coal power plants are now being designed as 'carbon capture ready' to meet new regulatory policies. These new plants will potentially be based on coal gasification and oxyfuel coal combustion processes and will require tonnage oxygen supply to deliver clean energy.

Currently large scale oxygen separation is carried out by cryogenic distillation. Apart from its complexity, cryogenic distillation is expensive and energy intensive because it operates at very low temperatures (–200°C) and at elevated pressures. Coupling a cryogenic air separation unit at the

© Woodhead Publishing Limited, 2011

front end of a coal gasifier or oxyfuel coal power plant is likely to reduce power generation efficiencies from current best practice of around 40% down to 30%. These energy penalties must be tackled in order to improve the viability of clean energy delivery technologies. Ceramic membranes offer the potential to separate oxygen from air and to reduce oxygen production costs by 35% or more (Stiegel and Maxwell, 2001; Bücker *et al.*, 2005) with lower efficiency penalties.

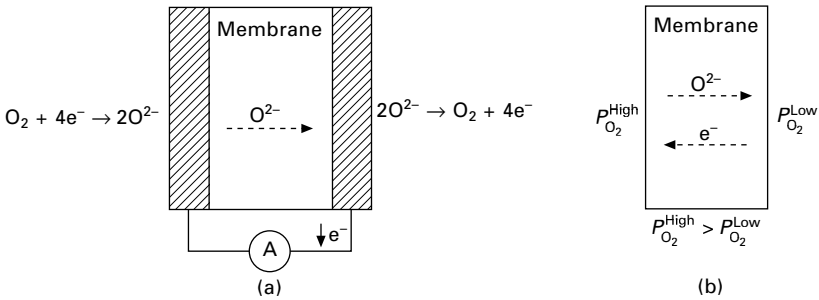
Other oxygen production processes include pressure swing adsorption (PSA) (Smith and Klosek, 2001), polymeric or ceramic membranes (Leo *et al.*, 2009a), chemical looping combustion, electrolysis of water or the electrolytic degradation of oxides or oxoacids (Emsley, 2001). Among these processes, PSA is a mature technology which can deliver high purity oxygen (up to 99.9%) at the small or medium scale (Jee *et al.*, 2005). Chemical looping combustion has been proposed, although the development of stable metal oxides is at early stage of laboratory research. Polymeric membranes can be used to enrich air with oxygen while the other processes, involving electrolytic degradation, may not be economically viable for tonnage oxygen production. In terms of market share, the higher capacity market is still dominated by cryogenic air separation followed by PSA (Koros and Fleming, 1993).

The new technology that is making inroads into the air separation market is dense ceramic membranes which operate at high temperatures (700–1000°C). In 2010, Air Products (USA) had operated a pilot plant for over 2 years, delivering 5 tonnes of oxygen per day. Large scale commercial plants using dense ceramic membranes are envisaged to be deployed within the next 10 years. Therefore, this chapter focuses on dense ceramic membranes for oxygen separation, from a materials point of view, to oxygen transport phenomena, in addition to discussion of the integration of dense ceramic membranes in energy systems whilst also addressing several other key technological issues.

9.2 Oxygen transport membrane materials, development and design

The two main types of oxygen separation systems based on ceramic membranes are illustrated in Fig. 9.1. The pure oxygen conducting membranes require an electrical potential gradient as the driving force for the permeation of oxygen. This is the case for ceramic materials that are limited to ionic conductivity only and thus require electrodes and a circuit as an electron pathway. An advantage of this system is the level of control over the oxygen flux through the application of an external electric current. In comparison the other type of oxygen separation system mixed ionic electronic conducting (MIEC) materials, does not require electrodes and the ceramic properties

© Woodhead Publishing Limited, 2011



9.1 Dense ceramic oxygen conducting membranes: (a) solid electrolyte for O^{2-} conduction and (b) mixed ionic electronic conductor.

allow the conduction of both ionic and electron species. The driving force for a MIEC membrane is associated with the chemical potential gradient of oxygen, which is related to the oxygen partial pressure difference across the membrane.

The MIEC membranes are the most common ceramic membrane technology for oxygen production and they will be the focus on this chapter. The primary classes of interest for these materials are perovskites (ABO_3), fluorites (AO_2), brownmillerites ($A_2B_2O_5$), Ruddlesden–Popper series ($A_{n+1}B_nO_{3n+1}$), and $Sr_4Fe_{6-x}Co_xO_{13}$ compounds, which are described in the following sections.

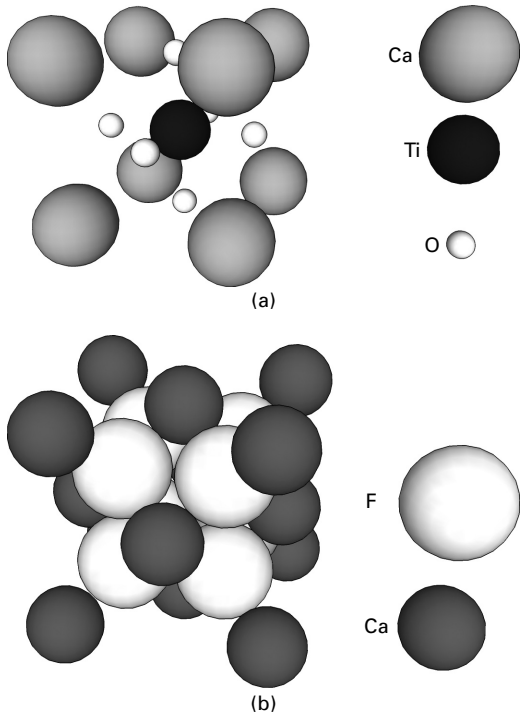
9.2.1 Materials

Oxides with the perovskite crystal structure have been the most studied MIEC materials, delivering the highest oxygen permeability reported to date. Figure 9.2(a) shows the perovskite structure with the formula ABO_3, where the A-cations and the B-cations are coordinated 12-fold and 6-fold with oxygen ions, respectively. In the pure cubic structure, the BO_6 octahedra are arrayed corner-shared (Bhalla *et al.*, 2000). The A-sites are occupied by alkaline-earth metals or the rare earth elements of the La-series, whereas the B-sites are occupied with transition metals. Goldschmidt introduced the tolerance factor, t (Equation [9.1]):

$$t = \frac{r_A + r_O}{\sqrt{2}(r_B + r_O)} \qquad [9.1]$$

with r_A, r_O, and r_B the radii of the A-cation, oxygen ion, and B-cation, respectively. The cubic perovskite structure is stable if the tolerance factor is close to one. With decreasing t, the structure is distorted to tetragonal, orthorhombic, or rhombohedral structures. As a rule, the cubic structure gives the highest oxygen permeability and any distorting of this structure leads to lower performance.

© Woodhead Publishing Limited, 2011



9.2 (a) Perovskite structure (example $CaTiO_3$) and (b) fluorite structure.

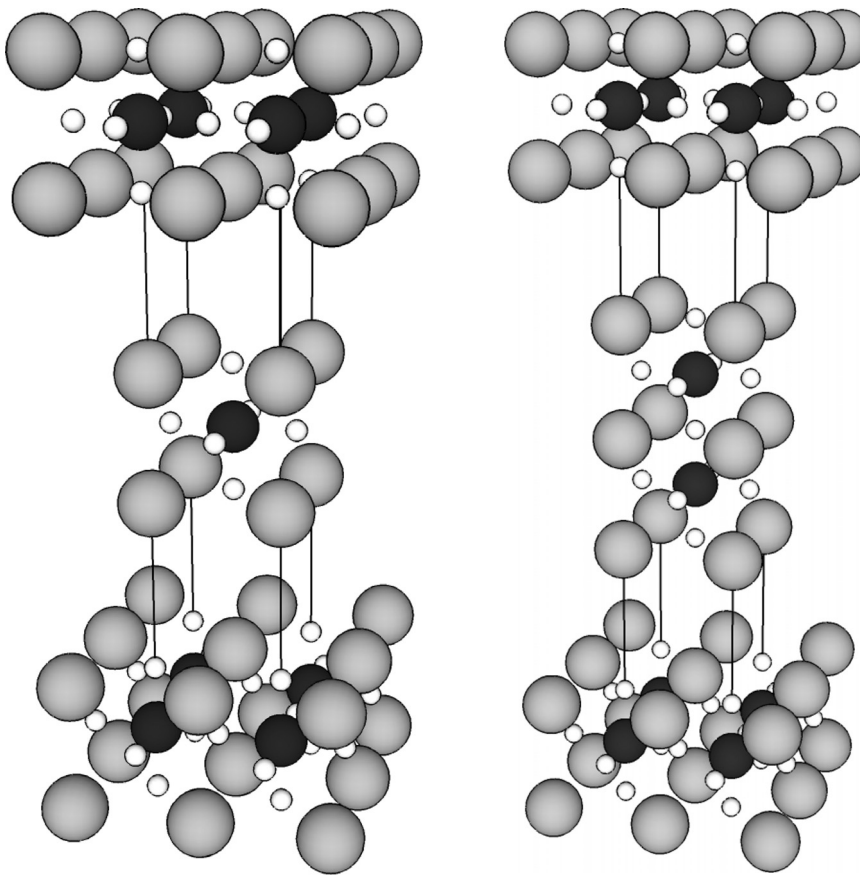
Fluorites (Fig. 9.2(b)) are also one of the most prominent oxygen conductive materials. Zirconia, a fluorite, in its pure form has three polymorphs, cubic at high temperature, tetragonal at intermediate temperature and monoclinic at low temperature. The cubic phase can be stabilized to room temperature by doping with MgO, CaO, Y_2O_3 and CeO_2 to form cubic stabilized zirconia. This has attracted great interest because of its high ionic conductivity, particularly as an electrolyte in solid oxide fuel cells (SOFC) (Badwal and Ciacchi, 2001). However, zirconia does not show electronic conductivity, which is essential to meet the requirements of MIEC materials for oxygen transport membranes, instead requiring a separate electronic conducting phase.

Another material of interest is brownmillerite ($A_2B_2O_5$), a layered structure of BO_6-octahedra and BO_4-tetrahedra. It can also be described as perovskite with an ordered oxygen vacancy structure aligned in the [001]-direction. The transition from perovskite to brownmillerite is accompanied by a strong drop in the ionic conductivity. This is attributed to the lower mobility of the oxygen vacancies in the polycrystal due to anisotropic diffusion properties (McIntosh *et al.*, 2006; Shaula *et al.*, 2006). Owing to the low permeabilities

© Woodhead Publishing Limited, 2011

brownmillereites are normally not considered applicable as oxygen transport membranes.

The Ruddlesden–Popper series consists of alternating layers of perovskite- and rock salt-structure with the formula $A_{m+1}B_mO_{3m+1}$ ($AB{\cdot}mABO_3$). The index m indicates how many combined perovskite layers are separated by one rock salt layer as depicted in Fig. 9.3(a) and (b). Accordingly, $m = \infty$ corresponds to a pure perovskite structure. La_2NiO_4 crystallizing in $K_2NiF_{4+\delta}$ where $m = 1$, is the composition which is mostly commonly investigated as an oxygen transport membrane material (Greenblatt, 1997, Kharton *et al.*, 2004; Naumovich and Kharton, 2010). The oxygen conductivity occurs in both the perovskite and the rock salt layers; however, in the latter, oxygen is transported via interstitial sites rather than vacancies. With increasing temperature, conductivity via interstitial sites is overwhelming (Kharton *et*



9.3 Ruddlesden–Popper structure with (*a*) $m = 1$ and (*b*) $m = 2$.

© Woodhead Publishing Limited, 2011

al., 2001; Yang *et al.*, 2005). The layered structure is thermodynamically more stable than pure perovskites (Breard *et al.*, 2002; Al Daroukh *et al.*, 2003); however, the layered structure also results in strongly anisotropic conductivity. Correspondingly, the oxygen permeation rates of polycrystalline membranes are low compared to cubic perovskites.

The final materials of interest are those of the $Sr_4Fe_{6-x}Co_xO_{13}$ structure, for example $Sr_4Fe_6O_{13}$ which consists of layers of perovskites and $Fe_2O_{2.5}$. The addition of Co ($x \geq 1.8$) results in the formation of several phases with spinel or perovskite structures (Xia *et al.*, 2000). High oxygen permeation and good long-term stability were observed under high oxygen partial pressure gradients (Balachandran *et al.*, 1998), but low permeability under more realistic oxygen partial pressure gradients has meant that these materials are not currently considered for oxygen transport membranes (Kim *et al.*, 1998; Manthiram *et al.*, 2002).

MIEC materials do not have to be limited to a single phase. For those materials which demonstrate good ionic conduction but limited by electronic conduction, it is possible to introduce a second phase of electron conducting material in the matrix of the membrane. These are known as dual phase membranes and the electronic and ionic charge carriers are transported separately by different phases. In order to achieve oxygen permeation, a percolation of the two phases is essential and this is normally possible if the two phases are inert to each other (Kharton *et al.*, 2003; Yi *et al.*, 2006; Yin *et al.*, 2006; Chang *et al.*, 2006) and the amount of both phases is approx. 40–60 (vol%). The electronic conductivity is most commonly delivered by noble metals such as platinum (Pt) and palladium (Pd) (Chen *et al.*, 1995). The high cost associated with incorporating noble metals and the significant reduction in effective membrane area caused by the presence of two phases, makes the dual phase membrane concept commercially unattractive at this time.

9.2.2 Chemical and structural modification

The most promising class of materials for oxygen transport membranes are pervoskites and fluorites. As a result, these materials have been investigated both by the research community and by industry. This section focuses on the general principles of material development that are leading the drive for high oxygen permeation performance.

Perovskites (ABO_3)

Oxygen diffusion in classical perovskites of the formula ABO_3 is limited. The general approach to improve oxygen flux is to increase the number of defects or oxygen vacancies in the perovskite structure. This can be achieved

© Woodhead Publishing Limited, 2011

by doping either of the cation sites (A or B) with other cations (A′ or B′) of different sizes and valences, resulting in a perovskite crystal structure of the formula $A_xA'_{1-x}B_yB'_{1-y}O_{3-\delta}$, where δ represents the number of oxygen vacancies. This approach was pioneered by Teraoka and co-workers in 1985 who developed perovskite membranes based on $(La,Sr)(Co,Fe)O_{3-\delta}$ (Teraoka *et al.*, 1985a, 1985b). Since then, a large array of materials has been developed as shown in Table 9.1. The common elements in the $A_xA'_{1-x}$ site are Ba, La and Sr, whilst the $B_yB'_{1-y}$ site is dominated by cobalt (Co) and iron (Fe). Generally oxygen fluxes reported in the literature are below 1 ml m^{-2} min^{-1}, although a few materials have shown higher fluxes, in excess of 3 ml m^{-2} min^{-1} such as BZCF ($BaZr_xCo_yFe_{1-x-y}O_{3-\delta}$), BTCF ($Ba_xTi_{1-x}Co_yFe_{1-y}O_{3-\delta}$), LSC ($L_xSr_{1-x}Co_yO_{3-\delta}$) and SCF ($Sr_xCo_yFe_{1-y}O_{3-\delta}$). Although the results in Table 9.1 are illustrative only, a note of caution should be taken here, as membrane thickness, temperature, oxygen partial pressures and testing conditions may differ for every result shown.

The major reason for these materials generally incorporating strontium (Sr) or Co is that it has been found that the mixed conductivity of MIEC ceramics increased as a function of Sr and Co content. It was also observed that a $SrCoO_{3-\delta}$ perovskite structure was stabilized by partly substituting Co with Fe, forming $SrCo_{0.8}Fe_{0.2}O_{3-\delta}$ (Nagai *et al.*, 2007). The stabilization of the perovskite structure was further improved by partial substitution of Sr with barium (Ba), forming $Ba_{0.5}Sr_{0.5}Co_{0.8}Fe_{0.2}O_{3-\delta}$ (BSCF) (Shao *et al.*,

Table 9.1 Representative oxygen fluxes of perovskite membranes

Compound	Temperature (°C)	Flux (ml min^{-1} cm^{-2})	Reference
$BaBi_{0.4}Co_{0.2}Fe_{0.4}O_{3-\delta}$	925	0.80438	Shao *et al.* (2000a)
$BaCe_{0.15}Fe_{0.85}O_{3-\delta}$	950	0.52295	Zhu *et al.* (2004)
$BaCo_{0.4}Fe_{0.5}Zr_{0.1}O_{3-\delta}$	950	0.91567	Tong *et al.* (2002)
$Ba_{0.5}Sr_{0.5}Co_{0.8}Fe_{0.2}O_{3-\delta}$	950	4.38950	Liu and Gavalas (2005)
$Ba_{0.5}Sr_{0.5}Zn_{0.2}Fe_{0.8}O_{3-\delta}$	975	3.49978	Wang *et al.* (2005a)
$BaTi_{0.2}Co_{0.4}Fe_{0.4}O_{3-\delta}$	950	8.99942	Tong *et al.* (2003)
$Gd_{0.6}Sr_{0.4}CoO_{3-\delta}$	820	1.58458	Teraoka *et al.* (1988)
$La_{0.6}Ba_{0.4}Co_{0.8}Fe_{0.2}O_{3-\delta}$	860	2.06438	Teraoka *et al.* (1988)
$La_{0.6}Ca_{0.4}Co_{0.8}Fe_{0.2}O_{3-\delta}$	860	1.83322	Teraoka *et al.* (1988)
$La_{0.6}Sr_{0.4}CoO_{3-\delta}$	850	2.99981	Miura *et al.* (1995)
$La_{0.6}Sr_{0.4}Co_{0.8}Cu_{0.2}O_{3-\delta}$	860	1.90445	Teraoka *et al.* (1988)
$La_{0.6}Sr_{0.4}Co_{0.8}Ni_{0.2}O_{3-\delta}$	860	1.44614	Teraoka *et al.* (1988)
$La_{0.8}Sr_{0.2}Ga_{0.7}Co_{0.3}O_{3-\delta}$	1000	1.48378	Ishihara *et al.* (2000)
$Nd_{0.6}Sr_{0.4}CoO_{3-\delta}$	820	1.02897	Ishihara *et al.* (2000)
$Pr_{0.6}Sr_{0.4}CoO_{3-\delta}$	820	0.92602	Teraoka *et al.* (1988)
$Sm_{0.6}Sr_{0.4}CoO_{3-\delta}$	820	1.19105	Teraoka *et al.* (1988)
$SrCo_{0.8}Fe_{0.2}O_{3-\delta}$	870	3.33984	Teraoka *et al.* (1985a)
$SrCo_{0.89}Fe_{0.1}Cr_{0.01}O_{3-\delta}$	880	0.63168	Kharton *et al.* (1999)
$Y_{0.05}Ba_{0.95}CoO_{3-\delta}$	900	0.52416	Brinkman *et al.* (1994)

© Woodhead Publishing Limited, 2011

2000b). This composition possesses the highest oxygen permeability ever reported and has hence attracted great interest from the research community (Wang *et al.*, 2005b, Vente *et al.*, 2006b; Zeng *et al.*, 2007; Zwick and Pfaff, 2008; Baumann *et al.*, 2010). However, recent reports indicate that BSCF suffers from thermal and chemical stability problems (Arnold *et al.*, 2007; Švarcová *et al.*, 2008).

Fluorite (AO_2)

$Ce_{1-x}Gd_xO_{2-\delta}$ (CGO) as well as $Ce_{1-x}Pr_xO_{2-\delta}$ (CPO) are very good oxygen ion conductors owing to similar host and dopant radii of Ce^{4+} and the substituents Gd^{3+} and Pr^{3+} (Navarro *et al.*, 1997; Jurado, 2001) leading to high solubility and high oxygen vacancy concentrations. The application of CGO as an electrolyte is generally considered at intermediate temperatures (500–700°C) because of considerable electronic conductivity at higher temperatures, particularly in reducing atmospheres. In the case of CPO, an additional electronic conductivity occurs at higher oxygen partial pressures owing to the mixed valence of the Pr^{3+}/Pr^{4+} pair (Lübke and Wiemhöfer, 1999). Accordingly, CPO shows enhanced p-type conductivity when compared with CGO. Additional enhancement of the electronic conductivity can be achieved by doping with transition metals such as Co (Kleinlogel and Gauckler, 2000). Further, the electronic conductivity of $Ce_{0.8}Gd_{0.2-x}Pr_xO_{2-\delta}$ increases with increasing Pr content (Fagg *et al.*, 2006; Schmale *et al.*, 2010).

Bismuth (Bi) oxide in its pure form is also the subject of constant research owing to its very high ionic conductivity, which can reach 1 S cm^{-1} for the δ form (fcc (face centred cubic) structure) at 800°C. This is attributed to the high oxygen vacancy concentration by the occupancy of only three out of four oxygen sites in the fluorite lattice (Bouwmeester *et al.*, 1992). Unfortunately, this material has a low melting point of 830°C and a dramatic phase transition at 730°C which is accompanied by a large volume change and results in large mechanical strains across the membrane. The high temperature form of the δ phase can be stabilized at room temperature by cation substitution for Bi achieved through the incorporation of Er_2O_3 (Bouwmeester *et al.*, 1992), Gd_2O_3 (Takahashi *et al.*, 1975) or Dy_2O_3 (Verkerk *et al.*, 1983), but these substitutions also lower the ionic conductivity. Solid solutions of bismuth oxide with CaO, BaO and SrO have resulted in stabilized rhombohedral phases with high conductivity at high temperature (Boivin and Thomas, 1981; Goodenough, 2003). As with perovskites, a large array of fluorite materials for oxygen production has been developed, as shown in Table 9.2. The O_2 fluxes reported in the literature for fluorite-based MIEC membranes are generally orders of magnitude below those reported for perovskite membranes, the solitary exception being BYSm which reported an oxygen flux of 0.85 ml m^{-2} min^{-1}.

© Woodhead Publishing Limited, 2011

Table 9.2 Representative oxygen fluxes of fluorite membranes

Compound	Temperature (°C)	Flux (ml min^{-1} cm^{-2})	Reference
$(Bi_2O_3)_{0.73}(CaO)_{0.27}$	680	0.00444	Capoen *et al.* (2006)
$(Bi_2O_3)_{0.75}(Er_2O_3)_{0.25}$	810	0.00868	Capoen *et al.* (2006)
$(Bi_2O_3)_{0.6}(Tb_2O_{3.5})_{0.4}$	650	0.02419	Bouwmeester and Burggraaf (1996)
$(Bi_2O_3)_{0.75}(Y_2O_3)_{0.25}$	950	0.04504	Zeng and Lin (2000)
$Bi_{0.75}Y_{0.5}Cu_{0.75}O_3$	850	0.01425	Han *et al.* (1997)
$Bi_{1.5}Y_{0.3}Sm_{0.2}O_3$	950	0.05689	Zeng and Lin (2001)
$Bi_{2.02}Co_{0.13}V_{0.85}O_z$	650	0.00022	Capoen *et al.* (2006)
$Ce_{0.8}Pr_{0.2}O_{2-\delta}$	950	0.04502	Fagg *et al.* (2006)
$Gd_{0.2}Ce_{0.6}Pr_{0.2}O_{2-\delta}$	950	0.03576	Fagg *et al.* (2006)
$(ZrO_2)_{0.85}(CaO)_{0.15}$	870	0.02275	Teraoka *et al.* (1985a)
$(ZrO_2)_{0.7}(Tb_2O_{3.5})_{0.3}$	900	0.00003	Cao (1994)
$(ZrO_2)_{0.7}(Tb_2O_{3.5})_{0.25}(Y_2O_3)_{0.05}$	900	0.00003	Cao (1994)

9.3 Principles of oxygen membrane separation

9.3.1 Oxygen transport membranes

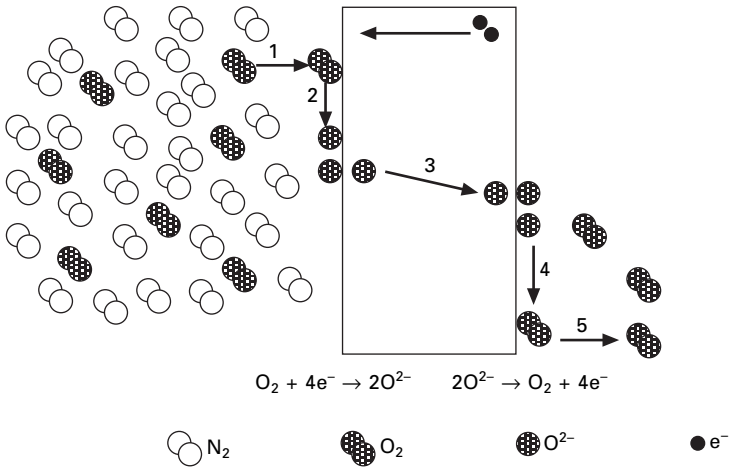
An intrinsic property of materials used in oxygen transport membranes is that they conduct oxygen ions at high temperatures, preferentially in excess of 700°C. Oxygen ions diffuse through the crystal lattice of ceramics by hopping through oxygen vacancy defect sites. This transport phenomenon in MIEC materials results in the occupancy of oxygen vacancy sites within the crystal structure and the formation of two electron holes, as given by Equation 9.2, where $V_o^{\bullet\bullet}$ represents an oxygen vacancy, O_o^x is a lattice oxygen and $h^{\bullet}$ is an electron hole.

$$V_o^{\bullet\bullet} + \tfrac{1}{2}\, O_2 \leftrightarrow O_o^x + 2h^{\bullet} \qquad [9.2]$$

In terms of membrane operation, oxygen transport involves five progressive steps shown schematically in Fig. 9.4.

- Step 1: feed side gas transport – the oxygen molecule is transported from the gas phase to the membrane surface by gas-to-gas diffusion.
- Step 2: dissociation (surface reaction) onto interface I (feed side) – the oxygen molecule adsorbs to the membrane surface and then disassociates owing to catalytic activity of the ceramic material.
- Step 3: ionic transport (bulk diffusion) – the oxygen ions diffuse through the ceramic crystal lattices, driven by a partial pressure gradient of oxygen across the membrane. Electrons are transported in the opposite direction to maintain the electrical neutrality of the membrane.
- Step 4: association (surface reaction) on interface II (permeate side) – the oxygen ions recombine into oxygen molecules and desorb from the membrane surface.

© Woodhead Publishing Limited, 2011



9.4 Schematic of O_2 permeation through a perovskite membrane.

- Step 5: permeate side gas transport – the oxygen molecules are transported to the permeate stream by gas-to-gas diffusion.

The O_2 fluxes in steps 2 and 4 are controlled by the kinetics of the surface dissociation/association reaction, whilst the flux in step 3 is controlled by the membrane's intrinsic permeability and thickness. An important concept associated with oxygen transport membranes is that of the critical length, L_c, which is defined as the thickness of a membrane at which the transport resistances due to surface kinetics and bulk diffusion are equal. In general terms, O_2 flux can be increased by reducing the thickness of the membrane until reaching the membrane's critical length. At this point, any further reduction in membrane thickness will not result in a corresponding increase in O_2 flux, as this becomes limited by the kinetics of the surface exchange reaction. In the case of BSCF perovskite membranes, the critical length is approximately 0.7–1.1 mm between 800–900°C (Hong and Choi, 2010). Thus, a BSCF hollow fibre with a thickness in the region of 200–300 μm, will be operating in the surface kinetics controlled regime. Catalysts can be employed to overcome surface kinetics limitations of thin membranes, thereby continuing to enhance oxygen flux (Leo *et al.*, 2006, 2009b).

In the case of fluorite-based compounds, some materials have very high ionic conductivity compared to their electronic conductivity. This represents a special transport limitation, as the oxygen flux is controlled by the electronic conductivity, as in most bismuth oxide and zirconia-based compounds (Dou *et al.*, 1985; Bouwmeester *et al.*, 1992; Cao, 1994; Nigara *et al.*, 1995; Han *et al.*, 1997; Kim and Lin, 2000; Zeng and Lin, 2000; Capoen *et al.*, 2006; Fagg *et al.*, 2006). Nevertheless, as the membrane thickness is decreased beyond L_c, the controlling step will no longer be bulk diffusion but instead be

© Woodhead Publishing Limited, 2011

the kinetics of the surface exchange reaction (Dou *et al.*, 1985; Bouwmeester *et al.*, 1992; Cao, 1994).

9.3.2 Bulk diffusion

The oxygen flux through oxygen transport membranes can be generally determined by the Wagner Equation [9.3] (Gellings and Bouwmeester, 1992):

$$J_{O_2} = \frac{1}{4^2 F^2 L} \int_{\mu_{O_2}(II)}^{\mu_{O_2}(I)} t_i t_e \sigma_t d\mu_{O_2} \quad [9.3]$$

$$t_i = \frac{\sigma_i}{\sigma_i + \sigma_e} = \frac{\sigma_i}{\sigma_t} \quad [9.4]$$

where J_{O_2} represents the oxygen flux, F is Faraday's constant, L is the thickness of the transport layer, t_i and t_e are the ionic and electronic transfer numbers ($0 \le t \le 1$), respectively; σ_i, σ_e and σ_t are the ionic, electronic and overall conductivity, respectively and μ_{O_2} is the chemical potential of the hypothetical neutral oxygen in the oxide.

The Wagner equation indicates that both ionic and electronic conductivity are very important material properties in determining the oxygen flux through membranes. There is a general trend reported in the literature for perovskites ($A_xA'_{1-x}B_yB'_{1-y}O_{3-\delta}$) indicating the use of lanthanum (La) (a rare earth element) and Sr or Ba (alkali earth elements) as dopants for A site cations and copper (Cu), nickel (Ni) or Fe (transition metals) as dopants for B site cations. These substitutions lead to increased ionic and electronic conductivity (0.2–1.0 S cm^{-1}) at high temperatures (> 1000°C), whilst also providing good thermal stability of the synthesized material (Badwal *et al.*, 2000). In terms of fluorites, Bi_2O_3 doped with metal oxides (Y_2O_3, Gd_2O_3, Er_2O_3, Dy_2O_3, Nb_2O_5, Ta_2O_5) becomes an oxygen-ion conductor with significantly higher conductivity of around 0.2 S cm^{-1} at lower temperatures (500°C) than doped zirconia and ceria at high temperatures (1000°C) (Verkerk *et al.*, 1980).

If there is good correlation between the oxygen ionic conductivity and oxygen partial pressure (Equation [9.5]), then the Wagner equation can be simplified to Equation [9.6] (Qi *et al.*, 2000):

$$\sigma_i = \sigma_i^o P_{O_2}^{-n} \quad [9.5]$$

$$J_{O_2} = \frac{RT\sigma_i^o}{4F^2 L}(p'^n_{O_2} - p''^n_{O_2}) \quad [9.6]$$

where J_{O_2} represents the oxygen flux, F is the Faraday's constant, L is the thickness of the transport layer; σ_i^o is the ionic conductivity at 1 atm and

© Woodhead Publishing Limited, 2011

p'_{O_2} and p''_{O_2} are the oxygen partial pressures on the feed and permeate sides, respectively. In terms of bulk diffusion, there are three regimes which can limit oxygen flux:

- oxygen vacancies
- electrons, or
- electron holes.

In the case where there are electron or electron hole transport limitations, it was found that generally $n = 1/4$ where n is the experimentally determined index of bulk diffusion. Assuming that bulk diffusion is the limiting step, the Wagner equation can be further simplified to Equation [9.7]:

$$J_{O_2} = \frac{RT\sigma_e\sigma_i}{16F^2L(\sigma_e + \sigma_i)} \ln\left(\frac{p'_{O_2}}{p''_{O_2}}\right) \quad [9.7]$$

However, one must bear in mind that these simplified versions of the Wagner equation are based on several assumptions and fitting experimental data (Lin *et al.*, 1994). In addition, there is strong evidence that different MIEC materials will behave in different ways owing to the complexity of the crystal structure and defects derived from doping with different cations. Therefore, a more comprehensive approach is required to determine the transport properties of these materials, which is outside the scope of this chapter.

9.3.3 Surface kinetics

The Wagner equation is no longer applicable when the oxygen flux is controlled by the surface exchange oxygen reaction. Hence, other relationships have been developed to explain the oxygen flux in the surface kinetics limited regime. Surface-exchange reactions for the dissociation of O_2 can be represented sequentially by (1) adsorption from the gas phase followed by (2) the charge transfer reaction between the adsorbed species and the bulk, whilst the association of O_2 can be represented by the reversed steps, that is (2) followed by (1) (Chen *et al.*, 1995). A proportionality constant, K, represents the reaction equilibrium constant for an O^x species on the membrane surface. The O^x concentration can be determined by Equation [9.8]:

$$[O^x_{(w')}] = \frac{K_{O^x_{(w')}} K^{\frac{1}{2}}_{O_{(w')}} [V^{\bullet\bullet}_{O_{(w')}}] p^{\frac{1}{2}}_{O_2}}{p^2_{(w')}} \quad [9.8]$$

where the w subscript represents the surface phase species and the single and double primes refer to interface I and II. For example, $[V^{\bullet\bullet}_{O_{(w')}}]$ is the concentration of oxygen vacancies in the surface of interface I. K is specific for each type of reaction as indicated in its subscript which refers to the primary product of the reaction (Equations [9.9] and [9.10]):

© Woodhead Publishing Limited, 2011

$$K_{O_{(w')}} = \frac{[O_{(w')}]^2}{p_{O_{2(g')}}} \quad [9.9]$$

$$K_{O^x_{(w')}} = \frac{[O^x_{(w')}]\, p^2_{(w')}}{[O_{(w')}][V^{\bullet\bullet}_{O_{(w')}}]} \quad [9.10]$$

If the oxygen flux is proportional to the concentration of species O^x, then the oxygen flux can be represented by Equation [9.11]:

$$J_{O_2} = \alpha (p'^n_{O_2} - p''^n_{O_2}) \quad [9.11]$$

where J_{O_2} represents the oxygen flux, α is the surface permeation constant and p'_{O_2} and p''_{O_2} are the oxygen partial pressures at the feed and permeate side, respectively.

The *nth* order of this equation approaches ½ for thin films and ¼ for thick films (Dou *et al.*, 1985). As with the bulk diffusion limited regime, there is also strong evidence that different MIEC materials will give different surface reaction equilibrium constants owing to the intrinsic properties of each material and the species involved in the actually rate limiting step, for example O_2^-, O_2^{2-}, O^-. For instance, erbia-stabilized bismuth oxide membranes were proposed to have $n = 5/8$ (Bouwmeester *et al.*, 1992). Therefore, a more comprehensive approach is required to determine the transport properties of MIEC materials in the surface reaction limited regime, which is again outside the scope of this chapter

9.4 Application and integration in power plants

Energy consumption is increasing worldwide and there is a great need to retain security of energy supply whilst reducing greenhouse gas emissions. Consequently, there is an increasing requirement in the construction of the next generation of fossil fuel power generation plants that they must be designed to be carbon capture ready (CCR). To meet the engineering requirements in this technological race, the first generation CCR plants are likely to operate in post combustion carbon capture mode, where conventional and mature technologies will be employed. However, there is a raft of options available to power generators, who are seeking simpler solutions to replace the complexities and inefficiencies of first generation carbon capture technologies such as amine adsorption/strippers. Within this theme, two power generation processes are attracting significant attention and investment from governments and industry around the world, namely oxyfuel coal combustion and coal gasification. Oxygen is a central feedstock for these power generating processes underlining the importance of an air separation unit capable of delivering tonnage oxygen.

© Woodhead Publishing Limited, 2011

9.4.1 Oxyfuel coal combustion

The oxyfuel coal combustion process, incorporating a membrane unit for air separation, is schematically illustrated in Fig. 9.5. This process differs from conventional coal combustion in that the coal is combusted in the presence of pure O_2 rather than air. As a result, oxyfuel coal combustion generates a flue gas that consists predominately of CO_2 and water, with small amounts of nitrogen and sulfur oxides, ash and trace elements (Wall *et al.*, 2009). Water and ash can be easily removed through conventional condensation and filtration respectively, leaving a flue gas stream containing highly concentrated CO_2 (80–90%). The small concentration of nitrogen oxides is mainly associated with nitrogen contained within the coal and small leaks in the boiler, pipelines and other plant equipment. The flue gas stream can be further purified by partial liquefaction and phase separation to increase the purity of CO_2 to 96% (Kakaras *et al.*, 2007; Hadjipaschalis *et al.*, 2009). Economics will determine whether further purification will be required, as the cost of purification will have to be balanced against storage requirements and costs. The purified CO_2 stream can then be transported and safely stored by a number of new technological methods under development as reported elsewhere (Doctor *et al.*, 1997; Bachu, 2000, 2002; Flett *et al.*, 2007).

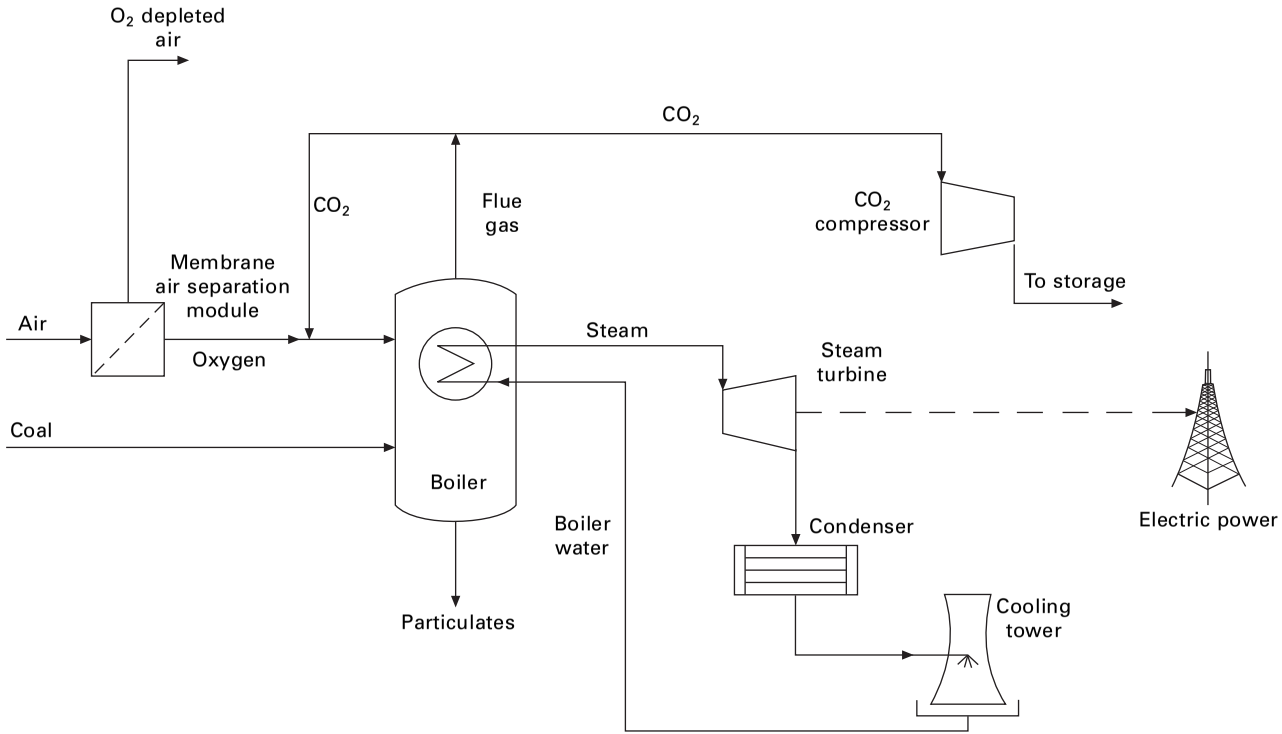
The steam generated in the boiler is used to drive the turbine via a Rankine cycle, thus producing electrical power via a generator. Combustion of coal with pure oxygen generates elevated temperatures, beyond the thermal limitations of current boiler designs. One way of overcoming this challenge is to recycle the concentrated CO_2 flue gas back into the boiler as a heat sink. In other words, CO_2 from the flue gas stream is used to dilute the oxygen feed before combustion, thus controlling the temperature in the boiler (Leo *et al.*, 2009a). The recycling rates of CO_2 flue gas will largely depend upon on the coal properties and boiler operation, nevertheless dilutions of approximately 30% O_2 in CO_2 will give similar burner flame temperatures to standard air blown boilers (Wall *et al.*, 2009).

9.4.2 Coal gasification

Coal gasification or pre-combustion is an old process used as early as the 1900s to generate town gas, now known as syngas, a mixture of predominately carbon monoxide (CO) and hydrogen (H_2). Current technical developments suggest efficiencies of up to 50% are possible as an 'integrated gasification combined cycle' (IGCC) which could employ fuel cells as part of a topping cycle, as illustrated in Fig. 9.6, making this process very attractive (Haupt *et al.*, 2003; Beér, 2007; Descamps *et al.*, 2008; Pérez-Fortes *et al.*, 2009). In the IGCC process, coal is gasified under pressure with steam and oxygen, less than required for combustion, to make syngas. The particulates (e.g.

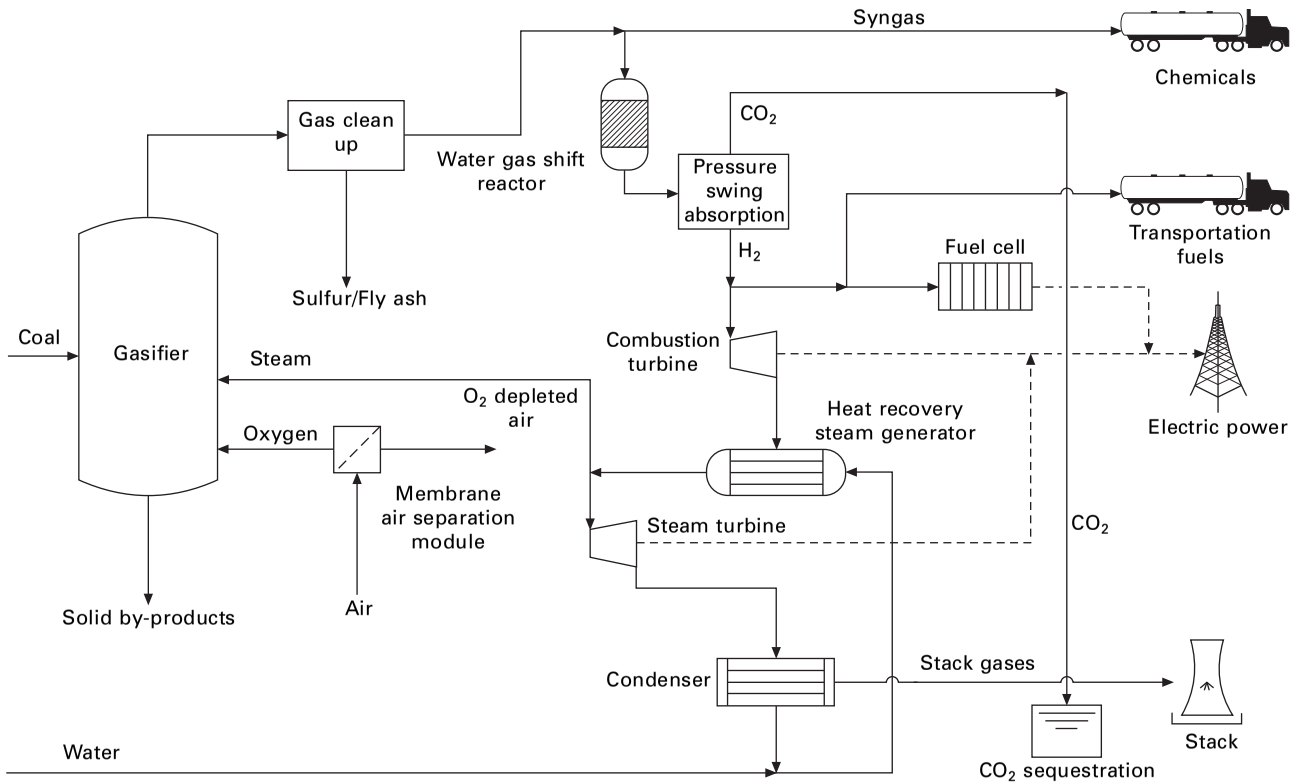
© Woodhead Publishing Limited, 2011

© Woodhead Publishing Limited, 2011



9.5 Schematic of an oxyfuel coal combustion power plant with a membrane air separation unit.

© Woodhead Publishing Limited, 2011



9.6 Schematic of a IGCC with a carbon capture and membrane air separation unit.

ash) entrained in the syngas stream are initially trapped in candle filters or other hot gas cleaning technologies at temperatures up to 600°C (Eriksson *et al.*, 1993; Mazaheri *et al.*, 2003; Sharma *et al.*, 2008). The sulfur in the coal is reduced to H_2S during coal gasification. This compound has a major impact on downstream reaction or separation processes and, as a result, a desulfurization unit precedes any further syngas processing.

The CO component in the syngas can be converted via the water gas shift reaction to produce more H_2, although CO is converted into CO_2. The H_2 component of the syngas can be combusted in a gas turbine or used directly in a fuel cell to generate power, while the heat contained in the turbine exhaust or generated by the fuel cell can be recovered and used to generate more power via a Rankine cycle, yielding high overall efficiencies. In addition, IGCC departs from the conventional power generation paradigm, as the plant can also deliver syngas for gas to liquids (GTL) production of fuels and H_2 production for energy and transportation fuel cell systems. Syngas and/or H_2 both attract higher value-added margins compared to electricity, which can confer an IGCC process with major economic advantages over conventional power generation systems for carbon capture and storage (Smart *et al.*, 2010).

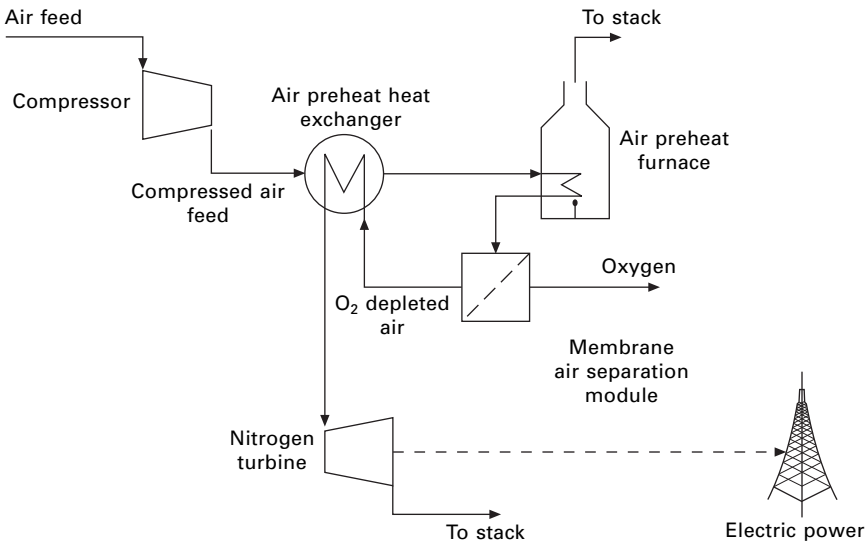
9.4.3 Process integration

A key enabling technology in both oxyfuel coal combustion and IGCC is the air separation unit. There are two common technical problems for the integration of ceramic membranes into both processes. First, MIEC membranes operate efficiently and deliver relatively high oxygen fluxes only at elevated temperatures (900°C), hence heat integration becomes paramount. Second, the partial pressure of oxygen in atmospheric air is approximately 21 kPa, which is too low to generate any significant driving force across the membrane. Hence, air must be compressed to pressures preferably above 2 MPa. A final point of interest is that process safety is a major concern, particularly when handling pure O_2 at these high temperatures.

Mixed ion electronic conducting (MIEC) membranes in oxyfuel coal power plants

Figure 9.7 shows a process flow diagram of a membrane system supplying oxygen to an oxyfuel coal power plant, where a membrane-based air separation train is integrated at the front end of the plant. Air is initially compressed to at least 1 MPa to induce the required O_2 partial pressure gradient across the membrane. This compression from initial atmospheric conditions to a variable pressure, P_f, and temperature, T_f, is energy intensive and represents a significant energy penalty for the separation train (Schneider *et al.*, 2007).

© Woodhead Publishing Limited, 2011



9.7 Schematic of MIEC membrane air separation unit supplying pure oxygen to an oxyfuel coal power plant.

The temperature at the outlet of the compressor (T_f) will reach 300–350°C, depending on the isentropic efficiency of the compressor and the overall process conditions. This temperature is still below the high temperatures (> 900°C) currently required for large-scale air separation using MIEC membranes. Hence, further heat is required, some of which can be obtained using traditional heat integration with the hot nitrogen-enriched air stream leaving the MIEC membrane unit, or the hot flue gas stream leaving the oxyfuel boiler. However, both these sources will be unable to supply the high grade heat required to reach optimal operating temperatures of > 900°C. Thus, it will be necessary to deploy a furnace, burning extra coal or natural gas, to preheat the air via heat exchangers to 900°C or more (Leo *et al.*, 2009a). The advantage of the preheater unit is that it utilizes waste heat and reduces consumption of fuel in the furnace. The outlet of the MIEC membrane unit, called the retentate stream, consists of oxygen-depleted or nitrogen-enriched air which retains significant energy content owing to the high pressure and high temperature operating conditions of the unit. Some of the excess heat can be recovered via the preheater unit, while the remainder of the heat and mechanical energy can be recovered by expanding the gas through a turbine to generate additional electricity. The process described and illustrated in Fig. 9.7, is a simplified version of the more comprehensive configurations possible in oxyfuel coal power plant design.

The oxygen flux through an MIEC membrane depends on the oxygen partial pressure gradient established across the permeate and retentate streams.

© Woodhead Publishing Limited, 2011

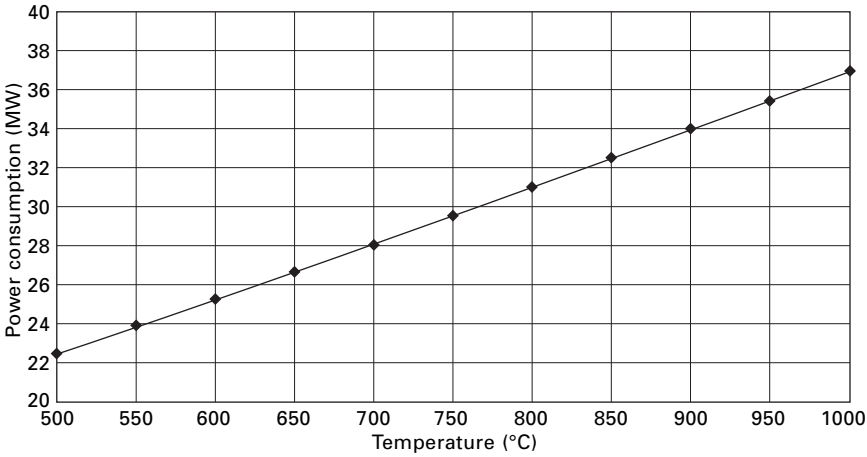
For instance, if the partial pressure of O_2 in the permeate stream is kept at approximately atmospheric pressure (101 kPa), then the partial pressure in the oxygen-depleted retentate stream will always have to exceed 101 kPa. If the oxygen partial pressure gradient drops to zero, then equilibrium is reached and no oxygen flux is observable through the membrane. As the oxygen flux is proportional to the partial pressure gradient across the membrane, it can be increased by increasing the oxygen partial pressure on the feed side and/or by reducing the partial pressure of oxygen in the permeate stream. The former can be accomplished through conventional compressors, as discussed above, whilst the latter can be achieved using vacuum pumps or a sweep gas stream. The concept of recycling the flue gas containing a high concentration of CO_2 into the oxyfuel boiler can be taken a step further by utilizing it as a sweep gas for the permeate stream of the MIEC membrane unit (Engels *et al.*, 2010; Stadler *et al.*, 2011). Although this concept would be beneficial in terms of process operation, the reality is that MIEC membranes are chemically unstable to carbon dioxide and would quickly deteriorate, rendering them ineffective for further oxygen separation from air.

Effective energy recovery is paramount for MIEC membranes to surpass traditional cryogenic air separation. Using AspenPlus™ software, the energy consumption for the process flow diagram in Fig. 9.7 was modelled. The base case was an oxyfuel coal power plant exporting 100 MW and an air compressor with 72% isentropic efficiency. We found that increasing the operating pressure from 1 to 5 MPa while maintaining the operating temperature at 900°C resulted in almost no significant increase in overall energy consumption. Whilst the air compressor could consume as much as 32 MW for a P_f of 1 MPa, approximately 75% of this energy can be recovered by the nitrogen turbine. In other words, the highest consumer of process energy was the air preheat furnace. As an example, Fig. 9.8 shows the AspenPlus™ modelling results of varying the operating temperature for the membranes, whilst keeping the amount of oxygen delivered by the membrane unit the same. It is observed that reducing the operating temperature from 1000 to 500°C, allows a reduction in energy consumption from 36.9 to 22.5 MW, equivalent to 39%. This simple example illustrates the necessity of further reducing the operating temperature of the membranes to below 700°C, for easy heat integration and increased process efficiency.

MIEC membranes in integrated gasification combined cycle (IGCC) plants

The integration of MIEC membranes in IGCC power plants could be accomplished through the same process as the oxyfuel coal power plant as shown in Fig. 9.6. However, there are several additional options for process integration of MIEC membranes in IGCC plants. An IGCC plant can produce

© Woodhead Publishing Limited, 2011



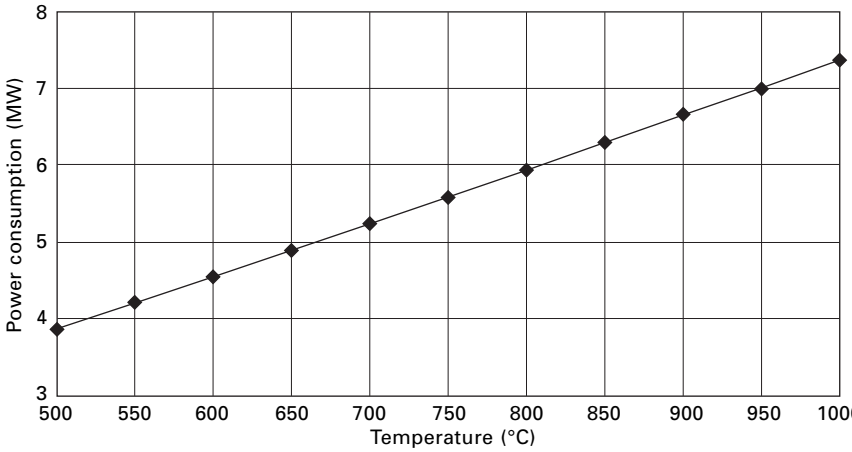
9.8 Power consumption of a MIEC membrane air separation unit for a 100 MW power output oxyfuel coal power plant.

hydrogen by separating it from the syngas stream prior to or following the water gas shift reaction. The major advantage here is that gas turbines burning pure hydrogen generate high temperatures, and theoretically deliver more power and increased efficiencies. In reality, this process configuration depends on the next generation of staged turbines utilizing exotic high temperature materials which are currently not available. Hence, one option is to dilute (or combust depending on the oxygen depletion) the hydrogen with the nitrogen-enriched air from the retentate stream of the MIEC module in the turbine (Shah, 2006). This would reduce combustion temperatures and control flame speed (Shah *et al.*, 2005).

The energy and economic penalties for integrating MIEC membrane modules in an IGCC plant are lower than for oxyfuel coal power plants for several reasons. First, the oxygen consumption in oxyfuel combustion is a more critical component for CO_2 capture than in an IGCC plant, because the latter also uses water as a reactant. Therefore, oxyfuel coal combustion may require up to three times the amount of oxygen compared to an IGCC process. This translates to smaller MIEC membrane air separation units in IGCC systems, reducing the capital costs and overall plant footprint. Second, the syngas stream leaving the gasifier (Fig. 9.6) provides waste heat at a higher duty with temperatures between 1000–1100°C, so the potential for heat integration is greater. Third, the syngas produced by the coal gasifier can be used as a fuel in the air preheat furnace to reach the required operating temperatures of the membrane module. Hence, this eliminates the capital cost, operating costs and storage requirements associated with the purchase of natural gas, or excess coal to run these burners.

Nevertheless, Fig. 9.9 shows the likely energy consumption of a MIEC

© Woodhead Publishing Limited, 2011



9.9 Power consumption of a MIEC membrane air separation unit for a 100 MW power output IGCC power plant.

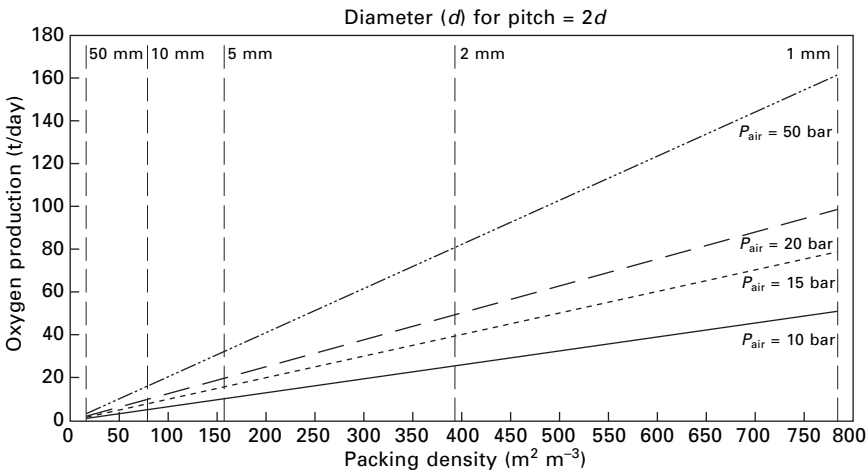
membrane air unit (operating as shown in the process flow diagram in Fig. 9.7) in an IGCC power plant. The base case here is again supplying pure oxygen for an IGCC plant exporting 100 MW. It is observed that the energy consumption varies between ~4–7.5 MW, which is almost one order of magnitude below the energy consumption for oxyfuel coal power plants. This clearly demonstrates the potential attractiveness of attaching a MIEC membrane air separation unit at the front end of an IGCC power plant. Again heat to take the air to high operating temperatures is the major energy consuming item. Thus reducing the operating temperature from 1000 to 500°C gives 52% energy savings provided that the oxygen permeation rates can be kept constant by applied research.

9.5 Oxygen transport membranes

9.5.1 Membrane geometries

There are a number of membrane geometries that could be assembled into membrane modules for air separation. The major membrane configurations currently being pursued by both industry and research groups around the world, include the flat membranes developed by Air Products and Chemicals, Inc., tubes, monoliths and hollow fibres. In industrial applications, the footprint area of an air separation unit should be small, a principle that benefits membrane unit operations with a large surface area to unit volume ratio such as hollow fibre geometries. For instance, Fig. 9.10 shows an ideal calculation of oxygen production based on Equation [9.6] and an air separation module operating with tubular MIEC membrane geometries

© Woodhead Publishing Limited, 2011



9.10 Oxygen production versus membrane packing density.

of diameter (d) at 900°C with a total feed air pressure (P_f) of 50 bar and delivering a permeate stream of pure oxygen at a flux of 10 ml m^{-2} min^{-1} at 1 bar. These results clearly indicate that high oxygen production can be achieved only through high feed air pressures, small membrane diameters and high packing densities. The highest value of 160 tonnes of oxygen per day is delivered by a module incorporating membranes with diameters of 1 mm, equivalent to hollow fibre dimensions. Increasing the diameter of the membranes leads to a large decrease in oxygen production.

The complete design of MIEC membrane modules will have to take into consideration engineering parameters and the mechanical properties of the membrane materials. One of the problems of using hollow fibres is that high gas velocities in the inner shell of the hollow fibre may lead to turbulent oxygen flow. Coupled with high temperatures (> 900°C), this may result in high shear stresses on the walls of the hollow fibre, causing internal erosion and possibly leading to failure of the membrane. Further, the problem of gas velocities is associated with the length of membrane. Abdel-Jawad and co-workers (Abdel-Jawad *et al.*, 2007) developed computational fluid dynamics modelling of gas flow fields on both sides of the membrane and demonstrated that gas velocities tend to increase along the membrane length towards the exit of the membrane permeate stream. This means that the risk of hollow fibre failure could increase at the oxygen air exit. Further, ceramic hollow fibres *per se* are mechanically fragile and sealing them is complicated. This all alludes to the fact that the length of hollow fibres in MIEC membrane modules will be limited. These engineering design challenges are likely to be similar for flat membrane geometries, but less so for tube geometries.

Studies performed at the Energy Centre of the Netherlands have investigated membrane modules using tubes, flat and hollow fibre membranes (Vente *et*

© Woodhead Publishing Limited, 2011

al., 2006a). Their base case considered the design of a full-scale air separation unit with a total capacity of 30 000 Nm^3 oxygen per hour, requiring 5000 m^2 membrane area, and allowed a maximum gas velocity in the module of 25 m s^{-1}. They found that a minimum of 32 modules were required for single-hole tubes (d = 19 mm), followed by 39 modules containing multi-channel monoliths (d = 100 mm), 120 modules with multiple tube-and-plate assemblies (d = 70 mm) and finally 1800 modules containing hollow fibres (d = 1 mm). These results clearly indicate that whilst the high surface area to volume ratio and packing density of hollow fibres is attractive, the gas velocity limitations mean that the number of hollow fibre modules is excessive for large scale oxygen production, and a solution towards tube or plate geometries may be preferred.

9.5.2 Membrane sealing

Membrane sealing is one of the areas of highest risk in membrane technology, particularly for ceramic membranes operating at high temperatures (> 900°C) and pressures (> 10 atmospheres). For these applications the seal technology must deliver a gas tight membrane without substantially affecting the mechanical and chemical properties of the ceramic membranes. For instance, excessive radial pressure with compressive seals can lead to the failure of ceramic tubes (Duke *et al.*, 2004). A second issue is that high temperature seals often include exotic ceramic materials for interconnecting various tubes or flat cells and are likely to have a low thermal cycling capacity. These issues emphasize the fact that reducing the sealing area per membrane area will also reduce the risk of failure at the membrane/seal interface.

Owing to the high temperature operation of MIEC membranes, glasses or ceramic seals are the best candidates to deliver gas tight seals. Borosilicate glass is commonly the primary ingredient although mixtures of glass with ceramics have also been tested. Ideally glass–ceramic seals should have good wettability for the membrane and the module casing, suitable viscosity and rigidity to seal the membrane interface and membrane casing, and good thermal expansion compatibility with all materials used in the membrane and its casing (Qi *et al.*, 2000). Metal materials such as silver (as a solid ring or liquid paste) and gold (as a solid ring) have also been used as a sealant (Xu and Thomson, 1998; Kim and Lin, 2000; Kobayashi *et al.*, 2006). In the case of the paste, the sealant is usually heated up to a temperature where the solvent is evaporated to form intact seals. These sealants can also be softened to ensure they are gas tight at high temperature prior to permeation or reaction. Solid metal rings achieve gas tightness by exerting compression, normally applied through spring clamps, between the metal ring and membrane. The drawback is the increased risk of crack formation induced from compression forces and thermal stresses.

© Woodhead Publishing Limited, 2011

The choice of membrane sealant is strongly dependent on the application and operation conditions and sealing MIEC membranes at high temperatures and pressures remains one of the major unresolved engineering issues. For instance, the inertness of glass seals containing exotic materials is largely questioned. During high temperature operation, diffusion of the sealant material into the ceramic membrane or even onto the membrane surface area is a possibility if some of the sealant materials become volatile. As a result, this may reduce the effective surface area and lead to performance degradation (Qi *et al.*, 2001). Metals such as silver or gold are attractive owing to their chemical inertness and durability at high temperature.

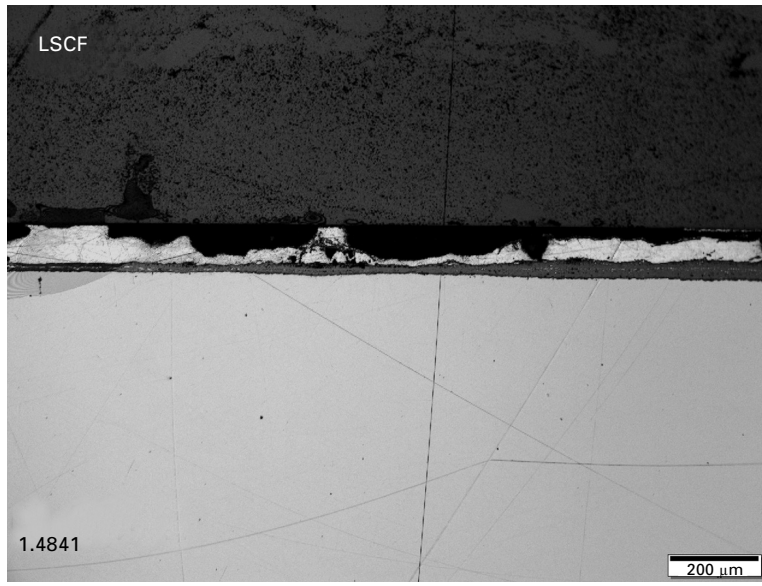
Figure 9.11(a) shows a joining and sealing assembly containing a LSCF membrane disk followed by an AgCu seal and 1.4841 (314 AISI) stainless steel. A similar set up was also employed using an AgCuTi sealant and/or BSCF membrane disks. Table 9.3 presents the gas leak rate for different sealing compounds on LSCF and BSCF disks, using helium as the gas leakage probe. These results indicate that the gas leak rate was orders of magnitude lower for sealing LSCF assemblies compared with the BSCF assembly. One point of consideration here is that the variation in surface tension between ceramics and metals (Bhalla *et al.*, 2000) causes low wettability of metal pastes for the ceramic surface, leading to non-gas-tight membranes. An example is depicted in Fig. 9.11(b) for a silver-based metal paste.

9.5.3 Structural and chemical stability

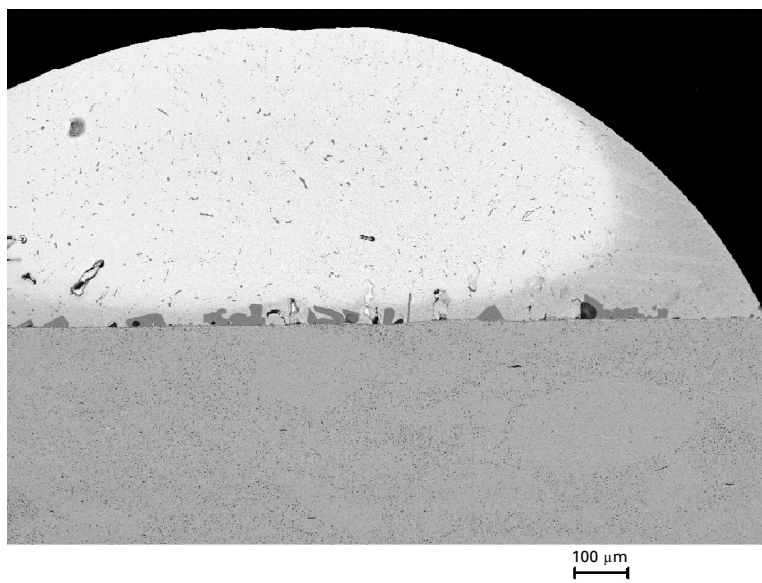
The chemical and structural stability of MIEC membranes is paramount for their successful adoption in industrial air separation units. To this end, membranes are expected to operate continuously, with an expected lifetime in excess of two years or longer. One of the stability problems in MIEC membranes is linked to creep, a common behaviour under the high operating temperatures in a wide range of perovskites such as LSFC ($La_xSr_{1-x}Co_yFe_{1-y}O_{3-\delta}$) and BSCF among many other compositions (Wolfenstine *et al.*, 1996, 2000; Majkic *et al.*, 2000, 2002; De Arellano-López *et al.*, 2001). Creep causes deformation of the ceramic crystal structure and is attributed to grain boundary sliding. The latter occurs because the formation of oxygen vacancies in MIEC materials is associated with the formation of free space within the crystal structure. Consequently, some of the cations of the MIEC materials may diffuse into the free space resulting in creep. The creep rate increases as a function of oxygen vacancies, which in turn increases with high temperatures (Lein *et al.*, 2006; Yi *et al.*, 2009). Hence, creep can be reduced by operating MIEC membranes well below 900°C. Creep can also be caused by crystal phase transition from hexagonal to cubic structure as reported for BSCF between 880 and 905°C (Yi *et al.*, 2009).

MIEC materials should preferably have stable cubic phase crystal

© Woodhead Publishing Limited, 2011



(a)



(b)

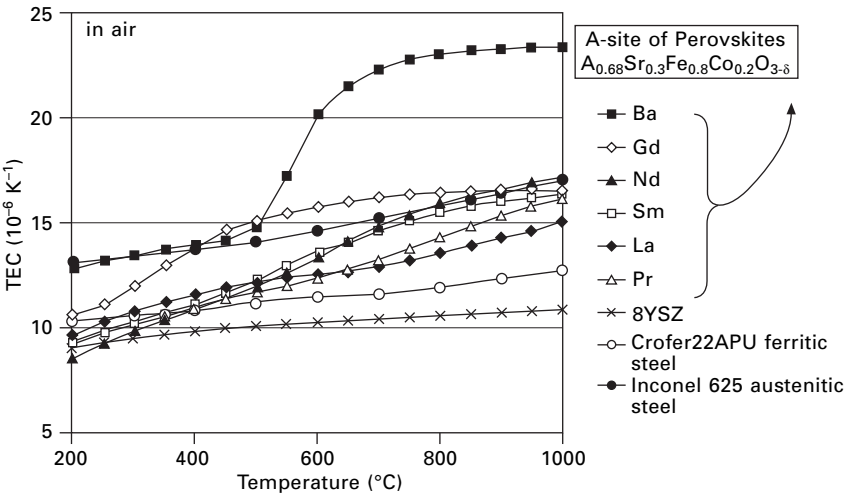
9.11 (a) LSCF metal paste LP17 (AgCu) and brazing 1.4811 assembly, (b) non-wettability of a metal paste containing Ag on the surface of a ceramic material.

structures. However, a number of compounds with good oxygen ionic transport properties experience a phase transition in the crystal structure from a cubic structure to a non-cubic structure. This phenomenon can lead to a

© Woodhead Publishing Limited, 2011

Table 9.3 Gas leakage rate to MIEC disk membranes using metal pastes and brazings

He leakage rate (mbar l s^{-1})	Single disk only	AgCu sealant	AgCuTi sealant
BSCF	1×10^{-7}	3×10^{-7}	2×10^{-6}
LSCF	6×10^{-8}	5×10^{-8}	4×10^{-8}



9.12 Thermal expansion coefficient (TEC) for a range of MIEC materials and reference materials. Data sourced from Serra *et al.* (2008).

sudden volumetric change as well as a sudden decrease of oxygen flux at the transition temperature (Kruidhof *et al.*, 1993). One approach to suppress this unwanted phase transition in order to stabilize the cubic structure is the partial substitution of the MIEC compounds with other metal cations. Examples include Ba doping onto the A-site of $SrCo_{0.8}Fe_{0.2}O_{3-\delta}$ (Shao *et al.*, 2001), Ce and Zr doping onto the B-site of $BaFeO_{3-\delta}$ (Zhu *et al.*, 2006; Watanabe *et al.*, 2009), La doping onto the A-site of $SrCoO_{3-\delta}$, Ce, Cr, Nb, Sc, Sn, Ti, V, Y, Zr doping onto the B-site of $SrCoO_{3-\delta}$ (Nagai *et al.*, 2007) and Bi doping onto the A-site and B-site of $BaSc_{0.1}Co_{0.9}O_{3-\delta}$ (Sunarso *et al.*, 2010).

The effects of temperature and chemistry on the thermal expansion coefficient (TEC) of MIEC membranes are illustrated in Fig. 9.12. The TEC is generally non-linear as a function of temperature for a large number of perovskite compounds based on $A_{0.68}Sr_{0.3}Fe_{0.8}Co_{0.2}O_{3-\delta}$, where the A site ($A_{0.68}$) was replaced by several oxides. BSCF in particular shows a highly non-linear behaviour, especially between 500 and 600°C. The change in TEC

© Woodhead Publishing Limited, 2011

is chemically induced by the increase in the number of oxygen vacancies in the perovskite structure and expansion of the oxygen octahedral. On the other hand, the fluorite 8YSZ demonstrates an almost linear increase in TEC with increased temperature. Two stainless steels from Crofer (ferritic) and Inconel (austenic) have been included to demonstrate the mismatch in TEC of the module casing compared to the membrane. LSCF is the only perovskite material that gives an almost linear thermal expansion behaviour above 400°C, being slightly non-linear below this temperature.

Material instability can also be induced by process conditions and the detrimental effects caused by CO_2, water and sulfur on MIEC membranes are well documented. These substances are routinely found in air and give a clear indication that air cleaning guard beds may be required prior to the MIEC membrane module. At high temperatures, CO_2 reacts with alkaline earth elements to form carbonates. Carbonates do not conduct ions and hence are detrimental to oxygen flux; in addition their formation disrupts the MIEC crystal structure leading to the degradation of the membrane.

BSCF materials are particularly prone to chemical instability and exposure to CO_2 results in a membrane completely impermeable to oxygen (Arnold *et al.*, 2007). Severe degradation can also occur by the synergistic effect of water and CO_2 forming bicarbonates (Yi *et al.*, 2005). LSCF also undergoes a carbonation reaction that leads to the formation of $SrCO_3$, La_2O_3, $Fe_{21.34}O_{32}$ and CoO during CO_2 adsorption and desorption at 800°C (Yang *et al.*, 2006). Similar effects were observed for other MIEC compounds such as $Sr_{0.95}Ca_{0.05}Co_{0.5}Fe_{0.5}O_{3-\delta}$ (Homonnay *et al.*, 2002). The presence of sulfur in air also destabilizes the structure of $BaCo_xFe_yZr_zO_{3-\delta}$ (BCFZ) membranes and results in Ba segregation from the BCFZ matrix, leading to lower oxygen fluxes (Wang *et al.*, 2006).

The long-term integrity of MIEC materials is also influenced by other important process considerations. For example, stable oxygen fluxes were obtained for LSCF (Schlehuber *et al.*, 2010) and BSCF (Shao *et al.*, 2000b) membranes operating for 3000 and 1000 hours under air/helium and air/argon, respectively. However, these tests are far from industrial conditions, which will require a gradient of air/oxygen. The effect of operating under oxidative conditions warrants further research and development. In addition, BSCF membranes are particularly prone to mechanical/thermal failure. Replacing strontium in BSCF with zirconium, forming BCFZ, resulted in superior mechanical integrity. The BSCF membranes cracked after 500 hours while the BCFZ membranes showed no failure after 2200 hours of testing (Schiestel *et al.*, 2005). As discussed at length, operating temperature and temperature cycling are also important parameters for MIEC membranes and process integration. Whilst reducing the operating temperature is highly desirable, this can induce phase transitions in BSCF materials in particular (Švarcová *et al.*, 2008). The evaluation of BCFZ membranes at low temperature operation

© Woodhead Publishing Limited, 2011

(400–500°C) was successful by Caro's group in Germany (Wang *et al.*, 2008). Although the oxygen flux declined over time, the BCFZ membrane could be regenerated by thermal treatment at 925°C for 1 hour in air.

9.6 Future trends

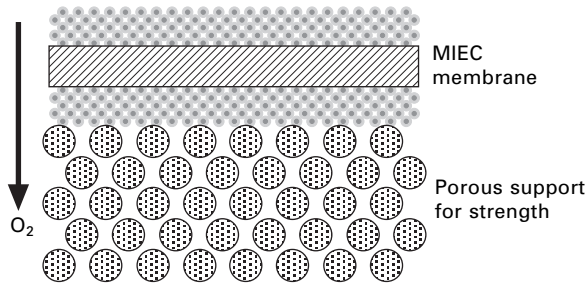
Membrane systems offer great advantages as they can operate at varying temperatures, pressure loads and flow regimes and offer great flexibility in process integration. As the development of MIEC materials advances, there is a need to depart from ideal laboratory conditions to industrial operation, where the membrane systems will have to cope with impurities, fouling, material degradation, sealing, thermal and chemical expansion of materials, in addition to non-standard operating conditions such as cooling and heating cycles, start up and shut down. Prolonged stable operation under all process conditions is crucial to meet industrial and commercial viability. This means that the MIEC membranes must be able to withstand exposure to feed air containing some CO_2 and H_2O, and traces of SO_X and NO_X. Long-term oxygen permeation data from realistic air atmospheric feeds containing CO_2 and H_2O is presently lacking. In addition, there are substantial issues with the fabrication and lifetime of MIEC membranes in terms of gas tight seals and thermal cycling. Degradation of these materials in operation leads to a decrease in the oxygen flux and any defects or cracks leads to catastrophic mechanical failure.

While the oxygen flux improves with temperature, both the IGCC and oxyfuel process economics favour operating these membranes at temperatures < 900°C. In order to operate the devices at a low temperature, it is essential to use thin films (< 100 μm) of MIEC materials on a stronger porous substrate. At these thicknesses, the membrane strength needs to be augmented by incorporation of another metallic or ceramic phase, as schematically illustrated in Fig. 9.13. In this case, the MIEC membrane is sandwiched between two porous layers, while one side of the porous layer is anchored to a larger and stronger porous support. This conceptual design has many advantages:

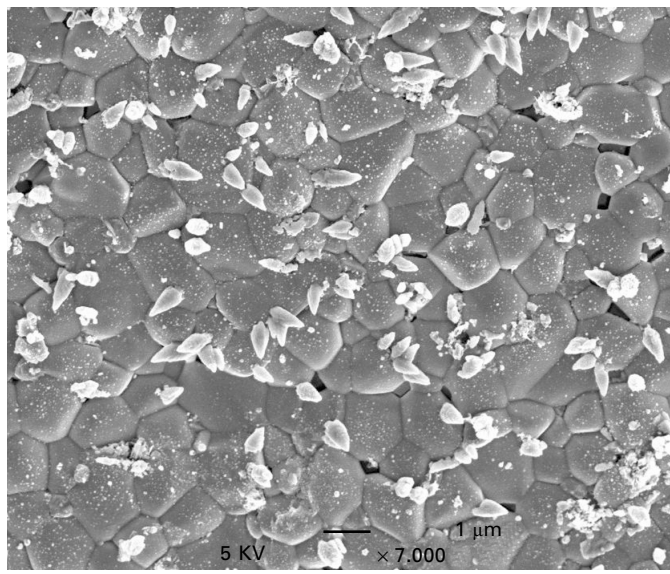
1. The porous layers adjacent to the MIEC film increase the mechanical and thermal stability of the membrane, while the porous substrate adds mechanical robustness.
2. The porous layers can be designed to match the TEC of both MIEC film and porous substrates.

On the other hand, the use of porous materials brings disadvantages as it reduces the effective area for oxygen transport through the MIEC membrane. Furthermore, many MIEC materials have highly non-linear thermal expansion behaviour (Fig. 9.12) and matching the TEC for different materials may prove challenging.

© Woodhead Publishing Limited, 2011



9.13 Conceptual design of a thin film MIEC membrane sandwiched between porous layers and anchored on a porous support.



9.14 SEM micrograph of a BSCF coated with silver nano-catalysts.

As the film thickness is reduced below 100 μm, bulk diffusion of oxygen ions is no longer the rate limiting step in oxygen permeation. Figure 9.14 shows the surface of a BSCF membrane coated with silver nano-catalysts. The silver coated BSCF membranes demonstrated up to 100% increase in oxygen permeation at 700°C (Leo *et al.*, 2009b), an attractive solution for operating MIEC membranes at low temperatures. However, the positive effect of the catalyst was less prominent at higher temperatures (950°C), only achieving a 10% improvement in O_2 permeation compared to non-coated membranes (Leo *et al.*, 2009b). This demonstrates that the right balance must be attained between the catalyst, the MIEC membrane and the operating conditions. If correctly balanced and optimized, the layers adjacent to the MIEC membrane

© Woodhead Publishing Limited, 2011

in Fig. 9.13 could well be made of porous catalysts, and/or mixed catalysts and ceramics.

Despite the initial discoveries about oxygen transport membranes that were made over 30 years ago, a large concerted effort by the research community, committed to the development of MIEC materials, remains. The bulk of research and development (R&D) of MIEC membranes is still at the development stage. On the other hand, the deployment of CCS schemes and the press for clean energy from fossil fuels is increasing and there is need to take MIEC technology to demonstration. Current R&D is mainly focused on materials; however, one area that requires immediate attention is the mechanical engineering design of MIEC modules, particularly given the design constraints related to high temperature operation, gas tight sealing systems and differing TECs in the MIEC materials and the materials of construction. It is imperative that innovative mechanical engineering designs are developed to meet the future needs of large membrane modules integrated into CCS enabled IGCC and oxyfuel power plants (Smart *et al.*, 2010).

One example of innovative mechanical engineering design is the flat membrane wafer configuration developed by Air Products and Chemicals as depicted in Fig. 9.15. The membrane wafers can be assembled in stacks and have a central oxygen collector tube (permeate stream). This design reduces the sealing area per membrane area, whilst also providing a large MIEC membrane packing density, translating to high oxygen fluxes per unit volume. Air Products and Chemicals has scaled up this design to deliver 5 tonnes of oxygen per day and this module has now been tested for over 515 days. This MIEC membrane design currently represents the closest air separation unit to commercialization.

9.7 Conclusions

There has been a concerted effort for the last three decades to improve the oxygen flux of ceramic membrane technology. A large array of compounds have been synthesized and tested and best performance has been achieved with perovskite followed by fluorite compounds. In all cases, the high operating temperature (> 900°C) remains an impediment to the industrial uptake of this technology. Separating oxygen from air at high operating conditions attracts severe energy penalties, adding up to 25% in energy losses. In addition, high temperature operation to heat air in excess of 900°C requires a furnace and burning fuel, thus adding extra plant capital and operating costs.

In terms of integrating ceramic membranes into industrial plants, process engineering principles point to low temperature operations, preferably below 700°C. However, at this temperature oxygen fluxes are very low, thus requiring large membrane air separation units to deliver tonnage oxygen supply. This adds extra capital cost to the plant. Hence, it is necessary to trade off the

© Woodhead Publishing Limited, 2011



9.15 Planar ITM ceramic membrane stacks. (Copyright 2010 Air Products and Chemicals, Inc. All rights reserved.)

membrane's oxygen fluxes versus temperature, which in tandem also affect capital and operating costs.

The engineering of ceramic air separation units is an area that warrants further development. The mechanical design of these units requires clever designs owing to the non-linear coefficient of expansion of many ceramics which must match the robust metal design of the pressure vessel. Sealing membranes at high temperatures and pressures remains an area of high risk, in particular for delivering the high purity oxygen required in many industrial processes. Finally, long-term chemical stability is paramount for the integration of ceramic air separation units in industrial process. These challenges will provide many research and development opportunities for years to come.

9.8 Acknowledgements

The authors would like to acknowledge financial support from the European Community Framework Project (FP7) project NASA-OTM, under grant number NMP3-SL-2009-228701. Simon Smart and Joao C. Diniz da Costa

© Woodhead Publishing Limited, 2011

also acknowledge financial support from the Australian Research Council Discovery Program under grant number DP0878849.

9.9 References

Abdel-Jawad, M. M., Gopalakrishnan, S., Duke, M. C., Macrossan, M. N., Schneider, P. S. and Diniz Da Costa, J. C. (2007) 'Flowfields on feed and permeate sides of tubular molecular sieving silica (MSS) membranes'. *Journal of Membrane Science*, **299**, 229–35.

Al Daroukh, M., Vashook, V. V., Ullmann, H., Tietz, F. and Arual Raj, I. (2003) 'Oxides of the AMO3 and A2MO4-type: structural stability, electrical conductivity and thermal expansion'. *Solid State Ionics*, **158**, 141–50.

Arnold, M., Wang, H. and Feldhoff, A. (2007) 'Influence of CO_2 on the oxygen permeation performance and the microstructure of perovskite-type $(Ba_{0.5}Sr_{0.5})(Co_{0.8}Fe_{0.2})O_{3-\delta}$ membranes'. *Journal of Membrane Science*, **293**, 44–52.

Bachu, S. (2000) 'Sequestration of CO_2 in geological media: criteria and approach for site selection in response to climate change'. *Energy Conversion and Management*, **41**, 953–70.

Bachu, S. (2002) 'Sequestration of CO_2 in geological media in response to climate change: road map for site selection using the transform of the geological space into the CO_2 phase space'. *Energy Conversion and Management*, **43**, 87–102.

Badwal, S. P. S. and Ciacchi, F. T. (2001) 'Ceramic membrane technologies for oxygen separation'. *Advances Materials*, **13**, 993–6.

Badwal, S. P. S., Ciacchi, F. T. and Milosevic, D. (2000) 'Scandia–zirconia electrolytes for intermediate temperature solid oxide fuel cell operation'. *Solid State Ionics*, **136–7**, 91–9.

Balachandran, U., Ma, B., Maiya, P. S., Mieville, R. L., Dusek, J. T., Picciolo, J. J., Guan, J., Dorris, S. E. and Liu, M. (1998) 'Development of mixed-conducting oxides for gas separation'. *Solid State Ionics*, **108**, 363–70.

Baumann, S., Schulze-Küppers, F., Roitsch, S., Betz, M., Zwick, M., Pfaff, E. M., Meulenberg, W. A., Mayer, J. and Stöver, D. (2010) 'Influence of sintering conditions on microstructure and oxygen permeation of $Ba_{0.5}Sr_{0.5}Co_{0.8}Fe_{0.2}O_{3-\delta}$ (BSCF) oxygen transport membranes'. *Journal of Membrane Science*, **359**, 102–9.

Beér, J. M. (2007) 'High efficiency electric power generation: The environmental role'. *Progress in Energy and Combustion Science*, **33**, 107–34.

Bhalla, A. S., Guo, R. Y. and Roy, R. (2000) 'The perovskite structure - a review of its role in ceramic science and technology'. *Materials Research Innovations*, **4**, 3–26.

Boivin, J.-C. and Thomas, D. J. (1981) 'Crystal chemistry and electrical properties of bismuth-based mixed oxides'. *Solid State Ionics*, **5**, 523–5.

Bouwmeester, H. J. M. and Burggraaf, A. J. (1996) 'Dense ceramic membranes for oxygen separation'. *Fundamentals of Inorganic Membrane Science and Technology.* Burggraaf, A. J. and Cot, L. (eds), Elsevier Science B.V., Amsterdam.

Bouwmeester, H. J. M., Kruidhof, H., Burggraaf, A. J. and Gellings, P. J. (1992) 'Oxygen semipermeability of erbia-stabilized bismuth oxide'. *Solid State Ionics*, **53–6**, 460–8.

Breard, Y., Michel, C., Hervieu, M., Studer, F., Maignan, A. and Raveau, B. B. (2002) 'Large oxygen deficiency in a $n = 2$ member of the RP series: Sr_3FeCoO_{7-x} ($x <= 1.55$)'. *Chemistry of Materials*, **14**, 3128–35.

© Woodhead Publishing Limited, 2011

Brinkman, H. W., Kruidhof, H. and Burggraaf, A. J. (1994) 'Mixed conducting yttrium-barium-cobalt-oxide for high oxygen permeation'. *Solid State Ionics*, **68**, 173–6.

Bücker, D., Holmberg, D. and Griffin, T. (2005) 'Techno-economic evaluation of an oxyfuel power plant using mixed conducting membrane'. *Carbon Dioxide Capture for Storage in Deep Geologic Formations*. Elsevier Science, Amsterdam.

Cao, G. Z. (1994) 'Electrical conductivity and oxygen semipermeability of terbia and yttria stabilized zirconia'. *Journal Applied Electrochemistry*, **24**, 1222–7.

Capoen, E., Steil, M. C., Nowogrocki, G., Malys, M., Pirovano, C., Löfberg, A., Bordes-Richard, E., Boivin, J. C., Mairesse, G. and Vannier, R. N. (2006) 'Oxygen permeation in bismuth-based materials. Part I: Sintering and oxygen permeation fluxes'. *Solid State Ionics*, **177**, 483–8.

Chang, X., Zhang, C., Jin, W. and Xu, N. (2006) 'Match of thermal performances between the membrane and the support for supported dense mixed-conducting membranes'. *Journal of Membrane Science*, **285**, 232–8.

Chen, C. S., Boukamp, B. A., Bouwmeester, H. J. M., Cao, G. Z., Kruidhof, H., Winnubst, A. J. A. and Burggraaf, A. J. (1995) 'Microstructural development, electrical properties and oxygen permeation of zirconia-palladium composites'. *Solid State Ionics*, **76**, 23–8.

De Arellano-López, A. R., Balachandran, U., Goretta, K. C., Ma, B. and Routbort, J. L. (2001) 'High-temperature deformation of Sr(FeCo)1.5O_x ceramics'. *Acta Materialia*, **49**, 3109–16.

Descamps, C., Bouallou, C. and Kanniche, M. (2008) 'Efficiency of an integrated gasification combined cycle (IGCC) power plant including CO_2 removal'. *Energy*, **33**, 874–81.

Doctor, R. D., Molburg, J. C. and Thimmapuram, P. R. (1997) 'Oxygen-blown gasification combined cycle: Carbon dioxide recovery, transport, and disposal'. *Energy Conversion and Management*, **38**, S575–S580.

Dou, S., Masson, C. R. and Pacey, P. D. (1985) 'Mechanism of oxygen permeation through lime-stabilized zirconia'. *Journal of the Electrochemical Society*, **132**, 1843–9.

Duke, M., Rudolph, V., Lu, G. Q. and Diniz Da Costa, J. C. (2004) 'Scale-up of molecular sieve silica membranes for reformate purification'. *AIChE Journal*, **50**, 2630–4.

Emsley, J. (2001) *Nature's Building blocks : an A-Z guide to the elements*, Oxford University Press, Oxford.

Engels, S., Beggel, F., Modigell, M. and Stadler, H. (2010) 'Simulation of a membrane unit for oxyfuel power plants under consideration of realistic BSCF membrane properties'. *Journal of Membrane Science*, **359**, 93–101.

Eriksson, T., Isaksson, J., Ståhlberg, P., Kurkela, E. and Helanti, V. (1993) 'Durability of ceramic filters in hot gas filtration'. *Bioresource Technology*, **46**, 103–12.

Fagg, D. P., Marozau, I. P., Shaula, A. L., Kharton, V. V. and Frade, J. R. (2006) 'Oxygen permeability, thermal expansion and mixed conductivity of $Gd_xCe_{0.8-x}Pr_{0.2}O_{2-\delta}$, x = 0, 0.15, 0.2'. *Journal of Solid State Chemistry*, **179**, 3347–56.

Flett, M., Gurton, R. and Weir, G. (2007) 'Heterogeneous saline formations for carbon dioxide disposal: Impact of varying heterogeneity on containment and trapping'. *Journal of Petroleum Science and Engineering*, **57**, 106–18.

Gellings, P. J. and Bouwmeester, H. J. M. (1992) 'Ion and mixed conducting oxides as catalysts'. *Catalysis Today*, **12**, 1–101.

Goodenough, J. B. (2003) 'Oxide-ion electrolytes'. *Annual Review of Materials Research*, **33**, 91–128.

Greenblatt, M. (1997) 'Ruddlesden–Popper $Ln_{n+1}Ni_nO_{3n+1}$ nickelates: structure and properties'. *Current Opinion in Solid State and Materials Science*, **2**, 174–83.

© Woodhead Publishing Limited, 2011

Hadjipaschalis, I., Kourtis, G. and Poullikkas, A. (2009) 'Assessment of oxyfuel power generation technologies'. *Renewable and Sustainable Energy Reviews*, **13**, 2637–44.

Han, J., Zeng, Y. and Lin, Y. S. (1997) 'Oxygen permeation through fluorite-type bismuth-yttrium-copper oxide membranes'. *Journal of Membrane Science*, **132**, 235–43.

Haupt, G., Zimmermann, G., Pruschek, R., Oeljeklaus, G., Gale, J. and Kaya, Y. (2003) 'IGCC – the best choice for producing low-CO_2 power'. *Greenhouse Gas Control Technologies – 6th International Conference*, Pergamon, Oxford.

Homonnay, Z., Nomura, K., Juhasz, G., Gal, M., Solymos, K., Hamakawa, S., Hayakawa, T. and Vertes, A. (2002) 'Simultaneous probing of the Fe and Co sites in the CO_2-absorber perovskite $Sr_{0.95}Ca_{0.05}C_{0.5}Fe_{0.5}O_{3-\delta}$: a Mossbauer study'. *Chemistry of Materials*, **14**, 1127–35.

Hong, W. K. and Choi, G. M. (2010) 'Oxygen permeation of BSCF membrane with varying thickness and surface coating'. *Journal of Membrane Science*, **346**, 353–60.

Ishihara, T., Yamada, T., Arikawa, H., Nishiguchi, H. and Takita, Y. (2000) 'Mixed electronic-oxide ionic conductivity and oxygen permeating property of Fe-, Co- or Ni-doped $LaGaO_3$ perovskite oxide'. *Solid State Ionics*, **135**, 631–6.

Jee, J.-G., Kim, M.-B. and Lee, C.-H. (2005) 'Pressure swing adsorption processes to purify oxygen using a carbon molecular sieve'. *Chemical Engineering Science*, **60**, 869–82.

Jurado, J. R. (2001) 'Present several items on ceria-based ceramic electrolytes: synthesis, additive effects, reactivity and electrochemical behaviour'. *Journal of Materials Science*, **36**, 1133–9.

Kakaras, E., Koumanakos, A., Doukelis, A., Giannakopoulos, D. and Vorrias, I. (2007) 'Oxyfuel boiler design in a lignite-fired power plant'. *Fuel*, **86**, 2144–50.

Kharton, V. V., Yaremchenko, A. A., Kovalevsky, A. V., Viskup, A. P., Naumovich, E. N. and Kerko, P. F. (1999) 'Perovskite-type oxides for high-temperature oxygen separation membranes'. *Journal of Membrane Science*, **163**, 307–17.

Kharton, V. V., Viskup, A. P., Kovalevsky, A. V., Naumovich, E. N. and Marques, F. M. B. (2001) 'Ionic transport in oxygen-hyperstoichiometric phases with K_2NiF_4-type structure'. *Solid State Ionics*, **143**, 337–53.

Kharton, V. V., Kovalevsky, A. V., Viskup, A. P., Shaula, A. L., Figueiredo, F. M., Naumovich, E. N. and Marques, F. M. B. (2003) 'Oxygen transport in $Ce_{0.8}Gd_{0.2}O_{2-\delta}$-based composite membranes'. *Solid State Ionics*, **160**, 247–58.

Kharton, V. V., Yaremchenko, A. A., Shaula, A. L., Patrakeev, M. V., Naumovich, E. N., Logvinovich, D. I., Frade, J. R. and Marques, F. M. B. (2004) 'Transport properties and stability of Ni-containing mixed conductors with perovskite- and K_2NiF_4-type structure', *Journal of Solid State Chemistry*, **177**, 26–37.

Kim, J. and Lin, Y. S. (2000) 'Synthesis and oxygen permeation properties of ceramic-metal dual-phase membranes'. *Journal of Membrane Science*, **167**, 123–33.

Kim, S., Yang, Y. L., Christoffersen, R. and Jacobson, A. J. (1998) 'Determination of oxygen permeation kinetics in a ceramic membrane based on the composition $SrFeCo_{0.5}O_{3.25-\delta}$'. *Solid State Ionics*, **109**, 187–96.

Kleinlogel, C. M. and Gauckler, L. J. (2000) 'Mixed electronic-ionic conductivity of cobalt doped cerium gadolinium oxide'. *Journal of Electroceramics*, **5**, 231–43.

Kobayashi, K., Nishioka, M., Sato, K., Inoue, T., Hamakawa, S. and Tsunoda, T. (2006) 'Synthesis and oxygen permeation properties of 75 mol% $Ce_{0.75}Nd_{0.25}O_{1.875-25}$ mol% $Nd_{1.8}Ce_{0.2}CuO_4$ composite'. *Journal of Solid State Electrochemistry*, **10**, 629–34.

Koros, W. J. and Fleming, G. K. (1993) 'Membrane-based gas separation'. *Journal of Membrane Science*, **83**, 1–80.

© Woodhead Publishing Limited, 2011

Kruidhof, H., Bouwmeester, H. J. M., Van Doorn, R. H. E. and Burggraaf, A. J. (1993) 'Influence of order-disorder transitions on oxygen permeability through selected nonstoichiometric perovskite-type oxides'. *Solid State Ionics*, **63–5**, 816–22.

Lein, H. L., Wiik, K., Einarsrud, M. A. and Grande, T. (2006) 'High-temperature creep behavior of mixed conducting $La_{0.5}Sr_{0.5}Fe_{1-x}Co_xO_{3-\delta}$ ($0.5 <= x <= 1$) materials'. *Journal of the American Ceramic Society*, **89**, 2895–8.

Leo, A., Liu, S., Diniz Da Costa, J. C. and Shao, Z. (2006) 'Oxygen permeation through perovskite membranes and the improvement of oxygen flux by surface modification'. *Science and Technology of Advanced Materials*, **7**, 819–25.

Leo, A., Liu, S. and Diniz Da Costa, J. C. (2009a) 'Development of mixed conducting membranes for clean coal energy delivery'. *International Journal of Greenhouse Gas Control*, **3**, 357–67.

Leo, A., Liu, S. and Diniz Da Costa, J. C. (2009b) 'The enhancement of oxygen flux on $Ba_{0.5}Sr_{0.5}Co_{0.8}Fe_{0.2}O_{3-\delta}$ (BSCF) hollow fibers using silver surface modification'. *Journal of Membrane Science*, **340**, 148–53.

Lin, Y. S., Wang, W. J. and Han, J. H. (1994) 'Oxygen permeation through thin mixed-conducting solid oxide membranes'. *AiChE Journal*, **40**, 786–98.

Liu, S. and Gavalas, G. R. (2005) 'Oxygen selective ceramic hollow fiber membranes'. *Journal of Membrane Science*, **246**, 103–8.

Lübke, S. and Wiemhöfer, H. D. (1999) 'Electronic conductivity of Gd-doped ceria with additional Pr-doping'. *Solid State Ionics*, **117**, 229–43.

Majkic, G., Wheeler, L. and Salama, K. (2000) 'Creep of polycrystalline $SrCo_{0.8}Fe_{0.2}O_{3-\delta}$. *Acta Materialia*, **48**, 1907–17.

Majkic, G., Wheeler, L. T. and Salama, K. (2002) 'High-temperature deformation of $La_{0.2}Sr_{0.8}Fe_{0.8}Cr_{0.2}O_{3-\delta}$ mixed ionic-electronic conductor'. *Solid State Ionics*, **146**, 393–404.

Manthiram, A., Prado, F. and Armstrong, T. (2002) 'Oxygen separation membranes based on intergrowth structures'. *Solid State Ionics*, **152–3**, 647–55.

Mazaheri, A. R., Ahmadi, G. and Gamwo, I. K. (2003) 'Hot-gas flow and particle transport and deposition in a candle filter vessel'. *Advanced Powder Technology*, **14**, 111–25.

McIntosh, S., Vente, J. F., Haije, W. G., Blank, D. H. A. and Bouwmeester, H. J. M. (2006) 'Phase stability and oxygen non-stoichiometry of $SrCo_{0.8}Fe_{0.2}O_{3-\delta}$ measured by *in situ* neutron diffraction'. *Solid State Ionics*, **177**, 833–42.

Miura, N., Okamoto, Y., Tamaki, J., Morinaga, K. and Yamazoe, N. (1995) 'Oxygen semipermeability of mixed-conductive oxide thick-film prepared by slip casting'. *Solid State Ionics*, **79**, 195–200.

Nagai, T., Ito, W. and Sakon, T. (2007) 'Relationship between cation substitution and stability of perovskite structure in $SrCoO_{3-\delta}$ based mixed conductors'. *Solid State Ionics*, **177**, 3433–44.

Naumovich, E. N. and Kharton, V. V. (2010) 'Atomic-scale insight into the oxygen ionic transport mechanisms in La_2NiO_4-based materials'. *Journal of Molecular Structure: THEOCHEM*, **946**, 57–64.

Navarro, I., Marques, F. and Frade, J. (1997) 'n-type conductivity in gadolinia-doped ceria'. *Journal of the Electrochemical Society*, **144**, 267–73.

Nigara, Y., Mizusaki, J. and Ishigame, M. (1995) 'Measurement of oxygen permeability in CeO_2 doped CSZ'. *Solid State Ionics*, **79**, 208–11.

Pérez-Fortes, M., Bojarski, A. D., Velo, E., Nougués, J. M. and Puigjaner, L. (2009) 'Conceptual model and evaluation of generated power and emissions in an IGCC plant'. *Energy*, **34**, 1721–32.

© Woodhead Publishing Limited, 2011

Qi, X. W., Lin, Y. S. and Swartz, S. L. (2000) 'Electric transport and oxygen permeation properties of lanthanum cobaltite membranes synthesized by different methods'. *Industrial and Engineering Chemistry Research*, **39**, 646–53.

Qi, X., Akin, F. T. and Lin, Y. S. (2001) 'Ceramic-glass composite high temperature seals for dense ionic-conducting ceramic membranes'. *Journal of Membrane Science*, **193**, 185–93.

Schiestel, T., Kilgus, M., Peter, S., Caspary, K. J., Wang, H. and Caro, J. (2005) 'Hollow fibre perovskite membranes for oxygen separation'. *Journal of Membrane Science*, **258**, 1–4.

Schlehuber, D., Wessel, E., Singheiser, L. and Markus, T. (2010) 'Long-term operation of a $La_{0.58}Sr_{0.4}Co_{0.2}Fe_{0.8}O_{3-\delta}$ membrane for oxygen separation'. *Journal of Membrane Science*, **351**, 16–20.

Schmale, K., Janssen, M., Grünebaum, M., Baumann, S., Schulze-Küppers, F. and Meulenberg, W. A. (2010) 'Electronic conductivity of ceria co-doped with Gd, Pr and Co.' *E-MRS Spring 2010,* Strasbourg, France.

Schneider, P. S., Duke, M. C., Liu, S., Abdel-Jawad, M. and Diniz Da Costa, J. C. (2007) 'Energetics for gas separation in microporous membranes'. *International Journal of Nanotechnology*, **4**, 468–81.

Serra, J. M., Vert, V. B., Betz, M., Haanappel, V. A. C., Meulenberg, W. A. and Tietz, F. (2008) 'Screening of A-substitution in the system $A_{0.68}Sr_{0.3}Fe_{0.8}Co_{0.2}O_{3-\delta}$ for SOFC cathodes'. *Journal of the Electrochemical Society*, **155**, B207–B214.

Shah, M. M. (2006) 'Advanced clean coal technologies for CO_2 capture'. *Pittsburgh Coal Conference*. Pittsburgh.

Shah, M. M., Raybold, T., Jamal, A., Drnevich, R. F., Bonaquist, D. B. and Jones, R. (2005) 'IGCC – CO_2 capture ready?' *Gasification Technologies Conference*. San Francisco.

Shao, Z., Xiong, G., Cong, Y. and Yang, W. (2000a) 'Synthesis and oxygen permeation study of novel perovskite-type $BaBi_xCo_{0.2}Fe_{0.8-x}O_{3-\delta}$.' *Journal Membrane Science*, **164**, 167–76.

Shao, Z. P., Yang, W. S., Cong, Y., Dong, H., Tong, J. H. and Xiong, G. X. (2000b) 'Investigation of the permeation behavior and stability of a $Ba_{0.5}Sr_{0.5}Co_{0.8}Fe_{0.2}O_{3-\delta}$ oxygen membrane'. *Journal of Membrane Science*, **172**, 177–88.

Shao, Z., Xiong, G., Tong, J., Dong, H. and Yang, W. (2001) 'Ba effect in doped $Sr(Co_{0.8}Fe_{0.2})O_{3-\delta}$ on the phase structure and oxygen permeation properties of the dense ceramic membranes'. *Separation and Purification Technology*, **25**, 419–29.

Sharma, S. D., Dolan, M., Park, D., Morpeth, L., Ilyushechkin, A., McLennan, K., Harris, D. J. and Thambimuthu, K. V. (2008) 'A critical review of syngas cleaning technologies – fundamental limitations and practical problems'. *Powder Technology*, **180**, 115–21.

Shaula, A. L., Pivak, Y. V., Waerenborgh, J. C., Gaczyñski, P., Yaremchenko, A. A. and Kharton, V. V. (2006) 'Ionic conductivity of brownmillerite-type calcium ferrite under oxidizing conditions'. *Solid State Ionics*, **177**, 2923–30.

Smart, S., Lin, C. X. C., Ding, L., Thambimuthu, K. and Diniz Da Costa, J. C. (2010) 'Ceramic membranes for gas processing in coal gasification'. *Energy and Environmental Science*, **3**, 268–78.

Smith, A. R. and Klosek, J. (2001) 'A review of air separation technologies and their integration with energy conversion processes'. *Fuel Processing Technology*, **70**, 115–34.

Stadler, H., Beggel, F., Habermehl, M., Persigehl, B., Kneer, R., Modigell, M. and Jeschke,

© Woodhead Publishing Limited, 2011

P. (2011) 'Oxyfuel coal combustion by efficient integration of oxygen transport membranes'. *International Journal of Greenhouse Gas Control*, **5**, 7–15.

Stiegel, G. J. and Maxwell, R. C. (2001) 'Gasification technologies: the path to clean, affordable energy in the 21st century'. *Fuel Processing Technology*, **71**, 79–97.

Sunarso, J., Motuzas, J., Liu, S. and Costa, J. C. D. D. (2010) 'Bi-doping effects on the structure and oxygen permeation properties of $BaSc_{0.1}Co_{0.9}O_{3-\delta}$ perovskite membranes'. *Journal of Membrane Science*, **361**, 120–5.

Švarcová, S., Wiik, K., Tolchard, J., Bouwmeester, H. J. M. and Grande, T. (2008) 'Structural instability of cubic perovskite $Ba_xSr_{1-x}Co_{1-y}Fe_yO_{3-\delta}$'. *Solid State Ionics*, **178**, 1787–91.

Takahashi, T., Esaka, T. and Iwahara, I. (1975) 'High oxide ion conduction in sintered oxides of the system Bi_2O_3-Gd_2O_3'. *Journal Applied Electrochemistry*, **5**, 197–202.

Teraoka, Y., Zhang, H. M., Furukawa, S. and Yamazoe, N. (1985a) 'Oxygen permeation through perovskite-type oxides'. *Chemistry Letters*, 1743–6.

Teraoka, Y., Zhang, H. M. and Yamazoe, N. (1985b) 'Oxygen-sorptive properties of defect perovskite-type $La_{1-x}Sr_xCo_{1-y}Fe_yO_{3-\delta}$'. *Chemistry Letters*, 1367–70.

Teraoka, Y., Nobunaga, T. and Yamazoe, N. (1988) 'Effect of cation substitution on the oxygen semipermeability of perovskite-type oxides'. *Chemistry Letters*, 503–6.

Tong, J., Yang, W., Zhu, B. and Cai, R. (2002) 'Investigation of ideal zirconium-doped perovskite-type ceramic membrane materials for oxygen separation'. *Journal of Membrane Science*, **203**, 175–89.

Tong, J., Yang, W., Cai, R., Zhu, B., Xiong, G. and Lin, L. (2003) 'Investigation on the structure stability and oxygen permeability of titanium-doped perovskite-type oxides of $BaTi_{0.2}Co_xFe_{0.8-x}O_{3-\delta}$ (x = 0.2–0.6)'. *Separation and Purification Technology*, **32**, 289–99.

Vente, J. F., Haije, W. G., Ijpelaan, R. and Rusting, F. T. (2006a) 'On the full-scale module design of an air separation unit using mixed ionic electronic conducting membranes'. *Journal of Membrane Science*, **278**, 66–71.

Vente, J. F., McIntosh, S., Haije, W. G. and Bouwmeester, H. J. M. (2006b) 'Properties and performance of $Ba_xSr_{1-x}Co_{0.8}Fe_{0.2}O_{3-\delta}$ materials for oxygen transport membranes'. *Journal of Solid State Electrochemistry*, **10**, 581–8.

Verkerk, M. J., Keizer, K. and Burggraaf, A. J. (1980) 'High oxygen ion conduction in sintered oxides of the Bi_2O_3–Er_2O_3 system'. *Journal of Applied Electrochemistry*, **10**, 81–90.

Verkerk, M. J., Hammink, M. W. J. and Burggraaf, A. J. (1983) 'Oxygen transfer on substituted ZrO_2, Bi_2O_3 and CeO_2 electrolytes with platinum electrodes'. *J. Electrochem. Soc.*, **130**, 70–8.

Wall, T., Liu, Y., Spero, C., Elliott, L., Khare, S., Rathnam, R., Zeenathal, F., Moghtaderi, B., Buhre, B., Sheng, C., Gupta, R., Yamada, T., Makino, K. and Yu, J. (2009) 'An overview on oxyfuel coal combustion–State of the art research and technology development'. *Chemical Engineering Research and Design*, **87**, 1003–16.

Wang, H., Tablet, C., Feldhoff, A. and Caro, J. (2005a) 'A cobalt-free oxygen-permeable membrane based on the perovskite-type oxide $Ba_{0.5}Sr_{0.5}Zn_{0.2}Fe_{0.8}O_{3-\delta}$'. *Advanced Materials*, **17**, 1785–8.

Wang, H., Tablet, C., Feldhoff, A. and Caro, J. (2005b) 'Investigation of phase structure, sintering, and permeability of perovskite-type $Ba_{0.5}Sr_{0.5}Co_{0.8}Fe_{0.2}O_{3-\delta}$ membranes'. *Journal of Membrane Science*, **262**, 20–6.

Wang, H., Schiestel, T., Tablet, C., Schroeder, M. and Caro, J. (2006) 'Mixed oxygen ion and electron conducting hollow fiber membranes for oxygen separation'. *Solid State Ionics*, **177**, 2255–9.

© Woodhead Publishing Limited, 2011

Wang, H., Tablet, C. and Caro, J. (2008) 'Oxygen production at low temperature using dense perovskite hollow fiber membranes'. *Journal of Membrane Science*, **322**, 214–17.

Watanabe, K., Takauchi, D., Yuasa, M., Kida, T., Shimanoe, K., Teraoka, Y. and Yamazoe, N. (2009) 'Oxygen permeation properties of Co-free perovskite-type oxide membranes based on $BaFe_{1-y}Zr_yO_{3-\delta}$'. *Journal of the Electrochemical Society*, **156**, E81–E85.

Wolfenstine, J., Goretta, K. C., Cook, R. E. and Routbort, J. L. (1996) 'Use of diffusional creep to investigate mass transport in (La, Sr)MnO_3'. *Solid State Ionics*, **92**, 75–83.

Wolfenstine, J., Huang, P. and Petric, A. (2000) 'High-temperature mechanical behavior of the solid-state electrolyte: $La_{0.8}Sr_{0.2}Ga_{0.85}Mg_{0.15}O_{2.825}$'. *Journal of the Electrochemical Society*, **147**, 1668–70.

Xia, Y., Armstrong, T., Prado, F. and Manthiram, A. (2000) 'Sol-gel synthesis, phase relationships, and oxygen permeation properties of $Sr_4Fe_{6-x}Co_xO_{13+\delta}$ (0<=x<=3)'. *Solid State Ionics*, **130**, 81–90.

Xu, S. J. and Thomson, W. J. (1998) 'Stability of $La_{0.6}Sr_{0.4}Co_{0.2}Fe_{0.8}O_{3-\delta}$ perovskite membranes in reducing and nonreducing environments'. *Industrial and Engineering Chemistry Research*, **37**, 1290–9.

Yang, Q., Lin, Y. S. and Bulow, M. (2006) 'High temperature sorption separation of air for producing oxygen-enriched CO_2 stream'. *AiChE Journal*, **52**, 574–81.

Yang, W. S., Wang, H. H., Zhu, X. F. and Lin, L. W. (2005) 'Development and application of oxygen permeable membrane in selective oxidation of light alkanes'. *Topics in Catalysis*, **35**, 155–67.

Yi, J. X., Feng, S. J., Zuo, Y. B., Liu, W. and Chen, C. S. (2005) 'Oxygen permeability and stability of $Sr_{0.95}Co_{0.8}Fe_{0.2}O_{3-\delta}$ in a CO_2- and H_2O-containing atmosphere'. *Chemistry of Materials*, **17**, 5856–61.

Yi, J., Zuo, Y., Liu, W., Winnubst, L. and Chen, C. (2006) 'Oxygen permeation through a $Ce_{0.8}Sm_{0.2}O_{2-\delta}$–$La_{0.8}Sr_{0.2}CrO_{3-\delta}$ dual-phase composite membrane'. *Journal of Membrane Science*, **280**, 849–55.

Yi, J. X., Lein, H. L., Grande, T., Yakovlev, S. and Bouwmeester, H. J. M. (2009) 'High-temperature compressive creep behaviour of the perovskite-type oxide $Ba_{0.5}Sr_{0.5}Co_{0.8}Fe_{0.2}O_{3-\delta}$'. *Solid State Ionics*, **180**, 1564–8.

Yin, X., Hong, L. and Liu, Z.-L. (2006) 'Oxygen permeation through the LSCO–80/CeO_2 asymmetric tubular membrane reactor'. *Journal of Membrane Science*, **268**, 2–12.

Zeng, P., Chen, Z., Zhou, W., Gu, H., Shao, Z. and Liu, S. (2007) 'Re-evaluation of $Ba_{0.5}Sr_{0.5}Co_{0.8}Fe_{0.2}O_{3-\delta}$ perovskite as oxygen semi-permeable membrane'. *Journal of Membrane Science*, **291**, 148–56.

Zeng, Y. and Lin, Y. S. (2000) 'Oxygen permeation and oxidative coupling of methane in yttria doped bismuth oxide membrane reactor'. *Journal Catalysis*, **193**, 58–64.

Zeng, Y. and Lin, Y. S. (2001) 'Oxidative coupling of methane on improved bismuth oxide membrane reactors'. *AIChE Journal*, **47**, 436–44.

Zhu, X., Wang, H. and Yang, W. (2004) 'Novel cobalt-free oxygen permeable membrane'. *Chemical Communications*, 1130–1.

Zhu, X., Wang, H. and Yang, W. (2006) 'Structural stability and oxygen permeability of cerium lightly doped $BaFeO_{3-\delta}$'. *Solid State Ionics*, **177**, 2917–21.

Zwick, M. and Pfaff, E. M. (2008) 'Microstructure optimization of $Ba_{0.5}Sr_{0.5}Co_{0.8}Fe_{0.2}O_{3-\delta}$ perovskite for OTM reactors', *32nd International Conference on Advanced Ceramics and Composites*. Daytona Beach, Florida, USA.

© Woodhead Publishing Limited, 2011

10
Membranes for hydrocarbon fuel processing and separation

A. GUGLIUZZA, A. IULIANELLI and A. BASILE,
Institute on Membrane Technology of the Italian
National Research Council, ITM-CNR, Italy

Abstract: The role of the membrane technology in hydrocarbon fuel processing and separation is discussed, spotlighting various classes of materials used for membranes. The advantages and shortcomings are considered in relation to the molecules being separated, examining efforts to overcome the conventional trade-off relationship between selectivity and permeability. The scale-up from fundamental research to large-scale industry is analysed considering important opportunities in design, rationalization and optimization of innovative industrial production. Novel processes are proposed in order to preserve the environment and improve the quality of life through production of alternative green energy and rational recycling of raw materials. Heterogeneous catalysis in the petrochemical industry and biofuels production from steam reforming of hydrocarbons are discussed.

Key words: biofuel production, heterogeneous catalysis, hydrocarbons and gas separation, nanocomposite membranes, steam reforming.

10.1 Introduction

In the last few years, integrated unit membrane operations have become competitive with traditional and well-established cryogenic distillation, absorption and pressure-swing adsorption (Koros, 2002; Ghosal and Freeman 1994), yielding an attractive and cost-effective option for chemical and petrochemical industrial processes. Over the last few decades, the effectiveness of membrane technology has been demonstrated for resource recovery of C_2^+ hydrocarbons, including olefins, paraffins and halo-hydrocarbons, from waste gas/liquid streams (Semenova, 2004; Smitha *et al*., 2004). If we consider that a large amount of hydrogen and methane together with small amounts of higher hydrocarbons (C_3^+) form natural gas, the use of this developing technology for the treatment of hydrocarbon streams represents an attractive challenge. Also, the removal of more condensable vapours is needed to reduce the dewpoint and heating value of natural gas to pipeline specifications in order to prevent its condensation during transportation or use at low temperature (Baker and Wijmans, 1994; Baker *et al*., 1991; Ahmad *et al*., 2007). At the same time, the recovery of valuable hydrocarbons is fundamental in several

© Woodhead Publishing Limited, 2011

chemical applications. Polypropylene is, for example, one of the most used raw materials in several chemical processes and its separation from a mixture containing propane is an important requirement of the chemical industry (Bai *et al.*, 1998). The separation of olefins from paraffins analogues, as well as the removal of perfluorinated and chlorinated compounds from air and liquid streams, including municipal and wastewater, is regarded as an important issue because of their direct impact on environmental safety (O'Reilly *et al.*, 2001; Battelle, 2007; ECSA, 2008) and its commercial implications in advanced segments of the industry, such as the microelectronics (Cummins *et al.*, 1997). Undoubtedly, membrane technology is a viable alternative to more conventional methodologies, if economics and eco-sustainability are considered.

The successful outcome of the membrane processes with regard to separation and conversion events, depends significantly on the type of membranes operated and the engineering process. Structural and chemical features of the material, together with sophisticated technology, can decide the final performance of the overall membrane operation. Solubility-selective materials such as rubbery and ultra-high free volume polymers are, for instance, optimal candidates for separating hydrocarbons according to mechanisms that favour the transport of larger condensable components over smaller supercritical gases. A lot of work has been done on the behaviour of these classes of high-performance polymers for production and separation of higher C_2^+ hydrocarbons (Semenova, 2004; Smitha *et al.*, 2004). However, an ambitious target for the next few years is to design breakthrough membranes, enabling the conventional trade-off relationship between selectivity and gas permeability in polymers to be overcome. Traditionally, an increase in selectivity is expected to correspond to a decrease in permeability and *vice versa*. The immediate challenge, therefore, is to combine high permeability with high selectivity through a molecular design that addresses the rational manipulation of the distribution of interconnected free volume elements as well as the enhancement of reciprocal materials–hydrocarbon affinity. In this perspective, mixed matrixes can be considered to be a promising next generation class of robust membranes that meet the requirements of high permeability, high selectivity and long-term stability. Indeed, higher selectivity has been demonstrated to join higher productivity, challenging the processability of high-performance polymers and the robustness of inorganic materials. Attractively, hybrid nanocomposite membranes have the advantage of maintaining superior permselectivity features in presence of complex and aggressive gas and liquid streams, resulting in better scalability and durability. In this chapter, an overview of classes of membrane materials for particular applications involving hydrocarbon streams is provided, suggesting the membrane technology is a powerful tool that can be rationally integrated into industrial processes dedicated to the production of greener energy and

© Woodhead Publishing Limited, 2011

recycling of add-value raw materials. All this is expected to bring important benefits to environmental safety and the quality of life.

10.2 Membrane materials, development and design for hydrocarbon processing

Depending on the chemical and mechanical robustness of materials under specific operating conditions, as well as their durability and scalability, any desirable features of the processing membranes used in hydrocarbon separation must be competitive economically. In this respect, the efficiency of a membrane arises from its intrinsic constituents which, combined with the engineering process, produce the final performance of the membrane operation.

10.2.1 Functional materials for hydrocarbon separation through membrane technology

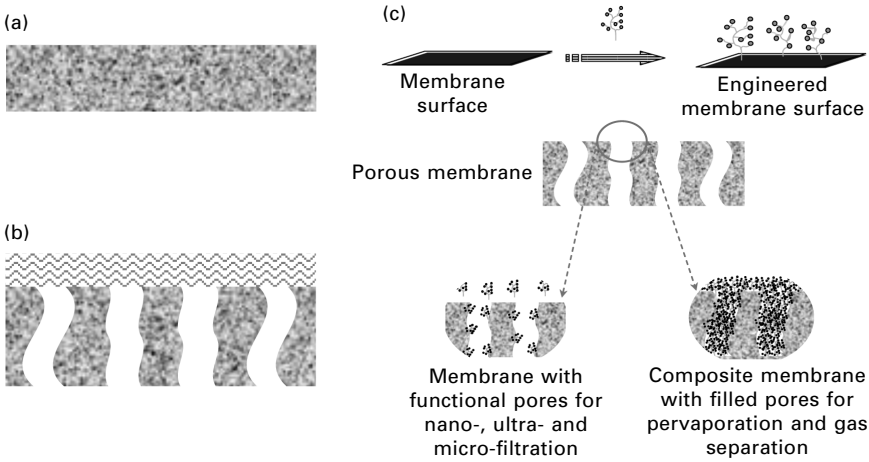
The development of the next generation of membranes is regarded as a good opportunity to revolutionize traditional conversion and separation technologies, enabling the achievement of challenging targets in a more-effective, greener and economically advantageous way. Hereafter, the performance of various types of polymeric, inorganic and mixed membranes for hydrocarbon separations is illustrated, elucidating the nature of the materials, fabrication procedures and membrane effectiveness in terms of selectivity and flux through well-controlled structure–transport property relationships.

10.2.2 Polymeric membranes for hydrocarbon separations: molecular design and structure–property relationships

Even though polymeric membranes have limited chemical, mechanical and thermal resistance under harsh operating conditions and relatively high sensitivity to compaction, ageing or swelling, their use in the recovery and separation of higher C_2^+ hydrocarbons from refinery hydrogen purge streams or methane in natural-gas processing is considered a key issue in research in the next few years. Indeed, their low cost of fabrication, good processability and feasibility for large-scale application make them more competitive than traditional inorganic membranes (Koros, 2002).

Customarily, homogeneous symmetric and composite dense polymeric membranes as well as engineered surface membranes (MSE) are used in lab scale set-ups for the separation of organic mixtures (Fig. 10.1). In order to meet the requirement of enhanced high-performance materials and

© Woodhead Publishing Limited, 2011



10.1 Schematic structures of membranes used in pervaporation and gas separation: (a) symmetric self-standing dense polymer membranes; (b) composite membranes with thin dense skin layer on the top of a porous support; (c) composite porous membranes with filled pores.

effectiveness, two different arrangements are usually adopted to tailor make composite polymeric membranes that are permeable to hydrocarbon vapours: (a) matrixes formed by a porous support coated with a thin selective dense layer; (b) porous films whose pores are filled with interacting molecular compounds. A large category of polymers within glasses and rubbers can be distinguished as suitable materials. Glassy membranes are processed at temperatures below the glass transition temperature (T_g) and achieve high selectivity using size-molecular discrimination mechanisms, resulting in 100 times more permeability, for instance, for hydrogen (kinetic diameter = 2.89 Å) than for methane (kinetic diameter = 3.8 Å). Rubbery membranes operate at temperatures below the T_g and exhibit reverse selectivity deriving from their ability to discern between components with different solubilities in the polymeric matrix. Rubbery membranes are often suggested for removal of higher hydrocarbons from natural gas and hydrogen streams, because the hydrocarbons are better at condensing than light gases. When a large quantity of organic vapour is predominant, rubbery membranes are preferred to minimize the membrane-area and compression requirements, yielding more economically competitive processes.

High separation factors for vapours over light gases can be achieved in any relationships where diffusivity selectivity and solubility selectivity are considered (Freeman and Pinnau, 1997). Polymeric membranes exhibit high permeability and selectivity to organic vapours when materials are selected with a chemical and molecular structure suitable to achieve diffusivity

© Woodhead Publishing Limited, 2011

selectivity as near unity as possible ($D_{\text{organic vapour}}/D_{\text{light gas}} \leq 1$) and solubility selectivity higher than unity ($S_{\text{organic vapour}}/S_{\text{light gas}} > 1$). In this respect, two classes of polymers, including super-glassy materials like poly(1-trimethylsilyl-1-propyne) (PTMSP) (Toy and Pinnau, 1996; Morisato *et al.*, 1996; Pinnau and Toy, 1996a and 1996b; Baschetti *et al.*, 2005; Syrtsova *et al.*, 2007; Consolati *et al.*, 1996; Matteucci *et al.*, 2006) and rubbers (Semenova, 2004; Matteucci *et al.*, 2006; Pinnau and He, 2004; Raharjo *et al.*, 2007a; Hirayama *et al.*, 1999) seem to meet these requirements.

Poly(1-trimethylsilyl-1-propyne) (PTMSP): an extraordinary example of a glassy polymer for effective hydrocarbon separation

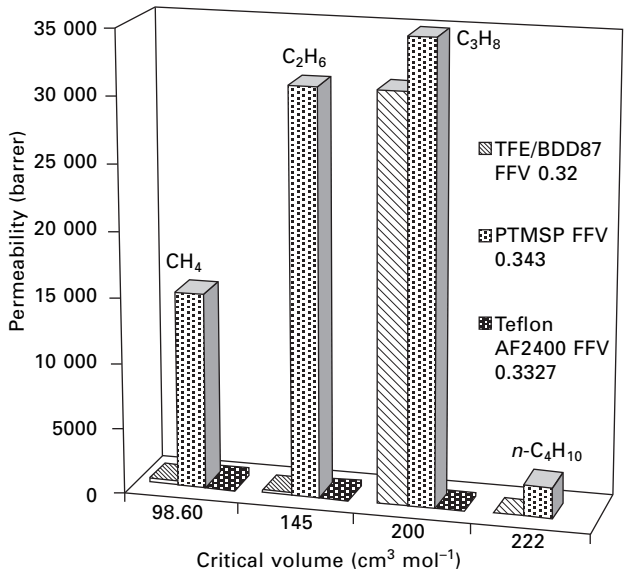
PTMSP has been demonstrated to be a super-glassy polymer with an excess fractional free volume (FFV: 0.343). Large holes are interconnected forming nanoscale channels through packed polymer chains (Wang *et al.*, 2004). PTMSP can really be regarded as a nanoporous material, where the FFV is the result of the ability of the rigid double bond and bulky trimethylsilyl moiety to prevent the polymer backbone from moving freely. Positron annihilation lifetime spectroscopy (PALS) confirms (Consolati *et al.*, 1996, Shantarovich *et al.*, 2000; Hofmann *et al.*, 2002 and 2003) that the network of these channels produces a bimodal size distribution of free volume with average radii of about 4.5–7.5 Å, compared with about 3 Å estimated for common glassy polymers, providing free pathways for permeation of organic vapours. The good performance of PTMSP is ascribed to the high degree of interconnected holes and high distribution of free cavities, enabling larger penetrants to be processed easily as clearly shown in Fig. 10.2. Indeed, glassy polymers that have comparable FFVs to PTMSP but different average cavities exhibit different permeabilities to hydrocarbons as the critical volume rises (Pinnau and Toy, 1996a and 1996b, Wang *et al.*, 2004, Srinivasan *et al.*, 1994; Nunes and Peinemann, 2006; Roizard *et al.*, 2007).

Enhanced permeability and selectivity can be regarded as a result of the competitive solubility of higher hydrocarbons into accessible cavities, preventing lesser condensable gases from diffusing through the blocked channels. An increase in permeability can be observed with rising critical temperature (Fig. 10.3). PTMSP is a super-glassy material that has recently been discovered to be more permeable than more traditional rubbery poly(dimethylsiloxane) (PDMS) (Table 10.1).

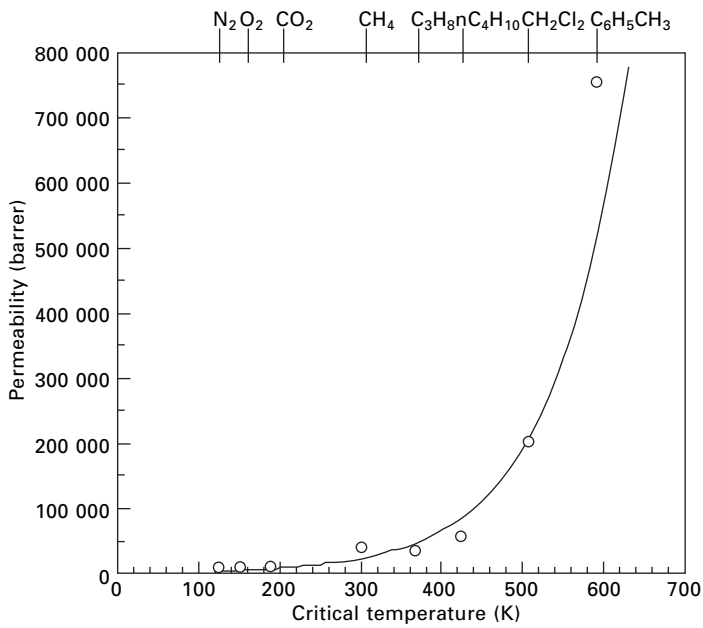
Decay in PTMSP hydrocarbon permeability and strategies to control ageing

One property to be considered in high-performance membranes is undoubtedly their long-term stability. An ideal system would preserve its intrinsic

© Woodhead Publishing Limited, 2011



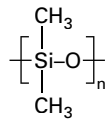
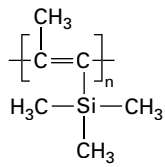
10.2 Comparison of hydrocarbon permeability values estimated for three different glassy polymers with dissimilar fractional free volumes (FFV) (Pinnau and Toy, 1996a, 1996b; Wang *et al.*, 2004).



10.3 Increasing permeability vs rising critical temperature measured through PTMSP membranes (Srinivasan *et al.*, 1994; Nunes and Peinemann, 2006; Roizard *et al.*, 2007).

© Woodhead Publishing Limited, 2011

Table 10.1 Hydrocarbon permeability and selectivity estimated for rubbery (PDMS) and glassy (PTMSP) membranes, respectively

Structure	Permeability (barrer)			
	Acronym	CH_4	C_3H_8	n-C_4H_{10}
	PDMS	1300[a]	7400[a]	14 000[b]
	PTMSP	6500[c]	33 800[c]	53 500[d]

[a] Values measured at 35°C, P_{feed}: 4.4 atm; $P_{permeate}$: 1 atm (Pinnau and He, 2004). [b] Data reported by Raharjo *et al.* (2007a, 2007b). [c] Values measured at 25°C (Roizard *et al.*, 2007). [d] Data reported by Nunes and Peinemann (2006).

permselectivity with time. Unfortunately, a dramatic decrease in productivity and efficiency is often observed. Despite its excellent permselectivity, PTMSP is a typical polymer that loses its own transport properties dramatically in a few weeks. This may be ascribed to chemical and physical phenomena including the oxidation of the double bonds in the main backbone (chemical ageing), absorption of materials in the membranes when processed (contamination) or relaxation of the non-equilibrium excess of free volume (physical ageing) (Odani and Masuda, 1992; Dorkenoo and Pfromm, 2000; Starannikova *et al.*, 2004; Wang *et al.*, 2006; Nakagawa *et al.*, 2010). PTMSP also has limited solvent resistance, which prohibits its use in most industrial applications. In order to control the decay in gas and hydrocarbon permeability through PTMSP, different attempts to stabilize the fractional free volume have been proposed, including physically blending PTMSP with other polymers such as poly(tert-butyl acetylene) (PTBA) (Nakagawa *et al.*, 2010) and poly(1-phenyl-1-propyne) (PPP) (Morisato *et al.*, 1996) as well as addition of crosslinked (bis(azide)s), fumed silica nanoparticles and poly(siloxysilsesquioxane) (Jia and Baker, 1998; Douglas, 2008; Kelman *et al.*, 2008a and 2008b). Despite enhanced structural stability, a decrease in transport properties has unfortunately been estimated when there are changes in the free volume and diffusional mobility of the penetrants. In this respect, the molecular design of new advanced polymers resembling the structural features of PTMSP

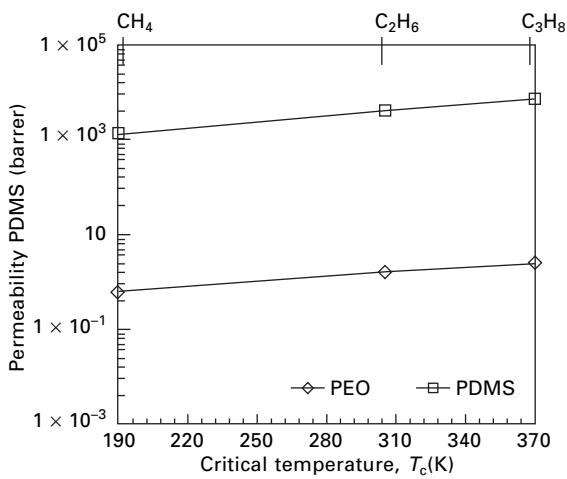
© Woodhead Publishing Limited, 2011

needs to overcome the limitations of the chemical and physical stability of this extraordinary polymer.

Solubility-selective membranes and plasticization as key factors in removing extra organic vapours from permanent gases

Rubbery membranes work as suitable selective interfaces for the removal of largely soluble hydrocarbons. In this case, the contribution of vapour/gas diffusion selectivity through this type of membranes is irrelevant to the overall selectivity, being a ratio of less than one. However, the vapour/gas solubility selectivity becomes a discriminating factor, when related to condensability and relative affinity with rubbery polymer matrixes of the highest hydrocarbons, including poly(ethylene oxide) (PEO) (Lin and Freeman, 2004) and PDMS (Pinnau and He, 2004; Raharjo *et al.*, 2007b). Despite both polymers being permeable to hydrocarbons, isotropic PDMS membranes usually exhibit higher performance than semi-crystalline PEO films, because the solubility selectivity overcomes significantly the diffusivity selectivity causing an important plasticization in PDMS, which is responsible for significant changes in permeability and selectivity (Fig. 10.4).

PDMS is one of the rubbery materials currently used to tailor self-standing (Raharjo *et al.*, 2007a and 2007b; Leemann *et al.*, 1996) and supported membranes (Jiang and Kumar, 2006; Jannatduost *et al.*, 2010) owing to its superior performance in removing extra hydrocarbons from feed (Baker, 2004; Yeom *et al.*, 2002). PDMS membranes have, for instance, been used



10.4 Comparison of permeability values estimated for semicrystalline poly(ethylene oxide) (PEO) and polydimethylsiloxane (PDMS) at 35°C and 4.4 atm (445.83 kPa).

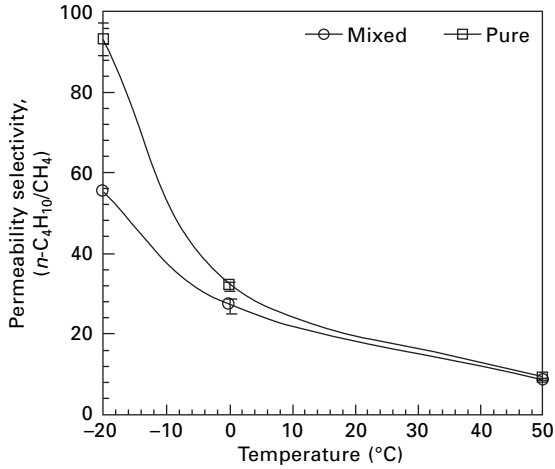
© Woodhead Publishing Limited, 2011

to separate hydrogen (Pinnau and He, 2004) and nitrogen (Jiang and Kumar 2006) from hydrocarbons in the presence of binary and multicomponent gaseous streams in place of hydrogen-selective membranes such as glassy polysulfone and polyimide. Indeed, the tendency of PDMS to swell when in contact with condensable molecules is strategically used in combination with sub-ambient operating temperatures. When organic vapour mixtures are used, increasing the content of strongly sorbing hydrocarbons in the feed at constant temperature induces swelling of the polymer chains, yielding larger local segmental motion and/or increased fractional free volume. The plasticization caused by the condensation of the penetrant in the polymer matrix is, hence, reflected in the enhanced penetrant diffusivity. An increase in higher organic compounds in the vapour, for example *n*-butane, with respect to smaller components, for example methane, can be regarded as a result of the greater diffusive motion of the largest molecules. An increase in *n*-butane concentration in the upstream from 1 to 8 vol% causes an enhancement of 1.4 fold in the *n*-butane permeability, resulting in a higher *n*-butane/methane selectivity from 10 to 12 (Pinnau and He, 2004). This selectivity is amplified when the fugacity of *n*-butane increases and the feed temperature is lowered down to sub-ambient values, for example –20°C, producing an increase in the separation factor of almost an order of magnitude as a consequence of the larger contribution of negative heat of the sorption values (H_s) to the activation energy for *n*-butane permeation (Pinnau and He, 2004; Raharjo *et al.*, 2007a and 2007b). It has also been demonstrated how the permeability, diffusivity and selectivity values for the vapour-couple *n*-C_4H_{10}/CH_4 in a mixture are comparable to pure vapour values at high temperature. In contrast, discrepancies and the increasing standard deviation can be appreciated at sub-ambient temperatures and higher *n*-butane fugacity. In this case, lower values are estimated for the mixed vapours (Figs 10.5 and 10.6).

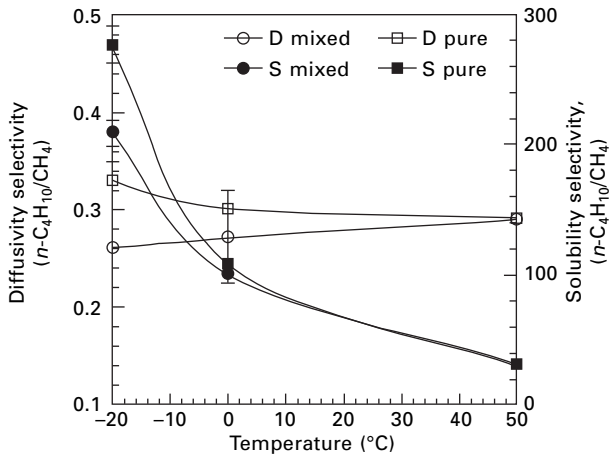
This can be ascribed to the dependence of the methane permeability, diffusivity and solubility on the *n*-butane fugacity in a mixture. Indeed, large amounts of sorbed *n*-butane plasticize the polymer matrix, causing an increase in the diffusivity of the organic vapours, that is *n*-butane and methane. Moreover, an increase in *n*-butane provides a thermodynamically favourable environment for methane dissolution into the matrix, reducing the separation factor (Raharjo *et al.*, 2007a, 2007b).

The effects of pendant groups in the backbone of PDMS on the transport of hydrocarbons at increasing kinetic diameter have also been discussed by Semenova (Semenova, 2004). Variation in the structure of organosilicon polymers can effectively influence the diffusivity more than the solubility of vapours, owing to an increase in glass transition temperature which means restriction of the local segmental mobility of the polymer chains.

© Woodhead Publishing Limited, 2011



10.5 Comparison of selectivity values for pure methane and a mixed *n*-butane/methane couple at various operating temperatures (Raharjo *et al.*, 2007a, 2007b).



10.6 Comparison of diffusivity and solubility selectivity values for pure methane and a mixed *n*-butane/methane couple at various operating temperatures (Raharjo *et al.*, 2007a, 2007b).

10.2.3 Inorganic membranes: from preparation to application in hydrocarbon separations

In the last few years, inorganic membrane separation technology has experienced a rapid growth and innovation. Several membrane separation processes have been developed and new processes are constantly being studied in both the academic and industrial research areas.

© Woodhead Publishing Limited, 2011

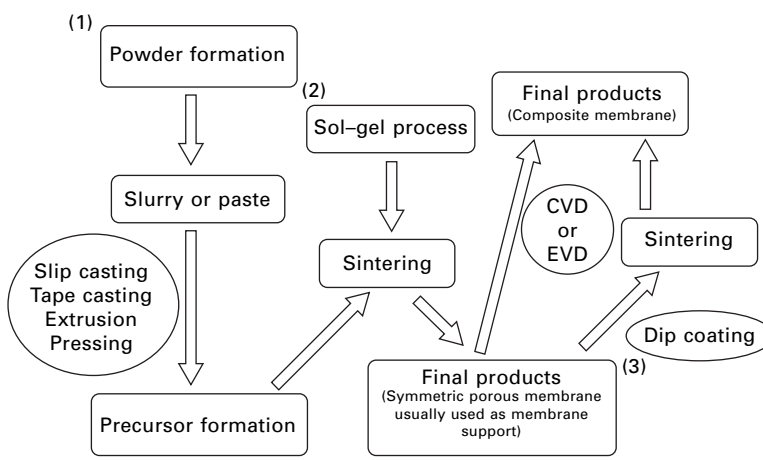
In particular, there is an interesting variety of inorganic membranes, commonly made up of different materials such as ceramics, carbon, silica, zeolite, oxides (alumina, titania, zirconia) as well as palladium, silver and their alloys. Inorganic membranes possess several advantages over organic membranes such as resistance towards solvents, a well-defined stable pore structure (in the case of porous inorganic membranes), high mechanical stability and elevated resistance at high operating temperatures of 500–800°C for metal membranes and over 1000°C for ceramic ones. However, they exhibit brittleness, are expensive to fabricate and are difficult to scale up. There follows an overview of the main fabrication procedures for inorganic membranes and some of their main applications in hydrocarbon separation are discussed.

Ceramic membranes

Commonly, the preparation of ceramic membranes involves several stages:

- formation of particle suspensions;
- packing of the particles in the suspensions into a membrane precursor with a particular shape such as flat sheet, monolith or tube;
- consolidation of the membrane precursor by heat treatment at high temperatures.

A generalized procedure for the preparation of symmetric and composite ceramic membranes is illustrated in Fig. 10.7 reporting different methods such as casting, tape casting, extrusion and pressing. Composite membranes (multi-layer membranes) can further be produced on a membrane support



10.7 Conventional methods for preparation of ceramic membranes.

© Woodhead Publishing Limited, 2011

through a coating step using dip-coating, sol–gel, chemical vapour deposition (CVD) or electrochemical vapour deposition (EVD) processes, followed by a cycling firing step.

Slip casting

Slip casting is one of the most commonly used traditional methods of membrane preparation, although the casting time is usually very long (Fig. 10.8(a)). Moreover, during the casting procedure it is difficult to control the wall thickness. A comprehensive discussion of the theory of slip casting has been given by Tiller and Tsai (1986) who provided a method for selection of the mould with an optimum pore diameter. However, the pore size of the membrane is mainly dependent on the particle size of the powders used in the slip. Nowadays, if the powders are prepared via a sol–gel process, a pore size range of the prepared membrane as small as 3–6 nm can be obtained.

Tape casting

The tape casting procedure is another well-known method for producing flat sheet ceramic membranes. Figure 10.8(b) illustrates the basic principle of the tape casting process. The process consists of a stationary casting knife, a reservoir for powder suspensions, a moving carrier and a drying zone. In preparing flat sheet ceramic membranes, the powder suspension is poured into a reservoir behind the casting knife and the carrier to be cast upon is set in motion.

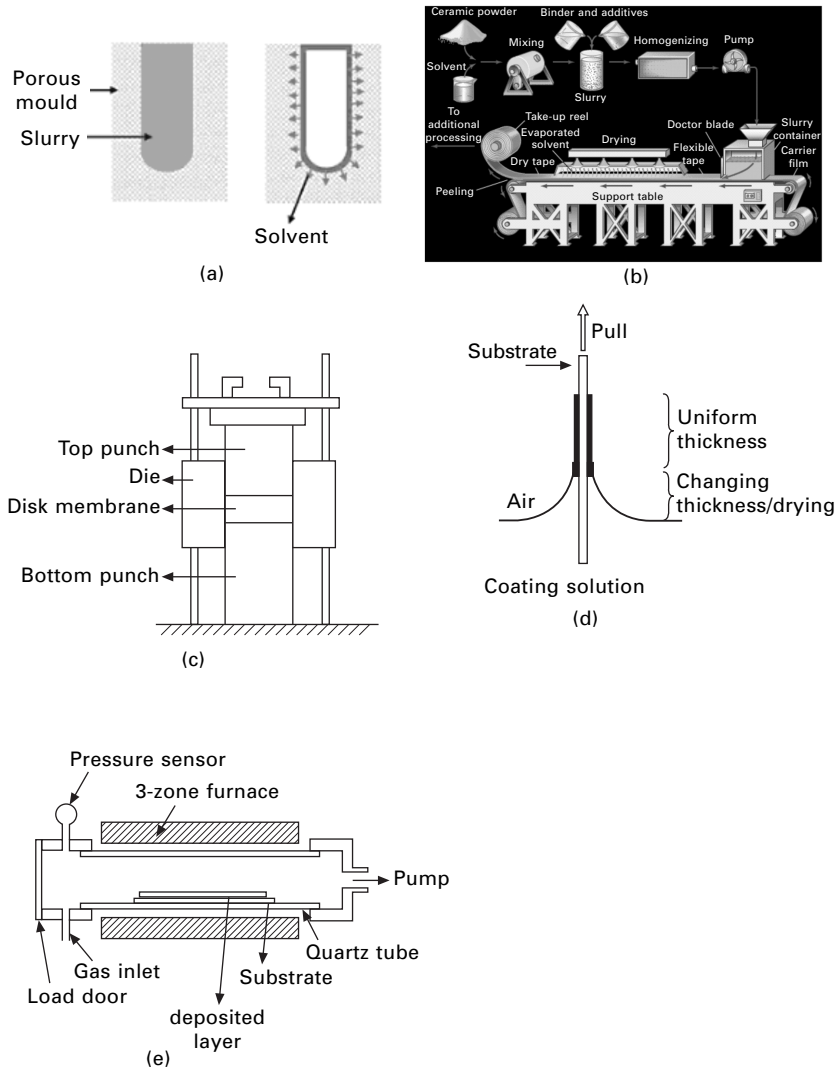
Pressing

Pressing is a commonly used procedure for preparing disc inorganic membranes. As illustrated in Fig. 10.8(c), particle consolidation into a dense layer occurs by an applied force. A special press machine is able to apply more than 100 MPa pressure to press powders into a compacted disc. The diameter of the disc is usually a few centimetres, while the thickness is often around 0.5 mm and the disc is dense after firing.

Dip coating

The critical factors in dip coating are the viscosity of the particle suspension and the coating speed or time (Fig. 10.8(d)). The drying process starts simultaneously with the dip coating, when the substrate is in contact with the atmosphere at a relative humidity below 100%. In a multiple step process, after calcination of the first layer, the complete cycle of dipping, drying and calcinations is repeated.

© Woodhead Publishing Limited, 2011



10.8 Techniques used for the fabrication of ceramic membranes.

Chemical vapour deposition

Chemical vapour deposition (CVD) is a technique that enables the properties of membrane surfaces to be modified by depositing a layer of the same or a different compound via chemical reactions in a gaseous medium surrounding the component at elevated temperatures. The CVD system includes a mixture of reactive and carrier gases, a heated reaction chamber and a system for the treatment and disposal of exhaust gases (Fig. 10.8(e)).

© Woodhead Publishing Limited, 2011

The gas mixture, which typically consists of hydrogen, nitrogen or argon and reactive gases such as metal halides and hydrocarbons, is carried into the reaction chamber and heated at the desired temperature. A typical application of this technique is the formation of a nickel aluminide film on the surface of nickel by reaction of aluminium trichloride and hydrogen from the vapour with the surface of nickel at high temperature.

Metal membranes

Dense metal membranes have attracted the interest of many researchers owing to their permselective characteristics which could permit complete separation of products from gaseous mixtures. Taking into account the so-called 'hydrogen economy', a short résumé of preparation techniques of palladium membranes is reported in Table 10.2.

Application of inorganic membranes to the treatment of hydrocarbon streams

Several inorganic membranes applications include processes such as dehydrogenation, hydrogenation and oxidation reactions such as formation of butadiene from butane, styrene production from ethyl benzene by means of dehydrogenation, water–gas shift reaction and oxidative coupling of methane in membrane reactor (Hsieh, 1996).

Dehydrogenation

An example of dehydrogenation of cyclohexane to benzene with 99% cyclohexane conversion has been proposed by Itoh (Itoh, 1987) through a Pd/Ag membrane tube packed with 0.5% Pt/Al_2O_3 catalyst. The reaction was carried out at 200°C and 1 atm (1.01×10^5 Pa), using an argon stream saturated with cyclohexane vapour and the feed rate was kept very low in order to obtain high cyclohexane conversion. Moreover, the sweep gas was used to collect the H_2 permeating through the Pd membrane. Kikuchi and co-workers (Kikuchi *et al.*, 1989; Kikuchi, 1995, 1997; Maksudu *et al.*, 1993) also used a Pd alloy coated onto a mesoporous membrane support for the dehydrogenation of isobutane. In their study, isobutane was passed over a Pt/Al_2O_3 catalyst packed into the membrane. The yield of isobutylene increased from the equilibrium value of 6% to 23% at 400°C using this kind of membrane.

Ethylbenzene dehydrogenation to styrene is another dehydrogenation reaction worthy of mention in the petrochemical industry. Liu *et al.* (1993) have proposed using a two-stage packed bed reactor followed by a membrane reactor, where the mesoporous membrane is packed with a commercial

© Woodhead Publishing Limited, 2011

Table 10.2 Advantages and limitations of the methods of preparation of dense palladium membranes

Method	Advantages	Limitations
Cold rolling	The material possesses good characteristics, good electronic properties, corrosion resistance and high catalytic activities.	This treatment can enhance H_2 solubility in palladium and its alloys owing to the accumulation of H_2 excess in the stress field around dislocations.
Physical vapour deposition (PVD)	Materials can be deposited with improved properties compared to the substrate material. Almost any type of inorganic material can be used as well as some kinds of organic materials.	It is a line-of-sight technique meaning that it is extremely difficult to coat undercuts and similar surface features; High capital cost; Some processes operate at high vacuums and temperatures requiring skilled operators; Processes requiring large amounts of heat require appropriate cooling systems; The rate of coating deposition is usually quite slow.
Spray pyrolysis	Very simple technique.	Shows quite low separation factor.
Sputtering and magnetron sputtering (MS)	The sputtered film consists of smaller grains with better adhesion to the substrates. Composition may be controlled by the evaporation rates. The growth surface is constantly under electron bombardment and thus is highly energetic.	The main disadvantage, in this case, is a strong decrease in the substrate ion current when increasing the substrate-to-target distance. Direct deposition of alloys is not easily controlled owing to different partial pressures and evaporation rates from the melting of the components.
Solvated metal atom deposition	The method allows the easy introduction of the metal phase on to the inner surface of a tubular membrane.	Need of metal vapour
Electroplating (EP)	Deposit is extremely hard and wear resistant; Thick deposits can be machined for repair/tolerance applications; Simple, well-understood technology. Wide range of applications; Surface offers good lubricity characteristics; In combination with nickel underplating, it can offer good corrosion resistance.	Slow rate of deposition; multiple coats often needed; Machining needed to get uniform thickness; Susceptible to H_2 embrittlement; Exhibits brittleness, leading to micro-cracking and reduced corrosion resistance; Decontamination of plating solutions is difficult.

© Woodhead Publishing Limited, 2011

Table 10.2 Continued

Method	Advantages	Limitations
Electroless plating deposition (ELP)	Uniformity of deposits on complex shapes and hardness.	Difficult thickness control, costly losses of palladium in the bath, purity of the deposit not guaranteed.
Electrochemical vapour deposition (EVD)	The growth rate of the film can be controlled by the reactant concentration, reaction temperature and pressure. Uniform thickness layer.	High reaction temperature, presence of corrosive gases, and relatively low deposition rate

potassium-promoted iron oxide catalyst for styrene production. In this system, an enhancement of the 4% yield of styrene has been observed.

Oxidative coupling of methane (OCM)

Porous ceramic membrane reactors can be used for oxidative coupling of methane (OCM). There are mainly two methods, direct or indirect routes, that have been studied in converting methane to chemicals and liquid fuels. The direct route is the oxidative coupling of methane (OCM) into C_2 hydrocarbons such as ethane and ethylene. The indirect route is the production of syngas (H_2 and CO mixture) by steam reforming or a partial oxidative reaction of methane followed by a further conversion into higher hydrocarbons by the Fischer–Tropsch process. Comparatively, the direct route is economically more promising if the C_2 yield can be considerably improved.

Coronas *et al*. (1994) used a porous α-alumina membrane improving the membrane surface area and related acidity by depositing silica sol inside the porous alumina structure and further impregnating with Li_2CO_3 solution. The membrane reactor was packed with Li/MgO catalyst. At 750°C and a feed molar ratio CH_4/O_2 of 4/1, there was 28% CH_4 conversion and C_2 selectivity of 60–65%. Wang *et al*. (2005) achieved 70% CH_4 conversion and 70% C_2 selectivity using a reactor of dense membrane tubes made from $Ba_{0.5}Sr_{0.5}Co_{0.8}Fe_{0.2}O_{3-\delta}$, packed with La-Sr/CaO catalyst at 850°C.

Methane steam reforming (MSR)

Nowadays, methane steam reforming (MSR) is used to produce H_2 and syngas economically. This reaction is carried out at high temperature and pressure, but if H_2 is selectively removed from the reaction system, the reactants are shifted towards the products, obtaining an efficient conversion of CH_4 to CO_2 and H_2. Indeed, the MSR reaction can be performed in an inorganic Pd-based membrane reactor at lower operating temperatures obtaining higher

© Woodhead Publishing Limited, 2011

H_2 production than conventional processes (Kikuchi, 2000). Uemiya *et al.* (1991) demonstrated that MSR can be enhanced using Pd/Ag alloy membrane coated onto a porous glass tube packed with an alumina supported Ni catalyst. At a H_2O/CH_4 feed molar ratio of 3/1, they achieved 80% CH_4 conversion at 1 atm and 500°C versus an equilibrium value of ~ 42%.

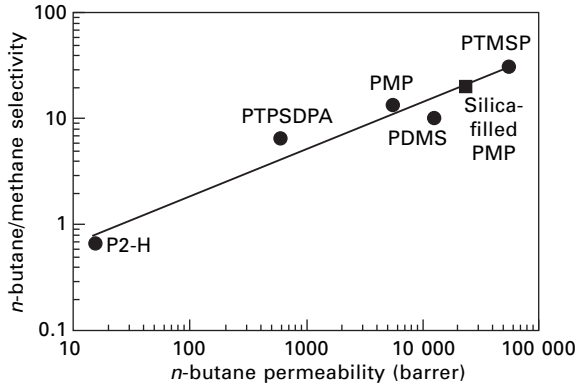
10.2.4 Organic–inorganic nanocomposite membranes for developed hydrocarbon separations

Nanocomposite hybrid materials are the result of the integration of two apparently conflicting classes of materials. Nanocomposite structures have the advantage of combining, in well-defined textures, the extraordinary mechanical and thermal stability of inorganic materials with the flexibility, processability, permselectivity and scalability of organic polymers. An improvement in the transport properties is often a result of this union. Hybrid systems have been realized through a rational design and combination of pore size, chemical moieties and a suitable ratio between inorganic and organic components (Javaid *et al.*, 2006). The loading of inorganic nanoparticles, as well as the compatibility between the inorganic and organic phase, plays a decisive role in the redistribution of free volume and modulation of the affinity for penetrating molecules.

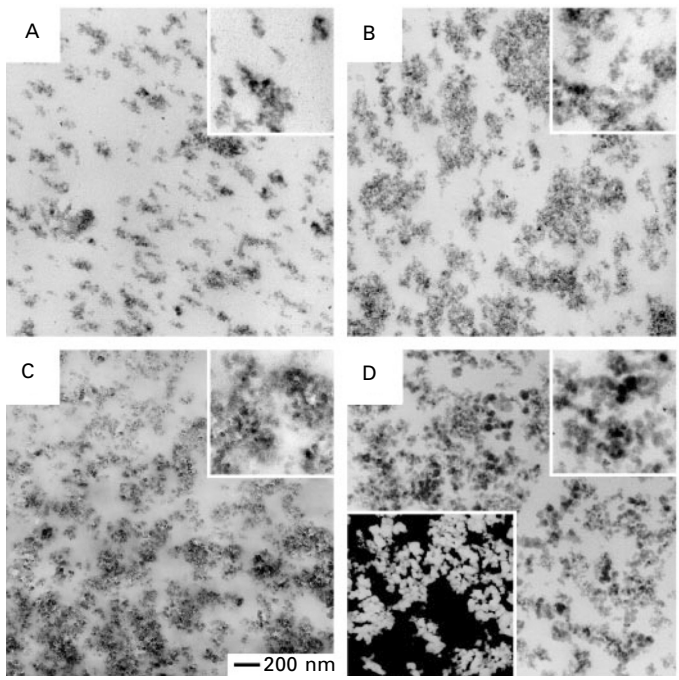
He *et al.* (2002) proposed nanocomposite membranes based on poly(4-methyl-2-pentyne) (PMP) and nano-sized fumed silica fillers as an alternative to the less chemically resistant PTMSP, yielding an interesting indication about the attractive performance of these materials in removing C_2^+ hydrocarbons. Specifically, a *n*-butane/methane separation factor of 26 and a *n*-butane permeability of 19 000 barrer have been estimated when 30% of hydrophilic silica has been added to PMP (Fig. 10.9). Most surprising was a simultaneous increase in *n*-butane/methane selectivity and *n*-butane permeability, contrary to more conventional trade-off relationship between selectivity and permeability in polymers. Indeed, the addition of fumed silica to PMP enables this polymer to challenge the efficiency and productivity of PTMSP by disrupting the molecular packing by fillers that cause a redistribution of the free volume (Fig. 10.10) (Merkel *et al.*, 2002).

It has been observed that nanoparticles smaller than 50 nm cause a significant increase in permeability owing to the high polymer/particle interfacial area, resulting in amplified *d*-spacing (Fig. 10.10). In contrast, a restriction of the diffusional pathway was observed when cloisite Na^+ nanoclays were added to poly(ethylene-*co*-vinyl acetate) (EVA) in the separation of chloroform from acetone via pervaporation (Anilkumar *et al.*, 2008). In this case, an ultra-thin dispersion of exfoliated silicates promotes strong interactions between the polymer chains and the layered nanoclays, resulting in ten-fold higher chloroform/acetone selectivity: $\alpha = 3.8$ for unfilled membranes and

© Woodhead Publishing Limited, 2011



10.9 Mixed-gas n-C_4H_{10}/CH_4 selectivity vs n-C_4H_{10} permeability measured for different polymers (He *et al.*, 2002).



10.10 TEM images obtained from PMP containing hydrophilic fumed silica (TS-530) at (a) 15/6 wt%/vol; (b) 30/13 wt%/vol; (c) 40/19 wt%/vol and (d) hydrophilic fumed silica (L-90) at 40/19 wt%/vol. The matched contrast-inverted image is a Si image (d), which confirms that the particles are siliceous. Image reproduced from Merkel *et al.* (2002) with the permission of *Science*.

© Woodhead Publishing Limited, 2011

$\alpha = 36$ for membrane containing 3% nanoclays. The reduced permeability is a direct consequence of an increase in the tortuosity of the path. In this case, the membrane has been demonstrated to act as a third phase that breaks the chloroform/acetone azeotrope, overcoming the limits of evaporative selectivity.

Desirable *n*-butane/hydrogen permselectivity with higher permeability was also achieved when tubular ceramic supports were coated by PDMS solutions (Jannatduost *et al.*, 2010). In this case, the ceramic membranes work as mechanical supports, whereas the thin PDMS film is the real active layer revealing a separation dominated by the solution–diffusion mechanism.

Engineered membranes have been proposed from a combination of mesoporous support and dendimetric organic phases for the removal of propane from nitrogen (Yoo *et al.*, 2009). In contrast to PDMS ($\alpha_{C_3H_8/N_2} = 18$), an increase up to 70 in propane/nitrogen selectivity has been achieved as a result of the action of hyperbranched structure of the dendrimetric structure, which is responsible for an enhanced solubility selectivity and a high free volume with a ratio of diffusivity close to unity. A similar approach had been exploited to remove toluene from nitrogen (Javaid *et al.*, 2006). Octadecyltrichlorosilane (OTS), phenyltrichlorosilane (PTS) and triazine-based hyperbranched molecules have been chemically and physically attached to the surfaces of mesoporous (~5 nm) alumina substrates in order to afford simultaneous control over both the chemistry and free volume. Different toluene/nitrogen selectivity and toluene permeability values have been achieved as a function of the chemical moieties and/or molecular shape of the organic modifiers (Javaid *et al.*, 2006). This is reasonably difficult to obtain with purely organic or inorganic materials.

A viable alternative to more conventional polymer and inorganic membranes is also represented by embedding carbon nanotubes (CNTs) in polymer matrixes which seems to overcome any limitations in terms of costs of fabrication, long-term stability, handling and permselectivities (Ismail *et al.*, 2009). Nanoscale confinement causes differences in the adsorption and diffusion of penetrating molecules when compared to the bulk. Any studies based on computer simulation (Mao and Sinnott, 2001; Cao and Wu, 2004; Lee and Sinnott, 2004) have, for example, demonstrated that the diffusion of hydrocarbon binary mixtures, that is methane/ethane, methane/*n*-butane and methane/isobutene mixtures, depends mainly on the diameter of CNTs on the nanometer scale, resulting in a higher dynamic flow of the penetrant through larger CNTs and slower flow dynamics when strong reciprocal interactions occur in effect causing an increased density of molecules inside the channels. Predictive models suggest that the molecular structure is a critical issue for the diffusion of hydrocarbons in nanotubes. The separation factor is predicted to decrease with rising CNT diameters, whereas larger hydrocarbons are expected to adsorb more readily to the interior walls of

© Woodhead Publishing Limited, 2011

CNTs, especially if they have a linear molecular structure (Mao and Sinnott, 2001; Cao and Wu, 2004; Lee and Sinnott, 2004).

10.3 Separation of olefins and paraffins

Low molecular weight olefins represent an important resource for the chemical industry, especially for the production of valuable polyolefins such as polyethylene, polypropylene, polystyrene and so on. Their separation from their paraffin analogues is, however, a critical concern if we consider the narrow range of boiling temperatures. Once more, membrane technology can be regarded as a cost-effective and energy-saving alternative to conventional distillation (Eldridge, 1993). Much effort has been expended to separate olefin/paraffin mixtures via membrane processes (Semenova, 2004). Polyimides with bulky substituents such as dicarboxy phenylhexafluoropropane dianhydride (6FDA) dianhydrides, trimethyl phenylene diamine (TrMPD) diamines, tetramethylphenyldiamine (TeMPD), dimethyldiaminobenzo thiophene dioxide (DDBT) thiophenes together with poly(phenylene oxide) (PPO), polysulfone, ethyl cellulose (EC) and PDMS have been among the most used polymeric materials for the separation of ethylene/ethane ($\alpha = 2.9–4.4$), propylene/propane ($\alpha = 30$) and 1,3-butadiene/*n*-butane ($\alpha = 67–190$) (Tanaka *et al.*, 1996; Okamoto *et al.*, 1997; Staudt-Bickel and Koros, 2000). The performance of these glassy polymers under various operating conditions has largely been discussed in relation to diffusion selectivity and solubility selectivity, arguing the dependence of olefin/paraffin selectivity on partial pressure of the penetrants and temperature, respectively (Semonova, 2004).

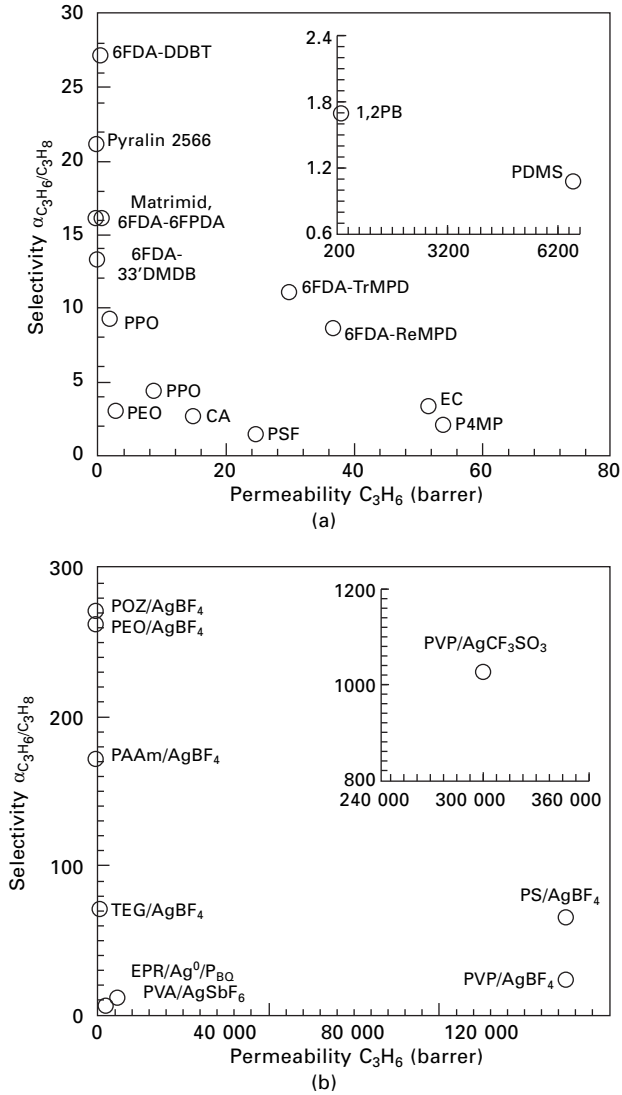
Interesting behaviour has been observed for poly(ethyleneoxide) (PEO). Despite the lowest critical temperature, the olefins exhibit higher solubility than their paraffin analogues, resulting in a propylene/propane separation factor of 2.7 and solubility selectivity of 1.7 at infinite dilution (Lin and Freeman, 2004). Similar behaviour can be ascribed to the favourable interactions of the olefins with the polar ether oxygen included in the backbone of PEO.

10.3.1 Facilitated transport membranes

The tendency of the olefins to form complexes, especially with metal ions, has been successfully exploited in separation processes based on facilitated transport mechanisms (Azhin *et al.*, 2008). This approach appears to be more effective than traditional use of purely glassy and rubbery polymeric membranes (Azhin *et al.*, 2008; Burns and Koros, 2003), since higher permeability and selectivity can be achieved (Fig. 10.11).

In chemical facilitated transport, olefins selectively form complexes with the carrier dissolved in a liquid phase immobilized within the pores

© Woodhead Publishing Limited, 2011

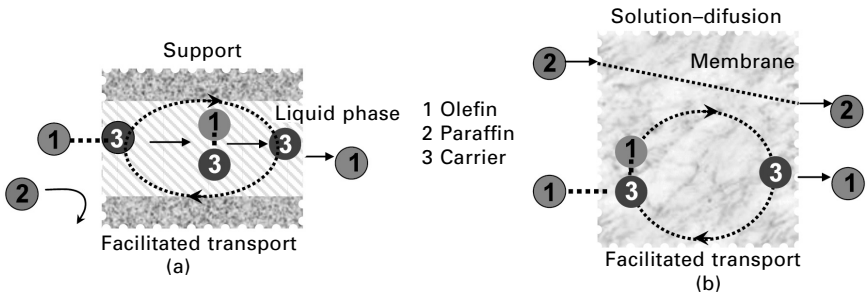


10.11 Propylene/propane selectivity vs propylene permeability: (a) data obtained by solution–diffusion transport through dense membranes (Lin and Freeman, 2004; Azhin *et al.*, 2008); (b) data obtained through facilitated transport through polymeric membranes (Azhin *et al.*, 2008).

of a microporous support (ILM) or embedded in a solid matrix forming an electrolyte membrane (EM) (Fig. 10.12(a,b)).

In contrast, the paraffin cannot interact with the metal ion (M^+) and its mass transfer through the membrane occurs exclusively via a solution–diffusion

© Woodhead Publishing Limited, 2011



10.12 Scheme of facilitated transport through (a) the liquid phase immobilized within pores of a microporous support (ILM) and (b) a solid matrix (EM).

mechanism. The formation of a reversible carrier–olefin complex usually takes place at the upstream membrane surface, involving weak intermolecular interactions such as van der Waals forces via chemisorption or coupled transport mechanisms according to Equations [10.1]–[10.3]:

$$M^+ + \text{olefin} \underset{K_1}{\longleftrightarrow} [M(\text{olefin})]^+ \qquad [10.1]$$

$$[M(\text{olefin})]^+ + M^+ \underset{K_2}{\longleftrightarrow} [M_2(\text{olefin})]^{2+} \qquad [10.2]$$

$$[M(\text{olefin})]^+ + \text{olefin} \underset{K_3}{\longleftrightarrow} [M(\text{olefin})_2]^+ \qquad [10.3]$$

where M^+ is the metal ion and K_1, K_2 and K_3 are the kinetic constants of the complexation reactions of the olefin with metal ion and successive complexes, respectively. Then, the complex is delivered to permeate membrane side, where the olefin is released following the break up of the weak bonds with re-establishment of the carrier.

Despite being effective, immobilized liquid membranes suffer mechanical and chemical instability caused by frequent carrier poisoning and/or drying of the supported liquid phase. This seriously limits the lifetime of the membrane. Doped polymer electrolytes have been developed to overcome these shortcomings. Carriers have been embedded in solid polymers by directing chemical or physical bonds (Park *et al.*, 2001, 2007; Teramoto *et al.*, 2002). High-performance membranes without a permeability–selectivity trade-off have been fabricated (Kim *et al.*, 2004a). An example is given by poly(2-ethyl-2-oxazoline) (POZ)-based membranes which embed $AgBF_4$ electrolytes at (C=O):(Ag) = 1:1 in the separation of propylene/propane mixtures. Similarly, a better performance has been exhibited by PEO membranes containing $AgBF_4$ at 80 wt% with ethylene/ethane and propylene/propane pure-gas selectivity higher than 5500 and 4000, respectively (LeBlanc *et al.*,

© Woodhead Publishing Limited, 2011

1980). Enhanced ethylene/ethane solubility selectivity (α_s) up to 700 was also estimated for PA12-PTMO membranes containing the 70 wt% $AgBF_4$ (Morisato *et al.*, 2002).

The choice of the metal ion is crucial in deciding the productivity of the process, since π-complexation depends on the metal atom electronegativity. Ideal values of electronegativity for a good and reversible complexation range from 1.6 to 2.3, while Ag(I) and Cu(I) are preferable for their capability to form complexes with alkenes easily and reversibly (Azhin *et al.*, 2008). The selection of the counteranion of the salt is also important to facilitate the formation of a weak ionic bond with the cation, resulting in higher dissolution in the polymer. The lattice energies of various anions have been discussed and useful indications have been yielded about the most suitable ion pairs to form solid polymer electrolytes complexes (Azhin *et al.*, 2008). Table 10.3 provides a résumé of the performance of some facilitated transport polymeric membranes for C_2–C_5 olefin separation from mixtures containing paraffin analogues.

10.4 Removal of hydrocarbons from liquid streams

Pervaporation (PV) is a profitable membrane-based technology used successfully for the separation of aromatic/non-aromatic hydrocarbon mixtures in place of the energy-consuming and more expensive conventional distillation, rectification, extraction and crystallization (Razdan *et al.*, 2003; Smitha *et al.*, 2004). An example of an integrated pilot plant which uses the pervaporation technology for the separation of aromatics/aliphatics is displayed in Fig. 10.13 (Matuschewski and Schedler, 2008). This technology is usually used in three main applications, including (i) dehydration of aqueous–organic mixtures, (ii) removal of trace volatile and organic compounds from aqueous solution and (iii) separation of organic–organic solvent mixtures (Smitha *et al.*, 2004, Yamaguchi *et al.*, 1991, 1992; Wang *et al.*, 1998).

10.4.1 Aromatic/aliphatic separation

An exhaustive description of the performance of various polymeric materials used for aromatic/aliphatic hydrocarbon separations has been reported by Smitha *et al.* (2004). Here, we only report some interesting examples of high-performance polymeric membranes for this specific separation (Table 10.4).

In all these operations, the separation is directed by sorption–diffusion transport mechanisms, yielding solubility (β_s) or diffusivity (β_d) selective processes as a function of the material selected to form the membranes (Semenova, 2004). Hydrocarbon sorption into the polymer matrix can, for instance, be directed by the ratio of the boiling temperatures of the

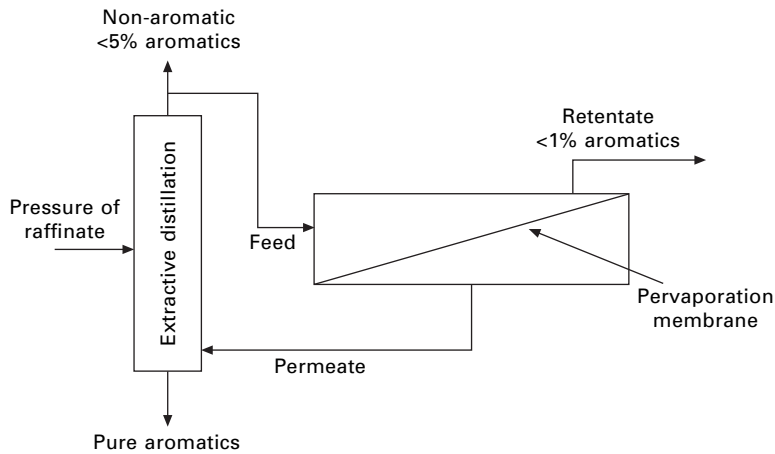
© Woodhead Publishing Limited, 2011

Table 10.3 Permeability and selectivity values estimated for facilitated transport polymeric membranes

Polymer	Permeability (barrer)	Selectivity	Remarks	Reference
		C_2H_4/C_2H_6		
SPEEK	10 000	2700	Hollow fibre	Nymeijer *et al.* (2004)
6M $AgNO_3$ aqueous solution	5130	1000	Supported liquid membrane	Hughes *et al.* (1986)
PEO 10M $AgNO_3$	1200	290	Supported liquid membrane	Teramoto *et al.* (2005)
NAFION 6M $AgBF_4$	700	400	Immobilized liquid membrane (humid gas)	Eriksen *et al.* (1993)
		C_3H_6/C_3H_8		
PVP/$AgCF_3SO_3$ (mol% 0.5)	310 000	1000	Polyelectrolyte membrane	Kim *et al.* (2003)
PS/$AgBF_4$ (mol% 0.5)	110 000	65	Polyelectrolyte membrane	Kim J.H. *et al.* (2004b); Kim S.H. *et al.* (2004c)
SIS (PS 22 wt%)/ $AgBF_4$	40 000	60	Polyelectrolyte membrane	Lee *et al.* (2009)
POZ/$AgBF_4$ (40% humidity)	200	270	Polyelectrolyte membrane	Hong *et al.* (2000)
6FDA-TrMPD	27	10	Dense	Tanaka *et al.* (1996)
		C_4H_8/C_4H_{10}	membranes	
SR-g-AA-Ag^+	2400	2.91	Complex membranes	Yang and Hsiue (1997)
7.5 M $AgNO_3$-glycerol	260	850	Immobilized liquid membrane	Kovvali *et al.* (2002)
PTMSP-g-AA-Ag^+	1000 (*i*-C_4H_8) 4590 (*trans*-C_4H_8)	6.0 (*i*-C_4H_8/*i*-C_4H_{10}) 4.4 (*trans*-C_4H_8/n-C_4H_{10})	Polyelectrolyte membrane	Yang and Hsiue (1996)
		C_5H_8/C_5H_{12}		
$AgBF_4$-CA	390 000	83	Polyelectrolyte membrane	Kim *et al.* (2004a and 2004b)

CA is poly(cellulose acetate); 6FDA-TrMPD is 4,4′-hexafluoroidopropylidene of diphthalic acid-2,4,6-tetramethyl-1,3-phenylenediamine; NAFION® is tetrafluoroethylene (TFE)-perfluorovinyl ether (PSEPVE) copolymer; PVP is poly(N-vinyl pyrrolidone); SR-g-AA is silicone rubber-grafted-poly(acrylic acid); SIS is poly(styrene-*b*-isoprene-*b*-styrene) and SPEEK is sulfonated poly(ether-ether) ketone.

© Woodhead Publishing Limited, 2011



10.13 Integrated pilot plant for separation of aromatics by pervaporation.

components being separated and/or by specific penetrant/polymer segment interactions.

A predictive model to describe the behaviour of aromatic–non aromatic liquid mixtures has recently been proposed by Ghoreyshi *et al.* (2009). The Flory–Huggins (FH) thermodynamic model has been used to describe the sorption step, while the Maxwell–Stefan formulation has been used to describe the transport steps, suggesting dense poly(urethane) membranes as potential effective interfaces working in pervaporation processes in the separation of aromatic/non aromatic hydrocarbons.

The selective removal of aromatic from aliphatic or alicyclic compounds is usually promoted by the introduction of π-acceptor moieties into the polymer matrix. The establishment of favourable π-interactions causes enhanced solubility selectivity, increasing the separation factor. Ethynyl (Takeichi *et al.*, 1994; Gao *et al.*, 1996), phosphorylate (Cabasso, 1983), sulfone (Hao *et al.*, 1997), acrylate (Wang *et al.*, 1999) and phenyl groups (Sun and Ruckenstein, 1995) have been introduced into polymeric membranes in order to increase the membrane affinity for aromatic species. These π-electron acceptor groups also increase the cohesion energy of the polymer, increasing the rigidity of the polymer segment chains and preventing swelling phenomena through the establishment of hydrogen bonding, dipole–dipole, van der Waals interactions and so on. Enhanced diffusion selectivity can be regarded as a result of the reduction of the polymer backbone mobility. This can reasonably be ascribed to the ability of the functional polymer/modifier moieties to form intermolecular interactions (Tsubouchi and Yoshikawa, 1998). Depending on rigidity of the polymer chains, together with the ratio of the molecular size of the compounds being separated, the diffusion parameter of the separation

© Woodhead Publishing Limited, 2011

Table 10.4 Performance of polymeric membranes for aromatic/aliphatic hydrocarbon separation

System (binary liquid mixtures)	Membrane material	Selectivity (α)	Flux (kg μm m^{-2} h^{-1})	Temperature (°C)
Toluene (10–70%)/*n*-hexane	Polyurethane	2.8–5.8	1.1–3.5	25
Toluene (11%)/*n*-octane	Sulfonyl containing polyimide	155	1.1	40
Toluene (50%)/*i*-octane	Ionically cross-linked copolymers of methyl, ethyl, *n*-butyl acrylate with AA	2.5–13	20–1000	40
Benzene (8%)/*n*-hexane	Plasma grafted membrane	210	0.9	70
Benzene/*n*-hexane	Sulfonyl containing polyimide	22	1.2	40
Benzene (60%)/cycloxane	HDPE-g-GMA	19–22	3–3.7	70
Benzene (50%)/cycloxane	PS/PAA	48.4	9.6	20
Benzene (10%)/cycloxane	Carbon graphite-Nylon 6 composite	435	–	–
Benzene/cycloxane (5/15)	PERVAP® 2200 (composite membrane)	71	76.7	25
Benzene/cycloxane (5/15)	PERVAP® 2200 (composite membrane)	68	151	25
p-Xylene (10%)/*o*–xylene	Co-polyimides of 6FDA with DABA	20–300	–	60

(HDPE-g-GMA) = glycidyl methacrylate grafted high density polyethylene, (DABA) = 3,5-diamino benzoic acid, (PS/PAA) = polystyrene/polyamidoamine block copolymers.

factor component (β_d) can decide the final performance of the hydrocarbon separation via pervaporation (Semenova, 2004). For instance, a different type of diffusion has been observed for the benzene/cycloexane and toluene/*i*-octane couples through copolyimides (Fang *et al.*, 1999). In this case, the difference was dependent on the ratios of the minimum cross-sections of the hydrocarbons. In cross-linking treatments the swelling was suppressed, resulting in a reduction in higher diffusion of aromatics over branched or aliphatics and a toluene/*i*-octane separation factor over 300 (Fang *et al.*, 1999).

High-performance inorganic membranes also find suitable application in the separation of hydrocarbon mixtures (Table 10.5), suggesting zeolites as

© Woodhead Publishing Limited, 2011

Table 10.5 Performance of inorganic membranes for aromatic/aliphatic hydrocarbon separation

System (liquid mixtures)	Membrane material	Selectivity (α)	Flux (kg μm m^{-2} h^{-1})	Temperature (°C)
Bz/Cx (5 kPa/5 kPa)	Faujasite-type zeolite membrane	160	561	160
Toluene/*n*-heptane	Faujasite-type zeolite membrane	45	–	60
p-Xylene (10%)/*m*-xylene	Polycrystalline ZSM-5 membrane	0 (high)	Very low	26–75
n-Hexane (45%)/2,2-dimethylbutane	Zeolite membranes on alumina support	243.2	High	300
n-Hexane (10–80%)/2,2-dimethylbutane	Tubular ZSM-5 zeolite membrane	650	–	100
n-Heptane (40%)/*i*-octane (40%)/benzene (20%)	Silicate zeolite membrane	72–34, 68–35	–	86–91

providing ideal resistance interfaces to separate organic molecules, owing to their preferential adsorption, preferential diffusion or pure molecular sieving (Smitha *et al.*, 2004).

10.4.2 Halogenated hydrocarbon separation

Chlorofluorocarbons (CFCs) are largely used as refrigerants, solvents, degreasing agents in the electronic industry, blowing agents in plastic formation and propellants for aerosol cans. Unfortunately, they are inert and may remain in the atmosphere for 40–150 years and cause the destruction of the ozone layer above the earth (Molina and Rowland, 1974). Similarly, the use of disinfectants for wastewater and drinking water causes the formation of halogenated compounds, well-known as disinfectant by-products, resulting in a major source of water pollution (Matamoros and Bayona, 2008). Their recovery and separation from air and water is, therefore, an emergency for environmental safety and health security. In this respect, membrane technology has been envisaged as an economically competitive methodology, while the performance of different membrane materials has been analysed for removal of CFCs from gas and vapour streams, including polyimides (Chung *et al.*, 1995), cross-linked membranes of polymethacrylates with PEO and perfluorononyl moieties (Hirayama *et al.*, 1999), PDMS, PTMSP and 2,2-bistrifluoromethyl-4,5-difluoro-1,3-dioxole/tetrafluoroethylene (Teflon AF 2400) (Pinnau and Toy, 1996a and 1996b; Merkel *et al.*,

© Woodhead Publishing Limited, 2011

1999) and so on. In the last case, it was observed that fluorocarbons are more soluble in fluorinated matrixes (tetrafluoroethylene/trifluoromethyl difluorodioxide copolymers) than their hydrocarbon analogues. Also, low levels of fluorocarbon solubility have been observed in PDMS and PTMSP as a result of unfavourable interactions of the halogenated penetrants with the chemical environment (Merkel *et al.*, 1999). As aforementioned, hybrid composite materials have also been used to remove chlorinated hydrocarbons from liquid mixtures. Poly(ethylene-*co*-vinyl acetate)–clay nanocomposite membranes have been processed in pervaporation operations to remove chloroform from mixtures containing acetone, achieving ten-fold selectivity more than that estimated for unfilled membranes (Anilkumar *et al.*, 2008). Similarly, higher performance has been observed for PDMS membranes filled with amorphous silica, yielding higher CCl_4 and C_2HCl_3 fluxes than water in water exclusion mechanisms (Dotremont *et al.*, 1997). Liu and Xiao (2004) proposed silicalite-filled poly(siloxane imide) membranes for the removal of volatile organic compounds (VOCs) from water, achieving fluxes of 280 g m^{-2} h^{-1} and a separation factor of chloroform over water of 53.2.

10.5 Nanotechnologies from fundamental research to large-scale industry

The market for functional nano-materials is quickly expanding for their enormous applicability in advanced industrial areas such as oil refinery, chemistry and petrochemistry, food and pharmaceutical industries, environmental protection and power engineering. The development of new value-added products and the implementation of innovative technologies are in high demand for (a) modernizing the oil-refining, chemical and petrochemical industries including the treatment of aromatic hydrocarbons and olefins, (b) producing new green energy, (c) preserving the environment and (d) recycling as well as increasing the value of resources, raw materials and energy. Membrane nanotechnology is key to promoting the scale-up from fundamental research to large-scale industry, because it offers attractive opportunities in the design, rationalization and optimization of innovative products. An industrial process can integrate different operations, yielding important benefits in product quality, plant compactness, environmental impact and energetic aspects. High competitiveness and innovation are expected from integrated membrane reactor technologies in many segments of industrial activity, especially in sectors such as the production of hydrogen from steam reforming and shift conversion of natural gas or other hydrocarbons, the production of new greener alternative energy sources such as bio-fuel and the production of new polyolefin-based composite chemicals. Hereafter, two examples of integrated membrane technology processes are discussed:

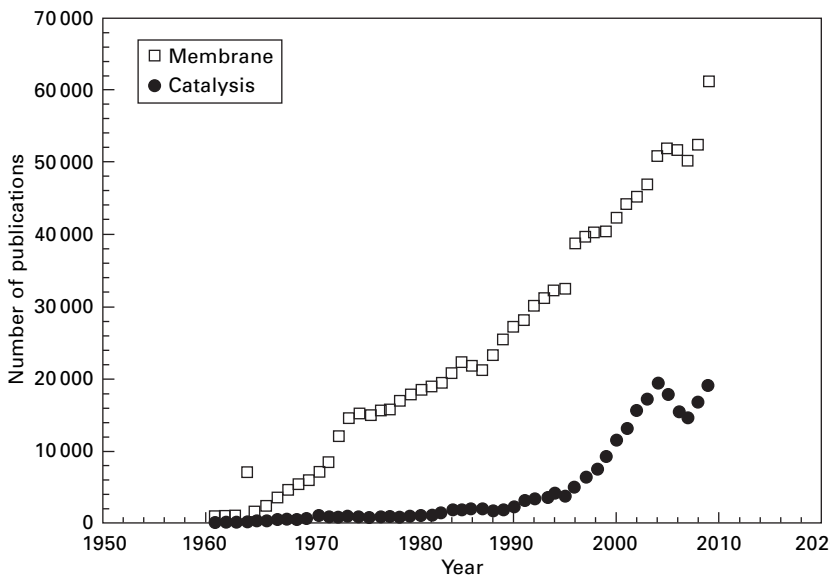
© Woodhead Publishing Limited, 2011

heterogeneous catalysis in the petrochemical industry and bio-fuels production from steam reforming of hydrocarbons.

10.5.1 Membrane catalysis in the petrochemical industry

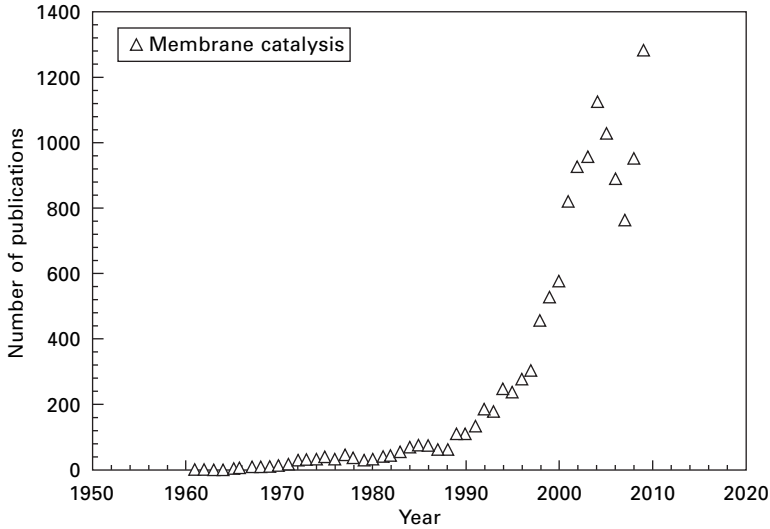
Membrane reactor (MR) technology combines two distinct sciences: catalysis and membranes technology. For many researchers, the difficulty consists in evaluating which of them has more relevance in MR development. However, it is reasonable to believe that catalyst performance is certainly an important factor, in particular to improve hydrogen production units, for example fulfilling the requirements of the integration of fuel processors with fuel cells. Significant progress in both the membrane and catalysis fields is reflected in the increasing number of publications, as shown in Fig. 10.14. Moreover, in the last few decades, membrane catalysis has been studied by several researchers and significant progress in this field is summarized in Fig. 10.15.

Catalytic MR technology can be considered for application in petroleum refineries. For example, when the hydrogen content of the refinery gas is greater than 50% by volume, the hydrogen could be recovered by means of a membrane. In particular, in the field of high purity hydrogen permeation, several Pd-based membranes offer hydrogen permselectivity as a benefit



10.14 Number of publications vs time on membrane technology and catalysis (Data reported were found using the Elsevier Scopus database research: http://scopees.elsevier.com).

© Woodhead Publishing Limited, 2011



10.15 Number of publications vs time on membrane catalysis (Data reported were found using the Elsevier Scopus database research: http://scopees.elsevier.com).

and there are a number of interesting process applications being considered, such as dehydrogenation, oxydehydrogenation and decomposition reactions. Furthermore, permselective hydrogen membranes could be used to perform selective hydrogenations of organic substrates and coupled reactions (Dittmeyer *et al.*, 2001; Gobina and Hughes, 1996a and 1996b). In particular, these membranes allow the hydrogen production to be enhanced in processes such as steam reforming, the water–gas shift reaction or the conversion of natural gas to syngas and liquid fuels (Basile 2008; Basile *et al.*, 2008a, 2008b and 2008c; Mendes *et al.*, 2009; Farris and Armor, 1993).

10.5.2 Hydrogen production from steam reforming of hydrocarbons via membrane reactors technology: opportunity to exploit biofuels

The development of a strategy to exploit alternative and renewable energy sources represents an important scientific issue when considering climate change and the increasing cost of oil and gas. The combination of hydrogen, as a novel energy carrier, and proton exchange membrane fuel cells (PEMFCs), as efficient energy converters, may play an important role on this respect.

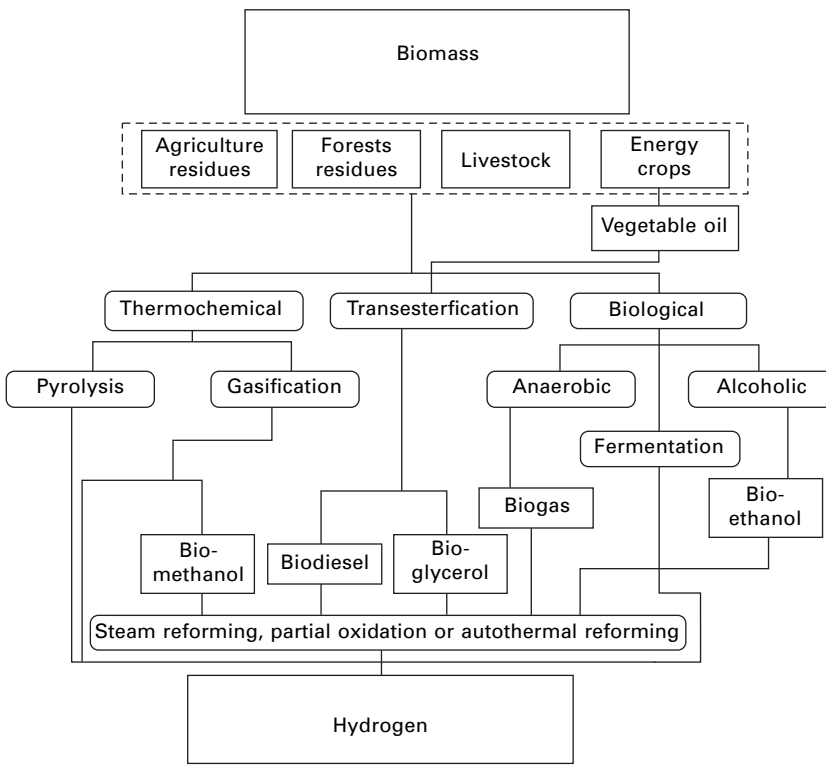
The steam reforming (SR) reaction of biofuels (bioethanol, glycerol, acetic acid, etc.) could be used to produce a hydrogen-rich gas that could be purified as CO_x-free hydrogen to supply a PEMFC. An outline of hydrogen

© Woodhead Publishing Limited, 2011

production via different biosources is shown in Fig. 10.16 and a list of the main biofuels is reported below:

- Bioethanol contains ethanol, water and other by-products, produced from biomass and/or the biodegradable fraction of general or agricultural waste;
- Biomethanol: methanol produced from biomass;
- Biodiesel: a methyl-ester produced from vegetable or animal oil;
- Bioglycerol: glycerol produced as a by-product of biodiesel;
- Biogas: a fuel gas produced from biomass and/or the biodegradable waste that can be treated in a purification plant in order to achieve a quality similar to natural gas.

SR of biofuels, performed in fixed bed reactors (FBRs), produces a hydrogen-rich gas stream containing other by-products such as mainly CO, CH_4 and CO_2. Therefore, in order to supply a PEMFC, which can tolerate only few ppm of CO (<10), hydrogen from a reformer needs to be purified by the following processes: water gas shift (WGS) reactors, pressure swing adsorption (PSA) and/or Pd membrane separation, and so on.



10.16 Selected hydrogen production technologies from biomass.

© Woodhead Publishing Limited, 2011

As an innovative technology, dense self-supported Pd/Ag MRs could be proposed as an alternative solution to the conventional systems for pure or CO_x-free hydrogen production (Basile, 2008; Basile *et al.*, 2008a, 2008b and 2008c; Cheng *et al.*, 2002; Damle, 2009; Matsumura and Tong, 2008; Tosti *et al.*, 2000; Valenti and Macchi, 2008).

In particular, with respect to the FBRs, MR technology is able:

- to combine chemical reaction and hydrogen separation in one system, reducing the capital costs;
- to favour the conversion enhancement of equilibrium-limited reactions. In fact, by selective removal of one or more products from the reaction side, thermodynamic equilibrium restrictions can be overcome, owing to the so-called 'shift effect';
- to achieve higher conversions than FBRs, operating under the same MR conditions, or in contrast, the same conversion, but operating under milder conditions;
- to improve the hydrogen yield and hydrogen selectivity;
- to produce high purity hydrogen.

A short overview on the membrane type, operative conditions and performances (reaction conversion and hydrogen recovery defined as the molar ratio between the CO_x-free hydrogen permeated stream and the total hydrogen really produced) obtained carrying out SR of different biosources in MRs is reported in Table 10.6. It illustrates the ability of MR to obtain almost complete reactant conversion under different reactions, as well as, in particular, the further advantage of producing pure or, at least, CO_x-free hydrogen supply, for example, to a PEMFC by using a Pd-based MR in the temperature range between 250°C and 600°C.

Only a few studies of bioethanol steam reforming reaction focus on MRs in detail. As illustrated in Table 10.6, Pd/Ag MR technology makes it possible for this process to reach around 95%, hydrogen recovery working at 3.0 bar reaction pressure and almost complete bioethanol conversion (Gernot *et al.*, 2006; Iulianelli and Basile, 2010; Iulianelli *et al.*, 2010a). These great results in terms of high conversion and hydrogen recovery are emphasized when high pressure and temperature are used as a consequence of the well-known membranologist's 'shift effect'. In practice, high reaction pressures affect the hydrogen permeation driving force positively, allowing a higher hydrogen permeating flux through the Pd/Ag membrane to be realized. This involves higher bioethanol conversion as well as higher hydrogen production and, in particular, a greater hydrogen stream permeating through the membrane.

The approach of a single step membrane reformer using Pd/Ag membranes was also demonstrated in reforming of liquid hydrocarbon fuels such as butane and methanol in order to produce pure hydrogen. Table 10.6 confirms

© Woodhead Publishing Limited, 2011

Table 10.6 Overview of operative conditions and performances of MRs used to carry out the SR reaction of biosources

Membrane	Catalyst	Temperature (°C)	H_2-recovery (%)	Conversion (%)	Ref.
Bioethanol steam reforming					
Composite Pd-based	–	600	–	100	Gernot *et al.* (2006)
Dense Pd/Ag	Co/Al_2O_3	400	30	95	Iulianelli and Basile (2010)
Dense Pd/Ag	Co/Al_2O_3	400	95	100	Iulianelli *et al.* (2010a)
Methanol steam reforming					
$Pd_{75}Ag_{25}$		300	96		Wieland *et al.* (2002)
$Pd_{60}Cu_{40}$			78		
Pd/V/Pd			–		
Dense Pd/Ag	$Cu/ZnO/Al_2O_3$	250		80	Basile *et al.* (2005)
TiO_2/Al_2O_3 asymmetric porous	Ru/Al_2O_3	350		30	Gallucci *et al.* (2007);
commercial membrane with a Pd/Ag deposit		600		100	Basile *et al.* (2006)
Commercial asymmetric porous ceramic		350		45	
membrane with a Pd/Ag deposit		550		65	
Pinhole free Pd/Ag membrane tube		350		87	
Dense Pd/Ag	$CuOAl_2O_3ZnOMgO$	450		100	Basile (2008); Basile *et al.* (2008a, 2008b and 2008c)
		300		100	
Dense Pd/Ag	Cu/Zn/Mg-based	300	93		Iulianelli *et al.* (2008a and 2008b)
Pd/Ag based	–	450	15	76	Damle (2009)
		550	45	73	
		600	50	72	
			53	71	
			60	75	
Bioglycerol steam reforming					

Continued

© Woodhead Publishing Limited, 2011

Table 10.6 Continued

Membrane	Catalyst	Temperature (°C)	H_2-recovery (%)	Conversion (%)	Ref.
Bioethanol steam reforming					
Dense Pd/Ag	Co/Al_2O_3	400	60	94	Iulianelli *et al.* (2010a)
Dense Pd/Ag	Ru/Al_2O_3	400	16	20	Iulianelli *et al.* (2010b)
Dimethyl ether steam reforming		350			
Porous stainless steel supported membrane	Cu/Al_2O_3	450	–	50 100	Park *et al.* (2008)
Acetic acid steam reforming					
Dense Pd/Ag	Ni/Al_2O_3	400	32 36	100 100	Basile, (2008); Basile *et al.* (2008a, 2008b and 2008c)
Dense Pd/Ag	Ni/Al_2O_3 – Ru/Al_2O_3	450	26 32	92 98	
Dense Pd/Ag	Ni/Al_2O_3	400	70		Iulianelli *et al.* (2008c)
Methane steam reforming					
Dense Pd/Ag	Ni/Al_2O_3	450	70	50	Iulianelli *et al.* (2011)
Dense Pd/Ag	Ni/ZrO	450	83	70	Iulianelli *et al.* (2010c)
n-butane dehydrogenation					
Supported Pd/Ag	Pd/Al_2O_3	410	99	40	Gobina and Hughes (1996a and 1996b)
Propane dehydrogenation					
Pd/Ag composite	Pt/Al_2O_3	450	–	42	Wu *et al.* (2009)
Isobutane dehydrogenation					
Pd/Ag composite	Cr_2O_3/Al_2O_3	500	–	70	Guo *et al.* (2003)

© Woodhead Publishing Limited, 2011

the validity of this technology, reflecting high methanol conversion, in some cases equal to 100%.

Furthermore, the specialized literature reported in Table 10.6 shows that glycerol, as a by-product of biodiesel production, can be largely converted (94% conversion) via the steam reforming reaction using Pd/Ag MRs, further recovering hydrogen at medium reaction pressure (4.0 bar) (Iulianelli *et al.*, 2010b and 2011). Table 10.6 in particular reports the results of dimethyl ether reforming performed in non-palladium-based stainless steel-supported composite membranes. In this case, the absence of the selective removal of hydrogen, typically realized through palladium-based membranes, is reflected in lower performances in terms of conversion and hydrogen recovery.

The methane steam reforming reaction is conventionally the most used reaction for producing hydrogen. It has been largely studied in both fixed bed and membrane reactors (Pistonesi *et al.*, 2007; Matsumura and Nakamori, 2004; Hou and Hughes, 2001; Chen *et al.*, 2007, 2008; Levent *et al.*, 2003; Tong and Matsumura, 2005, 2006; Profeti *et al.*, 2008; Kikuchi *et al.*, 2000; Lin *et al.*, 2003) and Table 10.6 shows some novel results achieved by adopting dense Pd/Ag self-supported membrane reactors (Iulianelli *et al.*, 2010c; Basile *et al.*, 2011).

Even the dehydrogenation reaction of hydrocarbons has been extensively studied exploiting the ability of MRs that allow the continuous removal of hydrogen from the reaction zone during dehydrogenation, thus offering the possibility of substantially increasing the conversion and/or lowering the reaction temperature in endothermic, equilibrium-limited reactions of this type. Table 10.6 sketches few results concerning the application of Pd/Ag-based MRs to the dehydrogenation reaction of hydrocarbons such as *n*-butane, isobutane and propane. However, although there is relevant research in literature concerning MR technology applied to exploit hydrocarbons and biofuels for hydrogen production, some deficiencies need to be overcome before implementation on larger scales. Moreover, future research should be devoted to the preparation of defect-free membranes able to work for long periods at high temperatures and pressures as well as to MR technology cost evaluation for larger scale applications.

10.6 References

Ahmad F, Mukhtar H, Man Z and Dutta B K (2007), 'Predicting separation of lower hydrocarbon from natural gas by a nano-porous membrane using capillary condensation', *Chem Eng Technol*, **30**, 1266–73.

Anilkumar S, Kumaran M G and Thomas S (2008), 'Characterization of EVA/Clay nanocomposite membranes and its pervaporation performance', *J Phys Chem B*, **112**, 4009–15.

Azhin M, Kaghazchi T and Rahmani M (2008), 'A review on olefin/paraffin separation using reversible chemical complexation technology', *J Ind Eng Chem*, **14**, 622–38.

© Woodhead Publishing Limited, 2011

Bai S, Sridhar S and Khan A A (1998), 'Metal-ion mediated separation of propylene from propane using PPO membranes', *J Membrane Sci*, **147**, 131–9.

Baker R W (2004), *Membrane Technology and Applications*, John Wiley & Sons, New York.

Baker R W and Wijmans J G (1994), 'Membrane separation of organic vapors from gas streams', in *Polymeric gas separation membranes*, D.R. Paul, Y.P. Yampolskii (eds), CRC Press, Boca Raton, 353–97.

Baker R W, Cussler E L, Eykamp W, Koros W J, Riley R L and Strathmann H (1991), *Membrane Separation Systems: recent development and future directions*, Noye Data Corporation, Park Ridge, NJ.

Baschetti M G, Ghisellini M, Quinzi M, Doghieri F, Stagnaro P, Costa G and Sarti G C (2005), 'Effects on sorption and diffusion in PTMSP and TMSP/TMSE copolymers of free volume changes due to polymer ageing', *J Mol Struct*, **739**, 75–86.

Basile A (2008), 'Hydrogen production using Pd–based membrane reactors for fuel cells', *Top Catal*, **51**, 107–22.

Basile A, Gallucci F and Paturzo L (2005), 'A dense Pd/Ag membrane reactor for methanol steam reforming: Experimental study', *Catal Today*, **104**, 244–50.

Basile A, Tosti S, Capannelli G, Vitulli G, Iulianelli A, Gallucci F and Drioli E (2006), 'Co-current and counter-current modes for methanol steam reforming membrane reactor: Experimental study', *Catal Today*, **118**, 237–45.

Basile A, Gallucci F, Iulianelli A, Borgognoni F and Tosti S (2008a), 'Acetic acid steam reforming in a Pd–Ag membrane reactor: The effect of the catalytic bed pattern', *J Membrane Sci*, **311**, 46–52.

Basile A, Gallucci F, Iulianelli A and Tosti S (2008b), 'CO-free hydrogen production by ethanol steam reforming in a Pd-Ag membrane reactor', *Fuel Cells*, **8**, 62–8.

Basile A, Parmaliana A, Tosti S, Iulianelli A, Gallucci F, Espro C and Spooren J (2008c), 'Hydrogen production by methanol steam reforming carried out in membrane reactor on Cu/Zn/Mg-based catalyst', *Catal Today*, **137**, 17–22.

Basile A, Campanari S, Manzolini G, Iulianelli A, Longo T, Liguori S, De Falco M and Piemonte V (2011), 'Methane steam reforming in a Pd–Ag membrane reformer: an experimental study on the reaction pressure influence at middle temperature', *Int J Hydrogen Energy*, **36**, 1531–9.

Battelle (2007), *The Business of Innovation in Sediment Toxicity of Petroleum Hydrocarbon Fractions*', Report for Massachusetts Department of Environmental Protection Office of Research and Standards, Duxbury, MA, 1–89.

Burns R L and Koros W J (2003), 'Defining the challenges for C_3H_6/C_3H_8 separation using polymeric membranes', *J Membrane Sci*, **211**, 299–309.

Cabasso I (1983), 'Organic liquid mixtures separation by permselective polymer membranes. 1. Selection and characteristics of dense isotropic membranes employed in the pervaporation process', *Ind Eng Chem Prod Res Dev*, **22**, 313–19.

Cao D and Wu J (2004), 'Self-diffusion of methane in single–walled carbon nanotubes at sub- and supercritical conditions', *Langmuir*, **20**, 3759–65.

Chen L, Hong Q, Lin J and Dautzenberg F M (2007), 'Hydrogen production by coupled catalytic partial oxidation and steam methane reforming at elevated pressure and temperature', *J Power Sources*, **164**, 803–8.

Chen Y, Wang Y, Xu H and Xiong G (2008), 'Efficient production of hydrogen from natural gas steam reforming in palladium membrane reactor', *Appl Catal B: Env*, **80**, 283–94.

Cheng Y S, Pena M A, Fierro J L, Hui D C W and Yeung K L (2002), 'Performance of

© Woodhead Publishing Limited, 2011

alumina, zeolite, palladium, Pd–Ag alloy membranes for hydrogen separation from Towngas mixture', *J Membrane Sci*, **204**, 329–40.

Chung I J, Lee K R and Hwang S T (1995), 'Separation of CFC-12 from air by polyimide hollow-fiber membrane module', *J Membrane Sci*, **105**, 177–85.

Consolati C, Cenco I, Pecoraro M and Zanderichi L (1996), 'Positron annihilation lifetime (PAL) in poly(1-(trimethylsilyl) propine) (PTMSP): free volume determination and time dependence of permeability', *J Polym Sci: Part B: Polym Phys*, **34**, 357–67.

Coronas J, Menendez M and Santamaria J (1994), 'Methane oxidative coupling using porous ceramic membrane reactors: II. Reaction studies', *Chem Eng Sci*, **49**, 2015–25.

Cummins W R, Dupuis G, Kesari S, Miner D, Trilli K and Fleming G (1997), 'The future of perfluorocarbon capture and recycling: Membrane technology', *Semiconductor Int*, **20**, 265–72.

Damle A S (2009), 'Hydrogen production by reforming of liquid hydrocarbons in a membrane reactor for portable power generation – Experimental studies', *J Power Sources*, **186**, 167–77.

Dittmeyer R, Höllein V and Daub K (2001), 'Membrane reactors for hydrogenation and dehydrogenation processes based on supported palladium', *J Molecular Catal A: Chem*, **173**, 135–84.

Dorkenoo K D and Pfromm P H (2000), 'Accelerated physical aging of thin poly(1-(trimethylsilyl)-1-propyne) films', *Macromolecules*, **33**, 3747–51.

Dotremont C, Vankelecom I F J, Morobe M, Uytterhoeven J B and Vandecasteele C (1997), 'Zeolite-filled PDMS membranes. 2. Pervaporation of halogenated hydrocarbons', *J Phys Chem B*, **101**, 2160–3.

Douglas K S (2008), *Cross-linking and Stabilization of High Fractional Free Volume Polymers for the Separation of Organic Vapors from Permanent Gases*, D. Eng. Thesis Dissertation, University of Texas, Austin.

ECSA (2008), *Solvents Emissions Directive, Chlorinated Solvents Users*, Guidance, http://www.eurochlor.org/

Eldridge R B (1993), 'Olefin/paraffin separation technology: A review', *Ind Eng Chem Res*, **32**, 2208–12.

Eriksen O I, Aksnes E and Dahl I M (1993), 'Facilitated transport of ethene through Nafion membranes. Part I. Water swollen membranes', *J Membrane Sci*, **85**, 89–106.

Fang J, Tanaka K, Kita H and Okamoto K (1999), 'Pervaporation properties of ethynyl-containing copolyimide membranes to aromatic/non-aromatic hydrocarbon mixtures', *Polymer*, **40**, 3051–9.

Farris T S and Armor J N (1993), 'Liquid-phase catalytic hydrogenation using palladium alloy membranes', *Appl Catal A: Gen*, **96**, 25–32.

Freeman B D and Pinnau I (1997), 'Separation of gases using solubility-selective polymers' *TRIP*, **5**, 167–73.

Gallucci F, Basile A, Tosti S, Iulianelli A and Drioli E (2007), 'Methanol and ethanol steam reforming in membrane reactors: an experimental study', *Int J Hydrogen Energy*, **32**, 1201–10.

Gao C, Paventi M and Hay A S (1996), 'Thermally crosslinkable polyimides containing the 1,2-diphenylcyclopropane or diphenylacetylene moiety', *J Polym Sci A*, **34**, 413–20.

Gernot E, Aupretre F, Deschamps A, Epron F, Merecot P, Duprez D and Etievant C (2006), 'Production of hydrogen from bioethanol in catalytic membrane reactor', *16th Confèrence Mondiale de l 'Hydrogène Energie* (WHEC16), Lyon (France), http://www.ceth.fr/download/presse/art_ceth_3.pdf.

© Woodhead Publishing Limited, 2011

Ghoreyshi A, Najafpour G D and Ebrahimi Z (2009), 'A predictive model for the selective separation of aromatic/non aromatic hydrocarbon mixtures by pervaporation using dense homogenous polymer membranes', *World Appl Sci J*, **6**, 24–34.

Ghosal K and Freeman B D (1994), 'Gas separation using polymer membranes: an overview', *Polym Adv Technol*, **5**, 673–97.

Gobina E and Hughes R (1996a), 'Reaction assisted hydrogen transport during catalytic dehydrogenation in a membrane reactor', *Appl Catal A: Gen*, **137**, 119–27.

Gobina E and Hughes R (1996b), 'Reaction coupling in catalytic membrane reactors', *Chem Eng Sci*, **51**, 3045–50.

Guo Y, Lu G, Wang Y and Wang R (2003), 'Preparation and characterization of Pd–Ag/ceramic composite membrane and application to enhancement of catalytic dehydrogenation of isobutene', *Sep Purif Techn*, **32**, 271–9.

Hao J, Tanaka K, Kita H and Okamoto K (1997), 'The pervaporation properties of sulfonyl–containing polyimide membranes to aromatic/aliphatic hydrocarbon mixtures', *J Membrane Sci*, **132**, 97–108.

He Z, Pinnau I and Morisato A (2002), 'Nanostructured poly(4-methyl-2-pentyne)/silica hybrid membranes for gas separation', *Desalination*, **146**, 11–15.

Hirayama Y, Tanihara N, Kusuki Y, Kase Y, Haraya K and Okamoto K (1999), 'Permeation properties to hydrocarbons, perfluorocarbons and chlorofluorocarbons of cross-linked membranes of polymethacrylates with poly(ethylene oxide) and perfluorononyl moieties', *J Membrane Sci*, **163**, 373–81.

Hofmann D, Heuchel M, Yampolskii Y, Khotimskii V and Shantarovich V (2002), 'Free volume distributions in ultrahigh and lower free volume polymers: comparison between molecular modeling and positron lifetime studies', *Macromolecules*, **35**, 2129–40.

Hofmann D, Entrialgo-Castano M, Lerbret A, Heuchel M and Yampolskii Y (2003), 'Molecular modeling investigation of free volume distributions in stiff chain polymers with conventional and ultrahigh free volume: Comparison between molecular modeling and positron lifetime studies', *Macromolecules*, **36**, 8528–38.

Hong S U, Jin J H, Won J and Kang Y S (2000), 'Solid polymer electrolytes containing silver ions and their application to facilitated transport membranes', *Adv Mater*, **12**, 968–71.

Hou K and Hughes R (2001), 'The kinetics of methane steam reforming over a Ni/a–Al_2O_3 catalyst', *Chem Eng J*, **82**, 311–28.

Hughes R D, Mahoney J A and Steigelmann E F (1986), 'Olefin separation by facilitated transport membranes', *Recent Development in Separation Science*, CRC Press, Boca Raton, FL.

Hsieh H P (1996), *Inorganic Membranes for Separation and Reaction*, Elsevier Science, Amsterdam.

Ismail A F, Goh P S, Sanip S M and Aziz M (2009), 'Transport and separation properties of carbon nanotube–mixed matrix membrane', *Sep Purif Tech*, **70**, 12–26.

Itoh N (1987), 'A membrane reactor using palladium', *AIChE J*, **33**, 1576–8.

Iulianelli A and Basile A (2010), 'An experimental study on bio-ethanol steam reforming in a catalytic membrane reactor. Part I: temperature and sweep-gas flow configuration effects', *Int J Hydrogen Energy*, **35**, 3170–7.

Iulianelli A, Longo T and Basile A (2008a), 'Methanol steam reforming in a dense Pd-Ag membrane reactor: The pressure and WHSV effects on CO-free H_2 production', *J Membrane Sci*, **323**, 235–40.

Iulianelli A, Longo T and Basile A (2008b), 'Methanol steam reforming reaction in a Pd-Ag membrane reactor for CO-free hydrogen production', *Int J Hydrogen Energy*, **33**, 5583–8.

© Woodhead Publishing Limited, 2011

Iulianelli A, Longo T and Basile A (2008c), 'CO-free hydrogen production by steam reforming of acetic acid carried out in a Pd-Ag membrane reactor: The effect of co-current and counter-current mode', *Int J Hydrogen Energy*, **33**, 4091–6.

Iulianelli A, Liguori S, Longo T, Tosti S, Pinacci P and Basile A (2010a), 'An experimental study on bio-ethanol steam reforming in a catalytic membrane reactor. Part II: reaction pressure, sweep factor and WHSV effects', *Int J Hydrogen Energy*, **35**, 3159–64.

Iulianelli A, Longo T, Liguori S and Basile A (2010b), 'Production of hydrogen via glycerol steam reforming in a Pd-Ag membrane reactor over Co-Al_2O_3 catalyst', *Asia-Pac J Chem Eng*, **5**, 138–45.

Iulianelli A, Manzolini G, De Falco M, Campanari S, Longo T, Liguori S and Basile A (2010c), 'H_2 production by low pressure methane steam reforming in a Pd-Ag membrane reactor over a Ni-based catalyst: experimental and modelling', *Int J Hydrogen Energy*, **35**, 11514–24.

Iulianelli A, Seelam P K, Longo T, Liguori S, Keiski R, Calabrò V and Basile A (2011), 'Hydrogen production for PEM fuel cell by gas phase reforming of glycerol as by-product of bio-diesel. The use of a Pd-Ag membrane reactor at middle reaction temperature', *Int J Hydrogen Energy*, **36**, 3827–34.

Jannatduost E, Babaluo A A, Abbasi F, Akhfash Ardestani M and Peyravi M (2010), 'Surface modification of nanocomposite ceramic membranes by PDMS for condensable hydrocarbons separation', *Desalination*, **250**, 1136–9.

Javaid A, Gonzalez S O, Simanek E E and Ford D M (2006), 'Nanocomposite membranes of chemisorbed and physisorbed molecules on porous alumina for environmentally important separations', *J Membrane Sci*, **275**, 255–60.

Jia A and Baker G L (1998), 'Cross-linking of poly(1-(trimethylsilyl)-1-propyne) membranes using bis(aryl azides)', *J Polym Sci*, *Part B: Polym Phys*, **36**, 959–68.

Jiang X and Kumar A (2006), 'Silicone-coated polymeric membrane for separation of hydrocarbons and nitrogen at sub-ambient temperatures', *J Membrane Sci*, **286**, 285–92.

Kelman S D, Rowe B W, Bielawski C W, Pas S J, Hill A J, Paul D R and Freeman B D (2008a), 'Crosslinking poly(1-(trimethylsilyl)-1-propyne) and its effect on physical stability', *J Membrane Sci*, **320**, 123–34.

Kelman S D, Raharjo R D, Bielawski C W and Freeman B D (2008b), 'The influence of crosslinking and fumed silica nanoparticles on mixed gas transport properties of poly(1-(trimethylsilyl)-1-propyne)', *Polymer*, **49**, 3029–41.

Kikuchi E (1995), 'Palladium-ceramic membranes for selective hydrogen permeation and their application to membrane reactor', *Catal Today*, **25**, 333–7.

Kikuchi E (1997), 'Hydrogen-permselective membrane reactor', *Cattech*, **1**, 67–74.

Kikuchi E (2000), 'Membrane reactor application to hydrogen production', *Catal Today*, **56**, 97–101.

Kikuchi E, Uemiya S, Sate N, Inoue H, Ando H and Matsuda T (1989), 'Membrane reactor using microporous glass-supported thin film of palladium. Application to the water gas shift reaction', *Chem. Lett.*, **3**, 489–92.

Kikuchi E, Nemoto Y, Kajiwara M, Uemiya S and Kojima T (2000), 'Steam reforming of methane in membrane reactors: comparison of electroless-plating and CVD membranes and catalyst packing modes', *Catal Today*, **56**, 75–81.

Kim J H, Min B R, Won J, Kang Y S (2003), 'Facilitated transport of ethylene across polymer membranes containing silver salt: effect of HBF_4 on the photoreduction of silver ions', *J Membrane Sci*, **212**, 283–8.

Kim J H, Park S M, Won J and Kang Y S, (2004a), 'Dependence of facilitated olefin

© Woodhead Publishing Limited, 2011

transport on the thickness of silver polymer electrolyte membranes', *J Membrane Sci*, **236**, 209–12

Kim J H, Won J and Kang Y S (2004b), 'P-complexes of polystyrene with silver salts and their use as facilitated olefin transport membranes', *J Polym Sci: Part B: Polym Phys*, **42**, 2263–9.

Kim S H, Kim D B, Choi D K, Lee H, Kim H S and Won J (2004c), 'Isoprene/pentane separation using facilitated transport membranes', *J Membrane Sci*, **233**, 113–17.

Koros W J (2002), 'Gas separation membranes needs for combined materials science and processing approaches', *Macromol Symp*, **188**, 13–22.

Kovvali A S, Chen H and Sirkar K K (2002), 'Glycerol-based immobilized liquid membranes for olefin-paraffin separation', *Ind Eng Chem Res*, **41**, 347–56.

LeBlanc O H, Ward W J, Matson S L and Kimura S G (1980), 'Facilitated transport in ion-exchange membranes', *J Membrane Sci*, **6**, 339–43.

Lee D H, Kang Y S and Kim J H (2009), 'Olefin separation performances and coordination behaviors of facilitated transport membranes based on poly(styrene-*b*-isoprene-*b*-styrene)/silver salt complexes', *Macromol Res*, **17**, 104–9.

Lee K H and Sinnott S B (2004), 'Computational studies of non-equilibrium molecular transport through carbon nanotubes', *J Phys Chem B*, **108**, 9861–70.

Leemann M, Eigenberger G and Strathmann H (1996), 'Vapour permeation for the recovery of organic solvents from waste air streams: separation capacities and process optimization', *J Membrane Sci*, **113**, 313–22.

Levent M, Gunn D J and El-Bousi M A (2003), 'Production of hydrogen-rich gases from steam reforming of methane in an automatic catalytic microreactor', *Int J Hydrogen Energy*, **28**, 945–59.

Lin H and Freeman B D (2004), 'Gas solubility, diffusivity and permeability in poly(ethylene oxide)', *J Membrane Sci*, **239**, 105–17.

Lin Y M, Liu S L, Chuang C H and Chu Y T (2003), 'Effect of incipient removal of hydrogen through palladium membrane on the conversion of methane steam reforming. Experimental and modeling', *Catal Today*, **82**, 127–39.

Liu P, Gallaher G and Gerdes T (1993), 'Experimental evaluation of dehydrogenation using catalytic membrane processes', *Sep Sci Tech*, **28**, 309–26.

Liu Q L and Xiao J (2004), 'Silicalite-filled poly(siloxane imide) membranes for removal of VOCs from water by pervaporation', *J Membrane Sci*, **230**, 121–9.

Maksudu T, Koike I, Kubo N and Kikuchi E (1993), 'Dehydrogenation of isobutene to isobutene in a palladium membrane reactor', *Appl Catal A: Gen*, **96**, 3–13.

Mao Z and Sinnott S B (2001), 'Separation of organic molecular mixtures in carbon nanotubes and bundles: molecular dynamics simulations', *J Phys Chem B*, **105** 6916–24.

Matamoros V and Bayona J M (2008), in *Emerging Contaminants from Industrial and Municipal Waste*, *Removal Technologies*', D. Barcelò and M. Petrovic (eds), Springer–Verlarg, Berlin, 199–217.

Matsumura Y and Nakamori T (2004), 'Steam reforming of methane over nickel catalysts at low reaction temperature', *Appl Catal A: Gen*, **258**, 107–14.

Matsumura Y and Tong J (2008), 'Methane steam reforming in hydrogen-permeable membrane reactor for pure hydrogen production', *Top Catal*, **51**, 123–32.

Matteucci S, Yampolskii Y, Freeman B D and Pinnau I (2006), 'Transport of gases and vapors in glassy and rubbery poly' in *Materials Science of Membranes for Gas and Vapor Separation*, Y. Yampolskii, I. Pinnau and B.D. Freeman (eds), John Wiley & Sons, New York, 1–47.

© Woodhead Publishing Limited, 2011

Matuschewski H and Schedler U (2008), 'MSE – modified membranes in organophilic pervaporation for aromatics/aliphatics separation', *Desalination*, **224**, 124–31.

Mendes D, Mendes A, Madeira L M, Iulianelli A, Sousa J M and Basile A (2009), 'The water-gas shift reaction: from conventional catalytic systems to Pd-based membrane reactors – A review', *Asia-Pac J Chem Eng*, **5**, 111–37.

Merkel T C, Bondar V, Nagai K and Freeman B D (1999), 'Perfluorocarbon sorption in polydimethylsiloxane, poly(1-trimethylsilyl)-1-propyne), and random copolymers of tetrafluoroethylene and 2,2-bistrifluoromethyl-4,5-difluoro-1,3-dioxole', *Macromolecules*, **32**, 370–4.

Merkel T C, Freeman B D, Spontak R J, He Z, Pinnau I, Meakin P and Hill A J (2002), 'Ultrapermeable, reverse-selective nanocomposite membranes', *Science*, **296**, 519–21.

Molina M J and Rowland F S (1974), 'Stratospheric sink for chlorofluoromethanes: chlorine atom-catalysed destruction of ozone', *Nature*, **249**, 810–12.

Morisato A, Shen H C, Sankar S S, Freeman B D, Pinnau I and Casillas C C (1996), 'Polymer characterization and gas permeability of poly(1-trimethylsilyl-1-propyne) (PTMSP), poly(1-phenyl-1-propyne) (PPP), and PTMSP/PPP blends', *J Polym Sci: Part B: Polym Phys*, **34**, 2209–22.

Morisato A, He Z, Pinnau I and Merkel T C (2002), 'Transport properties of PA 12-PTMO/AgBFd solid polymer electrolyte membranes for olefin/paraffin separation', *Desalination*, **145**, 347–51.

Nakagawa T, Watanabe T, Mori M and Nagai K (2010), 'Aging of gas permeability in poly(1-(trimethylsilyl)-1-propyne) (PTMSP) and PTMSP-Poly(tert-butylacetylene) blends', in *Polymer Membranes for Gas and Vapor Separation ACS Symposium Series*, **733**, B D Freeman and I Pinnau (eds), North Carolina State University, Division of Polymeric Materials: Science and Engineering, 68–84.

Nunes S P and Peinemann K V (2006), *Membrane Technology in Chemical Industry*, Wiley-VCH, Venheim.

Nymeijer K, Visser T, Assen R and Wessling M (2004), 'Super selective membranes in gas–liquid membrane contactors for olefin/paraffin separation', *J Membrane Sci*, **232**, 107–14.

O'Reilly K T, Megaw R I and Rixey W G (2001), 'Predicting the effect of hydrocarbon and hydrocarbon-impacted soil on', *Amer Petroleum Inst*, **14**, 1–14.

Odani and Masuda T (1992), 'Design of polymer membranes for gas separation', in *Polymer for Gas Separation*, N. Toshima (ed), VCH, New York, 107–44.

Okamoto K, Noborio K, Hao J, Tanaka K and Kita H (1997), 'Permeation and separation properties of polyimide membranes to 1,3-butadiene and *n*-butane', *J Membrane Sci*, **134**, 171–9.

Park J H, Park K H and Kim D P (2007), 'Superparamagnetic Si_3N_4–Fe-containing ceramics prepared from a polymer-metal complex', *J Ind Eng Chem*, **13**, 27–32.

Park S J, Lee D W, Yu C Y, Lee K Y and Lee K H (2008), 'Hydrogen production from a DME reforming-membrane reactor using stainless steel-supported Knudsen membranes with high permeability', *J Membrane Sci*, **318**, 123–8.

Park Y S, Won J and Kang Y S (2001), 'Facilitated transport of olefin through solid PAAm and PAAm-graft composite membranes with silver ions', *J Membrane Sci*, **183**, 163–70.

Pinnau I and He Z (2004), 'Pure- and mixed-gas permeation properties of polydimethylsiloxane for hydrocarbon/methane and hydrocarbon/hydrogen separation', *J Membrane Sci*, **244**, 227–33.

© Woodhead Publishing Limited, 2011

Pinnau I and Toy L G (1996a), 'Transport of organic vapors through poly(1-trimethylsilyl-1-propyne)', *J Membrane Sci*, **116**, 199–209.

Pinnau I and Toy L G (1996b), 'Gas and vapor transport properties of amorphous perfluorinated copolymer membranes based on 2,2-bistrifluoromethyl-4,5-difluoro-l,3-dioxole/tetrafluoroethylene', *J Membrane Sci*, **109**, 125–33.

Pistonesi C, Juan A, Irigoyen B and Amadeo N (2007), 'Theoretical and experimental study of methane steam reforming reactions over nickel catalyst', *Appl Surf Sci*, **253**, 4427–37.

Profeti L P R, Ticianelli E A and Assaf E M (2008), 'Co/Al_2O_3 catalysts promoted with noble metals for production of hydrogen by methane steam reforming', *Fuel*, **87**, 2076–81.

Raharjo R D, Freeman B D, Paul D R, Sarti G C and Sanders E S (2007a), 'Pure and mixed gas CH_4 and *n*-C_4H_{10} permeability and diffusivity in poly(dimethylsiloxane)', *J Membrane Sci*, **306** 75–92.

Raharjo R D, Freeman B D and Sanders E S (2007b), 'Pure and mixed gas CH_4 and *n*-C_4H_{10} sorption and dilation in poly(dimethylsiloxane)', *J Membrane Sci*, **292**, 45–61.

Razdan U, Joshi S V and Shah V J (2003), 'Novel membrane processes for separation of organics', *Current Sci*, **85**, 761–71.

Roizard D, Favre E, Teplyakov V and Khotimisky V (2007), 'Organic membranes and related molecular separation processes: input in energy and environment areas', *Names*, 3rd France-Russia Seminar, Metz, France, 7–9 November 2007, EDP Sciences, France, 167–70.

Semenova S I (2004), 'Polymer membranes for hydrocarbon separation and removal', *J Membrane Sci*, **231**, 189–207.

Shantarovich V P, Kevdina I B, Yampolskii Y P and Alentiev A Y (2000), 'Positron annihilation lifetime study of high and low free volume glassy polymers: effects of free volume sizes on the permeability and permselectivity', *Macromolecules*, **33**, 7453–66.

Smitha B, Suhanya D, Sridhar S and Ramakrishna M (2004), 'Separation of organic–organic mixtures by pervaporation – A review', *J Membrane Sci*, **241**, 1–21.

Srinivasan R, Auvil S R and Burban P M (1994), 'Elucidating the mechanism(s) of gas transport in poly (1-(trimethylsilyl)-1-propyne) (PTMSP) membranes', *J Membrane Sci*, **86**, 67–86.

Starannikova L, Khodzhaeva V and Yampolskii Yu (2004), 'Mechanism of aging of poly(1-(trimethylsilyl)-1-propyne) and its effect on gas permeability', *J Membrane Sci*, **244**, 183–91.

Staudt-Bickel C and Koros W J (2000), 'Olefin/paraffin gas separations with 6FDA-based polyimide membranes', *J Membrane Sci*, **170**, 205–14.

Sun F and Ruckenstein E (1995), 'Sorption and pervaporation of benzene-cyclohexane mixtures through composite membranes prepared via concentrated emulsion polymerization', *J Membrane Sci*, **99**, 273–84.

Syrtsova D A, Borisevich O B, Shkrebko O A, Teplyakov V V, Grinshpan D D, Khotimskii V S and Roizard D (2007), 'The permeability of gases and light hydrocarbons through new polymeric composite membranes based on poly (1-trimethylsilylpropyne)', *Sep Purif Techn*, **57**, 435–9.

Takeichi T, Takahashi N and Yokota R (1994), 'High modulus polyimide/polyimide molecular composite films that utilize acetylene unit as a crosslink site', *J Polym Sci A*, **32**, 167–74.

Tanaka K, Taguchi A, Hao J Q, Kita H and Okamoto K (1996), 'Permeation and

© Woodhead Publishing Limited, 2011

separation properties of polyimide membranes to olefins and paraffins', *J Membrane Sci*, **121**, 197–207.

Teramoto M, Takeuchi N, Maki T and Matsuyama H (2002), 'Ethylene/ethane separation by facilitated transport membrane accompanied by permeation of aqueous silver nitrate solution', *Sep Purif Technol*, **28**, 117–24.

Teramoto M, Shimizu S, Matsuyama H and Matsumiya N (2005), 'Ethylene/ethane separation and concentration by hollow fiber facilitated transport membrane module with permeation of silver nitrate solution', *Sep Purif Technol*, **44**, 19–29.

Tiller F M and Tsai C D (1986), 'Theory of filtration of ceramics: I, slip casting', *J Amer Ceram Soc*, **69**, 882–7.

Tong J and Matsumura Y (2005), 'Effect of catalytic activity on methane steam reforming in hydrogen-permeable membrane reactor', *Appl Catal A: Gen*, **286**, 226–31.

Tong J and Matsumura Y (2006), 'Pure hydrogen production by methane steam reforming with hydrogen-permeable membrane reactor', *Catal Today*, **111**, 147–52.

Tosti S, Bettinali L and Violante V (2000), 'Rolled thin Pd and Pd–Ag membranes for hydrogen separation and production', *Int J Hydrogen Energy*, **25**, 319–25.

Toy L G and Pinnau I (1996), *Natural Gas Treatment Process using PTMSP Membrane*, US Patent 5501722.

Tsubouchi K and Yoshikawa M (1998), 'Pervaporation separation of benzene/cyclohexane mixtures through polyamide-polyether block copolymer membranes', *Membrane (Maku)*, **23**, 322–6.

Uemiya S, Sato N, Ando H, Matsuda T and Kikuchi E (1991), 'Steam reforming of methane in a hydrogen-permeable membrane reactor', *Appl Catal*, **67**, 223–30.

Valenti G and Macchi F (2008), 'Proposal of an innovative, high efficiency, large-scale hydrogen liquefier', *Int J Hydrogen Energy*, **33**, 3116–21.

Wang H, Lin X, Tanaka K, Kita H and Okamoto K (1998), 'Preparation of plasma-grafted polymer membranes and their morphology and pervaporation properties toward benzene/cyclohexane mixtures', *J Polym Sci*, **36**, 2247–59.

Wang H, Tanaka K, Kita H and Okamoto K (1999), 'Pervaporation of aromatic/non-aromatic hydrocarbon mixtures through plasma-grafted membranes', *J Membrane Sci*, **154**, 221–8.

Wang H, Cong Y and Yang W (2005), 'Oxidative coupling of methane in $Ba_{0.5}Sr_{0.5}Co_{0.8}Fe_{0.2}O_3$ tubular membrane reactors', *Catal Today*, **104**, 160–7.

Wang X Y, Lee K M, Stone M T, Sanchez I C and Freeman B D (2004), 'Cavity size distributions in high free volume glassy polymers by molecular simulation', *Polymer*, **45**, 3907–12.

Wang X Y, Willmore F T, Raharjo R D, Wang X, Freeman B D, Hill A J and Sanchez I C (2006), 'Molecular simulations of physical aging in polymer membrane materials', *J Phys Chem B.*, **110**, 16685–93.

Wieland S, Melin T and Lamm A (2002), 'Membrane reactors for hydrogen production', *Chem Eng Sci*, **57**, 1571–6.

Wu Z, Hatim I M D, Kingsbury B F K, Gbenedio E and Li K (2009), 'A novel inorganic hollow fiber membrane reactor for catalytic dehydrogenation of propane', *AIChE J*, **55**, 2389–98.

Yamaguchi T, Nakao S and Kimura S (1991), 'Tin ditriflate-promoted addition of 1-alkynes to aldehydes', *Macromolecules*, **24**, 5522–7.

Yamaguchi T, Nakao S and Kimura S (1992), 'Solubility and pervaporation properties of the filling-polymerized membrane prepared by plasma-graft polymerization for pervaporation of organic-liquid mixtures', *Ind Eng Chem Res*, **31**, 1914–19.

© Woodhead Publishing Limited, 2011

Yang J S and Hsiue G H (1996), 'C4 olefin/paraffin separation by poly((1-trimethylsilyl)-1-propyne)-graft-poly(acrylic acid)-Ag+ complex membranes', *J Membrane Sci*, **111**, 27–38.

Yang J S and Hsiue G H (1997), 'Selective olefin permeation through Ag(I) contained silicone rubber-graft-poly(acrylic acid) membranes', *J Membrane Sci*, **126**, 139–49.

Yeom C K, Lee S H, Song H Y and Lee J M (2002), 'A characterization of concentration polarization in a boundary layer in the permeation of VOCs/N_2 mixtures through PDMS membrane', *J Membrane Sci*, **205**, 155–74.

Yoo S N, Yeua S, Sherman R L, Simanek E E, Shantza D F and Ford D M (2009), 'Reverse-selective membranes formed by dendrimers on mesoporous ceramic supports', *J Membrane Sci*, **334**, 16–22.

10.7 Appendix: list of symbols

C_n^+: hydrocarbons
D: diffusion coefficient
$D_{\text{organic vapour}}/D_{\text{light gas}}$: diffusivity selectivity for vapour–gas pair
H_s: heat of the sorption values
K_n: kinetic constants of the complexation reactions
S: solubility coefficient
$S_{\text{organic vapour}}/S_{\text{light gas}}$: solubility selectivity for vapour–gas pair
T_g: glass transition temperature
α: overall selectivity
α_s: solubility selectivity
α_d: diffusion selectivity
β_s: sorption component of separation factor in pervaporation processes
β_d: diffusion component of separation factor in pervaporation processes

© Woodhead Publishing Limited, 2011

11

Polymeric membranes for natural gas processing

S. E. KENTISH, CRC for Greenhouse Gas Technologies (CO2CRC), University of Melbourne, Australia

Abstract: This chapter provides an outline of the use of polymeric membranes for processing natural gas. It describes the current range of natural gas sweetening operations in which such membranes are used and gives a summary of the membrane materials that are employed. This is followed by discussion of the operational and performance issues that can occur with membrane use and how these issues can be minimized by effective pretreatment and staging within a gas sweetening operation. The advantages and limitations of membrane processes in this application are outlined. The chapter concludes with a discussion of future trends for this industry and provides resources for further study.

Key words: carbon dioxide, methane, natural gas, polymeric membrane.

11.1 Introduction

Natural gas accounted for 24.1% of world energy use in 2008, with 3066 billion cubic litres produced in that year (BP, 2009). Owing to its small carbon footprint relative to coal, use is expected to continue to increase. However, based on current production rates and proven reserves, this fuel will continue to supply the world with a relatively clean source of energy for the next 60 years.

The main application of membranes to natural gas processing is in the removal of carbon dioxide in order to meet pipeline standards and this will be the major focus of this chapter. However, membranes have also been utilized to remove water, hydrocarbons and nitrogen and these applications will also be considered.

11.2 Polymeric membrane operations in natural gas processing

When first extracted, natural gas contains a number of constituents other than methane, including water, heavier hydrocarbons, hydrogen sulfide, nitrogen, helium and carbon dioxide. The water content within the gas must be reduced immediately, to reduce the risk of pipe corrosion and to limit the formation of gas hydrates. Similarly, acid gases such as CO_2 and H_2S must

© Woodhead Publishing Limited, 2011

be removed to limit corrosion. The extent of removal of inert gases, which includes CO_2 but also nitrogen and argon, relates to the intended purpose of the gas. If the gas is to be transported by pipeline, then moderate levels of inert gases are acceptable (see Table 11.1). Conversely, if the gas is to be liquefied for either storage or ship transport then much more stringent standards are required for the inert gas content, as otherwise the liquefaction process becomes difficult. In this case, total inert gas contents of less than 100 ppm are desired (Kohl and Nielsen, 1997) with levels of less than 50 ppm being common. Heavier hydrocarbons are often removed to reduce the dewpoint of the gas to acceptable levels (Baker and Lokhandwala, 2008) and because they can be of more value if sold separately.

Traditionally, acid gases like CO_2 and H_2S were removed from natural gas using solvents such as methyldiethanolamine (MDEA). Membranes were first used as an alternative approach in the 1980s. Two of the first units were installed in the Sacroc facility in Texas in 1983 (Parro, 1984; Kohl and Nielsen, 1997), where they were used in combination with a potassium carbonate absorption process to process around 200 MMscfd of gas (220 000 Nm^3h^{-1}). A later expansion in 1997 saw the membrane process displace carbonate absorption completely.

Table 11.1 Standard specifications for natural gas compositions for pipeline delivery (Standards Association of Australia, 2005; Woodcock and Gottlieb, 2000; Younger, 2004; International Organisation for Standardisation, 2006)

	Australian Standard	US Standards	International Standards Organisation
		Maximum limit	
Oxygen	0.2 mol%	0–0.4 ml%	
Total sulfur		23 mg m^{-3}	120 mg m^{-3}
Hydrogen sulfide	5.7 mg m^{-3}	5.7–6 mg m^{-3}	5 mg m^{-3}
Water	Dewpoint 0°C at the highest transmission pressure (in any case, no more than 112.0 mg m^{-3})	64–112 mg m^{-3}	30 mg m^{-3} at 20 MPa and –20°C
Hydrocarbon dewpoint	2.0°C at 3500 kPa gauge	264.9K at 5.5 MPa	<1% liquid at lowest temperature
Free oxygen			3 mol%
Carbon dioxide		1–3 mol%	3 mol%
Total inert gases	7.0%		

1 m^3 means 1 cubic metre of dry gas under standard conditions.

© Woodhead Publishing Limited, 2011

Over the years, processing units have increased in size and number. Current installations range in size from 1–265 MMscfd (1100–300 000 Nm^3h^{-1}), with newer units in design or construction proposed to handle feed volumes of up to 700 MMscfd (780 000 Nm^3h^{-1}) (Sanders, 2003). However, membrane processes still only represent about 1% of the market for natural gas sweetening operations (White, 2010), so there is significant opportunity for further growth.

Specific examples of large scale operations include:

- the Pailin field in the Gulf of Thailand, which processes 250 MMscfd (280 000 Nm^3h^{-1}) of 36% CO_2 to produce a product of < 23% CO_2 using hollow fibre cellulose acetate membranes (NATCO Cynara);
- the CPOC platform in the Gulf of Thailand which was due to commence production in late 2009 to process 650 MMscfd (725 000 Nm^3h^{-1}) of 43% CO_2 to produce a product of 23% CO_2 using hollow fibre cellulose actetate membranes (NATCO Cynara);
- the Kadanwari system is a two-stage unit designed to treat 210 MMscfd (230 000 Nm^3h^{-1}) of feed gas at 90 Bar. The CO_2 content is reduced from 12% to less than 3% (UOP, cellulose acetate spiral wound);
- the Separex membrane system in Qadirpur, Pakistan is designed to process 265 MMscfd (300 000 Nm^3h^{-1}) of natural gas at 59 Bar. The CO_2 content is reduced from 6.5% to less than 2% (UOP, cellulose acetate spiral wound);
- the Medal membrane system in Argentina operates in a 3-stage setup to treat 43 000 $Nm^3\ h^{-1}$ (36 MMscfd) of natural gas with 19% CO_2 (Air Liquide, polyimide hollow fibre);
- Air Products PRISM membranes are used to dry 3.2 MMscfd (3600 Nm^3h^{-1}) of natural gas for AGIP in Italy.

11.3 Membrane materials, development and design for natural gas processing

There have been a plethora of materials tested at the laboratory scale for natural gas processing and in particular for CO_2/CH_4 separation. The relative performance of these materials can be compared on a plot of permeability(P) versus selectivity(α) as first identified by Robeson (1991). The most recent depiction of this relationship (Robeson, 2008) for CO_2/CH_4 is shown in Fig. 11.1.

The slope of the upper bound line in Fig. 11.1 can be related to the kinetic diameter of the gas species (Freeman, 1999). Most recently, Robeson *et al.* (2009) were able to show that permeability data for a large array of polymers could be described by a simple relationship:

$$P_j = P_i^n \qquad [11.1]$$

© Woodhead Publishing Limited, 2011

where the exponent (n) can be simply related to the upper bound slope (n_u) by:

$$\frac{1}{n_u} = 1 - n \qquad [11.2]$$

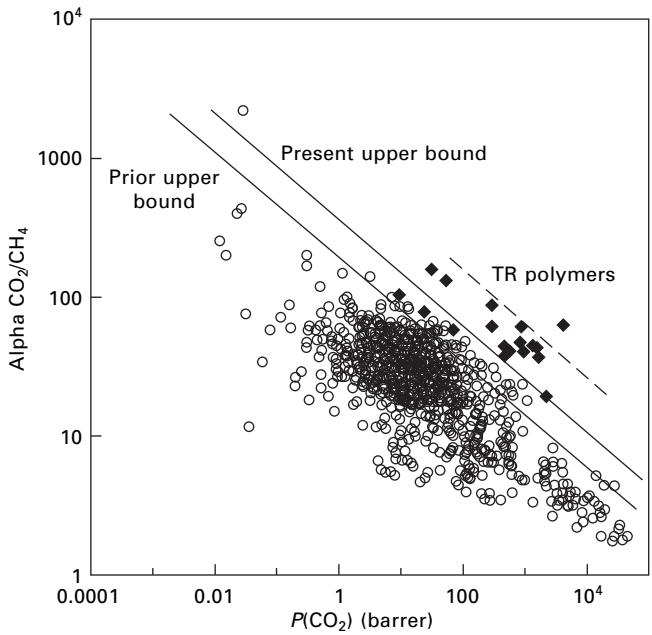
For the CO_2/CH_4 gas pair, this results in (see Figure 11.2):

$$P_{CH_4} = 0.0176\, P_{CO_2}^{1.3034} \qquad [11.3]$$

where both permeabilities are quoted in barrer.

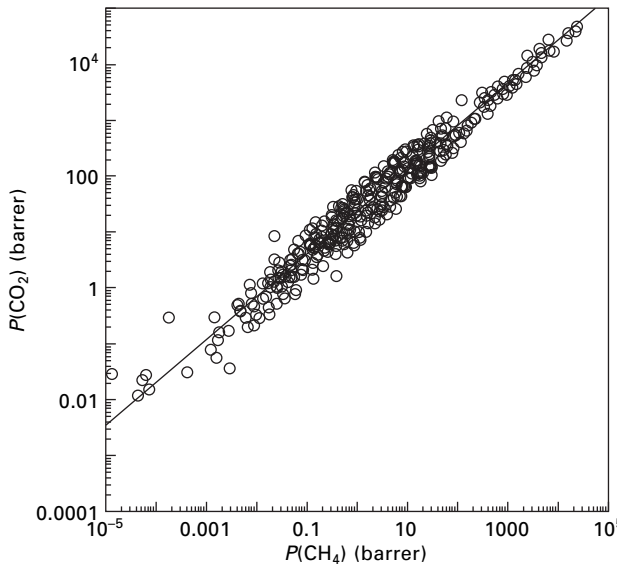
While Fig. 11.1 and 11.2 show the very large range of materials that have been considered for CO_2/CH_4 separation, less than ten materials have been commercialized for this purpose (Abetz *et al.*, 2006).

The original membrane material deployed was cellulose acetate (Fig. 11.3) and this material continues to provide by far the greatest volume of natural gas processing needs. The major advantage of this material is its low price. However, it is a very hygroscopic material that can be easily damaged by exposure to either liquid water or the glycol used in natural gas

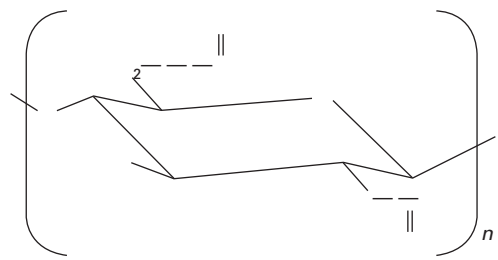


11.1 Upper bound correlation for CO_2/CH_4 separation, where $P(CO_2)$ is the permeability of carbon dioxide and Alpha is the CO_2/CH_4 selectivity. TR refers to thermally rearranged polymers and is indicated by the solid diamonds (reprinted with permission from Robeson, 2008).

© Woodhead Publishing Limited, 2011



11.2 CO_2/CH_4 permeability correlation (reprinted with permission from Robeson *et al.,* 2009).

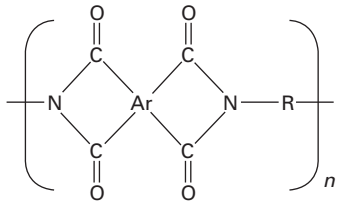


11.3 Chemical structure of cellulose acetate.

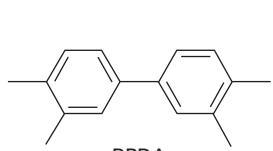
dehydration units. Plasticization of the membrane structure from exposure to high pressures of carbon dioxide is also an issue. It can be formed into either a spiral wound or hollow fibre format.

Polyimides and fluorinated polyimides (Fig. 11.4) were developed at a later stage as a replacement for cellulose acetate. These materials offer better CO_2/CH_4 selectivity than cellulose acetate and are mechanically stronger, but are more expensive. This is particularly the case because they are exclusively supplied as intrinsically skinned hollow fibres. As the full thickness of the fibre must be supplied from the expensive polymer, the price differential can be significant. These materials are more resistant to water and glycol, but can be susceptible to plasticization due to exposure to hydrocarbons or high partial pressures of carbon dioxide (Staudt-Bickel and Koros, 1999).

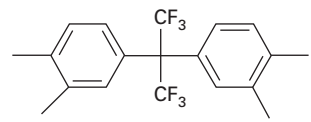
© Woodhead Publishing Limited, 2011



Examples of Ar:

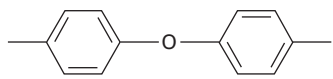


BPDA

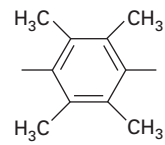


6FDA

Examples of R:



DADE



TMPDA

11.4 Chemical structures of some typical polyimides (adapted from Kase, 2008). BPDA – prepared from biphenyltetracarboxylic dianhydride, 6FDA – prepared from 4,4′-(hexafluoroisopropylidene) diphthalic anhydride, TMPDA – prepared from 2,3,5,6-tetramethyl-1,4-phenylenediamine, DADE – prepared from diaminodiphenyl ether.

Poly ether ether ketone (PEEK, marketed by Porogen) is a membrane material that is more robust towards plasticization meaning that much less pretreatment is required (Smith, 2009). This allows a range of gas impurities (water, CO_2, H_2S and hydrocarbons) to be removed in a single stage. These membranes have been field tested and are approaching commercialization, particularly for natural gas dehydration applications (Smith, 2009). The membrane is prepared by melt extrusion.

The company MTR is marketing similar natural gas sweetening systems based on a perfluorocarbon polymer prepared in a composite membrane format on a microporous support (Hale and Lokhandwala, 2004; Baker and Lokhandwala, 2008). Marketed as Z-Top®, these polymers are also resistant to plasticization by hydrocarbons and aromatics (Prabhakar *et al.*, 2004), so that pretreatment costs can be reduced. Applications have been successful for flow rates ranging from 0.2 MMscfd up to 90 MMscfd (220–100 000 Nm^3h^{-1}) and pressures from 3.4–64 Bar (Hale and Lokhandwala, 2004).

© Woodhead Publishing Limited, 2011

Polysulfone (marketed as PRISM® by Air Products) has been commercialized for both natural gas dehydration as well as CO_2 removal. However, this membrane material lends itself better to oxygen/nitrogen separation processes and has a more limited share of the natural gas market. Indeed, the use of membranes for natural gas dehydration is itself limited. This is not because membranes are not selective for water. Rather, a flow of water across the membrane can only occur if the partial pressure of water on the feed side of the membrane is greater than the partial pressure of water on the permeate side of the membrane (Baker, 2002). The rapid flow of water across the membrane leads to a build-up of water on the permeate side, which ultimately limits the effectiveness of this approach.

Silicone rubber polymers can be used to remove propane and heavier hydrocarbons. These are usually provided in a composite format, with a thin silicone rubber layer coated on a porous support. The most commonly used membranes in this service were commercialized by GKSS and use a polyacrylonitrile support which is resistant to compaction (Abetz *et al.*, 2006).

Glassy perfluorinated polymer membranes have also been commercialized quite recently by MTR for the removal of nitrogen from natural gas, under the trade name Nitrosep™. Table 11.2 provides a cost comparison of these membrane systems to other alternatives, namely cryogenic distillation and pressure swing adsorption (PSA). For the N_2/CH_4 pair, separation can be based upon either solubility or size selectivity. That is, for glassy polymers, nitrogen will tend to permeate, with a maximum α_{N_2/CH_4} selectivity of ~ 2.5 (Lokhandwala *et al.*, 1997) whereas for rubbery polymers, methane will preferentially permeate, with α_{CH_4/N_2} selectivity of ~ 3.5 (Lokhandwala *et al.*, 1997). In the Nitrosep™ process, glassy perfluorinated polymers were chosen, as they show high selectivity and permeability, owing to the unusual sorption properties of these materials (Lokhandwala *et al.*, 1997).

Initial installations of gas separation membranes used the spiral wound format that is also common in water treatment applications. This configuration has a number of advantages. The relatively wide permeate channels reduce

Table 11.2 Cost comparison for various technologies currently available for removal of 8% nitrogen from subquality natural gas (Lokhandwala *et al.,* 1997). Costs are sourced from Changela *et al.* (1990)

Technology	Total capital cost (US$/Mscfd plant capacity)	Processing cost (US$/Mscf)
Cryogenic distillation	1184	1.30
PSA	1320	1.65
Membranes	277	0.30

© Woodhead Publishing Limited, 2011

pressure drop on this side and hence allow a low back pressure. The feed spacers promote turbulence and hence reduce concentration polarization effects. However, these feed spacers can also act to trap condensed liquids (Isa and Azhar, 2009), leading to performance decline caused by plasticization. This arrangement can also be easily damaged by compaction if high differential pressures (>125 Bar) are utilized. Further, the units operate essentially in a cross-flow mode, which is less thermodynamically efficient than countercurrent flow.

GKSS has commercialized an alternative module where a sequence of membrane envelopes manufactured from flat sheets are stacked together. This arrangement is said to result in reduced concentration polarization, a reduced permeate path, a relatively low number of gaskets and an absence of glue (Abetz *et al.*, 2006). This type of module has been deployed mainly for the recovery of hydrocarbon vapours from both natural gas and other process streams.

The hollow fibre format was introduced later and has the primary advantage of providing a much greater membrane area per unit volume. This can be particularly important in offshore applications where space is often limited. Further, flow can be engineered to approach countercurrent operation, leading to greater separation (Smith, 2009). However, this arrangement is more readily blocked with particulates owing to the narrow spaces between fibres.

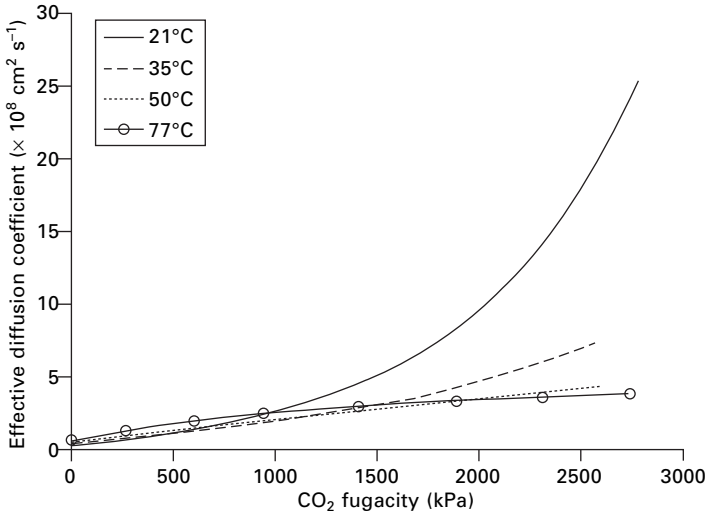
Whether hollow fibre or spiral wound, the module size is increasing as a mechanism for cost reduction. While a typical module size has been 8 inches (20 cm) diameter and 40 inches (1 metre) in length, modules of up to 30 inches (76.2 cm) in diameter and 72 inches (183 cm) in length are now available (Sanders, 2003).

11.4 Operation and performance issues and analysis

The performance of a membrane in the field can differ significantly from that measured under ideal conditions within the laboratory.

Plasticization is a swelling of the membrane structure due to the sorption of a penetrant within the polymer matrix. It generally leads to an increase in the fractional free volume of the membrane. In turn this increases the diffusion of all gas species through the membrane (Fig. 11.5) and there is thus an increase in permeability but a loss of selectivity (Fig. 11.6). Plasticization also tends to lead to a loss of mechanical strength and this can result in total membrane failure due to the collapse of the support structure. Plasticization can be caused by a number of gases that are readily sorbed within the membrane including carbon dioxide, water and a range of linear hydrocarbons and aromatics. For example, plasticization by the BTEX aromatics at 200–1000 ppm can reduce membrane selectivity by 30–50% (Vu and Koros, 2002). Many authors suggest that plasticization only occurs

© Woodhead Publishing Limited, 2011



11.5 Plot of the Fickian diffusion coefficient for 6FDA-TMPDA as a function of temperature and CO_2 fugacity (reprinted with permission from Duthie *et al.,* 2007).

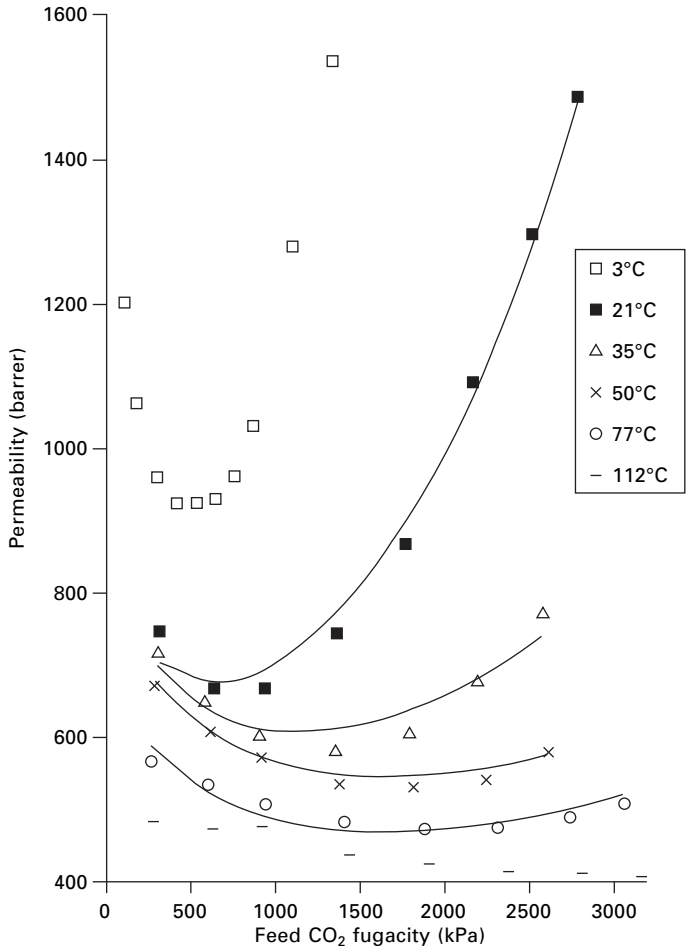
once a critical concentration of penetrant within the membrane is exceeded (Bos *et al.*, 1999). This critical concentration is reflected in the 'plasticization pressure', that is, the penetrant pressure above which membrane swelling is observed. However, it has been noted more recently that this plasticization pressure is much lower in thinner membrane layers (< 2 μm) than in dense films (Wessling *et al.*, 2001; Scholes *et al.*, 2010).

Ageing of membranes is essentially the reverse of plasticization in that it represents a compaction of the membrane structure over time and thus a loss of fractional free volume. This results in a loss of permeability, but an increase in selectivity. Membranes that initially have a higher fractional free volume suffer most from this phenomenon. Again, there is evidence that ageing is accelerated in thinner membrane layers (Pfromm and Koros, 1995). Compaction of the membrane support structure may also occur as a direct result of the application of a large pressure differential across the membrane.

A further factor influencing membrane performance is the competitive sorption from other species present in the gas, that is, the presence of one gas species can affect the solubility of another gas species. This can affect both rubbery and glassy polymers to varying extents. For rubbery polymers, the effects can be described by Flory–Huggins theory, that is, the solubility of a pure gas A in the polymer is described by:

$$\ln(S_A) = \ln(K_A) + \sigma_A C_A \qquad [11.4]$$

© Woodhead Publishing Limited, 2011



11.6 CO_2 permeability of 6FDA-TMPDA as a function of fugacity at various temperatures (reprinted with permission from Duthie *et al.*, 2007).

where K_A is the Henry's Law coefficient, C_A is the volume of gas dissolving in 1 cm^3 of unswollen polymer and σ_A is given by:

$$\sigma_A = \frac{2(1 + \chi_A)V_A}{V_G} \qquad [11.5]$$

where V_A is the molar volume and χ_A is the Flory–Huggins parameter of gas A, while V_G is the molar volume of a gas at STP, which is 22 400 cm^3/mol^{-1}.

© Woodhead Publishing Limited, 2011

The presence of a contaminant B changes this solubility to:

$$\ln S_{AB} = \ln(K_A) + \sigma_{AB} C_B + \sigma_A C_A \quad [11.6]$$

where:

$$\sigma_{AB} = \left(\chi_A - \chi_{AB} + (1 + \chi_B) \frac{V_A}{V_B} \right) \frac{V_B}{V_G} \quad [11.7]$$

where χ_{AB} characterizes mixing between gas A and B. In this case, the presence of species B can lead either to an increase or to a decrease in the solubility of species A.

For glassy polymers, competitive sorption affects the Langmuir component of the gas solubility most strongly. In this case, the solubility always decreases according to:

$$S_{AB} = K_A + \frac{C'_{HA} b_A}{(1 + b_A f_A + b_B f_B)} \quad [11.8]$$

where C'_{HA} is the maximum adsorption capacity of species A, while b is the ratio of rate coefficients of adsorption and desorption for each species, or the Langmuir affinity constant. There is a strong correlation between the value of b and the critical temperature of the species, with highly condensing gases such as water and hexane having the greatest impact upon the solubility of the less condensable natural gas components CO_2 and CH_4.

Temperature is an important parameter in any analysis of membrane performance. Most laboratory measurements are conducted at 35°C but processing conditions can differ substantially from this value. For rubbery polymers, permeability generally increases with temperature, with selectivity falling. Conversely, low temperatures increase the condensability of all gases and this can lead to greater permeability and solubility selectivity in glassy membranes. To counteract this, the higher solubility leads to greater plasticization (Fig. 11.5 and 11.6) which increases permeability but decreases selectivity. Conversely, higher temperatures can lead to accelerated ageing in all systems.

11.5 Application and integration into natural gas operations

The effectiveness of natural gas membrane operations relies heavily on an efficient pretreatment system. As discussed in Section 11.4, the presence of significant quantities of condensable contaminants results in plasticization and competitive sorption. Contamination of the membrane surface or support structure with liquids reduces mass transfer by providing a further resistance to flow (Echt, 2002). In the simplest scenario, these condensables

© Woodhead Publishing Limited, 2011

are removed by 'dew-pointing', That is, the gas stream is cooled to condense such contaminants and then reheated to ensure that the gas is at least 10–15°C above the dew point.

A more complete pretreatment operation could involve a number of steps (Echt 2002):

1. a chiller or cooler, to reduce temperature and thus cause condensation of contaminants;
2. a coalescing filter, knock-out drum or a mist eliminator vessel to remove particulate matter and entrained liquids;
3. a guard bed using an adsorbent such as activated carbon to remove the heaviest hydrocarbon fractions, including compressor oil;
4. a downstream particle filter to capture any fines from the guard bed;
5. a pre-heater to heat the gas stream above the dew point, to ensure that condensation of liquids does not occur even on the permeate side of the membrane. This pre-heater also ensures that the membrane is operated at a uniform temperature and hence provides consistent performance.

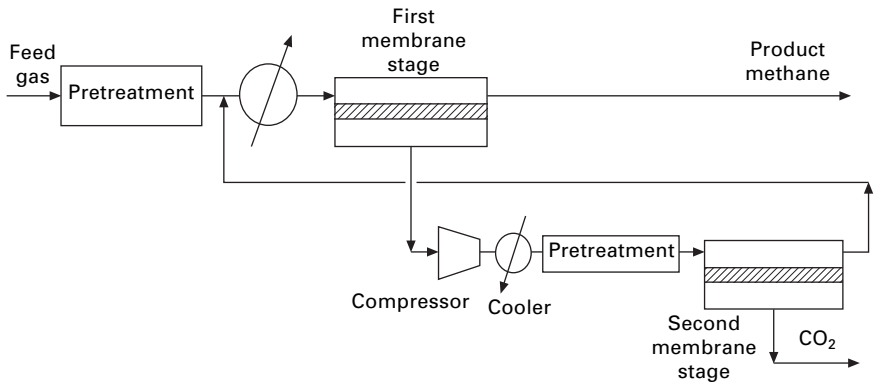
Other pretreatment options include thermal swing absorption using silica gel to remove heavy hydrocarbons (Anderson and Siahann, 2005). While not a necessary step for membrane processing, mercury is often also removed at this stage using an adsorbent guard bed, to prevent amalgamation and embrittlement of aluminium and other metals in downstream piping.

A decision must be made as to whether a hollow fibre or spiral wound module format will be utilized. Hollow fibre modules give more membrane area per unit volume but will have a higher pressure drop on both retentate and permeate sides. The feed gas is usually supplied to the shell side of the module to minimize this pressure drop and to reduce compaction; hollow fibres are much stronger under compression than expansion (Kohl and Nielsen 1997). A number of modules can be employed in series and this will lead to higher recoveries, but a greater pressure drop.

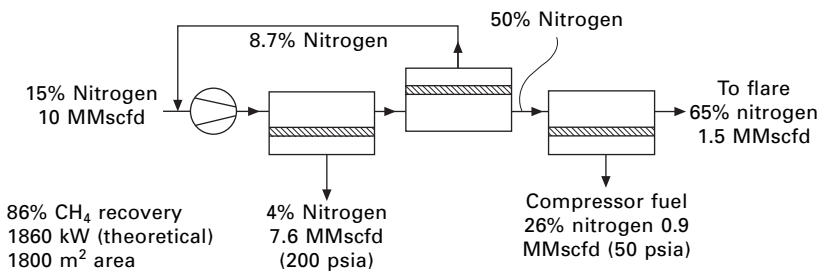
In many cases, the use of a single membrane stage would lead to unacceptable losses of product methane. In such cases, two membrane stages are usually employed (Fig. 11.7). While these reduce hydrocarbon loss, the need for a compressor adds to both operating and capital costs.

Another option often utilized is to place a single membrane stage upstream of a solvent absorption unit. This hybrid arrangement provides a better product purity than can be achieved by a single stage membrane unit and lower energy and operating costs than is possible with a solvent system alone (Echt, 2002). This approach can be particularly attractive for an offshore gas supply. The more compact and lighter weight membrane skid can be placed offshore to remove the majority of the CO_2, reducing the capital and operating costs associated with bringing this gas onshore. The CO_2 permeate can often be reinjected directly into the well, increasing recovery rates and

© Woodhead Publishing Limited, 2011



11.7 Two-stage natural gas sweetening arrangement (adapted from Echt, 2002).



11.8 Flow scheme required to bring 200 psia natural gas streams with 8–15 mol% nitrogen content to pipeline specification (≤ 4% nitrogen) using membrane-based separations (reprinted with permission from Lokhandwala *et al.,* 2010).

minimizing the carbon footprint. An onshore solvent absorption unit then increases the purity of the product methane.

For N_2 separation from natural gas, a single stage is sufficient for feed streams of 6–8% N_2. For higher nitrogen concentrations, two stages are necessary (Lokhandwala *et al.*, 1997). For example, for feeds of 8–15% N_2 (Fig. 11.8), the first stage is used to remove pipeline quality natural gas as permeate, but the retentate retains significant quantities of methane. This retentate is thus directed to a second stage for additional methane recovery. The permeate from this stage, containing 6–10% nitrogen is recycled to the feed stream. The retentate can be used directly as a compressor fuel or sent to a third stage for enhancement of the heating value prior to such use.

11.6 Advantages and limitations

The major advantage of membrane processes for natural gas separation is their light weight and small physical footprint. This makes them more practical

© Woodhead Publishing Limited, 2011

for offshore use, which is their major application. They can be installed and operated in any orientation, a further advantage within the limited confines of an offshore platform. There is no solvent and chemical make-up that will require additional space on the platform for chemical handling and storage. The absence of the need to replenish solvent and chemicals also reduces logistics and transportation costs (Isa and Azhar, 2009). Relative to solvent absorption, they have low environmental impact as no chemicals are involved. The modular construction means that scale up and turndown is more readily achieved than with a solvent absorption analogue and delivery to site is also simplified. They are simple to operate, requiring little operator attention and generally maintenance costs are low. The lack of rotating machinery for a single stage operation reduces energy demand and can avoid a potential source of ignition in an otherwise hazardous release of hydrocarbon gases (Isa and Azhar, 2009). However, energy demand increases significantly if two stages are needed owing to the use of gas compression.

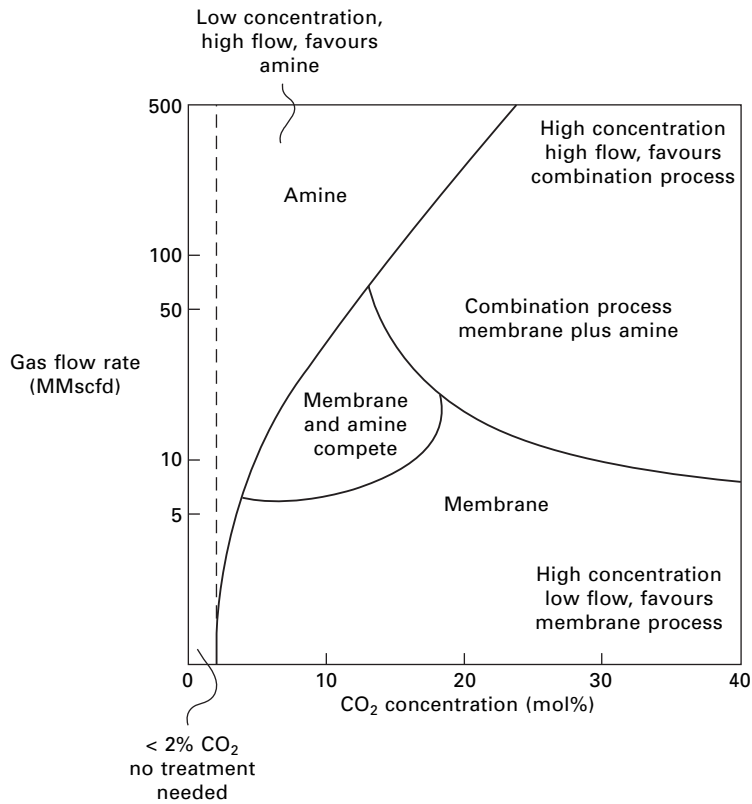
An important distinction is that water permeates with the carbon dioxide, thus leaving the retentate dry. This can obviate the need for downstream dehydration of the product natural gas (Isa and Azhar, 2009). Conversely, if the carbon dioxide is to be used for enhanced oil recovery or carbon storage, this permeate stream will need to be dried.

The costs of membrane processes generally scale with the total volume of feed gas to be processed. Conversely, solvent absorption scales with the volume of solvent required and thus with the volume of CO_2 to be recovered. Thus, membranes are ideal for bulk removal of high concentrations of CO_2 at relatively low flow rates (Fig. 11.9) (Baker and Lokhandwala, 2008). In general, membranes are best suited to situations when the feed contains 10–85 vol% of the more permeable gas, when the feed is already at moderate to high pressure (15–150 bar gauge) and at moderate temperature (0–70°C). Gas pretreatment can be expensive, up to 60% of the cost of the whole operation (Sanders, 2003) and this must be factored into any capital cost estimation. Membranes will also not provide the product purity that is possible with a reactive solvent absorption process (see Fig. 11.10). If a product purity of less than 2% CO_2 is required, for example for liquefied natural gas, then a hybrid process may be employed, as described in Section 11.5 above.

11.7 Future trends

There is active research worldwide into the development of more robust and higher performing membranes for carbon dioxide permeation. Many of these new membranes fall on or above Robeson's bound (Fig. 11.1). These include the use of block copolymers (Bondar *et al.*, 1999) and polymers with intrinsic microporosity (PIMS) (Ilinitch *et al.*, 1999; Ghanem *et al.*, 2009; McKeown and Budd, 2010). There is also an increasing focus on mixed matrix

© Woodhead Publishing Limited, 2011

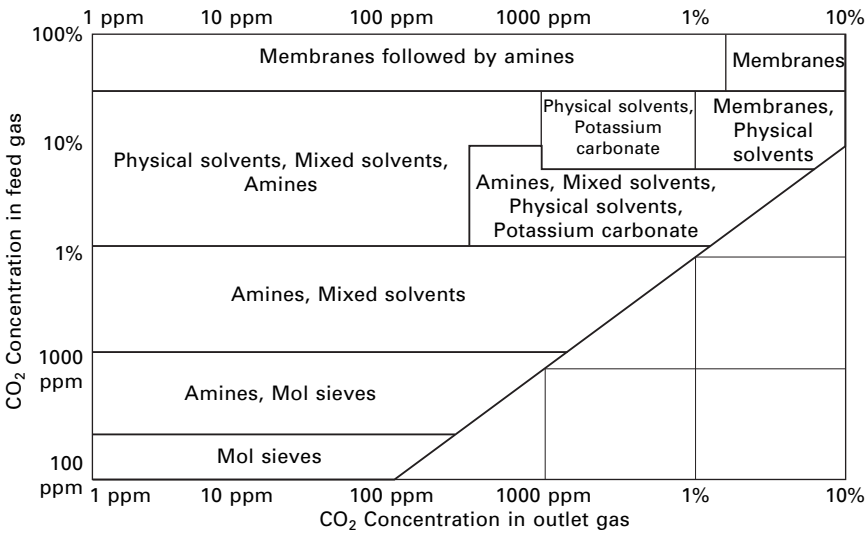


11.9 Schematic plot illustrating the effect of gas flow rate and carbon dioxide concentration in the gas on the choice of carbon dioxide removal technology (reprinted with permission from Baker and Lokhandwala, 2008).

membranes which incorporate an inorganic filler into a polymeric structure (see for example Ahn *et al.*, 2008; Choi *et al.*, 2008; Huang *et al.*, 2006; Chung *et al.*, 2007; Merkel *et al.*, 2002). These mixed matrix membranes generally increase permeability by offering a path of relatively high free volume through a polymer matrix that is less permeable but provides the necessary selectivity.

An approach that has been around for a number of years has been the preparation of nanoporous carbon membranes by the pyrolysis of polymer substrates (Fuertes and Centeno, 1998; Hagg *et al.*, 2003; Lagorsse *et al.*, 2004; Ogawa and Nakano, 2000; Rao and Sircar, 1993; Vu and Koros, 2002). These membranes have excellent performance, above Robeson's bound, can be operated at high temperatures and resist plasticization and competitive sorption by impurities. However, commercial uptake has been poor owing to the brittle nature of the membranes and failure in the presence

© Woodhead Publishing Limited, 2011



11.10 Guide to selection of natural gas sweetening processes (adapted from Manning and Thompson, 1991).

of oxygen. More recently, thermally rearranged (TR) polymers have been developed (Park *et al.*, 2007; Choi *et al.*, 2010), which are annealed at more moderate temperatures at which the polymer structure rearranges to form a more open lattice but does not carbonize. This approach appears to provide the advantages of carbon membranes (see Fig. 11.1), but without the loss in flexibility that has plagued these systems.

An alternative approach is the use of facilitated transport (Chen *et al.*, 2000; Noble and Koval, 2006; Meldon *et al.*, 1982). In this case a reactive species is embedded within the membrane itself. The CO_2 reacts with this species at one surface of the membrane and is transported across the membrane as a complex such as a carbonate or carbamate species. It is then released on the permeate side of the membrane. This type of membrane provides large CO_2 permeabilities with very good selectivities at low partial pressures, but selectivity decreases strongly as the CO_2 partial pressure increases (Chen *et al.*, 2000) owing to carrier saturation. Further, they usually require a highly hydrated feed stream to maintain the facilitation (Laciak *et al.*, 1990; Zou *et al.*, 2007). This can be a particular issue at the downstream end of a module when most of the water has already permeated, leaving a dry gas.

Membrane contactors act differently again (Gabelman and Hwang, 1999; deMontigny *et al.*, 2001). In this case, a classical absorption solvent flows on one side of a microporous membrane. The membrane itself is non-selective, but acts simply as a semi-permeable barrier that permits the passage of gaseous CO_2, but limits the flow of liquid solvent. A highly hydrophobic membrane is required to limit wetting of the membrane pores with the liquid solvent as

© Woodhead Publishing Limited, 2011

this leads to higher mass transfer resistance (Rangwala, 1996; Franco *et al.*, 2008). This approach was taken to the pilot scale for both the dehydration of natural gas and the capture of carbon dioxide by Kvaerner systems in the 1990s using polytetrafluoroethylene (PTFE) membranes (Falk-Pedersen *et al.*, 2000, 2005) but the programme was halted owing to the high cost of the membranes and the need for a sophisticated and expensive pressure control system.

While research into novel membrane materials is extensive, the ability to convert these materials into durable and cheap modules has been less well studied. One area of focus is the development of dual layer hollow fibres. These allow an expensive CO_2 selective polymer to be used only as a thin selective layer with the bulk of the hollow fibre composed of an inexpensive support material (Hosseini *et al.*, 2010; Li *et al.*, 2008; Jiang *et al.*, 2004). While this approach appears promising, there can be issues with delamination at the interface between the two layers.

11.8 Sources of further information and advice

A very good textbook on the general principles of natural gas purification is *Gas Purification* (Kohl and Nielsen, 1997). Textbooks specific to membrane separation include *Materials Science of Membranes for Gas and Vapor Separation* (Freeman *et al.*, 2006), *Membrane Gas Separation* (Freeman and Yampol'skii 2010) and the *Membrane Handbook* (Ho and Sirkar, 2001). There is also an excellent Chapter on gas separation membranes within the *Handbook of Separation Process Technology* (Koros and Chern, 1987). There are a number of comprehensive review articles that investigate the types of membranes generally available for gas separation (Baker, 2002; Lin and Freeman, 2005; Scholes *et al.*, 2010; Maiser, 1998; Stern, 1994). The reader is also directed to relevant manufacturer websites:

- Air Products: www.airproducts.com/Products/Equipment/PRISMMembranes/default.htm
- Cynara: www.natcogroup.com/products-cynara-membranes
- Medal: www.medal.airliquide.com
- MTR: www.mtrinc.com
- Porogen: www.porogen.com/
- UOP: www.uop.com/

as well as other websites:

- American Natural Gas Supply Association: www.naturalgas.org
- BP Statistical Review of World Energy: www.bp.com/statisticalreview

© Woodhead Publishing Limited, 2011

11.9 References

Abetz V, Brinkmann T, Dijkstra M, Ebert K, Fritsch D, Ohlrogge K, Paul D, Peinemann K-V, Pereira-Nunes S, Scharnagl N and Schossig M (2006) 'Developments in membrane research: from material via process design to industrial application', *Advanced Engineering Materials*, **8**(5), 328–58.

Ahn J, Chung W-J, Pinnau I and Guiver M D (2008) 'Polysulfone/silica nanoparticle mixed-matrix membranes for gas separation', *Journal of Membrane Science*, **314**(1+2), 123–33.

Anderson C L and Siahann A (2005) 'Case study: membrane CO_2 removal from natural gas, Grissik Gas Plant, Sumatra, Indonesia', *Laurence Reid Gas Conditioning Conference*, Norman, OK, USA.

Baker R W (2002) 'Future directions of membrane gas separation technology', *Industrial & Engineering Chemistry Research*, **41**(6), 1393–411.

Baker R W and Lokhandwala K (2008) 'Natural gas processing with membranes: An overview', *Industrial & Engineering Chemistry Research*, **47**(7), 2109–21.

Bondar V I, Freeman B D and Pinnau I (1999) 'Gas sorption and characterization of poly(ether-*b*-amide) segmented block copolymers', *Journal of Polymer Science*, *Part B: Polymer Physics*, **37**(17), 2463–75.

Bos A, Punt I G M, Wessling M and Strathmann H (1999) 'CO_2-induced plasticization phenomena in glassy polymers', *Journal of Membrane Science*, **155**(1), 67–78.

BP (2009) *Statistical Review of World Energy*, 2010 (online), available: http://www.bp.com/productlanding.do?categoryId=6929&contentId=7044622 (accessed July 2010).

Changela M K, McKee R L, Heshan H, Pathak V K, Quinlan M D and Strickland J F (1990) *Evaluation of Natural Gas Process Technology*, Task 3, Vol. II, Echterchoff L W and Reading G J (eds) Topical Report to Gas Research Institute, No. GRI-9110230 (September 1990).

Chen H, Kovvali A S and Sirkar K K (2000) 'Selective CO_2 separation from CO_2–N_2 mixtures by immobilized glycine–Na–glycerol membranes', *Industrial & Engineering Chemistry Research*, **39**(7), 2447–58.

Choi J I, Jung C H, Han S H, Park H B and Lee Y M (2010) 'Thermally rearranged (TR) poly(benzoxazole-*co*-pyrrolone) membranes tuned for high gas permeability and selectivity', *Journal of Membrane Science*, **349**(1–2), 358–68.

Choi S, Coronas J, Lai Z, Yust D, Onorato F and Tsapatsis M (2008) 'Fabrication and gas separation properties of polybenzimidazole (PBI)/nano porous silicates hybrid membranes', *Journal of Membrane Science*, **316**(1+2), 145–52.

Chung T S, Jiang L Y, Li Y and Kulprathipanja S (2007) 'Mixed matrix membranes (MMMs) comprising organic polymers with dispersed inorganic fillers for gas separation', *Progress in Polymer Science*, **32**, 483–507.

deMontigny D, Tontiwachwuthikul P and Chakma A (2001) 'Parametric studies of carbon dioxide absorption into highly concentrated monoethanolamine solutions', *Canadian Journal of Chemical Engineering*, **79**(1), 137.

Duthie X, Kentish S, Powell C, Nagai K, Qiao G and Stevens G (2007) 'Operating temperature effects on the plasticization of polyimide gas separation membranes', *Journal of Membrane Science*, **294**(1+2), 40–9.

Echt W (2002) 'Hybrid systems: combining technologies leads to more efficient gas conditioning', in *Laurance Reid Gas Conditioning Conference*, Norman, Oklahoma, USA, 24–27 February 2002.

Falk-Pedersen O, Dannstrom H, Gronvold M, Stuksrud D and Ronning O (2000) 'Gas

© Woodhead Publishing Limited, 2011

treatment using membrane gas/liquid contactors', *5th International Conference on Greenhouse Gas Control Technologies*, Cairns, Australia, 13–16 August, 2000.

Falk-Pedersen O, Gronvold M S, Nokleby P, Bjerve F and Svendsen H F (2005) 'CO_2 capture with membrane contactors', *International Journal of Green Energy*, **2**, 157–65.

Franco J, Demontigny D, Kentish S, Perera J and Stevens G (2008) 'A study of the mass transfer of CO_2 through different membrane materials in the membrane gas absorption process', *Separation Science and Technology*, **43**(2), 225–44.

Freeman B D (1999) 'Basis of permeability/selectivity tradeoff relations in polymeric gas separation membranes', *Macromolecules*, **32**, 375.

Freeman B D and Yampol'skii Y (eds) (2010) *Membrane Gas Separation*, John Wiley & Sons, Chichester, UK.

Freeman B D, Yampol'skii Y and Pinnau I (eds) (2006) *Materials Science of Membranes for Gas and Vapor Separation*, John Wiley & Sons, Chichester, UK.

Fuertes A B and Centeno T A (1998) 'Preparation of supported carbon molecular sieve membranes', *Journal of Membrane Science*, **144**, 105–11.

Gabelman A and Hwang S (1999) 'Hollow fibre membrane contactors', *Journal of Membrane Science*, **159**, 61.

Ghanem B S, McKeown N B, Budd P M, Al-Harbi N M, Fritsch D, Heinrich K, Starannikova L, Tokarev A and Yampolskii Y (2009) 'Synthesis, characterization, and gas permeation properties of a novel group of polymers with intrinsic microporosity: PIM-polyimides', *Macromolecules*, **42**(20), 7881–8.

Hagg M, Lie J A and Lindbrathen A (2003) 'Carbon molecular sieve membranes: a promising alternative for selected industrial applications', *Annals of the New York Academy of Sciences*, **984**(Advanced Membrane Technology), 329–45.

Hale P and Lokhandwala K A (2004) 'Advances in membrane materials provide new solutions in the gas business', in *Laurance Reid Gas Conditioning Conference*, Norman, Oklahoma, USA, February 2004.

Ho W S W and Sirkar K K (2001) *Membrane Handbook*, Kluwer Academic, Boston.

Hosseini S S, Peng N and Chung T S (2010) 'Gas separation membranes developed through integration of polymer blending and dual-layer hollow fiber spinning process for hydrogen and natural gas enrichments', *Journal of Membrane Science*, **349**(1–2), 156–66.

Huang Z, Li Y, Wen R, Teoh M M and Kulprathipanja S (2006) 'Enhanced gas separation properties by using nanostructured PES-zeolite 4A mixed matrix membranes', *Journal Applied Polymer Science*, **101**(6), 3800–5.

Ilinitch O M, Fenelonov V B, Lapkin A A, Okkel L G, Terskikh V V and Zamaraev K I (1999) 'Intrinsic microporosity and gas transport in polyphenylene oxide polymers', *Microporous and Mesoporous Materials*, **31**(1–2), 97–110.

International Organisation for Standardisation (2006) *International Standard: Natural Gas — Natural gas for use as a compressed fuel for vehicles* (ISO 15403), International Organisation for Standardisation, Geneva.

Isa M F M and Azhar M A (2009) 'Meeting technical challenges in developing high CO_2 gas field offshore', in *24th World Gas Conference*, Buenos Airies, Argentina.

Jiang L Y, Chung T S, Li D F, Cao C and Kulprathipanja A (2004) 'Fabrication of matrimid/polyethersulfone dual-layer hollow fiber membranes for gas separation', *Journal of Membrane Science*, **240**(1–2), 91–103.

Kase Y (2008) 'Gas Separation by polyimide membranes', in *Advanced Membrane Technology and Applications*, Li NN, Fare AG, Ho WSW and Matsuura T (eds) John Wiley and Sons, Hoboken, NJ, USA.

© Woodhead Publishing Limited, 2011

Kohl A L and Nielsen R B (1997) *Gas Purification*, 5th edn, Gulf Publishing (Elsevier), Houston, TX, USA.

Koros W J and Chern R T (1987) 'Separation of gaseous mixtures using polymer membranes' in *Handbook of Separation Process Technology*, Rousseau, R W (ed) John Wiley and Sons, New York 862–953.

Laciak D V, Quinn R, Pez G P, Appleby J B and Puri P S (1990) 'Selective permeation of ammonia and carbon dioxide by novel membranes', *Separation Science and Technology*, **25**, 1295–305.

Lagorsse S, Magalhaes F D and Mendes A (2004) 'Carbon molecular sieve membranes. Sorption, kinetic and structural characterization', *Journal of Membrane Science*, **241**(2), 275–87.

Li Y, Chung T S and Xiao Y C (2008) 'Superior gas separation performance of dual-layer hollow fiber membranes with an ultrathin dense-selective layer', *Journal of Membrane Science*, **325**(1), 23–7.

Lin H and Freeman B D (2005) 'Materials selection guidelines for membranes that remove CO2 from gas mixtures', *Journal of Molecular Structure*, **739**, 57–74.

Lokhandwala K A, Ringer M, Wijmans J G and Baker R W (1997) *Nitrogen Removal from Natural Gas Using Membranes*, NG8-2 available: http://www.netl.doe.gov/kmd/cds/disk28/NG8-2.PDF [accessed 6th April, 2010].

Lokhandwala K A, Pinnau I, He Z, Amo K D, DaCosta A R, Wijmans J G and Baker R W (2010) 'Membrane separation of nitrogen from natural gas: A case study from membrane synthesis to commercial deployment', *Journal of Membrane Science*, **346**, 270–9.

Maiser G (1998) 'Gas separation with polymer membranes', *Angewandte Chemie International Edition*, **37**, 2960.

Manning F S and Thompson R (1991) 'Oilfield processing', *Natural Gas*, Volume 1, PennWell Publishing, Tulsa, OK, USA.

McKeown N B and Budd P M (2010) 'Exploitation of intrinsic microporosity in polymer-based materials', *Macromolecules*, **43**(12), 5163–76.

Meldon J H, Stroeve P and Gregoire C E (1982) 'Facilitated transport of carbon dioxide: a review.', *Chemical Engineering Communications*, **16**, 283–300.

Merkel T C, Freeman B D, Spontak R J, He Z, Pinnau I, Meakin P and Hill A J (2002) 'Ultrapermeable, reverse-selective nanocomposite membranes', *Science*, **296**(5567), 519–22.

Noble R D and Koval C A (2006) 'Review of facilitated transport membranes' in *Membrane Gas Separation*, Yampol'skii Y P, Pinnau I and Freeman B D (eds), John Wiley & Sons, Chichester.

Ogawa M and Nakano Y (2000) 'Separation of CO_2/CH_4 mixture through carbonized membrane prepared by gel modification', *Journal of Membrane Science*, **173**(1), 123–32.

Park H B P, Chul H J, Lee Y M, Hill A J, Pas S J, Mudie S T, Wagner E V, Freeman B D and Cookson D J (2007) 'Polymers with cavities tuned for fast selective transport of small molecules and ions', *Science*, **318**, 254–8.

Parro D (1984) 'Membrane CO_2 separation proves out at SACROC tertiary recovery project', *Oil and Gas Journal*, (September 24), 85–8.

Pfromm P H and Koros W J (1995) 'Accelerated physical ageing of thin glassy polymer films: evidence from gas transport measurements', *Polymer*, **36**(12), 2379–87.

Prabhakar R S, Freeman B D and Roman I (2004) 'Gas and vapor sorption and permeation

© Woodhead Publishing Limited, 2011

in poly(2,2,4-trifluoro-5-trifluoromethoxy-1,3-dioxole-*co*-tetrafluoroethylene)', *Macromolecules*, **37**(20), 7688–97.

Rangwala H (1996) 'Absorption of carbon dioxide into aqueous solutions using hollow fiber membrane contactors', *Journal of Membrane Science*, **112**, 229–40.

Rao M B and Sircar S (1993) 'Nanoporous carbon membranes for separation of gas mixtures by selective surface flow', *Journal of Membrane Science*, **85**, 253–64.

Robeson L M (1991) 'Correlation of separation factor versus permeability for polymeric membranes', *Journal of Membrane Science*, **62**(2), 165–85.

Robeson L M (2008) 'The upper bound revisited', *Journal of Membrane Science*, **320**(1–2), 390–400.

Robeson L M, Freeman B D, Paul D R and Rowe B W (2009) 'An empirical correlation of gas permeability and permselectivity in polymers and its theoretical basis', *Journal of Membrane Science*, **341**(1–2), 178–85.

Sanders E S (2003) *Large Scale Membrane-based Separations*, North American Membrane Society, Jackson Hole, Wyoming.

Scholes C A, Chen G Q, Stevens G W and Kentish S E (2010) 'Plasticization of ultra-thin polysulfone membranes by carbon dioxide', *Journal of Membrane Science*, **346**(1), 208–14.

Smith L W (2009) 'Emerging membrane technology for natural gas dehydration', in *16th Annual Natural Gas STAR Annual Implementation Workshop*, San Antonio, TX, October 19–21.

Standards Association of Australia (2005) *Australian Standard: specification for general purpose natural gas* (AS4564–2005), Standards Australia, Sydney.

Staudt-Bickel C and Koros W J (1999) 'Improvement of CO_2/CH_4 separation characteristics of polyimides by chemical crosslinking', *Journal of Membrane Science*, **155**(1), 145–54.

Stern S (1994) 'Polymers for gas separation: the next decade', *Journal of Membrane Science*, **94**, 1–65.

Vu D Q and Koros W J (2002) 'High pressure CO_2/CH_4 separation using carbon molecular sieve hollow fiber membranes', *Industrial and Engineering Chemistry Research*, **41**, 367–80.

Wessling M, Lopez M L and Strathmann H (2001) 'Accelerated plasticization of thin-film composite membranes used in gas separation', *Separation and Purification Technology*, **24**, 223–33.

White L S (2010) 'Evolution of natural gas treatment with membrane systems' in *Membrane Gas Separation*, Freeman, B D and Yampol'skii Y P (eds), Wiley, Chichester, UK.

Woodcock K E and Gottlieb M (2000) 'Natural gas' in *Kirk–Othmer Encyclopedia of Chemical Technology Volume 12*, Kirk R E and Othmer D F, (eds), Wiley, New York, 365–86.

Younger A H (2004) *Natural Gas Processing Principles and Technology: Part 1 (University of Calgary Course Text)*, University of Calgary, Calgary, Canada.

Zou J, Huang J and Ho W S W (2007) 'CO_2-selective water gas shift membrane reactor for fuel cell hydrogen processing', *Industrial and Engineering Chemistry Research*, **46**, 2272–9.

© Woodhead Publishing Limited, 2011

11.10 Appendix: list of symbols

Symbol	Definition	Units
b	Langmuir affinity constant	atm^{-1}
C	Concentration	$cm^3(STP)\ cm^{-3}$
C'_H	Maximum adsorption capacity	$cm^3(STP)\ cm^{-3}$
f	Fugacity	atm
K	Henry's Law coefficient	$cm^3(STP)\ cm^{-3}\ atm^{-1}$
P	Permeability	barrer
S	Solubility	$cm^3(STP)\ cm^{-3}\ atm^{-1}$
V	Molar volume	$cm^3\ mol^{-1}$
V_G	Molar volume of a gas at STP = 22 400	$cm^3\ mol^{-1}$
α	Selectivity	
σ	Concentration dependent component of the solubility	
χ	Flory–Huggins interaction parameter	
Superscripts		
n	Exponent	
Subscripts		
A	Species A	
B	Species B	
i	Species i	
j	Species j	
u	Upper bound slope	

© Woodhead Publishing Limited, 2011

12
Membranes for advanced biofuels production

S. CURCIO, University of Calabria, Italy

Abstract: Bioenergy is regarded as the utilization of biomass as starting material for the production of sustainable fuels. First generation biofuels, primarily produced from food crops and oil seeds, however, are limited in their ability to achieve the desired targets for biofuel production, climate change mitigation and economic growth. These concerns have increased interest in developing second generation biofuels produced from non-food feedstocks. The present contribution is intended to present an overview of the application of membrane processes and, particularly, of membrane bioreactors in bioenergy, pointing out the engineering aspects related to some of the bio-catalytic processes involved in biofuels production.

Key words: bioenergy, biofuels, biomass, bioreactors, modelling.

12.1 General overview of second-generation biofuels

Before the advent of an economy based on fossil fuels, biomass was the main source of energy. Energy efficiency in the conversion of biomass was, however, very low. Fossil fuel energy, instead, represented a more economical alternative for the developing society of the nineteenth century. With increasing industrialization worldwide, energy demands have now reached a stage where fossil fuel energy is not able to meet the required sustainable growth in the world economy. Recognition that crude oil reserve is finite and its depletion is occurring much faster than previously predicted has determined a new interest in biomass, which is considered to be one of the few current sustainable resources for producing renewable energy (Klass, 1998). Moreover, the environmental deterioration resulting from the over-consumption of petroleum-derived products is seriously menacing the sustainability of human society. As an example, to comply with a 10% target in the European Union from domestic production, the actual feedstocks supply is not enough to meet the current demand and the land requirements for biofuels production would be more than the potential available arable land for bioenergy crops. Extensive pressure for land use change and an increase in cultivated fields may lead to land competition and biodiversity loss, owing to cutting down existing forests and the utilization of ecologically important

© Woodhead Publishing Limited, 2011

areas (Renewable Fuel Agency, 2008). Second generation biofuels, instead, offer a possible solution to the current problems since they contribute to a reduction in land requirements because of their presumed higher energy yields per hectare as well as their non-requirement for agricultural land. Processes with high biomass-to-energy conversion efficiency are therefore required. In this context, the role of bioengineering is crucial to make the transition from a fossil fuel economy to a biomass-based economy a reality, although currently there are no obvious routes to achieve this.

12.1.1 Biodiesel production

Biodiesel has gained greater and greater importance owing to its ability to substitute for fossil fuels, which are expected to run out within a century. The environmental issues related to the emission of exhaust gases, mainly CO_2, characterizing the combustion of fossil fuels have encouraged the utilization of biodiesel which can be considered to be a carbon neutral fuel since the carbon present in the exhaust was originally fixed from the atmosphere. Biodiesel is a mixture of mono-alkyl esters that can be obtained from either vegetable oils or from other sources like animal fat, waste cooking oil, greases and algae (Peterson, 1986; Ranganathan *et al.*, 2008). The utilization of vegetable oils as biodiesel is achieved by blending the oils with traditional diesel in a suitable ratio even though these ester blends are stable only for a short period. The direct usage of the so-obtained blended oils, however, is not adequate for long-term use in commercial diesel engines, especially in the last generation ones, owing to high viscosity, acid contamination, carbon deposition and free fatty acid formation and polymerization (Ma and Hanna, 1999). Vegetable oils do actually require further processing to attain properties similar to those of conventional diesel fuel, thus allowing direct utilization in available diesel engines. However, to become a more viable alternative fuel and to survive in the market, biodiesel must compete economically with diesel. Additionally, biodiesel needs to have a lower environmental impact and ensure the same level as performance as existing fuels (Mata *et al.*, 2010).

The end cost of biodiesel mainly depends on the price of the feedstocks which accounts for 60–75% of the total cost (Canakci and Sanli, 2008). In order to not compete with edible vegetable oils, low-cost and profitable biodiesel should be produced from low-cost feedstocks such as non-edible oils, used frying oils, animal fats, soap-stocks and greases. Three different techniques are actually exploited to convert the vegetable oils into a fuel form, pyrolysis, microemulsification and transesterification (Ranganathan *et al.*, 2008), the latter being the most widespread process on an industrial scale.

Transesterification represents the alcoholysis of triglyceric esters resulting

© Woodhead Publishing Limited, 2011

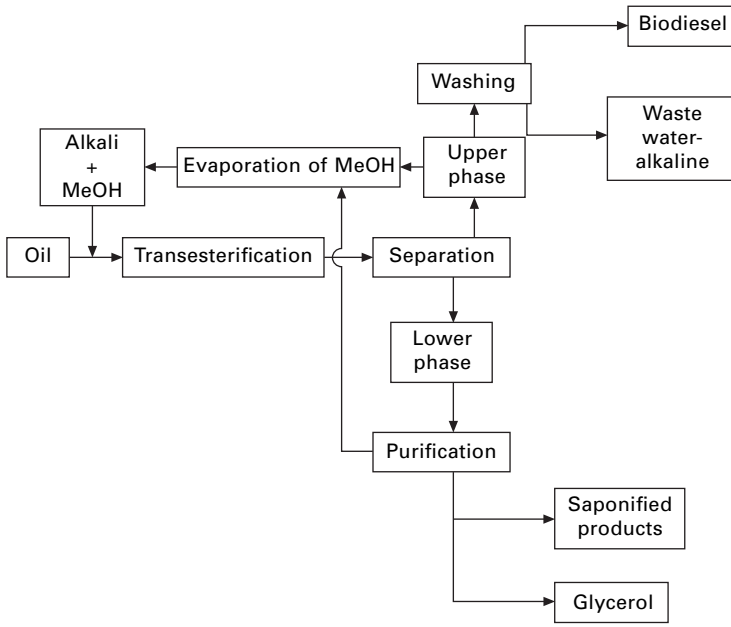
in a mixture of mono-alkyl esters and glycerol. The high viscosity compound, glycerol, is separated and removed so as to achieve a low-viscosity final product similar to conventional diesel fuel; a mixture of these mono-alkyl esters does indeed represent a rather good substitute for fossil fuels. The transesterification process can be performed in different ways, namely by an alkaline catalyst, by an acid catalyst or by a biocatalyst that could be entrapped in a proper support, for example a membrane. In the alkaline process either sodium hydroxide or potassium hydroxide is employed as catalyst together with methanol, or ethanol, or isopropanol, or butanol, although methanol is the most common owing to its low cost and availability. During the process, an alcoxy species is first formed by the reaction between the catalyst and the alcohol. Then the alcoxy species is reacted with any vegetable oil to form biodiesel and glycerol. Glycerol and biodiesel are eventually separated in a decanter exploiting their different densities (Barnwal and Sharma, 2005). This process is actually very efficient and is characterized by a high reaction rate even at an operating temperature of 333K (Fukuda *et al.*, 2001).

A reasonable alternative to the alkaline process is represented by the utilization of an acid catalyst instead of a base. Any mineral acid can be used to catalyse the process, but the most common acids are actually sulfuric acid or sulfonic acid. The yield of biodiesel is high, albeit the acids may cause damage to the equipment (Freedman *et al.*, 1984). Compared to both alkaline and acid catalysts, the utilization of enzymes, such as lipase obtained from microorganisms like *Mucor miehei*, *Rhizopus oryzae*, *Candida antarctica* and *Pseudomonas cepacia*, offers several advantages that may allow more rational transesterification processes to be designed (Watanabe *et al.*, 2000; Hama *et al.*, 2007; Noureddini *et al.*, 2001; Ricca *et al.*, 2009). Enzymes, in fact, can be immobilized thus allowing the reutilization of biocatalyst without any additional separation; moreover, the operating temperature of the process is lower (up to 323K) than the other techniques. Finally, it is not necessary to make use of any strong alkaline or acid compound that, eventually, needs to be properly disposed of. Enzymatic processes, however, also have some disadvantages that concern the inhibition effects observed when methanol is added to the mixture, the decay of enzyme activity and the rather high cost of enzymes. Research works mostly focus on ways of overcoming these problems and on modelling, designing and controlling efficient membrane bioreactors with immobilized enzymes in which to perform biodiesel production on an industrial scale.

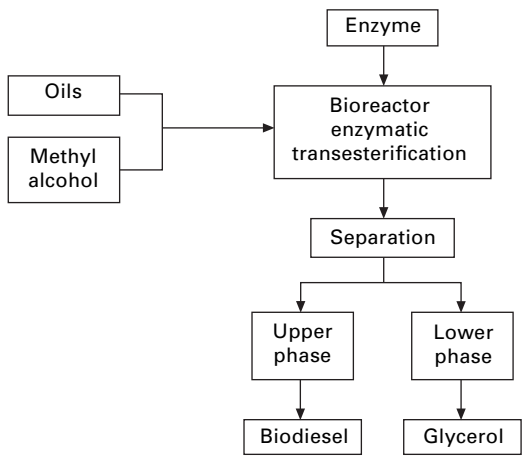
At present, of all of the above-mentioned processes, only the alkaline route is performed on an industrial scale owing to its cost effectiveness and its higher efficiency. However, the downstream processing is far complicated since the separation of both catalyst and unreacted methanol from biodiesel is actually quite difficult. The removal of the catalyst does indeed present many problems since biodiesel has to be repeatedly washed to achieve the required

© Woodhead Publishing Limited, 2011

purity. Figures 12.1 and 12.2 show a comparison between the downstream operations of alkaline and enzymatic processes. Production of biodiesel by a biocatalytic process reduces most of the disadvantages characterizing the



12.1 Production of biodiesel by the alkaline process (adapted from Ranganathan *et al.*, 2008).



12.2 Production of biodiesel by the enzymatic process (adapted from Ranganathan *et al.*, 2008).

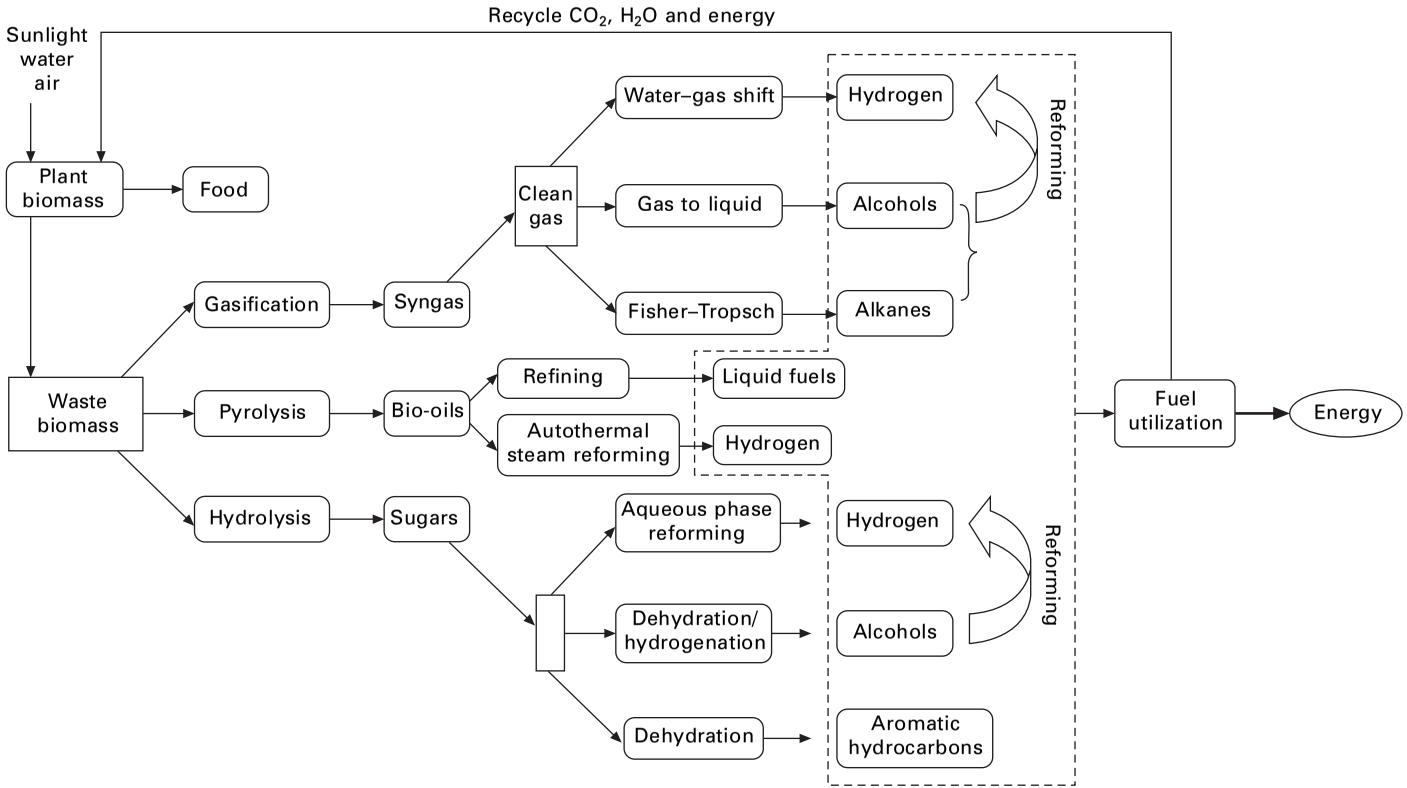
© Woodhead Publishing Limited, 2011

alkaline process and allows a very high purity final product to be obtained with little or no downstream operations (Ranganathan *et al.*, 2008).

12.1.2 Hydrogen production

Hydrogen is considered to be one of the few long-term sustainable clean energy carriers, emitting only water vapour as a by-product during the combustion or oxidation process. Although it is possible to use hydrogen as a fuel in internal combustion engines, its use in fuel cells is more attractive because of its higher efficiency (Crane and Scott, 1992). Various resources can be utilized to produce hydrogen, including both renewable and non-renewable ones. An established technology, such as the steam reforming of methane or natural gas, is most likely adopted initially, because of its wide use and economic feasibility (Tanksale *et al.*, 2010). However, the benefits of a true hydrogen economy can only be achieved if the hydrogen is derived from renewable and carbon neutral resources. In the long term, it is indeed expected that the technology will evolve towards more renewable resources such as biomass or water electrolysis, greatly reducing NO_x and CO_x emissions. The technologies aimed at hydrogen production can be classified in three categories, where hydrogen is produced with (a) net positive emission of CO and CO_2, (b) CO_2 free emissions and (c) CO_2 neutral emissions. Examples of type (a) include steam reforming, partial oxidation and autothermal reforming of hydrocarbons such as natural gas (Nielsen, 2001), as well as the shift reaction of the gaseous products of coal gasification (Lin *et al.*, 2002). Carbon dioxide-free hydrogen production can be achieved through methane decomposition (Steinberg, 1998) and methane aromatization. However, hydrogen production can be environmentally friendly only if the resource used to obtain it is carbon neutral. Resources like natural gas and coal require a lot of energy for mining and processing, thus producing an increase of CO_2 emissions and, therefore, a rise in the environmental impact characterizing hydrogen production from these sources. Biomass-derived hydrogen, instead, can be classified as 'carbon neutral' since the CO_2 released during hydrogen production is consumed by further biomass generation. This well-established idea is actually true if the CO_2 produced during the operation of hydrogen production unit is neglected. CO_2 neutral hydrogen production can be achieved by several routes, for example conversion of biomass via gasification (Chen *et al.*, 2004), pyrolysis of bio-oils, steam reforming of alkanes and alcohols derived from biomass (Nielsen, 2001) and aqueous phase reforming of oxygenated hydrocarbons (Cortright *et al.*, 2002). For some of the above processes it is actually necessary to perform a preliminary step, the hydrolysis of cellulose, which allows the production of sugar monomers that actually represent the basis for the subsequent downstream processes aimed at obtaining different classes of biofuels. Figure 12.3 (Tanksale *et al.*, 2010;

© Woodhead Publishing Limited, 2011



12.3 Hydrogen and liquid fuels production from biomass sources. The waste CO_2, H_2O, and energy produced from these fuels can be utilized to produce move biomass (adapted from Tanksale *et al.*, 2010 and Huber and Dumesic, 2006).

© Woodhead Publishing Limited, 2011

Huber and Dumesic, 2006) summarizes the above-mentioned routes which can be followed to produce other types of biofuels, for example bioethanol, from biomass. In synthesis, syngas can be converted to hydrogen by the water–gas shift reaction, however, any remaining CO must be removed from the gas stream. Pyrolysis bio-oil can be converted to liquid fuel but the processes are complex and the conversion is low. Hydrogen can also be produced from the bio-oil by autothermal reforming with high conversion efficiency, especially with the use of catalytic membrane reactors. Aqueous phase reforming can be used to convert sugars and sugar alcohols into hydrogen.

Lignocellulosic biomass (plant biomass) represents the most abundant form of biomass; it contains approximately 40–50% cellulose, 20–30% hemicellulose and 0–20% lignin (Lynd *et al.*, 1999). Lignocellulosic biomass can be obtained from various resources: (a) forestry wastes such as logging wastes, sawmill wood waste, and the residues of the trees and shrubs, (b) agricultural residues like animal and crop wastes and (c) energy crops like corn, sugarcane, grasses and aquatic plants. Residues from energy crops, such as corn stover, sugarcane or sorghum bagasse, have high energy content per unit mass (Towler *et al.*, 2004) and, therefore, are very attractive for biomass conversion. Hydrogen produced from biomass can be used as a fuel in polymer electrolyte membrane (PEM) fuel cells to produce electricity for transportation purposes. In the short to medium term, this hydrogen can also be used for traditional purposes to minimize the environmental effects of the hydrogen derived from fossil fuels.

12.2 Hydrolysis of biomass to produce sugars

The hydrolysis of biomass is a crucial step in biofuels technology since it allows sugar monomers to be produced that are subsequently processed to obtain either hydrogen or bioethanol. Biomass hydrolysis can be classified as: (1) diluted acid hydrolysis (Karimi *et al.*, 2006), (2) concentrated acid hydrolysis, (3) alkaline hydrolysis (Bobleter, 1994), (4) enzyme hydrolysis catalysed by cellulases (Sun and Cheng, 2002) and (5) near- and super-critical water hydrolysis. The utility cost of enzymatic hydrolysis is low compared to acid or alkaline hydrolysis since enzymes operate under mild conditions (pH 4.8 and temperature ranging between 45 and 50°C) and corrosion problems have been found (Duff and Murray, 1996). Cellulases are usually a mixture of several enzymes. At least three major groups of cellulases are involved in the hydrolysis process: (1) endoglucanase (EG, *endo*-1,4-D-glucanohydrolase), which attacks regions of low crystallinity in the cellulose fibre, creating free chain-ends, (2) exoglucanase or cellobiohydrolase (CBH, 1,4-*b*-D-glucan cellobiohydrolase), which further degrades the molecule by removing cellobiose units from the free chain-ends and (3) β-glucosidase (EC 3.2.1.21) which hydrolyses cellobiose to produce glucose (Coughlan

© Woodhead Publishing Limited, 2011

and Ljungdahl, 1988). The enzymatic hydrolysis of cellulose is, therefore, a multi-step reaction occurring in a heterogeneous system, in which insoluble cellulose is initially broken down at the solid–liquid interface via the synergistic action of both EG and CBH (Zhang and Lynd, 2004). This initial degradation is accompanied by further liquid phase hydrolysis of soluble intermediate products, for example short cellulo-oligosaccharides and cellobiose, which are catalytically cleaved to produce glucose by the action of β-glucosidase (BG) (Andric *et al.*, 2010). The substrate heterogeneity generally determines variations in the rates of the enzymatic hydrolysis of the cellulose depending on the site where the enzymatic attack of the substrate actually occurs.

Since the reactions are catalysed by several enzymes, which operate on insoluble and heterogeneous lignocellulosic materials, the simple Michaelis–Menten equation is not adequate to describe the actual kinetic mechanisms properly and has to be modified in order to account for the different phenomena involved in the process. Therefore, a wide number of kinetic models for enzyme-catalysed hydrolysis of cellulose have been proposed in the literature (Zhang and Lynd, 2004; Kadam *et al.*, 2004).

The enzymatic hydrolysis of cellulose is strongly affected by the type and nature of substrates, by the enzyme activity and by the reaction conditions (temperature, pH, but also other parameters). To improve the yield and the rate of the enzymatic hydrolysis, research has mostly focused on designing improved bioreacting systems and on enhancing the activity of cellulases (Cantwell *et al.*, 1988). Substrate concentration is one of the main factors affecting the yield and the initial reaction rate. At low substrate levels, an increase of substrate concentration results in an increase of both the yield and the hydrolysis reaction rate (Cheung and Anderson, 1997). In contrast, high substrate concentration can cause substrate inhibition, which may strongly lower the rate of the hydrolysis; the extent of substrate inhibition does actually depend on the ratio of total substrate to total enzyme (Sun and Cheng, 2002).

A key requirement in developing cost-efficient lignocellulosic biomass processing is, therefore, to design and to operate reacting systems capable of ensuring high conversion of the cellulose with low enzyme dosage; enzymes, in fact, are still one of the most important cost terms in lignocellulose-to-biofuels processing (Lynd *et al.*, 2008).

Actually, the effective use of the catalyst, defined as the yield of glucose obtained per unit of enzyme(s) and the efficient bioconversion of the substrate itself, defined as the amount of product per unit of substrate, are considered to be the most important parameters for the design and operation of a bioreactor aimed at lignocellulosic biomass conversion. The maximization of product concentration and the optimization of volumetric productivity, for example the mass flow rate of glucose formed per reactor volume, represent two additional meaningful parameters for attaining economically viable and sustainable

© Woodhead Publishing Limited, 2011

enzyme processing, especially on the large scale and in a continuous mode. Compared to other enzyme-catalysed reactions, the volumetric productivity of bioreactors for cellulose conversion are limited by the inherently slow rate of the enzyme-catalysed degradation of lignocellulose to glucose (Gan *et al.*, 2002). For non-complexed cellulose systems this slow rate is mainly ascribed to the insoluble and partly crystalline nature of the cellulose substrate (Zhang and Lynd, 2004).

It is worthwhile remarking that a too low rate of glucose formation per reactor volume may even prevent feasible processing as it can require unrealistic reactor dimensions; for this reason, it is necessary to make use of selected classes of enzymes. Both bacteria and fungi can produce cellulases. These microorganisms can be aerobic or anaerobic, mesophilic or thermophilic. Bacteria belonging to *Clostridium*, *Cellulomonas bacillus*, *Thermomonospora*, *Ruminococcus*, *Bacteriodes*, *Erwinia*, *Acetovibrio*, *Microbispora* and *Streptomyces* can produce cellulases. Fungi that have been reported to produce cellulases include *Sclerotium rolfsii*, *Phanerochaete chrysosporium* and species of *Trichoderma*, *Aspergillus*, *Schizophyllum* and *Penicillium* (Duff and Murray, 1996). Cellulase activity, however, is inhibited by cellobiose and to a lesser extent by glucose. Several methods have been proposed to reduce the inhibition, including use of high concentrations of enzymes, addition of β-glucosidases during the hydrolysis, removal of the produced sugars by ultrafiltration or the simultaneous saccharification and fermentation (SSF).

12.2.1 Bioethanol production

Ethanol, in being both renewable and environmentally friendly, is believed to be one of the best alternatives to traditional fuels; it is indeed one of the most important renewable fuels contributing to the reduction of the negative environmental impact generated by the worldwide use of fossil fuels. As Fig. 12.3 shows, some transformations involved in hydrogen production from lignocellulosic biomass, for example the hydrolysis of cellulose, have to be performed preliminarily to obtain bioethanol finally. Lignocellulosic biomass, in fact, has to be conditioned and treated so as to obtain sugars that can be then fermented by yeasts into ethanol. The aqueous solutions of ethanol so obtained are subsequently concentrated, thus attaining hydrous ethanol which is used as an oxygenate for gasoline, that is the trade form in which ethanol is mostly employed in the transportation sector.

The complexity of the above-described process partly explains why fuel ethanol has not yet played a leading role in comparison to cheaper oil-derived fuels. Only in the last few years, because of rising environmental concerns and the periodic crises in some of the larger oil exporting countries, has bioethanol become a viable and realistic alternative in the energy market.

© Woodhead Publishing Limited, 2011

Therefore, the development of cost-effective technologies for fuel ethanol production is a priority for many research centres, universities, private firms and even governments. Analysis of integration features of the overall process of fuel ethanol production from different feedstocks represents one of the main objectives of the current studies.

As in the case of hydrogen, bioethanol can also be produced from raw materials containing fermentable sugars, like sugar cane and beet, which are rich in sucrose (Bai *et al.*, 2008). Bioethanol may also be produced from some polysaccharides, which can be then transformed to obtain sugars that can be converted into ethyl alcohol or, directly, from the lactose contained in the dairy industry wastes (Sansonetti *et al.*, 2009, 2010). Lignocellulosic biomass, however, is the most promising feedstock considering its great availability and low cost, but large-scale commercial production of fuel ethanol from lignocellulosic materials has not yet been implemented. To design fuel ethanol production processes, an assessment of the utilization of different feedstocks is required considering the large share that raw materials take in ethanol costs. Sugar cane, either in the form of cane juice or cane molasses, is the most important feedstock utilized in tropical and sub-tropical countries for producing ethanol. Conversion of sucrose into ethanol is easier compared with starchy materials and lignocellulosic biomass because the preliminary hydrolysis of feedstock is not required since this disaccharide can be broken down by the yeast cells; in addition, the conditioning of the cane juice or molasses promotes the hydrolysis of sucrose. In terms of the design of ethanol production processes from sucrose-containing biomass, the availability and transport costs of the feedstock play a key role when new cost-effective production facilities are being projected despite the relative maturity of the conversion technologies involved.

To produce ethanol from starch it is necessary to break down the chains of this carbohydrate to obtain glucose syrup, which can be then converted into ethanol by yeasts. This type of feedstock is the most utilized for ethanol production in North America and Europe, with corn and wheat being mainly employed. In tropical countries, other starchy crops like tubers (e.g. cassava) can be used for commercial production of fuel ethanol.

Currently, a large number of studies regarding the utilization of lignocellulosic biomass as a feedstock for producing fuel ethanol are being carried out worldwide. For countries where it is difficult to cultivate energy crops, lignocellulosic materials represent an attractive option (Bungay, 2002). The main challenge in the conversion of biomass into ethanol is represented, however, by the complex processes preceding the sugar fermentation step. Owing to the structure of the lignocellulosic complex, a pretreatment is required to allow its degradation, the removal of lignin, partial or total hydrolysis of a hemicellulose and the decrease in the fraction of crystalline cellulose with respect to amorphous cellulose, the most suitable form for the

© Woodhead Publishing Limited, 2011

subsequent hydrolysis process. As described in the previous section, during hydrolysis, cellulose undergoes a series of biocatalytic reactions that produce glucose which is then transformed into ethanol by process microorganisms. Eventually, the sugars released during the hydrolysis of hemicellulose can be converted into ethanol as well. Consequently, the technologies involved are more complex, leading to higher ethanol production costs compared to cane, beet or corn. However, the fact that many lignocellulosic materials are by-products of agricultural activities, industrial residues or domestic wastes and, therefore, are not competitive with foodstuffs offers huge possibilities for the production of fuel ethanol on the large scale as well as its global consumption as a renewable fuel. It is believed that lignocellulosic biomass will become the main feedstock for ethanol production in the near future (Fukuda *et al*., 2009).

Among many microorganisms that have been exploited for fermentation of sugars into ethanol, *Saccharomyces cerevisiae* still remains as the principal species. *Zymomonas mobilis* has also been extensively studied over the past three decades and repeatedly claimed by several researchers to replace *S. cerevisiae* in ethanol production, because this species possesses some 'superior characteristics' compared to its counterpart *S. cerevisiae* (Cardona and Sanchez, 2007).

12.3 Key role of process engineering for second-generation biofuels production

Owing to the large number of existing and incompletely developed technologies for the production of biofuels it is necessary to exploit process engineering tools to overcome some of the inherent difficulties accompanying the development of novel technologies. Process engineering includes the design of innovative process configurations aimed at reducing production costs. Through process design it is possible to develop environmentally friendly technologies, utilizing different design approaches. The design of cost-effective processes for biofuels production implies the selection and definition of a suitable process configuration that allows the conversion of raw materials into the desired biofuel(s), meeting given specifications. The task of defining a proper configuration of the process requires the generation and assessment of many alternative process flowsheets to find those that show improved performance indicators. In this way, the impact of specific technologies on the global process and production costs can be elucidated. This step is called process synthesis, during which the structure of the synthesized flowsheets is established providing a more detailed insight with which to improve the process. In both the above-mentioned steps, process modelling and simulation play a significant role in the successful design of alternative configurations for biofuels production. This is particularly true in

© Woodhead Publishing Limited, 2011

the case of continuous processes where a proper dynamic analysis is crucial for an appropriate design.

One of the most important approaches in the design of more intensive and cost-effective process configurations is process integration. In the case of biofuels production, process integration is involved to integrate all the single unit operations involved in the process. This can be achieved through the development of integrated bioprocesses that combine different steps into one single unit. Thus, reaction–separation integration removes, for instance, the product(s) from the biotransformation zone offering several opportunities to increase process yield and consequently reduce product costs. Process integration is attracting more and more interest owing to the advantages of its application in the production of biofuels allowing a reduction in energy costs, a decrease in both the size and number of process units and an intensification of the biological and downstream processes.

Process optimization is another crucial tool employed within the framework of process design. Optimization plays a decisive role during the experimental stage as well as during the design steps. This is particularly the case for second-generation biofuels, where production costs can be significantly reduced since it is believed that some current technologies have reached their inherent limits and the exploitation of novel and less expensive alternatives is therefore required. Consequently, advanced models should be developed for optimization of biofuels production costs utilizing a systemic approach that allows opportunities to be identified for overcoming the present technological barriers.

A detailed analysis of all the above-mentioned techniques is far beyond the scope of this chapter. In the following, however, some of the most important engineering aspects will be elucidated with reference to the characterization and improvement of membrane bioreactors performance.

12.4 Membrane bioreactors

In the last few decades membrane science and technology have offered a considerable contribution to the development of biotechnology and, more specifically, of enzyme reactors engineering that will provide efficient and innovative systems in which to perform biocatalytic conversion of one or more substrate(s) into the desired product(s). When an enzyme operates in its native form and is dissolved in a homogeneous batch solution several drawbacks are encountered. These drawbacks include high enzyme purification costs, low productivity, difficult and expensive recovery and reuse of enzyme or cellular microorganisms, product pollution and difficulties in maintaining a standard product quality (Chibata, 1978). Confining the biocatalysts in a well-defined space, where they can retain their catalytic activity and can be repeatedly and continuously used enables these disadvantages to be overcome.

© Woodhead Publishing Limited, 2011

Confinement of biocatalyst allows reactants/products and enzymes to be kept separate at any time, so that the enzyme can be reused and product can be easily separated from the reaction mixture. In addition, biocatalyst stability is enhanced, operating costs and enzyme consumption costs are significantly reduced and the process operates with a higher productivity (Messing, 1975).

The immobilization of microorganisms instead of purified enzymes represent an interesting alternative route, which can be suitably carried out when enzymes are intracellular, when the enzyme, extracted from cells, is unstable during and after immobilization, as well as when the microorganism does not contain any stable interfering enzyme. Furthermore, the immobilization of whole cells is preferred when mass transport of both substrate and product(s) to the catalytic sites is not limited. In these cases, the immobilization of whole cells permits some significant advantages to be achieved compared to purified enzyme immobilization. In particular, a significant cost reduction is achieved since enzyme extraction and purification are not necessary and can therefore be skipped; moreover, the enzyme remains in its natural environment, thus preserving a high initial activity.

Another advantage offered by immobilization of cells is the possibility of performing multi-step reactions, each catalysed by a different type of enzyme contained within the cell (Cheryan and Mehaia, 1986), as is required by cellulose hydrolysis. Biocatalysts immobilization techniques are various and range from the confinement in a gel, to the encapsulation in cellulose or alginate beads, from physical adsorption on a solid surface, to covalent chemical binding to an insoluble support and from copolymerization with a proteic carrier, to entrapment within a polymeric matrix (Bailey and Ollis, 1986).

Synthetic membranes are a well-assessed support for the immobilization of biological catalysts, such as enzymes or whole cells, under milder conditions than techniques that require the establishment of a chemical bound. A synthetic membrane, with a suitable molecular weight cut-off (MWCO), somehow artificially replicates the cell membrane function, ensuring the protection of the enzymes against contaminants and inhibitors. In a membrane bioreactor the biocatalyst is confined in a well-defined space by a selective membrane, or immobilized by absorption or entrapment within the polymeric structure of a membrane. Enzymes are precluded, due to their molecular size, from diffusing out or permeating through the membrane, while substrates and products can readily permeate or diffuse through the membrane.

Although diffusion is the primary mass transfer mechanism, membrane bioreactors may be operated with ultrafiltration fluxes through the membrane wall. These fluxes are generally promoted by the application of a trans-membrane pressure difference (TMP). If significant TMP values are achieved, the mass transfer rate is significantly enhanced by the addition of a convective

© Woodhead Publishing Limited, 2011

component to the diffusive mass transfer mechanism (Calabrò *et al.*, 2002). Membrane bioreactors offer the possibility of coupling a separation process to a (bio)-chemical reaction, resulting in plant simplification and in further costs cut-off. The removal of a reaction product from the reaction environment is easily achieved thanks to membrane selective permeability and this would be a great advantage in thermodynamically unfavourable conditions, such as reversible reactions or product-inhibited enzyme reactions. The behaviour of membrane bioreactors, however, is strongly affected by mass transfer limitations and a detailed understanding of the transport phenomena involved in the biocatalytic process is required.

Different kinds of membrane bioreactors are:

- enzyme membrane reactors (EMR)
- enzyme gel-layer membrane reactors
- membrane segregated enzyme reactors
- membrane bound enzymes in continuous flow reactors
- whole cells or enzymes immobilized in capillary membrane reactors.

For the sake of brevity, in the present general overview of the engineering aspects of membrane bioreactors to be used in the production of second-generation biofuels, attention will be focused on particular problems, analysing bioreactors that have real significance owing to their possible utilization on a pilot/industrial scale where:

- the biocatalyst is continuously separated by a membrane system and then recycled back to the reaction tank;
- the biocatalyst is immobilized on the surface of a membrane by covalent bonding;
- the biocatalyst is immobilized/entrapped within the porous structure of an ultrafiltration (UF) membrane.

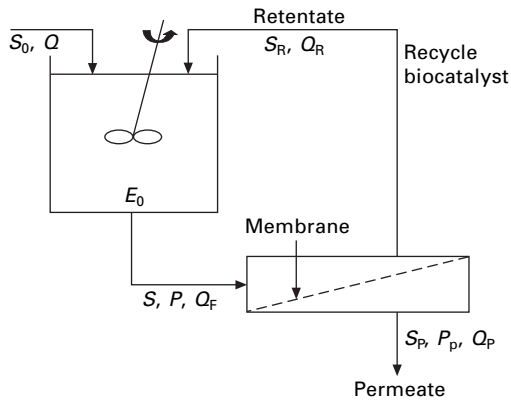
In particular, it will be shown, with reference to some very general cases, how the formulation of good theoretical models is helpful in characterizing the actual behaviour of membrane bioreactors. In this way, it is possible to determine how to operate each type of bioreactor so as to improve its performance and maximize its productivity.

12.5 Biocatalyst continuously separated by a membrane system and recirculated into the reaction tank

This type of bioreactor (Fig. 12.4) is realized by coupling a continuous stirred tank reactor, loaded with a known amount of enzyme in its native state, to a cross-flow filtration unit.

The enzyme is continuously recirculated to the reaction tank where the

© Woodhead Publishing Limited, 2011



12.4 Schematic of a membrane bioreactor with continuous biocatalyst recirculation. See text and Appendix for symbols.

greatest part of the reaction occurs. Depending on the membrane properties and the substrate characteristics either partial or total substrate rejection can be achieved. It is supposed that the reaction products are contained only in the permeate (this can be achieved by a proper choice of membrane characteristics), which is continuously removed from the system; this configuration, therefore, is particularly useful in those cases in which the biocatalytic reaction is product inhibited. Moreover, compared to a classical enzyme membrane reactor composed of a stirred tank equipped with a UF membrane, this bioreactor exhibits much fewer concentration polarization phenomena, which significantly limit the process efficiency. Finally, this type of bioreactor is characterized by a rather large surface-to-volume ratio and by a greater compactness, which make the system more suitable for large scale operations, as required in most industrial applications.

A simplified analysis aimed at predicting the actual system behaviour will be briefly presented so as to estimate two fundamental parameters, the degree of conversion and the reactor productivity. It is assumed that polarization phenomena occurring in the membrane module are modelled by the film theory according to which the permeate flux through the membrane depends on the mass transfer coefficient, k_L. A correct estimation of k_L values is necessary and can be achieved by the semi-empirical correlations available in the literature (Bird *et al.*, 1960), taking into account the dependence of the Sherwood number upon both the Reynolds and the Schmidt numbers, that is $Sh = f(Re, Sc)$, where:

$$Sh = \frac{D \cdot k_L}{Diff} \text{ Sherwood number (dimensionless)}$$

$$Re = \frac{D \cdot U}{\nu} \text{ Reynolds number (dimensionless)}$$

© Woodhead Publishing Limited, 2011

$$Sc = \frac{\nu}{Diff} \text{ Schmidt number (dimensionless)}$$

in which D is a characteristic length of the system (for example the fibre diameter), U is the characteristic velocity (for example the cross-flow velocity in the membrane module), ν is the kinematic viscosity and *Diff* is the diffusion coefficient.

If the substrate is partially rejected by the membrane, it can be assumed that the substrate concentration both in the permeate, S_P, as well as in the retentate, S_R, does not change with respect to the concentration, S, of the solution fed to the membrane; this concentration, according to the hypothesis of a continuous stirred reactor, is equal to that measured in the bioreactor where the reaction mostly occurs.

The above assumption of $S = S_R = S_P$, which is valid when a low permeate flux is observed (Iorio and Calabrò, 1994), allows the analysis for the determination of the bioreactor key parameters to be simplified. A mass balance on the substrate contained in the EMR can be formulated under steady-state conditions. Assuming that the reaction kinetics can be expressed by a Michaelis–Menten equation rate:

$$R = \frac{R_{MAX} \cdot S}{K_M + S} \qquad [12.1]$$

where, R and $R_{MAX} = k_2 E_0$ are, respectively, the actual and the maximum reaction rates, S is the substrate concentration, K_M is the Michaelis constant and the following relationship is obtained:

$$Q S_0 + Q_R S_R - Q_F S - R V = 0 \qquad [12.2]$$

On the basis of the above hypotheses and assuming that the permeate flow rate, Q_P, is equal to the solution flow rate, Q, so as to keep a constant volume, V, in the bioreactor, the following equation is obtained:

$$S_0 - S - \frac{R_{MAX} S}{K_M + S} \tau_R = 0 \qquad [12.3]$$

in which τ_R, representing the residence time in the bioreactor, is defined as:

$$\tau_R = \frac{V}{Q} = \frac{V}{J A_m} \qquad [12.4]$$

where, J is the permeate flux through the membrane and A_m is the membrane area.

A set of characteristic dimensionless variables can be introduced:

$$\chi = \frac{S}{S_0} \text{ dimensionless substrate concentration} \qquad [12.5]$$

© Woodhead Publishing Limited, 2011

$$\theta = \frac{K_M}{S_0} \text{ saturation factor} \qquad [12.6]$$

The dimensionless saturation factor is actually a measure of enzyme saturation that allows the Michaelis–Menten reaction rate to be approximated either to the first order ($\theta >> 1$) or to the zero-order ($\theta << 1$).

Equation [12.3] can be rearranged, thus obtaining:

$$(1 - \chi) - \left(\frac{k_2 \cdot E_0}{S_0} \cdot \tau_R\right) \cdot \frac{\chi}{\theta + \chi} = 0 \qquad [12.7]$$

in which two groups, representing the process operating parameters, τ_R and the ratio k_2E_o/S_o, are present. It is worthwhile observing that k_2E_0/S_o corresponds to the reciprocal of a characteristic kinetic time, which is multiplied to another characteristic time of the system under study, the residence time τ_R. The solution of Equation [12.7] is straightforward; if the above two characteristic times are grouped in a single variable, B, expressing a comparison between the relative importance of residence time with respect to the kinetic time:

$$B = \left(\frac{k_2 \cdot E_0}{S_0} \cdot \tau_R\right) \qquad [12.8]$$

Equation [12.7] can be simplified to:

$$(1 - \chi) - B \cdot \frac{\chi}{\theta + \chi} = 0 \qquad [12.9]$$

giving the following two roots :

$$\chi = \frac{-(\theta + B - 1) \pm \sqrt{(\theta + B - 1)^2 + 4\theta}}{2} \qquad [12.10]$$

of which only the positive one has a physical significance.

The degree of conversion, α, defined as:

$$\alpha = \frac{S_0 - S}{S_0} = 1 - \chi = 1 - \frac{\sqrt{(\theta + B - 1)^2 + 4\theta} - (\theta + B - 1)}{2} \qquad [12.11]$$

is therefore easily calculated.

The productivity of the present enzyme membrane reactor at a generic time t can be defined as:

$$\Theta_{EMR} = \frac{\text{total amount of product formed at time } t}{\text{total amount of enzyme}} \qquad [12.12]$$

which, on the basis of the above hypotheses and after some rearrangement, gives:

© Woodhead Publishing Limited, 2011

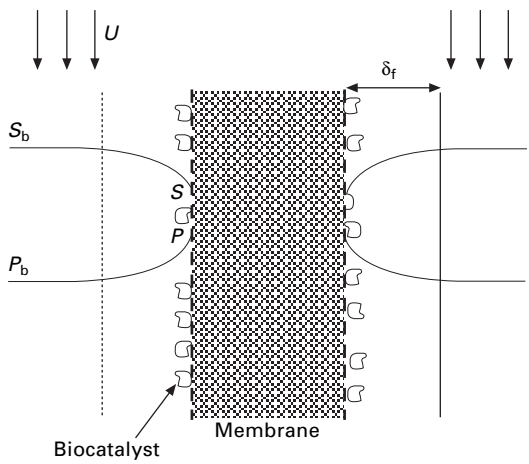
$$\Theta_{EMR} = \frac{P\ (J\ A_m)\ t}{E_0\ V} = \frac{(S_o - S)}{E_0} \cdot \frac{t}{\tau_R} = \frac{\alpha \cdot S_0}{E_0} \cdot \frac{t}{\tau_R} \qquad [12.13]$$

The productivity, therefore, is expressed as a function of the degree of conversion α; furthermore, it is a linear function of the ratio t/τ_R, which represents a kind of volumetric renewal occurring in the bioreactor. With reference to the biocatalytic reactions involved in biofuels production, both the Equations [12.11] and [12.13] give very useful indications about bioreactor behaviour; moreover, they can be used to determine the set of operating conditions that can be exploited to maximize either the degree of conversion or the bioreactor productivity.

12.6 Biocatalyst immobilized onto the membrane surface

This is a typical case of enzyme immobilization by either physical adsorption or the establishment of a chemical bond between the enzyme and the membrane material. Figure 12.5 shows a schematic of a membrane pellet with a biocatalyst immobilized on its surface.

As far as mass transfer is concerned, the enzyme reaction process can be modelled, in terms of the film theory combined with a description of the surface reaction. In other words, it is assumed that the substrate mass transfer resistance is concentrated in a thin film adjacent to the membrane surface where the enzyme molecules have been entrapped. The substrate diffuses through the film and reacts on the membrane surface. With reference to the



12.5 Schematic of a biocatalyst immobilized on the membrane surface. The film thickness δ_f, where transport resistances are localized, is shown. The qualitative concentration profiles of both substrate S_b and product P_b are also reported.

© Woodhead Publishing Limited, 2011

membrane surface, where no accumulation occurs, it is assumed that all the substrate arriving from the bulk by diffusion through the film is consumed by the reaction:

$$k_s \cdot a \cdot (S_b - S) = \frac{R_{MAX} \cdot S}{K_M + S} \quad [12.14]$$

In this case a Michaelis–Menten equation (Equation 12.1) is also used to express the reaction rate. R_{MAX}, expressed in terms of the amount of enzyme immobilized on the support, $E_{m,V}$, is defined as the moles of substrate that react for each unit of support and unit of time:

$$R_{MAX} = k_2 \cdot E_{m,V} \quad [12.15]$$

In Equaton [12.14], a is the specific membrane surface, defined as the ratio between the membrane surface A_m and its volume V_m:

$$a = \frac{A_m}{V_m} \quad [12.16]$$

k_s, instead, is the mass transfer coefficient in the liquid film and is estimated by semi-empirical correlations available in the literature, expressing the Colburn factor, j_D, as a function of the Reynolds number (Bird *et al.*, 1960; Perry and Green, 1997):

$$j_D = \frac{Sh}{Re \cdot Sc} \cdot (Sc)^{2/3} = \frac{k_s}{U} \cdot (Sc)^{2/3} = f(Re) \quad [12.17]$$

Equation [12.14] can be rewritten in terms of the already defined dimensionless variables, χ and θ (Equations 12.5] and [12.6], and of the Damköhler number, a dimensionless parameter, which compares the maximum reaction rate to the overall mass transfer resistances occurring outside the immobilized enzyme:

$$Da = \frac{R_{MAX}}{(k_s \cdot a) \cdot S_b} \quad [12.18]$$

thus obtaining:

$$\frac{1 - \chi}{Da} = \frac{\chi}{\chi + \theta} \quad [12.19]$$

It is worthwhile remarking that when $Da << 1$, the process is limited by the reaction; whereas, when $Da >> 1$, an extremely fast reaction occurs, so that the process is limited by the diffusion outside the immobilized biocatalyst. Equation [12.19] can be solved; of the two roots, the one with physical significance is:

$$\chi = \frac{1}{2}\left(1 - \theta - Da + \sqrt{1 + 2\theta - 2Da + \theta^2 + 2\theta\, Da + Da^2}\right) \quad [12.20]$$

© Woodhead Publishing Limited, 2011

Equation [12.20] expresses the dependence of the substrate dimensionless concentration upon both the Damköhler number and the saturation factor.

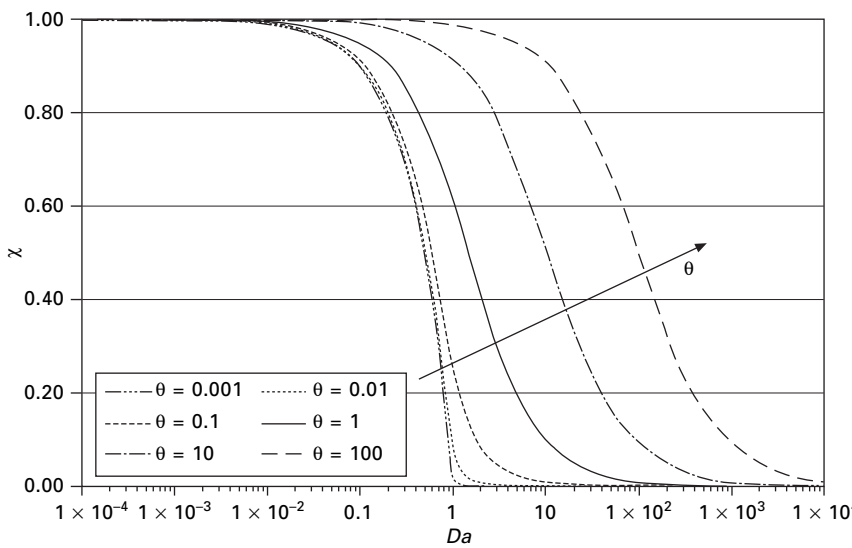
Figure 12.6 shows the dimensionless substrate concentration profile as a function of the Damköhler number, at various values of the saturation factor. It is worthwhile observing that when the process is limited by the reaction rate, the substrate concentration does not change significantly; this effect is even more significant when the enzyme saturation is high ($\theta >> 1$), that is when the reaction rate approximates a first order kinetic.

The effect of mass transfer limitation on the overall process can be also expressed in terms of the effectiveness factor η, which compares the actual reaction rate to that which would have been observed if the catalyst surface were exposed to the substrate concentration S_b measured in the bulk solution, that is without any diffusive resistance outside the enzyme molecule (Bird *et al.*, 1960):

$$\eta = \frac{\text{actual reaction rate}}{\text{reaction rate without external diffusional resistance}} \qquad [12.21]$$

In the case under investigation, the effectiveness factor is defined as:

$$\eta = \frac{R(S) \cdot A_m}{R(S_0) \cdot A_m} = \frac{\dfrac{R_{MAX} \cdot S}{K_M + S}}{\dfrac{R_{MAX} \cdot S_0}{K_M + S_o}} \qquad [12.22]$$



12.6 Substrate dimensionless concentration χ as a function of Damköhler number, *Da*, at different saturation factors, θ.

© Woodhead Publishing Limited, 2011

which, in dimensionless form and according to Equation [12.19], becomes:

$$\eta = \frac{\chi \cdot (1 + \theta)}{\chi + \theta} = \frac{(1 + \theta)}{Da} \cdot (1 - \chi) \qquad [12.23]$$

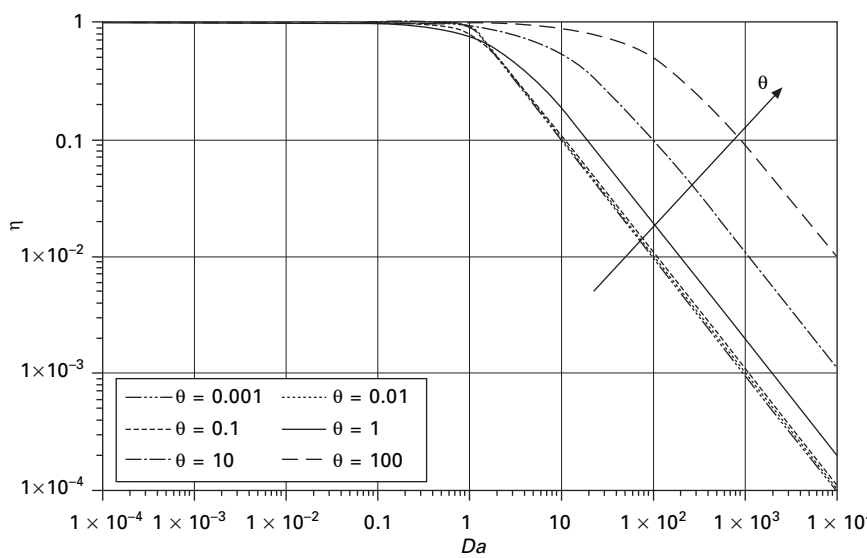
Figure 12.7 is a log–log plot showing the dependence of the effectiveness factor on the Damköhler number at various values of saturation factor, as calculated by Equation [12.23]. It can be observed that when the process is controlled by kinetics ($Da << 1$) and the substrate concentration is uniform throughout the film at the S_b (Fig. 12.6), the effectiveness factor tends to unity. In this case, the actual process rate R_P corresponds to the reaction rate,

$$R_P = \frac{R_{MAX} \cdot S}{K_M + S}$$

which, in dimensionless variables, can be written as:

$$\frac{R_P}{R_{MAX}} = \frac{\chi}{\theta + \chi}$$

Under diffusive control ($Da >> 1$), the reaction is considered to be so fast that the substrate concentration vanishes very rapidly, that is as soon as the substrate molecules come in contact with the enzyme immobilized on the membrane surface. The effectiveness factor can be calculated by simplifying Equation [12.23] as follows ($\chi \to 0$):



12.7 Effectiveness factor η as a function of Damkhöler number, *Da*, at widely varying values of saturation factor, θ.

© Woodhead Publishing Limited, 2011

$$\eta = \frac{1 + \theta}{Da} \qquad [12.24]$$

which tends to zero as Da tends to infinity. In this case, the process rate R_P can be expressed as:

$$R_P = k_s \cdot a \cdot S_b \qquad [12.25]$$

which, in dimensionless form, gives:

$$\frac{R_P}{R_{MAX}} = \frac{1}{Da} \qquad [12.26]$$

In the diffusive control region, a linear dependence between η and Da can be observed in a log–log plot:

$$\log\eta = \log (1 + \theta) - \log Da \qquad [12.27]$$

The saturation factor plays a significant role since at higher values of θ, the region where kinetics controls the process is wider. To improve system efficiency, the external concentration gradients must be minimized; this can be attained, for instance, by a proper choice of system fluid dynamics, provided that the enzyme–membrane bonds are strong enough to avoid any biocatalyst removal by mechanical shear.

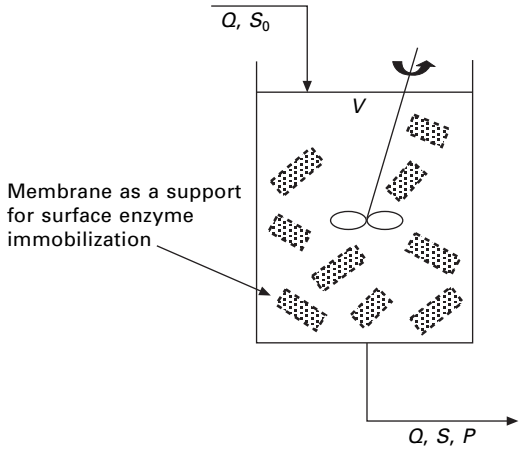
Biocatalyst immobilized on the membrane surface is a common system, which can be used in different bioreactor configurations and geometries. As an example, a continuous stirrer tank bioreactor in which the bioconversion is promoted by an enzyme immobilized on the surface of a flat sheet membrane will be described in the following section.

12.7 Continuous stirred tank reactor with biocatalyst immobilized on the membrane surface (CSTMB)

Figure 12.8 shows the schematic of the system under investigation. It consists of a bioreactor continuously fed by stream characterized by a substrate concentration equal to S_0.

Small pieces of a flat sheet membrane with biocatalyst immobilized on the external surfaces are uniformly distributed in the tank. The geometrical characteristics of the pellets are not actually significant in this case, since only the external mass transfer resistance is taken in consideration. The behaviour of the CSTMB under consideration depends on an additional parameter: the void fraction ε in the tank, defined by the following relationship, which accounts for the true volume occupied by the pellets in which the enzyme has been immobilized:

© Woodhead Publishing Limited, 2011



12.8 Schematic of a continuous stirred membrane bioreactor (CSTMB) in which biocatalyst is immobilized on the membrane surface.

$$1 - \varepsilon = \frac{\text{pellets volume}}{\text{reactor volume}} = \frac{m_p/\gamma_p}{V} \qquad [12.28]$$

where γ_p and m_p are, respectively, the pellet density and the mass of pellets fed to the reactor. A mass balance on the substrate can be formulated under the assumption of steady-state conditions:

$$Q \cdot S_0 - Q \cdot S - \eta \cdot R \cdot (1 - \varepsilon) \cdot V = 0 \qquad [12.29]$$

where R, the actual reaction rate, is referred to the volume of membrane support, V_P, given as:

$$V_p = (1 - \varepsilon) \cdot V \qquad [12.30]$$

When the reaction rate is modelled by the Michaelis–Menten equation, Equation [12.29] can be rewritten as:

$$Q \cdot S_0 - Q \cdot S - \eta \cdot \frac{R_{MAX} \cdot S}{K_M + S} \cdot (1 - \varepsilon) \cdot V = 0 \qquad [12.31]$$

where, R_{MAX} was already defined by Equation [12.15]. Introducing the residence time, $\tau_R = \dfrac{V}{Q}$, and the dimensionless variables χ and θ, Equation [12.31] becomes:

$$1 - \chi - \eta \cdot (1 - \varepsilon) \cdot \left(\frac{k_2 \cdot E_0}{S_0} \cdot \tau_R \right) \cdot \frac{\chi}{\chi + \theta} = 0 \qquad [12.32]$$

The solutions of Equation [12.32] are:

© Woodhead Publishing Limited, 2011

$$\chi = \frac{-B1 \pm \sqrt{B1^2 + 4\,\theta}}{2} \qquad [12.33]$$

where the variable $B1$ groups the following parameters:

$$B1 = \theta - 1 + \eta \cdot (1 - \varepsilon) \cdot \left(\frac{R_{MAX}}{S_0} \cdot \tau_R \right) \qquad [12.34]$$

The positive root of Equation [12.33] is the only one which has physical significance and is exploited to calculate the degree of conversion α:

$$\alpha = \frac{S_0 - S}{S_0} = 1 - \chi = 1 - \frac{\sqrt{B1^2 + 4\theta} - B1}{2} \qquad [12.35]$$

The productivity Θ for unit enzyme can be estimated, too:

$$\Theta_{CSTMB} = \frac{P \cdot Q \cdot t}{E_{m,V} \cdot (1 - \varepsilon) \cdot V} = \frac{(S_o - S)}{E_{m,V} \cdot (1 - \varepsilon)} \cdot \frac{t}{\tau_R} = \frac{\alpha \cdot S_0}{E_{m,V} \cdot (1 - \varepsilon)} \cdot \frac{t}{\tau_R} \qquad [12.36]$$

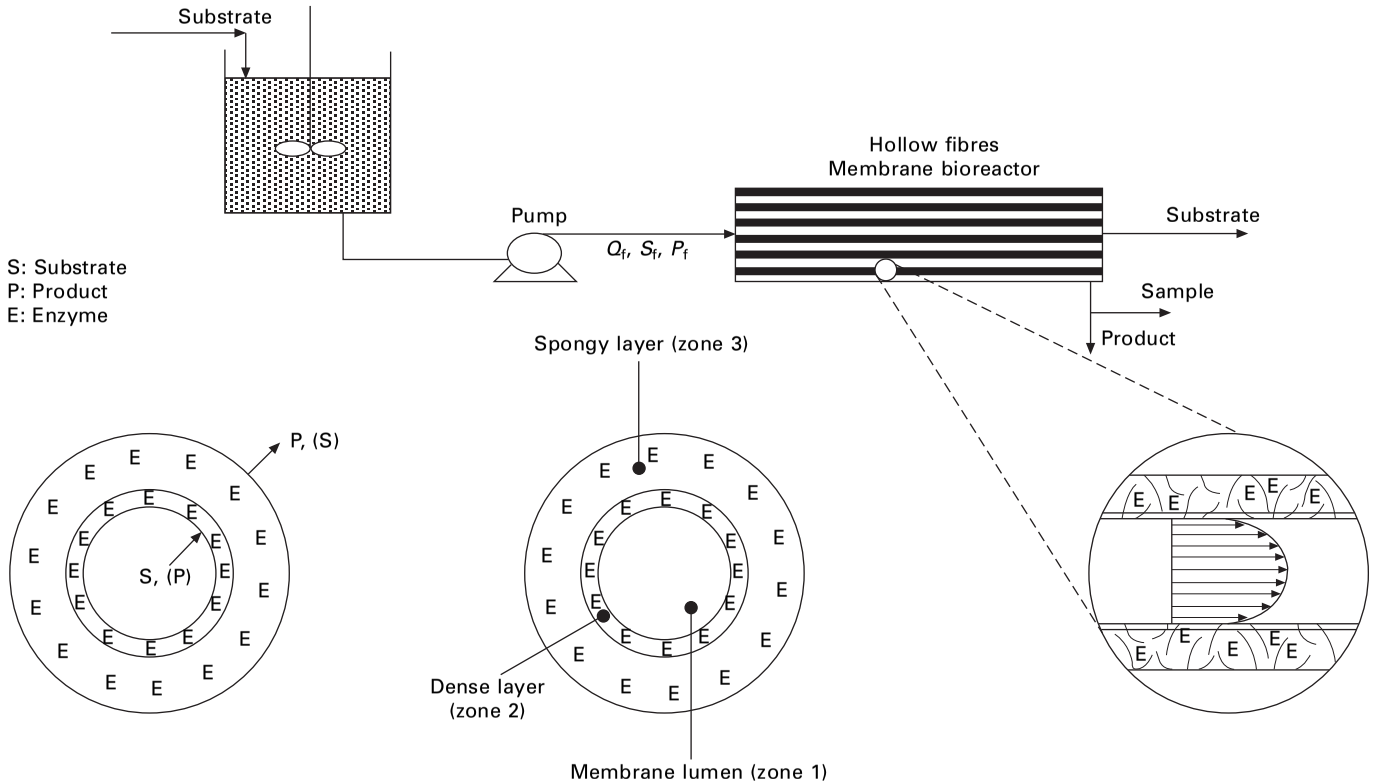
The productivity of CSTMB is very close to the productivity of EMR as given by Equation [12.13]; in both Equation [12.36] and Equation [12.13], the substrate/enzyme ratio, the conversion degree and the residence time play a similar role.

12.8 Single pass membrane bioreactor

This type of membrane bioreactor consists of a bundle of ultrafiltration hollow fibres assembled in a cylindrical cartridge according to a tube and shell configuration (Fig. 12.9). The fibres are asymmetric membranes where the enzyme has been previously immobilized or entrapped; the membrane is composed of a thin skin supported on a porous matrix, which provides the fibres their structural integrity. To develop a theoretical model aimed at predicting the bioreactor behaviour, a single fibre is considered. Within the fibre three regions can be distinguished: the membrane lumen (region 1), where substrate continuously flows mainly in the axial direction and partially in the radial direction; the membrane dense layer or 'skin' (region 2) and the membrane spongy layer (region 3). It is supposed that the enzyme molecules or, in general, the whole cells are actually confined only in regions 2 and 3.

Substrate is forced by ultrafiltration to permeate through the membrane wall where it comes in contact with the immobilized enzyme. The biocatalytic reaction thus occurs; the product(s) and the unconverted substrate are continuously removed in the radial direction from the permeate stream and in axial direction as retentate, respectively.

© Woodhead Publishing Limited, 2011



12.9 Schematic of a hollow fibre membrane bioreactor.

© Woodhead Publishing Limited, 2011

The solution of the problem consists in the determination of velocity and of concentration profiles in each fibre region. The present theoretical model is based on the evaluation of the mass transfer resistances that are localized in a liquid film surrounding each immobilized enzyme molecule, both in the dense and in the spongy layers. Evaluation of the resistances is achieved by defining a local Sherwood number, modified to account for the pores size distribution of the different fibre regions and by the estimation of the membrane specific surface area.

The hypotheses used to formulate the theoretical model are (Calabrò *et al.*, 2002):

1. the system is isothermal;
2. the system operates under steady state conditions;
3. the diffusion mechanism is governed by the Fick's law;
4. axial diffusion, as well as back diffusion of products, are negligible in all the fibre regions;
5. the flow regime within the fibre lumen is laminar;
6. the physical and the transport parameters (viscosity and diffusivity) are constant;
7. the bio-chemical reaction occurs only in regions 2 and 3;
8. the substrate flows in the axial and in radial directions only in the lumen, whereas in the dense and in the spongy layers the flux occurs in a radial direction;
9. the trans-membrane pressure (TMP) is assumed to be constant:

$$TMP = \frac{P_0 + P_L}{2} - P_{atm} \qquad [12.37]$$

where P_{atm} is the atmospheric pressure and P_0 and P_L are, respectively, the pressures measured at the fibre inlet and outlet sections. In a laminar flow regime, for 10-cm long fibres with an internal diameter of 5.5×10^{-4} m, the pressure drop can be estimated as 65 Pa (less than 0.05% of P_0) and, therefore, the assumption is absolutely reasonable.

The reaction rate can be expressed, in a general case, by a modified Michaelis–Menten equation which accounts for both substrate and product inhibition effects:

$$R = \frac{R_{max} \cdot S}{K_m \cdot \left(1 + \frac{P}{k_i}\right) + (1 + k_p) \cdot S} \qquad [12.38]$$

where, with respect to a classical Michaelis–Menten equation, both the product and the substrate inhibition, expressed in terms of the kinetic constants k_i and k_p, respectively, are considered.

Starting from these hypotheses, the momentum and the mass transport

© Woodhead Publishing Limited, 2011

equations were obtained and put in a dimensionless form, introducing a proper set of characteristic dimensionless variables.

12.8.1 Momentum analysis

A preliminary fluid dynamic analysis of the system is necessary to determine the concentration profiles developing in the membrane bioreactor. The axial and the radial velocity profiles in the fibre lumen were derived from the analytical solution of momentum and continuity equations formulated by Apelblat *et al*. (1974). In regions 2 and 3 the porous matrix severely hinders fluid transport in the axial direction; therefore, only the radial velocity component was considered. The calculated velocity profiles for each region of a single fibre are (Calabrò *et al*., 2002):

Lumen side

$$v_z(r, z) = \frac{2Q_o}{\pi R_l^2 N_f}\left(1 - \frac{Q_{pb}}{Q_o}\frac{z}{L}\right)\cdot\left(1 - \frac{r^2}{R_l^2}\right) \qquad [12.39]$$

where $v_z(r, z)$ is the velocity profile in the axial direction, r and z are, respectively, the radial and the axial generic coordinates, Q_0 is the total feed flow rate in the axial direction, Q_{pb} is the permeate flow rate, R_1 and L represent, respectively, the lumen radius and its length, and N_f is the number of hollow fibres assembled in the cylindrical cartridge.

The above solution represents a modified form of the Poiseuille equation, where a dependence on the axial coordinate is superimposed on the radial parabolic profile. This dependence is expressed by a term containing the permeation ratio $\frac{Q_{pb}}{Q_0}$, which is constant once the trans-membrane pressure and the axial flow rate have been fixed.

As far as the radial velocity profile, $v_{r1}(r, z)$, is concerned, application of the continuity equation gives:

$$v_{r1}(r, z) = \frac{Q_{pb}}{2\pi R_1 L N_f}\left(2\cdot\frac{r}{R_1} - \frac{r^3}{R_1^3}\right) \qquad [12.40]$$

Dense and spongy layers

The velocity profiles in both the dense and the spongy layer are obtained after utilization of the continuity conditions referred to the different regions of the membrane:

$$v_{r,i}(r) = \frac{1}{\varepsilon_i} L_p \cdot TMP\,\frac{R_1}{r} \quad i = 2,3 \text{ and } R_1 < r < R_3 \qquad [12.41]$$

© Woodhead Publishing Limited, 2011

where the term L_p is the membrane hydraulic permeability and the product between L_p and *TMP* (Equation [12.37]) represents the permeation velocity, v_p, in the radial direction; ε_i is the porosity of each of the two regions.

12.8.2 Mass transfer analysis

The formulation of continuity and mass balance equations allows, for the three regions of the hollow fibre, a system of differential equations to be obtained for both the substrate and the product concentrations.

The mass balance equations, in their dimensionless form, are:

1. Membrane lumen
substrate:

$$\frac{\partial^2 S_1^*}{\partial \rho^2} + \frac{1}{\rho}\frac{\partial S_1^*}{\partial \rho} - Pe_{\text{rad}} v_{r1}^* \frac{\partial S_1^*}{\partial \rho} - Pe_{\text{ax}} \left(\frac{R_1^2}{L^2}\right) v_z^* \frac{\partial S_1^*}{\partial \zeta} = 0 \qquad [12.42]$$

product:

$$\frac{\partial^2 P_1^*}{\partial \rho^2} + \frac{1}{\rho}\frac{\partial P_1^*}{\partial \rho} - Pe_{\text{rad}} \left(\frac{D_{\text{AB}}}{D_{\text{PB}}}\right) v_{r1}^* \frac{\partial P_1^*}{\partial \rho} - Pe_{\text{ax}} \left(\frac{R_1^2}{L^2}\right) \left(\frac{D_{\text{AB}}}{D_{\text{PB}}}\right) v_z^* \frac{\partial P_1^*}{\partial \zeta} = 0 \qquad [12.43]$$

2. Dense layer
substrate:

$$\frac{\partial^2 S_2^*}{\partial \rho^2} + \frac{1}{\rho}\cdot\frac{\partial S_2^*}{\partial \rho} - v_{r2}^* \cdot Pe_{\text{rad}} \cdot \frac{\partial S_2^*}{\partial \rho} - \frac{\lambda^2 \cdot (E_2/E_0) \cdot S_{2\text{E}}^*}{\theta + \frac{K_{\text{m}}}{k_{\text{i}}} P_{2\text{E}}^* + (1 + k_{\text{p}})\, S_{2\text{E}}^*} = 0 \qquad [12.44]$$

product:

$$\frac{\partial^2 P_2^*}{\partial \rho^2} + \frac{1}{\rho}\cdot\frac{\partial P_2^*}{\partial \rho} - v_{\text{r}_2}^* \cdot Pe_{\text{rad}} \left(\frac{D_{\text{AB}}}{D_{\text{PB}}}\right) \frac{\partial P_2^*}{\partial \rho} + \frac{\lambda^2 \cdot (D_{\text{AB}}/D_{\text{PB}})(E_2/E_0) \cdot S_{2\text{E}}^*}{\theta + \frac{K_{\text{m}}}{k_{\text{i}}} P_{2\text{E}}^* + (1 + k_{\text{p}})\, S_{2\text{E}}^*} = 0 \qquad [12.45]$$

3. Spongy layer
substrate:

$$\frac{\partial^2 S_3^*}{\partial \rho^2} + \frac{1}{\rho}\cdot\frac{\partial S_3^*}{\partial \rho} - v_{r3}^* \cdot Pe_{\text{rad}} \cdot \frac{\partial S_3^*}{\partial \rho} - \frac{\lambda^2 (E_3/E_0) \cdot S_{3\text{E}}^*}{\theta + \frac{K_{\text{m}}}{k_{\text{i}}} P_{3\text{E}}^* + (1 + k_{\text{p}})\, S_{3\text{E}}^*} = 0 \qquad [12.46]$$

© Woodhead Publishing Limited, 2011

product:

$$\frac{\partial^2 P_3^*}{\partial \rho^2} + \frac{1}{\rho}\cdot\frac{\partial P_3^*}{\partial \rho} - v_{r3}^*\cdot Pe_{\text{rad}}\left(\frac{D_{\text{AB}}}{D_{\text{PB}}}\right)\cdot\frac{\partial P_3^*}{\partial \rho} + \frac{\lambda^2\cdot(D_{\text{AB}}/D_{\text{PB}})(E_3/E_0)\cdot S_{3\text{E}}^*}{\theta + \frac{K_{\text{m}}}{k_{\text{i}}}P_{3\text{E}}^* + (1+k_{\text{p}})\,S_{3\text{E}}^*} = 0 \quad [12.47]$$

where S_i^* and P_i^* are, respectively, the dimensionless concentration for both substrate and product in each of the three fibre regions (i = 1, 2, 3); $\rho = \frac{r}{R_1}$ is the dimensionless radial coordinate and $\zeta = \frac{z}{L}$ is the dimensionless axial coordinate. The mass transfer equations have been obtained, by introducing an appropriate set of dimensionless parameters, such as the axial Peclet number, $Pe_{\text{ax}} = \frac{v_0 L}{D_{\text{AB}}}$, the radial Peclet number, $Pe_{\text{rad}} = \frac{v_{\text{p}} R_1}{D_{\text{AB}}}$, the square Thiele modulus, $\lambda^2 = \frac{k_2 E_0 R_1^2}{C_0 D_{\text{AB}}}$, the dimensionless Michaelis constant (saturation factor), $\theta = \frac{K_{\text{m}}}{S_0}$, and the ratios E_2/E_0 and E_3/E_0, which, respectively, represent the amount of biocatalyst immobilized in the membrane dense layer (skin) and in the porous layer (sponge), compared to the total amount of immobilized enzyme. In the above equations the terms $S_{2\text{E}}^*$, $S_{3\text{E}}^*$, $P_{2\text{E}}^*$, and $P_{3\text{E}}^*$, are the dimensionless forms of substrate and product concentrations at the enzyme–substrate interface and at the enzyme–product interface in the dense and in the spongy layers, respectively. These substrate and product interface concentrations, S_{iE}^* and P_{iE}^* (i = 2, 3), are generally different from the corresponding bulk concentration values, S_{i}^* and P_i^* (i = 2, 3), owing to mass transfer resistances occurring outside the immobilized biocatalyst molecules.

The system of partial differential Equations [12.42] – [12.47] is completed by a proper set of boundary conditions:

$$\text{B.C.1} \quad \zeta = 0 \quad \forall\rho \quad S_1^* = 1 \quad [12.48a]$$

$$\text{B.C.1}' \quad \zeta = 0 \quad \forall\rho \quad P_1^* = 1 \quad [12.48b]$$

$$\text{B.C.2} \quad \rho = 0 \quad \forall\zeta \quad \frac{\partial S_1^*}{\partial \rho} = 0 \quad [12.48c]$$

$$\text{B.C.2}' \quad \rho = 0 \quad \forall\zeta \quad \frac{\partial P_1^*}{\partial \rho} = 0 \quad [12.48d]$$

$$\text{B.C.3} \quad \rho = 1 \quad \forall\zeta \quad S_1^* = S_2^* \quad [12.48e]$$

© Woodhead Publishing Limited, 2011

$$\text{B.C.3}'\quad \rho = 1 \quad \forall\zeta \quad P_1^* = P_2^* \qquad [12.48f]$$

$$\text{B.C.4}\quad \rho = 1\ \forall\zeta \quad -\frac{\partial S_1^*}{\partial\rho} + Pe_{\text{rad}}\cdot S_1^* = -\varepsilon_2\cdot\frac{\partial S_2^*}{\partial\rho} + Pe_{\text{rad}}\cdot S_2^* \qquad [12.48g]$$

$$\text{B.C.4}'\quad \rho = 1\ \forall\zeta \quad -\frac{\partial P_1^*}{\partial\rho} + Pe_{\text{rad}}\left(\frac{D_{\text{AB}}}{D_{\text{PB}}}\right)P_1^* = -\varepsilon_2\cdot\frac{\partial P_2^*}{\partial\rho} + Pe_{\text{rad}}\left(\frac{D_{\text{AB}}}{D_{\text{PB}}}\right)P_2^* \qquad [12.48h]$$

$$\text{B.C.5}\quad \rho = \frac{R_2}{R_1} \quad \forall\zeta \quad S_2^* = S_3^* \qquad [12.48i]$$

$$\text{B.C.5}'\quad \rho = \frac{R_2}{R_1} \quad \forall\zeta \quad P_2^* = P_3^* \qquad [12.48j]$$

$$\text{B.C.6}\quad \rho = \frac{R_2}{R_1} \quad \forall\zeta \quad -\varepsilon_2\frac{\partial S_2^*}{\partial\rho} + \frac{R_1}{R_2}Pe_{\text{rad}}S_2^* = -\varepsilon_3\frac{\partial S_3^*}{\partial\rho} + \frac{R_1}{R_2}Pe_{\text{rad}}S_3^* \qquad [12.48k]$$

$$\text{B.C.6}'\quad \rho = \frac{R_2}{R_1} \quad \forall\zeta \quad -\varepsilon_2\frac{\partial P_2^*}{\partial\rho} + \frac{R_1}{R_2}Pe_{\text{rad}}\left(\frac{D_{\text{AB}}}{D_{\text{PB}}}\right)P_2^* = -\varepsilon_3\frac{\partial P_3^*}{\partial\rho} + \frac{R_1}{R_2}Pe_{\text{rad}}\left(\frac{D_{\text{AB}}}{D_{\text{PB}}}\right)P_3^* \qquad [12.48l]$$

$$\text{B.C.7}\quad \rho = \frac{R_3}{R_1} \quad \forall\zeta \quad \frac{\partial S_3^*}{\partial\rho} = 0 \qquad [12.48m]$$

$$\text{B.C.7}'\quad \rho = \frac{R_3}{R_1} \quad \forall\zeta \quad \frac{\partial P_3^*}{\partial\rho} = 0 \qquad [12.48n]$$

The BCs from Equation [12.48e] to [12.48l] express the continuity of substrate and product concentrations and of the molar fluxes at the interfaces between the three regions defining the hollow fibre. Equations [12.48m] and [12.48n] are two Danckwerts-type conditions, which express the vanishing substrate and product concentrations gradients at the interface between the spongy layer and the bioreactor shell side.

The interfacial concentrations, $S_{i\text{E}}^*$ and $P_{i\text{E}}^*$ (i = 2, 3), are evaluated by means of a mass balance at the enzyme catalytic site supposing that the mass transfer resistances are localized in a liquid film close to the biocatalyst particle. In steady state conditions it can be stated that:

© Woodhead Publishing Limited, 2011

Amount of substrate reaching the biocatalyst surface

= Amount of substrate reacted owing to the chemical reaction

that is, for both the membrane regions:

$$k_s A_{m,i}(S_i - S_{iE}) = \frac{k_2 \cdot E_0 \cdot (E_i/E_0) \cdot S_{iE}}{K_m\left(1 + \frac{P_{iE}}{k_i}\right) + (1 + k_p)\, S_{iE}}\, \varepsilon_i\ V_{m,i} \qquad [12.49]$$

where, k_s is the mass transport coefficient evaluated in the liquid film, $V_{m,i}$ is total available volume of each of two membrane regions and $A_{m,i}$ is the surface actually in contact (wetted) with the liquid containing the substrate. Defining a mean specific surface for both the dense and the spongy layers (a_i), as the ratio between the total surface of membrane region where the reaction takes place and the total volume of the considered region:

$$a_i = \frac{\text{total wetted surface}}{\text{total volume}} = \frac{A_{m,i}}{V_{m,i}} \qquad [12.50]$$

After some manipulation, the dimensionless form of Equation [12.49] is obtained for both the skin and the dense layers (i = 2, 3):

$$Sh \cdot a_i^* \cdot (S_i^* - S_{iE}^*) = \frac{\lambda^2 (E_i/E_0) \cdot S_{iE}^*}{\theta + \frac{K_m}{k_i} \cdot P_{iE}^* + (1 + k_p) \cdot S_{iE}^*} \qquad [12.51]$$

where $Sh = \frac{k_s R_1}{D_{AB}}$ is the Sherwood number and $a_i^* = (a_i/\varepsilon_i)\, R_1$ is the dimensionless specific surface of each membrane region. A good estimate of the Sherwood number and of the dimensionless mean specific surface area (a_2^*, a_3^*) either for the dense and the spongy layer is needed to evaluate correctly the terms S_{2E}^*, S_{3E}^*, P_{2E}^*, and P_{3E}^*, used in mass balance equations. A semi-empirical correlation (Bird *et al.*, 1960), obtained for porous media is used to estimate the Sherwood number by means of the Colburn factor:

$$j_D = \frac{Sh}{Re \cdot Sc^{1/3}} = 0.91 \cdot \psi \cdot Re^{-0.51} \qquad [12.52]$$

where Sc is the Schimdt number and ψ is a shape factor characteristic of the porous medium equal to 0.86 for irregular shapes like membranes.

In the Equation [12.52], the Reynolds number, Re, is defined through a characteristic length that is the reciprocal of the mean specific surface area a_i, and not the usual fibre pore diameter:

$$Re_i = \frac{v_p}{a_i \cdot \upsilon \cdot \psi} \qquad [12.53]$$

© Woodhead Publishing Limited, 2011

12.8.3 Relevant parameters for bioreactor performances analysis

On the basis of theoretical results, expressed in terms of substrate and product dimensionless concentration profiles, two characteristic parameters have been defined to describe the overall bioreactor performances as functions of the operating conditions: the performance index (PI) and the effectiveness factor (η).

The performance index is defined as the ratio of the amount of substrate reacted in the membrane and that of the substrate fed to the fibres (Equation [12.54]) and represents a measure of the relative significance of mass transfer mechanisms and of chemical reaction. An effectiveness factor has also been introduced to evaluate how the diffusion resistance in the liquid film close to the biocatalyst surface affects the overall conversion process. It is calculated as the ratio between the actual reaction rate and the reaction rate that would have been observed in absence of mass transfer limitations (Equation [12.55]).

$$PI = \frac{\text{substrate reacted in membrane}}{\text{substrate fed to the fibres}} = \frac{2\cdot\lambda^2}{Pe_{ax}(R_1/L)^2}\left(\begin{array}{l}\dfrac{E_2}{E_0}\,\varepsilon_2\int_0^1\int_1^{\frac{R_2}{R_1}}\dfrac{S^*_{2E}}{\theta+(1+k_p)S^*_{2E}+\dfrac{K_m}{k_i}P^*_{2E}}\rho d\rho d\xi \\ +\dfrac{E_3}{E_0}\,\varepsilon_3\int_0^1\int_{\frac{R_2}{R_1}}^{\frac{R_3}{R_1}}\dfrac{S^*_{3E}}{\theta+(1+k_p)S^*_{3E}+\dfrac{K_m}{k_i}P^*_{3E}}\rho d\rho d\xi\end{array}\right) \quad [12.54]$$

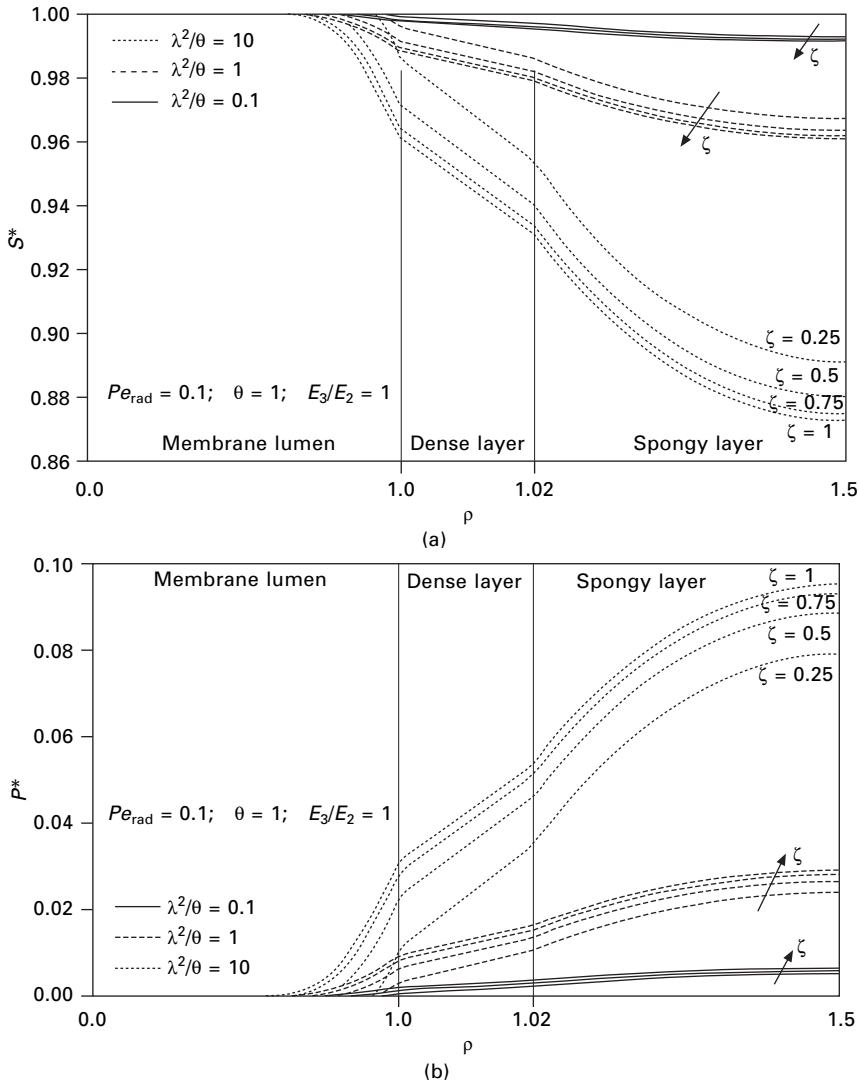
$$\eta = \frac{\text{actual reaction rate}}{\text{reaction rate in absence of mass transfer limitations}} = \frac{2(\vartheta+1)R_1^2}{\varepsilon_2(R_2^2-R_1^2)+\varepsilon_3(R_3^2-R_2^2)} + \left(\begin{array}{l}\dfrac{E_2}{E_0}\,\varepsilon_2\int_0^1\int_1^{\frac{R_2}{R_1}}\dfrac{S^*_{2E}}{\theta+(1+k_p)S^*_{2E}+\dfrac{K_m}{k_i}P^*_{2E}}\rho d\rho d\xi \\ +\dfrac{E_3}{E_0}\,\varepsilon_3\int_0^1\int_{\frac{R_2}{R_1}}^{\frac{R_3}{R_1}}\dfrac{S^*_{3E}}{\theta+(1+k_p)S^*_{3E}+\dfrac{K_m}{k_i}P^*_{3E}}\rho d\rho d\xi\end{array}\right) \quad [12.55]$$

Some of the results that can be obtained by the proposed theoretical model are presented in the following. First, the dimensionless substrate and

© Woodhead Publishing Limited, 2011

product concentration profiles in the radial direction are shown at various values of the squared Thiele modulus (λ^2). Then, attention is focused on the influence of some of the most significant dimensionless parameters, related to the system operating conditions, on the performance index, in order to predict the conditions that may optimize the bioreactor performance.

Figure 12.10(a) and 12.10(b) show the effect of the λ^2/θ ratio, which, for fixed values of all the other physical and operating parameters and of the



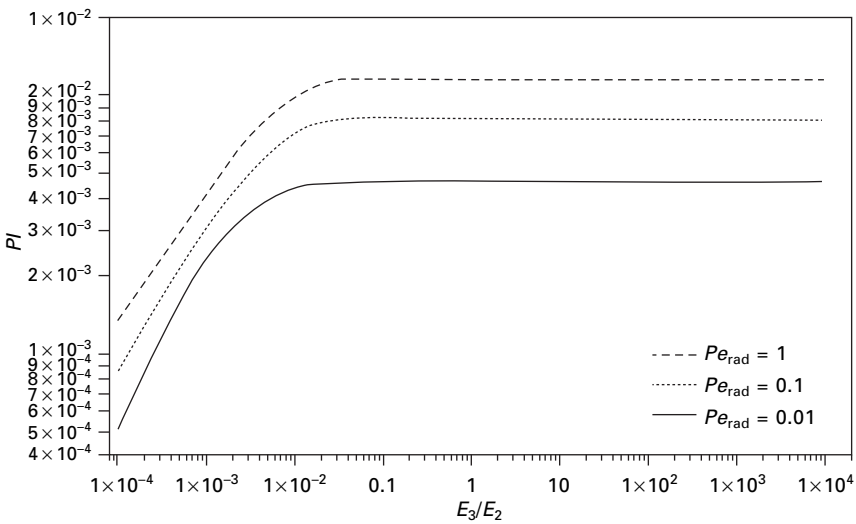
12.10 (a) Dimensionless substrate concentration profiles in the membrane at different values of Thiele modulus. (b) Dimensionless product concentration profiles in the membrane at different values of Thiele modulus.

© Woodhead Publishing Limited, 2011

feed substrate concentration, expresses a direct measure of the total amount of entrapped enzyme, on substrate and product dimensionless concentrations occurring in the radial direction at different axial positions. An increase in substrate consumption and a greater amount of product formed are in agreement with a higher λ^2/θ ratio.

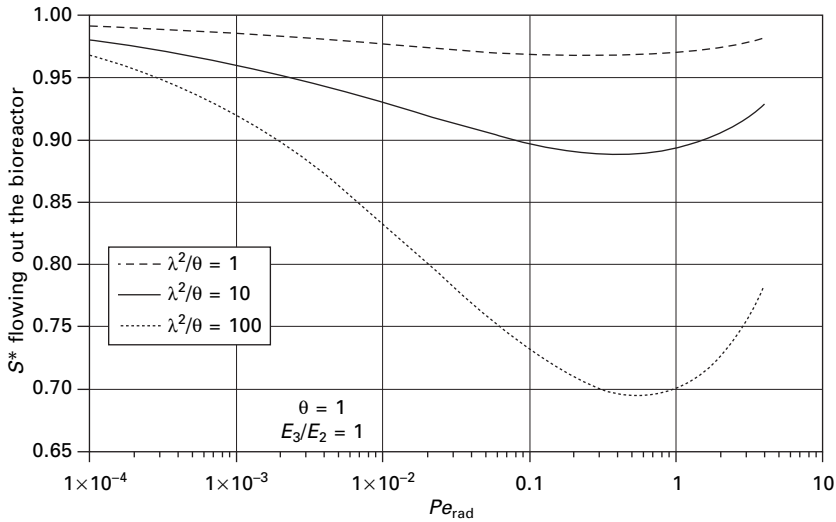
Figure 12.11 shows that it is possible to choose a set of operating conditions in order to obtain a significant yield of desired product and then high values of the performance index. This figure clearly explains that performance index is practically the same for E_3/E_2 ranging from 0.05 to 10^4. Therefore, having reached a definite value of enzyme distribution function, the bioreactor behaviour is no longer affected by E_3/E_2. This result is of particular importance in bioreactor optimization since it can be affirmed that it would be more advantageous to immobilize all the biocatalyst in the spongy layer of the membrane because the bioreactor productivity, for all the tested values of Pe_{rad}, reaches a maximum either when the enzyme is equally distributed in the membrane regions or when it is mostly entrapped in the fibre spongy layer. The latter conclusion is noteworthy for the design of membrane bioreactors because it suggests that the enzyme immobilization should only be performed in the spongy layer; this immobilization, by the way, is simpler from a technological point of view and much cheaper than other immobilization techniques.

Finally, Fig. 12.12 represents another remarkable example that testifies how the proposed approach can be successfully utilized as a powerful tool



12.11 Performance index vs enzyme distribution function at different values of Pe_{rad}.

© Woodhead Publishing Limited, 2011



12.12 Dimensionless outlet substrate concentration vs Pe_{rad} number at different values of squared Thiele modulus.

for bioreactor optimization. In fact, it is shown that a minimum value of outlet substrate concentration (optimal value) can be identified as a function of the radial Peclet number. This result suggests that it is necessary to choose a precise value of the operating *TMP* which, at the same time, has to allow lowering of the outside diffusive resistances, but permitting sufficient contact time between the substrate and the immobilized enzyme so as to increase the substrate conversion. This optimal value belongs to the range of Pe_{rad} between 0.1 and 1. It is worthwhile observing that the lowest value of substrate concentration (corresponding to the highest substrate conversion) is attained for Pe_{rad} equal to 0.18 when $\lambda^2/\theta = 0.1$ (not shown in figure), for $Pe_{rad} = 0.31$ when $\lambda^2/\theta = 1$, for $Pe_{rad} = 0.40$ when $\lambda^2/\theta = 10$ and, finally, for $Pe_{rad} = 0.57$ when $\lambda^2/\theta = 100$. This shift towards higher and higher values of radial Peclet number is ascribed to the higher resistances that the system has to overcome in order to reach the biocatalyst molecules. Indeed, an increase of the radial Peclet number has, in general, a beneficial effect on the reduction of the external mass transfer resistances, but determines, for Pe_{rad} higher than 1, a too fast passage of substrate within the membrane regions where the enzyme has been actually immobilized and, therefore, an unacceptable substrate conversion.

The above model provides very useful indications about bioreactor performance. In the following section a further improvement will be presented and briefly discussed.

© Woodhead Publishing Limited, 2011

12.9 Hollow fibre membrane bioreactor with recycling of unreacted substrate

This type of bioreactor consists of a feed tank and a hollow fibre bioreactor assembled in a cylindrical cartridge according to a tube and shell configuration (Fig. 12.13). Substrate is forced by ultrafiltration to permeate through the membrane wall where it comes into contact with the immobilized enzyme and reacts. Products and unconverted substrate are continuously removed in a radial direction from the permeate stream; the retentate stream, still containing substrate and a certain amount of products, is instead recycled back to the feed tank (Curcio *et al.*, 2006).

The formulation of a theoretical model describing the behaviour of the present bioreactor is based on the general equation of motion (in unsteady-state conditions) and on the continuity equation written to describe the flow field in the lumen; these equations are coupled to the Brinkman (in unsteady-state conditions) and continuity equations written for both the dense and the spongy layer of the fibre.

12.9.1 Lumen side

$$\gamma\left[\frac{\partial \mathbf{u}_1}{\partial t} + (\mathbf{u}_1 \cdot \nabla)\,\mathbf{u}_1\right] = -\,\boldsymbol{\nabla} p_i + \boldsymbol{\nabla} \cdot \mu\,\{\boldsymbol{\nabla}\mathbf{u}_i + (\boldsymbol{\nabla}\mathbf{u}_i)^T\} \qquad [12.56]$$

$$\boldsymbol{\nabla} \cdot \mathbf{u}_i = \mathbf{0} \qquad [12.57]$$

where γ denotes the solution density, μ is its viscosity, $\mathbf{u}_1$ is the velocity vector and p_1 the pressure.

12.9.2 Dense and spongy layers

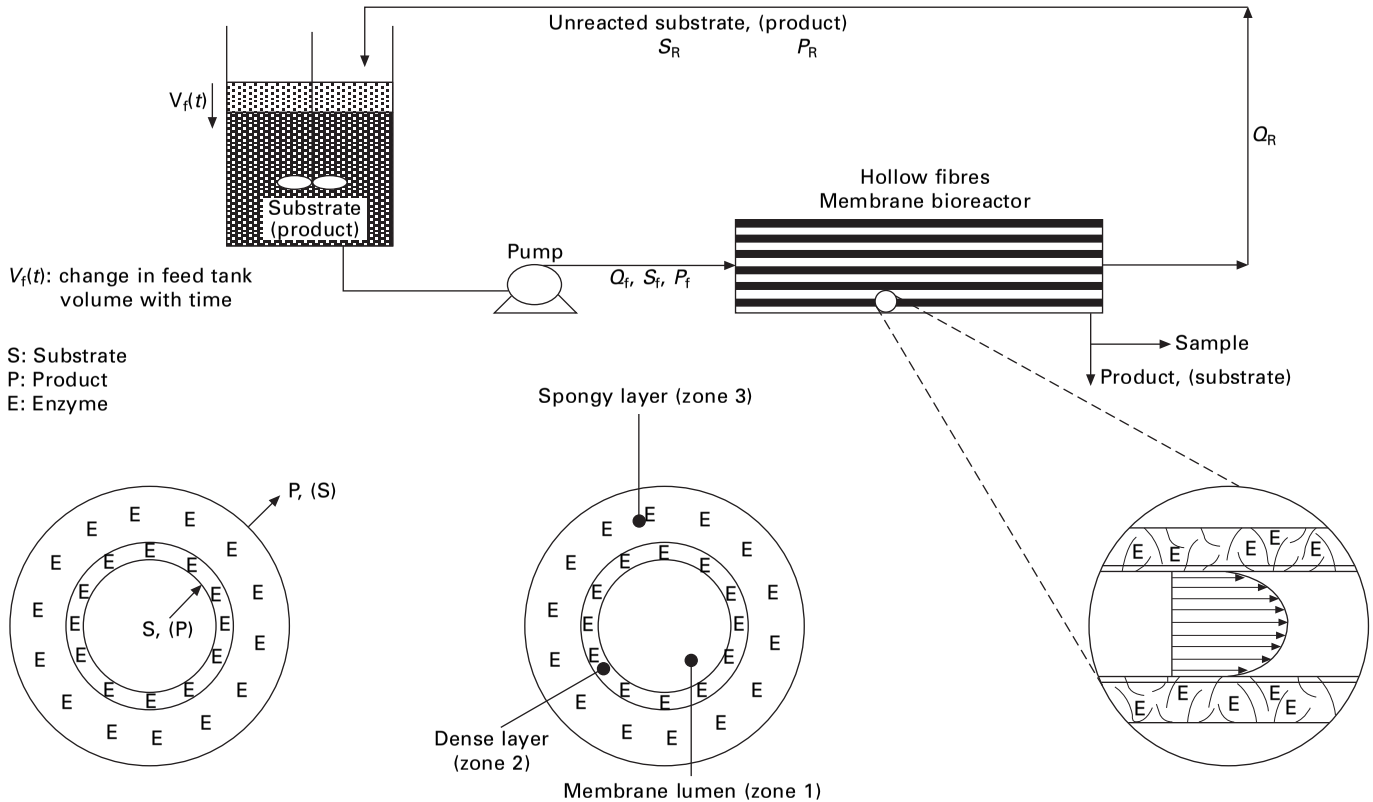
$$\gamma\,\frac{\partial \mathbf{u}_i}{\partial t} + \frac{\mu}{h_i}\,\mathbf{u}_i = -\,\boldsymbol{\nabla} p_i + \boldsymbol{\nabla} \cdot \mu\,\{\boldsymbol{\nabla}\mathbf{u}_i + (\boldsymbol{\nabla}\mathbf{u}_i)^T\} \qquad [12.58]$$

$$\boldsymbol{\nabla} \cdot \mathbf{u}_i = \mathbf{0} \qquad [12.59]$$

where the subscript $i = 2,3$ refers to dense and spongy layers respectively, $\mathbf{u}_i$ is the superficial velocity vector which, according to Bird *et al.* (1960), accounts for the porosity ε_i of the two regions, p_i is the pressure and h_i denotes the permeability of the porous media (i.e. the dense and the spongy layers of the membrane).

The mass transfer analysis actually accounts for the behaviour of both the feed tank and the hollow fibre membrane bioreactor. As far as feed tank is concerned, the overall mass balance together with the substrate, S_f, and the product, P_f, mass balances are needed to express the time evolution of

© Woodhead Publishing Limited, 2011



12.13 Schematic of a hollow fibre membrane bioreactor in recycling configuration.

© Woodhead Publishing Limited, 2011

mixture volume in the feed tank and the composition of the stream fed to the hollow fibres. The corresponding system of ordinary differential equations and their initial conditions are:

Total mass balance

$$dV_f/dt = Q_R - Q_f$$

Initial condition

$$\text{(IC): } V_f\,(t = 0) = V_0 \qquad [12.60]$$

Mass balance on the substrate

$$d(V_f\,S_f)/dt = Q_R\,S_R - Q_f\,S_f$$

$$\text{IC: } S_f\,(t = 0) = S_0 \qquad [12.61]$$

Mass balance on the product

$$d(V_f\,P_f)/dt = Q_R\,P_R - Q_f\,P_f$$

$$\text{IC: } P_f\,(t = 0) = 0 \qquad [12.62]$$

where, V_f is the volume of the mixture contained in the feed tank, Q_R is the volumetric flow rate leaving the bioreactor in the axial direction and recycled back to the tank, Q_f is the volumetric flow rate actually fed to the bioreactor, and S_R and P_R are the average substrate and product concentrations flowing from the bioreactor and recycled to the feed tank. It is worthwhile observing that the flowing stream may contain an amount of product formed on the inner surface of the fibre where a certain amount of enzyme adheres. Finally, V_0 and S_0 represent, respectively, the initial volume and substrate concentration chosen to perform each numerical simulation.

As far as the three different regions of hollow fibre are concerned, the mass transfer is based on the classical time-dependent convection–diffusion–reaction balance equation that is written for both the substrate, S and the product, P:

substrate:

$$\frac{\partial S_i}{\partial t} + \nabla\cdot\,(-D_{ABeff,i}\nabla S_i) = -R_i - \mathbf{u}_i\cdot\nabla S_i \qquad [12.63]$$

product:

$$\frac{\partial P_i}{\partial t} + \nabla\cdot\,(-D_{PBeff,i}\nabla P_i) = R_i - \mathbf{u}_i\cdot\nabla P_i \qquad [12.64]$$

where, the subscript i (i =1, 2, 3) indicates the actual fibre region where each mass balance equation is referred, R_i (i = 2, 3 since no reaction takes

© Woodhead Publishing Limited, 2011

place in the lumen) is the reaction rate $\left(R_i = \frac{R_{\max} \cdot S_{Ei}}{K_m \cdot \left(1 + \frac{P_{Ei}}{k_i}\right) + (1 + k_p) \cdot S_{Ei}} \right)$ written for the dense and the spongy layers only and accounting for the actual interfacial concentrations (S_{Ei} and P_{Ei}), and $D_{AB,eff}$ and $D_{PB,eff}$ are, instead, the effective diffusion coefficient of both substrate and product in water, calculated accounting for the void fractions, ε_i, of each region (for luminal side $\varepsilon = 1$). The general Equations [12.56]–[12.59] and [12.63]–[12.64] and the corresponding boundary conditions (not reported for sake of brevity) have been adapted to the fibre geometry referring to a system of cylindrical coordinates and, thus, properly defining the components of both the vector differential operator, $\boldsymbol{\nabla}$, and the velocity vector, $\mathbf{u}_i$. They have then been put in their dimensionless form introducing exactly the same set of dimensionless variables defined in the previous section.

The dimensionless modelling equations so obtained, together with the corresponding dimensionless boundary conditions, constitute a system of non-linear partial differential equations which can be solved only by a numerical procedure. In this case, the finite elements method (FEM), implemented by a commercial CFD code, was used. Each hollow fibre has been discretized into 19523 finite elements with a thicker mesh in the dense layer. On a 1.4 GHz Intel personal computer running under Windows XP, the bioreactor behaviour over a time horizon of 6 hours was simulated, on average, in about 1 hour. It is worthwhile remarking that the proposed model does not need any adjustment of parameters, but only the specification of a set of input variables that can be varied within a specific range of physical significance to simulate the bioreactor performance under different operating conditions. The proposed transport model, moreover, is very general as it may describe the behaviour of different types of heterogeneous reacting systems by just accounting for the correct reaction rate expression and utilizing a set of kinetic constants typical of the reactions involved in biofuels production.

The results of the theoretical model suggest the definition, in analogy with the case presented in the previous section, of some characteristic indexes describing the instantaneous bioreactor performance as functions of the operating conditions. In particular, the effectiveness factor, $\eta(t)$, is defined as the ratio between the actual reaction rate integrated within the membrane fibre at any time t and the reaction rate that would have been observed if all the immobilized biocatalyst were uniformly exposed to the instantaneous feed substrate/product concentration $S_f(t)$, $P_f(t)$.

© Woodhead Publishing Limited, 2011

$$\eta(t) = \frac{2\left(\vartheta + \frac{K_m}{k_i}\frac{P_f}{S_0} + \frac{S_f}{S_0}\right)\left(\begin{array}{l}\frac{E_2}{E_0}\varepsilon_2\int_0^1\int_1^{\frac{R_2}{R_1}}\frac{S^*_{E2}}{\theta + S^*_{E2} + \frac{K_m}{k_i}P^*_{E2}}\rho d\rho d\zeta \\ + \frac{E_3}{E_0}\varepsilon_3\int_0^1\int_{\frac{R_2}{R_1}}^{\frac{R_3}{R_1}}\frac{S^*_{E3}}{\theta + S^*_{E3} + \frac{K_m}{k_i}P^*_{E3}}\rho d\rho d\zeta\end{array}\right)}{\frac{S_f}{S_0}\left[\varepsilon_2\frac{E_2}{E_0}\left(\frac{R_2^2}{R_1^2} - 1\right) + \varepsilon_3\frac{E_3}{E_0}\left(\frac{R_3^2}{R_1^2} - \frac{R_2^2}{R_1^2}\right)\right]} \quad [12.65]$$

The degree of conversion in the membrane, $\alpha(t)$, gives instead an indication of enzyme activity compared to the mass transfer mechanisms affecting the transport phenomena in those regions where enzyme is actually immobilized. It is defined as the ratio between the actual reaction rate integrated within the membrane fibre at any time t and the overall (convective and diffusive) substrate instantaneous molar flow at the inner fibre surface:

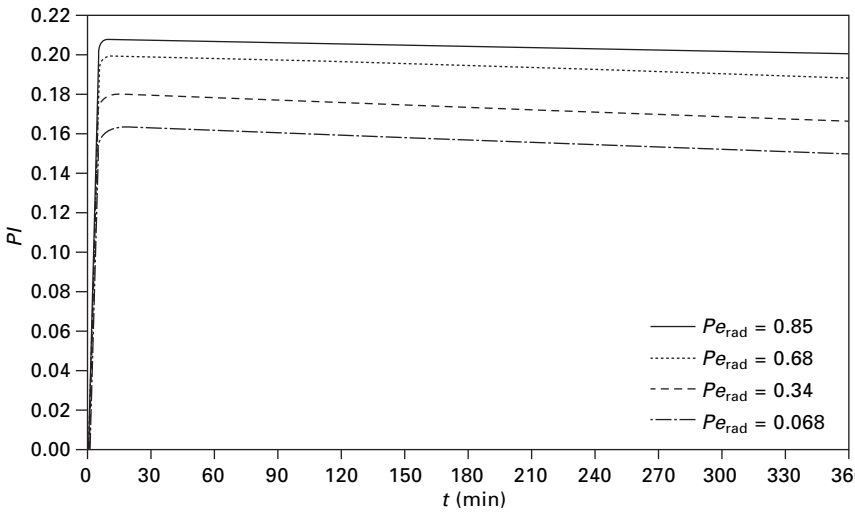
$$\alpha(t) = \frac{\lambda^2\left(\begin{array}{l}\frac{E_2}{E_0}\varepsilon_2\int_0^1\int_1^{\frac{R_2}{R_1}}\frac{S^*_{E2}}{\theta + S^*_{E2} + \frac{K_m}{k_i}P^*_{E2}}\rho d\rho d\zeta \\ + \frac{E_3}{E_0}\varepsilon_3\int_0^1\int_{\frac{R_2}{R_1}}^{\frac{R_3}{R_1}}\frac{S^*_{E3}}{\theta + S^*_{E3} + \frac{K_m}{k_i}P^*_{E3}}\rho d\rho d\zeta\end{array}\right)}{Pe_{rad}\int_0^1\left[\left(S_1^*\frac{u_{r1}}{v_p}\right)_{|\rho=1} - \frac{1}{Pe_{rad}}\frac{\partial S_1^*}{\partial\rho_{|\rho=1}}\right]d\zeta} \times 100 \quad [12.66]$$

The performance index, $PI(t)$, is finally defined as the ratio between the actual reaction rate integrated within the membrane fibre at any time t and the instantaneous substrate flow rate fed to the fibres; like the degree of conversion, it also represents a measure of the relative significance of mass transfer mechanisms and chemical reaction, referred, however, to the whole bioreactor:

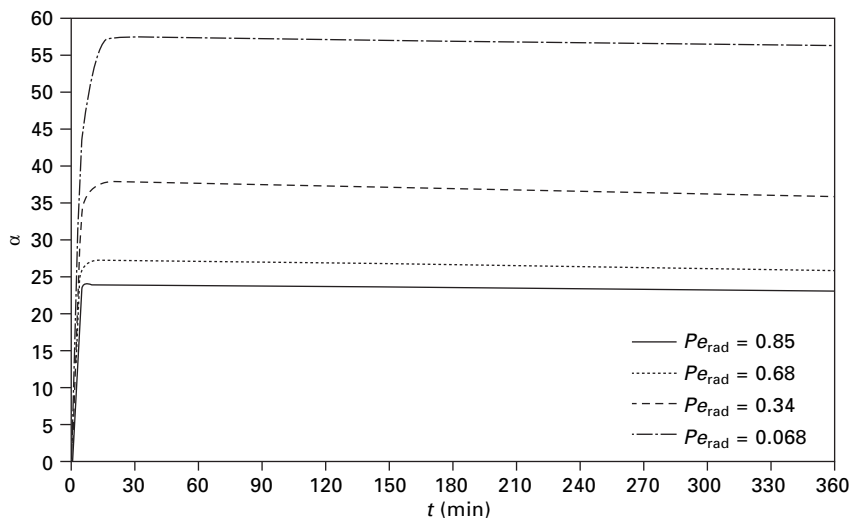
$$PI(t) = \frac{2\cdot\lambda^2\left(\begin{array}{l}\frac{E_2}{E_0}\varepsilon_2\int_0^1\int_1^{\frac{R_2}{R_1}}\frac{S^*_{E2}}{\theta + S^*_{E2} + \frac{K_m}{k_i}P^*_{E2}}\rho d\rho d\zeta \\ + \frac{E_3}{E_0}\varepsilon_3\int_0^1\int_{\frac{R_2}{R_1}}^{\frac{R_3}{R_1}}\frac{S^*_{E3}}{\theta + S^*_{E3} + \frac{K_m}{k_i}P^*_{E3}}\rho d\rho d\zeta\end{array}\right)}{Pe_{ax}(R_1/L)^2(S_f/S_0)} \quad [12.67]$$

© Woodhead Publishing Limited, 2011

Among the possible results that the proposed model allows, those shown in Fig. 12.14 and 12.15 are particularly interesting since they might configure a classical optimization problem. In fact, a trade-off exists between the high conversions (typical of low Pe_{rad} values) and the increase of both bioreactor productivity and external mass transfer coefficient (typical of high Pe_{rad} values).



12.14 Effect of the radial Peclet number on the dynamic evolution of bioreactor performance index (Pe_{ax} = 10^5; θ = 1; λ^2 = 10; E_3/E_2 = 1).



12.15 Effect of the radial Peclet number on the degree of conversion in the membrane (Pe_{ax} = 10^5; θ = 1; λ^2 = 10; E_3/E_2 = 1).

© Woodhead Publishing Limited, 2011

As a matter of fact, the optimization of membrane bioreactor operation with respect to radial Peclet number often depends on the specificity of downstream processes. For instance, a difficult product separation might suggest high conversion in the membrane and, therefore, low values of Pe_{rad}, whereas an easier product separation might suggest high values of Pe_{rad} to increase bioreactor productivity.

12.10 Conclusions

The present contribution was intended to evidence the importance of engineering in the development of novel technologies and in the characterization of innovative systems aimed at biofuels production. In particular, it was shown that membrane science may offer a great contribution to the progress of biotechnology and, more specifically, to an improvement in enzyme membrane bioreactors engineering that pursues the objective of realizing and operating efficient reacting systems in which to perform the biocatalytic conversion of one or more substrate(s) into the desired product(s). It was shown how the definition of characteristic indexes, for example the degree of conversion, the effectiveness factor, the bioreactor productivity and the performance index, provided useful indications about the actual behaviour of membrane bioreactors and could be exploited so as to identify the set of operating conditions that allow the yields of each biocatalytic reaction to increase. As a matter of fact, it was proved that when the process is reaction rate controlled, the effectiveness factor approaches unitary values, whereas when the process is controlled by external mass transfer, the effectiveness factor sharply decreases to very low values. Moreover, in the case of hollow fibres membrane bioreactors that offer more interesting perspectives for possible utilization on a pilot/industrial scale, it was demonstrated that:

- The system productivity is strongly affected by the radial Peclet number, Pe_{rad}, the squared Thiele modulus, λ^2, and the enzyme distribution ratio, E_3/E_2.
- An increase in squared Thiele modulus determines a continuous improvement in substrate conversion, against a significant decrease in biocatalyst efficiency.
- An optimal value of radial Peclet number can be identified. It represents a trade-off between overcoming of diffusive resistances in the liquid film outside the biocatalyst particle, typical of high Pe_{rad} values, and sufficient contact time between the substrate and the enzyme, typical of low Pe_{rad}.
- It is better to immobilize the enzyme predominantly in the membrane spongy layer; this procedure is easier from a technological point of view and cheaper from an economic one.

© Woodhead Publishing Limited, 2011

12.11 Sources of further information and advice

USDA Economic Research Service at http://www.ers.usda.gov/features/bioenergy/

Biomass & Bioenergy at www.elsevier.com/locate/biombioe

Biofuels from Biomass: Technology and Policy Considerations (overview from MIT): http://web.mit.edu/professional/short-programs/courses/biofuels_biomass.html

Caye Drapcho, Nhuan Phú Nghiêm and Terry Walker (August 2008). *Biofuels Engineering Process Technology*, McGraw-Hill Education.

IChemE Energy Conversion Technology Subject Group (May 2009). *A Biofuels Compendium*, IChemE, UK.

Towards sustainable production and use of resources: assessing biofuels: http://www.unep.fr/scp/rpanel/pdf/Assessing_Biofuels_Full_Report.pdf

12.12 References

Andric, P., Meyer, A. S., Jensen, P. A. and Dam-Johansen, K. (2010), 'Reactor design for minimizing product inhibition during enzymatic lignocelluloses hydrolysis: I. Significance and mechanism of cellobiose and glucose inhibition on cellulolytic enzymes', *Biotechnology Advances*, **28**, 308–24.

Apelblat, A., Katzir-Katchalsky, A. and Silberberg, A. (1974), 'A mathematical analysis of capillary tissue fluid exchange', *Biorheology*, **11**, 1–49.

Bai, F. W., Anderson, W. A. and Moo-Young M. (2008), 'Ethanol fermentation technologies from sugar and starch feedstocks', *Biotechnology Advances*, **26**, 89–105.

Bailey, J. E. and Ollis, D. F. (1986), *Biochemical Engineering Fundamentals*, McGraw Hill Book Company, Singapore, MA.

Barnwal, B. K. and Sharma, M. P. (2005), 'Prospects of biodiesel production from vegetable oils in India', *Renewal Sustainable Energy*, **9**(4), 363–78.

Bird, R. B., Stewart, W. E. and Lighfoot, E. N. (1960), *Transport Phenomena*, J. Wiley & Sons, New York.

Bobleter, O. (1994), 'Hydrothermal degradation of polymers derived from plants', *Progress Polymer Science*, **19**, 797–841.

Bungay, H. R. (2002), 'Confessions of a bioenergy advocate', *Trends in Biotechnology*, **22**, 67–71.

Calabrò, V., Curcio, S. and Iorio, G. (2002), 'A theoretical analysis of transport phenomena in a hollow fibre membrane bioreactor with immobilized biocatalyst', *Journal of Membrane Science*, **206**(1–2), 217–41.

Canakci, M. and Sanli, H. (2008), 'Biodiesel production from various feedstocks and their effects on the fuel properties', *Journal of Industrial Microbiology and Biotechnology*, **35**, 431–41.

Cantwell, B. A., Sharp, P. M., Gormley, E. and McConnell, D. J. (1988), 'Molecular cloning of bacillus β-glucanases', in *Biochemistry and Genetics of Cellulose Degradation*, Aubert, J. P., Beguin, P. and Millet, J. (eds), Academic Press, San Diego, CA, 181–201.

Cardona, C. A. and Sanchez, O. J. (2007), 'Fuel ethanol production: Process design trends and integration opportunities', *Bioresource Technology*, **98**, 2415–57.

© Woodhead Publishing Limited, 2011

Chen, G., Andries, J., Spliethoff, H., Fang, M. and van de Enden, P. J. (2004), 'Biomass gasification integrated with pyrolysis in a circulating fluidized bed', *Solar Energy*, **76**, 345–9.

Cheryan, M. and Mehaia, M. A. (1986), 'Membrane bioreactors', in *Membrane Separations in Biotechnology*, Mc Gregor, W.C. (ed), Marcel Dekker, New York.

Cheung, S. W. and Anderson, B. C. (1997), 'Laboratory investigation of ethanol production from municipal primary wastewater', *Bioresource Technology*, **59**, 81–96.

Chibata, I. (1978), *Immobilized Enzymes, Research and Development*, Halsted Press, New York, USA.

Cortright, R. D., Davda, R. R. and Dumesic, J. A. (2002), 'Hydrogen from catalytic reforming of biomass-derived hydrocarbons in liquid water', *Nature*, **418**, 964–7.

Coughlan, M. P. and Ljungdahl, L. G. (1988), 'Comparative biochemistry of fungal and bacterial cellulolytic enzyme system', in *Biochemistry and Genetics of Cellulose Degradation*, Aubert, J. P., Beguin, P. and Millet, J. (eds), Academic Press, San Diego, CA, 11–30.

Crane, P. and Scott, D. S. (1992), 'Efficiency and carbon dioxide emission analysis of pathways by which methane can provide transportation services', *International Journal of Hydrogen Energy*, **17**, 543–50.

Curcio, S., Calabrò, V. and Iorio, G. (2006), 'A theoretical and experimental analysis of a membrane bioreactor performance in recycle configuration', *Journal of Membrane Science*, **273**(1–2), 129–42.

Duff, S. J. B. and Murray, W. D. (1996), 'Bioconversion of forest products industry waste cellulosics to fuel ethanol: a review', *Bioresource Technology*, **55**, 1–33.

Freedman, B., Pryde, E. H. and Mounts, T. L. (1984), 'Variables affecting the yields of fatty esters from tranesterified vegetable oils', *Journal of American Oil Chemical Society*, **61**(10), 1638–43

Fukuda, H., Kondo, A. and Noda, H. (2001), 'Biodiesel fuel production by transesterification of oils', *Journal Bioscience Bioengineering*, **92**(5), 405–16

Fukuda, H., Kondo, A. and Tamalampudi, S. (2009), 'Bioenergy: Sustainable fuels from biomass by yeast and fungal whole-cell biocatalysts', *Biochemical Engineering Journal*, **44**, 2–12.

Gan, Q., Allen, S. J. and Taylor, G. (2002), 'Design and operation of an integrated membrane reactor for enzymatic cellulose hydrolysis', *Biochemical Engineering Journal*, **12**, 223–9.

Hama, S., Yamaji, H., Fukumizu, T., Numata, T., Tamalampudi, S., Kondo, A., Nodac, H. and Fukuda, H. (2007), 'Biodiesel fuel production in a packed-bed reactor using lipase-producing *Rhizopus oryzae* cells immobilized within biomass support particles', *Biochemical Engineering Journal*, **34**, 273–8.

Huber, G. W. and Dumesic, J. A. (2006), 'An overview of aqueous-phase catalytic processes for production of hydrogen and alkanes in a biorefinery', *Catalysis Today*, **111**, 119–32.

Iorio G. and Calabrò, V. (1994), 'Enzyme membrane reactors', in *Membrane Processes in Separation and Purification*, Crespo, J.G. and Boddeker, K.W. (eds), Kluwer Academic Publishers, NL, 149–67.

Kadam, K. L., Rydholm, E. C. and McMillan, J. D. (2004), 'Development and validation of a kinetic model for enzymatic saccharification of lignocellulosic biomass', *Biotechnology Progress*, **20**, 698–705.

Karimi, K., Kheradmandinia, S. and Taherzadeh, M. J. (2006), 'Conversion of rice straw to sugars by dilute-acid hydrolysis', *Biomass and Bioenergy*, **30**, 247–253.

© Woodhead Publishing Limited, 2011

Klass, D. L. (1998), *Biomass for Renewable Energy, Fuels, and Chemicals*, Academic Press, San Diego, CA.

Lin, S., Harada, M., Suzuki, Y. and Hatano, H. (2002), 'Hydrogen production from coal by separating carbon dioxide during gasification', *Fuel*, **81**, 2079–85.

Lynd, L. R., Wyman, C. E. and Gerngross, T. U. (1999), 'Biocommodity engineering', *Biotechnology Progress*, **15**, 777–93.

Lynd, L. R., Laser, M. S., Bransby, D., Dale, B. E., Davison, B., Hamilton, R., Himmel, M., Keller, M., McMillan, J. D., and Sheehan, J. (2008), 'How biotech can transform biofuels', *Nature Biotechnology*, **26**, 169–72.

Ma, F. and Hanna, M. A. (1999), 'Biodiesel production: a review', *Bioresource Technology*, **70**, 1–15.

Mata, T. M., Martins, A. A. and Caetano, N. C. (2010), 'Microalgae for biodiesel production and other applications: A review', *Renewable and Sustainable Energy Reviews*, **14**, 217–32.

Messing, R. A. (1975), *Immobilised Enzymes for Industrial Reactors*, Academic Press, New York, USA.

Nielsen, R., JR. (2001), 'Conversion of hydrocarbons and alcohols for fuel cells', *Physical Chemistry Chemical Physical*, **3**, 283–8.

Noureddini, H., Gao, X. and Phikana, R. S. (2001), 'Immobilized *Pseudomonas cepacia* lipase for biodiesel fuel production from soyabean oil', *Bioresource Technology*, **96**, 767–77.

Perry, R. H. and Green, D. W. (1997), *Perry's Chemical Engineers' Handbook*, 7th edition, McGraw-Hill, New York.

Peterson, C. L. (1986), 'Vegetable oil as a diesel fuel: Status and research priorities', *ASAE Transactions*, **29**(5), 1413–22

Ranganathan, S.V., Narasimhan, S. L. and Muthukumar, K. (2008) 'An overview of enzymatic production of biodiesel', *Bioresource Technology*, **99**, 3975–81.

Renewable Fuel Agency (2008), *The Gallagher Review of the Indirect Effects of Biofuels Production*, http://www.renewablefuelsagency.gov.uk/reportsandpublications/reviewoftheindirecteffectsofbiofuels See also: http://dft.gov.uk/pgr/sustainable/biofuels/

Ricca, E., De Paola, M.G., Calabrò, V., Curcio, S. and Iorio, G. (2009), 'Olive husk oil transesterification in a fluidized bed reactor with immobilized lipases', *Asia-Pacific Journal of Chemical Engineering*, **4**(3), 365–8.

Sansonetti, S., Curcio, S., Calabrò, V. and Iorio, G. (2009), 'Bio-ethanol production by fermentation of ricotta cheese whey as an effective alternative non-vegetable source', *Biomass and Bioenergy*, **33**(12), 1687–92.

Sansonetti, S., Curcio, S., Calabrò, V. and Iorio, G. (2010), 'Optimization of ricotta cheese whey (RCW) fermentation by response surface methodology', *Bioresource Technology*, **101**(23), 9156–62.

Steinberg, M. (1998), 'Production of hydrogen and methanol from natural gas with reduced CO_2 emission', *International Journal of Hydrogen Energy*, **23**, 419–25.

Sun, Y. and Cheng, J. (2002), 'Hydrolysis of lignocellulosic materials for ethanol production: a review', *Bioresource Technology*, **83**, 1–11.

Tanksale, A., Beltramini, J. N. and Lu, G. Q. M. (2010), 'A review of catalytic hydrogen production processes from biomass', *Renewable and Sustainable Energy Reviews*, **14**, 166–82.

Towler, G. P., Oroskar, A. R. and Smith, S. E. (2004), 'Development of a sustainable liquid fuels infrastructure based on biomass', *Environmental Progress*, **23**, 334–41.

© Woodhead Publishing Limited, 2011

Watanabe, Y., Shimada, Y., Sugihara, A., Noda, H., Fukuda, H. and Tominaga, Y. (2000), 'Continuous production of biodiesel fuel from vegetable oil using immobilized *Candida antarctica* lipase', *Journal of American Oil Chemical Society*, **77**, 355–60.

Zhang, Y. P. and Lynd, L. R. (2004), 'Toward an aggregated understanding of enzymatic hydrolysis of cellulose: non-complexed cellulase systems', *Biotechnology and Bioengineering*, **88**, 797–824.

12.13 Appendix: list of symbols

12.13.1 Symbols

a	specific membrane surface	$[m^{-1}]$
A_m	membrane surface	$[m^2]$
$A_{m,i}$	total surface of each membrane region	$[m^2]$
B	dimensionless parameter (Equation [12.8])	
$B1$	dimensionless parameter (Equation [12.34])	
D	characteristic length of the system	[m]
Da	Damköhler number	
D_{AB}	substrate diffusivity	$[m^2\ s^{-1}]$
$D_{AB,eff}$	effective substrate diffusivity	$[m^2\ s^{-1}]$
$Diff$	diffusion coefficient	$[m^2\ s^{-1}]$
D_{PB}	product diffusivity	$[m^2\ s^{-1}]$
$D_{PB,eff}$	effective product diffusivity	$[m^2\ s^{-1}]$
E_0	enzyme concentration loaded to the bioreactor	$[mol_{enzyme}\ m^{-3}]$
E_i	enzyme concentration immobilized in each membrane region	$[mol\ m^{-3}]$
$E_{m,V}$	Amount of enzyme immobilized on the support (Equation [12.14])	$[mol_{enzyme}\ m^{-3}{}_{support}]$
h_i	hydraulic permeability in the Brinkman equation	$[m^2]$
J	permeate flux	$[m^3\ m^{-2}\ s^{-1}]$
j_D	Colburn factor	
k_2	kinetic constant in Michaelis–Menten equation	$[mol/(mol_{enzyme}\ s)]$
k_i	product inhibition kinetic constant in Michaelis–Menten equation	$[mol\ m^{-3}]$
k_L	mass transfer coefficient	$[m\ s^{-1}]$
K_M	Michaelis constant	$[mol\ m^{-3}]$
k_p	substrate inhibition kinetic constant in Michaelis–Menten equation	$[mol\ m^{-3}]$

© Woodhead Publishing Limited, 2011

k_s	mass transfer coefficient in the liquid film (Equation [12.14])	[m s^{-1}]
L	Fibre lumen length	[m]
L_p	membrane hydraulic permeability	[m s^{-1} Pa^{-1}]
m_P	total mass of the pellets fed to the bioreactor	[kg]
N_f	number of hollow fibres	
P	product concentration	[mol m^{-3}]
$P^* = P/C_0$	dimensionless product concentration	
P_0	module inlet pressure	[Pa]
p_1	pressure in the lumen	[Pa]
P_{atm}	atmospheric pressure	[Pa]
P_b	product concentration in the bulk (Fig. 12.5)	[mol m^{-3}]
P_f	product concentration fed to bioreactor (Fig. 12.9 and 12.13)	[mol m^{-3}]
$Pe_{ax} = \frac{v_0 L}{D_{AB}}$	axial Peclet number	
$Pe_{rad} = \frac{v_p R_1}{D_{AB}}$	radial Peclet number	
PI	performance index	
p_i	pressure in the dense or in the spongy layers	[Pa]
P^*_{iE}	interfacial dimensionless product concentration	
P_L	module outlet pressure	[Pa]
P_P	product concentration in the permeate (Fig. 12.4)	[mol m^{-3}]
P_R	recycle product concentration (Fig. 12.13)	[mol m^{-3}]
Q	volumetric flow rate fed to the system in Fig. 12.4	[m^3 s^{-1}]
$Q_0 = N_f v_0 \pi R_1^2$	total feed flow rate in the axial direction	[m^3 s^{-1}]
$Q_{pb} = N_f 2\pi R_1 L\, L_p\, TMP$	bioreactor permeate flow rate	[m^3 s^{-1}]
Q_f	volumetric flow rate fed to the bioreactor (Fig. 12.9 and 12.13)	[m^3 s^{-1}]
Q_F	volumetric flow rate fed to the membrane module (Fig. 12.4)	[m^3 s^{-1}]
Q_P	volumetric permeate flow rate (Fig. 12.4)	[m^3 s^{-1}]

© Woodhead Publishing Limited, 2011

Q_R	recycle volumetric flow rate (Fig. 12.4 and 12.13)	[$m^3\ s^{-1}$]
R	actual reaction rate	[mol $m^{-3}\ s^{-1}$]
r	radial generic coordinate	[m]
R_1	fibre lumen radius	[m]
R_{MAX}	maximum reaction rate	[mol $m^{-3}\ s^{-1}$]
$Re_i = \frac{v_p}{a_i \cdot \nu \cdot \psi}$	Reynolds number (Equation [12.53])	
S	substrate concentration	[mol m^{-3}]
$S^* = S/S_0$	dimensionless substrate concentration	
S_0	initial or feed substrate concentration	[mol m^{-3}]
S_b	substrate concentration in the bulk (Fig. 12.5)	[mol m^{-3}]
S_f	substrate concentration fed to bioreactor (Fig. 12.9 and 12.13)	[mol m^{-3}]
S^*_{iE}	interfacial dimensionless substrate concentration	
S_P	substrate concentration in the permeate (Fig. 12.4)	[mol m^{-3}]
S_R	recycle substrate concentration (Fig. 12.4 and 12.13)	[mol m^{-3}]
t	time	[s]
U	characteristic velocity	[m s^{-1}]
$\mathbf{u}_1$	velocity vector in the lumen	[m s^{-1}]
$\mathbf{u}_i$	generic velocity vector in each membrane region	[m s^{-1}]
V	bioreactor volume (Fig. 12.4)	[m^3]
V_0	initial volume of the mixture in the feed tank (Fig. 12.13)	[m^3]
V_2	dense layer volume	[m^3]
V_3	spongy layer volume	[m^3]
V_f	volume of the mixture in the feed tank (Fig.13)	[m^3]
V_m	membrane volume	[m^3]
$V_{m,i}$	total volume of each membrane region	[m^3]
V_P	volume of the pellets	[m^3]
$v_0 = \frac{Q_0}{\pi R_1^2}$	feed velocity in axial direction	[m s^{-1}]

© Woodhead Publishing Limited, 2011

$v_p = L_p\, TMP$	permeation velocity in radial direction	[m s^{-1}]
$v_r(r, z)$	radial velocity profile	[m s^{-1}]
$v^*_{ri} = \frac{v_r(r, z)}{v_p}$	dimensionless radial velocity profile in each fibre region	
$v_z(r, z)$	velocity profile in the axial direction	[m s^{-1}]
$v^*_{zi} = \frac{v_z(r, z)}{v_0}$	dimensionless axial velocity profile in each fibre region	
z	axial generic coordinate	[m]

12.13.2 Greek symbols

∇	Vector differential operator (nabla); for a cylindrical coordinate system: $\nabla = \left\{\frac{\partial}{\partial r}, \frac{1}{r}\frac{\partial}{\partial \phi}, \frac{\partial}{\partial z}\right\}$	
α	degree of conversion	
χ	dimensionless substrate concentration (Equation [12.5])	
δ_F	film thickness (Fig. 12.5)	[m]
ε	bioreactor void fraction	
γ	solution density	[kg m^{-3}]
γ_P	pellet density	[kg m^{-3}]
η	effectivess factor	
$\lambda^2 = \frac{k_2 E R_1^2}{C_0 D_{AB}}$	squared Thiele modulus	
μ	solution viscosity	[kg(m^{-1} s^{-1})]
ν	kinematic viscosity	[m^2 s^{-1}]
Θ	bioreactor productivity	[$mol_{product}/mol_{enzyme}$]
θ	saturation factor (Equation [12.6])	
$\rho = \frac{r}{R_1}$	dimensionless radial generic coordinate	
τ_R	bioreactor residence time	[s]
ψ	shape factor	
$\zeta = \frac{z}{L}$	dimensionless axial generic coordinate	

© Woodhead Publishing Limited, 2011

12.13.3 Subscripts and superscripts

$i = 1, 2, 3$	(membrane region)
1	membrane lumen
2	membrane dense layer
3	membrane spongy layer
T	Transpose

© Woodhead Publishing Limited, 2011

13

Ion exchange membranes for vanadium redox flow batteries

S. S. HOSSEINY, Aachener Verfahrenstechnik-Chemische Verfahrenstechnik, RWTH-Aachen University, Germany and M. WESSLING, Aachener Verfahrenstechnik-Chemische Vefahrenstechnik, RWTH-Aachen University, Germany and University of Twente, The Netherlands

Abstract: Ion exchange membranes play a crucial role in flow batteries. Such batteries comprise an electrochemical cell in which oxidation and reduction processes can store and release electrons during charge and discharge operations. The electrical energy is stored in a liquid in large reservoirs. Vanadium redox flow batteries are considered here in particular. This chapter reviews (a) principles of electrochemical energy storage and (b) the properties of polymeric and hybrid membrane materials that are suitable for redox flow batteries.

Key words: ion exchange, membranes, polymeric membranes, redox flow batteries, vanadium.

13.1 Electrochemical energy storage

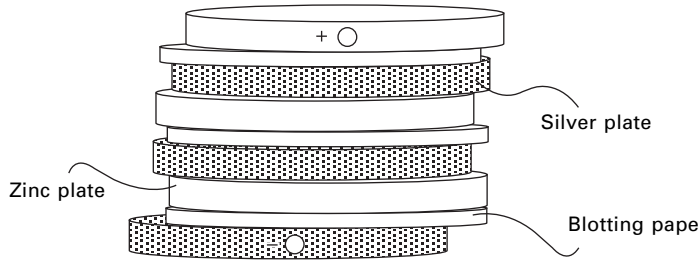
13.1.1 Motivation

With vanishing resources of fossil fuels and the rise of solar power generation, society will be facing the task to store electrons stemming from photovoltaic photon-to-electron conversions. Such storage systems need to be flexible, scalable and reliable. Electrochemical storage systems are one of the most viable technological solutions for electricity storage. This chapter sketches today's situation in general, but focuses in particular on flow batteries and the membranes used for these systems. Such batteries may offer in the near future a viable process for efficient energy storage.

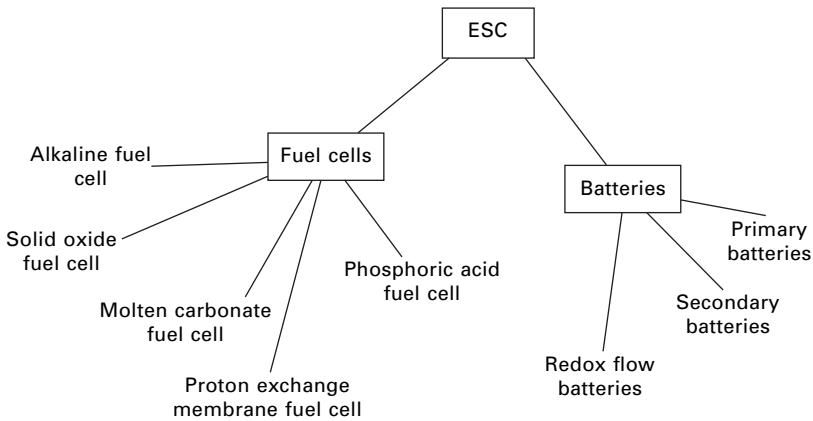
13.1.2 Historic background

In the late 1700s and early 1800s the basis of electrochemical energy storage and conversion (ESC) was manifested by Luigi Galvani and Alessandro Volta. Figure 13.1 depicts the first battery system, the volta pile, comprising alternatingly silver (or copper) and zinc plates separated by blotting paper soaked in brine (electrolyte) to increase the electrolyte conductivity.

© Woodhead Publishing Limited, 2011



13.1 Volta pile.



13.2 ESC systems.

During the last few decades, a wide range of ESC systems have been developed and commercialized. Nowadays, ESC systems belong to our daily life and are used for a wide range of applications like starting, lighting and ignition (SLI) of emergency units, portable electronic devices, spacecraft, electronic vehicles and so on. In addition, in applications like power quality management and electrification of automobiles ESC systems have taken a critical role. There are two main types of ESC system (Fig. 13.2).

In fuel cells, chemical energy is converted into electrical energy by feeding the cell with a chemical fuel (hydrogen or methanol, for instance) which is then turned via a catalytic reaction into energy and chemical reaction products. Fuel cells will deliver electrical energy as long as they are fed with fuel. The reaction products cannot be returned to the original chemicals. Batteries (especially secondary and redox flow batteries) are different: in batteries the electrical energy is also gained by conversion of chemical energy, however, the chemical nature can be regained after discharge through a re-charging process. Hence, the chemical reactants can be contained within the limited space of the battery. This also limits in turn the amount of electrical energy

© Woodhead Publishing Limited, 2011

stored per unit volume of the battery. This chapter focusses on the use of polyelectrolyte membranes in battery applications, in particular vanadium-based batteries.

Since the first battery system was developed 100 years ago, we now use batteries almost every day and every situation. Over time the field of battery research and development has grown very rapidly and can be demonstrated by three different types of battery:

- primary
- secondary
- redox flow.

13.1.3 Primary batteries

Primary batteries, also called 'disposable batteries', still use the basic idea of a voltaic pile. Here the electrochemical energy produced by the decomposition of electrode material and electrolyte will break down once the electrode or the electrolyte are degraded. Since this procedure is irreversible, the battery needs to be replaced by a new battery. A primary battery is a battery in which the electrochemical reaction is not reversible. Table 13.1 presents some of the common primary battery systems. However, such systems are expensive and environmentally unfriendly owing to their disposable character.

13.1.4 Secondary batteries

Facing a time of energy crises and environmental protection, ways to store energy efficiently and in large quantities with reversible systems has recently inspired the field of battery technology. Secondary batteries present such a reversible system as they do not need to be replaced after every discharge cycle, owing to the reversible nature of electrochemical charging and discharging of the system. Many secondary batteries have been developed and commercialized in the past and some are depicted in Table 13.2.

Table 13.1 Some common primary battery systems (Kiehne, 2003)

Battery system	Cell reaction	Potential (V)
Leclanché	$Zn + 2MnO_2 + 2NH_4Cl \rightarrow ZnNH_3Cl_2 + Mn_2O_3$	1.5
Manganese alkaline	$Zn + 2MnO_2 + 2H_2O \rightarrow ZnO + Mn_2O_3$	1.5
Silver oxide/zinc	$Zn + Ag_2O + H_2O \rightarrow Zn(OH)_2 + 2Ag$	1.6
Air/zinc (alkaline)	$2Zn + O_2 \rightarrow 2ZnO$	1.45
Lithium/manganese dioxide	$Li + Mn^{4+}O_2 \rightarrow Mn^{3+}O_2 + (Li^+)$	3.5
Thionyl chloride	$4Li + 2SOCl_2 \rightarrow 4LiCl + S + SO_2$	3.9

© Woodhead Publishing Limited, 2011

Such systems are not only environmentally friendly but also cheap since with every recharge the price drops, compared with a primary battery. However, secondary batteries also have a specific lifetime and need to be replaced after a certain number of charge–discharge cycles, depending on the charge–discharge conditions. Another disadvantage is that current secondary batteries have major drawbacks with regard to large scale energy storage, as summarized by Table 13.3 for three large scale systems.

13.1.5 Redox flow batteries

Redox flow batteries are a relatively new technology for storing large quantities of energy. This system increases the flexibility, minimises the environmental risk and improves the response time to demand. Rather than the electrolyte system being encapsulated between the electrodes, and being limited to the volume of the secondary battery, in flow batteries the electroyte can be circulated from a reservoir tank. The tank volume gives the extent of energy storage. In the past many systems have been developed to achieve a stable and cheap way of storing large quantities of energy. Table 13.4 summarizes the systems and their characteristics.

All of the above-mentioned systems can be up-scaled in order to increase the power of the cells. This happens usually by increasing the size of the electrodes, stacking the systems with bipolar electrodes (10–200) or connecting the systems in series or parallel. To increase the storage capacity the concentration and volume of the electrolyte solution can be increased. Power and storage capacity are separate and can be influenced independently.

Table 13.2 Some common secondary battery systems (Kiehne, 2003)

Battery system	Cell reaction	Potential (V)
Lead/acid	$Pb + PbO_2 + 2H_2SO_4 \leftrightarrow 2PbSO_4 + 2H_2O$	2
Nickel/cadmium	$Cd + 2NiOOH + 2H_2O \leftrightarrow 2Ni(OH)_2 + Cd(OH)_2$	1.3
Nickel/metal hydride	$H_2 + 2NiOOH \leftrightarrow 2Ni(OH)_2$	1.3
Lithium-ion	$Li_xC_6 + Li_{1-x}Mn_2O_4 \leftrightarrow C_6 + Li_xMn_2O_4$	3.6

Table 13.3 Secondary batteries as large scale energy storage systems (Chen *et al.*, 2009)

Battery system	Drawbacks
Lead/acid	Very limited life (500–1000 cycles), low power density, low temperature performance
Nickel/cadmium	High cost (US$1000/ kWh), toxicity, memory effect
Sodium-sulfate	High operation temperature (300–350°C)

© Woodhead Publishing Limited, 2011

Table 13.4 Redox flow battery systems

Redox flow battery system	Cell reactions		Cell potential (V)	Reference
	Charge	Discharge		
Bromide/Polysulfide	$3Br^- \rightarrow Br_3^- + 2e^-$ $S_4^{2-} + 2e^- \rightarrow 2S_2^{2-}$	$Br_3^- + 2e^- \rightarrow 3Br^-$ $2S_2^{2-} \rightarrow S_4^{2-} + 2e^-$	1.35	Price *et al.* (1999)
All-Vanadium	$VO^{2+} + H_2O \rightarrow VO_2^+ + 2H^+ + e^-$ $V^{3+} + e^- \rightarrow V^{2+}$	$VO_2^+ + 2H^+ + e^- \rightarrow VO^{2+} + H_2O$ $V^{2+} \rightarrow V^{3+} + e^-$	1.26	Skyllas-Kazacos *et al.* (1988)
Vanadium/Bromine	$2VBr_3 + 2e^- \rightarrow 2VBr_2 + 2Br^-$ $2Br^- + Cl^- \rightarrow ClBr_2^- + 2e^-$	$2VBr_2 + 2Br^- \rightarrow 2VBr_3 + 2e^-$ $ClBr_2^- + 2e^- \rightarrow 2Br^- + Cl^-$	1.3	Leon *et al.* (2006)
Iron/Chromium	$Fe^{2+} \rightarrow Fe^{3+} + e^-$ $Cr^{3+} + e^- \rightarrow Cr^{2+}$	$Fe^{3+} + e^- \rightarrow Fe^{2+}$ $Cr^{2+} \rightarrow Cr^{3+} + e^-$	1.18	Hagedorn (1982)
Zinc/Bromine	$3Br^- \rightarrow Br_3^- + 2e^-$ $Zn^{2+} + 2e^- \rightarrow Zn$	$Br_3^- + 2e^- \rightarrow 3Br^-$ $Zn \rightarrow Zn^{2+} + 2e^-$	1.85	Lex *et al.* (1999)
Vanadium/Air	$2H_2O \rightarrow 4H^+ + O_2 + 4e^-$ $4V^{3+} + 4e^- \rightarrow 4V^{2+}$	$4H^+ + O_2 + 4e^- \rightarrow 2H_2O$ $4V^{2+} \rightarrow 4V^{3+} + 4e^-$	1.49	Hosseiny *et al.* (2011)
Zinc/Cerium	$2Ce^{3+} \rightarrow 2Ce^{4+} + 2e^-$ $Zn^{2+} + 2e^- \rightarrow Zn$	$2Ce^{4+} + 2e^- \rightarrow 2Ce^{3+}$ $Zn \rightarrow Zn^{2+} + 2e^-$	2.4	Clarke *et al.* (2007)

© Woodhead Publishing Limited, 2011

This is one of the most important features of these systems. A redox flow battery system will be characterized in the following terms:

$$\text{Voltage efficiency} \quad \eta_V = \frac{V_{cc}\,(\text{discharge})}{V_{cc}\,(\text{charge})} \qquad [13.1]$$

$$\text{Charge efficiency} \quad \eta_C = \frac{Q\,(\text{discharge})}{Q\,(\text{charge})} \qquad [13.2]$$

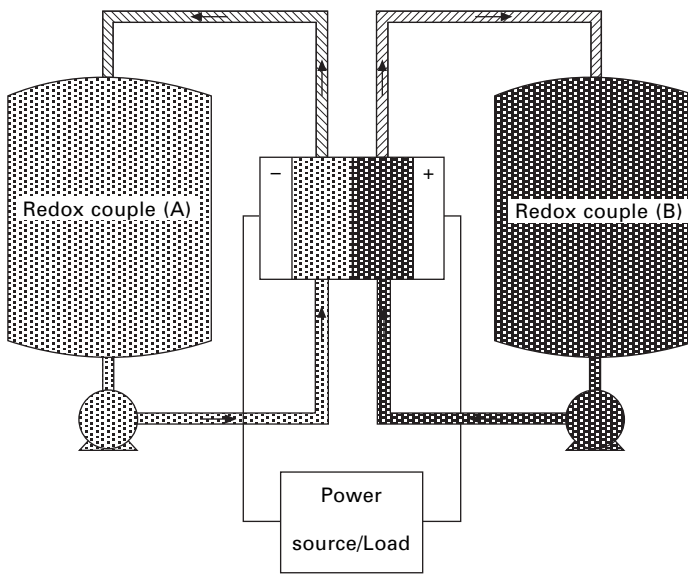
$$\text{Energy efficiency} \quad \eta_e = \frac{E\,(\text{discharge})}{E\,(\text{charge})} \qquad [13.3]$$

The concept of a redox flow battery is depicted in Fig. 13.3. The main element of Fig. 13.3 is the electrochemical cell, where the redox reaction of the battery takes place. The electrochemical cell is mainly composed of two half cells, separated by an ion exchange membrane. The electrodes are included in the half cells. To run the system, the electrolyte flows through the electrochemical cell containing the oxidized and reduced species. The membrane, electrodes and the electrolyte need to fulfill different tasks.

13.2 Vanadium redox flow batteries

13.2.1 Principles

The all vanadium redox flow battery (VRFB) is an electrochemical energy storage system invented by Maria Skyllas-Kazacos in 1984. It consists of



13.3 Overview of a redox flow battery.

© Woodhead Publishing Limited, 2011

two electrochemical half cells, separated by an ion exchange membrane (Fig. 13.4).

Since vanadium can exsist in four different oxidation states, the positive half cell employs VO^{2+}/VO_2^+ while the negative half cell contains V^{2+}/V^{3+}. When the vanadium battery is charged, the VO^{2+} ions in the positive half cell are converted to VO_2^+ ions when electrons are removed from the positive terminal of the battery. Similarly in the negative half cell, electrons are introduced converting the V^{3+} ions into V^{2+}. During discharge this process is reversed.

Equations [13.4] and [13.5] summarize the electrochemical reactions during charging and discharging:

Charge: $VO^{2+} \rightarrow VO_2^+ + e^-$

$$V^{3+} + e^- \rightarrow V^{2+} \qquad [13.4]$$

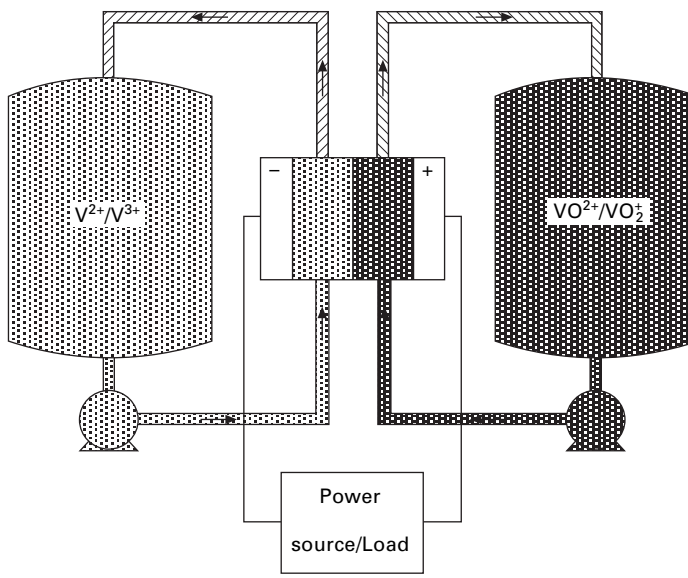
Discharge: $VO_2^+ + e^- \rightarrow VO^{2+}$

$$V^{2+} \rightarrow V^{3+} + e^- \qquad [13.5]$$

The VRFB potential is calculated by the redox potentials of the half cell reactions and is presented by Equation [13.6].

$$E_{(\mathrm{VRFB})} = E^0_{(V^{2+/3+})} - E^0_{(VO^{2+}/VO_2^+)}$$

$$E_{(\mathrm{VRFB})} = 0.26\ \mathrm{V} - (-1.00\ \mathrm{V})$$



13.4 Overview of a vanadium redox flow battery.

© Woodhead Publishing Limited, 2011

$$E_{(\mathrm{VRFB})} = 1.26\ \mathrm{V} \qquad [13.6]$$

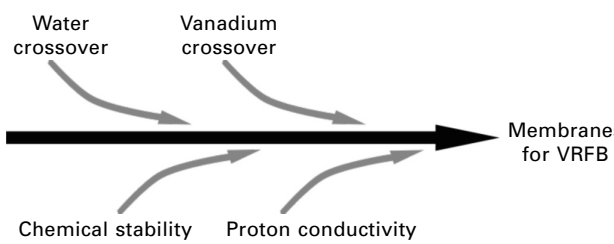
The VRFB has been chosen as a special type of redox flow system, since the crossover of vanadium redox couples through the ion exchange membrane (seperator) will not damage the battery system as it would in several other systems like iron-chromium, zinc-bromine and zinc-cerium. However, crossover still remains a critical issue for the ion exchange membrane in the VRFB next to other issues such as water crossover, conductivity and chemical stability.

13.2.2 Critical issues

Since the discovery of the vanadium redox flow battery (VRFB) in 1984 by Maria Skyllas-Kazacos VRFBs have gone a long way and have recently reached commercialization. However, there is still ongoing research on improving the system in terms of stability and performance. One main research area beside the electrode and the electrolyte is dedicated to the polyelectrolyte membrane. Polyelectrolyte membranes used as a separator in the VRFB have the important task of separating efficiently the half cells and conducting anions or protons to equilibrate the ionic strength during the charge and discharge procedures. Besides ion conductivity and separation properties, the membrane has to withstand the harsh conditions inside the VRFB since the vanadium electrolyte solvent will be 3–6 molar sulfuric acid and VO_2^+, which will be produced during charging, has very strong oxidative properties. Because of this limitation the polyelectrolyte membranes still show some issues which will decrease the performance or the lifetime of the VRFB. These issues are depicted in Fig. 13.5.

13.2.3 Crossover

The phenomenon of crossover in VRFB describes the undesired permeation of chemical species (H_2O and vanadium ions) through the ion exchange membranes.



13.5 Issues which need to be overcome in order to develop a suitable membrane for VRFBs.

© Woodhead Publishing Limited, 2011

Vanadium and water crossover

The unique chemistry of VRFB prevents the system from irreversible degradation since vanadium will be applied in both half cells of the system; this avoids any irreversible mixing of chemcially different species and downgrading of the electrolyte quality. Yet the crossover of vanadium will influence the cell performance, since undesired self discharge can take place if the following reactions occur by crossover of vanadium ions [13.7]:

$$V^{2+} + VO_2^+ \rightarrow V^{3+} + VO^{2+}$$
$$V^{3+} + VO_2^+ \rightarrow 2VO^{2+} \qquad [13.7]$$

Looking at the vanadium chemistry it appears that VO_2^+ and VO^{2+} show a rather complicated dissociation reaction in sulfuric acid. Sukkar and Skyllas-Kazacos, (2003) showed that a vanadium redox flow battery with 2M vanadium solution in the negative half cell and 2M vanadium solution in the positive half cell, both using a sulfuric acid with 5M total sulfate content as the solvent, will have the following composition at a state of charge of 50%.

Positive half cell:

$$1\ M\ VOSO_4 + 0.4\ M\ VO_2^+ + 0.6\ M\ VO_2SO_4^- + 3.4\ M\ HSO_4^- + 3.6\ M\ H^+$$

Negative half cell:

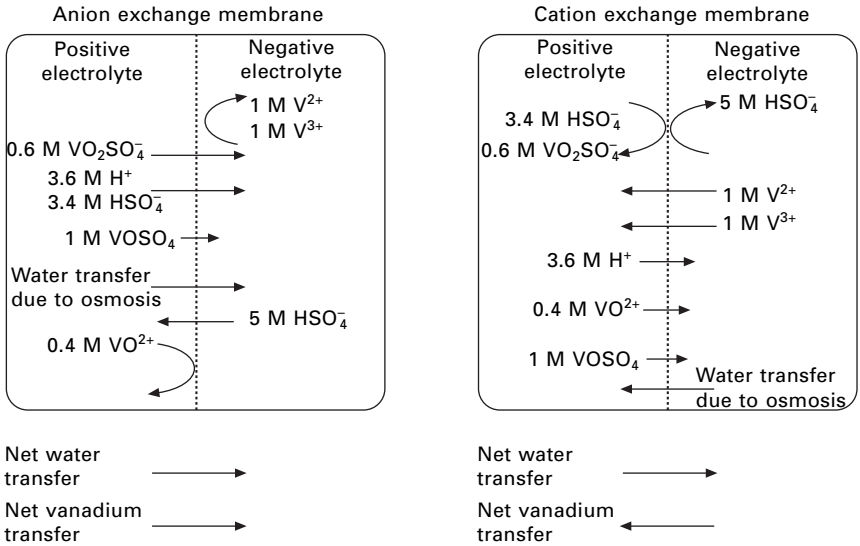
$$1\ M\ V^{3+} + 1\ M\ V^{2+} + 2.5\ M\ HSO_4^- + 2.5\ M\ SO_4^{2-} + 2.5\ M\ H^+$$

This variation in dissociation behaviour leads to different ionic strengths, which will result, when applied in the vanadium redox flow battery, in osmosis. Osmosis presents an issue in the VRFB since the concentration of electrolyte will change leading to concentration of electrolyte in one half cell and dilution of electrolyte in the other half cell (Mohammadi *et al.* 1997, Sukkar *et al.*, 2003, Sum *et al.*, 2010.). By this the osmotic pressure difference will increase as well, leading to more vanadium crossover and a faster self discharge behaviour. It is important to understand water crossover in the VRFB in order to improve its performance. Two methods of water transfer have been investigated recently by Sun *et al.* (2010) and Sukkar *et al.* (2003) in which it was shown that the vanadium crossover and the water crossover are related to each other. Figure 13.6 depicts the dependence of the water transfer on the vanadium-proton cross over and osmotic pressure difference.

13.2.4 Ion conductivity

The issue of ion conductivity has been tackled before in the development of efficient membranes for the VRFB. The ion conductivity of a membrane in

© Woodhead Publishing Limited, 2011



13.6 Expected water and ion transfer for anion and cation exchange membranes applied in a 50% state of charge for a VRFB (redrawn from Sukkar et al. (2003).

a VRFB system defines the ability to conduct protons or anions (e.g. SO_4^{2-}), in both directions during charge and discharge in order to balance the charge differences occuring during these reactions. Since the ion conductivity of polyelectrolyte determines the resistance and the voltage drop inside the electrochemical cell, a suitable polyelectrolyte needs to have an ion conductivity in order to achieve a good performing and efficient redox flow battery..

The ion conductivity of a polyelectrolyte comes from fixed charged groups on the polymer backbone of the membrane. According to the charge on the fixed groups the ions are transported through the ion channels inside the membrane. Fixed negative charges in the ion channels will promote conduction of positive charges (cation exchange membranes) and positively charged fixed groups will promote conduction of negatively charged ions (anion exchange membranes). Not only does the ion conductivity need to be reasonable but also the crossover of the vanadium ions through the membrane also needs to be low to avoid self-charge. Cases in which a Nafion membrane gives lower energy efficiency than a lower ion conductive membrane are reported. This was the case where the developed polyelectrolytes showed lower vanadium permeability than Nafion.

13.2.5 Chemical stability

A VRFB produces during charge in the positive half cell VO_2^+ ions, which have a very strong oxidizing potential. Since the vanadium ion is in its

© Woodhead Publishing Limited, 2011

highest oxidation state it will act as a electron acceptor and fall back in the more stable oxidation state of 4+. Furthermore, the vanadium solution needs to have a high acidity, owing to poor vanadium solubility in neutral solution. The membranes applied in the VRFB need to be chemically stable at these harsh conditions.

Many pathways have been described in the literature for enhancing the chemical stability of ion exchange membranes for other types of energy conversion and storage systems, like fuel cells. However, the stability issue for membranes in the VRFB has been noted in the scientific literature, but never been considered as a major topic in quantifying and understanding degradation pathways. Even though VO_2^+ is mostly claimed to be the major degradation agent other states like V^{2+} have also a high degradation potential, since V^{2+} is a very strong reducing agent. Finally, to the knowledge of the authors, no scientific work has been done on the long-term stability of polyelectrolytes in contact with strong reducing agents like V^{2+}.

The majority of publications on VRFB deal with the application of (a) sulfonated perfluorinated polymers like Nafion, (b) partly sulfonated fluorinated polymers as well as (c) sulfonated polyarylenes with conjugated π bonds. For the latter, for example sulfonated poly(ether ketone) the polymers need to be sulphonated first. This sulfonation will also set limits on the stability (chemical and mechanical).

Little work has been done on the field of anion exchange membranes compared to the amount of work done on cation exchange membranes (mostly sulfonated polymers). In the scientific literature only a few anion exchange membranes have been prepared and observed for application in VRFBs.

In conclusion, a suitable membrane for the VRFB needs to deal with very harsh environments. More work needs to be done on the chemical stability of polyelectrolytes for VRFBs in order to understand the degradation procedures to engineer a cheap, conductive but stable membrane for this promising energy storage application.

13.3 Membranes

Several commercially available ion exchange membranes from Asahi Glass (Selemion and Flemion), Dow Chemicals (Dow XUSI 3204.01), Asahi Chemicals (K142) and Du Pont(Nafion) (Mohammadi *et al.*, 1995b) have been applied and tested in the past for the VRFB application.Two of the above mentioned membranes (Flemion and Nafion) have been identified as suitable for the VRFB. But these ion exchange membranes are fairly expensive and show a quite high vanadium crossover. Researchers have been screening several material classes in order to produce a cheap, stable, proton conductive and selective membrane with little vanadium crossover. Next to cation exchange membranes (CEM), anion exchange membranes

© Woodhead Publishing Limited, 2011

(AEM) as well as amphotheric ion exchange membranes (AIEM) have been studied.

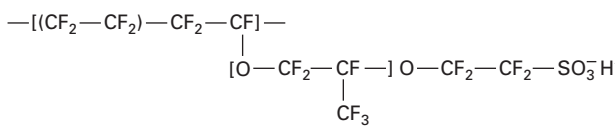
13.3.1 Cation exchange membranes

The CEM is the most reported membrane for the VRFB application in the scientific literature due to the high transport rates for protons. However, the vanadium species are mobile as well and will also permeate through the CEM. According to that the challenge is to apply a high proton conductive but a low vanadium permeable membrane for the VRFB in order to achieve a highly efficient system. Nafion is the most used CEM due to its chemical stability and excellent proton conductivity. Nafion is a sulfonated perfluorinated polymer with a copolymer molecule structure (Fig. 13.7). The polymer consists of a strong hydrophobic backbone and regularly spaced shorter perfluoro vinylether side chains, each terminated by a strong hydrophilic sulfonic acid group. Nafion shows good phase separation between the hydrophilic and hydrophobic phases, leading to a very well interconnected hydrophilic phase due to the highly flexible fluorocarbon backbone of the polymer. The fluorocarbon backbone is also the reason that this polymer shows excellent chemical stability. Since the hydrophilic groups are responsible for proton conductivity by dissociation in contact with protic and polar solvents, among a large list of commercial polymers Nafion has chemical stability but also good proton conductivity.

The two major disadvantages of Nafion for VRFB applications are the cost and the vanadium crossover. The high costs are mainly due to the complex production method. Vanadium permeation is due to well interconnected hydrophilic and broad channels (Jia *et al.*, 2010). Figure 13.8 depicts the difference between a swollen Nafion membrane and a glassy polyelectrolyte (in this case sulfonated poly (ether ketone) (SPEK), Kreuer (2001). The illustration expresses the highly permeable phase separation of Nafion and the dead end and narrow channels of SPEEK which do not contribute as effectively to the ion conductivity.

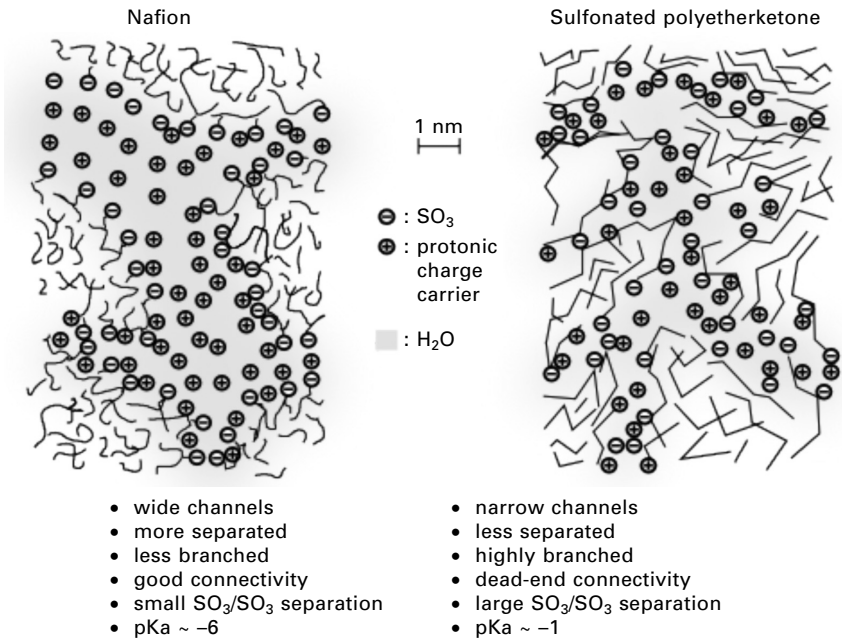
This leads to the two main issues of Nafion in VRFB:

- Self discharge and low energy efficiency due to vanadium permeation (cross-over)
- Dilution and concentrating of the electrolyte solutions



13.7 Chemical structure of Nafion.

© Woodhead Publishing Limited, 2011



13.8 Illustration of a swollen sulfonated poly(ether ether ketone) (SPEEK) and Nafion membrane model (redrawn from Kreuer, 2001).

In the search for alternatives for Nafion, considerable work has been done on modification methods of CEMs.

The following methods were applied to CEMs in order to produce low vanadium permeable CEMs:

- Soaking of porous non conductive membranes with polyelectrolytes (Mohammadi *et al.*, 1995a; Chienga *et al.*, 1992; Tian *et al.*, 2004; Miyake, 2002, Mohammadi *et al.*, 1995c)
- Synthesis of organic/inorganic composite membrane
  - *In situ* sol–gel
  - Blending of the polyelectrolyte with inorganic particles
- Modification with polyelectrolyte multilayers.

Two major modifications have been proved to decrease vanadium crossover and show long-term stability in a running VRFB. These methods are described in the next section.

Synthesis of organic/inorganic composite membranes

Composite ion exchange membranes with inorganic materials such as silica (Antonucci *et al.*, 1999; Jiang *et al.*, 2006; Jung *et al.*, 2002), zirconia

© Woodhead Publishing Limited, 2011

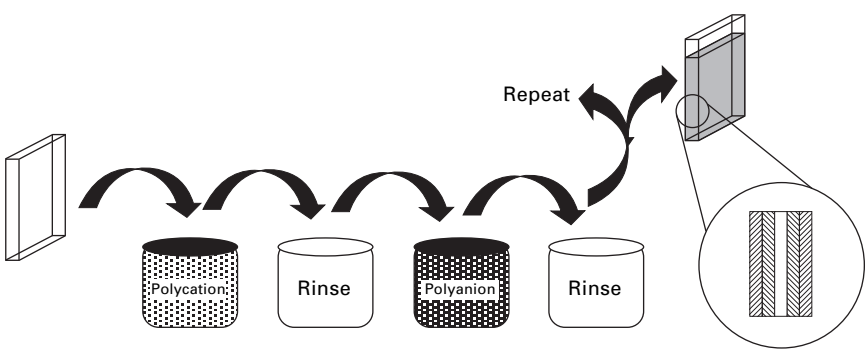
(Arbizzani *et al*., 2010; Bauer and Willert-Porada, 2004), silica titanium oxide (Daiko *et al*., 2006), zeolites (Yildrim *et al*., 2009) and silicon-aluminum oxide (Ismail *et al*., 2009) have been the focus of research in the field of direct methanol fuel cells in order to reduce methanol crossover. In particular, Nafion has been modified by these inorganic nanoparticles to introduce winding pathways for methanol, since the crossover of methanol presents a serious issue in direct methanol fuel cells. The crossover of methanol is caused by two different effects: (1) the protonic drag of methanol, where methanol is easily transported together with protons through the membrane and (2) diffusion through waterfilled channels. Since these effects may also be the origin of vanadium crossover, research was done into incorporation of inorganic particles into CEMs suitable for VRFBs.

Xi *et al*. (2007) for example, employed successfully a Nafion/SiO_2 (prepared by the sol–gel route) membrane to the VRFB system. The results showed that the incorporation of the SiO_2 decreased efficiently the vanadium crossover. This was attributed to the filling of the polar clusters of Nafion by silica nanoparticles. This results in a better coulomb and energy efficiency but also in lower self-discharge rate of the VRFB.

Modification with polyelectrolyte multilayers

Layer by Layer (LbL) deposition of polyelectrolytes represents a surface modification method. In the LbL, polyelectrolyte membranes which have to be modified on the surface (in this case Nafion) will be immersed first in a positively charged polyelectrolyte solution followed by a washing step with deionized water (Fig. 13.9).

After the washing step the same membrane is immersed into a negatively charged polyelectrolyte solution. Repeating these steps a mono layer of self assembled cationic and anionic charged layers will accumulate on the surface, which is stabilized by ionic interactions. By this simple method



13.9 Layer-by-layer surface modification.

© Woodhead Publishing Limited, 2011

the modification of a polyelectrolyte membrane by thin stacked oppositely charged thin layer polyelectrolytes thin films can be achieved, within the nanoscale (Chao *et al.*, 1991; Decher, 1997).

In DMFC applications LbL modified membranes are mainly applied to decrease the methanol crossover (Jiang *et al.*, 2006). However, in VRFB, it has been observed (Xi *et al.*, 2008) that LbL modified Nafion membranes show a lower vanadium crossover and with that an increase of coulomb and energy efficiency but also a lower self-discharge rate.

However, research also has to be done on CEM materials in order to reduce the vanadium crossover and the price. New materials and modified CEMs used in VRFB application are listed in Table 13.5.

13.3.2 Anion exchange membranes

Anion exchange membranes (AEM) are membranes which have positively charged functional groups. These membranes allow the transport of anions, while rejecting cations. A recent review summarizes the properties of AEMs for use in alkaline fuel cells (Merle *et al.*, 2011). However, the properties of the AEMs initiated some work in the field of polyelectrolyte membrane separators for the VRFB to obtain low vanadium crossover and low water crossover. Since the AEMs are positively charged only anions can pass: the crossover of positively charged vanadium ions will be decreased drastically. Due to the decreased crossover of the vanadium species, the water crossover will be minimized as well, since it is dependent on the vanadium crossover. Even though the AEM rejects cations, protons will diffuse through the membrane since their exclusion by the anion exchange membrane is less effective. In fact, it is desired to use a so-called proton-leaking AEM so that proton transport happens through 'leakage' as well as vanadium rejection. The chemical stability seems to be less under the harsh conditions in the VRFB (Zhang *et al.*, 2010) compared with CEMs. These issues might have been the reason for the little research on AEMs for VRFB application.

13.3.3 Amphoteric ion exchange membranes

The amphoteric ion exchange membranes (AIEM) contain cationic as well as anionic exchange groups as first proposed in 1932 by Sollner (1932). The advantage of AIEM is that the adjustment of the composition and the external conditions allows the control the ion exchange properties. Because of this, AIEMs show high potential in different applications (Qiu *et al.*, 2009b). However, only this research group has been investigating the AIEM in the VRFB (Qiu *et al.*, 2009b). The study shows that owing to adjustments in the cation and anion exchange group composition, vanadium as well as water crossover can be decreased drastically leading to an open circuit

© Woodhead Publishing Limited, 2011

Table 13.5 Cation exchange membranes for VRFB application

Membrane material	Conductivity (mS/cm)	VRFB performance (developed) membrane/Nafion			Reference
		CE%	EE%	VE%	
Sulfonated poly fluorenyl ether ketone	17	79.5 / 76.8	49.7/40.2	–	Chen *et al.* (2010b)
Sulfonated poly ether ether ketone/ tungstophosphoric acid/polypropylene	18.4	93/–	87/–	93/–	Jia *et al.* (2010)
Nafion/TiO_2	17.8	94.8/90.8	77.9/77	77.9/77	Teng *et al.* (2009b)
Nafion/SiO_2	57.5	95.8/92.1	87.4/73.8	96.5/94.4	Teng *et al.* (2009a)
Nafion/poly(diallyldimethylammonium chloride)/poly(sodium styrene sulfonate)	48.8–51.8	97.6/90	83.9/73.5	92.5/90	Xi *et al.* (2008)
Poly(vinylidenedifluoride)/ polystyrene/polymaleic anhydride	up to 200	–	–	–	Qiu *et al.* (2008)
Poly(vinylidene fluoride)/graft-poly(styrene sulfonic acid)	32.2	90 / 90	75.8 / 74.7	–	Luo *et al.* (2005)
Nafion/polyethylenimine	–	96.2–97.3/93.8	81.1–85.1/85.0	88.4–83.3/90.7	Luo *et al.* (2008a)
Nafion/sulfonated poly ether ether ketone	6.25	97.6/93.8	83.3/85.6	85.3/90.7	Luo *et al.* (2008b)
Sulfonated poly(fluorenyl ether ketone)/SiO_2	31.8	90.8/82.5	–	–	Chen *et al.* (2010a)
Sulfonated poly(tetramethydiphenyl ether ether ketone)	–	91.1–98.5/91.7	84.0–87.5/84.7	86.3–88.8/92.3	Mai *et al.* (2011)
Nafion/SiO_2	56.2	85/72.5	79.9/73.8	95/95	Xi *et al.* (2007)
Nafion/ZrP	14–17	–	–	–	Sang *et al.* (2007)
Sulfonated polystyrene	–	90/–	73/–	81/–	Skyllas-Kazacos *et al.* (1987)
Sulfonated polysulfone	–	97.8/95	83.7/83.3	–	Kim *et al.* (2010)
Nafion/polypyrrole	0.77–7.8	–	–	–	Zeng *et al.* (2008)
Fluorene-containing sulfonated poly(arylene ether sulfone)	8.2	70.9/62.9	–	–	Chen *et al.* (2010c)

© Woodhead Publishing Limited, 2011

Table 13.6 Anion exchange membranes for VRFB application

Membrane material	Conductivity (mS/cm)	VRFB performance (developed) membrane/Nafion			Reference
		CE%	EE%	VE%	
Poly(methacryloxyethyl dimethylammonium chloride)	3.04	–	–	–	Qiu *et al.* (2007)
Quaternized poly (phthalazinone ether sulfone)	up to 10	98.7/95.9	83.4/86	84.5/89.7	Xing *et al.* (2010)
Chloromethylated poly(phthalazione ether sulfone)	–	–	–	–	Xing *et al.* (2009)
Crosslinked new selemion	–	–	82/–	87.7/–	Hwang and Ohya (1997)

Table 13.7 Amphoteric ion exchange membranes for VRFB application

Membrane material	Conductivity (mS/cm)	VRFB performance (developed) membrane/Nafion			Reference
		CE%	EE%	VE%	
Poly(vinylidenefluodiride)/Styrene/ dimethylaminoethyl methacrylate	19–52	–	–	–	Qiu *et al.* (2009a)
Poly(ethylene-co-tetra fluoroethylene)/styrene/ dimethylaminoethylmethacrylate	39–48	95.6/87.9	75.1/72.6	78.6/82.6	Qiu *et al.* (2009b)
Sulfonated AMV	–	96/–	79.2/–	82.5/–	Mohammadi and Skyllas-Kazacos (1996)
Poly(sodium 4-styrenesulfoanate) selemion	–	100/–	83.4/–	83.4/–	Mohammadi and Skyllas-Kazacos (1996)

© Woodhead Publishing Limited, 2011

potential which is 100 times more stable than using Nafion 117 as a CEM for the VRFB. The adjustment of the oppositely charged and fixed groups of the polyelectrolyte will decrease the vanadium permeability for the same reason as in the case of LbL modified membranes. Unfortunately the work presented does not include any CE, EE and VE measurements. The same group investigated the amphoteric membranes prepared by grafting (Qui *et al.*, 2009b). Here the result showed clearly that the application of a membrane bearing positive and negative charges can indeed increase the performance of the VRFB. This is also due to the 130 to 200 times lower vanadium permeability. The membrane stability in the VRFB was tested up to ~ 45 cycles. The values for the voltage efficiency, energy efficiency and coulomb efficiency showed more deviation in the last cycles from cycle number 30. However, this was not commented in the publication, which might be to our opinion an instability of the membrane itself.

13.4 Conclusions

Energy storage systems such as the VRFB rely on ion-exchange based membranes. We report on state-of-the-art materials and reflect on their properties in terms of conductivity, chemical stability and crossover properties. In contrast to fuel cell applications where the scientific literature gives exhaustive details of the technical aspects involved, the literature on energy storing redox flow batteries is much less developed. As energy storage research intensifies over the coming decade, so will research for better membrane materials. A decrease in vanadium crossover at high ionic conductivity and extensive material lifetime are desirable.

13.5 References

Antonucci PL, and Aricò AS, and Cretì P and Ramunnic E, and Antonucci V (1999). Investigation of a direct methanol fuel cell based on a composite Nafion®-silica electrolyte for high temperature operation. *Solid State Ionics*, **125**(1–4): 431–437.

Arbizzani C, and Donnadio A, and Pica M, and Sganappa M, and Varzi A, and Casciola M, and Mastragostino M (2010). Methanol permeability and performance of Nafion–zirconium phosphate composite membranes in active and passive direct methanol fuel cells. *Journal of Power Sources*, **195**(23): 7751–7756.

Bauer F, and Willert-Porada M (2004). Microstructural characterization of Zr-phosphate–Nafion® membranes for direct methanol fuel cell (DMFC) applications. *Journal of Membrane Science*, **233**(1–2): 141–149.

Chao, L. and Charles, M.R. (1991). Composite membranes from photochemical synthesis of ultrathin polymer films. *Nature* **352**: 50–52

Chen D, and Wang S, and Xiao M, and Han D, and Meng Y (2010a). Sulfonated poly (fluorenyl ether ketone) membrane with embedded silica rich layer and enhanced

© Woodhead Publishing Limited, 2011

proton selectivity for vanadium redox flow battery. *Journal of Power Sources*, **195**(22): 7701–7708.

Chen D, and Wang S, and Xiao M, and Meng Y (2010). Preparation and properties of sulfonated poly(fluorenyl ether ketone) membrane for vanadium redox flow battery application. *Journal of Power Sources*, **195**(7): 2089–2095.

Chen D, and Wang S, and Xiao M, and Meng Y (2010c). Synthesis and properties of novel sulfonated poly(arylene ether sulfone) ionomers for vanadium redox flow battery. *Energy Conversion and Management*, **51**(12): 2816–2824.

Chen H, and Cong TN, and Yang W, and Tan C, and Li Y, and Ding Y (2009). Progress in electrical energy storage system: A critical review. *Progress in Natural Science*, **19**: 290–312.

Chienga SC, and Kazacosa M, Skyllas-Kazacos M (1992). Modification of Daramic, microporous separator, for redox flow battery applications. *Journal of Membrane Science*, **75**(1–2): 81–91.

Clarke RL, and Dougherty BJ, and Harrison S, and Millington JP, and Mohanta S. (2007). Battery with bifunctional electrolyte.

Daiko Y, and Klein LC, and Kasuga T, and Nogami M (2006). Hygroscopic-oxides/Nafion® hybrid electrolyte for direct methanol fuel cells. *Journal of Membrane Science*, **281**(1–2): 619–625.

Decher G (1997). Fuzzy nanoassemblies: toward layered polymeric multicomposites. *Science*, **277**(5330): 1232–1237.

Hagedorn NH and Thaller LH (1982). *Design flexibility of redox flow systems*. Technical report, TM-82854, DOE/NASA/12726-16, NASA.

Hosseiny SS, and Saakes M, and Wessling M (2011). A polyelectrolyte membrane based vanadium/air redox flow battery. *Electrochemistry Communications*, DOI:10.1016/j.elecom.2010.11.025.

Hwang G-J, and Ohya H (1997). Crosslinking of anion exchange membrane by accelerated electron radiation as a separator for the all-vanadium redox flow battery. *Journal of Membrane Science*, **132**(1): 55–61.

Ismail AF, and Othmana NH, and Mustafa A (2009). Sulfonated polyether ether ketone composite membrane using tungstosilicic acid supported on silica–aluminium oxide for direct methanol fuel cell (DMFC). *Journal of Membrane Science*, **329**(1-2): 18–29.

Jia C, and Liu J, and Yan C (2010). A significantly improved membrane for vanadium redox flow battery. *Journal of Power Sources*, **195**(13): 4380–4383.

Jiang R, and Russell Kunz H, and Fenton JM (2006). Composite silica/Nafion® membranes prepared by tetraethylorthosilicate sol–gel reaction and solution casting for direct methanol fuel cells. *Journal of Membrane Science*, **272**(1–2): 116–124.

Jung DH, and Cho SY, and Peck DH, and Shina DR, and Kim JS (2002). Performance evaluation of a Nafion/silicon oxide hybrid membrane for direct methanol fuel cell. *Journal of Power Sources*, **106**(1–2): 173–177.

Kiehne HA (2003). *Battery Technology Handbook*. Expert Verlag, Renningen-Malsheim, Germany.

Kim S, and Schwenzer B, and Zhang J, and Li L, and Liu J, and Yang Z, and Hickner MA (2010). Cycling performance and efficiency of sulfonated poly(sulfone) membranes in vanadium redox flow batteries. *Electrochemistry Communications*, **12**(11): 1650–1653.

Kreuer KD (2001). On the development of proton conducting polymer membranes for hydrogen and methanol fuel cells. *Journal of Membrane Science*, **185**(1): 29–39.

© Woodhead Publishing Limited, 2011

Lex P, and Jonshagen B (1999). The zinc/bromine battery system for utility and remote area applications. *Power Engineering Journal,* **13**(3), 142–48.

Liu C, and Martin CR (1991). Composite membranes from photochemical synthesis of ultrathin polymer films. *Nature*, **352**(6330): 50–52.

Luo Q, and Zhang H, and Chen J, and Qian P, and Zhai Y (2008b). Modification of Nafion membrane using interfacial polymerization for vanadium redox flow battery applications. *Journal of Membrane Science*, **311**(1–2): 98–103.

Luo Q, and Zhang H, and Chen J, and You D, and Sun C, and Zhang Y (2008a). Preparation and characterization of Nafion/SPEEK layered composite membrane and its application in vanadium redox flow battery. *Journal of Membrane Science*, **325**(2): 553–558.

Luo X, and Lu Z, and Xi J, and Wu Z, and Zhu W, and Chen L, and Qiu, X (2005). Influences of permeation of vanadium ions through PVDF-g-PSSA membranes on performances of vanadium redox flow batteries. *The Journal of Physical Chemistry B*, **109**(43): 20310–20314.

Mai Z, and Zhang H, and Li X, and Bi C, and Dai H (2011). Sulfonated poly(tetramethydiphenyl ether ether ketone) membranes for vanadium redox flow battery application. *Journal of Power Sources*, **196**(1): 482–487.

Merle G, and Wesslinga M, and Nijmeijer K (2011). Anion exchange membranes next term for alkaline fuel cells: A review. *Journal of Membrane Science*, DOI: 10.1016/j.memsci.2011.04.043, **337**, issues 1–2, 1–35.

Miyake S (2002). *Battery Diaphragm*. US Patent, No. US 6461772 B1.

Mohammadi T, and Skyllas-Kazacos M (1995a). Characterisation of novel composite membrane for redox flow battery applications, *Journal of Membrane Science*, **98**(1–2): 77–87.

Mohammadi T, and Skyllas-Kazacos M (1995b). Preparation of sulfonated composite membrane for vanadium redox flow battery applications. *Journal of Membrane Science*, **107**(1–2): 35–45.

Mohammadi T, and Skyllas-Kazacos M (1995c). Use of polyelectrolyte for incorporation of ion-exchange groups in composite membranes for vanadium redox flow battery applications. *Journal of Power Sources*, **56**(1): 91–96.

Mohammadi T, and Skyllas Kazacos M (1996). *Journal of Power Sources*, **63**(2): 179–186.

Mohammadi T, and Chieng S C, and Skyllas Kazacos M (1997). Water transport study across commercial ion exchange membranes in the vanadium redox flow battery. *Journal of Membrane Science*, **133**(2): 151–159.

Ponce de León, C., Frias-Ferrer, A, González-García, J, Szánto, D.A. and Walsh, F.C. (2006). *Journal of Power Sources*, **160**(1): 716–732.

Price A, and Bartley S, and Male S, and Cooley G (1999). A novel approach to utility-scale energy storage. *Power Engineering Journal*, **13**(3): 122–129.

Qiu J, and Li M, and Ni J, and Zhai M, and Peng J, and Xu L, and Zhou H, and Li J, and Wei G (2007). Preparation of ETFE-based anion exchange membrane to reduce permeability of vanadium ions in vanadium redox battery. *Journal of Membrane Science*, **297**(1–2): 174–180.

Qiu J, and Zhai M, and Chenb J, and Wang Y, and Peng J, and Xu L, and Li J, and Wei G (2009b). Performance of vanadium redox flow battery with a novel amphoteric ion exchange membrane synthesized by two-step grafting method. *Journal of Membrane Science*, **342**(1–2): 215–220.

Qiu J, and Zhang J, and Chen J, and Peng J, and Xu L, and Zhaia M, and Li J, and Weia G (2009a). Amphoteric ion exchange membrane synthesized by radiation-induced

© Woodhead Publishing Limited, 2011

graft copolymerization of styrene and dimethylaminoethyl methacrylate into PVDF film for vanadium redox flow battery applications. *Journal of Membrane Science*, **334**(1–2): 9–5.

Qiu J, and Zhao L, and Zhai M, and Ni J, and Zhou H, and Peng J, and Li J, and Wei G (2008). Pre-irradiation grafting of styrene and maleic anhydride onto PVDF membrane and subsequent sulfonation for application in vanadium redox batteries. *Journal of Power Sources*, **177**(2): 617–623.

Sang S, and Wu Q, and Huang K (2007). Preparation of zirconium phosphate (ZrP)/ Nafion1135 composite membrane and H+/VO2+ transfer property investigation. *Journal of Membrane Science*, **305**(1–2): 118–124.

Skyllas-Kazacos M (2003). Novel vanadium chloride/polyhalide redox flow battery. *Journal of Power Sources*, **124**(1): 299–302.

Skyllas-Kazacos, M. and Grossmith, F. (1987). Efficient vanadium redox flow cell. *Journal of the Electrochemical Society*, ECS, **134**: 2950–2953.

Skyllas-Kazacos M, and Rychick M, and Robins R (1988). All-vanadium redox battery.

Sollner K (1932). On mosaic membranes. *Biochem. Z.*, **244**: 370–381.

Sukkar T, and Skyllas-Kazacos M (2003). Modification of membranes using polyelectrolytes to improve water transfer properties in the vanadium redox battery. *Journal of Membrane Science*, **222** (1–2): 249–264.

Sun C, and Chen J, and Zhang H, and Han X, and Luo Q (2010). Investigations on transfer of water and vanadium ions across Nafion membrane in an operating vanadium redox flow battery. *Journal of Power Sources*, **195**(3): 890–897.

Teng X, and Zhao Y, and Xi J, and Wu Z, and Qiu X, and Chen L (2009b). Nafion/ organically modified silicate hybrids membrane for vanadium redox flow battery. *Journal of Power Sources*, **189**(2): 1240–1246.

Teng X, and Zhao Y, and Xi J, and Wu Z, and Qiu X, and Chen L (2009a). Nafion/organic silica modified TiO2 composite membrane for vanadium redox flow battery via *in situ* sol-gel reactions. *Journal of Membrane Science*, **341**(1–2): 149–154.

Tian B and Yan CW, and Wang FH (2004). Proton conducting composite membrane from Daramic/Nafion for vanadium redox flow battery. *Journal of Membrane Science*, **234**(1–2): 51–54.

Xi J, and Wu Z, and Qui, X, and Chen L (2007). Nafion/SiO_2 hybrid membrane for vanadium redox flow battery. *Journal of Power Sources*, **166**(2): 531–356.

Xi J, and Wu Z, and Teng X, and Zhao Y, and Chen L, and Qiu X (2008). Self-assembled polyelectrolyte multilayer modified Nafion membrane with suppressed vanadium ion crossover for vanadium redox flow batteries. *Journal of Materials Chemistry*, **18**(11): 1232–1238.

Xing D, and Zhang S, and Yin C, and Yan C, and Jian X (2009). Preparation and characterization of chloromethylated/quanternized poly(phthalazinone ether sulfone) anion exchange membrane. *Materials Science and Engineering: B*, **157**(1–3): 1–5.

Xing D, and Zhang S, and Yin C, and Zhang B, and Jian X (2010). Effect of amination agent on the properties of quaternized poly(phthalazinone ether sulfone) anion exchange membrane for vanadium redox flow battery application. *Journal of Membrane Science*, **354**(1–2): 68–73.

Yildirim MH, and Roca Curòs A, and Motuzas J, and Julbe A, and Stamatialis DF, and Wessling M (2009). Nafion/H-ZSM-5 composite membranes with superior performance for direct methanol fuel cells. *Journal of Membrane Science*, **338**(1–2): 75–83.

© Woodhead Publishing Limited, 2011

Zeng J, and Jiang C, and Wang Y, and Chen J, and Zhu S, and Zhao B, and Wang R (2008). Studies on polypyrrole modified nafion membrane for vanadium redox flow battery. *Electrochemistry Communications*, **10**(3): 372–375.

Zhang S, and Yin C, and Xing D, and Yang D, and Jian X (2010). Preparation of chloromethylated/quaternized poly(phthalazinone ether ketone) anion exchange membrane materials for vanadium redox flow battery applications. *Journal of Membrane Science*, **363**(1–2): 243–249.

© Woodhead Publishing Limited, 2011

14
Membranes for lithium batteries

R. BONGIOVANNI and J. RAVI NAIR, Politecnico di Torino, Italy; C. GERBALDI, Italian Institute of Technology and Politecnico di Torino, Italy and A. M. STEPHAN, Central Electrochemical Research Institute, India

Abstract: By virtue of their high energy efficiency, lithium batteries can provide an energy return factor higher than conventional batteries and are expected to become the power source of choice for sustainable transport. High performing innovative materials are crucial for large-scale diffusion of Li-based cells. The electrodes need to have greater capacity and durability, while the electrolyte, currently in the liquid state, should be a solid membrane capable of high ionic conductivity even at ambient temperature, with good mechanical and interfacial properties. After a general introduction to lithium batteries, this chapter describes polymeric membranes that have up until now been proposed as electrolytes.

Key words: cross-linked membranes, electrolyte, gel polymers, lithium batteries, polymeric electrolytes, solid polymers.

14.1 Introduction

Electrochemical systems, such as batteries and supercapacitors, play a crucial role in the modern era as they can efficiently store and deliver energy on demand in stand-alone power plants and, in addition provide power quality and load levelling of the electrical grid in integrated systems. Because they have a high energy efficiency, lithium-based batteries are expected to provide an energy return factor greater than that assured by conventional batteries. In addition, they are also regarded as the preferred power source for sustainable transport and are becoming the best option for the increasing use of hybrid electric vehicles.

Lithium-ion batteries represent one of the major successes of modern electrochemistry (Scrosati, 1995). They are compact, lightweight, rechargeable power sources and are stable for over 700 cycles; because of their higher energy and power density, they outperform many other conventional systems, such as the lead–acid, nickel–cadmium and nickel–metal hydride batteries. They allow design flexibility and can be fabricated in different sizes ranging from few micrometres to large-scale batteries; they are commonly used in laptops because they are smaller and lighter than alternative power sources.

© Woodhead Publishing Limited, 2011

They could replace the nickel–metal hydride batteries used in electric vehicles (EVs) and hybrid-electric vehicles (HEVs); by reducing weight, they help cut costs, reduce the environmental impact and improve fuel economy. Finally lithium batteries are based on components that are considered environmentally acceptable.

Although these batteries are already commercially successful, with the electrodes and electrolytes currently used they have reached the limits of their performance, which strongly depends on the materials employed. So the development of innovative, low cost, ecologically friendly and safe materials is of crucial importance for advances in battery technology (Goodenough and Kim, 2010; Scrosati and Garche, 2010); these materials can boost new generations of rechargeable lithium batteries for application in consumer electronics, as well as clean energy storage and hybrid electric vehicles (Fergus, 2010). Therefore nowadays a main research stream concerns the preparation of electrode materials that assure increased energy density, faster discharge kinetics and better stability; in this area the nanostructuring of materials has proved to be one of the best strategies. Another fundamental research theme is the development of materials that will be safer and more reliable electrolytes, replacing the currently used liquid solutions of lithium salts, which mainly employ organic carbonates as solvent. The goal is to obtain a solid membrane capable of high ionic conductivity even at ambient temperature, guaranteeing good mechanical properties, appropriate interfacial properties and stable electrochemical performances, being easily processable and of low cost. This challenge is the focus of this chapter.

14.2 Types of lithium battery and basic operating principles

A battery is an electrochemical power source composed of several units called cells, connected in series or parallel (or a combination of both) depending on the desired output voltage and capacity. A battery stores energy in chemical form in its active materials and can directly convert it into electrical energy on demand, typically by means of a spontaneous electrochemical oxidation–reduction (redox) reaction (Linden, 1994). Each cell consists of three major components, a positive and a negative electrode (both sources of chemical reactions) and an electrolyte separating them. Typically the electrolyte contains dissociated salts and enables ion transfer between the two electrodes. Once these electrodes are externally connected, the chemical reactions proceed in tandem at both electrodes, thereby liberating electrons and enabling the current to be tapped by the user. In particular, a rechargeable battery is made of electrodes that can be reconstituted to their original condition, after discharge, by passing electricity back through them.

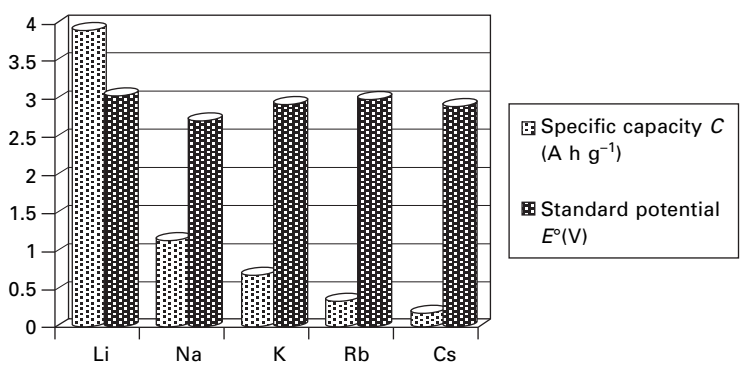
© Woodhead Publishing Limited, 2011

A rechargeable battery is also called a secondary battery, storage battery or accumulator, as it can be reused many times.

The most well-known rechargeable battery is the wet cell lead–acid battery. Although its design is very old and it has one of the worst energy-to-weight ratios, it is still in use, as the power-to-weight and energy-to-volume ratios can be quite good, it is cheap and can supply the high surge currents needed to start a motor. More portable rechargeable batteries include several 'dry cell' types, which are sealed units and are, therefore, useful in appliances like mobile phones and laptops. Cells of this type (in order of increasing power density and cost) include nickel–cadmium (Ni-Cd) and nickel–metal hydride (Ni-MH) cells. The progressively increasing demand for energy density arising from the market of portable devices stimulated the development of more advanced technologies than Ni–Cd and Ni–MH. In order to maximize the voltage, the natural choice was the use of the most electropositive alkali metal, that is lithium, which is also the lightest element of the series and is more easily handled than other alkali metals (Fig. 14.1).

The substitution of aqueous by non-aqueous electrolytes then became compulsory, thus expanding the electrochemical stability window of the batteries in the presence of water (ΔV = 1.23 V); this led to a higher cell voltage and, consequently, to a higher energy density.

Lithium and its compounds will probably remain a good choice for decades to come, because they can readily produce free electrons and Li^+ ions which are light (low mass density), small in size and have both a high mobility and a fast transport speed. This gives Li-based batteries a net advantage over many other battery systems; they are also preferred for being more environmentally friendly than Ni-Cd cells and Pb-acid cells which contain toxic and fairly heavy elements (cadmium and lead, respectively). Lithium is present in the upper 16 km of the Earth's crust to the extent of ca. 0.006% wt/wt; it is the 27th most abundant element and the lightest metal in the periodic table with



14.1 Specific capacity and standard potential of the alkali metals series.

© Woodhead Publishing Limited, 2011

an equivalent weight of 6.94 g mol^{-1} and a specific gravity of 0.53 g cm^{-3}. This last property is very attractive for the development of a lightweight battery, together with the electrochemical properties of the metal. Lithium has a specific capacity of 3.86 A h g^{-1} (Tarascon and Armand, 2001) and a high electrochemical potential of – 3.045 V versus the standard hydrogen electrode (SHE), which holds out the promise of a >3 V battery when combined with a suitable positive electrode, thus facilitating the design of storage systems with a high energy density.

In the 1970s, a new Li-ion secondary cell chemistry was proposed based on 'intercalation/de-intercalation' or 'insertion/de-insertion' processes. This means that rather than a traditional redox galvanic action, the electrochemical mechanism is based on Li^+ ions entering and exiting the electrode materials.

During charge, the Li^+ ions are de-inserted from the positive electrode, with relative oxidation of the active material $Li_xM_yY_z$, according to the reaction:

$$Li_xM_yY_z \leftrightarrow Li_{(x-n)}M_yY_z + nLi^+ + ne^- \quad [14.1]$$

Then they migrate across the electrolyte and are inserted into the crystal structure of the negative active material, which is reduced. At the same time, the compensating electrons travel through the external circuit and are accepted by the host to balance the reaction.

The discharge process is just the opposite:

$$A_mB_w + nLi^+ + ne^- \leftrightarrow Li_nA_mB_w \quad [14.2]$$

Accordingly, the overall reaction can be generalized as follows:

$$Li_xM_yY_z + A_mB_w \leftrightarrow Li_{(x-n)}M_yY_z + Li_nA_mB_w \quad [14.3]$$

The process is completely reversible. Thus, the lithium ions pass back and forth between the electrodes during charging and discharging. This has given rise to the names 'rocking chair' (Scrosati, 1992), 'swing' (Brandt, 1994) or 'shuttlecock' (Ohzuku *et al.*, 1993) to describe the Li-ion cells. As a rule, the term 'intercalation' is used mostly when the host substance has a layered morphology, while the term 'insertion' is preferred for those substances with a three-dimensional framework containing cavities connected by narrow channels. As a consequence of the new chemistry, the active materials for Li-based batteries had to be both electronic as well as ionic conductors as the current flow depends not only on electronic conductivity but also on the mobility of Li^+ ions. This led to the development of rechargeable lithium batteries using lithium insertion compounds as positive electrodes and lithium metal as the negative electrode. These systems can provide both very high voltage and outstanding specific capacity, resulting in excellent energy density. The first cell of this kind appeared when Exxon tried to commercialize a

© Woodhead Publishing Limited, 2011

system using TiS_2 as the positive electrode, Li metal as the negative electrode and lithium perchlorate in dioxolane as the electrolyte. It was simply called a 'lithium battery', but now it is identified as the Li-metal battery which has lithium metal as the negative electrode (Whittingham, 1976).

During the 1980s, scientific research showed that lithium metal at the negative electrode has stability problems during cycling. In fact, it was found that cycling alters the lithium metal electrode, thereby reducing its thermal stability and causing potential thermal runaway. Whenever this happens, the cell temperature quickly approaches the melting point of lithium, which causes a violent reaction and can even lead to explosion hazards.

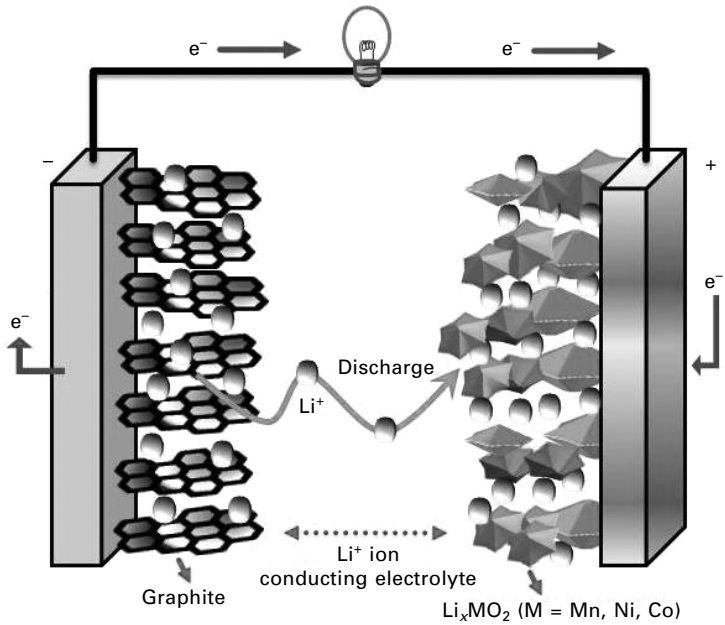
To circumvent the safety issues connected to the use of lithium metal, several alternatives were pursued in which either the electrolyte or the negative electrode were modified. The first approach (Scrosati, 1992) involved replacing metallic lithium by a second insertion host with a significantly lower standard reduction potential than that of the hosts used for the positive electrode (Whittingham, 2008). This concept was first demonstrated by Murphy *et al*. (1978) and then by Lazzari and Scrosati (1980). At the end of the 1980s and in early 1990s the so called lithium-ion (Li-ion) battery appeared. The Li-ion battery defines the state of lithium at the anode as Li^+, not Li^0; thus the active anode material is an intercalation compound of Li ions, which are extracted from/inserted into the active materials. Because of the presence of lithium in its ionic form rather than in the metallic state, Li-ion cells solve the problem of stability and in principle, are inherently safer than Li-metal cells, although providing a lower voltage and a lower capacity.

In the early 1980s, Mizushima *et al*. (1980) and Thackeray *et al*. (1983), proposed the use of high voltage metal oxides (Li_xMO_2, where M = Ni, Co or Mn); these are still the most commonly used cathodes in commercial Li-ion cells. Later, the discovery of a highly reversible, low voltage lithium intercalation/de-intercalation process in carbonaceous material (Mohri *et al*., 1989) led to the creation of the first Li-ion cell based on $C/LiCoO_2$, which was commercialized by Sony Corporation (Nagaura and Tozawa, 1990). This type of cell has an operational voltage of 3.6 V (three times higher than alkaline systems), energy densities as high as 120–150 Wh kg^{-1} (two to three times those of standard Ni-Cd batteries) and a cycle life of at least 700 deep discharges; it is found in most of today's high-performance portable electronic devices.

The working principle of a secondary Li-ion battery is explained in Fig. 14.2.

Besides substituting lithium metal with less reactive and safer materials to avoid reaction of metallic lithium with the liquid electrolyte, in the 1980s replacement of the latter by a solid electrolyte was proposed. The obvious advantage of this approach is that it avoids leakage of electrolyte solution, which is one of the most undesirable features of many batteries.

© Woodhead Publishing Limited, 2011



14.2 Schematic representation of a common lithium-ion battery. Negative electrode – graphite, positive electrode – Li_xMO_2 (for example $LiCoO_2$), separated by a non-aqueous liquid electrolyte $LiPF_6$ ethylene carbonate/dimethyl carbonate (Mohri *et al.*, 1989). The removal of lithium ions by the simultaneous oxidation of M (e.g. cobalt) in the cathode and insertion of lithium ions into the graphite anode charges the battery. Electricity is produced when ions move in the opposite direction and the M (e.g. cobalt) is reduced.

The goal was then to identify solid materials that would provide a single-ion conduction mechanism, a permanent interface with Li metal and high total ionic conductivity. Not only could polymers satisfy these requirements, but they also assure flexibility, ease of manufacturing and low cost.

For the last three decades extensive effort has been dedicated to the development of Li-metal polymer batteries, in order to improve their cycle life, while maintaining their excellent energy density and high voltage (Tarascon and Armand, 2001). At the end of the twentieth century, Li-ion polymer batteries (usually called Li polymer batteries) were also introduced into the market in the form of thin-film cells (Tarascon *et al.*, 1996).

The next sections report a wide range of polymeric materials used as electrolytic membranes for lithium batteries.

© Woodhead Publishing Limited, 2011

14.3 Polymer electrolyte membranes for advanced lithium batteries

As mentioned earlier, internal short circuits, leaks, corrosive reactions and combustible reaction products at the electrode surface associated with liquid electrolytes can be prevented to a large extent by using polymeric membranes as electrolytes. Polymer electrolytes can be classified as follows:

- solid polymer electrolytes (SPEs)
- composite or nanocomposite polymer electrolytes (CPEs and NCPEs)
- gel/plasticized polymer electrolytes (GPEs)

SPEs are neat polymers which serve as both solvents to dissolve lithium salts and mechanical matrices to support processability. GPEs, also called polymer liquid electrolytes, are based on polymer gels where the polymer encages a liquid electrolyte solution and the polymer, swollen by the solvent, mainly provides dimensional stability. In a composite electrolyte, alternatively called 'composite polymer electrolytes' high surface area particulate fillers such as ZrO_2, TiO_2, Al_2O_3 and hydrophobic fumed silica are incorporated into the polymer matrices, eventually obtaining a dispersion at the nanoscale. These organic–inorganic systems can then be used either as all solid electrolytes or as gel electrolytes.

For each class, further groups based on the chemical architecture of the polymer matrix, namely thermoplastic polymers and cross-linked ones can be distinguished (i.e. elastomers or thermoset polymers). This last group will be discussed specifically later in the chapter.

Owing to poor ion conductivities ($\sigma = 10^{-6}$ S cm^{-1}), at present SPEs remain a topic of academic interest, with a remote chance of practical application; on the other hand, GPEs have shown much higher feasibility. The proximity of GPEs to conventional non-aqueous electrolytes, both for physical and electrochemical aspects, including their electrochemical stability on various electrodes and corresponding interfacial chemistry, makes them viable candidates for practical applications.

14.3.1 Solid polymer electrolyte (SPE) membranes

Wright and co-workers were the first to discover that an ether-based polymer, poly(ethylene oxide) (PEO), can dissolve inorganic salts and exhibit ion conduction at room temperature (Fenton *et al.*, 1973). Sequira and Hooper (1983) described the electrochemical properties of solid lithium systems. PEO-based electrolytes offer very low σ values that range from 10^{-8} to 10^{-4} S cm^{-1} at temperatures between 40 and 100°C, which excludes ambient temperature applications.

© Woodhead Publishing Limited, 2011

These novel materials were at the centre of electrolyte research by Armand (1994). The advantages that polymer electrolytes can offer are:

- excellent processability and flexibility that could enable the fabrication of ultrathin lithium cells with various geometric shapes so that high energy and power density can be achieved for versatile applications;
- higher safety owing to the absence of flammable organic solvents and the much lower reactivity of macromolecules toward lithium;
- possible prevention of the growth of Li dendrites upon cycling;
- high dimensional stability;
- improvement in energy density and reduction of manufacturing cost by simplified cell configuration and enhanced packing efficiency of the cell elements.

Ionic motion in polymer is closely associated with local structural relaxations of the macromolecule, which in turn can be adjusted either by changing the polymer architecture or introducing plasticizers. These polymer salt complexes exhibit mechanical properties, which are similar in most ways to those of true solids owing to chain entanglement of the polymer host. The microscopic environment remains liquid-like for the lithium ion, and the ion conductivity is 'coupled' to the local segmental motion of the polymer. The latter property is often characterized by the glass–rubbery phase transition temperature (T_g) of the polymer, which to a great extent determines the mechanical strength and hence processability of a polymer material. Ideally, polymers should have a T_g high enough to give the mechanical properties of a solid, but low enough to maintain mobility at room temperature as if they were liquid, thus preserving lithium ion conductivities similar to those of a typical liquid electrolyte system.

Various new polymers with low T_g have been investigated and are still under investigation. In addition to PEO, there is flexible polypropylene oxide that remains completely amorphous at room temperature, polysiloxanes (Rossi and West, 2009; Jiang and Fang, 2006) and polyphosphazene-based structures (Takeuchi *et al.*, 2001).

Comb-like polyethers have also been developed in which ether linkages are attached as side chains to the backbone so that more flexible segmental motion is possible. In the last two decades, following the initial work by Armand (1994), little progress has been made concerning the actual application of SPEs, where poor ion conduction is a seemingly insurmountable barrier. Owing to the low ionic conductivity, little has been known about the electrochemical stability of these polymer electrolytes on various intercalation-type electrode materials.

Operation at high temperature seems to be a solution for poor ion conductivity, but a high rate of degradation results, as indicated by the fading capacity of these cells. Angell and co-workers proposed an innovative

© Woodhead Publishing Limited, 2011

approach of 'polymer-in-salt' to bypass the poor ion conductivity of the 'salt-in-polymer' solid polymer electrolytes (Angell *et al.*, 1993). It consists of an 'ionic rubber', a polymer material with high molecular weight but low T_g, added in a low amount to the conductive liquid electrolyte to provide a fair mechanical strength and film processability. Conductivities are therefore similar to those of the liquid electrolytes, since most ions are free of coordination with polymer segments, owing to its small concentration.

The limitations of the ionic conductivity of amorphous polymers, despite significant improvements over the last 30 years, has led to the exploration of the use of crystalline polymer electrolytes (Bruce, 2008). Encouraged by the recognition that the ionic conductivity of ceramic electrolytes is higher than the best amorphous polymers, Gadjourova and co-workers (Gadjourova *et al.*, 2001) reported the first examples of ionically conducting crystalline PEO electrolytes, with a stoichiometry PEO_6:$LiXF_6$ (where, X = P, As, Sb). They have a crystal structure composed of pairs of PEO chains that fold to form tunnels within which Li^+ ions reside and migrate, the anions being located between the tunnels. The ionic conductivity achieved by these stoichiometric materials proved to be too low for practical application, but modified complexes raised the conductivity by up to three orders of magnitude. Modelling studies recognized and explained ion transport in these crystalline polymer electrolytes (Johansson and Jacobsson, 2003). The polymer film is composed of many grains each of which is composed of many crystallites. Alternating current (AC) impedance has shown no evidence of resistance to ion transport across the grain boundaries. Although the misalignment of crystallites within the grains may introduce some tortuosity for ion transport, experiments with tortuosity in ceramic conductors suggested that such effects are small (Staunton *et al.*, 2007). Modifying the chain ends can also raise the conductivity. Replacing the methyl $–CH_3$ groups, normally used to terminate the PEO chains, with bulkier groups, for example the ethyl $–C_2H_5$, results in retention of the same crystal structure but with a small shift in the lattice parameters. Although the structure and hence pathways for Li^+ migration are the same, additional disruption at the chain ends makes the coordination of Li^+ ions in these regions more difficult, that is less stable, hence more defects and higher conductivity are observed (Staunton *et al.*, 2007).

14.3.2 Composite and nanocomposite polymer electrolyte membranes

One of the most promising ways to improve the electrochemical and mechanical properties of polymer electrolytes is the addition of ceramic fillers (Manuel Stephan and Nahm, 2006; Croce *et al.*, 1998, 1999; Itoh *et al.*, 2003). It is well established that ceramic fillers improve the conductivity of the polymer hosts and enhance their interfacial properties when in contact with the lithium

© Woodhead Publishing Limited, 2011

electrode. An increase in ionic conductivity takes place when the polymer chains become more amorphous and recrystallization is hindered (Appetecchi *et al.*, 2000). In all the cases, the particle size and characteristics of the ceramic fillers play a key role in determining the electrochemical properties of the electrolytes.

In general, ceramic particles used in the polymer matrix are broadly classified into two categories: active fillers and passive fillers. The active fillers, such as Li_2N and $LiAl_2O_3$ materials, take part in the conduction process, while inactive materials such as Al_2O_3, SiO_2 and MgO are not involved in the lithium transport process. The selection of fillers between active and passive components is quite arbitrary. In a pioneering research work, Weston and Steele (Weston and Steele, 1982) first demonstrated the effect of incorporating inert filler (α-alumina) in the PEO system. The mechanical strength and the ionic conductivity were significantly enhanced upon the addition of inert particles in the polymer composite systems. Entropy effects of the introduction of alumina in PEO and PEO blend-based systems were also reported (Wieczorek, 1992).

The specific interactions involved between the surface groups of the ceramic particles and both the PEO segments and the lithium salt anions are further interpreted in terms of Lewis acid–base interactions (Wieczorek *et al.*, 1996). The Lewis acid groups of the added ceramic particles (e.g. the –OH groups on the Al_2O_3 surface) are likely to compete with the Lewis acid lithium cations for the formation of complexes with the PEO chains, as well as with the anions of the added LiX salt (Croce *et al.*, 2001). The ceramic's surface –OH groups are expected to favour interactions (via hydrogen bonding) with both the lithium salt anion and the PEO segments, with a consequent increase in salt dissociation and in the local PEO amorphous phase fraction; these changes are reflected in the enhancements of lithium ion transference number (T_{Li}^{+}) and ionic conductivity. The contribution of Al_2O_3 varies if the surface groups change. With neutral alumina, owing to the lower extent of the ceramic's surface groups, weaker interactions with both the lithium salt anion and the PEO segments are expected, with less important enhancements both in T_{Li}^{+} and in ionic conductivity. Finally, in the case of basic Al_2O_3, few surface effects are expected and thus, no macroscopic changes of ionic transport properties with respect to ceramic-free polymer electrolytes are foreseen. In summary, the extent of structural modifications induced by the ceramics should increase according to the following sequence: Al_2O_3 acidic > Al_2O_3 neutral > Al_2O_3 basic.

The filler content generally influences the ionic conductivity. The dilution effect which tends to depress the conductivity is efficiently contrasted by the specific interactions of the ceramic surface, which can promote fast ion transport. Thus, the net result is a progressive enhancement of the conductivity. At high filler content, the dilution effect predominates and the conductivity

© Woodhead Publishing Limited, 2011

decays. Thus, a maximum in the conductivity versus composition curve is expected, generally occurring around 8–10 wt% (Croce *et al.*, 2001). The enhancement in conductivity when the polymer is in its amorphous state is precise evidence of a promoting effect resulting from specific interactions at the surface of the ceramics. T_{Li^+} showed a progressive increase from the ceramic-free material to the three composites which in turn have basic, neutral and acidic Al_2O_3. Panero *et al.* (1992) observed that the addition of up to 30 wt% inert filler, γ-$LiAlO_2$, improved the mechanical properties but had a negligible effect on ionic conductivity.

There have been many more studies into understanding the effect of solid fillers, quantity of filler, size, type, nature, and so on. All kinds of particles have been studied by different research groups. The most studied ceramic fillers include: SiO_2, γ-$LiAlO_2$, ferroelectric materials ($BaTiO_3$, $PbTiO_3$, $LiNbO_3$), MgO, TiO_2, ZrO_2, SiC and zeolites (Kumar and Scanlon, 1994; Borghini *et al.*, 1995; Kim *et al.*, 2003; Golodnitski *et al.*, 2002; Shin and Passerini, 2004). Every material has its peculiarities and influences on the final properties. In every case either conductivity and/or mechanical properties are improved along with some improvements in transport characteristics.

14.3.3 Gel polymer electrolyte (GPE) membranes

Dry polymer electrolyte systems, typically represented by PEO/LiX systems, offer very low ionic conductivity at ambient temperature which excludes this type of membrane from practical applications. Hence, large research efforts have been devoted to expanding the region of operation of the PEO/LiX matrix. The most common approach is the addition of low molecular weight liquid plasticizers such as cyclic carbonic acid esters and chain-like esters (e.g. propylene carbonate, dimethyl carbonate, diethyl carbonate, etc.) (Manuel Stephan, 2006). The plasticized electrolytes are much closer to actual applications than SPEs. They inherit important properties from the bulk liquid electrolytes, including ion conduction, electrochemical stability of the anode and various metal oxide cathode materials, assuring at the same time better safety and tolerance against mechanical and electrical abuses. Certainly, the concomitant consequence of the low polymer content in GPEs is their poorer mechanical strength compared to the pure SPEs. So either chemical or physical cross-linking is frequently necessary for the dimensional stability of such gel materials (as it will be discussed later). Since the polymer mainly serves as swollen matrix to provide dimensional integrity, the ether linkage of PEO (CH_2–CH_2–O–) with its complexing ability is no longer the sole macromolecular structure of choice. A list of polymers frequently used in GPEs as host matrices is reported in Table 14.1.

© Woodhead Publishing Limited, 2011

Table 14.1 Some common polymers used as matrices, their chemical formulae and thermal transitions temperatures

Polymer host	Repeating unit	T_g (°C)	T_m (°C)
Poly(ethylene oxide), PEO	$-(CH_2CH_2O)_n-$	–64	65
Poly(propylene oxide), PPO	$-(CH(-CH_3)CH_2O)_n-$	–60	–
Poly(acrylonitrile), PAN	$-(CH_2CH(-CN))_n-$	85	317
Poly(methyl methacrylate), PMMA	$-(CH_2C(-CH_3)COOCH_3)_n-$	105	–
Poly(vinyl chloride), PVC	$-(CH_2CHCl)_n-$	82	–
Poly(vinylidene fluoride), PVdF	$-(CH_2CF_2)_n-$	–62	171
Poly(vinylidene fluoride)-hexafluoropropylene, PVdF-HFP	$-(CH_2CF_2)_x(CF_2CF\text{-}CF_3)_y-$	–62	140

Poly(ethylene oxide), PEO

Large research efforts have been devoted to PEO-based electrolyte systems since Wright's discovery of ionic conductivity in alkali metal salt complexes of PEO. In order to improve the room temperature ionic conductivity of PEO complexed with lithium salts, the role of various additives was examined (Kelly *et al.*, 1985). It was also found that partial substitution of high molecular weight PEO with a lower molecular weight PEO has the effect of increasing the solubility of crystalline polymer/salt complexes as well as lowering the effective melting and glass transition temperature of the polymer. Ito and co-workers (Ito *et al.*, 1987) made ionic conductivity measurements on PEO–$LiCF_3SO_3$ complexes with poly(ethylene glycol) (PEG) as plasticizer. They observed that the ionic conductivity increases with an increase in PEG content. The increase in conductivity has been mainly attributed to a reduction of crystallinity and increase of free volume of the system. The increase in ionic conductivity was adversely accompanied by poor interfacial properties owing to the presence of the hydroxyl end-groups of PEG. In order to avoid this problem, few researchers have attempted to replace the hydroxyl end groups of PEG by methoxy ones CH_3O- (Sandner *et al.*, 1992). The crown ethers have also been used as plasticizers to enhance the ionic conductivity of polymer electrolytes (Morita *et al.*, 1996). Others (Benedict *et al.*, 1998) explored the possibility of using dibutyl phthalate (DBP) as plasticizer for PEO–$LiAsF_6$ complexes. The activation energy of the system was considerably reduced upon the addition of DBP in the system.

The thermal stability of PEO–$LiCF_3SO_3$ with a combination of plasticizers like ethylene carbonate (EC) and propylene carbonate (PC) was analysed in air as well as in argon atmosphere by Shodai *et al.* (1994). Their results revealed that the PEO-based electrolytes have a lower decomposition temperature than PEO and the decomposition rate is accelerated. Recently, the possibility of using low cost lithium-ion batteries comprising $LiFePO_4$/PEO-gel electrolytes/natural graphite system was also explored (Zaghib

© Woodhead Publishing Limited, 2011

et al., 2004). This system has shown excellent capacity retention and was found to be more suitable for hybrid electric vehicle applications. Review papers also document the development and general characteristics of blends of PEO with other polymers (Meyer, 1998; Bruce, 1995).

Poly(propyleneoxide) PPO

PPO systems were investigated by a few researchers (Teeters and Frech, 1986; Bruce *et al.*, 1987). The ionic conductivity of amorphous mixtures of lithium salt with PPO is considerably lower than the equivalent mixture with PEO because PPO has a lower dielectric constant ε (F m^{-1}) and the methyl group hinders the segmental motion of the polymer chain and thus reduces its conductivity.

Poly(acrylonitrile), PAN

The PAN-based electrolytes offer homogenous, hybrid electrolyte films in which the salt and the plasticizer are molecularly dispersed. Watanabe *et al.* (1982) used a combination of plasticizers EC and PC to plasticize PAN and complexed it with $LiClO_4$. They concluded that the PAN host is inactive in the ionic transport mechanism but acts as a matrix for structural stability. PAN-based gels were found to have lithium ion transference numbers higher than 0.5 because of the absence of oxygen atoms in the PAN matrix (Appetecchi and Scrosati, 1998).

PAN-based electrolytes were prepared by encapsulating Li-salt solutions obtained by dissolving $LiN(CF_3SO_2)_2$, $LiAsF_6$, $LiCF_3SO_3$ and $LiPF_6$ in a plasticizer mixture of EC and PC (Choe *et al.*, 1997). Cyclic voltammetry studies revealed that the electrolytes have an inherent oxidation stability window exceeding 5 V vs Li^+/Li. These electrolytes exhibited high ionic conductivity and a high lithium transference number.

Despite the several advantages of PAN-based electrolytes, like high ionic conductivity of the order of 10^{-3} S cm^{-1} at 20°C, good electrochemical stability of 4.5 V and a Li-transference number around 0.6, its poor compatibility with the Li metal anode precludes their use in practical applications. Their application in rechargeable lithium polymer batteries is hindered and this is attributed to the instability of Li electrode interface. It has been found that Li^+ ions strongly interact with the C≡N groups of PAN (Wang *et al.*, 1996). It is very difficult to observe the interaction between the ions and the molecules at a concentration as low as 5% Li^+ ions, because of the high intensity of the characteristic vibration of the C≡N group of PAN. Other studies clearly revealed that the Li electrode undergoes serious passivation when in contact with PAN-based electrodes and this affects cyclability and eventually leads to safety hazards (Scrosati, 1992).

© Woodhead Publishing Limited, 2011

Poly(methyl methacrylate), PMMA

In 1985, it was found that PMMA could be used as a gelling agent for Li-batteries membranes (Iijima *et al*., 1985). Later, Appetecchi *et al*. (1995) focused their attention on PMMA gel electrolytes with different plasticizers. These authors concluded that the electrochemical stability window depends on the polymer host and lithium salt complexes. Although better scalability has been obtained with PMMA when compared with PAN, the voltammetry results and the efficiency tests revealed that a consistent fraction of lithium is lost upon cycling and thus a large excess of lithium would be eventually required to assure an acceptable life for the battery.

The rheological and electrochemical properties of a PMMA-$LiClO_4$/PC membrane were examined (Bohnke *et al*., 1992). At low concentrations of PMMA, the gelatinized electrolyte can be considered as a liquid electrolyte encaged in a loose polymer matrix. The addition of PMMA in various proportions (higher than 20%wt/wt) increased the viscosity of the macromolecule solution, while the conductivity was considerably reduced. However, the room temperature conductivity remained unvaried and close to the conductivity of the liquid electrolytes. A model that emphasized the importance of the PMMA-lithium solvation effect of ion-pairing and the cross-linking action of cations at high PMMA concentration has also been reported (Bohnke *et al*., 1993a,b).

Interesting DSC, nuclear magnetic resonance (NMR) and electrical conductivity studies have been done by Stallworth *et al*. (1995) for gel electrolytes prepared from PMMA and various lithium salts ($LiClO_4$, $LiAsF_6$, $LiN(CF_3SO_2)_2$). The results are in accordance with those reported for PMMA electrolytes by other groups (Croce *et al*., 1993). Vondrak *et al*. (2001) prepared PMMA gel electrolytes with PC as plasticizer, complexed with salts of various perchlorates with different cation sizes including lithium. The gel electrolyte exhibited maximum conductivity with lithium and this was attributed to the small ionic radius of the cation. Even though it has many favourable merits, the poor mechanical strength of plasticized PMMA precludes these electrolytes from practical applications.

Poly(vinyl chloride), PVC

Complexed poly(vinyl chloride) (PVC) with lithium bis(trifluoromethyl sulfonyl) imide (LiTFSI), plasticized with dibutyl phthalate (DBP) and dioctyl adipate (DOA) was described as a polymer electrolyte (Sukeshini *et al*., 1996). The ionic conductivity of the membranes increased considerably when the PVC content decreased. The electrochemical stability domain was close to 4.0 V at 60°C, established by cyclic voltammetry using Ni-ultra microelectrodes. The value was limited on the cathodic side by Li deposition

© Woodhead Publishing Limited, 2011

and stripping processes and on the anodic side by the oxidation of the polymer. The efficiency of lithium stripping followed by deposition was found to be poor and was attributed to the reaction of DBP or DOA with Li. Many membranes based on PVC show ionic conductivity of 10^{-3} S cm^{-1} under ambient conditions. However, compatibility with a Li metal anode was not satisfactory enough for any direct application in lithium batteries.

PVC/PMMA blend

The possibility of using PVC/PMMA blend electrolytes was explored by Rhoo *et al*. (1997) and Manuel Stephan *et al. (*1999). The problem caused by the poor mechanical strength of PMMA was circumvented. A 7:3 PMMA:PVC blend electrolyte at 70 wt% plasticizer content was found to be optimal in terms of mechanical strength and conductivity. Although the mechanical strength was increased upon the addition of PVC in the blend, it leads to poor interfacial properties and thus poor cycling.

Poly(vinylidene fluoride), PVdF

By virtue of its attractive thermal and mechanical properties, PVdF has been chosen as a polymer host for lithium battery applications. PVdF-based polymer electrolytes possess high anodic stability owing to the presence of a strong electron-withdrawing functional group (—C—F); the polymer itself has a $\varepsilon = 8.4$, which promotes greater dissolution of lithium salts and subsequently supports a high concentration of charge carriers. Earlier reports indicate that a homogenous hybrid film can be obtained with PVdF when EC/PC and lithium salts are used in the correct proportions (Watanabe *et al*., 1981). Tsuchida examined plasticized PVdF gel electrolytes and found that viscosity, and not the dielectric constant of the plasticizer plays a major role in the conductivity (Tsuchida *et al*., 1983).

A novel polymer electrolyte comprising PVdF-EC-PC and a lithium salt ($LiCF_3SO_3$, $LiPF_6$ or $LiN(SO_2CF_3)_2$) was prepared by a thermal extrusion method (Jiang *et al*., 1997). The mechanical strength of the polymer electrolyte film varied widely and depended on the PVdF content. The viscosity of the medium, the concentration of the charge carriers, which are directly related to the weight ratio of PVdF-EC-PC, and the kind of Li salt studied were the main influences on the conductivity of the electrolyte. The authors showed that although the PVdF-based electrolytes offer excellent electrochemical properties, this fluorinated polymer alone is not stable towards Li, leading to poor interfacial properties between lithium and fluorine, although the interface can be improved by the addition of organic solvents and by choosing a suitable salt. A compatibility study of Li metal anode with a PVdF-EC-PC-$LiN(SO_2CF_3)_2$ polymer electrolyte reveals that

© Woodhead Publishing Limited, 2011

these electrolytes may have a good shelf life at room temperature. However, the low Li cycling efficiency data suggested that these electrolytes may be better suited for primary rather than secondary batteries when the anode is Li metal. When they are used in Li-ion batteries where Li metal is replaced by graphitic carbon, the current collector and an appropriate Li salt must be chosen to match the oxidation stability of the electrolyte with the charging potential of the cathode.

A rechargeable all-plastic battery was fabricated with a PVdF-PC-$LiClO_4$ membrane as electrolyte using polyacetylene film as an active electrode material. This battery has been found to be feasible for small power source for low current electronic devices. However, the problems associated with the ionic conductivity of polymer electrolyte, the degradation of battery performance and adhesion between the acetylene films and polymer electrolyte need to be solved (Nagamoto *et al*., 1987). Recently, the electrochemical and dielectric properties of PVdF polymer hosts have been reviewed (Mohamed and Arof, 2004).

Poly(vinylidene fluoride)-hexafluoro propylene, PVdF-HFP

The disadvantages of PVdF-based systems were rectified to an extent by copolymerization with hexafluoro propylene (HFP). Gel polymer electrolytes based on a copolymer of PVdF-HFP and a solution of EC, diethyl carbonate (DEC) and $LiN(CF_3SO_2)_2$ as a salt were prepared by changing the ratio of the polymer/salt solution (Capiglia *et al*., 2000). The ionic conductivity, thermal stability and compatibility of PVdF-HFP gel electrolytes with a combination of EC and PC as plasticizers and three different lithium salts ($LiCF_3SO_3$, $LiBF_4$ and $LiClO_4$) have been examined by other authors (Manuel Stephan *et al*., 2005; Saikia and Kumar, 2004). The PVdF-HFP film exhibited a higher conductivity and transport number than PVdF. The higher conductivity of PVdF-HFP films was attributed to the lower crystallinity of the copolymers. On the other hand, PVdF has a higher degree of crystallinity, which results in lower conductivity, but higher mechanical resistance.

Porous polymer electrolytes with high ionic conductivity at ambient temperature and good mechanical and thermal stability have been described (Appetecchi *et al*., 1995). In this case the copolymer consists of two phases, the amorphous domain which helps to trap a large amount of liquid electrolyte and the crystalline phase, which acts as a mechanical support for freestanding membranes.

Other polymer hosts

Investigations of the physical and electrochemical properties of many other polymer host systems have been carried out. Phase changes caused by

© Woodhead Publishing Limited, 2011

dissolution of Li salt in linear poly(ethylene imine) have been investigated by various authors (Chiang *et al*., 1986; York *et al*., 2001a). Raman and infrared (IR) studies on poly(ethylene imine) (LPEI) complexed with $LiCF_3SO_3$ and $NaCF_3SO_3$ showed the presence of free ions, contact ion pairs and other complex charged species.

Studies have also been done on copolymer of PEO-PPO (Ishikawa *et al*., 1990), poly(MEEMA) (polymethoxy ethoxy ethyl methacrylate) (Selvaraj *et al*., 1995) and ter-polymer of PMMA with ethylene oxide and propylene oxide (Wieczorek and Stevens, 1997). Sung *et al*. (1998) reported that PVC-based electrolytes suffer from solvent exudation and suggested the replacement of PVC with polyvinylacetate (PVAc) copolymer. High molecular weight comb polymers based on ethylene oxide and methoxy ethoxy ethyl glycidyl ether (MEEGE) have also been analysed by Nishimoto *et al*. (1998) as matrices for polymer electrolyte. An apparent decrease in crystallinity was observed when the content of MEEGE in the copolymer was increased and subsequently, an increase in conductivity was found. The interfacial properties of P(EO-MEEGE) matrices with Li metal anode were reported by Watanabe *et al*. (1999).

Comb-shaped high molecular weight poly (oxyethylene) with tri(oxyethylene) side chains as solid polymer electrolyte was synthesized and characterized by Ikeda *et al*. (2000). The presence of tri(oxyethylene) side chains was found to decrease the crystallinity of oxyethylene segments. Polymer electrolytes were prepared from poly(acrylonitrile-co-Li methacrylate), EC and $LiClO_4$ and studies of their ionic conductivity were reported (Lee *et al*., 2000).

Mehta *et al*. (2000) developed a new type of high performance polymer electrolytes, based on interconnecting networks of boroxine rings.

A hyper branched poly[bis(hexaethylene glycol) benzoate] with terminal acetyl groups was prepared and the ionic conductivity, thermal properties and electrochemical stability of the polymer electrolyte with $LiN(CF_3SO_3)_2$ were investigated (Itoh *et al*., 2001).

A new copolymer poly(acrylonitrile-*co*-bis[2-(2-methoxy ethoxy) ethyl] itaconate) (PANI) was synthesized and its ionic conductivity and DSC thermogram were reported (Kim *et al*., 2001b). The PAN-PANI blend gel electrolyte had better electrochemical stability and was more stable towards the lithium electrode than pristine PAN-based electrolytes, although it exhibited slightly low mechanical rigidity when the PAN matrix becomes more amorphous. Kuratomi *et al*. (2001) developed a long-life lithium battery using a $LiCoO_2$/Li electrode system with a cross-linked random copolymer of ethylene oxide (EO) and propylene oxide (PO). The battery performance was found to depend on the species and concentration of lithium salts used.

The thermal transition, ionic association and ionic conductivity have been measured as a function of $LiCF_3SO_3$ concentration in polydioxolane-based electrolytes by Silva *et al*. (2001).

© Woodhead Publishing Limited, 2011

Gel polymer electrolytes composed of acrylonitrile–methyl methacrylate (AM) copolymer and $LiClO_4$-EC/PC were prepared by Kim *et al.* (2001a). The system shows no solvent exudation from the polymer matrix owing to enhanced compatibility between AM copolymer and the organic liquid electrolyte.

A comparative vibrational spectroscopy study on a series of polymer electrolytes composed of poly(oligoethyleneoxy phosphazane) containing dissolved lithium triflate was done by York *et al.* (2001b). Novel gels comprising methyl methacrylate–acrylonitrile–styrene terpolymer with a combination of ethylene carbonate and diethyl carbonate plasticizers and $LiClO_4$ as a salt were synthesized (Kim *et al.*, 1999) and employed as separators in cells. There have been attempts to incorporate siloxane structures into the polymer electrolytes both as part of the polymer matrix as well as side branches grafted on the main polymer backbone in order to improve the interfacial properties (Trapa *et al.*, 2005a, 2005b).

Separators

We can include a short discussion on separators in the description of gel polymer electrolyte (Arora and Zhang, 2004). They are porous membranes placed between electrodes of opposite polarity, permeable to ionic flow but preventing electric contact of the electrodes and usually between 25 and 35 μm thick. While the previous GPE membranes are non-porous and the membrane polymer structure is crucial because transport occurs through the polymer itself, in separators the function of the polymer is mainly to provide sufficient mechanical stability. As batteries have become more sophisticated, the separator function has also become more demanding and complex; they should be very good electronic insulators and have the capability of conducting ions by soaking electrolyte. The material should also be soft and flexible enough to be laid between the electrodes. Starting with cedar shingles and sausage casing, separators have been manufactured from many different polymeric materials from cellulosic papers and cellophane to nonwoven fabrics, foams, ion exchange membranes and microporous flat sheet membranes. For example using PVdF-HFP polymer, a porous membrane was prepared by Tarascon *et al.* (1996) extracting the plasticizer and then substituting liquid electrolyte during the final stage of cell processing. The system more specifically can be described as a heterogeneous, phase separated, plasticizer-free polymer separator.

Oriented polyolefins, such as polyethylene and polypropylene with micropores, are the most widely used separators. Celgard® is an example of a microporous polyolefin separator (http://www.celgard.com/) bonded to the electrodes. The material itself is cheap, but the processing technology needed to obtain micropores makes it very expensive.

© Woodhead Publishing Limited, 2011

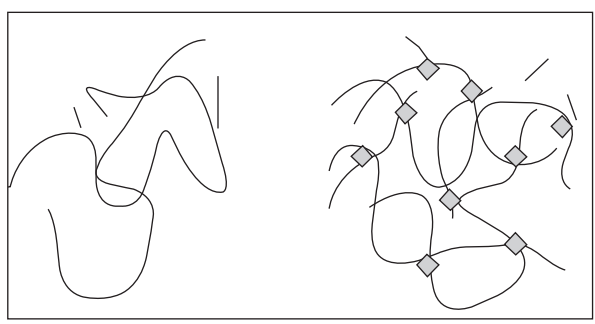
14.3.4 Cross-linked polymer electrolyte membranes

As mentioned before, GPEs can have poor mechanical strength. In the field of polymeric materials, the strategies for improving their mechanical properties are based either on promoting crystallization, or by introduction of fillers or by cross-linking. When it comes to application as an electrolytic membrane, crystallization is not advisable because it hinders ionic conduction. Examples of composites membranes have already been discussed in Section 14.3.2, however in most cases, fillers are used to improve ionic conductivity and are not added in such a high amount that they will strongly influence the mechanical modulus and resistance of the polymer. Cross-linking is a versatile pathway, as the process can be induced in different ways (i.e. thermally, photochemically, in the presence of coreactants or catalyst), can be applied to many matrices (i.e. many of the linear polymers mentioned before) and can be controlled to give an appropriate cross-linking density therefore tailoring the final properties of the network by changing its architecture. Figure 14.3 is a sketch of entangled linear polymeric chains (thermoplastic materials) and a network where the small shaded diamonds are the knots which typically correspond to covalent bonding of the chains (physical networks also exist).

When cross-linking polymers have to be used as electrolytes, sufficient mobility must be maintained in the polymeric systems. This is also the case for elastomeric materials. Therefore two main guidelines have to be followed:

- the linear prepolymer to be cross-linked has to be rubbery with low T_g values;
- the degree of cross-linking has to be low and the network has to be a loosely linked network in the rubbery state.

An interesting example in this context is the preparation of a self-supported mixed matrix membrane containing an ion conductive polymer electrolyte,



14.3 Schematic representation of the architecture of a linear polymer (on the left) and of a network (on the right).

© Woodhead Publishing Limited, 2011

that is an immiscible blend of polymethacrylates (PMAs) with poly(ethylene carbonate *co*-ethylene oxide) side chains (PMA-PEC-EO) blended with poly(vinylidenefluoride-*co*-hexafluoropropylene) (PVDF-HFP) (Elmer and Jannasch, 2007). Films of the macro monomer PMA-PEC-EO, blended with the fluoropolymer, containing lithium bis(trifluoromethyl-sulfonyl) imide (LiTFSI) salt and an ultra violet (UV) initiator were cast, followed by irradiation with UV light to polymerize the methacrylate units. UV irradiation was also used during *in situ* preparation of mixed matrix silica/poly(ethylene oxide) (PEO)-immobilized electrolyte membranes (Liu *et al.*, 2004), by sol–gel synthesis of silica particles, along with the UV polymerisation of the macromonomers in one step, enabling the simultaneous formation of the polymer network and the inorganic nanoparticles. Many different polymers cross-linked after polymerization by a UV-induced process are described in patents (Jannasch and Gavelin, 2001; Michot *et al.*, 2002). A cross-linked polyurethane acrylate was prepared by end capping 2,6-toluene diisocyanate/poly(ethylene glycol)-based prepolymer with hydroxybutyl methacrylate. Significant interactions between lithium ions and soft/hard segments of the polymer were observed when complexed with $LiClO_4$. The membrane showed a high electrochemical stability window and good compatibility with lithium metal (Santhosh *et al.*, 2006).

Cross-linked membranes can be also prepared starting from monomers with appropriate functionalities and polymerizing them. Photo-induced polymerization is a well established polymerization technique for making networks. Under UV light a liquid poly-functional monomer containing a proper photoinitiator forms a solid cross-linked membrane upon irradiation. The process is a consolidated technique for the production of coatings and inks; it is widely applied in the field of photolithography for the production of electronic and optical devices and is well known for being fast and environmentally friendly, as the energy consumption is low (just the irradiation) and there is no emission of volatile organic compounds (Fouassier and Rabek, 1993). Photo-cross-linked membranes were first proposed in a patent by 3M (Chen and Huang, 1996). The authors describe thiolene systems containing polyethylene oxide units (PEO), cured by UV light. Reiche *et al.* (1998) synthesized PEO acrylate membranes, then modified them by addition of cyanomethacrylate (Sandner *et al.*, 1998). Lee *et al.* (2001) studied cross-linked polymer electrolytes prepared by polymerization of polyethylene glycol dimethacrylate (PEGDMA) and an alkyl monomer in the presence of liquid electrolyte 1.3 M $LiPF_6$/EC. The flexibility and ionic conductivity of the electrolyte were improved when the monomer content was varied. Song *et al.* (2002) followed this research line, investigating acrylic membranes. A few other membranes, based on acrylates containing poly(ethylene oxide) chains are described in the literature (Hwang and Liu, 2002; Jiang and Fang, 2006; Nair *et al.*, 2008; Gerbaldi *et al.*, 2008; Penazzi *et al.*, 2009).

© Woodhead Publishing Limited, 2011

Recently a work has been published reporting the results on siloxane-containing photopolymers giving a σ value of 4×10^{-3} S cm^{-1} (at room temperature) and high cyclability for low and stable surface resistance, owing to the good interfacial properties of the membrane (Gerbaldi *et al.*, 2010a).

The polymer electrolytes mentioned above are gel membranes, obtained by swelling a previously prepared UV-cured network with liquid lithium electrolyte. However, Gerbaldi *et al.* (2010b) already demonstrated that Li-X salt can be introduced directly during polymerization, thus completely avoiding the time consuming activation of the membranes by swelling into a liquid electrolyte. Using this method, the complete electrolyte preparation takes less than five minutes (Gerbaldi *et al.*, 2009).

Attempts to prepare solid polymer electrolytes by UV polymerization are reported by Gerbaldi (2010) and Nair *et al.* (2010). Conductivities are comparable to those of the solid membrane described in Section 14.3.1 while the membrane preparation is faster and in principle can be done directly onto the battery electrodes.

14.4 Conclusions and future trends

Worldwide demand for ultra-thin, ultra-light, long living rechargeable batteries will continue to increase. Lithium-ion polymer batteries are the most technically advanced rechargeable power source available and the technology is just at the onset of a commercial exploitation. Development of new materials is a key strategy for better performance. In the field of solid electrolytes there is considerable room for examining new polymer structures, eventually considering biodegradable systems.

As far as gel–polymer electrolytes are concerned, the trend is to introduce alternative liquids as electrolyte solvents. Ionic liquids (ILs), which can be defined as room-temperature molten salts, have attracted a lot of attention as new 'green solvents'. They meet all of the requirements of plasticizing salts and offer potential advantages such as low vapour pressure, high ionic conductivity and greater thermal and electrochemical stability (Susan *et al.*, 2005; Welton, 1999; Egashira *et al.*, 2005; Ahmad and Deepa, 2007; Ferrari *et al.*, 2010; Abitelli *et al.*, 2010). However, highly conducting IL-based polymer electrolytes are yet to be realized (Tokuda *et al.*, 2004).

The manufacture of batteries with a full plastic structure is a present goal (Scrosati, 2002) as they are expected to be cheaper and more easily scaled up. The other advantages of the system are the substitution of a rigid metallic packing case by a lightweight plastic container, allowing improvement in energy density and the fabrication of batteries in any desired shape and size. However, to achieve this goal it is also necessary to develop suitable electrodes and new electronic and ionic conductive materials.

© Woodhead Publishing Limited, 2011

Research is in progress toward fully flexible polymer devices. Recently researchers have combined carbon nanotubes and nanoporous cellulose to make lithium-ion batteries and supercapacitors that are both lighter and more flexible than existing devices (Scrosati, 2007; Pushparaj *et al.*, 2007.) The novelty of these devices lies in their mechanical flexibility, which allows them to change shape to meet the space requirements of modern devices, and the elegance of the design, with all the components (the electrode, electrolyte and separator) being integrated into a single unit that acts as a building block for the final battery structure. Paper-based energy storage devices are also under investigation, with the distinctive advantages of bio-based materials and their environmental friendliness, flexibility, cost and versatility (Nyholm *et al.*, 2011).

14.5 Sources of further information and advice

14.5.1 Electrochemistry

Bagotsky V S (2006), *Fundamentals of Electrochemistry*, 2nd edition, John Wiley & Sons, Hoboken, NJ.

Hamann C H, Hamnett A and Vielstich W (1998), *Electrochemistry*, Wiley-VCH, Weinheim, Germany.

Newman J and Thomas-Alyea K E (2004), *Electrochemical Systems*, 3rd edition, John Wiley & Sons, Hoboken, New Jersey.

Rieger P H (1994), *Electrochemistry*, 2nd edition, Chapman & Hall, New York.

14.5.2 Lithium batteries and related materials

Crompton T R (2000), *Battery Reference Book*, 3rd edition, Reed Educational and Professional Publishing, Oxford.

Gabano J P (1983), *Lithium Batteries*, Academic Press, London and New York.

Julien C and Stoynov Z (2000), *Materials for Lithium-ion Batteries*, Springer Science + Business Media, New York.

Linden D (1994), *Handbook of Batteries & Fuel Cells*, McGraw-Hill, New York.

Murphy D W, Broadhead J and Steele B C H (1980), *Materials for Advanced Batteries*, Plenum Press, New York.

Nazri G A and Pistoia G (2009), *Lithium Batteries Science and Technology*, Springer Science + Business Media, New York.

Osaka T and Datta M (2000), *Energy Storage Systems for Electronics*, Gordon and Breach Science Publishers, New York.

Ozawa K (2009), *Lithium Ion Rechargeable Batteries: Materials, Technology and New Applications*, Wiley-VCH, Weinheim, Germany.

© Woodhead Publishing Limited, 2011

Van Gool W (1973), *Fast Ion Transport in Solids*, North-Holland/American Elsevier, New York.
Van Schalkwijk W A and Scrosati B (2002), *Advances in Lithium Ion Batteries*, Kluwer Academic/Plenum Publisher, New York.
Wakihara M and Yamamoto O (1998), *Lithium Ion Batteries: Fundamentals and Performance*, Kodansha International LTD, Tokyo.

14.5.3 Polymer science and technology, polymer electrolytes

Flory P J (1953), *Principles of Polymer Chemistry*, Cornell University Press, New York.
Fouassier J P and Rabek J F (1993), *Radiation Curing in Polymer Science and Technology*, Elsevier, London.
Linford R G (1990), *Electrochemical Science and Technology of Polymers*, Volume 2, Elsevier Applied Science, London.
MacCallum J R and Vincent C A (1989), *Polymer Electrolyte Reviews*, Elsevier Science, Crown House, Essex, UK.
Mulder M (1996), *Basic Principles of Membranes Technology*, Kluwer Academic, Dordrecht, The Netherlands.
Scrosati B (1993), *Applications of Electroactive Polymers*, Chapman & Hall London.

14.5.4 Ionic liquids

Gaune-Escard M (2002), *Molten Salts: from Fundamentals to Applications*, Springer Science + Business Media, New York.
Ohno H (2005), *Electrochemical Aspects of Ionic Liquids*, John Wiley & Sons, Hoboken, NJ.
Rogers R D and Seddon K R (2002), *Ionic Liquids: Industrial Applications for Green Chemistry*, American Chemical Society, Washington.

14.5.5 Internet sources

Batteries in a Portable World, a handbook on rechargeable batteries for non-engineers, http://www.buchmann.ca/default.asp
Batteries Wholesale, Specializing in Custom and Consumer Battery Technologies, http://www.batterieswholesale.com/index.html
Battery University, http://batteryuniversity.com/
Celgard®, Lithium Battery Separators, http://www.celgard.com/
The Electropaedia, Battery and Energy Technologies, http://www.mpoweruk.com/index.htm

© Woodhead Publishing Limited, 2011

14.6 References

Abitelli E, Ferrari S, Quartarone E, Mustarelli P, Magistris A, Fagnoni M, Albini A and Gerbaldi C (2010), 'Polyethylene oxide electrolyte membranes with pyrrolidinium-based ionic liquids', *Electrochim Acta*, **55**, 5478–84.

Ahmad S and Deepa M (2007), 'Ionogels encompassing ionic liquid with liquid like performance preferable for fast solid state electrochromic devices', *Electrochem Commun*, **9**, 1635–8.

Angell C A, Liu C and Sanchez E (1993), 'Rubbery solid electrolytes with dominant cationic transport and high ambient conductivity', *Nature*, **362**, 137–9.

Appetecchi G B and Scrosati B (1998), 'A lithium ion polymer battery', *Electrochim Acta*, **43**, 1105–7.

Appetecchi G B, Croce F and Scrosati B (1995), 'Kinetics and stability of the lithium electrode in poly(methylmethacrylate)-based gel electrolytes', *Electrochim Acta*, **40**, 991–7.

Appetecchi G B, Croce F, Persi L, Ronci F and Scrosati B (2000), 'Transport and interfacial properties of composite polymer electrolytes', *Electrochim Acta*, **45**, 1481–90.

Armand M (1994), 'The history of polymer electrolytes', *Solid State Ionics*, **69**, 309–19.

Arora P and Zhang Z (2004), 'Battery separators', *Chem Rev*, **104**, 4419–62.

Benedict T J, Banumathi S, Veluchamy A, Gangadharan R, Ahmed A Z and Rajendran S (1998), 'Characterization of plasticized solid polymer electrolyte by XRD and AC impedance methods', *J Power Sources*, **75**, 171–4.

Bohnke O, Rousselot C, Gillet P A and Truche C (1992), 'Gel electrolyte for solid-state electrochromic cell', *J Electrochem Soc*, **139**, 1862–5.

Bohnke O, Frand G, Rezrazi M, Rousselot C and Truche C (1993a), 'Fast ion transport in new lithium electrolytes gelled with PMMA. 1. Influence of polymer concentration', *Solid State Ionics*, **66**, 97–104.

Bohnke O, Frand G, Rezrazi M, Rousselot C and Truche C (1993b), 'Fast ion transport in new lithium electrolytes gelled with PMMA. 2. Influence of lithium salt concentration', *Solid State Ionics*, **66**, 105–12.

Borghini M C, Mastragostino M, Passerini S and Scrosati B (1995), 'Electrochemical properties of polyethylene oxide-Li[$(CF_3SO_2)2N$]-gamma-$LiAlO_2$ composite polymer electrolytes', *J Electrochem Soc*, **142**, 2118–21.

Brandt K (1994), 'Historical development of secondary lithium batteries', *Solid State Ionics*, **69**, 173–83.

Bruce P G (1995), 'Structure and electrochemistry of polymer electrolytes', *Electrochim Acta*, **40**, 2077–85.

Bruce P G (2008), 'Energy storage beyond the horizon: Rechargeable lithium batteries', *Solid State Ionics*, **179**, 752–60.

Bruce P G, Evans J and Vincent C A (1987), 'A dc technique for measurement of solid electrolyte conductivity', *Solid State Ionics*, **25**, 255–62.

Capiglia C, Saito Y, Kataoka H, Kodama T, Quartarone E and Mustarelli P (2000), 'Structure and transport properties of polymer gel electrolytes based on PVdF-HFP and $LiN(C_2F_5SO_2)_2$', *Solid State Ionics*, **131**, 291–9.

Chen K and Huang H (1996) *Polymer Electrolyte Composition Based Upon Thiol-ene Chemistry*. PCT Patent WO 96/35238.

Chiang C K, Davis G T, Harding C A and Takahashi T (1986), 'Polymeric electrolyte based on poly(ethylene imine) and lithium salts', *Solid State Ionics*, **18–19**, 300–5.

© Woodhead Publishing Limited, 2011

Choe H S, Carroll B G, Pasquariello D M and Abraham K M (1997), 'Characterization of some polyacrylonitrile-based electrolytes', *Chem Mater*, **9**, 369–79.

Croce F, Brown S D, Greenbaum S G, Slane S M and Salomon M (1993), 'Lithium-7 NMR and ionic conductivity studies of gel electrolytes based on polyacrylonitrile', *Chem Mater*, **5**, 1268–72.

Croce F, Appetecchi G B, Persi L and Scrosati S (1998), 'Nanocomposite polymer electrolytes for lithium batteries', *Nature*, **394**, 456–8.

Croce F, Curini R, Martinelli A, Persi L, Ronci F, Scrosati B and Caminiti R (1999), 'Physical and chemical properties of nanocomposite polymer electrolytes', *J Phys Chem B*, **103**, 10632–8.

Croce F, Persi L, Scrosati B, Serraino-Fiory F, Plichta E and Hendrickson M A (2001), 'Role of the ceramic fillers in enhancing the transport properties of composite polymer electrolytes', *Electrochim Acta*, **46**, 2457–61.

Egashira M, Nakagawa M, Watanabe I, Okada S and Yamaki T (2005), 'Cyano-containing quaternary ammonium-based ionic liquid as a "co-solvent" for lithium battery electrolyte', *J Power Sources*, **146**, 685–8.

Elmer A M and Jannasch P (2007), 'Polymer electrolyte membranes by *in situ* polymerization of poly(ethylene carbonate-co-ethylene oxide) macromonomers in blends with poly(vinylidene fluoride-co-hexafluoropropylene)', *J Polym Sci B: Polym Phys*, **45**, 79–90.

Fenton D E, Parker J M and Wright P V (1973), 'Complexes of alkali metal ions with poly(ethylene oxide)', *Polymer*, **14**, 589.

Fergus J W (2010), 'Ceramic and polymeric solid electrolytes for lithium-ion batteries', *J Power Sources*, **195**, 4554–69.

Ferrari S, Quartarone E, Mustarelli P, Magistris A, Fagnoni M, Protti S, Gerbaldi C and Spinella A (2010), 'Lithium ion conducting PVdF-HFP composite gel electrolytes based on N-methoxyethyl-N-methylpyrrolidinium bis(trifluoromethanesulfonyl)-imide ionic liquid', *J Power Sources*, **195**, 559–66.

Fouassier J P and Rabek J F (1993), *Radiation Curing in Polymer Science and Technology*, Elsevier, London.

Gadjourova Z, Andreev Y G, Tunstall D P and Bruce P G (2001), 'Ionic conductivity in crystalline polymer electrolytes', *Nature*, **412**, 520–23.

Gerbaldi C (2010), 'All-solid-state lithium-based polymer cells for high-temperature applications', *Ionics*, **16**, 777–86.

Gerbaldi C, Nair J, Bonatto Minella C, Meligrana G, Mulas G, Bodoardo S, Bongiovanni R, Penazzi N (2008), 'Development of gel-polymer electrolytes and nano-structured electrodes for Li-ion polymer batteries', *J Appl Electrochem*, **38**, 985–92.

Gerbaldi C, Nair J, Meligrana G, Bodoardo S, Bongiovanni R, Penazzi N (2009), 'Highly ionic conducting methacrylic-based gel-polymer electrolytes by UV-curing technique', *J Appl Electrochem*, **39**, 2199–207.

Gerbaldi C, Nair J R, Meligrana G, Bongiovanni R, Bodoardo S, Penazzi N (2010a), 'UV-curable siloxane-acrylate gel-copolymer electrolytes for lithium-based battery applications', *Electrochim Acta*, **55**, 1460–7.

Gerbaldi C, Nair J R, Ahmad S, Meligrana G, Bongiovanni R, Bodoardo S, Penazzi N (2010b), 'UV-cured polymer electrolytes encompassing hydrophobic room temperature ionic liquid for lithium batteries', *J Power Sources*, **195**, 1706–13.

Golodnitsky D, Ardel G and Peled E (2002), 'Ion-transport phenomena in concentrated PEO-based composite polymer electrolytes', *Solid State Ionics*, **147**, 141–55.

Goodenough J B and Kim Y (2010), 'Challenges for rechargeable Li batteries', *Chem Mater*, **22**, 587–603.

© Woodhead Publishing Limited, 2011

Hwang J J and Liu H J (2002), 'Influence of organophilic clay on the morphology, plasticizer-maintaining ability, dimensional stability, and electrochemical properties of gel polyacrylonitrile (PAN) nanocomposite electrolytes', *Macromolecules*, **35**, 7314–19.

Iijima T, Toyoguchi Y and Eda N (1985), 'Quasi-solid organic electrolytes gelatinized with polymethylmethacrylate and their applications for lithium batteries', *Denki Kagaku*, **53**, 619–23 [in Japanese].

Ikeda Y, Wada Y, Matoba Y, Murakami S and Kohjiya S (2000), 'Characterization of comb-shaped high molecular weight poly(oxyethylene) with tri(oxyethylene) side chains for a polymer solid electrolyte', *Electrochim Acta*, **45**, 1167–74.

Ishikawa K, Sugihara T, Oshima Y, Kato T and Imai A (1990), 'Li ion conductive polymer electrolyte based on polyglycerine', *Solid State Ionics*, **40–41**, 612–16.

Ito Y, Kanehori K, Miyauchi K and Kudo T (1987), 'Ionic conductivity of electrolytes formed from PEO-$LiCF_3SO_3$ complex low molecular weight poly(ethylene glycol)', *J Mater Sci*, **22**, 1845–9.

Itoh T, Hirata N, Wen Z, Kubo M and Yamamoto O (2001), 'Polymer electrolytes based on hyperbranched polymers', *J Power Sources*, **97**, 637–40.

Itoh T, Miyamura Y, Ichikawa Y, Uno T, Kubo M and Yamamoto O (2003), 'Composite polymer electrolytes of poly(ethylene oxide)/$BaTiO_3$/Li salt with hyperbranched polymer', *J Power Sources*, **119–121**, 403–8.

Jannasch P and Gavelin P (2001), *Polymer Gel Electrolyte*, PCT Patent WO 01/47047.

Jiang H and Fang S B (2006), 'All solid-state comb-like network polymer electrolytes based on poly(methylsiloxane)', *J Power Sources*, **159**, 673–8.

Jiang Z, Carroll B and Abraham K M (1997), 'Studies of some poly(vinylidene fluoride) electrolytes', *Electrochim Acta*, **42**, 2667–77.

Johansson P and Jacobsson P (2003), 'An *ab initio* approach to the single ion transport in crystalline $LiPF_6PEO_6$', *Electrochim Acta*, **48**, 2279–81.

Kelly I E, Owen J R, and Steele B C H (1985), 'Poly(ethylene oxide) electrolytes for operation at near room temperature', *J Power Sources*, **14**, 13–21.

Kim D W, Oh B K and Choi Y M (1999), 'Electrochemical performance of lithium-ion polymer cell using gel polymer electrolyte based on acrylonitrile-methyl methacrylate-styrene terpolymer', *Solid State Ionics*, **123**, 243–9.

Kim D W, Ko J M and Chun J H (2001a), 'Electrochemical characteristics of Li/$LiMn_2O_4$ cells using gel polymer electrolytes', *J Power Sources*, **93**, 151–5.

Kim Y W, Gong M S and Choi B K (2001b), 'Ionic conduction and electrochemical properties of new poly(acrylonitrile-itaconate)-based gel polymer electrolytes', *J Power Sources*, **97–98**, 654–6.

Kim J W, Ji K S, Lee J P and Park J W (2003), 'Electrochemical characteristics of two types of PEO-based composite electrolyte with functional SiO_2', *J Power Sources*, **119–121**, 415–21.

Kumar B and Scanlon L G (1994), 'Polymer-ceramic composite electrolytes', *J Power Sources*, **52**, 261–8.

Kuratomi J, Iguchi T, Bando T, Aihara Y, Ono T and Kuwana K (2001), 'Development of solid polymer lithium secondary batteries', *J Power Sources*, **97–98**, 801–3.

Lazzari M and Scrosati B (1980), 'A cyclable lithium organic electrolyte cell based on two intercalation electrodes', *J Electrochem Soc*, **127**, 773–4.

Lee K H, Park J K and Kim W J (2000), 'Electrochemical characteristics of PAN ionomer based polymer electrolytes', *Electrochim Acta*, **45**, 1301–6.

Lee K H, Kim K H and Lim H S (2001), 'Studies on a new series of cross-linked

© Woodhead Publishing Limited, 2011

polymer electrolytes for a lithium secondary battery', *J Electrochem Soc*, **148**, A1148–A1152.

Linden D (1994), *Handbook of Batteries & Fuel Cells*, McGraw-Hill, New York.

Liu Y, Lee J Y and Hong L (2004), '*In situ* preparation of poly(ethylene oxide)–SiO_2 composite polymer electrolytes, *J Power Sources*, **129**, 303–11.

Manuel Stephan A (2006), 'Review on gel polymer electrolytes for lithium batteries', *Europ Polym J*, **42**, 21–42.

Manuel Stephan A and Nahm K S (2006), 'Review on composite polymer electrolytes for lithium batteries', *Polymer*, **47**, 5952–64.

Manuel Stephan A, Thirunakaran R, Renganathan N G, Sundaram V, Pitchumani S, Muniyandi N and Ramamoorthy P (1999), 'A study on polymer blend electrolyte based on PVC/PMMA with lithium salt', *J Power Sources*, **81–82**, 752–8.

Manuel Stephan A, Gopu Kumar S, Renganathan N G and Anbu Kulandainathan M (2005), 'Characterization of poly(vinylidene fluoride-hexafluoropropylene) (PVdF–HFP) electrolytes complexed with different lithium salts', *Europ Polym J*, **41**, 15–21.

Mehta M A, Fujinami T, Inoue S, Matsushita K, Miwa T and Inoue T (2000), 'The use of boroxine rings for the development of high performance polymer electrolytes', *Electrochim Acta*, **45**, 1175–80.

Meyer W H (1998), 'Polymer electrolytes for lithium-ion batteries', *Adv Mater*, **10**, 439–48.

Michot C, Vallee A, Harvey P, Gauthier M and Armand M (2002), *Polymers Obtained from Monomers Allowing a Sequential Polymerization, and their use for Preparing Ionic Conductors*. US Patent 2002/018364.

Mizushima K, Jones P C, Wiseman P J and Goodenough J B (1980), 'Li_xCoO_2 ($0<x<-1$): A new cathode material for batteries of high energy density', *Mat Res Bull*, **15**, 783–9.

Mohamed N S and Arof A K (2004), 'Investigation of electrical and electrochemical properties of PVDF-based polymer electrolytes', *J Power Sources*, **132**, 229–34.

Mohri M, Yanagisawa N, Tajima Y, Tanaka H, Mitate T, Nakajima S, Yoshida M, Yoshimoto Y, Suzuki T and Wada H (1989), 'Rechargeable lithium battery based on pyrolytic carbon as a negative electrode', *J Power Sources*, **26**, 545–51.

Morita M, Tanaka H, Ishikawa M, Matsuda Y (1996), 'Effects of crown ethers on the electrochemical properties of polymeric solid electrolytes consisting of poly(ethylene oxide)-grafted poly(methylmethacrylates), *Solid State Ionics* **86–88**, 401–405.

Murphy D W, Di Salvo F J, Carides J N and Waszczak J V (1978), 'Topochemical reactions of rutile related structures with lithium', *Mat Res Bull*, **13**, 1395–402.

Nagatomo T, Ichikawa C and Omoto O (1987), 'All-plastic batteries with polyacetylene electrodes', *J Electrochem Soc*, **134**, 305–8.

Nagaura T and Tozawa K (1990), 'Lithium ion rechargeable battery', *Prog Batteries and Solar Cells*, **9**, 209.

Nair J R, Gerbaldi C, Meligrana G, Bongiovanni R, Bodoardo S, Penazzi N, Reale P and Gentili V (2008), 'UV-cured methacrylic membranes as novel gel-polymer electrolyte for Li-ion batteries', *J Power Sources*, **178**, 751–7.

Nair J R, Gerbaldi C, Destro M, Bongiovanni R and Penazzi N (2010), 'Methacrylic-based solid polymer electrolyte membranes for lithium-based batteries by a rapid UV-curing process', *React Funct Polym*, **71**(4), 409–41.

Nishimoto A, Watanabe M, Ikeda Y and Kohjiya S (1998), 'High ionic conductivity of new polymer electrolytes based on high molecular weight polyether comb polymers', *Electrochim Acta*, **43**, 1177–84.

© Woodhead Publishing Limited, 2011

Nyholm L, Nyström G, Mihranyan A and Strømme M (2011), 'Toward flexible polymer and paper-based energy storage devices', *Adv. Mater.*, **XX**, 1–19.

Ohzuku T, Iwakoshi Y and Sawai K (1993), 'Formation of lithium–graphite intercalation compounds in nonaqueous electrolytes and their application as a negative electrode for a lithium ion (shuttlecock) cell', *J Electrochem Soc*, **140**, 2490–8.

Panero S, Scrosati B and Greenbaum S G (1992), 'Ionic conductivity and ^{7}Li NMR study of poly(ethylene glycol) complexed with lithium salts', *Electrochim Acta*, **37**, 1533–9.

Penazzi N, Bodoardo S, Bongiovanni R, Gerbaldi C, Meligrana G, Mulas G and Nair J (2009), 'Nanostructured electrodes and gel–polymer electrolyte for an improved li-ion battery', *Fuel Cells*, **9**, 273–6.

Pushparaj V L, Shaijumon M M, Kumar A, Murugesan S, Ci L, Vajtai R, Linhardt R J, Nalamasu O and Ajayan P M (2007), 'Flexible energy storage devices based on nanocomposite paper', *Proc. Natl Acad. Sci. USA*, **104**, 13574–7.

Reiche A, Tubke J, Sandner R S, Werther A, Sandner B and Fleischer G (1998), 'Cationic transport in gel electrolytes on basis of oligo(ethylene glycol) dimethacrylate', *Electrochim Acta*, **43**, 1429–34.

Rhoo H J, Kim H T, Park J K and Hwang T S (1997), 'Ionic conduction in plasticized PVC/PMMA blend polymer electrolytes', *Electrochim Acta*, **42**, 1571–9.

Rossi N A A and West R (2009), 'Silicon-containing liquid polymer electrolytes for application in lithium ion batteries', *Polym Int*, **58**, 267–72.

Saikia D and Kumar A (2004), 'Ionic conduction in P(VDF-HFP)/PVDF–(PC+DEC)–$LiClO_4$ polymer gel electrolytes', *Electrochim Acta*, **49**, 2581–9.

Sandner B, Steurich T, Wiesner K and Bischoff H (1992), 'Solid polymer electrolytes based on oligo(ethylene glycol)methacrylates', *Polym Bull*, **28**, 355–60.

Sandner B, Weinkauf A, Reiche A, Siury K, Tübke J, Wartewig S and Shashkov S (1998), 'Properties of gel electrolytes based on crosslinked copolymers of oligo(ethylene glycol) dimethacrylate and cyanomethyl methacrylate', *Electrochim Acta*, **43**, 1263–9.

Santhosh P, Gopalan A, Vasudevan T and Lee K (2006), 'Evaluation of a cross-linked polyurethane acrylate as polymer electrolyte for lithium batteries', *Mat Res Bull*, **41**, 1023–37.

Scrosati B (1992), 'Lithium rocking chair batteries: an old concept?', *J Electrochem Soc*, **139**, 2776–81.

Scrosati B (1995), 'Challenge of portable power', *Nature*, **373**, 557–8.

Scrosati B (2002), *Advances in Lithium Ion Batteries*, Kluwer Academic/Plenum Publisher, New York.

Scrosati B (2007), 'Nanomaterials: Paper powers battery breakthrough', *Nature Nanotechnology*, **2**, 598–9;

Scrosati B and Garche J (2010), 'Lithium batteries: status, prospects and future', *J Power Sources*, **195**, 2419–30.

Selvaraj I I, Chaklanobis S and Chandrasekar V (1995), 'Conductivity studies on poly (methoxyethoxyethylmethacrylate)-lithium salt complexes', *J Electrochem Soc*, **142**, 366–70.

Sequeira C A C and Hooper A (1983), 'The study of lithium electrode reversibility against $(PEO)_xLiF_3CSO_3$ polymeric electrolytes', *Solid State Ionics*, **9–10**, 1131–8.

Shin J H and Passerini S (2004), 'PEO-$LiN(SO_2CF_2CF_3)_2$ polymer electrolytes', *J Electrochem Soc*, **151**, A238–A245.

Shodai T, Owens B B, Ohtsuka H and Yamaki J (1994), 'Thermal stability of the polymer electrolyte $(PEO)_8LiCF_3SO_3$', *J Electrochem Soc*, **141**, 2978–81.

© Woodhead Publishing Limited, 2011

Silva R A, Silva G G, Furtado C A, Moreira R L and Pimenta M A (2001), 'Structure and conductivity in polydioxolane/$LiCF_3SO_3$ electrolytes', *Electrochim Acta*, **46**, 1493–8.

Song M, Cho J, Cho B W and Rhee H (2002), 'Characterization of UV-cured gel polymer electrolytes for rechargeable lithium batteries', *J Power Sources*, **110**, 209–15.

Stallworth P E, Greenbaum S G, Croce F, Slane S and Salomon M (1995), 'Lithium-7 NMR and ionic conductivity studies of gel electrolytes based on poly(methylmethacrylate)', *Electrochim Acta*, **40**, 2137–41.

Staunton E, Andreev Y G and Bruce P G (2007), 'Factors influencing the conductivity of crystalline polymer electrolytes', *Faraday Discuss*, **134**, 143–56.

Sukeshini M A, Nishimoto A and Watanabe M (1996), 'Transport and electrochemical characterization of plasticized poly(vinyl chloride) solid electrolytes', *Solid State Ionics*, **86–88**, 385–93.

Sung H Y, Wang Y Y and Wan C C (1998), 'Preparation and characterization of poly(vinyl chloride-co-vinyl acetate)-based gel electrolytes for Li-ion batteries', *J Electrochem Soc*, **145**, 1207–11.

Susan M A B H, Kaneko T, Noda A and Watanabe M (2005), 'Ion gels prepared by *in situ* radical polymerization of vinyl monomers in an ionic liquid and their characterization as polymer electrolytes', *J Am Chem Soc*, **127**, 4976–83.

Takeuchi M, Shuichi N, Takashi O, Nishioka, Ayako N and Masaaki N (2001), *Polymerizable Compound, Solid Polymer Electrolyte Using the Same and Use Thereof*. JP Patent 4–253771.

Tarascon J M and Armand M (2001), 'Issues and challenges facing rechargeable lithium batteries', *Nature*, **414**, 359–67.

Tarascon J M, Gozdz A S, Schmutz C, Shokoohi F and Warren P C (1996), 'Performance of Bellcore's plastic rechargeable Li-ion batteries', *Solid State Ionics*, **86–88**, 49–54.

Teeters D and Frech R (1986), 'Temperature-dependent spectroscopic studies of poly(propylene oxide) and poly(propylene oxide)-inorganic salt complexes', *Solid State Ionics*, **18–19**, 271–6.

Thackeray M M, David W, Bruce P G and Goodenough J B (1983), 'Lithium insertion into manganese spinels', *Mat Res Bull*, **18**, 461–72.

Tokuda H, Hayamizu K, Ishii K, Susan M A B H and Watanabe M (2004), 'Physicochemical properties and structures of room temperature ionic liquids. 1. Variation of anionic species', *J Phys Chem B*, **108**, 16593–600.

Trapa P E, Acar M H, Sadoway D R and Mayes A M (2005a), 'Synthesis and characterization of single-ion graft copolymer electrolytes', *J Electrochem Soc*, **152**, A2281–A2284.

Trapa P E, Won Y Y, Mui S C, Olivetti E A, Huang B, Sadoway D R, Mayes A M and Dallek S (2005b), 'Rubbery graft copolymer electrolytes for solid-state, thin-film lithium batteries', *J Electrochem Soc*, **152**, A1–A5.

Tsuchida E, Ohno H and Tsunemi K (1983), 'Conduction of lithium ions in polyvinylidene fluoride and its derivatives', *Electrochim Acta*, **28**, 591–5.

Vondrak J, Sedlarikova M, Velicka J, Klapste B, Novak V and Reiter J (2001), 'Gel polymer electrolytes based on PMMA', *Electrochim Acta*, **46**, 2047–8.

Wang Z, Huang B, Huang H, Xue R, Chen L and Wang F (1996), 'A vibrational spectroscopic study on the interaction between lithium salt and ethylene carbonate plasticizer for PAN-based electrolytes', *J Electrochem Soc*, **143**, 1510–14.

Watanabe M, Kanba M, Matsuda H, Tsunemi K, Mizoguchi K, Tsuchida E and Shinohara I (1981), 'High lithium ionic conductivity of polymeric solid electrolytes', *Macromol Chem Rapid Comm*, **2**, 741–4.

© Woodhead Publishing Limited, 2011

Watanabe M, Kanba M, Nagaoka K and Shinohara I (1982), 'Ionic conductivity of hybrid films based on polyacrylonitrile and their battery application', *J Appl Polym Sci*, **27**, 4191–8.

Watanabe M, Endo T, Nishimoto A, Miura K and Yanagida M (1999), 'High ionic conductivity and electrode interface properties of polymer electrolytes based on high molecular weight branched polyether', *J Power Sources*, **81–82**, 786–9.

Welton T (1999), 'Room-temperature ionic liquids solvents for synthesis and catalysis', *Chem Rev*, **99**, 2071–84.

Weston J E and Steele B C H (1982), 'Effects of inert fillers on the mechanical and electrochemical properties of lithium salt-poly(ethylene oxide) polymer electrolytes', *Solid State Ionics*, **7**, 75–9.

Whittingham M S (1976), 'Electrical energy storage and intercalation chemistry. Li/TiS_2 with $LiPF_6$ or $LiClO_4$ electrolyte at ambient temperature', *Science*, **192**, 1226–7.

Whittingham M S (2008), 'Inorganic nanomaterials for batteries', *Dalton Trans*, **40**, 5424–31.

Wieczorek W (1992), 'Entropy effects on conductivity of the blend-based and composite polymer solid electrolytes', *Solid State Ionics*, **53–56**, 1064–70.

Wieczorek W and Stevens J R (1997), 'Impedance spectroscopy and phase structure of polyether–poly(methyl methacrylate)–$LiCF_3SO_3$ blend-based electrolytes', *J Phys Chem B*, **101**, 1529–34.

Wieczorek W, Stevens J R and Florjanczyk Z (1996), 'Composite polyether based solid electrolytes. The Lewis acid–base approach', *Solid State Ionics*, **85**, 67–72.

York S, Frech R, Snow A and Glatzhofer D (2001a), 'A comparative vibrational spectroscopic study of lithium triflate and sodium triflate in linear poly(ethylenimine)', *Electrochim Acta*, **46**, 1533–7.

York S, Kellam III E C, Allcock H R and Frech R (2001b), 'A vibrational spectroscopic study of lithium triflate in polyphosphazenes with linear oligoethyleneoxy side-chains of different lengths', *Electrochim Acta*, **46**, 1553–7.

Zaghib K, Striebel K, Guerfi A, Shim J, Armand M and Gauthier M (2004), '$LiFePO_4$/polymer/natural graphite: low cost Li-ion batteries', *Electrochim Acta*, **50**, 263–70.

© Woodhead Publishing Limited, 2011

15
Proton exchange membranes for fuel cells

V. ARCELLA, L. MERLO, A. GHIELMI,
Solvay Solexis S.p.A., Italy

Abstract: This chapter deals with proton exchange membranes (PEM) for fuel cells (FC). Starting with the requirements that a PEM should ideally satisfy, it describes currently employed membrane materials, designs and fabrication processes. It also addresses the issues related to the operation of a PEM in a FC and the methods employed to assess performance and degradation. These aspects are complemented by a short introductory section on fuel cell basics and two sections in which applications and advantages/limitations of PEM FCs are discussed. The chapter ends by indicating possible future trends in PEM research and citing comprehensive references for a deeper study of the various subjects.

Key words: Aquivion® membranes, ionomer membranes, PEM fuel cell, polymer electrolyte FC, proton exchange membranes.

15.1 Introduction

Fuel cells (FC) are galvanic cells, in which the free energy of a chemical reaction is converted into electrical energy by continuously feeding the reactants (a fuel and an oxidant) to the electrodes of the cell. Their invention dates back to the middle of the nineteenth century, however development towards economically viable systems for energy generation started with a certain vitality only around the 1980s. One of the major factors determining the highly intense development of fuel cells in the last 30 years has been increasing concern about the environmental impact of fossil fuel use in electricity generation and vehicle propulsion. Fuel cells may contribute to reducing our dependence on fossil fuels and decrease emissions into the atmosphere, since they have higher efficiencies compared to heat engines. When pure hydrogen is used as a fuel, they produce only water, thus eliminating locally all emissions otherwise caused by electricity production and vehicle circulation, independently of the hydrogen source. As enablers of a truly emission-free energy generation technology, fuel cells using hydrogen would require this to be produced by completely renewable sources. The share of renewable energy from sun, wind and water will increase but these are not suited to cover the base load of energy request owing to their irregular availability. Employing these sources to produce hydrogen in combination with its use in fuel cells is, however, a practicable option for future power

© Woodhead Publishing Limited, 2011

generation. In addition, if compared to the direct combustion of fossil fuels in internal combustion engines (ICE), the use of hydrogen in FC vehicles shows a higher overall 'well-to-wheel' efficiency even when derived from the same fossil fuels.

Proton exchange membranes (PEM) are key electrolyte components in PEM fuel cells which, owing to their low operating temperature and high power density, are the most promising and versatile among the different FC technologies for low to medium power generation, especially under discontinuous or dynamic operation (e.g. uninterrupted power supply, vehicle propulsion).

This chapter gives an overview of membrane technology in PEM fuel cells by describing materials and production processes and analyzing the functional abilities of currently available products, thus including their shortcomings, ideal product design and related development trends. Exemplification of statements by experimental data will mostly be made referring to the so-called short-side-chain (SSC) perfluorosulfonic acid (PFSA) ionomer membranes, which are being developed at the authors' company and sold under the trade name Aquivion®. Incidentally, the SSC PFSA ionomer is currently recognized as the best available polymer electrolyte for fuel cell applications (see e.g. Kreuer *et al.*, 2008).

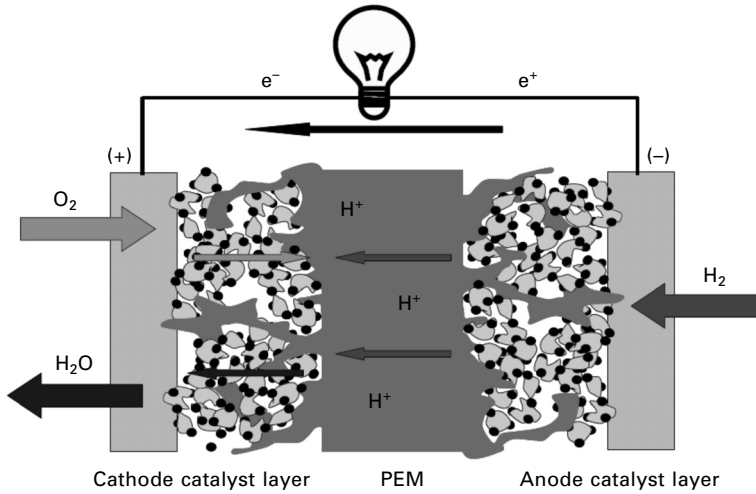
15.2 Basic operating principles and types of fuel cell

The operating principle of a fuel cell is extremely simple in its base concept. A fuel is continuously fed to the anode of the fuel cell and oxidized. Symmetrically, an oxidant is fed to the cathode and reduced. Positively charged ions that are formed at the anode as a result of fuel oxidation or, alternatively (depending on the electrolyte), negatively charged ions that are formed at the cathode as a result of oxidant reduction migrate through the electrolyte and react at the opposite electrode. Electrons need to flow through an external circuit from the anode to the cathode for the reaction to occur. The working principle is illustrated for a PEM FC with H_2 as the fuel and O_2 as the oxidant in Fig. 15.1.

Hydrogen and methanol are the most typical fuels supplied to the anode for direct oxidation. Hydrocarbon fuels can also be directly fed to the cell in high-temperature fuel cells (> 550°C) and the reaction typically occurs through reforming the fuel in the first part of the cell and then oxidation of the resulting hydrogen and carbon monoxide species. The cathode reaction in fuel cells is typically oxygen reduction, in most cases from air.

Fuel cells are usually classified according to the type of electrolyte they use, which largely determines the temperature of use and the type of reactants. The most relevant exceptions are direct-methanol fuel cells (DMFCs), which can, however, be considered as a sub-type of PEM fuel cells, with methanol

© Woodhead Publishing Limited, 2011



15.1 Working principle of a H_2/O_2 PEM fuel cell.

Table 15.1 Fuel cell types and their main characteristics

Type	Electrolyte	Typical working temperature range (°C)	Conducting ion
Alkaline	KOH	60–90	OH^-
PEM	PFSA ionomer	60–90	H^+
Phosphoric acid	H_3PO_4	170–220	H^+
Molten carbonate	Li_2CO_3–K_2CO_3 or Li_2CO_3–Na_2CO_3	550–800	CO_3^{2-}
Solid oxide	$Zr_{0.92}Y_{0.08}O_{1.96}$	800–1000	O^{2-}

PFSA = perfluoro sulfonic acid

fed directly to the anode. Other liquid reagents, such as ethanol or formic acid, can also be fed directly to the anode of a PEM FC. These reagents, however, have still not demonstrated up until today performances comparable to DMFC. Fuel cell types and their main characteristics are summarized in Table 15.1.

In a FC the voltage differential ΔV_0 that theoretically develops between the electrodes of a single cell is related to the Gibbs free energy change ΔG of the chemical reaction via the relationship $\Delta G = -nF\Delta V_0$, where n is the number of electrons involved in the reaction and F is the Faraday constant. Non-reversible losses in practice cause the cell potential to be lower than the theoretical one, even when the power extracted from the FC is zero, due to the non-ideality of the real system (e.g. gas permeability of the separator). Relevant deviations from the thermodynamic voltage are observed especially moving away from equilibrium conditions, that is at increasing cell currents.

© Woodhead Publishing Limited, 2011

These losses typically include electrode overpotential losses, ohmic losses given by electrolyte resistance to ion transport and mass transport losses caused by reactant diffusion limitations in the electrodes. Single cells are normally stacked in series to form what is referred to as a FC stack, the voltage of the stack ΔV^S being the sum of the individual cell voltages (ΔV^S ~ 1 V × number of cells at zero current).

15.3 Membrane materials, design and fabrication processes

15.3.1 Defining membranes

FC membranes are referred to as 'separation membranes' with better permeability and selectivity values than films or electrolytes because their function is, in short, to allow transport of protons from one side to the other with the lowest possible resistance while preventing fuel and oxidant from coming in contact with each other. The ideal membrane material is theoretically one which has the highest proton conductivity $\sigma(H^+)$ coupled to the lowest fuel and oxygen permeability $P(i)$ (over all operating conditions). A selectivity value $S(i) = \sigma(H^+)/P(i)$ can be defined for the individual reactant i (i = oxygen, hydrogen or methanol fuel) and this should be the highest possible. This parameter characterizes in principle both material and membrane, since the characteristic distance (membrane thickness) over which protons and gases move are the same. However, it should be best measured on the membrane inside the system, in order to account correctly for surface and interface resistance effects, which are increasingly important for very thin membranes.

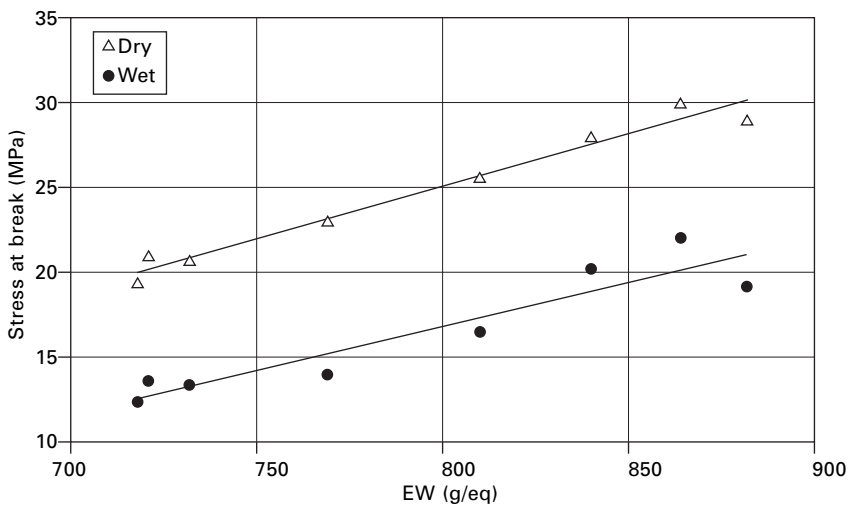
While higher membrane selectivities $S(i)$ are always welcome, membrane selection is based in practice on a balance of properties which strongly depends on system design and operation mode, and also the capability of the membrane to show only minor degradation of its properties throughout the desired life of the fuel cell. For instance, in systems where hydrogen is fed to the cell with no excess compared to that required to sustain the current ('dead-end' operation mode), the amount of nitrogen passing from the air to the hydrogen side is critical in defining how often the anode side must be purged to keep the hydrogen concentration high enough, and therefore in defining the system fuel efficiency. In this case, the maximum nitrogen permeability $P(N_2)$ must also be specified, although this is normally not the case for systems where some unreacted hydrogen is discharged continuously from the anode outlet. Another example relates to oxygen and hydrogen permeability: while calculations purely related to fuel efficiency (Gasteiger and Mathias, 2002) show that for a 25 μm membrane, typically used PFSA materials stand in acceptable permeability ranges (note: for hydrogen just

© Woodhead Publishing Limited, 2011

at the border of acceptability), it has however been reported (see e.g. Liu *et al.*, 2006) that reactants permeating through the membrane give rise to peroxide species which attack and degrade the polymer electrolyte, causing it to fail. The mechanical and chemical stability of the membrane will in this case define the maximum admitted reactant permeability. Since this relationship is extremely complex to quantify, normally empirical tests are carried out to check whether the membrane stability in time is sufficient. A third noteworthy example is one related to conductivity and mechanical properties: one possibility of increasing the conductivity $\sigma(H^+)$ of the polymer electrolyte is to decrease its equivalent weight EW (grams of polymer per equivalent of ion-transporting groups). However this typically implies decreasing the mechanical properties of the polymer (see e.g. Fig. 15.2) which can obviously have a negative impact on membrane durability.

DMFC membranes require a similar but separate consideration. For these polymer electrolyte fuel cells, the well known current challenge is to increase the membrane selectivity $S(CH_3OH)$ by decreasing methanol permeability $P(CH_3OH)$ through the membrane without substantially decreasing $\sigma(H^+)$, rather than further increasing $\sigma(H^+)$. In fact, methanol permeating through the membrane from the anode to the cathode side is at the origin of substantial fuel and voltage losses in these kinds of fuel cells.

One further important requirement to be mentioned is the necessity for a PEM FC membrane to transport water properly. Considering that water is generated at the cathode and that it also moves from the anode to the



15.2 Stress at break (by ASTM D1708) of extruded Aquivion® membranes as a function of EW. 'Dry': conditioned and measured at 23°C and 50% relative humidity (RH). 'Wet': conditioned in boiling water and immediately measured at 23°C and 50% RH.

© Woodhead Publishing Limited, 2011

cathode together with the protons (the so-called 'water drag' effect), it is fundamental that water rapidly back-diffuses from the cathode to the anode to prevent anode dry-out and subsequent decrease of reaction efficiency. This is especially true in hydrogen PEM FCs operating with dry inlet gases. In addition to this, while in an idealized system (the one desired by any system engineer) electrolyte conductivity is high and independent of relative humidity (RH), in reality currently employed PEMS show high dependencies of conductivity $\sigma(H^+)$ on RH. In this respect, fast water diffusion through the membrane keeps the membrane well hydrated through its entire thickness, and thus working efficiently.

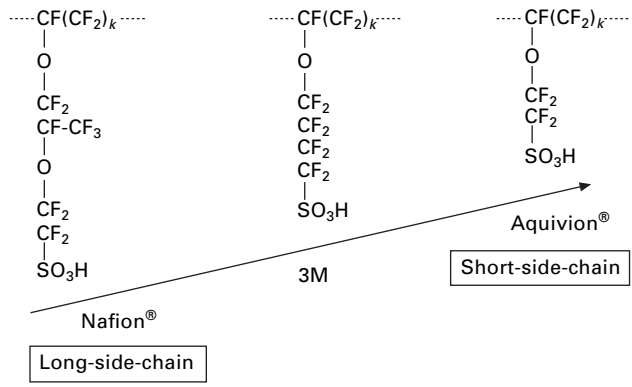
15.3.2 Membrane materials

One of the key enablers of the revival of fuel cells in the last decades of the twentieth century was the availability of perfluorosulfonic acid (PFSA) ionomers, first developed and commercialized by Dupont under the tradename Nafion®. Ionomers are defined as polymers where a fraction of the monomer units carries an ionic functionality (polymers where all monomer units are ionic in nature are normally referred to as polyelectrolytes).

After the introduction of Nafion®, other companies have developed and introduced PFSA ionomers to the market, namely Asahi Glass (Flemion®) and Asahi Chemical (Aciplex®). Around the 1980s, Dow Chemical developed a very interesting new PFSA (see e.g. Ezzell *et al.*, 1982 and Tant *et al.,* 1989), characterized by a short-side-chain (SSC) carrying the ionic functionality. Although the superior properties (higher crystallinity, higher glass transition temperature) of the SSC ionomer and their possible implications for FC application were soon recognized (Eisman, 1986) and significant improvements in FC performance actually obtained (Prater, 1990), Dow never brought this PFSA ionomer to a commercial scale. More recently Solvay Solexis introduced a simpler chemical route to the synthesis of the SSC monomer sulfonic precursor (Arcella *et al.*, 2003), which allowed the development of SSC PFSA membranes to be restarted (Ghielmi *et al.*, 2005) now commercially available under the tradename Aquivion®. Another PFSA ionomer recently developed by 3M has a side chain with a length intermediate between Aquivion® and Nafion® and correspondingly intermediate properties (Hamrock, 2009). Figure 15.3 reports the three structures of commercially available PFSA ionomers. Flemion® and Aciplex® are normally described as being long-side-chain (LSC) type ionomers (see. e.g. Doyle and Rajendran, 2003; Grot, 2008).

PFSA ionomers are normally described as having micro-segregated structures, resulting from the strongly hydrophobic fluorinated polymer portions that separate from the ionic domains constituted by the clustered ion-exchange groups. Small angle X-ray scattering and neutron scattering

© Woodhead Publishing Limited, 2011



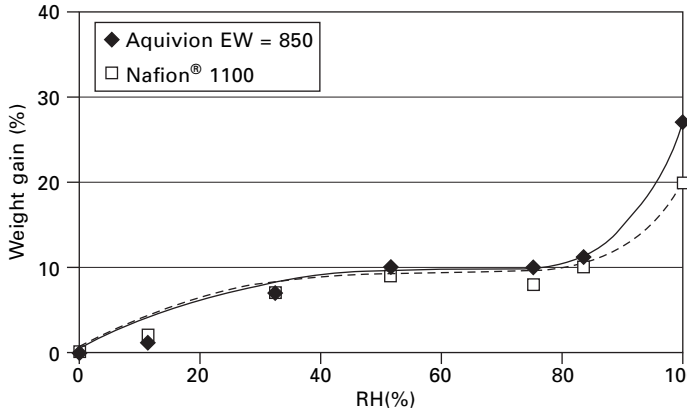
15.3 Main structures of commercially available PFSA ionomers.

experiments provide clear evidence of this kind of micro-phase separated morphology. Several conceptual models have been developed to describe it. One of the earliest and surely the most popular is the 'cluster network model' proposed by Hsu and Gierke (1982). This model represents the ionomer as constituted by spherical ionic clusters (3–4 nm in diameter) dispersed within the fluorinated matrix and interconnected by cylindrical ionic channels (~1 nm in diameter). Gierke *et al*. (1981) had previously calculated the cluster diameter to be ca. 4 nm for a 1200 EW Nafion® ionomer at 20% water uptake by weight, while the existence and size of the interconnecting channels was postulated to justify on one hand the continuity of ionic transport through the ionomer and on the other hand the OH^- exclusion characteristics that enable high current efficiencies in the chloralkali application.

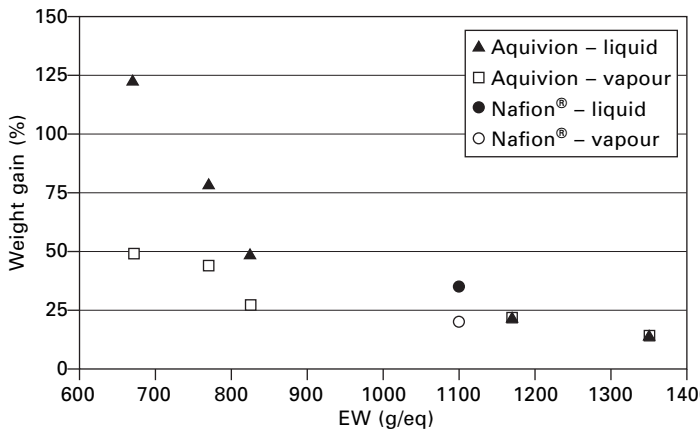
PFSA ionomers have a high affinity to water as a result of their ionic nature. Hydration is a strong function of RH, especially in the high humidity region (see Fig. 15.4). Moreover, uptake from the saturated vapour and liquid water do not show the same values, commonly referred to as the Schroeder paradox. Actually, this phenomenon first described for Nafion®, does not appear at sufficiently low ionic contents while it is more and more apparent at decreasing EWs (see Fig. 15.5), where uptake from liquid water strongly increases. As a matter of fact, at sufficiently low EWs (below 650 g/eq for SSC), liquid water uptake diverges, as shown in Fig. 15.6. The result is that the ionomer is completely dissolved. This is primarily due to the crystallinity of the polymer becoming so low, as a result of the increased number of side chains in the polymer, that the interactions of the ionic groups with the polar solvent become energetically dominant.

Figure 15.7, where data for SSC ionomers in the range 550–950 g/eq are collected, shows interpolated crystallinity falling to zero at EW = 600 g/eq (linear interpolation). Figure 15.7 shows that a small residual crystallinity persists below EW = 600 g/eq, which can be theoretically predicted by

© Woodhead Publishing Limited, 2011



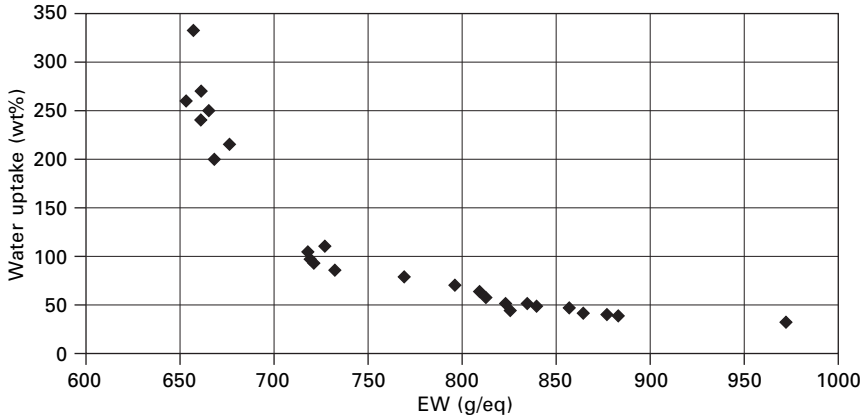
15.4 Water uptake of SSC and LSC PFSA extruded membranes from the vapour phase at 30°C as a function of relative humidity.



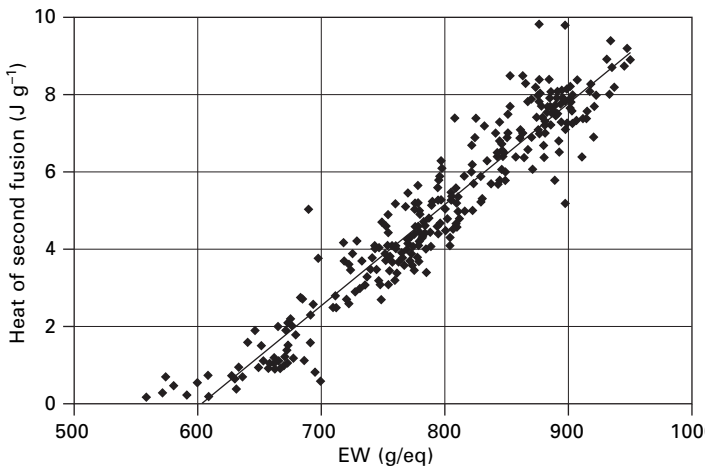
15.5 Water uptake of different ionomers (extruded membranes) from the vapour phase and the liquid phase at 100°C as a function of EW.

calculation of the distribution of -CF_2- sequences by using a classical statistical polymerization model (representative reactivity ratios for the monomers can be found in Kirsh *et al.*, 1990). However, this residual crystallinity is insufficient to hold the polymer chains together in boiling water. Insolubility and good mechanical properties in hot water are normally prerequisites for a FC membrane, since water is the product of the FC reaction and conditions where water is present in the liquid state are frequently experienced, especially for dynamic applications (exceptions might be stationary applications working in the higher temperature range with controlled shut-down strategies to avoid any water condensation).

© Woodhead Publishing Limited, 2011



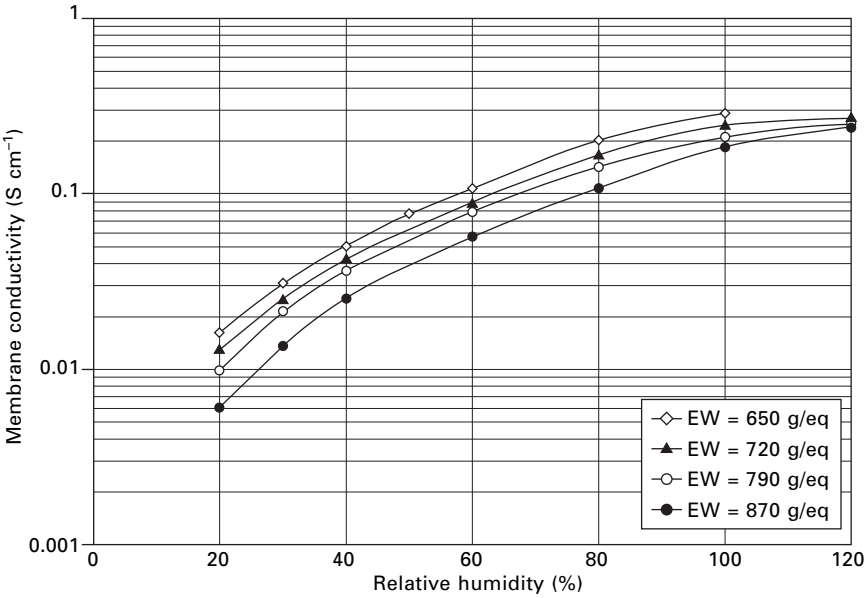
15.6 Weight uptake from boiling water as a function of EW (SSC ionomers).



15.7 Crystallinity, expressed by the heat of second fusion in differential scanning calorimetry (DSC) measurements, as a function of EW (SO_2F precursors of SSC ionomers).

Low EW ionomers are of great importance when confronted with the conductivity targets set out by car manufacturers. As a matter of fact, the conductivity of PFSA ionomers is a strong function of water content, which is in turn strongly related to relative humidity (Doyle and Rajendran, 2003). Figure 15.8 shows both the strong dependence of conductivity on RH and the fact that membrane conductivity increases with decreasing EW. Based on system simplification requirements for automotive application, conductivities around 0.1 S cm^{-1} are described as 'desirable' in the 50–67% RH range and as 'ideal' in the 25–33% range for a 20–25 μm membrane (Gasteiger

© Woodhead Publishing Limited, 2011



15.8 Membrane conductivity at 80°C as a function of RH for SSC ionomers with different EWs. RH at 120% refers to a condition of oversaturation obtained by saturating the inlet gases at a temperature higher than the measurement temperature.

and Mathias, 2002). A 25% RH inlet humidification, calculated in the same publication, would allow the stack to operate up to 120°C with no additional water recirculation and air compression requirements compared to a state-of-the art 80°C stack operating at full humidification. It is calculated that a temperature of 120°C is required in order to be able to reject the heat produced during peak operation of the engine without the need for higher heat rejection areas, that is oversized front radiators, compared to the ones currently utilized (Masten and Bosco, 2003). Incidentally, note that 120°C operation additionally requires that the ionomer is physically stable under such operating conditions. The higher glass transition temperature of the SSC ionomer (130–165°C, see Ghielmi *et al.*, 2005) makes it an ideal candidate among commercially available structures for such high temperature operation.

Going back to the conductivity targets, Fig. 15.8 shows that conductivity values approaching the 'desirable' ones are obtained with SSC low EW ionomers still in the range of semi-crystalline materials (EW = 650). Conductivity values approaching 'ideal' can be obtained with a SSC ionomer with EW below 500, but as shown above these ionomers are not physically stable in hot water. It may be possible to circumvent this problem by crosslinking the polymer. Approaches have been proposed which consider both radical crosslinking

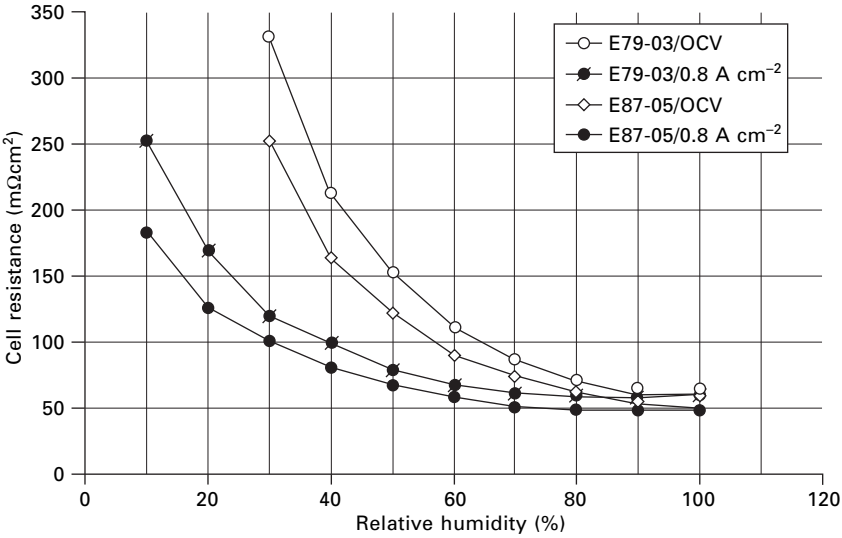
© Woodhead Publishing Limited, 2011

by introduction of cure sites during the polymerization (Arcella *et al.*, 2002) and ionic crosslinking through the functional groups of the ionomer. On one hand, these approaches typically involve quite complex chemistry of the membrane film once it is already formed, which is rather inconvenient from the production point of view. On the other hand, crosslinked membranes showing the 'ideal' conductivity values in combination with the chemical and mechanical stability properties required by the application still have to be proven.

Feeding fuel cells with dry reactant gases would give the highest level of system simplification. This is especially true on the air side, since hydrogen can be more easily recirculated from the outlet stream to provide some level of humidification at the inlet or can even come in already highly moist from the hydrocarbon reforming process. To handle zero-humidification inlet conditions, two strategies are being followed. The first is to develop materials that do not require water to conduct protons, which can be referred to as 'intrinsic' proton conductors. Such materials would have to comply with the conductivity requirements discussed above, that is, they should be as conductive, in the absence of water, as the highly acidic aqueous system provided by a PFSA ionomer under full humidification. This is a highly challenging task. The alternative strategy is to design membranes which can very quickly transfer the water produced in the cell to humidify the membrane sides (and electrodes) in contact with the dry gas at the inlet area. In this respect, it is useful to operate the fuel cell with the fuel and the oxidant flowing counter-current, so that the dry inlet on one side of the cell corresponds to the moist outlet on the other side. As for the conductivity, improvements in membrane water permeability are obtained by decreasing the EW, owing to the lower crystallinity of the material and the higher water sorption. Another possibility is to decrease the membrane thickness. This is more relevant to membrane design rather than to materials and is thus discussed in Section 15.3.3. Both approaches (reducing EW and reducing thickness) pose the challenge of decreased membrane mechanical properties and increased gas permeability.

Figure 15.9 shows the effect of the water produced when operating the fuel cell at the resistance of the membrane electrode assembly (MEA). In this specific case, the MEA resistance is more than halved under dry conditions when operating the cell at 0.8 A cm^{-2}. Note that in automotive applications, currents more than twice as high are typically targeted at peak power, which means more than twice the water produced. In Fig. 15.9 the beneficial effect of a thinner and lower EW membrane can also be noticed. Despite the lower mechanical properties, when the cell is operated with dry inlet gases, lower EW membranes can ensure a homogeneous distribution of the water produced in the cell, avoiding local dry-out of the MEA and thus leading to longer lifetimes.

© Woodhead Publishing Limited, 2011

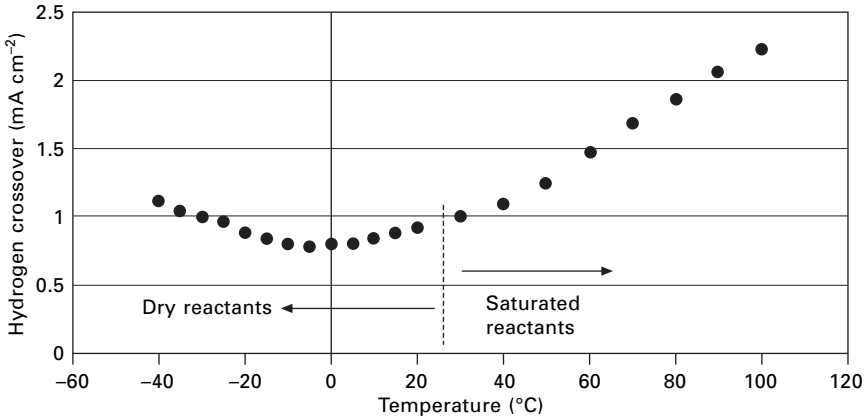


15.9 MEA resistance as a function of inlet RH under OCV (open-circuit voltage) and with current applied for two extruded Aquivion® membrane types (E79-03: EW = 790 g/eq, thickness = 30 μm; and E87-05: EW = 870 g/eq, thickness = 50 μm). Test conditions: H_2 and air, cell temperature = 75°C, cell pressure = 1.5 bar abs, anode inlet RH = cathode inlet RH.

Apart from being able to conduct protons under dry conditions, fuel cell membranes must ensure sufficient conductivities at sub-zero temperatures. This is obviously true for systems which need to work exposed to ambient conditions, for example car engines. A change in the slope of the Arrhenius-form conductivity–temperature plot is measured for PFSA around the water freezing point, which highlights a change in the activation energy of the proton transport mechanism; however, no discontinuity in the conductivity curve occurs (Merlo *et al.*, 2007a). Moreover, the drop in conductivity (increase in the conductivity–temperature slope) is not dramatic at sub-zero conditions, owing to the good conductivity properties retained by water in the solid state and the presence of non-freezable water inside the membrane structure. Similar conductivities at such low temperatures represent another high challenge for 'intrinsic' proton conductors. Sub-zero start-up in FCs equipped with PFSA membranes has been widely proven.

Gas permeability requirements have been discussed in Section 15.3.1. In order to exemplify typical values and trends, Fig. 15.10 reports H_2 crossover through a SSC ionomer membrane as a function of temperature over the full working temperature range (at least for current PEM FCs). The H_2 crossover is measured and expressed as an equivalent crossover current. Measurements were taken at full humidification above 25°C and with dry inlet gases below

© Woodhead Publishing Limited, 2011

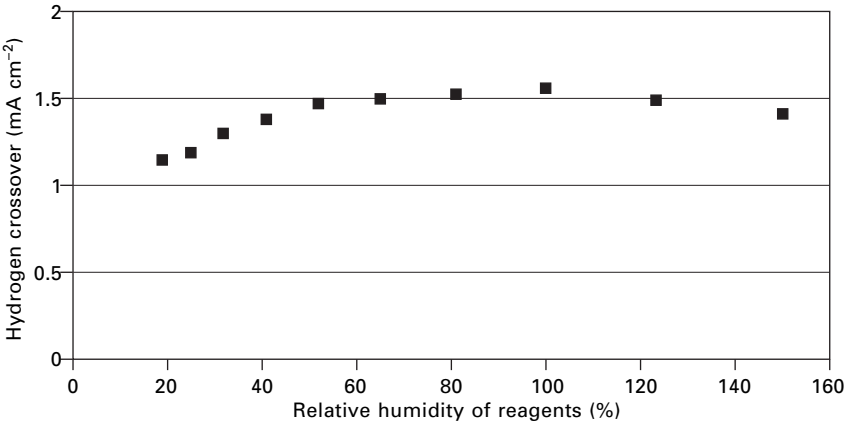


15.10 H_2 crossover as a function of temperature for an Aquivion® E87-05 extruded membrane. The crossover is measured as an electric current by imposing a voltage on the cathode side (operated in N_2) such that all the permeated hydrogen is oxidized and transported back as H^+ to the electrode fed on hydrogen. N_2 pressure: 1 bar abs; H_2 pressure: 1.5 bar abs.

this temperature. Three points are worth noting when observing Fig. 15.10. First, is that permeability increases as temperature increases towards 100°C. This must be taken in account when developing thinner membranes fit for dry operation at these temperatures. Second, is that a minor discontinuity arises when passing from dry to fully humidified conditions at 25°C. This is due to the fact that relatively small differences in H_2 crossover are measured passing from high to low RH, with values decreasing in moving towards the dry state (see Fig. 15.11). Third, it can be observed that the curve has an inversion of tendency around the freezing point of water, with permeability values slightly increasing when moving towards deep freezing temperatures.

Another important characteristic of fuel cell membranes is their chemical stability in the highly aggressive environment of the fuel cell. Though Nafion® PFSA ionomers were originally selected for their high chemical inertness, as demonstrated by lifetimes in excess of 57 000 hours (Prater, 1990), in recent years it became evident that measures needed to be taken to ensure that there is sufficient durability under operation conditions required to make the technology viable. The originally proposed materials proved to be insufficient under operating conditions where high voltages, low humidity and/or dry/wet cycling conditions are frequently experienced. These conditions are typical, for example, of an automotive drive cycle. Degradation of the ionomer has been recognized to occur as a result of the presence of the hydroxyl OH• and hydroperoxyl HO_2• species that form as a consequence of reactant crossover and is highlighted by the evolution of fluorides in the outlet water, increase of hydrogen crossover, membrane thinning and formation of pin holes. It

© Woodhead Publishing Limited, 2011



15.11 H_2 crossover as a function of RH for an Aquivion® E87-05 extruded membrane at 60°C. N_2 pressure: 1 bar abs; H_2 pressure: 1.5 bar abs.

has been shown that H_2, O_2 and a catalytic surface are required to obtain membrane degradation (Liu *et al.*, 2006). Hydrogen peroxide has been detected in both anode and cathode condensate in a concentration directly proportional to the membrane gas crossover (Liu and Zuckerbrod, 2005). Hydrogen peroxide is well known to lead to the formation of the above radicals, especially by catalytic action of Fenton metal ions such as Fe^{2+}. Actually, contamination by Fe^{2+} ions has been proven to increase strongly the rate of membrane degradation (Liu *et al.*, 2009).

PFSA ionomer degradation is recognized to occur via attack of the weak carboxylic end groups of the fluorinated chains, leading to an 'unzipping' of the same, according to the following mechanism (Curtin *et al.*, 2004):

$$R_f\text{–}CF_2COOH + OH\bullet \rightarrow R_f\text{–}CF_2\bullet + CO_2 + H_2O$$

$$R_f\text{–}CF_2\bullet + OH\bullet \rightarrow R_f\text{–}CF_2OH \rightarrow R_f\text{–}COF + HF$$

$$R_f\text{–}COF + H_2O \rightarrow R_f\text{–}COOH + HF$$

where R_f is the fluorinated ionomer backbone chain.

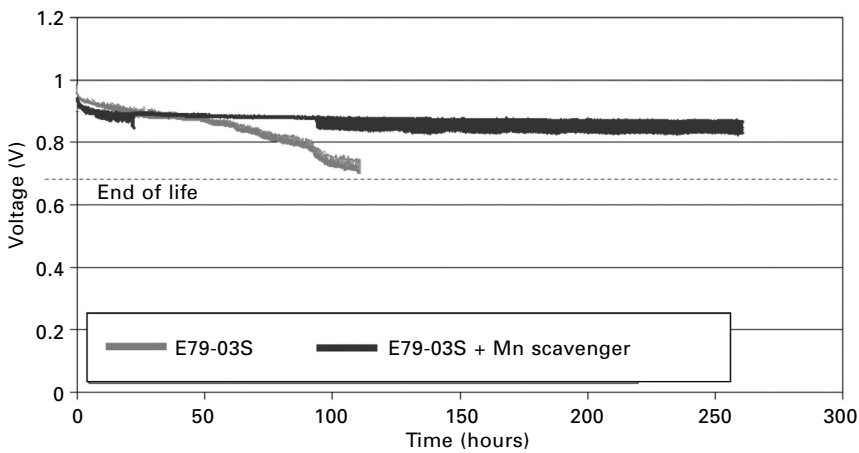
Large improvements have been obtained by reducing or eliminating the weak end groups (Curtin *et al.*, 2004; Merlo *et al.*, 2007b). This can be achieved by, for example direct fluorination of the polymer, thermally or UV-assisted; $-CF_3$ end groups are obtained. These PFSA ionomers are typically referred to as 'stabilized'. However, it has also been shown that under very dry or dry/wet operating conditions, the advantage of stabilized ionomers over unstabilized ones disappears (Liu *et al.*, 2009). As a matter of fact, under dry conditions mechanisms are active which lead to chain scission and consequent formation of carboxylic groups in the polymer (Hommura *et al.*,

© Woodhead Publishing Limited, 2011

2008). Significant chain length reduction is also physically apparent from the extreme embrittlement that membranes experience. According to such findings, carboxylic end groups are formed in dry conditions and unzipping of the chain subsequently follows under wet conditions starting from these weak terminals. Exposure of the membrane to H_2O_2 in dry conditions followed by exposure in wet conditions, gives, in fact, the most pronounced membrane degradation (Liu *et al.*, 2009). It is therefore evident that under automotive drive cycles, where dry and wet conditions alternate, stabilizing ionomers by weak chain-end elimination is insufficient.

Alternative stabilization approaches have been developed by adding stabilizer molecules to the ionomer in the membrane (or in the electrode), normally referred to as 'scavengers'. The stabilizer molecules typically act as catalysts to the decomposition of the reactive radicals or as radical traps, with kinetics that must be obviously faster than the reaction of the radicals with the ionomer chain. These kinetics have recently been measured by spin trapping electron spin resonance (ESR) for the Ce^{3+} scavenger ion (Danilczuk *et al.*, 2010). Incidentally, the same paper shows that Aquivion® and 3M ionomers, that is linear side-chain ionomers, are more stable to radical attack than Nafion®-type ionomers due to the absence of the tertiary carbon in the side chain.

A large number of papers and patents have recently appeared related to the introduction of radical scavengers in fuel cell membranes. Among the scavengers with catalytic activity, Mn^{2+} and Ce^{3+} have been reported to be among the most active (Coms *et al.*, 2008). Figure 15.12 shows the



15.12 OCV hold durability test for an extruded Aquivion® E79-03S membrane and the same membrane type with Mn scavenger. Test conditions: H_2 and oxygen, cell temperature = 90°C, cell pressure = 1 bar abs, 25% inlet RH (both anode and cathode), BASF LT250EW electrodes on both sides.

© Woodhead Publishing Limited, 2011

improvement in durability obtained in an OCV (open-circuit-voltage) hold test in dry conditions when an extruded Aquivion® membrane was partially neutralized by manganese ions (4% mol of sulfonic groups neutralized).

Finally it is worth regarding hydrocarbon ionomers for use in FC membranes. Significant improvement has been achieved in these materials in the last few years, the aim being to develop cheaper alternatives to fluorinated polymers (Gross *et al*., 2009). Hydrocarbon-based membranes, however, typically show low conductivities when moving away from fully humidified conditions, as a result of lower acid strengths compared to PFSAs. To achieve acceptable conductivity levels, the ion-exchange capacity has to be increased greatly, leading to undesirably high water swelling. Another drawback is that hydrocarbon materials are often mechanically quite stiff; this may lead to problems in creating tenacious bonding of the electrodes to the membrane, with a detrimental effect on durability. Finally, hydrocarbon polymers are in general less chemically stable than fluorinated polymers, owing to lower intramolecular bond energies; long-term stability of membranes based on such materials still needs to be proven in those PEM FC applications where the chemical stress on the membrane is the highest, for example automotive.

The main advantage of hydrocarbon membranes relates to their very low reactant permeability. In this respect, hydrocarbons are very promising candidates for DMFC application, since the high swelling of PFSA ionomers in methanol typically leads to relevant fuel crossover. Also, DMFC is an application where the environment is not chemically very aggressive to the membrane owing to high humidity and typically non-dynamic operation; therefore, it is more suited for less stable membrane materials such as hydrocarbons. Though Nafion® is still the current reference for DMFC application, possible replacements have been reported with lower methanol crossover at similar proton conductivities and/or higher DMFC power densities. An excellent review of polymer electrolyte membranes for DMFC can be found in Deluca and Elabd (2006).

15.3.3 Membrane design

Although many examples can be found in the technical literature of asymmetric membranes for fuel cells (e.g. multi-layers of different EW or incorporating barrier layers for methanol in the case of DMFC), symmetric membranes are the option widely used in practice for FCs.

One possibility to classify FC PEMs according to their design is to distinguish ‘dense’ (or ‘unsupported’) membranes and ‘reinforced’ (or ‘supported’) membranes. Dense membranes are homogenously constituted through their thickness by the ionomer, normally alone, or eventually in intimate mixtures with other polymers doped with scavenging molecules. Reinforced membranes, instead, incorporate a microporous support, which

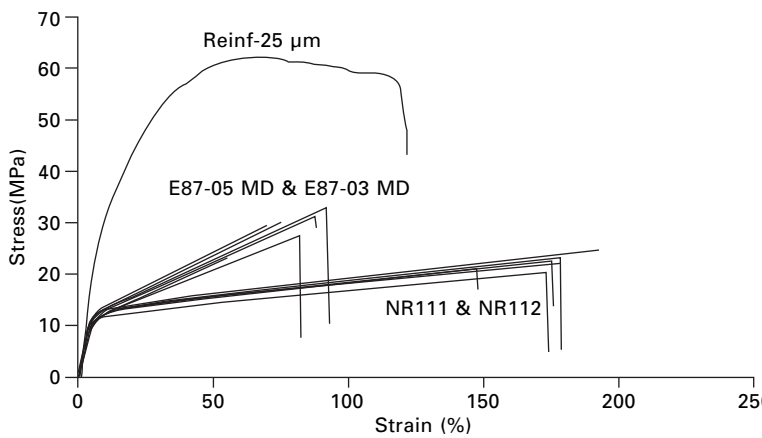
© Woodhead Publishing Limited, 2011

has the function of stabilizing the membrane mechanically. The support is usually embedded inside the membrane, leaving two peripheral layers of dense ionomer. Dense membranes can be isotropic or anisotropic in the plane, according to their production process. Typically, membranes obtained by melt extrusion are anisotropic owing to the stretching that occurs in machine direction during the extrusion process. This anisotropy is readily detected by, for example, different linear swelling upon soaking in water and different mechanical properties in the two directions of the plane. Solvent-cast membranes are instead typically isotropic in the plane.

Reinforced membranes are typically isotropic or moderately anisotropic in the plane, in relation to the properties of the support material. For instance, when biaxially expanded films are used as reinforcement, differences in the stretching ratio in the two directions will define the level of anisotropic behaviour of the final membrane product.

ePTFE (expanded polytetrafluoroethylene) is the most well known and well studied microporous material for reinforcement of FC membranes. It was introduced for the purpose in the 1990s (Verbrugge *et al.*, 1992; Kolde *et al.*, 1995; Bahar *et al.*, 1996). Although not mechanically outstanding, this material is considered ideal for a number of its properties: very high void volume (> 80%), very fine and regular pore structure defined by thin fibrils, good compatibility with PFSA ionomers, extremely high chemical inertness and extremely low thickness availability (down to <10 μm).

Figure 15.13 shows stress–strain curves for different membrane types. Comparison is made between cast membranes (Nafion® NR), extruded membranes (Aquivion® E87) and an experimental reinforced membrane

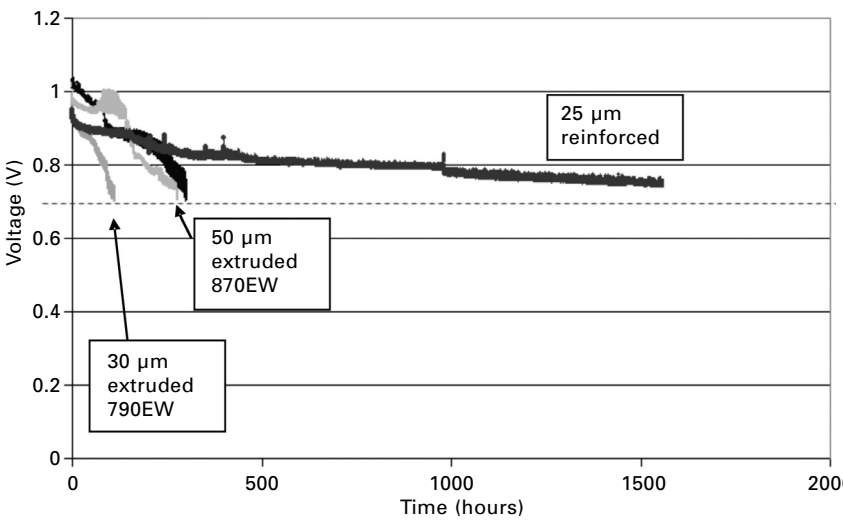


15.13 Stress–strain curves for cast Nafion® membranes (NR111, N112), extruded Aquivion® membranes (E87-03, E87-05) and an experimental ePTFE-based reinforced membrane. Test conditions: 23°C, 50% RH.

© Woodhead Publishing Limited, 2011

obtained by impregnating ePTFE with a commercial ionomer dispersion. On one hand it can be seen that extruded membranes show a higher stress than cast membranes after the yield point and a lower strain at break. This is due to the fact that the measurement was taken in the machine direction, that is the direction in which the material is oriented during processing. On the other hand, it can be seen that the reinforced membrane shows both a high modulus and an elevated strain at break, that is overall improved mechanical properties. This is due to the interaction of the PFSA ionomer with the fine fibrillated PTFE structure which creates a composite structure in the membrane, that is two extensively interacting solid phases.

Other microporous materials are under investigation as reinforcing materials, especially targeting improved mechanical properties of the membrane. Examples are porous bi-stretched polyethylene (Mallant *et al.*, 1998) and porous PVDF (Nasef *et al.*, 2006). Higher durabilities can be obtained by introducing a microporous reinforcement in the membrane. Figure 15.14 shows the result of a durability test (OCV hold) for an experimental reinforced membrane produced with EW = 830 g/eq Aquivion® compared to a number of other dense Aquivion® membranes obtained by melt extrusion with different ionomers and thicknesses (the first two digits after the 'E' represent the EW and the last two digits the thickness in tens of micrometres, for example E87-05 has an EW of 870 g/eq and a thickness of 50 μm; the final 'S' stands for stabilized ionomer). Despite the fact that the ionomer in



15.14 OCV hold durability test for an experimental Aquivion® reinforced membrane (25 μm thickness) compared to Aquivion® extruded (E) membranes with different EWs and thicknesses. Test conditions as in Fig. 15.12.

© Woodhead Publishing Limited, 2011

this reinforced membrane is not stabilized and that the membrane is in the low thickness range, the effect of the reinforcement is evident in limiting the decay under these test conditions. Actually, while the ionomer in a dense membrane is at the same time delivering functional and mechanical characteristics, in a supported membrane these are at least partially subdivided between ionomer (functional) and reinforcement (mechanical). Therefore, even if the mechanical characteristics of the ionomer are degraded by chain scission under the chemically aggressive conditions of the test in Fig. 15.14, the reinforcement is still able to confer sufficient mechanical stability to the membrane. However, by virtue of the composite nature of the membrane, if the ionomer is extremely degraded, a reinforced membrane with a highly inert support material will also fail.

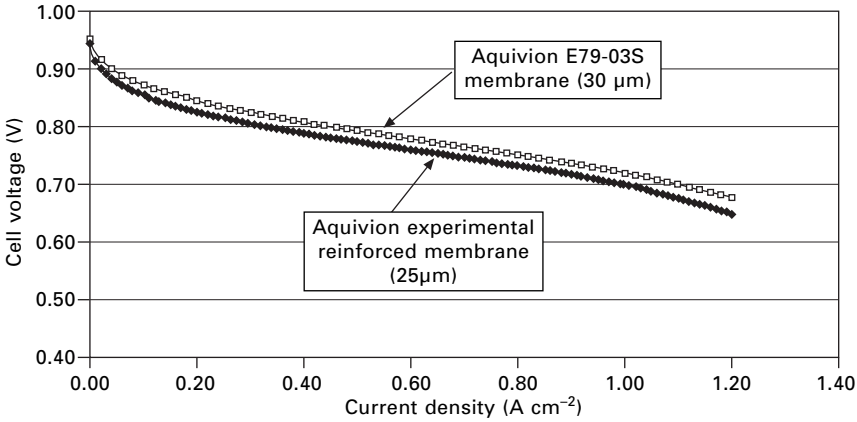
Note that while extruded membranes are typically not fit to survive under the dry high voltage test conditions shown in Fig. 15.14 (failure in few 100 hours), they can guarantee very high lifetimes under high RH conditions with current constantly drawn from the a cell (typical stationary application conditions): a cell operation of 20 000 hours has been recently achieved on an Aquivion® E87-05S membrane with no detectable membrane degradation (Merlo *et al.*, 2010).

While introduction of reinforcement can deliver significant durability improvements, as shown above, it obviously affects the conductivity of the membrane, owing to the presence of the inert support material. It was also recognized in early studies that water permeability is reduced (Verbrugge *et al.*, 1992). Proper optimization of the membrane construction (choice of support, impregnation parameters, etc.) can limit these drawbacks. Moreover, the introduction of the support allows lower thicknesses without compromising durability, which helps to compensate for conductivity and water permeability losses. Figure 15.15 shows that better performances (voltage at given current) are achieved with a reinforced membrane (experimental membrane of thickness 25 μm) compared to an extruded 30 μm Aquivion® E79-03S membrane.

In recent years, the general trend for membranes in H_2/air FC applications, especially for automotive applications, has been to move to lower thicknesses. Ultra-thin membranes (<10 μm) have been shown to be able to preserve the cell voltage under very dry conditions if electrical current is drawn from the cell. For instance, Kinoshita and Shimoda (2008) have shown limited voltage losses in H_2/air operation at 10% inlet RH, 95°C, 150 kPa and 2 A cm^{-2} with 5 μm thick membranes. This is related to the efficient transport by the thin membrane of the water produced at the cathode to keep the whole MEA well hydrated.

Membranes with such low thickness obviously pose the problem of higher gas crossover and lower durability. The latter is obviously related to the lower membrane strength but also to the higher gas permeability, which

© Woodhead Publishing Limited, 2011



15.15 Polarization curve for an experimental Aquivion® reinforced membrane (25 μm thickness) compared to an Aquivion® extruded E79-03S membrane (30 μm thickness, EW = 790 g/eq). Test conditions: H_2 and air, cell temperature = 75°C, cell pressure = 2.5 bar abs, anode inlet RH = cathode inlet RH = 100%, Pt loading anode = Pt loading cathode = 0.5 mg cm^{-2}.

enhances the radical degradation mechanisms described in Section 15.3.2. Significant advances in materials and design must be made before ultra-thin membranes can achieve the lifetimes required to be considered mature enough for introduction in fuel cell systems.

15.3.4 Membrane fabrication processes

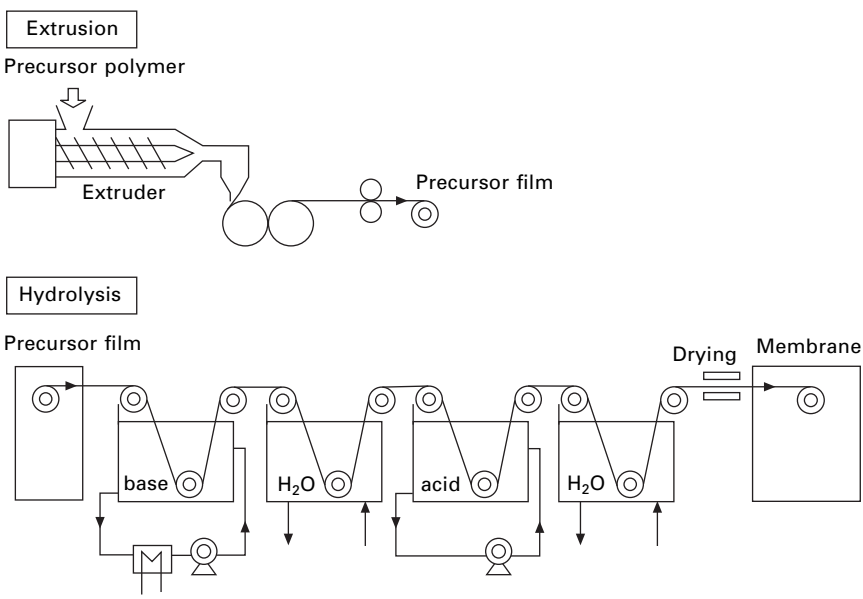
Although many different fabrication processes have been reported for fuel cell PEMs, the ones currently employed in practice are mainly three: melt extrusion, solvent casting and impregnation. These processes respectively result in the membrane types described in the previous section: extruded, cast and reinforced membranes. The processes will be briefly illustrated with reference to PFSA ionomers. Analogous ones apply for hydrocarbon ionomers.

In melt extrusion, the ionomer in its precursor (-SO_2F) and molten form is fed to an extruder where it is formed into a thin film. Typical temperatures are around 250°C or above, but can be lower for highly modified low melting grades (low EWs). Special screw and barrel materials (Ni alloys) are required to handle the fluorinated polymer at these temperatures. The film is stretched at the exit of the extruder to achieve the required thickness, cooled on rolls to allow crystallization of the polymer and wound up. At this point, the film is ready to be transformed into its ionic form by wet treatment. This typically implies immersion in an alkali solution (e.g. KOH) followed by rinsing in water, immersion in an acid solution (e.g. HNO_3) and final

© Woodhead Publishing Limited, 2011

rinsing. The -SO_2F group will thus be transformed to -SO_3K and eventually exchanged to the protonated form. Typically, the slow step in this process is the basic treatment. However, this can be considerably accelerated (>100 times) by addition of a polar aprotic solvent to the basic solution which, besides swelling the ionomer and facilitating entry of the alkali into the polymer matrix, strongly enhances the kinetics of substitution of F^- by OH^-, as typical for S_N2 nucleophilic substitution reactions. Fig. 15.16 reports the schematic of a PEM fabrication process by melt extrusion.

Melt extrusion is generally considered to be adequate for PEM membranes which are not too thin (≥ 30 μm). Extruded membranes generally possess good mechanical properties within the family of pure ionomer dense membranes. This is a consequence of adequate crystallization of ionomers of standard equivalent weight during film formation from the precursor molten state. The fact that wet chemistry must be applied to the film for hydrolysis to take place is instead considered to be a limitation: on one hand it induces dimensional variations that are difficult to handle especially for low EW membranes and low thicknesses and on the other hand it limits the use of eventual fillers or additives to those which are stable in strongly basic environments (stability in strongly acid environments is of course a prerequisite for any PEM additive). A possibility to circumvent this problem is to insert the additives, when possible, as a final step on the protonated membrane. This can easily be done for example for scavenger cations. An alternative approach is to



15.16 Fabrication process for extruded PFSA ionomer PEMs. Melt-extrusion is followed by hydrolysis treatment (base and acid).

© Woodhead Publishing Limited, 2011

introduce these additives through the electrodes, which are in contact with the membrane and will normally diffuse into the film.

In PEM manufacturing by solvent casting, the PFSA ionomer in its ionic form is first dissolved in a polar solvent. Different dissolution techniques have been reported, the most typical being dissolution at high temperature (150–250°C) in mixtures of water and a polar organic solvent miscible with water (Grot, 1984). Fine ionomer colloidal dispersions, rather than real solutions, are normally obtained by these methods. These dispersions are then formulated to the correct ionomer content, viscosities and surface tensions by addition of other solvent(s) after concentration by evaporation. The dispersion is then cast onto a moving substrate film (normally a polymer film) at a defined wet thickness, to obtain the desired final dry thickness. The water and solvents are then evaporated by heating and the membrane is finally annealed. This final annealing step is required to consolidate the film by sintering individual polymer particles and regenerating the crystalline structure. In the absence of this step, membranes are mechanically unstable and partially or totally soluble in water or water/solvent mixtures (cf. for instance Zook and Leddy, 1996). The annealing temperature must typically not exceed 230–250°C if the polymer is in the acid form in order not to have degradation of the functional groups.

Solvent casting has the advantage over extrusion in that no chemistry is done on the thin film if the membrane is cast in the protonated form. All the chemistry is done upstream of film formation in chemical reactors. Eventual additives can be added after the chemistry is finalized, just prior to final formulation of the ionomer dispersion or casting of the membrane. Very thin membranes can be easily produced. High speed casting processes can be adopted and the limiting step for productivity normally becomes drying or annealing of the membrane. This can be easily remedied by increasing the oven length. Because of these characteristics, casting would be the most tailored process for mass manufacture that will be required for fuel cells in cars, if membranes with sufficient durability can be demonstrated by this process.

While extrusion and casting typically deliver dense membranes, reinforced membranes are typically (though not uniquely) obtained by impregnation of a pre-existing microporous support. Impregnation can be carried out by dipping. The process has many of the features of the casting process even if the ionomer dispersion needs to be properly adapted. Ionomer particle size, first of all, has to be compatible with the pore size of the support material to avoid size-exclusion effects, which may mean very small particles (few tens of nanometres) if supports with low average pore size are employed ($\leq$ 0.2 μm). Penetration of the dispersion in the support is driven by capillary forces according to the Young–Laplace equation $\Delta p = 2\,\gamma \cos\theta / r$, where Δp represents the wicking pressure, γ the surface tension of the liquid, θ the

© Woodhead Publishing Limited, 2011

contact angle of the liquid on the solid surface and r the radius of the pore. This equation shows that the best impregnation is given by an optimal balance between surface tension and contact angle, resulting in solvent compositions typically different from those employed for solvent casting.

Microporous supports have a strong tendency to shrink in the plane during the drying and annealing phases of the process. This is due to the strong polymer–polymer interaction during contraction of the liquid film consequent to solvent evaporation. If the film roll is handled at the edges only, high tensions develop along these lines, leading to possible damage of the film at these locations and shrinkage in the area in between. If during the drying–annealing phase the film is instead adhered to a stable backing film, these tensions are homogeneously distributed in the whole membrane area, resulting in homogeneous and dimensionally stable membranes. This allows realization of reinforced membranes including low EW ionomers, such as those typically targeted with SSC ionomers, with improved dimensional stability (Arcella *et al.*, 2006).

15.4 Membrane performance in operation: issues and analysis

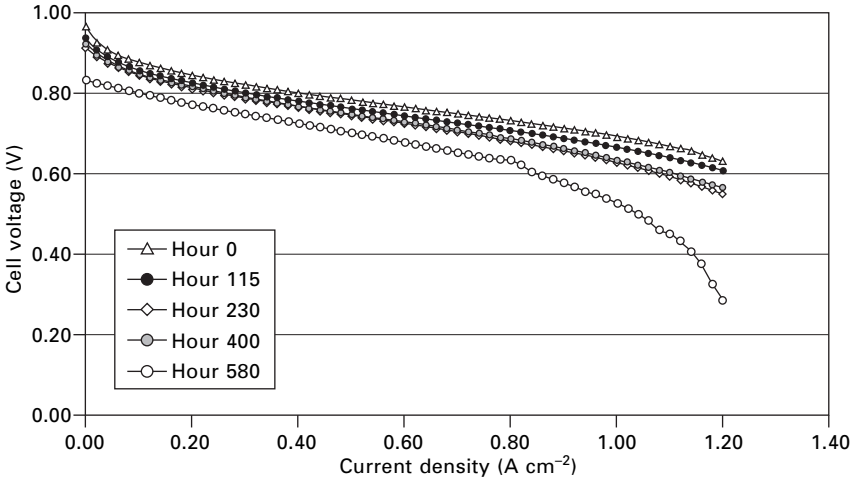
Once the membrane has been qualified for performance within an MEA (between electrodes and gas diffusion layers), that is has been proven to deliver the required voltage at given current densities over the range of temperatures, pressures, inlet RH and reactant flows that will then be experienced in field, durability tests are started to test the membrane capability to retain the performance in time.

Failures related to membrane degradation are normally experienced as diffuse or local thinning of the membrane, or weakening of its mechanical properties, resulting in a more or less pronounced increase of hydrogen crossover and final formation of a pin hole. This is normally evidenced by a decrease of the OCV (due to the mixed potential given by hydrogen diffusing to the cathode) and final shortening of the cell in extreme cases.

Figure 15.17 shows the degradation in performance of an experimental Aquivion® reinforced membrane in an aggressive accelerated durability test carried out at 120ºC and 25% RH up to 680 hours. It can be seen that at 570 hours the cell delivers lower performance and the OCV has dropped considerably, which is related to the membrane having lost its initial good gas barrier properties. It must however be considered that 680 hours under 120°C operation is a remarkable result with regards to the possibility of using PFSA membranes at target automotive peak temperatures.

Accelerated tests are carried out to gather data about membrane chemical and mechanical degradation which would be lengthy to obtain operating under real application conditions. In fact, for stationary applications, where

© Woodhead Publishing Limited, 2011



15.17 Durability test at 120°C and 25% inlet RH (both air and H_2) for an experimental Aquivion® reinforced membrane. The cell was operated at a constant voltage of 0.6 V during the durability hold. The polarization curves were taken at 75°C and 100% RH at the reported test times to check the performance decay.

durability of 40 000 h is targeted, it would be just too lengthy and expensive to wait for example 10 000 h (over one year) to discover that the membrane is not durable enough. Accelerated tests are typically designed to challenge the membrane with respect to chemical and/or mechanical durability.

OCV tests carried out under high RH conditions typically provide indications that especially relate to chemical stability. Large differences are seen for example between non-stabilized and stabilized ionomer membranes, as shown, for example, in Merlo *et al.* (2007b).

OCV tests carried out under low RH conditions are typically representative of both the chemical and mechanical stability of the membrane, since chemical mechanisms are active which strongly impair the mechanical properties of the membrane, as explained in Section 15.3.2. The chemical stability contribution can be seen in Fig. 15.12, where addition of a scavenger improves the lifetime over a membrane otherwise absolutely identical, while the mechanical stability contribution can be seen in Fig. 15.14, where introduction of a mechanical reinforcement enhances the durability in comparison to non-reinforced membranes, even without the use of a stabilized ionomer.

Accelerated tests have also been developed which highlight in particular the mechanical stability of a membrane. In these tests the membrane is typically cycled between wet and dry conditions under no potential difference (air on both sides), causing the membrane to swell and shrink and to fail by fatigue mechanisms if it is not mechanically resistant (Mathias *et al.*, 2005). The chemical degradation aspect can be combined in this purely mechanical stress

© Woodhead Publishing Limited, 2011

test by operating under a voltage difference, for example OCV conditions in H_2 and air, to deliver a combined mechanical and chemical durability stress test.

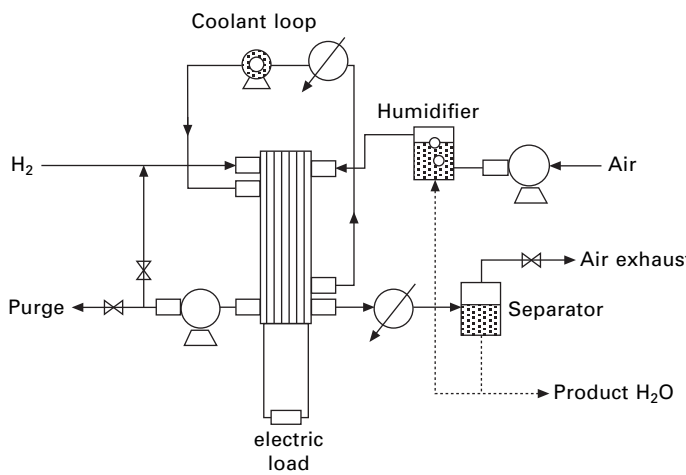
Some parameters are typically monitored during a durability fuel cell test. These are performance (current–voltage characteristic curve, including the OCV value), hydrogen crossover (normally measured electrochemically) and cell resistance (by electrochemical impedance spectroscopy). Fluoride release from the cell can also be measured in the product water when using PFSA ionomers, which is indicative of membrane chemical degradation.

So-called 'post-mortem' analysis of the membrane after the cell is dismantled is sometimes also very useful in identifying the reason for membrane failure. Aspects that can be considered are, for instance: location and type of the failure, eventual membrane thinning (by SEM image analysis), contamination of the membrane (e.g. formation of the Pt-band caused by dissolution of Pt from the catalyst and re-precipitation within the membrane) and chemical modification (by structural analysis).

15.5 Integration and application of proton exchange membrane (PEM) fuel cell systems

An example of integration of a PEM FC stack in a system is shown in Fig. 15.18, which reports a simplified scheme in one of the possible configurations. Typically, it could represent the FC system on board a car.

In the fuel circuit, H_2 is supposed to be fed from a compressed tank and thus requires no further compression. Two different fuel feeding strategies



15.18 Schematic of a H_2 PEM fuel cell system comprising a hydrogen loop, air inlet humidification, water recovery and liquid cooling.

© Woodhead Publishing Limited, 2011

are typically implemented: the so-called 'dead-end' mode and the 'hydrogen recirculation' mode. In the 'dead-end' mode, hydrogen is accumulated on the anode side of the fuel cell and periodically purged to remove accumulated water and nitrogen coming from the cathode side. In the 'hydrogen recirculation' mode, the hydrogen is recirculated in a loop from the outlet to the inlet, where a fresh gas portion is added. Also in this latter case a periodical purge is foreseen. Air is taken from the ambient surroundings and requires compression. At the outlet of the cathode, the water generated in the cell is collected and used for humidification of the inlet air. A recirculating liquid is used to cool the stack and cooled in an exchanger (the radiator, in the case of a car). The stack supplies electricity to the load.

A number of variations can be considered for the system, for example hydrogen can be delivered from a reforming reactor, air can be fed with no prehumidification, temperature control of the stack can be obtained by air cooling and hydrogen and air can be fed counter-flow instead of co-flow, and so on. Also, additional electrical components which are usually required, such as an inverter or a transformer (e.g. if the system is connected to the grid or in parallel to a secondary battery), are not reported in Fig. 15.18.

Target use of hydrogen PEM FC is typically, but not exclusively, for small to medium power systems (≤ 250 kW) to be operated dynamically and/or with frequent stops. Owing to their low operating temperature, PEM FCs have the advantage that a much faster start-up time can be achieved compared with high-temperature systems such as solid oxide fuel cells (SOFC) and molten carbonate fuel cells (MCFC). Typical applications are single- or multiple-home power generation, distributed generation for appliances in remote locations, uninterrupted power supply, auxiliary power systems on-board vehicles and a main power supply for transportation applications (e.g. buses and cars). While competition from other FC systems (especially SOFC) is high in the area of stationary applications, it appears today that PEM FC is the technology of choice for cars.

Projects for demonstration of hydrogen PEM FC in higher power stationary generation plants are ongoing, for example for the production of electrical energy where hydrogen is already available as a by-product in chemical plants. A good example is the 1 MW PEM FC system under construction at the Solvay electrolysis plant in Lillo, Belgium (see Solvay Press Release, 2010).

The application of DMFC goes instead in the direction of small systems for portable power, this term indicating units ranging from few watts to about 1 kW which are intended to be moveable and not used for powering vehicles. DMFC are not suitable for higher power applications owing to insufficient energy efficiency. Despite the expectation at the beginning of the millennium that DMFC would be the first widespread FC technology, used for powering cell phones and laptops, reported numbers of installed

© Woodhead Publishing Limited, 2011

systems were still not relevant in 2006 (Crawley, 2007). Today, DMFCs appear rather to have a future in systems working in power ranges of tens to hundreds of watts for consumer leisure (mainly as battery range extenders), remote sensors and as mobile power sources in the military sector (device powering and battery recharge).

15.6 Advantages and limitations of PEM fuel cells

Compared to other types of fuel cells, hydrogen PEM FCs have a number of advantages and disadvantages. Among the advantages, the main ones are related to the high power density, dynamic and flexible operation and the fact that the electrolyte is a solid film which poses limited problems of handling and corrosion. Compared to alkaline FCs (including solid-alkaline fuel cells, see Section 15.7) the electrolyte is CO_2-insensitive. The main disadvantages, are as follows: they require precious metal catalysts such as Pt owing to the acid environment, they cannot run on direct hydrocarbon feed (need for reforming), they are poisoned by CO (need to purify extensively if the H_2 comes from reforming), they need proper water management and they have rather slow oxygen reduction kinetics.

Despite the list of disadvantages, the definite advantages make PEM FC the technology of choice for the applications described in Section 15.5.

In DMFC technology some of the main disadvantages of H_2 PEM FC are amplified. Especially, they require very high precious metal loadings (even ten times the quantity used in PEM FC). Cathode as well as anode kinetics are slow (slow methanol oxidation at low temperatures). The main advantage is obviously related to the fact that the fuel is liquid and widely available.

15.7 Future trends

Future trends of research into FC membranes are closely linked to the open challenges which have been discussed in the previous sections of this chapter. The key challenge regarding performance of H_2 PEM FCs, is to develop membranes capable of working under dry conditions and possibly higher temperatures. This is typically addressed by lowering the EW of the ionomer, employing fillers and additives, using crosslinked or higher T_g materials and designing thinner and thinner membranes, which require the gas crossover of the other side of the membrane material to be reduced without losing water permeability characteristics. Improvements in durability are continuously sought in membrane chemical and mechanical stability by developing improved ionomers, new scavenger systems and new reinforcement concepts.

The main trend regarding DMFC membranes is the development of ionomers that show greatly reduced methanol permeability compared to

© Woodhead Publishing Limited, 2011

the current reference (Nafion®), without losing conductivity. Membranes with such characteristics have been obtained but need now to be integrated and demonstrated in working systems in addition to considering their durability.

Finally a field of development of fuel cell membranes which is still at quite an early stage is worth mentioning: anion exchange membranes (AEM) for solid-alkaline fuel cells (SAFC). Such systems are in principle able to work without the need of precious metals such as Pt, owing to the alkaline environment. This is their main advantage, but they offer a number of other advantages especially when working with liquid fuels (e.g. alcohols), such as facilitated fuel oxidation on the anode side. An excellent review can be found in Varcoe and Slade (2005).

15.8 Sources of further information and advice

A very exhaustive reference book on fuel cells is the *Handbook of Fuel Cells*, 2003–2009 from J. Wiley and Sons, some chapters of which are cited in the reference section.

Grot (2008), Deluca and Elabd (2006) and Varcoe and Slade (2005) provide very useful overviews of the field of perfluorinated ionomers, DMFC membranes and SAFC membranes, respectively.

15.9 References

Arcella V, Ghielmi A, Apostolo M and Abusleme J (2002), *Fluorinated Ionomers,* European Patent 1,167,400.

Arcella V, Ghielmi A and Tommasi G (2003), 'High performance perfluoropolymer films and membranes', *Ann NY Acad Sci*, **984**, 226–44.

Arcella V, Vaccarono P and Ghielmi A (2006), *Composite Ionomeric Membrane*, European Patent 1,702,668.

Bahar B, Hobson A R, Kolde J A and Zuckerbrod D (1996), *Ultra-thin Integral Composite Membrane*, US Patent 5,547,551.

Coms F D, Liu H and Owejan J E (2008), 'Mitigation of perfluorosulfonic acid membrane chemical degradation using cerium and manganese ions', *ECS Trans*, **16**, 1735–47.

Crawley G (2007), 'Direct methanol fuel cells (DMFC)', *Fuel Cell Today*, August 2007, www.fuelcelltoday.com

Curtin D E, Lousenberg R D, Henry T J, Tangeman P C and Tisack M E (2004), 'Advanced materials for improved PEMFC performance and life', *J Power Sources*, **131**, 41–8.

Danilczuk M, Perkowski A J and Schlick S (2010), 'Ranking the stability of perfluorinated membranes used in fuel cells to attack by hydroxyl radicals and the effect of Ce(III): a competitive kinetics approach based on spin trapping ESR', *Macromolecules*, **43**, 3352–8.

Deluca N W and Elabd Y A (2006), 'Polymer electrolyte membranes for the direct methanol fuel cell: a review', *J Polym Sci Polym Phys Ed*, **44**, 2201–25.

© Woodhead Publishing Limited, 2011

Doyle M and Rajendran G (2003), 'Perfluorinated membranes', in *Handbook of Fuel Cells – Fundamentals, Technology and Applications, Volume 3: Fuel Cell Technology and Applications*, Chapter 30, Wiley & Sons Chichester.

Eisman G A (1986), 'The physical and mechanical properties of a new perfluorosulfonic acid ionomer for use as a separator/membrane in proton exchange processes', *Proceedings of the 168th Electrochemical Society Meeting*, **83 13**, 156–71.

Ezzell B R, Carl W P and Mod WA (1982), *Novel Polymers having Acid Functionality*, US Patent 4,330,654.

Gasteiger H A and Mathias M F (2002), 'Fundamental research and development challenges in polymer electrolyte fuel cell technology', in *Proton Conducting Membrane Fuel Cells III, Electrochemical Society Proceedings*, Salt Lake City, 2002–31, 1–24. http://books.google.de/books?id=JhFMwms8szMC&printsec=frontcover&dq=Proton+Conducting+Membrane+Fuel+Cells+I+Symposium&source=bl&ots=00POJ_mjX9&sig=2Sk5FjFLIAP7d5som8Mr4BDjiAo&hl=de&ei=9iqjTdmJLYaCOrSCgTU&sa=X&oi=book_result&ct=result&resnum=4&ved=0CD4Q6AEwAw#v=onepage&q&f=false

Ghielmi A, Vaccarono P, Troglia C and Arcella V (2005), 'Proton exchange membranes based on the short-side-chain perfluorinated ionomer', *J Power Sources*, **145**, 108–15.

Gierke T D, Munn G E and Wilson F C (1981), 'Morphology of Nafion perfluorosulfonated membrane products, as determined by wide- and small-angle X-ray studies', *J Polym Sci Polym Phys Ed*, **19**, 1687–704.

Gross M, Maier G, Fuller T, MacKinnon S and Gittleman C (2009), 'Design rules for the improvement of the performance of hydrocarbon-based membranes for proton exchange membrane fuel cells (PEMFC)', in *Handbook of Fuel Cells – Fundamentals, Technology and Applications*, *Volume 5: Advances in Electrocatalysis, Materials, Diagnostics and Durability*, Chapter 18, Wiley & Sons, Chichester.

Grot W (1984), US Patent 4,433,082.

Grot W (2008), *Fluorinated Ionomers*, William Andrew Publishing, Norwich NY.

Hamrock S J (2009), 'New fuel cell membrane development at 3M', *Fuel Cell Seminar and Exposition*, Palm Springs, CA, November 2009, Abstract LRD33-2, 125–7.

Hommura S, Kawahara K, Shimohira T and Teraoka Y (2008), 'Development of a method for clarifying the perfluorosulfonated membrane degradation mechanism in a fuel cell environment', *J Electrochem Soc*, **155**, A29–A33.

Hsu W Y and Gierke T D (1982), 'Elastic theory for ionic clustering in perfluorinated ionomers', *Macromolecules*, **15**, 101–5.

Kinoshita S and Shimoda H (2008), 'Performances of highly durable PFSA polymer based MEAs at high temperature, low RH & dry-wet conditions', presented at *Progress MEA 2008*, *1st International Carisma Conference* 21–24 September 2008, La Grande Motte, France.

Kirsh Y E, Smirnov S A, PopKov Y M and Timashev S F (1990), 'Perfluorinated carbon-chain copolymers with functional groups and cation exchange membranes based on them: synthesis, structure and properties', *Russ Chem Rev*, **59**, 560–74.

Kolde J A, Bahar B, Wilson M S, Zawodzinski T A and Gottesfeld S (1995), 'Advanced composite polymer electrolyte fuel cell membranes', in *Proton Conducting Membrane Fuel Cells I, Electrochemical Society Proceedings*, **1995 23**, 193–201.

Kreuer K D, Schuster M, Obliers B, Diat O, Traub U, Fuchs A, Klock U, Paddison S J and Maier J (2008), 'SSC proton conducting PFSA ionomers: why they perform better in PEM fuel cells', *J Power Sources*, **178**, 499–509.

Liu H, Gasteiger H A, Laconti A B and Zhang J (2006), 'Factors impacting chemical

© Woodhead Publishing Limited, 2011

degradation of perfluorinated sulfonic acid ionomers', *ECS Transactions*, **1**, 283–93.

Liu W and Zuckerbrod D (2005), '*In situ* detection of hydrogen peroxide in PEM fuel cells', *J Electrochem Soc*, **152**, A1165–A1170.

Liu W K, Cleghorn S J C, Delaney B E and Crum M (2009), 'Chemical and mechanical membrane degradation', in *Handbook of Fuel Cells – Fundamentals, Technology and Applications*, *Volume 5: Advances in Electrocatalysis, Materials, Diagnostics and Durability*, Chapter 26, Wiley & Sons, Chichester.

Mallant R, Calis G and De Bruijn F (1998), *Electronic Membrane, Method of Manufacturing it and Use*, Patent WO9820063.

Masten D A and Bosco A D (2003), 'System design for vehicle applications: GM/Opel', in *Handbook of Fuel Cells – Fundamentals, Technology and Applications, Volume 4: Fuel Cell Technology and Applications*, Chapter 53, Wiley & Sons, Chichester.

Mathias M F, Makharia R, Gasteiger H A, Conley J J, Fuller T J, Gittleman C J, Kocha S S, Miller D P, Mittelsteadt C K, Xie T, Yan S G and Yu P T (2005), 'Two fuel cell cars in every garage?', The Electrochemical Society *Interface*, Fall 2005. http://www.electrochem.org/dl/interface/fal/fal05/IF8-05_Pg24-35.pdf

Merlo L, Ghielmi A, Cirillo L, Gebert M and Arcella V (2007a), 'Membrane electrode assemblies based on Hyflon® Ion for an evolving fuel cell technology', *Separation Sci Technol*, **42**, 2891–908.

Merlo L, Ghielmi A, Cirillo L, Gebert M and Arcella V (2007b), 'Resistance to peroxide degradation of Hyflon® Ion membranes', *J Power Sources*, **171**, 140–7.

Merlo L, Escribano S, Holber M and Haug A (2010), 'Degradation study of PFSA membranes in DECODE project', presented at *Progress MEA 2010*, *2nd International Carisma Conference*, 19–22 September 2010, La Grande Motte, France.

Nasef M M, Zubir N A, Ismail A F, Khayet M, Dahlan K Z M, Saidi H, Rohani R, Ngah T I S and Sulaiman N A (2006), 'PSSA pore-filled PVDF membranes by simultaneous electron beam irradiation: preparation and transport characteristics of protons and methanol', *J Membrane Sci*, **268**, 96–108.

Prater K (1990), 'The renaissance of the solid polymer fuel cell', *J Power Sources*, **29**, 239–50.

Solvay Press Release, 2010, February 10, www.solvinpvc.com/static/wma/pdf/1/7/2/7/2/Pile%20combustible_EN.pdf

Tant M R, Darst K P, Lee K D and Martin C W (1989), 'Structure and properties of short-side-chain perfluorosulfonate ionomers', in *Multiphase Polymers: Blends and Ionomers, ACS Symp Ser*, **395**, 370–400.

Varcoe J R and Slade R C T (2005), 'Prospects for alkaline anion-exchange membranes in low temperature fuel cells', *Fuel Cells*, **5**, 187–200.

Verbrugge M W, Hill R F and Schneider E W (1992), 'Composite membranes for fuel-cell applications', *AIChE Journal*, **38**, 93–100.

Zook L A and Leddy J (1996), 'Density and solubility of Nafion: recast, annealed, and commercial films', *Anal Chem*, **68**, 3793–6.

15.10 Appendix: list of symbols

ΔG Gibbs free energy change of the FC chemical reaction

Δp wicking pressure for the ionomer dispersion into a microporous reinforcement

© Woodhead Publishing Limited, 2011

ΔV_0	theoretical voltage differential of a FC (single cell)
ΔV^S	voltage of the FC stack
γ	surface tension of the ionomer dispersion
$\sigma(H^+)$	membrane proton conductivity
θ	contact angle of the ionomer dispersion on the reinforcement material surface
n	number of electrons involved in the FC reaction
F	Faraday constant
$P(i)$	permeability of reactant or gas i through the membrane
$S(i)$	membrane proton-to-reactant transport selectivity
r	pore radius of the microporous reinforcement

© Woodhead Publishing Limited, 2011

16

Functional ceramic hollow fibre membranes for catalytic membrane reactors and solid oxide fuel cells

Z.T. WU, M. H. D. OTHMAN,
B. F. K. KINGSBURY and K. LI,
Imperial College London, UK

Abstract: This chapter introduces major developments and use of functional ceramic hollow fibre membranes, that is a membrane design consisting of a dense outer layer for separation supported on a highly porous inner catalytic substrate layer, for energy utilization in methane conversion and micro-tubular solid oxide fuel cells (SOFCs). The advantages of the dual-layer hollow fibre membrane design and the single-step co-extrusion and co-sintering process employed to achieve this membrane design are addressed. The key factors that affect the fabrication and performance of the developed membranes are discussed and future technology challenges are also outlined.

Key words: co-extrusion, co-sintering, dual-layer hollow fibre membrane, membrane reactor, SOFC

16.1 Introduction

As a relatively new type of ceramic membrane, hollow fibres have been characterized as having outstanding surface area/volume ratios and a considerably reduced membrane thickness in contrast to their disk/flat-sheet and tubular counterparts (Li, 2007). The distinguishing characteristics of this configuration are a significant increase in permeation rate per unit volume, a greater processing capacity for the corresponding membrane modules and lower material costs, thus promoting and expanding the use of ceramic hollow fibre membranes in membrane separation and catalytic membrane reactor applications (Li, 2007). The main purpose of this chapter is to introduce the concept and fabrication process of ceramic hollow fibre membranes with more advanced structures, that is a functional dual-layer structure, and the application of membranes of this type in energy utilization. After a brief introduction to the fundamentals of functional ceramic dual-layer hollow fibre membranes, a single-step co-extrusion and co-sintering process for fabricating such membranes is addressed. The developed membranes are finally used in a catalytic membrane reactor (CMR) and a solid oxide fuel cell (SOFC) as two typical applications in energy utilization.

© Woodhead Publishing Limited, 2011

16.1.1 Fundamentals of membrane separation

A membrane is a permeable or semi-permeable barrier, which restricts the motion of certain species (Scott, 1995). In contrast to conventional separation processes such as adsorption, absorption and distillation, membrane separation can be more economical and lead to large energy savings. Transport processes across the membrane result from a driving force, which is typically associated with a gradient of concentration, pressure, temperature, electric potential, and so on (Marcano and Tsotsis, 2002). Although a broad range of membranes have been developed, they can be classified by:

- materials used to construct the membrane, i.e. polymer, ceramic or metal etc.
- size of the pores in the membrane, i.e. microfiltration (MF), ultrafiltration (UF), nanofiltration (NF), gas and vapour separation (GS), pervaporation (PV) and dense membranes.
- macrostructures of the membrane, i.e. symmetric or asymmetric membranes
- geometry of the membrane, i.e. flat-sheet, tubular or hollow fibre membranes.

The mechanism of membrane separation is based either on sieving (porous membrane) or on control of relative transport rates through the membrane (dense membrane). The separation performance of a membrane is normally indicated by two factors, permeability and selectivity. The permeability is defined as the permeation flux (molar or volumetric flow per unit membrane area) scaled with respect to membrane thickness and driving force (Marcano and Tsotsis, 2002). Permeance, which is permeation flux scaled with respect to driving force, is more practically useful because of the difficulties in determining the true membrane thickness. Selectivity, which characterizes the ability of a membrane to separate two given molecular species, is typically defined as the ratio of the individual permeabilities for the two species (Marcano and Tsotsis, 2002).

16.1.2 Dense ceramic membranes in energy utilization

Dense ceramic membranes are widely used for the purpose of energy utilization, such as in CMR and SOFC. The selectivity of such membranes is theoretically infinite as a result of the nature of the membrane materials, while the permeation flux is determined by a number of factors such as membrane material, membrane thickness and morphology. Taking mixed ionic–electronic conducting (MIEC) membranes as an example, higher mixed conductivity, lower membrane thickness and larger effective membrane surface area contribute to achieve higher oxygen permeation flux, while

© Woodhead Publishing Limited, 2011

the selectivity of the membranes for oxygen should be close to infinity, as oxygen ions and electrons are the only transportable species. Although the extremely high selectivity of the dense membranes can be considered to be an advantage, compared with their porous counterparts, membrane stability is the main concern as a consequence of high operating temperatures and the presence of reducing agents. For example, MIEC materials with high oxygen permeation fluxes always suffer from poor stability in CMR for methane conversion, owing to the formation of hydrogen and CO as products. As a result, oxygen permeation flux and membrane stability are normally considered to be the most critical factors, indicating the performance of dense ceramic membranes.

The most direct and challenging route to improve MIEC membrane performance is to develop membrane materials with both high mixed conductivity and greater stability. However, the trade-off between oxygen permeation and membrane stability is still a challenge in this research field. Alternatively, stable MIEC materials with less oxygen permeation flux can be used, leading to the development of thinner membranes with larger surface areas that allow higher oxygen permeation fluxes. In contrast to disk/flat-sheet or tubular ceramic membranes, ceramic membranes in a hollow fibre configuration possess the highest surface area/volume ratio to date, while a thinner membrane can be achieved by developing an asymmetric or supported membrane in which the oxygen separation layer is deposited onto a highly porous substrate with the necessary mechanical properties. A combination of the advantages of these two membrane designs results in a more advanced membrane structure, a ceramic dual-layer hollow fibre membrane.

16.1.3 Functional ceramic dual-layer hollow fibre membranes

A ceramic dual-layer hollow fibre membrane consists of a thin dense layer that will facilitate separation, deposited onto a highly porous substrate layer. It has a similar structure to asymmetric or supported membranes, which has only been achieved previously for disk- or short tubular-membranes using multistep fabrication processes. Although a design of this type integrates the advantages of a thin separation layer and high permeate rate, its main function is limited to separation. Additional catalyst, either packed or coated on to membrane surface, is still necessary for energy utilization. As a result, we aim to develop a functional ceramic dual-layer hollow fibre membrane, in which the porous substrate layer is, in the same time, catalytically active for certain reactions. For example, the thin and dense separation layer can be used to separate oxygen from ambient air (CMR) or allow the transport of oxygen ions (electrolyte of SOFC), while the porous substrate layer may form a catalytic layer for methane conversion (CMR) or an anode layer in

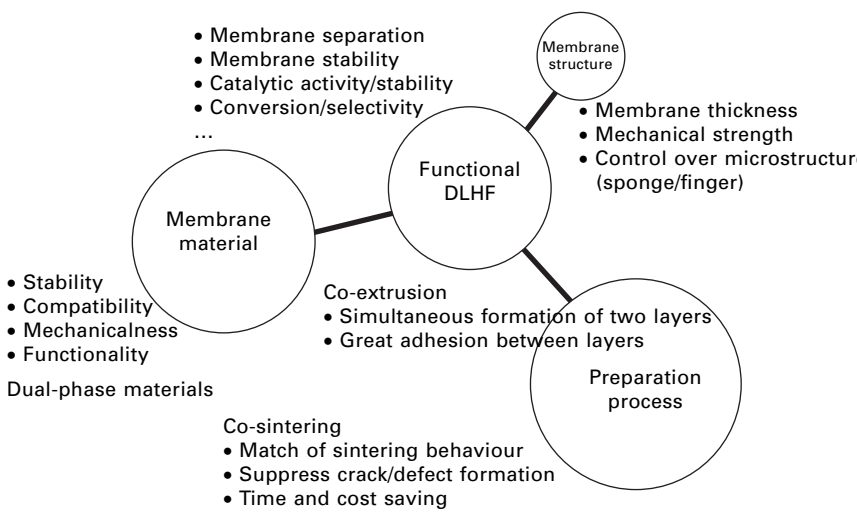
© Woodhead Publishing Limited, 2011

SOFC for energy conversion. As a result, functional ceramic dual-layer hollow fibre membranes can be used directly as a device for energy utilization.

In addition to the design itself, an efficient process to achieve such a design has to be developed as well. As a consequence of high surface area and curvature, it is challenging to fabricate high quality ceramic dual-layer hollow fibre membranes using conventional multistep fabrication processes, in which a time-consuming coating and sintering cycle has to be repeated a number of times, further increasing the possibility of crack formation. Furthermore, the macrostructure of the membrane, which is normally largely determined by the fabrication process, greatly affects the membrane performance. If control over membrane structure can be achieved during the fabrication process, its performance can be optimized for various applications without post-modification. Therefore, a series of interactive factors must be taken into consideration before a functional ceramic dual-layer hollow fibre membrane can be developed. The interrelationship between these factors, which also addresses how to develop such membranes, is summarized and schematically shown in Fig. 16.1.

16.2 Membrane materials issues

Up till now, a large number of ceramics have been developed for the fabrication of ceramic membranes. It is still a challenge to select the proper membrane materials for functional dual-layer hollow fibre membranes. In general, use



16.1 Schematic diagram of the development of high quality multifunctional ceramic dual-layer hollow fibre membranes.

© Woodhead Publishing Limited, 2011

of ceramic membranes for energy utilization normally involves a number of conditions, such as high operating temperature and the presence of reducing reactants/products, which set a high level of requirement on the chemical and thermal stabilities of membrane materials. For single phase MIEC membrane materials, such as those with perovskite or perovskite-related structures, better stability is always at the expense of oxygen permeation flux. When taking into account membrane configuration like hollow fibres, mechanical strength is another issue that needs to be addressed. Forming a dual-layer structure which is free of defects/cracks, needs the sintering behaviour of materials of the two layers to be well matched. This is normally difficult for single-phase membrane materials, as the sintering behaviour of MIEC materials in the separation layer is usually quite different from substrate layer materials with good mechanical properties. Consequently, it is challenging to achieve simultaneously a dense separation layer and a porous substrate layer. Moreover, a possible solid-state reaction between two layers of different single-phase materials would seriously affect membrane performance. Finally, functionalization of a single-phase membrane material with catalytic activity is quite difficult, which is partially due to a significant loss of surface area after high temperature sintering. As a result, single-phase materials are not suggested for fabricating functional ceramic dual-layer hollow fibre membranes.

In contrast to their single-phase counterparts, dual-phase materials made of two individually continuous and uniform phases are more 'adjustable' to tackle the problems above. Each phase with a certain 'selective' property can be very stable at high temperatures in the presence of reducing agents. The correct combination of such 'selective' properties would result in a functional ceramic dual-layer hollow fibre membrane for a specific application. For example, the oxygen separation layer of a dual-layer hollow fibre membrane reactor (DL-HFMR) may be composed of a continuous ionic conductive phase together with another continuous electronic conductive phase, while the catalytic support layer may consist of the same ionic conductive phase as in the oxygen separation layer but with an additional metal oxide phase such as NiO. NiO can be easily reduced to Ni using hydrogen, which not only generates a type of catalytic activity, but also produces a highly interconnected porous structure. A similar idea can be used to fabricate a porous anode layer for a micro-tubular SOFC. Another major advantage of employing 'adjustable' dual-phase membrane materials is in the fabrication of dual-layer hollow fibre membranes, where the sintering behaviours of the two layers can be matched by adjusting the ratios between the phases, which will be introduced in the next section.

Generally, there is a phase coexistence in both layers. This phase should possess great mechanical properties, while at the same time contributing to achieving specific functions for each layer. For the example above of DL-

© Woodhead Publishing Limited, 2011

HFMR, an ionic conductive phase exists in both the separation layer, allowing transportation of oxygen ions, and in the catalytic substrate layer for good mechanical properties as well as catalytic activity. More importantly, this ionic conductive phase acts as a 'bridge', building up a strong connection between the two layers, contributing to matching sintering behaviour as well as strengthening adhesion between the two layers.

Although each individual phase in a dual-phase material may be very stable even at high temperatures and under reducing atmospheres, a simple combination of two stable phases may still lead to a solid-state reaction between them, which can cause membrane performance such as permeation flux, catalytic activity and mechanical strength to deteriorate either rapidly or over a longer time period. As a result, compatibility between the two phases must be investigated prior to membrane fabrication. Moreover, in order to achieve proper functionality, the volume ratio between the two phases, which is dependent on the nature of the materials, particle size or even particle shape, is another factor that must be considered.

16.3 Membrane development routes and macrostructure control

Up until now, most single-layer ceramic hollow fibre membranes have been fabricated using a combined phase inversion/sintering process which is an adaption of the immersion induced phase inversion method first described by Loeb and Sourirajan (1963). The concept of a phase inversion based co-extrusion process has been widely used in the preparation of polymer dual-layer hollow fibre membranes. The first example of using a co-extrusion and co-sintering process to fabricate dual-layer alumina hollow fibre membranes (De Jong *et al.*, 2004) appeared in the literature in 2004, with little further progress achieved to date. This slow progress is probably due to limited knowledge and understanding of this process, which includes membrane fabrication, control of membrane structure and selection of the correct membrane materials. As a result, this section starts with a brief introduction to the fundamentals of the combined phase inversion/sintering process.

16.3.1 Combined phase inversion/sintering process

The phase inversion process has been widely used for the fabrication of polymer hollow fibre membranes and was employed to produce ceramic counterparts around 2000. Two typical morphologies have so far been observed in both polymer and ceramic hollow fibre membranes, finger-like voids and a sponge-like structure. Besides high temperature sintering, the major difference in the membrane fabrication process between polymer and ceramic hollow fibre membranes is the role of the polymer. In ceramic membrane fabrication

© Woodhead Publishing Limited, 2011

the polymer acts only as a binder, instead of a membrane material, it serves only to hold the ceramic particles together during spinning and is only present in small quantities in the spinning suspension. As a result, control and understanding of the formation mechanisms of polymer membranes can only be selectively applied to ceramic membrane fabrication.

A combined phase inversion/sintering process for fabricating ceramic hollow fibre membranes usually consists of three steps: preparation of the spinning suspension, wet or dry-wet spinning of hollow fibre precursors and finally sintering. A spinning suspension is a homogeneous mixture consisting of a predetermined amount of a ceramic powder or powder mixtures, a polymer binder (sometimes with additional additives) and a solvent. The properties of the spinning suspension may significantly vary with a number of factors, such as the amount and particle size of the ceramic powder, the ratio between ceramic powder and polymer binder, the type of polymer and solvent and so on. A certain initial suspension viscosity (at a particular shear rate) is preferred so that the fibres can be formed easily and smoothly. During spinning, the spinning suspension is extruded through a tube-in-orifice spinneret into a precipitation bath containing a non-solvent for the polymer. Simultaneously, an internal precipitant is supplied through the central tube of the spinneret into the lumen of the nascent fibre. Control over the membrane morphology, that is finger-like voids and sponge-like structure, can be achieved by adjusting the extrusion rate of the suspension, the flow rate of the internal precipitant and the air gap (the distance between spinneret and external precipitation bath). These factors mainly affect how the viscosity in nascent fibres changes during the spinning process and largely determine the morphology of the resultant membranes. The macrostructure of the hollow fibre precursor formed during the phase inversion process is retained during sintering (calcination/heat treatment). Finger-like voids above a certain size are not usually eliminated, although at elevated sintering temperatures sponge-like regions would densify and eventually become gas tight for some ceramic materials.

16.3.2 Co-extrusion and co-sintering

In a similar way to the combined phase inversion/sintering process, the single-step co-extrusion and co-sintering process is composed of three main steps: preparation of spinning suspensions, co-extrusion and co-sintering. The principles for preparing spinning suspensions are often similar and only the last two steps will be discussed.

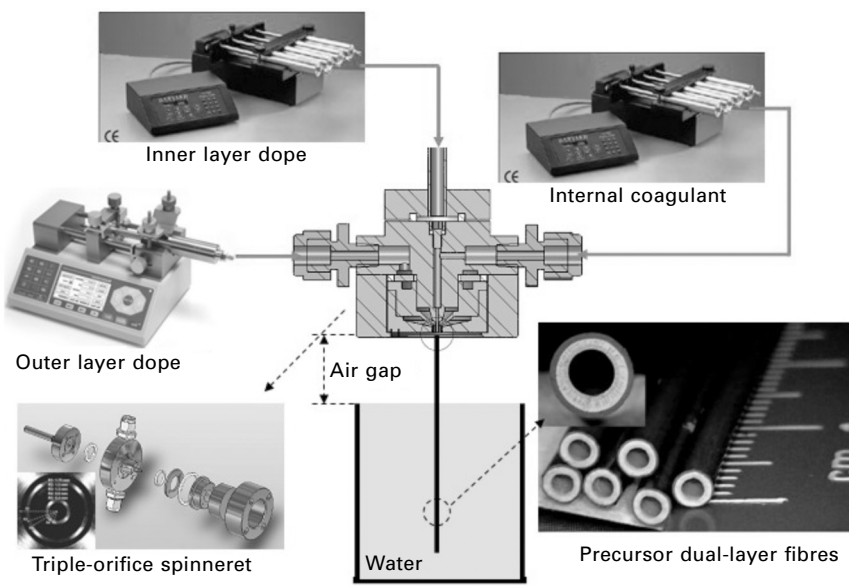
Co-extrusion process

The phase inversion-based co-extrusion process is a very convenient way of producing ceramic dual-layer hollow fibre membranes with adjustable

© Woodhead Publishing Limited, 2011

structures. During spinning, suspensions for the outer separation layer and the inner functional support layer are simultaneously extruded through a triple-orifice spinneret, passing through an air gap and into the external precipitation bath, as shown in Fig. 16.2. At the same time, a stream of internal precipitant is supplied through the central bore of the spinneret. In the simultaneous formation of a dual-layer structure, accurate control over the extrusion rates, which are dependent on the dimensions of the spinneret and the viscosity of the spinning suspensions, is critically important to avoid delamination of the two layers. Moreover, the properties of the spinning suspensions are preferably similar, such as the amount and type of polymer binder and solvent employed. In common with the combined phase inversion/sintering process, the macrostructure of the dual-layer precursor fibres can be controlled by adjusting the spinning parameters and is largely determined during the co-extrusion process.

After co-extrusion, precipitated polymer forms a sort of skeleton structure in both layers, where ceramic particles are fixed. This indicates that good adhesion between layers in a precursor fibre mainly arises from the great uniformity of such polymeric skeleton structures across layers and throughout the whole fibre. If the properties of the inner and outer layer spinning suspensions are too different from each other, a delamination (gap) would form between the layers and consequently affect the uniformity of polymeric skeleton structure, weakening connection between the layers.



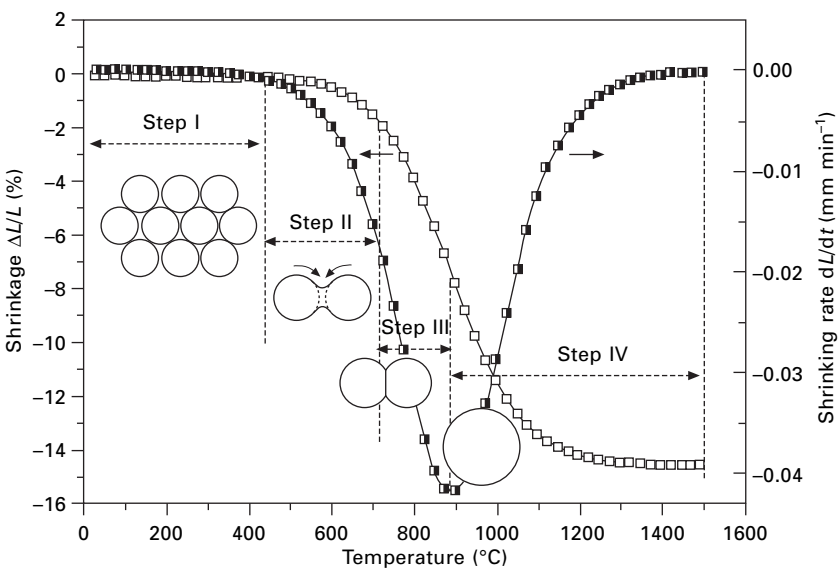
16.2 Schematic diagram of the phase inversion based co-extrusion process.

© Woodhead Publishing Limited, 2011

Co-sintering process

During the co-sintering process, two layers are simultaneously sintered after passing through a number of steps such as removal of adsorbed moisture and thermolysis of the polymer binder (Li, 2007). Sintering is normally thought to occur in three stages, an initial stage, intermediate stage and final stage (Reed, 1995) as the temperature is increased. The redistribution of atoms varies at each stage of sintering and may result in densification, grain coarsening and pore closing, depending on the mechanism.

In principle, the sintering process would not begin until the temperature exceeds one-half to two-thirds of the melting temperature of the ceramic material. As a result, only absorbed water and polymer binder would be removed from the precursor fibres in Step I in Fig. 16.3, where ceramic particles are brought into contact with each other. A further increase in temperature leads to a significant level of atomic diffusion in solid state sintering or significant diffusion and viscous flow when a liquid phase is present or is generated by a chemical reaction. This leads to the formation of a 'neck' between particles, which reduces the surface free energy. At the 'neck', the radius of curvature is negative and the vapour pressure is lower than in other areas, facilitating the transfer of materials to this region. Diffusion along grain boundaries and through the lattice initially leads to 'neck' growth as the temperature is increased and finally to grain growth in



16.3 Schematic diagram of sintering of ceramic hollow fibre membranes.

© Woodhead Publishing Limited, 2011

the latter stages of sintering. In the meantime, the membrane shrinks as a result of the reduction in both pore volume and pore size.

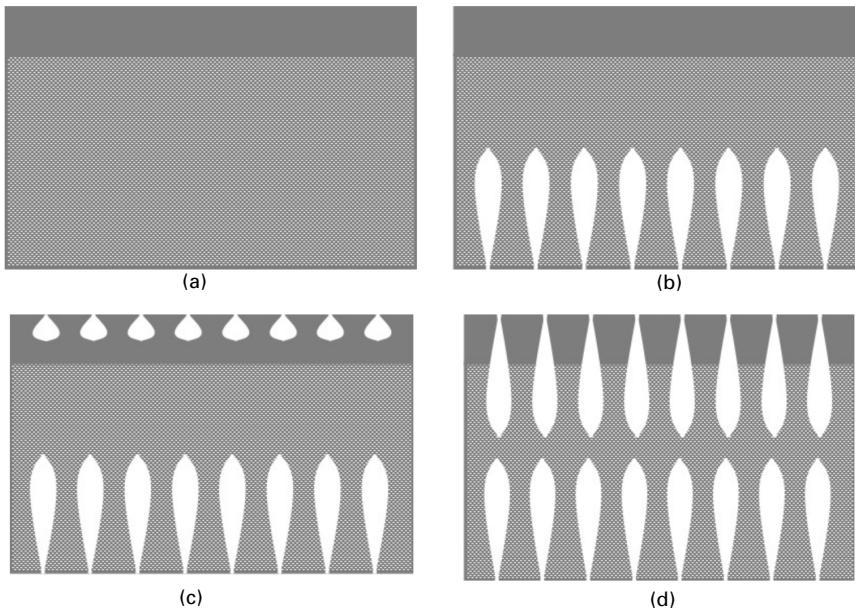
The membrane starts to shrink at a low rate (Step II) which significantly increases with increasing temperature (Step III). The maximum shrinking rate is obtained at a certain temperature, over which the shrinking rate dramatically decreases, finally tending to zero as the temperature is increased further (Step IV). The shrinkage rate slows down and stabilizes at a particular value, indicating the end of the sintering process. The density of the membrane is very close to the theoretical density at this stage owing to the elimination of pores. With increasing sintering temperature, the number of grain boundaries decreases owing to an increase in grain size, while the mechanical strength of the membrane is seen to increase until the point where the material is 'over-sintered' and a reduction in mechanical strength is observed.

In order to obtain high quality ceramic dual-layer hollow fibre membranes, a good match between the sintering behaviour of the two layers is critically important. Any kind of discrepancy in sintering behaviour would produce a level of stress in the membrane and may result in the formation of cracks or the breakdown of the membrane. This is also one of the main reasons that dual-phase membrane materials are preferred for a dual-layer structure, as the sintering behaviour of the two layers can be adjusted to match each other by changing the material compositions, something that is quite challenging for single-phase membrane materials.

16.3.3 Control over the macrostructures of dual-layer hollow fibre membranes

Functional ceramic dual-layer hollow fibre membranes consist of a thin and fully dense separation layer supported on a highly porous catalytic substrate layer. A symmetric structure in both layers, shown in Fig. 16.4 (a), is always preferred for fewer defects in the separation layer and better mechanical strength from the substrate layer. However, a number of other macrostructures are commonly observed, as shown in Fig. 16.4 (b)–(d), in which a finger-like structure forms during the co-extrusion process caused by the viscous fingering phenomenon (Kingsbury and Li, 2009). Although the finger-like structure in the substrate layer (Fig. 16.4 (b)) can be used for catalyst deposition when the substrate layer shows no catalytic activity, it reduces mechanical strength and is consequently not preferred for functional ceramic dual-layer hollow fibre membranes. A tiny finger-like structure in the separation layer (Fig. 16.4(c)) is acceptable as long as it is not penetrated through the boundary between layers, as there is still a dense region in the separation layer. The worst situation is that finger-like structures that have developed from both the inner and outer surfaces and the one from the separation layer surface run across the boundary between layers (Fig. 16.4

© Woodhead Publishing Limited, 2011



16.4 Schematic diagram of the macrostructures of dual-layer ceramic hollow fibre membranes: (a) symmetric structures in both layers, (b) symmetric outer layer with asymmetric inner layer, (c) asymmetric structures in both layers with short fingers in the outer layer, (d) asymmetric structures in both layers with long fingers penetrating through the outer layer.

(d)), resulting in low mechanical strength as well as poor gas tightness of the separation layer.

One of the most efficient ways to prevent such finger-like structure formation is to increase the suspension viscosities of both layers to a certain level, for example by replacing an amount of solvent with water or ethanol, because viscous fingering would not occur if the initial viscosity of the spinning suspension exceeds a 'threshold' value (Kingsbury and Li, 2009). However, there is still a limit to this method because a very viscous suspension, especially one for a thin separation layer, would significantly increase extrusion pressure to an extremely high level when the suspension is extruded through spinneret orifices. Moreover, too high a viscosity would affect the adhesion between the layers. As a result, some other spinning parameters, such as extrusion rate, air gap and internal precipitant flow rate, can be used to adjust the macrostructure of ceramic dual-layer hollow fibre membranes.

© Woodhead Publishing Limited, 2011

16.4 A multifunctional dual-layer hollow fibre membrane reactor (DL-HFMR) for methane conversion

16.4.1 Background

A membrane reactor is a device that combines membrane separation and catalytic chemical reaction in one unit (Li, 2007). As a consequence of the advantages of this type of reactor design, much lower operating costs result from coupling reaction with separation. The use of dense ceramic membranes to control the addition and distribution of oxygen from ambient air to chemical reactions, such as partial oxidation of methane (POM) to syngas, has been widely studied in the last few decades (Balachandran *et al.*, 1997; Bouwmeester, 2003; Liu and Tan, 2006), stemming from a number of technological advantages over conventional techniques. Great progress has been achieved, particularly in the light of the development of membrane materials with higher oxygen permeation fluxes and better high temperature stability in reducing atmospheres (Sunarso *et al.*, 2008; Thursfield and Metcalfe, 2004). In addition, technical breakthroughs in the fabrication of dense ceramic hollow fibre membranes greatly improve surface area/volume ratios and significantly reduce membrane thicknesses (Tan and Li, 2007; Tan *et al.*, 2001, 2008) when compared to most disk and tubular counterparts. However, there are still several fundamental concerns over the design of dense ceramic membrane reactors: (1) the trade-off between oxygen permeation and the lifetime of ceramic membranes, which is more significant for the POM reaction owing to the formation of reducing products such as H_2 and CO; (2) the surface area per unit volume and the volume productivity of most of the current membrane reactor designs, in which catalyst is usually packed directly on the membrane surface, are still very limited, challenging the scale-up process for industrial applications.

These major concerns can be met by developing functional dual-layer hollow fibre membranes. The outer oxygen separation layer consists of a mixture of $La_{0.8}Sr_{0.2}MnO_{3-\delta}$ (LSM, 40 vol%) and yttria-stabilized zirconia (YSZ, 60 vol%), which has been widely used as a composite cathode material in SOFC, as the two materials have excellent compatibility and stability in reducing atmospheres (Steele and Heinzel, 2001), as well as similar sintering temperatures and thermal expansion coefficients (Li *et al.*, 2009; Minh, 1993), while the inner functional layer is made of NiO (30 vol%) and YSZ (70 vol%). The inner layer transforms into a highly porous structure without the use of pore formers when NiO is reduced into Ni, which is also catalytically active for a POM reaction when combined with YSZ (Yin *et al.*, 2007, 2008; You *et al.*, 2007). As a result, the inner layer functions not only as the support for the membrane, but also as the catalyst in the DL-HFMR, substantially

© Woodhead Publishing Limited, 2011

increasing the surface area/volume ratio of the membrane reactor design by significantly reducing the space taken up by extra packing of catalyst.

16.4.2 Single-step fabrication of DL-HFMR for methane conversion

Compositions of the spinning suspensions of the outer oxygen separation layer and the inner catalytic support layer are listed in Table 16.1. In a typical process to prepare the suspensions, the desired quantity and ratio of the ceramic powders, the solvent and the additive were premixed and ball-milled (mainly to break up the agglomerates of the ceramic particles) in a high speed shimmy ball mill (MTI Corporation, SFM-1 (QM-3SP2)) for 48 h. After addition of the polymer binder, ball milling was continued for a further 48 h in order to obtain homogeneous spinning suspensions. The resultant spinning suspensions were then degassed while stirring under vacuum for about 2 h to remove air bubbles present in the suspension. After degassing, the suspensions for the outer layer and the inner layer were transferred to stainless steel syringes with a maximum volume of 100 ml and 200 ml, respectively, and were simultaneously extruded through a triple-orifice spinneret (Fig. 16.2) into an external coagulation bath containing around 120 litres of tap water with an air gap of 25 cm. The extrusion rates of the two spinning suspensions as well as the flow rate of the internal coagulant were accurately controlled and monitored by a KDS410 high pressure syringe pump and two Harvard PHD 22/2000 Hpsi syringe pumps, ensuring the uniformity of the prepared fibre precursors.

The precursor fibres formed were cut to the required length, heated in an Elite tubular furnace at 600°C for 2 h to remove the organic polymer binder and were finally sintered at 1400°C for 5 h with heating and cooling rates of 5°C min^{-1} and 3°C min^{-1}, respectively.

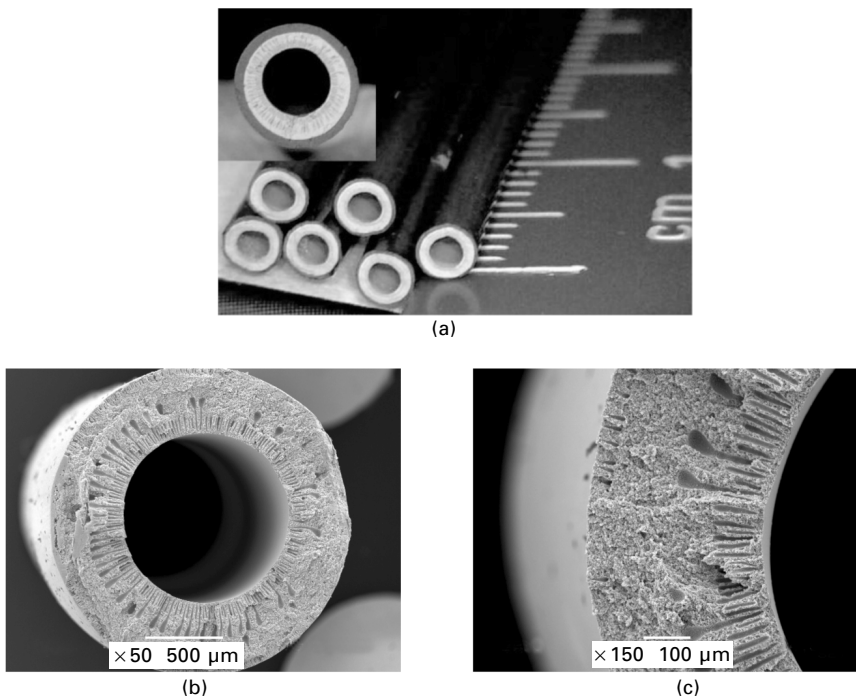
Table 16.1 Compositions of the spinning suspensions and co-extrusion parameters

	Outer oxygen separation layer (wt%)	Inner support/ catalytic layer (wt%)
LSM	27.4	–
YSZ	37.6	45.6
NiO	–	22.4
DMSO (dimethyl sulfoxide)	28.0	25.1
Polyether sulfone	6.5	6.8
Additive	0.5	0.1
Extrusion rate (ml min^{-1})	4.5–6.5	8
Temperature (°C)	25	
Air gap (cm)	25	
Internal precipitant (ml min^{-1})	10	

© Woodhead Publishing Limited, 2011

16.4.3 Morphology of dual-layer precursor hollow fibre membranes

A photographic image of the precursor fibres (before co-sintering) is shown in Fig. 16.5 (a). As can be seen, a thin outer layer has been uniformly coated around an inner layer with a clear interface between them. The outer layer benefits from the accurate control of the extrusion rates of the two layers, as well as similar spinning suspension properties and compositions, the types of ceramic powder, the polymer binder and the solvent used and is well bonded to the inner layer with a consistent thickness and uniform macrostructure for the whole batch of prepared fibres. The outer diameter (OD) and inner diameter (ID) of the dual-layer precursor fibres were measured as 1935.9 and 1064.1 μm, respectively, according to the SEM images shown in Fig. 16.5(b). The interface between the layers is less visible in Fig. 16.5(c) because of the polymer binder present in the precursor fibres. Tiny finger-like voids are found in the outer layer, while the inner layer is composed of both a sponge-like layer and a finger-like layer. The finger-like structure, which is formed as a result of viscous fingering phenomena during the phase inversion



(a)

(b)

(c)

16.5 (a) Photographic; and SEM images (b) of a whole view and (c) cross-section of precursor dual-layer hollow fibre membranes.

© Woodhead Publishing Limited, 2011

process (Kingsbury and Li, 2009), contributes to reduce the resistance of gas permeation through the inner layer, but at the cost of mechanical strength. It should be noted here that the finger-like structures of this type can be eliminated by further optimizing the spinning parameters, such as the viscosity of the spinning suspension (Kingsbury and Li, 2009).

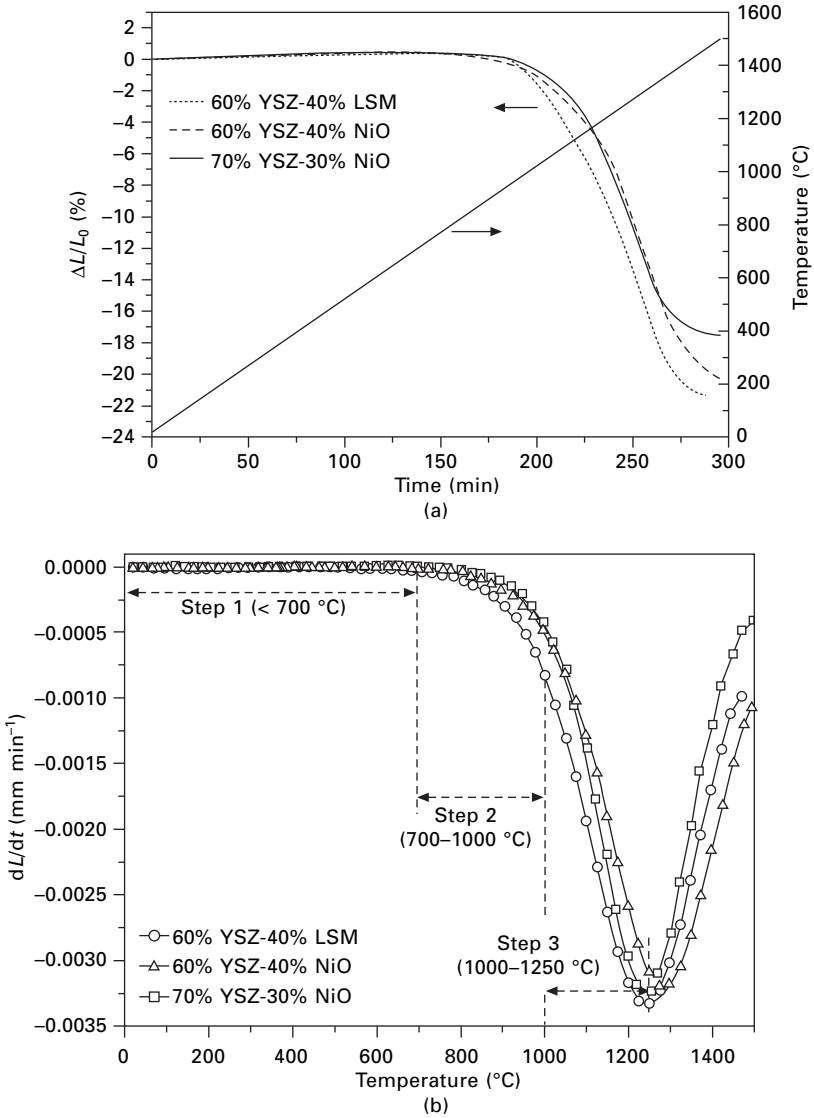
16.4.4 Co-sintering of LSM-YSZ/NiO-YSZ hollow fibre membranes

During co-sintering of a ceramic membrane with a dual-layer structure, which is also referred to as a supported or asymmetric structure for disk-type membranes (Chang *et al.*, 2006, Jin *et al.*, 2001), matching the sintering behaviour of the two layers made from different materials is critically important to achieve simultaneously a dense oxygen separation layer and a porous support layer free of defects. In contrast to supported/asymmetric disk-type membranes with a limited surface area, which are prepared by conventional multi-step fabrication processes, there is a considerably higher possibility of crack formation during co-sintering of dual-layer hollow fibre membranes, owing to a much higher surface area and curvature. As a result, the sintering behaviour of the different membrane materials must be investigated prior to co-sintering.

The advantages of the co-extrusion process allow excellent adhesion between the two layers of the precursor dual-layer hollow fibres, which has been discussed above. Dual-phase materials are employed in both the inner and the outer layers, which contain a large amount of YSZ. YSZ with excellent mechanical properties can, in this case, be considered to be the matrix of the hollow fibres which dominates the co-sintering process and helps to match the sintering behaviour of the two layers. Figure 16.6 shows the sintering curves as the well as sintering rate curves of the outer layer (LSM (40 vol%)-YSZ (60 vol%)) and the inner layer (NiO-YSZ) materials. In order to highlight the importance of the material composition to the sintering behaviour, two types of NiO-YSZ inner layer materials with different NiO concentrations, 30 vol% and 40 vol%, were tested for comparison.

As can be seen in Fig. 16.6(a), LSM-YSZ starts to shrink at a lower temperature and shows a higher final shrinkage compared with NiO-YSZ. When more YSZ is used in the inner layer material, the final shrinkage is reduced from 20.31% to 17.53%, which is even less than that of LSM-YSZ at 21.41%. In addition to the nature of the materials, the final shrinkages of the membrane materials are substantially dependent on the green packing density, which can be affected by a number of factors such as particle size, particle shape and the distance between particles. As the particle size of YSZ is about half that of NiO, the use of more YSZ would reduce the distance between particles, increase the green packing density of the corresponding

© Woodhead Publishing Limited, 2011



16.6 Sintering curves and sintering rate curves of the dual-layer hollow fibre materials, (a) sintering curves and (b) sintering rates.

sample and result in a lower final shrinkage. The values of final shrinkage from the sintering curves are still insufficient to give an insight into the co-sintering process because they are not able to reflect how the materials change during high temperature sintering, especially when there is an interaction between the two layers.

© Woodhead Publishing Limited, 2011

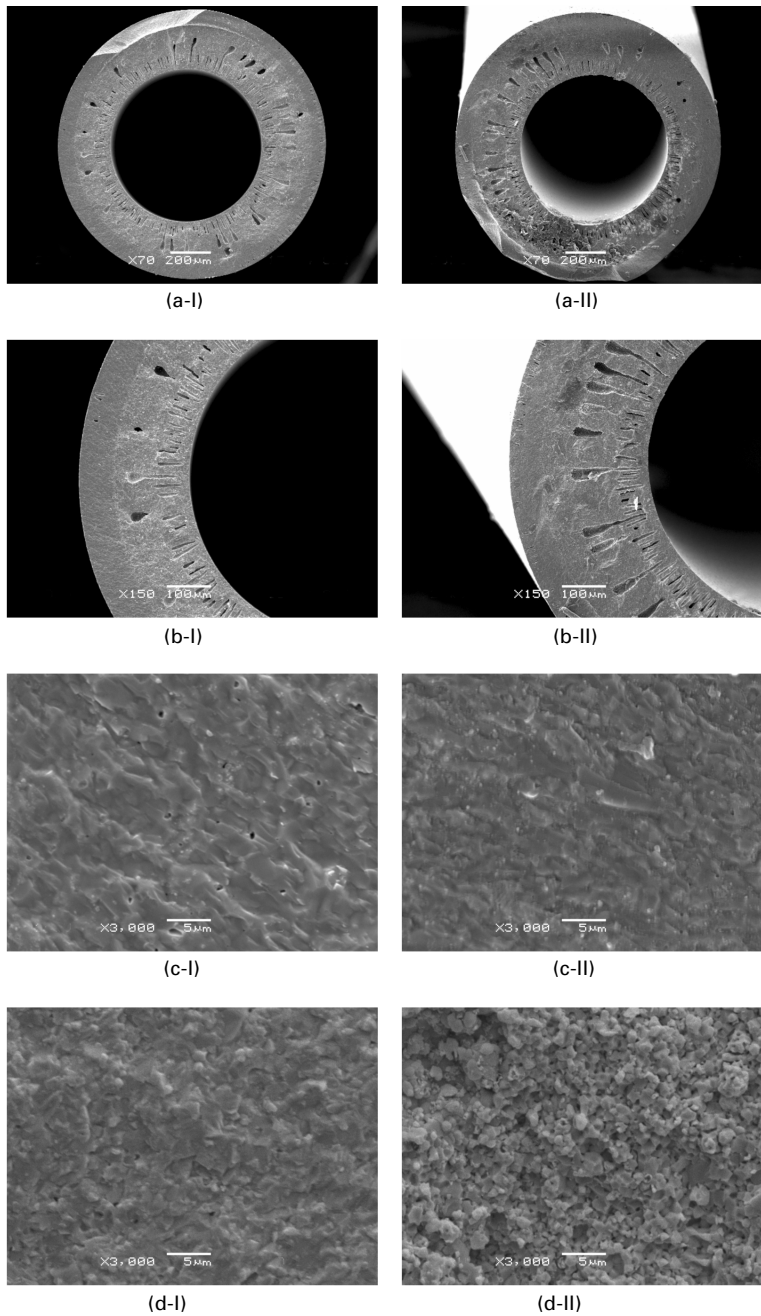
Based on the sintering curves in Fig. 16.6(a), the sintering rate curves that reveal the most critically important and useful information about the sintering process are shown in Fig. 16.6(b). As can be seen, there is little sintering below 700°C, at which temperature the polymers in the precursor fibres have been removed. With increasing temperature, ceramic membrane materials start to sinter at a very low rate which then slowly increases with increasing temperature up to about 1000°C. When the sintering temperature is above 1000°C, there is a significant increase in the sintering rate which reaches a maximum value at about 1250°C. As a result, step 3 is the most important stage in the co-sintering process because the difference in sintering rates at this stage is one of the main reasons for the formation of cracks or defects which result in poor integrity and mechanical strength of the resultant membranes. If the difference in the sintering rate is too large, the membrane cannot even survive the co-sintering process. For example, although the final shrinkage of 60 vol%YSZ-40 vol%NiO is closer to that of LSM-YSZ, when compared with 70 vol%YSZ-30 vol% NiO (Fig. 16.6(a)), its sintering rate curve is quite different from that of LSM-YSZ and as a consequence the corresponding dual-layer hollow fibres break into several parts with very poor mechanical properties after co-sintering. In contrast, 70 vol%YSZ-30 vol%NiO is more suitable as the inner layer material. Moreover, the use of larger amounts of YSZ in the inner layer improves the mechanical properties of the resultant hollow fibre membranes.

16.4.5 Mechanical properties and macrostructure of dual-layer hollow fibres

The precursor fibres of 40 cm in length, which are composed of a 40 vol% LSM-60 vol% YSZ outer oxygen separation layer supported by a 30 vol% NiO-70 vol% YSZ inner catalytic support layer are then co-sintered at 1400°C for 5 h. The mechanical properties of the developed dual-layer hollow fibres are investigated and compared with an inner single-layer fibre prepared separately under identical conditions. As can be seen in Table 16.2, the dual-layer fibres are stronger than their inner single-layer counterparts in terms of the higher force/loading needed to break the samples, as a result of the additional outer oxygen separation layer. However, the bending strengths of these two types of samples are quite similar to each other, because the ODs of the dual-layer fibres are larger than those of the inner single-layer fibres, while the IDs of both fibres are the same, giving a greater fibre wall thickness to the dual-layer fibres. The bending strengths, which are normalized to the fibre dimensions are shown in Equation [16.1]:

$$\sigma_F = \frac{8F_m L_h D_o}{\pi(D_o^4 - d_i^4)} \qquad [16.1]$$

© Woodhead Publishing Limited, 2011



(a-I) (a-II)

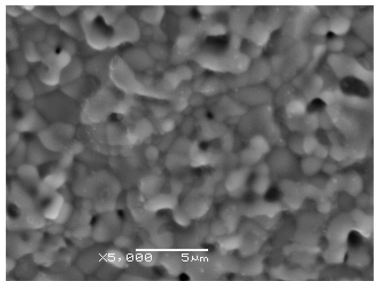
(b-I) (b-II)

(c-I) (c-II)

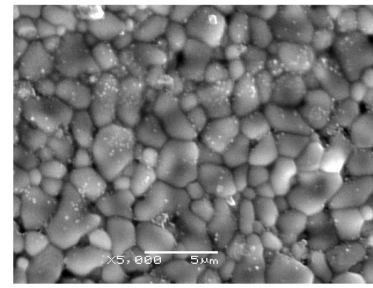
(d-I) (d-II)

16.7 SEM images of dual-layer hollow fibres after co-sintering (I) and after reduction (II), (a) whole view, (b) cross-section, (c) outer layer cross-section, (d) inner layer cross-section, (e) outer layer surface, (f) inner layer surface.

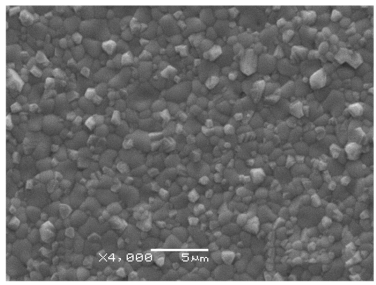
© Woodhead Publishing Limited, 2011



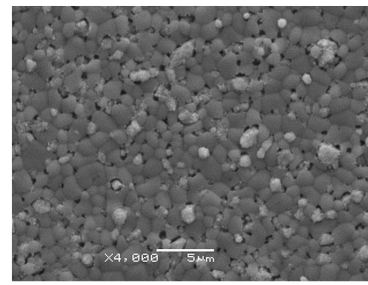
(e-I)



(e-II)



(f-I)



(f-II)

16.7 Continued

Table 16.2 Three-point bending of single-layer and dual-layer hollow fibres

	Inner single-layer fibres		Dual-layer fibres	
	Load (N)	Bending strength (MPa)	Load (N)	Bending strength (MPa)
Sample 1	5.61	298.80	8.24	311.91
Sample 2	5.07	270.04	7.33	277.47
Sample 3	5.26	280.15	7.49	283.52
Average	5.31	283.00	7.69	290.97

where σ_F is the bending strength (MPa), F_m is the force/loading applied at breaking point (N), L_h is the the length of the fibre (m), D_o is the fibre outer diameter (m) and d_i is the fibre inner diameter (m).

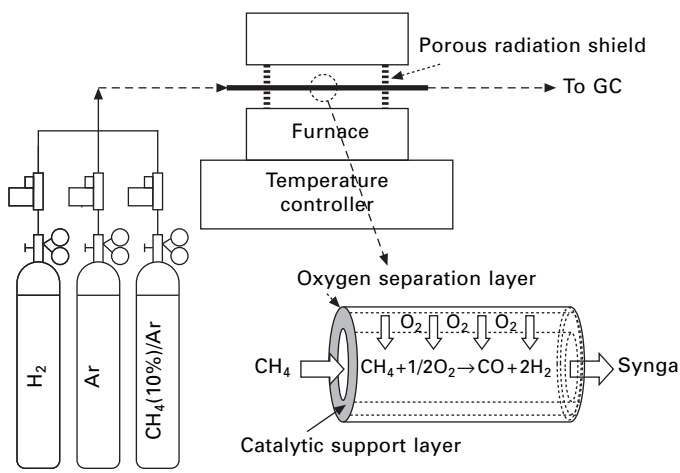
The force/loading needed to break these fibres is slightly higher than that of a YSZ hollow fibre with a similar asymmetric structure (Wei and Li, 2008) owing to the thicker hollow fibre wall. The comparable bending strengths between the dual-layer and the inner single-layer fibres in Table 16.2 further indicate that, because of the well matched sintering behaviour of the outer oxygen separation layer and the inner support layer materials (Fig. 16.6), the formation of structural defects or cracks during the co-sintering process can be much reduced, further demonstrating the excellent integrity of the developed dual-layer hollow fibres.

© Woodhead Publishing Limited, 2011

After co-sintering, the average length of the fibres is reduced to 28.7 cm, while the OD and ID of the resultant dual-layer fibres decrease to approximately 1309.1 and 736.4 μm, respectively (Fig. 16.7 (a-I)), resulting in a surface area/volume ratio of up to 2769.7 m^2/m^3. The thickness of the outer oxygen separation layer is measured to be 75.0 μm (Fig. 16.7 (b-I)). No cracks were found after co-sintering and there is a clear interface between the two layers. The cross-sections of the outer (Fig. 16.7 (c-I)) and the inner (Fig. 16.7 (d-I)) layers, as well as the inner surface (Fig. 16.7 (f-I)), are densified, although dead-end pores are observed on the outer surface (Fig. 16.7 (e-I)). No obvious macro-structural changes in the outer layer were observed when NiO in the inner layer was reduced to Ni (Fig. 16.7 (a), (b), (c-II) and e-II)), indicating excellent material stability under a reducing atmosphere. The cross-section (Fig. 16.7 (d-II)) and the inner surface (Fig. 16.7 (f-II)) of the inner layer transform into a highly porous structure after reduction. In addition, the porous structure formed as a result of the reduction is highly interconnected in the inner layer, providing a high catalytic surface area in the resultant DL-HFMR for methane conversion.

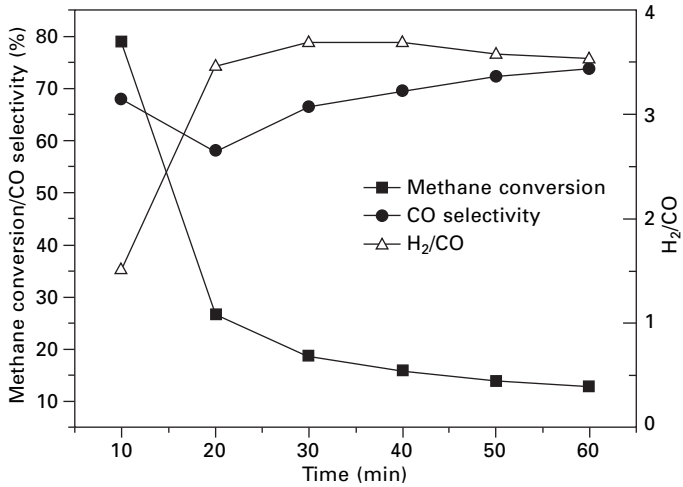
16.4.6 DL-HFMR for methane conversion

The developed dual-layer hollow fibre membranes are then directly used as a membrane reactor for methane conversion using the experimental set-up shown in Fig. 16.8. Prior to the reaction, NiO in the inner layer was reduced to Ni at 550°C for 30 min using a hydrogen stream with a flow rate of 20 ml min^{-1}, in order to generate catalytic activity for methane conversion. Figure 16.9 shows that an initial methane conversion as high as 78.94% at 750°C



16.8 Schematic diagram of experimental set-up for POM reaction.

© Woodhead Publishing Limited, 2011



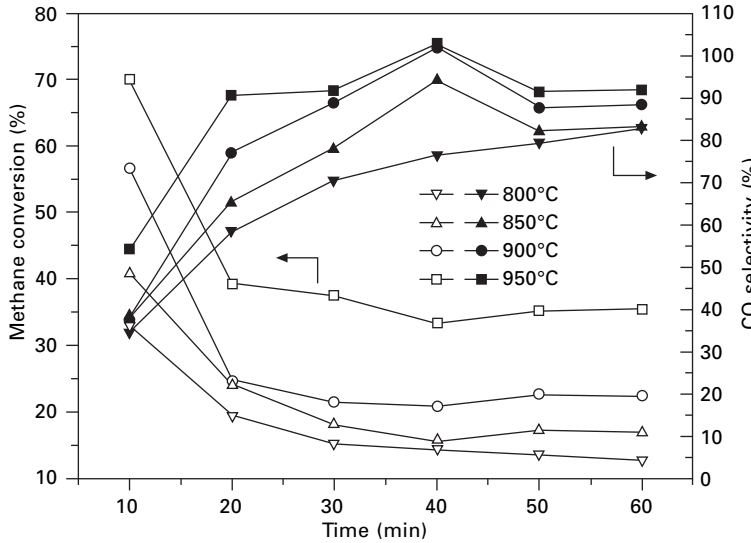
16.9 Time dependent performance of DL-HFMR at 750°C.

can be achieved after 10 min of reaction. However, methane conversion drops to 12.75% within one hour of operation. This is in good agreement with the report of Yin *et al.* (2008), in which a mixture of NiO and YSZ-8 (1:1 by weight) was used as the catalyst for a POM reaction. The reason for the drop in methane conversion was considered to be a consequence of coke accumulation on Ni(0) grain surfaces which hindered the access of methane to the catalyst active sites (Yin *et al.*, 2008) and which was proved by X-ray diffraction (XRD) analysis (Yin *et al.*, 2007). Figure 16.9 further indicates that, after 20 min of reaction at 750°C, CO selectivity increases with reaction time while the H_2/CO ratio is only slightly affected and is stabilized at about 3.5.

After one hour of reaction at 750°C, the reactant stream was switched to argon at 20 ml min^{-1} for 30 min, after which the argon was switched back to the reactant stream. In the meantime, the operating temperature was increased from 750 to 800, 850, 900 and 950°C with a heating rate of 5°C min^{-1}. Only CO is detectable in the product stream when the methane stream is switched to argon, which indicates that coke is removed by the permeated oxygen, agreeing well with the work of Yin *et al.* (2007, 2008). In addition, only trace amounts of nitrogen at approximately 1.4×10^{-4} ml cm^{-2} s^{-1} can be detected in the product stream of the DL-HFMR during the reaction, further proving the excellent integrity of the membrane at high temperatures.

As can be seen in Fig. 16.10, methane conversion and CO selectivity increase with increasing temperature between 800°C and 950°C. At the same temperature, methane conversion drops sharply from a high initial value and stabilizes within one hour of reaction, while CO selectivity increases with

© Woodhead Publishing Limited, 2011

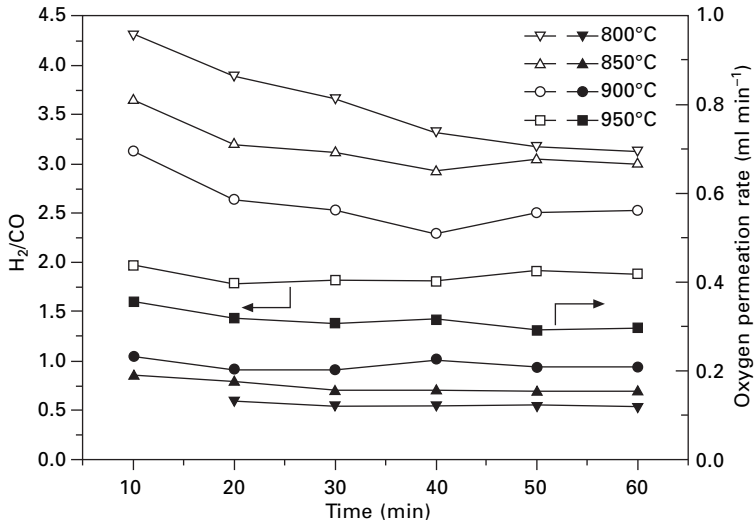


16.10 Time dependent methane conversion (open symbols) and CO selectivity (solid symbols) of DL-HFMR between 800 and 950°C.

reaction time, which is similar to the trend at 750°C. A sudden increase in CO selectivity is observed after 40 min reaction when the temperature is above 850°C, the reason for which is still under investigation and may be related to the consumption of coke accumulated on the inner layer during the reaction. At 950°C, the stabilized methane conversion and CO selectivity are 35.54% and 91.98%, respectively. With increasing temperature, as shown in Fig. 16.11, the oxygen permeation rate increases while the H_2/CO ratio decreases. At the same temperature, the oxygen permeation rate varies slightly with reaction time while the H_2/CO ratio decreases and is finally stable at a certain value after one hour of operation between 800°C and 900°C. In contrast, the H_2/CO ratio at 950°C is less dependent on the reaction time and is stable at around 2, although there is also a sharp drop in methane conversion after 10 min of reaction at this temperature (Fig. 16.10).

It has been reported that the coke deposition rate on Ni-YSZ increases with increasing temperature (Ke *et al.*, 2006), which is in line with the larger drop in methane conversion at higher temperatures shown in Fig. 16.10. However, a higher oxygen permeation rate through the LSM-YSZ outer layer at elevated temperatures (Fig. 16.11) contributes to an increase the methane conversion and CO selectivity and results in H_2/CO ratios closer to the value of 2. As a result, less coking on the inner catalytic support layer and a higher oxygen permeation rate of the outer oxygen separation layer are helpful in further improving the performance of the DL-HFMR for methane conversion, which can be achieved by replacing Ni-YSZ with

© Woodhead Publishing Limited, 2011



16.11 Time dependent H_2/CO (open symbols) and oxygen permeation rate (solid symbols) of DL-HFMR between 800 and 950°C.

more coking-resistant materials and further reducing the thickness of the outer layer using the same membrane production process, respectively.

16.5 Dual-layer hollow fibres for a micro-tubular solid oxide fuel cell (SOFC)

16.5.1 Background

The solid oxide fuel cell (SOFC) has been considered as a promising electricity generation technology because of its high efficiency in converting chemical energy to electrical power (Singhal and Kendall, 2003). To date, two types of SOFC designs, planar and tubular SOFC, have been widely studied. Although planar SOFC in a highly compact configuration shows great power density, a design of this type is challenged by the need for high temperature sealing near the edges of the cell because only few sealants can endure the thermal cycles experienced during operation (Weil *et al.*, 2004). Another concern with this design is the relatively long start-up times that are required in order to prevent crack formation in thin planar configurations. In contrast, a tubular geometry is more reliable and can be operated in the absence of high temperature seals, consequently showing excellent resistance to rapid thermal cycling. However, it is more difficult to achieve high power density owing to less efficient cell packing and higher cell losses associated with elongated electronic pathways. In order to improve the volumetric power density, the diameter of tubular designs needs to be reduced from a few

© Woodhead Publishing Limited, 2011

centimeters (e.g. Siemens-Westinghouse cell) to the order of 1 mm, namely micro-tubular SOFC, as they are often referred to in the literature. A design of this type can significantly increase the specific surface area of electrodes, improve mechanical properties and more importantly, speed up the start-up and the shut-down processes. As a result of these advantages, micro-tubular SOFCs have attracted increasing interest in recent years.

Conventionally, the supports of micro-tubular SOFC, that is the anode or cathode layers, are fabricated by extrusion followed by high temperature sintering. The electrolyte layer is then deposited using a number of techniques such as dip coating, chemical vapour deposition (CVD) and spraying techniques, followed by additional sintering. The whole fabrication process is usually time-consuming and cost-intensive. A structure of this type, for example anode–support–electrolyte, can be achieved by using the single-step co-extrusion and co-sintering process.

16.5.2 Single-step fabrication of electrolyte/anode dual-layer hollow fibres

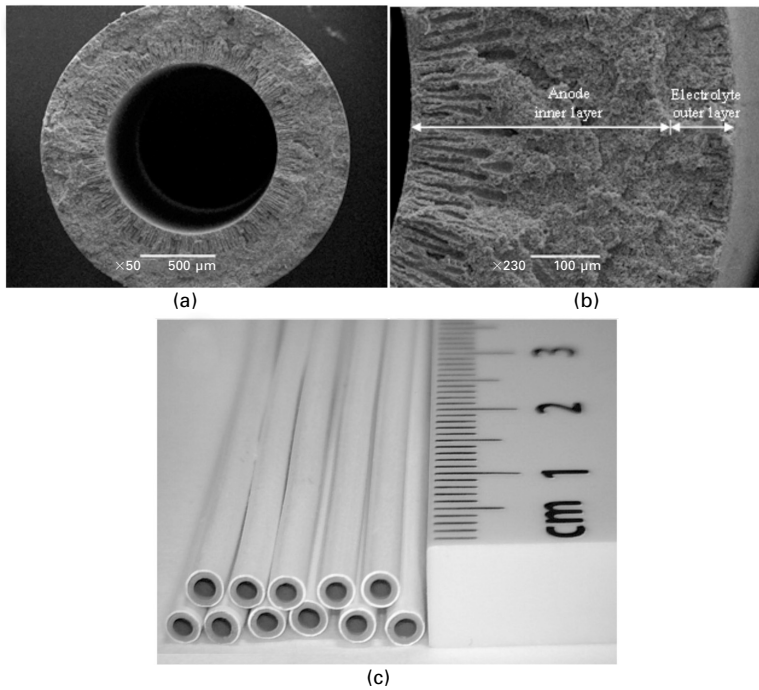
$Ce_{0.9}Gd_{0.1}O_{1.95}$ (CGO)/Ni-CGO electrolyte/anode dual-layer hollow fibres for intermediate temperature micro-tubular SOFC are prepared using the co-extrusion process with the spinning suspension compositions listed in Table 16.3. As can be seen in Fig. 16.12, fabrication of precursor fibres with a consistent and uniform dual-layer structure has been achieved. The cross-section of the inner layer exhibits an asymmetric structure with short finger-like structures originating from the inner surface to approximately 35% of the inner layer thickness, whereas the remaining 65% consists of a sponge-like structure. The cross-section of the outer layer also has short finger-like structures near the outer surface and a sponge-like structure occupying the rest of the layer.

In contrast to the dual-layer hollow fibre membranes used for catalytic membrane reactors, in which both of the inner and outer layers are made of dual-phase materials, the material compositions of $Ce_{0.9}Gd_{0.1}O_{1.95}$ (CGO)/ Ni-CGO electrolyte/anode dual-layer hollow fibres are less 'adjustable' owing to the special functions of each individual layer. Consequently, the sintering

Table 16.3 Compositions of the spinning suspensions for $Ce_{0.9}Gd_{0.1}O_{1.95}$ (CGO)/ Ni-CGO electrolyte/anode dual-layer hollow fibres

Layer	Composition (wt%)					
	NiO	CGO	PESf	Arlacel P135	DMSO	Viscosity at 50 s^{-1} (cP)
Anode	42.00	28.00	7.00	0.12	22.88	32 500
Electrolyte	–	64.00	6.40	0.12	29.48	14 900

© Woodhead Publishing Limited, 2011

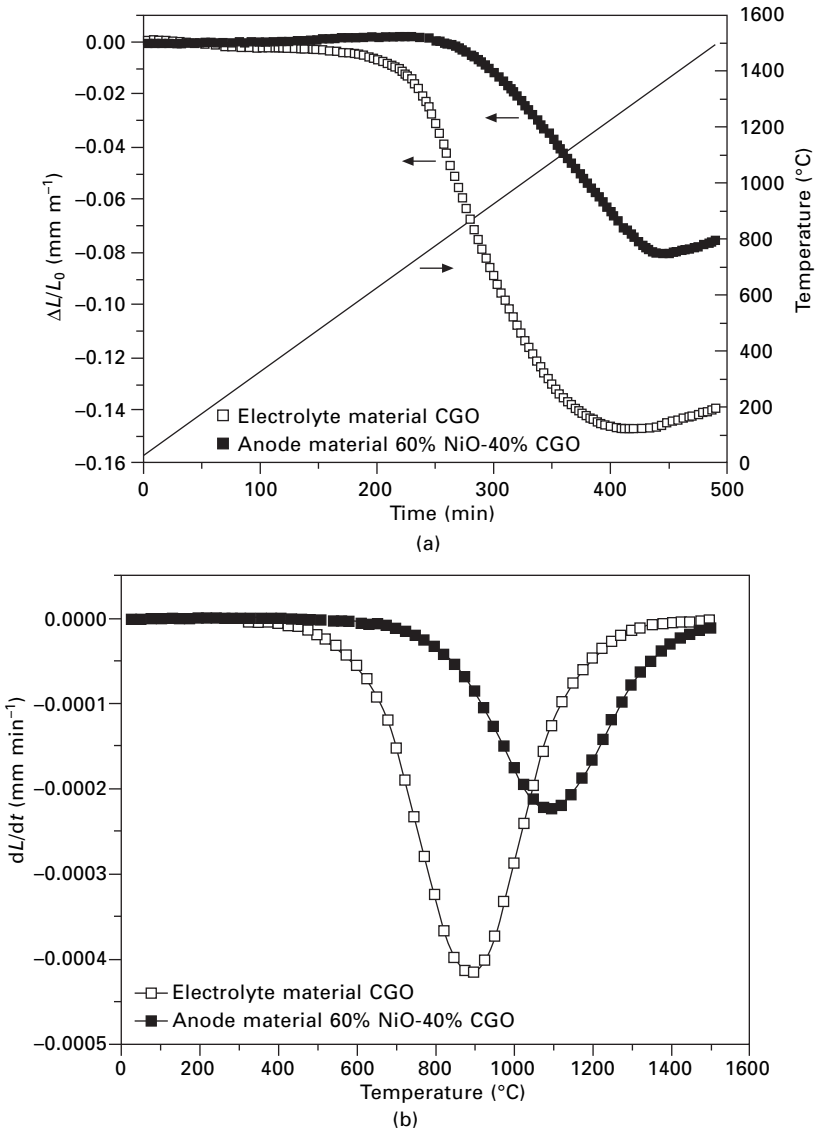


16.12 (a) Overall view (SEM), (b) cross-section (SEM) and (c) photographic image of the CGO/NiO-CGO dual-layer hollow fibre precursors.

behaviour of the CGO electrolyte layer and the Ni-CGO anode, which are quite different from each other and are shown in Fig. 16.13, cannot be matched easily by changing the material compositions. As a result, a heating rate as high as 15°C min^{-1} has to be used during the co-sintering process, below which the fibres cannot survive the sintering process. At the beginning of this work, the dual-layer hollow fibre precursor was co-sintered at 1550°C for 12 hours and followed by a simple reduction process at 550°C for 2.5 hours.

After depositing a $La_{0.6}Sr_{0.4}Fe_{0.8}Co_{0.2}O_3$ (LSCF)-CGO composite cathode onto the CGO electrolyte layer, an intermediate temperature micro-tubular SOFC can be obtained with the clear triple-layer structure shown in Fig. 16.14. This cell produced maximum power densities of 420 W m^{-2} and 800 W m^{-2} at 450°C and 550°C, respectively (Droushiotis *et al.*, 2009a), approximately one order of magnitude lower than those of micro-tubular SOFC prepared by a conventional extrusion and sintering method (Suzuki *et al.*, 2009). This can be attributed to a number of factors such as the lower porosity of the Ni-CGO anode inner layer owing to the high co-sintering temperature used (1550°C) and the relatively thicker CGO electrolyte layer (around 80 μm). In an attempt to improve the porosity of the anode layer,

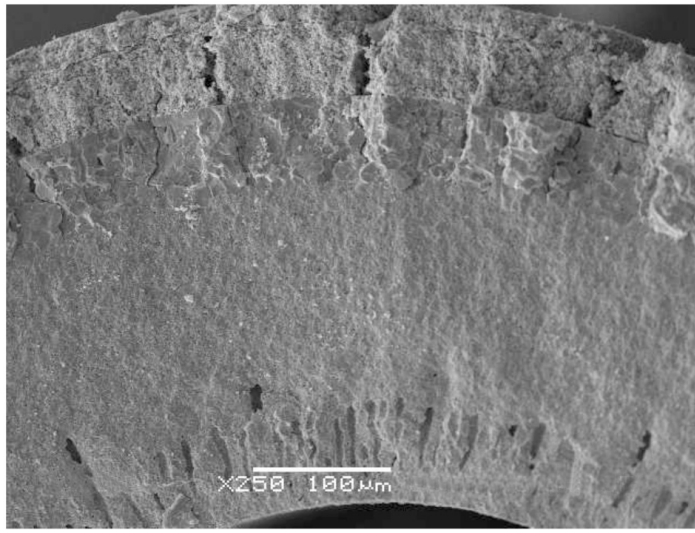
© Woodhead Publishing Limited, 2011



16.13 (a) Sintering curves and (b) sintering rate curves of the inner and outer layer materials.

studies on the effects of co-sintering temperature and anode macrostructure have been carried out and will be discussed in the following sections. The power outputs of the corresponding SOFC have been improved to 1186–5864 W m^{-2} at between 450°C and 570°C, when a more porous anode and a better current collection method are employed.

© Woodhead Publishing Limited, 2011



16.14 Cross-sectional SEM image of the micro-tubular HF-SOFC showing anode/electrolyte/cathode layers after anode reduction.

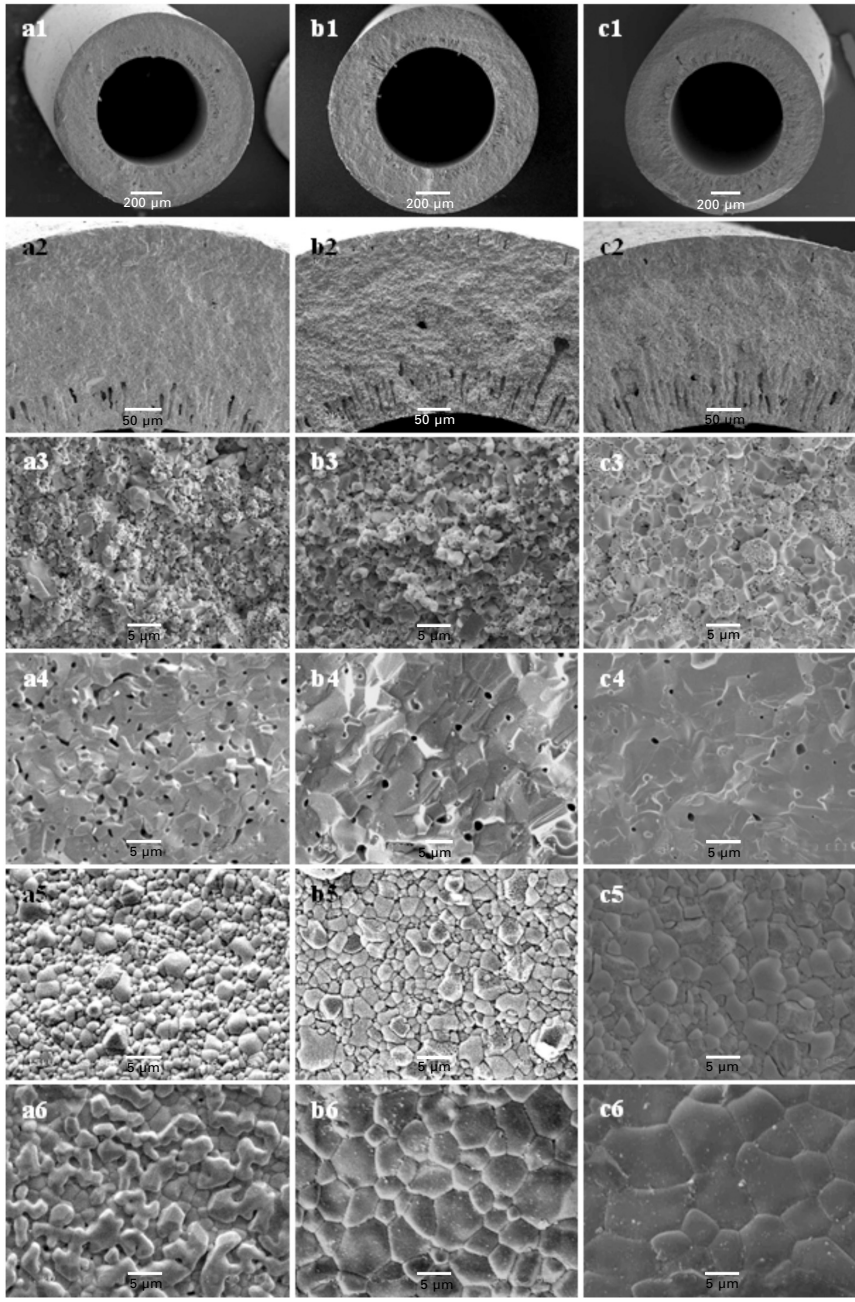
16.5.3 Effect of co-sintering temperatures on CGO/Ni-CGO electrolyte/anode dual-layer hollow fibres

Although the macrostructure of the precursor fibres is largely determined during the spinning process, its microstructure, such as porosity and pore size, are closely dependent on the sintering process. A reduction in the co-sintering temperature facilitates the diffusion of the fuel by increasing the porosity and average pore size of the sponge-like layer of the anode, which contributes to improving the efficiency. However, this is at the expense of mechanical strength and the electrical conductivity of the anode layer, together with the gas tightness of the outer electrolyte layer. As a result, a suitable co-sintering temperature for CGO/Ni-CGO electrolyte/anode dual-layer hollow fibres needs to be determined.

Microstructure

The microstructures of CGO/Ni-CGO dual-layer hollow fibres, which are co-sintered between 1450°C and 1550°C for 12 h followed by a reduction in NiO, are shown in Fig. 16.15. The OD and the ID are less dependent on the co-sintering temperatures and are measured to be approximately 1400 µm, and 800 µm respectively (Fig. 16.15(a1)–(c1)), with uniform thicknesses of the inner and the outer layers of *ca*. 220 µm and 80 µm, respectively. The macrostructure of the CGO/Ni-CGO dual-layer hollow fibre, which is free of cracks, (Fig. 16.15(a2)–(c2)) is almost identical to their CGO/NiO-CGO

© Woodhead Publishing Limited, 2011



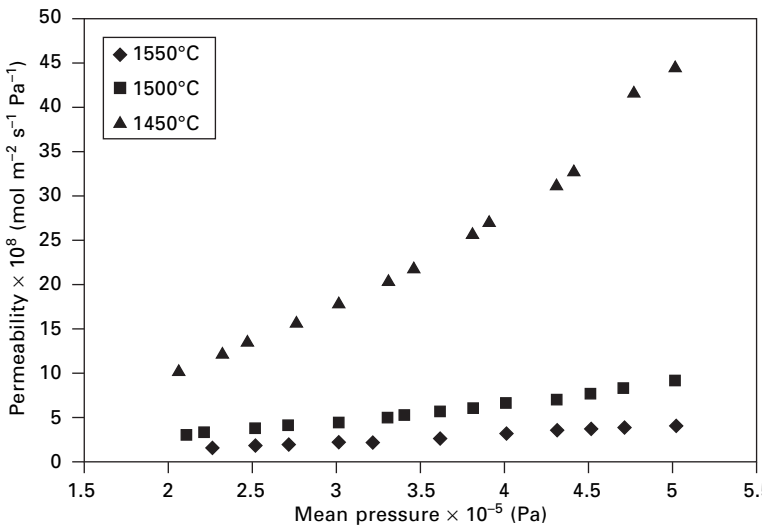
16.15 SEM images of the CGO/Ni-CGO dual-layer HF at different co-sintering temperatures: (a) 1450°C, (b) 1500°C (c) 1550°C, and from different perspectives: (1) overall view of the HF, (2) cross-section of the HF, (3) anode cross-section of the HF, (4) electrolyte cross-section of the HF, (5) inner surface of the HF, (6) outer surface of the HF.

© Woodhead Publishing Limited, 2011

precursor counterparts, indicating that the co-sintering process removed only the organic materials without significantly changing the membrane morphology.

With an increase of the co-sintering temperature from 1450–1550°C, the electrolyte layer becomes denser and smoother, together with a significant growth in CGO grain sizes (Fig. 16.15(a4)–(c4), (a5)–(c5), (a6)–(c6)). The average CGO grain size is visually estimated at approximately 2.7, 5.9 and 9.6 μm at co-sintering temperatures of 1450, 1500 and 1550°C, respectively. A similar trend was also observed for the inner layer. Although the overall porosity of the inner layer decreases with the increasing co-sintering temperatures, its cross-section and inner surface are still relatively porous, as pores of this type are formed as a result of the reduction of NiO to Ni. Such an interconnected pore structure is desirable to facilitate the diffusion of the fuel into the anode. Furthermore, the tiny finger-like voids near the outer surface of the outer layer almost disappear after the co-sintering process.

Another way to demonstrate the effect of the co-sintering temperature on the porous structure is to investigate the gas permeation, such as the nitrogen permeation, through the inner anode layer, which is achieved by fabricating single-layer Ni-CGO hollow fibres using identical spinning parameters to their dual-layer counterparts. Figure 16.16 shows that the nitrogen permeability drops significantly when the sintering temperature is increased from 1450–1500°C, compared with a temperature increase from 1500–1550°C. Moreover, with an increase of the sintering temperature, the nitrogen permeability is less dependent on the mean pressure, in other words the slope of a plot of



16.16 N_2 permeation through a Ni-CGO hollow fibre anode as a function of sintering temperature.

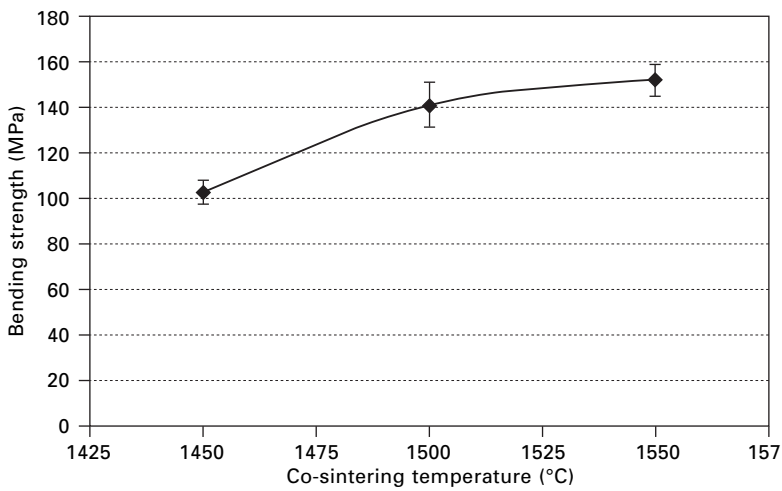
© Woodhead Publishing Limited, 2011

permeability against pressure is closer to 0, which indicates that the average pore size in the anode layer decreases with an increase in sintering temperature, in agreement with the results shown in Fig. 16.15.

Mechanical strength and gas tightness

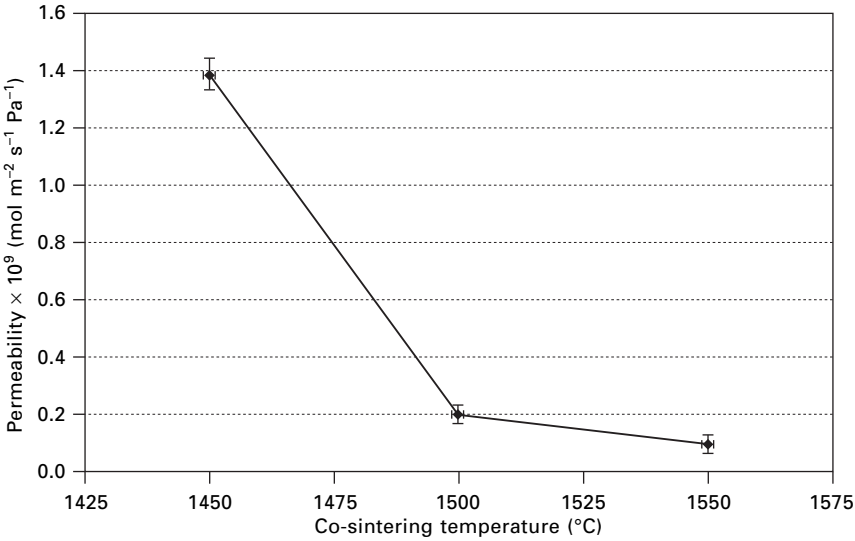
The effect of co-sintering temperatures on the mechanical properties of the developed CGO/Ni-CGO dual-layer hollow fibres is investigated using a three-point bending test and is shown in Fig. 16.17. As can be seen, a significant increase in the mechanical strength of around 38% is observed when the co-sintering temperature is increased from 1450–1500°C, while an increase of less than 8% is observed when the temperature is further increased to 1550°C. This agrees well with the change in nitrogen permeation shown in Figure 16.16. The mechanical strength of CGO/Ni-CGO fibres sintered at 1500°C for 12 h is approximately 141.1 MPa, which is comparable with a Ni-YSZ tube or hollow fibre with similar dimensions and Ni content (Dong *et al.*, 2007; Droushiotis *et al.*, 2009b; Du and Sammes, 2004; Yang *et al.*, 2008). The mechanical strength can be further improved by optimizing the asymmetric structure of the anode layer, for example by reducing the length of the finger-like voids, which will be briefly introduced in the following sections.

In contrast to the inner anode layer, the electrolyte layer of SOFC must be impermeable to any gas to prevent direct contact between the fuel and oxidizer. According to Tan *et al.* (2005), a ceramic membrane can be considered gas-tight if the measured nitrogen permeability is close to 10^{-10} mol m^{-2} s^{-1}



16.17 Bending strength of the CGO/Ni-CGO dual-layer hollow fibres as a function of co-sintering temperature.

© Woodhead Publishing Limited, 2011



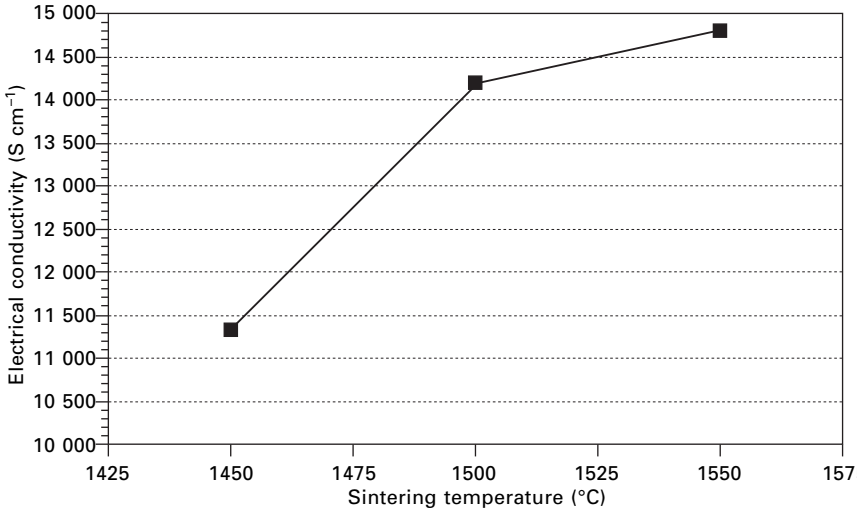
16.18 Gas-tightness of the CGO/Ni-CGO dual-layer hollow fibres as a function of co-sintering temperature.

Pa^{-1}. As can be seen in Fig. 16.18, the nitrogen permeability of the CGO/Ni-CGO co-sintered at 1450°C is 13.9×10^{-10} mol m^{-2} s^{-1} Pa^{-1}; this value decreases dramatically to 2.02×10^{-10} mol m^{-2} s^{-1} Pa^{-1} at 1500°C, and further reduces slightly to 0.96×10^{-10} mol m^{-2} s^{-1} Pa^{-1} at 1550°C. This is in agreement with the changes in mechanical strength and nitrogen permeation discussed above and indicates that a co-sintering temperature of 1500°C is high enough to achieve a fully dense electrolyte layer for SOFC.

Electrical conductivity

The electrical conductivity of the Ni-CGO anode, which is critically important to minimize the ohmic losses in the cell, is investigated using a four-probe DC technique at room temperature. The conductivity obtained is mainly from the contribution of the Ni phase in the anode because CGO shows no electronic conductivity at room temperature. As can be seen in Fig. 16.19, electrical conductivity increases with the sintering temperature as it is increased from 1450–1550°C. The increasing sintering temperatures strengthen the connection between NiO particles, resulting in a more continuous Ni phase after reduction and consequently higher electrical conductivity of the anode (Droushiotis *et al.*, 2009b; Yang *et al.*, 2008). In contrast with data from previous studies, such as 1700 S cm^{-1} (Ni-YSZ hollow fibre with a sandwich-like structure and 50 wt% Ni) (Droushiotis *et al.*, 2009b) and 772 S cm^{-1} (Ni-YSZ hollow fibre with an asymmetric structure) (Yang *et al.*, 2008),

© Woodhead Publishing Limited, 2011



16.19 Electrical conductivity of Ni-CGO hollow fibre anode as a function of sintering temperature.

the conductivity in Fig. 16.19 is significantly higher as a result of a greater proportion of sponge-like structure, fewer and shorter finger-like voids and a more uniform Ni distribution. Such a structure is also expected to increase the length of triple phase boundary (TPB) regions and, as a result, minimize the activation polarization in the anode.

The small enhancement of electrical conductivity from 1500–1550°C indicates that a sintering temperature at 1500°C is recommended to fabricate CGO/Ni-CGO dual-layer hollow fibres for the construction of micro-tubular SOFC, in conjunction with the changes in microstructure, nitrogen permeation, mechanical strength and gas-tightness as a function of sintering temperatures.

16.5.4 Control over the macrostructure of Ni-CGO anode

In addition to variation of co-sintering temperatures, the performance of the Ni-CGO anode support layer, in terms of electrical conductivity, mechanical strength and how efficiently a fuel is able to diffuse into the anode, can be improved by controlling the asymmetric structure of the anode layer, that is the ratio between the thickness of the sponge- and finger-like layers. The formation of finger-like structures is believed to be initiated by hydrodynamically unstable viscous fingering developed when a less viscous fluid (non-solvent) is in contact with a higher viscosity fluid (spinning suspension containing invertible polymer binder) (Kingsbury and Li, 2009).

Finger-like void growth occurs only below a critical suspension viscosity,

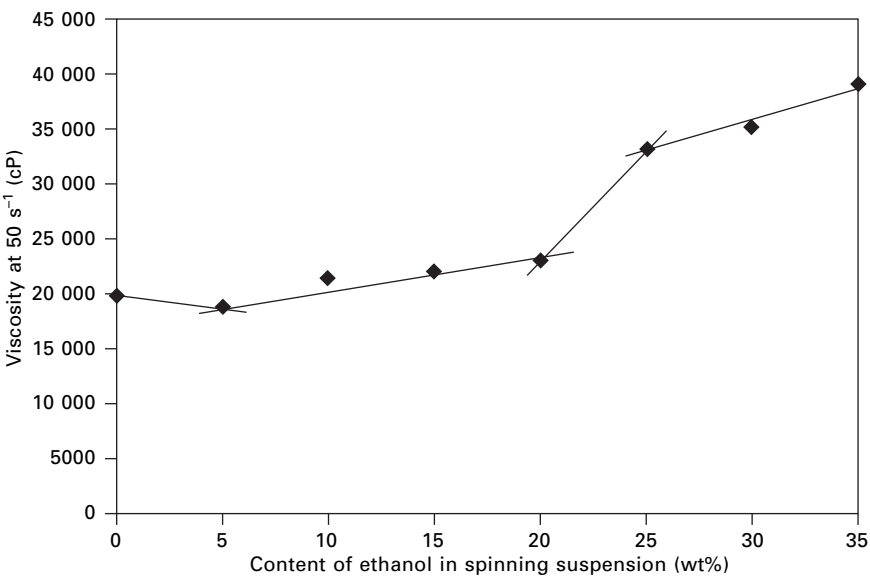
© Woodhead Publishing Limited, 2011

above which a sponge-like structure is observed over the entire hollow fibre cross-section. Although a number of factors, such as extrusion rate, air gap and bore liquid flow rate, may affect the morphology of ceramic hollow fibres, viscosity is determined to be the dominating factor for ceramic systems (Kingsbury and Li, 2009). As a result, ethanol as a poor solvent or water as a non-solvent can be employed to adjust the initial property of the spinning suspensions to allow control over the membrane morphology.

Effects of ethanol on Ni-CGO hollow fibre macrostructure

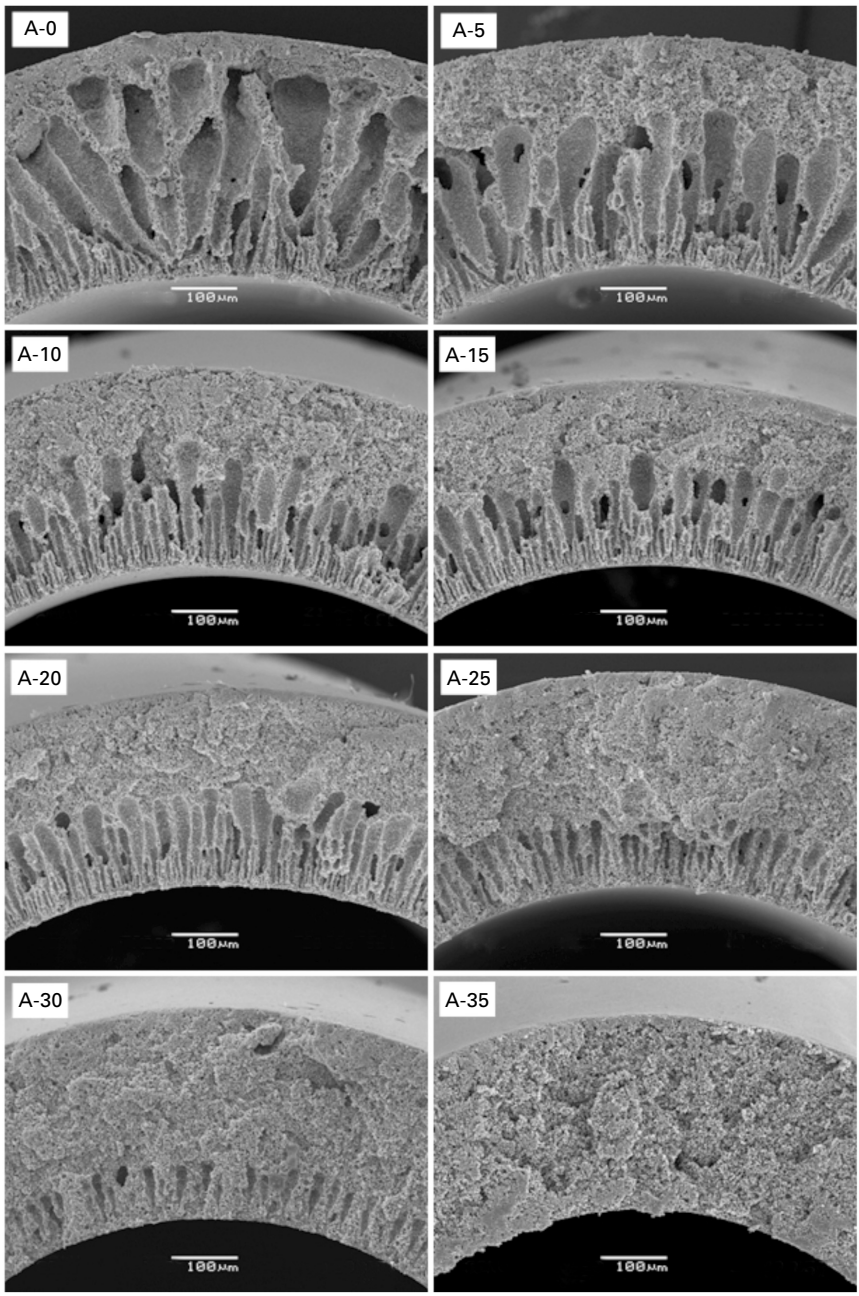
For the NiO-CGO system, the main reason for replacing certain amounts of solvent with ethanol (Table 16.4), instead of water, to manipulate spinning suspension viscosity is that ethanol acts as a good dispersant for NiO-CGO mixture without use of additional polymeric additives. As can be seen in Fig. 16.20, replacing 5% of NMP with ethanol brings little change in suspension viscosity. Use of more ethanol (from 10%–20%) results in a gradual enhancement of viscosity from 21 400–22 900 cP. A further addition of ethanol from 25–35% leads to a significantly faster increase in viscosity from 33 100–39100 cP.

This change in suspension viscosity as a result of replacing N-methyl-2-pyrrolidone (NMP) with ethanol leads to a significant variation of hollow fibre macrostructure. As can be seen in Fig. 16.21, hollow fibres with 0 wt% ethanol have a typical asymmetric structure of long finger-like voids



16.20 Viscosity of spinning suspensions prepared with 0–35 wt% ethanol (as a percentage of the total NMP-ethanol content).

© Woodhead Publishing Limited, 2011



16.21 SEM images of the NiO-CGO precursor hollow fibres with 0–35 wt% ethanol (as a percentage of the total NMP-ethanol content) where, for example, A0 is 0% ethanol content and A35 is 35% ethanol content.

© Woodhead Publishing Limited, 2011

Table 16.4 Composition of spinning suspensions with different amounts of ethanol

Fibre	Composition (wt%)					NMP – ethanol composition (wt%)
	NiO	CGO	PESf	Arlacel P135	NMP + ethanol	
A-0						100–0
A-5						95–5
A-10						90–10
A-15	42.00	28.00	7.00	0.12	22.88	85–15
A-20						80–20
A-25						75–25
A-30						70–30
A-35						65–35

originating from the inner fibre surface and occupying up to 85% of the fibre thickness, with the remaining fibre region taken up by a sponge-like layer. Although 5% ethanol results in little change in suspension viscosity, there is still an observable reduction in the length of the finger-like voids. This is because less NMP takes part into solvent–non-solvent exchange during the phase inversion process, which speeds up the increase of suspension viscosity during spinning, inhibits further viscous fingering and results in shorter finger-like voids.

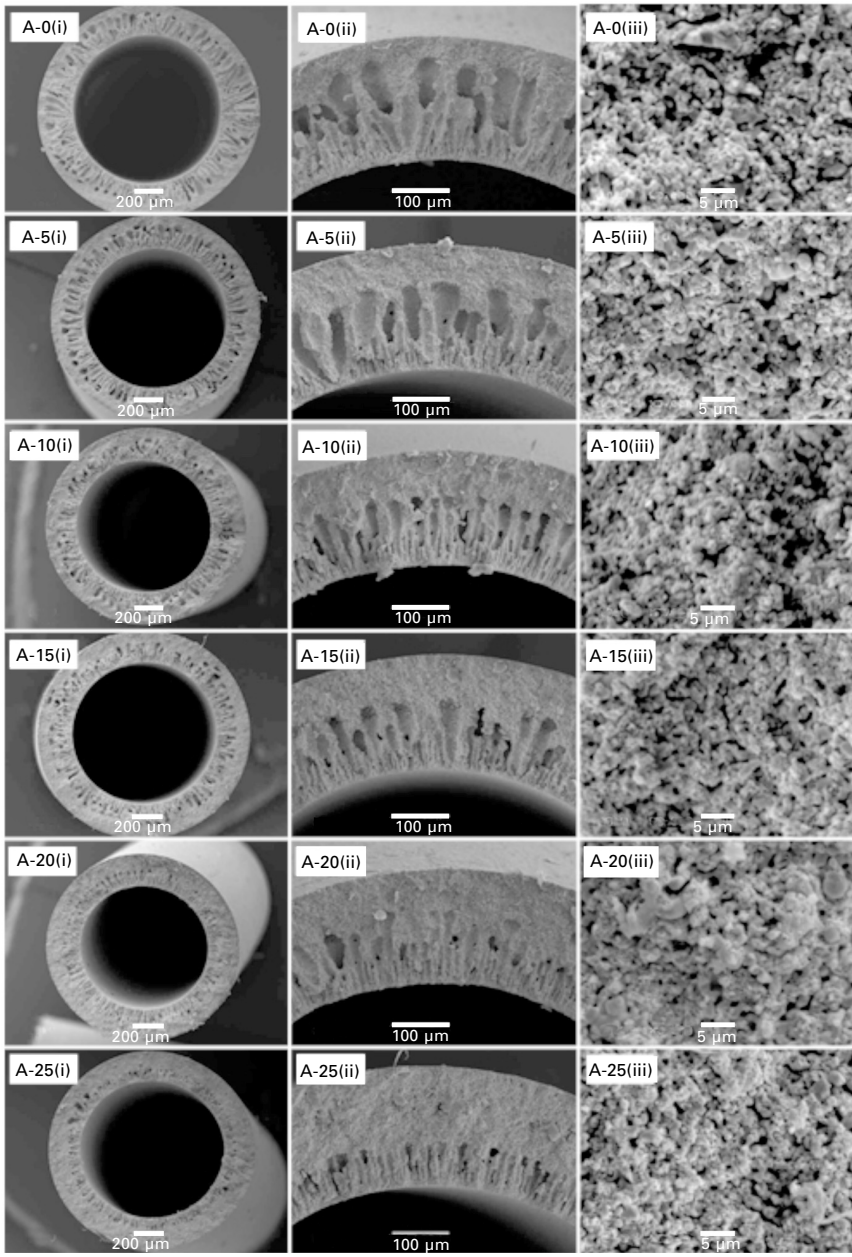
The relative thicknesses of finger-like layers are further gradually reduced to approximately 60%, 55% and 50% when the ethanol content is increased to 10 wt%, 15 wt% and 20 wt%, respectively, as shown in SEM images of A-10, A-15 and A-20 in Fig. 16.21. In agreement with the changes in suspension viscosity (Fig. 16.20), the finger-like layer is abruptly reduced to about 30% and 20% of the cross-section with 25 wt% and 30 wt% ethanol, respectively, in spinning suspensions. And a further increase in suspension viscosity by using 35 wt% of ethanol reaches the 'threshold' value where viscous fingering would not occur, resulting in a fully sponge-like structure.

These hollow fibres were then sintered (1450°C for 6 hours) and reduced (550°C for 2.5 h) in order to obtain a Ni-CGO anode hollow fibre. Apart from the shrinking size, the macrostructures of the hollow fibres are largely retained after sintering and reduction processes, as shown in Fig. 16.22, while reduction of NiO to Ni turns the sintered fibres into a highly interconnected porous structure and as a result alters the microstructures of these hollow fibres.

Microstructure of Ni-CGO fibres

Microstructures of Ni-CGO anode hollow fibres were investigated using a mercury porosimeter. As shown in Fig. 16.23, three types of pore structures

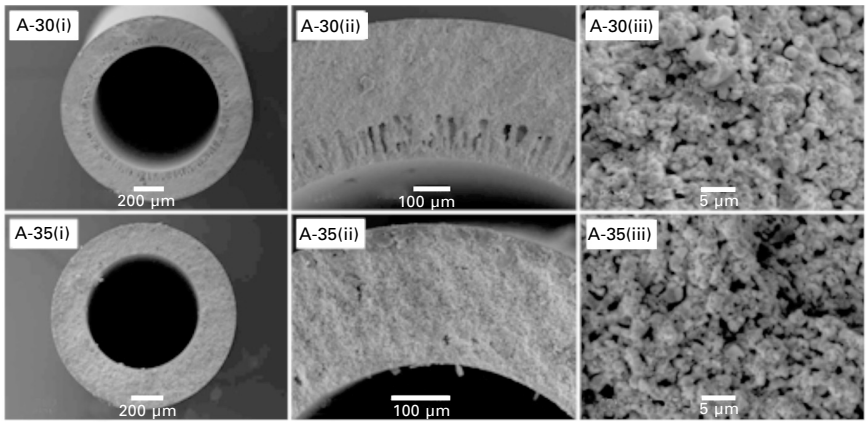
© Woodhead Publishing Limited, 2011



16.22 SEM images of the (i) overall view, (ii) cross-section, and (iii) the sponge-like structure region of Ni-CGO anode hollow fibres. A0, A5, A10, A15, A20, A25, A30, A35 refer to ethanol content as Fig. 16.21.

Continued overleaf

© Woodhead Publishing Limited, 2011



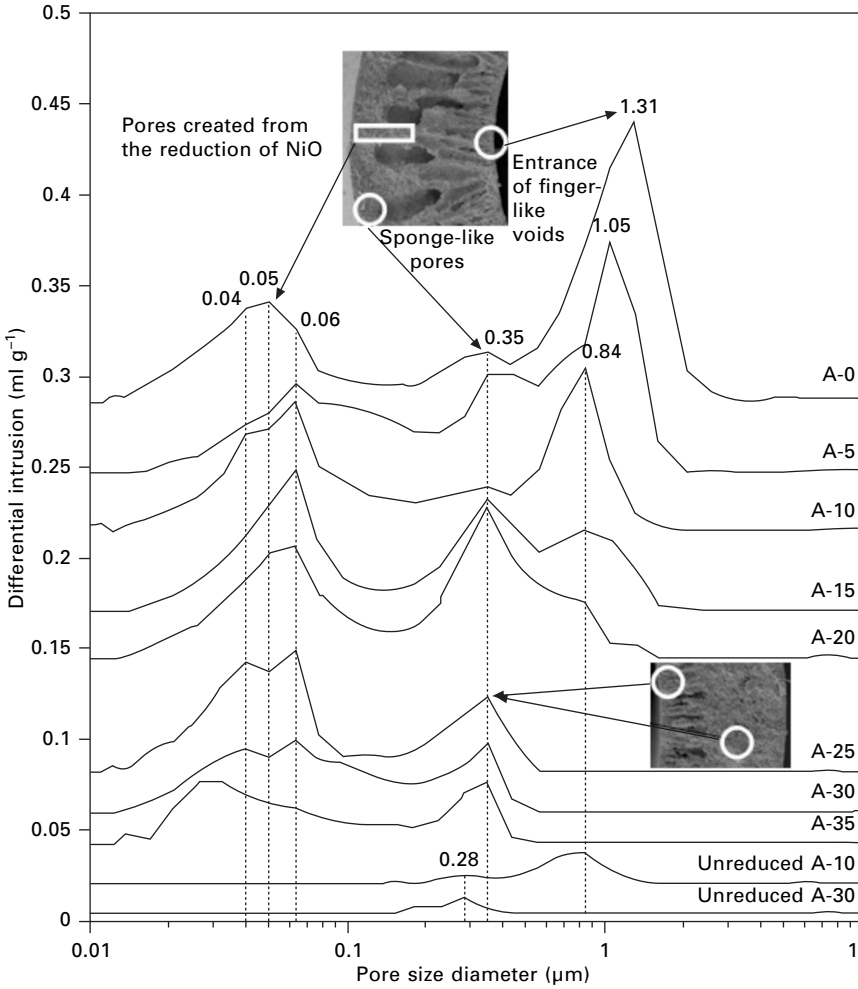
16.22 Continued

are observed in the Ni-CGO hollow fibres, which are, in an order of decreasing pore size, the entrances of finger-like voids, the packed pores in the sponge-like region that survived the sintering (sintering at 1450°C for 6 h can still densify NiO-CGO mixture and leave some packed pores in the sintered fibres) and the pores formed as a result of reduction of NiO to Ni.

As can be seen in Fig. 16.23, fibres A-0 show a pore size distribution consisting of a peak at approximately 1.31 μm, which represents the pores at inner fibre surface that form the entrances to finger-like voids, a smaller peak at 0.35 μm representing the packed pores and a broad peak at a range 0.04–0.06 μm representing the pores from the reduction of NiO. With increasing ethanol concentration in spinning suspensions, the peak of finger-like void entrances at 1.31 μm is shifted to 1.05 and 0.84 μm for fibres A-5 and A-10, respectively, indicating that the entrance of the finger-like voids reduces with decreasing length of finger-like voids.

The intensity of the peak at 0.84 μm is reduced by more than half and the peak at 0.35 μm appears more significantly for fibres A-15 and A-20. The peak at 0.84 μm is totally absent for A-25 and A-30 and this can be attributed to the suspension viscosity trend shown in Fig. 16.20. As there is a huge increase in the viscosity after the addition of 25 wt% ethanol to the spinning suspension, the viscous fingering phenomenon is almost inhibited during phase inversion, resulting in the formation of tiny finger-like voids that do not originate from the inner surface of the fibres. Figure 16.22 (A-25ii) and (A-30ii), shows a very thin sponge-like porous structure in the region between the inner surface and the entrance to the finger-like voids and it is expected that the size of entrance to the finger-like voids is reduced to a size similar to that of the sponge-like layer. Therefore, it is believed that the peak at 0.35 μm for fibres A-25 and A-30 not only represents the sponge-like pores but also the entrance pores for finger-like voids. As expected, only two

© Woodhead Publishing Limited, 2011



16.23 Pore size distributions of the Ni-CGO anode hollow fibres with various macrostructures. A0–A35 have the same meaning as Fig. 16.21 and Fig. 16.22.

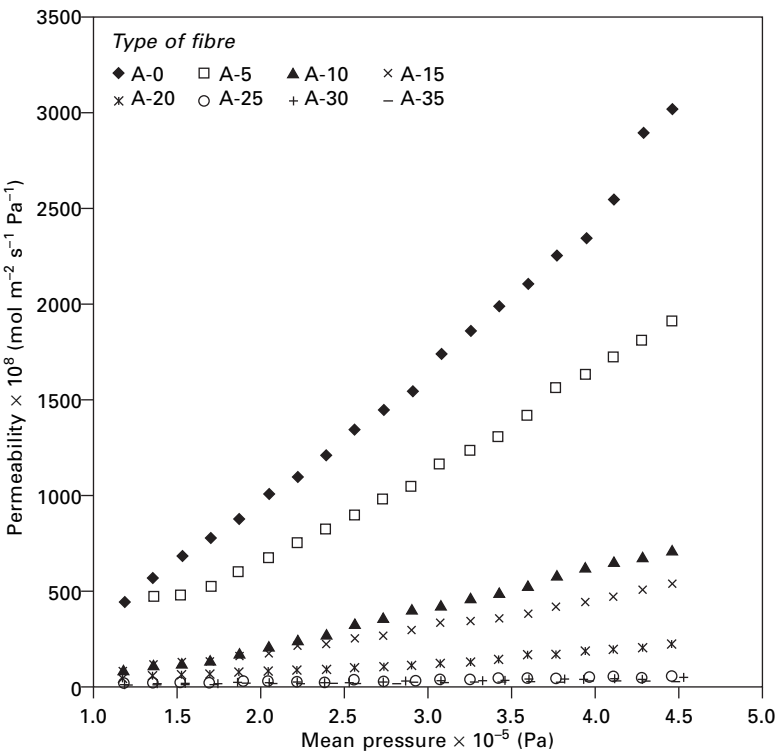
significant peaks appear for A-35, at 0.35 μm and 0.03 μm, which represent the packed pores and the pores from the reduction of NiO, respectively.

Figure 16.23 also shows that the unreduced fibres have relatively low intensity peaks for the entrance pores of finger-like voids and packed pores as can be seen in the trend of unreduced A-10 and A-30. This indicates that the pore size for the sponge-like structure and finger-like voids structure increase after the reduction process. This also confirms that the reduction process would significantly increase the porosity of the fibres although the fibres were sintered at a relatively high temperature.

© Woodhead Publishing Limited, 2011

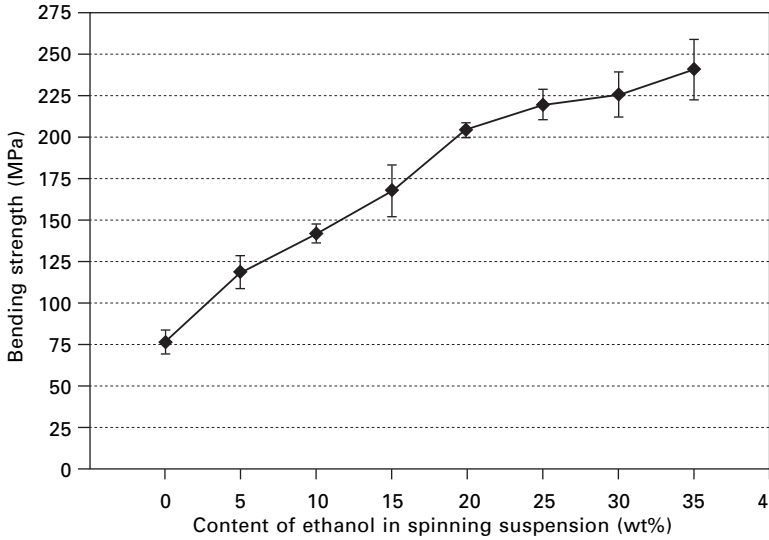
Effect of morphology on Ni-CGO anode performance

The performance of anode hollow fibre is affected by a number of factors, such as electrical conductivity, resistance to diffusion of fuel into the anode and mechanical strength. Nitrogen permeation results shown in Fig. 16.24 indicate how efficiently fuel is able to diffuse into the anode layer. Larger finger-like voids, when less ethanol is used in spinning suspensions, reduce gas permeation resistance, allowing better contact between fuel and anode. However, larger finger-like voids also decrease the sponge-like region, which consequently reduces the mechanical strength (Fig. 16.25) as well as the electrical conductivity (Fig. 16.26) of the anode layer. All these indicate that the performance of anode hollow fibre is quite sensitive to its macrostructure. As a result, one of the major benefits of controlling the macrostructure of Ni-CGO anode hollow fibres, that is the ratio between the sponge-like layer and finger-like layer, by adjusting the spinning suspension viscosity with ethanol is that it will help to determine the most suitable anode morphology for micro-tubular SOFC.

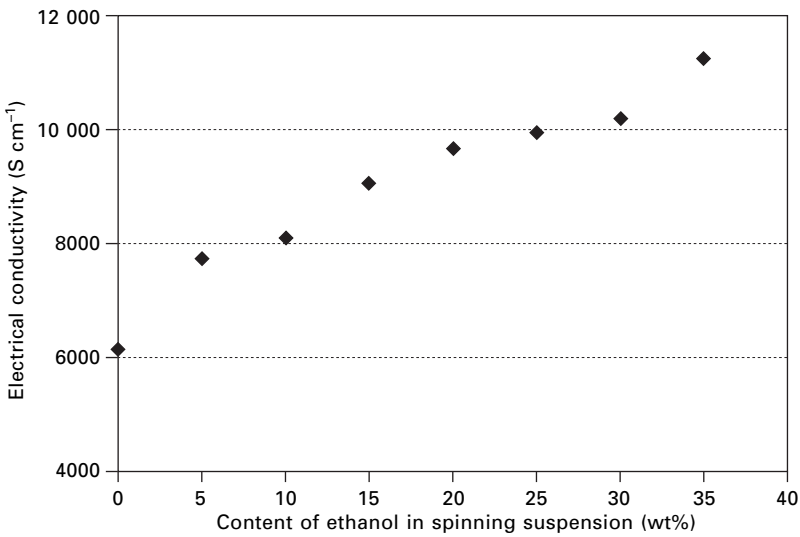


16.24 The N_2 permeation results for the Ni-CGO anode hollow fibres.

© Woodhead Publishing Limited, 2011



16.25 Bending strength of the Ni-CGO anode hollow fibres with different ethanol contents in the spinning suspension.



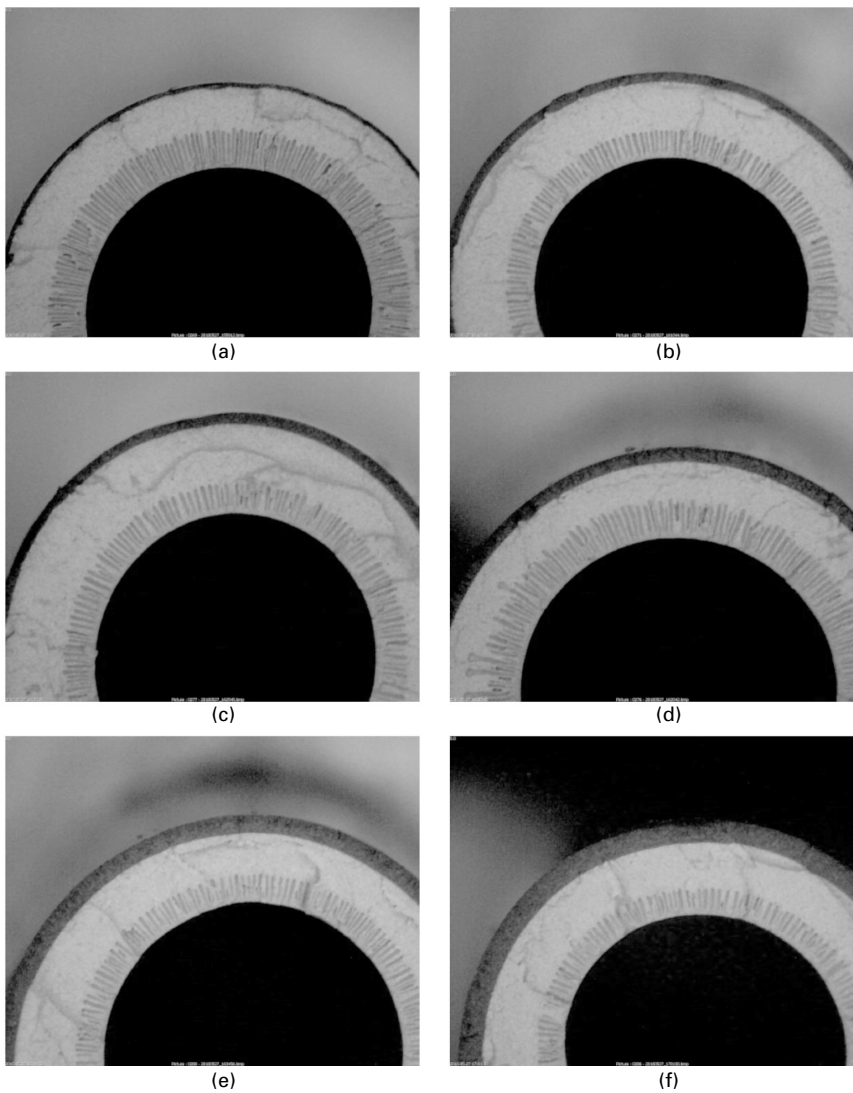
16.26 Electrical conductivities of the Ni-CGO anode layer hollow fibres.

16.6 Other ways of improving ceramic dual-layer hollow fibres

In addition to improving the inner catalytic substrate layer, another efficient way of improving performance of ceramic dual-layer hollow fibre membranes

© Woodhead Publishing Limited, 2011

is to reduce the thickness of the outer dense layer used for separation. This can be conveniently achieved and accurately controlled in the co-extrusion process by maintaining the extrusion rate of the inner layer suspension, while varying that of the outer layer suspension. The minimum thickness of the outer layer is dependent on a number of factors, such as the size of the spinneret outer orifice and viscosity of the suspension. Figure 16.27



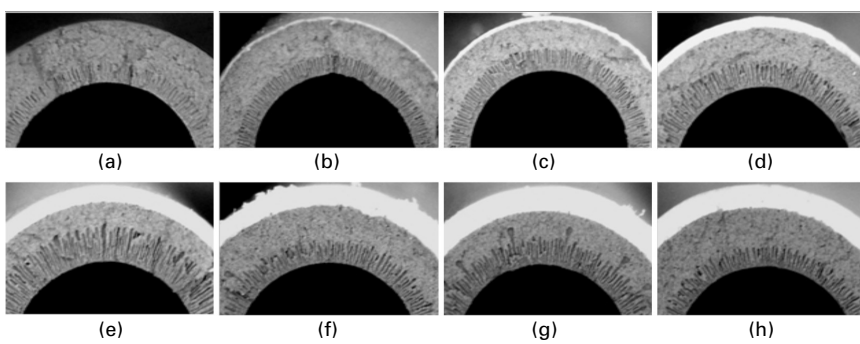
16.27 Photographic images of precursor fibres with varied outer layer thickness for multifunctional DL-HFMR. (a) 0.5 ml min^{-1}, (b) 1.0 ml min^{-1}, (c) 2.0 ml min^{-1}, (d) 3.0 ml min^{-1}, (e) 4.0 ml min^{-1}, (f) 5.0 ml min^{-1}.

© Woodhead Publishing Limited, 2011

and Fig. 16.28 show precursor dual-layer hollow fibres for multifunctional DL-HFMR and micro-tubular SOFC, respectively, with varied outer layer thicknesses. In both cases, the minimum outer layer extrusion rate is at 0.5 ml min^{-1}, below which the outer layer is not able to be uniformly coated. Use of an extrusion rate of 0.5 ml min^{-1} results in a uniform outer layer thickness of around 10 μm after co-sintering.

16.7 Conclusions

The design of ceramic dual-layer hollow fibre membranes consisting of a thin layer for separation supported on a highly porous substrate layer integrates a number of distinguishing advantages that are critically important in meeting the challenges of membrane separation and membrane reactor processes. These advantages include a large surface area/volume ratio, outstanding processing capacity, lower material cost, higher permeation flux and reduced gas permeation resistance. The phase inversion based single-step co-extrusion and co-sintering technique provides a versatile, time and cost effective process for the production of high quality ceramic dual-layer hollow fibre membranes with controllable asymmetric structures. By functionalizing each individual layer, ceramic dual-layer hollow fibre membranes of this type can be applied to various kinds of applications, such as multifunctional hollow fibre membrane reactors and electrolyte/anode fibres for micro-tubular solid oxide fuel cells. The generic advantages of the design of functional ceramic dual-layer hollow fibre membranes and the single-step membrane fabrication process can be transferred to the development of other inorganic membranes with more advanced structures, expanding and speeding up the development of membrane separation and membrane reactor processes.



16.28 Photographic images of precursor fibres with varied outer layer thickness for micro-tubular SOFC. Extrusion rate for outer layer is (a) 0 ml min^{-1}, (b) 0.5 ml min^{-1}, (c) 1 ml min^{-1}, (d) 2 ml min^{-1}, (e) 3 ml min^{-1}, (f) 4 ml min^{-1}, (g) 5 ml min^{-1}, (h) 6 ml min^{-1}.

© Woodhead Publishing Limited, 2011

Besides all these advantages, the major concern over such hollow fibre designs is the mechanical properties. The mechanical strength of ceramic hollow fibres is normally less than their tubular counterparts, as a consequence of smaller diameter and thinner wall thickness which are, at the same time, the advantages of hollow fibre membranes. In order to promote its strength, hollow fibres can be integrated into a bundle in which every individual fibre is surrounded and supported by other fibres. At the same time, improvement in the mechanical properties of each single hollow fibre is also important and can be achieved by using stronger membrane materials, optimizing hollow fibre morphology and adjusting wall thickness and so on.

Although there is still a lot to do prior to a practical engineering use of hollow fibre membranes and reactors, the advantages of a ceramic hollow fibre configuration over its conventional flat-sheet/tubular counterparts are a strong and persistent driving force behind related research in this field. Any sort of breakthrough in membrane material, membrane fabrication process and application process may significantly speed up development in the near future, requiring closer joint efforts by both material scientists and chemical engineers.

16.8 References

Balachandran U, Dusek JT, Maiya PS, Ma B, Mieville RL, Kleefisch MS, Udovich CA, Fleisch TH and Bose AC (1997), 'Development of dense ceramic membranes for methane conversion', *Stud. Surf. Sci. Catal.*, **107**, 409–14.

Bouwmeester HJM (2003), 'Dense ceramic membranes for methane conversion', *Catal. Today*, **82**, 141–50.

Chang XF, Zhang C, Jin WQ and Xu NP (2006), 'Match of thermal performances between the membrane and the support for supported dense mixed-conducting membranes', *J. Membr. Sci.*, **285**, 232–8.

De Jong J, Benes NE, Koops GH and Wessling M (2004), 'Towards single step production of multi-layer inorganic hollow fibers', *J. Membr. Sci.*, **239**, 265–9.

Dong DH, Gao JF, Liu XQ and Meng GY (2007), 'Fabrication of tubular NiO/YSZ anode-support of solid oxide fuel cell by gelcasting', *J. Power Sources*, **165**, 217–23.

Droushiotis N, Othman MHD, Doraswami U, Wu ZT, Kelsall G and Li K (2009a), 'Novel co-extruded electrolyte-anode hollow fibres for solid oxide fuel cells', *Electrochem Commun*, **11**, 1799–802.

Droushiotis N, Doraswami U, Kanawka K, Kelsall GH and Li K (2009b), 'Characterization of NiO-yttria stabilised zirconia (YSZ) hollow fibres for use as SOFC anodes', *Solid State Ionics*, **180**, 1091–9.

Du YH and Sammes NM (2004), 'Fabrication and properties of anode-supported tubular solid oxide fuel cells', *J. Power Sources*, **136**, 66–71.

Jin WQ, Li SG, Huang P, Xu NP and Shi J (2001), 'Preparation of an asymmetric perovskite-type membrane and its oxygen permeability', *J. Membr. Sci.*, **185**, 237–43.

Ke K, Gunji A, Mori H, Tsuchida S, Takahashi H, Ukai K, Mizutani Y, Sumi H, Yokoyama M and Waki K (2006), 'Effect of oxide on carbon deposition behavior of CH4 fuel

© Woodhead Publishing Limited, 2011

on Ni/ScSZ cermet anode in high temperature SOFCs', *Solid State Ionics*, **177**, 541–7.

Kingsbury BFK and Li K (2009), 'A morphological study of ceramic hollow fibre membranes', *J. Membr. Sci*., **328**, 134–40.

Li K (2007), *Ceramic Membranes for Separation and Reaction*, Wiley, Chichester, UK.

Li W, Liu JJ and Chen CS (2009), 'Hollow fiber membrane of yttrium-stabilized zirconia and strontium-doped lanthanum manganite dual-phase composite for oxygen separation', *J. Membr. Sci*., **340**, 266–71.

Liu YY, Tan XY and Li K (2006), 'Mixed conducting ceramics for catalytic membrane processing', *Catal. Rev.*, **48**, 145–98.

Loeb S and Sourirajan S (1963), 'Sea water demineralisation by means of an osmotic membrane', *Adv. Chem. Ser.*, **38**, 117.

Marcano JGS and Tsotsis TT (2002), *Catalytic Membranes and Membrane Reactors*, Wiley-VCH, Weinheim.

Minh NQ (1993), 'Ceramic fuel-cells', *J. Am. Ceram. Soc*., **76**, 563–88.

Reed JS (1995), *Principles of Ceramic Processing*, John Wiley & Sons, New York.

Scott K (1995), *Handbook of Industrial Membranes*, Elsevier Science Publishers, Oxford, UK.

Singhal SC and Kendall K (2003), *High-temperature Solid Oxide Fuel Cells: Fundamentals, Design and Applications*, Elsevier Advanced Technology, Oxford.

Steele BCH and Heinzel A (2001), 'Materials for fuel-cell technologies', *Nature*, **414**, 345–52.

Sunarso J, Baumann S, Serra JM, Meulenberg WA, Liu S, Lin YS and da Costa JCD (2008), 'Mixed ionic-electronic conducting (MIEC) ceramic-based membranes for oxygen separation', *J. Membr. Sci*., **320**, 13–41.

Suzuki T, Funahashi Y, Yamaguchi T, Fujishiro Y and Awano M (2009), 'Effect of anode microstructure on the performance of micro tubular SOFCs', *Solid State Ionics*, **180**, 546–9.

Tan XY and Li K (2007), 'Oxygen production using dense ceramic hollow fiber membrane modules with different operating modes', *AIChE J*., **53**, 838–45.

Tan XY, Liu SM and Li K (2001), 'Preparation and characterization of inorganic hollow fiber membranes', *J. Membr. Sci*., **188**, 87–95.

Tan XY, Liu YT and Li K (2005), 'Mixed conducting ceramic hollow-fiber membranes for air separation', *AIChE J*., **51**, 1991–2000.

Tan XY, Pang ZB and Li K (2008), 'Oxygen production using $La_{0.6}Sr_{0.4}Co_{0.2}Fe_{0.8}O_3$-alpha (LSCF) perovskite hollow fibre membrane modules', *J. Membr. Sci*., **310**, 550–6.

Thursfield A and Metcalfe IS (2004), 'The use of dense mixed ionic and electronic conducting membranes for chemical production', *J. Mater. Chem*., **14**, 2475–85.

Wei CC and Li K (2008), 'Yttria-stabilized zirconia (YSZ)-based hollow fiber solid oxide fuel cells', *Ind. Eng. Chem. Res*., **47**, 1506–12.

Weil KS, Coyle CA, Hardy JS, Kim JY and Xia G-G (2004), 'Alternative planar SOFC sealing concepts', *Fuel Cells Bulletin*, 11–16.

Yang NT, Tan XY and Ma ZF (2008), 'A phase inversion/sintering process to fabricate nickel/yttria-stabilized zirconia hollow fibers as the anode support for micro-tubular solid oxide fuel cells', *J. Power Sources*, **183**, 14–19.

Yin X, Hong L and Liu ZL (2007), 'Asymmetric tubular oxygen-permeable ceramic membrane reactor for partial oxidation of methane', *J. Phys. Chem. C*, **111**, 9194–202.

© Woodhead Publishing Limited, 2011

Yin X, Hong L and Liu ZL (2008), 'Integrating air separation with partial oxidation of methane – A novel configuration of asymmetric tubular ceramic membrane reactor', *J. Membr. Sci.*, **311**, 89–97.

You HX, Abuliti A, Ding XW and Zhou YH (2007), 'Reactions of low and middle concentration dry methane over Ni/YSZ anode of solid oxide fuel cell', *J. Power Sources*, **165**, 722–7.

© Woodhead Publishing Limited, 2011

17

Proton-conducting ceramic membranes for solid oxide fuel cells and hydrogen (H_2) processing

W. A. MEULENBERG, M. E. IVANOVA, Forschungszentrum Jülich GmbH, Germany, J. M. SERRA, Instituto de Tecnología Química (UPV – CSIC), Spain and S. ROITSCH, Ernst-Ruska Centre for Microscopy and Spectroscopy with Electrons, RWTH Aachen University of Forschungszentrum Jülich GmbH, Germany

Abstract: The reduction of greenhouse gas emissions such as CO_2 is a major subject of current socioeconomic, environmental and political discussion. Of a special interest is electricity production using alternative energy sources, as well as reduction in the CO_2 levels emitted by existing electricity generation power plants fuelled by coal or gas. This goal can be achieved by developing innovative technologies that make use of ceramic membranes. Proton-conducting ceramic membranes are relevant for a variety of energy-related applications and hence it is necessary to develop materials with improved functional properties and durability. The present chapter will review the fundamentals and relevant application-oriented properties of different proton-conducting ceramic materials for membrane manufacturing for a variety of applications.

Key words: ceramic membranes, hydrogen flux, hydrogen separation, proton-conducting ceramic materials, protonic conductivity.

17.1 Introduction

A reduction in CO_2 emissions from power plants fired by coal or gas is a major subject in current socioeconomic, environmental and political discussion on reducing greenhouse gas emissions such as CO_2. This goal can be achieved by introducing gas separation techniques making use of membrane technology that has significantly lower efficiency losses compared to conventional separation techniques.

Depending on the kind of power plant process, different membrane types (ceramic, polymer, metal) can be implemented to accomplish specific separation tasks. CO_2/N_2 separation is the main target in the post-combustion process. Air separation (O_2/N_2) is the focus of the oxyfuel process. In the pre-combustion process, an additional H_2/CO_2 separation is included. All

© Woodhead Publishing Limited, 2011

separation concepts imply different process requirements but what they have in common is the need for a membrane with high permeability, selectivity and stability.

In addition to separation tasks, ceramic membranes are also used as the solid dense electrolyte in proton-conducting solid oxide fuel cells (PC-SOFCs). PC-SOFCs represent an alternative technology for clean electricity production that offers benefits in terms of fuel utilization, overall efficiency and system simplicity with reformed fossil fuels as well as hydrogen from renewables. A PC-SOFC electrolyte needs to exhibit high protonic conductivity with a very low electronic contribution while the dense ceramic material of a H_2-separating membrane has to be a mixed protonic-electronic conductor.

This chapter will give an overview of proton-conducting ceramic materials for membrane manufacturing comprising material diversity and relevant properties in terms of application.

17.2 Operation principle of proton-conducting ceramic membranes and demands on materials

17.2.1 Membrane as a solid electrolyte in a proton-conducting solid oxide fuel cell (PC-SOFC)

Proton-conducting fuel cells differ from traditional solid oxide fuels in that the electrolyte membrane transports protons instead of oxygen ions. These fuel cells can operate at lower temperatures owing to the higher mobility of protons in comparison to oxygen ions while proton conductivity decreases at high temperatures (above 800°C) owing to the lower proton (water) solubility in the oxide, that is a lower concentration of proton charge carriers. The high proton conductivity at intermediate temperatures helps to alleviate problems caused by the high operating temperatures of traditional solid oxide fuel cells.

Starting with the anode side of the cell, hydrogen is oxidized to protons and is then conducted through the electrolyte until it finally combines with oxygen to produce water at the cathode. The electrons from the anode partial reaction are routed through an external circuit and thus electricity is produced and the circuit is closed by returning the electrons to the cathode. The protons must move through the electrolyte, therefore, a membrane material with dominant protonic conductivity at elevated temperatures and in a wide range of p_{O_2} is required as the PC-SOFC electrolyte (minor electronic conductivity contributions are tolerable). High redox stability accompanied by a high mechanical and thermal stability is also required in terms of durability and optimal operation.

© Woodhead Publishing Limited, 2011

17.2.2 Membrane for hydrogen (H_2) separation

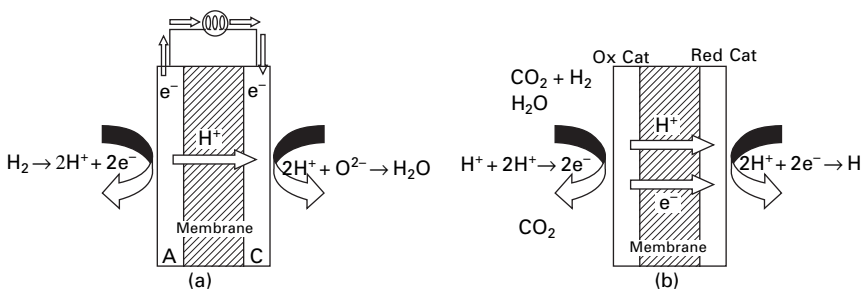
Dense ceramic membranes for H_2 separation can be implemented in the pre-combustion CO_2 capture concept, offering an efficient way to produce high-purity hydrogen for a variety of applications, along with CO_2 sequestration, which can be identified as a major benefit of great environmental relevance. The pre-combustion approach consists of several stages. Stage I is the partial oxidation of fossil fuel (methane, natural gas or gasified coal) with pure O_2 resulting in a synthesis gas (CO + H_2); Stage II is the water gas shift reaction (WGSR) to transform the carbon monoxide from the synthesis gas to carbon dioxide; Stage III includes CO_2/H_2 separation by means of a mixed protonic–electronic conducting (MPEC) membrane. Typical operating conditions in Stage III of a pre-combustion power plant are temperatures in the range of 400–900°C, pressures between 2 and 50 bar, as well as an environment containing CO_2, H_2, H_2S (about 5–200 ppm) and H_2O. Hence, a membrane material is required with mixed protonic–electronic conductivity and pronounced chemical stability under reducing and hydrothermal conditions.

The operation principles of a PC-SOFC and a membrane for H_2 separation are presented schematically in Fig. 17.1(a) and (b) respectively.

17.2.3 Membrane for steam electrolysis

Hydrogen can be produced industrially from the electrolysis of water but at a high energy cost. High-temperature electrolysis offers higher power efficiency and hence significant cost savings over conventional low-temperature electrolysers. There have been relatively few investigations of ceramic electrolysers so far and most work has been done on low-temperature alkaline and proton exchange membrane (PEM) electrolysers which are considered to be state-of-the-art technology in electrolysis.

Elevated temperatures are required in order to optimize the cost effectiveness of the electrolysis cell. Hence ceramic materials are interesting candidates



17.1 Schematic illustration of the operating principle of (a) PC-SOFC and (b) H_2-separating membranes.

© Woodhead Publishing Limited, 2011

for high-temperature cells operating at high to intermediate temperatures. The following reactions take place in an electrolysis cell. At the anode water is split according to:

$$H_2O = 2H^+ + \frac{1}{2} O_2 + 2e^-$$

while at the cathode, reduction of hydrogen takes place:

$$2e^- + 2H^+ = H_2$$

with an overall reaction:

$$H_2O = H_2 + \frac{1}{2} O_2$$

In order to be used as a solid membrane in an electrolysis cell, ceramic materials need to exhibit predominantly protonic conductivity.

17.2.4 Membrane as a H_2 sensor

High-temperature proton conductors find several applications as gas sensors. They can be applied principally for the quantification of H_2 (and CO) and humidity while gas sensing can be performed not only in hot gas streams but also in molten salts or metals. The advantages of the high-temperature proton conducting oxide sensors entail sensitivity, accuracy, a wide H_2 concentration detection range, robust construction and possible miniaturization. Typically, in pure proton conductors, the EMF voltage depends on the hydrogen concentration gradient across the electrolyte, while the electrolyte conductivity varies as a function of the water concentration in the electrolyte gas environment (Wang and Virkar, 2004), since the hydration degree determines the concentration of charge carriers. These two phenomena, together with the kinetic effects of surface reactions when the electrolyte surface is covered with specific sensing electrode materials (electrocatalysts), allow the development of sensors for H_2, CO (Yamazoe and Miura, 1988) and water for very particular applications. Several proton conducting materials hava been tested in a variety of H_2 sensors, for example Yb-doped $SrCeO_{3-\delta}$ (Kosacki and Arderson, 1998), Gd-doped $BaCe_{3-\delta}$ (Bonanos *et al.*, 1991), $BaZr_{0.4}Ce_{0.4}In_{0.2}O_{3-\delta}$ (Du and Nowick, 1996) and $KCa_2Nb_3O_{10}$ (Sakthivel and Weppner, 2007). Most of these electrolyte materials were used as potentiometric sensors (monitoring the EMF response) albeit depending on the application and sensor arrangement, they can be used as conductimetric or amperometric sensors. Further details of sensor configuration, performance and sensing electrodes can be found in Korotcenkow *et al.* (2009). Probably, the most important application of high-temperature solid electrolyte H_2 sensors is the quantification of hydrogen in molten metals, for example aluminium or copper, in the metallurgical industry (Fukatsu and Kurita, 2005). Specifically, high-quality aluminium alloy manufacture requires strict control of the solved

© Woodhead Publishing Limited, 2011

hydrogen in the molten metal during the casting process. The best sensor for this application makes uses of a galvanic cell (Yajoma *et al.*, 1993) based on Pt || $CaZr_{0.9}In_{0.1}O_{3-\delta}$ || Pt and allows precise measurement of the hydrogen concentration in the temperature range 700–800°C.

In summary, the applications considered above define specific demands on the candidate ceramic proton-conducting materials, for example in terms of material transport properties, stability under relevant operating conditions, and so on. In terms of their electrical properties, materials with dominant pure proton conductivity are mainly suitable for application as dense solid electrolytes for PC-SOFC, while materials with mixed proton–electronic conductivity are applicable as H_2-separating membranes. Along with the required pure protonic or mixed proton–electronic conductivity, candidate materials for these applications need to exhibit a high chemical, thermal and mechanical stability under a variety of operating conditions (e.g. redox when material is applied as an electrolyte in PC-SOFC or reducing when operating as a H_2-separating membrane). These strict requirements greatly limit the range of candidate materials that can operate efficiently under the relevant conditions, maintaining their functionality and durability in the long term without significant performance degradation.

17.3 Protons and proton conductance in ceramics

17.3.1 Formation of proton defects in oxide ceramics and defect equilibrium

In atmospheres containing water (water vapour) or hydrogen, protons are dissolved in the oxide lattice thus forming positively charged defects according to the following quasi-chemical reaction written in Kröger–Vink notation:

$$H_2O_{(v)} + V_O^{\bullet\bullet} + O_O^X \Leftrightarrow 2OH_O^{\bullet} \qquad [17.1]$$

$$K_{OH\bullet} = \frac{[OH_O^{\bullet}]^2}{([V_O^{\bullet\bullet}]\,[O_O^X]p_{H_2O})} \qquad [17.2]$$

where $V_O^{\bullet\bullet}$ is an oxygen vacancy with an effective charge (2+), O_O^X is an oxygen atom on its ordinary place (subscript O) in the crystal lattice with a neutral charge (expressed by superscript X), $OH_O^{\bullet}$ is a proton defect effectively charged (1+), e′ is an electron with charge (1–), $K_{OH\bullet}$ is the equilibrium constant of proton defect formation reaction, $[OH_O^{\bullet}]$ is the concentration of the proton defect, $[V_O^{\bullet\bullet}]$ is the concentration of the oxygen vacancy, $[O_O^X]$ is the concentration of oxygen atoms on their ordinary place in the crystal lattice and p_{H_2O} is the partial pressure of water vapour.

According to Kreuer (2003), for large band gap oxide materials (e.g. Ce/Zr/Ti-based perovskites), proton defects are formed at moderate temperatures

© Woodhead Publishing Limited, 2011

through a dissociative absorption of water that requires the presence of oxygen ion vacancies (Norby, 1999). Water from the gas phase dissociates to hydroxide ion and a proton. The hydroxide ion is adsorbed by the oxygen vacancies and the proton forms a covalent bond with the lattice oxygen. Thus two positive proton defects, $OH_O^{\bullet}$, are generated.

17.3.2 Stability of proton defects in oxide ceramics

The formation of proton defects is accompanied by a significant weight increase (often determined via thermogravimetry). The concentration of proton defects changes with temperature and water partial pressure thus giving information about the thermodynamic stability of proton defects. The equilibrium of the hydration reaction Equation [17.1] shifts to the left with increasing temperatures since the reaction is exothermic: the more negative the hydration enthalpy, the higher the proton content and the dehydration temperature. Several factors strongly affect the stability and mobility of proton defects, for example crystal symmetry, chemical nature (acid–base sites), electronegativities of cations that interact with the lattice oxygen and repulsive forces between the proton and its surroundings (Kreuer, 1996, 1997, 1999, 2000, 2003, 2004; Ricote *et al.*, 2009).

17.3.3 Proton diffusion mechanisms

When a hydrogen atom is absorbed into a structure it usually loses its electron and turns into a proton. The charge densities of protons are too large to exist as separate entities in the structure and they tend to associate with electronegative atoms, such as oxygen ions, in the parent structure.

Proton diffusion mainly occurs by two mechanisms: the free proton mechanism (Grotthuss mechanism) and the vehicle-facilitated mechanism (Kreuer, 1996). The Grotthuss mechanism consists of proton jumps from a stationary oxygen atom to a neighbouring oxygen atom after it has rotated to the correct position between the two oxygen atoms.

In the vehicle mechanism, protons attach to an oxygen ion and move together with this 'vehicle' (via translational diffusion). The hydroxide ions thus formed diffuse through the structure, much like ordinary oxygen ions. Hydroxide ions may possibly have a lower activation energy of diffusion than oxygen ions owing to their smaller size. Hydroxide ions can diffuse through the structure using vacancy diffusion or interstitial diffusion. The electroneutrality balance is maintained by the counterdiffusion of unprotonated vehicles or most probably by oxygen vacancies.

According to Kreuer, for structural reasons, the Grotthuss-type mechanism is more likely to be found in oxides than the migration of hydroxyl ions. For perovskite structures it is considered that the proton transfer between

© Woodhead Publishing Limited, 2011

two neighbouring lattice oxygens is the rate-limiting step. With increasing temperature a gradual transition from the Grotthuss to the vehicle type of mechanism (translational diffusion) can be expected owing to elongation and breaking of the hydrogen bonds that may suppress proton transfer and release the translational degree of freedom.

17.3.4 Proton mobility, proton conductivity and H_2 flux

The mobility and conductivity of proton defects is given according to Equations [17.3] and [17.4]:

$$\mu_{H^+} = \mu_0 T^{-1} \exp\left(-\frac{\Delta H_{mob}}{kT}\right) \quad [17.3]$$

$$\sigma_{H^+} = zFc_{H^+}\mu_{H^+} = \frac{z^2 F c_{H^+} D_{H^+}}{kT} \quad [17.4]$$

where

$$D = \frac{\mu kT}{z} \text{ (acc. to Einstein–Smoluchowski)} \quad [17.5]$$

and μ_{H^+} is the mobility of protons, T is the temperature in K, ΔH_{mob} is the enthalpy of mobility, k is the Boltzmann constant, σ_{H^+} is the proton conductivity, z is the electrical charge, F is the Faraday constant, c_{H^+} is the concentration of protons and D_{H^+} is the proton diffusion coefficient.

The mobility of proton defects and proton conductivity has an Arrhenius-type temperature dependence, meaning that they depend exponentially on the temperature. Proton concentration is also dependent on the temperature in terms of its thermodynamic stability when the protons are incorporated into the crystal lattice (as discussed above). The total activation energy ΔE_{act} for proton conduction consists of energetic terms required mainly for proton defect formation and proton migration.

The Wagner theory defines the H_2 flux through a dense ceramic material according to:

$$j_{H^+} = \frac{-RT}{2F^2 L} \int_I^{II} \sigma_{H^+} t_e \mathrm{d} \ln p_{H_2} \quad [17.6]$$

where j_{H^+} is the hydrogen flux, R is the universal gas constant, L is the membrane thickness, t_e is the transport number of electrons and p_{H_2} is the partial pressure of hydrogen.

17.3.5 Defect generation by aliovalent doping

In the case of dense ceramic ionic conductors operating at elevated temperatures, lattice diffusion of point defects (vacancies, interstitial defects, protons) is

© Woodhead Publishing Limited, 2011

the dominating mechanism for the transport of charge carriers through the crystal lattice. Point defects may be formed intrinsically by varying the ratios of the basic components of the material or extrinsically by acceptor doping. In this sense, doping plays a crucial role in creating defects in the primary crystal structure. Hence, doping is a very frequently used strategy to modify and control the properties of the material by (i) distorting the crystal lattice (geometrical factor, e.g. ionic radius), (ii) influencing the chemical properties by introducing elements with a different chemical nature (electronegativity, chemical properties), or/and (iii) modifying the electrical properties by controlling the concentration and the type of electro-balancing charge carriers that are formed within the structure as a result of the doping.

In a very common case when the acceptor doping route is followed, positively charged species are generated to maintain the electroneutrality of the lattice. Positively charged species are electron holes ($h^{\bullet}$), oxygen vacancies ($V_O^{\bullet\bullet}$) and proton defects ($OH_O^{\bullet}$). In accordance with the mass action law, under definite conditions (p_{O_2}, p_{H_2O}, and T) the existing defects are in dynamic equilibrium. For each set of equilibrium conditions, there are values of po_2, p_{H_2O} and T that determine the domination of a definite pair of defects (represented by Brouwer diagrams). Under dry oxidizing conditions, oxygen is built up in the crystal lattice, so that the concentration of the oxygen vacancies diminishes simultaneously with the generation of electron holes which are needed to neutralize the negative charge generated by the aliovalent doping element.

$$\frac{1}{2}\,O_{2(gas)} + V_O^{\bullet\bullet} \rightarrow O_O^X + 2h^{\bullet} \qquad [17.7]$$

$$K_h = \frac{[O_O^X][h^{\bullet}]^2}{[V_O^{\bullet\bullet}]p_{O_2}^{1/2}} \qquad [17.8]$$

where $h^{\bullet}$ is the electron hole with charge (1+), K_h is the equilibrium constant of electron hole formation, $[h^{\bullet}]$ is the concentration of electron holes and p_{O_2} is the partial pressure of oxygen.

Under dry reducing conditions, the crystal lattice starts losing oxygen, so that oxygen vacancies are formed together with the generation of electrons:

$$O_O^X \rightarrow V_O^{\bullet\bullet} + 2e' + \frac{1}{2}\,O_2 \qquad [17.9]$$

$$K_e = \frac{[V_O^{\bullet\bullet}][e']^2 p_{O_2}^{1/2}}{[O_O^X]} \qquad [17.10]$$

where K_e is the equilibrium constant of electron formation and $[e']$ is the concentration of electrons.

In water- and hydrogen-containing environments proton defects in the

© Woodhead Publishing Limited, 2011

oxide contribute considerably to the conductivity and have to be taken into account with respect to defect chemistry and defect equilibrium.

In order to obtain considerable electron conduction levels within the material, a host lattice element is replaced by a doping element *M* with a variable oxidation state. As an example, the following quasi-chemical reactions describe the defect formation under oxidizing [17.11] and reducing [17.12] conditions, respectively:

$$M_2O_3 - 2e' = MO_2 - 2h^{\bullet};\ MO_2 \xrightarrow{AO_2} 2M_M^X + 2h^{\bullet}\ (OX) \qquad [17.11]$$

$$MO_2 + 2e' = M_2O_3 + 2h^{\bullet};\ M_2O_3 \xrightarrow{AO_2} 2M'_M + 3O_0^8 + V_O^{\bullet\bullet} + 2e'\ (red) \qquad [17.12]$$

where M_2O_3 is the oxide compound of doping element M where M has a charge (3+), MO_2 is the oxide compound of doping element M where M has a charge (4+) and AO_2 is the host oxide lattice formed by host lattice element A and oxygen.

And finally, independently of the kind of the doping scheme used, when thermodynamic and chemical equilibrium are maintained, the equality of all positive and negative species generated within the crystal lattice is also maintained.

17.4 Conductivity and hydrogen (H_2) flux of selected classes of ceramic membrane materials

17.4.1 Perovskites

Proton conductivity in the perovskite type of oxide ceramics was first discovered by Iwahara *et al.* (1981) in the early 1980s. The most extensively studied high-temperature proton-conducting ceramic materials with a perovskite structure are $SrCeO_3$, $BaCeO_3$, $SrZrO_3$, as well as complex perovskites of types $A_2B'B''O_6$ and $A_3B'B''O_9$. Materials with a perovskite structure having a general formula $A^{2+}B^{4+}O_3$ (type II–IV), where when A is Ba and B is Ce, Zr, Tb or Th they exhibit the best proton conductivities of above 10^{-2} S cm^{-1} (Davies *et al.*, 1999; Fontaine *et al.*, 2008; Iwahara, *et al.*, 1981, 1993; Kreuer, 1996, 1999, 2003; Kreuer *et al.*, 2001; Krug *et al.*, 1995; Meulenberg *et al.*, 2010; Norby, 2009; Schober *et al.*, 1995; Schober and Bohn, 2000; Stotz and Wagner, 1966; Yamanaka *et al.*, 2005). They have large negative hydration enthalpies and the lowest activation energies for proton conduction. As summarized by Norby (2009), when the A-site is occupied by Sr instead of Ba, the conductivity drops to between 10^{-2} and 10^{-3} S cm^{-1} ($SrZrO_3$, $SrCeO_3$). Calcium-based perovskites are also proton conductors, especially $CaZrO_3$. Within perovskite type I-V ($A^{1+}B^{5+}O_3$) there

© Woodhead Publishing Limited, 2011

are some examples such as $KTaO_3$ for which a very low conductivity was reported (Lee *et al.*, 1986).

Cerates and zirconates have been extensively studied for hydrogen separation membranes. Selected examples of doped cerates and zirconates are summarized in Table 17.1. The H_2 flux data published in the literature about cerates point to Yb-doped $SrCeO_3$ as the best state-of-the-art perovskite-based material for H_2 separation applications. However, there are several disadvantages that limit the application range of these materials. Briefly, chemical stability under reducing atmospheres especially concerns the cerates. Because of their basicity they react easily with CO_2 and $H_2S/SO_2/SO_3$ at moderate and with H_2O at low temperatures and form alkaline earth carbonates, sulphates and hydroxides, respectively (Scholten *et al.*, 1993; Shirsat *et al.*, 2004). Consequently, their mechanical properties become poor owing to formation of reaction products at the grain boundaries.

Zirconate-based materials were found to be attractive for membrane applications mainly because of their higher stability of zirconates under reducing atmospheres, in particular in CO_2 environments. However, existing experimental data about the hydrogen flux through zirconate-based membranes are rather limited in comparison to the data available for the cerate class of membranes. Despite their better stability in reducing environments, zirconates exhibit high grain boundary resistance that negatively influences their electrical performance. Furthermore, manufacturing of membranes with high gas tightness requires extremely high sintering temperatures (e.g. ~ 1700°C or even higher for zirconates). In an attempt to lower grain boundary resistance and sintering temperatures, much work has been done in recent years. Examining the influence of different dopants (Naoki *et al.*, 2008; Tao and Irvine, 2007) or manufacturing routes (Duval *et al.*, 2007; Gibson *et al.*, 2009; Guillaume *et al.*, 2005; Meulenberg *et al.*, 2006; Serra and Meulenberg, 2007; Serra *et al.*, 2007) does not lead to a significant improvement in the electrical properties but in some cases results in better sinterability of the investigated zirconates.

17.4.2 Rare earth oxides

Norby and Kofstad found that Y_2O_3 conducts protons although the conductivity values are low (Norby and Kofstad, 1984, 1986). Furthermore, proton conduction in numerous undoped and doped rare earth oxides of type Ln_2O_3 and $LnBO_3$ (Ln is lanthanide element) have been investigated and it was found that they also exhibit proton conduction at elevated temperatures (Larring and Norby, 1995; Norby, 1990; Norby *et al.*, 1992; Norby and Larring, 1997). An extensive study of the equilibrium between water vapour, protons and oxygen vacancies in rare earth oxides Nd_2O_3 and Sm_2O_3 doped on the A-site with 1 and 2 mol% Ca was conducted by Larring and

© Woodhead Publishing Limited, 2011

Table 17.1 Selected literature examples of ceramic membrane materials for H_2 separation

Material	Membrane thickness (mm)	H_2 flux (ml cm^{-2} min^{-1})	T (°C)	Additional data	Reference
$SrCe_{0.95}Tm_{0.05}O_3$	0.15	0.126	900	10% H_2/He(upstream) Air (downstream)	Cheng *et al.* (2005)
$SrCe_{0.95}Tm_{0.05}O_{3-\delta}$	1.6	0.039	900	10% H_2/He (upstream) 20% O_2/N_2 (downstream) No electrodes	Qi and Lin (2000)
	3	0.028	900	10% H_2/He (upstream) 20% O_2/N_2 (downstream) No electrodes	
$SrCe_{0.95}Yb_{0.05}O_{3-\delta}$	1,6	0.023	900	1% H_2/Ar (upstream) 20% O_2/Ar (downstream) Pt catalyst (electrode)	Qi and Lin (2000) Hamakawa *et al.* (1994)
$SrCe_{0.95}Y_{0.05}O_{3-\delta}$	1.6	0.028 (extrapolated)	900	4% H_2/Ar (upstream) Ar (downstream) 2 Pt-electrodes (short-circuited)	Qi and Lin (2000) Guan *et al.* (1998)
$SrCe_{0.80}Y_{0.20}O_{3-\delta}$	1.6	0.048 (extrapolated)	900	4% H_2/N_2 (upstream) Ar (downstream) 2 Pt-electrodes (short-circuited)	Qi and Lin (2000) Balachandran *et al.* (1998)
$SrCe_{0.95}Tb_{0.05}O_3$	1 (eff. area 1.8 cm^2)	1.4×10^{-2} 1.6×10^{-2}	900 900	0.001 atm CO (downstream) 0.1 atm CO (downstream)	Wei *et al.* (2009)
$SrCe_{0.95}Y_{0.05}O_{3-\delta}$	0.05 0.62	0.102 7 times less	950	80% H_2/He (upstream) Ar (downstream)	Zhan *et al.* (2009)
$SrCe_{0.95}Yb_{0.05}O_{3-\delta}$	0.002 (layer)	13.44	677	H_2 (upstream) N_2/O_2 and He (downstream)	Hamakawa *et al.* (2002)
$SrCe_{0.95}Eu_{0.05}O_3$	1.72	3.085×10^{-3}	850	Dry H_2 Wet H_2 (p_{H_2O} = 0.028 atm)	Song *et al.* (2005)
		3.018×10^{-3}	850	Wet H_2 (p_{H_2O} = 0.051 atm)	
		2.683×10^{-3}	850	Wet H_2 (p_{H_2O} = 0.086 atm)	
		2.548×10^{-3}	850	He (downstream)	

Continued overleaf

© Woodhead Publishing Limited, 2011

Table 17.1 Continued

Material	Membrane thickness (mm)	H_2 flux (ml cm^{-2} min^{-1})	T (°C)	Additional data	Reference
$SrCe_{0.95}Sm_{0.05}O_3$	1.72 (thickness) and 24 (in diameter)	3.125×10^{-3}	850	Dry H_2	Song *et al.* (2004)
		1.623×10^{-3}	850	Wet H_2 (p_{H_2O} = 0.028 atm) He (downstream)	
$BaCe_{0.8}Y_{0.1}Ru_{0.1}O_3$	0.5	8.68×10^{-2}	800	H_2/Ar (upstream) Ar (downstream)	Matsumoto *et al.* (2005)
$BaCe_{0.95}Nd_{0.05}O_3$	0.7	2.6×10^{-2}	925	15% H_2 (upstream) Ar +Ne (downstream)	Cai *et al.* (2009)
Nd_6WO_{12}	0.51	2.3×10^{-2}	1000	Wet 20% H_2/He (upstream) Ar (downstream)	Escolástico *et al.* (2009)

© Woodhead Publishing Limited, 2011

Norby,1997). It was found that these rare earth oxides are mixed proton, ion and p-type electron conductors depending on the conditions. They are nearly pure proton conductors at moderate temperatures and under wet conditions.

17.4.3 Phosphates

The phosphates (e.g. zirconium phosphates and uranylphosphates) have been widely studied as proton conductors at moderate temperatures. Proton conductivity at higher temperatures was found relatively recently in materials that have no structural protons such as Li_3PO_4, other alkali phosphates (Mellander and Zhu, 1993) and β-$Ca(PO_3)_2$ (Greenblatt *et al.*, 1990). $LaPO_4$ was suggested as an interesting candidate owing to its stability and ability to dissolve and transport protons. Ca- and Sr-substituted $LnPO_4$ ortho-phosphates, where Ln is La, Nd, and Gd were studied by Norby and Christiansen (1995). The conductivity of Ca- and Sr-substituted $LaPO_4$ was found to be mainly of the proton type except at the highest temperatures and driest conditions, where the native conductivity dominates.

17.4.4 Pyrochlores

Pyrochlore-structured $La_2Zr_2O_7$ was reported to show proton conductivity which was not found in the isostructural Ti-containing oxide (Labrincha *et al.*, 1997). Shimura *et al.* (1996) found that $Y_2Ti_{1.8}M_{0.2}O_{7-\delta}$ with M = In on Mg did not show measurable proton transport. The conductivity of undoped $La_2Ti_2O_7$ was previously measured at relatively high temperatures (800–1000°C) and with no special emphasis on possible effects of protons and proton transport (Balachandran and Eror, 1982). Haugsrud and Norby (2005) studied 2% Ca-doped $La_2Ti_2O_7$ and proton conductivity was determined to be $\sim 5 \times 10^{-5}$ S cm^{-1} at 800°C. The hydrogen flux across Ca-doped $La_2Ti_2O_7$ film with a thickness of 10 μm was estimated on the basis of measurement of partial conductivities. It was estimated that such a membrane would yield a hydrogen flux in the order of 0.1 ml_N cm^{-2} min^{-1} at 750°C, where subscript N stands for normalized flux, this value being lower by a factor of ~5 compared to that of 5% Yb-doped $SrCeO_3$ under the same conditions. However, the protonic conductivity of rare earth oxides, phosphates and pyrochlores is far too low for these materials to be implemented and efficiently operated in the envisaged applications.

Dense H_2-conducting ceramic materials achieve much lower values of H_2 flux compared to dense metallic membranes (based on Pd alloys) and microporous silica membranes, which display much better performance. However, these membranes face serious degradation problems when integrated in processes of coal gasification and/or steam reforming. Moreover,

© Woodhead Publishing Limited, 2011

these two material classes (dense metallic and ceramic microporous materials) are not the subject of this paper and they will not be considered here.

17.4.5 Rare earth ortho-niobates and tantalates

Rare earth ortho-niobates ($LnNbO_4$) and tantalates ($LnTaO_4$) are materials with a fergusonite structure (monoclinic symmetry) that changes to a scheelite structure (tetragonal symmetry). The temperature of phase transition is different for these two classes (see Section 17.5.3). Proton conductivity was found in several acceptor-doped rare earth ortho-niobates and ortho-tantalates ($LnNbO_4$ and $LnTaO_4$) at elevated temperatures and in a humid atmosphere (Haugsrud and Norby, 2006). Tantalates exhibit a proton conductivity approximately one order of magnitude lower than that of niobates (Norby and Haugsrud, 2007). The total conductivity of undoped $LaNbO_4$ was found to be about $4–5 \times 10^{-5}$ S cm^{-1} at 1000°C (Mokkelbost *et al.*, 2008) compared to the A-site-doped (Haugsrud and Norby, 2006; Mokkelbost *et al.*, 2008) material $La_{0.99}Ca_{0.01}NbO_4$, which exhibits conductivity of less than 2×10^{-3} S cm^{-1} in a wet O_2 atmosphere and conductivity of about 7×10^{-4} S cm^{-1} in a wet H_2 environment, both at 1000°C. At 800°C the total conductivity of $La_{0.99}Ca_{0.01}NbO_4$ in wet O_2 is ~$7.5–8 \times 10^{-4}$ S·cm^{-1} and less than 6×10^{-4} S cm^{-1} in wet H_2 (Haugsrud and Norby, 2006), while the conductivity of undoped $LaNbO_4$ at the same temperature is ~8×10^{-6} S × cm^{-1}.

A variety of studies on rare earth ortho-tantalates with a general formula $LnTaO_4$ have shown that these materials exhibit proton conductivity at lower temperatures, but this conductivity is generally an order of magnitude lower than that of niobates (Norby and Haugsrud, 2007). At 1000°C $La_{0.99}Ca_{0.01}TaO_4$, for example, exhibits a total conductivity of about 4×10^{-4} S cm^{-1} and a protonic conductivity of ~2×10^{-4} S cm^{-1}. At the same temperature, the values of the total and protonic conductivities for $Nd_{0.99}Ca_{0.01}TaO_4$ are σ_{tot} ~2×10^{-4} S cm^{-1} and $\sigma_H < 2 \times 10^{-4}$ S cm^{-1}; for $Gd_{0.99}Ca_{0.01}TaO_4$ are $\sigma_{tot} \sim 8 \times 10^{-5}$ S cm^{-1} and $\sigma_H < 5 \times 10^{-5}$ S cm^{-1}, and for $Er_{0.99}Ca_{0.01}TaO_4$ are $\sigma_{tot} \sim \sigma_H = 4 \times 10^{-5}$ S cm^{-1}, respectively. With decreasing ionic radius in the row La→Nd→Gd→Er, the activation energy for proton conduction increases and the same tendency is true both for ortho-niobates and ortho-tantalates.

17.4.6 Rare earth tungstates

Rare earth tungstates (Ln_6WO_{12}) are materials with a defective fluorite structure, although the crystal symmetry is not completely clarified. A correlation was found between the type of the lanthanide element and the crystal lattice symmetry that shows a tendency toward reducing the crystal symmetry from cubic through tetragonal and finally to rhombohedral when Ln changes in the order La→Nd→Er.

© Woodhead Publishing Limited, 2011

Shimura *et al*. (2001) studied $La_{5.8}WO_{11.7}$ in electrochemical hydrogen pumping experiments and proton conduction for this material was demonstrated. The proton transport number was determined to be between 0.7 and 0.9 in a H_2-containing atmosphere. A proton conductivity of 5×10^{-3} S cm^{-1} was measured in wet H_2 at 900°C. Haugsrud (Haugsrud, 2007) studied defects and transport properties in Ln_6WO_{12} where Ln is La, Nd, Gd and Er. A general feature of these materials is that they exhibit protonic conductivity in wet atmospheres, below ~900°C. Under oxidizing and reducing conditions and at elevated temperatures, Ln_6WO_{12} becomes predominantly an electronic semiconductor. Maximal conductivity was observed for undoped La_6WO_{12} compared to La_6WO_{12} doped with 0.05 mol% Ca on the A-site.

In several publications, the feasibility of tungstates as membranes for H_2 separation was studied by flux measurements or estimated theoretically (Escolástico *et al*., 2009; Haugsrud and Kjølseth, 2008; Norby and Haugsrud, 2007; Shimura *et al*., 2001). Haugsrud and Kjølselh (2008) compared the ambipolar conductivity of undoped La_6WO_{12} to that of 5%-Yb-doped $SrCeO_3$ (state-of-the-art material) and came to the conclusion that the undoped La_6WO_{12} is a good candidate for membrane applications. A permeability data prediction was communicated by Norby *et al*. (Norby and Haugsrud, 2007) for La_6WO_{12}, $SrCeO_3$ and Er_6WO_{12}. The flux was calculated for 10-μm-thick layers with a feedside pressure of 10 atm H_2 and assuming that the flux was ruled by the Wagner equation, that is via a bulk diffusion mechanism. The predicted hydrogen permeation for La_6WO_{12} at 800°C has a value of about 2.0 ml_N cm^{-2} min^{-1}, which is higher compared to $SrCeO_3$ and Er_6WO_{12} yielding a hydrogen flux at the same temperature of about 1.0 ml_n cm^{-2} min^{-1} and less than 0.1 ml_n cm^{-2} min^{-1}, respectively.

Table 17.1 presents a summary of selected examples of ceramic materials developed and tested or theoretically evaluated for H_2-separating membrane applications.

17.5 Structure of selected classes of proton-conducting materials

Proton conductivity can be observed for a variety of materials. The most common crystal structures of proton-conducting materials are described in this section.

17.5.1 Perovskites

The cubic perovskite structure is observed in many compounds featuring a composition ABX_3, whereby A and B are cations with different oxidation numbers and X is an anion. The A-cation occupies the centre of the unit cell, while the B cation and the X anions are arranged at the corners and the edges

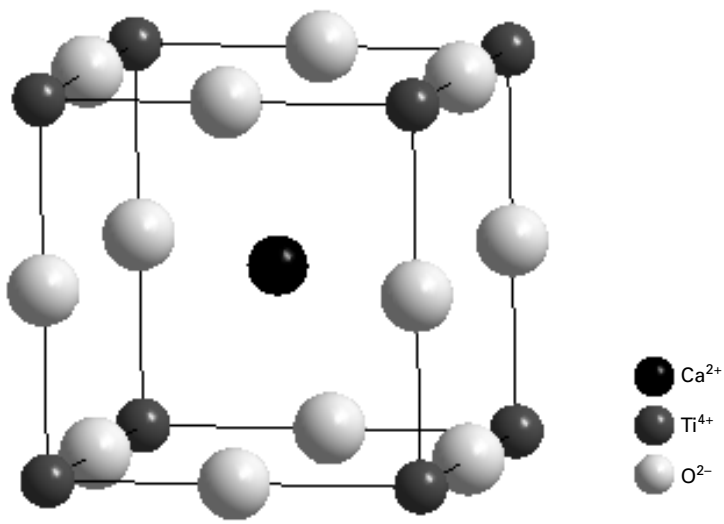
© Woodhead Publishing Limited, 2011

of the unit cell, respectively. Figure 17.2 shows the unit cell of $CaTiO_3$ as an example of the perovskite structure. Owing to steric constraints, caused by different combinations of ion radii, the unit cell of most perovskites is slightly distorted. A perfect cubic unit cell is only present within $SrTiO_3$.

Proton-conducting compounds with a perovskite structure are, for example, the acceptor-doped lanthanum rare earths $LaErO_3$ (Larring and Norby, 1994) and $LaScO_3$ (Fujii *et al.*, 1998). In so-called complex perovskites, significant non-stoichiometries are used in order to enhance the proton conductivity. A prominent example with a high cation non-stoichiometry is $Ba_3Ca_{1.18}Nb_{1.82}O_{8.73}$ (BCN18) (Norby, 1999). Hydration of proton-conducting perovskites with high oxygen deficiency allows for increased proton contents. $Ba_2InSnO_{5.5}$ and $Ba_2In_2O_5$, for example, may take up 0.5 protons (Schober, 1998) and one proton (Fischer *et al.*, 1999) per unit cell, respectively.

17.5.2 Pyrochlores

A number of titanates featuring the composition $A_2Ti_2O_7$ with A = Y, and the elements in the row from Sm to Yb as well as some zirconates, for example $La_2Zr_2O_7$ and $Gd_2Zr_2O_7$, crystallize in the pyrochlore structure. The classical pyrochlore composition is $(Na,Ca)_2(Nb,Ti)_2(O,F)_6(O,F)$ [= $A_2B_2X_6Y$] and is sometimes referred to in the literature as anion-deficient fluorite derivative (Jona *et al.*, 1955). Basic building components are arrays of corner-connected tetrahedra formed by the A atoms while the Y atoms



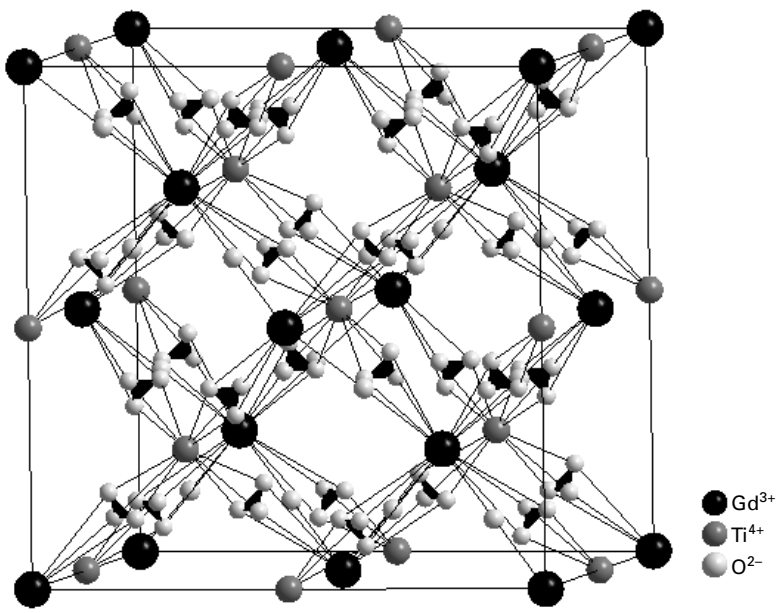
17.2 Example of a unit cell of the perovskite structure: the case of $CaTiO_3$.

© Woodhead Publishing Limited, 2011

occupy the centres of the tetrahedra. Each A atom is coordinated by six X atoms arranged in a puckered hexagon and a pair of Y atoms normal to the mean plane of the hexagon, resulting in hexagonal–bipyramid coordination (Nyman and Andersson, 1978). Figure 17.3 presents the unit cell of $Gd_2Ti_2O_7$ as an illustration of the pyrochlore structure.

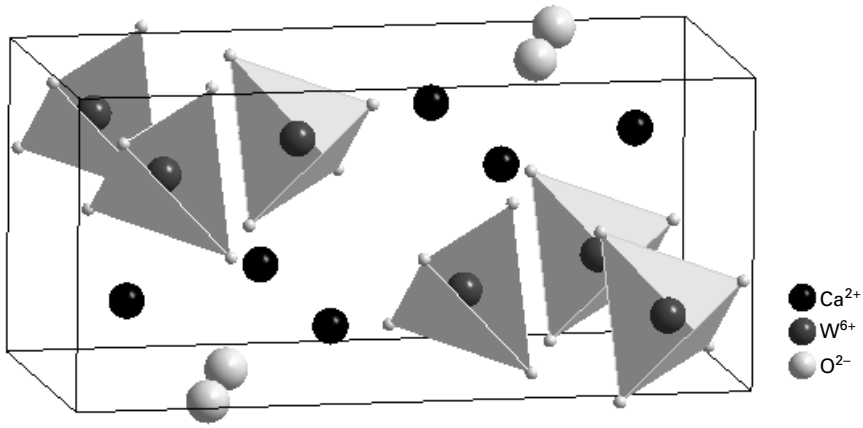
17.5.3 Niobates and tantalates

As described in Section 17.4.5, rare earth ortho-niobates ($LnNbO_4$) [= ABO_4] and rare earth ortho-tantalates ($LnTaO_4$) possess proton conductivity. In these material classes a phase transition takes place from a monoclinic crystal structure (fergusonite type) at low temperatures to a tetragonal crystal structure (scheelite type) at high temperatures. In the case of the niobates, the transition temperature ranges from about 500–800°C and increases with decreasing radii of the rare earth cations (Gingerich and Bair, 1964). The transition temperature of the tantalates is significantly higher and ranges from 1300–1450°C (Stubican, 1964). The scheelite structure can be described as two intercalated diamond lattices, one for A cations and the other for B cations. The A cations are coordinated by eight oxygen anions and the B cations are tetrahedrally coordinated by the oxygen anions. Figure 17.4 shows



17.3 Example of a unit cell of the pyrochlore structure: the case of $Gd_2Ti_2O_7$.

© Woodhead Publishing Limited, 2011



17.4 Unit cell of the mineral scheelite ($CaWO_4$).

the unit cell of the mineral scheelite ($CaWO_4$). The fergusonite structure can be considered as a distorted scheelite structure. Each A cation is surrounded by eight oxygen anions and each B cation is surrounded by four oxygen sites and two additional near oxygen sites. As reported by Errandonea *et al*. (2004), the scheelite-to-fergusonite transition can be described as a shear transformation in which the scheelite structure is partially conserved while certain sheets are slightly shifted.

17.5.4 Tungstates

Rare earth tungstates with a stoichiometry close to Ln_6WO_{12} (including Y_6WO_{12}) are interesting material candidates in terms of proton conductivity (e.g. Haugsrud, 2007). The crystal structures of most materials of this class, however, have not yet been completely solved. Detailed structure reports are only given in the case of Y_6WO_{12} and Ho_6WO_{12} (Diot *et al*., 2000). Diot *et al*. report that the rhombohedral structure of these compounds can be described by an arrangement of seven edge-sharing cubes, where the central cube is occupied by W cations.

The crystal symmetries of the lanthanide tungstates were published by McCarthy *et al*. (1972) in 1972. The crystal symmetry depends on the rare earth element and is cubic in the case of La, Ce and Pr, pseudo-tetragonal from Nd to Gd, and is rhombohedral from Tb to Lu and for Y. The structure of the rare earth tungstates is related to the fluorite structure and is therefore frequently referred to in the literature as an ordered defective fluorite structure or as a disordered pyrochlore structure (e.g. Diot *et al*., 2001). Magrasó *et al*. (2009) reported that the structure of La_6WO_{12} is closely related to the cubic fluorite structure and is characterized by an ordering of the La and

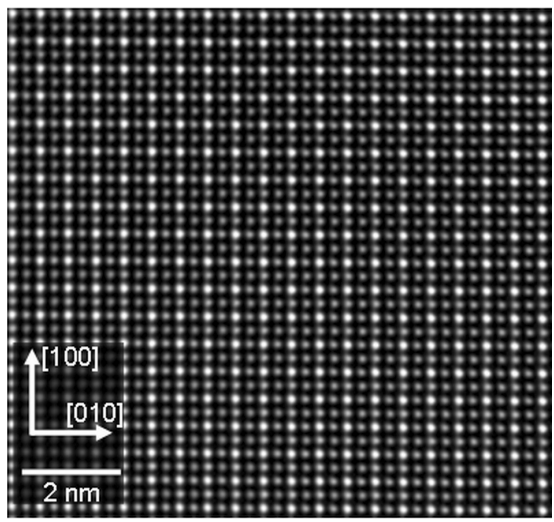
© Woodhead Publishing Limited, 2011

the W atoms, in other words a superstructure is present. This finding is also confirmed by transmission electron microscopy (TEM). Figure 17.5 shows a high-resolution TEM micrograph of La_6WO_{12} in the [001] orientation. Atom columns along this direction consisting of La atoms and W atoms appear as white spots on a dark background. Owing to the contrast-forming conditions applied, oxygen sites are not visible within this image. Because of their higher electron-scattering power, W atoms appear with higher intensity. The superstructure of the cations is clearly visible as an ordering of the brighter and darker spots.

In a contrast to the structures considered above, the phosphates and rare earth oxides are not classified by their structure but by their elements. This makes an attempt to summarize and describe the existing great variety of different structures amongst these material classes a rather difficult task even when common structural features are applied. Therefore, presenting a structural overview of these groups of materials in this general structural section of the chapter was not found to be relevant nor of benefit to the reader.

17.6 Chemical stability of selected classes of ceramic membrane materials

Perovskitic proton-conducting materials are principally based on the type $A^{II}B^{IV}O_3$. As a result, these materials contain large proportions of alkaline-earth elements, basically Sr and Ba. However, as previously mentioned, the high



17.5 High-resolution TEM micrograph of La_6WO_{12} in the [001] orientation. Atom sites appear as bright spots on a dark background.

© Woodhead Publishing Limited, 2011

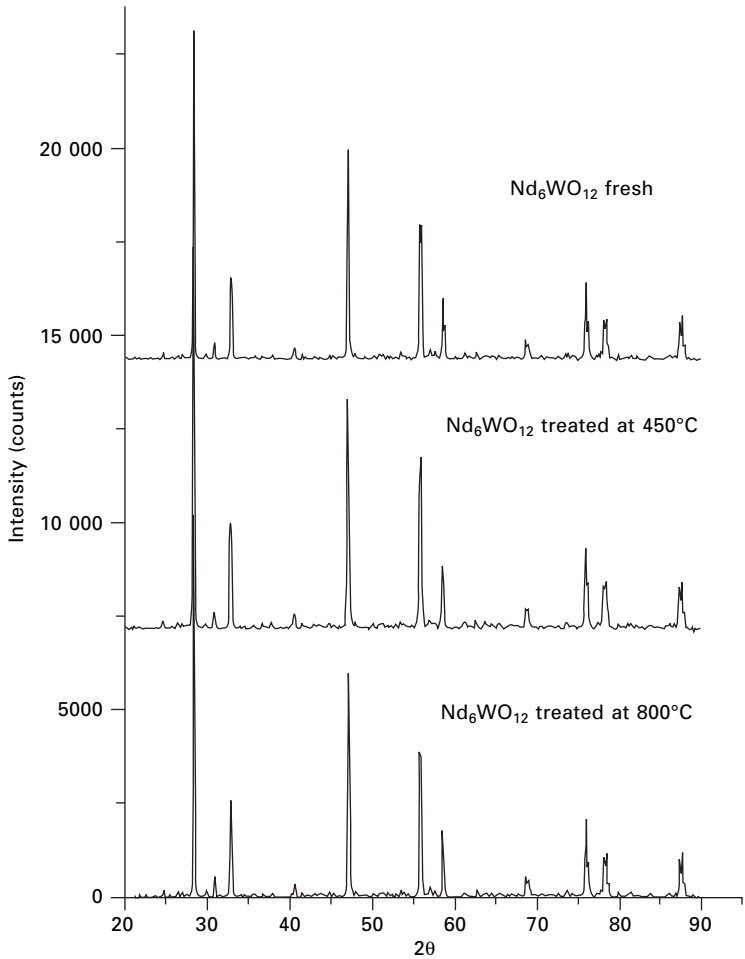
basicity of these elements results in the high stability of the corresponding Ba-Sr carbonates and sulphates (with respect to the mixed oxide compound) and, therefore, these proton conductors tend to react with acid gases (CO_2 and S-containing gases) under the envisaged operating conditions and decompose irreversibly. The stability of the perovskite compound depends on the specific lattice composition and the kind of transition metal present in the B-atom position is particularly crucial. The order for the three main metals used as B-atoms is (in decreasing order of stability): titanates, zirconates and cerates (Kreuer *et al.*, 2001). In general, it seems that there is an opposing trend between mixed oxide stability and proton conductivity, that is the higher the stability, the lower the proton conductivity. Doped $SrCeO_3$ and $BaCeO_3$ are thermodynamically stabilized slightly with regard to decomposition into the single oxides while they react rapidly with CO_2 even at low concentrations. This fact prevents their use in realistic applications entailing the conversion of hydrocarbons or syngas. Nevertheless, the choice of the acceptor dopant would allow stability to be increased and a balanced stability to be achieved between perovskite oxide and protonic defects principally caused by modification of local symmetry.

A realistic stability test was carried out using powdered membrane materials based on several doped $BaZrO_3$ and $BaCeO_3$. The test period was three days and the conditions were 800°C and 700°C (independent tests) respectively under wet CO_2-rich reducing conditions, that is CO_2+CH_4 gas (1/9 molar ratio) at atmospheric pressure (Serra and Escolástico, unpublished results). All doped zirconates remained stable during the treatment as revealed by X-ray diffraction (XRD) diffraction while all doped cerates reacted dramatically to form carbonates and CeO_2-based oxides.

Another stability test comprised the treatment of a similar set of samples under wet CO_2-rich reducing and corrosive conditions, that is in gas flow 115 ppm H_2S, 4.43% CO_2, 2.12% CO and 92.09% H_2 at 30 bar for three days under continuous flow of 50 ml min^{-1}. Again, the zirconates successfully passed the test while the cerate decomposed to form carbonates and sulphates.

Ln_6WO_{12} membrane materials are believed to possess high chemical stability to carbonation owing to the absence of highly basic cations in their structure. The most H_2 permeable material reported up to now consists uniquely of undoped La_6WO_{12}. Similar tests to those reported above confirmed the stability to carbonation and in the presence of significant amounts of H_2S, as concluded from XRD investigations. Nevertheless, a long-term stability test is needed to assess the applicability of these materials. Moreover, at high temperatures, Ln_6WO_{12} shows high reactivity with other ceramic compounds such as YSZ, CeO_2 and NiO. Figure 17.6 illustrates the high stability of Ln_6WO_{12} (where Ln is Nd) in a wet H_2 atmosphere at elevated temperatures. A similar situation was observed for the compounds $LaNbO_4$ and $LaTaO_4$, which remained stable after treatment in CO_2. However, it was observed

© Woodhead Publishing Limited, 2011



17.6 XRD patterns corresponding to Nd_6WO_{12} powdered samples before and after treatment in wet hydrogen for one week.

that some specific multidoped $LaNbO_4$ compounds decomposed under wet CO_2-rich reducing and corrosive conditions.

17.7 Conclusions

Inorganic proton conducting membranes can be implemented in a variety of applications and therefore the ceramic materials have to meet the corresponding requirements. During the past 20 years significant progress in research and development (R&D) has been made, mostly motivated by the benefits that these membranes offer in a number of applications. Improved proton conductivity and stability under relevant operating conditions are of a

© Woodhead Publishing Limited, 2011

particular importance. Proton conductivity is rather sensitive to temperature owing to the thermodynamic stability of proton defects in terms of proton content that contributes to the total conductivity of the material. Moreover, the stability and mobility of proton defects is unique for each kind of material. It strongly depends on the crystal structure, chemical nature and concentration of doping elements. However, as seen in the literature, the stability of protons is not an indication of either the chemical stability of the material or high proton conductivity. In this context, it should be mentioned that proton defects have the highest stability in cerates followed by the zirconates but in terms of chemical stability zirconates are more stable to carbonation than cerates. In order to illuminate the basics of these phenomena and complex dependencies for different classes of materials, intensive research is strongly required. In any case, proton–electron or dominant proton conductivity, the stability/mobility of proton defects and chemical stability must be balanced by a trade-off for obtaining the optimal properties of the membrane.

Strategies for the development of novel, application robust membranes rely on progress in materials science-based improvements as well as technology-driven optimization of the process and application conditions. R&D activities are consequently directed towards mechanically robust porous structures and functional layers in the nanometre range and the development of mixed-conducting oxides by means of theoretical approaches like atom modelling and experimental screening, based both on prior knowledge and modelling outcome. Decisive results based on a parallel investigation of (i) new materials, design and processing of components and equipment, (ii) integration into power plants and the related process engineering and (iii) energy systems analysis will pave the way to efficient and affordable membrane technologies including carbon capture and storage and hydrogen generation from carbon-based fuels by means of new gasification processes for fossil and biomass energy carriers.

17.8 Acknowledgements

The authors acknowledge the Initiative and Networking Fund of the Helmholtz Association, contract HA-104 ('MEM-BRAIN'), German Federal Ministry of Education and Research (BMBF) through the Northern European Innovative Energy Research Project, contract 03SF0330 ('N-INNER') and Spanish Ministry for Science and Innovation (Project ENE2008-06302).

17.9 References

Balachandran U and Eror N (1982), 'Non-stoichiometric disorder in $La_2Ti_2O_7$ at elevated temperatures', *J. Less-Common Met.*, **85**, 111–20.

Balachandran U, Guan J, Dorris S E, Bose A C and Stiegel G J (1998), *Proceedings*

© Woodhead Publishing Limited, 2011

5th International Conference on Inorganic Materials, A-410, Nagoya, Japan, June 22–26.

Bonanos N, Ellis B and Mahmood M N (1991), 'Construction and operation of fuel-cells based on the solid electrolyte $BaCeO_3$-Gd', *Solid State Ionics*, **44**, 305–11.

Cai M, Liu S, Efimov K, Caro J, Feldhoff A and Wang H (2009), 'Preparation and hydrogen permeation of $BaCe_{0,95}Nd_{0,05}O_{3-\delta}$ membranes', *J. Mem. Sci.*, **343**, 90–6.

Cheng S, Gupta V and Lin Y S (2005), 'Synthesis and hydrogen permeation properties of asymmetric proton-conducting ceramic membranes', *Solid State Ionics*, **176**, 2653–62.

Davies R A, Islam M S and Gale J D (1999), 'Dopant and proton incorporation in perovskite-type zirconates', *Solid State Ionics*, **126**, 323–35.

Diot N, Bernard-Rocherulle P, Marchand R (2000), 'X-ray powder diffraction data and Rietveld refinement for Ln_6WO_{12} (Ln = Y, Ho)', *Powder Diffr.*, **15**, 220.

Diot N, Larcher O, Marchand R, Kempf J Y, Macaudière P (2001), 'Rare-earth and tungsten oxynitrides with a defect fluorite-type structure as new pigments', *J. Alloys Compd.*, **45**, 323–4.

Du Y and Nowick A S (1996), 'Galvanic cell measurements on a fast proton conducting complex perovskite electrolyte', *Solid State Ionics*, **91**, 85–91.

Duval, S B C, Holtappels P, Vogt UF, Pomjakushina E, Conder K, Stimming U and Graule T (2007), 'Electrical conductivity of the proton conductor $BaZr_{0,9}Y_{0,1}O_{3-\delta}$ obtained by high temperature annealing', *Solid State Ionics*, **178**, 1437–41.

Errandonea D, Manjón F J, Somayazulu M and Häusermann D (2004), 'Effects of pressure on the local atomic structure of $CaWO_4$ and $YLiF_4$: mechanism of the scheelite-to-wolframite and scheelite-to-fergusonite transitions', *J. Solid State Chem.*, **177**, 1087.

Escolástico S, Vert V B and Serra J M (2009), 'Preparation and characterization of nanocrystalline mixed proton-electronic conducting materials based on the system Ln_6WO_{12}', *Chem. Mater.*, **21**, 3079–89.

Fischer W, Reck G and Schober T (1999), 'Structural transformation of the oxygen and proton conductor $Ba_2In_2O_5$ in humid air: an *in-situ* X-ray powder diffraction study', *Solid State Ionics*, **116** (3–4), 211–15.

Fontaine M L, Norby T, Larring Y, Grande T and Bredesen R (2008), 'Oxygen and hydrogen separation membranes based on dense ceramic conductors', *Membrane Science and Technology*, Vol. 13, Chapter 10, Elsevier B.V., Amsterdam, 401–58.

Fujii H, Katayama Y, Shimura T, Iwahara H (1998), 'Protonic conduction in perovskite-type oxide ceramics based on $LnScO_3$ (Ln = La, Nd, Sm or Gd) at high temperature', *J. Electroceramics*, **2**, 119.

Fukatsu N and Kurita N (2005), 'Hydrogen sensor based on oxide proton conductors and its application to metallurgical engineering', *Ionics*, **11**, 54–65.

Gibson St, Ivanova M, Meulenberg W A, Sebold D and Etsell Th (2009), 'On the preparation and characterization of ceria-based perovskite layers for potential use in proton conducting fuel cells', *Proceedings of the 3rd European Fuel Cell Technology and Applications Conference EFC09*, December 15–18, Rome, Italy, 135–6.

Gingerich K A and Bair H E (1964), 'Relation between ionic radii and transformation temperature in rare earth niobates', *Adv. X-Ray Anal.*, **7**, 22.

Greenblatt M, Tsai P, Kodama T and Tanase S (1990), 'Humidity sensor with sintered β-$Ca(PO_3)_2$ for high temperature use', *Solid State Ionics*, **40/41**, 444–7.

Guan J, Dorris SE, Balachandran U and Liu M (1998), 'Transport properties of $SrCe_{0.95}Y_{0.05}O_{3-\delta}$ and its application for hydrogen separation', *Solid State Ionics*, **110**, 303–10.

© Woodhead Publishing Limited, 2011

Guillaume B, Boschini F, Garcia-Cano I, Rulmont A, Cloots R and Ausloos M (2005), 'Optimization of $BaZrO_3$ sintering by control of the initial powder size distribution; a factorial design statistical analysis', *J. Eur. Ceram. Soc.*, **25**(16) 3593–604.

Hamakawa S, Hibino T and Iwahara H (1994), 'Electrochemical H_2 permeation in a proton-hole mixed conductor and its application to a membrane reactor', *J. Electrochem. Soc.*, **141**(7), 1720–5.

Hamakawa S, Li L, Li A and Iglesia E (2002), 'Synthesis and hydrogen permeation properties of membranes based on dense $SrCe_{0,95}Yb_{0,05}O_{3-\alpha}$ thin films', *Solid State Ionics*, **48**, 71–81.

Haugsrud R (2007), 'Defects and transport properties in Ln_6WO_{12} (Ln = La, Nd, Gd, Er)', *Solid State Ionics*, **178**, 555–60.

Haugsrud R and Norby T (2005), 'On the mixed ionic-electronic conductivity in Ca-doped $La_2Ti_2O_7$', *Proceedings of the 26th Risø International Symposium on Materials Science: Solid State Electrochemistry*, S. Linderoth, A. Smith, N. Bonanos, A. Hagen, L. Mikkelsen, K. Kammer, D. Lybye, P.V. Hendriksen, F.W. Poulsen, M. Mogensen and W.G. Wang (eds), Risø National Laboratory, Roskilde, Denmark.

Haugsrud R and Kjølseth Ch (2008), 'Effects of protons and acceptor substitution on the electrical conductivity of La_6WO_{12}', *J. Phys. Chem. Sol.*, **69**, 1758–65.

Haugsrud R and Norby T (2006), 'Proton conduction in rare-earth ortho-niobates and ortho-tantalates', *Nature Mater.*, **5**, 193–6.

Iwahara H, Esaka T, Uchida H and Maeda N (1981), 'Proton conduction in sintered oxides and its application to steam electrolysis for hydrogen production', *Solid State Ionics*, **3–4**, 359–63.

Iwahara H, Yajima T, Hibino T, Ozaki K and Suzuki H (1993), 'Proton conduction in calcium, strontium and barium zirconates', *Solid State Ionics*, **61**, 65–9.

Jona F, Shirane G and Pepinsky R (1955), 'Dielectric, X-ray, and optical study of ferroelectric $Cd_2Nb_2O_7$ and related compounds', *Phys. Rev.*, **98**, 903.

Korotcenkow G, Han S D, Stetter J R (2009), 'Review of electrochemical hydrogen sensors', *Chem. Rev.*, **109**, 1402–33.

Kosacki I and Anderson H I (1998), 'Nanostructured oxide thin films for gas sensors', *Sens. Actuators B*, **48**, 263–9.

Kreuer K D (1996), 'Proton conductivity: Materials and applications', *Chem. Mater.*, **8**, 610–41.

Kreuer K D (1997), 'On the development of proton conducting materials for technological applications', *Solid State Ionics*, **97**, 1–15.

Kreuer K D (1999), 'Aspects of the formation and mobility of protonic charge carriers and the stability of perovskite-type oxides', *Solid State Ionics*, **125**, 285–302.

Kreuer K D (2000), 'On the complexity of proton conduction phenomena', *Solid State Ionics*, **136–137**, 149–60.

Kreuer K D (2003), 'Proton conducting oxides', *Annu. Rev. Mater. Res.*, **33**, 333–59.

Kreuer K D (2004), 'Transport in proton conductors for fuel-cell applications: simulations, elementary reactions, and phenomenology', *Chem. Rev.*, **104**, 4637–78.

Kreuer K D, Adams St, Münch W, Fuchs A, Klock U and Maier J (2001), 'Proton conducting alkaline earth zirconates and titanates for high drain electrochemical applications', *Solid State Ionics*, **145**, 295–306.

Krug F, Schober T and Springer T (1995), 'In situ measurements of the water uptake in Yb doped $SrCeO_3$', *Solid State Ionics*, **81**, 111–18.

Labrincha J, Frade J and Marques F (1997), 'Proton conduction in $La_2Zr_2O_7$-based pyrochlore materials', *Solid State Ionics*, **99**(1–2), 33–40.

© Woodhead Publishing Limited, 2011

Larring Y and Norby T (1994), 'Protons in $LaErO_3$', *Solid State Ionics*, **70/71**, 305–10.

Larring Y and Norby T (1995), 'Protons in rare earth oxides', *Solid State Ionics*, **77**, 147–51.

Larring Y and Norby T (1997), 'The equilibrium between water vapour, protons, and oxygen vacancies in rare earth oxides', *Solid State Ionics*, **97**, 523–8.

Lee W K, Nowick A S and Boatner L A (1986), 'Protonic conduction in acceptor-doped $KTaO_3$ crystals', *Solid State Ionics*, **18–19**, 989–93.

Magrasó A, Frontera C, Marrero-López D and Núnez P (2009), 'New crystal structure and characterization of lanthanum tungstate "La_6WO_{12}" prepared by freeze-drying synthesis', *Dalton Trans*., 10273.

Matsumoto H, Shimura T, Higuchi T, Tanaka H, Katahira K, Otake T, Kudo T, Yashiro K, Kaimai A, Kawada T and Mizusaki J (2005), 'Protonic-electronic mixed conduction and hydrogen permeation in $BaCe_{0,9-x}Y_{0,1}Ru_xO_{3-\delta}$', *J. Electrochem. Soc*., **152**(3), A488–A492.

McCarthy G J, Fisher R D, Johnson G G Jr and Gooden C E (1972), 'Crystal chemistry and compound formation in the systems rare earth sesquioxide–WO_3', in *National Bureau St. Special Publication 364, Solid State Chemistry, Proceedings of the 5th Materials Research Symposium*, 397.

Mellander B and Zhu B (1993), 'High temperature protonic conduction in phosphate-based salts', *Solid State Ionics*, **61**, 105–10.

Meulenberg W A, Serra J M and Schober T (2006), 'Preparation of proton conducting $BaCe_{0,8}Gd_{0,2}O_3$ thin films', *Solid State Ionics*, **177**, 2851–6.

Meulenberg W A, Ivanova M, van Gestel T, Bram M, Buchkremer H P, Stöver D, Alfaro-Serra J M (2010), 'State of the art of ceramic membranes for hydrogen separation', in *Hydrogen Energy*. D Stolten (ed), Wiley-VCH, Weinheim, 321–49.

Mokkelbost T, Kaus I, Haugsrud R, Norby T, Grande T and Einarsrud M A (2008), 'High-temperature proton-conducting lanthanum ortho-niobate-based materials. Part II: Sintering properties and solubility of alkaline earth oxides', *J. Am. Ceram. Soc*., **91**(3), 879–86.

Naoki I, Matsumoto H, Kawasaki Y, Okada S and Ishihara T (2008), 'Introduction of In or Ga as second dopant to $BaZr_{0,9}Y_{0,1}O_{3-\delta}$ to achieve better sinterability', *Solid State Ionics*, **179**, 324–9.

Norby T (1990), 'Proton conduction in oxides', *Solid State Ionics*, **40/41**, 857–62.

Norby T (1999), 'Solid-state protonic conductors: principles, properties, progress and prospects', *Solid State Ionics*, **125**, 1–11.

Norby T (2009), 'Proton conduction in perovskite oxides'. *Perovskite Oxides for Solid Oxide Fuel Cells*', (*Fuel Cells and Hydrogen Energy*), T. Ishihara (ed), Springer Science+Business Media, Chapter 11, 217–41.

Norby T and Christiansen N (1995), 'Proton conduction in Ca- and Sr-substituted $LaPO_4$', *Solid State Ionics*, **77**, 240–3.

Norby T and Haugsrud R (2007), 'High temperature proton conducting materials for H_2-separation', *Invited lecture at Forschungszentrum Jülich (FZJ) Workshop*, Forschungszentum Jülich, Germany, November 16, 2007.

Norby T and Kofstad P (1984), 'Electrical conductivity and defect structure of Y_2O_3 as a function of water vapor pressure', *J. Am. Ceram. Soc*., **67**(12), 786.

Norby T and Kofstad P (1986), 'Proton and native-ion conductivities in Y_2O_3 at high temperatures', *Solid State Ionics*, **20**, 169–84.

Norby T and Larring Y (1997), 'Concentration and transport of protons in oxides', *Curr. Opin. Solid State Mater. Sci*., **2**(5), 593–9.

© Woodhead Publishing Limited, 2011

Norby T, Dyrlie O and Kofstad P (1992), 'Protons in Ca-doped La_2O_3, Nd_2O_3 and $LaNdO_3$', *Solid State Ionics*, **53–56**, 446–52.

Nyman H and Andersson S (1978), 'The pyrochlore structure and its relatives', *J. Sol. State Chem.*, **26**(2), 123–31.

Qi X and Lin Y S (2000), 'Electrical conductivity and hydrogen permeation through mixed proton-electron conducting strontium cerate membranes', *Solid State Ionics*, **130**, 149–56.

Ricote S, Bonanos N and Caboche G (2009), 'Water vapour solubility and conductivity study of the proton conductor $BaCe_{(0.9-x)}Zr_xY_{0.1}O_{(3-\delta)}$', *Solid State Ionics*, **180**, 990–7.

Sakthivel M and Weppner W (2007), 'Application of layered perovskite type proton conducting $KCa_2Nb_3O_{10}$ in H_2 sensors: Pt particle size and temperature dependence', *Sens. Actuators B*, **125**, 435–40.

Schober T (1998), 'Protonic conduction in $BaIn_{0.5}Sn_{0.5}O_{2.75}$', *Solid State Ionics*, **109**(1–2), 1–11.

Schober T and Bohn H G (2000), 'Water vapor solubility and electrochemical characterization of the high temperature proton conductor $BaZr_{0,9}Y_{0,1}O_{2,95}$', *Solid State Ionics*, **127**, 351–60.

Schober T, Friedrich J and Condon J B (1995), 'Effective hydrogen diffusivity in $SrCe_{0,95}Yb_{0,05}O_{3-\alpha}$ and $SrZr_{0,95}Yb_{0,05}O_{3-\alpha}$', *Solid State Ionics*, **77**, 175–9.

Scholten M J, Schoonman J, Miltenburg J C van and Oonk H A J (1993), 'Synthesis of strontium and barium cerate and their reaction with carbon dioxide', *Solid State Ionics*, **61**, 83–91.

Serra J M and Meulenberg W A (2007), 'Thin-film proton $BaZr_{0.85}Y_{0.15}O_3$ conducting electrolytes: toward an intermediate-temperature solid oxide fuel cell alternative', *J. Am. Ceram. Soc.*, **90**(7), 2082–9.

Serra J M, Büchler O, Meulenberg W A and Buchkremer H P (2007), 'Thin $BaCe_{0.8}Gd_{0.2}O_{3-\delta}$ protonic electrolytes on porous $Ce_{0.8}Gd_{0.2}O_{1.9}$–Ni substrates', *J. Electrochem. Soc.*, **154**(3), B334–B340.

Shimura T, Komori M and Iwahara H (1996), 'Ionic conduction in pyrochlore-type oxides containing rare earth elements at high temperature', *Solid State Ionics*, **86–88**, 685–9.

Shimura T, Fujimoto S and Iwahara H (2001), 'Proton conduction in non-perovskite-type oxides at elevated temperatures', *Solid State Ionics* **143**, 117–23.

Shirsat A N, Kaimal K N G, Bharadwaj S R and Das D (2004), 'Thermodynamic stability of $SrCeO_3$', *J. Solid State Chem.*, **177**, 2007–13.

Song S J, Wachsman E D, Rhodes J, Dorris S E, Balachandran U (2004), 'Hydrogen permeability of $SrCe_{1-x}M_xO_{3-\delta}$ (x = 0,05, M = Eu, Sm)', *Solid State Ionics*, **167**, 99–105.

Song S J, Wachsman E D, Rhodes J, Yoon H S, Lee K H, Zhang G, Dorris S E and Balachandran U (2005), 'Hydrogen permeability and effect of microstructure on mixed protonic-electronic conducting Eu-doped strontium cerate', *J. Mater. Sci.*, **40**, 4061–6.

Stotz S and Wagner C (1966), 'Die Lösigkeit von wasserdampf und Wasserstoff in festen Oxiden', *Ber. Bunsenges.Phys.Chem. Bd*, **70**(8), 781–8.

Stubican V S (1964), 'High-temperature transitions in rare-earth niobates and tantalates', *J. Am. Ceram. Soc.*, **47**, 55–8.

Tao S and Irvine J T S (2007), 'Conductivity studies of dense yttrium-doped $BaZrO_3$ sintered at 1325°C', *J. Solid State Chem.*, **180**, 3493–503.

Wang W and Virkar A V (2004), 'A conductimetric humidity sensor based on proton conducting perovskite oxides', *Sens. Actuators B*, **98**, 282–90.

© Woodhead Publishing Limited, 2011

Wei X, Kniep J and Lin Y S (2009), 'Hydrogen permeation through terbium doped strontium cerate membranes enabled by presence of reducing gas in the downstream', *J. Mem. Sci.*, **345**, 201–6.

Yajoma T, Koide K, Fukatsu N, Ohashi T and Iwahara H (1993), 'A new hydrogen sensor for molten aluminum', *Sens. Actuators B*, **13–14**, 697–9.

Yamanaka S, Kurosaki K, Maekawa T, Matsuda T, Kobayashi S and Uno M (2005), 'Thermochemical and thermophysical properties of alkaline-earth perovskites', *J. Nucl. Mater*, **344**, 61–6.

Yamazoe N and Miura N (1988), *Proton Conductor Gas Sensor and Method of Detecting Gas using Proton Conductor Gas Sensor*', US Patent 4,718,991 to Figaro Engineering Inc.

Zhan S, Zhu X, Ji B, Wang W, Zhang X, Wang J, Yang W and Lin L (2009), 'Preparation and hydrogen permeation of $SrCe_{0.95}Y_{0.05}O_{3-\delta}$ asymmetrical membranes', *J. Mem. Sci.*, **340**, 241–8.

© Woodhead Publishing Limited, 2011

18
Membrane electrolysers for hydrogen (H_2) production

P. MILLET, University of Paris, France

Abstract: Ion-conducting membrane materials are used in electrolysers for the dual purpose of carrying electric charge between electrodes and separating the products formed at each electrode. The aim of this chapter is to provide an overview of the main membrane materials and associated technological processes. After a brief introduction, the basic principles of electrolysis are introduced in Section 18.2. The main membrane materials (chemical composition and ion-transport properties) are described in Section 18.3 and the main physical properties are discussed in Section 18.4. Industrial applications are described in Section 18.5. The limitations of current materials are discussed in Section 18.6 and prospective issues are evoked in Section 18.7.

Key word: electrolysers, electrolysis, ionic-conductors, membranes.

18.1 Introduction

18.1.1 Brief historical review of electrolysis

The word 'electrolysis' comes from a combination of two Greek words: *elektron* (amber) and *lýsis* (to separate). Electrolysis is therefore the process in which a direct electric current passing between two electrodes through an ionic substance (that is either molten such as a molten salt or dissolved in a suitable solvent) is used to perform a non-spontaneous chemical reaction and to separate reaction products. The principles of electrolysis were discovered in 1800 by two English scientists, William Nicholson (1753–1815) and Anthony Carlisle (1768–1842) who employed a voltaic pile to liberate hydrogen and oxygen from water[1] and initiated the science of electrochemistry:

$$H_2O_{(liq)} \rightarrow H_{2(g)} + \tfrac{1}{2}\, O_{2(g)}$$

The laws of electrolysis were published in 1834 by Michael Faraday.[2] Electrolysis was used in the nineteenth century for the synthesis of several chemical elements. Sir Humphrey Davy discovered potassium, sodium, barium, calcium and magnesium in 1807. Henri Moissan discovered fluorine in 1886. Aluminium was obtained in 1886 using the Hall–Héroult process and sodium hydroxide was obtained in 1890 using the Castner–Kellner process. A large variety of extremely important electrochemical processes

© Woodhead Publishing Limited, 2011

are used in the industry. Many key chemicals produced in the world such as chlorine, soda (NaOH) and aluminium are obtained from electrochemical processes.[3,4]

18.1.2 Membranes

In biology and chemistry, a membrane is often defined as a thin sheet of natural or synthetic material that is permeable to substances in solution. This means that the membrane is impregnated with the solvent and that the solute can move freely across the membrane. Among various kinds of membranes, an ion-exchange membrane is a thin sheet or film of ion-exchange material which may be used to separate ions by allowing the preferential transport of either cations (in the case of a cation-exchange membrane) or anions (in the case of an anion exchange membrane). If the membrane material only contains the ion-exchanging material, it is called a homogeneous ion-exchange membrane. If the ion-exchange material is embedded in an inert binder, it is called a heterogeneous ion-exchange membrane. Ion-conducting membrane materials are used in electrolysers for the double purpose of carrying electric charges (ions) between electrodes and separating the products of the electrochemical transformation formed at each electrode. In the electrochemical industry, different materials are used as solid electrolytes and cell separators: (i) inert porous materials impregnated with a liquid electrolyte; (ii) ion-conducting polymers; (ii) ion-conducting ceramics. The choice and selection of a material for a given application depends on the operating conditions and, most importantly, on the temperature at which the electrochemical process is conducted.

18.1.3 Gap cells, zero-gap cells and solid polymer electrolyte (SPE) cells

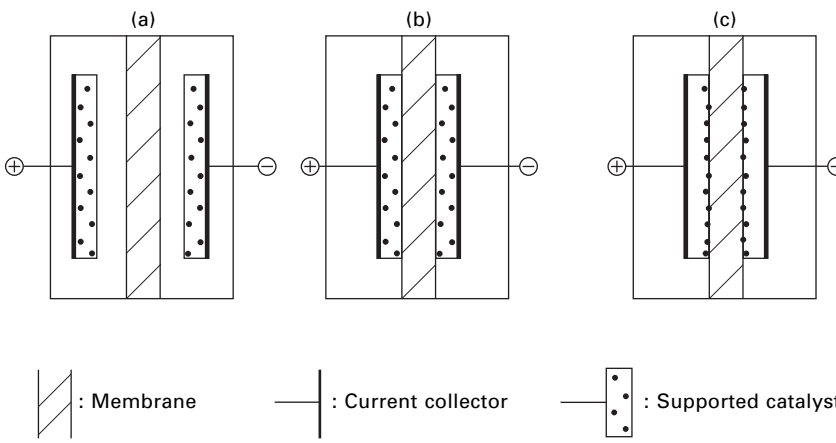
The device used to perform electrolysis is called an electrolyser. An electrolyser is made by the interconnection of several elementary electrolysis cells. The key component of an electrolysis cell is the interface between a metal (an electron conductor or electrode) and an electrolyte (an ionic conductor). Electrons are highly reactive species and cannot exist freely in the electrolyte. Therefore, the charge (electron) transfer process at the interface, driven by an external power supply, leads to redox chemical transformations at the interface, on the electrolyte side. A second metal/electrolyte interface, facing the first one, is introduced in the cell to collect electrons and equilibrate charge transfers. The anode is the electrode where an oxidation takes place and the cathode is the electrode where a reduction takes place. Thus basically, an electrolysis cell is a galvanic (electrochemical) chain obtained (in the simplest and most common case) by the series connection of three

© Woodhead Publishing Limited, 2011

different phases, one electronic conductor, one ionic conductor and a second electron conductor. Usually, planar geometry is preferred over cylindrical geometry (more largely found in electrochemical generators) because it is more appropriate for the design of large systems.

From a thermodynamic viewpoint, an electrolyser can be seen as a device which can convert electrical energy into chemical energy. Electrolysis is sometimes referred to as 'electricity-driven chemical reaction'. This means that the chemical transformation is a non-spontaneous process. In most cases, the reverse reaction, however, is spontaneous and therefore, it is necessary to prevent the spontaneous recombination of chemical products produced at the anode and the cathode during electrolysis. Liquid electrolytes are not efficient separators because chemicals can be transported rapidly from one electrode to the other by diffusion and/or convection. Solids are more efficient and in practical cases, a charge-conducting separator (a membrane) is inserted between the anode and the cathode. Basically, three different cell concepts are used in the industry (Fig. 18.1).

The first concept is called a 'gap cell' (Fig. 18.1(a)). This is the most conventional configuration. Two planar electrodes (in fact, a cheap electron-conducting substrate surface covered by a thin layer of electrocatalyst) are placed face-to-face in an electrolyte and a membrane is inserted in the liquid electrolyte, to prevent recombination of products. The membrane can be an inert and porous material (sometimes called a diaphragm), impregnated with the liquid electrolyte. Since transport of electric charges in an electrolyte follow Ohm's law, then the larger the distance between the two electrodes, the larger the ohmic losses and the lower the cell efficiency. Therefore, cell design is of the uppermost significance. When the electrolysis leads to the



18.1 Two dimensional schematic diagrams of (a) a gap-cell, (b) a zero-gap cell and (c) a SPE cell.

© Woodhead Publishing Limited, 2011

formation of gaseous products (for example H_2 and O_2 during the electrolysis of water), the maximum current density is limited to a few hundreds of milliamps per square centimetre (mA cm^{-2}). This is because non-conducting gaseous films tend to form over the electrode surfaces. Therefore, the concept of gap cell pictured in Fig. 18.1(a) is not efficient, and not appropriate for gas-evolving electrodes.

The second concept is called a 'zero-gap cell' (Fig. 18.1(b)). In this case, porous electrodes are pressed onto the membrane separator, to reduce as much as possible the distance between anode and cathode (and corresponding ohmic losses). Products are released through the pores at the back of the electrodes. This is an interesting concept when gases are produced, at least at one electrode. Significantly larger current densities can be achieved without significant extra losses. However, a liquid electrolyte is still needed.

The third concept is called a 'SPE cell' (Fig. 18.1(c)). SPE, which is a registered trademark of Hamilton Standard Corp., stands for solid polymer electrolyte. In such cells, ions which convey electric charges from one electrode to the other are immobilized inside the membrane which acts as a solid electrolyte. There is no liquid electrolyte in circulation in the electrolyser. This concept was first proposed for application in H_2/O_2 fuel cells in 1950, at the dawn of the US space program, to solve the problems associated with operation in a low gravity environment and those caused by the corrosion of metals in acidic media. The idea was used later for the development of water electrolysers. In the literature, it is referred to as SPE water electrolysis or PEM (proton exchange membrane or polymer electrolyte membrane) water electrolysis. In a PEM water electrolysis cell, electrodes are deposited at the surface of the membrane and porous current collectors are pressed on each side of the cell. There is no liquid electrolyte. Only deionised water is circulated in the anodic chamber to feed the electrochemical reaction. The same concept is used at high temperature, with oxide-ion conducting membranes.

18.2 Basic principles of electrolysis

In the following, the electrolysis of water is used as an example to introduce the general features of electrolysis.

18.2.1 Thermodynamics

In a water electrolysis cell, electricity is used to split water molecules into gaseous hydrogen and oxygen. When an acidic electrolyte is used, water splitting occurs according to the following half-cell reactions:
anode:

$$H_2O(liq) \rightarrow \tfrac{1}{2}\, O_2(g) + 2\, H^+ + 2\, e^- \qquad [18.1]$$

© Woodhead Publishing Limited, 2011

cathode:

$$2\ H^+ + 2\ e^- \rightarrow H_2(g) \qquad [18.2]$$

full reaction:

$$H_2O(liq) \rightarrow H_2(g) + \tfrac{1}{2}\ O_2(g) \qquad [18.3]$$

Solvated protons formed at the oxygen-evolving anode of the PEM cell migrate through the SPE membrane to the cathode where they are reduced into molecular hydrogen. Liquid water is consumed at the anode to form oxygen but is also released at the cathode when hydrated protons are reduced (so-called electro-osmosis drag). At equilibrium, the amount of electricity (nFE) required to split one mole of water is equal to the change in Gibbs free energy ΔG_d of the water dissociation reaction [18.3]:

$$\Delta G_d - n\ F\ E = 0 \qquad \text{where} \qquad \Delta G_d > 0 \qquad [18.4]$$

where $n = 2$ (number of electrons exchanged during the electrochemical splitting of water), $F \approx 96\ 485$ C mol^{-1} (Faraday constant), E is the thermodynamic electrolysis voltage (V) associated with reaction [18.3] and ΔG_d is the free energy change (J mol^{-1}) associated with reaction [18.3].

ΔG_d is a function of both operating temperature and pressure and thus:

$$\Delta G_d(T, P) = \Delta H_d(T, P) - T\ \Delta S_d(T, P) > 0 \qquad [18.5]$$

where $\Delta H_d\ (T, P)$ and $\Delta S_d\ (T, P)$ are respectively the enthalpy change (J mol^{-1}) and entropy change (J mol^{-1} K^{-1}) associated with reaction [18.3]. To split one mole of water, ΔG_d (J mol^{-1}) of electricity and T ΔS_d (J mol^{-1}) of heat are required. The thermodynamic electrolysis voltage E (in volts, V) is defined as:

$$E(T, P) = \frac{\Delta G_d(T, P)}{n\ F} \qquad [18.6]$$

The thermo-neutral voltage V (V) is defined as:

$$V(T, P) = \frac{\Delta H(T, P)}{n\ F} \qquad [18.7]$$

Under standard conditions of temperature and pressure (T = 298K, P = 1 atm), water is liquid and H_2 and O_2 are gaseous. Standard free energy, enthalpy and entropy changes for reaction [18.3] are:

$$\Delta G_d^0\,(H_2O) = 237.22\ \text{kJ mol}^{-1} \Rightarrow E^0 = \Delta G_d^0\,(H_2O)/2F$$
$$= 1.2293\ \text{V} \approx 1.23\ \text{V}$$
$$\Delta H_d^0\,(H_2O) = 285.840\ \text{kJ mol}^{-1} \Rightarrow V^0 = \Delta H_d^0\,(H_2O)/2F$$
$$= 1.4813\ \text{V} \approx 1.48\ \text{V}$$

© Woodhead Publishing Limited, 2011

$$\Delta S_d^0 (H_2O) = 163.15 \text{ J mol}^{-1} \text{ K}^{-1}$$

A voltage term $T\Delta S_d^0/(2F) = 0.25$ V must be added to the thermodynamic voltage E to provide the heat required by reaction [18.3].

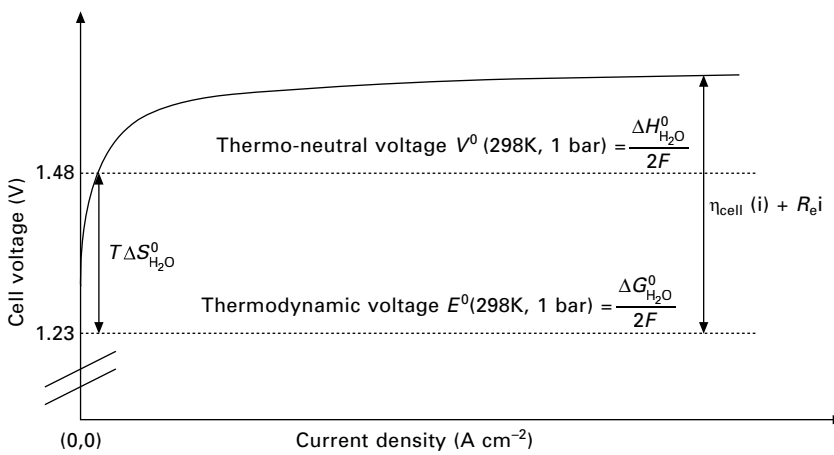
18.2.2 Kinetics

The free energy change (ΔG_d) of the reaction corresponds to the minimum energy required to transform one mole of reactant. However, there is no practical interest in performing electrolysis close to equilibrium. On the contrary, it is necessary to increase significantly the operating current density in order to reduce investment costs. In conventional electrolysers, current densities ranging from 100 mA cm^{-2} up to several A cm^{-2} are achieved.

To reach such values, it is necessary to overcome different kinds of current-dependent irreversibilities such as interface overvoltages associated with charge transfer processes (η in V) or ohmic drop across the electrolyte caused by the resistance (R_e) of the electrolyte. The amplitude of such voltage losses increases with operating current density. As a result, an increasing amount of electrical energy is transformed into heat and the efficiency of the electrochemical cell decreases. A typical polarization curve (a plot of the cell voltage as a function of the operating current density) measured during PEM water electrolysis is plotted in Fig. 18.2.

18.2.3 Cell efficiency

The efficiency ε of an electrolysis cell relates the theoretical amount of energy W_t required to split one mole of reactant to the real amount of energy W_r



18.2 Schematic diagram of a voltage–current density polarization curve during PEM water electrolysis.

© Woodhead Publishing Limited, 2011

required by the process. Because of the above-mentioned irreversibilities, $W_r > W_t$. The cell efficiency is defined as:

$$\varepsilon = \frac{W_t}{W_r} \qquad [18.8]$$

where: $W_r = (U_{cell}\, I\, t)$, U_{cell} is the actual cell voltage (V), I is current (A) and t is the duration(s); W_t can be defined from the thermodynamic voltage E, $W_{t,\Delta G} = (E\, I\, t)$ and W_t can also be defined from the thermo-neutral voltage V; $W_{t,\Delta H} = (V\, I\, t)$.

Therefore, two different definitions can be used to express the efficiency of the electrolysis cell. Since E and V are both functions of operating temperature (T) and operating pressure (P), and since U_{cell} is also a function of the operating current density j, the two different cell efficiencies can also be expressed as a function of T, P, j:

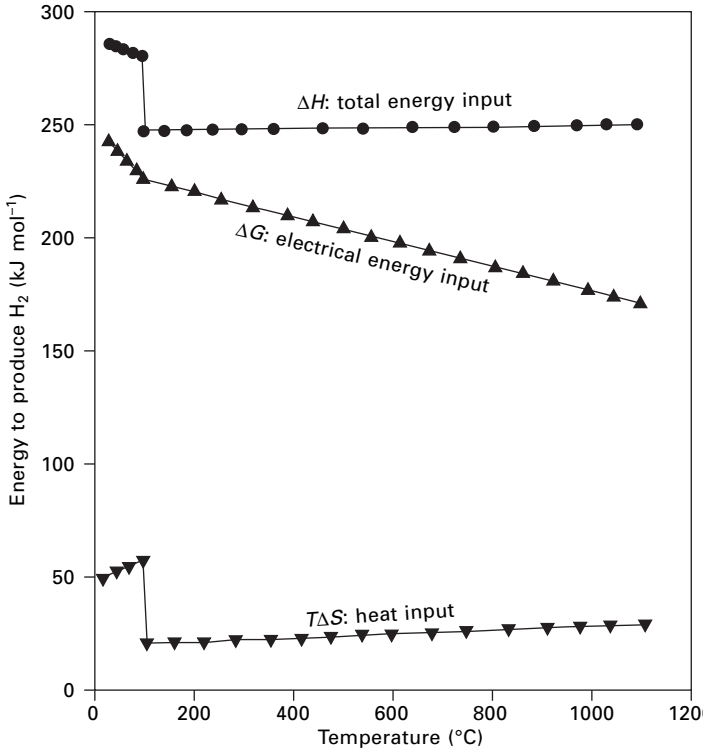
$$\varepsilon_{\Delta G}(T, P, j) = \frac{E(T, P)}{U_{cell}(T, P, j)} \qquad \varepsilon_{\Delta H}(T, P, j) = \frac{V(T, P)}{U_{cell}(T, P, j)} \qquad [18.9]$$

At low current densities, cell efficiencies close to 100% are obtained. In conventional water electrolysers, $\varepsilon_{\Delta H} \approx 70\%$ at 1 A cm^{-2}, $T = 90°C$ and $P = 1$ bar. The efficiency of the electrolysis cell is a critical parameter responsible for the energy cost of the process. Operation at high current density is necessary to reduce investment costs but since efficiency decreases when current density increases, a compromise has to be found between energy and investment costs.

18.3 Membrane materials

An important operating parameter in electrolysis technology is the temperature of operation of the cell. For many electrochemical processes, $\Delta H(T)$ remains almost constant over a large range of temperature (–50°C up to 1000°C) at constant operating pressure. In contrast, $\Delta G(T)$ tends to decrease and $T\Delta S_d(T)$ tends to increase with temperature. This is the case for the water splitting reaction (Fig. 18.3). As a result, the higher the operating temperature, the less electricity and the more heat are required to perform the reaction. From a thermodynamic viewpoint, when a source of heat is available at high (800–1000°C) temperature, there is an interest in performing electrolysis at such elevated temperatures because the electricity consumption is reduced compared to the amount required at lower temperatures. Another benefit of higher operating temperature is an increase in cell efficiency due to improved kinetics. Whereas liquid electrolytes using water as solvent are restricted to temperature values less than 100°C (or slightly above under pressure), solid electrolytes are required for operation at higher temperatures. There is a large variety of solid ion-conductors for operation in the +100°C to

© Woodhead Publishing Limited, 2011



18.3 $\Delta G(T)$, $\Delta H(T)$ and $T\,\Delta S(T)$ plots associated with the water splitting reaction.

+1000°C temperature range. The main materials used in practical applications are listed below.

18.3.1 Materials used as diaphragms with liquid electrolytes

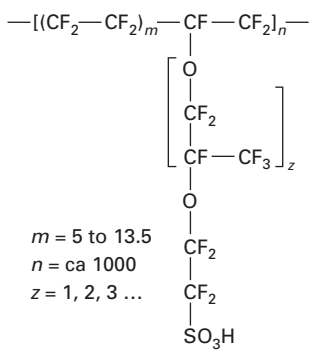
In low temperature processes, abundant and cheap water is commonly used as a solvent. Acidic liquid electrolytes are seldom found in practical applications, mostly because of corrosion problems. Sodium chloride and potassium hydroxide are two examples of ionic compounds used in electrochemical processes. The ionic conductivity of an electrolyte depends markedly on the concentration of ionic species dissolved in the solvent and concentrations as high as 26 wt% (brine electrolysis) and 40 g l^{-1} (alkaline water electrolysis) are used. Most cell separators found in electrolysis cells with liquid electrolytes are called diaphragms. Asbestos has been largely used in alkaline water electrolysis. Asbestos is a naturally occurring silicate mineral exploited commercially for its physical properties (mainly

© Woodhead Publishing Limited, 2011

its sound absorption, average tensile strength, and its resistance to heat, electrical and chemical damage). It is used in electrochemical cells because of some interesting properties such as wettability and chemical resistance to electrolytes. It is formed of characteristic fibrous crystals. The inhalation of asbestos fibres can cause serious illnesses (lung cancer). This is why all use of asbestos and extraction, manufacture and processing of asbestos products have been banned by the European Union. Less hazardous materials can be used alternatively. For example, diaphragms of porous sinter metal oxidized to metal oxide can be used for alkaline water electrolysis.[5]

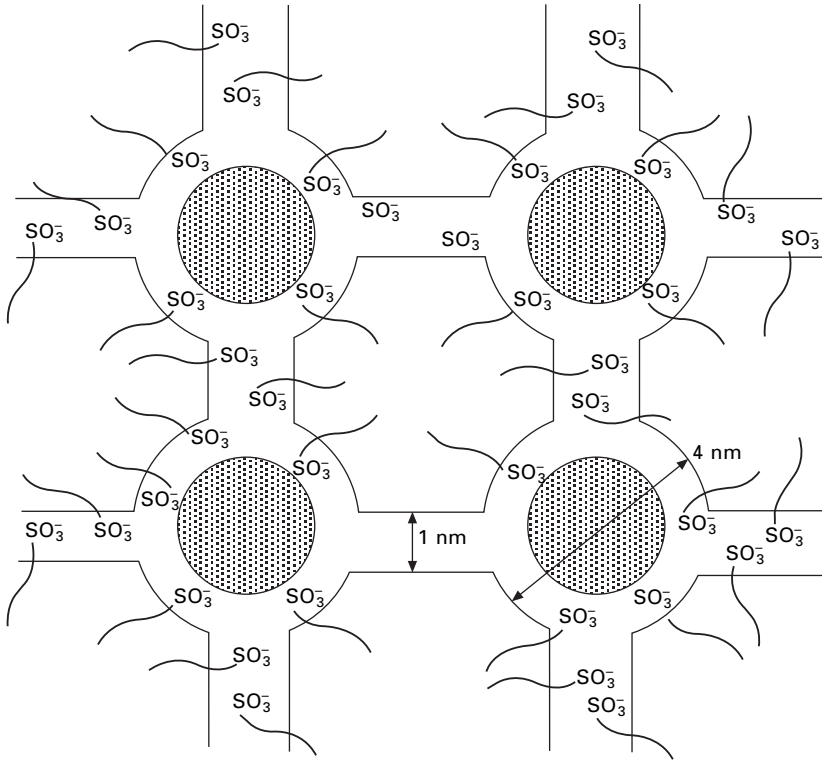
18.3.2 Polymeric proton conductors

In PEM water electrolysis technology, chemically stable sulfonated tetrafluoroethylene based fluoropolymer–copolymer membranes (W. Grot, E.I. DuPont Co., Nafion® products) are commonly used as SPE (Fig. 18.4). Nafion® products are characterized by their equivalent weight (EW), that is the number of grams of dry Nafion® per mole of sulfonic acid groups when the material is in the acid form. EW can be ascertained by acid–base titration. Such materials gather a number of physical properties which are necessary for operation in PEM water electrolysis cells: (i) a high ionic conductivity (>10 mS cm^{-1}), (ii) a poor electronic conductivity, (iii) a good chemical and mechanical stability, (iv) a high thermal conductivity (>0.1 J s^{-1} m^{-1} K^{-1}) and (v) a limited permeability to hydrogen and oxygen. Proton conductivity, water management, relative affinity to water, hydration stability at high temperatures, electro-osmotic drag, and mechanical, thermal, and oxidative stability of these materials are directly determined by their chemical microstructure. From a historical perspective, the cluster-network model of Gierke *et al.*[6] has been used for many years to interpret the properties of Nafion® membranes (especially ion and water transport and ion permselectivity). In this model (Fig. 18.5), it is assumed that there are ≈ 40 Å diameter clusters



18.4 Structural unit of Nafion®.

© Woodhead Publishing Limited, 2011



18.5 Gierke model of nanoclusters in perfluorosulfonic acid materials.

of sulfonate-ended perfluoroalkyl ether groups that are organized as inverted micelles and arranged on a lattice. These micelles are connected by pores or channels that are ≈ 10 Å in size. These -SO_3^--coated channels were invoked to account for inter-cluster transfer of cations and ion conductivity.

Among the earliest concepts that were set forth regarding microstructure are those of Yeager and Steck.[7] Compared to the model of Gierke *et al.*, the clusters do not have a strict geometry and their geometrical distribution has a lower degree of order. Most importantly, intermediate interphase domains are found between hydrophobic and hydrophilic regions. For the development of PEM water electrolysis applications, Nafion® can be considered as a homogeneous two-phase medium, a mixture of hydrophobic regions containing fluoro-carbon backbones and hydrophilic regions containing water, where proton conductivity takes place.

18.3.3 Polymeric hydroxyl-ion conductors

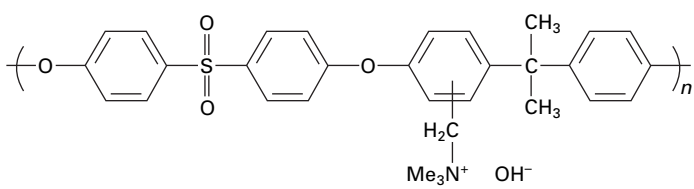
Hydroxyl-ion conducting polymers are increasingly studied for application in alkaline fuel cell technology (so-called alkaline anion-exchange membranes

© Woodhead Publishing Limited, 2011

fuel cells). High power densities (up to 400 mW cm^{-2}) and high current densities (up to 1 A cm^{-2}) have been recently reported.[8] The advantages and disadvantages of OH^- conducting membranes have been described in detail in recent reviews.[9,10] State-of-the-art materials are conductive, chemically and thermally stable quaternary-ammonium-containing polymers (Fig. 18.6). Cross-linked (OH^- exchanging but water insoluble) alkaline interface polymers that allow the preparation of membrane electrode assemblies (MEAs) for alkaline anion-exchange membranes applications have been successfully developed.[11] The counter ions (quaternary ammonium groups) to the OH^- conduction species are bound to the polymer backbone in the same manner as the counter ions (SO_3^- groups) are bound to the polymer backbone in commercial proton-conducting polymers such as Nafion®. For example, quaternary-ammonium polysulfone (Fig. 18.6) shows a microstructure similar to that of Nafion, that is a continuous hydrophobic network penetrated by interlinked and nano-sized hydrophilic domains. Such materials are reported to provide both high ionic conductivity (>10^{-2} S cm^{-1} at room temperature) and excellent mechanical strength (>1000 MPa in Young's modulus), opening the way to fuel cell and electrolysis applications.

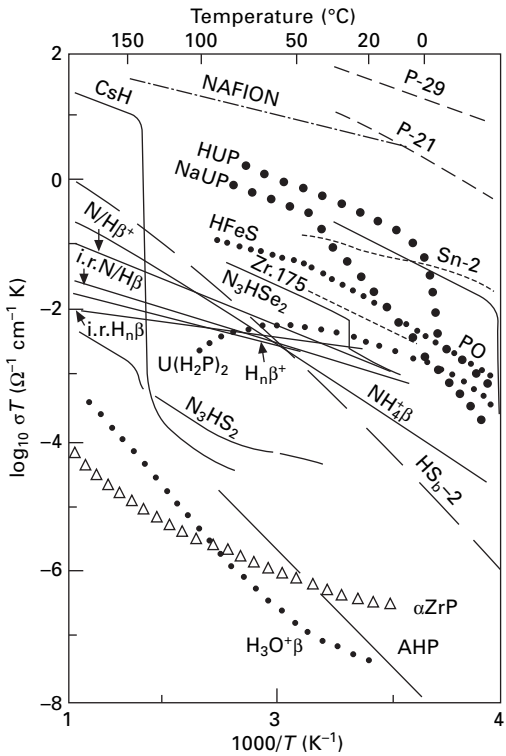
18.3.4 Non-organic proton conductors

The mechanism of proton conduction in most organic proton conductors (such as ion-conducting polymers) requires water. These materials can be employed at temperatures less than 150°C. Although there are many good non-organic protonic solid conductors (Fig. 18.7),[12] most of them are unstable at temperatures above 300°C and decompose to liberate water. Some perovskite-type oxides are proton conductors at elevated (400–1000°C) temperatures.[13] In particular, some perovskites (simples or mixes) present a high ionic conductivity when exposed to water vapour (Fig. 18.8). They can potentially be used as thin (<100 μm) solid electrolyte for manufacturing water electrolysis cells. For example, $Sr[Ce_xZr_{1-x}]_{0.95}Yb_{0.05}O_3$ which shows a maximum of conductivity for $x = 0.8$[14] can be used in solid oxide electrochemical applications. Another example is given by $La_{0.6}Ba_{0.4}ScO_{2.8}$.



18.6 Structural unit of quaternary ammonium polysulfone.

© Woodhead Publishing Limited, 2011

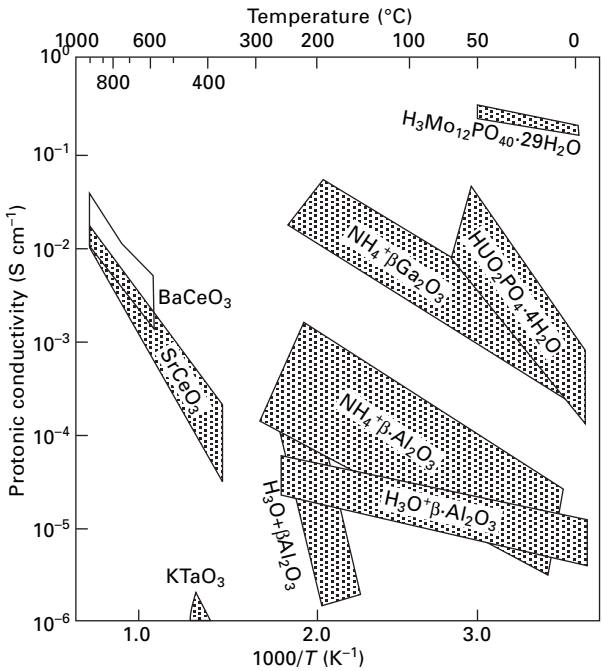


18.7 Low temperature proton conductors (see reference 12 for more details about chemical compositions).

18.3.5 Oxide-ion conductors

Solid electrolytes operating at high (800–1000°C) temperature must be chemically stable in the presence of oxygen, good ionic conductors and poor electronic conductors. In this temperature range, proton conductors are replaced by anionic conductors such as oxygen ions. Yttria-stabilized zirconia (YSZ) is a zirconium oxide based ceramic, in which the particular crystal structure of zirconium oxide is made stable at room temperature by addition of yttrium oxide. These oxides are commonly called 'zirconia' (ZrO_2) and 'yttria' (Y_2O_3), hence the name. The addition of yttria to pure zirconia replaces some of the Zr^{4+} ions in the zirconia lattice with Y^{3+} ions. This produces oxygen vacancies, as three O^{2-} ions replace four O^{2-} ions. It also permits yttrium stabilized zirconia to conduct O^{2-} ions, provided there is sufficient vacancy site mobility, a property that increases steadily with temperature. This high ionic conductivity by O^{2-} ions makes yttria-stabilized zirconia one of the most useful electroceramics, well suited for applications in solid oxide fuel cells and solid oxide water electrolysis cells.

© Woodhead Publishing Limited, 2011



18.8 High temperature proton conductors.

18.4 Membrane performance

For application in electrolysis cells, membranes must satisfy a number of criteria, among them are (i) good ionic and thermal conductivity, (ii) poor electronic conductivity, (iii) good chemical and mechanical stability, (iv) good thermal stability, (v) ease of manufacture and easily produced in the form of large surface membrane of homogeneous thickness and (vi) showing low gas solubility. Some quantitative figures are discussed in this section.

18.4.1 Ionic conductivity

The first role of a membrane in an electrolysis cell is to convey electric charges (ions) between electrodes. Therefore, the ionic conductivity is a key physical property of membrane materials. In conventional electrolysers, the operating current density ranges from a few hundred mA cm^{-2} to 1 A cm^{-2}. A maximum ohmic drop of 100 mV at 1 A cm^{-2} is a good target for electrolysers. Therefore, the surface resistance should be less than 0.1 Ω cm^2.

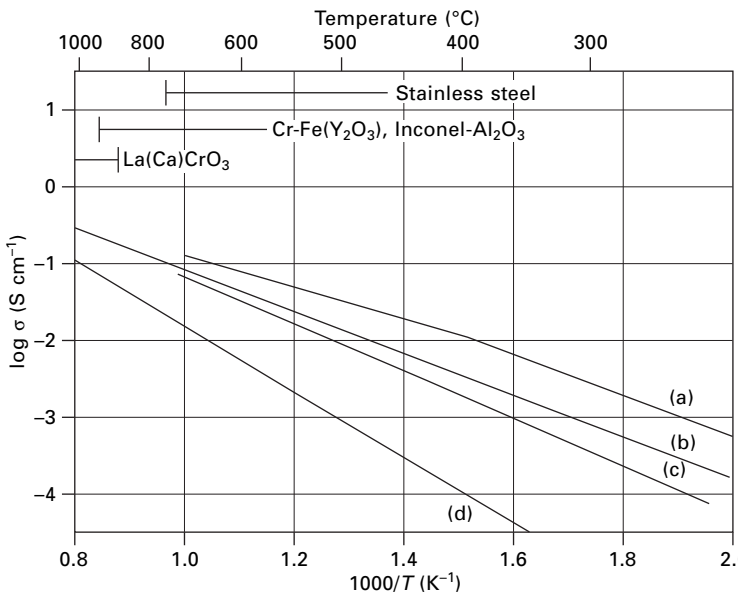
In PEM water electrolysis, membranes have a typical thickness of 200 μm (this is the case for commercial Nafion® products). At room temperature, the resistivity of 1100 EW Nafion® in H^+ form is $\rho < 5.0$ Ω cm and the corresponding conductivity is $\sigma > 0.2$ S cm^{-1}.[15] The surface resistance of

© Woodhead Publishing Limited, 2011

the membrane is therefore 0.1 Ω cm^2. The conductivity of Nafion is due to both proton migration in the aqueous phase and to proton tunnelling between adjacent sulfonate groups in narrow pores. Different materials can be used as oxygen-ion conductors, (Fig. 18.9). Stabilized zirconia is one of the most studied oxide-ion conducting solid electrolytes. The experimental values of the ionic conductivity of ZrO_2-12 mol% Y_2O, single crystals in the temperature range 200–1600°C show that in the upper temperature range, the conductivity is sufficient for application in devices such as solid oxide water electrolysis.[16,17] At 1000°C, $\sigma = 0.1$ S cm^{-1}. Therefore, 100 μm thick membranes are required to reach the target surface resistance of 0.1 Ω cm^2.

18.4.2 Permselectivity

Permselectivity is the term used to define the preferential permeation of certain ionic species through ion-exchange membranes.[22] When the membrane is used in a gap cell or in a zero-gap cell (Fig. 18.1) with a liquid electrolyte, both cations and anions participate in the transport of electric charges according to their charge and individual mobility. Donnan exclusion effects must also be considered. However, when the membrane is used in



18.9 Ionic conductivity of some oxygen-ion conductors. (a) $Bi_2V_{0.9}Cu_{0.1}O_{5.35}$,[18] (b) $Ce_{0.9}Gd_{0.1}O_{1.95}$,[19] (c) $La_{0.9}Sr_{0.1}Ga_{0.8}Mg_{0.2}O_{2.85}$,[20] and (d) $(ZrO_2)_{0.9}(Y_2O_3)_{0.1}$.[21] Top : conductivity of SOFC bipolar plate materials are given for comparison.

© Woodhead Publishing Limited, 2011

a SPE cell (no liquid electrolyte), there is only one kind of charge carrier: cations in cation-exchange materials (for example protons in PEM water electrolysis cells or sodium ions in brine electrolysis cells) and anions in anion-exchange materials.

18.4.3 Gas permeability

The second role of a membrane in an electrolysis cell is to prevent recombination of reaction products formed during electrolysis at the electrodes. When the electrochemical reaction produces gases at high pressure (this is the case in a high pressure PEM water electrolysis cell), the gas permeability P^{m} of the membrane becomes a critical physical property. P^{m} is defined as:

$$P^{m} = \frac{u}{\Delta P}\frac{\delta}{A}\ (\mathrm{cm}^2\ \mathrm{Pa}^{-1}\ \mathrm{s}^{-1}) \qquad [18.10]$$

where u is the rate of gas permeation ($Nm^3\ s^{-1}$; where Nm^3 is a normal cubic metre under normal conditions of temperature (0°C) and pressure (1 bar)), ΔP is the difference in gas pressure across the membrane (Pa), δ is the thickness of the membrane (m) and A is the section of the membrane (m^2). Figure 18.10 shows that P^{m} varies markedly with both temperature and water content of the polymer membrane, in a range between the values measured for poly(tetrafluoroethylene) (PTFE) and for liquid water. From these data, it is interesting to notice that the transport of dissolved gases across Nafion® takes place mainly through ionic (hydrated) clusters. In a PEM water electrolyzer, liquid water is electrolysed. The membrane is fully hydrated and therefore, H_2 and O_2 permeabilities are significant. To estimate permeation flows, it is necessary to determine the value of diffusion coefficients. Gas permeability of species i is related to the diffusion coefficient D_i (in $cm^2\ s^{-1}$) through the relationship:

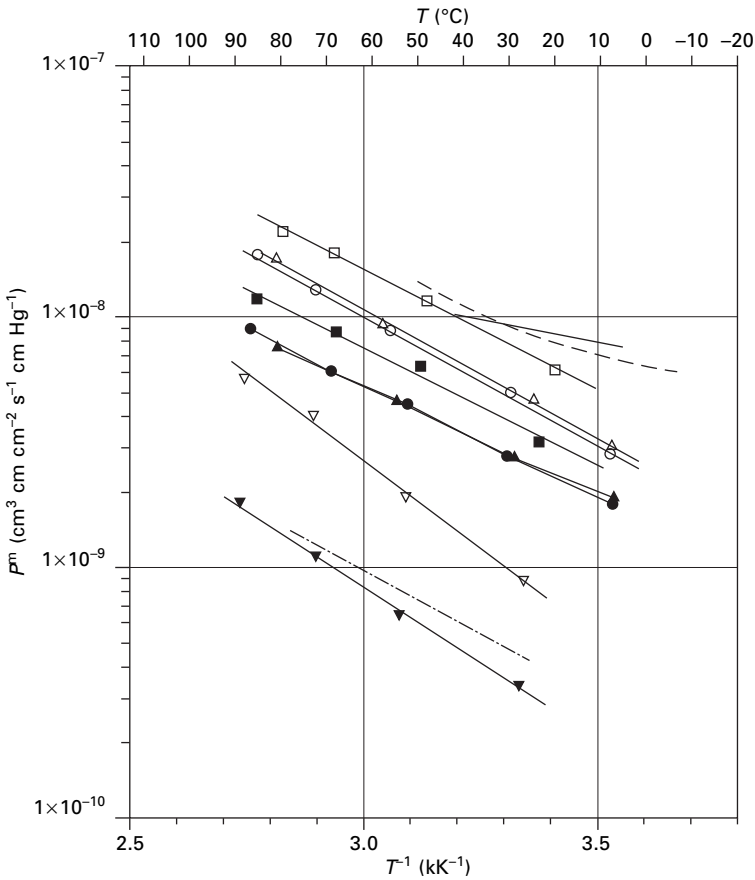
$$D_i = P_i^m\ RTC_i \qquad [18.11]$$

where R is the constant of perfect gas (82×10^5 Pa $cm^3\ K^{-1}\ mol^{-1}$), T is the temperature (K) and C_i is the concentration of species i (mol cm^{-3}). Hydrogen and oxygen diffusion coefficients in Nafion® 117 at different operating temperatures are compiled in Table 18.1. D_{H_2} is larger than D_{O_2} by about a factor of two over the conventional 0–100°C temperature range of operation.

18.4.4 Thermal conductivity

During operation in an electrolysis cell, an ionic current flows across the membrane. According to Ohm's law, energy is dissipated as heat. Therefore, the thermal conductivity of the membrane must be sufficiently high to transfer

© Woodhead Publishing Limited, 2011



18.10 Hydrogen and oxygen permeability of Nafion® 117 with temperature and water content:[23] – – –, H_2 in pure water; — O_2 in pure water. H_2 is represented by open symbols and O_2 is represented by closed symbols: □, ■ Nafion 117, 100 % H_2O; △, ▲ Nafion 117, 50 % H_2O; ○, ● Nafion 117, 34 % H_2O; ▽, ▼ dry Nafion 117; – . – ., PTFE.

Table 18.1 H_2 and O_2 permeability and diffusion coefficients in fully hydrated Nafion 117 at different temperatures

T (°C)	10	20	40	60	85
$P^m_{O_2}$ (cm^2 Pa^{-1} s^{-1})	2.1×10^{-12}	2.3×10^{-12}	3.7×10^{-12}	5.3×10^{-12}	8.4×10^{-11}
D_{O_2} (cm^2 s^{-1})	2.1×10^{-7}	2.5×10^{-7}	4.2×10^{-7}	6.5×10^{-7}	1.1×10^{-6}
$P^m_{H_2}$/(cm^2 Pa^{-1} s^{-1})	3.8×10^{-12}	4.6×10^{-12}	7.6×10^{-12}	1.2×10^{-11}	2.0×10^{-11}
D_{H_2} (cm^2 s^{-1})	3.9×10^{-7}	4.9×10^{-7}	8.7×10^{-7}	1.5×10^{-6}	2.6×10^{-6}
D_{H_2} /(D_{O_2})	1.9	2.0	2.1	2.3	2.4

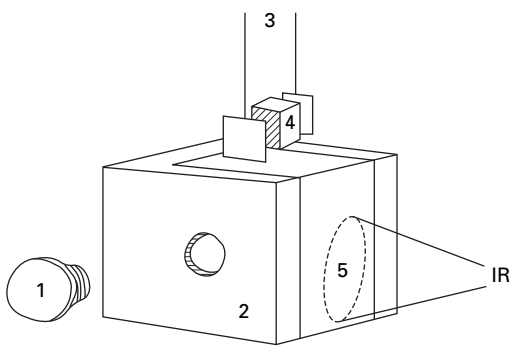
© Woodhead Publishing Limited, 2011

this heat to the surroundings (for example to the current collectors in the PEM stack) to avoid unacceptable heat peaks that could provoke irreversible damage. This is particularly significant when the cell is operating at high current density (several A cm^{-2} can be achieved in PEM water electrolysis cells). Heterogeneous temperatures provoke heterogeneous membrane swelling and membrane perforation. The thermal dissipation in an electrolysis cell can be observed experimentally using an infra red (IR) camera. This technique has been used for the characterization of PEM cells (Fig. 18.11 and 18.12).[24] The MEA (4) is clamped between two Pt electrodes (3) and inserted in a polysulfone cell (2). During water electrolysis, the IR camera (5) is used to measure thermograms from which temperature profiles can be determined and modelled (Fig. 18.12). Results indicated that the thermal conductivity of the SPE (Nafion®) is sufficient to avoid the formation of hot points during electrolysis, even at high current density (1 A cm^{-2}), but care must be taken when designing a PEM stack to introduce thermal bridges that favour heat transmission to the surroundings.

The thermal conductivity of dry Nafion® is known to vary slightly with operating temperature (Fig. 18.13): 160 ± 30 mW m^{-1} K^{-1} at room temperature and 130 ± 20 mW m^{-1} K^{-1} at 65°C. The thermal conductivity of hydrated Nafion® is a function of water content: $\lambda = 180$ mW m^{-1} K^{-1} (relative humidity, RH = 10%) and $\lambda = 300$ mW m^{-1} K^{-1} (RH = 100%).[25] Over the usual 0–100°C temperature range of operation, the thermal conductivity of Nafion® is closer to the thermal conductivity of PTFE (λ = 210–270 mW m^{-1} K^{-1})[26] than to the thermal conductivity of water (λ = 600–653 mW m^{-1} K^{-1}).

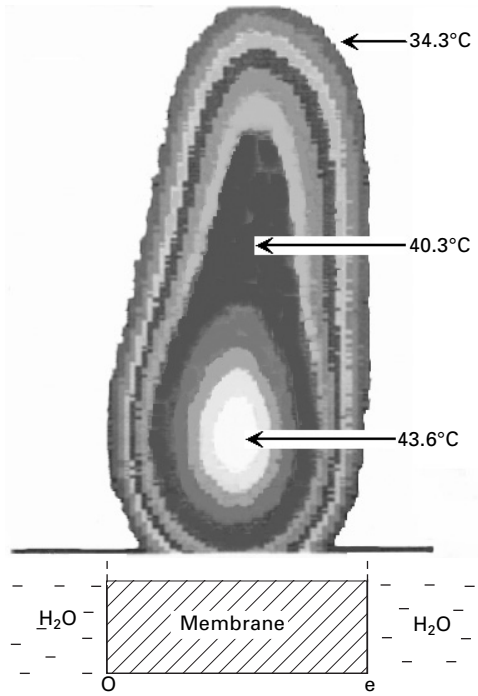
18.4.5 Mechanical properties

Tensile strength σ (Pa) is indicated by the maxima of a stress–strain curve. This is an important parameter of engineering materials. The main mechanical

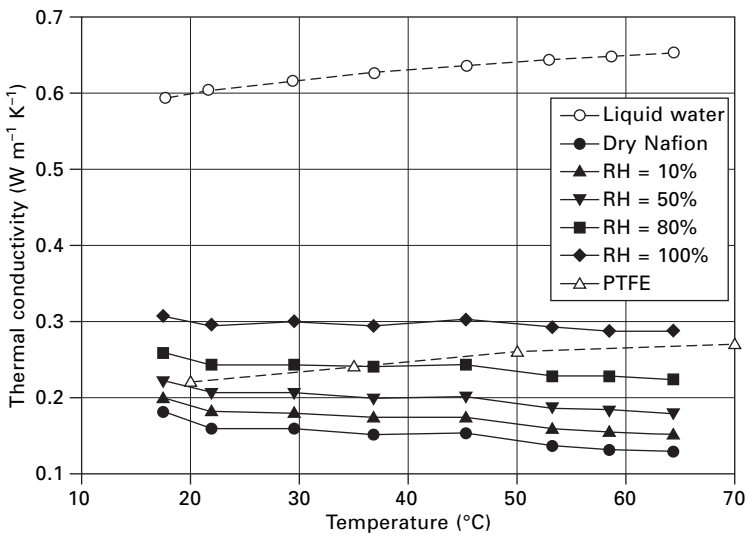


18.11 Schematic diagram of the cell used to measure temperature profiles in the PEM cell. (1) screw, (2) polysulfone cell, (3) electrodes, (4) MEA, (5) IR window.

© Woodhead Publishing Limited, 2011



18.12 Typical temperature profile measured in a 0.42 mm thick PEM cell at 0.4 A cm^{-2}.



18.13 Thermal conductivity of Nafion® (1100 EW) at different humidity ratios. The thermal conductivity variation of pure water and PTFE are shown as reference values.

© Woodhead Publishing Limited, 2011

properties of Nafion® are compiled in Table 18.2.[27] The mechanical stability of these polymer materials is sufficient to design electrolysis cells several square meters in size. The situation is somewhat different when ceramics are used as the SPE. Ceramics are brittle and their mechanical properties can be seriously damaged by thermal cycling. Improvement of these properties to meet the requirements of practical applications remains a challenging issue in material science.

18.5 Application and integration of electrolyser systems

18.5.1 Alkaline water electrolysis

Principles

In an alkaline water electrolysis cell, electricity is used to split water molecules into gaseous hydrogen and oxygen. Water splitting occurs according to the following half-cell reactions (Fig. 18.14):
anode:

$$2\ OH^- \rightarrow \tfrac{1}{2}\ O_2 + H_2O(liq) + 2\ e^- \qquad [18.12]$$

cathode:

$$2\ H_2O(liq) + 2\ e^- \rightarrow H_2(g) + 2\ OH^- \qquad [18.13]$$

full reaction:

$$H_2O(liq) \rightarrow H_2(g) + \tfrac{1}{2}\ O_2(g) \qquad [18.14]$$

Water molecules are reduced to molecular hydrogen and hydroxyl ions

Table 18.2 Main mechanical properties of Nafion® (RH : relative humidity (%); MD : machine direction; TD : transverse direction)

Physical property	RH = 50% (23°C)	Water soaked (23°C)	Water soaked (100°C)
Tensile modulus (MPa)	249 (36)	114 (16)	64 (9.4)
Maximum tensile strength (MPa)	43 (6.2) in MD, 32 (4.6) in TD	34 (4.9) in MD, 26 (3.8) in TD	25 (3.6) in MD, 24 (3.5) in TD
Elongation at break (%)	225 in MD, 310 in TD	200 in MD, 275 in TD	180 in MD, 240 in TD
Initial tear resistance (g mm^{-1})	6000 in MD, TD	3500 in MD, TD	3000 in MD, TD
Propagating tear resistance (g mm^{-1})	>100 in MD, >150 in TD	92 in MD, 104 in TD	74 in MD, 85 in TD
Electrical conductivity (S cm^{-1})			0.083
Acid capacity (meq g^{-1})	0.89	0.89	0.89

© Woodhead Publishing Limited, 2011

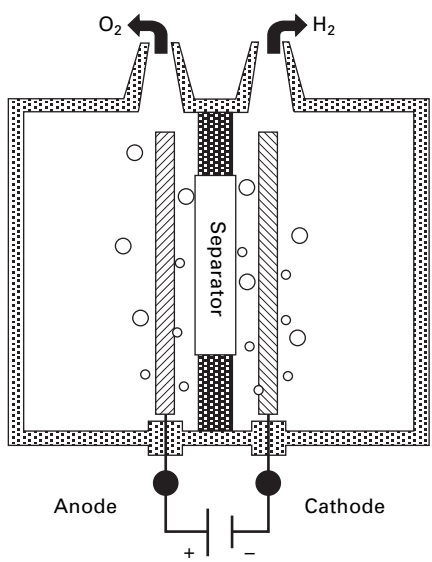
at the cathode of the alkaline cell. Solvated hydroxyl ions migrate through the electrolyte to the anode where they are oxidized into molecular oxygen (Fig. 18.14).

Performance and technological developments

In industry, hydrogen and oxygen of electrolytic grade are produced using 'zero gap' alkaline cells. As can be seen from Fig. 18.15, electrode overvoltages and electrolyte resistance both contribute to efficiency losses. A photograph of a conventional alkaline water electrolyser which can deliver 485 Nm^3 H_2 h^{-1} is provided in Fig. 18.16. In France, electrolysis units of several MW input power were used in the 1970s in space applications (production of pure hydrogen and oxygen for the cryogenic engine of Ariane launchers). These systems can operate at 120°C, at pressures up to 30 bars and at current densities of several hundred mA cm^{-2}. Large scale water electrolysis has also been (and still is) considered for the regulation of electric power production from nuclear plants.

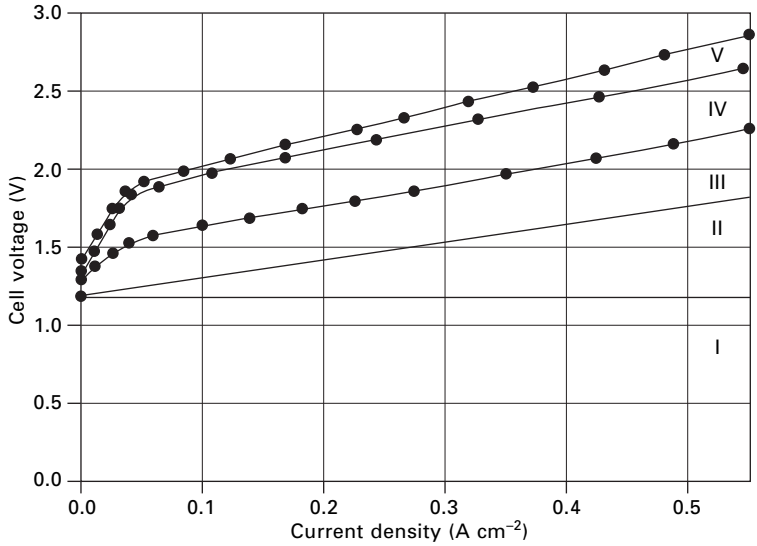
Challenges and perspectives

Two areas that have a significant impact on cell efficiency are electrocatalysts and cell membranes. Research efforts reported in the literature have been made to increase the efficiency of the water electrolysis cell by preparing



18.14 Schematic diagram of an alkaline 'gap cell' water electrolysis cell.

© Woodhead Publishing Limited, 2011



18.15 Electrochemical performance of a conventional alkaline 'membrane cell' water electrolyser at 90°C, (I) Thermodynamic voltage (1.18 V), (II) ionic ohmic drop across electrolyte, (III) anodic (O_2) overvoltage, (IV) cathodic (H_2) overvoltage, (V) electronic ohmic drop of electrodes.

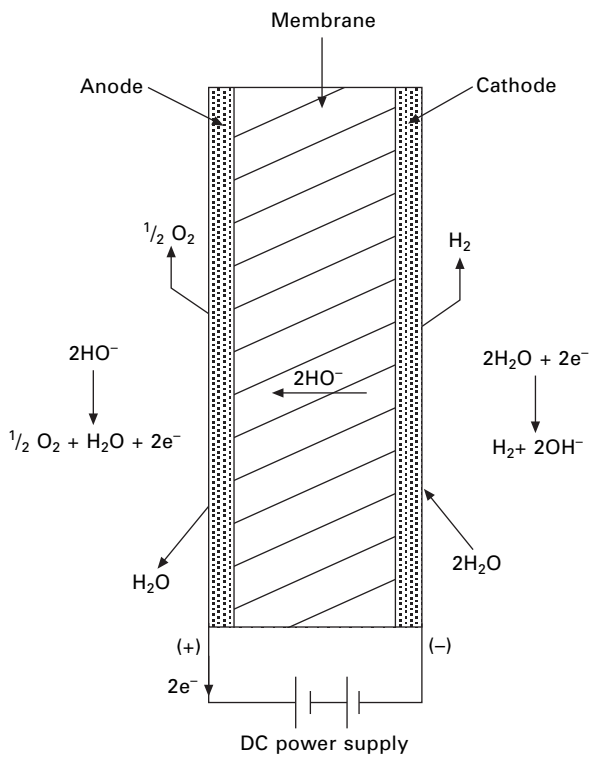


18.16 Norsk-Hydro alkaline water electrolyser operating at 5 bars (485 Nm^3 H_2 h^{-1}, 4.1 kWh Nm^{-3}). (Image courtesy Hydrogen Technologies AS, Norway).

© Woodhead Publishing Limited, 2011

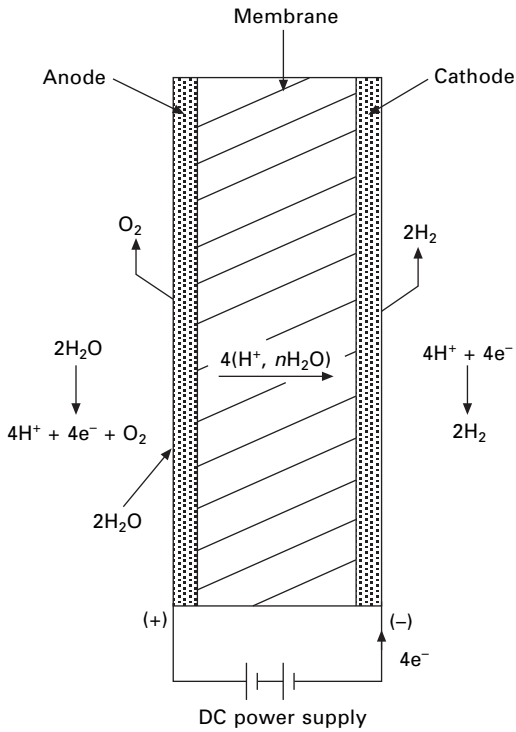
and evaluating (a) electrocatalysts based on non-precious metals (nickel, cobalt, molybdenum and others), transition metal macrocycles and (b) alkaline exchange membranes that primarily conduct hydroxyl ions in the cell electrolyte. The ultimate design of such cells is the HEM cell (using a hydroxyl-ion exchange membrane as SPE in place of a proton-conducting membrane) in which no liquid electrolyte is used (Fig. 18.17). This is a concept symmetrical to the PEM cell of Fig. 18.18. The principles of this concept have already been described in the open literature but there is little information available in terms of electrochemical performance and system development. The potential advantages of HEM cells are:

- No liquid alkaline electrolyte is used; this is beneficial for safety and maintenance issues;
- Thin SPEs are used and a reduced ohmic drop is expected, as in PEM technology;
- Possibility of using non-precious catalysts and reducing MEA cost;
- A large variety of low-cost polymers are available;
- Lower cathode sensitivity to poisoning by potential deposition of trace amounts of metals.



18.17 Schematic diagram of a HEM water electrolysis cell.

© Woodhead Publishing Limited, 2011



18.18 Schematic diagram of a PEM water electrolysis cell.

Some identified disadvantages are:

- Necessity to use perfluorinated hydroxyl-conducting SPEs to maintain chemical stability on the anodic side, thus reducing the advantage in terms of cost compared to PEM cells;
- Larger ohmic drop across the SPE than in PEM cells owing to the lower mobility of hydroxyl ions compared to protons.

18.5.2 Proton exchange membrane (PEM) water electrolysis

Principles

In a PEM water electrolysis cell, electricity is used to split water molecules into gaseous hydrogen and oxygen, according to the following half-cell reactions (Fig. 18.18):

anode:

$$H_2O(liq) \rightarrow \tfrac{1}{2}\ O_2(g) + 2\ H^+ + 2\ e^- \qquad [18.1]$$

© Woodhead Publishing Limited, 2011

cathode:

$$2\ H^+ + 2\ e^- \rightarrow H_2(g) \qquad [18.2]$$

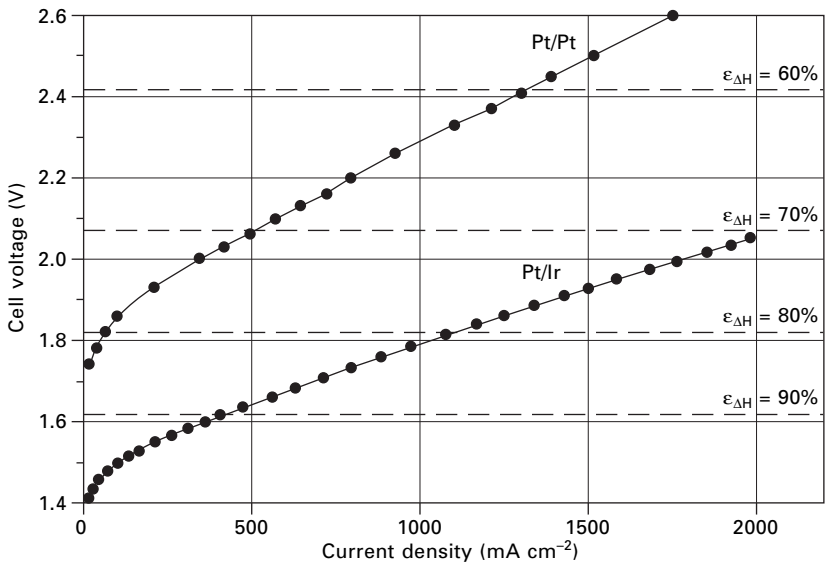
full reaction:

$$H_2O(liq) \rightarrow H_2(g) + \tfrac{1}{2}\ O_2(g) \qquad [18.3]$$

Solvated protons formed at the oxygen-evolving anode of the PEM cell migrate through the SPE membrane to the cathode where they are reduced to molecular hydrogen. Liquid water is consumed at the anode for oxygen generation but is also released at the cathode when solvated protons are reduced to hydrogen (so-called electroosmosis drag).

Performance and technological developments

Typical polarization curves are plotted in Fig. 18.19. At low current densities, cell efficiencies close to 100% are obtained. In conventional PEM water electrolysers, $\varepsilon_{\Delta H} \approx 80\%$ at 1 A cm^{-2}, $T = 90°C$ and $P = 1$ bar. The efficiency of a PEM water electrolysis cell is a critical parameter responsible for the energy cost of the process. Operation at high current density is necessary to reduce investment costs but since efficiency decreases when current density increases, a compromise has to be found between energy and investment



18.19 Typical polarization curves measured on a PEM cell using (top) Pt as anodic and cathodic catalyst; (bottom) Pt for the HER and Ir for the OER.

© Woodhead Publishing Limited, 2011

costs. Commercial systems able to deliver a few cubic metres of hydrogen per hour are currently available (Fig. 18.20).

Challenges and perspectives

State-of-art PEM water electrolysers are still penalized by a number of factors which limit the large scale dissemination of the technology to the market of electrolytic hydrogen and oxygen. The main challenges are (i) the replacement of platinum with non-noble electrocatalysts at the cathode of PEM cells, (ii) the replacement of iridium with non-noble electrocatalysts at the anode of PEM cells, and (iii) the development of new proton conducting polymers for operation at more elevated temperatures (100–150°C). Recently, low cost cobalt clathrochelates and polyoxometalates have been successfully tested in place of platinum.[28]

18.5.3 Solid oxide water electrolysis

Principles

The concept of high temperature (900–1000°C) electrolysis of water vapour originates from studies made on solid oxide fuel cells (SOFC). In the literature, it is sometimes referred to as 'solid oxide water electrolysis'. In



18.20 A PEM water electrolyser (5 Nm^3 H_2 h^{-1}) powered by a set of photovoltaic panels. (Image courtesy CETH, France).

© Woodhead Publishing Limited, 2011

a high temperature water electrolysis cell, electricity is used to split water molecules into gaseous hydrogen and oxygen, according to the following half-cell reactions (Fig. 18.21):

anode:

$$O^{2-} \rightarrow \tfrac{1}{2}\, O_2(g) + 2\, e^- \qquad [18.15]$$

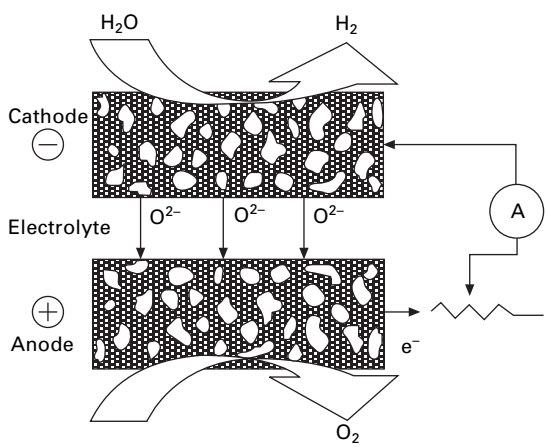
cathode:

$$H_2O(vap) + 2\, e^- \rightarrow H_2(g) + O^{2-} \qquad [18.16]$$

full reaction:

$$H_2O(vap) \rightarrow H_2(g) + \tfrac{1}{2}\, O_2(g) \qquad [18.17]$$

The electrolyte is an oxide-ion conducting ceramic, typically an yttrium-stabilized ZrO_2 membrane. Similar to PEM technology, the role of the membrane is dual: it acts as a solid electrolyte which conveys electric charges from one electrode to the other and acts as a separator to prevent the recombination of reaction products. Water vapour is introduced into the cathodic compartment. The main advantages of the high temperature operation are (i) lower electricity consumption ($\approx$ 3 kWh/Nm^3 H_2 at 900°C against $\approx$ 4 kWh/Nm^3 H_2 at 80°C) owing to a reduced ΔG and improved kinetics, (ii) reduced costs because no electrocatalyst is required at these temperatures and (iii) the technique is well-suited for the centralized production of large amounts of hydrogen, using the high temperature heat released by nuclear reactors. On the less positive side, the main drawbacks come from a reduced lifetime of the cell components owing to the high temperature of operation: material degradation (phase transformation, decreasing ionic conductivity) in relation to temperature and thermal cycling and gas tightness. The technique



18.21 Schematic diagram of a HT water electrolysis cell.

© Woodhead Publishing Limited, 2011

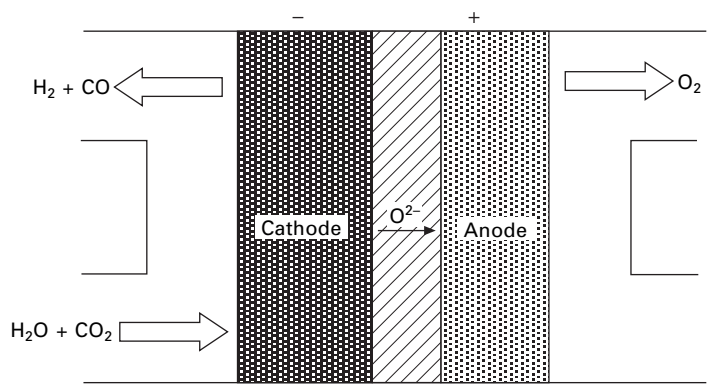
is not appropriate for intermittent operation. The same concept in a cell can also be used for the oxidation of methane (Fig. 18.21) or for the co-electrolysis of water vapour and CO_2 for the production of syngas (Fig. 18.22), opening the way to the production of synthetic fuels.

Performance and technological developments

A photograph of a prototype solid oxide water electrolysis stack is provided in Fig. 18.23. The maximum power reported in the literature for a single stack is close to 20 kW. A similar concept in a cell can be used for the co-electrolysis of water vapour and carbon dioxide.[29] Technological developments in this field are limited to the manufacturing and testing of prototypes for demonstration purposes.

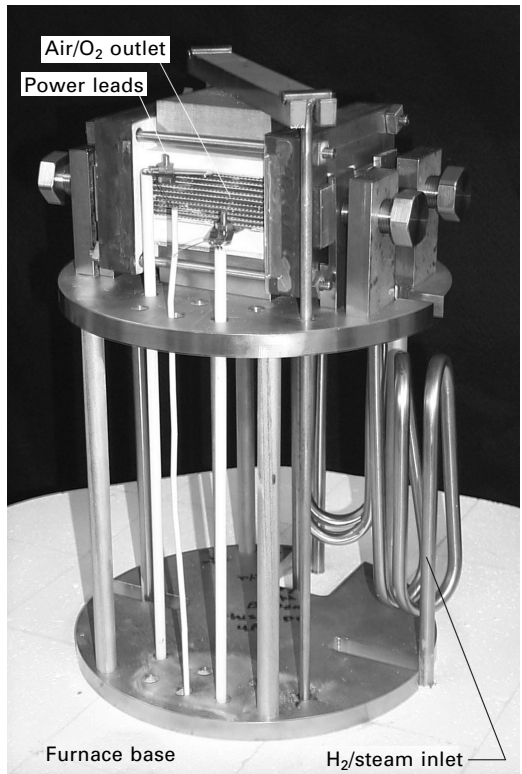
Challenges and perspectives

At these elevated temperatures, the most significant challenges concern material science (material dilatation, material stability and corrosion issues). In the current technology, material resistance to thermal gradients and thermal cycling remains rather poor and largely contributes to high investment costs. An option would be to reduce the operating temperature down to the 700–800°C range, where however the ionic conductivity of yttrium stabilized ZrO_2 is still insufficient. In this lower temperature range, catalysts are required. Some nickelates (Ruddlesden–Popper compounds) such as $Ln_{1+n}M_nO_{3n+1\pm\delta}$, where n = 1, 2 or 3, Ln = La, Nd or Pr and M is preferably Ni, are currently being investigated.[30] The chemical composition can be adjusted by performing simple or double cationic substitutions for higher anodic efficiency. Such compounds can be easily powdered and used



18.22 Schematic diagram of a cell used for the co-electrolysis of CO_2 and water vapour.

© Woodhead Publishing Limited, 2011



18.23 Prototype high temperature water electrolysis stack from CERAMATEC company (25 cells, 200 cm^2, 17 kW). (Image courtesy CERAMATEC and Idaho National Laboratory, USA).

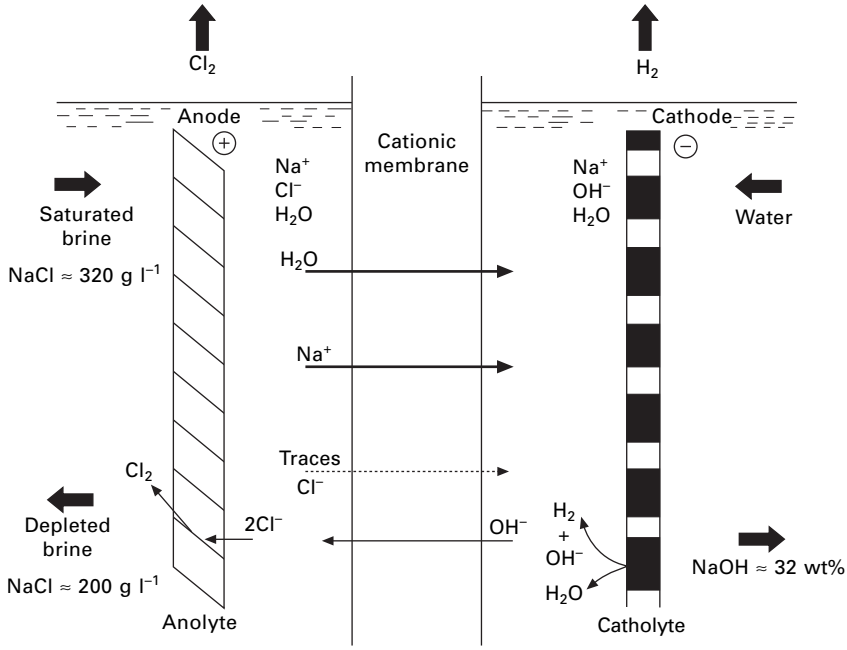
in catalytic ink compositions for the automated production of large scale and homogeneous catalytic layers.

18.5.4 Brine electrolysis

Principles

Chlorine and sodium hydroxide (caustic soda) are among the top ten chemicals produced in the world. They are involved in the manufacture of a wide variety of products used in day-to-day life, including pharmaceuticals, detergents, deodorants, disinfectants, herbicides, pesticides and plastics. In a brine electrolysis cell, electricity is used to produce chlorine at the anode and reduce water into hydrogen at the cathode. Caustic soda (sodium hydroxide) is also produced at the cathode (Fig. 18.24):

© Woodhead Publishing Limited, 2011



18.24 Schematic diagram of a brine electrolysis cell using a 'gap cell'.

anode:

$$2\ Cl^- \rightarrow Cl_2(g) + 2\ e^- \qquad [18.18]$$

cathode:

$$2\ H_2O(liq) + 2\ e^- \rightarrow H_2(g) + 2\ OH^- \qquad [18.19]$$

full reaction:

$$2\ NaCl(liq) + 2\ H_2O(liq) \rightarrow Cl_2(g) + H_2(g) + 2\ NaOH \qquad [18.20]$$

There are three types of electrolytic cells used for the production of chlorine and caustic soda. The main difference in these technologies lies in the manner by which the chlorine gas and the sodium hydroxide are prevented from mixing with each other to ensure generation of pure products. The membrane process uses a gap or zero-gap cell (Fig. 18.1). A cationic ion-exchange membrane is placed between the anode and the cathode. The transport of current across the membrane is ensured selectively by hydrated sodium ions Na^+. In most cases, the separator is a bi-layer membrane made of perfluorocarboxylic and perfluorosulfonic acid-based films, to prevent the transport of caustic soda from the cathodic to the anodic compartment.

© Woodhead Publishing Limited, 2011

Performance and technological developments

A picture of a typical production plant is provided in Fig. 18.25. The main electrochemical characteristics of brine electrolysis cells using membranes are: (i) operating current density is 300–500 mA cm^{-2}, (ii) cell voltage is 3.0–3.6 V, (iii) NaOH concentration is 33–35 wt%, (iv) energy consumption is 2650 kWh/Mt Cl_2 at 500 mA cm^{-2}, (v) efficiency is 50% and (vi) steam consumption to concentrate NaOH to 50% is 180 kWh/Mt Cl_2.

Perspectives

In the membrane process, there are separate anodic and cathodic circuits. It is therefore possible to use solid salt (sodium chloride) directly in place of saturated brine. To prevent the pollution of the membrane (mostly by calcium and magnesium cationic species) the NaCl-saturated brine is purified by addition of NaOH + Na_2CO_3 (Ca and Mg concentration are then reduced down to the 1–5 ppm range) and then filtrated using ion-exchange resins (to further reduce the Ca/Mg concentration down to the 0.02 ppm range). It is also necessary to reduce the concentration of other constituents such as Al, Fe, SiO_2, iodine, sulfates, chlorates, Ba and Sr. Under such operating conditions, the lifetime of the membranes is reported to be approximately three years. Compared to the diaphragm and mercury cells, the main advantages of the membrane process are: (i) high purity chlorine, (ii) low energy consumption and (iii) high flexibility. On the less positive side (i) a high purity brine is



18.25 Chlorine-alkali cell room with BL-2.7 membrane cells (Image courtesy of Uhde GmbH, Germany).

© Woodhead Publishing Limited, 2011

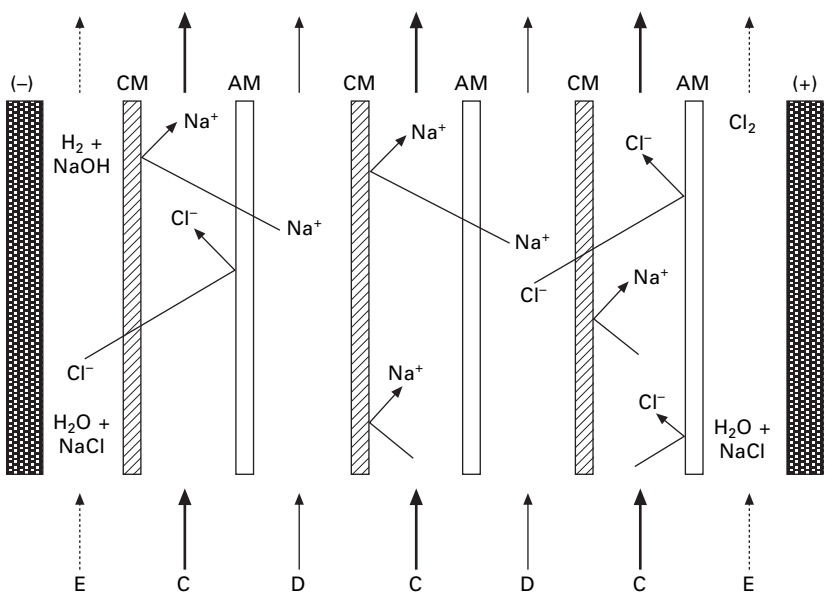
required, (ii) and membranes are very sensitive to the presence of trace amounts of poisonous chemicals and (iii) membranes are expensive.

18.5.5 Electrodialysis

Principles

In an electrodialysis cell, electricity is used to concentrate effluents. An important application is the desalination of seawater but there are many others (nitrate removal in drinking water, adjustment of pH in wine and food products, etc.). Interest in an electrodialysis cell does not come from the electrochemical reactions which are taking place at the end electrodes, but from ion-transport phenomena in the intermediate cells which lead to an increase in salt concentration in some cells. In almost all practical processes, multiple electrodialysis cells are connected in series to form an electrodialysis stack, with alternating anion (AM) and cation (CM) exchange membranes forming the multiple electrodialysis cells (Fig. 18.26).

A simple electrodialysis cell consists of (i) a feed (diluate) compartment, (ii) a concentrate (brine) compartment and (iii) an electrode compartment. The diluate (D) feed stream (from which salt is eliminated), a brine or concentrate (C) stream (where salt is concentrated) an and electrode (E) stream (where electrode processes are taking place) are allowed to flow



18.26 Schematic diagram of a electrodialysis cell.

© Woodhead Publishing Limited, 2011

through the appropriate cell compartments formed by the pair of AM and CM ion exchange membranes. When an electrical potential difference is applied between the two end-electrodes, the negatively charged ions (e.g. chloride) in the diluate stream migrate towards the positively charged anode, passing through the positively charged anion exchange membrane (AM). They are prevented from further migration toward the anode by the negatively charged cation exchange membrane (CM) and therefore stay in the C stream, which becomes concentrated with anions. The positively charged species (e.g. sodium) in the D stream migrate toward the negatively charged cathode, passing through the negatively charged cation exchange membrane. These cations also stay in the C stream, prevented from further migration toward the cathode by the positively charged anion exchange membrane. As a result of ion migration, electric current flows between the cathode and anode.

The overall result of the electrodialysis process is that the salt concentration increases in the concentrate stream with a depletion of salt in the diluate solution feed stream. The electrochemical reactions (charge transfer processes) which are taking place at the terminal electrodes of the cell stack are those of brine electrolysis:

anode:

$$2\ Cl^- \rightarrow Cl_2(g) + 2\ e^- \qquad [18.18]$$

cathode:

$$2\ H_2O(liq) + 2\ e^- \rightarrow H_2(g) + 2\ OH^- \qquad [18.19]$$

full reaction:

$$2\ H_2O(liq) + 2\ NaCl \rightarrow H_2(g) + Cl_2(g) + 2\ NaOH \qquad [18.20]$$

Alternatively, the E-streams contain different species (e.g. sodium sulfate) to prevent chlorine evolution at the anode.

Performance and technological developments

Filter-press electrodialysis stacks using several tens of individual cells can be used to produce desalinated water from sea water. The unit represented in Fig. 18.27 was developed by Eurodia Co. It contains 76 active cell pairs and is equipped with membranes that have 0.4 m^2 effective area. The cation membranes are Neosepta CMX and anion membranes are Neosepta AM1. The stack can be used with different electrodes for different applications: (i) nickel anodes and cathodes for operation with a NaOH electrode rinse solution, (ii) dimensionally stable anode (DSA) iridium coated anodes and graphite cathodes for operation with a $NaNO_3$ electrode rinse solution and (iii) DSA/ruthenium coated anodes and graphite 2 cathodes for electrode rinse solutions containing HCl. Power is supplied to the electrodialysis stack by a

© Woodhead Publishing Limited, 2011



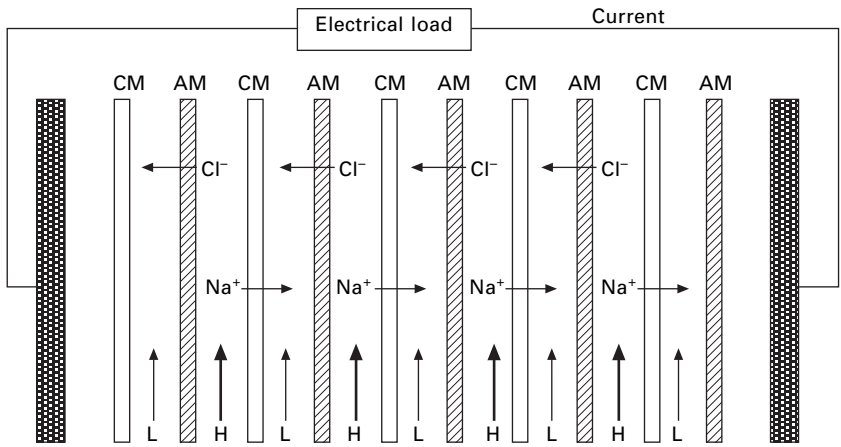
18.27 An electrodialysis pilot plant tested at Argonne National Laboratory. (Image courtesy Argonne National Laboratory, USA).

Rapid Power DC rectifier specified to provide up to 575 A and 100 V. The stack has a pressure rating of 5 bar and can be operated at current densities up to several hundred mA cm^{-2}. A problem comes from the high resistance of the diluate which increases energy consumption.

Perspectives

The extraction of the 'osmotic energy' from two salt solutions showing a large difference in salt concentration is called salinity gradient power (SGP).[31] The potential energy available is significantly high (the osmotic energy in 1 m^3 of seawater is 0.75 kWh). To exploit this energy: (a) pressure retarded osmosis and (b) reverse electrodialysis have been suggested in the literature. In reverse electrodialysis, cation and anion conductive membranes are placed in an alternating way in order to produce dilute and concentrate compartments as illustrated in Fig. 18.28. The combination of a cation conductive membrane, an anion conductive membrane and the two corresponding compartments form a cell pair. The concentrate compartment (HIGH) is then filled with the high concentration salt solution while the dilute compartment (LOW) is filled with the low concentration salt solution. The salt concentration difference (salt gradient) between both compartments in the cell pair invokes a Nernst potential across the cell pair which causes an electrical current to

© Woodhead Publishing Limited, 2011



18.28 Principle of reverse electrodialysis. H : high salt concentration, L : low salt concentration, CM : cationic membrane, AM : anionic membrane.

flow through the electrical load connected to the electrodes. The electrical resistance within the LOW compartment when filled with fresh water (typical conductivity < 0.05 S m^{-1}) is high when compared to the HIGH compartment filled with seawater (typical conductivity of 4.8 S m^{-1}). As a result the LOW compartment with the fresh water completely dictates the overall resistance of the cell pair. The situation can be improved by using seawater as a dilute source and concentrated brine as a concentrated source. Then, it can be estimated that 18.8 MJ can be extracted from each m^3 of brine.[32] Considerable progress has been achieved during the past years. According to Veerman *et al.*,[33] a power density of 1.2 W m^{-2} has been demonstrated. Although it has been concluded that the main limiting factor in the power density is the cell resistance, membrane properties and degradation issues still require research and development (R&D) to improve the system efficiency.

18.6 Some advantages and limitations of current membrane materials

18.6.1 Polymeric proton conductors

Perfluorinated ion-exchange polymers used as SPE in state-of-the-art PEM technology have adequate physical properties. Their main drawback is increased cost (partly due to manpower costs resulting from the fluorination step) which may be prohibitive for large scale dissemination of the technology. Another disadvantage comes from gas solubility and associated cross-permeation effects which become critical when the electrochemical cell is operating at elevated gas pressures (for example pressurized PEM water electrolysis,

© Woodhead Publishing Limited, 2011

when the storage of pressurized hydrogen and oxygen is required). In such cases, cross-permeation effects are such that the hydrogen content in the oxygen produced at the anode of a PEM cell is not zero and conversely, the oxygen content in the hydrogen produced at the cathode is also not zero. This is due to the fact that H_2 and O_2 solubility and mobility in perfluorinated membranes, although small, have finite values. The driving force for the transfer of dissolved gases from one side of the cell to the other is the gradient of chemical potential set across the SPE during operation, resulting from the gradient of pressure (concentration). The mass transport mechanism is mostly diffusion controlled (convection has also been reported but found to be less significant since the size of ionic clusters in the SPE is very small, as shown in Fig. 18.5). The most striking point concerning cross-permeation phenomena in PEM cells is that dissolved gases which diffuse across the SPE membrane can be released across the porous electrodes without being totally reoxidized (hydrogen at the anode) or reduced (oxygen at the cathode). In fact, these gases are partly consumed at the electrodes and this is the reason why the faradic yield at each interface is less than unity. But it should be kept in mind that they are dissolved in liquid water and the kinetics of oxidation (H_2) or reduction (O_2) is much lower than in the gas phase (as in fuel cells). As a result, a significant quantity of these gases can come across the porous electrodes and can be released in the opposite compartment of the PEM cell, thus polluting the gaseous production.

There are different reports available in the literature on gas (H_2 and O_2) solubility in Nafion® materials.[34,35] The quantitative relationship between gas concentration in the polymer and partial pressure in the gas phase is approached by Henry's Law:

$$P_i = H_i C_i \qquad [18.21]$$

where P_i is the partial pressure of gas in the gas phase (Pa) (the partial pressure of water vapour must be taken into account in the calculations), H_i is the solubility coefficient (Henry's constant) of species i (mol cm^{-3} Pa^{-1}) and C_i is the concentration of species i (mol cm^{-3}). Henry's Law constants for H_2 and O_2 are mainly a function of equivalent weight (EW) of the polymer, water content, temperature and pressure. Gas solubility values in water can be taken, as a first approximation, for gas solubility in Nafion®. For H_2, the following relations can be used in the 0–100°C temperature range and the 1–10 atm pressure range:[36]

For $0°C < T < 45°C$:

$$H_{H_2}^{H_2O} = 7.9 \times 10^6 \exp(-545/T) \times (1 + 0.000\,071\, P_{H_2}^3) \quad (\text{atm mol}^{-1}\ \text{cm}^3) \qquad [18.22]$$

© Woodhead Publishing Limited, 2011

For 45°C < T < 100°C:

$$H_{H_2}^{H_2O} = 8.3 \times 10^5 \exp(-170/T) \times (1 + 0.000\,071\, P_{H_2}^3) \quad (\text{atm mol}^{-1}\ \text{cm}^3) \quad [18.23]$$

For O_2, the following relations can be used in the 0–100°C temperature range, at 1 atm:

For 0°C < T < 45°C:

$$H_{O_2}^{H_2O} = 1.3 \times 10^8 \exp(-1540/T)\ (\text{atm mol}^{-1}\ \text{cm}^3) \quad [18.24]$$

For 45°C < T < 100°C:

$$H_{O_2}^{H_2O} = 5.1 \times 10^6 \exp(-500/T)\ (\text{atm mol}^{-1}\ \text{cm}^3) \quad [18.25]$$

A model of cross-permeation phenomena has been proposed by Fateev *et al.*[37] The H_2 content in O_2 (at constant temperature and pressure) is inversely proportional to current density. Experiments show that this is not exactly the case, in particular at low current densities (Fig. 18.29).

This is due to the faradic efficiency at the anode, which for a given PEM cell, is a function of current density, temperature and pressure. As can be seen from Fig. 18.29 (curves (a) and (b) at 2 and 30 bars are reported, whereas results at intermediate pressures are not plotted), the efficiency decreases significantly at low current densities. By taking into account experimental values of current efficiencies (also plotted in Fig. 18.29), it is possible to obtain a reasonable fit to the experimental values of H_2 concentration in O_2 (Fig. 18.29, full lines).

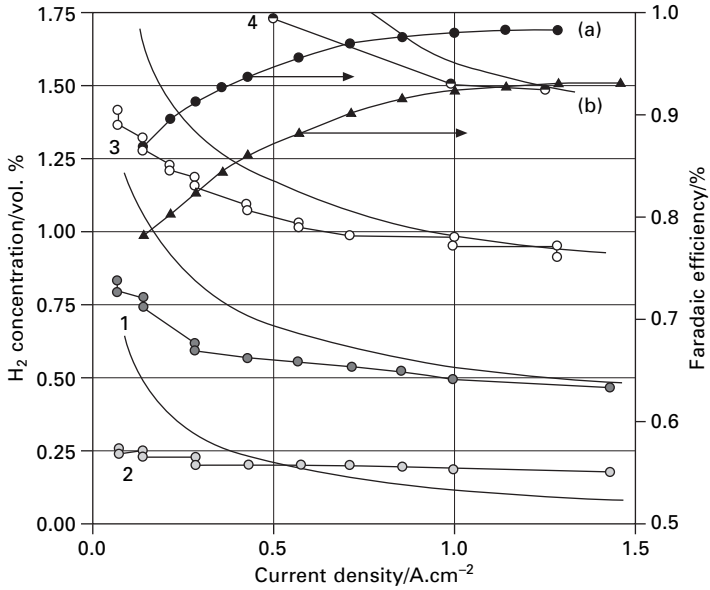
18.6.2 Polymeric hydroxyl-ion conductors

Potentially, some of the polymers used as alkaline anion-exchange membranes in fuel cell technology can also be used as solid polymer electrolyte for water electrolysis applications. The main expected benefits are: (1) enhanced electro-kinetics: (ii) significant cost reduction with the potential use of non-noble metal catalysts; (iii) lower sensitivity of catalysts to trace amounts of cations and the possibility of electrolysing less-purified water than in PEM technology. R&D on such issues is still in progress, with only proof-of-concept available. Critical issues include chemical stability at the anode with a high potential value under oxygen evolution.

18.6.3 Oxide-ions conductors

Among the different properties, the ionic conductivity of the membrane material used as oxide-ion conductor for solid oxide water electrolysis is a

© Woodhead Publishing Limited, 2011



18.29 (Left) hydrogen content (vol%) in the anodic oxygen–water vapour mixture, measured at different pressures as a function of operating current density: 50 cm^2 mono-cell; Pt for the hydrogen evolution reaction, Ir for the oxygen evolution reaction and Nafion 117 as SPE, T = 85°C. (1) 1 bar (current collector is platinized); (2) 1 bar (current collector not platinized); (3) 6 bar (current collector is platinized); (4) 30 bar (current collector is platinized); full lines are model curves from Fateev *et al.*[37] (Right) current efficiency at the cathode at (a) 2 bar and (b) 30 bar, as a function of operating current density.

critical parameter. Energy cost requirements are such that a specific resistivity of 0.1–0.2 $\Omega\,cm^2$ is required for practical applications. The ionic conductivity of yttria-stabilized zirconia (YSZ) is such that, for a self-supported membrane (thickness ≈ 150 μm), an operating temperature greater than 950°C is required to reach the target resistivity value. In conventional technology,[38] a thin (30–40 mm thick) layer of YSZ is coated onto a porous tubular cathode of lanthanum strontium manganite (LSM). Conventional ceramic routes, such as the deposition of YSR powders and subsequent sintering, are constrained by the need to restrict temperatures to less than 1250°C, to avoid reaction between LSM and YSZ. An electrochemical vapour deposition process can be used alternatively but cost considerations require cheaper fabrication routes. Alternative oxide-ion conductors such as $Ce_{0.9}Gd_{0.1}O_{1.95}$ or $Bi_2V_{0.9}Cu_{0.1}O_{5.35}$ (Fig. 18.9) have been identified as promising materials to replace YSR.

© Woodhead Publishing Limited, 2011

18.7 Future trends

Most R&D activities are aimed at developing new materials for operation over extended temperature ranges.

18.7.1 High temperature polymeric proton conductors

Research in solid polymer electrolyte technology is driven by potential applications in the H_2/O_2 fuel cell technology for automotive applications. Since most of the energy delivered by such fuel cells is released as heat, operation at conventional (80–90°C) temperatures requires a larger heat exchanger compared to those used in internal combustion engine-driven cars. An operating temperature close to 150°C would be more appropriate. A lot of R&D activity is currently underway in the European Community to find alternative and less expensive materials. For example, different perfluorinated polymers (Hyflon® from Solvay Solexis Co.), stable at these temperatures, offer interesting new perspectives.

18.7.2 Low water-content polymeric proton conductors

An additional problem in fuel cell technology comes from water management issues. Feed gases must be appropriately hydrated and the water produced at the cathode from the reduction of oxygen must be removed to avoid condensation and loss of performance. These problems are critical and a new trend in research is to develop new polymers involving new proton conduction mechanisms and operating in quasi dry conditions. It is expected that the results of all this research will also benefit PEM water electrolysis, bringing to the market new polymer materials for operation at higher temperatures.

18.7.3 New oxide-ion conducting ceramics

The development of alternative oxide-ion conducting ceramics suitable for application in solid oxide electrochemical technology remains a challenging task. Reports on Sr- and Mg- doped $LaGaO_3$ perovskite as an alternative electrolyte to YSZ can be found in the literature.[39] However, so far, little progress has been made and material issues remain critical in developing of more efficient technologies.

18.8 Sources of further information and advice

Faraday M (1834), Experimental researches in electricity, *The London and Edinburgh Philosophical Magazine and Journal of Science*, **5**, 27.

Bockris J O'M and Reddy A A K (1982) *Comprehensive Treatise of Electrochemistry*, Plenum Press, New York.

© Woodhead Publishing Limited, 2011

Hamann C H, Hamnett A and Vielstich W (1998), *Electrochemistry*, Wiley-VCH, Weinheim, Germany.

Mauritz K A and Moore R B, (2004) 'State of understanding of Nafion', *Chemical Reviews*, **104**, 4535–85.

18.9 References

1 *Encyclopedia Britannica*, 2010 Edition.

2 Ehl R G and Ihde A (1954), 'Faraday's electrochemical laws and the determination of equivalent weights', *Journal of Chemical Education*, **31**(May), 226–32.

3 Goodridge F and Scott K (1995), *Electrochemical Process Engineering: A Guide to the Design of Electrolytic Plant*, Plenum Publishing Corporation, New York.

4 Wendt H and Kreysa G (1999), *Electrochemical Engineering: Science and Technology in Chemical and Other Industries*, Springer, Germany

5 Divisek J and Murgen J (1983), *Diaphragms for Alkaline Water Electrolysis and Method for Production of the Same as Well as Utilization Thereof'*, United States Patent 4394244.

6 Gierke T D, Munn G E and Wilson F C (1981), 'The morphology in Nafion perfluorinated membrane products, as determined by wide and small-angle X-ray studies', *Journal of Polymer Science B: Polymers Physics*, **19**(11), 1687–704.

7 Yeager H L and Steck A (1981), 'Cation and water diffusion in Nafion ionexchange membranes: influence of polymer structure', *Journal Electrochemical Society*, **128**, 1880–4.

8 Piana M, Boccia M, Filpi A, Flammia E, Miller H, Orsini M, Salusti F, Santiccioli S, Ciardelli F and Pucci A (2010), 'H_2/air alkaline membrane fuel cell performance and durability using novel ionomer and non platinum group metal cathode catalyst', *Journal Power Sources*, **195**, 5875–81.

9 Varcoe J R and Slade R C T (2005), 'Prospects for alkaline anion-exchange membranes in low temperature fuel cells', *Fuel Cells*, **5**, 187–200.

10 Wang Y, Li L, Hu L, Zhuang L, Lu J and Xu B (2003), 'A feasibility analysis for alkaline membrane direct methanol fuel cell: thermodynamic disadvantages versus kinetic advantages', *Electrochemistry Communications*, **5**, 662–6.

11 Varcoe J R, Slade R C T and How Yee E L (2006), 'An alkaline polymer electrochemical interface: a breakthrough in application of alkaline anion-exchange membranes in fuel cells', *Chemical Communications*, **13**, 1428.

12 Sandra S (1989), *Proton Conductors in Superionic Solids and Solid Electrolytes*, A Laskar and S Chandra (eds), Academic Press, London 185–226.

13 Iwahara H (1992), *Proton Conductors*, *Solids*, *Membranes and Gels*, *Materials and Devices*, P. Colomban (ed), Chapter 8, Cambridge University Press, Cambridge, 122–137.

14 Sata N (1999), 'Proton conduction in mixed perovskite-type oxides' *Solid State Ionics*, **125**, 383–7.

15 Tsampas M N, Pikos A, Brosda S, Katsaounis A and Vayenas C G (2006), 'The effect of membrane thickness on the conductivity of Nafion', *Electrochimica Acta*, **51**(13), 2743–55.

16 Solier J D, Cachadina I and Dominguez-Rodriguez A (1993), 'Ionic conductivity of ZrO_2-12 mol % Y_2O_3 single crystals', *Physical Review B*, *Condensed Matter*, **48**(6), 3704–12.

© Woodhead Publishing Limited, 2011

17 Steele B C H and Heinzel A (2001), 'Materials for fuel cell technology', *Nature*, **414**, 345–352.
18 Nimat R K, Joshi R S and Pawar S H (2007), 'Temperature dependent conductivity and dielectric properties of $Bi_2V_{0.9}Cu_{0.1}O_{5.35}$ solid electrolyte thin films', *Materials Science and Engineering B*, **137**, 93–8.
19 Cheng J G, Zha S W, Jia H, Liu X Q and Meng G Y (2003), 'Sintering behavior and electrical conductivity of $Ce_{0.9}Gd_{0.1}O_{1.95}$ powder prepared by the gel-casting process', *Materials Chemistry and Physics*, **78**, 791–5.
20 Yamaji K, Horita T, Ishikawa M, Sakai, N and Yokokawa H (1998), 'Compatibility of $La_{0.9}Sr_{0.1}Ga_{0.8}Mg_{0.2}O_{2.85}$ as the electrolyte for SOFCs', *Solid State Ionics*, **108**, 436–42.
21 Colomer M T and Jurado J R (2002), 'Structure, microstructure, and mixed conduction of $[ZrO_2)_{0.92}(Y_2O_3)_{0.08}]_{0.9}(TiO_2)_{0.1}$', *Journal of Solid State Chemistry*, **165**, 79–88.
22 *IUPAC Compendium of Chemical Terminology* (1993), **65**, 856.
23 Sakai T, Takenaka H, Wakabayashi N, Kawami Y and Torikai E (1985), 'Gas permeation properties of solid polymer electrolyte (SPE) membranes,' *Journal Electrochemical Society*, **132**, 1328–32.
24 Millet P (1990), 'Water electrolysis using EME technology: temperature profile inside a Nafion membrane during electrolysis', *Electrochimica Acta*, **36**, 263–7.
25 Khandelwal M and Mench M M (2006), 'Direct measurement of through-plane thermal conductivity and contact resistance in fuel cell materials', *Journal of Power Sources*, **161**, 1106–15.
26 Price D C and Jarratt M (2000), 'Thermal conductivity of PTFE and PTFE composites', *Proceedings of the 28th Conference of the North-American Thermal Analysis Society*, October 4-6, Orlando, Florida.
27 *DuPont, Nafion® PFSA Membranes N-112, NE-1135, N-115, N-117, NE-1110, Perfluorosulfonic Acid Polymer*, Nafion® commercial leaflet, November 2002.
28 Millet P, Ngameni R, Grigoriev S.A., Mbemba N., Brisset F, Ranjbari A and Etiévant C (2010), 'PEM water electrolyzers: from electrocatalysis to stack development', *International Journal of Hydrogen Energy*, **35**, 5043–52.
29 Stoots C, O'Brien J E, Hawkes G L, Herring J S and Hartvigsen J J (2006), 'High temperature steam and carbon dioxide electrolysis at INL', *Workshop on High Temperature Electrolysis,* Roskilde, Denmark, September 18–19.
30 Stevens P, Bassat J-M, Mauvy F, Grenier J-C and Lalanne C (2006), *Matériaux d'Anode pour SOEC*, Brevet EDF/CNRS WO 2006/008390.
31 Pattle R E (1954), 'Production of electric power by mixing fresh and salt water in the hydroelectric pile', *Nature*, **174**, 660.
32 Brauns E (2010), 'An alternative hybrid concept combining seawater desalination, solar energy and reverse electrodialysis for a sustainable production of sweet water and electrical energy', *Desalination and Water Treatment*, **13**, 53–62.
33 Veerman J, de Jong R M, Saakes M, Metz S J and Harmsen G J (2009), 'Reverse electrodialysis: Comparison of six commercial membrane pairs on the thermodynamic efficiency and power density', *Journal of Membrane Science*, **343**, 7–15.
34 Ogumi Z, Takehara Z and Yoshizawa S (1984), 'Gas permeation in SPE method', *Journal Electrochemical Society*, **131**, 769–73.
35 Sakai T, Takenaka H and Torikai E (1986), 'Gas diffusion in the dry and hydrated Nafion', *Journal Electrochemical Society*, **133**, 88–92.
36 Mann R E, Amphlett J C, Peppley B A and Thurgood C P (2006), 'Henry's law

© Woodhead Publishing Limited, 2011

and the solubilities of reactant gases in the modeling of PEM fuel cells', *Journal of Power Sources*, **161**, 768–74.
37 Fateev V, Grigoriev S, Millet P, Korobtsev S, Porembskiy V and Auprêtre F (2010), 'High pressure PEM water electrolysis and corresponding safety issues', *International Journal of Hydrogen Energy*, **36**, 2721–8.
38 Minh NQ and Takahashi T (1995), *Science and Technology of Ceramic Fuel Cells*, Elsevier, Amsterdam.
39 Huang K, Wan J and Goodenough JB (2001), 'Oxide-ion conducting ceramics for solid oxide fuel cells', *Journal of Materials Science*, **36**, 1093–8.

18.10 Appendix: nomenclature

18.10.1 Symbols

A	Membrane area (m^2)
C_i	Concentration of species i (mol m^{-3})
D_i	Diffusion coefficient of species i (m^2 s^{-1})
E	Thermodynamic electrolysis voltage (V)
F	Faraday constant (96 485 C mol^{-1})
G	Gibbs free energy (J mol^{-1})
H	Enthalpy (J mol^{-1})
H_i	Henry's constant of gas solubility (mol cm^{-3} Pa^{-1})
I	Current (A)
i	Current density (A cm^{-2})
J_i	i component flux through the membrane (mol m^{-2} s^{-1})
n	Number of electrons exchanged during the electrochemical reaction
P	Pressure (Pa)
P_i	Partial pressure of component i in a gas mixture (Pa)
P^m	Membrane permselectivity (m^2 Pa^{-1} s^{-1})
R	Resistance (Ω)
r	Specific resistance (Ω m^2)
R_{PG}	Perfect gas constant (0.082 J K^{-1} mol^{-1})
S	Entropy (J mol^{-1} K^{-1})
t	Time (s)
T	Absolute temperature (K)
U_{cell}	Cell voltage (V)
u	Rate of gas permeation (m^3 s^{-1})
V	Thermo-neutral electrolysis voltage (V)
W	Electrical work (J)

18.10.2 Greek symbols

δ	Membrane thickness (m)

© Woodhead Publishing Limited, 2011

Δ	Difference
ε	Cell efficiency (%)
η	Overvoltage (V)
λ	Thermal conductivity (W m^{-1} K^{-1})
ρ	Electrical resistivity (Ω m)
σ	Tensile strength (Pa)
σ	Electrical conductivity (S m^{-1})

18.10.3 Subscripts or superscripts

$^\circ$	Standard conditions (298 K, 1 bar)
cell	Electrolysis cell
d	Dissociation
e	Electrolyte
i	Species *i*
r	Real
t	Theoretical

© Woodhead Publishing Limited, 2011

19

Biomimetic membrane reactors for hydrogen (H_2) production

S. BENSAID and G. SARACCO,
Politecnico di Torino, Italy

Abstract: This chapter addresses the theoretical background and technical challenges behind the direct production of hydrogen via photo-splitting of water in biomimetic devices. Natural systems for water splitting via natural sunlight (photosystem II) and for hydrogen synthesis (hydrogenase enzymes), as well as artificial molecules obtained to mimic the properties of natural ones, are reviewed and discussed. Given the properties of these systems, a theoretical efficiency of 10% was estimated based on the thermodynamics of a fully optimized system in terms of materials and engineering design. Finally, the main advances in theoretical knowledge and engineering research required to assemble these functionalities into a solar-to-fuel device, which may compete with photovoltaic cells, are presented.

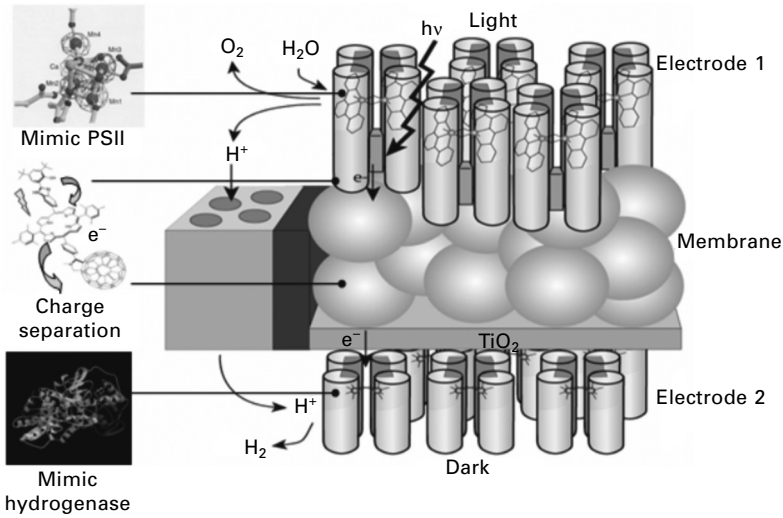
Key words: artificial leaf, biomimetic systems, hydrogen production, photosynthesis, solar-to-fuel conversion, water photo-splitting.

19.1 Introduction

Leaves and algae can split water into oxygen and hydrogen (in the form of reducing equivalents) under ambient conditions that exploit sunlight. Photosystem II is the enzyme that governs this process. In photosynthesis, the reducing equivalents derived from H_2O splitting are used to reduce CO_2 giving rise to the various organic compounds of living organisms, including those which provide fuel (biomass, sugars, vegetable oils), as well as being the origin of the fossil fuels. However, in certain types of photosynthetic organisms and under some conditions, a specific enzyme, hydrogenase, can bypass the CO_2 fixation process and can lead to non-negligible H_2 formation. Drawing inspiration from this biological background, an artificial or biomimetic device (see Fig. 19.1) capable of splitting water to produce hydrogen at ambient temperature can be devised. It is composed of:

- **an anode** exposed to sunlight carrying photosystem II (PSII) or a PSII-like chemical mimic. PSII from microalgae known as cyanobacteria might indeed be isolated by high water splitting activity and immobilized for attachment to the electrically conducting membrane. In this way the generation of electrons and protons from water at the anodic surface

© Woodhead Publishing Limited, 2011

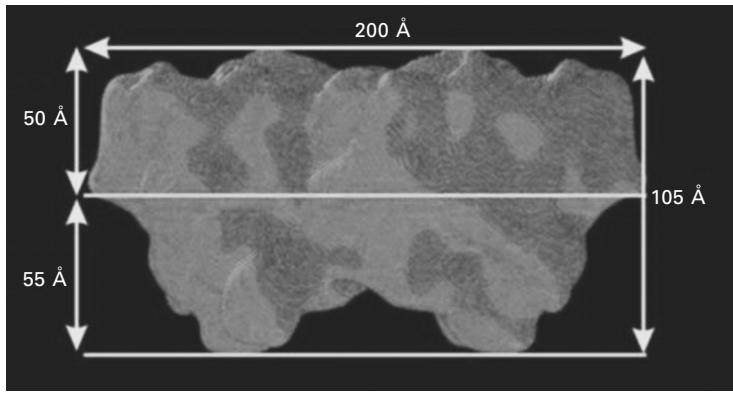


19.1 Scheme of the biomimetic H_2-production device concept, based on the original idea by Dutton and Moser (personal communication).

will use a natural light harvesting system, charge separation machinery and the water oxidation site of PSII. Synthetic metal clusters which can bring about light-driven directional charge separation are most likely to be exploited, thus mimicking the natural photosynthetic reaction centre and using the oxidizing potential of the 'hole' to split water on a specifically tailored electrochemically active catalyst. The main reasons for preferring a mimic are linked to the short lifetime of the PSII enzyme, which cannot withstand more than about 20 water splitting cycles, thereby requiring complex recovery processes, and the size of the PSII enzyme itself (Fig. 19.2), which is simply too large to achieve sufficient solar energy conversion into hydrogen per unit illuminated surface (as discussed later).

- **a cathode** carrying a hydrogenase or an artificial hydrogenase catalyst in order to recombine protons and electrons into molecular hydrogen. Here again, initial studies involve immobilizing the natural enzymes, including those with low sensitivity to oxygen. Also, as for the water splitting site on the anodic side of the membrane, the longer term goal will be to synthesize a catalytic site which mimics hydrogenase activity in order to produce hydrogen gas.
- **a membrane** enabling transport of both electrons and protons via, for example, carbon nanotubes or TiO_2 connecting the two electrodes and ion-exchange resins, like Nafion or sulfonated polyether ether ketone (SPEEK), respectively.

© Woodhead Publishing Limited, 2011



19.2 PSII dimeric core of *T. elongates* (side view) (J. Duncan, J. Nield and J. Barber, unpublished).

The membrane should be tailored to provide the minimum transfer resistance to protons and electrons thus achieving maximum conversion efficiencies, as well as hampering oxygen permeation in order to preserve hydrogen synthesis activity at the cathode. Nafion can indeed play a role both as an enzyme immobilization medium over electrode materials and as a solvated proton conductor (similar to proton exchange membrane (PEM) fuel cells). This will offer a wonderful opportunity to design a system that can readily catch the protons where they are generated and drive them by diffusion towards the cathodic electrode where H_2 is formed, owing to the injection of excited electrons derived from the chlorophyll/dye dependent photoactivated water splitting reaction.

The main technical and scientific objectives of this challenging and ever growing research field are:

- development of an innovative device capable of using sunlight to produce hydrogen from water splitting in the most cost-effective way, with routes based on photovoltaics coupled with electrochemically driven catalysis. An ambitious efficiency target is 10% conversion of solar energy into pure hydrogen, which will be proved to be feasible in Section 19.4, where a comparison with alternative intensive micro-algal growth systems, aimed at producing hydrogen or vegetable oils as fuels, is made;
- the device must be robust with long operational times. Ideally, the same duration of photovoltaics must be targeted;
- to disclose wide potential application opportunities, the above targets must be reached without using expensive noble metals or materials. They should use assembling techniques that are amenable for mass production.

© Woodhead Publishing Limited, 2011

In the following, the authors will demonstrate that a sort of artificial leaf, mimicking nature to produce hydrogen effectively from solar light and water, has indeed a great potential and possibly can be developed in the near future.

19.2 General background to the concept

At Imperial College London, the molecular details of the catalytic site where water splitting occurs in photosynthetic organisms were recently revealed by Prof. J. Barber. This discovery led to the award of the 2005 Italgas Prize, the 2006 Novartis Medal and Prize and the 2007 Wheland Medal and Prize. The water splitting site is located in the so-called photosystem II (PSII) enzyme and is composed of four manganese atoms (Mn) and a calcium ion (Ca^{2+}) surrounded by a highly conserved protein matrix. Professor Barber has published a large number of papers about PSII (Barber, 2006; Ferreira *et al.*, 2004; Bibby *et al.*, 2003; Barbato *et al.*, 1995).

A great deal is being learnt about how the hydrogenase enzymes, either the iron–nickel (Fe-Ni) or all iron (Fe-Fe) types, catalyse the production of molecular hydrogen from energized electrons and protons like those produced by the splitting of water by PSII (King *et al.*, 2006; Vincent *et al.*, 2005). This new information provides a framework on which could be elucidated the unique chemistry that underpins Nature's solution to energy problems and provides mankind with a new avenue to explore for generating hydrogen as a fuel. In depth knowledge of enzyme stabilization (Fantuzzi *et al.*, 2006, 2004) and surface functionalization (Fiorilli *et al.*, 2007; Geobaldo *et al.*, 2004) will also be vital for cathode development. Appropriate references can also be listed for the developments required in membranes (Saracco, 1997; Saracco and Specchia, 1994; Sgroi *et al.*, 2007; Icardi *et al.*, 2008; Parcero *et al.*, 2006; Roeder *et al.*, 2005, 2006) carbon nanotubes (Parcero *et al.*, 2006; Roeder *et al.*, 2006; Porro *et al.*, 2007) and semi-conductor performance and stability (Abdelkrim *et al.*, 2007), such as porous TiO_2 (Grätzel, 2005; Hinsch *et al.*, 2001; Vlachopoulos *et al.*, 1988).

Finally, the possibility of mimicking the light-driven water splitting reaction is being actively pursued particularly by groups in the USA like those of Nocera at MIT (Betley *et al.*, 2008), Myers at North Carolina (Liu *et al.*, 2008), Brudvig/Crabtree at Yale (Limberg *et al.*, 1999), Dismukes at Princeton (Wu *et al.*, 2006) as well as the artificial photosynthesis group of Hammarström and Styring in Uppsala University in Sweden (Hammarström and Styring, 2008).

© Woodhead Publishing Limited, 2011

19.3 An ambitious goal with numerous challenges

19.3.1 Challenge of electron transfer to and from the electrodes

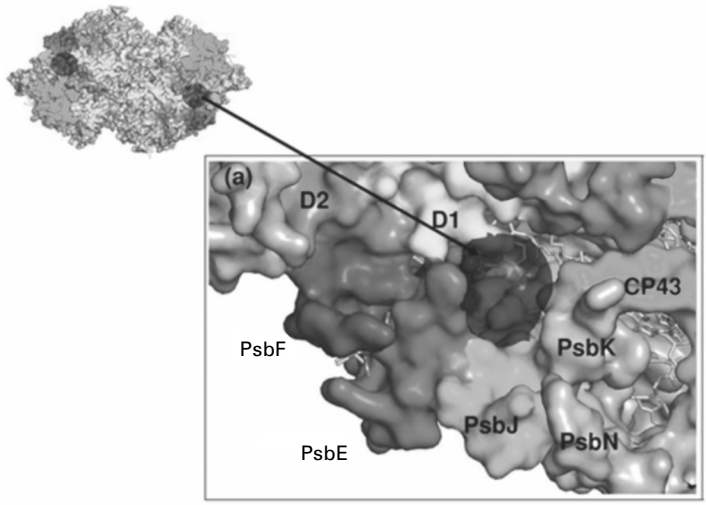
The immobilization of biological enzymes on electrode surfaces has the advantage of using their highly specialized catalytic activities, but the disadvantage that they are not robust enough for long-term application. This is true for the natural enzymes, namely PSII and algal/bacterial hydrogenases. Nevertheless, it has been shown in both cases that these and related enzymes, in their isolated states, can be immobilized, stabilized and electronically coupled to electrode surfaces (Giardi and Pace, 2005; Vincent *et al.*, 2007).

Badura *et al.* (2006) used His-tagged (Histidine-tagged) PSII isolated from *Thermosynechococcus elongatus* to demonstrate that this enzyme could be attached to an electrode surface and generate photocurrent commensurate with their high catalytic activity. In this work, isolated PSII was attached to the surface of a gold electrode, modified with thiolates bearing Ni(II)-nitrilotriacetic acid (NTA) groups. A good coverage density of about 0.3 pmol protein cm^{-2}, corresponding to a monomolecular film covering the surface, was achieved. Upon illumination (in presence of 2,6-dichloro1,4-benzoquinone (DCBQ) as a mediator) current densities of up to 14 $\mu A\ cm^{-2}$ were recorded which is equivalent to the highest oxygen evolution rates measured prior to immobilization. This current flux was more than 1000 times better than previous efforts to use PSII in this way. The success of this work reflects the very high activity of the PSII dimeric core complex isolated from the thermophile *T. elongatus* and the ability to immobilize the complex as an orientated monolayer on the gold surface using the His-NTA linkage. The work also clearly demonstrated that the electron transfer mediator DCBQ could access the Q_B site within the enzyme. James Barber has shown through his crystallographic studies of PSII that there is a 'hole' on the stromal surface of the *T. elongatus* PSII which links to the Q_B pocket (see Fig. 19.3). This 'hole' almost certainly provides a conduit for mediators to transfer electrons efficiently from the enzyme to the electrode surface as demonstrated by the work of Badura *et al.* (2006).

19.3.2 Challenge of enzyme stability

Badura *et al.* (2006) did not report details of the stability of their PSII-gold electrode system but there is every reason to believe that, after optimization, the activity could be maintained for several days or longer. For example, immobilized PSII is already incorporated into biosensors designed to monitor herbicides levels in the aqueous environment, which rely on its water splitting activity for days (Touloupakis *et al.*, 2005). In this case PSII is stabilized by treatment with an albumin glutaraldehyde matrix before being immobilized on

© Woodhead Publishing Limited, 2011



19.3 Stromal surface of the PSII dimer complex, showing the opening of a cavity which links to Q_B-site thus providing a conduit for electron transfer with the aid of a mediator. The enlarged image shows the details of the surrounding subunits.

the surface of a screen-printed graphite electrode. Tetramethyl-*p*-benzoquinone and potassium ferricyanide are used as electron transfer mediators between PSII and the electrode surface. A wide range of herbicides tightly bind to the Q_B-site of PSII leading to inhibition of the photo-generated signal and this inhibition is the basis for the diagnostic activity of this biosensor. At present this device uses PSII isolated from plants but given the significantly higher stability of the equivalent from *T. elongatus* there is no obvious reason why the lifetime of water splitting activity cannot be sustained for longer periods of time. Indeed, from Barber's experience of handling *T. elongatus* PSII isolated for crystallography, samples and crystals can remain active for months at room temperature if treated appropriately. The shortening of their lifetimes is brought about by illumination where oxidative damage is accelerated. This damage should be significantly reduced by maintaining a low oxygen partial pressure by flushing with nitrogen gas. Similar precautions will initially have to be taken with hydrogenase where again oxygen can inhibit activity.

Despite this problem, it is well established, especially through the work of Armstrong and colleagues (Vincent *et al.*, 2007, Lamle *et al.*, 2003) that hydrogenases can be deposited on a variety of electrode surfaces (including graphite) and show excellent electrochemical coupling. Moreover, under optimal conditions, it has been shown that [NiFeSe]-hydrogenase from *Desulfomicrobium bactulatum* bound to electrode surfaces can maintain activity for several weeks (Armstrong, personal communication, 2008).

© Woodhead Publishing Limited, 2011

19.3.3 Challenge of mimicking natural enzymes.

As mentioned in the Introduction, natural enzymes are not likely at all to guarantee sufficient durability to compete with current photovoltaics. For this reason the development of stable, smaller and possibly more active mimics will be mandatory.

Metalloenzymes such as PSII and hydrogenases have catalytic sites which are composed of metal ions arranged in a specific manner surrounded by amino acid side chains, which in part provide a scaffold and a ligand field, but usually also play key roles in the chemistry, the latter being facilitated. The evolutionary origins of these metalloenzymes probably stem back to inorganic catalysts which were incorporated into proteins and optimized through mutation over a very long period of time. Nature had to use metals which were readily available like Mn or Fe and Ni, as found in PSII and hydrogenases respectively, and initially had to employ protein scaffolds which had already evolved and were readily available. In this way catalysts were arrived at which 'worked' but were not necessarily the best solution. It is against this background that artificial catalysts could be constructed using the knowledge of 'how nature did it' but not necessarily using the same materials. For example, natural proteins are very unstable and are easily denatured. In principle, it should be possible to construct chemical systems with high catalytic activities, but which are more robust than their biological counterparts. This challenge has become more realistic with the successful determinations of the crystal structures of a wide range of metalloproteins.

Spurred on by this detailed structural information, there is considerable effort to mimic the chemistry of PSII and hydrogenase. In the case of mimicking PSII, there has been a flurry of activity in recent years with the emphasis on using Ru rather than Mn. Perhaps, the most impressive achievement stems from the work of Thomas Meyer, who successfully used *cis cis*$[(bpy)_2(H_2O))Ru^{III}ORu^{III}(H_2O)(bpy)_2]^{4+}$ also known as the 'blue dimer' (bpy = 2,2-bipyridine), to split water using visible light energy (Liu *et al.*, 2008). We will, however, focus on using Mn as the high potential multivalency metal to develop our artificial water splitting system since it is plentiful (thus cheap) and highly suitable for water oxidation chemistry as demonstrated by its use in the natural system. Although there is a high risk, here the proponents are encouraged by the success of others, such as Brudvig/Crabtree (in Limberg *et al.*, 1999) and Dismukes (in Wu *et al.*, 2006), in synthesizing redox active Mn compounds able to catalyse O—O bond formation. Moreover, Christou and colleagues have synthesized a Mn_4Ca cluster very similar to that proposed for the natural system (Glatzel *et al.*, 2004; Pizarro *et al.*, 2004). The work of Nocera and colleagues at MIT (Betley *et al.*, 2008) using high potential metal oxides is revealing ways to construct the right geometry for O—O bond formation while at

© Woodhead Publishing Limited, 2011

the same time taking care of proton coupled electron transfer (PCET) (see Fig. 19.4(a)). Hammarström and Styring in Uppsala (Hammarström and Styring, 2008) have successfully tethered a Ru-porphyrin to a dinuclear Mn molecule and demonstrated multiple light induced oxidation on the Mn ions (see Fig. 19.4(b)). Our strategy of focusing on the synthesis and use of Mn_xCaO_x complexes will complement the work of others and will evolve as this rapidly advancing subject yields new possibilities.

Shifting to hydrogenase, both Fe and Ni-Fe hydrogenases are remarkably efficient catalysts for the high turnover number (in the range of 1000–9000 per second), and the mild conditions (room temperature, aqueous solution and neutral pH) at which the reaction occurs. The natural enzymes catalyse proton reduction at potentials close to –400 mV vs standard hydrogen electrode (SHE) and are thus as effective as Pt, but less sensitive than Pt to poisoning by carbon monoxide. Most known molecular H_2 evolution catalysts, based either on the structure of the active site of hydrogenases or on metal complexes having simple macrocyclic ligands, catalyse H_2 evolution in organic solvents at fairly negative potentials, from –1.1 to -2 V vs a saturated calomel electrode (SCE).

The major challenge in developing suitable mimics for the hydrogenase is represented by producing robust bio-inspired catalysts that maintain the exceptional qualities of natural enzymes:

- low overpotential necessary for hydrogen production
- use of low cost, that is sustainable, metals such as iron and nickel as catalysts
- good efficiency under mild operating conditions
- easy synthesis of metal complex with the appropriate coordination geometry.

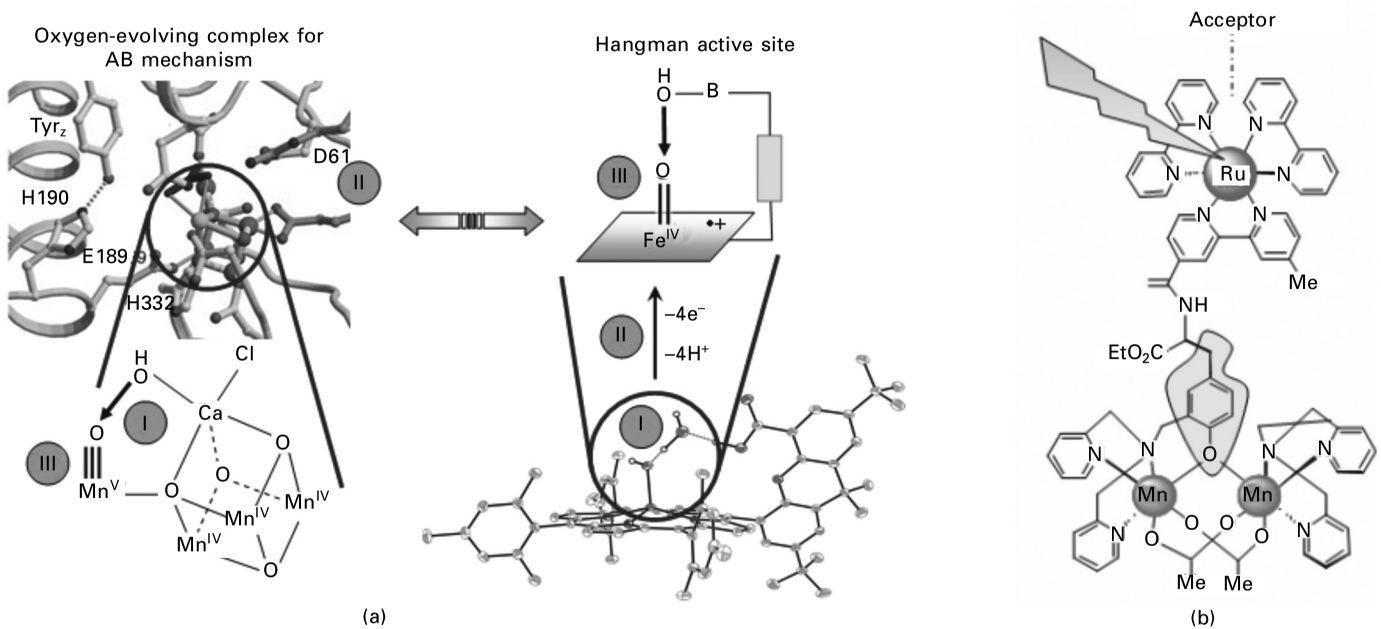
Some inorganic complexes mimicking the Fe-Fe cluster have been proposed for hydrogen production particularly by Pickett and colleagues (Tard *et al.*, 2005). A large ligand L_{cav} is proposed to stabilize the 4Fe4S cluster in place of the protein scaffold (Fig. 19.5).

Models of the active site in [NiFe]hydrogenase enzymes have proved to be challenging to prepare: for accurate bimetallic models the coordinating geometry is not easily reproduced by organic synthesis (Fig. 19.6). In particular NiS_4 complexes, to be used as metallothiolate ligands on iron organometallic centres, are difficult to synthesize since a square planar geometry is preferred in the presence of high-field donor ligands (Canaguier *et al.*, 2008).

A paramagnetic dinuclear nickel–ruthenium complex (Fig. 19.7(a)) was recently characterized by a bridging hydrido ligand from the heterolytic cleavage of H_2 by a dinuclear NiRu aqua complex in water under ambient conditions (20°C and 1 atm pressure). The structure of the hexacoordinate Ni(μ-H)Ru complex approaches closely to an effective analogue of the core

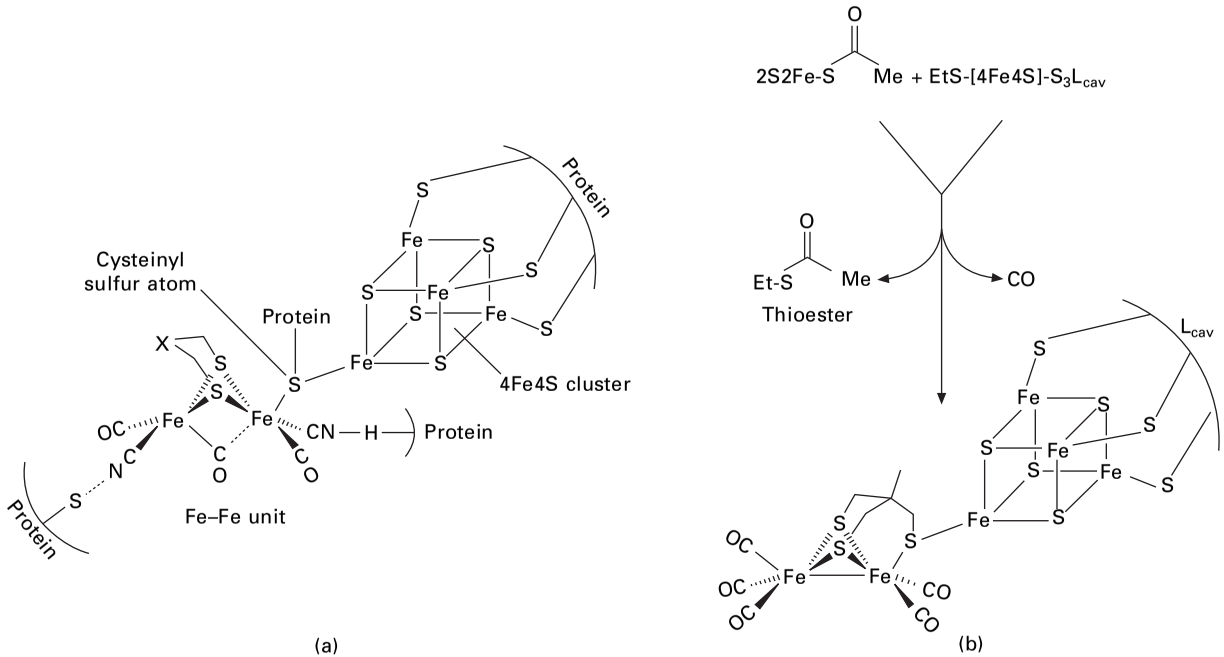
© Woodhead Publishing Limited, 2011

© Woodhead Publishing Limited, 2011

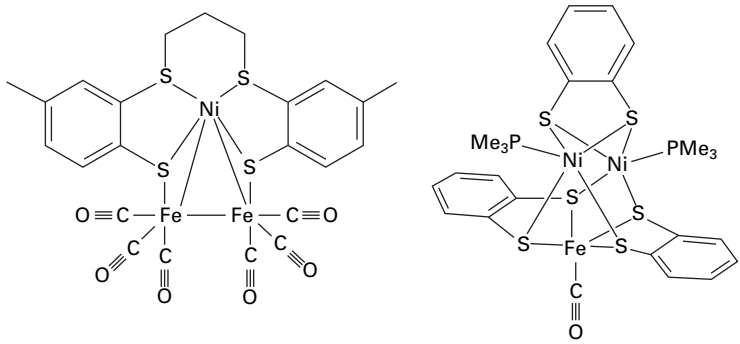


19.4 Progress in mimicking the PS II system: (a) the water oxidation centre in photosystem II (Ferreira *et al.*, 2004) and the Hangman porphyrin (I) assemble the oxygens from two water molecules for coupling, (II) activate the water to oxo by PCET and (III) position a high valent oxo along the reactive metal hydroxide vector. Although the resting state of the Hangman is a Fe^{III}-OH...H_2O complex, the Hangman porphyrin is prepared by the introduction of an Fe^{II} into the porphyrin core and the assembly of two water molecules. Production of the compound I intermediate of the Hangman thus results from an overall ($4e^-$,$4H^+$) process (from Betley *et al.*, 2008; reproduced by permission of The Royal Society). (b) A Ru-Mn_2 complex capable of light-induced cumulative electron transfer from the Mn_2 to the photo-oxidized Ru-unit (from Hammarström and Styring, 2008; reproduced by permission of The Royal Society).

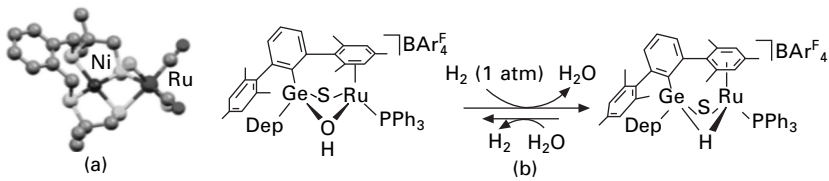
© Woodhead Publishing Limited, 2011



19.5 (a) Active site, or 'H-cluster', of the all-iron hydrogenase, a cube-shaped 4Fe4S cluster bridged to an Fe–Fe organometallic unit by a cysteinyl sulfur atom. (b) Synthetic analogue of the H-cluster from sulfur-containing precursors. L_{cav} is a large, bowl-shaped (cavitand) ligand used to prevent expansion of the 4Fe4S cluster (reprinted by permission from Macmillan Publishers, Darensbourg, 2005).



19.6 Two functional mimics of [NiFe]-hydrogenase (from Canaguier *et al.*, 2008; reproduced by permission of The Royal Society of Chemistry).



19.7 Interesting molecular structures for hydrogenase mimicking: paramagnetic dinuclear nickel-ruthenium complex (from Ogo *et al.*, 2007; Reprinted with permission from AAAS) and hydroxo/sulfido-bridged dinuclear ruthenium-germanium complex (Reprinted in part with permission from Matsumoto *et al.*, 2008; Copyright 2008 American Chemical Society).

structure of the proposed [Ni(μ-H)Fe] species, believed to be the active form of the hydrogenase (Ogo *et al.*, 2007). A hydroxo/sulfido-bridged dinuclear ruthenium–germanium complex (Fig. 19.7(b)) was recently demonstrated to be a functional hydrogenase model for reversible hydrogen production (Matsumoto *et al.*, 2008).

Ni–Ru complexes are functional bio-inspired dinuclear electrocatalysts for H_2 production (Oudart *et al.*, 2006). They are easy to prepare, highly stable and are able to catalyse the reduction of weak acids with high yields and turnover numbers (Canaguier *et al.*, 2008). However, they suffer from a major drawback, namely the important overvoltage required for catalysis. In addition, Ru is much less economically viable and sustainable than Fe, which is selected by living organisms for its bioavailability and made functional by the unique features of the protein scaffold of the natural catalyst hydrogenase.

An important recent finding, from studies of mononuclear Ni complexes, concerns the crucial role of basic sites in the close vicinity of the active metal centre to enhance the activity of a catalyst for H_2 production or uptake.

© Woodhead Publishing Limited, 2011

Since a proton exchange site is indeed found at the active site of both FeFe (with the putative azadithiolate bridge) and NiFe hydrogenases (with a terminal cysteinate residue), these should, in the future, be included in the next generation of bioinspired catalysts, taking into account the particular role of the protein moiety in proton exchange.

Both for Fe-only and Ni Fe-hydrogenase mimics a key point still to be tackled in detail concerning how to replace the role of the protein in stabilizing and tuning functional hydrogenase mimics, although a recently published paper suggested peptides as simplified scaffolds for functional clusters (de Hatten *et al.*, 2007).

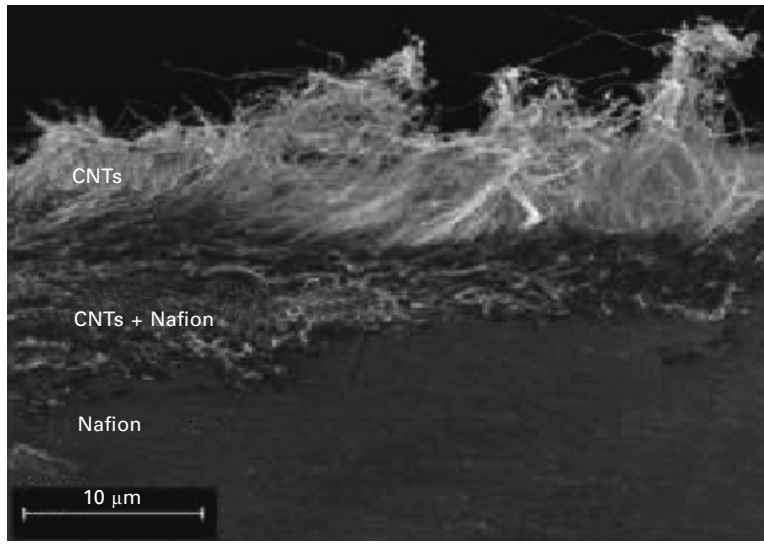
19.3.4 Problem of assembling a mixed conducting membrane

Mixed ion and electron conductive ceramic materials, like perovskites, are under investigation as membranes for gas separation at high temperature by many groups. However while pure proton conductive membranes like Nafion are also the subject of worldwide research, polymeric proton–electron mixed conductive materials have not been explored much. One of few approaches is the development of mixed conductive polymer blends (e.g. SPEEK/PANI (polyaniline), Nafion/PANI), as reported by Roeder *et al.* (2006, 2005) and Barthet and Guglielmi (1996). To make the biomimetic H_2 production systems feasible, high electron conductivity is required and a promising approach was chosen, namely the dispersion of electron conductive fillers like carbon nanotubes (CNT) or TiO_2 in a proton conductive matrix. CNTs offer a unique combination of properties for membrane preparation: high aspect ratio/high surface area, electron conductivity, simple functionalization, easy dispersion in organic polymers and capability to enhance mechanical strength. Taking advantage of mixed ionic conduction, attempts to prepare optimized membrane electrode assemblies (MEAs) using carbon nanotubes have been reported recently (Tang *et al.*, 2007; Li *et al.*, 2005). CNTs loaded with catalysts have been deposited or incorporated in the carbon paper or cloth, by dispersion and electrophoretic deposition, by growing the CNTs directly onto the carbon paper or alternatively by filtration of a CNT dispersion which is then deposited onto a commercial Nafion® membrane and hot pressed with the carbon backing layer. Preliminary results for membrane assemblies with aligned nanotubes as electrodes coated with Pt catalyst have been obtained (Prehn *et al.*, 2008) (Fig. 19.8). One can actually see this membrane as a sort of short circuited PEM fuel cell membrane.

Important requirements for an effective mixed conduction composite membrane are:

- percolation of the electron conductive particles, keeping the conductivity as high as possible;

© Woodhead Publishing Limited, 2011



19.8 Nafion/CNT membranes for fuel cell application (from Prehn *et al.*, 2008 with permission from Elsevier).

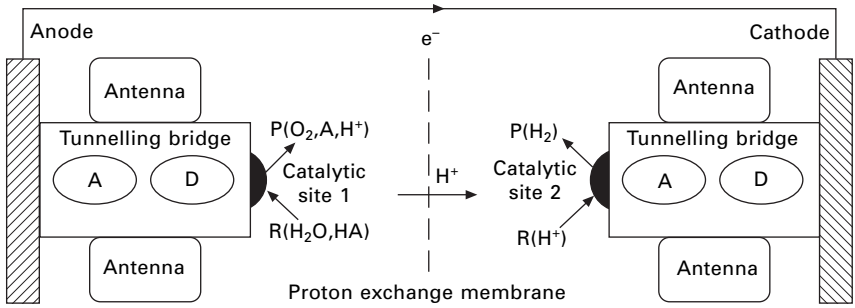
- good adhesion between the proton and electron conductive phases;
- fine dispersion of fillers;
- direct accessibility or even covalent attachment of the catalyst both to electron and conductive components.

To attain these requirements, functionalization of fillers and eventually also of the polymer will probably be necessary. Attachment of the biomimicking catalysts to the filler and/or to the polymer should improve the system efficiency (Karthikeyan *et al.*, 2005; Ponce *et al.*, 2008).

19.4 Thermodynamic limitations and device design

The biomimetic H_2 generation nanoreactor has the mandate to bridge between long distance energy transfer on the short timescale of fluorescence, ca. 10^{-9} s, and short distance proton-coupled electron transfer and storage on the much longer time scale of catalysis, ca. 10^{-3} s (Lubitz *et al.*, 2008; Pandit *et al.*, 2006). As a consequence, a modular approach has to be taken, allowing the design of nanostructured optimized topologies, with a tunnelling bridge for electrons, to integrate storage with catalysis, and with the optimization of proton chemical potentials, to mimic the proton coupled electron transfer processes in photosystem II and hydrogenase. A perhaps clearer scheme of the components of this modular approach is provided in Fig. 19.9. Compared to the concept in Fig. 19.1, Fig. 19.9 schematically decouples the electron transfer in an external wire from the proton transfer through the membrane,

© Woodhead Publishing Limited, 2011



19.9 Solar energy-driven photoelectrochemistry for production of H_2 with high efficiency (schematic). System integration of modules will combine a light-harvesting antenna system and photochemical reaction centre containing a donor (D) and an acceptor (A) to produce a stable photocurrent that drives novel catalysts for multi-electron reactions (R → P). Such 'smart matrices' build upon knowledge about natural photosynthesis and hydrogenase in order to extract electrons from water and produce fuel(s) from protons (from de Groot, 2010; with kind permission from Springer Science+Business Media).

separating the two electrodes. It goes without saying that this is a practical option, less compact than the previous one, which can:

- allow use of a membrane similar to those employed in PEM fuel cells
- allow application of a potential bias, over the wire, if the potential losses are too high to enable proton recombination (see later).

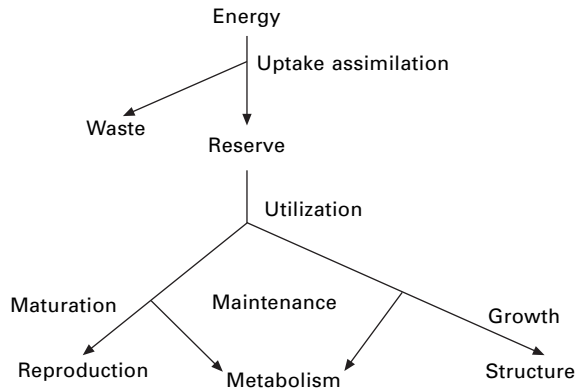
In the following, thermodynamic limitations of systems based on natural enzymes and bioartificial ones will be discussed, showing that the target of 10% solar energy conversion into hydrogen can actually be achieved.

19.4.1 Natural photosynthesis

In nature, the photosynthetic apparatus is connected to a steady-state network of catalytic conversion reactions in the organism that is continuously dissipating energy and generating entropy (Fig. 19.10). From a biological perspective, photosynthesis is an expensive process in terms of required resources, and organisms generally produce only the photosynthetic capacity that they need to serve their requirements within the limits of the environmental and developmental constraints.

This is the reason why solar energy conversion into fuels achievable via the growth, harvesting and conversion of energy crops into fuels is rather low (see Table 19.1). At low light intensities, however, the productive storage of energy is an efficient chemical thermodynamic process, which is optimized against depletion by wasteful back reactions that feed into the decay of the

© Woodhead Publishing Limited, 2011



19.10 Energy use in the biological steady state.

Table 19.1 Biomass yields, specific power and solar energy conversion efficiency for different crops. Basic assumption: assuming an average irradiance of 150 Wm^{-2} (midwest USA) and a thermal equivalent of 1 g dry weight = 17 kJ

Crop	Biomass tdw $ha^{-1}yr^{-1}$	Specific Power (W m^{-2})	Efficiency (%)
Corn	7	0.38	0.25
Sugarcane	80	4.3	2.9
Swithgrass	15	0.8	0.54
Rape seed	3	0.16	0.1
Arthrospira	60	3.3	2.2

tdw = total dry weight.

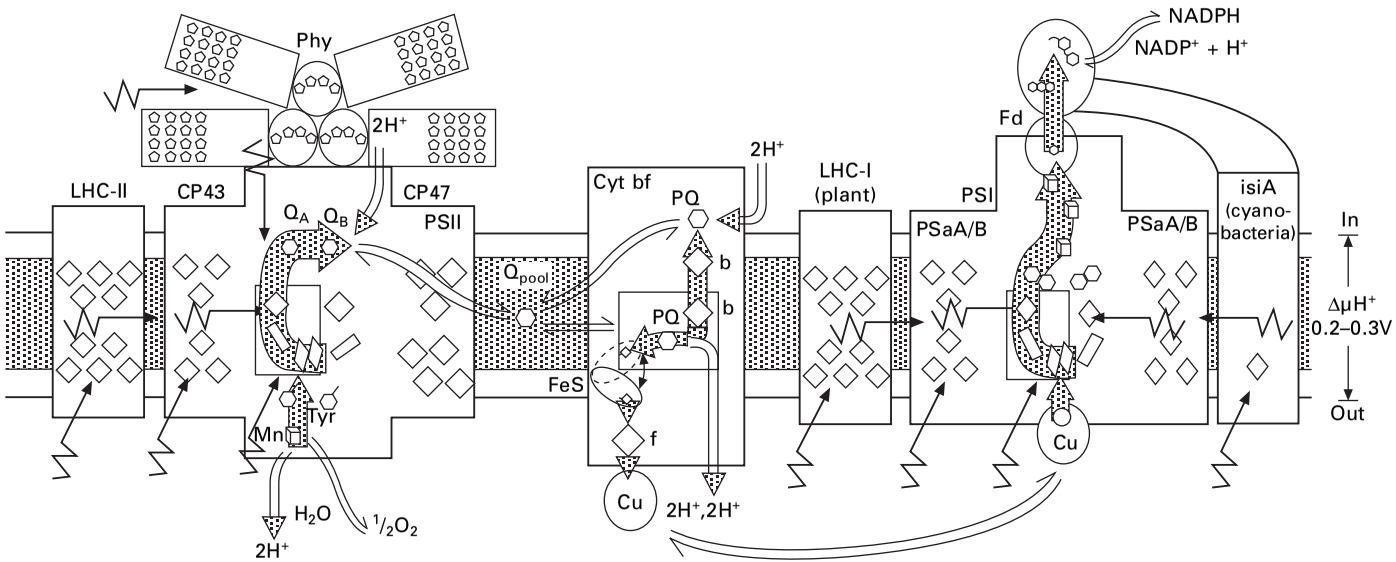
absorber at a rate $g = 1/\tau$ from the excited chlorophyll state into the ground state at the start of the conversion chain (Ross and Calvin, 1967).

Natural photosynthesis requires coupling of primary conversion into biochemical networks and catalytic cycles that are subject to regulation for protection against excess light, leading to limited photosynthetic capacity (Fig. 19.11 and Fig. 19.12).

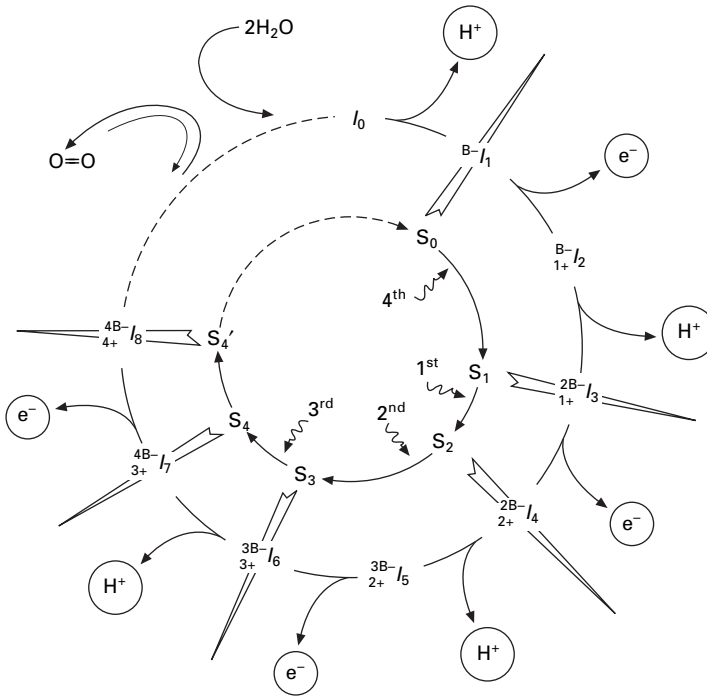
To complete an overall process, including oxygen evolution and hydrogen exploitation in nicotinamide adenine dinucleotide phosphate (NADPH), an overall amount of eight photons are required, four of which are exploited in the PSI and four in the PSII systems. Figure 19.13 provides more details about this process, including the potential levels achieved by the reacting system along the complete water splitting pathway. Particularly, hydrogen fixation requires high potentials that cannot be guaranteed by PSII alone, owing to the occurrence of potential decay accompanying the reaction steps. Hence, PSI has to sum up the effect of four other photons to bring the potential level at this location down to the required –1400 mV. A careful evaluation of the potential level required by natural hydrogenase or its mimics is required to

© Woodhead Publishing Limited, 2011

© Woodhead Publishing Limited, 2011



19.11 Schematic representation of cofactors in light harvesting, reaction centre and bc_1 proteins of photosynthetic organisms and particularly plant membranes with photosystem I (PSI), photosystem II (PSII) and b_6f analogous to bc_1 complex; light-energy excitation or energy transfer (zig-zag arrows) between (bacterio)chlorophylls (diamonds) leads eventually to charge separation in reaction centres (inner rectangular boxes) and electron tunnelling (thick grey arrows) from centre to centre in a chain across the membrane (grey, low dielectric region) to create a transmembranal electric field. Proton binding and release (double arrows–solid head) occur at chains terminating in quinones (hexagons), generating a transmembranal proton gradient. In addition, reduced quinone and oxidized cytochrome c or plastocyanin diffuse (double arrows–half head) to connect membrane complexes (from Noy *et al.*, 2006; with permission from Elsevier).



19.12 Cyclic operation of water splitting to oxygen in natural photosynthesis (PSII).

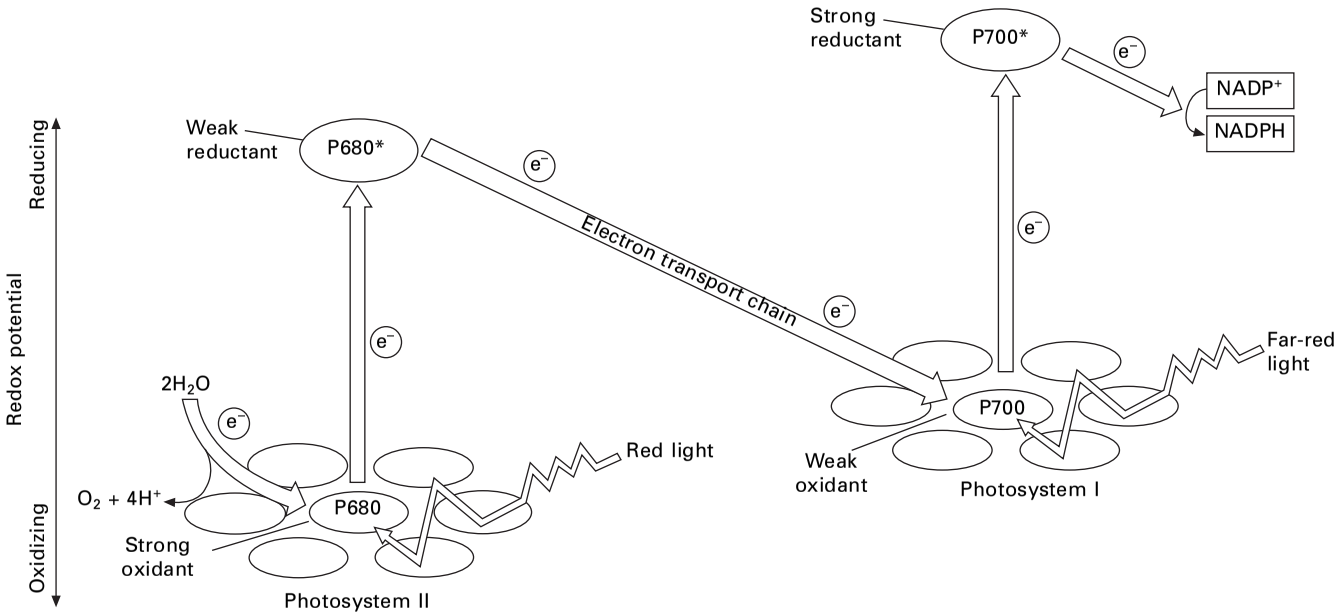
promote hydrogen recombination. In the case where natural PSII is employed, it seems quite likely that additional energy capture should be required. This is represented by the presence of an antenna not only at the anode side, but also at the cathode side of the nanodevice represented in Fig. 19.9. This is also due to the fact that natural photosynthetic pathways exploit 'red photons' (Fig. 19.14), whose energy level (1.8 eV) is not the highest in the light spectrum (Fig. 19.14). Blue photons might indeed inject more energy into a potential bioartificial system, so that the entire set of reactions leading to O_2 evolution and hydrogen fixation, can occur in a row.

Another weak point of natural photosynthesis, which limits the achievable conversion efficiency, lies in the fact that just 50% of the overall spectrum of solar light is actually exploited. Some algae (*Acaryochloris marina*; Fig. 19.15) were recently discovered in which the coverage of the light spectrum is actually wider, leading to a 10% increase of the exploited solar energy. This points the way towards a clear goal for bioartificial systems, in line with recent developments on tandem photovoltaic cells.

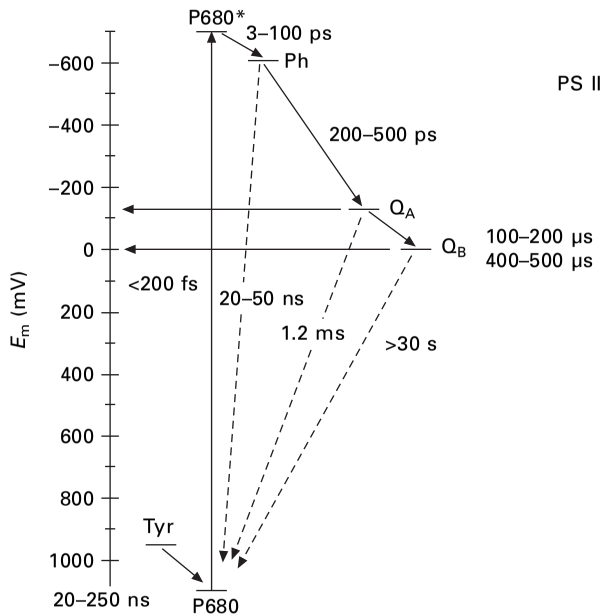
Keeping as a reference ideal 'Carnot efficiency' cycles with an (overrated) 80% conversion efficiency, one can expect natural photosynthesis to achieve theoretically 40% conversion (accounting for the 50% limitation

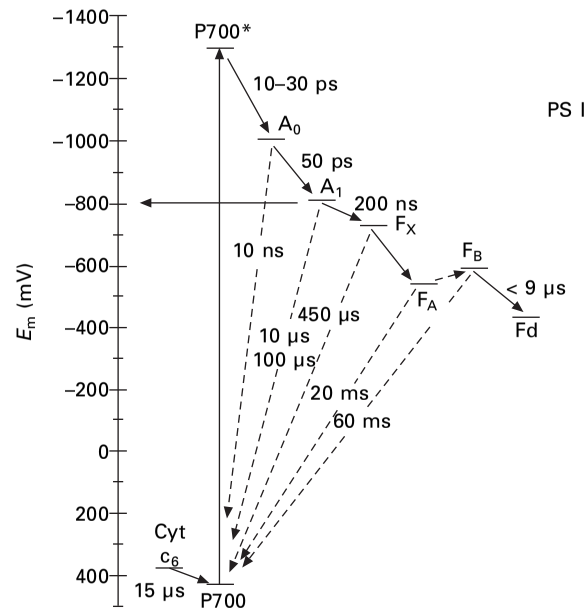
© Woodhead Publishing Limited, 2011

© Woodhead Publishing Limited, 2011



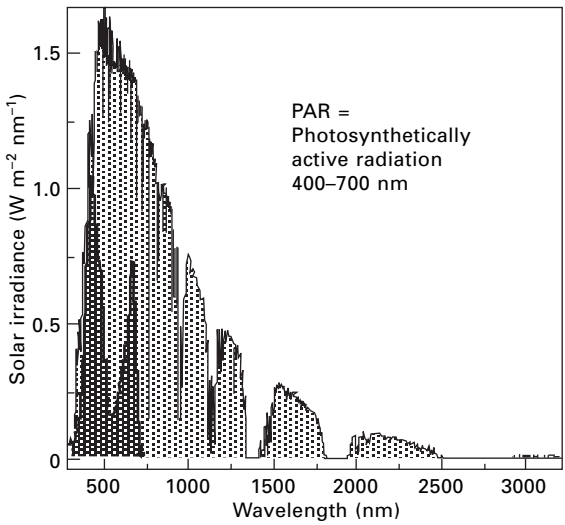
19.13 Comparison of the redox potentials of photosystem I with photosystem II. The primary electron donors and the quinones are offset from one another by about 700 mV. The cofactors are highly similar in both instances, indicating that the protein environment is what modulates the midpoint potential of a given electron transfer component.



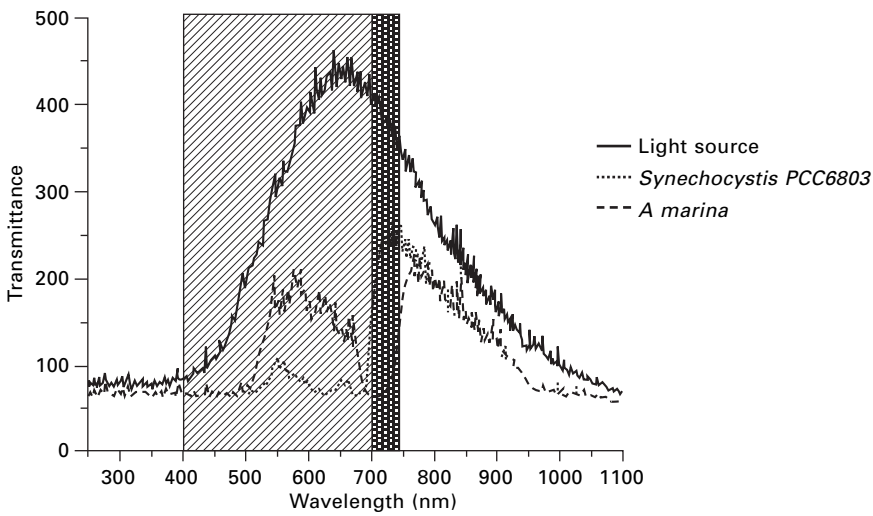


19.13 Continued

© Woodhead Publishing Limited, 2011



19.14 Chlorophyll range of adsorption (dark shading) vs. overall spectrum of solar energy.



19.15 Improved light absorption range of *Acaryochloris marina* (dashed line) compared to conventional microorganisms (dotted line).

in capturing sunlight). An additional half-cut of the conversion efficiency is due to irreversible phenomena occurring to NADPH and ATP along the way, thereby leading to a maximum achievable 20% value, which is a sort of overall target for the formation of hydrogen (for example) in a biochemical device based on natural systems. An additional limit to the

© Woodhead Publishing Limited, 2011

natural photosynthesis is linked to the fact that the size of the antennae developed by natural plants (Fig. 19.16) is rather large if one expects leaves to be able to capture the whole intensity of solar energy, even in the hottest daytime hours. Conversely, as a consequence of a non-optimized antenna size, a saturation asymptote is reached beyond which additional sunlight intensity cannot simply be exploited (Fig. 19.17).

As a result of the above constraints, Fig. 19.18 shows the overall solar energy conversion efficiencies that can be expected in natural and biomimetic systems.

19.4.2 Artificial photosynthesis

In artificial photosynthesis, the minimal design requirements for the most efficient solar-to-fuel conversion process must be considered, operating close to the theoretical limits of solar energy conversion. To understand how thermodynamic constraints can guide the design of artificial systems for photochemical storage, it is better to start from minimal models that consider the thermodynamic constraints of the photovoltaic or photochemical solar energy conversion by exploring an analogy with efficient conversion in the solar or photovoltaic cell (Ross and Calvin, 1967; Noy *et al.*, 2006; Markvart and Landsberg, 2002; Wurfel, 2002; Shockley and Queisser, 1961). In productive photochemical conversion, storage or downstream utilization is described as a single step conversion of solar energy into Gibbs free energy. Like the silicon solar cell, the photosynthetic solar cell is in its simplest form a molecular absorber that is excited and produces energy conversion by charge separation into an electron and hole, at a certain rate I (see definition in Equation [19.3]), in dynamic equilibrium with the absorber (Fig. 19.19). The excitation of a molecular chlorophyll (Chl) absorber in exchange with the field of solar irradiation leads to a difference in chemical potential:

$$\Delta\mu_{abs} = h\nu_0 + k_B T \ln(p/p_0) \qquad [19.1]$$

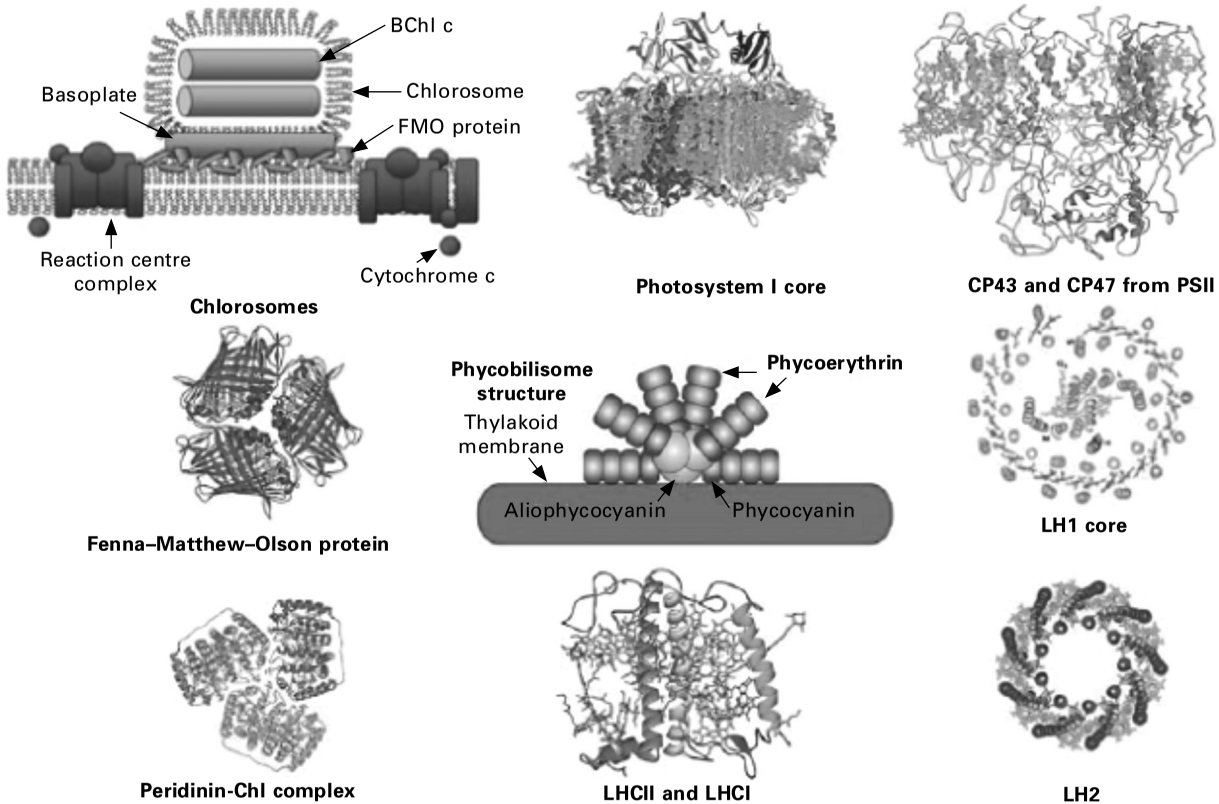
with p and p_0 being the populations of the excited and ground state of the absorber (Shockley and Queisser, 1961). In the dark, the excited and ground state are in equilibrium and $\Delta\mu_{abs} = 0$, leading to $p/p_0 = \exp(-h\nu_0/k_B T)$, the Boltzmann distribution.

For Chl *a* in green plants $h\nu_0 = 1.8$ eV. A detailed balance has been used to calculate the upper limit at the absorber stage, which leads to maximum efficiency $\eta = 1 - 4T/3T_S = 93\%$, for reversible operation, owing to entropic losses originating from the different temperatures of the incoming radiation at $T_S \sim 5800$K and of the heat reservoir at $T \sim 300$K (Noy *et al.*, 2006; Wurfel, 2002; Shockley and Queisser, 1961).

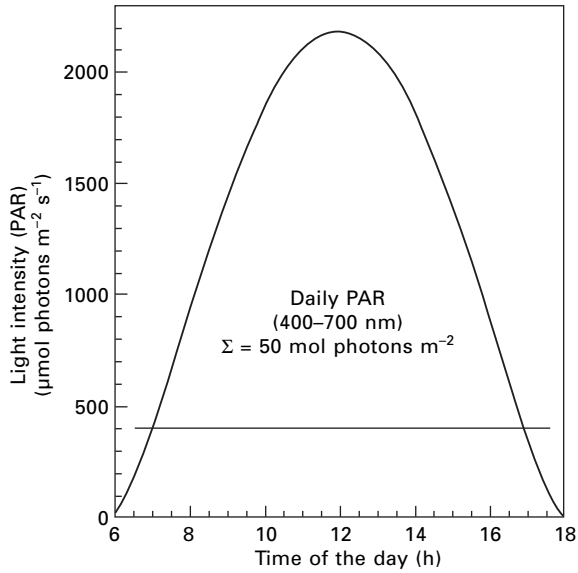
A photovoltaic (PV) solar cell produces electricity, while a photosynthetic reaction centre produces a photochemical steady state with a voltage over the

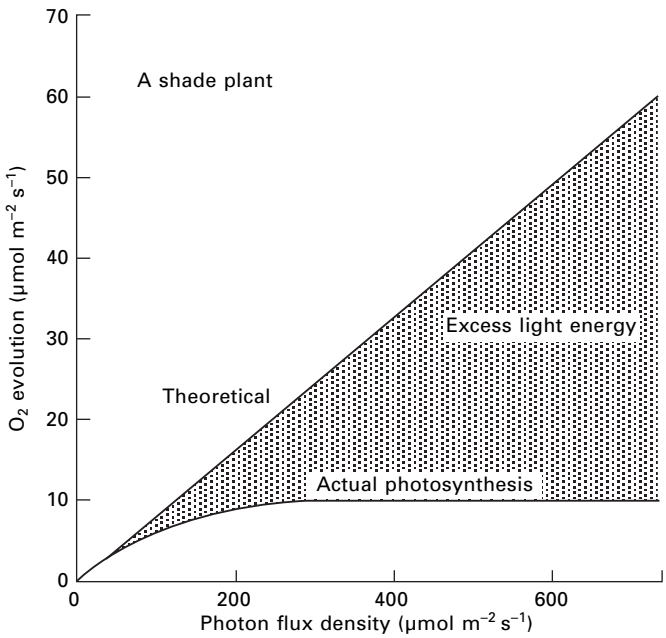
© Woodhead Publishing Limited, 2011

© Woodhead Publishing Limited, 2011



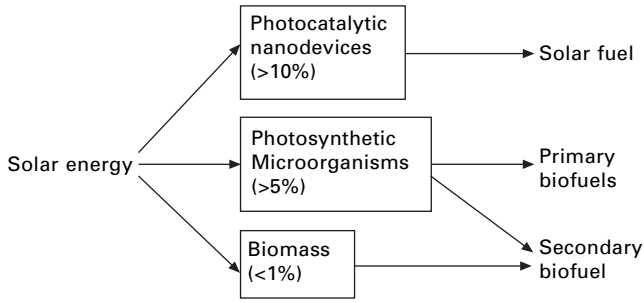
19.16 Extreme diversity of antenna systems strongly suggests multiple independent evolutionary origins. BChl c oligomers are light-harvesting pigments in chlromosomal bacteriochlorophyll.



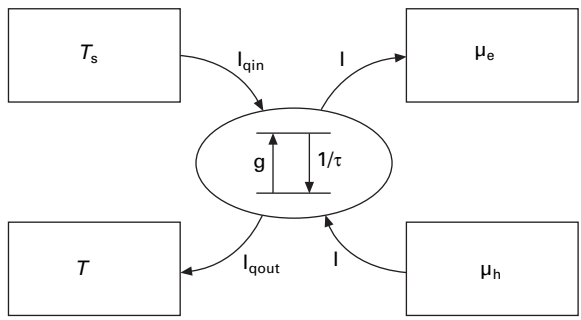


19.17 Another structural limit of natural photosynthesis: as a consequence of large antenna dimensions, photosynthesis reaches a saturation asymptote.

© Woodhead Publishing Limited, 2011



19.18 Reasonable efficiency targets for solar energy conversion into fuels via the growth of biomass (energy crops) or photosynthetic microorganisms (algae) or the development of a photocatalytic nanodevice as in Fig. 19.9.



19.19 Basic electrochemistry and energetics of the photosynthetic solar cell (from Markvart and Landsberg, 2002; with permission from Elsevier). A chlorophyll molecule is connected to a reservoir at ambient temperature $T \sim 300$K, and emitting heat at a rate I_{qout}, is excited by the heat flow I_{qin} from the solar reservoir at temperature T of 5800K at a rate g to an excited state separated by energy $\eta\nu_0$ from the ground state. The excited chlorophyll state either decays with loss rate of $1/\tau$ or produces an electron–hole pair with a net charge separation rate I and free energy $\Delta\mu = \mu_e - \mu_h$

membrane and charge separation in dynamic equilibrium with the absorber. Recently, solar energy conversion has been considered in a general setting, including both the photochemical and photovoltaic mechanisms (Markvart and Landsberg, 2002). The equation:

$$\Delta\mu_{e-h} = e\,\Delta\psi + k_B T \ln(p'q'/p_0'q_0') \qquad [19.2]$$

represents the difference in chemical potential or free energy produced by light-induced charge separation and contains an electronic term $e\Delta\psi$. In addition, a photochemical term $k_B T \ln(p'q'/p_0'q_0')$ measures the concentration $p'q'$ of the charge separated state, that is the probabilities of electron and

© Woodhead Publishing Limited, 2011

hole occupation of the acceptor and donor states in the light relative to the concentration $p'_0q'_0$ in the dark. This term is proportional to the temperature. Equation [19.2] illustrates how the electrochemical potential $\Delta\mu_{e-h}$ can comprise a light-induced electrostatic potential of charge separation $e\Delta\psi$, a photochemical one $k_BT \ln(p'q'/p'_0q'_0)$, or both, as in photosynthesis (Markvart and Landsberg, 2002).

The net production rate of the charge separation and energy storage in a photosynthetic process can then be described by the solar cell equation:

$$I = I_f - I_b(e^{\Delta\mu/k_BT} - 1) \quad [19.3]$$

where I_f and I_b are the forward and backward reaction rates, respectively (Shockley and Queisser, 1961; Archer and Bolton, 1990). The difference I represents the rate of energy extraction. For photovoltaics (PV) this is electrical energy, and for artificial photosynthesis I is the net flow of energy into proton coupled electron transfer and temporary storage, followed by the multi-electron chemical reaction that oxidizes water or produces fuel.

The second principle of thermodynamics, stating that entropy cannot be destroyed, limits the efficiency of solar energy conversion to 0.93 for reversible operation (Shockley and Queisser, 1961). Extraction of energy implies a non-reversible process with a theoretical limit less than the 93% for the reversible process (Ross and Calvin, 1967). Processing the incident solar energy current is thus not possible without lowering the efficiency and Equation [19.2] can be generalized according to:

$$\Delta\mu_{st} = \Delta\mu_{max} + k_BT \ln(\delta) \quad [19.4]$$

with a quantum yield

$$\eta_{st} = [I_f/(\tau^{-1} + I_f)] \cdot (1 - \delta) \quad [19.5]$$

Here the first factor is due to the kinetics of the steady state, while δ measures the thermodynamic activity of the trap (Ross and Calvin, 1967). Hence, in order to favour the forward reaction over the backward process, the energy of the combined products is lower than for the excited state by at least $k_BT\ln(\delta)$. The maximum power is generated for $\delta \sim k_BT/\mu_{max}$, a compromise between high conversion efficiency and high storage efficiency.

Since multi-electron catalysis for water oxidation or hydrogen production requires storage for downstream accumulation of electronic charges at longer timescales than the initial light absorption process, a catalytic site in an artificial photosynthesis device will be in Boltzmann equilibrium with the initial excited state throughout the entire process, both during the accumulation of charge and during the actual catalytic reaction. This means that the processes of storage and catalysis have to go hand in hand. Catalytic processes operate on the ms timescale and the accumulation of several electrons or holes on this timescale is rate limiting. Thus, $\Delta\mu_{st}$ inside the catalyst should be

© Woodhead Publishing Limited, 2011

sufficiently low to trap electrons or holes allowing multi-electron catalysis to proceed against back reactions. For efficient solar-to-fuel conversion, the overall rate of energy extraction has to be close to the net rate of excitation of the molecular absorber at the start of the conversion chain.

When the absorber operates at an energy $h\nu_0$ with an excited state lifetime τ, the theoretical limit of the electrochemical potential $\Delta\mu_{st}$ that can be established inside the catalyst in a reversible process in a multi-electron catalytic chain will depend on the required storage time t for accumulation prior to the actual catalytic process, according to Pandit *et al.* (2006), and van Gorkom (1986):

$$\Delta\mu_{st} = h\nu_0 + k_B T \ln(t/\tau) \qquad [19.6]$$

and will decrease in order to establish a net energy flow I through the catalyst for the chemical reaction, in line with Equations [19.3]–[19.5].

19.5 Integrated engineering approach for solar-to-fuel conversion

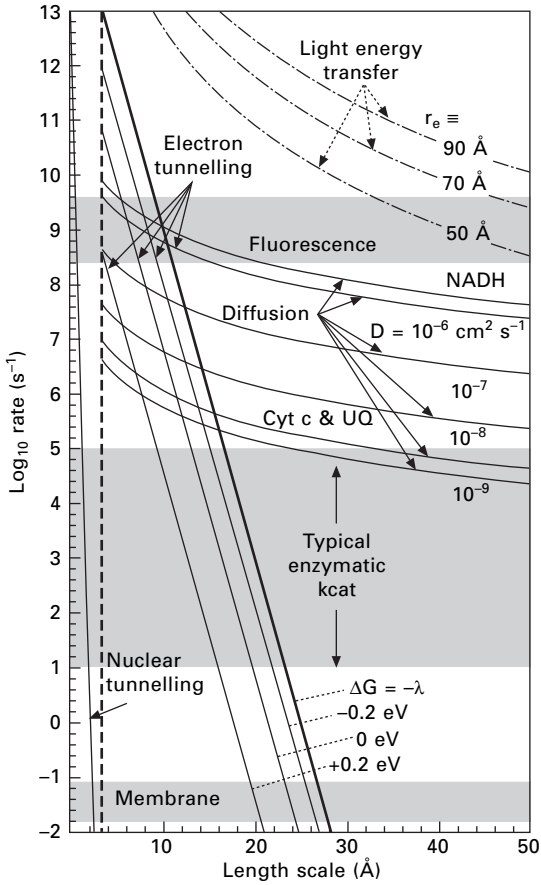
The fundamental limits of solar energy conversion in photosynthesis have been described many times in the literature. The crucial point about Equation [19.6] is, however, that it links the timescale of the chemical process to the electrochemical potential that is established inside the catalyst and the free energy difference $h\nu_0 - \Delta\mu_{st}(t)$ which is minimally required to achieve the desired steady state for thermodynamic reasons. It puts a fundamental restraint on how to match length scales, energy scales and timescales, and allows for the design of nanostructured artificial solar-to-fuel conversion topologies based on knowledge of the length scales, timescales and energy scales from natural photosynthesis that have been discussed extensively (van Gorkom, 1986) (Fig. 19.20).

In Fig. 19.9, catalysis is integrated with storage to allow a multi-electron process. The reaction centre dimension is an important parameter; in fact nanostructured support affords tens to hundreds of catalytic sites per square nanometre. The turnover frequency (number of oxygen molecules produced per second per nanocluster) and size of the catalyst determine the degree to which an integrated system featuring this catalyst will be able to keep up with the rate of incident solar photons.

For example surface sites of nanoclusters of Co are substantially more efficient catalytically (by a factor of 16) than those of micrometre-sized particles (Jiao and Frei, 2009). So using Co oxide nanoclusters (a few nanometres rods) an efficiency comparable to the nature's photosystem II occurs (sized 105×200Å, as depicted in Fig. 19.2), in which the majority of the space is taken up by the light-harvesting system rather than the catalyst.

When operating a multi-electron catalyst in artificial photosynthesis, part

© Woodhead Publishing Limited, 2011



19.20 Rates of key transfer phenomena for design of an artificial nanodevice for the conversion of solar energy into fuels. Length scales for light energy transfer, electron tunnelling and proton tunnelling and diffusion (indicated by arrows). Fluorescence decay times, enzymatic turnover times (kcat) and membrane potential decay (indicated by shaded horizontal areas) represent basic engineering time constraints. Fluorescence heralds the end of the energy transfer time domain (from Noy *et al.*, 2006; with permission from Elsevier).

of the initial free energy stored in the solar energy assimilation $h\nu_0$ will be necessary to produce a free energy difference $h\nu_0 - \Delta\mu_{st}(t)$. This free energy difference is inevitable, and must be put to use in promoting confinement of electrons or holes inside catalytic sites, in line with Equation [19.6]. Viewed in this way, the term $k_B T \ln(t/\tau)$ leads to a nanostructure design concept that is fundamentally different from alternatives that work from delocalized electrons at moderately functionalized extended semiconductor interfaces,

© Woodhead Publishing Limited, 2011

or try to combine the different required functions of storage and catalysis into essentially one or two complex molecules that perform all the functions of an anode or a cathode.

In particular, the incorporation of insulating tunnelling bridges between the catalyst and the electrode is critical to the design. Inside the nanostructure, $e\Delta\psi$ and $k_B T \ln(p'q'/p'_0q'_0)$ are interchangeable, as described by Equation [19.2]. During accumulation, energy is preserved locally, initially in the form of $e\Delta\psi$, followed by chemical coupling into a proton process to temporarily neutralize the charge. It may appear counterintuitive at first sight, but the tunnelling bridge ensures that the overvoltage for catalysis produces a suitable confinement potential for electrons or holes in the catalytic sites. A tunnelling bridge of ~ 20 Å will allow the accumulation of charges on a timescale necessary for multi-electron catalysis (van Gorkom, 1986). Similarly, the spatial orientation and separation between the antenna and the donor–acceptor pairs will be adjusted for optimal excitation trapping and charge separation (van Gorkom, 1986).

While it is essential for the free energy difference to be operational in confining electrons and holes, it will be equally essential that the subsequent chemical conversion can proceed downhill, without any restraints. This implies that there should not be a potential barrier between the proton exchange membrane and the catalytic nanostructure, to allow for barrierless proton coupled electron transfer and smooth charge transfer across the proton exchange membrane. Previous attempts to perform multi-electron catalysis on an electrode often work by catalysts embedded in proton exchange membranes optimized for proton conduction, such as Nafion, with a pKa ~ –6. In this case the chemical potential for protons at the catalytic site is very high. While such an approach may work well for hydrogen production at a photocathode, for water oxidation at a photoanode it will give rise to a free energy difference that competes with the tunnelling barrier, quenching catalysis. For a photoanode it would be preferable to work from an alkaline environment to produce a low proton chemical potential and to tune the chemical potential of intermediates in the multi-electron pathway for optimal proton coupled electron transfer and a charged resting state. This is in line with the mechanisms in natural photosynthesis that have been resolved by electron paramagnetic resonance (EPR), by Lubitz *et al*. (2008), and recently also by nuclear magnetic resonance (NMR) and theoretical analyses (Rossmeisl *et al*., 2007; Alia *et al*., 2009). This fact is indeed favoured by a very high membrane permeability to protons, to keep proton concentrations as low as possible where they are generated. On the other hand, low proton concentrations would lower the reaction kinetics at the cathode side. This once again requires a compromise that will affect the overall performance of the artificial leaf. It is likely that different ion exchange resins would provide a better environment than Nafion, despite this, the polymer can

© Woodhead Publishing Limited, 2011

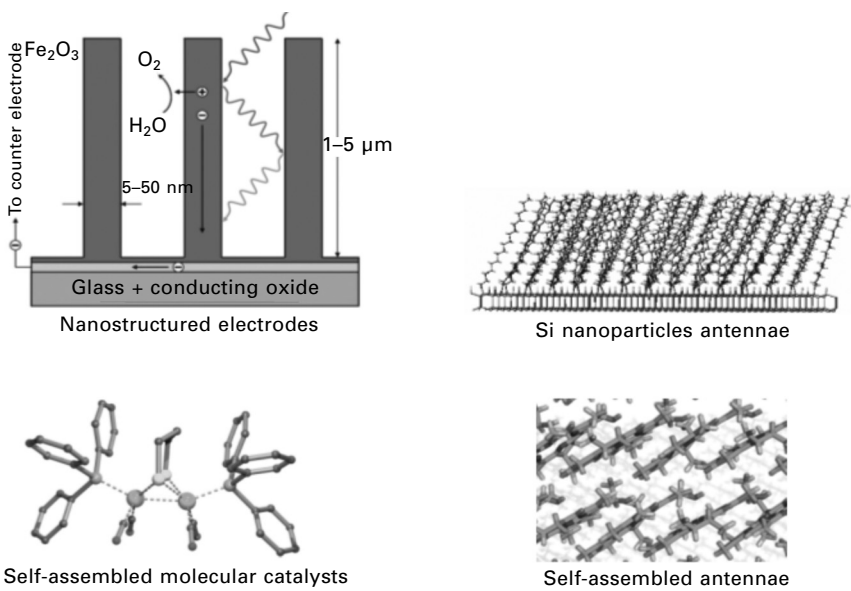
achieve conductivities higher than 10 S m^{-1} and thicknesses as low as 25 μm, which help to lower the potential loss across the membrane.

Adequate engineering of antennae, reactive sites, electrodes, membrane will have to be achieved to avoid bottlenecks and to maximize the efficiency of the artificial leaf (Fig. 19.21). Guidelines for this process are reported in Table 19.2.

19.6 Conclusions

The potential of nanodevices for solar energy conversion into hydrogen has been discussed. Thermodynamic margins for a fruitful exploitation of this biomimicking technology are present to guarantee success against competing opportunities (e.g. a photovoltaic panel coupled with an electrolyser). Formidable challenges stand along the pathway to practical exploitation. With reference to the concept outlined in Fig. 19.1, the following conclusions can be drawn based on the analysis carried out above:

(1) The natural process requires two photons to store one H+ and the co-current action of PSI and PSII. Using just PSII in the bioartificial system with no additional antennae to increase the energy of electrons getting to the hydrogenase is probably a paramount task. Attention must be paid to the level of energy of the electrons that can actually be delivered to the hydrogenase and whether they are energetic enough to promote the



19.21 Nanodesign of electrodes, catalysts and antennae.

© Woodhead Publishing Limited, 2011

Table 19.2 Engineering guidelines for the design of biomimetic H_2 production nanodevices (from Noy *et al.*, 2006; with permission from Elsevier)

Process	Constraint	Guideline[a]
Light absorption	Incoming photon flux is rate limiting.	Increase absorption cross-section by using dense arrays of pigments. Use multiple chromophores with complementary absorption spectra that match the spectral distribution of incoming photons. *Expand the useful spectral range by utilizing lower energy photons. This requires lowering the driving force of the charge separation reaction.*
EET	Excitation energy should be trapped by the RC.	Interconnect several cofactors to allow multiple EET pathways within LH pigments and between LH and RC. *Adjust site energies of cofactors to form an energy funnel from the periphery to the RC.*
EET	Strongly coupled dimers may become non-radiative, unproductive traps.	Avoid placing pigments less than 10 Å from each other. *Restrict relative orientations of pigments such that EET is preferred over non-radiative decay.*
EET	ET to/from the RC may create harmful radicals in the LH unit.	Form a *cordon sanitaire* around the RC beyond which ET rates to/from RC are marginal compared to EET rate.
ET	Single step electron tunnelling across transmembranal distances is prohibitively slow.	Use chain of redox cofactors spaced within 14 Å (edge to edge) from each other.
ET	ET from the excited state competes with relaxation to the ground state.	Place acceptor within 5 Å of the photoexcited donor.

[a]Guidelines in italics improve yield but are not critical.
EET = excitation energy transfer, ET = electron transfer, LH = light-harvesting, RC = reaction centre.

© Woodhead Publishing Limited, 2011

desired H_2 evolution. If not, a new antenna system has to be added to the hydrogenase enzyme or a bias system has to be employed.

(2) The dimensions of the PSII system and of its antennae are large and not fitted to the intensified pattern of light harvesting that is required for a >10% efficiency targeted conversion.

(3) The natural photosynthetic conversion pathway has intrinsic limitations that might be circumvented by the design of a fully nano-artificial device, covering a wider range of the spectrum with antennae short and powerful enough to tolerate the highest solar radiation intensities.

(4) Photochemical devices that mimic the photosynthesis of plant leaves and produce renewable fuels from solar energy using water as a raw material, require the integration of efficient light harvesting and photo-catalysis in nano-structured 'smart matrices', based on powerful biochemical and biophysical insights into natural water splitting and hydrogenases to address the complex chemistry of conversion and storage by multi-electron photocatalysis.

(5) A proper balance between time, space and energy scales has to be found to achieve the best results and overpass the 10% efficiency target. A set of guidelines for such a design have been proposed in this chapter and will have to be exploited if artificial leaf hydrogen production devices are to become a reality.

19.7 References

Abdelkrim M, Loulou M, Gharbi R, Fathallah M, Pirri C F and Tresso E (2007), 'Static and dynamic electrical study of a-SiC:H based *p–i–n* structure, effect of hydrogen dilution of the intrinsic layer', *Solid State Electron*, **51**, 137–41.

Alia A, Wawrzyniak P K, Janssen G J, Buda F, Matysik J and de Groot H J M (2009), 'Differential charge polarization of axial histidines in bacterial reaction centers balances the asymmetry of the special pair', *J Am Chem Soc*, **131**, 9626–7.

Archer M D and Bolton J R (1990), 'Requirements for ideal performance of photochemical and photovoltaic solar energy converters', *J Phys Chem*, **94**, 8028–36.

Armstrong F (2008), private communication to James Barber, St John's College, Oxford.

Badura A, Esper B, Ataka K, Grunwald C, Woll C, Kuhlmann J, Herberle J and Rogner M (2006), 'Light-driven water splitting for (bio-)hydrogen production: photosystem 2 as the central part of a bioelectrochemical device', *Photochem Photobiol*, **82**, 1385–90.

Barbato R, Friso G, Pontikos M and Barber J (1995), 'Characterization of the light-induced cross-linking of the alpha-subunit of cytochrome B(559) and the D1 protein in isolated photosystem-II reaction centers', *J Biol Chem*, **270**, 24032–7.

Barber J. (2006) 'Photosystem II; The Engine of Life'. *The Biochemist*, **28**, 7–11.

Barthet C and Guglielmi M (1996), 'Aspects of the conducting properties of Nafion doped polyaniline', *Electrochim Acta*, **41**, 2791–8.

Betley T A, Surendranath Y, Childress M V, Alliger G E, Fu R, Cummins C C and Nocera D G (2008), 'A ligand field chemistry of oxygen generation by the oxygen-

© Woodhead Publishing Limited, 2011

evolving complex and synthetic active sites', *Philos Trans Roy Soc B*, **363**, 1293–303.

Bibby T S, Mary I, Nield J, Partensky F and Barber J (2003), 'Low-light-adapted *Prochlorococcus* species possess specific antennae for each photosystem', *Nature*, **424**, 1051–4.

Canaguier S, Artero V and Fontecave M (2008), 'Modelling NiFe hydrogenases: nickel-based electrocatalysts for hydrogen production', *Dalton Trans*, **21**, 315–25.

Darensbourg M Y (2005), 'Synthetic chemistry – Making a natural fuel cell', *Nature*, **433**, 589–91.

de Groot H J M (2010), 'Integration of catalysis with storage for the design of multi-electron photochemistry devices for solar fuel', *Appl Magn Reson*, **37**(1-4), 497–503.

de Hatten X, Cournia Z, Huc I, Smith J C and Metzler-Nolte N (2007), 'Force-field development and molecular dynamics simulations of ferrocene-peptide conjugates as a scaffold for hydrogenase mimics', *Chem-Eur J*, **13**, 8139–52.

Fantuzzi A, Fairhead M and Gilardi G (2004), 'Direct electrochemistry of immobilized human cytochrome P450 2E1', *J Am Chem Soc*, **126**, 5040–1.

Fantuzzi A, Meharenna Y T, Briscoe P B, Sassone C, Borgia B and Gilardi G (2006), 'Improving catalytic properties of P450 BM3 haem domain electrodes by molecular Lego', *Chem Commun*, **28**, 1289–91.

Ferreira K N, Iverson T M, Maghlaoui K, Barber J and Iwata S (2004), 'Architecture of the photosynthetic oxygen-evolving center', *Science*, **303**, 1831–8.

Fiorilli S, Onida B, Barolo C, Viscardi G, Brunel D and Garrone E (2007), 'Tethering of modified Reichardt's dye on SBA-15 mesoporous silica: the effect of the linker flexibility', *Langmuir*, **23**, 2261–8.

Geobaldo F, Rivolo P, Uglieng P and Garrone E (2004), 'A new route to the surface functionalisation of porous silicon', *Sensors Actuator*, **100**, 29–32.

Giardi M T and Pace E (2005), 'Photosynthetic proteins for technological applications', *Trends Biochem Sci*, **23**(5), 257–63.

Glatzel P, Bergmann U, Yano J, Visser H, Robblee J H, Gu W, de Groot F M, Christou G, Pecoraro V L, Cramer S P and Yachandra V K (2004), 'The electronic structure of Mn in oxides, coordination complexes, and the oxygen-evolving complex of photosystem II studied by resonant inelastic X-ray scattering', *J Am Chem Soc*, **126**, 9946–59.

Grätzel M (2005), 'Solar energy conversion by dye-sensitized photovoltaic cells', *Inorg Chem*, **44**, 6841–51.

Hammarström L and Styring S (2008), 'Coupled electron transfers in artificial photosynthesis', *Philos Trans Roy Soc B*, **363**, 1283–91.

Hinsch A, Kroon J M, Kern R, Uhlendorf I, Holzbock J, Meyer A and Ferber J (2001), 'Long-term stability of dye-sensitised solar cells', *Prog Photovoltaics*, **9**, 425.

Icardi U A, Specchia S, Fontana G J R, Saracco G and Specchia V (2008), 'Compact direct methanol fuel cells for portable applications', *J Power Sources*, **176**, 460–7.

Jiao F and Frei H (2009), 'Nanostructured cobalt oxide clusters in mesoporous silica as efficient oxygen-evolving catalyst', *Angew Chem Int Edit*, **48**, 1841–4.

Karthikeyan C S, Nunes S P, Prado L A S A, Ponce M L, Silva H, Ruffmann B and Schulte K (2005), 'Polymer nanocomposite membranes for DMFC application', *J Membrane Sci*, **254**, 139–46.

King P W, Posewitz M C, Ghirardi M L and Seibert M (2006), 'Functional studies of [FeFe] hydrogenase maturation in an *Escherichia coli* biosynthetic system', *J Bacteriol.*, **188**, 2163–72.

© Woodhead Publishing Limited, 2011

Lamle S E, Vincent K A, Halliwell M, Abracht S P and Armstrong F A (2003), 'Hydrogenase on an electrode: a remarkable heterogeneous catalyst', *Dalton Trans*, **21**, 4152–7.

Li W, Wang X, Chen Z, Waje M and Yan Y (2005), 'Carbon nanotube film by filtration as cathode catalyst support for proton-exchange membrane fuel cell', *Langmuir*, **21**, 9386–9.

Limberg J, Vrettos J S, Liable-Sands L M, Rheingold AL, Robert H, Crabtree R H and Brudvig G W (1999), 'A functional model for O–O bond formation by the O_2-evolving complex in photosystem II', *Science*, **283**, 1524–7.

Liu F, Concepcion J J, Jurss J W, Cardolaccia T, Templeton JL and Meyer T J (2008), 'Mechanisms of water oxidation from the blue dimer to photosystem II', *Inorg Chem*, **47**, 1727–52.

Lubitz W, Reijerse E J and Messinger J (2008), 'Solar water-splitting into H_2 and O_2: design principles of photosystem II and hydrogenases', *Energ Environ Sci*, **1**, 15–31.

Markvart T and Landsberg P T (2002), 'Thermodynamics and reciprocity of solar energy conversion', *Physica E*, **14**, 71–7.

Matsumoto T, Nakaya Y, Itakura N and Tatsumi K A, (2008), 'Functional hydrogenase model: reversible interconversion of H_2 and H_2O by a hydroxo/sulfido-bridged dinuclear ruthenium-germanium complex', *J Am Chem Soc*, **130**, 2458–9.

Noy D, Moser C C and Dutton P L (2006), 'Design and engineering of photosynthetic light-harvesting and electron transfer using length, time, and energy scales', *Biochim Biophys Acta*, **1757**, 90–105.

Ogo S, Kabe R., Uehara K., Kure B., Nishimura T., Menon S. C., Harada R., Fukuzumi S., Higuchi Y, Ohhara T, Tamada T and Kuroki R (2007), 'A dinuclear Ni(mu-H)Ru complex derived from H_2', *Science*, **316**, 585–7.

Oudart Y, Artero V, Pécaut J and Fontecave M (2006), '[Ni(xbsms)Ru$(CO)_2Cl_2$]: a bioinspired nickel-ruthenium functional model of [NiFe] hydrogenase', *Inorg Chem*, **45**, 4334–6.

Pandit A, de Groot H J M and Holzwarth A (2006), *Harnessing Solar Energy for the Production of Clean Fuels*, European Science Foundation, White Paper.

Parcero E, Herrera R and Nunes S P (2006), 'Phosphonated and sulfonated polyhphenylsulfone membranes for fuel cell application', *J Membrane Sci*, **285**, 206–13.

Pizarro S A, Glatzel P, Visser H, Robblee J H, Christou G, Bergmann U and Yachandra V K (2004), 'Mn oxidation states in tri- and tetra-nuclear Mn compounds structurally relevant to photosystem II: Mn K-edge X-ray absorption and KÃŸ X-ray emission spectroscopy studies', *Phys Chem Chem Phys*, **6**, 4864–70.

Ponce M L, Gomes D and Nunes S P (2008), 'One-pot synthesis of high molecular weight sulfonated poly(oxadiazole–triazole) copolymers for proton conductive membranes', *J Membrane Sci*, **319**, 14–22.

Porro S, Musso S, Giorcelli M, Chiodoni A and Tagliaferro A (2007), 'Optimization of a thermal-CVD system for carbon nanotubes growth', *Physica E*, **37**, 16–20.

Prehn K, Adelung R, Heinen M, Nunes S P and Schulte K (2008), 'Catalytically active CNT-polymer-membrane assemblies: from synthesis to application', *J Membrane Sci*, **321**, 123–30.

Roeder J, Silva H, Nunes S P and Pires A (2005), 'Mixed conductive blends of SPEEK/PANI', *Solid State Ionics*, **176**, 1411–17.

Roeder J, Zucolotto V, Shishatskiy S, Bertolino J R, Nunes S P and Pires A (2006), 'Mixed conductive membrane: aniline polymerization in an acid SPEEK matrix', *J Membrane Sci*, **279**, 70–5.

© Woodhead Publishing Limited, 2011

Ross R T and Calvin M (1967), 'Thermodynamics of light emission and free-energy storage in photosynthesis', *Biophys J*, **7**, 595–614.

Rossmeisl J, Dimitrievski K, Siegbahn P and Norskov J K (2007), 'Comparing electrochemical and biological water splitting', *J Phys Chem C*, **111**, 18821–3.

Saracco G (1997), 'Transport properties of monovalent-ion-permselective membranes', *Chem Eng Sci*, **52**, 3019–31.

Saracco G and Specchia V (1994), 'Catalytic inorganic membrane reactors: present experience and future opportunities', *Catal Rev*, **36**, 305–84.

Sgroi M, Bollito G, Innocenti G, Saracco G, Specchia S and Icardi UA (2007), 'Study of an electrochemical alcohol concentration sensor: optimization of the anode structure', *J Fuel Cell Sci Tech*, **4**, 345–9.

Shockley W and Queisser H J (1961), 'Detailed balance limit of efficiency of *p-n* junction solar cells', *J Appl Phys*, **32**, 510–19.

Tang J M, Jensen K, Waje M, Li W, Larsen P, Pauley K, Chen Z, Ramesh P, Itkis M E, Yan Y, Yushan H and Haddon R C (2007), 'High performance hydrogen fuel cells with ultralow Pt loading carbon nanotube thin film catalysts', *J Phys Chem C*, **111**, 17901–4.

Tard C, Liu X, Ibrahim S K, Bruschi M, De Gioia L, Davies SC, Yang X, Wang LS, Sawers G and Pickett C J (2005), 'Synthesis of the H-cluster framework of iron-only hydrogenase', *Nature*, **433**, 610–13.

Touloupakis E, Giannoudi L, Piletsky S A, Guzzella L, Pozzoni F and Giardi M T (2005), 'A multi-biosensor based on immobilized photosystem II on screen-printed electrodes for the detection of herbicides in river water', *Biosens Bioelectron*, **20**, 1984–92.

van Gorkom H J (1986), 'Photochemistry of photosynthetic reaction centres'. *Bioelectroch Bioener*, **16**, 77–87.

Vincent K A, Cracknell J A, Lenz O, Zebger I, Friedrich B and Armstrong F A (2005), 'Electrocatalytic hydrogen oxidation by an enzyme at high carbon monoxide or oxygen levels', *Proc Natl Acad Sci USA*, **102**, 16951–4.

Vincent K A, Parkin A and Armstrong F A (2007), 'Investigating and exploiting the electrocatalytic properties of hydrogenases', *Chem Rev*, **107**, 4366–413.

Vlachopoulos N, Liska P, Augustynski J and Grätzel M J (1988), 'Very efficient visible light energy harvesting and conversion by spectral sensitization of high surface area polycrystalline titanium dioxide films', *J Am Chem Soc*, **110**, 1216–20.

Wu J Z, Angelis F D, Carrell T G, Yap G P A, Sheats J, Car R and Dismukes G C (2006), 'Tuning the photoinduced O_2-evolving reactivity of $Mn_4O_4^{7+}$, $Mn_4O_4^{6+}$, and $Mn_4O_3(OH)^{6+}$ manganese-oxo cubane complexes', *Inorg Chem*, **45**, 189–95.

Wurfel P (2002), 'Thermodynamic limitations to solar energy conversion', *Physica E*, **14**, 18–26.

© Woodhead Publishing Limited, 2011

20

Membranes for industrial microfiltration and ultrafiltration

A. CASSANO and A. BASILE,
Institute on Membrane Technology of the Italian National Research Council, (ITM-CNR), Italy

Abstract: In this chapter a general overview of industrial microfiltration (MF) and ultrafiltration (UF) processes is given. Basic principles, membrane materials, membrane preparation technologies, membrane module configurations and process designs involved in these operations are described. Membrane fouling and concentration polarization phenomena, as well as methods to control and reduce their effects on membrane performance, are also discussed. Finally the main applications of UF and MF membranes and their integration on a large technical scale are reviewed.

Key words: concentration polarization, membrane fouling, membrane processes, microfitration (MF), ultrafiltration (UF).

20.1 Introduction

Microfiltration (MF) and ultrafiltration (UF) are typical pressure-driven membrane operations that can be considered, together with reverse osmosis (RO), to be well-established industrial separation technologies. These processes are based on the use of polymeric membranes and represent a valid approach to solving separations problems involving particulate material and macromolecules. They are a valid alternative to competitive separation processes like distillation, extraction, fractionation, and adsorption, since the separation process is athermal and involves no phase change or chemical agents. Additional advantages are the relative simplicity of operation, low energy consumption, easy scale-up, low weight and space requirements, modularity and the possibility of carrying out the separation continuously (Bilstad, 1997).

The utilization of MF and UF processes on an industrial scale is relatively recent, spanning only 40 years. Up until 1945, membrane filters were used primarily for removal of microorganisms and particles from liquid and gaseous streams, for sizing of macromolecules and for culturing bacteria cells. The development of a RO cellulose acetate membrane with an asymmetric structure in the early 1960s (Loeb and Sourirajan, 1962) is considered to be a milestone in membrane science and technology. Soon, other synthetic

© Woodhead Publishing Limited, 2011

polymers were used as basic materials for synthetic membranes. UF was an offshoot of RO and really came into use only in the 1960s when MF on a smaller scale was already well established. The first commercially successful industrial UF system was installed in 1969 by Abcor to recover electrocoated paint from automobile paint shop rinsewater (Goldsmith *et al.*, 1971).

Today the market for UF and MF membranes and related equipment is well developed in a wide range of industrial applications with annual sales higher than one billion US $.

20.2 Basic principles of microfiltration and ultrafiltration

In both MF and UF processes the separation mechanism is mainly based on molecular sieving using porous membranes with increasingly fine pores (size exclusion). In general, MF is used to separate suspended particles with diameters between 0.1 and 10 μm from a fluid mixture; this size range includes a wide variety of natural and industrial particles. Typically solutes separated by MF are larger than those separated by UF and RO; consequently, the osmotic pressure for MF is negligible. Also, the membrane pore size and permeate flux are typically larger for MF than for UF and RO (Ho and Sirkar, 1992).

Membranes used in UF are characterized by pore sizes in the range 1–100 nm capable of retaining species in the molecular weight range 300–500 000 Da. Typical rejected species include dissolved macromolecules (such as proteins, sugars, polymers, biomolecules) and colloidal particles, whilst solvent and salts will pass through the membrane.

The driving force for transport across MF and UF membranes is a pressure differential which forces the suspending fluid and small solutes to pass through the membrane where they are collected as permeate; particles retained by the filter medium are collected as retentate. Because MF and UF membranes do not typically reject salts, osmotic pressure differentials are small compared to RO; consequently, the operative pressure required is relatively small (typically 1–10 bar).

The observed solute rejection R_i for a given species i is:

$$R_i = 1 - \frac{C_{i\mathrm{p}}}{C_{i\mathrm{r}}} \qquad [20.1]$$

where $C_{i\mathrm{p}}$ and $C_{i\mathrm{r}}$ are the concentrations (mol m^{-3}) in the permeate and retentate side, respectively. R can be ≤ 1 and is a function of the particle size, the pore size and pore size distribution.

The rejection characteristics of MF and UF membranes are usually expressed as nominal molecular weight cut-off (MWCO), defined as the smallest molecular weight species for which the membrane has more than

© Woodhead Publishing Limited, 2011

90% rejection. The permeate flux through the filter medium is affected by the applied pressure difference across the membrane, the resistance of the membrane and the viscosity of the fluid being filtered. The volumetric flux is given by:

$$J_v = \frac{P(\Delta p - \Delta\pi)}{l} \quad [20.2]$$

where P is a permeability coefficient (mol $m^{-1} s^{-1} Pa^{-1}$), Δp the hydrostatic pressure difference (Pa), $\Delta\pi$ the osmotic pressure difference (Pa) between feed and permeate phases and l the membrane thickness (m).

MF and UF membranes can be used both in dead-end and cross-flow mode. In the former, the feed solution is forced perpendicularly through the membrane under pressure; rejected particles accumulate on the membrane surface and the pressure needed to maintain the required flow increases, until at some point the membrane must be replaced. In the cross-flow configuration, feed material sweeps tangentially across the membrane surface producing a clean, particle-free permeate and a retentate containing the particles. The equipment is more complex but flux rates and membrane lifetime are maximized if compared to the dead-end filtration.

20.3 Membrane materials and membrane preparation technology

Materials for fabrication of commercial MF and UF membranes include synthetic polymers (polypropylene, perfluoropolymers, polyamides, polysulphones, etc.), cellulose derivatives, ceramics, inorganics and metals (Table 20.1). Membrane materials must be chemically resistant to both feed and cleaning solutions, mechanically and thermally stable and characterized by high selectivity and permeability.

Hydrophilic materials are not suitable for MF and UF membranes since water molecules act as plasticizers affecting mechanical strength and thermal stability. On the other hand, crystalline polymers show high chemical resistance and thermal stability since the crystalline domain contributes to the effect of cross-linking between amorphous domains and hinders the free rotation of polymer segments (Osada and Nakagawa, 1992). MF membranes generally consist of crystalline polymers. Polytetrafluoroethylene (PTFE), poly(vinylidene fluoride) (PVDF) and polypropylene (PP) are typical hydrophobic materials commonly used as MF membranes. Hydrophobic membranes are also widely used to minimize adsorption phenomena which reduce permeate fluxes and create difficulties in membrane cleaning.

Aliphatic polyamides such as nylon 4-6, nylon-6 and nylon 6-6, also widely used as MF membranes, are characterized by good chemical, thermal and mechanical stability. Amorphous polymers are generally used to produce UF

© Woodhead Publishing Limited, 2011

Table 20.1 Most common materials for MF and UF membrane preparation

Materials		Application	
		MF	UF
Polymers	Cellulose acetate (CA)	X	X
	Cellulose triacetate	X	X
	Cellulose esters	X	
	Cellulose nitrate (CN)	X	
	Blend CA/CN	X	
	Poly(vinyl alcohol)	X	X
	Polyacrylonitrile		X
	Poly(vinyl chloride) (PVC)	X	
	PVC copolymer	X	X
	Acrylic copolymer	X	
	Aromatic polyamide	X	X
	Aliphatic polyamide	X	X
	Polyimide	X	X
	Polysulphone	X	X
	Sulphonated polysulphone		X
	Polyethersulphone		X
	Polyetheretherketone (PEEK)	X	X
	Polycarbonate	X	
	Polyester	X	
	Polypropylene	X	
	Polyethylene	X	
	Poly(phenylene sulphide)	X	X
	Polytetrafluoroethylene (PTFE)	X	X
	Poly(vinylidene difluoride) (PVDF)	X	X
	Polybenzimidazole	X	
	Teflon	X	X
Ceramics	Alumina	X	X
	Zirconia/alumina	X	
	Zirconia/sintered material	X	
	Zirconia/carbon	X	X
	Silica	X	X
	Silica carbide	X	
	Pyrolysed carbon		X
Sintered metal	Type 316 stainless steel	X	
	Other alloys	X	

membranes owing to their convenient regulation and control of small pores size. Polymeric materials which have a high glass transition temperature are generally employed. In particular, polyacrylonitrile (PAN), widely used for general aqueous systems because of its resistance to solvents and chemicals, also exhibits relatively low protein binding owing to its hydrophilic properties. Polysulphone (PS), also widely used in the production of UF membranes, has good mechanical strength and good resistance to heat and pH; in contrast it exhibits poor resistance to solvents.

© Woodhead Publishing Limited, 2011

In terms of structure, MF and UF membranes can be either symmetric or asymmetric. Symmetric membranes are characterized by identical structure and transport properties over the entire cross-section of the membrane. In asymmetric membranes structural and transport properties vary over the membrane cross-section; typically, a relatively dense thin selective layer (0.1–1 μm) is supported by a much thicker (100–200 μm) porous substrate. The mass flux is determined mainly by the thickness of the selective layer, whereas the porous sub-layer provides mechanical strength and has little effect on the separation characteristics of the membrane. MF membranes can be prepared by several methods: slip coating-sintering, stretching, phase inversion and track-etching.

Thermoplastic polymers can be melted and extruded through a die producing a macroporous membrane whose pore structure is induced by stretching the material. The partially crystalline polymeric material is stretched perpendicularly to the direction of extrusion so that crystalline regions are located parallel to the direction of extrusion. Under mechanical stress, small slit-like ruptures (generally 0.2 μm in length and 0.02 μm in width) occur in the membrane (Kesting, 1985). Pore diameters of the produced membrane are in the range 0.1–3 μm, while the porosity can approach 90%. PP and PTFE are materials typically used in the production of these membranes.

Ceramic membranes for UF and MF made from aluminium, titanium or silica oxides are generally realised by a slip coating-sintering process (Strathmann *et al.*, 2006). In this process a porous ceramic support tube is made by pressing a dispersion of a fine-grain ceramic material and then heating at high temperature. By using the correct sintering temperature, the interface between the particles disappears producing a porous structure. One surface of the tube is then coated with a suspension of finer particles in a solution of a cellulosic polymer or polyvinyl alcohol which acts as a binder and viscosity enhancer to hold the particles in suspension. When this mixture, called a slip suspension, is dried and sintered at high temperature, a finely porous surface layer remains. Several slip-coated layers formed by suspensions of progressively finer particles can be applied in series producing an asymmetric structure. Pore diameters in ceramic membranes for MF and UF are in the range from 0.01–10 μm.

An ideal form of porous membrane is a dense polymer with cylindrical pores. Such membranes can be produced by track-etching (Fleischer *et al.*, 1969). This procedure involves irradiation of a thin polymer film (about 10 μm thick) with fission particles from a nuclear reactor or other radiation source: the highly energetic ions pierce the polymeric film and break the polymer chains leaving 'tracks' in the membrane material (tracking). In the etching step, the tracked film is immersed in an acid (or alkaline) solution in which tracks are converted into cylindrical pores with a uniform diameter and a narrow pore size distribution. The exposure time of the film to radiation

© Woodhead Publishing Limited, 2011

controls the number of membrane pores (pore density), while the etching time determines the pore diameter which can range between 0.2 μm and 10 μm. Membranes prepared by the track-etching procedure are symmetrical and the permeate flux is proportional to the membrane thickness; consequently, they have to be thinner than asymmetric microporous membranes in order to have a comparable flux. Polycarbonate or polyester films are the usual materials used for track-etched membranes. The porosities of these membranes are of the order of 10%.

Most polymeric MF and UF membranes are prepared by the phase inversion process (Baker, 2000). In this process a colloidal dispersion (sol) is converted, by removal of solvent, into a swollen three-dimensional macromolecular network (gel) which ultimately forms a solid matrix, the membrane. Thus the phase inversion process can be considered a sol–gel transition. The dope mixture (i.e. casting solution) contains the polymer, the solvent (which is the most volatile component), and may include a swelling agent and/or a non-solvent as well as ingredients, such as lithium or magnesium salts, that influence the kinetics of the phase separation process. After a specific period of maturation, the casting solution is cast as a film either as a flat sheet on a smooth surface (i.e. a glass plate) or inside a porous tube or extruded through a spinnerette as a hollow fibre. Following a period of evaporation of the solvent, the cast film is transferred to a non-solvent gelation bath (usually a water bath) where exchange occurs between solvent and non-solvent leading to polymer precipitation. The procedure produces a liquid phase forming the membrane pores and a solid phase forming the membrane structure, which may be either symmetric or asymmetric (Strathmann, 1985).

The performance of phase inversion membranes, in terms of flux and selectivity, is affected by different parameters such as polymer concentration, evaporation time before immersion, humidity, temperature, composition of the casting solution and the coagulation bath composition.

In the Accurel process developed by Enka (Schneider, 1982) PP is mixed with *N*,*N*-bis(2-hydroxyethyl)hexadecylamine to form a binary system, which is miscible at 150°C but immiscible at lower temperatures (50°C). Phase separation is obtained by extruding the note dope, as films, tubes or fibres into a cooled bath of the hexadecylamine. This phase inversion technique, named thermal phase inversion, produces a symmetric microporous membrane with a relatively narrow distribution of effective pore size.

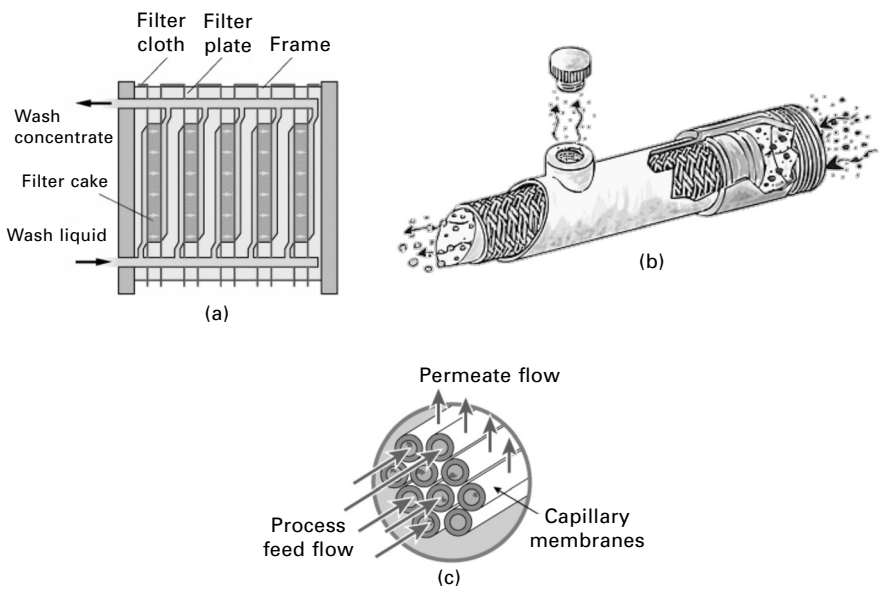
20.4 Module configuration and process design

MF and UF membranes used at the industrial level are installed in a device generally called a membrane module. The choice of the membrane module depends on different parameters such as the production cost, packing density, energy consumption and especially the control of concentration polarization

© Woodhead Publishing Limited, 2011

and membrane fouling. On a large industrial scale, membrane modules are available in five basic designs: hollow fibre, spiral wound, tubular, plate and frame and capillary (Fig. 20.1). They are quite different in their design, mode of operation, production costs and energy requirement for pumping the feed solution through the module.

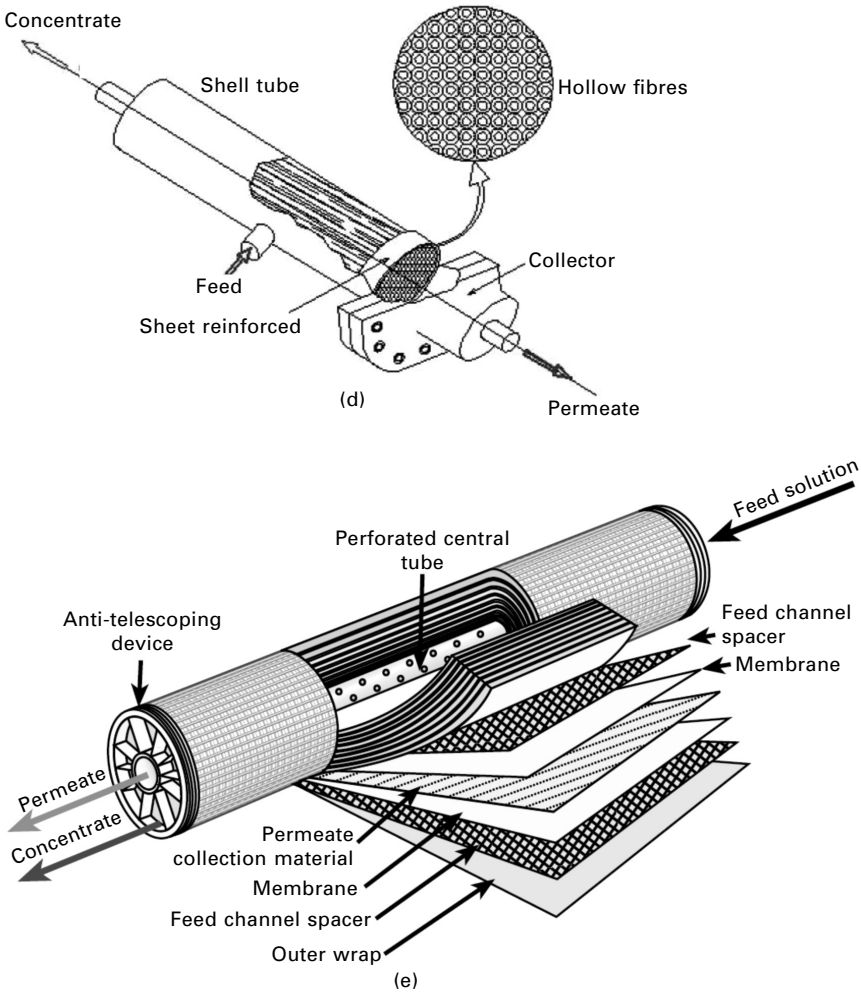
In the following the basic concepts of the principal module types used in cross flow MF and UF are discussed. The design of the plate-and-frame module (Fig. 20.1(a)) has its origin in the conventional filter press concept. Membranes, feed flow spacers and porous permeate support plates are layered together between two endplates and placed in a housing. The sheets are either in the form of circular discs, elliptical sheets or rectangular plates. The feed mixture is pressurized in the housing and forced across the membrane surface. A portion passes through the membrane, enters the permeate channel and makes its way to a central permeate collection manifold. Plate-and-frame units are mainly used for small-scale applications (production of pharmaceuticals, bioproducts or fine chemicals); these units, however, are quite expensive and the membrane replacement is labour intensive. They are used in a limited number of UF applications with highly fouling feeds. The feed channels are often less than 1 mm thick and, although more sensitive to fouling, are easier to clean as no mesh support is used.



20.1 Schematic drawing illustrating basic configurations of membrane modules: (a) plate and frame module, (b) tubular module, (c) capillary module, (d) hollow-fibre module, (e) spiral-wound module.

Continued overleaf

© Woodhead Publishing Limited, 2011



20.1 Continued

The tubular membrane module (Fig. 20.1(b)) consists of membrane tubes surrounded by porous paper or fibreglass supports. The pressurized feed solution flows internally along the tubes and the permeate is collected on the outer side of the porous support. Tube diameters are in the range 1–2.5 cm and a number of tubes are placed in one pressure housing in order to increase the module productivity. Tubular modules can also be made by welding flat sheet membranes that are cast on a mechanically strong porous polyester support. These tubes, which have a diameter of 0.5–1 cm, do not require an additional support if operated at pressures of less than 4 bar. They are typically used in UF at low hydrostatic pressure.

© Woodhead Publishing Limited, 2011

Concentration polarization and membrane fouling phenomena can be easily controlled in tubular membrane modules; moreover, plugging of the membrane module can be avoided even with feed solutions containing a very high concentration of solid matter. On the other hand the low surface area that can be installed in a given unit volume and the high costs are the main drawbacks of the tubular design. Consequently, tubular membranes are generally used when feed solutions containing high solid content and with high viscosity have to be treated (i.e. industrial effluents or treatment of solutions coming from the food and pharmaceutical industries).

The capillary membrane module (Fig. 20.1(c)) is essentially constituted by a large number of membrane capillaries with an inner diameter of 0.5–3 mm arranged in parallel as a bundle in a shell tube. The feed solution is pumped into the lumen of the membranes and the permeate is collected in the shell tube. Fibres are open at both ends with the tube-fibre bank sealed in epoxy blocks. UF capillary membranes are available in a wide range of polymers including PS, PAN and chlorinated polyolefins.

The capillary membrane module is characterized by a high membrane area per module volume and low production costs; another advantage is the possibility of controlling concentration polarization and membrane fouling through a physical process called back flushing in which the permeate flow is reversed allowing the fouling material to be dislodged from the membrane surface. The main drawbacks of the capillary membrane module are the required low operating pressure which cannot exceed values of 4–6 bar owing to the limited stability of the membranes.

Hollow fibre membrane modules (Fig. 20.1(d)) consist of a bundle of several membrane fibres with the free ends potted with an epoxy resin into a cylindrical housing or shell. Fibres with diameters in the range 50–200 μm are usually called fine hollow fibres. The selective layer is on the outside of the fibres where the feed fluid is applied while the permeate is removed down the fibre bore. Such fibres can withstand very high hydrostatic pressures applied from the outside and they are typically used in RO desalination of sea water or in high-pressure gas separation. When the fibre diameter is between 200 μm and 500 μm, the feed solution is commonly applied to the inside bore of the fibre and the permeate is removed from the shell side. These fibres are used for low-pressure gas separation and for UF applications. Fibres with diameters greater than 500 μm are called capillary fibres.

The hollow fibre membrane module is characterized by the highest packing density compared with other configurations and its production is very cost effective. Its drawbacks are related to the difficulty in controlling concentration polarization and membrane fouling. Consequently an extensive pretreatment of the solution is needed in order to remove particles, macromolecules or other materials which can precipitate at the membrane surface.

The spiral wound membrane module (Fig. 20.1(e)) is characterized by a

© Woodhead Publishing Limited, 2011

simple design consisting of an envelope containing the feed flow channel spacer, the membrane and a porous membrane support rolled around a perforated central collection tube; the module is placed inside a tubular pressure housing made from stainless steel or polyvinyl chloride (PVC). The feed solution passes axially through the feed channel across the membrane surface. The permeate moves along the permeate channel and is collected in the collection tube. Small spiral wound modules for laboratory applications consist of a single envelope wrapped around the collection tube. These units have a membrane area in the range 0.2–1 m^2. Industrial scale modules are realised according to a multi-leaf arrangement with several membrane envelopes, each one with an area of 1–2 m^2, wrapped around the central collection tube. This design permits the pressure drop encountered by the permeate fluid moving down the permeate channel to the central pipe to be minimized. In particular, in a single membrane envelope the path taken by the permeate to reach the collection tube would be several metres long resulting in a large pressure drop in the permeate collection channel. UF spiral wound modules are produced in standard module sizes and have a diameter of 0.05, 0.1 and 0.2 m and lengths between 0.15 and 1.2 m corresponding to membrane areas up to 15 m^2 depending upon channel width. The spiral wound configuration is compact and provides a relatively large area per unit volume that is relatively inexpensive but prone to particulate fouling (thus pre-filtration is needed). Commercially available membrane modules for UF and MF applications are summarized in Table 20.2.

Selection of the correct membrane in MF and UF applications is one of the most important factors for achieving a desired separation. However, the process design is equally important since it determines: (1) the technical feasibility and the economics of the process, (2) the achievable recovery rate, (3) the maximum concentration of a component in the retentate and (4) the lifetime of the membranes (the process design is an important factor for the control of concentration polarization and membrane fouling). In these processes the driving force in transporting specific compounds through a semi-permeable membrane is the difference in hydrostatic pressure applied between the two sides of the membrane. As a result the feed solution is

Table 20.2 Commercially available membrane modules for UF and MF applications

Type	Membrane area per unit volume (m^2 m^{-3})	Investment costs/ installed area	Control of concentration polarization	Ease of clearing
Plate-and-frame	400–800	Medium	Good	Good
Spiral-wound	800–1200	Low	Good	Medium
Tubular	20–100	Very high	Very good	Very good
Capillary	600–1200	Low	Good	Poor
Hollow fibre	2000–5000	Very low	Very poor	Very poor

© Woodhead Publishing Limited, 2011

converted into a permeate and a retentate stream according to the scheme reported in Fig 20.2. The performance of a MF or UF membrane is expressed in terms of permeate flux and separation properties. They are a function of the membrane permeability for different compounds in the feed solution and the applied hydrostatic pressure. In addition, they are also a function of the process design.

The separation capability of a MF or UF membrane is expressed as membrane rejection according to Equation [20.1]. However, the concentrations in the retentate and permeate streams depend not only by the membrane rejection but also by the recovery rate (Δ) which is given by:

$$\Delta = \frac{V_p}{V_0} \qquad [20.3]$$

where $V_p = V_p(t)$ and V_0 are the permeate volume and the initial feed volume (m^3), respectively, and t is the time. The recovery rate ranges between 0 and 1. Sometimes data are also presented as volume concentration ratio (VCR):

$$\text{VCR} = \frac{V_0}{V_r} \qquad [20.4]$$

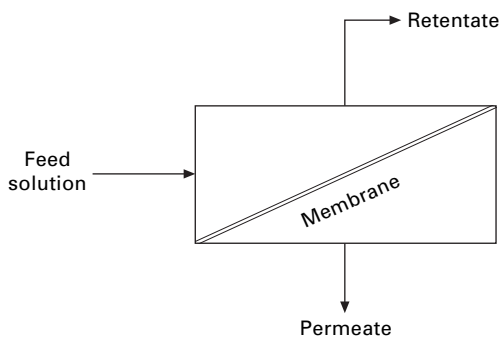
where $V_r = V_r(t)$ is the retentate volume (m^3).

The concentration of a solute at any time in the process is a function of both volume concentration ratio and rejection according to Equation [20.5]:

$$C_r = C_0 (VCR)^R \qquad [20.5]$$

where C_r and C_0 are the solute concentration in the retentate and in the initial feed solution, respectively.

The yield (Y) of a specific component is defined as the fraction of that component in the original feed recovered in the final retentate:



20.2 Schematic representation of microfiltration and ultrafiltration processes.

© Woodhead Publishing Limited, 2011

$$Y = \frac{C_r V_r}{C_0 V_0} \quad [20.6]$$

Equation [20.7] is obtained by combining Equations [20.4], [20.5] and [20.6]:

$$Y = (VCR)^{R-1} \quad [20.7]$$

According to Equation [20.7], the yield of a specific compound is an exponential function of the decreasing volume of the feed in the system (Cheryan, 1998). The most common process configurations in MF and UF are:

- total recycle
- batch concentration (with full or partial recycle of retentate)
- single-pass processing
- feed-and-bleed process
- diafiltration
- multistage recycle operation.

A schematic representation of these operation modes is reported in Fig. 20.3.

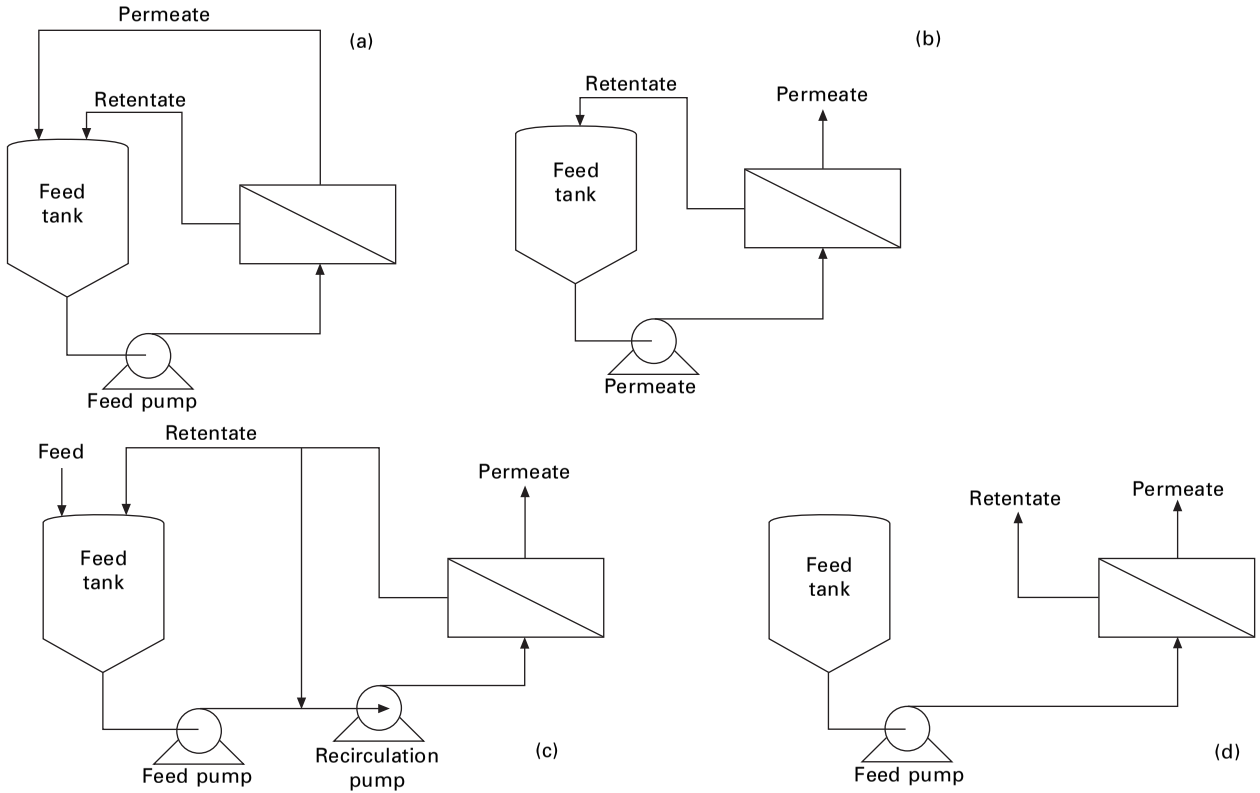
In the total recycle configuration (Fig. 20.3(a)), the permeate and retentate streams are returned to the feed reservoir and no net concentration of particles occurs. This configuration is mainly used in order to study the effect of different operating parameters on the permeate flux.

In the batch concentration configuration, the retentate is returned to the feed reservoir and the permeate is collected separately (full recycle of retentate) (Fig. 20.2(b)). This approach requires the minimum membrane area and one pump can be used for both feed and recirculation. The batch concentration with partial recycle of retentate (Fig. 20.3(c)) configuration is used when a continuous feedstream has to be processed. Batch operations are used when the permeate is the product of interest such as in fruit juice clarification or treatment of effluents in which the retentate has to be discharged. In this approach the residence time of particles within the system is longer than in other configurations.

In single-pass processing (Fig. 20.3(d)), the feed solution is continuously fed into the filtration device: in most cases the recirculation flow rate is higher than the permeate flux. This approach results in a very low permeate volume and low recovery rate unless a very large membrane area is used. In this case the residence time of particles in the system is minimized. Higher recovery rates can be obtained by applying the feed-and-bleed operation mode in which the permeate is removed from the system together with a small part of the retentate (Fig. 20.3(e)). Most of the retentate is recycled and mixed with the feed solution to maintain a high tangential velocity in the membrane module. A feed pump and a recirculation pump are required

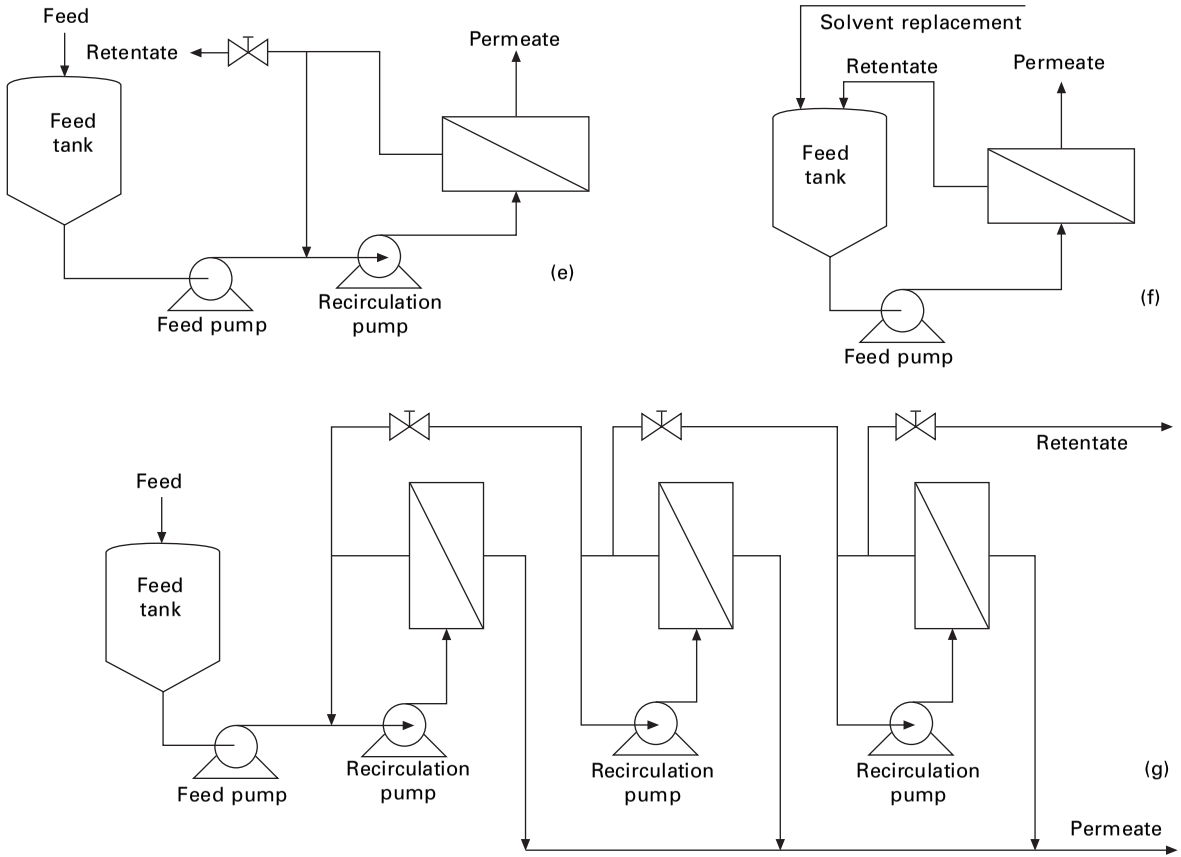
© Woodhead Publishing Limited, 2011

© Woodhead Publishing Limited, 2011



20.3 Schematic diagram of different operation modes in MF and UF processes: (a) total recycle, (b) batch concentration with full recycle of retentate, (c) batch concentration with partial recycle of retentate, (d) single-pass continuous filtration, (e) feed-and-bleed operation, (f) diafiltration, (g) multistage filtration.

© Woodhead Publishing Limited, 2011



20.3 Continued

to provide the transmembrane pressure and the cross-flow, respectively. If a component is not completely retained by the membrane, its concentration is proportional to the retentate concentration and is increased by increasing the recovery rate. Since the process loop is operated continuously at a concentration factor equivalent to the final concentration of a batch system, the permeate flux is lower than the average flux in a batch mode and the membrane area required is correspondingly higher.

In diafiltration the retentate is recycled to the feed reservoir and the permeate is replaced by an equal volume of pure solvent (Fig. 20.3(f)). This configuration is often used when more complete separation of micro- and macrosolutes is required (Porter and Michaels, 1971). Diafiltration is used, for example, to remove salts from a mixture containing macromolecular compounds such as proteins. The variation of the permeate and retentate concentration with time during the diafiltration process is given by:

$$\frac{V_p C_{ip}}{t} = -V_0 \frac{dC_{ir}}{dt} \qquad [20.8]$$

where C_{ip} and C_{ir} are the concentration of the component i in the permeate and in the feed tank, and V_0 and V_p the volumes of the feed tank and the permeate, respectively. Introducing $V_p = V_w$ and $C_{ip} = (1 - R)\, C_{ir}$ into Equation [20.8], and integrating over a certain time period, the concentration in the feed tank will be given by:

$$C_{ir} = C_{ir}^{0} \exp - (1 - R)\frac{V_w}{V_0} \qquad [20.9]$$

where C_{ir} and C_{ir}^{0} are the concentrations in the feed tank at time t (s) and at the beginning of the filtration, V_0 is the volume of the feed tank, V_w is the volume of the solvent added during time t and R the rejection of the membrane towards the component i. The ratio V_w/V_0, named the diavolume coefficient, is a parameter used to evaluate the diafiltration process.

Finally, the multistage recycle operation (Fig. 20.3(g)) permits the low flux disadvantage of the feed-and-bleed operation to be overcome. In this case, a multitude of filtration devices is arranged in series and the individual devices are referred to as stages. Only the final stage operates at the highest concentration and lowest flux, while the other stages operate at lower concentrations with higher fluxes. This permits the total membrane area to be reduced in comparison with a single stage operated in a feed-and-bleed configuration.

20.5 Concentration polarization and membrane fouling

Concentration polarization and membrane fouling are typical phenomena affecting the performance of MF and UF processes. The general effect of

© Woodhead Publishing Limited, 2011

these phenomena is a reduction in the permeate flux through the formation of an additional barrier caused by the retention of feed solution compounds with a consequent increase in the mass transfer resistance.

When a feed solution containing a solvent and a solute or suspended solids is filtered through a porous membrane, some components permeate the membrane under a given driving force while others are retained. This results in a higher local concentration of the rejected solute at the membrane surface, compared to the bulk, with formation of a viscous or gelatinous cake layer. This phenomenon is referred to as concentration polarization (Aimar *et al.*, 1989; Cheryan, 1998; Mulder, 1991). It is not to be confused with the membrane fouling phenomenon that is essentially caused by deposition of retained particles onto the membrane surface or in the membrane pores.

Two mechanisms have been proposed to explain the reduction in flux in polarization-limited systems. In the former, the increased solute concentration at the membrane surface leads to an increase in the osmotic pressure and thus to a decrease in the driving force (P_T-$\Delta\pi$) and flux at constant applied pressure. This mechanism can be considered valid in RO systems in which the feed solutions have a considerable osmotic pressure. In UF and MF, only macromolecules are retained by the membrane: consequently, the osmotic pressure of the feed solution is generally small. Owing to the high molecular weight of the retained compounds, their diffusion back from the membrane surface to the bulk is relatively low. According to the second mechanism, the retained components are precipitated to form a solid layer at the membrane surface. This consolidated layer affects the performance of the process by both reducing the membrane flux and modifying the rejection towards lower molecular weight compounds.

A mathematical model generally accepted to describe the concentration polarization in MF and UF processes is the well-known film theory (Fig. 20.4). This relates the solute concentration at the membrane surface to that in the bulk and permeate solutions, the membrane flux and fluid flow conditions in the boundary layer between membrane surface and bulk solution. The film model assumes that the solute is brought to the membrane surface by convective transport at a rate J_s (mol m^{-2} s^{-1}) defined as:

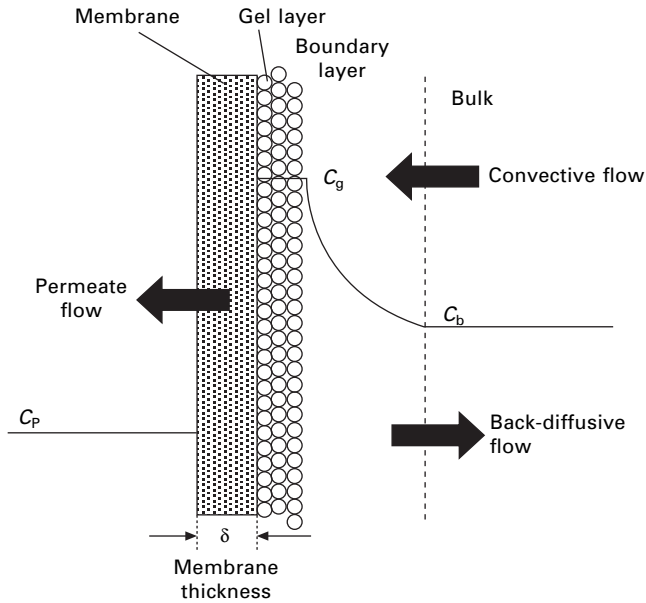
$$J_s = J_v C_b \qquad [20.10]$$

where J_v is the membrane volume flux (m s^{-1}) and C_b the bulk concentration of the rejected solute.

The resulting concentration gradient causes a diffusive flux of the retained material back into the bulk solution at a rate given by:

$$J_s = -D\frac{dC}{dx} \qquad [20.11]$$

© Woodhead Publishing Limited, 2011



20.4 Schematic diagram of the concentration polarization phenomenon according to the film model (C_g is the solute concentration at the membrane surface, C_P is the solute concentration in the permeate and C_b is the solute concentration in the bulk solution).

where D is the solute diffusion coefficient ($m^2\ s^{-1}$) and dC/dx the concentration gradient of the solute in the boundary layer.

In the steady state, the convective transport is counterbalanced by the diffusive flux and Equations [20.10] and [20.11] can be equated and integrated over the boundary layer leading to:

$$J_v = \frac{D}{\delta} \ln \frac{(C_g - C_P)}{(C_b - C_P)} \qquad [20.12]$$

where C_g is the solute concentration at the membrane surface (gel concentration), C_P is the permeate solute concentration and δ is the boundary layer thickness (m).

Since the membrane rejection R is given by Equation [20.1], the combination of Equations [20.1] and [20.12] leads to:

$$\frac{C_g}{C_b} = \frac{\exp \frac{J_v \delta}{D}}{R + (1 - R) \exp \frac{J_v \delta}{D}} \qquad [20.13]$$

According to Equation [20.13], the concentration polarization is expressed

© Woodhead Publishing Limited, 2011

as the ratio of the solute concentration at the membrane surface and the solute concentration in the bulk. It is a function of the membrane flux J_v, the boundary layer thickness δ (m), the solute diffusion coefficient in the boundary layer D and the membrane solute rejection R.

The concentration polarization can be described in various feed flows conditions introducing a solute mass transfer coefficient k (which has the same units as the flux J_v, m s^{-1}) given by:

$$k = \frac{D}{\delta} \qquad [20.14]$$

Introducing k into Equation [20.13] leads to:

$$\frac{C_g}{C_b} = \frac{\exp \frac{J_v}{k}}{R + (1 - R) \exp \frac{J_v}{k}} \qquad [20.15]$$

in which the concentration polarization is a function of the membrane flux, the membrane rejection and the mass transfer coefficient.

The mass transfer coefficient can be estimated by using the following general equation (Sherwood *et al.*, 1965):

$$Sh = a Re^b Sc^C \left(\frac{d_h}{L}\right)^d \qquad [20.16]$$

where Sh, Re and Sc are the Sherwood, Reynolds and Schmidt numbers, respectively, L is the length (m) of the feed flow channel (or tube), d_h is the hydraulic diameter (m) of the feed channel and a, b, c and d are characteristic constants for different geometries to be experimentally determined.

The Schmidt number is given by:

$$Sc = \frac{\nu}{D} \qquad [20.17]$$

where ν is the viscosity (m^2 s^{-1}).

The Reynolds number in a channel (or in a tube) is given by:

$$Re = \frac{d_h u}{\nu} \qquad [20.18]$$

where u is the fluid velocity (m s^{-1}).

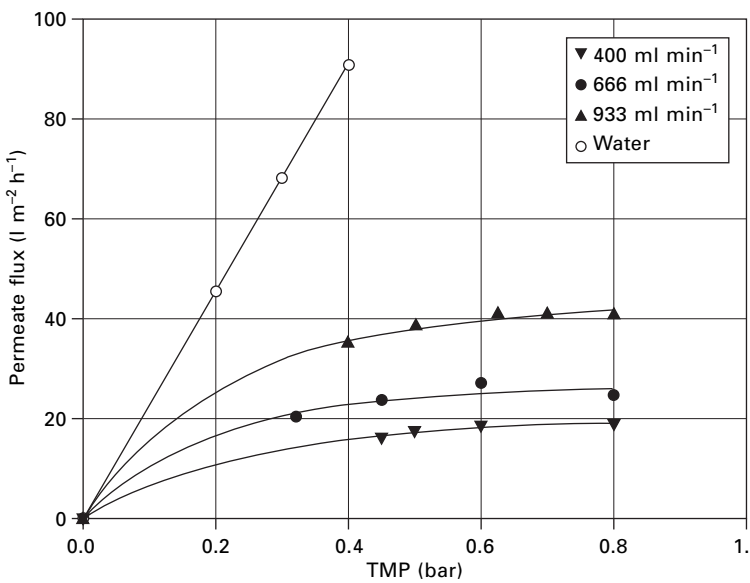
In general, Re values less than 1800 are considered to be laminar flow and Re greater than 4000 is turbulent flow. The film model can be used to describe the concentration polarization in both the turbulent and laminar flow regimes. In the turbulent flow regime entrance effects can be neglected: in this case the exponent d in Equation [20.16] is zero. In the laminar flow regime entrance effects cannot be neglected and the Sherwood number is expressed as (Bird *et al.*, 1965):

© Woodhead Publishing Limited, 2011

$$Sh = \left(a\, Sc\, Re\, \frac{d_h}{L} \right)^{0.33} \qquad [20.19]$$

and the concentration polarization can be obtained as a function of the flow velocity, the channel height and the channel length by combining Equations [20.15] and [20.19].

The film model is not always applicable in MF and UF because the feed solutions contain macromolecular compounds or suspended particles with low diffusion coefficients; consequently, the diffusive mass transport of retained compounds from the membrane surface back into the bulk solution is slower than the convective mass transport towards the membrane. When the solute concentration at membrane surface exceeds the solubility of the feed constituents it can precipitate forming a solid layer on the membrane surface. This layer results in an additional hydrodynamic resistance to the membrane flux. In these conditions, if the transmembrane pressure is increased, more solutes are transported towards the membrane increasing the layer thickness at the membrane surface without a corresponding increase in flux. The experimental evidence of this concept is illustrated in Fig. 20.5 referred to the UF of a macromolecular solution, such as a kiwifruit juice (Cassano *et al.*, 2008). Here permeate fluxes in the steady state are reported as a function of the applied transmembrane pressure at different feed flow rates. At low



20.5 Clarification of kiwifruit juice by UF. Effect of transmembrane pressure (TMP) on the permeate flux at different feed flow rates (operating temperature, 30°C).

© Woodhead Publishing Limited, 2011

pressures, the permeate flux is proportional to the applied pressure. When the particles start to deposit on the membrane surface the rate of increase of flux decreases. Further increases in pressure determine an increase in the thickness of the particle layer and when the concentration polarization layer reaches a limiting concentration, the flux becomes independent of the pressure. The gel-polarized layer is assumed to be dynamic. Higher flow rates tend to remove the deposited material reducing the hydraulic resistance through the membrane: consequently, higher permeate fluxes can be obtained.

Membrane fouling is the major limiting step in MF and UF processes. The term fouling is referred to a long term flux decline caused by the deposition of retained particles (colloids, suspended particles, macromolecules, etc.) onto the membrane surface and/or within the pores of the membrane. The fouling behaviour is specific to the system of interest and is strongly affected by the physicochemical nature of the membrane, the solutes and the fluid dynamic system design.

Membrane fouling can also be a consequence of concentration polarization phenomena. Gel or cake layer formation may be caused by inorganic precipitates (such as $CaSO_4$ and metal hydroxides), organic materials (such as proteins, lipids, humic acids and other macromolecular materials) and biological components (such as microorganisms and products of their metabolism). However, membrane fouling can be also caused by adsorption of specific substances onto the membrane surface owing to hydrophobic interactions, van der Waals force attractions or electrostatic forces (Strathmann *et al.*, 2006).

Both polarization concentration and fouling determine a reduction of permeate flux in MF and UF processes. However, they can have an opposite effect on the observed rejection: the concentration polarization determines a reduction in the rejection. In the case of fouling, if the build-up of solids on the membrane is significant enough, it may act as a secondary membrane and change the effective sieving and transport properties of the system: consequently, the rejection can be increased or maintained constant. While the concentration polarization is a reversible process based on diffusion taking place over a few seconds, fouling is generally irreversible and the flux decline is a long-term process. A constant flux is not generally reached at all. Finally, the concentration polarization can be described by a simple mathematical model and minimized by means of hydrodynamics, such as the feed flow velocity and the membrane module design; in contrast, the control and description of membrane fouling are more difficult.

The attachment of biological materials, such as proteins, organic acids, polysaccharides and microorganisms to membrane surfaces is recognized as biofouling. A general model accepted for bacterial fouling in water systems includes the attachment of organisms to a specific surface, followed by the adsorption of simple organic molecules that fuel further metabolic actions

© Woodhead Publishing Limited, 2011

and a final step in which a polysaccharide, named glycocalyx, is generated stabilizing the microorganism–surface interaction. The consequences of biofouling are in terms of loss of performance, incresase in energy input and costly cleaning. Methods generally accepted for controlling and minimizing fouling phenomena can be summarized as: feed pretreatment, modification of membrane properties, modification of operating conditions, flow manipulation and membrane cleaning with the correct chemical agents.

Pretreatment methods for feed solutions include coagulation, sedimentation, precipitation, prefiltration, pH adjustment, chlorination and carbon adsorption. The modification of membrane properties is another approach for reducing the extent of fouling. For example, hydrophobic membranes, which strongly adsorb proteins, can be modified by introducing hydrophilic characteristics. This can be achieved by mixing hydrophilic and hydrophobic polymers, or by pretreatment of hydrophobic membranes with hydrophilic surfactants or enzymes or by surface modification (Strathmann *et al.*, 2006). Surface modifications include plasma treatment, polymerization or grafting of the surface initiated by heat, chemicals or UV light, interfacial polymerization and introduction of ionic or polar groups by chemical reaction.

Process parameters such as temperature, flow rate, pressure and feed concentration have great influence on membrane fouling. Generally, an increasing temperature results in an increasing permeate flux. However in some cases, such as in the UF of cheese whey, a flux decreasing at a temperature lower than 30°C has been observed owing to a decrease in the solubility of calcium phosphate (Cheryan, 1998). In addition, in most UF applications concerning biological systems, the adsorption of proteins generally increases with temperature. In many cases, an increase in the shear rate generated at the membrane surface tends to shear off deposited material and thus reduces the hydraulic resistance of the fouling layer. When the polarization layer reaches a limiting concentration, an increase in operating pressure does not improve the performance of the system and the flux remains practically unchanged. High pressures may also cause severe fouling in MF and UF processes owing to compaction of the fouling layer.

Removal of foreign material from both the membrane surface and membrane pores is defined as membrane cleaning. Typical systems used for membrane cleaning are based on mechanical, hydraulic, chemical or electrical methods. Hydraulic cleaning is generally performed by backflushing conducted by pumping permeate back into the feed channel to lift deposited material off the membrane surface. In most cases, backflushing is done with permeate for 1–5 s at a frequency of 1–10 times/min at 1–10 bar. Backflushing is effective with many kinds of foulants, in particular with materials that are not linked to the membrane as adherent films.

Mechanical cleaning is generally obtained by forcing foam balls down tubular modules at high velocities. The balls create turbulence at the membrane

© Woodhead Publishing Limited, 2011

surface dislodging fouling materials. Electrical cleaning methods are based on the use of electrical pulsing which is able to remove charged species from the membrane surface. Special modules are required to introduce the charge to the membrane surface which is generally realised in metallic form.

The most important method of controlling and minimizing membrane fouling is chemical cleaning. It aims to solubilize or disperse the foulant or soil. The choice of cleaning agent depends upon the type of foulant, type of membrane and the severity of fouling. Typical cleaning agents are acids, alkalis, detergents, enzymes, complexing agents and disinfectants. Alkaline solutions containing NaOH or KOH, sometimes supplemented with hypochlorite, are particularly effective for solubilizing fats and proteins. Sodium carbonate, soda ash or phosphates are used as buffering compounds to control the pH during the cleaning. Mineral acids, polyacrylates and ethylenediaminetetraacetic acid (EDTA) are used essentially to remove salt precipitates and mineral scalants. Phosphoric acid is largely used because it is not very aggressive; in addition, it also has a detergent action because of the phosphate groups. Citric acid combines acidity with detergency and chelating ability and is preferred, especially for iron removal. Blends of acids may be also particularly effective. HCl and sulphuric acid are very corrosive and should be avoided.

Enzymatic cleaners based on either proteases, amylases, glucanases, and so on, are used at neutral pH for specific instances followed by sanitization with an oxidizing solution such as sodium hypochlorite or hydrogen peroxide. Surfactants possess both hydrophobic and hydrophilic functional groups. Their main purpose in a cleaning solution is to enhance wettability and rinsability, improve contact between the foulants and cleaning agents and reducing water usage and cleaning time. Surfactants can be anionic (soaps and alkylsulphonates), cationic (quaternary ammonium compounds) or non-ionic (phenol compounds and ethylene oxide).

Cleaning solutions should be recirculated through membrane modules at low pressure and at high velocity to prevent deeper penetration of foulants within the porous substructure of the membrane. Several companies sell chemical cleaners, as powders or liquid, specifically for membranes and for the most usual foulants. For new process applications the most effective cleaning protocol must be established experimentally.

20.6 Applications

At the industrial level MF is widely used in both dead-end and cross-flow configurations. Applications of dead-end MF are generally in the areas of purification, clarification, sterilization and analysis. A wide range of applications in the pharmaceutical industry including antibiotic processing, production of therapeutic proteins, ophthalmic preparations, fermentation,

© Woodhead Publishing Limited, 2011

injectable drugs (parenterals), and so on, have already been consolidated (Scott, 1995). Antibiotic processing includes a variety of treatments such as the bulk clarification after the fermentation step, filtration of solvents and processing the bulk final solution in a solvent-based process involving the use of MF membranes. In the production of biologicals from mammalian cells, applications of microporous systems include cell-harvesting, perfusion of continuous cell culture vessels, clarification of biologicals and pre-column clarification. In the fermentation process used in the production of antibiotics, hormones, aminoacids and enzymes, the inlet and outlet air is filtered to remove airborne microorganic contaminants from the fermentor. MF applications also include the sterile filtration of the nutrient feed and liquid product and 0.22-μm-rated filters are usually used. These filters are also used to sterilize heat-sensitive ophthalmic components.

In processing parenterals, MF is primarily used for final sterilization from heat labile products, reduction of the bacterial burden before the final sterilization by autoclave and removal of particles from parenteral solutions and aerosols generated during their processing. The use of MF in the food industry can be considered the most consolidated application of membrane technology at the industrial level. A wide range of materials can be processed, including milk, vinegar, edible oils, drinking water, alcoholic beverages (beer, wine, whiskies) and soft drinks.

In the dairy industry MF is used to remove bacteria and spores from milk in order to extend its shelf-life as an alternative to the ultrapasteurization. In the Bactocatch system developed by Alfa Laval (Holm *et al.*, 1986) raw milk is separated into skimmed milk and cream. The resulting skimmed milk is treated by MF obtaining a permeate with a bacterial concentration less than 0.5% of the original value. The retentate containing nearly all the bacteria and spores is submitted to a conventional high heat treatment (130°C, 4 s) and then mixed with the permeate before the pasteurization step. In this process only a small volume of milk is treated at high temperatures, preserving its sensory qualities. Another promising application is the fractionation of milk proteins: the separation of micellar casein from whey proteins can be achieved by ceramic MF membranes producing a retentate enriched in native casein that can be used for cheese making. In whey processing MF can be used to remove bacteria and spores from the initial feed, obtaining a permeate that can be submitted to the UF step for the production of high quality whey protein concentrate and isolates.

Cross-flow MF is a valid approach for removing dirt, coagulated proteins, fats and other particles from raw gelatine derived from selective hydrolysis of collagen. Suspended solids can be also removed by MF from glucose solutions employed in syrups and sweeteners production. Several applications of both dead-end and cross-flow MF can be found in wine production. In particular, the use of cross-flow MF in wine production

© Woodhead Publishing Limited, 2011

offers significant advantages over conventional processing steps in terms of reduced use of SO_2, improved quality and brilliance of wine, reduced costs for the disposal of diatomaceous earths with no changes in the wine composition. Cross-flow MF membranes are used for the clarification of both white and red wines before storage as an alternative to the use of fining substances and filter materials. Other applications include cold sterilisation of unfermented must, the last cellar filtration after ageing in a storage tank, cold sterilization of wine before bottling and filtration of water used for bottle cleaning. Sterile venting of unfermented must tanks, sterile filtration of compressed air to remove unfermented must and filtration of steam and air using disposable filter capsules and cartridges are typical dead-end MF applications. Plate-and-frame MF modules are commonly used to remove yeast, microorganisms and haze in the clarification step of beer without affecting its taste.

In the electronics industry, MF membranes are used to remove microparticles from a variety of chemicals such us sulphuric acid, nitric acid, ammonia and hydrogen peroxide, in the production of ultrapure water. These membranes are typically made of polyethylene, PVDF and PTFE with a 0.1 μm pore diameter or less. Teflon MF membranes are also used to remove particles from a variety of reactive gases and solvents employed in the electronics industry.

Tubular MF membranes are used in treating the sludge from the treatment of sewage and chemical coagulation of surface water, as alternative to the common use of polyelectrolytes, centrifugation and plate and frame filter presses. Typical applications also include the removal of oil and fine metals from industrial wastewaters, the removal of precipitated metals (metal hydroxide flakes) from industrial effluents and the processing of fruit juices. Table 20.3 summarizes main applications of the MF process at the industrial level.

The first large application of UF was the recovery of electrocoat paint in an automobile plant (Cardew and Le, 1998). The UF system removes ionic impurities from the paint tank, producing a clean permeate, which is sent to the countercurrent rinsing operation, and a concentrated paint that is returned to the paint tank. Tubular modules were used in the first plants; recently, capillary and spiral wound modules have also been used.

Significant applications of UF exist in the food industry especially in the dairy industry and in the production of fruit juices, beer and wine. During cheese production, milk proteins are precipitated and the solid fraction (curd) formed is sent to the cheese fermentation plant. The supernatant liquor (whey) containing most of the dissolved solids and sugars present in the original milk and about 25% of the original protein content create remarkable disposal problems for the dairy industry. The protein fraction is removed from the whey by UF in order to obtain a concentrated protein, which can be

© Woodhead Publishing Limited, 2011

Table 20.3 Industrial applications of the MF process

Industrial sector	Application
Pharmaceutical	Sterile filtration: parenterals, ophthalmic solutions, fermentation products (antibiotics, vaccines and bioengineered proteins), tissue culture media; removal of microorganisms and particulates from air and other gases (vent filters, filtration of air or nitrogen used in fermentors)
Electronic	Sterile filtration: final point-of-use filters for ultrapure water
Nuclear	Removal of corrosion products in the primary coolant loop of boiling water reactors
Food/beverage	Sterile filtration: wine, beer, bottled water, gases, sugar solutions, edible oil, syrups, vinegar, whisky, brandy; clarification of cheese whey, defatting and reduction of microbial load in milk; clarification of wine, beer, fruit juices, vinegar, bottled water, beet and sugar cane solutions, purification of dextrose stream
Medical	Haemodialysis, biohybrid organs, analytical and diagnostic devices
Biotechnology	Downstream processing (concentration, clarification); marine biotechnology; biological conversions by membrane bioreactors (membrane recycle bioreactors, plug flow bioreactors)
Water treatment	Process water, treatment of grinding and polishing waters, finely dispersed suspension; retention of activated carbons, recovery of process water, filtration of process chemicals, solvents; removal of heavy metals as hydroxides, removal of lignin, removal of oil water effluents
Bulk chemicals/ petrochemical	Sterile filtration: solvents and reagents, inorganic solutions, fatty acids, waxes, polymer fibers and films
Paints/coatings	Painting solutions, hydraulic fluid inks, foam, plating solutions, wastewaters
Sugar refining	Removal of colloidal and macromolecular impurities from raw juice, clarification of thin juice
Vegetable oils	Removal of waxes from sunflower oil
Corns and other grains	Dextrose clarification

successively dehydrated by evaporation, and a permeate enriched in lactose and salts. Since whey proteins are characterized by both nutritional and functional properties (gelling, emulsifying and foaming properties), they can be exploited in a wide range of applications (nutritional foods, beverages, processed meats, etc.).

Typically, a first UF step is used to achieve a 5- to 10- fold volume reduction and remove most of the lactose; the feed is then diluted with water and reconcentrated in a second UF step in order to remove the remaining lactose. The permeate can be discharged to a biological wastewater treatment

© Woodhead Publishing Limited, 2011

plant or submitted to a concentration step by RO. UF can be also used to treat whole or skimmed milk in order to produce a pre-cheese concentrate (MMV process) that can be used directly to produce soft cheese (Camembert, mozzarella and feta) and yogurt (Maubois *et al*., 1980). Another application of UF is the standardization of proteins and total solids in milk for use in fermented dairy products (yogurt, cream and cottage cheeses) (Rosemberg, 1995).

UF is successfully applied in the clarification of fruit juices. In particular, UF represents a valid alternative to the use of traditional fining agents such as gelatine, bentonite and silica sol, which cause problems of environmental impact caused by their disposal (Eykamp, 1995). This process can be used to separate juices into a fibrous concentrated pulp and a clarified fraction free of spoilage microorganisms. Then, the clarified fraction can undergo non-thermal membrane concentration, such as membrane or osmotic distillation and, in the case of whole juice reconstitution, by combination with pasteurised pulp to obtain a product with improved sensorial properties (De Barros *et al*., 2003). Other advantages of UF over conventional methods include the production of clarified juices by a continuous simplified process, elimination of filter aids and filter presses, reduction in the filtration time, increased juice yield, better product quality and reduced enzyme usage (Fukumoto *et al*., 1998). UF polymeric and ceramic membranes with a MWCO of 10–50 kDa, packaged as tubular or capillary hollow-fibre modules, are generally used.

In winemaking, UF can be used before the fermentation in order to remove colloids, high molecular weight tannins, haze proteins, suspended solids and microorganisms from musts. After fermentation, UF can be used as alternative to fining agents (i.e. bentonite) to remove haze proteins from the wine (especially white wine) to improve the stability of the finished wine. Flavour compounds, generally removed by fining agents, can be preserved during the UF treatment. Additionally, UF membranes are able to remove enzymes such as polyphenol oxidase that causes the formation of undesirable brown compounds, increasing the colour/flavour stability of the wine. A wide range of vinegar types can be clarified by UF as a substitute for conventional methodologies. The process allows the removal of undesirable compounds such as proteins, pectins, yeast, fungi, bacteria and colloids and a reduction of the storage time.

Other well-established UF applications in the food industry are related to the concentration and purification of animal blood plasma, concentration of whole-egg and the egg-white and concentration of agar, agarose, carrageenan, gelatine, apple and citrus pectin (Lipinzki, 2010). Spent oil-water emulsions used in automated machining operations (automobile plants, steel rolling mills, etc.) can be treated by UF to recover the oil component for reuse and to obtain a dilute permeate that can be discharged or reused. The removal

© Woodhead Publishing Limited, 2011

of microparticles, ions and microorganisms from water in the production of ultrapure water used in the manufacture of semiconductor devices is another consolidate application of the UF process (Cheryan, 1998). Finally, UF membranes can be used in surface water treatment (such as natural organic matter and pathogen removal), in membrane bioreactors (MBRs), in pretreatment processes for RO and nanofiltration (NF), and in many other industrial applications (Aoustin *et al*., 2001; Van der Bruggen *et al*., 2003, Durham *et al*., 2001; Jarusutthirak and Amy, 2001). Main applications of industrial UF are summarized in Table 20.4.

20.7 Microfiltration and ultrafiltration in integrated processes

MF and UF can be integrated with conventional processes (centrifugation, evaporation, liquid–liquid extraction and adsorption) or other membrane operations in different productive sectors according to the process intensification strategy. Significant advantages can be obtained in terms of improvement of product quality, reduction of energy consumption and environmental impact, recovery and reuse of water and chemicals.

Traditionally, precipitation, filtration and ion-exchange are used in the production of industrial water. These processes can be replaced by MF, RO and electrodialysis (ED). Integrated processes including water softening, MF, RO, UF, UV-sterilization and mixed bed ion-exchange have been proposed for purifying well or surface waters (Strathmann *et al*., 2006).

The combination of bioreactors and UF membranes (MBRs) permits an innovative and effective cleaning process for both municipal and industrial wastewaters to be obtained. The bioreactor is an oxygenated feed tank in which the dissolved organic substances are decomposed by microorganisms into nitrogen, water and carbon dioxide. The biomass is separated from the effluent by the UF membrane and recycled in the feed tank. Using this treatment high molecular weight substances are rejected by the membrane and can be further decomposed. The biomass concentration in the system can reach values 10 times higher than those obtained in conventional plants (Zenon Environmental b.v., 1995). A highly concentrated activated sludge process has also been combined with rotary disk type UF membranes in the treatment of fermentation wastewaters (Lu *et al*., 1999).

The recovery of water, toxic and valuable compounds from water and wastewaters in the chemical industry, to avoid pollution of the environment, is another interesting field of application (Reynolds, 1996). The application of ED with MF, UF and ion-exchange processes provides a good solution for recovering and recycling valuable compounds (nickel, cadmium, copper) from rinse solutions in the metal processing industry. An integrated membrane process based on the use of UF and NF has been proposed by Cassano *et*

© Woodhead Publishing Limited, 2011

Table 20.4 Industrial applications of the UF process

Industrial sector	Application
Pharmaceutical	Sterile filtration: parenterals, ophthalmic solutions, fermentation products (antibiotics, vaccines and bioengineered proteins), tissue culture media
Food/beverage	Clarification of fruit and vegetable juices, must, wine, beer and vinegar; fractionation of cheese whey, preconcentration of milk for cheese manufacture
Biotechnology	Downstream processing: separation and harvesting of microbial cells from the suspending medium, recovery of enzymes from plant and microbial sources; biological conversions by membrane bioreactors (membrane recycle bioreactors, plug flow bioreactors)
Water treatment	Process water, water treatment in drinking water production; treatment of metalworking oily waste, recovery of brine (NaCl) in cheese manufacture, treatment of wash water from printing process, final polishing of laundry wastewaters, removal of heavy metals by micellar-enhanced UF
Textile	Recovery of synthetic warp sizing agents, treatment of wool scouring effluents, dyes recovery
Chemicals	Treatment of latex emulsions
Pulp and paper	Colour removal from kraft mill bleaching effluents, concentration of dilute spent sulphite liquor, recovery of lignin from kraft black liquor, recovery of paper coatings
Tanning and leather	Sulphide recovery from spent dehairing bath, recovery of vegetable tanning baths, chromium recovery from spent chromium liquors
Electrocoat paint	Recovery of paint from electrocoat painting solutions
Sugar refining	Removal of colloidal and macromolecular impurities from raw juice, clarification of thin juice
Soybean and vegetable proteins	Removal of oligosaccharides, phytic acid and trypsin inhibitors from soybean; removal of undesirable compounds from vegetable proteins
Vegetable oils	Removal of reverse micelles from oil–hexane mixtures; removal of fatty acids from oil
Corns and other grains	Separation of corn proteins
Animal products	Treatment of wastewaters from meat processing plants, reduction in low molecular weight components from gelatine, removal of glucose from egg white, recovery of proteins from effluents of fish processing

al. (2001) for the recovery of chromium from spent tanning liquors in the leather industry. Osmota GmbH (Germany) proposed a treatment scheme for the recovery and recycling of water and sulphuric acid from the rinse of a lead battery production line including MF, NF, ED and RO (Strathmann, 2004). Kim *et al*. (2006) reported a pilot-scale wastewater treatment and

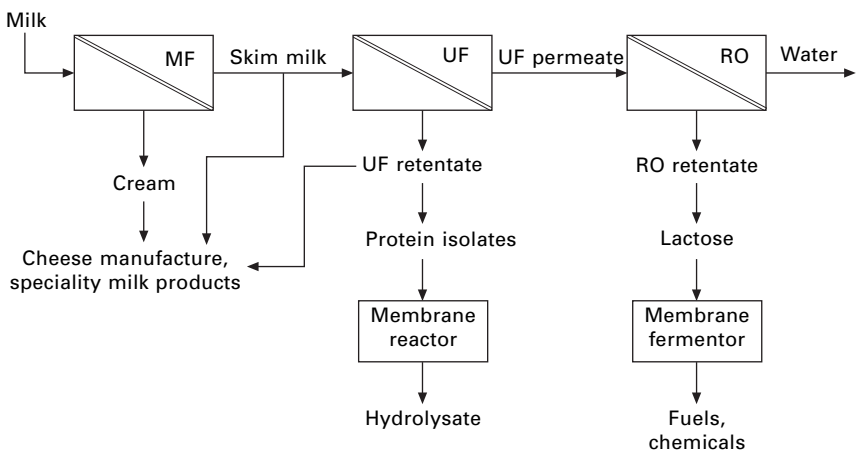
© Woodhead Publishing Limited, 2011

reuse system by integrating MF and ED. MF removes suspending solids and heavy metal ions (immobilized by separating materials) from sewage, while the following ED operation further purifies and desalinates the outlet. UF and RO can be also integrated to recover dyes from wastewaters produced by the textile industry (Short, 1993).

In the food and beverage industry, integrated membrane operations including MF and UF can be successfully applied for clarification, concentration, fractionation, desalting, recycling, recovery and purification. In this field, the use of membrane technology is dominated mainly by the application in the treatment of whey and milk followed by beverages, wine, beer and fruit juices.

A general scheme of integrated membrane processes in milk processing is depicted in Fig. 20.6. The UF concentrated milk is used to formulate speciality milk-based beverages (such as beverages with a high calcium content and relatively low content of fat and cholesterol) and for a pre-cheese mixture production which is then processed into hard or soft cheese (Cheddar, Camembert, Roquefort, etc.). Milk protein concentrates, containing 50–58% protein, can be produced by an integrated MF/UF process. These concentrates are used in the production of food additives in which the functionality of proteins has to be guaranteed.

Whey protein concentrates, lactose and waste streams with reduced biological oxygen demand (BOD) can be produced by integrating UF and RO processes. Integrated processes involving MF and UF are also efficient in whey fractionation. In particular, MF membranes retain fats, precipitated salts, bacteria and casein as particulate. UF can be used to fractionate β-lactoglobulin and α-lactoglobulin from other proteins (lactoferrin, albumin, immunoglobuline, etc.) (Zydney, 1998).



20.6 Integrated membrane process in milk processing (adapted from Cheryan, 1998).

© Woodhead Publishing Limited, 2011

High-strength citrus juice concentrates can be produced by using UF or MF as a pretreatment to separate the pulp from the serum, followed by a combination of high- and low-retention RO membranes (Cheryan and Alvarez, 1995). A pilot scale system investigating an integrated process for the clarification (by UF), concentration (by thermal evaporation) and aroma compounds recovery (by pervaporation, PV) from apple juice has been exploited by Alvarez *et al*. (2000). Integrated membrane processes for the clarification (by UF), preconcentration (by RO) and concentration (by osmotic distillation, OD) of different fruit and vegetable juices (orange, carrot, lemon, kiwifruit and cactus-pear) have been also proposed by Cassano *et al*. (2003, 2004, 2007). In wine production, the UF step can be used before fermentation to remove microorganisms, colloids and high molecular weight compounds from the must before its fermentation. This process can be integrated to a second membrane step (MF) in order to remove yeasts from the wine. A final step before bottling could be a sterile filtration by using MF membranes.

In a typical recovery process for intracellular products made by fermentation, MF and UF processes are typically used for the medium purification (MF), cell harvesting (UF), concentration of products (UF) and pyrogen removal (UF).

20.8 Advantages and limitations

As already mentioned, in most applications MF and UF processes are characterized by several advantages compared to conventional procedures. Typically, these processes are energy efficient, do not require the addition of chemical compounds or phase changes, are modular and easy to scale up and down, yield a higher quality product and offer the possibility of carrying out the separation continuously. In addition they operate at ambient temperature avoiding any change or degradation of products. This is a very important feature in separation, concentration and purification processes involving thermosensitive products such as food and pharmaceutical products. However, in many MF and UF applications extensive pretreatments are needed in order to limit concentration polarization and membrane fouling phenomena. The low mechanical resistance of the membrane, in some cases, is an additional drawback which can lead to the membrane breaking when there are uncorrected operating procedures.

20.9 Future trends

The market for dead-end cartridge MF membranes used in microelectronics and pharmaceutical applications is well developed. A potential increase of the cross-flow MF market is expected in some areas of interest such as

© Woodhead Publishing Limited, 2011

drinking water production, tertiary treatment of sewage and replacement of conventional depth filtration in food industries. Ceramic MF membranes with long lifetimes are available for this purpose but their high cost is the main drawback for large scale application. The development of cheaper MF membranes characterized by long lifetimes could offer new perspectives in market growth related to the areas mentioned.

Further membrane fouling and gel layer formation are inherent characteristics of MF and UF processes, which affect membrane fluxes and membrane lifetimes and consequently increasing operating costs. Significant progresses have been made in controlling and limiting these phenomena in the last few years, and thus the development of fouling-resistant membranes and membrane modules is expected. Investigations concerning the modification of membrane surface absorption properties and the reduction of the deposited layer-membrane surface link are promising approaches for this purpose.

Similar to the MF process, ceramic UF membranes could replace polymeric membranes in many applications if their cost were to be competitive. The development of new applications of MF and UF processes will be driven by economic and environmental targets. An additional driver for these processes is the high growth rate of the market for functional foods, a segment in which membrane operations have a high potential. Finally, MF and UF membranes have great potential as systems to improve the design of chemical transformations. In particular, the properties of catalysts immobilized in polymeric membranes and membrane bioreactors offer new perspectives in the production and purification of specific bioactive compounds.

20.10 Sources of further information and advice

http://www.millipore.com
http://www.gea-liquid.dk
http://kochmembranesystems.com
http://www.thomasnet.com

20.11 References

Aimar P, Howell JA and Turner M (1989), 'Effects of concentration boundary layer development on the flux limitations of ultrafiltration', *Chem Eng Res Des*, **67**, 255–61.

Alvarez S, Riera FA, Alvarez R, Coca J, Cuperus FP, Bouwer S, Boswinkel G, van Gemert RW, Veldsink JW, Giorno L, Donato L, Todisco S, Drioli E, Olsson J, Trägårdh G, Gaeta SN and Panyor L (2000), 'A new integrated membrane process for producing clarified apple juice and apple juice aroma concentrate', *J Food Eng*, **46**, 109–25.

Aoustin E, Schafer AI, Fane AG, Waite TD (2001), 'Ultrafiltration of natural organic matter', *Sep Purif Technol*, **22–23**, 63–78.

Baker RW (2000), *Membrane Technology and Applications*, McGraw-Hill, New York.

© Woodhead Publishing Limited, 2011

Bilstad T (1997), 'Membrane operations', *Wat Sci Tech*, **36**, 17–24.
Bird RB, Stewart WE, Lightfoot EN (1965), *Transport Phenomena*, John Wiley & Sons, New York.
Cardew PT and Le MS (1998), *Membrane Processes: a Technology Guide*, Royal Society of Chemistry, Cambridge.
Cassano A, Molinari R, Romano M and Drioli E (2001), 'Treatment of aqueous effluents of the leather industry by membrane processes. A review', *J Membrane Sci*, **181**, 111–26.
Cassano A, Drioli E, Galaverna G, Marchelli R, Di Silvestro G and Cagnasso P (2003), 'Clarification and concentration of citrus and carrot juices by integrated membrane processes', *J Food Eng*, **57**, 153–63.
Cassano A, Jiao B and Drioli E (2004), 'Production of concentrated kiwifruit juice by integrated membrane processes', *Food Res Int*, **37**, 139–48.
Cassano A, Conidi C, Timpone R, D'Avella M and Drioli E (2007), 'A membrane-based process for the clarification and the concentration of the cactus pear juice', *J Food Eng,* **80**, 914–21.
Cassano A, Donato L, Conidi C, Drioli E (2008), 'Recovery of bioactive compounds in kiwifruit juice by ultrafiltration', *Innov Food Sci Emerg*, **9**, 556–62.
Cheryan M (1998), *Ultrafiltration and Microfiltration Handbook*, Technomic Publishing, Lancaster.
Cheryan M and Alvarez J (1995), 'Food and beverage industry applications', in *Membrane Separations Technology. Principles and Applications*, Noble RD and Stern SA (eds), Elsevier, Amsterdam.
De Barros STD, Andrade CMG, Mendes ES and Peres L (2003), 'Study of fouling mechanism in pineapple juice clarification by ultrafiltration', *J Membrane Sci*, **215**, 213–24.
Durham B, Bourbigot MM, Pankratz T (2001), 'Membranes as pretreatment to desalination in wastewater reuse: operating experience in the municipal and industrial sectors', *Desalination*, **138**, 83–90.
Eykamp W (1995), 'Microfiltration and ultrafiltration', in *Membrane Separation Technology – Principles and Applications*, Noble RD and Stern SA (eds), Elsevier, Amsterdam.
Fleischer RL, Price PB and Walker RM (1969), 'Nuclear tracks in solids', *Sci Am*, **220**, 30–9.
Fukumoto LR, Delaquis P and Girard B (1998), 'Microfiltration and ultrafiltration ceramic membranes for apple juice clarification', *J Food Sci*, **63**, 845–50.
Goldsmith RL, de Filippi RP, Hossain S and Timmins RS (1971), 'Industrial ultrafiltration', in *Membrane Processes in Industry and Biomedicine*, Bier M (ed), Plenum Press, New York.
Ho WSW and Sirkar KK (1992), *Membrane Handbook*, Chapman & Hall, New York.
Holm S, Malmberg R and Svensson K (1986), *Method and Plant for Producing Milk with Low Bacterial Content*', Patent WO86/001687.
Jarusutthirak C and Amy G (2001), 'Membrane filtration of wastewater effluents for reuse: effluent organic matter rejection and fouling', *Water Sci Technol*, **43**, 225–32.
Kesting RE (1985), *Synthetic Polymeric Membranes*, Wiley, New York.
Kim JO, Jeong JT, Kim SK, Kim RH and Lee YJ (2006), 'Development of novel wastewater reclamation system using microfiltration with advanced new membrane material and electrodialysis', *Mater Sci Forum*, **510–511**, 586–9.
Lipinzki F (2010), 'Cross-flow membrane applications in the food industry', in *Membrane Technology, Volume 3: Membranes for Food Applications*, Peinemann KV, Nunes SP and Giorno L (eds), Wiley-VCH, Weinheim, 1–24.

© Woodhead Publishing Limited, 2011

Loeb S and Sourirajan S (1962), 'Seawater demineralization by means of a semipermeable membrane', *Advances in Chemistry, ACS Series No. 38*, in Gould R (ed), American Chemical Society, Washington, 117–32.

Lu SG, Imai T, Ukita M, Sekine M, Fukagawa M and Nakanishi H (1999), 'Fermentation wastewater treatment in a membrane bioreactor', *Environ Technol*, **20**, 431–6.

Maubois JL, Mocquot G and Vassal L (1980), *Preparation of Cheese Using Ultrafiltration*', US Patent 4,205,080.

Mulder M (1991), *Basic Principles of Membrane Technology*, Kluwer Academic, Dordrecht.

Osada Y and Nakagawa T (1992), *Membrane Science and Technology*, Marcel Dekker, New York.

Porter MC and Michaels AS (1971), 'Membrane ultrafiltration', *Chem Technol 1*, **56**, 248, 440 and 633.

Reynolds R (1996), *Unit Operations and Processes in Environmental Engineering*, PWS Publishing, Boston.

Rosemberg M (1995), 'Current and future applications of membrane processes in the dairy industry', *Trend Food Sci Tech*, **6**, 12–19.

Schneider K (1982), 'The concentration of suspensions by means crossflow-microfiltration', *Desalination*, **41**, 263–75.

Scott K (1995), *Handbook of Industrial Membranes*, Elsevier Advanced Technology, Oxford.

Sherwood TK, Brian PTL, Fischer RE and Dresner L (1965), 'Salt concentration of phase boundaries in desalination by reverse osmosis', *Ind Eng Chem Fundam*, **4**, 113.

Short JL (1993), *Membrane Industry News*, Westford, MA, November issue.

Strathmann H (1985), 'Production of microporous media by phase inversion processes', in *Material Science of Synthetic Membranes*, Lloyd DR (ed), American Chemical Society, Washington, ACS Symposium Series No. 269, 165.

Strathmann H (2004), *Ion-Exchange Membrane Separation Processes* (Membrane Science and Technology Series 9), Elsevier, Amsterdam.

Strathmann H, Giorno L and Drioli E (2006), *An Introduction to Membrane Science and Technology*, Consiglio Nazionale delle Ricerche, Roma.

Van der Bruggen B, Vandecasteele C, Van Gestel T, Doyen W and Leysen R (2003), 'A review of pressure-driven membrane processes in wastewater treatment and drinking water production', *Environ Prog*, **22**, 46–56.

Zenon Environmental B.V. (1995), 'Ultrafiltration combined with a bioreactor for the treatment of tannery effluents', *World leather*, **8**, 41–2.

Zydney AL (1998), 'Protein separation using membrane filtration: new opportunities for whey fractionation', *Int Dairy J*, **8**, 243–50.

© Woodhead Publishing Limited, 2011

21
Membranes for forward osmosis in industrial applications

N. K. RASTOGI and C. A. NAYAK,
Central Food Technological Research Institute, India

Abstract: Forward osmosis is recognized as one of the most promising membrane-based separation processes owing to its inherent advantages. It finds its application not only in food processing, but also in many other separation processes such as wastewater treatment or seawater/brackish water desalination. This review discusses the mechanism of water transport during forward osmosis, the principles involved as well as the factors affecting the flux. Recent advances and developments in forward osmosis membrane processes, its application and limitations have also been presented.

Key words: desalination, forward/direct osmosis, hydrophilic, membrane, osmosis.

21.1 Introduction

Osmosis is a physical phenomenon that has been extensively studied by scientists in various disciplines of science and engineering. Osmosis is defined as a net movement of water across a selectively permeable membrane driven by a difference in osmotic pressure across the membrane. Applications of osmosis extend from water treatment and food processing to production of electricity and novel methods of controlled drug release (Cath *et al.*, 2006, Cath, 2010, Wilf, 2010).

Evaporative concentration of fluid food results in heat-induced deterioration of the sensory and nutritional quality of the finished product. It is well known that in the first few minutes of evaporative concentration, most of the aroma compounds present in raw juice are lost and the profile of the aroma undergoes irreversible change (Lazarides *et al.*, 1990). Use of vacuum evaporation for juice concentration is highly energy intensive (Petrotos and Lazarides, 2001). Product quality improvement and energy savings have led to the development of alternative concentration techniques such as freeze concentration or reverse osmosis. The capital costs of a commercial-scale freeze-concentration plant are much higher than the cost of an evaporation plant for a similar throughput. Accordingly, the operating costs of freeze concentration are rather prohibitive. Reverse osmosis suffers from serious

© Woodhead Publishing Limited, 2011

limitations such as concentration polarization and membrane fouling, especially under the high pressures that are necessary to produce high product concentrations. Under such high pressures, membrane compaction is another major limitation. A potential solution to the above problems and an attractive alternative to evaporative concentration techniques was offered by a purely osmotic, low-pressure membrane technique, namely direct or forward osmosis (Dova *et al*., 2007a).

Forward osmosis is a membrane process, which employs a semi-permeable dense hydrophilic membrane that separates two aqueous solutions (feed and osmotic agent solution) that have different osmotic pressures. The difference in osmotic pressure acts as the driving force. An osmotic pressure driven process operates on the principle of osmotic transport of water across a semi-permeable hydrophilic membrane from a dilute feed solution into a concentrated osmotic agent or draw solution (Nayak and Rastogi, 2010a).

The expanding global population, increasing water pollution and increasing standards of living have relentlessly put pressure on water and energy resources. Low cost methods of purifying freshwater and desalting seawater are required to contend with this destabilizing trend. Production of purified water from salt water using membranes has become a viable alternative to evaporation-based technologies. The concept is similar to that used by Eastern European farmers for the concentration of fruit juices, wherein a bag filled with juice was immersed in a brine solution and resulted in a highly concentrated juice. But, the process was very slow, as the bags had to remain in the brine overnight (Cussler, 1984). A commercial process was developed, which involved filling a bag made of semi-permeable material (cellulose, polysulphones or animal intestines) with the feed (fruit juices, milk or dairy products) and then subjecting the bag to a bath of osmotic medium at an elevated temperature. The movement of the bag led to higher water fluxes and a significant reduction in time taken (Scott, 1975).

At first, Popper *et al*. (1966) demonstrated that fruit juice could be concentrated using first generation reverse osmosis membranes (cellulose acetate) in both a flat and tubular configuration forward osmosis process. The average osmotic flux was low and of the order of 2.5 l m^{-2} h^{-1}. It was initially called dialysis. Beaudry and Lampi (1990a, 1990b) utilized modified new generation thin film composite reverse osmosis membranes (thickness 25–85 μm). The selective layer was similar to that of tight reverse osmosis membranes, which allowed no passage to other food ingredients except water. These modifications resulted in enhanced turbulence, increased osmotic flux and minimized fouling. These membranes resulted in a higher magnitude of transmembrane flux 5–6 l m^{-2} h^{-1} and were used in a module with flat geometry (Herron *et al*., 1994).

Later, Petrotos *et al*. (1998, 1999) demonstrated that the membrane thickness and the viscosity of the osmotic fluid are the prime factors determining the

© Woodhead Publishing Limited, 2011

transmembrane flux. A thinner membrane and a low-viscosity osmotic medium such as NaCl solution are expected to yield a better performance compared to viscous carbohydrate syrups as osmotic agent solutions. Clarification of the juice either by plain filtration, microfiltration or ultrafiltration resulted in higher values of osmotic fluxes. Also, Petrotos and Lazarides (2001) developed an osmotic cell with a flat configuration to promote turbulence. The average flux was reported to be as high as 4.5 l m^{-2} h^{-1}. Herron *et al.* (1994) demonstrated that the forward osmosis concentrate was of superior quality in comparison to juice conventionally concentrated by a vacuum evaporator. This study contradicted the claims made by Bolin and Salunke (1971) regarding the negative effect of forward osmosis on the quality of osmotic fruit juice concentrates.

Initially this process could not be exploited commercially owing to low flux. In recent years, forward osmosis concentration is gaining importance in the concentration of liquid foods and natural colours (Popper *et al.*, 1966; Bolin and Salunke, 1971; Loeb and Bloch, 1973; Rodriguez-Saona *et al.*, 2001), wastewater treatment (Holloway *et al.*, 2007) and desalination of seawater as well as electricity generation (Kravath and Davis, 1975).

The main advantage of using forward osmosis is that it can concentrate feed at ambient pressure and temperature without significantly losing nutritional and bioactive components. Especially for concentration of fruit juices in the food industry, the forward osmosis technology is applied and has replaced the traditionally used technology of multi-stage vacuum evaporation for some applications (Jiao *et al.*, 2004; Petrotos and Lazarides, 2001; Herron *et al.*, 1994). As well as reduced energy consumption, the other advantages were higher product quality in terms of less loss of fresh fruit flavours, reduced colour degradation and a less cooked taste owing to lower thermal effects. Forword osmosis also results in high rejection of a wide range of contaminants and a lower propensity for membrane fouling than pressure-driven membrane processes (Babu *et al.*, 2006). There is no hydraulic pressure difference applied across the membrane and the dissolved as well as suspended solids in the feed are not forced against the membrane, so the membrane does not foul to a significant extent. Although there is a very little difference in the actual pressures of the two solutions, the driving force for the feed concentration is the osmotic pressure of the osmotic agent solution minus the osmotic pressure of the juice. The pressure involved in the forward osmosis process is due to flow resistance in the membrane module. Hence the equipment used in this process has a very simple construction (Cath *et al.*, 2005a, 2005b).

Unlike the pressure-driven membrane processes, the sole driving force for most forward osmosis processes is the osmotic pressure differential between the feed and the osmotic agent solution. When compared to pressure-driven membrane processes, such as reverse osmosis, forward osmosis

© Woodhead Publishing Limited, 2011

uses significantly less electrical energy. The overall energy cost of forward osmosis can be vastly lower than pressure-driven membrane processes if the osmotic agent solution can be easily recovered or discarded using less or lower quality energy (Garcia-Castello *et al.*, 2009). The main drawback relating to the forward osmosis process is that the recovery or disposal of osmotic agent solution may incur high energy and/or capital costs. This issue must be properly addressed before this technology can be used on a wider scale (McCutcheon *et al.*, 2005).

This chapter discusses the recent advances and developments in forward osmosis membrane processes and the mechanism of water transport as well as factors affecting the process, along with the applications and limitations.

21.2 Mechanism of forward osmosis

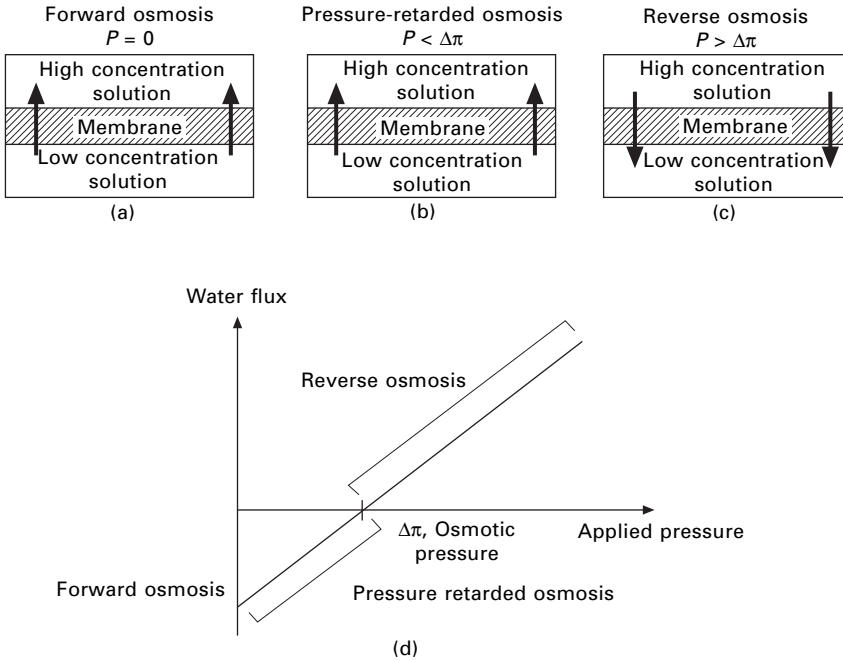
The transport of water across a selectively permeable membrane from a region of higher chemical potential to that of the lower chemical potential is known as osmosis. Forward osmosis uses the osmotic pressure differential ($\Delta\pi$) across the membrane, rather than the hydraulic pressure differential (as in reverse osmosis), as the driving force for transport of water through the membrane. The forward osmosis process results in a concentration of the feed stream and a dilution of the concentrated stream (referred to as the draw solution). Pressure-retarded osmosis can be viewed as an intermediate process between forward osmosis and reverse osmosis, where hydraulic pressure is applied in the opposite direction to the osmotic pressure gradient (similar to reverse osmosis) (Cath *et al.*, 2006; Xu *et al.*, 2010). However, the net water flux is still in the direction of the concentrated draw solution (similar to forward osmosis). Lee *et al.* (1981) characterized all three processes. The forward osmosis point, pressure-retarded osmosis zone and reverse osmosis zone, along with the flux reversal point and the direction of flux of the permeating water are illustrated in Fig. 21.1. The water flux in osmotic driven membrane processes is described as below:

$$J_w = a(\sigma \Delta \pi - \Delta P) \qquad [21.1]$$

where, J_w is the water flux (kg m^{-2} h^{-1} or Lm^{-2} h^{-1}), a is the water permeability of the membrane (m s^{-1} Pa^{-1}), σ is the reflection coefficient, ΔP is the difference in pressure (atm) (Xu *et al.*, 2010) and $\Delta\pi$ is the osmotic pressure difference across the membrane (the driving force) (atm).

The forward osmosis membrane process employs a semi-permeable dense hydrophilic membrane, which separates the feed and the osmotic agent solutions. The osmotic pressure difference between the feed and the osmotic agent solutions acts as a driving force for transport of water. The asymmetric membrane used in forward osmosis consists of two layers, one is a loosely bound support layer and other is a dense active membrane

© Woodhead Publishing Limited, 2011

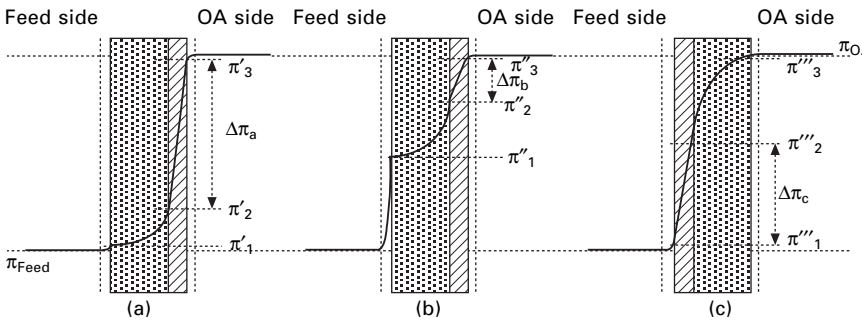


21.1 Direction and magnitude of water flux as a function of applied pressure in (a) forward osmosis, (b) pressure-retarded osmosis and (c) reverse osmosis. Forward osmosis takes place when the hydraulic pressure difference is zero. (d) The pressure retarded osmosis zone is where the applied pressure difference is between zero and the flux reversal point, and the reverse osmosis zone is where the applied pressure difference is greater than the osmotic pressure difference. (from Xu *et al.*, 2010)

layer. The membrane can be placed between the feed and the osmotic agent solutions in two different orientations such as feed towards the support layer (normal mode) and feed towards the active layer (reverse mode), which are referred as mode I and mode II, respectively (Gray *et al.*, 2006; Nayak and Rastogi, 2010a).

In mode I, when the feed is pure water, the water is diffused into the support layer and transferred to the osmotic agent side through the active membrane layer. Since the feed is water, it will not result in any external or internal polarization. An insignificant external polarization may take place in the boundary layer on the osmotic agent side. In this situation, if the feed (water) is replaced by a solution of low molecular weight compounds, it will lead to significant internal polarization (concentrative) and negligible external polarization on the feed as well as on the osmotic agent (OA) side (Fig. 21.2(a)). The internal concentration polarization occurs within the porous support layer and it cannot be mitigated by hydrodynamics such as

© Woodhead Publishing Limited, 2011



21.2 Mechanism of forward osmosis indicating water transport from the solution of low osmotic pressure to the solution of high osmotic pressure. (a) Feed solution containing low molecular weight compounds, (b) feed solution containing high molecular weight compounds, (c) feed solution containing low/high molecular weight compounds. $\Delta\pi_a$, $\Delta\pi_b$ and $\Delta\pi_c$ are the corresponding effective driving force, respectively. π_{Feed} and π_{OA} are the osmotic pressures of feed and osmotic agent (OA) solution, respectively (from Nayak and Rastogi, 2010a).

turbulence, hence drastically reducing the osmotic driving force (McCutcheon and Elimelech, 2007). Cath *et al*. (2006) pointed out that in this situation the extent of external polarization is much less than the internal polarization during forward osmosis.

When the feed is replaced by a solution containing high molecular weight compounds (Fig. 21.2(b)), the retained concentration of high molecular weight compounds will build up on the support layer resulting in significant external concentration polarization on the feed side. Mi and Elimelech (2008) have indicated that these high molecular weight compounds may be deposited within the porous structure of the membrane leading to cake layer formation owing to lack of shear force as well as hindered back diffusion in the porous structure. Further, it will also lead to significant internal polarization (concentrative) within the support layer. But, external polarization towards the osmotic agent side will be negligible as indicated in the earlier cases (Fig. 21.2(b)). Because of this the effective driving force ($\Delta\pi_b$) will be much less compared to the same situation in which a solution of low molecular weight compounds or water was taken as the feed ($\Delta\pi_b < \Delta\pi_a$), which, in turn, drastically reduces the transmembrane flux. Further, Mi and Elimelech (2010) also studied the fouling and cleaning behaviour of a forward osmosis membrane. The fouling of the forward osmosis membrane caused by alginate was reported to be almost fully reversible, with more than 98% recovery of permeate water flux possible after a simple water rinse without any chemical cleaning reagents. The fouling reversibility of the forward osmosis membrane was attributed to the less compact organic

© Woodhead Publishing Limited, 2011

fouling layer formed in the forward osmosis mode caused by the lack of hydraulic pressure.

When the porous support layer of an asymmetric membrane faces the feed solution, a polarized layer is established along the inside of the porous layer (Fig. 21.2(b)), which is referred to as concentrative internal concentration polarization. If this phenomenon takes place on the surface of the membrane, it is referred to as concentrative external concentration polarization (Nayak and Rastogi 2010a).

The resistivity of the membrane (support and active layer) during the forward osmosis process (mode I) can be calculated by the following equation presented for concentrative internal concentration polarization (Gray *et al.*, 2006; McCutcheon and Elimelech, 2007; Tan and Ng, 2008; Loeb *et al.*, 1997):

$$K = \left(\frac{1}{J_w}\right)\ln\left(\frac{B + A\pi_{OA} - J_w}{B + A\pi_{Feed}}\right) \qquad [21.2]$$

where J_w is the transmembrane flux during forward osmosis, K is the resistivity of the membrane (s m^{-1}) (support and active layer) and π_{OA} and π_{Feed} are the osmotic pressure of osmotic agent and feed (atm), respectively. The constants '*A*' (0.027 m/atm-day) and '*B*' (0.011 m/day) refer to the water and solute permeability coefficients of the active layer of the membrane, respectively (Gray *et al.*, 2006; Leob *et al.*, 1997).

In mode II, when the feed (solution containing high or low molecular weight compounds) is directed towards the active layer and the osmotic agent is directed towards the support layer, the water from the feed diffuses into the active layer, which, in turn, diffuses to the support layer and then to the bulk through the boundary layer. Since, the solute used as osmotic agent is generally of low molecular weight, it also diffuses into the support layer to the interior surface of the active layer before flux can occur. As water flux crosses the active layer into the support layer, the solute is diluted owing to convection. The solute diffuses back to the interior surface. A steady-state is quickly reached, but the concentration at the interior surface of the active layer is far lower than in the bulk solution (Gray *et al.*, 2006). The combined effect of both the diffusion of water through the active layer as well as the osmotic agent into the support layer results in the setting up of an internal concentration polarization (dilutive, Fig. 21.2(c)). In this case as well, the extent of external concentration polarization towards the support layer (feed) as well as the active layer (osmotic agent) will be much less than the internal polarization.

Nayak and Rastogi (2010a) have demonstrated that when the feed is directed towards the active layer (mode II), the external polarization on the feed side can be taken as negligible compared to the internal polarization and the molecular weight of the compounds in the feed do not have any effect

© Woodhead Publishing Limited, 2011

on the transmembrane flux. The effective driving force, in this case, will be less than the situation indicated in mode I ($\Delta\pi_c < \Delta\pi_a$), when low molecular weight compounds or water are taken as the a feed and, hence in this situation, mode I is most desirable. However, when a solution of high molecular weight compounds is taken as the feed, mode II is expected to give higher driving force ($\Delta\pi_c > \Delta\pi_b$) which, in turn, leads to higher transmembrane flux (Cath *et al.*, 2006). When the feed flows on the active layer of the membrane solutes build up at the active layer, this type of polarization is called concentrative external concentration polarization. Simultaneously, the draw solution in contact with the permeate side of the membrane is being diluted at the permeate–membrane interface by the permeating water resulting in dilutive external concentration polarization. Both concentrative and dilutive external concentration polarization phenomena reduce the effective osmotic driving force.

In forward osmosis applications for desalination and water treatment, the active layer of the membrane faces the feed solution (sea water or saline water) and the porous support layer faces the draw solution (sodium bicarbonate). As water permeates through the active layer, the draw solution within the porous substructure becomes diluted. This is referred to as dilutive internal concentration polarization (Fig. 21.2(c)).

The resistivity of the membrane (support and active layer) during forward osmosis process (mode II) can be calculated by the Equation [21.3] presented for dilutive internal concentration polarization (Gray *et al.*, 2006, McCutcheon and Elimelech, 2007, Tan and Ng, 2008; Leob *et al.*, 1997):

$$K = \left(\frac{1}{J_w}\right)\ln\left(\frac{B + A\pi_{OA}}{B + J_w + A\pi_{Feed}}\right) \qquad [21.3]$$

where J_w is the transmembrane flux during forward osmosis, K is the resistivity of the membrane (support and active layer) (s m^{-1}) and π_{OA} and π_{Feed} are the osmotic pressure of osmotic agent and feed, respectively (Gray *et al.*, 2006; Leob *et al.*, 1997).

Tang *et al.* (2010) investigated the effects of internal concentration polarization and fouling on forward osmosis flux behaviour. Both theoretical model and experimental results demonstrated that the forward osmosis flux was highly non-linear with respect to the apparent driving force (the concentration difference between the draw solution and the feed water) as a result of internal concentration polarization. Compared to the active layer facing draw solution (mode I) configuration, more severe internal concentration polarization was observed when the membrane active layer faced the feed water (mode II) as a result of dilutive internal concentration polarization in the forward osmosis support layer. Interestingly, the mode II configuration showed remarkable flux stability against both dilution of the bulk draw solution and membrane fouling. In contrast, the mode I configuration suffered severe flux reduction

© Woodhead Publishing Limited, 2011

as the porous membrane support faced humic acid containing the feed water. The flux loss in this configuration was probably due to the combined effects of the internal clogging of the forward osmosis support structure as well as the resulting enhanced internal concentration polarization in the support layer. The pore clogging enhanced internal concentration polarization mechanism probably played a dominant role in forward osmosis flux reduction at higher flux levels.

21.3 Membranes for forward osmosis

The ideal forward osmosis membrane must allow water to flow from the feed to the osmotic solution with virtually no cross-contamination of salts. Moreover, the forward osmosis membrane should be stable in the presence of the osmotic agent at the operating temperature.

Membrane selection is one of the most critical aspects of forward osmosis process design. Early researchers experimented with a number of available membrane materials, including bladders of pigs cattle and fish, collodion (nitrocellulose), rubber, porcelain and goldbeaters' skin (Cath *et al.*, 2006, Tang and Ng, 2008). Generally, any dense, non-porous, selectively permeable material can be used as a membrane for forward osmosis. However, a number of studies have indicated that membranes designed for reverse osmosis do not work well owing to extensive mass transfer resistance near the membrane interfaces and within the membrane support structure (McCutcheon *et al.*, 2005; Dova *et al.*, 2007b; McGinnis *et al.*, 2007; Gray *et al.*, 2006). These mass transfer resistances collectively attributed to concentration polarization and require very large osmotic driving forces to sustain adequate water flux.

In a pressure driven membrane process, mass transfer through the porous support layer and fabric backing the membrane has minor or insignificant resistance. Membrane fouling takes place from the feed side of the membrane where concentration polarization reduces the permeate water flux and induces scaling of the membrane. However, in the osmotic process, influence on mass transfer of the feed will occur on both sides of the membrane and not just the permeate side (Gray, 2006; McCutcheon *et al.*, 2006). The membranes for forward osmosis should consist of a high density active layer (for high solute rejection), with minimum porosity of the support layer (for low internal concentration polarization or higher water flux) and be hydrophilic (for enhanced flux and reduced membrane fouling). The rate of water removal is strongly influenced by the thickness of the membrane and on the attainment of intimate contact between the flowing solution and the membrane. The better the contact of the flowing solutions, the faster will be the rate of concentration.

Loeb *et al.* (1997) removed the support fabric layer bonded to the porous

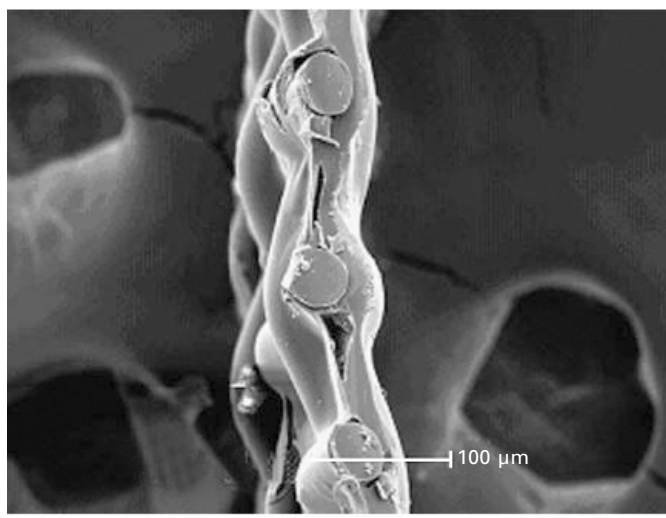
© Woodhead Publishing Limited, 2011

support layer of asymmetric Loeb–Sourirajan type membranes and used these membranes in the osmosis process, where they were affected by the membrane orientation. McCutcheon and Elimelech (2008) also studied the influence of the membrane support layer hydrophobicity on water flux in osmotically driven membrane processes and demonstrated that the membrane support layer significantly influences the water flux in osmotically driven membrane processes.

Goosens and Van-Haute (1978) used cellulose acetate membranes reinforced with mineral fillers to evaluate whether membrane performance under reverse osmosis conditions can be predicted through forward osmosis testing.

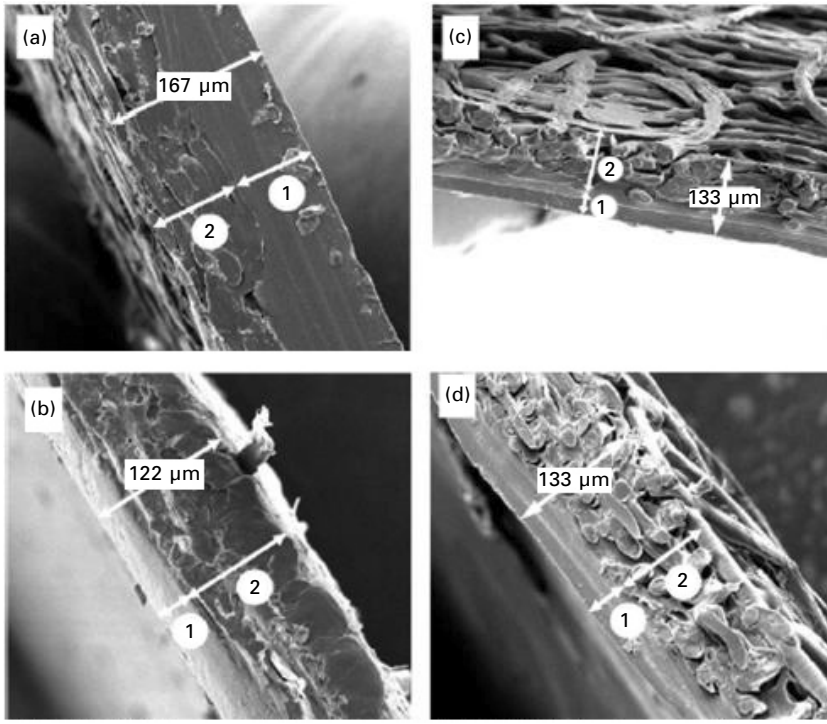
During the 1990s, a special membrane for forward osmosis made of cellulose triacetate (thickness less than 50 μm, Fig. 21.3) was developed by Hydration Technologies Inc., USA (HTI). The forward osmosis membrane was quite different from standard reverse osmosis membranes. Reverse osmosis membranes typically consisted of a very thin active layer (less than 10 μm) and a thick porous support layer. The cellulose triacetate forward osmosis membrane lacked a thick support layer. Instead, an embedded polyester mesh provided mechanical support (McCutcheon *et al.*, 2005). Ng *et al.* (2006) presented scanning electron microscope images of the cross-section of cellulose acetate, polyamide composite and cellulose triacetate membranes (Fig. 21.4).

A reverse osmosis membrane has to withstand significant pressure that



21.3 Cross-sectional SEM image of HTI's forward osmosis (FO) membrane. A polyester mesh is embedded within the polymer material for mechanical support. The membrane thickness is less than 50 μm (from McCutcheon *et al.*, 2005).

© Woodhead Publishing Limited, 2011



21.4 SEM images of the cross section of (a) cellulose acetate (CA) membrane, (b) polyamide composite (AD) membrane, (c) FO membrane and (d) FO membrane at higher resolution where '1' is the dense selective layer and '2' is the support layer (from Ng *et al.*, 2006).

drives the water from the retentate side to the permeate side. In a forward osmosis membrane, the water passes through the membrane by osmotic pressure. Diffusion of solids through the highly porous backing layer and porous sub-layer takes place in forward osmosis. Therefore, the support layer must be made up of very loose low resistance fibres and should allow water to diffuse easily. External and internal concentration polarizations significantly reduce the transmembrane flux of water across the membrane. The transmembrane flux for cellulose triacetate membranes and other reverse osmosis membranes used for forward osmosis is presented in Table 21.1.

Yang *et al*. (2009a, 2009b) developed a novel dual-layer hollow fibre nanofiltration membrane for protein enrichment/concentration in forward osmosis (without denaturing the component of interest) and to produce water by coextrusion technology, which consisted of an ultra-thin selective skin (around 10 μm), fully open-cell water channels underneath and a microporous sponge-like support structure. The membrane could achieve a high throughput for lysozyme enrichment and less protein fouling. In addition,

© Woodhead Publishing Limited, 2011

Table 21.1 Water flux through forward osmosis membrane and other reverse osmosis membranes used in forward osmosis (from Cath *et al.*, 2006)

Membrane used	Water flux (l m^{-2} h^{-1})
CTA- Osmotek	17.4
Osmonics-CD	1.90
Osmonics-CD	1.97
Hydraunautics –LFC1	0.54
Hydraunautics –LFC3	0.66

100 g l^{-1} NaCl solution and deionized water were used as the draw and feed solutions, respectively.

the high divalent salt rejection of Mg^{2+} at around 90% ensured an enriched lysozyme product with high purity without any change or denaturing.

Wang K Y *et al*. (2010a) designed forward osmosis membranes comprising a highly porous sublayer sandwiched between two selective skin layers via phase inversion. The double skin layers of the tailored membrane mitigated the internal concentration polarization by preventing the salt and other solutes in the draw solution from penetrating into the membrane porous support. The prototype double-skinned cellulose acetate membranes displayed a higher water flux and lower reverse salt transport caused by effective salt rejection by the double skin layers and the low water transport resistance within the porous support layer. Also, Wang R *et al*. (2010b) fabricated thin-film composite forward osmosis hollow fibres with an ultra-thin polyamide-based reverse osmosis-like skin layer (300–600 nm) on either the outer or inner surface of a porous hollow fibre substrate. The active layers presented excellent intrinsic separation properties with a hydrophilic rejection layer and good mechanical strength. The study suggested that the optimal forward osmosis membrane structure should possess a very small portion of sponge-like layer in a thin and highly porous substrate. Zhang *et al*. (2010) designed a double dense membrane structure using phase inversion of cellulose acetate that produced low salt leakage and resulted in less internal concentration polarization in the forward osmosis process.

Wang *et al*. (2009) developed high-flux and high-rejection forward osmosis membranes for water reuse and seawater desalination by fabricating polybenzimidazole nanofiltration hollow fibre membranes with a thin wall and the desired pore size via non-solvent induced phase inversion and chemical cross-linking modification. Cross-linking by *p*-xylylene dichloride finely tuned the mean pore size and enhanced the salt selectivity. The effect of the membrane morphology and operating conditions on water and salt transport through the membrane has also been investigated. Further, Su *et al*. (2010) developed a cellulose acetate nanofiltration hollow fibre membrane suitable for forward osmosis processes by subjecting it to a two-step heat-treatment

© Woodhead Publishing Limited, 2011

(60°C, 60 min and 95°C, 20 min), which effectively shrunk the membrane pores on the membrane surface with a denser outer skin layer (mean pore radius reduced from 0.63 to 0.30 nm). The resultant fibre has a high rejection for NaCl and $MgCl_2$ and low pure water permeability. Chou *et al*. (2010) described the characteristics and potential applications of a newly developed forward osmosis hollow fibre membrane, which was fabricated by interfacial polymerization on the inner surface of a polyethersulphone hollow fibre. This membrane presented excellent intrinsic separation properties, with a water flux of 42.6 l m^{-2} h^{-1} using 0.5 M NaCl as the draw solution and water as the feed with the active layer facing the draw solution orientation.

Yip *et al*. (2010) developed a high performance thin-film composite membrane for forward osmosis applications. The membrane consisted of a selective polyamide active layer formed by interfacial polymerization on top of a polysulphone support layer fabricated by phase separation onto a thin (40 μm) polyester nonwoven fabric. A mix of finger-like and sponge-like morphologies give significantly enhanced membrane performance. Using a 1.5 M NaCl draw solution and a pure water feed, the fabricated membranes produced water fluxes exceeding 18 l m^{-2} h^{-1}, while consistently maintaining observed salt rejection greater than 97%.

21.4 Forward osmosis membrane modules

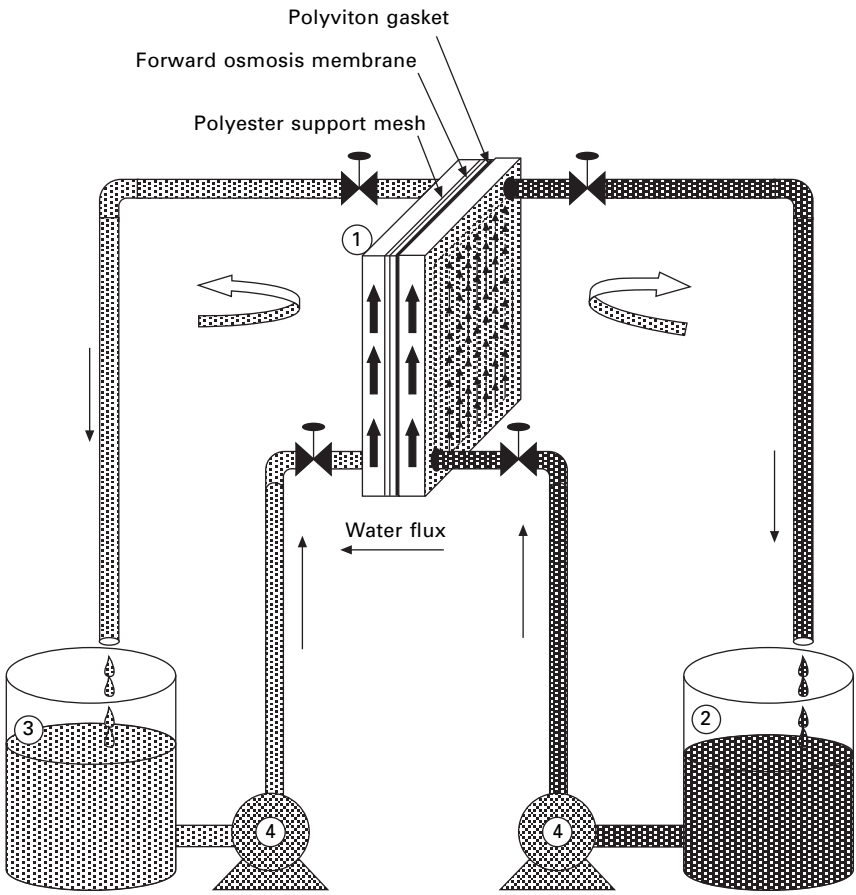
Forward osmosis can be configured in different modules to hold or pack membranes. Laboratory-scale modules are designed for use with either flat sheet or tubular/capillary membranes. Larger scale applications have been designed and built with flat sheet membranes in plate-and-frame configurations.

In continuous flow forward osmosis applications, the feed solution is recirculated on the feed side of the membrane and the concentrated draw solution is recirculated on the permeate side. For this reason, the module that uses flat sheet membrane is more complicated to build and operate for the forward osmosis process compared to pressure-driven processes. The spiral-bound module, which is one of the most common packing configurations in the membrane industry, cannot be used as such for forward osmosis because a liquid stream cannot be forced to flow on the support side.

21.4.1 Flat membrane module

The plate and frame module is the simplest device for packing flat sheet membranes. Plate-and-frame modules can be designed and developed in different orientations, sizes and shapes ranging from lab-scale devices that hold single, small-size membrane to systems that can hold series of membranes in plate and frame modules (Fig. 21.5). Two of the main limitations of plate-and-frame modules for membrane applications are the lack of adequate

© Woodhead Publishing Limited, 2011



21.5 Flat membrane module for forward osmosis: (1) flat membrane module, (2) feed reservoir, (3) osmotic agent reservoir, (4) peristaltic pump.

membrane support and low packing density. The lack of adequate membrane support limits the operation to low hydraulic pressure and/or operation at similar pressures on both sides of the membrane (requiring relatively high process control). Low packing density leads to a larger system footprint, higher capital and operating costs (labour for membrane replacement). Other limitations of the plate-and-frame configuration include problems with internal and external sealing, difficulty in monitoring membrane integrity and a limited range of operating conditions (e.g. flow velocities and pressures) (Cath *et al.*, 2006; Nayak and Rastogi, 2010b).

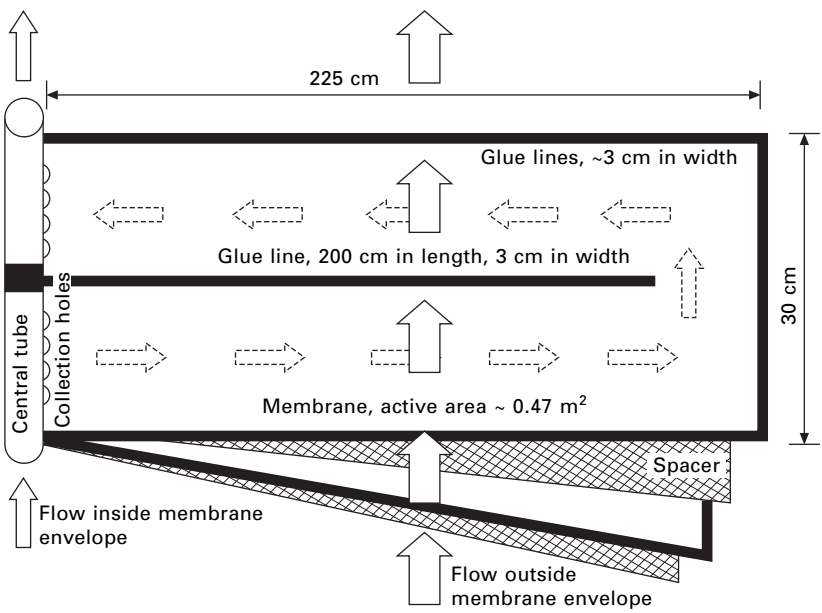
A flat sheet configuration for forward osmosis can also be made up as a hydration bag membrane. This is a double lined bag: the internal bag is made from a forward osmosis membrane and is filled with draw solution

© Woodhead Publishing Limited, 2011

(e.g., flavored sucrose) and the external bag is a sealed plastic bag. Upon immersing the bag in an aqueous solution, water diffuses into the bag owing to the osmotic pressure difference and slowly dilutes the draw solution. The concept of a hydration bag was developed for military, recreational and emergency relief situations where reliable drinking water was scarce or not available. The hydration bag is one of the few commercial applications of forward osmosis (Cath *et al.*, 2006).

21.4.2 Spiral wound membrane module

Commercially marketed spiral-wound membrane modules are operated with only one stream (the feed stream) flowing under direct control of its flow velocity tangential to the membrane. The permeate of the feed stream flows very slowly in the channel formed by the two glued membranes and its composition and flow velocity are controlled by the properties of the membrane and the operating conditions. Therefore, in its current design, spiral-wound membrane elements cannot be operated in the forward osmosis mode because the draw solution cannot be forced to flow inside the envelope formed by the membranes. Foreman, Worsley and co-workers (1977) designed and successfully tested a unique spiral wound module for forward osmosis. Both an outside-in and an inside-out operation can be used. In Fig. 21.6 (inside-out operation), the draw solution has been shown to flow through the spacers and between the



21.6 Experimental setup. An illustration of an open Hydrowell® spiral wound module (from Xu *et al.*, 2010).

© Woodhead Publishing Limited, 2011

rolled membranes, in the same way that a feed stream flows in a spiral-wound element for reverse osmosis (Xu *et al*., 2010). However, unlike reverse osmosis modules, the central collecting tube is blocked halfway through so that the feed solution cannot flow to the other side. Instead, an additional glue line at the centre of the membrane envelope provides a path for the feed to flow inside the envelope. In this configuration, the feed flows into the first half of the perforated central pipe, is then forced to flow into the envelope, and then flows out through the second half of the perforated central pipe. It is worth noting that this configuration can also be efficiently used for pressure-retarded osmosis. The draw solution outside the envelope can be pressurized in a similar way to spiral-wound membrane elements for reverse osmosis.

21.4.3 Tubular membrane module

For continuously operated forward osmosis processes, the use of tubular membrane (tubes or hollow fibres) modules is more practical. The tubular membranes are self-supported, can withstand hydraulic pressure without deformation and they can be easily packed in bundles directly inside a holding vessel. They are much simpler to fabricate and the packing density is relatively high. These modules allow liquids to flow freely on both sides of the membrane (Cath *et al*., 2006). The main difference between hollow fibre and tubular membranes is the flow regime that can be achieved on the bore side. In hollow fibres (internal diameter <1 mm), only laminar flow can be achieved and, therefore, mixing at the membrane surface is limited. Under these conditions, external concentration polarization, fouling and scaling can reduce mass transport across the membrane. In tubular membranes (internal diameter ≥ 2 mm), turbulence can be easily achieved and concentration polarization and fouling, as well as scaling, can be reduced.

Petrotos *et al*. (1998) have investigated the use of a tubular module for the concentration of tomato juice. The module consisted of an external stainless steel shroud accommodating internally a set of two identical reverse osmosis membrane tubes that have no lengthwise support but are properly sealed at their ends. A comparison was carried out using different draw solutions such as sodium chloride, calcium chloride, calcium nitrate, glucose, sucrose or polyethylene glycol 400. Sodium chloride was found to be the most effective osmotic agent among all the draw solutions.

21.5 Effect of various parameters on transmembrane flux

Apart from the membrane orientation, the other factors which affect the transmembrane flux are the type of membrane, osmotic agent concentration, flow rates of feed and osmotic agent and temperature.

© Woodhead Publishing Limited, 2011

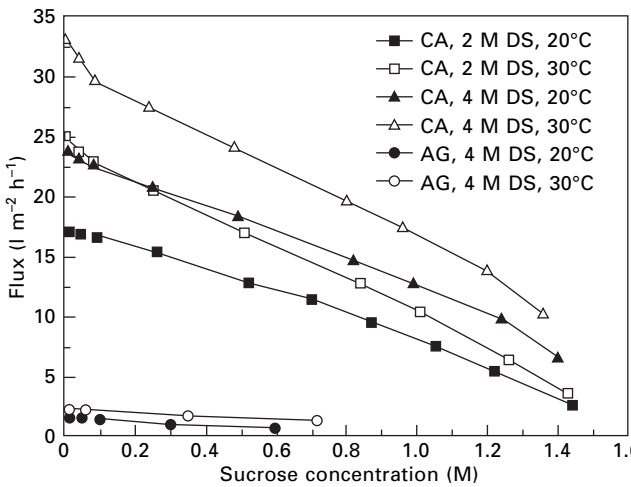
21.5.1 Types of membrane

A comparison of the performance of a cellulosic membrane from Hydration Technologies Inc. (designated CA) and a reverse osmosis membrane from General Electric Inc. (Osmonics) (designated AG) indicated that the water fluxes achieved for the AG membrane were only 7.7% of the CA membrane fluxes when deionized water was used as feed (Fig. 21.7, Garcia-Castello *et al.*, 2009). Similarly, McCutcheon *et al.* (2005) also indicted that the flux obtained using AG membrane was around 5% of the CA membrane, when NaCl and ammonium–carbon dioxide solutions were used as feed and osmotic agent solutions, respectively.

Osmotic flux was found to traverse the exponential trend with the thickness of membrane backing material and the active membrane layer being the same. A reduction in the thickness resulted in increase in osmotic flux (Petrotos *et al.*, 1998, Fig. 21.8).

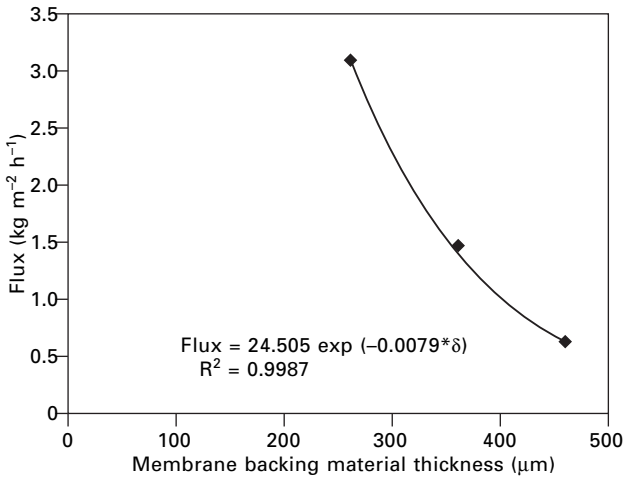
21.5.2 Effect of type and concentration of osmotic agent

Gray *et al.* (2006) demonstrated that a molar concentration of sodium chloride, dextrose or sucrose used as an osmotic agent solution directed towards the active layer of the membrane with water on the other side (mode I) did



21.7 Effect of temperature, draw solution (DS) concentration and sucrose feed solution concentration on permeate water flux for both the CA and AG membranes. Experimental conditions: feed solution (sucrose) concentration of 0–1.65 M (0–48 °Brix), draw solution concentration of 2 or 4 M NaCl, and cross-flow rate for draw and feed solutions of 1 l min^{-1} (1.67×10^{-5} m^3 s^{-1}) (from Garcia-Castello *et al.*, 2009).

© Woodhead Publishing Limited, 2011

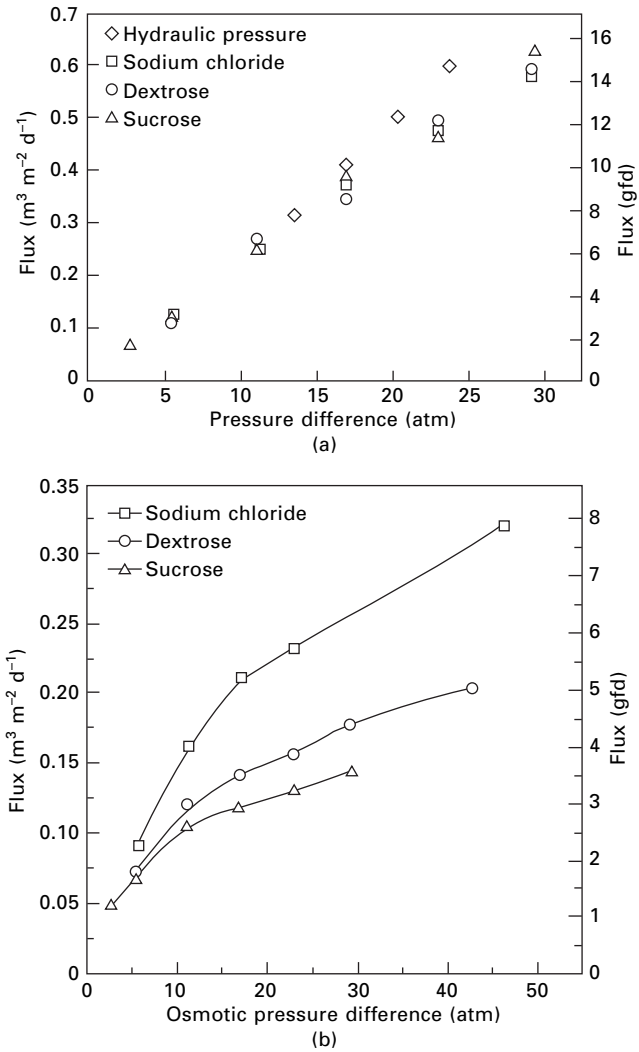


21.8 Correlation of tomato juice forward osmosis flux with the membrane backing material thickness (from Petrotos *et al.*, 1998).

not have significant effect on transmembrane flux (Fig. 21.9(a)) owing to insignificant internal and external concentration polarizations. In this situation, the molecular weight of solute had a negligible impact on performance and the flux varied linearly with the osmotic pressure, whereas, reversing the membrane orientation (mode II) resulted in reduced flux owing to substantial internal concentration polarization (Fig. 21.9(b)). Sodium chloride generates far more flux than dextrose at the same bulk osmotic pressure, which in turn generates more than sucrose. This may be attributed to the fact that larger molecular weight solutes cannot diffuse as quickly through the porous support of the membrane and dilutive internal concentration polarization will be more severe, resulting in lower flux.

The transmembrane fluxes both for pure water and for anthocyanin extract was found to increase in both modes I and II with an increase in osmotic agent (NaCl) concentration from 1.0–6.0M (Fig. 21.10). However, the transmembrane flux values in mode I were higher in comparison to mode II for the corresponding concentrations of osmotic agent solution. This may be attributed to the fact that during mode I, there will be negligible concentration polarization, but it will be significant in mode II owing to the diffusion of osmotic solute into the support layer resulting in the setting up of concentration gradient (Nayak and Rastogi, 2010a). Petrotos *et al.* (1998) pointed out a linear correlation between the brine concentration and osmotic flux. At the same time the mass transfer coefficient was shown to be inversely proportional to the brine concentration. Later, Dova *et al.* (2007a) also indicated that an increase in osmotic medium concentration (NaCl solution) resulted in an increase in transmembrane flux from the feed solution (sugar solution).

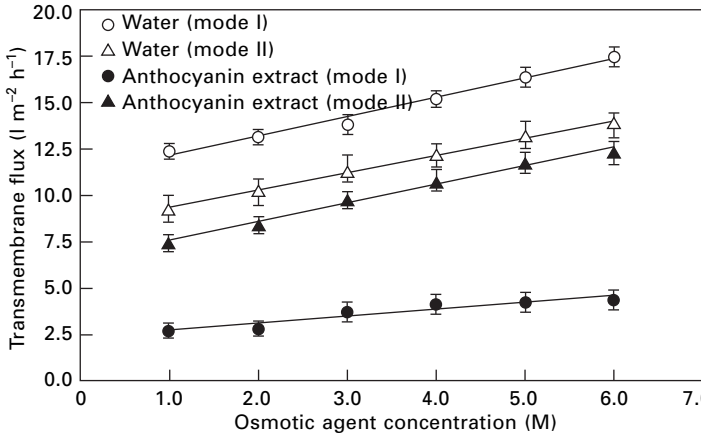
© Woodhead Publishing Limited, 2011



21.9 Water flux as a function of driving force (pressure difference). For FO runs with the three draw solutions, the osmotic pressure difference is generated by varying the draw solution concentration. (a) The draw solution was placed against the membrane active layer while the feed (deionized water) was placed against the support layer, (b) the draw solution was placed against the support layer of the membrane and the feed (deionized water) was placed against the active layer; gfd = gallons per square feet per day (from Gray *et al.*, 2006).

For the first time, Ling *et al.* (2010) used highly water-soluble magnetic nanoparticles as novel draw solutes in forward osmosis. The nanoparticles capped with polyacrylic acid yielded the highest driving force and subsequently

© Woodhead Publishing Limited, 2011



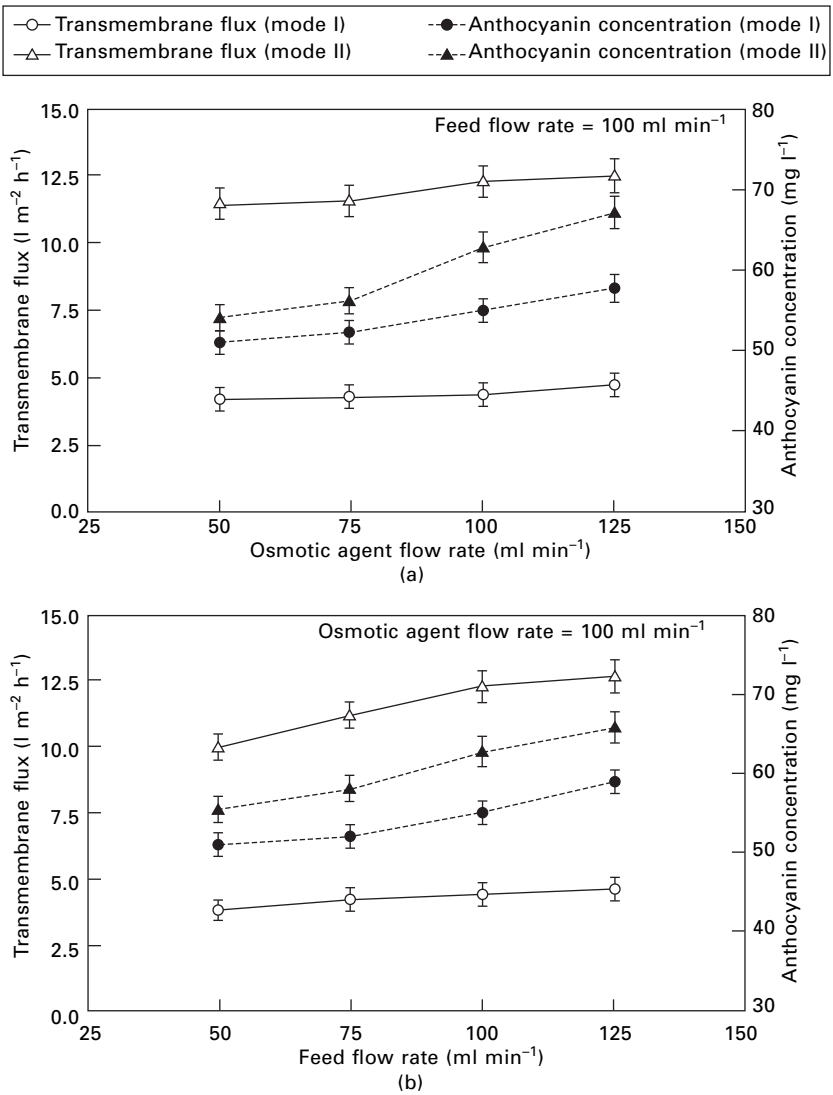
21.10 Effect of the osmotic agent concentration on transmembrane flux. Feed and osmotic agent flow rates were maintained at 100 ml min^{-1}. Modes I and II refer to the membrane orientation in which feed was directed towards the support layer and feed was directed towards active layer, respectively (from Nayak and Rastogi, 2010a).

the highest water flux. The used magnetic nanoparticles were captured by the magnetic field and recycled back into the stream as draw solutes in the forward osmosis process.

21.5.3 Effect of feed and osmotic agent flow rate on the transmembrane flux

With an increase in feed flow rate from 50–125 ml min^{-1}, the transmembrane flux was found to increase in both modes I and II (Fig. 21.11(a)). The osmotic agent flow rate and concentration during the experiments were maintained at 100 ml min^{-1} and 6.0 M, respectively. Similarly, transmembrane flux was found to increase in both modes I and II with an increase in osmotic agent flow rate (Fig. 21.11(b)). The feed flow rate and concentration of osmotic agent was maintained at 100 ml min^{-1} and 6.0 M, respectively. The anthocyanin concentration was found to increase for all the cases of an increase in transmembrane flux (Rastogi and Nayak, 2010a). Petrotos *et al.* (1998) demonstrated that a five-fold increase in flow rate (from 109–502 l h^{-1}) of tomato juice during forward osmosis flux resulted in an almost 32% increase of permeation flux. An increase in feed or osmotic agent flow rates resulting in an increase in transmembrane flux were also reported by Dova *et al.* (2007a) in the case when sugar solution is concentrated using NaCl solution as the osmotic agent solution.

© Woodhead Publishing Limited, 2011



21.11 Effect of (a) feed and (b) osmotic agent flow rate on transmembrane flux and anthocyanin concentration. Modes I and II refer to the membrane orientation in which feed was directed towards the support layer and feed was directed towards active layer, respectively. The osmotic agent concentration was maintained at 6.0 M (from Nayak and Rastogi, 2010a).

21.5.4 Effect of feed temperature

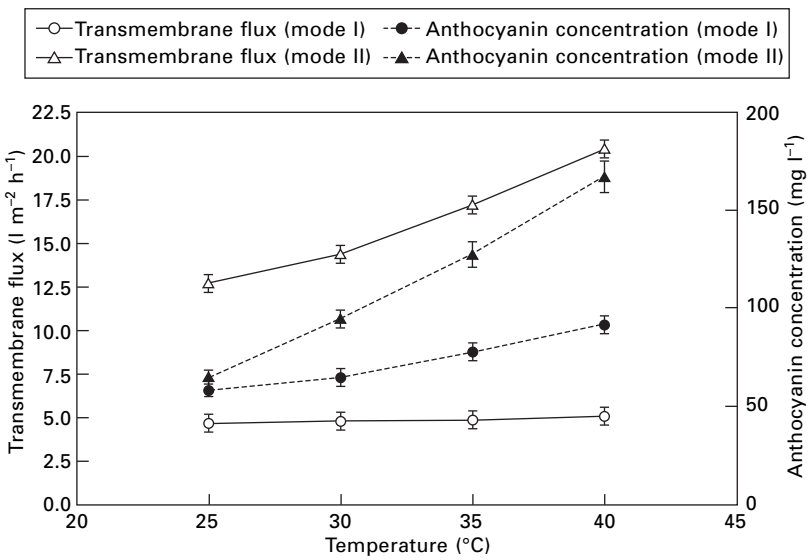
An increase in temperature yielded higher water flux (Fig. 21.7). The effect of temperature on permeate flux was described using an Arrhenius-type expression (McCutcheon *et al.*, 2006; Garcia-Castello *et al.*, 2009).

© Woodhead Publishing Limited, 2011

Nayak and Rastogi, (2010a) found that transmembrane flux in modes I and II increased with an increase in feed temperature (Fig. 21.12). The variation of the increase in transmembrane flux with temperature can be explained by the Wilke–Chang equation (Treybal, 1982), according to which the diffusion coefficient is proportional to the absolute temperature divided by the viscosity of the solvent. The increase in temperature reduces the viscosity of the solution and increases the diffusion coefficients, which results in an increase in transmembrane flux (Petrotos *et al.*, 1998; McCutcheon and Elimelech, 2006). At the same time, the anthocyanin content was also found to increase in modes I and II with an increase in temperature. Wrolstad *et al.* (1993) and Petrotos *et al.* (1998) have reported that in the forward osmosis process, an increase in temperature resulted in an increase in transmembrane flux when concentrating red raspberry juice and tomato juice, respectively.

21.5.5 Effect of viscosity of osmotic agent solution

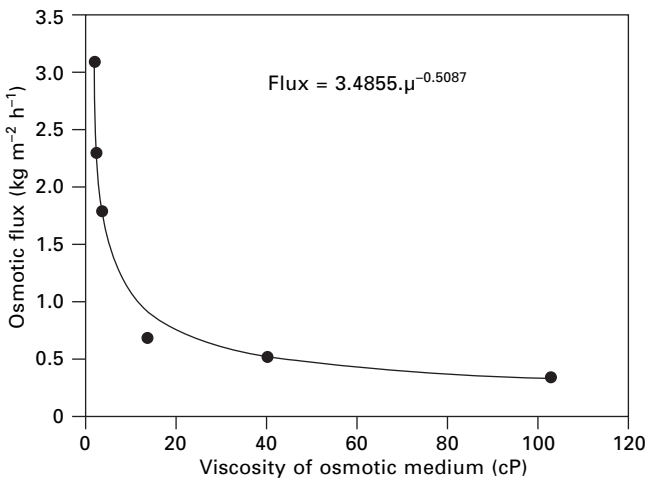
Petrotos *et al.* (1998) indicated that osmotic flux values had a strong exponential dependence on the viscosity of the osmotic solution. Flux values were found to be inversely proportional to the square root of the viscosity (Fig. 21.13).



21.12 Effect of feed temperature on transmembrane flux and anthocyanin concentration. Feed and osmotic agent flow rates were maintained at 125 ml min^{-1}. Modes I and II refer to the membrane orientation of the feed towards the support layer (I) and of the feed towards the active layer (II), respectively. The osmotic agent concentration was maintained at 6.0 M (from Nayak and Rastogi, 2010a).

© Woodhead Publishing Limited, 2011

The results indicated the importance of using a low viscosity osmotic medium in forward osmosis applications to enhance its performance. The calculated driving force for the separation and flux values indicated that there is only little correlation between these two parameters (the correlation coefficient $R = 0.10$, Table 21.2). This meant that the performance of the process of forward osmosis is dependent on the diffusion of water from the membrane active layer through the membrane backing material and osmotic medium polarized layer, which is in turn dependent on the physical properties of the osmotic solution used. A lower viscosity of an osmotic medium implies higher diffusivity (or lower resistivity) of the solute in the porous membrane backing material, which results in a lowering of internal polarization leading to higher osmotic fluxes.



21.13 Correlation of the forward osmosis flux with osmotic medium viscosity in direct osmosis concentration of tomato juice (from Petrotos *et al.*, 1998).

Table 21.2 Values of viscosity of the used osmotic media, the corresponding driving force and flux (from Petrotos *et al.*, 1998)

Osmotic medium	Viscosity (cP) (25°C)	$\Delta\pi$-ΔP (bar)	Flux (kg $m^{-2} h^{-1}$)
NaCl 22.24% (w/w)	1.90	280.30	3.10
$CaCl_2$ 29.07% (w/w)	2.30	548.00	2.33
$Ca(NO_3)_2$ 29.00% (w/w)	2.90	176.30	1.80
PEG400 49.97% (w/w)	14.00	303.00	0.70
Sucrose 58.29% (w/w)	40.50	134.80	0.55
Glucose 62.86% (w/w)	103.00	337.50	0.37

© Woodhead Publishing Limited, 2011

21.6 Applications of forward osmosis

A wide range of applications have been studied for forward osmosis membrane processes. The following section summarizes the applications of forward osmosis in food processing, wastewater treatment, water purification, seawater desalination and in power generation.

21.6.1 Food processing

Most of the information available for the concentration of beverages and liquid foods using forward osmosis are limited to the laboratory scale (Raghavarao *et al.*, 2005). The forward osmosis process utilizes ambient temperature and pressure, which promote high retention of sensory (e.g. taste, aroma, colour) and nutritional (e.g. vitamin) quality. High rejection and low membrane fouling compared to pressure-driven membrane processes like reverse osmosis are additional advantages. Several patents are available for the development of forward osmosis membranes, devices and methods for the concentration of liquid foods (Foreman *et al.*, 1977; Liu *et al.*, 2009). Work carried out by various researchers on forward osmosis for processing of food has been summarized in Table 21.3.

Popper *et al.* (1966) were the first to report the concentration of grape juice using a forward osmosis process involving a plate and frame filter press with a reverse osmosis type of membrane made of flat sheet cellulose acetate membranes. Sodium chloride was used as a draw solution. With moderate stirring, the grape juice was concentrated from 16–60° Brix with a flux of 2.5 l m^{-2} h^{-1}.

Rodriguez-Saona *et al.* (2001) developed a process for the concentration of red radish (anthocyanin) extract using forward osmosis as a potential natural red colourant. Concentrated extracts could be used as a food colourant with desirable colour attributes and minimal pigment degradation. Radish concentrates had colour characteristics close to FD&C Red #40. The extract was concentrated up to 30° Brix and contained anthocyanin levels of 800 mg/100 ml. Sensory evaluation showed that a combination of thermal evaporation and forward osmosis was found to considerably reduce the levels of undesirable radish aroma compounds.

Dova *et al.* (2007a) dealt with the impact of process parameters on performance of a pilot scale direct osmotic (membrane) concentration unit and studied its performance. The unit was built around a flat geometry membrane module with a contacting area of 0.09 m^2 (1.0 ft^2). Flat, square, reverse osmosis-type membrane sheets with varying characteristics were used with the osmotic module (cell). Model fluids, such as deionized water and low-concentration sucrose or glucose solutions, were utilized as feed fluids to study (and model) the impact of experimental parameters on process

© Woodhead Publishing Limited, 2011

Table 21.3 Work carried out by various researchers on forward/direct osmosis for the food processing industries

Juices/water/colorants	Osmotic agent	Membranes and their operating conditions	References
Grape juice	NaCl	Membrane: CA Module: plate and frame	Popper *et al.* (1966)
Red raspberry	HFCS	Module: Osmotek DOC cell S: 0.14 m^2	Wrolstad *et al.* (1993)
Orange Raspberry Tomato juice	PEG, HFCS	Module: Osmotek DOC cell CTA membrnae	Herron *et al.* (1994)
Tomato juice	NaCl $CaCl_2$ $Ca(NO_3)_2$	Tubular module AFC99 aromatic polyamide thin film	Petrotos *et al.* (1998)
Tomato juice	Brine	Flat sheet membrane module	Petrotos and Lazarides (2001)
Red radish	HFCS	Module: pilot plant (Osmotek Inc., Corvalis OR)	Rodriguez-Saona *et al.* (2001)
Pineapple juice	NaCl and sugar	Membrane: CTA Module: plate and frame	Babu *et al.* (2006)
Garcinia indica extract (natural food colorant)	NaCl	Membrane: CTA Module: plate and frame	Nayak and Rastogi (2010a) Nayak and Rastogi (2010b)

PEG = polyethylene glycol, HFCS = high fructose corn syrup.

performance. A solution of sodium chloride was used as an osmotic medium. Dova *et al*. (2007b) developed a generalized model for the direct osmotic concentration process.

Garcia-Castello *et al*. (2009) described concentrating sugar solutions using sodium chloride as a surrogate draw solution. This study demonstrated that forward osmosis is a viable alternative membrane process for concentration of sucrose solution. A concentration factor of 5.7 was achieved by forward osmosis with a starting sucrose concentration of 0.29 M, compared to reported concentration factors of up to 2.5 with reverse osmosis. Water fluxes were reported to be lower than those commonly obtained in reverse osmosis, which is a consequence of significantly higher concentration factors in conjunction with internal concentration polarization.

Wrolstad *et al*. (1993) studied the composition and sensory characterization of red raspberry juice concentrated by direct osmosis. Raspberry juice was concentrated up to 45 °Brix by evaporation as well as direct osmosis. The

© Woodhead Publishing Limited, 2011

study suggested that the direct osmosis concentrate is of premium quality, compared to that obtained by conventional evaporation. The osmotic concentrates were clustered closer to single strength juice in red raspberry in terms of flavour and aroma than the evaporation-concentrated sample. There were minor compositional differences between the osmotically concentrated and evaporation concentrated sample.

Wong and Winger (1999) reviewed the applications of forward osmosis for food processing. Fruit juices can be concentrated to a higher concentration than by reverse osmosis, even with high insoluble solid levels, and fouling has been reported to be minimal. The fluxes obtained with forward osmosis at present limit its full commercial acceptance in comparison to reverse osmosis.

Nayak and Rastogi (2010a, 2010b) demonstrated that the concentration of anthocyanin extract from *Garcinia indica* Choisy using forward osmosis has several advantages over thermal concentration in terms of higher stability, lower browning index and less conversion of hydroxy citric acid (HCA) to its lactone form. Anthocyanin was concentrated from 49 mg l^{-1} to 2.69 g l^{-1} (54-fold increase) using forward osmosis. In comparison to the concentrate produced by forward osmosis, the non enzymatic browning index and degradation constant for thermally concentrated sample were found to be approximately two (from 0.78 to 0.35) and eight (from 63.0×10^{-3} to 8.0×10^{-3} day^{-1}) times, respectively. The ratio of HCA lactone to HCA was also found to be higher for the sample produced by thermal concentration (2.84:1) compared to concentrate produced by forward osmosis (1.50:1) (Nayak and Rastogi, 2010a, 2010b)

It is evident that the forward osmosis process has enormous advantages over conventional concentration methods such as thermal evaporation and pressure-driven membrane processes for concentration of liquid foods. Low energy use, low operating temperatures and pressures and high product concentration are the main advantages of this process.

21.6.2 Electricity generation

Forward osmosis and pressure-retarded processes have been studied to yield energy by transmembrane osmotic pressure. A method of converting kinetic energy from the forward osmosis process to useful electricity generation is described by Irving (2005). The system comprised a solvent and pressure chambers to hold feed and draw solutions, respectively. Water effused across the membrane into the pressure chamber increasing the pressure, thereby generating hydrostatic energy. A conversion device converted the increased pressure in the pressure chamber to hydrostatic energy. The draw solution can be expelled and recycled after use.

The use of sea water in forward osmosis in the pressure-retarded mode

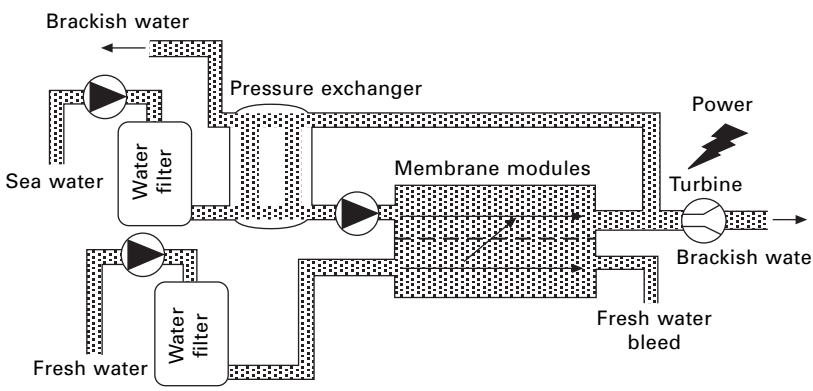
© Woodhead Publishing Limited, 2011

for generation of electric power has great potential (Achilli *et al*., 2009a, 2009b). The power generated is renewable with a limited environmental impact. Global osmotic power production potential is of the order of 2000 TWh per year (Aaberg, 2003). The layout for a pressure-retarded osmosis power process is illustrated in Fig. 21.14. The development and future success of pressure-retarded osmosis for power generation will have great impact on the success of forward osmosis for water treatment and desalination.

Pressure-retarded osmosis as a viable source of renewable energy was investigated by Achilli *et al*. (2009a, 2009b). In pressure-retarded osmosis, water from a low salinity feed solution permeated through a membrane into a pressurized, high salinity draw solution and power was obtained by depressurizing permeate through a hydroturbine. These results were reported for a flat-sheet cellulose triacetate forward osmosis membrane where sodium chloride was used as feed and draw solutions. Maximum power densities of 2.7 and 5.1 W/m^2 were observed for 35 and 60 g l^{-1} NaCl draw solutions, respectively, at 970 kPa hydraulic pressure. The power density was substantially reduced owing to internal concentration polarization in the asymmetric cellulose triacetate membranes and, to a lesser degree, to salt passage. External concentration polarization was found to exhibit a relatively small effect on reducing the osmotic pressure driving force.

21.6.3 Desalination

Desalination of sea (or saline) water has been practised regularly for over 50 years and is a well-established means of water supply in many countries. An increasing scarcity of fresh water sources fuelled a push towards alternative resources such as ocean water. In the 1970s, exploration began into using membranes for water desalination. As they proved to be successful



21.14 Simplified process layout for pressure-retarded osmosis power plant (from Aaberg, 2003).

© Woodhead Publishing Limited, 2011

in producing purified water from salt water, membranes became a viable alternative to evaporation-based technologies for water treatment. Desalination technologies are prohibitively expensive and energy intensive. Reverse osmosis is a commonly used desalination technology, which is significantly move expensive than the standard treatment of freshwater for potable use.

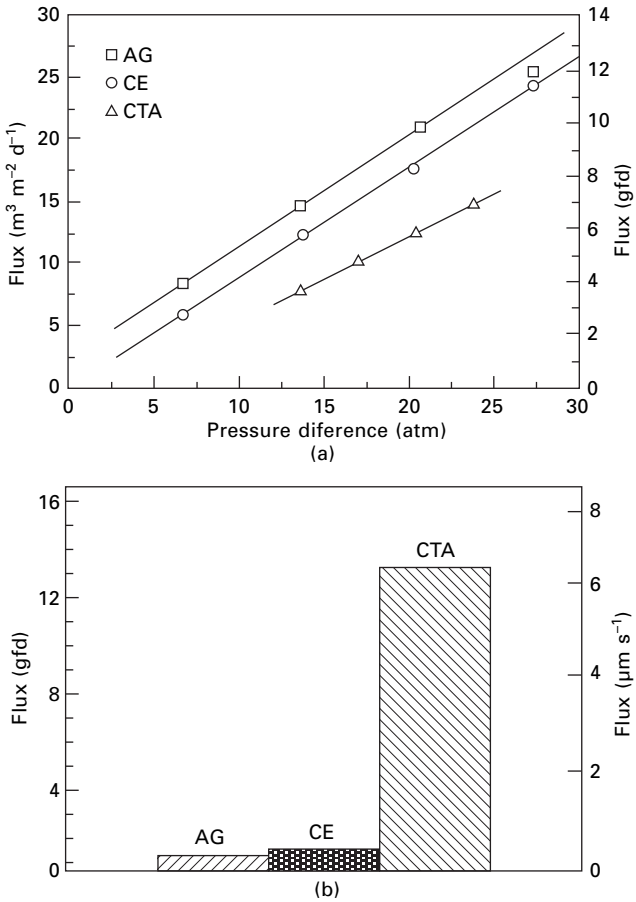
Over the years, purified water standards have become more stringent. However, membranes have risen to the challenge and continue to perform efficiently and effectively and forward osmosis membranes can be used for the desalination of water. Forward osmosis is a process that may be able to desalinate saline water sources at a notably reduced cost.

Frank (1972) described a method of forward osmosis using a solution of precipitable salt such as aluminum sulphate as an osmotic agent. The diluted osmosis agent solution was treated with calcium hydroxide, resulting in the precipitation of aluminim hydroxide and calcium sulphate. The precipitate was removed by standard methods leaving the fresh product water.

Kravath and Davis (1975) described a process of seawater desalination achieved by forward osmosis of water across a cellulose acetate membrane. Initial tests were conducted in a dialysis cell with glucose as the draw solute and seawater as the feed. Upon dilution, the salinity was reduced to a level where ingestion would be possible for short-term consumption. The performance of flat sheet cellulose acetate membranes was reported to be poor in terms of salt rejection. Stache (1989) used a semi-permeable membrane bag filled with concentrated fructose solution to desalinate small volumes of seawater while simultaneously creating a nutritious drink. Yaeli (1992) used a concentrated glucose solution as a draw solution and water was extracted from seawater by osmosis. The diluted glucose solution was fed to a reverse osmosis unit, where a low pressure reverse osmosis membrane separated potable water from the sucrose draw solution.

McCutcheon *et al.* (2006) demonstrated a novel forward osmosis desalination process, which involved an ammonium bicarbonate as an osmotic solution to extract water from saline feed water across a semi-permeable polymeric membrane. Very large osmotic pressures generated by the highly soluble ammonium bicarbonate osmotic solution yielded high water fluxes and resulted in very high feed water recoveries. Ammonium bicarbonate upon moderate heating can be decomposed into ammonia and carbon dioxide gases leaving the fresh product water. The water permeability (obtained from the slope of Fig. 21.15(a)) of the cellulose triacetate membrane was slightly lower than the AG and CE membranes (polyamide thin film composite membrane and cellulose acetate asymmetric membrane both have thick fabric backing layers), however, there was a great difference between the osmotic fluxes (Fig. 21.15(b)). The water permeability differences between the membranes did not account for the vast differences in water flux for the experiments described in Fig. 21.15(b). Since permeability does not account for this flux

© Woodhead Publishing Limited, 2011

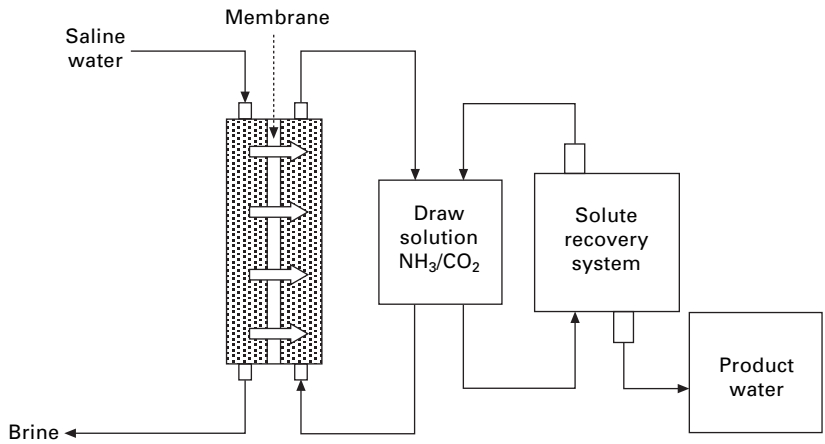


21.15 (a) Variation of pure water flux with hydraulic pressure. (b) Comparison of water flux in forward osmosis mode for the three membranes tested: AG and CE (reverse osmosis membranes) and CTA (forward osmosis membrane). Experimental conditions: 6 M ammonium bicarbonate draw solution, 0.5 M sodium chloride feed solution, and temperature of both feed and draw solutions 50°C (from McCutcheon *et al.*, 2005).

difference, the driving force must somehow be affected by certain membrane characteristics. It is expected that these thick fabric and porous support layers in both membranes contribute to the development of internal concentration polarization and, therefore, dramatically reduce the effective driving force and resulting water flux.

A schematic diagram of the ammonia–carbon dioxide forward osmosis desalination process to recover fresh water is presented in Fig. 21.16 (McGinnis and Elimelech, 2007). Low (2009) studied the performance of

© Woodhead Publishing Limited, 2011



21.16 Schematic diagram of the ammonia–carbon dioxide forward osmosis desalination process (from McGinnis and Elimelech, 2007).

forward osmosis with respect to different ammonia–carbon dioxide draw solutions and membranes. A simple forward osmosis test rig using a flat-sheet membrane was built. The internal concentration polarization lowered the flux. This phenomenon was found to be more prominent in higher concentration feeds. An increase in temperature was reported to improve flux but the effects were less significant for a higher concentration of feed.

McCutcheon *et al*. (2006, 2009) also reported that forward (direct) osmosis using semi-permeable polymeric membranes may be a viable alternative to reverse osmosis as a lower cost and more environmentally friendly desalination technology. The driving force was provided by a draw solution comprising the highly soluble gases ammonia and carbon dioxide. Water fluxes ranging from 3.6–36.0 l m^{-2} h^{-1} for a wide range of draw and feed solution concentrations were reported. Desalination of very high sodium chloride feed solutions (simulating 75% recovery of seawater) was also deemed possible, leading to the possibility minimization of brine discharge.

Lampi *et al*. (2007) integrated the forward osmosis process with a reverse osmosis process to generate potable water, particularly from water that has a high salt content. Forward osmosis was used to generate the significant hydraulic pressure used to drive the reverse osmosis process, wherein the reverse osmosis process can separate salt from sea water to generate potable water from water with high salt content.

Martinetti *et al*. (2009) compared vacuum-enhanced direct contact membrane distillation (VEDCMD) and forward osmosis for water recovery enhancement in desalination of brackish water. In both processes, high water recoveries were achieved; however, recoveries were limited by precipitation of inorganic salts on the membrane surface. Various cleaning techniques

© Woodhead Publishing Limited, 2011

were able to remove the scale layer from the membrane and restore water flux to almost initial levels. Forward osmosis achieved water recoveries up to 90% from the brines and VEDCMD achieved water recoveries up to 81% from the brines.

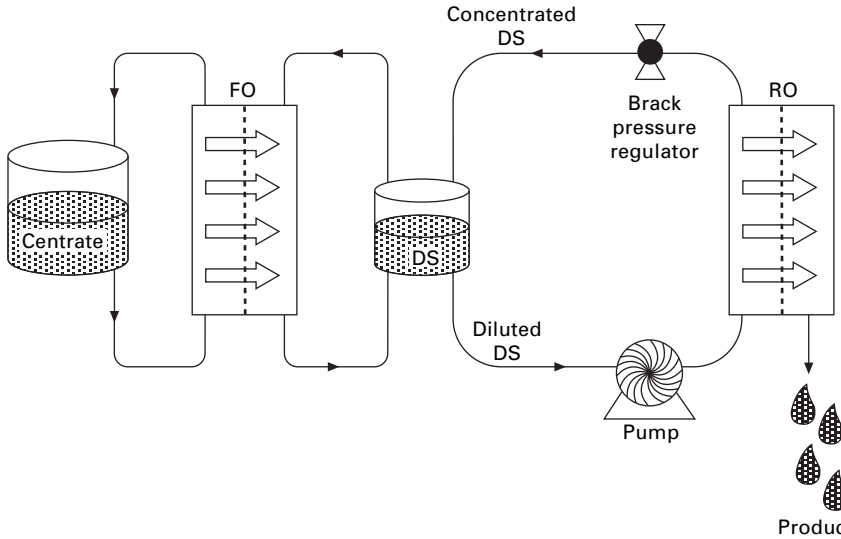
Bamaga *et al*. (2009) presented a design for an integrated desalination unit consisting of a closed forward osmosis and reverse osmosis process in which reverse osmosis brine was used as the osmotic draw solution so that the chemical energy stored in the reverse osmosis brine was recovered and utilized by the forward osmosis membrane process. In addition, the energy contained in the excess reverse osmosis brine pressure is used for brine circulation in the forward osmosis process loop. Choi *et al*. (2009, 2010) also investigated combined systems of forward osmosis and reverse osmosis for seawater desalination. A model to predict the performance of the combined systems was developed based on a solution–diffusion model and modified film theory considering internal concentration polarization. A pilot-scale combined system with forward osmosis resulted in higher recovery with higher quality and fluxes than conventional reverse osmosis-based desalination systems. Tan and Ng (2010) proposed a hybrid forward osmosis–nanofiltration process for seawater desalination. The process with two-pass nanofiltration regeneration was found to achieve good quality product water that met the recommended drinking water total dissolved solids guideline (500 mg l^{-1}). Lay *et al*. (2010) examined possible factors for the slower decline of flux in forward osmosis process based on a combined experimental and modelling approach. Low water fluxes, use of hydrophilic and smooth membranes and internal concentration polarization were found to be possible contributing factors. The transmission of draw solutes from the draw solution into the feed was found to have significant effect on performance.

21.6.4 Miscellaneous applications

Biosolids generated in excess during wastewater treatment are most often treated in an aerobic or anaerobic digester in order to destroy pathogens, reduce biochemical oxygen demand (BOD) and reduce the volume of the solid waste to be handled. Stabilized biomass and biogas are produced by this digester. When the digested biomass is dewatered using a centrifuge, a biosolids fraction and a liquid fraction (a centrate) are produced. Holloway *et al*. (2007) developed a process to mitigate the problems associated with centrate, removing both nitrogen and phosphorus or reducing the volume of centrate (Fig. 21.17). The continuous bench-scale system used forward osmosis as a pretreatment for reverse osmosis, which results in high water flux and high nutrient rejection along with the sustainable flux over an extended time period.

Tinge *et al*. (2007) introduced a new concept of dewatering aqueous

© Woodhead Publishing Limited, 2011



21.17 Continuous forward osmosis (FO)/reverse osmosis (RO) bench scale process setup. The first stage is a forward osmosis system for pretreatment of water and the second stage is a reverse osmosis system that concentrates the draw solution (DS) for the forward osmosis stage and produces purified water (from Holloway *et al.,* 2007).

caprolactam (the raw material of nylon-6) solutions using forward osmosis by employing the osmotic pressure of solutions of concentrated aqueous ammonium sulphate to reduce the overall energy costs associated with removal of water. In most of these commercial caprolactam processes a lot of water is involved for dilution and purification purposes. Since the end-product is sold as a molten liquid, almost all the water needs to be evaporated. This technology was shown to increase the sustainability of the overall caprolactam production process.

21.7 Conclusions

Recent developments in osmotic processes have prompted a flurry of research activity in the field of forward osmosis, which has recently been studied in many areas of science and engineering for food processing, water treatment, wastewater treatment, seawater/brackish water desalination, pharmaceutical drug delivery and electric power production. Basic research on forward osmosis and the development of new applications of forward osmosis are steadily growing despite the lack of new membranes and membrane modules. Forward osmosis membranes need to provide high water permeability, high rejection of solutes, substantially reduced internal concentration polarization,

© Woodhead Publishing Limited, 2011

high chemical stability and high mechanical strength. Membrane technologies may offer energy efficient methods of concentrating liquid foods when compared to energy intensive evaporative methods. Within the realm of these technologies, forward osmosis may be a more suitable, promising and sustainable alternative.

Owing to its inherent features, the forward osmosis process has attracted increasing interest in various disciplines and there is an increasing literature on both academic research and industrial applications. Presently, the major obstacles for the development of forward osmosis process are lack of good performance membranes and suitable draw solutions. The commercial application of forward osmosis needs membranes with an improved performance. As a consequence of the low water fluxes, very large membrane areas will be required to reach the desired concentration factors, resulting in high capital costs. Improved performance may be possible with the development of membranes specifically tailored for forward osmosis processes. Recent research work such as that on double-selective layer membranes may provide potential applications for forward osmosis in desalination and can pave the way to improving the membrane design for the forward osmosis process.

The lack of optimized membranes and processes for the effective recovery and regeneration of the draw solution are the main limitations to transforming forward osmosis into a full-scale process in the food industry.

21.8 Acknowledgements

The authors thank Dr V. Prakash, Director, CFTRI, Mysore for his encouragement and keen interest in downstream processing. Thanks are also due to Dr KSMS Raghavarao, Head, Department of Food Engineering, CFTRI for his support. The author Chetan A Nayak expresses his gratitude and sincere thanks to the Council of Scientific and Industrial Research, New Delhi for providing a Senior Research Fellowship.

21.9 References

Aaberg, R.J. (2003). 'Osmotic power-a new and powerful renewable energy source', *ReFocus*, **4**, 48–50.

Achilli, A., Cath, T.Y. and Childress, A.E. (2009a). 'Power generation with pressure retarded osmosis: An experimental and theoretical investigation', *Journal of Membrane Science*, **343**, 42–52.

Achilli, A., Cath, T.Y., Marchand, E.A. and Childress, A.E. (2009b). 'The forward osmosis membrane bioreactor: A low fouling alternative to MBR processes'. *Desalination*, **239**, 10–21.

Babu, B.R., Rastogi, N.K. and Raghavarao, K.S.M.S. (2006). 'Effect of process parameter on transmembrane flux during direct osmosis', *Journal of Food Science*, **280**, 185–94.

© Woodhead Publishing Limited, 2011

Bamaga, O.A., Yokochi, A. and Beaudry, E.G. (2009). 'Application of forward osmosis in pretreatment of seawater for small reverse osmosis desalination units', *Desalination and Water Treatment*, **5**, 183–91.

Beaudry, E.G. and Lampi, K.A. (1990a). 'Membrane technology for direct osmosis concentration of fruit juices', *Food Technology*, **44**, 121.

Beaudry, E.G. and Lampi, K.A. (1990b). 'Osmotic concentration of fruit juices', *Fluessiges Obst*, **57**, 652–64.

Bolin, H.R. and Salunke, D.K. (1971). 'Physicochemical and volatile flavor changes occurring in fruit juices during concentration and foam-mat drying', *Journal of Food Science*, **36**, 665–8.

Cath, T.Y. (2010). 'Osmotically and thermally driven membrane processes for enhancement of water recovery in desalination processes', *Desalination and Water Treatment*, **15**, 279–86.

Cath, T.Y., Gormly, S., Beaudry, E.G., Flynn, M.T., Adams, V.D. and Childress, A.E. (2005a). 'Membrane contactor processes for wastewater reclamation in space: Part I. Direct osmotic concentration as pretreatment for reverse osmosis', *Journal of Membrane Science*, **257**, 85–98.

Cath, T.Y., Adams, D. and Childress, A.E. (2005b). 'Membrane contactor processes for wastewater reclamation in space: II. Combined direct osmosis, osmotic distillation, and membrane distillation for treatment of metabolic wastewater', *Journal of Membrane Science*, **257**, 111–19.

Cath, T.Y., Childress, A.E. and Elimelech, M. (2006). 'Forward osmosis: Principles, applications, and recent developments', *Journal of Membrane Science*, **281**, 70–87.

Choi, Y.J., Choi, J.S., Oh, H.J., Lee, S., Yang, D.R., and Kim, J.H. (2009). 'Toward a combined system of forward osmosis and reverse osmosis for seawater desalination', *Desalination*, **247**, 239–46.

Choi, J.S., Kim, H., Lee, S., Hwang, T.M., Oh, H., Yang, D.R. and Kim, J.H. (2010). 'Theoretical investigation of hybrid desalination system combining reverse osmosis and forward osmosis', *Desalination and Water Treatment*, **15**, 114–20.

Chou, S., Shi, L., Wang, R., Tang, C.Y., Qiu, C. and Fane, A.G. (2010). 'Characteristics and potential applications of a novel forward osmosis hollow fiber membrane', *Desalination*, **261**, 365–72.

Cussler E.L. (1984). *Diffusion: Mass Transfer in Fluid Systems*, 3rd edn, Cambridge University Press, Cambridge, 384–5.

Dova, M.I., Petrotos, K.B. and Lazarides, H.N. (2007a). 'On the direct osmotic concentration of liquid foods. Part I: Impact of process parameters on process performance', *Journal of Food Engineering*, **78**, 422–30.

Dova, M.I., Petrotos, K.B. and Lazarides, H.N. (2007b). 'On the direct osmotic concentration of liquid foods: Part II. Development of a generalized model', *Journal of Food Engineering*, **78**, 431–7.

Foreman, G.E, Diego, S., Worsley, P.K. and Barbara, S. (1977). *Spiral Wound Membrane Module for Direct Osmosis Separations*. US Patent 4033878.

Frank, B.S. (1972). *Desalination of Sea Water*. US Patent 3,670,897.

Garcia-Castello, E.M., McCutcheon, J.R. and Elimelech, M. (2009). 'Performance evaluation of sucrose concentration using forward osmosis', *Journal of Membrane Science*, **338**, 61–6.

Goosens, I. and Van-Haute, A. (1978). 'The use of direct osmosis tests as complementary experiments to determine the water and salt permeabilities of reinforced cellulose acetate membranes', *Desalination*, **26**, 299–308.

© Woodhead Publishing Limited, 2011

Gray, G.T., McCutcheon, J.R. and Elimelech, M. (2006). 'Internal concentration polarization in forward osmosis: Role of membrane orientation', *Desalination*, **197**, 1–8.

Herron, J.R., Beaudry, E.G., Jochums, C.E. and Medina, L.E. (1994). *Osmotic Concentration Apparatus and Method for Direct Osmotic Concentration of Fruit Juices*. US Patent No 5,281,430.

Holloway, R.W., Childress, A.E., Dennett, K.E. and Cath, T.Y. (2007). 'Forward osmosis for concentration of anaerobic digester centrate', *Water Research*, **41**, 4005–14.

Irving, D. (2005). *Osmosis Process for Producing Energy*. WO2005/019643 A1.

Jiao, B., Cassano, A. and Drioli, E. (2004). 'Recent advantages on membrane processes for the concentration of fruit juices: a review', *Journal of Food Engineering*, **63**, 303–24.

Kravath, R.E. and Davis, J.A. (1975). 'Desalination of seawater by direct osmosis', *Desalination*, **16**, 151–5.

Lampi, K., Beaudry, E. and Herron, J. (2007). *Forward Osmosis Pressurized Device and Process for Generating Potable Water*. US Patent, 7,303,674 B2.

Lay, W.C.L., Chong, T.H., Tang, C.Y., Fane, A.G., Zhang, J. and Liu, Y. (2010). 'Fouling propensity of forward osmosis: Investigation of the slower flux decline phenomenon', *Water Science and Technology*, **61**, 927–36.

Lazarides, H.N., Iakovidis, A. and Schwartzberg, H.G. (1990). 'Aroma loss and recovery during falling film evaporation', in *Engineering and Food. Volume 3. Advanced processes*, W.E.L. Spiess and H. Schubert (eds), Elsevier Applied Science Publishers, Barking, UK, 96–105.

Lee, K.L., Baker, R.W. and Lonsdale, H.K. (1981). 'Membranes for power generation by pressure retarded process', *Journal of Membrane Science*, **8**, 141–71.

Ling, M.M., Wang, K.Y. and Chung, T.S. (2010). 'Highly water-soluble magnetic nanoparticles as novel draw solutes in forward osmosis for water reuse', *Industrial and Engineering Chemistry Research*, **49**, 5869–76.

Liu, L., Wang, M., Wang, D. and Gao, C. (2009). 'Current patents of forward osmosis membrane process', *Recent Patents on Chemical Engineering*, **2**, 76–82.

Loeb, S. and Bloch, M.R. (1973). 'Counter current flow osmotic processes for the production of solutions having a high osmotic pressure', *Desalination*, **13**, 207–15.

Loeb, S., Titelman, L., Korngold, E. and Freiman, J. (1997). 'Effect of porous support fabric on osmosis through a Loeb–Sourirajan asymmetric membrane', *Journal of Membrane Science*, **129**, 243–9.

Low, S.C. (2009). 'Preliminary studies of seawater desalination using forward osmosis', *Desalination and Water Treatment*, **7**, 41–6.

Martinetti, C.R., Childress, A.E. and Cath, T.Y. (2009). 'High recovery of concentrated RO brines using forward osmosis and membrane distillation', *Journal of Membrane Science*, **331**, 31–9.

McCutcheon, J.R. and Elimelech, M. (2006). 'Influence of concentrative and dilutive concentration polarization on flux behavior in forward osmosis', *Journal of Membrane Science*, **284**, 237–47.

McCutcheon, J.R. and Elimelech, M. (2007). 'Modeling water flux in forward osmosis, implications for improved membrane design', *AIChE Journal*, **53**, 1736–44.

McCutcheon, J.R. and Elimelech, M. (2008). 'Influence of membrane support layer hydrophobicity on water flux in osmotically driven membrane processes', *Journal of Membrane Science*, **318**, 458–66.

McCutcheon, J.R., McGinnis, R.L. and Elimelech, M. (2005). 'A novel ammonia–carbon dioxide forward (direct) osmosis desalination process', *Desalination*, **174**, 1–11.

© Woodhead Publishing Limited, 2011

McCutcheon, J.R., McGinnis, R.L. and Elimelech, M. (2006). 'Desalination by ammonia-carbon dioxide forward osmosis: Influence of draw and feed solution concentrations on process performance', *Journal of Membrane Science*, **278**, 114–23.

McCutcheon, J.R., McGinnis, R.L. and Elimelech, M. (2009). 'A novel ammonia–carbon dioxide forward (direct) osmosis desalination process', *Desalination*, **174**, 1–11.

McGinnis, R.L. and Elimelech, M. (2007). 'Energy requirements of ammonia–carbon dioxide forward osmosis desalination', *Desalination*, **207**, 370–82.

McGinnis, R.L., McCutcheon, J.R. and Elimelech, M. (2007). 'A novel ammonia-carbon dioxide osmotic heat engine for power generation', *Journal of Membrane Science,* **305**, 13–19.

Mi, B. and Elimelech, M. (2008). 'Chemical and physical aspects of organic fouling of forward osmosis membranes', *Journal of Membrane Science*, **320**, 292–302.

Mi, B. and Elimelech, M. (2010). 'Organic fouling of forward osmosis membranes: Fouling reversibility and cleaning without chemical reagents', *Journal of Membrane Science*, **348**, 337–45.

Nayak, C.A. and Rastogi, N.K. (2010a). 'Forward osmosis for the concentration of anthocyanin from *Garcinia indica* Choisy', *Separation and Purification Technology*, **71**, 144–51.

Nayak, C.A. and Rastogi, N.K. (2010b). 'Comparison of osmotic membrane distillation and direct osmosis membrane processes for concentration of anthocyanin', *Desalination and Water Treatment*, **16**, 134–45.

Ng, H.Y., Tang, W. and Wong, W.S. (2006). 'Performance of forward (direct) osmosis process, membrane structure and transport phenomenon', *Environmental Science and Technology*, **40**, 2408–13.

Petrotos, K.B. and Lazarides, H.N. (2001). 'Osmotic concentration of liquid foods', *Journal of Food Engineering*, **49**, 201–6.

Petrotos, K.B., Quantick, P. and Petropakis, H. (1998). 'A study of the direct osmotic concentration of tomato juice in tubular membrane– module configuration I. The effect of certain basic process parameters on the process performance', *Journal of Membrane Science*, **150**, 99–110.

Petrotos, K.B., Quantick, P.C. and Petropakis, H. (1999). 'Direct osmotic concentration of tomato juice in tubular membrane module configuration'. II. The effect of using clarified tomato juice on the process performance', *Journal of Membrane Science*, **160**, 171–7.

Popper, K., Camirand, W.M., Nury, F. and Stanley, W.L. (1966). 'Dialyzer concentrates beverages', *Food Engineering*, **38**, 102–4.

Raghavarao, K.S.M.S., Nagaraj, N., Patil, G., Babu, B.R. and Niranjan, K. (2005). 'Athermal membrane process for the concentration of liquid foods and natural colours', in *Emerging Technologies in Food Processing*, D. W. Sun (ed), Academic Press, Elsevier, London, 251–78.

Rodriguez-Saona, L.E., Giusti, M.M., Durst, R.W. and Wrolstad, R.E. (2001). 'Development and process optimization of red radish concentrate extract as potential natural red colourant', *Journal of Food Processing Preservation*, **25**, 165–82.

Scott, R.D. (1975). *Dehydration and Packaging of Foodstuffs*. US Patent No. 3,858,499.

Stache, K. (1989). *Apparatus for Transforming Sea water, Brackish Water, Polluted Water or the Like into a Nutritious Drink by Means of Osmosis*. US Patent 4,879,030.

Su, J., Yang, Q., Teo, J.F. and Chung, T.S. (2010). 'Cellulose acetate nanofiltration

© Woodhead Publishing Limited, 2011

hollow fiber membranes for forward osmosis processes', *Journal of Membrane Science*, **355**, 36–44.

Tan, C.H. and Ng, H.Y. (2008). 'Modified models to predict flux behavior in forward osmosis in consideration of external and internal concentration polarizations', *Journal of Membrane Science*, **324**, 209–19.

Tan, C.H. and Ng, H.Y. (2010). 'A novel hybrid forward osmosis–nanofiltration (FO–NF) process for seawater desalination: Draw solution selection and system configuration', *Desalination and Water Treatment*, **13**, 356–61.

Tang, W. and Ng, H.Y. (2008). 'Concentration of brine by forward osmosis: Performance and influence of membrane structure', *Desalination*, **224**, 143–53.

Tang, C.Y., She, Q., Lay, W.C.L., Wang, R. and Fane AG. (2010). 'Coupled effects of internal concentration polarization and fouling on flux behavior of forward osmosis membranes during humic acid filtration', *Journal of Membrane Science*, **354**, 123–33.

Tinge, J.T., Krooshof, G.J.P., Smeets, T.M., Vergossen, F.H.P., Krijgsman, J., Hoving, E. and Altink, R.M. (2007). 'Direct osmosis membrane process to de-water aqueous caprolactam with concentrated aqueous ammonium sulphate', *Chemical Engineering and Processing*, **46**, 505–12.

Treybal, R.E. (1982). *Mass Transfer Operations*, 3rd edn, McGraw-Hill Chemical Engineering Series, New Delhi.

Wang, K.Y., Yang, Q., Chung, T.S. and Rajagopalan, R. (2009). 'Enhanced forward osmosis from chemically modified polybenzimidazole (PBI) nanofiltration hollow fiber membranes with a thin wall', *Chemical Engineering Science*, **64**, 1577–84.

Wang, K.Y., Ong, R.C. and Chung, T.S. (2010a), 'Double-skinned forward osmosis membranes for reducing internal concentration polarization within the porous sublayer', *Industrial Engineering and Chemistry Research*, **49**, 4824–31.

Wang, R., Shi, L., Tang, CY., Chou, S., Qiu, C. and Fane, A.G. (2010b). 'Characterization of novel forward osmosis hollow fiber membranes', *Journal of Membrane Science*, **355**, 158–67.

Wilf, M. (2010). 'Future of the osmotic processes', *Desalination and Water Treatment*, **15**, 292–8.

Wong, M. and Winger, R.J. (1999). 'Direct osmotic concentration for concentrating liquid foods', *Food Australia*, **51**, 200–5.

Wrolstad, R.E., McDaniel, M.R., Durst, R.W., Micheals, R.W., Lampi, K.A., and Beaudry, E.G. (1993). 'Composition and sensory characterization of red raspberry juice concentration by direct osmosis or evaporation', *Journal of Food Science*, **58**, 633–41.

Xu, Y., Peng, X., Tang, C.Y., Shiang Fu, Q. and Nie, S. (2010). 'Effect of draw solution concentration and operating conditions on forward osmosis and pressure retarded osmosis performance in a spiral wound module', *Journal of Membrane Science*, **348**, 298–309.

Yaeli, J. (1992). *Method and Apparatus for Processing, Liquid Solutions of Suspensions Particularly Useful in the Desalination of Saline Water*. US Patent 5,098,575.

Yang, Q., Wang, K.Y. and Chung, T.-S. (2009a). 'A novel dual-layer forward osmosis membrane for protein enrichment and concentration', *Separation and Purification Technology*, **69**, 269–74.

Yang, Q., Wang, K.Y. and Chung, T.S. (2009b). 'Dual-layer hollow fibers with enhanced flux as novel forward osmosis membranes for water production', *Environmental Science and Technology*, **43**, 2800–5.

© Woodhead Publishing Limited, 2011

Yip, N.Y., Tiraferri, A., Phillip, Schiffman, J. and Elimelech, M. (2010). 'High performance thin-film composite forward osmosis membrane', *Environmental Science and Technology*, **44**, 3812–18.

Zhang, S., Wang, K.Y., Chung, T.S., Chen, H., Jean, Y.C. and Amy, G. (2010). 'Well-constructed cellulose acetate membranes for forward osmosis: Minimized internal concentration polarization with an ultra-thin selective layer', *Journal of Membrane Science*, **360**, 522–35.

© Woodhead Publishing Limited, 2011

22

Degradation of polymeric membranes in water and wastewater treatment

A. ANTONY and G. LESLIE, The University of New South Wales, Australia

Abstract: This chapter reviews the mechanisms and attendant operating problems associated with degradation of polymeric membranes in water treatment applications. Information is presented on the possible modes of membrane failure and associated operational issues in full scale applications. Specific details of the degradation mechanism for various membrane polymers in different aqueous environments are presented, in addition to information on tools to monitor, detect and prevent membrane degradation.

Key words: cleaning in place (CIP), membrane ageing, membrane degradation, membrane integrity.

22.1 Introduction

Membrane processes are used in the water industry in a variety of applications including the filtration of surface water, desalination of brackish and seawater and filtration of wastewater for a range of fit for purpose applications. The use of polymeric membranes in the water industry has become more prevalent as a result of technological developments and research that has improved the ruggedness, efficiency, reliability and cost effectiveness of the membranes. Membrane processes used in treatment applications are of two major types, (1) membrane processes such as microfiltration (MF) and ultrafiltration (UF) are porous structured with a convective transport mechanism and (2) semi-permeable membrane processes such as nanofiltration (NF) and reverse osmosis (RO) are dense structured with solution–diffusion transport. Integration of these processes into water treatment systems offers many advantages over traditional filtration processes including consistent product quality that is independent of feed water quality, effective removal of disinfectant-resistant pathogens and the potential to meet stringent water quality regulations.

Despite its potential in water treatment, a wider use of industrial membrane processes is impeded by some phenomena that lead to deterioration of permeate water quality, reduction in operating flux/increase in transmembrane pressure and shortening of membrane life. Membrane ageing and degradation is one of the challenges that membrane technology is facing that needs more research input. Membrane degradation followed by failure hastens membrane

© Woodhead Publishing Limited, 2011

replacement and substantially increases the cost of membrane filtration. Among the various probabilities that could lead to membrane degradation, routine use of chemicals is the major cause for membrane damage in an operational plant. Although chemical cleaning is inevitable in any membrane operation, many times the chemical incompatibility and ageing of membranes cause membrane degradation. The present article reviews state of the art understanding of membrane degradation and identifies the research needs and research trends expected in the near future.

22.2 Polymer materials and module design

Polymers used for membrane manufacture are expected to possess a high water permeation rate, good separation efficiency, mechanical stability, tolerance to chemicals, resistance to microbial attack and the ability to withstand a wide range of operating temperatures and pH values. Various polymeric materials used in membrane fabrication and general configuration are presented in Table 22.1.

A variety of polymer materials used for industrial water treatment applications vary in their hydrophilicity. Hydrophilic membranes are generally desired to give a stable filtration performance at high flux over a long period and are resistant to fouling from dissolved organic substances (Kubota *et al.*, 2008; Pearce, 2007a; Möckel *et al.*, 1999). In spite of the mechanical stability of polymers like PVDF, PES, PS and PAN, their relatively hydrophobic nature is limited, experiencing severe fouling. Therefore, these membranes are modified without any compromise to their mechanical stability by (i)

Table 22.1 Polymeric materials used for membrane fabrication

Application	General configuration	Separation mechanism	Polymer material
MF	Hollow fibre	Size exclusion	Polypropylene (PP), polytetrafluoroethylene (PTFE), polyvinylidene fluoride (PVDF), aliphatic polyamide (PA), polysulfone (PS), polyethersulfone (PES), polyether ether ketone (PEEK)
UF	Hollow fibre, spiral wound, tubular	Size exclusion	PVDF, aliphatic and aromatic PA, PS, PES, polyethylene (PE), PEEK, polyacrylonitrile (PAN), polyimide (PI), cellulose acetate (CA), PP, nylon6, polymethylmethacrylic acid (PMMA)
NF	Spiral wound, tubular	Size exclusion, diffusion	PES, PI, CA, aromatic PA
RO	Spiral wound	Diffusion	PI, CA, aromatic PA

© Woodhead Publishing Limited, 2011

modifying the base polymer before doping, (ii) combining the polymer with additives or (iii) surface modification of the final membrane, by physical adsorption of a hydrophilic component (Van der Bruggen, 2009). Hydrophilic polymers like polyvinyl pyrrolidone (PVP) and polyethylene glycol (PEG) are extensively used as membrane additives for membrane modification. The molecular mass and concentration of these additives also has an impact on the final membrane properties (Ochoa *et al.*, 2001; Idris *et al.*, 2007).

Commercial polymeric membrane modules applied for the water treatment applications have three major configurations, hollow fibre, spiral-wound and tubular. The membrane module configuration is generally selected based on the feed quality, expected product quality and operating parameters. Spiral wound modules are advantageous in terms of their mechanical robustness to operate at high pressures, however the fouling susceptibility is high and the ease of cleaning is relatively low. Hollow fibre modules possess high intrinsic integrity and hold up volume. The tubular configuration is generally preferred for water with high suspended solid content and high pore plugging potential. The objectives for selecting an appropriate configuration are to ensure sufficient circulation, and to limit the accumulation of materials adjacent to the surface of the membrane and the deposition and retention of materials on the surface of the membrane. The structural integrity of an individual membrane module or element is influenced to a certain extent by the configuration (Pearce, 2007b).

22.3 Membrane failure and operational issues

The chances of membrane degradation in membrane operations fall into two categories (Johnson and MacCormick, 2003):

1. Before installation, membrane damage could be during the manufacture, shipment and installation. However, quality controls and rigorous integrity testing of modules during installation can keep this damage to negligible.
2. During filtration, the chances of membrane damage are high during the membrane operation depending on the operating parameters and maintenance. The operational parameters include operational and backwash pressures, chemical usage and mechanical handling. However, the frequency of failure is also dependent on the manufacturer's record of accomplishment.

Statistical analysis of the data gathered from the literature, water treatment plants and membrane manufacturers shows that the strength of membrane material, the operation conditions and uncontrolled water quality incidents (such as the presence of material that can damage the membrane) are the factors responsible for fibre failure (Gijsbertsen-Abrahamse *et al.*, 2006).

© Woodhead Publishing Limited, 2011

In this survey, the annual rate of hollow fibre membrane failure is shown to typically to vary between 1 and 10 failures per 1 million fibres.

In a routine operation, the potential chances for membrane damage include pore expansion through use of routine cleaning chemicals (Arkhangelsky *et al.*, 2007b; Al-Qahtany and Al-Bastaki, 1995), damage by mechanical forces, shear forces and vibrations (Huisman and Williams, 2004), oxidation caused by disinfection and high operating pressures greater than manufacturer recommendations (Jacangelo *et al.*, 1991; Lake *et al.*, 2003).

22.3.1 Permeate flux restoration

A decrease in the permeate flux caused by irreversible membrane fouling is well recognised as the main problem in membrane operations. Membrane foulants can be classified into four major categories, colloidal, inorganic, organic and biological. Physical and chemical cleaning is an important task involved in industrial water treatment filtration to restore the membrane performance after fouling. Physical or hydrodynamic cleaning may involve aeration and backwash which apply turbulent and shear forces. Cleaning in-place (CIP) and chemically enhanced backwash operations are the common chemical restoration practices. CIP is the intermittent exposure of membranes to the cleaning solution for a specific time and temperature. Chemically enhanced backwash is a maintenance cleaning step where chemicals are mixed in a routine back flush; contact time and chemical aggressiveness are relatively less compared to CIP. CIP is performed when the normalised flux drops by 10–15%, normalised feed pressure increases by 10–15% or normalised permeate conductivity increases by 10–15% (Film Tec, 1995).

A wide range of cleaning chemicals can be grouped into acids, alkalis, oxidising agents, chelants, surfactants and enzymes. Selection of appropriate cleaning protocol ensures the removal of irreversible fouling and maximum flux restoration. Various membrane cleaning technologies, their efficiencies and mechanisms have been discussed in detail by many researchers in the past (Al-Amoudi and Lovitt, 2007; Le-Clech *et al.*, 2006; Porcelli and Judd, 2010; Liu *et al.*, 2001; Chen *et al.*, 2003). The key factors in selecting an appropriate cleaning protocol involve type and concentration of cleaning chemical, contact time, temperature and shear forces applied during cleaning. Chemical reactions remove foulants by loosening, dissolving and keeping the foulants in dispersion and solution to prevent the refouling of already cleaned surface (Madaeni and Mansourpanah, 2004). Amongst different cleaning chemicals, oxidising agents need a special mention in the context of membrane ageing. Oxidising agents are stand alone chemical disinfectants or sanitisers frequently used in water treatment plants to inactivate pathogenic microorganisms, mitigate biofouling and oxidise reduced inorganic solutes (Crittenden and Harza, 2005). Sodium hypochlorite is by far the most common

© Woodhead Publishing Limited, 2011

oxidising agent; however, other chemicals in use include chloramines, chlorine dioxide, hydrogen peroxide and ozone. Combining an oxidant in an alkaline cleaning step was seen to have complementary cleaning effects for organic foulants. In caustic environments, the fouling layer has an open structure allowing the chlorine to reach the inner layer of foulant materials (Hong and Elimelech, 1997; Zondervan and Roffel, 2007; Lin *et al.*, 2001; Causserand *et al.*, 2008; Kennedy *et al.*, 2008). Use of aggressive cleaning chemicals for the removal of membrane foulant may damage the membrane. Thus, upon routine membrane operation, repeated fouling and cleaning cycles result in ageing of membranes and performance decline. This typically shortens the expected lifetime of the membrane module. Membrane ageing has an impact on the membranes' mechanical, morphological and chemical properties causing the membrane to degrade or fail.

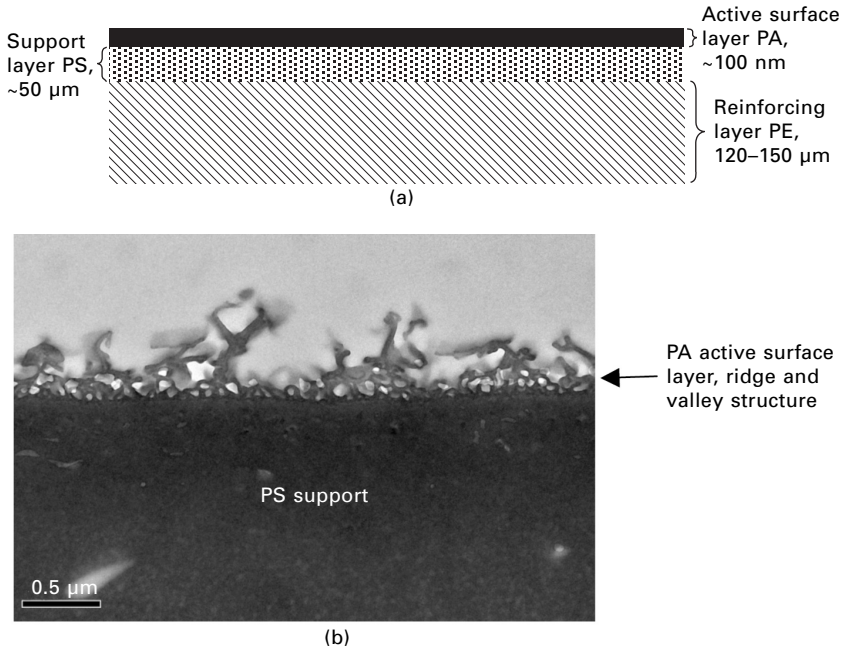
22.3.2 Disinfection of reverse osmosis systems

In the context of high pressure operations, PA thin film composite (TFC) membranes have become the most widely used RO membrane for water recycling and desalination applications. Typically, TFC membranes consist of three parts, as represented in Fig. 22.1(a). The top layer is the active surface layer of approximately 100 nm thickness. This is the PA layer, formed on the substrate after interfacial polycondensation reaction of acid chlorine with diamine. The middle layer is the microporous substrate, approximately 50 μm thick, mostly made of PS materials. The bottom layer is the reinforcing fabric support for additional mechanical strength, usually made from woven or nonwoven polyester materials approximately 120–150 μm thick. The transmission electron microscopy (TEM) cross-section of ESPA3 RO membrane given in Fig. 22.1(b) shows the active surface layer and PS support layer.

PA membranes can withstand a wide range of pH values and high recoveries (Glater *et al.*, 1994). A major limitation with these membranes are their poor tolerance of chlorine environments (Glater *et al.*, 1994; Antony *et al.*, 2010). RO membranes may become exposed to a chlorine environment in one of the two ways, (i) from chemical cleaning agents adopted for the flux recovery and (ii) from disinfection agents added to the RO upstream to mitigate biofouling.

To control biofouling in conventional RO desalination plants, a residual chlorine concentration of 0.2 to 4 mg l^{-1} and typical contact time of 15 and 30 min is maintained by continuous or intermittent chlorination. RO membrane manufacturers do not recommend continuous chlorine dosing owing to their poor tolerance to residual chlorine; the chlorine concentration in RO upstream is advised to be less than 0.1 mg l^{-1}. The excess chlorine is usually scavenged using sodium bisulfite before entering the membrane

© Woodhead Publishing Limited, 2011



22.1 (a) Schematic representation of a TFC membrane and (b) TEM cross-section image of RO membrane (ESPA3, Hydranautics).

system and rechlorinated before distribution. In spite of efforts taken to maintain the right amount of free chlorine concentration, uncontrollable factors like changes in feed water quality will alter the residual chlorine concentration. Similarly, in seawater RO systems, the presence of naturally occurring bromide ions disturbs the chlorine system (Shemer and Semiat, 2011). Thus, exposure to chlorine affects the structural integrity of the PA active layer, leading to impaired performance (Glater *et al.*, 1994, Light *et al.*, 1987, Petersen, 1993, Watters *et al.*, 1986).

22.3.3 Hollow fibre membrane failure

In the case of hollow fibre membranes, the impact of fibre failure on the overall integrity of the system depends on the system design and operation. Factors affecting membrane performance have been classified into common factors and system design factors (Johnson and MacCormick, 2003). The common factors are feed water quality, transmembrane pressure and removal efficiency of membrane fouling over time. The system design factors are the fibre internal diameter and number of fibres in a module, the mode of operation and the location of fibre break. Childress *et al.* (2005) performed research on membrane failure with respect to membrane mechanical properties,

© Woodhead Publishing Limited, 2011

particularly, membrane material, membrane symmetry, fibre modulus of elasticity, fibre diameter and thickness, module potting technique, module flow pattern and coliform breakthrough. The outcome was combined with mathematical modelling of a structure fluid interaction to assess the main factors responsible for maintaining the hollow fibre membrane integrity. The results illustrated that the additional stresses at the juncture of potting could be a potential cause for the formation of membrane fractures.

22.3.4 Membrane integrity

Membrane degradation affects the performance of filtration in three major ways, product quality, fouling propensity and mechanical strength. With membrane degradation, the functional properties/characteristics of the membrane gradually decrease affecting the product, both qualitatively and quantitatively. Membrane degradation changes the selectivity or rejection efficiency of the target contaminant and therefore the product quality is altered from that expected originally. Most importantly, in the drinking water production industry, membrane degradation and the resulting integrity breach could raise the microbial contamination risk of the product water (Antony *et al.*, in press). Health concerns are also an issue, where even a minor breach in the membrane could compromise the removal of bacteria and viruses in the drinking water treatment (Gitis *et al.*, 2006). The fouling propensity of the membrane is largely affected by the surface roughness, hydrophilicity and surface charge. Chemical exposure alters these properties and therefore the fouling propensity may change adversely in long-term operation (of cycling fouling and cleaning). This ends up requiring frequent cleaning at relatively short intervals. Finally, membrane degradation caused by chemical cleaning effects a major change on the mechanical properties, generally decreasing the tensile strength and reducing the membrane ductility. Membrane failure also extends to form hairline cracks, holes or complete membrane breaks, which all result in feed leak and direct mixing with the permeate.

22.4 Membrane degradation mechanisms

Understanding the impact of various chemicals used during membrane plant operation will help to optimise its use. But performing this in real time would take a very long time and therefore membrane ageing and degradation are generally studied as accelerated tests. Accelerated tests are performed under aggressive environments which include using high concentration of chemicals, lengthy contact times and aggressive temperature, pH and operating parameters.

Oxidants are the main class of chemicals that deteriorate the polymeric membranes under routine operation. The mechanism of degradation by

© Woodhead Publishing Limited, 2011

hypochlorite, free bromine, chloramines and hydrogen peroxide may be same, but the severity of damage differs from one chemical to another under same operating conditions (da Silva *et al.*, 2006; Tessaro *et al.*, 2005; Shemer and Semiat, 2011). Hypochlorite is the oxidising reagent extensively reported to cause membrane degradation upon exposure. The sanitisation effect and the degradation nature of hypochlorite are influenced by the ratio of its dissociated ion concentrations. Hypochlorite in water dissociates to give hypochlorous acid, HClO, which further dissociates to give hypochlorite ions, ClO^-:

$$NaClO + H_2O \leftrightarrow HClO + NaOH$$

$$HClO \leftrightarrow H^+ + ClO^-$$

In aqueous solution, the ratio of hypochlorous acid to hypochlorite ions is most dependent on but not limited to pH. The ClO^- form is the dominant form at pH >9 and HClO at low pH. Although both the forms are oxidants, the oxidising ability of HClO is much higher than ClO^-; the sanitising ability of the HClO form is approximately 50–100 times higher than ClO^-. Therefore, a lower pH is beneficial for the formation of HClO with greater chlorine sensitivity (Rouaix *et al.*, 2006; Gabelich *et al.*, 2005; Xu *et al.*, 2010).

For practical applications in the water industry, PVDF, PES, PS, CA and PA are widely used polymer materials in water treatment membrane materials (Thominette *et al.*, 2006; Arkhangelsky *et al.*, 2007b). PVDF, PES and PS membranes are generally said to be resistant to chlorine attack; however, they cannot be assured to be completely nonreactive in chemical environments. The degradation mechanism of these membranes is discussed in this section and summarised in Table 22.2.

22.4.1 Degradation of polyvinylidene fluoride (PVDF)

PVDF polymer is demonstrated to be reasonably resistant and capable of withstanding the typical cleaning concentration of hypochlorite upon ageing (Wang *et al.*, 2010; Puspitasari *et al.*, 2010). Accelerated cleaning of PVDF membrane with a hypochlorite exposure dose of 7.92 g h l^{-1} resulted in good flux recovery; however, the fouling severity increased with subsequent fouling–cleaning cycles (Wang *et al.*, 2010). In this study, chemical modification of the PVDF structure was not seen; however the mechanical properties were considerably altered. Cycling cleaning studies on a PDVF membrane with 1.7 g h l^{-1} of hypochlorite exposure clearly illustrated that over consecutive filtration–cleaning cycles, the fouling layer attaches to the membrane strongly and therefore fouling removal becomes difficult with successive cleaning operations (Puspitasari *et al.*, 2010). From the hydraulic performance assessed by X-ray photoelectron spectroscopy (XPS), Fourier

© Woodhead Publishing Limited, 2011

Table 22.2 Membrane degradation mechanism of common membrane materials

Membrane material	Key degradation step	Reference
PVDF	No major change in the chemical structure Selective elimination of surface modification additives	Puspitasari *et al.* (2010), Wang et al. (2010)
Cellulose acetate (CA)	Formation of carboxyl (-COOH), aldehyde (-CHO) and ketone (-C═O) end groups	Arkhangelsky *et al.* (2007a, 2008)
PES	Partial scission of Ph-S groups resulting in PES polymer chain terminated by sulfonic acid or phenyl chloride end groups Selective elimination of surface modification additives	Arkhangelsky *et al.* (2007a, 2007b), Yadav *et al.* (2009)
PS	Chain scission of polysulfone by radical oxidation, to yield alkenes and alcohols	Causserand *et al.* (2008), Gaudichet-Maurin and Thominette (2006)
PA	Electrophilic substitution of the aromatic ring/chlorination of amide nitrogen followed by rearrangement to form ring chlorinated products	Glater *et al.* (1994), Soice *et al.* (2003), Gabelich *et al.* (2005)
PVP	Chain scission and oxidation of PVP leading to ring opening of pyrrolidine	Wienk *et al.* (1995)

transform infrared spectroscopy (FTIR) and contact angle measurements, hypochlorite degradation and ageing of PVDF was suggested to take place in two steps. (1) Surface modification additives are gradually removed, resulting in increased membrane resistance and hydrophobicity with a potential chance of reduction in the average pore size. (2) When the surface modifiers are completely removed, the overall membrane resistance decreased and the membrane turned relatively more hydrophilic, possibly caused by the change in ionic strength of the membrane and pore enlargement.

22.4.2 Degradation of cellulose acetate (CA)

The attenuated total reflectance (ATR)-FTIR spectrum of CA membranes exposed to 18 g h l^{-1} hypochlorite showed a considerable reduction in the intensities of characteristic peaks corresponding to the O—C—O vibration (1760 cm^{-1}), C—O vibration (1230 cm^{-1}) and C—H vibration (1340 cm^{-1}) (Arkhangelsky *et al.*, 2007a, 2008). Significant peak reduction compared to virgin membrane suggests the oxidative degradation of CA to form carboxyl, aldehydes and ketone end products, also confirmed by XPS studies (Arkhangelsky *et al.*, 2008). In addition, a decline in mechanical strength

© Woodhead Publishing Limited, 2011

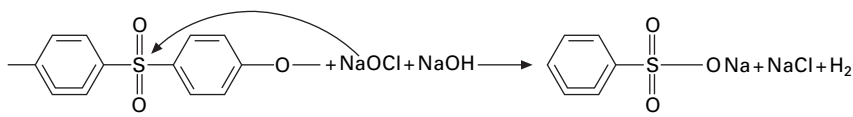
and pore enlargement was also demonstrated as a consequence of oxidative degradation.

22.4.3 Degradation of polyethersulfone (PES)

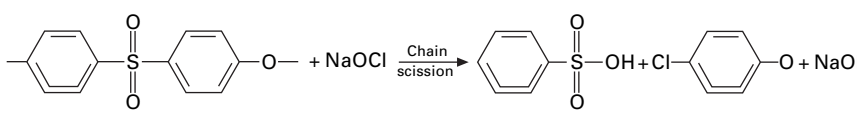
The reaction mechanism for the hypochlorite attack of PES was proposed to be partial scission of Ph—S bond by Arkhangelsky *et al.* (2007b) based on a previous study (Kice and Puls, 1977) as shown in Fig. 22.2.

This reaction scheme was predicted to progress by forming an intermediate step, where phenyl sulfinate $PhSO_2$ transforms to $PhSO_2^-$ followed by $PhSO_3^-$ formation. Later, Yadav *et al.* (2009) suggested a revision to this reaction path since the end product sodium sulfonate is likely to be an unstable compound. Moreover, uptake of chlorine by the membrane surface, evidenced from the surface characterisation techniques could be explained by this mechanism. The modified reaction scheme is given below in Fig. 22.3.

In addition, hypochlorite exposure of PES was shown to result in selective elimination of PVP from the membrane matrix (Arkhangelsky *et al.*, 2007b). PVP is an additive to promote hydrophilicity of polymer and therefore its leaching is expected to increase the hydrophobicity of the membrane, reflected as increased contact angle values (Wienk *et al.*, 1995). However, the contact angle values decreased with increasing hypochlorite concentration from 0–100 g h l^{-1} (Arkhangelsky *et al.*, 2007b); the likely causes for this were suggested to be (1) partial ionization of the membrane surface owing to the formation of charged compounds $PhSO_3^-$ and (2) formation of bigger pores owing to membrane degradation and consequent capillary action. Hypochlorite was effective in removing the foulant, but affected both surface and bulk characteristics. Hypochlorite exposure increased electronegativity, porosity and fouling tendency and decreased the mechanical strength of the cleaned membrane. On the other hand, a contradictory result was obtained in another study by Yadav *et al.* (2009), where ageing of the PES membrane at hypochlorite



22.2 Reaction scheme for the degradation of PES (Arkhangelsky *et al.*, 2007b).



22.3 Modified reaction scheme for the degradation of PES (Yadav and Morison, 2010).

© Woodhead Publishing Limited, 2011

concentrations of 240–600 g h l^{-1} resulted in surface modification which was evident from surface characterization techniques; however mechanical strength testing did not reflect a change in bulk properties.

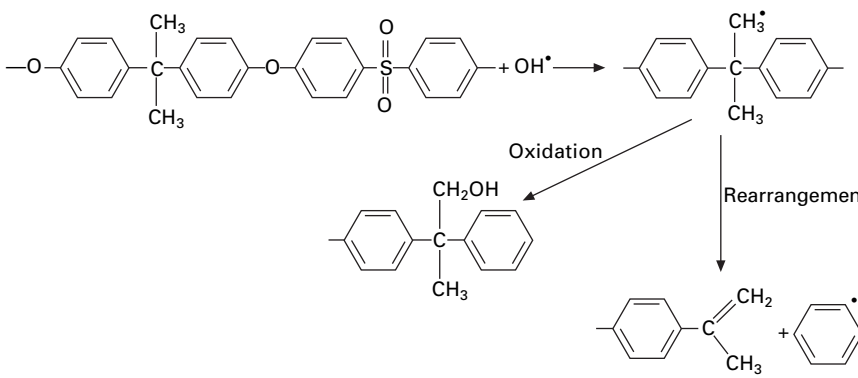
22.4.4 Degradation of polysulfone (PS)

Hypochlorite degradation of PS was comprehensively analysed by mechanical tests, spectroscopic analysis and molar mass distribution by Gaudichet-Maurin and Thominette (2006) who proposed the chain scission mechanism. They suggested a mechanism of radical oxidation of sulfone and isopropylidene bridges resulting in the formation of alkenes and alcohols. The suggested mechanism is given in Fig. 22.4.

Since this reaction has to be initiated by $OH^{\bullet}$ (free radical) in the chlorine environment, PS membrane degradation mainly depends on the chlorine chemistry. Formation of $OH^{\bullet}$ is decided by the availability of HClO, given as (Fukatsu and Kokot, 2001):

$$2HClO \rightarrow 2OH^{\bullet} + Cl_2$$

In addition, various conditions favourable for HClO will enhance the membrane degradation and *vice versa*. The presence of metal ions like Fe^{3+} and Cu^{2+} catalyse the radical oxidation reaction. On the other hand, the presence of an antiradical like tert-butanol inhibits oxidation of the PS structure (Causserand *et al.*, 2008).



22.4 Reaction scheme for PS degradation by a radical oxidation mechanism.

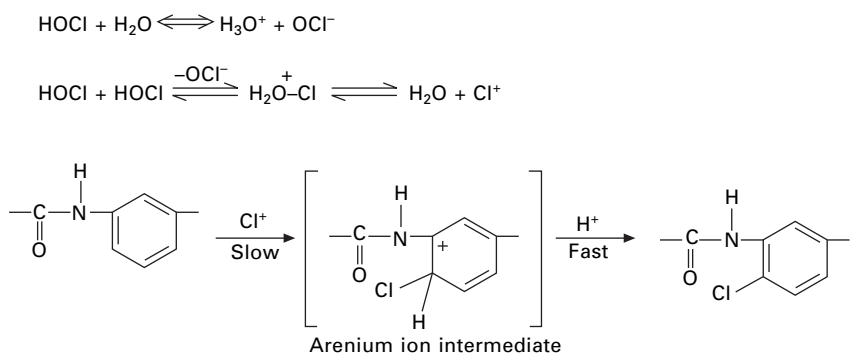
© Woodhead Publishing Limited, 2011

22.4.5 Degradation of aromatic polyamide (PA)

Oxidative degradation of PA membrane in a chlorine environment has been studied by many researchers and degradation takes place through two different mechanisms (Glater *et al*., 1994; Antony *et al*., 2010; Gabelich *et al*., 2005; Kang *et al*., 2007; Kwon and Leckie, 2006a, 2006b; Soice *et al*., 2003; Avlonitis *et al*., 1992).

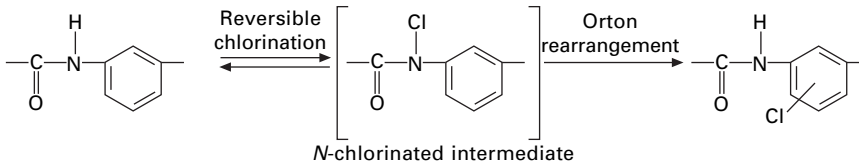
The first mechanism is by direct electrophilic aromatic substitution followed by Orton rearrangement. Aromatic rings are susceptible to electrophilic substitution by chlorine (March, 1992) but this chlorination is favoured only in the presence of an electron acceptor or Lewis acid (Solomons and Fryhle, 2008). In an aqueous chlorine environment, Cl^+ formed from HOCl acts as the Lewis acid, the primary driver for the chlorination reaction. This reaction proceeds through the formation of amide-substituted arenium ion followed by its rearrangement to form a ring-chlorinated product. The reaction mechanism proposed by Gabelich *et al*. (2005) is given below in Fig. 22.5. The first step forming the arenium ion intermediate is the slow and rate determining step. The energy of activation is greater for this step than the following rearrangement step.

The second mechanism of aromatic PA is by chlorination of amide nitrogen followed by Orton rearrangement. The amide nitrogen in the PA structure is susceptible to aqueous chlorine attack because of the electron withdrawing effects of the carbonyl group resulting in the formation of *N*-chloro derivatives (March, 1992; Challis and Challis, 1970). The degradation is proposed to take place in two steps (Glater *et al*., 1994). In the first step, the hydrogen atom on the amide nitrogen is substituted by chlorine to form a *N*-chlorinated intermediate. The second step is an intramolecular rearrangement: the *N*-chlorinated intermediate rearranges to from a ring-chlorinated end product. The *N*-chlorination reaction has also been claimed to be reversible, with the possibility of the *N*-chlorinated intermediate reverting back to the initial amide



22.5 Reaction scheme for PA degradation by electrophilic substitution of the aromatic ring to form ring-chlorinated products.

© Woodhead Publishing Limited, 2011



22.6 Reaction scheme for PA degradation by chlorination of amide nitrogen followed by Orton rearrangement.

structure with alkali treatment. The N-chlorination substituent was proposed to be a short-lived intermediate (Glater *et al.*, 1994; Kang *et al.*, 2007; Soice *et al.*, 2003). The suggested reaction path is given below in Fig. 22.6:

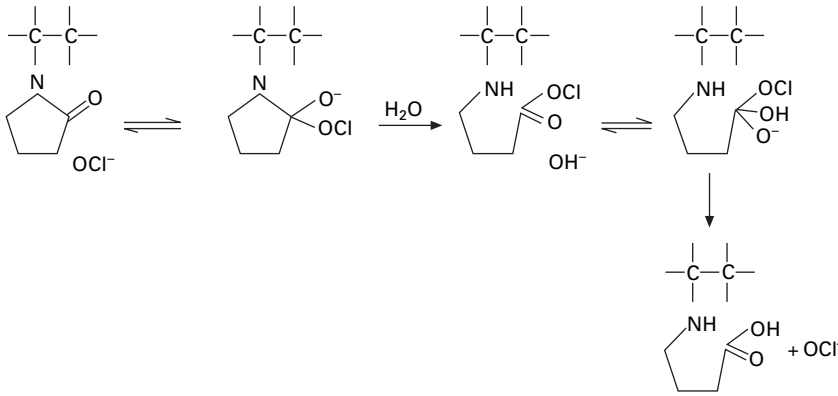
Antony *et al.* (2010) suggest that the *N*-chlorinated substituent may not be considered as a short-lived intermediate in view of the fact that chlorine substitution on nitrogen has been identified by FTIR. They suggested the reaction products could be both *N*-chlorinated products and ring-chlorinated compounds; most likely their existence is influenced by the operating parameters. More specifically, the rearrangement of the *N*-chlorinated substituent seems to be favoured under high pressure. Also, the ring-chlorination step seems to be the destructing step for the PA surface resulting in salt passage. Avlonitis *et al.* (1992) proposed that the chlorine attack of the PA membranes resulting in enhanced salt passage is due to the transition in morphology of the polymer, a more crystalline to a less crystalline (or more amorphous) state. In addition, oxidation of the PA membrane degradation in a chlorine environment was shown to be catalysed by the presence of metal ions like iron and aluminium (Gabelich *et al.*, 2005).

Soice *et al.* (2004) suggested that the chlorine degradation of PA does not lead to any chain scission but to separation of the barrier layer from the support; however this mechanism does not satisfy all pH conditions. For polymeric composite membranes, although the operating performance depends on the active surface layer, the porous support also has a minor effect on them. In this context, Benavente and co-workers studied the change in the transport parameters and chemical modifications of the PA active and PS porous sub-layer using ageing and chemical agents (Benavente and Vázquez, 2004; Benavente *et al.*, 2006). In these studies, both the active and support layers were shown to be affected on exposing the PA/PS membranes. An increase in permeability was observed upon treating with acids, whereas treatment with NaOH decreased the permeability.

22.4.6 Degradation of polyvinylpyrrolidone (PVP)

PVP is a common additive in membrane manufacture, as a pore former and hydrophiliser for naturally hydrophobic polymers like PS, PES, PAN and PVDF. During membrane ageing, a common degradation phenomenon is the

© Woodhead Publishing Limited, 2011



22.7 Reaction scheme for PVP by a ring-opening mechanism.

selective leaching of PVP. In other words, the polymer material by itself, for example PES is fairly resistant to hypochlorite, but the damaging effect on the membrane only takes place when PVP is present and is selectively leached from the porous membrane (Wienk *et al*., 1995; Gaudichet-Maurin and Thominette, 2006).

Wienk *et al*. (1995) proposed that the selective elimination of PVP from the membrane matrix could happen due to two distinct processes: (i) chain scission of PVP resulting in molecular weight reduction, which then gets washed out easily and (ii) oxidation of PVP in alkaline medium with pyrrolidine ring opening. The degradation mechanism of PVP by ring opening is shown in Fig. 22.7 (Wienk *et al*., 1995; Anderson *et al*., 1979):

Thus, the modification of the chemical structure minimises the interaction of PVP with the base polymer matrix and PVP elimination is facilitated. This mechanism was taken to be an advantage in synthesising high flux membranes with a narrow pore size distribution after hypochlorite treatment (Qin *et al*., 2003a, 2003b, 2005; Qin and Wong, 2002). Polyethylene glycol (PEG) is also often used as a pore former in polymeric membranes and can undergo radical degradation induced by hydroxyl radicals, with formation of aldehydic chain ends (Fukatsu and Kokot, 2001).

22.5 Identification and monitoring of membrane degradation

Several analytical tools are being used to detect, assess and understand the membrane degradation mechanism and its impact. Most of these tools are destructive in nature and are adopted in bench scale studies to elucidate the fundamentals of membrane degradation or in post operation membrane examination. In addition, in full scale operation, detection of membrane intactness is periodically monitored by various tests. So this section includes two

© Woodhead Publishing Limited, 2011

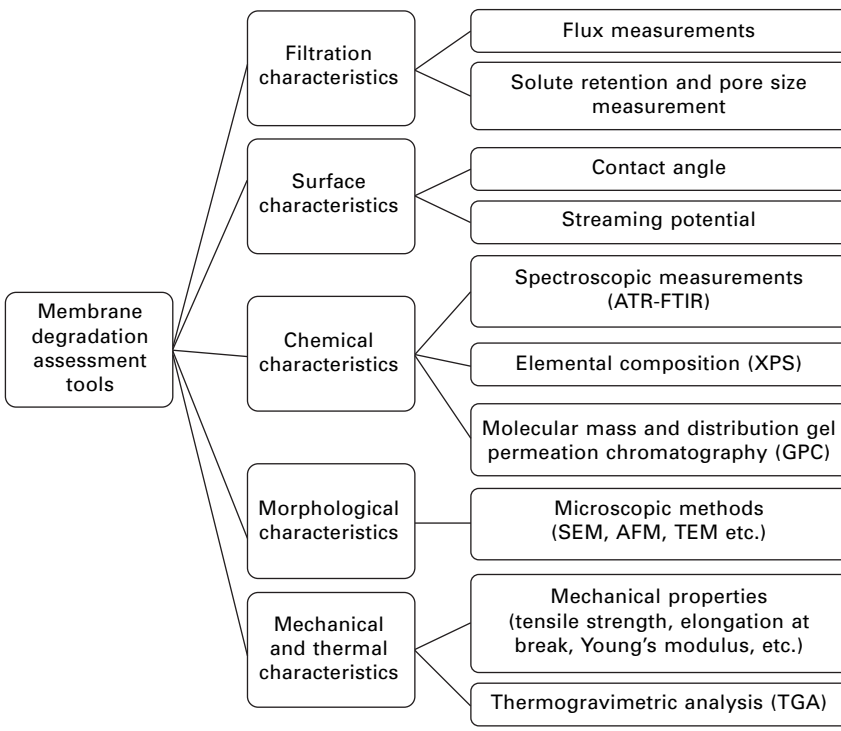
categories, analytical techniques performed to assess membrane degradation and tests adopted in operational plants to monitor the membrane integrity.

22.5.1 Membrane degradation assessment tools

Various analytical techniques adopted to assess and elucidate membrane degradation and its impact vary from use on the atomic scale to the macroscopic level. They also differ in their sensitivity, accuracy and reliability. These techniques can be classified into five major categories (Fig. 22.8) as tools to assess changes in filtration characteristics, surface characteristics, chemical/structural characteristics, mechanical and thermal characteristics and morphology.

Filtration characteristics

Filtration characteristics, permeability, membrane resistance and solute rejection are the fundamental, non-destructive and real time test methods for tracking changes in membrane properties after degradation. The principle of the membrane permeability method is defined by the capillary pore diffusion



22.8 Membrane degradation assessment tools.

© Woodhead Publishing Limited, 2011

model and the Hagan–Poiseuille equation, where the mean pore radius is calculated as a function of the water viscosity, membrane thickness, surface porosity, hydraulic permeability, water flux and the transmembrane pressure. Membrane permeability is a representation of intrinsic membrane hydraulic resistance and therefore commonly used as a direct measure of the extent of membrane flux restoration after cleaning. Membrane degradation is generally inferred when the flux restoration is greater than 100%. However hydraulic permeability is suspected to be relatively insensitive for predicting the small number of chain scission reactions compared to the change in membrane texture and mechanical properties (Causserand *et al.*, 2008). Membrane degradation is reflected in hydraulic permeability only when the deterioration reaches its final stage of gross integrity loss. Although hydraulic permeability is a decisive measurement of membrane filtration, it cannot be considered as a reliable tool for routine monitoring of membrane ageing or degradation.

Molecular weight cut off (MWCO) is a measure of pore size and can be correlated to the rejection of a spherical solute with a specific molecular weight. A change in rejection performance and pore size is usually measured by solute rejection tests using molecular weight markers (like PEG, dextran and polystyrene) of varying ranges (Arkhangelsky *et al.*, 2007b). Pore size measurement attributed to solute rejection is an approximate method that mainly considers the size exclusion aspect, compared to real membrane rejection which also involves charge interactions (Lee *et al.*, 2002). Testing solute changes depends on the membrane MWCO. For RO membranes, specific feed solutions or solutes like NaCl and glucose are used for rejection testing (Antony *et al.*, 2010; da Silva *et al.*, 2006; Gabelich *et al.*, 2005). In a membrane degradation study of PES membranes, using PEG markers resulted in a significant increase in the solute retention, tending to the conclusion that the hypochlorite exposure narrows the pore size and tightens the pore size distribution (Arkhangelsky *et al.*, 2007b). In reality, this observation is due to the increased affinity of phenyl sulfonate groups for PEG, resulting in PEG adsorption on the membrane surface and narrowing of the pore size. Direct pore size measurements based on bubble point and gas transport methods are a comparatively more precise way of measuring the pore size distribution changes caused by pore enlargements after membrane degradation.

Surface characteristics

Hydrophilicity and surface charge are key parameters that affect the fouling propensity of a membrane. A hydrophilic uncharged surface is considered to be resistant to fouling. Any chemical coming in contact with the membrane may alter the membrane surface by attaching or detaching some functional moieties, possibly bringing a change in the hydrophilicity and surface charge. Thus, contact angle and streaming potential can be considered as two important

© Woodhead Publishing Limited, 2011

measures to predict changes in the membrane fouling propensity. Moreover, these surface characteristics are related to surface roughness and membrane pore diameter. Membrane hydrophilicity is typically characterised by the contact angle obtained through the captive bubble contact angle or the sessile drop technique. The electrokinetic aspect of the membrane is measured by the streaming potential, which is used to characterise the membrane surface potential or zeta potential.

Given the fact that selective leaching of hydrophilizing polymeric additives is the ultimate change in the membrane, the membrane is expected to turn more hydrophobic. But chlorine-exposed membranes turned more hydrophilic, probably owing to formation of bigger pores and charged species by chain scission (Arkhangelsky *et al*., 2007b, Wang *et al*., 2010). Similarly, exposure of PES membrane to hypochlorite solution was shown to make it more negative owing to the formation of phenyl sulfonate after chain scission and subsequent increase in pore diameter (Arkhangelsky *et al*., 2007b). Contact angle and streaming potential measurements for chlorine-exposed PA membrane showed that chlorination made the membrane more hydrophilic and shifted it slightly to being more negative. This could be because the chlorine substitution generated dipole moments and/or gradual dissipation of surface coating layer that was applied to modify the membrane (Kwon and Leckie, 2006a).

Chemical/structural characteristics

Attenuated total reflectance – ATR - FTIR and XPS are two complementary techniques that are used by researchers to elucidate the chemical modification mechanism and degradation of membranes (Kwon and Leckie, 2006a, 2006b; Antony *et al*., 2010; Arkhangelsky *et al*., 2008, 2007b; Kang *et al*., 2007; Puspitasari *et al*., 2010; Rouaix *et al*., 2006). ATR - FTIR allows the detection of changes in the functional groups of the membrane by detecting bonds between atoms in a molecule and thus providing information about the functional groups and chemical structures of the membrane. XPS is a surface sensitive technique that measures elemental composition and provides information on chemical binding at the membrane surface, in the range 1–10 nm. XPS determines the surface composition of membrane samples and demonstrates their relative changes upon chemical treatment. XPS analysis of virgin and aged membrane allows the detection of chemical agent depositions on membrane surfaces and missing functional groups that are the result of chemical reaction between chemical agents and the membrane surface. ATR-FTIR is usually adopted as a qualitative measure of change in the chemical structure, whereas XPS is highly quantitative in nature.

The impact of chemical cleaning on the membrane is mostly directed through modification of the polymer backbone like chain breaking and

© Woodhead Publishing Limited, 2011

scission reactions. Chain scission resulting in a decrease of polymer chain length determined by gel permeation chromatography was demonstrated for PS and PVP (Rouaix *et al.*, 2006; Gaudichet-Maurin and Thominette, 2006; Wienk *et al.*, 1995). With an increase in the duration of hypochlorite exposure, the molar mass distribution decreased, showing that chain breaking forms low molar mass polymers.

Mechanical and thermomechanical characteristics

Membrane degradation caused by chemical exposure is generally observed to embrittle the macromolecules resulting in the loss of material ductility (Arkhangelsky *et al.*, 2008, 2007a, 2007b; Gaudichet-Maurin and Thominette, 2006; Rouaix *et al.*, 2006; Zondervan *et al.*, 2007). However Wang *et al.* (2010) reported the reverse; hypochlorite exposure of PVDF membranes resulted in a decline of tensile strength and Young's modulus, but ultimate elongation increased revealing that the membrane becomes more flexible. Gaudichet-Maurin and Thominette (2006) related the stress and yield stress patterns of macromolecules to the embrittlement mechanisms in polymer ageing. Physical ageing is expected to be characterized by an increase in the yield stress, whereas cross-linking is characterized by an increase in stress in the plastic zone and plasticization is characterzed by a decrease in yield stress.

Changes in the mechanical properties of the membranes were reported in terms of various parameters like ultimate tensile strength, elongation at break, yield stress and elasticity modulus. Ultimate tensile strength (the maximum resistance of the material to fracture is equivalent to the maximum load that can be carried by a specific unit area of the sample) is a commonly used macroscopic parameter used to detect microscopic changes in the membrane skin layer (Arkhangelsky *et al.*, 2007a). However, Rouaix *et al.* (2006) found that elongation at break is more sensitive than tensile strength. The estimated extent of damage would therefore be better understood by measuring more than one parameter.

Thermogravimetic analaysis (TGA) is used to detect the changes in the mass of the sample as a function of temperature and/or time. TGA is commonly used to determine the degradation temperatures of the polymer materials; however, its application in membrane degradation studies is limited. TGA was adopted to demonstrate thermal degradation of PES, when a small decrease in average molecular weight of the polymer was thought to be due to chain scission (Yadav *et al.*, 2009).

Morphological characteristics

Various microscopic methods like scanning electron microscopy (SEM), transmission electron microscopy (TEM), scanning probe microscopy (SPM),

© Woodhead Publishing Limited, 2011

and field emission scanning electron microscopy (FESEM) and atomic force microscopy (AFM) were used to help visualise the membrane surface in degradation studies (Arkhangelsky *et al.*, 2007a; Puspitasari *et al.*, 2010; Rouaix *et al.*, 2006; Kwon and Leckie, 2006a). Microscopic techniques produce very high-resolution images revealing detailed membrane characterisation in terms of membrane symmetry, diameter, thickness and pore size. SEM is often combined with an energy-dispersive X-ray spectroscopy (EDS) to provide detailed information on the morphological characteristics of chemical composition.

Among these techniques, AFM is widely employed as a powerful tool to study membrane surface morphology. AFM is one of the surface probe microscope techniques in which a precision tip interacts with the sample and the forces acting between them are measured. AFM produces micrograph images of the membrane surface and provides useful information about pore size distribution (MF/UF), surface roughness (NF/RO), surface forces, electrical properties and interactions between membrane and foulant (Wyart *et al.*, 2008; Hilal *et al.*, 2003; Arkhangelsky *et al.*, 2007b; Mitrouli *et al.*, 2010). Surface smoothness is an important factor affecting membrane fouling; a smooth surface is comparatively resistant to membrane fouling. More specifically, membrane roughness has been directly correlated to colloidal fouling of NF and RO membranes (Louie *et al.*, 2006; Vrijenhoek *et al.*, 2001; Mondal and Wickramasinghe, 2008). The chances of colloidal particles plugging the valleys of the relatively open structure is very high when the membrane surface is rough (Vrijenhoek *et al.*, 2001). The surface roughness of the membranes is generally reported in terms of peak-to-valley roughness, the average roughness and the root-mean-squared roughness. An increase in the severity of fouling with chemical exposure is expected to be due to the surface roughness of the membrane surface. But Kwon and Leckie (2006a) reported that no change in the surface roughness was seen for a chlorinated PA membrane, although chemical modification had been proved by other techniques.

In UF membranes, the surface roughness may also correlate with material characteristics such as the pore size distribution (Richard Bowen and Doneva, 2000). An increase in the surface roughness was reported for a PES UF membrane by Arkhangelsky *et al.* (2007b). The surface roughness, calculated as the peak-to-valley distance, which is the distance between the highest data point and the lowest data point, was found to be 14.5 nm for a fresh membrane and 9.8 nm for a chlorine-treated membrane. As a qualitative measure, the size of the sink (lowest 'valley' in the image) was related to the membrane pore size. Also, AFM images show that the chlorine-damaged surface possesses larger sinks, suggesting a larger pore size. Therefore AFM is a valuable supportive tool that provides an insight into the surface roughness and porosity of the membrane.

© Woodhead Publishing Limited, 2011

22.5.2 Membrane integrity monitoring tests

Membrane integrity is defined as the quality or state of the complete membrane in perfect condition. Generally, membrane integrity testing methodology is adopted to track incremental changes in membrane damage to allow for scheduled (or preventative) maintenance rather than the emergency (or reactionary) maintenance. Depending on the system design and mode of filtration, integrity tests provide a measure of system efficiency. The importance of membrane integrity monitoring was first raised in the pharmaceutical industry well before the extensive use of membranes in the water treatment industry. In pharmaceutical applications, a membrane could only be certified for sterilizing grade applications by demonstrating a log reduction value (LRV) of 7 by bacterial challenge tests (PDA, 1998). Membrane integrity tests are classified as either direct or indirect tests based on the form of the measurement. The detailed methodology for performing most these tests has been described in membrane filtration guidance manuals and ASTM standards (USEPA, 2005; ASTM, 2006, 2008). These techniques have been discussed in detail and reviewed by researchers (Antony *et al.*, in press; Crozes *et al.*, 2002; Sethi *et al.*, 2004; Guo *et al.*, 2010).

Direct tests measure a change in the integrity of the membranes themselves. Direct monitoring methods are performed on the membrane when it is off-line and the result is a direct measure of the extent of the breach in the membrane/module. A pressure decay test, diffusive air flow test, water displacement test and vacuum decay test are commonly employed direct integrity tests for various membrane operations.

Indirect tests measure the permeate quality and correlate this with the extent of loss of membrane integrity. Turbidity monitoring, particle counting and monitoring and surrogate measures (on-line or periodic measurement of water quality parameters like electrical conductivity, total organic carbon, colour, sulfate, UV absorbance at 254 nm and specific ion concentration) are used in practice as indirect integrity testing methods.

22.6 Materials degradation control strategies

The development of membranes resistant to chemical environment, particularly chlorine, is the most effective way of tackling membrane degradation. Some recent reviews elaborate the efforts made to develop new polymeric membranes and novel hydrophilic, fouling resistant, anti microbial, thermally stable and chlorine resistant membrane surfaces (Mansouri *et al.*, 2010; Li and Wang, 2010; Geise *et al.*, 2010).

The high cost involved in the dechlorination–rechlorination exercise created a quest for a chlorine-tolerant membrane and great efforts are being made for some time to develop a chlorine-resistant polymeric material. Based on

© Woodhead Publishing Limited, 2011

the ring chlorination mechanism, chlorine resistance is largely decided by the chemical structure of the monomer used. Some of the potential strategies considered for PA membranes are (Konagaya and Watanabe, 2000, Soice *et al.*, 2003, Glater *et al.*, 1994, Kawaguchi and Tamura, 1984, Yu *et al.*, 2009):

- Replacing the chlorine sensitive amide hydrogen with other moieties like methyl or phenyl groups
- Substituting the aromatic ring bonded to the amide nitrogen by aliphatic chain or cyclics
- Use of aliphatic or cycloaliphatic diamines with a secondary amino group or a short methylene chain length between end amino groups in the place of aromatic diamines
- Preventing the Orton rearrangement taking place by protecting the possible chlorination sites. As the N-H group is an *ortho*, *para* - directing group, attaching pendant groups at these positions can prevent chlorine attack.

Recently, Woongjin Chemical reported the development of a chlorine-resistant RO membrane (CRM), with higher resistance to chlorine than other RO membranes currently available in the market (CSM, 2007). In this novel membrane, surface modification is performed during the membrane manufacture itself, by elimination or modification of chlorine-sensitive sites, amide hydrogen and the aromatic ring bonded to the amide nitrogen. The CRM membrane module was tested comparatively with a regular polyamide TFC RO membrane operating under identical conditions and a chlorine exposure of 5 g h^{-1}. For the regular RO membrane, salt rejection significantly decreased at 0.5 g h l^{-1} itself, whereas CRM rejection maintained nearly 90% up to 2 g h l^{-1}. More precisely, the chlorine resistance of the CRM membrane was five times higher than the regular RO membrane (Brown and Quan, 2011).

Finding alternate materials for RO applications by avoiding the chlorine-sensitive amide linkages is a new platform in membrane applications that has received considerable attention in recent times. Polysulfones have been recognized as providing a suitable backbone with chlorine resistance, provided that water permeability and the hydrophilic ionic groups can be successfully incorporated (Noshay and Robeson, 1976). Highly chlorine-tolerant TFC has been prepared from sulfonated polysulfone materials, evaluated for water applications and demonstrated to be resistant to fouling (Park *et al.*, 2008; McGrath *et al.*, 2007). Likewise, cleaning protocols and operating conditions should be optimized before running them in a full scale operation. Performing a membrane autopsy at the end of pilot trials will provide valuable information on pretreatment effectiveness, fouling events, the cleaning efficiency of the implemented protocol and the chances of membrane degradation.

© Woodhead Publishing Limited, 2011

22.7 Future trends

A key limitation of membrane treatment systems is membrane degradation caused by chemical exposure. This challenge is being confronted by developing robust membrane materials. Extensive research performed in this field will be industrious when these materials are demonstrated to be a suitable end product for full scale operation.

In membrane degradation studies, the chlorine concentration is regularly reported as a product of two principle variables, concentration and time, g h l^{-1}. For example, reaching a chlorine exposure concentration of 10 g h l^{-1} in two ways (i) 0.1 g for 100 h and (ii) 10 g for 1 h is assumed to be same, however the free chlorine concentration is expected to have a more destructive effect compared to the contact time. Therefore, the present convention used for expressing chlorine exposure could be misleading (Adams, 1990). Detailed research is needed to address this and identify an appropriate way of denoting chlorine exposure concentration.

Most membrane ageing and degradation studies have been performed in the chlorine environment. A comprehensive study is required to address the impact of various cleaning chemicals at their operating conditions and to confirm their practical compatibility. Similarly, research input is needed to develop/identify reliable, *in situ* tools which will engage non-destructive analysis of the initial stages of membrane deterioration on a routine basis.

Currently, there are no protocols available to assess integrity loss during long-term use. Apart from integrity monitoring on a regular basis, both directly and indirectly as recommended in the USEPA *Membrane Filtration Guidance Manual*, a protocol to determine membrane breach caused by ageing over the long-term operation of the module is required and is especially vital in the drinking water production sector. Similarly, limited information is available on the effect of membrane ageing on the performance efficiency of various target contaminants. In a full scale operation, systematic study from the operating history of the decline in membrane performance as a function of time would be a great help in correlating the degradation mechanisms elucidated from bench scale studies.

22.8 Sources of further information and advice

Further information and details on this topic can be had from following sources:

1. L. Zeman and A. Zydney, *Microfiltration and Ultrafiltration: principles and applications*, Marcel Dekker, 1996.
2. J. Zabicky, *The Chemistry of Amides*, Interscience, 1970.
3. USEPA 2001. *Low Pressure Membrane Filtration for pathogen removal – Application, Implementation and Regulatory Issues*. United States

© Woodhead Publishing Limited, 2011

Environmental Protection Agency, Offfice of Water. *EPA 815-C-01-001*.
4. USEPA 2005, *Membrane Filtration Guidance Manual*, United States Environmental Protection Agency, Office of Water. *EPA.815-R-09-009*.
5 Khulbe, C. Feng and T. Matsuura, *Synthetic Polymeric Membranes: Characterization by Atomic Force Microscopy*, Springer, 2008.

22.9 Acknowledgements

The authors would like to thank Federico Pacheco, Stanford University, CA for providing the TEM image of RO membrane. The authors also thank Dianne Quan, Vitachem and Steve Brown, CSM, Woongjin Chemical Co Ltd for the details of CRM RO membranes.

22.10 References

Adams, W. R. (1990). 'The effects of chlorine dioxide on reverse osmosis membranes'. *Desalination*, **78**, 439–53.

Al-Amoudi, A. and Lovitt, R. W. (2007). 'Fouling strategies and the cleaning system of NF membranes and factors affecting cleaning efficiency'. *Journal of Membrane Science*, **303**, 6–28.

Al-Qahtany, H. I. and Al-Bastaki, N. M. S. (1995). 'Effect of aging on the performance of RO hollow fiber membranes in a section of an RO plant'. *Desalination*, **101**, 177–83.

Anderson, C. C., Rodriguez, F. and Thurston, D. A. (1979). 'Crosslinking aqueous poly(vinyl pyrrolidone) solutions by persulfate'. *Journal of Applied Polymer Science*, **23**, 2453–62.

Antony, A., Blackbeard, J. and Leslie, G. 'Removal efficiency and integrity monitoring techniques for virus removal by membrane processes'. *Critical Reviews in Environmental Science and Technology*, in press.

Antony, A., Fudianto, R., Cox, S. and Leslie, G. (2010). 'Assessing the oxidative degradation of polyamide reverse osmosis membrane–Accelerated ageing with hypochlorite exposure'. *Journal of Membrane Science*, **347**, 159–64.

Arkhangelsky, E., Kuzmenko, D., Gitis, N. V., Vinogradov, M., Kuiry, S. and Gitis, V. (2007a). 'Hypochlorite cleaning causes degradation of polymer membranes'. *Tribology Letters*, **28**, 109–16.

Arkhangelsky, E., Kuzmenko, D. and Gitis, V. (2007b). 'Impact of chemical cleaning on properties and functioning of polyethersulfone membranes'. *Journal of Membrane Science*, **305**, 176–84.

Arkhangelsky, E., Goren, U. and Gitis, V. (2008). 'Retention of organic matter by cellulose acetate membranes cleaned with hypochlorite'. *Desalination*, **223**, 97–105.

ASTM (2006). *Standard Practice for Integrity Testing of Water Filtration Membrane Systems* (D 6908–06).

ASTM (2008). *Standard Practices for Detecting Leaks in Reverse Osmosis and Nanofiltration Devices* (D3923–08).

© Woodhead Publishing Limited, 2011

Avlonitis, S., Hanbury, W. T. and Hodgkiess, T. (1992). 'Chlorine degradation of aromatic polyamides' *Desalination*, **85**, 321–34.

Benavente, J. and Vázquez, M. I. (2004). 'Effect of age and chemical treatments on characteristic parameters for active and porous sublayers of polymeric composite membranes'. *Journal of Colloid and Interface Science*, **273**, 547–55.

Benavente, J., Vázquez, M. I. and De Lara, R. (2006). 'Modification of active and porous sublayers of aged polyamide/polysulfone composite membranes due to HNO_3 treatment: Effect of treatment time'. *Journal of Colloid and Interface Science*, **297**, 226–34.

Brown, S. and Quan, D. (2011). *CSM, Chlorine resistant polyamide RO membrane*, personal communication.

Causserand, C., Rouaix, S., Lafaille, J.-P. and Aimar, P. (2008). 'Ageing of polysulfone membranes in contact with bleach solution: Role of radical oxidation and of some dissolved metal ions'. *Chemical Engineering and Processing: Process Intensification*, **47**, 48–56.

Challis, B.C. and Challis, J.A. (1970). *The Chemistry of Amides*, Wiley Interscience, New York.

Chen, J. P., Kim, S. L. and Ting, Y. P. (2003). 'Optimization of membrane physical and chemical cleaning by a statistically designed approach'. *Journal of Membrane Science*, **219**, 27–45.

Childress, A. E., Le-Clech, P., Daugherty, J. L., Chen, C. and Leslie, G. L. (2005). 'Mechanical analysis of hollow fiber membrane integrity in water reuse applications'. *Desalination*, **180**, 5–14.

Crittenden, J. and Harza, M. W. (2005). *Water treatment: Principles and Design*, John Wiley, Hoboken, NJ.

Crozes, G. F., Sethi, S., Mi, B., Curl, J. and Mariñas, B. (2002). 'Improving membrane integrity monitoring indirect methods to reduce plant downtime and increase microbial removal credit'. *Desalination*, **149**, 493–7.

CSM (2007). *Development of CSM CRM (chlorine resistant membrane)*, Woongijn Chemical Co Ltd [Online]. Available: http://www.csmfilter.com/csm/01com/Company_News_view.asp?num=299&pno=1&search_word=&search_jokun= [Accessed 12 December 2010].

Da Silva, M. K., Tessaro, I. C. and Wada, K. (2006). 'Investigation of oxidative degradation of polyamide reverse osmosis membranes by monochloramine solutions'. *Journal of Membrane Science*, **282**, 375–82.

Film Tec (1995). *FilmTec Membranes Technical Manual.*

Fukatsu, K. and Kokot, S. (2001). 'Degradation of poly(ethylene oxide) by electro-generated active species in aqueous halide medium'. *Polymer Degradation and Stability*, **72**, 353–9.

Gabelich, C. J., Frankin, J. C., Gerringer, F. W., Ishida, K. P. and Suffet, I. H. (2005). 'Enhanced oxidation of polyamide membranes using monochloramine and ferrous iron'. *Journal of Membrane Science*, **258**, 64–70.

Gaudichet-Maurin, E. and Thominette, F. (2006). 'Ageing of polysulfone ultrafiltration membranes in contact with bleach solutions'. *Journal of Membrane Science*, **282**, 198–204.

Geise, G. M., Lee, H.-S., Miller, D. J., Freeman, B. D., McGrath, J. E. and Paul, D. R. (2010). 'Water purification by membranes: The role of polymer science'. *Journal of Polymer Science Part B: Polymer Physics*, **48**, 1685–718.

Gijsbertsen-Abrahamse, A. J., Cornelissen, E. R. and Hofman, J. A. M. H. (2006). 'Fiber failure frequency and causes of hollow fiber integrity loss'. *Desalination*, **194**, 251–58.

© Woodhead Publishing Limited, 2011

Gitis, V., Haught, R. C., Clark, R. M., Gun, J. and Lev, O. (2006). 'Application of nanoscale probes for the evaluation of the integrity of ultrafiltration membranes'. *Journal of Membrane Science*, **276**, 185–92.

Glater, J., Hong, S.-K. and Elimelech, M. (1994). 'The search for a chlorine-resistant reverse osmosis membrane'. *Desalination*, **95**, 325–45.

Guo, H., Wyart, Y., Perot, J., Nauleau, F. and Moulin, P. (2010). 'Low-pressure membrane integrity tests for drinking water treatment: A review'. *Water Research*, **44**, 41–57.

Hilal, N., Mohammad, A. W., Atkin, B. and Darwish, N. A. (2003). 'Using atomic force microscopy towards improvement in nanofiltration membranes properties for desalination pre-treatment: A review'. *Desalination*, **157**, 137–44.

Hong, S. and Elimelech, M. (1997). 'Chemical and physical aspects of natural organic matter (NOM) fouling of nanofiltration membranes'. *Journal of Membrane Science*, **132**, 159–81.

Huisman, I. H. and Williams, K. (2004). 'Autopsy and failure analysis of ultrafiltration membranes from a waste-water treatment system'. *Desalination*, **165**, 161–4.

Idris, A., Mat Zain, N. and Noordin, M. Y. (2007). 'Synthesis, characterization and performance of asymmetric polyethersulfone (PES) ultrafiltration membranes with polyethylene glycol of different molecular weights as additives'. *Desalination*, **207**, 324–39.

Jacangelo, J. G., Laine, J.-M., Carns, K. E., Cummings, E. W. and Mallevialle, J. (1991). 'Low-pressure membrane filtration for removing *Giardia* and microbial indicators'. *Journal of Americal Water Works Association*, **83**, 97–106.

Johnson, W. and MacCormick, T. (2003). 'Issues of operational integrity in membrane drinking water plants'. *Water Science and Technology: Water Supply*, **3**, 73–80.

Kang, G.-D., Gao, C.-J., Chen, W.-D., Jie, X.-M., Cao, Y.-M. and Yuan, Q. (2007). 'Study on hypochlorite degradation of aromatic polyamide reverse osmosis membrane'. *Journal of Membrane Science*, **300**, 165–71.

Kawaguchi, T. and Tamura, H. (1984). 'Chlorine-resistant membrane for reverse osmosis. I. Correlation between chemical structures and chlorine resistance of polyamides'. *Journal of Applied Polymer Science*, **29**, 3359–67.

Kennedy, M. D., Kamanyi, J., Rodriguez, S. G. S., Lee, N. H., Schippers, J. C. and Amy, G. (2008). 'Water treatment by microfiltration and ultrafiltration'. In: *Advanced Membrane Technology and Applications*. Li, N. N., Fane, A. G., Ho, W. S. W. and Matsuura, T. (eds.), John Wiley and Sons, New Jersey.

Kice, J. L. and Puls, A. R. (1977). 'The reaction of hypochlorite with various oxidized derivatives of disulfides and with sulfinate ions'. *Journal of the American Chemical Society*, **99**, 3455–60.

Konagaya, S. and Watanabe, O. (2000). 'Influence of chemical structure of isophthaloyl dichloride and aliphatic, cycloaliphatic, and aromatic diamine compound polyamides on their chlorine resistance'. *Journal of Applied Polymer Science*, **76**, 201–7.

Kubota, N., Hasimoto, T. and Mori, Y. (2008). 'Microfiltration and ultrafiltration'. In: *Advanced Membrane Technology and Applications*. Li, N. N., Fane, A. G., Ho, W. S. W. and Matsuura, T. (eds.), John Wiley and Sons, New Jersey.

Kwon, Y.-N. and Leckie, J. O. (2006a). 'Hypochlorite degradation of crosslinked polyamide membranes: I. Changes in chemical/morphological properties'. *Journal of Membrane Science*, **283**, 21–6.

Kwon, Y.-N. and Leckie, J. O. (2006b). 'Hypochlorite degradation of crosslinked polyamide membranes: II. Changes in hydrogen bonding behavior and performance'. *Journal of Membrane Science*, **282**, 456–64.

© Woodhead Publishing Limited, 2011

Lake, R., Oxtoby, S., Burke, T., Leparc, J. and Mysore, C. (2003). 'An absolute barrier to *Cryptosporidium* – A British approach. In *Proceedings of the AWWA Membrane Technology Conference*, Atlanta, GA.

Le-Clech, P., Chen, V. and Fane, T. A. G. (2006). 'Fouling in membrane bioreactors used in wastewater treatment'. *Journal of Membrane Science*, **284**, 17–53.

Lee, S., Park, G., Amy, G., Hong, S.-K., Moon, S.-H., Lee, D.-H. and Cho, J. (2002,. 'Determination of membrane pore size distribution using the fractional rejection of nonionic and charged macromolecules'. *Journal of Membrane Science*, **201**, 191–201.

Li, D. and Wang, H. (2010). 'Recent developments in reverse osmosis desalination membranes'. *Journal of Materials Chemistry*, **20**, 4551–66.

Light, W. G., Chu, H. C. and Tran, C. N. (1987). 'Reverse osmosis TFC magnum elements for chlorinated/dechlorinated feedwater processing'. *Desalination*, **64**, 411–21.

Lin, C.-F., Liu, S.-H. and Hao, O. J. (2001). 'Effect of functional groups of humic substances on uf performance'. *Water Research*, **35**, 2395–402.

Liu, C., Caothien, S., Hayes, J., Caothuy, T., Otoyo, T. and Ogawa, T. (2001). 'Membrane chemical cleaning: from art to science. In: *Proceedings of AWWA Membrane Technology Conference*, 2001, San Antonio, TX.

Louie, J. S., Pinnau, I., Ciobanu, I., Ishida, K. P., Ng, A. and Reinhard, M. (2006). 'Effects of polyether-polyamide block copolymer coating on performance and fouling of reverse osmosis membranes'. *Journal of Membrane Science*, **280**, 762–70.

Madaeni, S. S. and Mansourpanah, Y. (2004). 'Chemical cleaning of reverse osmosis membranes fouled by whey'. *Desalination*, **161**, 13–24.

Mansouri, J., Harrisson, S. and Chen, V. (2010). 'Strategies for controlling biofouling in membrane filtration systems: challenges and opportunities'. *Journal of Materials Chemistry*, **20**, 4567–86.

March, J. (1992). *Advanced Organic Chemistry: Reactions, Mechanisms and Structures*, John Wiley, New York.

McGrath, J. E., Park, H. B. and Freeman, B. D. (2007). *Chlorine Resistant Desalination Membranes Based on Directly Sulfonated Poly(arylene ether sulfone) Copolymers*. WO Patent 2007/084759.

Mitrouli, S. T., Karabelas, A. J. and Isaias, N. P. (2010). 'Polyamide active layers of low pressure RO membranes: Data on spatial performance non-uniformity and degradation by hypochlorite solutions'. *Desalination*, **260**, 91–100.

Möckel, D., Staude, E. and Guiver, M. D. (1999). 'Static protein adsorption, ultrafiltration behavior and cleanability of hydrophilized polysulfone membranes'. *Journal of Membrane Science*, **158**, 63–75.

Mondal, S. and Wickramasinghe, S. R. (2008). 'Produced water treatment by nanofiltration and reverse osmosis membranes'. *Journal of Membrane Science*, **322**, 162–70.

Noshay, A. and Robeson, L. M. (1976). 'Sulfonated polysulfone'. *Journal of Applied Polymer Science*, **20**, 1885–903.

Ochoa, N. A., Prádanos, P., Palacio, L., Pagliero, C., Marchese, J. and Hernández, A. (2001). 'Pore size distributions based on AFM imaging and retention of multidisperse polymer solutes: Characterisation of polyethersulfone UF membranes with dopes containing different PVP'. *Journal of Membrane Science*, **187**, 227–37.

Park, H. B., Freeman, B. D., Zhang, Z.-B., Sankir, M. and McGrath, J. E. (2008). 'Highly chlorine-tolerant polymers for desalination'. *Angewandte Chemie International Edition*, **47**, 6019–24.

PDA (1998). Parenternal Drug Association, 'Sterilising filtration of liquids (Technical Report No. 26)'. *Journal Pharmaceutical Science Technology*, *Supplement*, **52**.

© Woodhead Publishing Limited, 2011

Pearce, G. (2007a). 'Introduction to membranes: Membrane selection'. *Filtration and Separation*, **44**, 35–7.

Pearce, G. (2007b). 'Water and wastewater filtration: Membrane module format'. *Filtration and Separation*, **44**, 31–3.

Petersen, R. J. (1993). 'Composite reverse osmosis and nanofiltration membranes'. *Journal of Membrane Science*, **83**, 81–150.

Porcelli, N. and Judd, S. (2010). 'Chemical cleaning of potable water membranes: A review'. *Separation and Purification Technology*, **71**, 137–43.

Puspitasari, V., Granville, A., Le-Clech, P. and Chen, V. (2010). 'Optimum cleaning and ageing effect of sodium hypochlorite on polyvinylidene fluoride (PVDF) membrane'. *Separation and Purification Technology*, **72**, 301–8.

Qin, J.-J. and Wong, F.-S. (2002). 'Hypochlorite treatment of hydrophilic hollow fiber ultrafiltration membranes for high fluxes'. *Desalination*, **146**, 307–9.

Qin, J.-J., Li, Y., Lee, L.-S. and Lee, H. (2003a). 'Cellulose acetate hollow fiber ultrafiltration membranes made from CA/PVP 360 K/NMP/water'. *Journal of Membrane Science*, **218**, 173–83.

Qin, J.-J., Wong, F.-S., Li, Y. and Liu, Y.-T. (2003b). 'A high flux ultrafiltration membrane spun from PSU/PVP (K90)/DMF/1,2-propanediol'. *Journal of Membrane Science*, **211**, 139–47.

Qin, J.-J., Oo, M. H. and Li, Y. (2005). 'Development of high flux polyethersulfone hollow fiber ultrafiltration membranes from a low critical solution temperature dope via hypochlorite treatment'. *Journal of Membrane Science*, **247**, 137–42.

Richard Bowen, W. and Doneva, T. A. (2000). 'Atomic force microscopy characterization of ultrafiltration membranes: correspondence between surface pore dimensions and molecular weight cut-off'. *Surface and Interface Analysis*, **29**, 544–7.

Rouaix, S., Causserand, C. and Aimar, P. (2006). 'Experimental study of the effects of hypochlorite on polysulfone membrane properties'. *Journal of Membrane Science*, **277**, 137–47.

Sethi, S., Crozes, G., Hugaboom, D., Mi, B. and Curl, J. M. (2004). *Assessment and Development of Low-pressure Membrane Integrity Monitoring Tools*, American Water Works Association.

Shemer, H. and Semiat, R. (2011). 'Impact of halogen based disinfectants in seawater on polyamide RO membranes'. *Desalination*, **273**, 179–83.

Soice, N. P., Maladono, A. C., Takigawa, D. Y., Norman, A. D., Krantz, W. B. and Greenberg, A. R. (2003). 'Oxidative degradation of polyamide reverse osmosis membranes: Studies of molecular model compounds and selected membranes'. *Journal of Applied Polymer Science*, **90**, 1173–84.

Soice, N. P., Greenberg, A. R., Krantz, W. B. and Norman, A. D. (2004). 'Studies of oxidative degradation in polyamide RO membrane barrier layers using pendant drop mechanical analysis'. *Journal of Membrane Science*, **243**, 345–55.

Solomons, T. and Fryhle, C. (2008). *Organic Chemistry*, 9th edn, Wiley, Hoboken, NJ.

Tessaro, I. C., Da Silva, J. B. A. and Wada, K. (2005). 'Investigation of some aspects related to the degradation of polyamide membranes: aqueous chlorine oxidation catalyzed by aluminum and sodium laurel sulfate oxidation during cleaning'. *Desalination*, **181**, 275–82.

Thominette, F., Farnault, O., Gaudichet-Maurin, E., Machinal, C. and Schrotter, J.-C. (2006). 'Ageing of polyethersulfone ultrafiltration membranes in hypochlorite treatment'. *Desalination*, **200**, 7–8.

© Woodhead Publishing Limited, 2011

USEPA (2005). *Membrane Filtration Guidance Manual. EPA.815-R-09-009.*

Van Der Bruggen, B. (2009). 'Chemical modification of polyethersulfone nanofiltration membranes: A review'. *Journal of Applied Polymer Science*, **114**, 630–42.

Vrijenhoek, E. M., Hong, S. and Elimelech, M. (2001). 'Influence of membrane surface properties on initial rate of colloidal fouling of reverse osmosis and nanofiltration membranes'. *Journal of Membrane Science*, **188**, 115–28.

Wang, P., Wang, Z., Wu, Z., Zhou, Q. and Yang, D. (2010). 'Effect of hypochlorite cleaning on the physiochemical characteristics of polyvinylidene fluoride membranes'. *Chemical Engineering Journal*, **162**, 1050–6.

Watters, J. C., Klein, E., Fleischman, M., Roberts, J. S. and Hall, B. (1986). 'Rejection spectra of reverse osmosis membranes degraded by hydrolysis or chlorine attack'. *Desalination*, **60**, 93–110.

Wienk, I. M., Meuleman, E. E. B., Borneman, Z., Boomgaard, T. V. D. and Smolders, C. A. (1995). 'Chemical treatment of membranes of a polymer blend: Mechanism of the reaction of hypochlorite with poly(vinyl pyrrolidone)'. *Journal of Polymer Science Part A: Polymer Chemistry*, **33**, 49–54.

Wyart, Y., Georges, G., Deumié, C., Amra, C. and Moulin, P. (2008). 'Membrane characterization by microscopic methods: Multiscale structure'. *Journal of Membrane Science*, **315**, 82–92.

Xu, J., Ruan, G., Zou, L. and Gao, C. (2010). 'Effect of chlorine and acid injection on hollow fiber RO for SWRO'. *Desalination*, **262**, 115–20.

Yadav, K. and Morison, K. R. (2010). 'Effects of hypochlorite exposure on flux through polyethersulphone ultrafiltration membranes'. *Food and Bioproducts Processing*, **88**, 419–24.

Yadav, K., Morison, K. and Staiger, M. P. (2009). 'Effects of hypochlorite treatment on the surface morphology and mechanical properties of polyethersulfone ultrafiltration membranes'. *Polymer Degradation and Stability*, **94**, 1955–61.

Yu, S., Liu, M., Lü, Z., Zhou, Y. and Gao, C. (2009). 'Aromatic-cycloaliphatic polyamide thin-film composite membrane with improved chlorine resistance prepared from m-phenylenediamine-4-methyl and cyclohexane-1,3,5-tricarbonyl chloride'. *Journal of Membrane Science*, **344**, 155–64.

Zondervan, E. and Roffel, B. (2007). 'Evaluation of different cleaning agents used for cleaning ultra filtration membranes fouled by surface water'. *Journal of Membrane Science*, **304**, 40–9.

Zondervan, E., Zwijnenburg, A. and Roffel, B. (2007). 'Statistical analysis of data from accelerated ageing tests of PES UF membranes'. *Journal of Membrane Science*, **300**, 111–16.

© Woodhead Publishing Limited, 2011

23

Membranes for photocatalysis in water and wastewater treatment

V. LODDO and L. PALMISANO, Università di Palermo, Italy and T. MARINO and R. MOLINARI, Università della Calabria, Italy

Abstract: The chapter reports the basic principles of heterogeneous photocatalysis together with a brief presentation of the types of membranes and membrane operations most widely used in this type of application. Coupling the two technologies with the aim of obtaining synergistic effects for conversion in liquid–solid systems is discussed and the relevant papers together with some case studies in pollutants abatement and reaction of synthesis are highlighted.

Key words: heterogeneous photocatalysis, membranes, pollutant abatement, synthesis reactions.

23.1 Introduction

Heterogeneous photocatalysis is a promising technique both for the abatement of organic and inorganic pollutants (Schiavello, 1995; Hoffmann *et al.*, 1995; Fujishima *et al.*, 1999) and for syntheses (Palmisano *et al.*, 2007a, 2007b; Yurdakal *et al.*, 2008, 2009). This method is based on the particular properties of semiconductor materials that can give rise to redox reactions when they are irradiated with light of suitable energy. Photocatalytic oxidation has recently been the subject of numerous investigations aiming to reduce the amounts of organic pollutants in wastewater.

A semiconductor catalyst is generally used as powder suspended in a liquid medium. The inconvenient aspect of this approach on the large scale is the catalyst-recovering step from the solution at the end of operation. Solid–liquid separation is an extremely important issue for the development of photocatalytic technology; indeed, the best possible recovery of particles must be ensured in order to prevent their wash out and consequently a decrease in their amount in the reactor system.

A promising approach for overcoming these problems is the combined application of photocatalysis and membrane processes. Photocatalytic membrane reactors (PMRs) are useful for catalyst separation and for the control of photooxidation products and/or by-products. The membrane may also ensure continuous operation in systems where the reaction of interest

© Woodhead Publishing Limited, 2011

and the separation of product(s) can occur in a single step. The membrane process can be carried out without chemical additives and has low energy requirements.

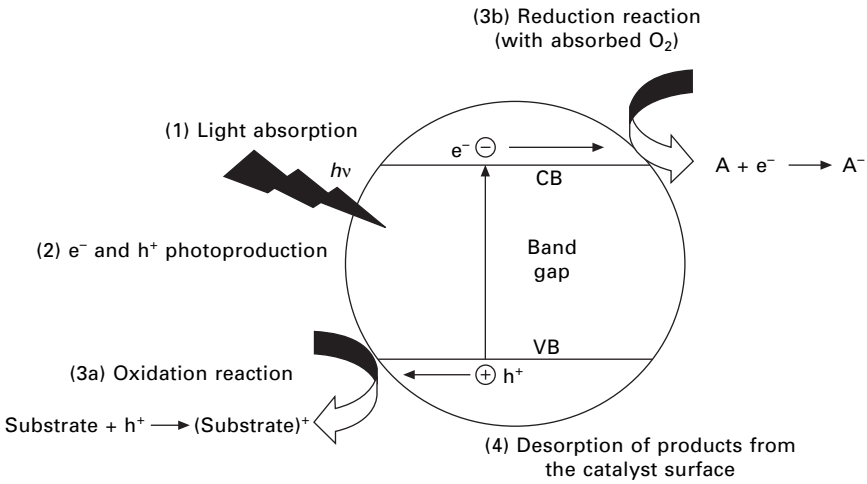
Different systems combining photocatalysis with pressure-driven membrane techniques, such as nanofiltration (NF) and ultrafiltration (UF) for the degradation of organic pollutants are described in the pertinent literature (Molinari *et al.*, 2000, 2002a, 2002b; Sopajaree *et al.*, 1999a, 1999b). One of the main drawbacks of these systems is membrane fouling. Coupling photocatalysis with membrane distillation (MD) could avoid this problem and an almost complete retention of total organic carbon (TOC) content is reported (Mozia *et al.*, 2005, 2007, Mozia and Morawski, 2006). Self-cleaning properties can be generated on a membrane by coating its surface with TiO_2 particles (Madaeni and Ghaemi, 2007, Kim *et al.*, 2003). Dialysis membranes were successfully coupled to a photoreactor in order to mineralize organic compounds contained in artificial turbid waters (Azrague *et al.*, 2007). Recently, it has been demonstrated that integration of heterogeneous photocatalysis with the pervaporation operation is a very promising method of improving the detoxification efficiency of water streams containing organic pollutants at low concentrations (Camera-Roda and Santarelli, 2007).

In order to understand the working principles of the photocatalytic processes satisfactorily, this chapter introduces some properties and definitions of semiconductors related mainly to TiO_2 together with the essentials of their thermodynamics and kinetics. Moreover, classification of the membranes based both on the materials used to produce them and on their morphological, structural and surface characteristics is also presented. Finally some case studies describing the coupling of the two processes with the advantages, drawbacks and future trends are highlighted.

23.2 Basic principles of heterogeneous photocatalysis

Irradiation of a semiconductor with light of energy equal or higher than its band-gap energy (E_g) gives rise to promotion of electrons (e^-) from the valence band (VB) to the conduction band (CB), leaving positive holes (h^+) in the valence band. The photogenerated electron–hole pairs can undergo different fates. They can: (i) recombine and dissipate their energy as heat, or (ii) get trapped in metastable surface states, or (iii) induce redox reactions with electron donor and electron acceptor species adsorbed on the semiconductor surface or located within the electrical double layer surrounding the charged particles. The space charge region allows separation of the photo-produced pairs; consequently the probability of their recombination decreases, while their availability for redox reactions increases. Figure 23.1 shows a scheme of the photoactivation of a semiconductor particle.

© Woodhead Publishing Limited, 2011



23.1 Scheme of the photocatalytic process occurring on an illuminated particle in contact with a redox system. The oxidizing agent A is O_2 and the reducing one is an organic substrate.

The reaction involving the species adsorbed onto the catalyst surface could occur only if the potential of the redox pair to which the species belongs (E^0_{redox}) is compatible with both the valence band and conduction band potentials, E_{VB} and E_{CB}, respectively. The redox potential, E^0_{redox}, should be less positive than E_{VB} (h^+, photo produced holes, can oxidize the reduced species of the pair), E^0_{redox} should be more positive than E_{CB} (e^-, the photo produced electron, is able to reduce the oxidized species of the pair).

Figure 23.2 shows the relative positions of the bands in different situations. The photocatalytic properties of a semiconductor depend on the position of the energetic levels, on the mobility and mean lifetime of the photogenerated electrons and holes, on the light absorption coefficient and on the nature of the interface. Moreover the photoactivity depends on the methods of preparation of the powders which allows many physicochemical properties of the semiconductor to be varied, like the crystalline structure, the surface area and the distribution of particle sizes.

The following scheme shows the events which can occur at the semiconductor–water interface when TiO_2 is used as the photocatalyst:

$$TiO + h\nu \rightarrow TiO_2(e^-_{(CB)} + h^+_{(VB)}) \quad [23.1]$$

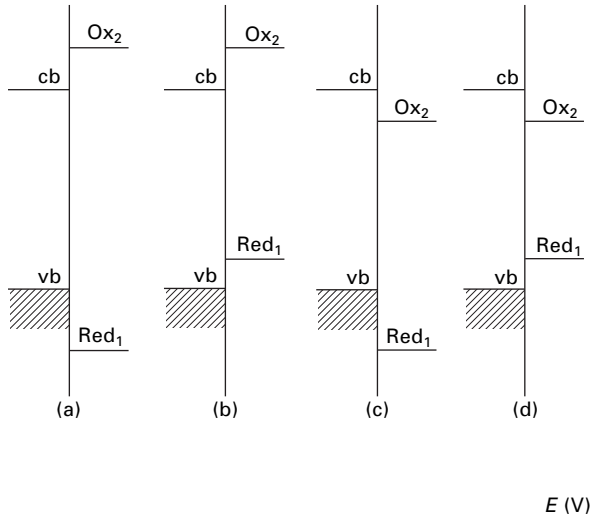
$$OH^- + h^+_{(VB)} \rightarrow {}^\bullet OH \quad [23.2]$$

$$O_2 + e^-_{(CB)} \rightarrow {}^\bullet O_2^- \quad [23.3]$$

$${}^\bullet O_2^- + H^+ \rightarrow {}^\bullet HO_2 \quad [23.4]$$

$$2{}^\bullet HO_2 \rightarrow O_2 + H_2O_2 \quad [23.5]$$

© Woodhead Publishing Limited, 2011



23.2 Relative positions of the valence and the conduction bands and the energies of two redox pairs. Both reduction and oxidation reactions are thermodynamically allowed only for (d). Ox_2 and Red_1 represent the oxidized and the reduced species, respectively, of two different redox pairs.

$$H_2O_2 + {}^{\bullet}O_2^- \rightarrow OH^- + {}^{\bullet}OH + O_2 \qquad [23.6]$$

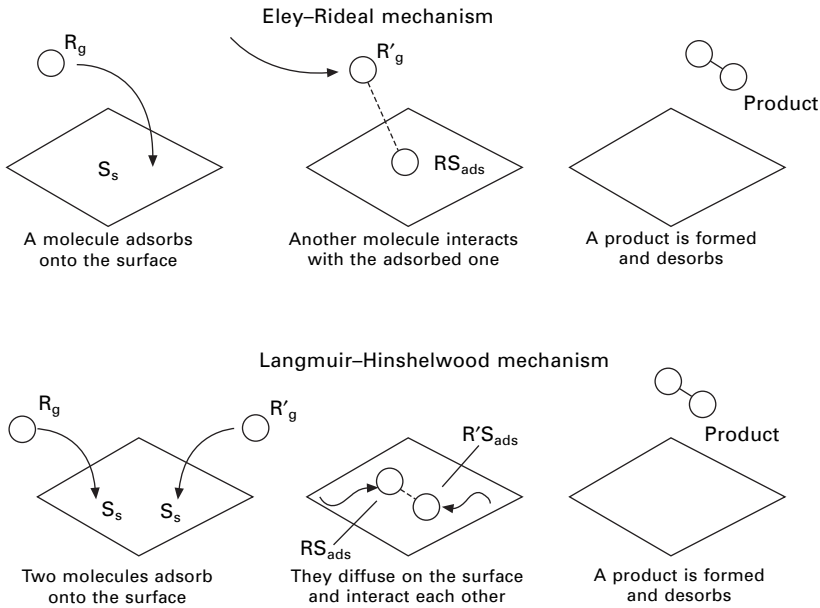
The photocatalytic method allows, moreover, many inorganic ionic pollutants present in water to be eliminated by reducing them to their elemental form on the surface of the catalyst particle. Photocatalysis is a 'change in the rate of a chemical reaction or its generation under the action of ultraviolet, visible, or infrared radiation in the presence of a substance – the photocatalyst – which absorbs light and is involved in the chemical transformations of the reaction partners' (Braslavsky *et al.*, 2011).

Generally, the interaction of radicals photogenerated by the adsorbed molecules can promote surface chemical processes by the Langmuir–Hinshelwood mechanism, whereas the interaction of molecules with surface active centres can initiate surface chemical processes by the Eley–Rideal mechanism. In the Eley–Rideal mechanism, proposed in 1938 by D. D. Eley and E. K. Rideal, only one of the molecules adsorbs and the other one reacts with it directly from the gas phase, without adsorbing. Figure 23.3 shows the scheme of the two different mechanisms.

23.3 Membrane materials developments and design for photocatalysis

A membrane can be defined as a selective separation barrier. The membrane module can act as a molecular filter allowing separation both of solid particles

© Woodhead Publishing Limited, 2011



23.3 Graphic models of the Eley–Rideal and Langmuir–Hinshelwood mechanisms. R_g and R'_g represent two general gaseous reagents and S_S a surface site.

and specific ions/molecules. The simplest classification of membranes is based on their nature and provides the main division into biological and synthetic membranes (organic and inorganic). Membranes can be solid or liquid, symmetric or asymmetric, homogeneous or heterogeneous. Another distinction is based on the morphology and structure of membranes. This type of classification is very important because the structure of the membrane can determine the separation mechanism and thus its application. A porous membrane allows permeation through its pores and then the mechanisms (Knudsen diffusion or microporous separation) are different depending on the pore size. In a dense membrane the permeate forms a solution with the membrane, then diffuses through the thickness allowing the separation. The differences between different types of morphologies can be both in the macroscopic structure (films, tubes, hollow fibres) and in the microscopic one (symmetrical, asymmetrical, porous, dense or mixed structure).

In symmetric membranes structural and transport properties are the same throughout its section and the thickness of the entire membrane determines the flow. In asymmetric membranes the structural and transport properties change along the membrane thickness. They are mainly used in separation processes that use hydrostatic pressure as the driving force. An asymmetric membrane consists of two parts: a dense thin layer supported by a porous layer which acts as mechanical support of the fragile skin layer and has a

© Woodhead Publishing Limited, 2011

small effect on separation and transport through the membrane. This type of structure combines the high selectivity of a dense membrane with the high permeation rate of a thin layer membrane.

Depending on membrane pore size, different pressure-driven processes can occur: reverse osmosis (RO), nanofiltration (NF), ultrafiltration (UF) and microfiltration (MF). Other characteristics that must be considered are the ability to transport electrical charges (ion exchange or bipolar mixed conduction) and the possibility of including, in the porous structure or deposited on the surface, a catalyst that has some affinity with the membrane. Another classification is based on surface properties of a membrane (hydrophobic/hydrophilic character).

Most of the photocatalytic membrane reactors (PMRs) in the literature involve the use of a catalyst in suspension, combined with pressure driven processes like MF, UF and NF. NF has the advantage of retaining molecules with a lower molecular weight than MF and UF membranes although these appear to be energetically more convenient. Other kinds of membrane operations used in processes coupled with photocatalysis are membrane distillation (MD) (Mozia and Morawski, 2006; Mozia *et al.*, 2007) and pervaporation (Augugliaro *et al.*, 2006).

The choice of the material used to produce membranes depends mainly on their different applications. For porous membranes (used for MF and UF processes) the material used is strongly determined by the requirements of the process, the tendency to give rise to fouling and the chemical and thermal stability of the materials. The performance depends directly on the material characteristics, for example dense non-porous membranes are generally used for pervaporation or gas separation applications.

23.3.1 Polymeric membranes

In photocatalysis polymeric membranes are generally used. The most used polymers for MF are poly(vinylidene fluoride) (PVDF), polytetrafluoroethylene (PTFE), polypropylene (PP), polysulfone (PSF) and cellulose acetate (CA) derivates.

PVDF is a partially fluorinated polymer with a high performance, characterized by good chemical resistance and good thermal stability. PVDF is also soluble in polar solvents, resistant to ultraviolet light and oxidant attack (Chin *et al.*, 2006). PVDF membranes have been used primarily in the construction of submerged modules, widely used in bioreactors owing to their lower costs with respect to other types of photocatalytic membranes (Sopajaree *et al.*, 1999a; Chin *et al.*, 2007; Jia *et al.*, 2006). Fu *et al.* (2006) described a submerged PVDF membrane photocatalytic reactor for the degradation of fulvic acid, whereas Chin *et al.* (2007) studied a low pressure PVDF submerged hollow fibre membrane module in direct contact with the

© Woodhead Publishing Limited, 2011

photooxidation medium. Different papers suggest the use of PVDF membranes for the construction of photocatalytically active modules.

Damodar *et al*. (2009) reported the preparation and testing of composite PVDF/TiO_2 membranes with self cleaning/antifouling, bactericidal and photoactive properties based on a UV/TiO_2 photocatalytic mechanism. Composite PVDF/TiO_2 membranes were prepared using the phase-inversion method. The casting solution, prepared by mixing 10 wt% PVDF with 0, 1, 2 and 4 wt% TiO_2 Degussa P25 in n-methyl-2-pyrrolidone solvent (60–65°C), was spread with a 200 μm thickness casting knife onto the non-woven sheet as a base substrate. Then the membranes were immersed in a tap water coagulation bath for 1 day (23–25°C) and the composite membranes obtained were washed with distilled water.

Bae and Tak (2005) reported the preparation of different types of membranes, including TiO_2 entrapped PVDF membranes, prepared by phase-inversion using the same method reported by Molinari *et al*. (2000). The casting solution consisted of PVDF, n-methyl-2-pyrrolidone and Degussa P25 TiO_2 particles. The TiO_2 ratio (w/w) of the casting solution was fixed at 0.3. The casting solution was spread with a 200 μm casting knife onto polyester non-woven fabric and, after evaporation, the membrane was immersed in a deionized water coagulation bath (18 ± 1°C). The higher affinity of metal oxides with water allowed the hydrophilicity of TiO_2 entrapped membrane to increase compared to the neat polymeric one.

Chin *et al*. (2006) showed that PTFE (a highly crystalline polymer that exhibits excellent thermal stability and high chemical resistance), like PVDF polymer, was quite stable after 30 days of UV-illumination. Damodar and You (2010) studied the photocatalytic mineralization of Reactive Black 5 dye in a photocatalytic membrane reactor, using a flat plate novel PTFE membrane module that was placed at the axis of the tank and surrounded by two UV lamps. The data obtained demonstrated that the membrane maintains a high performance even after cleaning, regaining its original behaviour. Moreover, the authors reported that no fouling occurred under the chosen operating conditions: the permeate flux 47–49 l $m^{-2}h^{-1}$ and transmembrane pressure (TMP) 1–1.5 inches Hg (3.39–5.08 kPa) remained constant throughout the photocatalytic runs.

Raja *et al*. (2007) reported the synthesis of PTFE/Co_3O_4 films and their testing for the fast decolouration of the azo-dye Orange II under visible light irradiation. Nanosized clusters of Co_3O_4 were formed on the PTFE surface by covering it with colloidal Co_3O_4. The Co-colloid was deposited on the PTFE film using a dip-coating technique. Then the film was dried, dipped into the Co_3O_4 sol and heated (280°C) to form the spinel crystallographic structure, allowing the diffusion of the oxide into the PTFE film.

Another hydrophobic polymer is polypropylene (PP). Owing to its excellent solvent resistance, PP is largely used in photocatalytic processes as reported

© Woodhead Publishing Limited, 2011

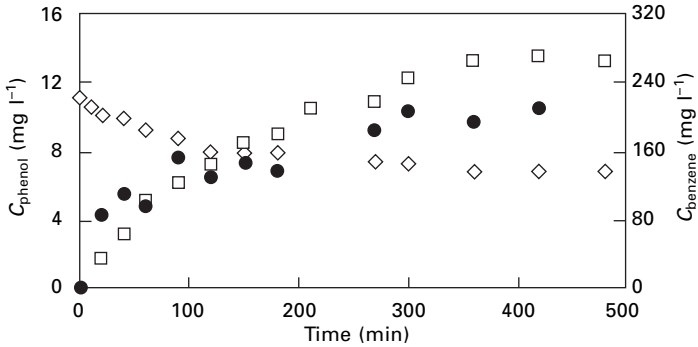
in the pertinent literature. PP membranes may be synthesized by stretching and phase-inversion. PP hollow fibre membranes were used by Erdim *et al.* (2009) to study the effect of natural organic matter (NOM) fouling. Synthetic and natural raw waters were used in their photocatalytic experiments. The data obtained showed that the increase in NOM concentration increased the pressure, and raw water experiments showed a higher pressure increase and lower removal efficiencies compared with that of synthetic water.

Because of their hydrophobic nature, PP membranes can be used in membrane distillation (MD), in fact they are not wetted by water or other liquids with a high surface tension (Mozia and Morawski, 2006; Mozia *et al.*, 2010; Grzechulska-Damszel *et al.*, 2009). Grzechulska-Damszel *et al.* (2009) studied various configurations of a photocatalytic membrane reactor for the removal of different azo-dyes. A PP membrane was used in a MD process using the permeate of the initial suspension as the feed. The non-volatile compounds were retained on the feed side whereas the volatile ones were transferred through the pores of the MD membrane and then condensed or dissolved in cold distillate. The authors reported a better removal of organic species from the treated solution by using the MD process than using a nanofiltration process.

Doll and Frimmel (2005) tested in a pilot plant membranes of different materials, including PP and PVDF, during the photodegradation process of three pharmaceutical compounds (carbamazepine, clofibric acid and iomeprol). The influence of periodical back washing in the presence of suspended TiO_2 with respect to abrasion was studied. Both the PP and PVDF membranes seem to be poorly resistant. Single channel ceramic membranes of α-alumina oxide showed good resistance to abrasion and back washing.

The use of PP membranes was also reported by Molinari *et al.* (2009) in a recent work regarding the study of the partial photooxidation of benzene to phenol. In the proposed system, the separation of phenol was obtained by using benzene both as reactant and extraction solvent. The organic phase was separated from the aqueous environment by means of a PP membrane according to previous studies (Soparajee *et al.*, 1999a, 1999b; Chin *et al.*, 2007). Benzene filled the PP membrane pores owing to the capillary force, but its passage into the aqueous reactive suspension was reduced by operating at a suitable pressure. In order to verify the efficiency of the phenol extraction with a PP membrane, preliminary transport tests were carried out. The results demonstrated that a PP membrane can be used for the separation of phenol from the aqueous phase. Moreover it assured a constant restock of benzene in the reactive suspension. The data obtained (Fig. 23.4), starting from two phases, a solution of phenol in water and a benzene phase separated by the membrane, showed that the equilibrium condition was reached after 360 minutes with a phenol extraction percentage of 24 ± 2% and a constant benzene concentration in the aqueous phase of about 200 mg l^{-1}. The phenol

© Woodhead Publishing Limited, 2011



23.4 Concentrations of phenol in aqueous and organic phases and benzene concentration in the aqueous phase during the transport test: ◇, phenol in aqueous solution; □, phenol in organic solution; ●, benzene in aqueous solution.

flux in the organic phase, measured in the first 180 minutes, was 1.7 mmol h^{-1} m^{-2}. Polymeric membranes consisting of hydrophilic materials have also been tested for photocatalytic applications. The best known class of these polymers is cellulose acetate (CA) based.

The performance of CA membrane was examined by Lee *et al.* (2001). The authors studied the photodegradation of humic acids in drinking water treatment by coupling a photocatalytic reaction and a cross-flow UF process using a plate-and-frame CA module. The CA membrane showed good resistance during the photocatalytic runs and ensured the separation of TiO_2 catalysts from the reaction environment. The experiments showed a partial photocatalytic mineralization of organic species and their transformation in less absorbable molecules enhanced the UF flux. A widely used material for membranes in photooxidation tests is cellulose triacetate (CTA).

Mounir *et al.* (2007) studied the photodegradation of Basic Red-46 under visible, UV and solar light, using two different catalysts based on cellulose fibres and TiO_2 particles. In the first case the TiO_2 catalyst was deposited on cellulose fibres (catalyst I), while in the second case it (catalyst II) consisted of three layers: a central one made of carbon fibres, one outer layer made of cellulose fibres containing the deposited TiO_2 and the other made of non-modified cellulose fibres. Catalyst (II) was more efficient than catalyst (I) in the photocatalytic process of dye degradation. By using sunlight, the discoloration yield was 100% for the most complex catalyst and 70% for catalyst (I), which had a simpler structure. The combination of cellulose membrane with active carbon and photocatalyst particles proved to be a promising technology for the photodegradation of harmful compounds. The performance of a cellulose triacetate (CTA) membrane with TiO_2 entrapped (CTA-TiO_2-A1-10) was studied by Molinari *et al.* (2004) in the

© Woodhead Publishing Limited, 2011

photodegradation of Congo Red dye. The results of photocatalytic tests were compared with those of other experiments with suspended TiO_2.

Cellulose triacetate membranes with entrapped TiO_2 were home prepared by using the phase-inversion process: 0.07 g of CTA was added to $CHCl_3$ (40°C). After three hours of agitation, TiO_2 as catalyst and 2-nitropheyloctylether (2-NPOE) as plasticizer were added. The polymerization process occurred in a Petri plate under room temperature during the evaporation of the solvent.

In other studies of photocatalytic membrane processes for water pollution purification proposed by the same authors, different membranes including cellulose modified with PP were tested. Ultrafiltration (UF) membranes are porous and most of them are prepared by phase-inversion. A very important class of polymers are polysulfone and polyethersulfone (PES), widely used as basic materials for UF membranes and as support for composite membranes. Another common polymer used for UF membranes tested in photocatalysis is polyacrilonitrile (PAN).

Molinari *et al*. (2000) studied different commercial membranes composed of various materials: polysulfone, polyamide, polyethersulfone, fluoride (FS) + PP, polyvinyl fluoride (PVF), PAN and cellulose + PP for photocatalytic purification of water. Preliminary analyses of membrane stability under UV irradiation, showed PAN, fluoride + PP and PP + PSF to be stable. These results were also confirmed by TOC analyses of the soaking water in which the membranes were immersed and irradiated for six hours. Other membranes exhibited an increase in the permeate flux after illumination, caused by membrane photodegradation, with an increased level of total organic carbon (TOC) (CA + PP, PVF).

A PAN supported TiO_2 membrane was chosen to carry out some photoreactivity experiments. The PAN membrane showed the highest permeate flux which was constant over time. Physical immobilization of TiO_2 on the membrane was done by ultrafiltration of suspensions containing various amounts (0.05, 0.1, 0.2 and 0.3 g l^{-1}) of TiO_2 in water. The amounts of immobilized TiO_2 were 0.76, 2.04, 4.08 and 6.12 mg cm^{-2} of membrane. The best uniform coverage was given by loading 4.08 mg cm^{-2} of TiO_2, although the best results for the photocatalytic reaction were obtained in a suspended TiO_2 system. 4-Nitrophenol was used as probe molecule and a degradation of 80% w/w was obtained in around 5 hours by using 0.5 g l^{-1} of suspended TiO_2, whereas in the system with deposited TiO_2 the degradation was around 51% w/w during the same irradiation time, independent of the amount of catalyst.

Moreover, Molinari *et al*. (2002a) reported the characterization of membranes used in photodegradation of pollutants, with different system configurations. Tests of photo-resistance under UV light were carried out by irradiating the membranes immersed in distilled water. Samples were periodically withdrawn, analysed by TOC and scanning electron microscopy

© Woodhead Publishing Limited, 2011

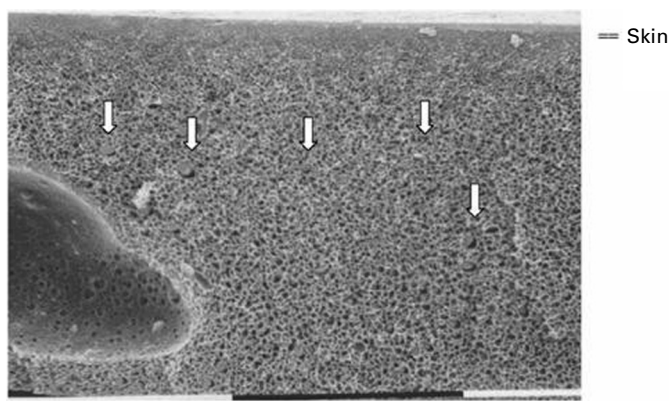
(SEM) in order to verify any damage to the membrane surface. Various types of commercial and home-made membranes with entrapped TiO_2, were used. Table 23.1 shows the commercial membranes used in UV irradiation tests.

The home-made membranes were prepared using the phase-inversion technique. The homogeneous polymeric solution consisted of commercial PSF, *N*-methyl-pyrrolidone (NMP) and 1-octanol. TiO_2 P25 Degussa was added to the polymeric solution. The best membrane morphology was obtained from a casting dope of composition: NMP:$C_8H_{17}OH$:PSF, 68:13:19, TiO_2, 16.7 wt% (TiO_2 + PSF), as shown in Fig. 23.5.

Table 23.1 Types of commercial membranes used in UV irradiation tests

Type of membrane	Manufacturer	Type of polymer	Cut-off pore size
MPPS 0000 u002	Separem	Polysulfone	15 kDa
MPPS 0000 u006	Separem	Polysulfone	40 kDa
MPCU 0000 u20	Separem	Polyamide	2.5 kDa
MPCU 0000 u25	Separem	Polyamide	2.0 kDa
P-12-10	Our lab	Polyether ether ketone (PEEK)	–
FS 50 PP	Dow	Fluoride + PP	50 kDa
PES	TechSep	Polyethersulfone	40 kDa
PVDF	TechSep	Polyvinylidenefluoride	0.1 kDa
GR 51 PP	TechSep	Polysulfone + PP	50 kDa
PAN	TechSep	Polyacrylonitrile	40 kDa
CA 600 PP	Dow	Cellulose acetate + PP	20 kDa

PP: polypropylene



23.5 Cross-section of the membrane obtained from the casting dope of composition: NMP:$C_8H_{17}OH$:PSF, 68:13:19, TiO_2, 16.7 wt% (TiO_2 + PSF). Coagulation bath ratio is water:NMP, 1:1. Arrows indicate particles of TiO_2 inside the membrane structure. Magnification: X 406 (Molinari *et al.*, 2002a).

© Woodhead Publishing Limited, 2011

Photocatalytic tests indicated a satisfactory photoactivity for TiO_2 content ≥ 30 wt%. Materials such as PSF are often used to prepare hollow fibres. Choo *et al*. (2008) proposed the use of a membrane module consisting of three hollow fibres for the photocatalytic removal of trichloroethylene in water. A better membrane system performance was obtained by using three fibres instead of a single one. The clogging of a single fibre did not affect the process.

The use of the photocatalytic reactor coupled with this membrane system allowed the complete separation of suspended catalyst from the reaction environment, which was also the case when the particle size of the catalyst was smaller than the pore size of the membrane. Indeed, the larger TiO_2 particles formed a layer on the membrane surface hindering the passage of the smaller ones. A reduction in the efficiency of the membrane occurred when humic acid was used as background species in the feedwater: the permeability decreased by 60% owing to membrane fouling. This phenomenon was due to the interaction between molecules of humic acid and particles of catalyst which accumulated on the membrane surface. To overcome the fouling problem, the cross-flow velocity should be controlled and kept above certain values.

Coupling photocatalysis and a NF membrane was also studied. NF membranes have the advantage of retaining low molecular weight molecules better in comparison to low pressure MF and UF modules. The membranes used are sulfonated or modified PSF, polyethersulfone and polyacrilonitrile (PAN). NF membranes can also be used as submerged modules, especially in bioreactors. Tsarenko *et al*. (2006) studied systems for purification of aqueous solutions containing organic matter with a commercial fine-pored NF membrane, using humic acid as the probe molecule.

A hybrid system built by coupling the photocatalytic reaction and membrane separation processes was proposed by Molinari *et al*. (2006) to degrade different pharmaceuticals (furosemide, ranitidine (hydrochloride), ofloxacine, phenazone, naproxen, carbamazepine and clofibric acid). Different NF membranes were used. Table 23.2 reports the main characteristic of these membranes.

It can be seen that the membrane retention depended both on the pH of the aqueous solution and on the chemical characteristics of the pharmaceuticals compounds. The membrane that showed the best rejection percentages for furosemide was NF PES 10 at alkaline pHs, NTR 7410 at neutral and alkaline pHs and N 30 F at acidic pHs, at pressures of 4–8 bar. NTR 7410 was the best membrane for ranitidine rejection, over the whole pH range, although its rejection at 8 bar was lower than that found for NF PES 10.

NF PES 10 and NTR 7410 were studied also for the photocatalytic removal of 4-nitrophenol (4-NP) and benzoic acid from aqueous solutions (Molinari *et al*., 2002b). In this paper, TiO_2 P25 Degussa was used as the catalyst,

© Woodhead Publishing Limited, 2011

Table 23.2 Main characteristics of the membranes employed

Membranes	Manufacturer	Characteristics	Material
NTR 7410	Nitto Denko, Tokyo	Rejection 10% with 0.2% NaCl at 4.9 bar, 25°C and pH 6.5	Sulfonated polysulfone
PAN GKSS HV3/T	GKSS, Germany	Cut-off = 30 kDa; water flux 423.1 $lh^{-1}m^{-2}$ at 2 bar and 846.2 $lh^{-1}m^{-2}$ at 4 bar	Polyacrylonitrile
N 30 F	Hoechst, Celgard, Germany	Rejection 25–35% with 0.2% NaCl and 85–95% with 0.5% of Na_2SO_4; water flux 40–70 $lh^{-1}m^{-2}$ at 40 bar and 20°C	Modified polysulfone
NF PES 10	Hoechst, Celgard, Germany	Rejection 10–20% with 0.5% NaCl and 40–70% with 0.5% of Na_2SO_4; water flux 200–400 $lh^{-1}m^{-2}$ at 40 bar and 20°C	Polyethersulfone

suspended or deposited on the polymeric membranes. It was found that the treatment of 4-NP solution in acidic medium allowed the total removal of the substrate by using a continuous system. NTR 7410 was also an efficient NF membrane for separating Congo Red and Direct Blue dyes from aqueous solutions (Molinari *et al.*, 2004). The membrane allowed the oxidation co-products to be retained until their complete photomineralization, thus obtaining a purified permeate solution.

23.3.2 Inorganic membranes

Inorganic membranes are attractive for PMR applications as they generally present higher chemical and thermal stability with respect to polymeric ones, but have the drawback of higher costs (Chin *et al.*, 2006; Moritz *et al.*, 2001).

Inorganic materials used for most photocatalytic membranes are ceramic based. Ceramics are prepared by the combination of a metal with a non-metal to form an oxide, nitride or carbide. Ceramic membranes prepared from materials like aluminium oxide and zirconium oxide or zirconia constitute the main class of inorganic membranes. Ceramic membranes can be prepared by different techniques like sintering (Auriol and Tritten, 1973; Terpstra *et al.*, 1985) and anodic oxidation (Hoar and Mott, 1959; Smith, 1973), but the most effective method is the sol–gel process (Alem *et al.*, 2009a, 2009b; Leenaars and Burggraaf, 1985; Klein and Gallagher, 1988).

Alem *et al.* (2009a) prepared a titania multilayer membrane, which consisted of an Al_2O_3 support, a colloidal sol–gel-derived intermediate layer and finally a sol–gel top layer. Methyl orange degradation was chosen to test the photoactivity of the obtained titania membrane. The results showed

© Woodhead Publishing Limited, 2011

a high stability and catalytic activity per unit mass of TiO_2, ensuring both the photodegradation reactions and the physical separation of pollutant.

The same authors reported the study of different techniques to prepare a crack-free mesoporous titania membrane on an alumina support. The titania colloidal sol was prepared by the sol–gel technique and its photocatalytic performance was evaluated by the photodegradation of methyl orange in aqueous solution. The best experimental conditions for synthesizing the colloidal titania sol were pH 1.0 and a temperature of 50.0°C. The membrane performance was strongly dependent on various factors, mainly the calcination time and temperature. An increase of calcination time and temperature caused a decrease in the specific surface area and in the photoactivity of the catalyst. Other factors, like crystallite size, allotropic phase of titania and membrane thickness, play an important role in the photocatalytic activity of the membrane.

23.4 Membrane operations performance issues and analysis: case studies

23.4.1 Fouling control

The main problem in membrane processes, especially for UF and MF separations, is the decrease of permeate flux caused by concentration polarization and fouling, whereas other membrane processes like gas separation and pervaporation are less affected. Different approaches have been studied to reduce fouling. Thiruvenkatachari *et al*. (2008) proposed intermediate pretreatment stages of the feed solution between the photocatalytic process and membrane separation: coagulation and sedimentation processes prior to membrane filtration were used with a consequent significant reduction of fouling. Another method of controlling and reducing fouling phenomena is based on control of the membrane properties. Hydrophilic modification of the polymeric membrane surface is a common method to reduce fouling.

Bae and Tak (2005) used entrapped and deposited TiO_2 membranes to study fouling in membrane bioreactors. The results showed that the deposited TiO_2 membrane was less affected by fouling than the entrapped TiO_2 one. This insight can be due to the greater amount of nanoparticles contained in the deposited TiO_2 membrane compared with the entrapped one. However, both types of surface modification showed fouling mitigation in membrane bioreactors processes.

The use of a modified membrane, with a titania layer deposited on an alumina microfilter, was reported also by Tsuru *et al*. (2008) in the photooxidation process of pollutants. An increase of the flux across the titania/alumina membrane showed the antifouling properties of this device. The advantage of controlling fouling and ensuring contemporaneously the

© Woodhead Publishing Limited, 2011

photodegradation of pollutants molecules, by using membrane reactors, was reported also by Lee *et al*. (2001). The photodegradation of humic acid in smaller molecules in the presence of natural organic matter using an UF separation system, represents a promising strategy for reduction of fouling during drinking water treatment.

23.4.2 Membrane reactor configurations

Different types of membrane operations (such as distillation, dialysis, nanofiltration, pervaporation and osmosis) were used in hybrid systems. The additional advantage of coupling is performed by the photocatalyst which prevents microbial fouling, offering a strong potential for the use of new types of thin film composite membranes. Some PMR configurations are described in the following.

Pressurized membrane reactors

Molinari *et al*. (2002a) described two different PMR configurations for the degradation of 4-NP where the permeate was obtained by pressurizing the membrane surface. TiO_2 catalyst was confined by the membrane and its irradiation was performed in the cell containing the membrane. Three sub-cases were studied:

- catalyst deposited on the membrane;
- catalyst suspended;
- catalyst entrapped in the membrane material.

The best system was the catalyst suspended in a recirculation batch, because it had the highest irradiation efficiency and the highest permeate flow rate.

Molinari *et al*. (2004) compared the photocatalytic performance of the process using a TiO_2 entrapped membrane with that of suspended photocatalyst. The data obtained demonstrated that the suspended system was the most efficient. The reduction of photoactivity of the TiO_2 entrapped membrane was probably due to the presence of polymer around the TiO_2 particles. The influence of UV irradiation on the photodegradation process was also studied. Experimental runs were carried out using two different photoreactor configurations: a cylindrical photoreactor with an external lamp and an annular one with an immersed lamp in the axial position. The results showed that the system with an immersed lamp was three times more efficient than that with an external lamp.

Submerged (depressured) membrane photoreactors

A submerged membrane system was studied to overcome the fouling. In this type of configuration, the membrane is immersed, the catalyst is suspended

© Woodhead Publishing Limited, 2011

in an open-air reaction environment and the permeate is withdrawn by means of a vacuum pump. Fu *et al.* (2006) investigated the effects of some operational parameters like TiO_2 concentration, pH and air flow on the photodegradation of fulvic acid. The results showed a reduction of fouling phenomena when nano-structured TiO_2 was used as the photocatalyst. The particle size of the photocatalyst used was greater than the P25 and a better system performance was obtained.

Sedimentation of the suspended semiconductor can be controlled by applying fine-bubble aeration and intermittent membrane filtration, as reported by Huang *et al.* (2007). An intermittent operative procedure was also employed by Choi (2006) to study the photodegradation of 4-chlorophenol using a submerged membrane photoreactor. The data obtained showed complete photodegradation of pollutant molecules and great sedimentation reduction.

23.4.3 Photocatalytic membrane contactors

Another type of separation which can be coupled with photocatalysis uses membrane contactors. They can be classified as gas–liquid (G-L) and liquid–liquid (L-L) contactors (Mulder, 1991). The performance of both configurations is determined mainly by the distribution coefficient of the transported species in the different phases where the membrane acts only as an interface. Photocatalytic membrane contactors have several advantages compared to the other types of reactor configuration. Indeed, they can be used to separate selectively the product(s) of interest during the photosynthetic process avoiding the occurrence of undesirable secondary reactions.

23.4.4 Membrane distillation–photocatalysis

In membrane distillation the separation process is based on the principle of vapour–liquid equilibrium. The non-volatile components are retained on the feed side and the volatile ones pass through a porous hydrophobic membrane and are condensed in distilled water. Mozia *et al.* (2008) reported the study of Acid Red 18 degradation using a PMR in which photocatalysis was coupled with a membrane distillation process. They compared the performance of a home-prepared anatase TiO_2 with that of Degussa P25. The membrane distillation system allowed the complete rejection of non-volatile compounds which were confined on the feed side. The results of photocatalytic experiments showed that the home-made TiO_2 allowed a degradation rate higher (49–64%) than that obtained using P25.

© Woodhead Publishing Limited, 2011

23.4.5 Pervaporation–photocatalysis

In order to enhance the efficiency of the photodegradation process, several studies propose systems in which photocatalysis is coupled with pervaporation. Camera-Roda and Santarelli (2007) used pervaporation to remove continuously and at a high rate the organic intermediates produced during the first step of a 4-chlorophenol oxidation reaction. They demonstrated that coupling pervaporation with photocatalysis is a very promising method of improving the efficiency of the detoxification of wastewater containing low concentrations of organic pollutants as the integration of the two methods generates a synergistic effect. Indeed the degradation of the probe molecule (4-chlorophenol) was 'intensified' by the presence of the membrane which eliminated some intermediates whose presence could slow down the photodegradation rate. Photocatalysis oxidized concurrently the weakly permeable substrate into organic compounds easily removed by pervaporation. Moreover, it was shown that intensification of the process depends on the optimization of the ratio between the characteristic rates of the two processes.

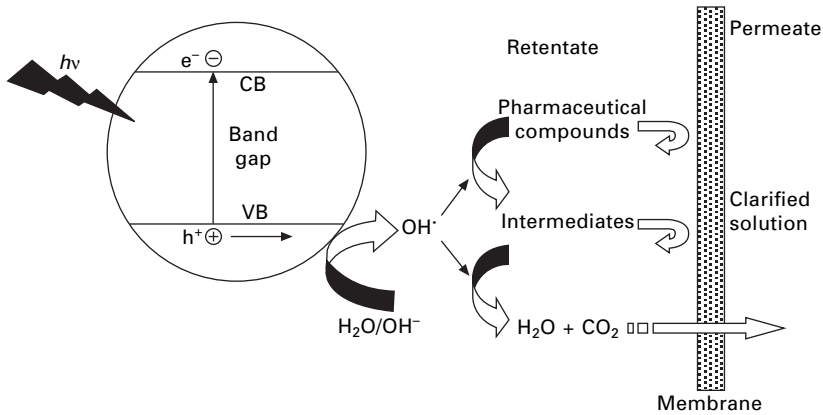
23.4.6 Dialysis–photocatalysis

Azrague *et al*. (2007) described an interesting process based on dialysis membranes used as contactor combined with a photocatalytic reactor for turbid water treatment. In the proposed system the membrane process allowed the transport of the 2,4-dihydroxybenzoic acid by diffusion from the feed tank side to the side where the photocatalytic reaction occurred. The driving force is the difference in concentration between the two membrane sides; no TMP is needed for this process. Complete pollutant mineralization was obtained, overcoming any fouling phenomena, with consequent benefits from an economic point of view.

23.4.7 Degradation of pharmaceutical compounds

The annual consumption of antibiotic type substances is similar in quantity to that of some pesticides; moreover drugs that are consumed but not metabolized by the organism are excreted through urine and faeces and their presence in the environment (especially in surface waters) is often found, owing to their resistance to common biotransformation mechanisms. Hybrid systems based on coupling membrane separation and photocatalytic process could represent an alternative pathway for their removal. Photocatalytic reaction allows a complete degradation of these organic molecules into harmless products and at the same time the recovery of catalysts (Fig. 23.6). The use of PMRs for the degradation of Gemfibrozil (GEM) and Tamoxifen (TAM)

© Woodhead Publishing Limited, 2011



23.6 Degradation process in a photocatalytic membrane reactor.

pharmaceuticals in water with suspended TiO_2 powder, was reported by Molinari *et al*. (2008).

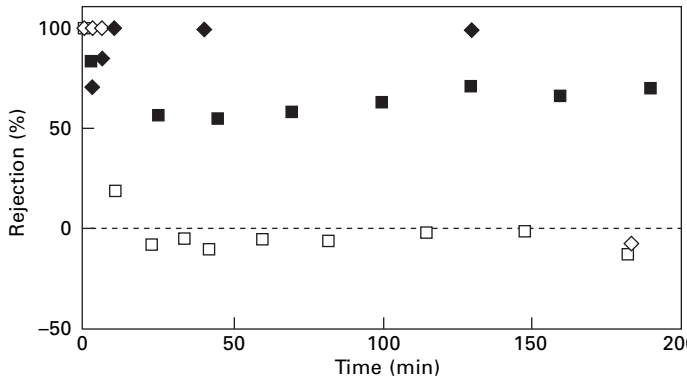
The experimental plant consisted of an annular photoreactor with an immersed UV lamp connected to the permeation cell in which a pressurized flat sheet membrane or a submerged membrane module were located. Closed and continuous procedures were used to investigate the behaviour of the pressurized membrane photoreactors. The data obtained for the closed membrane system showed complete photodegradation of GEM and TAM, with an abatement of 99% after 20 minutes and mineralization higher than 90% after approximately 120 minutes.

Catalyst deposition on the membrane surface and fouling caused a flux decline during the photocatalytic process. To overcome these problems, the depressurized (submerged) membrane system, in which the membrane module was located separately from the photoreactor, was studied. The results showed pharmaceuticals abatement of 100% after around 20 min and 44.5% mineralization after about 150 min in the retentate. The UF membrane used in the submerged system did not allow the rejection of GEM and of its oxidation products compared to the NF membranes in the pressurized system (Fig. 23.7). However, the submerged membrane photoreactor offered more advantages in terms of permeate flux than those obtained operating with the pressurized module.

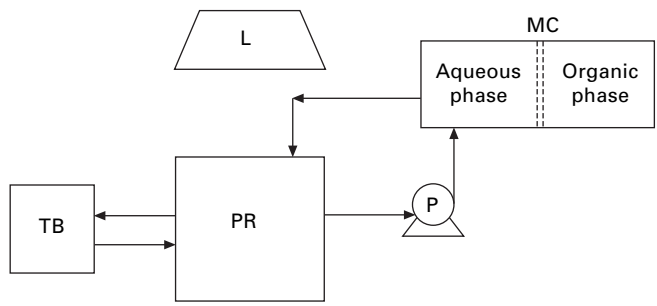
23.4.8 One-step synthesis and separation of phenol

Photocatalytic reactions can be also used in the syntheses of chemicals. Phenol represents an important substrate for the production of antioxidants, polymers and agrochemicals. Nowadays more than 90% of world production

© Woodhead Publishing Limited, 2011



23.7 Comparison between flat sheet and submerged continuous PMRs for the degradation of GEM (Molinari *et al.*, 2008): ◆, GEM with flat sheet PMRs; ◇, GEM with submerged PMRs; ■, TOC with flat sheet PMRs; □, TOC with submerged PMRs.



23.8 Scheme of the PMR: PR, photoreactor system; MC, membrane contactor; L, UV lamp; TB, thermostatic bath; and P, peristaltic pump (Molinari *et al.*, 2009).

is based on the multi-step cumene process which leads to acetone formation as a by-product.

The one-step conversion of benzene to phenol was studied by Molinari *et al*. (2009) in a photocatalytic membrane reactor (PMR) in which both the reaction and product separation occurred simultaneously by means of a membrane contactor. The system was operated using benzene both as reactant and extraction solvent, employing a polypropylene membrane to separate the organic phase from the aqueous one (Fig. 23.8). The PMR allowed the production and separation of phenol, although formation of intermediate oxidation by-products was observed. The operative pH of 3.1 did not influence significantly the phenol flux (J_{orgPh} = 1.27 mmol h^{-1} m^{-2}) with respect to pH 5.5 (J_{orgPh} = 1.06 mmol h^{-1} m^{-2}). Nevertheless, the most acidic condition allowed control of the selectivity towards the by-products.

© Woodhead Publishing Limited, 2011

23.5 Future trends

The wide literature examined in this chapter on coupling photocatalysis and membranes shows various advantages deriving from the synergy of these two techniques. It is foreseen that hybrid systems photocatalysis – membranes will have a significant impact in designing processes for pollutants abatement as well as processes for synthetic reactions. This last case has emerged particularly in the last few years for selective oxidation and/or selective reduction using, for example, hydrogen produced from water splitting employing sunlight as the energy source.

23.6 Sources of further information and advice

An exhaustive reference book on fundamentals and applications of heterogeneous photocatalysis, *Clean by Light Irradiation: Practical Applications of Supported TiO_2* by V. Augugliaro, V. Loddo, M. Pagliaro, G. Palmisano and L. Palmisano, RSC Publishing, Cambridge (UK), 2010, has been recently published. Information on membrane photoreactors can be found in the book *Simulation of Membrane Reactors*, A. Basile and F. Gallucci (eds), Nova Science Publishers, 2008.

23.7 References

Alem A, Sarpoolaky H and Keshmiri M (2009a), 'Sol-gel preparation of titania multilayer membrane for photocatalytic applications', *Ceramic Intern*, **35**, 1837–43.

Alem A, Sarpoolaky H and Keshmiri M (2009b), 'Titania ultrafiltration membrane: preparation, characterization and photocatalytic activity', *J Eur Ceramic Soc*, **29**, 629–35.

Augugliaro V, Litter M, Palmisano L and Soria J (2006), 'The combination of heterogeneous photocatalysis with chemical and physical operations', *J Photochem Photobiol C*, **7**, 127–44.

Auriol A and Tritten D (1973), *A Process for the Manufacture of Porous Supports*, French Patent 2463636.

Azrague K, Aimar P, Benoit–Marquié F and Maurette M T (2007), 'A new combination of a membrane and a photocatalytic reactor for the depollution of turbid water', *Appl Catal B-Environ*, **72**, 197–204.

Bae T-H and Tak T-M (2005), 'Effect of TiO_2 nanoparticles on fouling mitigation of ultrafiltration membranes for activated sludge filtration', *J Membr Sci*, **249**, 1–8.

Braslavsky S A, Braun A M, Cassano A E, Emeline A V, Litter M, Palmisano L, Parmon V N and Serpone N (2011), 'Glossary of terms used in photocatalysis and radiation catalysis, IUPAC Recommendations 2010', *Pure Appl Chem*, **83**, 931–1014.

Camera-Roda G and Santarelli F (2007), 'Intensification of water detoxification by integrating photocatalysis and pervaporation', *J Sol En Eng*, **129**, 68–73.

Chin S S, Chiang K and Fane A G (2006), 'The stability of polymeric membranes in a TiO_2 photocatalysis process', *J Membr Sci*, **275**, 202–11.

Chin S S, Lim T M, Chiang K and Fane A G (2007), 'Hybrid low-pressure submerged

© Woodhead Publishing Limited, 2011

membrane photoreactor for the removal of bisphenol A', *Desalination*, **202**, 253–61.

Choi W (2006), 'Pure and modified TiO_2 photocatalysts and their environmental applications', *Catal Surv Asia*, **10**, 16–28.

Choo K-H, Chang D-I, Park K-W and Kim M-H (2008), 'Use of an integrated photocatalysis/hollow fiber microfiltration system for the removal of trichloroethylene in water', *J Hazard Mater*, **152**, 183–90.

Damodar R A and You S-J (2010), 'Performance of an integrated membrane photocatalytic reactor for the removal of the Reactive Black 5', *Separ Purif Technol*, **71**, 44–49.

Damodar R A, You S-J and Chou H-H (2009), 'Study the self cleaning, antibacterial and photocatalytic properties of TiO_2 entrapped PVDF membranes', *J Hazard Mater*, **172**, 1321–28.

Doll T E and Frimmel F H (2005), 'Cross flow microfiltration with periodical back-washing for photocatalytic degradation of pharmaceutical and diagnostic residues-evaluation of the long-term stability of the photocatalytic activity of TiO_2', *Water Research*, **39**, 847–54.

Erdim E, Soyer E, Tasiyici S and Koyuncu I (2009), 'Hybrid photocatalysis/submerged microfiltration system for drinking water treatment', *Desal Water Treat*, **9**, 165–74.

Fu J, Ji M, Wang Z, Jin L and An D (2006), 'A new submerged membrane photocatalysis reactor (SMPR) for fulvic acid removal using a nano-structured photocatalyst', *J Hazard Mater*, **131**, 238–42.

Fujishima A, Hashimoto K and Watanabe T (1999), *TiO_2 Photocatalysis: Fundamentals and Applications*, BKC, Tokyo.

Grzechulska-Damszel J, Tomaskewska M and Morawski A W (2009), 'Integration of photocatalysis with membrane processes for purification of water contaminated with organic dyes', *Desalination*, **241**, 118–26.

Hoar T P and Mott N M (1959), 'Mechanism for the formation of porous anodic oxide films on aluminum', *J Phys Chem Solids*, **9**, 97–99.

Hoffmann M R, Martin T S, Choi W and Bahnemann D W (1995), 'Environmental applications of semiconductor photocatalysis', *Chem Rev*, **95**, 69–96.

Huang X, Meng Y, Liang P and Qian Y (2007), 'Operational conditions of a membrane filtration reactor coupled with photocatalytic oxidation', *Separ Purif Technol*, **55**, 165–72.

Jia Y, Wang R and Fane A G (2006), 'Atrazine adsorption from aqueous solution using powdered activated carbon–Improved mass transfer by air bubbling agitation', *Chem Eng J*, **116**, 53–59.

Kim S H, Kwak S-Y, Sohn B-H and Park T H (2003), 'Design of TiO_2 nanoparticle self-assembled aromatic polyamide thin-film-composite (TFC) membrane as an approach to solve biofouling problem', *J Membr Sci*, **211**, 157–65.

Klein L C and Gallagher D (1988), 'Pore structures of sol-gel silica membranes', *J Membr Sci*, **38**, 213–20.

Lee S A, Choo K-H, Lee C-H, Lee H-I, Hyeon T, Choi W and Known H-H (2001), 'Use of ultrafiltration membranes for the separation of the TiO_2 photocatalysis in drinking water treatment', *Ind Eng Chem Res*, **40**, 1712–19.

Leenaars A F M and Burggraaf A J (1985), 'The preparation and characterization of alumina membranes with ultra fine pores. Part 2. The formation of supported membranes', *J Colloid Interface Sci*, **105**, 27–40.

Madaeni S S and Ghaemi N (2007), 'Characterization of self-cleaning RO membranes coated with TiO_2 particles under UV irradiation', *J Membr Sci*, **303**, 221–33.

© Woodhead Publishing Limited, 2011

Molinari R, Mungari M, Drioli E, Di Paola A, Loddo V, Palmisano L and Schiavello M (2000), 'Study on a photocatalytic membrane reactor for water purification', *Catal Today*, **55**, 71–78.

Molinari R, Palmisano L, Drioli E and Schiavello M (2002a), 'Studies on various reactor configurations for coupling photocatalysis and membrane processes in water purification', *J Membr Sci*, **206**, 399–415.

Molinari R, Borgese M, Drioli E, Palmisano L and Schiavello M (2002b), 'Hybrid processes coupling photocatalysis and membranes for degradation of organic pollutants in water', *Catal Today*, **75**, 77–85.

Molinari R, Pirillo F, Falco M, Loddo V and Palmisano L (2004), 'Photocatalytic degradation of dyes by using a membrane reactor', *Chem Eng Process*, **43**, 1103–14.

Molinari R, Pirillo F, Loddo V and Palmisano L (2006), 'Heterogeneous photocatalytic degradation of pharmaceuticals in water by using polycrystalline TiO_2 and a nanofiltration membrane reactor', *Catal. Today*, **118**, 205–13.

Molinari R, Caruso A, Argurio P and Poerio T (2008), 'Degradation of the drugs Gemfibrozil and Tamoxifen in pressurized and de-pressurized membrane photoreactors using suspended polycrystalline TiO_2 as catalyst', *J Membr Sci*, **319**, 54–63.

Molinari R, Caruso A and Poerio T (2009), 'Direct benzene conversion to phenol in a hybrid photocatalytic membrane reactor', *Catal Today*, **144**, 81–86.

Moritz T, Benfer S, Arki P and Tomandl G (2001), 'Investigation of ceramic membrane materials by streaming potential measurements', *Colloid Surf A: Physicochem Eng Aspects*, **195**, 25–33.

Mounir B, Pons M N, Zahraa O, Yaacoubi A and Benhammou A (2007), 'Discoloration of a red cationic dye by supported TiO_2 photocatalyst', *J Hazard Mater*, **148**, 513–20.

Mozia S and Morawski A W (2006), 'Hybridization of photocatalysis and membrane distillation for purification of wastewater', *Catal Today*, **118**, 181–88.

Mozia S, Tomaszewska M and Morawski A W (2005), 'A new photocatalytic membrane reactor (PMR) for removal of azo-dye Acid Red 18 from water' *Appl Catal B: Environ*, **59**, 131–137.

Mozia S, Tomaszewska M and Morawski A W (2007), 'Photocatalytic membrane reactor (PMR) coupling photocatalysis and membrane distillation–Effectiveness of removal of three azo dyes from water'**,** *Catal Today*, **129**, 3–8.

Mozia S, Morawski A W, Toyoda M and Inagaki M (2008), 'Effectiveness of photodecomposition of an azo dye on a novel anatase-phase TiO_2 and two commercial photocatalysts in a photocatalytic membrane reactor (PMR)', *Separ Purif Technol*, **63**, 386–91.

Mozia S, Morawski A W and Toyoda (2010), 'Integration of photocatalysis and membrane distillation for removal of mono and poly-azo dyes from water', *Desalination*, **250**, 666–72.

Mulder M (1991), *Basic Principles of Membrane Technology*, 2nd edn, Kluwer Academic Publishers, Dordrecht.

Palmisano G, Addamo M, Augugliaro V, Caronna T, Di Paola A, García-López E, Loddo V, Marcì G, Palmisano L and Schiavello M (2007a), 'Selectivity of hydroxyl radical in the partial oxidation of aromatic compounds in heterogeneous photocatalysis', *Catal Today*, **122**, 118–27.

Palmisano G, Yurdakal S, Augugliaro V, Loddo V and Palmisano L (2007b), 'Photocatalytic selective oxidation of 4-methoxybenzyl alcohol to aldehyde in aqueous suspension of home-prepared TiO_2 catalyst', *Adv Synth Catal*, **349**, 964–70.

Raja P, Bensimon M, Klehm U, Albers P, Laub D, Kiwi-Minsker L, Renken A and Kiwi

© Woodhead Publishing Limited, 2011

J (2007), 'Highly dispersed PTFE/Co_3O_4 flexible films as photocatalyst showing fast kinetic performance for discoloration of azo-dyes under solar irradiation', *J Photochem Photobiol*, **187**, 332–38.

Schiavello M (1995), *Heterogeneous Photocatalysis*, John Wiley and Sons, New York.

Sopajaree K, Qasim S A, Basak S and Rajeshwar K (1999a), 'An integrated flow reactor-membrane filtration system for heterogeneous photocatalysis. Part I: Experiments and modelling of a batch-recirculated photoreactor', *J Appl Electrochem*, **29**, 533–39.

Sopajaree K, Qasim S A, Basak S and Rajeshwar K (1999b), 'An integrated flow reactor-membrane filtration system for heterogeneous photocatalysis. Part II: Experiments on the ultrafiltration unit and combined operation', *J Appl Electrochem*, **29**, 1111–18.

Smith A W (1973), 'Porous anodic alumina oxide membrane', *J Electrochem Soc*, **120**, 1068–69.

Terpstra R A, Bonekamp B C and Vering H G (1985), 'Preparation, characterization and some properties of tubular alpha alumina ceramic membranes for microfiltration and as a support for ultrafiltration and gas separation membranes', *J Desal*, **70**, 395–404.

Thiruvenkatachari R, Vigmeswaran S and Moon I S (2008), 'A review on UV/TiO_2 photocatalytic oxidation process', *Kor J Chem Eng*, **25**, 64–72.

Tsarenko S A, Kochkodan U M, Samsoni-Todorov A O and Goncharuk V V (2006), 'Removal of humic substancies from aqueous solutions with a photocatalytic membrane reactor', *Colloid J*, **68**, 341–4.

Tsuru T, Toyosada T, Yoshioka T and Asaeda M (2008), 'Photocatalytic reactions in a filtration system through porous titanium dioxide membranes', *J Chem Eng Jap*, **34**, 844–47.

Yurdakal S, Palmisano G, Loddo V, Augugliaro V and Palmisano L (2008), 'Nanostructured rutile TiO_2 for selective photocatalytic oxidation of aromatic alcohols to aldehydes in water', *J Am Chem Soc*, **130**, 1568–69.

Yurdakal S, Palmisano G, Loddo V, Alagöz O, Augugliaro V and Palmisano L (2009), 'Selective photocatalytic oxidation of 4-substituted aromatic alcohols in water with rutile TiO_2 prepared at room temperature', *Green Chem*, **11**, 510–16.

© Woodhead Publishing Limited, 2011

24

Membranes for nuclear power applications

S. TOSTI, ENEA, Italy and C. RIZZELLO, Tesi Sas, Italy

Abstract: Membrane technologies are applied to the treatment of air and liquid effluents of fission power plants and wastes produced by isotope laboratories and nuclear medicine facilities. Particularly, membrane pressure driven processes such as reverse osmosis, nanofiltration, ultrafiltration and microfiltration are widely used for liquid radioactive waste (LRWs) treatment, while purification of air effluents is carried out by filtration. Membranes are also applied to the nuclear fusion fuel cycle: hydrogen isotopes separation is proposed using Pd-based membranes. The main applications concern tritium recovery from breeding blankets, detritiation of gas streams (i.e. plasma exhausts) and water detritiation.

Key words: decontamination factor, detritiation, HEPA filters, liquid waste treatment, nuclear fuel cycle, tritium recovery.

24.1 Introduction

From a historical point of view, nuclear processes were among the first where membrane technologies were applied.[1] First attempts were made in the mid-1940s under the Manhattan project at the Oak Ridge laboratories where atomic bombs were produced which required the pure uranium 235 isotope. This isotope makes up only 0.7% of uranium found in nature, while the rest is isotope 238. Isotopes show the same chemical behavior and cannot be separated chemically: thus physical processes, based on the differences in mass and size, were required. Uranium separation was attained by converting uranium into gaseous UF_6 and pumping it through a porous membrane. The difference in mass and size results in a slight enrichment of ^{235}U in the stream crossing the membrane. The diffusion process involves forcing uranium hexafluoride gas under pressure through a series of porous membranes. As U^{235} molecules are lighter than the U^{238} molecules, they move faster and have a slightly better chance of passing through the pores of the membrane. The UF_6 molecules which diffuse through the membrane are thus slightly enriched in isotope 235. This process is repeated many times in a series of diffusion stages called a cascade. Each stage consists of a compressor, a diffuser and a heat exchanger to remove the heat of compression. The enriched UF_6 product is withdrawn from one end of the cascade while the depleted UF_6 is removed at the other end. The gas must be processed through some 1400

© Woodhead Publishing Limited, 2011

stages to obtain a product with a concentration of U^{235} in the range 3–4%. Presently, membranes are widely used to produce enriched uranium that will be burnt in nuclear power reactors. This technology is currently being replaced by more efficient centrifuges; however, membranes still provide more than 35% of the world uranium enrichment capacity.

Many applications in both nuclear fission and fusion require gas and liquid separation processes. In the main, separations in the nuclear field take advantage of some characteristics of membrane processes: continuous operation, flexibility, reliability, and so on. Purification of air effluents from the nuclear fission industry is carried out by filtration (high efficiency particulate air, HEPA filters) while the fuel cycle of fission reactors produces a large amount and different kinds of radioactive wastes mainly in liquid form. Liquid waste processing is necessary in order to ensure safe storage and disposal and to reduce the environmental impact.

Several examples of liquid radioactive wastes (LRWs) treated by pressure-driven processes such as reverse osmosis, nanofiltration, ultrafiltration and microfiltration are reported: a very extensive description is given in International Atomic Energy Agency (IAEA) reports.[2,3] These technologies are mature and are supported by well-defined process design and computer simulation and, as an important characteristic, these processes can be easily integrated with the traditional separation steps. Among the applications, at the Nine Mile Point nuclear power (boiling water reactor, BWR) plant (USA), reverse osmosis is used to obtain a reduction of the solid (secondary) wastes, which has great advantages compared to demineralizer systems. Ultrafiltration (as pretreatment) and reverse osmosis are applied at the Dresden and Comanche Peak nuclear power plants (both pressurized water reactors, PWR). After treatment the water is below the discharge activity limits: the decontamination factors are significantly higher than using demineralizer technology (up to a decontamination factor of 10^4 for the Comanche Peak plant). Ultrafiltration is also applied to processing contaminated waste from fuel reprocessing at Mound laboratory (USA) with retention of alpha radionuclides greater than 70%. AECL Chalk River laboratories (Atomic Energy of Canada Ltd) tested membrane technologies for the treatment of liquid radioactive waste (LRW) via microfiltration and reverse osmosis, attaining very high plant efficiency (close to 100%) while microfiltration was applied in order to demonstrate decontamination of groundwater and soils.

Nuclear fusion reactors need to burn hydrogen isotopes (deuterium and tritium) in order to produce energy: the fuel cycle of these machines is mainly focused on the separation of hydrogen and its isotopes in gaseous form. In the future, in fusion plants such as the ITER, a fusion reactor to be built in France (formerly International Thermonuclear Experimental Reactor) and DEMO (DEMOnstration Power Plant, a proposed nuclear fusion power plant) reactors,[4,5] tritium will be burnt with deuterium in order to sustain the

© Woodhead Publishing Limited, 2011

nuclear reaction: particularly, tritium will be produced in the Li-based breeding blanket surrounding the fusion chamber and its recovery is required both to ensure reactor self-sufficiency and to avoid releases to the environment. The important advantages of the membrane technologies permit cost reduction, higher reliability and, especially, a reduction of the tritium inventory which is a main aspect of the safe management of a fusion plant. Pd-based membranes and membrane reactors have been studied for such applications.[6,7] A series of Pd-Ag permeators and membrane reactors (PERMCAT, from permeation and catalyst) have been studied at the Tritium Laboratory of Karlsruhe for final clean-up of the tokamak exhausts in a continuous process. Tritiated gases containing up to 1% of tritium are fed into the lumen of a membrane reactor where protium is counter-currently sent on the shell side.[8] The performance of a membrane treatment for decontaminating a process stream can be assessed in terms of the decontamination factor (*DF*):

$$DF = \frac{\text{specific activity of feed}}{\text{specific activity of permeate}} \qquad [24.1]$$

The decontamination factor depends on the characteristics of the membrane (permeability, selectivity, surface area, etc.), the operating conditions (sweep mode, temperature, pressure, etc.) and the process design (pretreatments, recycles, etc.).

24.2 Membranes for nuclear fission applications

In the main, fission applications consist of the filtration of air effluents from nuclear facilities and the treatment of radioactive liquid wastes.

24.2.1 High efficiency particulate air (HEPA) filters applications

High efficiency filters, often called 'absolute' or 'HEPA', are widely used in the nuclear industry for the filtration of air effluent from nuclear facilities.[9] The first nuclear reactor fitted with effluent high-efficiency air filters was the X-10 reactor, a graphite moderated, air-cooled unit built at Oak Ridge National Laboratory. It entered into operation in November 1943 and supplied the Los Alamos laboratory with the first significant amounts of plutonium requested for the fabrication of nuclear weapons. Some years later, in 1948, a noticeable amount of radioactive particles (up to 600 μm in size) was discovered in the ground around the reactor stack. To prevent further emissions it was decided to filter the exhaust air stream. The filtering system, sized for 240 000 m^3 h^{-1}, was based on a modular unit of cellulose-asbestos fibres supported in plywood frames. Each module was 610 by 610 mm by 300 mm (depth) and its design efficiency was 99.9% for particles down to 0.1 μm.

© Woodhead Publishing Limited, 2011

Filters were preceded by fibreglass prefilters capable of capturing the coarse particles thus extending the life of the absolute filters. Filters and prefilters were arranged inside a reinforced concrete filter housing. High efficiency filters should be changed when airflow resistance increases from 1–5 inches (2.5–12.5 cm) of water. It was found that the service life of the absolute filters could be extended to more than 2 years by changing the prefilters two to three times per year. The characteristics of filtering media were developed from the gas masks employed during World War II: the most popular materials were cotton waste, asbestos and wool, manufactured on conventional papermaking machinery.

Filtration mechanisms

Great efforts were made to develop the theory and technology of aerosol filtration. At first, aerosol filtration theory was developed almost exclusively as an offshoot of water filtration knowledge. In reality, absolute filters are not membrane filters as sieving (removal of particles that are too large to pass through the openings of the filter) is not an important filtration mechanism. Sieving affects particles larger than 5 μm; these particles when collected on the surfaces of fibres form a coherent dust layer known as a filter cake. Although the filter efficiency increases proportionally with the thickness of the cake, the resistance of the filter to airflow increases at an accelerating rate in response to additional particle deposition and narrowing of the pathways. When cake filtration begins, the filter rapidly reaches its terminal designed airflow resistance. In conclusion, a sieve would make a poor air filter, even when containing sub-micrometric openings, since each collected particle closes up a sieve opening so that very soon no air can pass through.

In contrast, filters collect particles from air and gas streams in well-defined ways associated with the dynamic properties of airborne particles. Particles are mainly trapped by filters by one of the following mechanisms.

Usually, a particle entering the flow field surrounding the fibres must follow the curved path of the streamlines so it can pass around this obstacle. However, particles which possess sufficient inertia resist following the curvature of the airstream and come into contact with the fibre because their momentum is relatively higher than that of the conveying gas molecules. Accordingly, inertial impaction works on large and heavy particles suspended in the flow stream. It occurs when large particles are unable to adjust quickly to changes in the flow stream around the fibres. The particle, because of its inertia, impacts a fibre and is captured; this effect is dominant for particle sizes from around 0.5 μm up to 5 μm. After an airborne particle contacts a filter element, retention forces prevent re-entrainment under the influence of the drag of the air. For small particles, the principal retentive force is a surface phenomenon called the Van der Waals force, which is proportional

© Woodhead Publishing Limited, 2011

to the total area of contact and exceeds the re-entrainment force of the air drag.

Direct interception considers particles in the mid-range size that are not large enough to have inertia and not small enough to diffuse within the flow stream. These mid-sized particles follow the flow stream as it bends through the fibre spaces. Particles are intercepted or captured when they touch a fibre. With interception, particles following a line of flow in the airstream close to a fibre within one particle radius adhere to it. Particles that are farther than one particle diameter will not be removed by this process. Interception is independent of flow velocity and is enhanced when the diameter of the collecting fibre or granule approaches the geometric diameter of the particle. The more dense the filtering medium, the higher the probability of particle capture. This effect governs particles in the size range 0.1–1 μm.

Diffusion (also known as Brownian diffusion) operates on the smallest particles. Brownian diffusion is perhaps the most mysterious of the filtering effects since it tends to defy common sense. Very fine particles in the air stream will collide with gas molecules and create a random path through the media. The smaller the particle the longer the particle will zigzag around. This random motion increases the probability of the particle contacting a fibre. This effect is dominant for particles smaller than 0.1 μm. Separation of small particles by diffusion is enhanced by slower velocities through the filter.

The physical basis for particle retention on fibres or small granules was investigated by the Nobel laureate Irving Langmuir.[10] His analysis, indicated that the combined effects of these forces on a particle would be minimal when the particle was 0.3 μm in diameter. When particles with diameters greater or smaller than 0.3 μm were present, they would be removed at higher efficiencies than the test particles.

Since the first applications, some improvements have been made to HEPA filters although the principles of operation remain substantially unchanged. Actually, they are defined as a throwaway, extended-medium, dry-type filter with a minimum particle removal efficiency of 99.95% (later raised to 99.97%) for a 0.3 μm monodisperse particle cloud, a maximum resistance (when clean) 25 mm (1 inch) water gauge when operated at rated airflow capacity and a rigid frame 'casing' extending the full depth of the medium. HEPA filters have proved to be extraordinarily effective, reliable and economical devices for removing radioactive and non-radioactive sub-micrometre-sized particles with a high rate of collection efficiency.

High-efficiency filters are now made of a mixture of glass fibres with carefully graduated diameters that provide the required particle retention efficiency without exceeding the maximum airflow resistance criterion and meet a wide variety of physical and environmental requirements. The most important requirement is resistance to fire, as a fire in a nuclear facility

© Woodhead Publishing Limited, 2011

could mobilize some radioactive materials that must not be discharged to the environment. This implies the use of gaskets, frames and filtering media capable of resisting high temperatures.[11]

A method has been established to extract exhaust filters and insert new filters inside containment bags, without opening them to atmosphere, to reduce the spread of contamination during replacement. Methods have also been established to conduct in-place tests of filter installations. It was discovered as early as the initial installation of HEPA filters that full performance was not always achieved generally owing to incorrect installation, making it fundamental to test filters once installed. The basic procedure for in-place testing is described in detail in Military Standard MIL -STD-282.[12] An aerosol is generated and added to the stream of air reaching the filter and a light-scattering photometer is used to measure aerosol penetration. Traditionally the aerosol used for the test was made of was dioctyl phthalate (DOP); recently, this was substituted by less harmful substances like sodium chloride.

24.2.2 Treatment of liquid radioactive wastes

Liquid radioactive wastes are produced during the whole fuel cycle, from the uranium mines, to burnt and depleted fuel processing and the decommissioning of nuclear facilities. Other liquid radioactive wastes are produced by research laboratories and nuclear medicine facilities. Membrane processes are usually applied to low level liquid wastes. In fact, in order to reduce the radiation exposure of workers, apparatus that processes highly radioactive wastes should be remotely operated and maintained although this requirement is hard to attain with membrane equipment.

Liquid radioactive wastes are mainly processed via pressure-driven membrane processes: reverse osmosis, ultrafiltration, microfiltration and nanofiltration. Principally, these processes use well proven and largely diffused technologies which can remove a wide range of contaminants from large particles to ionic species. Besides the elimination of radioisotopes, a volume reduction of radioactive wastes is obtained so that the storage or disposal requirements can more easily or safely be met together with the production of decontaminated water that can be released into the environment or recycled into the nuclear plant.

When the radioisotopes present in the wastes are in the form of small ions or molecules which can easily pass through ultrafiltration membranes, special treatments have been studied. Small ions or molecules are bonded to other macromolecular compounds or adsorbers to enlarge their size. This process is called ‘complexation’ or ‘seeded ultrafiltration’ and allows the retention capacity of the ultrafiltration process to be increased. It can replace or supplement reverse osmosis as a final treatment of contaminated liquid streams.

© Woodhead Publishing Limited, 2011

Of the other membrane processes for the treatment of LRWs, electrodialysis and membrane distillation have been proposed. In these processes the driving forces of the separation are the electrical potential and the temperature gradient, respectively. The membrane system can be realized as transportable skid, stationary or mobile plants. Skid mounted systems are typically pilot plants capable of treating low liquid wastes feed flow rates. An example of a mobile system is the ECO series used in the Russian Federation.[13] Generally, these systems are not flexible enough to be applied to different sites with different treatment requirements for liquid wastes.

Reverse osmosis

The reverse osmosis characteristic of removing almost all contaminants from a solution permits its application to low level liquid wastes from nuclear fission plants. The purified streams present low activity so that they can be recycled to the power plant or directly discharged to the environment. In practice, reverse osmosis processes are used with conventional previously installed systems (i.e. evaporation or ion exchange) as well as with membrane (microfiltration, ultrafiltration) pretreatments. Thermex™ is a reverse osmosis system which is widely used in different operational schemes. At Chalk River Laboratories it is used to recover boric acid from radioactive wastes, which are concentrated by about 99%.[14] Thermex™ with conventional pretreatment (series of deep bed filters and a bag filter) is applied for decontamination of floor drain wastes,[15] while pretreatment by ultrafiltration is considered in a process for treating liquid wastes from the chemical cleaning of steam generators and heat exchangers at the Bruce power plant (Canada).[16]

Ultrafiltration

Ultrafiltration is capable of separating colloids and high molecular weight organic compounds. This technique is applied for removing radioactive metal ions which have previously been treated with complexing agents in order to form solid particles and less soluble species. Large volume reduction of the liquid wastes and high decontamination factors can be attained: a factor of 1000 for alpha (i.e. actinide wastes) species and 100 for beta and gamma species.[17–20]

Microfiltration and nanofiltration

Microfiltration is applied to concentrate liquid wastes generated in LWR plants with concentration factors of 100. Typical applications are the decontamination of soils and groundwaters via percolation and then leachate separation by microfiltration.[21] Nanofiltration applications have been considered

© Woodhead Publishing Limited, 2011

for treating boric acid wastewaters. In fact, nanofiltration membranes permit boric acid to pass through them while the radioactive particles remain in the retentate.

Electrodialysis

Although electrodialysis is a well-proven technology, there are no large scale applications for processing radioactive wastes. In fact, electrodialysis can attain high concentrations of the ion stream and operates with useful lifetimes but the formation of explosive and/or toxic gases limits its use for liquid radioactive wastes.[22] Other drawbacks are its incapability to remove uncharged particles, the formation of precipitates and the reduction in lifetime when operating at low pH values. Experimental applications are reported in the Russian Federation for liquid waste treatment at a Moscow plant,[23] in nuclear powered ice-breakers and submarines[24,25] and in Japanese laboratories.[26]

Membrane distillation

Temperature is the driving force in membrane distillation; volatile solvents are separated from the solution on a non-wetted microporous membrane. Radionuclides in the form of ions can be separated with large DFs.[27–30] Khayet *et al.*[31] studied direct contact membrane distillation coupled with a nuclear reactor to process simulated and real low and medium radioactive wastes, demonstrating the cost effectiveness of combining radioactive waste processing and water desalination.[31]

24.3 Membranes for nuclear fusion applications

The separation processes applied in the nuclear fusion machines are related to the purification of streams of hydrogen isotopes. The hydrogen isotopes protium (H), deuterium (D) and tritium (T) have atomic masses of 1, 2 and 3, respectively. Depending on the nuclear fusion reaction scheme being considered, different mixtures of the three hydrogen isotopes are used. The main on-going projects on nuclear fusion concern the tokamaks which are toroidal machines where a plasma of hydrogen isotopes is confined magnetically. The easiest and most promising nuclear fusion reaction from the energetic point of view is:

$$D + T \rightarrow {}^{4}He + n \qquad [24.2]$$

where n is a fast neutron (14.07 MeV).

Reaction [24.2] takes place in a toroidal plasma chamber and produces both useful energy and neutrons. In a Li-based blanket surrounding the

© Woodhead Publishing Limited, 2011

plasma chamber (the so called breeder), energy is recovered in the form of heat while neutrons are used to produce tritium. See the simplified scheme in Fig. 24.1. In fact, while deuterium is present in nature and can be separated from heavy water, tritium has to be produced artificially. In fusion plants, tritium is designed to be produced in a breeding blanket where the neutrons produced by the D+T reaction react with lithium according to:

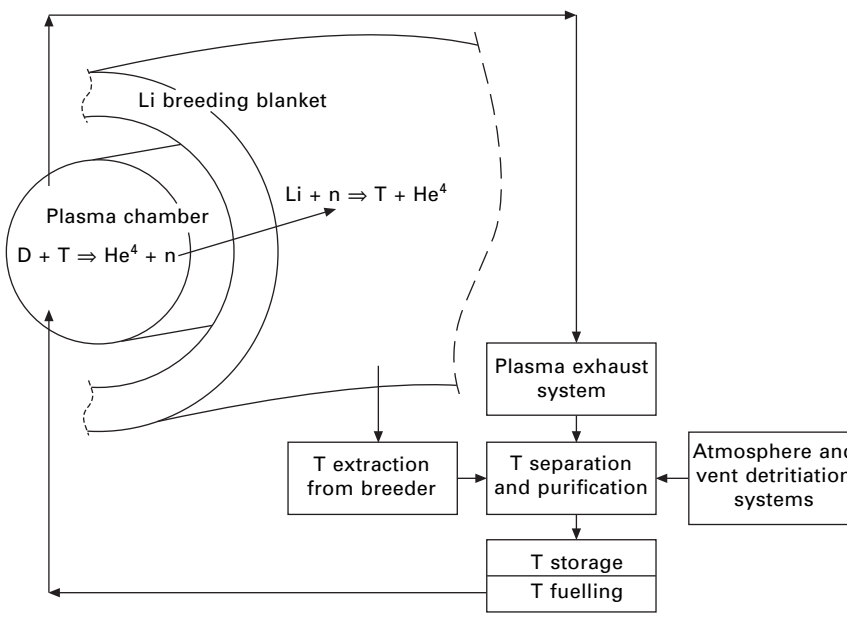
$$n + {}^{7}Li \rightarrow T + {}^{4}He + n' \quad [24.3]$$

$$n' + {}^{6}Li \rightarrow T + {}^{4}He \quad [24.4]$$

where n′ is a thermal (slow) neutron.

The breeding blanket contains a mix of lithium isotopes. Reaction [24.3] uses the fast neutrons coming from reaction [24.2] which is taking place in the plasma chamber to produce, via reaction [24.3], slow neutrons which produce another tritium by reacting with ^{6}Li according to reaction [24.4]. The fusion fuel cycle encompases the totality of the processes aimed at recovering tritium from the breeding blanket, purifying the tritium and then fuelling the fusion chamber in order to sustain reaction [24.2]. The main processes of a tokamak fuel cycle are:[5,32]

- storage and delivery of deuterium and tritium
- fuelling
- tritium extraction from the breeder



24.1 Simplified scheme of a tokamak fuel cycle.

© Woodhead Publishing Limited, 2011

- vacuum pumping from the torus and plasma exhaust treatment
- isotope separation
- water detritiation
- atmosphere and vent detritiation
- tritium analysis and accountability.

Applications of membrane technologies to the fusion fuel cycle are mostly studied for the extraction of tritium from the breeding blanket, plasma exhaust treatment and water detritiation. In particular, tritium and the other hydrogen isotopes are separated by means of Pd-based membranes. In fact, hydrogen isotopes selectively permeate a dense metal lattice. A wide literature has been written about hydrogen/metal interactions.[33–35] The mass transfer mechanism of hydrogen through metals is described by a general expression where the permeation flux is proportional to the hydrogen partial pressure difference and to the inverse of the membrane wall thickness:

$$F = P_i \frac{(p_{\text{up}}^n - p_{\text{down}}^n)A}{t} \qquad [24.5]$$

where F is the hydrogen permeation flow rate (mol s^{-1}), P_i is the hydrogen permeability (mol m^{-1} s^{-1} Pa^{-n}), p_{up} and p_{down} (Pa) are the hydrogen partial pressures at upstream and downstream side, respectively, n is the pressure factor, A is the membrane area (m^2) and t is the membrane thickness (m). When operating at low pressure the pressure factor is 0.5 and Equation [24.5] becomes Sieverts' law:

$$F = P_i \frac{(p_{\text{up}}^{0.5} - p_{\text{down}}^{0.5})A}{t} \qquad [24.6]$$

Among the metals, Pd and its alloys have been extensively studied and a Pd-Ag alloy with 20–25 wt% silver is commercially available for hydrogen separation applications. Several kinds of Pd-based membranes have been studied, mainly, composite membranes obtained by covering a porous (ceramic or metallic) support with thin Pd-based layers[36–40] or dense self-supported membranes.[41] Usually, composite membranes are characterized by higher permeability but incomplete hydrogen selectivity while the dense membranes have a lower permeability associated with complete hydrogen selectivity. Applications in the fusion fuel cycle require complete hydrogen selectivity to ensure very high decontamination factors and, especially, in order to avoid losses of tritium. Furthermore, membranes for fusion applications have to exhibit good stability in order to meet the safety requirements of a nuclear plant. In this sense, only dense Pd-Ag membranes can be applied to the separation processes in the fusion fuel cycle. When permeation of several hydrogen isotopes occurs, the mass transfer process has to take into consideration isotopic competition and Equation [24.6] is modified. For instance, the permeation flow rate of protium is expressed by:[42,43]

© Woodhead Publishing Limited, 2011

$$F_{H_2} = \frac{P_i}{t}\left(\frac{p_{H_{2up}}}{\sqrt{p_{H_{2up}} + p_{D_{2up}} + p_{T_{2up}}}} - \frac{p_{H_{2down}}}{\sqrt{p_{H_{2down}} + p_{D_{2down}} + p_{T_{2down}}}}\right)A \quad [24.7]$$

where p_{H_2}, p_{D_2} and p_{T_2} are the partial pressures of protium, deuterium and tritium, respectively, while the other symbols and units are the same as in Equation [24.5]. Similar expressions can be used for the permeation flow rates of deuterium and tritium.

The ITER project is aimed at realizing the largest tokamak machine which will operate with stable plasma in order to demonstrate the feasibility of fusion energy production. More than 1 kg of the tritium per year is expected to be burnt under normal operations during the final testing phase. Most of the tritium will be provided from outside and only small blanket modules will be used to test different breeder materials (solid ceramics or liquid lithium-lead).

24.3.1 Tritium extraction from breeding blanket

Tritium is designed to be recovered from solid breeding blanket modules in the ITER reactor via a helium purge stream which will operate under oxidizing conditions so that about half the tritium is expected to be in the form tritiated water; see the scheme in Fig. 24.2.[44] The tritiated water is separated from helium into a cryogenic trap (4) and collected in a tank (10) while tritium in gas form is separated by molecular sieve beds (6a and 6b) operating in batch mode. A gas stream containing tritium from the regeneration of the molecular sieve beds is sent into a Pd-based permeator (13) where the hydrogen isotopes are selectively separated from the carrier gas. The permeator works by using Pd-Ag thin wall permeators; operating at 350°C, the required permeation area is obtained using 28 tubes of thickness 50 μm, diameter 10 mm and length 300 mm.

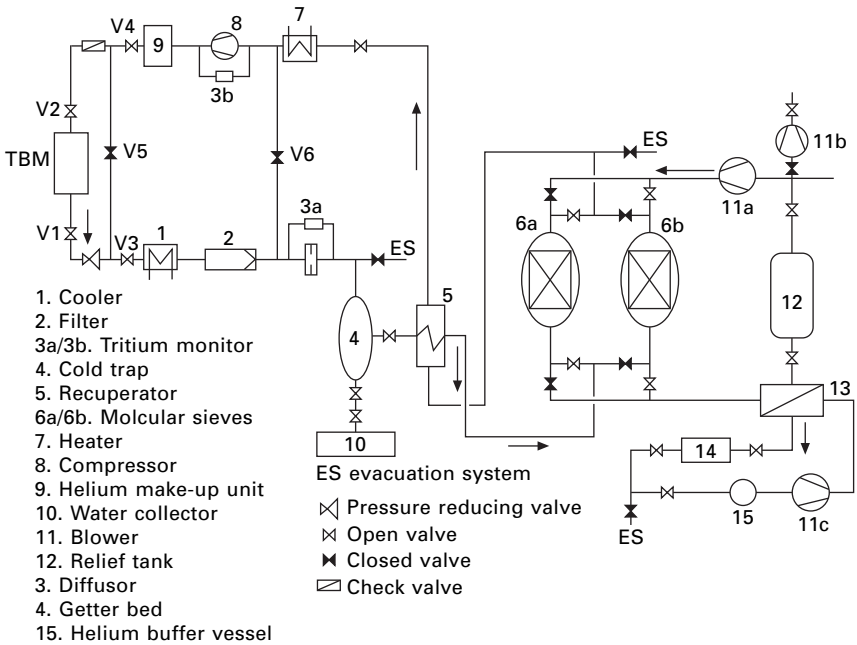
Tritium recovery from the tritiated water separated in the cold trap can be carried out by a membrane reactor where the water gas shift reaction takes place:

$$CO + HTO \Leftrightarrow HT + CO_2 \quad [24.8]$$

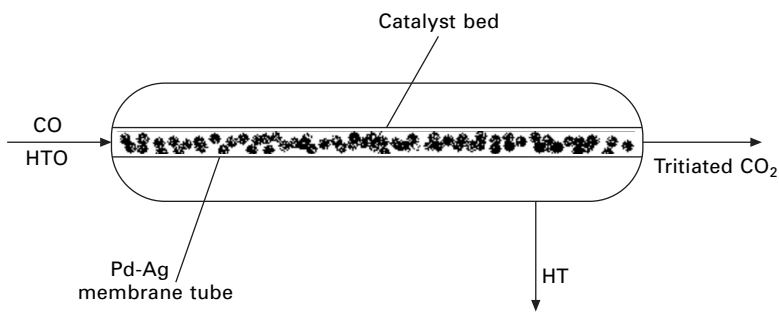
This is an equilibrium reaction which attains almost complete conversion in a Pd-Ag membrane reactor operating at 300–350°C while the reverse reaction takes place at 500°C.[45]

The membrane reactor consists of a dense defect-free Pd-Ag membrane tube filled with catalyst operating a water–gas shift reaction. As shown in Fig. 24.3, tritiated water (HTO) reacts with CO; the hydrogen isotopes (HT)

© Woodhead Publishing Limited, 2011



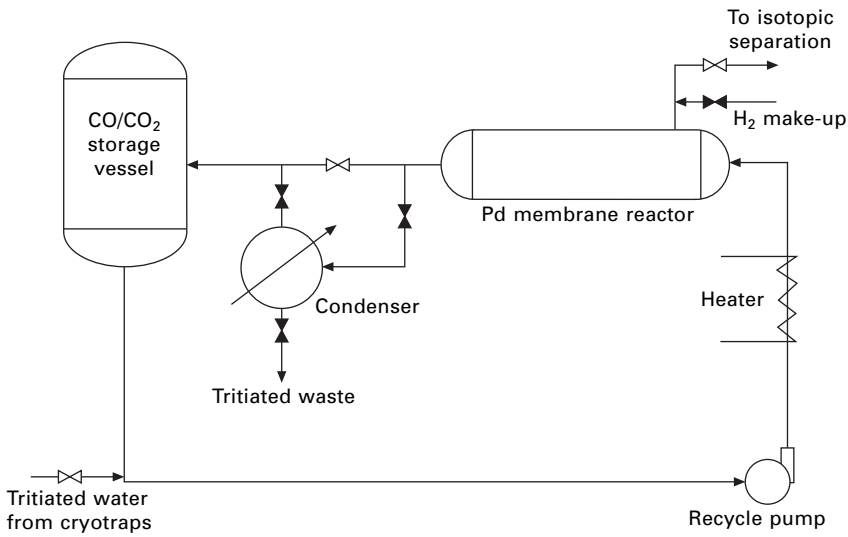
24.2 Tritium extraction from an ITER solid breeding blanket. Reprinted from: Basile A, Gallucci F and Tosti S (2008), 'Synthesis, characterization, and applications of palladium membranes', *Membrane Science and Technology*, **13**, 255–323.



24.3 Scheme of a tubular Pd-base membrane reactor for processing tritiated water via the water–gas shift reaction.

produced by the shift reaction selectively permeate the Pd-Ag permeator and are collected on the shell side of the reactor before proceeding to the isotopic separation units, while CO_2 and residual tritiated water leave the reactor lumen. Although the presence of the Pd-Ag membrane reactor allows operation with high reaction yields, the main drawbacks of this process are the large consumption of CO and the production of tritiated CO_2.

© Woodhead Publishing Limited, 2011



24.4 Closed loop process for processing tritiated water via the water–gas shift reaction. Reprinted from *Chemical Engineering Journal,* Tosti *et al.*[46]

In order to overcome these disadvantages, a closed loop process has been studied;[46] see the scheme in Fig. 24.4. This closed loop process operates in two phases: in the first process (in Fig. 24.4, the white valves are open), tritiated water reacts in a Pd-Ag tubular reactor at 300°C with CO from a storage vessel. Hydrogen isotopes (HT) produced by reaction [24.5] selectively permeate the Pd-Ag tube and are collected on the shell side of the reactor. This operation goes on until all the CO is converted into CO_2, when the second phase of the process is performed. Under these conditions (in Fig. 24.4, the black valves are open) the temperature of the reactor rises to 500°C. Hydrogen (protium) is fed into shell side of the reactor, it permeates the membrane tube and converts CO_2 into CO accordingly to the reverse water–gas shift reaction which also produces water separated by condensation. This step goes on until all the CO_2 is converted into CO. In practice, this loop process avoids the consumption of CO and produces very low activity wastes. In fact, the water produced during the second phase comes from the reaction of protium with CO_2 and, consequently, it may contain very minor tritiated impurities.

24.3.2 Plasma exhaust treatment

In addition to hydrogen isotopes and minor impurities, the gas stream leaving the plasma chamber contains tritiated gases from the interactions of plasma with the first wall. Depending on the characteristics of the first

© Woodhead Publishing Limited, 2011

wall, these tritiated gases can consist of a mixture of water, methane and other hydrocarbons with inert gases (nitrogen, helium). Tritium recovery from plasma exhaust is mainly proposed using Pd-based membranes and membrane reactors.

Willms *et al.*[47] tested a membrane reactor at the Los Alamos National Laboratory for processing fusion fuel impurities such as tritiated water and methane.[47] A Pd-Ag permeator tube 530 mm long, with a wall thickness of 200 μm and an outer diameter of 5 mm was assembled into a stainless steel shell in a finger-like configuration. The annulus between the permeator tube and the reactor shell was filled with a Ni-based catalyst where the water–gas shift reaction and methane steam reforming were performed, obtaining high hydrogen recovery values at 600°C. A Pd-Ag permeator was also studied at Los Alamos National Laboratory for processing mixtures of inert gases containing tritium.[48] A permeator consisting of a U-shaped tube with wall thickness 86 μm was fed with mixtures of hydrogen with Ar or nitrogen while the shell side of the membrane module was vacuum pumped. The tests demonstrated that hydrogen partial pressure equilibrium was achieved by such a permeator by operating in the temperature range 350–450°C.

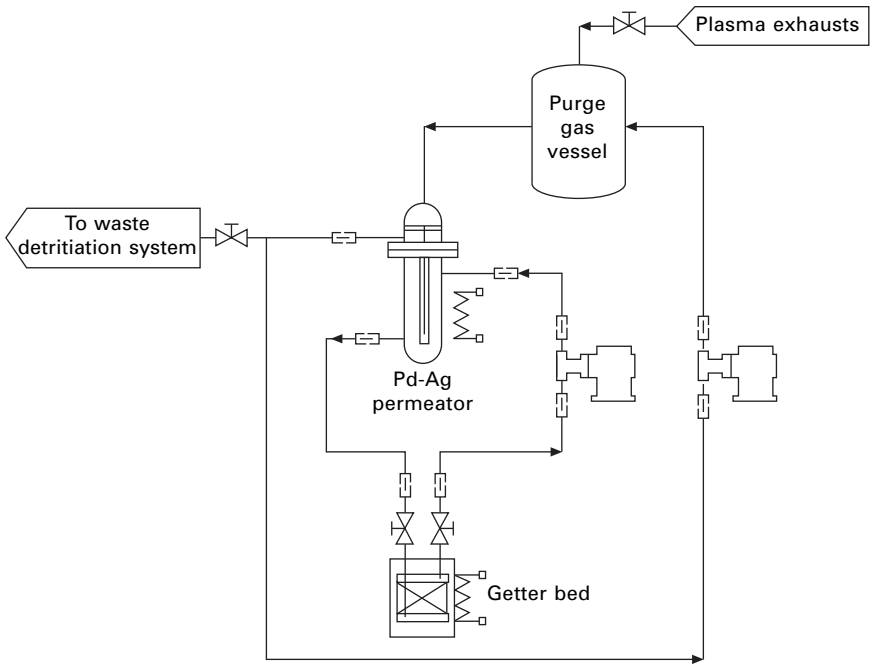
Plasma exhaust system IGNITOR

IGNITOR is an experimental tokamak machine designed to operate in high magnetic fields: the breeding blanket is not present and the fuel cycle is then simplified.[32] In the main tritium process strategy, plasma exhaust is sent into a dense Pd-Ag tube where the hydrogen isotopes are selectively separated from the other gases (helium and tritiated impurities), see the process scheme in Fig. 24.5. The hydrogen isotopes are stored in uranium getter beds and then sent for further processing while the other gases are oxidized so that tritium can easily be collected in the form of tritiated water. The permeator uses a Pd-Ag thin wall tube with a diameter of 20 mm, a length of 200 mm and a wall thickness of 40 μm: under the designed operating conditions, a permeation efficiency of 95% can be reached so that less than 5% of tritium in the form of water is sent to the waste detritiation system.

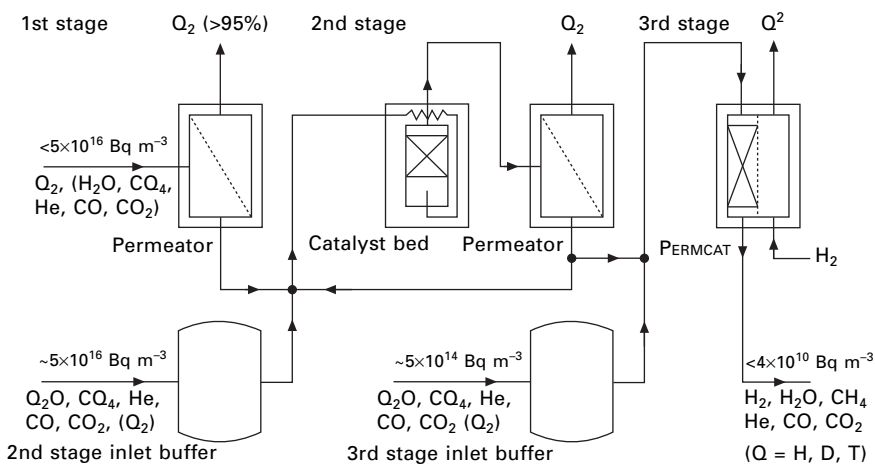
Plasma exhaust system ITER

An important system in the ITER fuel cycle is the plasma exhaust treatment, see Fig. 24.6. It consists of a three-step process for decontaminating gases containing up to 1% tritium in the form of water, hydrocarbons or molecular hydrogen isotopes.[5] The first stage uses a dense defect-free Pd-Ag permeator capable of selectively separating about 95% of the hydrogen isotopes in molecular form (i.e. a decontamination factor of about 20). In the second stage, the gas stream coming from the first permeator is sent to a Ni-based

© Woodhead Publishing Limited, 2011



24.5 Scheme of the IGNITOR plasma exhaust treatment. Reprinted from *Fusion Engineering and Design*, Rizzello and Tosti.[32]



24.6 ITER plasma exhaust process. Q represents protium, denterium or tritium. Reprinted from *Fusion Engineering and Design*, Glugla *et al.*[5]

catalyst where cracking and shift reactions produce molecular tritium which is separated in a second permeator. The final clean-up takes place in a membrane reactor (PERMCAT) capable of completing the detritiation process.[49]

© Woodhead Publishing Limited, 2011

The PERMCAT reactor consists of a dense defect-free Pd-Ag tube and a hydrogenation catalyst bed which promotes isotopic exchange reactions between tritiated and non-tritiated species. For example, a plasma exhaust gas stream may contain tritiated water vapour and methane and the following isotopic exchange reactions can be considered:

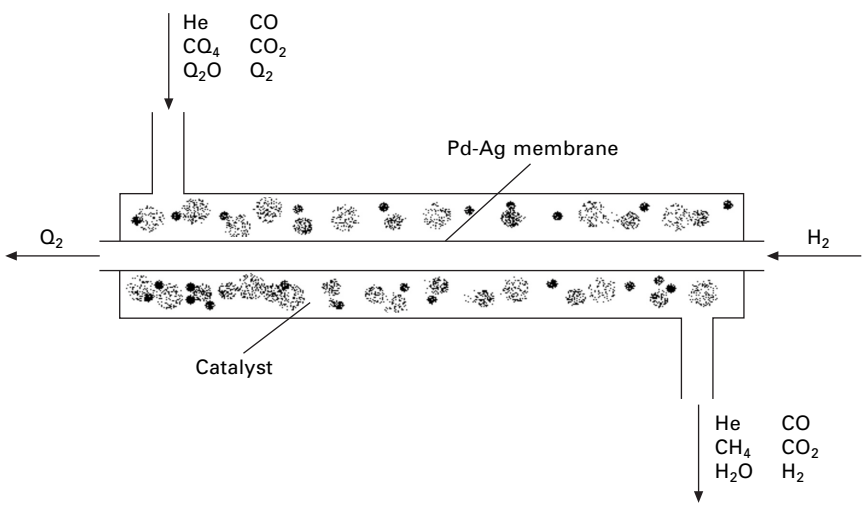
$$2H_2 + CQ_4 \Leftrightarrow CH_4 + 2Q_2 \quad [24.9]$$

$$H_2 + Q_2O \Leftrightarrow H_2O + Q_2 \quad [24.10]$$

where Q can represent one of the three hydrogen isotopes (protium, deuterium, tritium).

The tritiated gas stream from the plasma is fed into the membrane reactor while protium is counter-currently sent to the permeate side. As a consequence of combining the selective permeation of the hydrogen isotopes with reactions [24.9] and [24.10], detritiation of the feed stream occurs. The process is described in the scheme in Fig. 24.7 where the catalyst is located in the annulus between the membrane tube and the reactor shell.

The design of PERMCAT type reactors has to consider the use of long and thin wall permeator tubes in order to attain high decontamination factors. Furthermore, expansion of the Pd alloy consequent to hydrogenation has to be allowed in order to avoid harmful mechanical stress on the membrane tube. Many design configurations of the PERMCAT reactor have been studied: finger-like, use of metal bellows, use of corrugated membrane tube, catalyst in the membrane lumen or on the shell side, and so on. In fact, the operation of the reactor up to temperatures of 300–400°C starting at room temperature involves thermal and hydrogenation cycling with consequent elongation/



24.7 Scheme of PERMCAT reactor (catalyst on shell side).

© Woodhead Publishing Limited, 2011

contraction of the membrane tube. Experimental tests demonstrated that this Pd-Ag elongation can reach the values of 1.5–2%. Moreover, the wall thickness of the membrane tube has to be as thin as possible in order to ensure high hydrogen isotopes permeation fluxes and high decontamination factors. However, the narrow wall thickness of the permeator tubes involves reduced mechanical stiffness which has to be considered in the mechanical design.

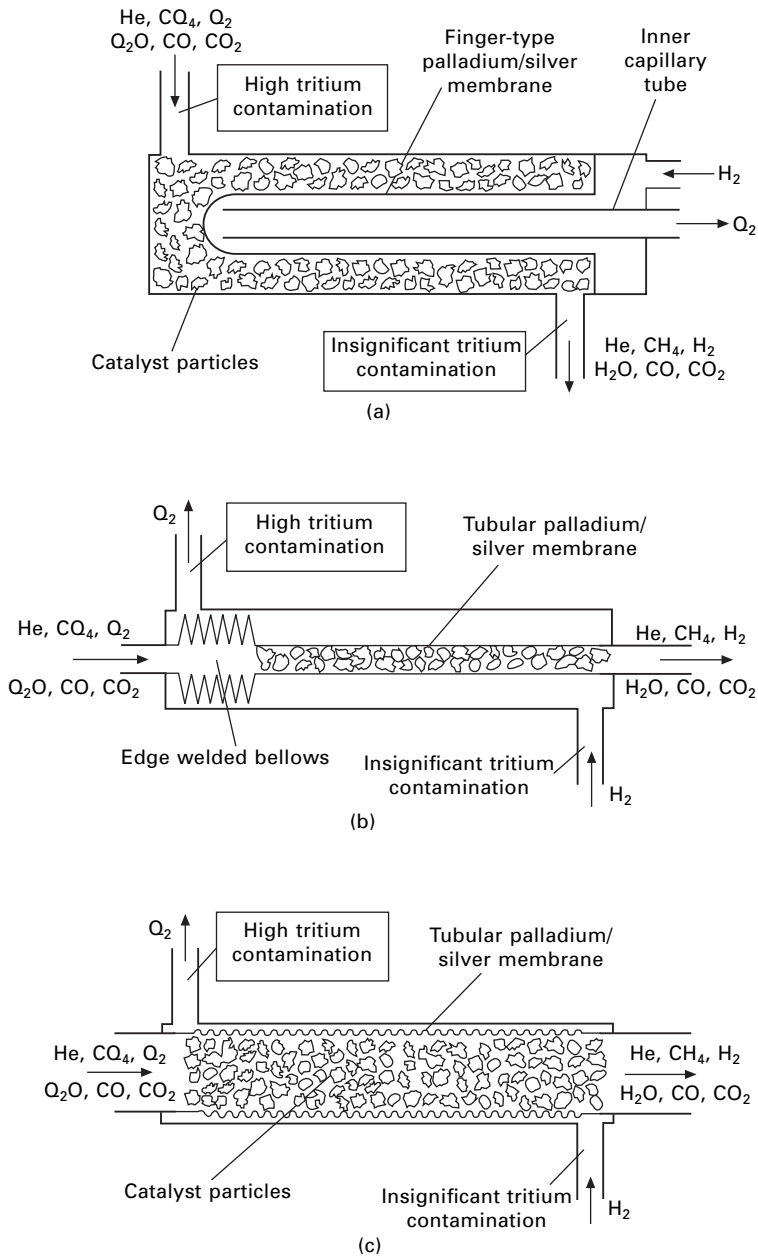
At the Tritium Laboratory of Karlsruhe, Pd-Ag membrane tubes with a wall thickness 100 μm have been developed, see Fig. 24.8.[50] First, a finger-like configuration has been studied: the Pd-Ag tube is fixed to the module only at one end so that the membrane can freely expand/contract under hydrogenation/dehydrogenation of the metal lattice. In a second design, a metal bellow with preliminary preloading was put in series with the membrane in order to compensate this expansion/contraction, while a third design uses a corrugated membrane. All three types of membrane have been tested by demonstrating the achievement of various decontamination factors.

The use of long thin wall permeator tubes permits high decontamination factors to be obtained. In fact, thin wall Pd-Ag tubes are characterized by high hydrogen permeability and complete selectivity. At the ENEA Frascati laboratories, a Pd-Ag tube with a wall thickness of 50 μm has been used to manufacture a PERMCAT-type reactor for separating hydrogen isotopes from plasma exhausts.[50–52] The use of a thinner wall membrane required a special module design aimed at avoiding any mechanical stress of the very weak tube. Among mechanical stresses, the compressive and bending stress is the most harmful for a thin and long tube. Therefore, a special assembly procedure has been studied in order to apply only tension stresses to the membrane tube. As shown in Fig. 24.9,[53] two pre-tensioned stainless steel metal bellows have been inserted between the Pd-Ag tube ends and the module. The experimentally assessed expansion of Pd-Ag is 1.5% which means an elongation of 7.5 mm for the 500 mm long tube. Accordingly, the permeator joined to the metal bellows is made shorter than the module by about 7.5 mm (Fig. 24.9(a)). Then the permeator tube is fixed by welding to the module by applying a traction force T which expands the bellows (Fig. 24.9(b)). During operation, when the hydrogenated Pd alloy tube expands, its elongation is compensated by the bellows so that no compressive stress (the traction force T is zero) is applied to the thin wall tube (Fig. 24.9(c)).

24.4 Conclusions

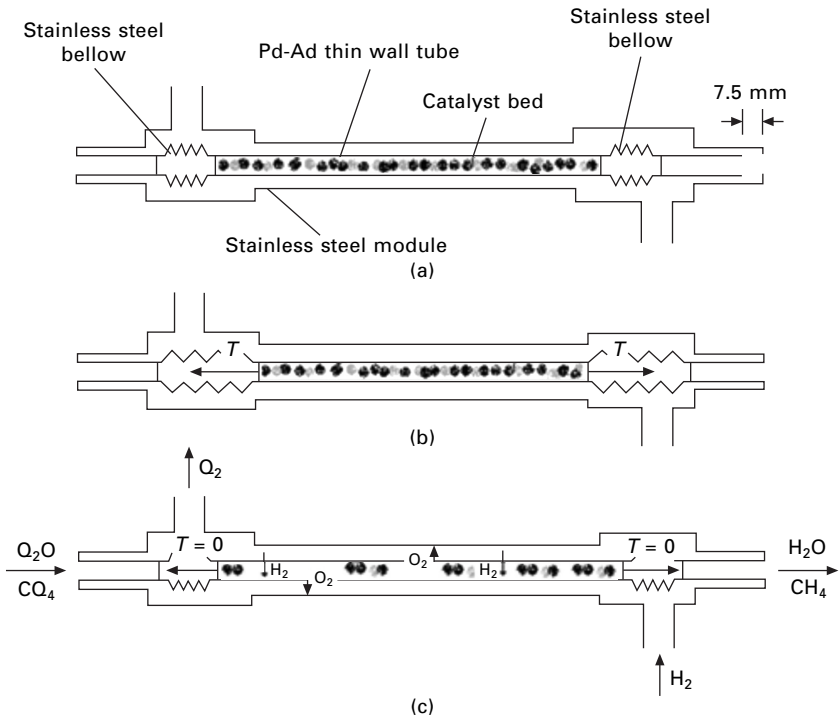
There are many applications of membrane technologies in the fuel cycle of both fission and fusion nuclear reactors. Other important applications concern the treatment of effluents from isotope laboratories and nuclear medicine facilities. In the nuclear field, separations take advantage of characteristics of

© Woodhead Publishing Limited, 2011



24.8 PERMCAT reactors developed at Tritium Laboratory of Karlsruhe. (a) finger-like configuration, catalyst shell side, (b) membrane tube with preloaded bellows, catalyst lumen side and (c) corrugated membrane tube, catalyst lumen side. Reprinted from *Fusion Engineering and Design*, Demange *et al.*[50]

© Woodhead Publishing Limited, 2011



24.9 Assembly procedure and operation scheme of the ENEA Pd-Ag membrane reactor (PERMCAT-kind). Reprinted from *International Journal of Hydrogen Energy,* Tosti.[53]

the membrane processes such as continuous operation, flexibility, reliability, and soon. In nuclear fission, well-known and proven technologies are applied such as reverse osmosis, nanofiltration, ultrafiltration and microfiltration for the treatment of the liquid radioactive wastes, while high efficiency filters ('absolute' or 'HEPA' filters) are widely used for the filtration of air effluents. These technologies are mature and are supported by well-defined process design and computer simulation. The nuclear fusion reactors fuel cycle uses membrane technologies to separate hydrogen isotopes in the gas phase. Pd-based membrane and membrane reactors have been proposed for these applications. Most recent studies have focused on optimizing the design of membrane reactors in order to ensure high hydrogen isotope permeation fluxes and complete and stable selectivity.

24.5 Future trends

Pressure-driven processes will remain in the future the most applied membrane processes in the nuclear fission industry, in particular, for the treatment of

© Woodhead Publishing Limited, 2011

large volumes of radioactive waste. Generally, the application of membranes in nuclear fission uses well-studied and proven technologies already in place in various industries (water treatment, pharmaceutical and fine chemistry plants, micro-electronics, food processing, etc.). Consequently, the majority of future progress and growth could be expected in the integration of membranes into traditional processes in order to attain further process optimization.

In nuclear fusion, Pd-based membrane and membrane reactors are used to separate hydrogen isotopes from gas mixtures. Currently, wide research work has considered the applicability of such dense Pd alloy permeators in processes developed for the fuel cycle in the tokamak projects. Future activities should involve membrane characterization in hot (tritium) long-term tests in order to verify their stability under the operating conditions of the fusion fuel cycle. In particular, complete hydrogen selectivity and the capability of separating high hydrogen permeation fluxes according to the decontamination factors required by the fusion fuel cycle will have to be experimentally verified. Furthermore, new designs of membrane modules will address the main results of experiment: design optimization should take into consideration the membrane module configuration and its heating system.

24.6 References

1 Noble RD and Stern SA (1995), *Membrane Separations Technology – Principles and Applications*, Elsevier Science B.V, Amsterdam.
2 IAEA (2004), *Application of Membrane Technologies for Liquid Radioactive Waste Processing*, IAEA Technical Reports series no 431, November 2004.
3 IAEA (2003), *Combined Methods for Liquid Radioactive Waste Treatment,* IAEA-TECDOC-1336, February 2003.
4 Konishi S, Nishio S and Tobita K (2002), 'The DEMO design team, DEMO plant design beyond ITER', *Fusion Eng Design*, **63–64**, 11–17.
5 Glugla M, Antipenkov A, Beloglazov S, Caldwell-Nichols C, Cristescu IR, Cristescu I, Day C, Doerr L, Girard JP and Tada E (2007), 'The ITER tritium systems', *Fusion Eng Design*, **82**, 472–87.
6 Yoshida H, Konishi S and Naruse Y (1983), 'Preliminary design of a fusion reactor fuel cleanup system by the palladium-alloy membrane method', *Nucl. Technol. Fusion*, **3**, 471–84.
7 Penzhorn RD, Rodriguez RD and Glugla M (1988), 'A catalytic plasma exhaust purification system', *Fusion Technol.*, **14**, 450–5.
8 Glugla M, Perevezentsev A, Niyongabo D, Penzhorn RD, Bell A and Herrmann P (2000), 'A PERMCAT reactor for impurity processing in the JET active gas handling', *Fusion Eng. Design*, **49/50**, 817–23.
9 DOE (2003), *Nuclear Air Cleaning Handbook*, Slawski JW, Fretthold JK, Hargan MR and Zaradaski RW (eds), DOE Handbook DOE-HDBK-1169-2003, US Department of Energy, Washington DC, November 2003.
10 Mott-Smith HM and Langmuir I (1926), 'The theory of collectors in gaseous discharges', *Phys. Rev.*, **28**, 727–63.
11 IAEA (2000), *Fire Safety in the Operation of Nuclear Power Plants*, IAEA Safety

© Woodhead Publishing Limited, 2011

Standards Series, Safety Guide no. NS-G-2.1, International Atomic Energy Agency, Vienna, July 2000.
12 Department of Defense Test Methods Standards (1956), *Protective Clothing, Gas-mask Components and Related Products: performance test method*, MIL-STD-282, 28 May 1956.
13 Karlin YU, Chuikov VY, Adamovich DV, Slastennikov YT, Il'in VA, Sumenko AV, Flit VY, Dmitriev SA and Sobolev IA (2001), 'Reprocessing of liquid radioactive wastes using mobile modular systems', *Atomic Energy*, **90**, 74–9.
14 Philip IP (1993), 'Commercial and research status report for inorganic membranes: Suggested uses in environmental and waste management processes', *Waste Management '93*. Proceedings Conference Tucson, AZ, Waste Management Symposia, Tucson, AZ, 1713–16.
15 Electric Power Research Institute (2001), *Performance Evaluation of Advanced LLW Liquid Processing Technology: Boiling Water Reactor Liquid Processing*, Report 1003063, Electric Power Research Institute, Palo Alto, CA.
16 Evans DW, Garamszeghy M, Solaimani HM and Stott JB (1995), 'Treatment of steam generator chemical cleaning wastes: Development and operation of the Bruce spent solvent treatment facility', in *Proceedings International Chemical Oxidation Association 5th Symposium, Chemical Oxidation: Technologies for the Nineties*, Nashville, Tennessee, February 1995.
17 Chaufer B and Dertani A (1988), 'Removal of metal ions by complexation-ultrafiltration using water-soluble macromolecules: Perspective of application to wastewater treatment', *Nucl. Chem. Waste Manag.*, **8**, 175–87.
18 Commission of the European Communities (1982), *First Annual Progress, Report of the European Community Programme 1980–1984*, Report EVR-8272, Luxembourg, CEC.
19 Roberts RC and Herald WR (1980), *Progress Report on Developments of Ultrafiltration and Inorganic Absorbents*, Report MLM-2684, Miamisburg, OH , Mound Laboratory.
20 Carley-Macauly KW, Gutman RG, Hooper EW, Jenkins JA, Turner AD, Wace PF, Chauvet P, Gauchon JP and Dippel T (1981), 'Radioactive waste: Advanced management methods for medium active liquid wastes EUR 7037', *Radioactive Waste Management*, Harwood, Essex, Vol. 1.
21 Buckley LP, Vijayan S and Wong CF (1993), 'Remediation process technology for ground water', *Proceedings of International Conference on Nuclear Waste Management and Environmental Remediation*, Prague, 1993, American Society of Mechanical Engineers, New York, 33.
22 Garcia RS (1996), *Commercially Available Low-level Radioactive and Mixed Waste Treatment Technologies*, Report DOE/LLW-240, Department of Energy, Washington, DC.
23 Demkin VI, Tubashov YA, Panteleev VI and Karlin YV (1987), 'Cleaning low mineral water by electrodialysis', *Desalination*, **64**, 367–74.
24 Dyers RS, Duffey RB, Penzin R and Sorlie A (1996), 'U.S. and Russian innovative technologies to process low-level liquid radioactive wastes: The Murmansk initiative', *Spectrum '96*, Proceedings of International Conference, Seattle, WA, American Nuclear Society, La Grange Park, IL, 470–4.
25 Dyers RS, Moskowitz PD, Czajkowski CJ, Cowgill M and Sullivan T (1997), 'Environmental security benefits arising from Russian/Norwegian/US cooperation in the high Arctic', *Waste Maragement '97*, Proceedings Conference, Tucson, AZ, WM Symposia, Tucson, AZ.

© Woodhead Publishing Limited, 2011

26 Sugimoto S (1987), 'Removal of radioactive ions from nuclear waste solutions by electrodialysis', *J. Nucl. Sci. Technol.*, **15**, 753–9.
27 Zakrzewska-Tezadel G, Harasimowicz M and Chemielewski AG (1999), 'Concentration of radioactive components in liquid low-level radioactive waste by membrane distillation', *Membr. Sci.*, **163**, 257–64.
28 Andersen SJ, Kjellnder N and Rodesio B (1985), 'Design and field tests of a new membrane distillation process', *Desalination*, **56**, 345.
29 Chemielewski AG, Zakrzewska-Tezadel G, Miljevie NR and Van Hook WA (1995), 'Membrane distillation employed for separation of water isotopic compounds', *Sep. Sci. Technol.*, **307**, 1653–67.
30 Zakrzewska-Trznadel G, Harasimowicz M and Chmielewski AG (2001), 'Membrane processes in nuclear technology application for liquid radioactive waste treatment', *Sep. Purif. Technol.*, **22–23**, 617–25.
31 Khayet M, Mengual JI and Zakrzewska-Trznadel G (2006), 'Direct contact membrane distillation for nuclear desalination, Part II: experiments with radioactive solutions reverse osmosis and membrane distillation', *Int. J. Nucl. Desalination*, **2**, 56–73.
32 Rizzello C and Tosti S (2008), 'Overview of the tritium system of Ignitor, *Fusion Eng. Design*', **83**, 594–600.
33 Shu J, Grandjean BPA, Van Neste A and Kalaguine S (1991), 'Catalytic palladium-based membrane reactors: a review', *Can. J. Chem. Eng.*, **69**, 1036–60.
34 Paglieri SN and Way JD (2002), 'Innovations in palladium membrane research', *Sep Purif. Methods*, **31/1**, 1–169.
35 Willms RS and Konishi S (1991), 'Fuel cleanup systems for fusion fuel processing', *Fusion Engi Design*, **18**, 53–60.
36 Uemiya S (1999), 'State-of-the-art of supported metal membranes for gas separation', *Sep. Purif. Methods*, **28/1**, 51–85.
37 Schramm O and Seidel-Morgenstrern A (1999), 'Comparing porous and dense membranes for the application in membrane reactors', *Chem. Eng. Sci.*, **54**, 1447–53.
38 Wu LQ, Xu N and Shu J (2000), 'Preparation of a palladium composite membrane by an improved electroless plating technique', *Ind. Eng. Chem. Res.*, **93**, 342–8.
39 Tosti S, Bettinali L, Castelli S, Sarto F, Scaglione S and Violante V (2002), 'Sputtered, electroless, and rolled palladium-ceramic membranes', *J. Membr. Sci.*, **196**, 241–9.
40 Shu J, Grandjean BPA, Ghali E and Kaliaguineet S (1993), 'Simultaneous depositing of Pd and Ag on porous stainless steel by electroless plating', *J. Membr. Sci.*, **77**, 181–95.
41 Tosti S and Bettinali L (2004), 'Diffusion Bonding of Pd-Ag membranes', *J. Mater. Sci.*, **39**, 3041–6.
42 Alvani C, Avon J, Casadio S, Futterer M A, Mancini MR, Nannetti CA, Ravel S, Roux N, Sedano L, Violante V, Terlain A, Tourasse M, Tosti S and Zanotti M (1996), 'Effect of purge gas oxidizing potential on tritium release from Li-ceramics and on its permeation through 316L Clads under irradiation (TRINE experiment)', *J. Nucl. Mater*, **233–237**, 1441–5.
43 Shiraishi T, Nishikawa M and Fukumatsu T (1998), 'Permeation of multi-component hydrogen isotopes through nickel', *J. Nucl. Mater*, **254**, 205–14.
44 Boccaccini LV (2005), *Design Description Document for the European Helium Cooled Pebble Bed (HCPB) Test Blanket Modules*, Report Forschungszentrum Karlsruhe, December, 2005.

© Woodhead Publishing Limited, 2011

45 Tosti S, Violante V, Basile A, Chiappetta G, Castelli S, De Francesco M, Scaglione S and Sarto F (2000), 'Catalytic membrane reactors for tritium recovery from tritiated water in the ITER fuel cycle', *Fusion Eng. Design*, **49–50**, 953–8.
46 Tosti S, Basile A, Chiappetta G, Rizzello C and Violante V (2003), 'Pd-Ag membrane reactors for water gas shift reaction', *Chem. Eng. J.*, **93**, 23–30.
47 Willms RS, Wilhelm R and Konishi S (1995), 'Performance of a palladium membrane reactor using an Ni catalyst for fusion fuel impurities processing', *Fusion Eng. Design*, **28**, 397–405.
48 Willms RS, Arzu PR, Honnell KG and Birdsell SA (2000), 'Initial testing of a low pressure permeator for tritium processing', *Fusion Eng. Design*, **49–50**, 963–70.
49 Bornschein B, Glugla M, Gunther K, Lasser R, Le TL, Simon KH and Welte S (2003), 'Tritium tests with a technical PERMCAT for final clean-up of ITER exhaust gases', *Fusion Eng. Design*, **69**, 51–6.
50 Demange D, Welte S and Glugla M (2007), 'Experimental validation of upgraded designs for PERMCAT reactors considering mechanical behavior of Pd/Ag membranes under H_2 atmosphere', *Fusion Eng. Design*, **82**, 2383–9.
51 Tosti S, Bettinali L, Borgognoni F and Murdoch DK (2007), 'Mechanical design of a PERMCAT reactor module', *Fusion Eng. Design*, **82**, 153–61.
52 Tosti S, Bettinali L and Marini F (2005), *Dispositivo per la Rimozione di Trizio da Correnti Gassose*', Italian Patent RM2005U000165.
53 Tosti S (2010), 'Overview of Pd-based membranes for producing pure hydrogen and state of art at ENEA laboratories', *Int. J. Hydrogen Energy*, **35**, 12650–9.

© Woodhead Publishing Limited, 2011

Index

Acaryochloris marina, 626
accumulator, 437
Aciplex, 470
adsorption, 65–6
adsorption selective carbon membranes, 192–3
advanced biofuels production, 361–410
  biocatalyst continuously separated by a membrane system and recirculated into the reaction bank, 374–8
    membrane bioreactor with continuous biocatalyst recirculation, 375
  biocatalyst immobilised onto the membrane surface, 378–82
    effectiveness factor as a function of function of Damköhler number, 381
    schematic representation, 378
    substrate dimensionless concentration as a function of Damköhler number, 380
  continuous stirred tank reactor with biocatalyst immobilised on the membrane surface, 382–4
    schematic of the system under investigation, 383
  hollow fibre membrane bioreactor with recycling of unreacted substrate, 396–402
    dense and spongy layers, 396
    lumen side, 396
    radial Peclet number on degree of conversion in the membrane, 401
    radial Peclet number on dynamic evolution of bioreactor performance index, 401
    schematic representation, 397
  hydrolysis of biomass to produce sugars, 367–71
    bioethanol production, 369–71
  membrane bioreactors, 372–4
  process engineering in second-generation biofuels production, 371–2
  second-generation biofuels, 361–7
    alkaline process, 364
    biodiesel production, 362–5
    enzymatic process, 364
    hydrogen and liquid fuels production from biomass sources, 366
    hydrogen production, 365–7
  single pass membrane bioreactor, 384–95
    dimensionless outlet substrate concentration vs radial Peclet number, 395
    dimensionless substrate concentration profiles and dimensionless product concentration profiles, 393
    hollow fibre membrane bioreactor, 385
    mass transfer analysis, 388–91
    momentum analysis, 387–8
    performance index vs enzyme distribution function, 394
    relevant parameters for bioreactor performance analysis, 392–5
aerosol filtration theory, 772
Air Products PRISM membranes, 341

© Woodhead Publishing Limited, 2011

alkaline water electrolysis, 586–90
alkaline 'gap cell' water electrolysis cell, 587
challenges and perspectives, 587–90
electrochemical performance of conventional alkaline 'membrane cell' water electrolyser, 588
HEM water electrolysis cell, 589
Norsk-Hydro alkaline water electrolyser, 588
PEM water electrolysis cell, 590
performance and technological developments, 587
principles, 586–7
amortisation factor, 95
amphoteric ion exchange membranes, 427, 429–30
anion exchange membranes, 422, 427, 428
anode, 569
Aquivion, 466, 470
aromatic/aliphatic separation, 317–21
asbestos, 575
Ashkelon SWRO desalination plant, 11
AspenPlus, 273
asymmetric Loeb–Sourirajan type membranes, 689
atomic absorption spectroscopy, 68
atomic force microscopy, 57, 736
autothermal reforming, 216
axial Peclet number, 389

β-glucosidase, 367–8
Barber, J., 613
batch concentration configuration, 658
battery, 436
bending strength, 512
biocatalyst immobilisation techniques, 373
biodiesel production, 362–5
bioethanol production, 369–71
biofouling, 667
biofuels
production, 15
steam reforming reaction, 324–9
biomass, 361–2
biomimetic systems
membrane utilisation for alternative hydrogen production, 610–40
challenges, 614–22
general background to concept, 613
solar-to-fuel conversion integrated engineering approach, 635–8
thermodynamic limitations and device design, 622–35
bioreactor, 13
bioreactor productivity, 394
block copolymers, 352
'blue dimer,' 616
Boltzmann distribution, 630
brine electrolysis, 595–8
chlorine-alkali cell room with BL-2.7 membrane cells, 597
performance and technological developments, 597
perspectives, 597–8
principles, 595–6
schematic diagram of cell using a 'gap cell,' 596
Brownian diffusion, 773
brownmillerite, 258–9
Brunauer, Emmett, Teller adsorption isotherm, 74

CACHET project, 206
capillary condensation, 188–9
capillary membrane module, 655
capillary pore diffusion model, 732
carbon capture ready, 267
carbon dioxide capture
conventional systems, 117, 119–23
oxy-fuel combustion capture, 120
post-combustion capture, 121–3
potential of technologies, 122
pre-combustion capture, 120
three different methods, 119
inorganic membranes, 184–207
carbon dioxide separation, 187–97
future trends, 207
industry characteristics, 186
membrane reactors for CO_2 capture, 197–205
number of published papers per year, 187
statistic evaluation of scientific studies of membrane-based processes, 186–7
techno-economic analysis of

© Woodhead Publishing Limited, 2011

the integrated gasification combined cycle and natural combined cycle, 205–7
membrane technology in power plants, 113–59
greenhouse gases distribution, 115
'Keeling curve' of atmospheric CO2 concentrations, 114
predicted global warming, 115
polymeric membranes, 160–80
advantages and limitations, 179
development and applications in power plants, 166–76
flue gas membrane separation, 163–6
future trends, 179–80
number of publications vs year, 162
operation and performance issues and analysis, 176–8
sequestration and environmental problems, 116–17
technology options for CO_2 separation, 118
carbon dioxide capture and storage, 161
carbon molecular sieve membranes, 58–63
micropore size distribution, 62–3
pore size distribution, 63
micropore volume and mean pore width, 61–2
characteristic curves of CO2 at 273K, 62
permeation of probing species, 60–1
adsorption equilibrium values, 61
pore network, 59–60
representation of species/wall interaction, 59
porous structure, 58
surface chemistry, 63
topography and integrity, 60
carbon nanotubes, 313, 621
'carbon neutral,' 365
carbon sequestration, 117
'Carnot efficiency,' 626
cascade, 769
casting solution, 752
catalytic membrane reactors
functional ceramic hollow fibre membranes, 496–538
dual-layer hollow fibres for micro-tubular SOFC, 518–35
membrane development routes and macrostructure control, 501–6
membrane materials issues, 499–501
multifunctional DL-HFMR for methane conversion, 507–18
other ways of improving ceramic dual-layer hollow fibres, 535–7
cation exchange membranes, 422, 424–7
layer-by-layer surface modification, 426
modification with polyelectrolyte multilayers, 426
Nafion chemical structure, 424
swollen SPEEK and Nafion membrane model, 425
synthesis of organic/inorganic composite membranes, 425–6
Celgard, 452
cellobiohydrolase, 367
cells, 436
cellulases, 367–8
cellulose acetate, 343, 689
membrane degradation, 726–7
cellulose membrane, 754
cellulose triacetate, 689–90, 754–5
cellulose triacetate membrane, 9
ceramic hollow fibre membranes
catalytic membrane reactors and solid oxide fuel cells, 496–538
dense ceramic membranes in energy utilisation, 497–8
diagram of development of high quality multifunctional ceramic dual-layer hollow fibre membranes, 499
dual-layer hollow fibres for micro-tubular solid oxide fuel cell, 518–35
anode/electrolyte/cathode layers after anode reduction, 522
bending strength of CGO/Ni-CGO dual-layer hollow fibres, 525
bending strength of Ni-CGO anode hollow fibres, 535
CGO/Ni-CGO dual-layer HF at different co-sintering temperatures, 523

© Woodhead Publishing Limited, 2011

CGO/NiO-CGO dual-layer hollow fibre precursors, 520
composition of spinning suspensions with different amounts of ethanol, 528
compositions of spinning suspensions, 519
control over the macrostructure of Ni-CGO anode, 527
effect of co-sintering temperatures, 522–7
electrical conductivities of Ni-CGO anode layer hollow fibres, 535
electrical conductivity of Ni-CGO hollow fibre anode, 527
gas-tightness of CGO/Ni-CGO dual-layer hollow fibres, 526
N_2 permeation results for Ni-CGO anode hollow fibres, 534
N_2 permeation through Ni-CGO, 524
Ni-CGO anode hollow fibres, 531–2
NiO-CGO precursor hollow fibres with 0-35 wt% ethanol, 530
pore size distributions of the Ni-CGO anode hollow fibres with various macrostructures, 533
single-step fabrication of electrolyte/anode dual-layer hollow fibres, 519–22
sintering curves and sintering rate curves of inner and outer layer materials, 521
viscosity of spinning suspensions prepared with 0-35 wt% ethanol, 529
functional ceramic dual-layer hollow fibre membranes, 498–9
fundamentals of membrane separation, 497
membrane development routes and macrostructure control, 501–6
co-extrusion and co-sintering, 502–5
combined phase-inversion/sintering process, 501–2
control over the macrostructures of dual-layer hollow fibre membranes, 505–6
diagram of sintering of ceramic hollow fibre membranes, 504
macrostructure of dual-layer ceramic hollow fibre membranes, 506
phase inversion based co-extrusion process, 503
membrane materials issues, 499–501
multifunctional dual-layer hollow fibre membrane reactor for methane conversion, 507–18
co-sintering of LSM-YSZ/NiO-YSZ hollow fibre membranes, 510–12
compositions of spinning suspensions and co-extrusion parameters, 508
DL-HFMR for methane conversion, 513, 515–18
dual-layer hollow fibres after co-sintering and after reduction, 514–15
experimental set-up for POM reaction, 515
mechanical properties and macrostructure, 512–13, 514–15
morphology of dual-layer precursor hollow fibre membranes, 509–10
single-step fabrication, 508
sintering curves and sintering rate curves of the dual-layer hollow fibre materials, 510
three-point bending of single-layer and dual-layer hollow fibres, 513
time dependent conversion and CO selectivity of DL-HFMR between 800 and 950 °C, 517
time dependent H_2/CO and oxygen permeation rate of DL-HFMR between 800 and 950°, 518
time dependent performance of DL-HFMR at 750 °C, 516
whole view and cross-section of precursor dual-layer hollow fibre membranes, 509

© Woodhead Publishing Limited, 2011

other ways of improving ceramic dual-layer hollow fibres, 535–7
precursor fibres with varied outer layer thickness for micro-tubular SOFC, 537
precursor fibres with varied outer layer thickness for multifunctional DL-HFMR, 536
ceramic membranes, 305–6, 758
conventional methods of preparation, 305
ceramics, 586
cerates, 550
chemical vapour deposition, 67, 190, 307–8
fabrication technique, 307
chlorination, 729
chlorofluorocarbons, 321
cleaning in-place, 721
'cluster network model,' 471
CO_2 enhanced separation and recovery, 143–4
coal gasification, 268, 271
schematics of IGCC, 270
Colburn factor, 379, 391
comparative analysis, 93
compensation effect, 46
complexation, 774
composite ceramic electrolyte, 441
composite polymer electrolyte membrane, 441, 443–5
concentration polarisation, 655, 662, 664
concentrative internal concentration polarisation, 686
continuous stirred tank membrane bioreactor, 382–4
cost of electricity production, 205
coupling photocatalysis, 757
CPOC platform, 341
cross-flow filtration, 17
cross-linking, 453
cross-permeation phenomena, 602, 603
Cryogenic CO_2 capture, 122–3
cyclohexane, 308

Damköhler number, 379, 380
Danckwerts-type conditions, 390
dead-end filtration, 17
'dead-end' mode, 490
decontamination factor, 771
degree of conversion, 377, 400
dehydrogenation, 308, 310
'demonstration hump,' 241
dense film *see* film
dense inorganic membranes, 193–7
H_2-selective dense inorganic membranes, 197
dense membranes, 218–19, 480–1
dense membranes models, 72–7
metal membranes, 74
polymer membranes, 72–4
sorption and diffusion parameters, 75–7
desalination, 10–11
Desulfomicrobium bactulatum, 615
detailed costs, 95–6
deuterium, 777
'dew-pointing,' 350
diafiltration, 661
dialysis, 681
dialysis-photocatalysis, 762
diavolume coefficient, 661
dibutyl phthalate, 446
dicarboxy phenylhexafluoropropane dianhydride, 314
diffusion, 43–4, 773
types of dependence of diffusion coefficients on penetrant concentration, 43
diffusion coefficient, 582
dilutive internal concentration polarisation, 687
dimensionless axial co-ordinate, 389
dimensionless Michaelis constant, 389
dimensionless radial co-ordinate, 389
dimensionless specific surface, 391
dimethyldiaminobenzo thiophene dioxide thiophenes, 314
dip coating, 306
fabrication technique, 307
direct electrophilic aromatic substitution, 729
direct-methanol fuel cells, 466, 490–1, 492
direct-methanol fuel cells membranes, 469
discount rate, 91
disposable batteries, 415
Donnan exclusion effects, 581
double-skinned cellulose acetate membranes, 691

© Woodhead Publishing Limited, 2011

Dow XUSI 3204.01, 423
drinking water purification, 9–10
dual-layer hollow fibres
co-sintering temperatures on CGO/Ni-CGO electrolyte/anode dual-layer hollow fibres, 522–7
bending strength, 525
CGO/Ni-CGO dual-layer HF at different co-sintering temperatures, 523
electrical conductivity, 526–7
electrical conductivity of Ni-CGO hollow fibre anode, 527
gas-tightness, 526
mechanical strength and gas tightness, 525–6
microstructure, 522–5
N_2 permeation through Ni-CGO, 524
control over the macrostructure of Ni-CGO anode, 527–35
bending strength, 535
composition of spinning suspensions with different amounts of ethanol, 528
effect of morphology on performance, 534–5
electrical conductivities, 535
ethanol on Ni-CGO hollow fibre macrostructure, 528–9
microstructure of Ni-CGO fibres, 529, 532–3
N_2 permeation results, 534
NiO-CGO precursor hollow fibres with 0-35 wt% ethanol, 530
overall view, cross-section and the sponge-like structure region, 531–2
pore size distributions with various macrostructures, 533
viscosity of spinning suspensions prepared with 0-35 wt% ethanol, 529
micro-tubular solid oxide fuel cell, 518–35
nanofiltration, 690
single-step fabrication of electrolyte/anode dual-layer hollow fibres, 519–22
CGO/NiO-CGO dual-layer hollow fibre precursors, 520
compositions of spinning suspensions, 519
micro-tubular HF-SOFC showing anode/electrolyte/cathode layers after anode reduction, 522
sintering curves and sintering rate curves of inner and outer layer materials, 521
Dubinin–Radushkevich equation, 61

economic analysis
membrane processes, 91–6
comparative analysis, 93
detailed costs, 95–6
internal rate of return method, 91–3
total cost ownership methods, 93–5
membrane technology, 142–4
'effective use of catalyst,' 368
effectiveness factor, 380–1, 392, 399
'efficient bioconversion of the substrate,' 368
'electricity-driven chemical reaction' *see* electrolysis
electrochemical energy storage, 413–18
common primary battery systems, 415
historical background, 413–15
ESC systems, 414
volta pile, 414
motivation, 413
primary batteries, 415
redox flow batteries, 416–18
concept, 418
systems and their characteristics, 417
secondary batteries, 415–16
common secondary battery systems, 416
large scale energy storage systems, 416
electrodeposition, 67
electrodialysis, 598–601
performance and technological developments, 599–600
perspectives, 600–1
pilot plant tested at Argonne National Laboratory, 600
principle of reverse electrodialysis, 601
principles, 598–9

© Woodhead Publishing Limited, 2011

schematic diagram of cell, 598
treatment of liquid radioactive wastes, 776
electroless plating, 67–8
electrolyser, 569
electrolysis, 568
electrolysis cell, 569–70
electron paramagnetic resonance, 637
electronegativity, 317
electronprobe microanalysis, 64
Eley–Rideal mechanism, 749
Elsam power station, 161
endoglucanase, 367
energy-dispersive X-ray spectroscopy, 68
energy storage and conversion, 413
enhanced oil recovery, 49
ESPA 3 RO membrane, 722
ethane, 310
ethanol, 369, 528
ethyl cellulose, 314
ethylbenzene, 308
ethylene, 310
ethylene carbonate, 446
exoglucanase, 367
expanded polytetrafluoroethylene, 481

facilitated transport membranes, 136
Faraday's constant, 265
fast gas, 12
fergusonite structure, 554, 557
Fick's first law of diffusion, 72
Fick's law, 24, 163, 219, 221
field energy scanning electron microscopy, 64
film, 26
film theory, 375, 662
filter cake, 772
Fischer–Tropsch, 215, 310
fixed costs, 94–5, 101
Flemion, 470
Flemium, 423
flexible polymer devices, 456
Flory–Huggins equation, 40–1
Flory–Huggins parameter of gas, 348
Flory–Huggins theory, 347
Flory–Huggins thermodynamic model, 319
flue gas, 160
flue gas membrane separation, 163–6
development of CO_2-selective membranes with high permeability and selectivity, 165
fluorinated polyimides, 343–4
fluorite, 262–3
representative oxygen fluxes, 263
forward osmosis, 681
applications, 703–11
ammonia–carbon dioxide forward osmosis desalination process, 709
continuous forward osmosis reverse osmosis bench scale process set-up, 711
desalination, 706–10
electricity generation, 705–6
food processing, 703–5
miscellaneous applications, 710–11
pressure-retarded osmosis power plant, 706
variation of pure water flux with hydraulic pressure, 708
effect of various parameters on transmembrane flux, 695–702
correlation of tomato juice direct osmosis flux with the membrane backing material thickness, 697
direct osmosis flux correlation with osmotic medium viscosity, 702
effect of feed temperature, 700–1
feed and osmotic agent flow rate, 699–700
osmotic agent concentration on transmembrane flux, 699
temperature, draw solution concentration and sucrose feed solution concentration, 696
type and concentration of osmotic agent, 696–9
types of membrane, 696
values of viscosity of used osmotic media, 702
viscosity of osmotic agent solution, 701–2
water flux as function of driving force, 698
industrial applications, 680–712
mechanism, 683–8

© Woodhead Publishing Limited, 2011

direction and magnitude of water flux as a function of applied pressure, 684
water transport from the solution of low osmotic pressure to solution of high osmotic pressure, 685
membrane modules, 692–5
flat membrane module, 692–4
flat membrane module for osmotic membrane distillation and direct osmosis, 693
open Hydrowell spiral wound module, 694
spiral wound membrane module, 694–5
tubular membrane module, 695
water flux as function of driving force, 698
membranes, 688–92
cross-section of CA, polyamide composite and cellulose triacetate membrane, 689
HTI's forward osmosis membrane, 689
water flux through forward osmosis membrane and other reverse osmosis membranes, 691
work carried out by various researchers on forward/direct osmosis for the food processing industries, 704
free volume, 38–9
polycarbonates value with fractional free volume, 39
free-volume network, 57
free volume theory, 32, 38
fuel cells, 465
basic operating principles and types, 466–8
types and their main characteristics, 467
fusion fuel cycle, 777

Galvani, L., 413
gap cell, 570–1
gas permeability, 582, 583
permeability of polymers, 48
polymers, 47–9
problems in membrane gas separation, 48
gas permeation membrane modules
modelling, 144–50
CO_2 permeate concentration, 147
CO_2 permeate concentration vs carbon dioxide recovery fraction, 148
CO_2 recovery ratio *versus* stage cut for 3 flow mode patterns, 146
complete mixing, parallel co-current flow and cross flow, 145
membrane area and CO2 permeate concentration vs carbon dioxide recovery fraction, 149
membrane properties, 147
poly(ethylene)oxide membrane properties, 146
gas permeation unit, 26
gas separation, 11–12
CO2 post-combustion capture, 104–6
Gas Separation Membranes for Zero-Emission Fossil Power Plants Project, 169
gel polymer electrolyte membrane, 441, 445–52
other polymer hosts, 450–2
poly(acrylonitrile), 447
poly(ethylene oxide), 446–7
poly(methyl methacrylate), 448
poly(propylene oxide), 447
poly(vinyl chloride), 448–9
poly(vinylidene fluoride), 449–50
poly(vinylidene fluoride)-hexafluoro propylene, 450
PVC/PMMA blend, 449
separators, 452
geological sequestration, 116
Gibbs free energy, 572, 630
glass transition temperature, 37–8
global permeability, 79
glycocalyx, 667
Grotthuss mechanism, 546–7

Hagan–Poiseuille equation, 732
halogenated hydrocarbon separation, 321–2
Henry's Law, 24, 40–1, 73, 163, 220, 348, 602
heterogeneous ion-exchange membrane, 569

© Woodhead Publishing Limited, 2011

heterogeneous photocatalysis
basic principles, 747–9
graphic models of the Eley–Rideal and Langmuir–Hinshelwood mechanisms, 750
relative positions of the valence and conduction bands and energies of two redox pairs, 749
scheme of photocatalytic process, 748
future trends, 765
membrane materials developments and design, 749–59
commercial membranes used in UV irradiation tests, 756
concentrations of phenol and benzene during transport test, 754
inorganic membranes, 758–9
main characteristics of the membranes employed, 758
polymeric membranes, 751–8
membrane reactor configurations, 760–1
pressurised membrane reactors, 760
submerged (depressured) membrane photoreactors, 760–1
membranes for photocatalysis in water and wastewater treatment, 746–65
operations performance issues and analysis, 759–64
degradation process in photocatalytic membrane reactor, 763
dialysis-photocatalysis, 762
flat sheet vs submerged continuous PMRs for Gemfibrozil degradation, 764
fouling control, 759–60
membrane distillation-photocatalysis, 761
one-step synthesis and separation of phenol, 763–4
pervaporation-photocatalysis, 762
pharmaceutical compounds degradation, 762–3
photocatalytic membrane contactors, 761
scheme of the PMR, 764
high temperature polymeric proton conductors, 605
high temperature proton conductors, 580
hollow fibre membrane, 723–4
hollow fibre membrane bioreactor with recycling of unreacted substrate, 396–402
hollow fibre membrane module, 655
homogeneous ion-exchange membrane, 569
hybrid-flow filtration, 17–18
hydrocarbon fuel
membrane technology for processing and separation, 295–338
hydrocarbons removal from liquid steams, 317–22
materials, development and design, 297–314
nanotechnologies, 322–9
olefins and paraffins separation, 314–17
‘hydrogen economy,’ 308
hydrogen permeation flow rate, 778
hydrogen peroxide, 478
hydrogen production, 365–7
background to concept, 613
challenges, 614–22
active site and synthetic analogue of H-cluster, 619
assembling mixed conducting membrane, 621–2
electron transfer to and from the electrodes, 614
enzyme stability, 614–15
functional mimics of [Ni-Fe]-hydrogenase, 620
mimicking natural enzymes, 616–20
molecular structures for hydrogenase mimicking, 620
Nafion/CNT membranes for fuel cell application, 622
progress in mimicking the PSII system, 618
stromal surface of PSII dimer complex, 615
membrane electrolysers, 568–609
advantages and limitations of current membrane materials, 601–4

© Woodhead Publishing Limited, 2011

application and integration of electrolyser systems, 586–601
basic principles of electrolysis, 571–4
future trends, 605
gap cells, zero-gap cells and solid polymer electrolyte cells, 569–71
historical review of electrolysis, 568–9
membrane materials, 574–80
membrane performance, 580–6
membranes, 569
membrane utilisation for alternative production in biomimetic systems, 610–40
biomimetic H_2-production device concept, 611
PSII dimeric core of *T.elongates,* 612
proton conducting ceramic membranes, 541–62
conductivity and hydrogen flux, 549–55
operation principle and demands on materials, 542–5
protons and proton conductance in ceramics, 545–9
structure of selected materials, 555–61
solar-to-fuel conversion integrated engineering approach, 635–8, 639
engineering guidelines for design of biomimetic H_2 production nanodevices, 639
nanodesign of electrodes, catalysts and antennae, 638
rates of key transfer phenomena for artificial nanodevice design, 636
thermodynamic limitations and device design, 622–35
artificial photosynthesis, 630–5
basic electrochemistry and energetics in photosynthetic solar cell, 633
biomass yields, specific power and solar energy conversion efficiency, 624
chlorophyll range of adsorption vs overall spectrum of solar energy, 629
cofactors in light harvesting, 625
cyclic operation of water splitting to oxygen in natural photosynthesis, 626
energy use in biological steady state, 624
extreme diversity of antenna systems, 631
improved light absorption range of *Acaryochloris marina,* 629
natural photosynthesis, 623–30
reasonable efficiency targets for solar energy conversion into fuels, 633
redox potentials of photosystem I vs photosystem II, 627–8
solar energy-driven photoelectrochemistry for H_2 production, 623
structural limit of natural photosynthesis, 632
'hydrogen recirculation' mode, 490
hydrogenase, 617
Hyflon, 605
hypochlorite, 724, 727

inductively coupled plasma optical emission spectroscopy, 68
industrial applications
membranes for forward osmosis, 680–712, 688–92
applications of forward osmosis, 703–11
effect of various parameters on transmembrane flux, 695–702
forward osmosis mechanism, 683–8
forward osmosis membrane modules, 692–5
Innovative CO2 capture, 143
inorganic membranes, 135–6, 758–9
carbon dioxide separation, 187–97
dense inorganic membranes, 193–7
porous inorganic membranes, 188–93
membrane reactors for CO_2 capture, 197–205

© Woodhead Publishing Limited, 2011

methane steam reforming membrane reactors, 201–5
water–gas shift membrane reactors, 197–201
pre-combustion carbon dioxide capture, 184–207
future trends, 207
preparation and application, 304–11
application to hydrocarbon streams treatment, 308
ceramic membranes, 305–6
chemical vapour deposition, 307–8
dehydrogenation, 308, 310
dip coating, 306
metal membranes, 308
methane steam reforming, 310–11
oxidative coupling of methane, 310
pressing, 306
slip casting, 306
tape casting, 306
synthesis gas processing, 214–54
application and integration in industry, 230–7
future trends, 241–4
membrane materials and development, 223–30
membrane modules, 237–41
membrane operation principles, 218–23
techno-economic analysis of the integrated gasification combined cycle and natural combined cycle, 205–7
performance and economic analysis of MemWGS and MemREF, 206
'insertion/de-insertion,' 438
integrated gasification combined cycle, 198, 205–7, 268, 271
'intercalation/de-intercalation,' 438
Intergovernmental Panel on Climate Change, 114, 116
internal rate of return method, 91–3
net present value vs discount rate, 99
International Energy Agency, 142
'intrinsic' proton conductors, 475
ion exchange membranes, 413–30
electrochemical energy storage, 413–18
common primary battery systems, 415
ESC systems, 414
historical background, 413–15
motivation, 413
primary batteries, 415
redox flow batteries, 416–18
secondary batteries, 415–16
volta pile, 414
membranes, 423–30
amphoteric ion exchange membranes, 427, 429–30
anion exchange membranes, 427, 428
cation exchange membranes, 424–7
vanadium redox flow batteries, 418–23
chemical stability, 422–3
critical issues, 420
crossover, 420–1
ion conductivity, 421–2
phenomena which need to be overcome in order to develop suitable membrane, 420
principles, 418–20
ionic conductivity, 580–1
ionomers, 470
isobutane, 308
isotopes, 769

K142, 423
Kadanwari system, 341
'Keeling curve,' 114
Knüdsen diffusion, 219–20
Knudsen flow, 11
Knudsen flux, 78
Knudsen mechanism, 188
Kröger–vink notation, 545
Kvaerner systems, 355
Kyoto Protocol, 114–15

Langmuir, I., 773
Langmuir affinity constant, 349
Langmuir sorption capacity constant, 41–2
Langmuir-type model, 222
Langmuir–Hinshelwood mechanism, 749
lanthanum strontium manganite, 604
layered double hydroxides, 241

© Woodhead Publishing Limited, 2011

Le Châtelier's principle, 232–4
Lennard-Jones parameters, 32–3
Li-metal battery, 439
Li polymer batteries, 440
lignocellulosic biomass, 367, 370
liquid radioactive wastes, 770
  treatment, 774–6
    electrodialysis, 776
    membrane distillation, 776
    microfiltration and nanofiltration, 775–6
    reverse osmosis, 775
    ultrafiltration, 775
lithium batteries, 435–56
  future trends, 455–6
  polymer electrolyte membranes, 441–55
    architecture of a linear polymer and of a network, 453
    common polymers used as matrices and their chemical formulae, 446
    composite and nanocomposite polymer electrolyte membranes, 443–5
    cross-linked polymer electrolyte membranes, 453–5
    gel polymer electrolyte membranes, 445–52
    solid polymer electrolyte membranes, 441–3
  types and basic operating principles, 436–40
    schematic representation of common lithium-ion battery, 440
    specific capacity and standard potential of the alkali metals series, 437
lithium ion battery, 439
Li_2ZrO_3 membrane, 193
low temperature proton conductors, 579
low water-content polymeric proton conductors, 605

mass transfer coefficient, 375, 664
mass transport mechanism, 71–9
  dense membranes models, 72–7
    metal membranes, 74
    permeate pressure representation, 76
    polymer membranes, 72–4
    sorption and diffusion parameters, 75–7
  models for porous membranes, 77–9
Matrimid, 127
Maxwell–Stefan equation, 220
Meares' equation, 46
Medal membrane system, 341
melt extrusion, 484–6
MemBrain, 169, 172
membrane bioreactors, 13–16, 374
  cellulosic ethanol production, 16
  enzyme immobilised in the membrane, 15
  wastewater treatment, 14
membrane catalysis
  petrochemical industry, 323–4
    number of publications vs time, 324
membrane configurations, 16–17
  hollow fibres membrane, 17
  spiral module, 16
  tubular membrane, 16–17
membrane crystallisation, 102
membrane degradation
  assessment tools, 732–6
    chemical/structural characteristics, 734–5
    classification, 732
    filtration characteristics, 732–3
    mechanical and thermomechanical characteristics, 735
    morphological characteristics, 735–6
    surface characteristics, 733–4
  control strategies, 737–8
  future trends, 739
  identification and monitoring, 731–7
  mechanisms, 724–31
    aromatic polyamide, 728–30
    cellulose acetate, 726–7
    common membrane materials, 726
    modified reaction scheme for PES degradation, 727
    polyethersulphone, 727–8
    polysulphone, 728
    polyvinylidene fluoride, 725–6
    polyvinylpyrrolidone, 730–1

© Woodhead Publishing Limited, 2011

membrane failure and operational issues, 720–4
disinfection of reverse osmosis systems, 722–3
hollow fibre membrane failure, 723–4
membrane integrity, 724
permeate flux restoration, 721–2
TFC membrane and RO membrane, 723
membrane integrity monitoring tests, 737
reaction scheme
PA degradation by chlorination of amide nitrogen, 730
PA degradation by electrophilic substitution, 729
PES degradation, 727
PS degradation by radical oxidation mechanism, 728
PVP by ring-opening mechanism, 731
water and wastewater treatment, 718–39
polymer materials and module design, 719–20
polymeric materials used for membrane fabrication, 719
membrane distillation, 102
treatment of liquid radioactive wastes, 776
membrane distillation-photocatalysis, 761
membrane electrode assembly, 475
membrane electrolysers
advantages and limitations of current membrane materials, 601–4
hydrogen content in the anodic oxygen-water vapour mixture, 604
oxide-ion conductors, 603–4
polymeric hydroxyl-ion conductors, 603
polymeric proton conductors, 601–3
application and integration of electrolyser systems, 586–601
alkaline water electrolysis, 586–90
brine electrolysis, 595–8
electrodialysis, 598–601
proton exchange membrane water electrolysis, 590–2
solid oxide water electrolysis, 592–5
basic principles of electrolysis, 571–4
cell efficiency, 573–4
kinetics, 573
thermodynamics, 571–3
voltage-current density polarisation curve during water electrolysis, 573
future trends
high temperature polymeric proton conductors, 605
low water-content polymeric proton conductors, 605
new oxide-ion conducting ceramics, 605
gap cells, zero-gap cells and solid polymer electrolyte cells, 569–71
two dimensional schematic diagrams, 570
hydrogen production, 568–609
historical review of electrolysis, 568–9
membranes, 569
membrane materials, 574–80
electrical energy, total energy and heat input plots associated with water splitting reaction, 575
Gierke model of nanoclusters in perfluorosulphonic acid materials, 577
high temperature proton conductors, 580
low temperature proton conductors, 579
materials used as diaphragms with liquid electrolytes, 575–6
non-organic proton conductors, 578–9, 580
oxide-ion conductors, 579
polymeric hydroxyl-ion conductors, 577–8
polymeric proton conductors, 576–7
quaternary ammonium polysulphone structural unit, 578

© Woodhead Publishing Limited, 2011

structural unit of Nafion, 576
membrane performance, 580–6
cell used to measuring temperature profiles in the PEM cell, 584
gas permeability, 582, 583
H_2 and O_2 permeability and diffusion coefficients in fully hydrated Nafion 117, 583
hydrogen and oxygen permeability of Nafion 117 with temperature and water content, 583
ionic conductivity, 580–1
ionic conductivity of some oxygen-ion conductors, 581
mechanical properties, 584, 586
Nafion main mechanical properties, 586
permselectivity, 581–2
temperature profile measured in 0.42 mm thick PEM cell, 585
thermal conductivity, 582, 584, 585
thermal conductivity of Nafion at different humidity ratios, 585
membrane fouling, 655, 666, 688
membrane integrity, 724, 737
membrane modules, 139–41, 237–41
advantages and disadvantages, 140
capillary fibres membranes, 139–41
comparison, 141
hollow fibres membranes, 139
scale-up and module design, 238–41
catalyst placement, 240
sealing, 237–8
spiral wound modules, 141
syngas processing, 230–2
process flow diagram of membrane unit incorporation, 230
process flow diagram of three membrane unit incorporation, 232
process flow diagram of two membrane unit incorporation, 231
membrane permeability, 733
membrane processes, 4–18
application of reverse osmosis, 8–11
carbon dioxide sequestration, 137–8
upper bound correlation for CO_2/N_2 separation, 138
case studies, 96–106
cost comparisons of gas separation membrane for CO_2, 106
detailed capital costs for CO_2 gas separation membrane, 107
gas separation membrane in CO2 post-combustion capture, 104–6
integrated fermentation, ultrafiltration and pervaporation systems, 97–9
integrated membrane systems for seawater desalination, 101–3
IRR from net present value vs discount rate, 99
ultrafiltration as pretreatment in sea water reverse osmosis, 100–1
economic analysis in industrial applications, 90–107
case studies, 96–106
economic analysis, 91–6
future trends, 106–7
gas separation, 11–12
membrane bioreactors, 13–16
membrane configurations, 16–17
microfiltration, 5–6
operating membrane systems, 17–18
reverse osmosis and nanofiltration, 7–8
science and engineering, 3–18
future trends, 18
ultrafiltration, 6–7
membrane reactor, 197–8, 222–3, 507
membrane rejection, 657
membrane sealing, 277–8
membrane technology
hydrocarbon fuel processing and separation, 295–338
hydrocarbons removal from liquid steams, 317–22
aromatic/aliphatic separation, 317–21
halogenated hydrocarbon separation, 321–2
inorganic membrane performance, 321
integrated pilot plant for aromatics separation, 319
permeability and selectivity values, 318
polymeric membrane performance, 320

© Woodhead Publishing Limited, 2011

materials, development and design, 297–314
functional materials for hydrocarbon separation, 297
inorganic membrane preparation and application, 304–11
mixed-gas n-C_4H_{10}/CH_4 selectivity vs n-C_4H_{10} permeability, 312
molecular design and structure-property relationships, 297–304
organic-inorganic nanocomposite membranes, 311–14
TEM images of hydrophilic fumed silica, 312
nanotechnologies, 322–9
hydrogen production via membrane reactor technology, 324–9
membrane catalysis in petrochemical industry, 323–4
olefins and paraffins separation, 314–17
facilitated transport membranes, 314–17
facilitated transport scheme, 316
propylene/propane selectivity vs propylene permeability, 315
membrane volume flux, 663
membranes, 26, 497
characterisation for energy and environmental applications, 56–89
mass transport characterisation, 71–9
polymer and carbon molecular sieve membranes, 56–63
zeolite and mixed matrix membranes, 64–71
forward osmosis in industrial applications, 680–712
applications of forward osmosis, 703–11
effect of various parameters on transmembrane flux, 695–702
forward osmosis mechanism, 683–8
forward osmosis membrane modules, 692–5
membranes for forward osmosis, 688–92
industrial microfiltration and ultrafiltration, 647–77
advantages and limitations, 676
applications, 668–73
basic principles of microfiltration and ultrafiltration, 648–9
concentration polarisation and membrane fouling, 661–8
integrated processes, 673–6
membrane materials and membrane preparation technology, 649–52
module configuration and process design, 652–61
nuclear power applications, 769–88
future trends, 787–8
nuclear fission applications, 771–6
nuclear fusion applications, 776–85
photocatalysis in water and wastewater treatment, 746–65
basic principles of heterogeneous photocatalysis, 747–9
future trends, 765
membrane materials developments and design for photocatalysis, 749–59
operations performance issues and analysis, 759–64
utilisation for alternative hydrogen production in biomimetic systems, 610–40
challenges, 614–22
general background to concept, 613
solar-to-fuel conversion integrated engineering approach, 635–8
thermodynamic limitations and device design, 622–35
membranologists, 161
metal membranes, 74, 308
advantages and limitations of preparation methods, 309–10
metalloenzymes, 616
methane steam reforming, 310–11
methane steam reforming membrane reactors, 201–5
evaluation of membrane stability, 204
membrane reactor stability test, 205
natural gas fired power plant with membrane reformer for CO_2, 203

© Woodhead Publishing Limited, 2011

methyldiethanolamine, 341
Meyer, T., 616
Michaelis–Menten equation, 368, 376, 379, 383, 386
micro-tubular solid oxide fuel cell, 518–35
co-sintering temperatures on CGO/Ni-CGO electrolyte/anode dual-layer hollow fibres, 522–7
bending strength of CGO/Ni-CGO dual-layer hollow fibres, 525
CGO/Ni-CGO dual-layer HF at different co-sintering temperatures, 523
electrical conductivity, 526–7
electrical conductivity of Ni-CGO hollow fibre anode, 527
gas-tightness of CGO/Ni-CGO dual-layer hollow fibres, 526
mechanical strength and gas tightness, 525–6
microstructure, 522–5
N_2 permeation through Ni-CGO, 524
single-step fabrication of electrolyte/anode dual-layer hollow fibres, 519–22
CGO/NiO-CGO dual-layer hollow fibre precursors, 520
compositions of spinning suspensions, 519
micro-tubular HF-SOFC showing anode/electrolyte/cathode layers after anode reduction, 522
sintering curves and sintering rate curves of inner and outer layer materials, 521
microfiltration, 4, 5–6, 647–77
advantages and limitations, 676
applications, 668–70, 671
industrial applications, 671
basic principles, 648–9
common materials for microfiltration and ultrafiltration membrane preparation, 650
concentration polarisation and membrane fouling, 661–8
clarification of kiwifruit juice, 665
concentration polarisation phenomenon according to film model, 663
future trends, 676–7
integrated processes, 673–6
integrated membrane process in milk processing, 675
membrane materials and membrane preparation technology, 649–52
module configuration and process design, 652–61
basic configurations of membrane modules, 653–4
commercially available membrane modules, 656
different operation modes, 659–60
schematic representation of process, 657
treatment of liquid radioactive wastes, 775–6
Military Standard MIL -STD-282, 774
Millipore water purification systems, 7
mineral sequestration, 117
minimum return rate, 91
mixed ionic electronic conducting materials, 256–7
integrated gasification combined cycle plants, 273–5
power consumption of a MIEC membrane air separation unit, 275
oxyfuel coal power plants, 271–3
power consumption of MIEC membrane air separation unit, 274
schematic of MIEC membrane air separation unit, 272
mixed matrix membranes, 69–71, 136
metal-organic framework membranes, 70
polymers with intrinsic microporosity membranes, 70–1
modified Poiseuille equation, 387
molecular mass, 38
molecular sieve carbon membranes, 192–3
molecular sieving, 189
molecular sieving silica membranes, 225–8
H_2 permanence of MSS-based membranes, 227

© Woodhead Publishing Limited, 2011

molecular weight cut off, 733
molecular weight cut-off, 4, 6
monoethanolamine, 121
multi-layer diffusion, 189
multifunctional dual-layer hollow fibre membrane reactor
  co-sintering of LSM-YSZ/NiO-YSZ hollow fibre membranes, 510–12
    sintering curves and sintering rate curves materials, 510
  DL-HFMR for methane conversion, 513, 515–18
    experimental set-up for POM reaction, 515
    time dependent conversion and CO selectivity of DL-HFMR between 800 and 950 °C, 517
    time dependent H_2/CO and oxygen permeation rate of DL-HFMR between 800 and 950 °C, 518
    time dependent performance of DL-HFMR at 750 °C, 516
  mechanical properties and macrostructure, 512–13, 514–15
    dual-layer hollow fibres after co-sintering and after reduction, 514–15
    three-point bending of single-layer and dual-layer hollow fibres, 513
  methane conversion, 507–18
  morphology of dual-layer precursor hollow fibre membranes, 509–10
    whole view and cross-section of precursor, 509
  single-step fabrication, 508
    compositions of spinning suspensions and co-extrusion parameters, 508
multistage recycle operation, 661

N-chlorination, 729
N-methyl-2-pyrrolidone (NMP), 528
Nafion, 422, 423, 470, 477, 492, 576, 621
  chemical structure, 424
nanofiltration, 7–8
  treatment of liquid radioactive wastes, 775–6
nanofiltration membrane, 757
Nanoglowa, 144
nanotechnologies, 322–9
  hydrogen production via membrane reactor technology, 324–9
    operative conditions and performances, 327–8
    selected production technologies from biomass, 325
  membrane catalysis in petrochemical industry, 323–4
    number of publications vs time, 323, 324
natural gas combined cycle, 198, 205–7
natural gas processing
  membrane materials, development and design, 341–6
    cellulose acetate chemical structure, 343
    CO_2/CH_4 permeability correlation, 343
    cost comparison for various technologies for removal of 8% nitrogen from subquality natural gas, 345
    polyimides and fluorinated polyimides, 344
    upper bound correlation for CO_2/CH_4 separation, 342
  operation and performance issues and analysis, 346–9
    CO_2 permeability of 6FDA-TMPDA, 348
    Fickian diffusion coefficient for 6FDA-TMPDA, 347
  polymeric membranes, 339–60
    advantages and limitations, 351–2
    application and integration into natural gas operations, 349–51
    flow scheme required to bring 200 psia natural gas streams with 8-15% nitrogen content, 351
    future trends, 352–5
    gas flow rate and CO_2 concentration in the gas on the choice of CO_2 removal technology, 353

© Woodhead Publishing Limited, 2011

guide to selection of natural gas sweetening processes, 354
operations, 340–1
standard specifications for pipeline delivery, 340
net present value, 91
NEWater, 10
NF PES 10, 757
nickel aluminide film, 308
niobates
conductivity and hydrogen flux, 554
structure, 557–8
Ni–Ru complexes, 620
Nitrosep, 345
non-organic proton conductors, 578–9, 580
NTR 7410, 757
nuclear fission applications, 771–6
future trends, 787–8
high efficiency particulate air filters applications, 771–6
filtration mechanisms, 772–5
treatment of liquid radioactive wastes, 774–6
electrodialysis, 776
membrane distillation, 776
microfiltration and nanofiltration, 775–6
reverse osmosis, 775
ultrafiltration, 775
nuclear fusion applications, 776–85
future trends, 787–8
plasma exhaust treatment, 781–5
assembly procedure and operation scheme of ENEA Pd-Ag membrane reactor, 787
ITER plasma exhaust process represents protium, denterium or tritium, 783
PERMCAT reactors developed at Tritium Laboratory of Karisruhe, 786
plasma exhaust system IGNITOR, 782
plasma exhaust system ITER, 782
scheme of PERMCAT reactor, 784
scheme of the IGNITOR plasma exhaust treatment, 783
simplified scheme of tokamak fuel cycle, 777
tritium extraction from breeding blanket, 779–81
closed loop process for processing tritiated water, 781
ITER solid breeding blanket, 780
scheme of tubular Pd-base membrane reactor for processing tritiated water, 780
nuclear power applications, 769–88
future trends, 787–8
nuclear fission applications, 771–6
high efficiency particulate air filters applications, 771–4
treatment of liquid radioactive wastes, 774–6
nuclear fusion applications, 776–85
plasma exhaust treatment, 781–5
tritium extraction from breeding blanket, 779–81
nylon-6, 132
nylon-12, 132

ocean sequestration, 116–17
octadecyltrichlorosilane, 313
olefins, 314–17
operating membrane systems, 17–18
cross-flow filtration, 17
dead-end filtration, 17
hybrid-flow filtration, 17–18
submerged filtration, 18
Orton rearrangement, 729
osmosis, 680, 683
oxidants, 724
oxidative coupling of methane, 310
oxide-ion conducting ceramics, 605
oxide-ion conductors, 579, 603–4
oxy-fuel combustion capture, 120
oxyfuel coal combustion, 268
schematics of a power plant, 269
oxygen transport membranes, 238, 275–82
application and integration in power plants, 267–75
coal gasification, 268, 271
oxyfuel coal combustion, 268
process integration, 271–5
dense ceramic membranes for power plant applications, 255–85
application and integration in power plants, 267–75

© Woodhead Publishing Limited, 2011

future trends, 282–4
materials, development and design, 256–63
chemical and structural modification, 260–3
materials, 257–60
perovskite and fluorite structures, 258
Ruddlesden–Popper structure, 259
schematic representation of oxygen separation systems, 257
membrane geometries, 275–7
oxygen production vs membrane packing density, 276
membrane sealing, 277–8
gas leakage rate, 280
joining and sealing assembly containing a LSCF membrane disk, 279
principles of oxygen membrane separation, 263–7
bulk diffusion, 265–6
surface kinetic, 266–7
structural and chemical stability, 278–82
thermal expansion coefficient, 280

Pailin field, 341
Palladium-based membranes, 67–9
membrane characterisation, 68–9
paper-based energy storage, 456
paraffins, 314–17
partial oxidation, 215–16
Pebax, 168–9, 171
Peclet number, 239
perfluorosulphonic acid, 470
performance index, 392, 394, 400
PERMCAT reactor, 771, 784
developed at Tritium Laboratory of Karisruhe, 786
scheme, 784
permeability, 38, 43–5, 497
see also gas permeability
types of dependence of the permeability coefficients on penetrant concentration, 45
permeability coefficient, 25
permeance, 497
'permeate,' 198
permeate flux restoration, 721–2
permeation ratio, 387
permporosimetry, 66–7
pattern for membrane defect assessment, 67
permselectivity, 221, 581–2
perovskites, 260–2
conductivity and hydrogen flux, 549–50, 551–2
representative oxygen fluxes, 261
schematic of O_2 permeation, 264
structure, 555–6
unit cell, 556
pervaporation-photocatalysis, 762
phase inversion, 652
phenyltrichlorosilane, 313
phosphates
conductivity and hydrogen flux, 553
photo-induced polymerisation, 454
photocatalysis, 749
photocatalyst, 749
photocatalytic membrane contactors, 761
photocatalytic membrane reactors, 746, 764
physical vapour deposition, 68
plasma exhaust treatment, 781–5
assembly procedure and operation scheme of ENEA Pd-Ag membrane reactor, 787
IGNITOR, 782
ITER, 782
ITER plasma exhaust process represents protium, denterium or tritium, 783
PERMCAT reactors developed at Tritium Laboratory of Karisruhe, 786
scheme of PERMCAT reactor, 784
scheme of the IGNITOR plasma exhaust treatment, 783
plasticisation, 302–4, 346–7
Poiseuille equation, 78
Polaris Membrane, 168, 171
poly ether ether ketone, 344
poly(4-methyl-2-pentyne), 311
poly(1-phenyl-1-propyne), 301
poly(1-trimethylsilyl-1-propyne), 299
hydrcarbon permeability values, 300
hydrocarbon permeability and selectivity, 301

© Woodhead Publishing Limited, 2011

hydrocarbon permeability and strategies to control ageing, 299, 301–2
increasing permeability vs rising critical temperature, 300
poly(acrylonitrile) (PAN), 447, 755
Polyactive, 171, 178
polyamide
degradation by chlorination of amide nitrogen, 730
degradation by electrophilic substitution, 729
membrane degradation, 728–30
polybenImidazole nanofiltration hollow fibre membranes, 691
polydimethylsiloxane, 302–3, 314
permeability values, 302
polyelectrolyte membranes, 420
polyethersulphone, 755
degradation reaction scheme, 727
membrane degradation, 727–8
modified reaction scheme for degradation, 727
poly(etherurea), 133
poly(etherurethane), 133
poly(ethylene-*co*-vinyl acetate), 311
poly(ethylene glycol), 446
poly(ethylene oxide), 132, 302, 314, 441, 446–7
polyimides, 343–4
polymer electrolyte membrane, 571
polymer membranes, 57–8
polymeric hydroxyl-ion conductors, 577–8, 603
polymeric membrane, 115, 751–8
carbon dioxide capture in power plants, 113–59
cost considerations and membrane technology, 142–4
future trends, 150–1
gas permeation membrane modules modelling, 144–50
membrane modules, 139–41
membrane processes performance, 137–8
power plant integration design, 141–2
degradation in water and wastewater treatment, 718–39
future trends, 739
identification and monitoring of membrane degradation, 731–7
materials degradation control strategies, 737–8
membrane degradation mechanism, 724–31
membrane failure and operational issues, 720–4
polymer materials and module design, 719–20
gas and vapour separation, 22–54
basic principles and definition, 23–32
objects of membrane gas separation, 47–9
temperature on transport parameters, 45–7
hydrocarbon separations, 297–304
decay in PTMSP hydrocarbon permeability, 299, 301–2
membrane structures in prevaporation and gas separation, 298
poly(1-trimethylsilyl-1-propyne), 299
solubility-selective membranes and plasticisation, 302–4
membrane technology review, 124–36
distribution of *o*/*p*-toluensulphonamide in 80PTMEO/PA12, 134–5
facilitated transport membranes, 136
gas permeability data for dense films incorporating polycarbonates, 129
gas permeability data for dense films incorporating polyimides, 128
gas permeability data for dense films incorporating polysulphone, 130
gas permeability data for polyarylate dense films, 129
gas permeability data for polypyrrole dense films, 129
glassy to rubbery membranes, 125–35
inorganic membranes, 135–6

© Woodhead Publishing Limited, 2011

mixed matrix membranes, 136
penetrant mobility, 126
published papers per year, 124
Pure gas separation properties of H2/CO2, 130
pure gas vs mixed gas separation, 131
scheme of different morphologies in gas separation, 126
membrane use in separation and sequestration, 123–4
natural gas processing, 339–60
advantages and limitations, 351–2
application and integration into natural gas operations, 349–51
future trends, 352–5
membrane materials, development and design, 341–6
operation and performance issues and analysis, 346–9
operations, 340–1
operation and performance issues and analysis, 176–8
CO_2 concentration in flue gas, 177–8
membrane configuration, 178
membrane performance, 178
pressure ratio, 176–7
post-combustion carbon dioxide capture, 160–80
advantages and limitations, 179
development and applications in power plants, 166–76
flue gas membrane separation, 163–6
future trends, 179–80
number of publications vs year, 162
pressure on transport parameters, 39–45
diffusion, 43–4
permeability, 43–5
sorption, 39–43
properties of penetrants and polymers, 32–9
diffusion coefficients in polymers with a cross section of diffusants, 33
effects of gas parameters, 32–7
polymer parameter, 37–9
polymeric proton conductors, 576–7, 601–3
polymers with intrinsic microporosity, 352
poly(methyl methacrylate), 448
poly(phenylene oxide), 314
polypropylene, 296, 752–3
poly(propylene oxide), 447
poly(siloxysilsesquioxane), 301
polysulphone, 314, 345, 755
degradation by radical oxidation mechanism, 728
membrane degradation, 728
poly(tert-butyl acetylene), 301
polytetrafluoroethylene, 355, 752
poly(tetramethyleneoxide), 132
poly(vinyl chloride), 448–9
polyvinylidene fluoride, 449–50, 751–2
membrane degradation, 725–6
poly(vinylidene fluoride)-hexafluoro propylene, 450
polyvinylpyrrolidone
membrane degradation, 730–1
ring-opening mechanism, 731
porous inorganic membranes, 188–93
capillary condensation, 188–9
CO_2-selective porous inorganic membranes, 194
H_2-selective porous inorganic membranes, 192
Knudsen mechanism, 188
molecular sieving, 189
multi-layer diffusion, 189
schematic representation, 189
surface diffusion, 188
porous membranes, 219–21
models, 77–9
porous stainless steel, 195
positron annihilation lifetime spectroscopy, 57–8, 64
post-combustion capture, 121–3
power law, 222
power plants
integration design, 141–2
membrane development and applications, 166–76
AFM phase image of Polyactive membrane, 172
CO_2 concentrations in different gas streams, 166

© Woodhead Publishing Limited, 2011

CO_2/N_2 selectivity as a function of CO_2 permeability, 170
effect of membrane properties on cost, 169
photographic image of Polyactive thin film membrane, 174
Polyactive membrane performance, 175
SEM image and performance of different polymeric membranes, 173
pre-combustion capture, 120
pressing, 306
fabrication techniques, 307
pressure swing adsorption, 185–6, 256
pressurised membrane reactors, 760
primary batteries, 415
PRISM, 345
process integration, 271–5, 372
MIEC membranes in integrated gasification combined cycle plants, 273–5
power consumption of a MIEC membrane air separation unit, 275
MIEC membranes in oxyfuel coal power plants, 271–3
power consumption of MIEC membrane air separation unit, 274
schematic of MIEC membrane air separation unit, 272
process optimisation, 372
process synthesis, 371
propylene carbonate, 446
proton conducting ceramic membranes
chemical stability of selected materials, 559–61
high stability of Ln_6WO_{12} in a wet H_2 atmosphere at elevated temperature, 561
conductivity and hydrogen flux, 549–55
perovskites, 549–50, 551–2
phosphates, 553
pyrochlores, 553–4
rare earth ortho-niobates and tantalates, 554
rare earth oxides, 550, 553
rare earth tungstates, 554–5
selected literature examples of ceramic membrane materials for H_2 separation, 551–2
operation principle and demands on materials, 542–5
membrane as a solid electrolyte in PC-SOFC, 542
membrane as H_2 sensor, 544–5
membrane for hydrogen separation, 542–3
membrane for steam electrolysis, 543–4
PC-SOFC and H_2-separating membranes operating principle, 543
protons and proton conductance in ceramics, 545–9
defect generation by aliovalent doping, 547–9
proton defects formation in oxide ceramics and defect equilibrium, 545–6
proton defects stability in oxide ceramics, 546
proton diffusion mechanics, 546–7
proton mobility, proton conductivity and H_2 flux, 547
solid oxide fuel cells and hydrogen processing, 541–62
structure of proton-conducting materials, 555–9
La_6WO_{12} in the [001] orientation, 559
mineral scheelite unit cell, 558
niobates and tantalates, 557–8
perovskite structure unit cell, 556
perovskites, 555–6
pyrochlore structure unit cell, 557
pyrochlores, 556–7
tungstates, 558–9
proton conducting solid oxide fuel cells, 542
proton diffusion mechanisms, 546–7
proton exchange membrane, 571
water electrolysis, 590–2
challenges and perspectives, 592
PEM water electrolyser powered by a set of photovoltaic panels, 592
performance and technological developments, 591–2

© Woodhead Publishing Limited, 2011

polarisation curves measured on PEM cell, 591
principles, 590–1
proton exchange membranes, 466
proton exchange membranes fuel cells, 465–95
advantages and limitations, 491
Aquivion E87-05 extruded membrane
H_2 crossover as function of RH for, 478
H_2 crossover as function of temperature, 477
basic operating principles and types of fuel cells, 466–8
fuel cell types and their main characteristics, 467
future trends, 491–2
integration and application, 489–91
schematic of H_2 PEM fuel cell system, 489
membrane design, 480–4
cast Nafion membranes, extruded Aquivion membranes and experimental ePTFE-based reinforced membrane, 481
membrane fabrication process, 484–7
fabrication process for extruded PFSA ionomer PEM, 485
membrane materials, 470–80
crystallinity as a function of equivalent weight, 473
main structures of commercially available PFSA ionomers, 471
MEA resistance as function of inlet RH under open-circuit voltage, 476
membrane conductivity at 80° as function of RH for SSC ionomers, 474
water uptake of different ionomers, 472
water uptake of SSC and LSC PFSA extruded membranes, 472
weight uptake from boiling water, 473
membrane materials, design and fabrication processes, 468–87
defining membranes, 468–70
stress at break of extruded Aquivion membranes, 469
membrane performance in operation, 487–9
durability test at 120 °C and 35% inlet RH, 488
open-circuit voltage hold durability test
experimental Aquivion reinforced membrane, 482
extruded Aquivion E79-03S membrane, 479
working principle of H_2/O_2 PEM FC, 467
PVC/PMMA blend, 449
pyrochlores
conductivity and hydrogen flux, 553–4
structure, 556–7
unit cell, 557

quaternary-ammonium polysulphone, 578

radial Peclet number, 389, 395
radial velocity profile, 387
Rankine cycle, 268
rare earth oxides
conductivity and hydrogen flux, 550, 553
rare earth tungstates
conductivity and hydrogen flux, 554–5
reaction rate, 379
Reactive Black 5 dye, 752
rechargeable battery, 437
recovery rate, 657
redox flow batteries, 416–18
concept, 418
systems and their characteristics, 417
reinforced membranes, 480–1
'retentate,' 198
retro-fitting, 121
reverse osmosis, 7–8
application, 8–11
desalination, 10–11
drinking water purification, 9–10
water and wastewater purification, 10
schematic of desalination, 9
systems disinfection, 722–3
treatment of liquid radioactive wastes, 775
reverse osmosis membrane, 722–3, 723
Reynolds number, 375, 391, 664

© Woodhead Publishing Limited, 2011

Richardson's equation, 74
RO water purification units, 10
Robeson's bound, 352, 353
Ruddlesden–Popper compounds, 259, 594

Saccharomyces cerevisiae, 371
scanning electron microscopy, 56, 64, 68
'scavengers,' 479
scheelite structure, 554, 557
Schmidt number, 375, 391, 664
Schroeder paradox, 471
sea water reverse osmosis, 11
  ultrafiltration pretreatment, 100–1
seawater desalination
  integrated membrane systems, 101–3
second-generation biofuels, 361–7
  alkaline process, 364
  biodiesel production, 362–5
  enzymatic process, 364
  hydrogen and liquid fuels production from biomass sources, 366
  hydrogen production, 365–7
secondary batteries, 415–16, 437
  common secondary battery systems, 416
  large scale energy storage systems, 416
seeded ultrafiltration, 774
selectivity, 27–32, 497
  correlation of solubility coefficients with critical temperature of penetrants in rubbery and glassy polymers, 35
  diffusion, solubility and permeability coefficients with critical volume of penetrants, 36–7
  permeability–selectivity diagram for the $C4H_{10}/CH_4$ pair in polymers, 31
  permeability–selectivity diagram for the H_2/CH_4 pair in polymersplain, 30
  permeability–selectivity diagram for the He/N_2 pair in polymers, 29
  permeability–selectivity diagram for the O_2/N_2 pair in polymers, 30
selectivity value, 468
Selemion, 423
semiconductor catalyst, 746
'separation membranes,' 468
separation processes, 23–32
  definition, 26–7
  historical background, 23
  selectivity, 27–32
  solution-diffusion mechanism, 24–6
separators, 452
Separex membrane system, 341
Sherwood number, 375, 391, 664–5
short-side-chain perfluorosulphonic acid (SSC PFSA) ionomer membranes, 466, 470
Sieverts' law, 74, 219, 778
silica membranes, 190–1
silicone rubber polymers, 345
Singapore Water Reclamation Study, 10
single component permeation, 60, 64–5
single pass membrane bioreactor, 384–95
  dimensionless outlet substrate concentration vs radial Peclet number, 395
  dimensionless substrate concentration profiles and dimensionless product concentration profiles, 393
  hollow fibre membrane bioreactor, 385
  mass transfer analysis, 388–91
  momentum analysis, 387–8
    dense and spongy layers, 387–8
  performance index vs enzyme distribution function, 394
  relevant parameters for bioreactor performance analysis, 392–5
single-pass processing, 658
Skyllas-Kazacos, M., 418
slip casting, 306
  fabrication techniques, 307
slip suspension, 651
solar cell equation, 634
sol–gel method, 191, 226
solid oxide fuel cells, 238, 258
  functional ceramic hollow fibre membranes, 496–538
    dual-layer hollow fibres for micro-tubular SOFC, 518–35
    membrane development routes and macrostructure control, 501–6
    membrane materials issues, 499–501

© Woodhead Publishing Limited, 2011

multifunctional DL-HFMR for methane conversion, 507–18
other ways of improving ceramic dual-layer hollow fibres, 535–7
proton conducting ceramic membranes, 541–62
conductivity and hydrogen flux, 549–55
operation principle and demands on materials, 542–5
protons and proton conductance in ceramics, 545–9
structure of selected materials, 555–61
solid oxide water electrolysis, 592–5
cell used for co-electrolysis of CO_2 and water vapour, 594
challenges and perspectives, 594–5
HT water electrolysis cell, 593
performance and technological developments, 594
principles, 592–4
prototype high temperature water electrolysis stack from CERAMATEC company, 595
solid polymer electrolyte cell, 571
solid polymer electrolyte membrane, 441–3
solubility-selective membranes, 302–4
diffusivity and solubility selectivity values for pure methane and a mixed *n*-butane/methane, 304
permeability values of PEO and PDMS, 302
selectivity values of methane and mixed n-butane/methane, 304
solute rejection, 648
solution–diffusion mechanism, 23, 24–6
Daynes-Barrer method, 25
gas transport scheme, 24
solvent casting, 486–7
sorption, 39–43
dual mode sorption model isotherm in glassy polymers, 42
typical shapes of sorption isotherms, 40
sorption enhanced water gas shift reactor, 241
SPE water electrolysis, 571
specific membrane surface, 379
spinning suspension, 502
spiral wound membrane module, 655–6
squared Thiele modulus, 389, 393
standard hydrogen electrode, 438
steam reforming, 215
storage battery, 437
submerged (depressured) membrane photoreactors, 760–1
submerged filtration, 18
sugar cane, 370
sulphonated poly(ether ether ketone), 424
surface diffusion, 188
surface roughness, 736
surface smoothness, 736
syngas, 310
production, 215–18
process flow diagram of methane reforming plant, 217
syngas processing
application and integration in industry, 230–7
clean up train for IGCC process with WGS membrane reactor, 235
integration as single WGS and as high and low temperature WGS membrane reactor, 233
membrane modules, 230–2
membrane reactor modules, 232–4
process integration limitations and opportunities, 235–7
inorganic membranes, 214–54
future trends, 241–4
technology maturity vs total investment, 242
membrane materials and development, 223–30
cobalt silica membranes coated onto various substrates, 224
dense metal membranes, 224–5
H_2 flux through different Pd-based membranes, 225
molecular sieving silica membranes, 225–8
zeolite membranes, 228–30
membrane modules, 237–41
scale-up and module design, 238–41
sealing, 237–8

© Woodhead Publishing Limited, 2011

membrane operation principles, 218–23
dense membranes, 218–19
membrane operation, 221–2
membrane reactor operation, 222–3
porous membranes, 219–21
synthetic tree, 163

tantalates
conductivity and hydrogen flux, 554
structure, 557–8
tape casting, 306
fabrication techniques, 307
terrestrial sequestration, 117
tetramethylphenyldiamine, 314
thermal conductivity, 582, 584, 585
thermal expansion coefficient, 280–1
Thermex, 775
thermodynamics electrolysis voltage, 572
thermogravimetric analysis, 735
Thermosynechococcus elongatus, 614
thin film composite, 722
membrane, 692, 723
time lag, 75
titania multilayer membrane, 758–9
tokamak fuel cycle, 777–8
Tokyo Gas, 244
tolerance factor, 257
total annual cost, 95
total cost ownership methods, 93–5
membrane replacement and cleaning, 94
other fixed costs, 94–5
other variable costs, 95
pretreatment, 94
various pretreatments of SWRO, 101
track-etching, 652
trans-membrane pressure, 373, 386
transesterification, 362–3
transition state theory, 31
transmission electron microscopy, 56
trimethyl phenylene diamine, 314
tritium, 777
extraction from breeding blanket, 779–81
closed loop process for processing tritiated water, 781
ITER solid breeding blanket, 780
scheme of tubular Pd-base membrane reactor for processing tritiated water, 780
tubular membrane module, 654
tungstates, 558–9

ultrafiltration, 4, 6–7, 647–77
advantages and limitations, 676
applications, 670–3, 674
industrial applications, 674
basic principles, 648–9
common materials for microfiltration and ultrafiltration membrane preparation, 650
concentration polarisation and membrane fouling, 661–8
clarification of kiwifruit juice, 665
concentration polarisation phenomenon according to film model, 663
future trends, 677
integrated processes, 673–6
integrated membrane process in milk processing, 675
membrane materials and membrane preparation technology, 649–52
module configuration and process design, 652–61
basic configurations of membrane modules, 653–4
commercially available membrane modules, 656
different operation modes, 659–60
schematic representation of process, 657
sea water reverse osmosis, 100–1
system for food industry wastewater, 8
treatment of liquid radioactive wastes, 775
unit product cost, 95
universal functional activity coefficient, 34
USEPA *Membrane Filtration Guidance Manual,* 739

vacuum-enhanced direct contact membrane distillation, 709–10
Van der Waals force, 772–3
vanadium redox flow battery, 418–23
chemical stability, 422–3

© Woodhead Publishing Limited, 2011

critical issues, 420
crossover, 420–1, 422
expected water and ion transfer for anion and cation exchange membranes, 422
ion conductivity, 421–2
ion exchange membranes applications, 413–30
phenomena which need to be overcome in order to develop suitable membrane, 420
principles, 418–20
overview, 419
variable costs, 95, 101
Vegard's law, 68
vehicle mechanism, 546–7
Volta, A., 413
volta pile, 413
volume concentration ratio (VCR), 657
von Wroblewski equation, 23

Wager theory, 547
Wagner Equation, 265–6
wastewater purification, 10
'water drag' effect, 470
water treatment
polymeric membranes degradation, 718–39
future trends, 739
identification and monitoring of membrane degradation, 731–7
materials degradation control strategies, 737–8
membrane degradation mechanism, 724–31
membrane failure and operational issues, 720–4
polymer materials and module design, 719–20
water vapour
content, 177
permeability, 178
water–gas shift, 185
water–gas shift membrane reactors, 185–6, 197–201
bench-scale membrane reactor setup, 201
CO conversion as function of the feed pressure and flow rate, 202
dense Pd-based membrane reactor, 198
natural gas fired power plant, 199
operative conditions and performance of MRs, 200
wet cell lead–acid battery, 437
Wilke–Chang equation, 701

X-10 reactor, 771
X-ray diffraction, 56
X-ray photoelectron spectroscopy, 64

Young–Laplace equation, 486
yttria, 570
yttria-stabilised zirconia, 579, 604

Z-Top, 344–5
zeolite membranes, 64–7, 228–30
H_2 permanence of zeolite membranes, 229
morphology, 64
SEM of MFI polycrystalline films, 65
permporosimetry, 66–7
general permporosimetry patterns, 67
pore structure and permeation mechanism, 64–6
schematics of generic permeation patterns, 66
zeolites, 189–90
Zero-Emission Fossil Power Plants Project, 169
zero-gap cell, 571
zirconates, 550
zirconia, 258, 579
Zymomonas mobilis, 371

© Woodhead Publishing Limited, 2011